General Disclaimer

One or more of the Following Statements may affect this Document

- This document has been reproduced from the best copy furnished by the organizational source. It is being released in the interest of making available as much information as possible.

- This document may contain data, which exceeds the sheet parameters. It was furnished in this condition by the organizational source and is the best copy available.

- This document may contain tone-on-tone or color graphs, charts and/or pictures, which have been reproduced in black and white.

- This document is paginated as submitted by the original source.

- Portions of this document are not fully legible due to the historical nature of some of the material. However, it is the best reproduction available from the original submission.

Produced by the NASA Center for Aerospace Information (CASI)

AD-761 559

PROCEEDINGS OF THE EIGHTH INTERNATIONAL SYMPOSIUM ON REMOTE SENSING OF ENVIRONMENT

VOL. 1

ENVIRONMENTAL RESEARCH INSTITUTE

PREPARED FOR
AIR FORCE OFFICE OF SCIENTIFIC RESEARCH/NPG

OCTOBER 1972

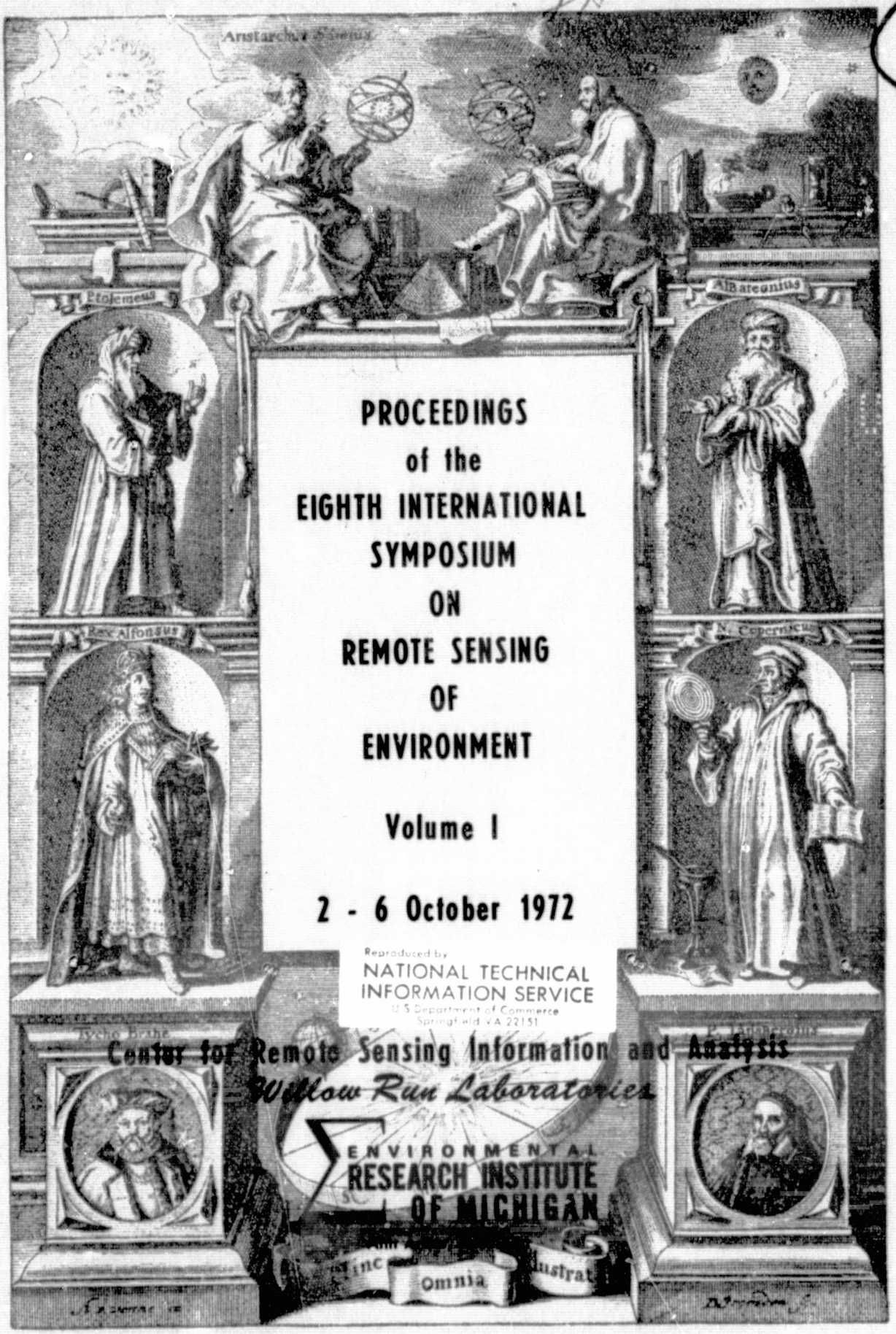
Distributed By:



National Technical Information Service
U. S. DEPARTMENT OF COMMERCE

AFOSR - TR-73-0980

AD 761559



PROCEEDINGS of the EIGHTH INTERNATIONAL SYMPOSIUM ON REMOTE SENSING OF ENVIRONMENT

Volume I

2 - 6 October 1972

Reproduced by
NATIONAL TECHNICAL
INFORMATION SERVICE
U S Department of Commerce
Springfield VA 22151

Center for Remote Sensing Information and Analysis
Willow Run Laboratories
ENVIRONMENTAL
RESEARCH INSTITUTE
OF MICHIGAN

N/R - PRIOR REPT

UNCLASSIFIED

Security Classification

DOCUMENT CONTROL DATA - R & D

(Security classification of title, body of abstract and indexing annotation must be entered when the overall report is classified)

1. ORIGINATING ACTIVITY (Corporate author)	2a. REPORT SECURITY CLASSIFICATION
Willow Run Laboratories of the Environmental Research Institute of Michigan, Ann Arbor	Unclassified
	2b. GROUP

3. REPORT TITLE

Proceedings of the Eighth International Symposium on Remote Sensing of Environment, Volume I, Ann Arbor, Michigan, 2-6 Oct 1972

4. DESCRIPTIVE NOTES (Type of report and inclusive dates)

Scientific.....Final

5. AUTHOR(S) (First name, middle initial, last name)

Jerald J. Cook

6. REPORT DATE	7a. TOTAL NO. OF PAGES	7b. NO. OF REFS
Oct 1972	xlix + 752	

8a. CONTRACT OR GRANT NO.	AFOSR-72-2372	9a. ORIGINATOR'S REPORT NUMBER(S)
b. PROJECT NO.	9751-04	195600-1-X
c.	61102F	9b. OTHER REPORT NO(S) (Any other numbers that may be assigned this report) AFOSR - TR - 73 - 0980
d.	681302	

10. DISTRIBUTION STATEMENT

This document has been approved for public release and sale; its distribution is unlimited.

11. SUPPLEMENTARY NOTES	12. SPONSORING MILITARY ACTIVITY
TECH, OTHER	AF Office of Scientific Research/NPG 1400 Wilson Boulevard Arlington, VA 22209

13. ABSTRACT

These Proceedings contain papers presented at the Eighth International Symposium on Remote Sensing of Environment, held October 2nd through 6th, 1972, on the campus of The University of Michigan. The symposium was conducted by the Center for Remote Sensing Information and Analysis of the Environmental Research Institute of Michigan (formerly The University of Michigan's Willow Run Laboratories) as a part of a continuing program investigating current activities in the field of remote sensing.

Presentations include those on the utilization of this technology by regional governmental units and by federal governmental agencies, as well as various applications in monitoring and managing the earth's resources and man's global environment. Ground-based, airborne, and spaceborne sensor systems and manual and machine-assisted data analysis and interpretation are included.

DD FORM 1 NOV 65 1473

UNCLASSIFIED

Security Classification

195600-1-X

Volume I

PROCEEDINGS of the EIGHTH INTERNATIONAL SYMPOSIUM ON REMOTE SENSING OF ENVIRONMENT

2 - 6 October 1972

This research was supported by the Geophysics Division, AFOSR

AFOSR-72-2372

Sponsored by

Center for Remote Sensing Information and Analysis
Environmental Research Institute of Michigan

Institute of Science and Technology
The University of Michigan

Office of Applications
National Aeronautics and Space Administration

Office of Research and Monitoring
U.S. Environmental Protection Agency

Federal Highway Administration
U.S. Department of Transportation

U.S. Geological Survey
U.S. Department of the Interior

Agricultural Research Service, Forest Service, and
Agricultural Stabilization and Conservation Service
U.S. Department of Agriculture

U.S. Air Force Office of Scientific Research

U.S. Navy Office of Naval Research

U.S. Coast Guard
U.S. Department of Transportation

National Oceanic and Atmospheric Administration
U.S. Department of Commerce

Division of Water Control Planning
Tennessee Valley Authority

VB

Willow Run Laboratories

ENVIRONMENTAL RESEARCH INSTITUTE OF MICHIGAN
Ann Arbor, Michigan

ia

PROGRAM COMMITTEE

Jerald J. Cook, Chairman
Environmental Research Institute of Michigan

R. H. Alexander, U. S. Geological Survey

J. S. Bailey, Office of Naval Research

W. H. Bailey, McLean, Virginia

L. R. Breslau, U. S. Coast Guard

A. J. Calio, National Aeronautics & Space Administration

W. O. Davis, National Oceanic & Atmospheric Administration

J. D. Herold, University of Michigan

R. F. Holmes, Environmental Protection Agency

M. R. Holter, Environmental Research Institute of Michigan

R. H. Miller, U. S. Department of Agriculture

V. E. Noble, U. S. Naval Oceanographic Office

A. B. Park, National Aeronautics & Space Administration

E. M. Risley, U. S. Geological Survey

J. E. Sater, Arctic Institute of North America

J. C. Wilkerson, U. S. Naval Oceanographic Office

G. J. Zissis, Environmental Research Institute of Michigan

Participating Societies

American Geophysical Union

American Institute of Biological Sciences

American Meteorological Society

American Society of Photogrammetry

Association of American Geographers

Geological Society of America

Society of American Foresters

PROGRAM

MONDAY OCTOBER 2

Registration, Rackham Lobby

Welcome and Introduction
W. M. BROWN, President, Environmental Research Institute of Michigan and Director, Willow Run Laboratories

PLENARY SESSION A
(Rackham Lecture Hall)

Chairman: J. C. KELLOGG, Executive Assistant to the Governor, State of Michigan, Lansing

Applications of Remote Sensing in Arizona State Government
C. WINIKKA, State of Arizona, and H. SCHUMANN, U. S. Geological Survey, Phoenix, Arizona

Remote Sensing, A Tool for State Planning-Management in Iowa
S. J. TUTHILL, State Geologist, and J. V. TARANIK, Chief of Remote Sensing, Iowa Remote Sensing Laboratory, Iowa Geological Survey, Iowa City, Iowa

Investigation of Land Resource Use in Southeast Michigan
J. G. AHL, M. G. BOYLAN, D. L. MOKMA, W. L. MYERS, S. W. SCHAR, R. D. VLASIN, Michigan State University, East Lansing, Michigan and I. J. SATTINGER, The University of Michigan, Willow Run Laboratories, Ann Arbor, Michigan

Development of a Practical Remote Sensing Water Quality Monitoring System
J. P. SCHERZ, Department of Civil and Environmental Engineering and Institute for Environmental Studies, The University of Wisconsin, Madison, Wisconsin

Users Report for the Northern Great Plains
F. A. WALTZ, V. I. MYERS, and L. R. HEINEMANN, Remote Sensing Institute, South Dakota State University, Brookings, South Dakota

Regional Land Inventory Systems Development in the Houston Area
J. E. DORNBACH, NASA, Manned Spacecraft Center, Houston, Texas, and J. B. HARRIS, Office of the Governor, Austin, Texas

Remote Sensing Applications in the Metropolitan Washington Council of Governments
H. J. MALLON, Director, Remote Sensing Project, Metropolitan Washington Council of Governments, Washington, D.C.

BREAK

The Role of Earth Resources Satellite Technology in Economic Development
M. W. CONITZ, University of Idaho, Moscow, Idaho

The Application of Remote Sensing to Locating and Monitoring Under-Utilised Land in Jamaica
W. G. COLLINS, University of Aston, Birmingham, England

An Integrated Resource Survey Using Orbital Imagery - An Example from South-East Spain
J. L. VAN GENDEREN, Department of Geography, University of Sheffield, Sheffield S10 2TN, United Kingdom

Enhancement of Earth Resources Technology Satellite (ERTS) and Aircraft Imagery Using Atmospheric Corrections
R. D. SHARMA, Department of Space Hq., Government of India, Bangalore, India, and Willow Run Labs (ERIM), University of Michigan

TUESDAY OCTOBER 3

PLENARY SESSION B
(Rackham Lecture Hall)

Chairman: W. E. BERG, Executive Secretary, Committee on Remote Sensing Programs for Earth Resources Surveys, National Research Council, Washington, D.C.

Use of Remote Sensing in Enforcement Activities: Present and Future
M. FELSHER, Environmental Protection Agency, Office of Enforcement and General Counsel, Office of Technical Analysis

BREAK

Results of the 1971 Corn Blight Watch Experiment
R. B. MACDONALD, NASA, M. E. BAUER, Purdue University, R. D. ALLEN, U. S. Department of Agriculture, J. W. CLIFTON, U. S. Department of Agriculture, J. D. ERICKSON, University of Michigan, and D. A. LANDGREBE, Purdue University

Keynote Address: Remote Sensing and International Affairs
B. LUNDHOLM, Swedish Natural Science Research Council, Stockholm, Sweden

TUESDAY OCTOBER 3

CONCURRENT SESSION 1
(Rackham Lecture Hall)

Chairman: W. H. BAILEY, McLean, Virginia

Microwave Radiometry at the DFVLR, Oberpfaffenhofen, Germany
M. VOGEL, DFVLR Institut fur Flugfunk und Mikrowellen, D 8031 Oberpfaffenhofen, Germany

Emission Properties of Natural Surfaces at Microwave Frequencies
V. V. MELENTYEV and YU. I. RABINOVICH, Council of Ministers of the USSR, Leningrad, USSR

Digital Data Processing from Scanners
J. L. BESSIS, French National Space Research Center (CNES), Bretigny, France

TUESDAY OCTOBER 3

CONCURRENT SESSION 2
(Rackham Amphitheater)

Chairman: J. H. SATER, Research Coordinator, Arctic Institute of North America, Washington D.C.

Satellite Detection of Melting Snow and Ice by Simultaneous Visible and Near-IR Measurements
D. F. MCGINNIS, U.S. Department of Commerce, National Oceanic and Atmospheric Administration, National Environmental Satellite Service, Hillcrest Heights, Maryland 20031

Locating Large Masses of Ground Ice with an Impulse Radar System
C. L. BERTRAM, K. J. CAMPBELL, and S. S. SANDLER, Geophysical Survey Systems, Inc., 16 Republic Road, No. Billerica, Massachusetts 01862

High Resolution Measurements of Snowpack Stratigraphy Using a Short Pulse Radar
R. S. VICKERS and G. C. ROSE, Colorado State University, Department of Electrical Engineering, Fort Collins, Colorado

Two-Dimensional Statistic Analysis of Radar Imagery of Sea Ice
A. A. ZAGORODNIKOV, V. S. LOSHCHILOV, K. B. CHELYSHEV, The Arctic and Antarctic Research Institute, Leningrad, USSR

Satellite Measurements of Microwave and Infrared Radiobrightness Temperature of the Earth's Cover and Clouds
A. E. BASHARINOV, A. S. GURVITCH, A. K. GORODEZKY, S. T. EGOROV, B. G. KUTUZA, A. A. KURSKAYA, D. T. MATVEEV, A. P. ORLOV, and A. M. SHUTKO, Institute of Atmospheric Physics Acad. Sci., USSR, Institute of Radioeng. and Electronics, Scad. Sci., USSR

WEDNESDAY OCTOBER 4

CONCURRENT SESSION 3
(Rackham Lecture Hall)

Chairman: R. H. ALEXANDER, Acting Chief Geographer, U. S. Geological Survey, Washington, D.C.

A Data Base for Comparisons Between Planned and Unplanned Urban Growth
F. H. OSTERHOUDT, Natural Resource Economics Division, Economic Research Service, U. S. Department of Agriculture

Urban Land Use from RB-57 Photography: Computer Graphics of the Boston Area
R. B. SIMPSON, Dartmouth College, Hanover, New Hampshire, R. S. YUILL, Central Michigan University, Mt. Pleasant, Michigan, and D. T. LINDGREN, Dartmouth College, Hanover, New Hampshire

Applications of Remote Sensing to Urban Recreation Planning
D. R. DUNN, College of Education, Temple University, Philadelphia, Pennsylvania

Remote Sensing in the Detection of Regional Change
J. E. ESTES and L. W. SENGER, Geography Remote Sensing Unit, University of California, Santa Barbara, California

BREAK

The Use of Small-Scale Multi-Band Photography for Detecting Land-Use Change
H. F. LINS, JR., and V. A. MILAZZO, Geographic Applications Program, U. S. Geological Survey, Washington, D.C. 20242

NASA Environmental Applications Demonstrations in Southeastern United States
C. T. N. PALUDAN, National Aeronautics and Space Administration, Marshall Space Flight Center, Alabama

Land Use Classification in the Southeastern Forest Region by Multispectral Scanning and Computerized Mapping
F. P. WEBER and R. C. ALDRICH, Pacific Southwest Forest and Range Experiment Station, Forest Service, U. S. Department of Agriculture, Berkeley, California and F. G. SADOWSKI and F. J. THOMSON, Environmental Research Institute of Michigan, (Formerly Willow Run Laboratories), The University of Michigan, Ann Arbor, Michigan

Utilizing Remote Sensing Data for Land Use Decisions for Indian Lands in South Dakota
C. J. FRAZEE, R. L. CAREY, and F. C. WESTIN, Remote Sensing Institute and Plant Science Department, South Dakota State University, Brookings, South Dakota and Branch of Land Operations, Bureau of Indian Affairs, Aberdeen, South Dakota

A Comprehensive Remote Sensing Legend System for the Ecological Characterization and Annotation of Natural and Altered Landscapes
C. E. POULTON, Director, Environmental Remote Sensing Applications Laboratory, Professor of Range Ecology, Rangeland Resources Program, Oregon State University, Corvallis, Oregon 97331

WEDNESDAY OCTOBER 4

CONCURRENT SESSION 4
(Rackham Amphitheater)

Chairman: W. O. DAVIS, Chief, Upper Atmosphere and Space Services, Office of Environmental Monitoring and Prediction, National Oceanic and Atmospheric Administration, Rockville, Maryland

Design and Performance Characteristics of the Vertical Temperature Profile Radiometer (VTPR) for Atmospheric Temperature Soundings
G. FALBEL, Barnes Engineering Company, Stamford, Connecticut

An Experimental Model for the Automated Detection, Measurement, and Quality Control of Low-Level Cloud Motion Vectors from Geosynchronous Satellite Data
R. BRADFORD, J. LEESE, and C. NOVAK, National Environmental Satellite Service, Washington, D.C. 20233

Structure of Dust Storms from ITOS-1 T.V. Images Obtained Over Iraq and the Gulf of Persia
B. V. VINOGRADOV, Moscow Institute, Aerospace Methods, Moscow, USSR, and A. A. GRIGORYEV and V. B. LIPATOV, University of Leningrad, Institute of Physics, Leningrad, USSR

BREAK

Remote Sensing of Atmospheric O_3 and H_2O to 70 km by Aircraft Measurements of Radiation at 1.64 mm Wavelength
J. W. WATERS, Massachusetts Institute of Technology, Department of Electrical Engineering and Research Laboratory of Electronics, Cambridge, Massachusetts 02139

Remote Sensing of Stratospheric Gases Using Submillimetre Radiation
J. E. HARRIES, Division of Electrical Science, National Physical Laboratory, Teddington, Middlesex, UK

Remote Sensing of Mesospheric Ozone
J. E. RUDZKI, JR., Air Force Avionics Laboratory, Dayton, Ohio

Some Results of Spectrophotometric Studies of Natural Formations from the Manned Spacecraft "Soyuz-9"
K. YA. KONDRATYEV, A. A. BUZNIKOV, O. B. VASILYEV, B. V. VINOGRADOV, V. M. ORLOV, V. I. SEVASTYANOV, and O. I. SMOKTY, Leningrad University, Institute of Physics, Leningrad, USSR

Airborne Infrared Polarimetry
D. L. COFFEEN, Lunar and Planetary Laboratory, University of Arizona 85721 and J. E. HANSEN, Goddard Institute for Space Studies, New York, 10025

Principles and Techniques of Polarimetric Mapping
J. HALAJIAN and H. HALLOCK, Grumman Aerospace Corporation, Bethpage, New York

WEDNESDAY OCTOBER 4

CONCURRENT SESSION 5
(Rackham Lecture Hall)

Chairman: R. F. HOLMES, Office of Monitoring, Environmental Protection Agency, Washington, D.C.

Eutrophication Assessment Using Remote Sensing Techniques
C. T. WEZERNAK and F. C. POLCYN, Environmental Research Institute of Michigan, (Formerly Willow Run Laboratories, The University of Michigan), Ann Arbor, Michigan

Investigation of Lake Water Quality in Eastern South Dakota with Remote Sensing Techniques
F. A. SCHMER, South Dakota State University, Brookings, M. J. TIPTON, South Dakota Geological Survey, Vermillion, D. W. RYLAND, South Dakota State University, Brookings, and J. HAYDEN and G. BEAVER, University of South Dakota, Vermillion

Calculating Water Quality Parameters Using Remotely Sensed Scanner DAta
W. L. BROWN, F. C. POLCYN, J. R. MCKIMMY, and O. E. PREWEIT, Willow Run Laboratories, The University of Michigan, Ann Arbor, Michigan

Location of Sawdust in the Penobcot River by a Multispectral Scanner
P. CHASE and A. CONROD, Bendix Aerospace Systems Division, Ann Arbor, Michigan, and E. IMHOFF, University of Maine, Orono, Maine

Multispectral Survey of Power Plant Thermal Effluents in Lake Michigan
F. C. POLCYN, W. L. BROWN, and S. R. STEWART, Environmental Research Institute of Michigan, (Formerly Willow Run Laboratories, University of Michigan), Ann Arbor, Michigan

BREAK

Investigation of Remote Sensing Techniques for Agricultural Feedlot Pollution Detection
F. A. SCHMER, D. W. RYLAND, and F. A. WALTZ, Remote Sensing Institute, South Dakota State University, Brookings, South Dakota

Application of a Pulsed Laser for Measurements of Bathymetry and Algal Fluorescence
G. D. HICKMAN, J. E. HOGG, E. J. FRIEDMAN, and A. H. GHOVANLOU. Sparcom, Inc., Alexandria, Virginia

Multispectral Remote Sensing of Elements of Water and Radiation Balances
W. A. MALILA and T. W. WAGNER, Environmental Research Institute of Michigan, (Formerly Willow Run Laboratories, University of Michigan), P. O. Box 618, Ann Arbor, Michigan

Salinity Surveys Using an Airborne Microwave Radiometer
J. F. PARIS, Lockheed Electronics Company, Inc., Earth Observations Department, Houston, Texas

Applications of Remote Sensing in Public Health
C. M. BARNES, C. E. FULLER, and H. J. SCHNEIDER, NASA Manned Spacecraft Center, Life Sciences Directorate, Health Services Division, Health Applications Office, Houston, Texas, and D. R. MORRISON, National Research Council Fellow, NASA Manned Spacecraft Center, Houston, Texas, and H. G. JONES, The Boeing Company, Houston, Texas

Water Quality Determinations in the Virgin Islands from ERTS-A Data
W. G. EGAN, Research Department, Grumman Aerospace Corporation, Bethpage, New York

WEDNESDAY OCTOBER 4

CONCURRENT SESSION 6
(Rackham Amphitheater)

Chairman: A. B. PARK, Chief, Earth Resources Survey, Earth Observations Programs, Office of Applications, National Aeronautics and Space Administration, Washington, D.C.

Utilization of Thermal Infra-Red Ground Measurements for Determination of Adequate Surveying Periods in Remote Sensing
F. BONN, P. CLEMENT, and collaborators: J. F. GADBOIS, C. JALBERT, M. LAJEUNESSE, and C. TRUDEL, Laboratoire de geographie physique, Universite de Sherbrooke, Sherbrooke, Quebec, Canada

Remote Sensing for Defining Aquifers in Glacial Drift
V. I. MYERS and D. G. MOORE, Remote Sensing Institute, South Dakota State University, Brookings, South Dakota

Thermal Structure of the Sand Desert from the Data of IR Aerophotography
B. V. VINOGRADOV, A. A. GRIGORYEV, V. B. LIPATOV, and A. P. CHERNENKO, Leningrad University, Leningrad, USSR

Radiometric Terrain Mapping at 3 MM Wavelength
E. SCHANDA, G. SCHAERER, and M. WUTHRICH, Institute of Applied Physics, University of Berne, Berne, Switzerland

Progress Report on Aircraft Gamma-Ray Surveys for Soil-Moisture Detection at a NOAA Test Site Near Phoenix, Arizona
D. R. WIESNET, National Environmental Satellite Service/NOAA, Washington, D.C., and E. L. PECK, National Weather Service/NOAA, Silver Spring, Maryland

BREAK

The Reliability of the Interpretation of Soils from Aerial Photographs in Highway Planning Practice
U. KIHLBLOM, Technical Director, B.A., VBB - member of SWECO, Stockholm, Sweden

Definition of Spectrally Separable Classes for Soil Survey Research
J. E. CIPRA, P. H. SWAIN, J. H. GILL, M. F. BAUMGARDNER, and S. J. KRISTOF, Laboratory for Applications of Remote Sensing, Purdue University, West Lafayette, Indiana

Automatic Terrain Mapping by Texture Recognition
E. E. TRIENDL, Institut fur Satellitenelektronik, Oberpfaffenhofen, Germany

Remote Sensing from an Earth Resource Rocket
B. S. E. BEATTIE, British Aircraft Corporation, Electronic and Space Systems, Bristol, England

THURSDAY OCTOBER 5

CONCURRENT SESSION 7
(Rackham Lecture Hall)

Chairman: D. LANDGREBE, Director, Laboratory for Applications of Remote Sensing, West Lafayette, Indiana

The Interpretation of Multispectral Imagery
R. D. MOWER, USAF, Department of Geography, Wright State University, Dayton, Ohio, and Aeronautical Systems Division, Directorate of Plans and Evaluation, Reconnaissance/Strike Group, Wright-Patterson AFB, Ohio

Performance Evaluation of Multispectral Scanner Classification Methods
R. B. CRANE and W. RICHARDSON, The University of Michigan, Willow Run Laboratories, Ann Arbor, Michigan

Adaptive Multispectral Recognition of Agricultural Crops
F. J. KRIEGLER, R. E. MARSHALL, H. HORWITZ, and M. GORDON, Environmental Research Institute of Michigan, P. O. Box 618, Ann Arbor, Michigan

The Effect of Subclass Numbers on Maximum Likelihood Gaussian Classification
A. G. WACKER, University of Saskatchewan, Saskatoon, Saskatchewan

BREAK

An Unsupervised Classification Technique for Multispectral Remote Sensing Data
M. Y. SU, Northrop Services, Inc., Huntsville, Alabama, and R. E. CUMMINGS, NASA Marshall Space Flight Center, Huntsville, Alabama

Signature Extension Techniques Applied to Multispectral Scanner Data
R. F. NALEPKA and J. P. MORGENSTERN, Environmental Research Institute of Michigan, P. O. Box 618, Ann Arbor, Michigan

Atmospheric Model for Correction of Spacecraft Data[1/]
R. E. TURNER and M. M. SPENCER, Environmental Research Institute of Michigan, P. O. Box 618, Ann Arbor, Michigan

Classifying Unresolved Objects from Simulated Space Data
R. F. NALEPKA and P. D. HYDE, Environmental Research Institute of Michigan, P. O. Box 618, Ann Arbor, Michigan

On a Model for Optimal Proportions Estimates for Category Mixtures
C. R. HALLUM, Lockheed Electronics Company, Inc., Houston Aerospace Systems Division, Houston, Texas 77058

A New Method for Evaluating and Mapping Colours in Aerial Photographs
H. S. HELBIG, Institut fur Satellitenelektronik der DFVLR, Oberpfaffenhofen, Germany

THURSDAY OCTOBER 5

CONCURRENT SESSION 8
(Rackham Amphitheater)

Chairman: V. E. NOBLE, Polar Oceanography Division, U. S. Naval Oceanographic Office, Washington, D.C.

Time Sensing and Analysis of Coastal Waters
M. NICHOLS, Virginia Institute of Marine Science, Gloucester Pt., Virginia 23062, and M. KELLY, Department of Environmental Sciences, University of Virginia, Charlottesville, Virginia 22093

Southern California Coastal Processes as Analyzed from Multi-Sensor Data
D. D. STELLER, L. V. LEWIS, and D. M. PHILLIPS, Earth Resources Operations, North American Rockwell Corporation, Downey, California

A Statistical-Temporal Image Merging Technique for Automatic Bathymetry Applied to Southern California Coastal Waters
D. T. HODDER and G. A. MCCUE, North American Rockwell Corporation, Sponsored by Geography Programs, Office of Naval Research under Contract N00014-72-C-0149

Isothermal Mapping of Temperature Patterns from Thermal Discharges in Italian Coastal Waters
D. BORGESE, G. DINELLI, and F. PARRINI, Ente Nazionale Per l'Energia Elettrica (ENEL), Centro Ricerca Termica e Nucleare, Milan, Italy, and D. T. HODDER and D. D. STELLER, Earth Resources Operations, North American Rockwell Corporation, Downey, California

BREAK

Remote Measurement of Water Temperature by Raman Scattering
C. H. CHANG and L. A. YOUNG, Avco Everett Research Laboratory, Everett, Massachusetts

Satellite Detection of Upwelling and Cold Water Eddies
A. E. STRONG, R. J. DERYCKE, and H. STUMPF, U. S. Department of Commerce, National Oceanic and Atmospheric Administration, National Environmental Satellite Service, Hillcrest Heights, Maryland 20031

Relationship Between Sea Wave Parameters and the Spectra of Aerial Photography and Radar Imagery of Sea Surface
A. A. ZAGORODNIKOV, V. S. LOSHCHILOV, and K. B. CHELYSHEV, Arctic and Antarctic Research Institute, Leningrad

The Use of Airborne Imagery for the Estimation of Area and Thickness of Marine Oil Spills: An Operational Example
R. R. THAMAN, J. E. ESTES, R. W. BUTLER, and J. M. RYERSON, University of California, Santa Barbara, California

Detection of Oil Spills Using a 13.3-GHz Radar Scatterometer
K. KRISHEN, Lockheed Electronics Company, Inc., Earth Observations Department, Houston, Texas

Charting the Loop Current by Satellite
M. SIDRAN, National Science Foundation Science Faculty Fellow, National Marine Fisheries Service, 75 Virginia Beach Drive, Miami, Florida 33149, and F. HEBARD, National Marine Fisheries Service, Department of Commerce, Washington, D.C. 20235

THURSDAY OCTOBER 5

CONCURRENT SESSION 9
(Rackham Lecture Hall)

Chairman: E. M. RISLEY, Staff Assistant for Program Development, EROS Program, U. S. Geological Survey, Washington, D.C.

Remote Sensing Aids Geologic Mapping
D. H. KNEPPER, JR., and R. W. MARRS, Colorado School of Mines, Golden, Colorado

Geological Evaluation of Remote Sensing Imagery of the Mesabi Range, Minnesota
A. S. WALKER, Department of Geology and Geophysics, University of Minnesota, Minneapolis, Minnesota

Thermal Activity of the Uson Kaldera Based on Infrared and Photographic Aerial Survey
B. V. SHILIN, N. A. GUSEV, E. I. VAVILOV, and E. J. KARIZHENSKI, Laboratory for Aeromethods, Leningrad, USSR

Geological Analysis of Aerial Thermography of the Canary Islands, Spain
R. S. WILLIAMS, JR., U. S. Geological Survey, Washington, D. C. 20242, and D. FERNANDOPULLE, UNESCO Canary Islands Project (SPA-15), Las Palmas de Gran Canaria, Canary Islands, Spain

Side-Looking Radar Imagery Applied in Seismic-Risk Mapping
E. Y. KEDAR and S. HSU, Department of Geography, State University of New York at Binghamton, Binghamton, New York 13901

BREAK

Research of Space Television Images - A Means of Comparative Planetology
I. I. BASHILOVA, V. K. EREMIN, G. V. MAKHIN, Ministry of Geology, Moscow, USSR

Metallogenic Significance of Alaskan Geostructures Seen from Space
E. H. LATHRAM and G. GRYC, U. S. Geological Survey, Menlo Park, California

The Use of Satellite Photography in Interpretation of Regional Geology
B. N. RAINA, Indian Photo-Interpretation Institute, Dehra Dun, India

An ERTS Multispectral Scanner Experiment for Mapping Iron Compounds
R. K. VINCENT, Willow Run Laboratories, The University of Michigan, Ann Arbor, Michigan

THURSDAY OCTOBER 5

CONCURRENT SESSION 10
(Rackham Amphitheater)

Chairman: R. H. MILLER, Remote Sensing Coordinator, U. S. Department of Agriculture, Washington, D. C.

Temporal Analysis of Multispectral Scanner Data
A. J. RICHARDSON, C. L. WIEGAND, and R. J. TORLINE, Agricultural Research Service, U. S. Department of Agriculture, Weslaco, Texas

Multispectral Scanner Imagery for Plant Community Classification
R. S. DRISCOLL, Rocky Mountain Forest and Range Experiment Station, U.S.D.A. Forest Service, Fort Collins, Colorado, and M. M. SPENCER, Environmental Research Institute of Michigan, P. O. Box 618, Ann Arbor, Michigan

On Microwave Remote Sensing of Vegetation
F. T. ULABY, R. K. MOORE, R. MOE, and J. HOLTZMAN, University of Kansas Center for Research, Inc., Lawrence, Kansas 66044

A Comparison of Four Remote Sensing Media for Assessing Salt Marsh Primary Productivity
J. L. GALLAGHER and R. J. REIMOLD, The University of Georgia Marine Institute, Sapelo Island, Georgia 31327, and D. E. THOMPSON, MAPCOtec, Inc., P. O. Box 310, Daytona Beach, Florida 32015

Detection of Small Fires and Mapping of Large Forest Fires by Infrared Imagery
K. YA. KONDRATYEV, L. N. DYACHENKO, V. I. BINENKO, and A. P. CHERNENKO, Leningrad University, Leningrad, USSR

BREAK

Photodensity and the Impact of Shifting Agriculture on Subtropical Vegetation: A Case Study in the Bahamas
R. BYRNE and J. C. MUNDAY, JR., Department of Geography, University of Toronto, Toronto, Canada

Remote Sensing of Coconut Plants in Kerala (India)
C. DAKSHINAMURTI and A. S. SUMMANWAR, Indian Agricultural Research Institute, New Delhi, India

Plant Canopy Models for Simulating Composite Scene Spectroradiance in the 0.4 to 1.05 Micrometer Region
J. A. SMITH and R. E. OLIVER, Department of Watershed Sciences, Colorado State University, Fort Collins, Colorado 80521

Remote Mapping of Standing Crop Biomass for Estimation of the Productivity of the Shortgrass Prairie, Pawnee National Grasslands, Colorado
R. L. PEARSON and L. D. MILLER, Department of Watershed Sciences, College of Forestry and Natural Resources, Colorado State University, Fort Collins, Colorado 80521

Remote Sensing of Fomes annosus in Forest Stands
C. E. OLSON, JR., School of Natural Resources, The University of Michigan, Ann Arbor, Michigan

Monitoring Levels of Existing Environmental Impact Utilizing Remote Sensing Techniques
M. M. MCCARTHY, Environmental Monitoring and Data Acquisition Group, Institute for Environmental Studies, and Department of Landscape Architecture/Environmental Awareness Center, University of Wisconsin, Madison, Wisconsin

FRIDAY OCTOBER 6

PLENARY SESSION C
(Rackham Lecture Hall)

Chairman: L. JAFFE, Deputy Associate Administrator, Office of Applications, National Aeronautics and Space Administration, Washington, D. C.

ERTS-1 Image Quality
R. WELCH, University of Georgia, Athens, Georgia 30601

A Computer Based System for Reading and Generalising Remote Sensing Data from ERTS-1
J. R. TARRANT, School of Environmental Sciences, University of East Anglia, Norwich, Norfolk, United Kingdom

Interdisciplinary Research on the Application of ERTS-1 Data to the Regional Land Use Planning Process
J. L. CLAPP, R. W. KIEFER, M. M. MCCARTHY, and B. J. NIEMANN, JR., The University of Wisconsin, Madison, Wisconsin

Satellite Geological and Geophysical Remote Sensing of Iceland
R. S. WILLIAMS, JR., U. S. Geological Survey, Washington, D. C. 20242

BREAK

Applications of ERTS-1 Imagery to Agricultural Resource Evaluation
W. C. DRAEGER and A. S. BENSON, Forestry Remote Sensing Laboratory, University of California, Berkeley, California 94270

The Usefulness of ERTS-1 and Supporting Aircraft Data for Monitoring Plant Development in Rangeland Environments
D. M. CARNEGGIE and S. D. DEGLORIA, Forestry Remote Sensing Laboratory, University of California, Berkeley, California

ERTS-1 Study of Reservoirs in Kansas
L. YARGER, J. C. COINER, G. W. JAMES, L. M. MAGNUSON, and J. R. MCCAULEY, The University of Kansas, Lawrence, Kansas, and G. R. MARZOLF, Kansas State University, Manhattan, Kansas

Application of ERTS-1 for Fishery Resource Assessment and Harvest
W. H. STEVENSON, National Marine Fisheries Service, Bay St. Louis, Mississippi, and B. H. ATWELL, NASA, Earth Resources Laboratory, Bay St. Louis, Mississippi, and P. M. MAUGHAN, Earth Satellite Corporation, Washington, D. C.

Canada Centre for Remote Sensing ERTS Program
W. M. STROME, Chief, Data Processing Division, Canada Centre for Remote Sensing, Department of Energy, Mines and Resources, Ottawa, and E. SHAW, ERTS Project Manager, Computing Devices of Canada, Ottawa

ERTS and Arctic Engineering Geology in Alaska
O. J. FERRIANS, JR., U. S. Geological Survey, Menlo Park, California

Cold Regions Environmental Analysis Based on ERTS-1 Imagery
R. K. HAUGEN, H. L. MCKIM, L. W. GATTO, and D. M. ANDERSON, U. S. Army Cold Regions Research and Engineering Laboratory, Hanover, New Hampshire 03755

Expected Results of Hydrologic and Geologic Studies Using ERTS Imagery of the Atacama Desert, Altiplano, and Puna de Atacama, South America (Southwest Bolivia, Northwest Argentina, and Northern Chile)
G. E. STOERTZ and G. E. ERICKSEN, U. S. Geological Survey, Washington, D. C. 20242

ABSTRACT

These Proceedings contain papers presented at the Eighth International Symposium on Remote Sensing of Environment, held October 2nd through 6th, 1972, on the campus of the University of Michigan. The symposium was conducted by the Center for Remote Sensing Information and Analysis of the Environmental Research Institute of Michigan (formerly the University of Michigan's Willow Run Laboratories) as a part of a continuing program investigating current activities in the field of remote sensing.

Presentations include those on the utilization of this technology by regional governmental units and by federal governmental agencies, as well as various applications in monitoring and managing the earth's resources and man's global environment. Ground-based, airborne, and spaceborne sensor systems and manual and machine-assisted data analysis and interpretation are included.

FOREWORD

The publication of these Proceedings of the Eighth International Symposium on Remote Sensing of Environment marks the end of the first decade of this series and the beginning of a new era in remote sensing. On 23 July 1972, the first Earth Resources Technology Satellite (ERTS-1) was launched into a sun-synchronous polar orbit, providing repetitive coverage of most of the earth once every 18 days. Initial results in the earth-resource application of these data were presented in a review at Goddard Space Flight Center on 29 September 1972. The following week that meeting was summarized and an additional 14 papers were presented at this symposium. These preliminary results provide a sound basis for the expectation that our next decade will more than duplicate the tremendous progress seen during the first.

All of you, the attendees and participants at the "Michigan Symposium" series, are to be congratulated for the truly remarkable progress which has been made since 1962. We are only beginning to realize the fruits of your labor, as a steadily growing community of earth-science users incorporate remote sensing data and processing techniques into their resource programs. For example, scan the first two sessions of the current meeting and note the breadth of application now being reported among various governmental units, or the following sessions with their now common-place continuum of reports on snow and ice, the sea surface, the atmosphere or land-use patterns. These Proceedings once again reflect an intense effort toward the development of machine-assisted data handling and interpretation techniques, in monitoring various environmental quality factors, or in delineating and assessing geological formations or vegetative parameters of importance in managing world resources.

Thus we, the remote sensing community, herewith submit the latest efforts in this continuing series, documenting activities aimed at the effective application of this far-reaching technology. At the end of this first decade these Proceedings continue to represent the most comprehensive compilation of remote sensing information available. This status is, as it will continue to be, due solely to the dedicated effort of the program committee, the participating societies, the guest speakers and session chairman, and of course, the scientific community who continue to present noteworthy papers at this meeting.

Finally, as the Willow Run Laboratories complete their separation from the University of Michigan, we should acknowledge the vast contribution, in pioneering and developing this technology, which has resulted from that long-standing illustricus association. The emergence of a new parent organization, the Environmental Research Institute of Michigan embodying essentially 100% of the former Willow Run Laboratories, will ensure an even more vigorous and multifaceted program of remote sensing research and development in the coming decade. The Center for Remote Sensing Information and Analysis, now an integral part of the new organization, will continue to host this series of symposia with the Ninth meeting now scheduled for April, 1974.

Jerald J. Cook
Chairman, Program Committee

EDITORIAL NOTE

The papers contained herein are in the order of presentation. Those manuscripts not received in time to meet publication deadlines have been represented by comprehensive summaries whereever possible. An author index and the revised program are included as a supplement to the table of contents.

All illustrative materials are reproduced in black and white unless individual authors elected to provide their own color prints. Readers are requested to contact specific authors where color prints of black and white figures are desired.

Additional copies of these Proceedings may be obtained from:

Center for Remote Sensing Information and Analysis
Environmental Research Institute of Michigan
P. O. Box 618
Ann Arbor, Michigan 48107

CONTENTS

Program Committee ii

Participating Societies ii

Program iii

Abstract x

Foreword xi

Editorial Note xii

Registrants xix

Welcome and Introduction, W. M. Brown 1

Plenary Session A

Applications of Remote Sensing in Arizona State Government, C. Winikka and H. Schumann . . 3

Application of Remote Sensing Technology to Resource Management Problems of State Government in California, J. B. Passerello and D. E. Schwarz 7

Remote Sensing, A Tool for State Planning-Management in Iowa, S. J. Tuthill and J. V. Taranik 11

A Study of the Feasibility of Applying Remotely Sensed Data in the Management of Natural Resources and the Improvement of Environmental Quality in Alabama, H. R. Henry, G. McDonough, and P. E. LaMoreaux 21

Investigation of Land Resource Use in Southeast Michigan, J. G. Ahl, et al 23

Development of a Practical Remote Sensing Water Quality Monitoring System, J. P. Scherz . . 35

Users Report for the Northern Great Plains, F. A. Waltz, V. I. Myers, and L. R. Heinemann . 47

Regional Land Inventory Systems Development in the Houston Area, J. E. Dornbach and J. B. Harris 53

Remote Sensing Applications in the Metropolitan Washington Council of Governments, H. J. Mallon 61

The Role of Earth Resources Satellite Technology in Economic Development, M. W. Conitz . . 99

The Application of Remote Sensing to Locating and Monitoring Under-Utilised Land in Jamaica, W. G. Collins 103

An Integrated Resource Survey Using Orbital Imagery - An Example from South-East Spain, J. L. van Genderen 117

Enhancement of Earth Resources Technology Satellite (ERTS) and Aircraft Imagery Using Atmospheric Corrections, R. D. Sharma 137

Plenary Session B

Use of Remote Sensing in Enforcement Activities: Present and Future, M. Felsher 153

Results of the 1971 Corn Blight Watch Experiment, R. B. MacDonald, et al 157

KEYNOTE ADDRESS: B. Lundholm 191

Concurrent Session 1

Microwave Radiometry at the DFVLR, Oberpfaffenhofen, Germany, M. Vogel 199

Emission Properties of Natural Surfaces at Microwave Frequencies, V. V. Melentyev and Yu. I. Rabinovich 217

Digital Data Processing From Scanners, J. L. Bessis 225

A Computer Controlled Precision Comparator-Densitometer, P. W. H. Blansjaar, et al 229

Concurrent Session 2

Satellite Detection of Melting Snow and Ice by Simultaneous Visible and Near-IR Measurements, D. F. McGinnis 231

Locating Large Masses of Ground Ice With an Impulse Radar System, C. L. Bertram, K. J. Campbell, and S. S. Sandler 241

High Resolution Measurements of Snowpack Stratigraphy Using a Short Pulse Radar, R. S. Vickers and G. C. Rose 261

Two-Dimensional Statistic Analysis of Radar Imagery of Sea Ice, A. A. Zagorodnikov, V. S. Loshchilov, and K. B. Chelyshev 279

Satellite Measurements of Microwave and Infrared Radiobrightness Temperature of the Earth's Cover and Clouds, A. E. Basharinov, et al 291

Concurrent Session 3

A Data Base for Comparisons Between Planned and Unplanned Urban Growth, F. H. Osterhoudt . 297

Urban Land Use From RB-57 Photography: Computer Graphics of the Boston Area, R. B. Simpson, R. S. Yuill, D. T. Lindgren 299

Applications of Remote Sensing to Urban Recreation Planning, D. R. Dunn 311

Remote Sensing in the Detection of Regional Change, J. E. Estes and L. W. Senger 317

The Use of Small-Scale Multi-Band Photography for Detecting Land-Use Change, H. F. Lins and V. A. Milazzo 325

NASA Environmental Applications Demonstrations in Southeastern United States, C. T. N. Paludan 345

Land Use Classification in the Southeastern Forest Region by Multispectral Scanning and Computerized Mapping, F. P. Weber, R. C. Aldrich, F. G. Sadowski, and F. J. Thomson . . 351

Utilizing Remote Sensing Data for Land Use Decisions for Indian Lands in South Dakota, C. J. Frazee, R. L. Carey, and F. C. Westin 375

A Comprehensive Remote Sensing Legend System for the Ecological Characterization and Annotation of Natural and Altered Landscapes, C. E. Poulton 393

Concurrent Session 4

Design and Performance Characteristics of the Vertical Temperature Profile Radiometer (VTPR) for Atmospheric Temperature Soundings, G. Falbel 409

An Experimental Model for the Automated Detection, Measurement, and Quality Control of Low-Level Cloud Motion Vectors from Geosynchronous Satellite Data, R. Bradford, J. Leese, and C. Novak 441

Structure of Dust Storms from ITOS-1 T. V. Images Obtained Over Iraq and the Gulf of Persia, B. V. Vinogradov, A. A. Grigoryev, and V. B. Lipatov 463

Remote Sensing of Atmospheric O_3 and H_2O to 70 km by Aircraft Measurements of Radiation at 1.64 mm Wavelength, J. W. Waters 467

Remote Sensing of Stratospheric Gases Using Submillimetre Radiation, J. E. Harries 475

Remote Sensing of Mesospheric Ozone, J. E. Rudzki 487

Some Results of Spectrophotometric Studies of Natural Formations From the Manned Spacecraft "SOYUZ-9", K. Ya. Kondratyev, et al 505

Airborne Infrared Polarimetry, D. L. Coffeen and J. E. Hansen 515

Principles and Techniques of Polarimetric Mapping, J. Halajian and H. Hallock 523

Concurrent Session 5

Eutrophication Assessment Using Remote Sensing Techniques, C. T. Wezernak and F. C. Polcyn 541

Investigation of Lake Water Quality in Eastern South Dakota With Remote Sensing Techniques, F. A. Schmer, et al 553

Calculating Water Quality Parameters Using Remotely Sensed Scanner Data, W. L. Brown, F. C. Polcyn, J. R. McKinmy, and O. E. Prewett 563

Location of Sawdust in the Penobcot River by a Multispectral Scanner, P. Chase, A. Conrod, and E. Imhoff 569

Multispectral Survey of Power Plant Thermal Effluents in Lake Michigan, F. C. Polcyn, W. L. Brown, and S. R. Stewart 583

Investigation of Remote Sensing Techniques for Agricultural Feedlot Pollution Detection, F. A. Schmer, D. W. Ryland, and F. A. Waltz 603

Application of a Pulsed Laser for Measurements of Bathymetry and Algal Fluorescence, G. D. Hickman, J. E. Hogg, E. J. Friedman, and A. H. Ghovanlou 617

Multispectral Remote Sensing of Elements of Water and Radiation Balances, W. A. Malila and T. W. Wagner 639

Salinity Surveys Using an Airborne Microwave Radiometer, J. F. Paris 665

Applications of Remote Sensing in Public Health, C. M. Barnes, et al 677

Water Quality Determinations in the Virgin Islands from ERTS-A Data, W. G. Egan 685

Concurrent Session 6

Utilization of Thermal Infra-Red Ground Measurements for Determination of Adequate Surveying Periods in Remote Sensing, F. Bonn, et al 709

Remote Sensing for Defining Aquifers in Glacial Drift, V. I. Myers and D. G. Moore 715

Thermal Structure of the Sand Desert From the Data of IR Aerophotography, B. V. Vinogradov, A. A. Grigoryev, V. B. Lipatov, and A. P. Chernenko 729

Radiometric Terrain Mapping at 3 MM Wavelength, E. Schanda, G. Schaerer, and M. Wüthrich. . 739

Progress Report on Aircraft Gamma-Ray Surveys for Soil Moisture Detection at a NOAA Test Site Near Phoenix, Arizona, D. R. Wiesnet and E. L. Peck 747

The Reliability of the Interpretation of Soils From Aerial Photographs in Highway Planning Practice, U. Kihlblom 755

Definition of Spectrally Separable Classes for Soil Survey Research, J. E. Cipra, et al . . 765

Automatic Terrain Mapping by Texture Recognition, E. E. Triendl 771

Remote Sensing From an Earth Resource Rocket, B. S. E. Beattie 777

Concurrent Session 7

The Interpretation of Multispectral Imagery, An Analysis of Automated Versus Human Interpretation Techniques, R. D. Mower 789

Performance Evaluation of Multispectral Scanner Classification Methods, R. B. Crane and W. Richardson 815

Adaptive Multispectral Recognition of Agricultural Crops, F. J. Kriegler, R. E. Marshall, H. Horwitz, and M. Gordon 833

The Effect of Subclass Numbers of Maximum Likelihood Gaussian Classification, A. G. Wacker 851

An Unsupervised Classification Technique for Multispectral Remote Sensing Data, M. Y. Su . 861

Signature Extension Techniques Applied to Multispectral Scanner Data, R. F. Nalepka and J. P. Morgenstern 881

Atmospheric Model for Correction of Spacecraft Data, R. E. Turner and M. M. Spencer . . . 895

Classifying Unresolved Objects From Simulated Space Data, R. F. Nalepka and P. D. Hyde . . 935

On a Model for Optimal Proportions Estimates for Category Mixtures, C. R. Hallum 951

A New Method for Evaluating and Mapping Colours in Aerial Photographs, H. S. Helbig and W. Tzschupke 959

Concurrent Session 8

Time Sensing and Analysis of Coastal Waters, M. Nichols and M. Kelly 969

Southern California Coastal Processes as Analyzed From Multi-Sensor Data, D. D. Steller, L. V. Lewis, and D. M. Phillips 983

A Statistical-Temporal Image Merging Technique for Automatic Bathymetry Applied to Southern California Coastal Waters, D. T. Hodder and G. A. McCue 999

Isothermal Mapping of Temperature Patterns From Thermal Discharges in Italian Coastal Waters, D. Borgese, et al 1017

Remote Measurement of Water Temperature by Raman Scattering, C. H. Chang and L. A. Young . 1049

Satellite Detection of Upwelling and Cold Water Eddies, A. E. Strong, R. J. DeRycke, and H. Stumpf 1069

Relationship Between Sea Wave Parameters and the Spectra of Aerial Photography and Radar Imagery of Sea Surface, A. A. Zagorodnikov, V. S. Loshchilov, and K. B. Chelyshev 1083

The Use of Airborne Imagery for the Estimation of Area and Thickness of Marine Oil Spills: An Operational Example, R. R. Thaman, J. E. Estes, R. W. Butler, and J. M. Ryerson 1093

Detection of Oil Spills Using a 13.3-GHz Radar Scatterometer, K. Krishen 1105

Charting the Loop Current by Satellite, M. Sidran and F. Hebard 1121

Concurrent Session 9

Remote Sensing Aids Geologic Mapping, D. H. Knepper and R. W. Marrs 1127

Geological Evaluation of Remote Sensing Imagery of the Mesabi Range, Minnesota, A. S. Walker 1137

Thermal Activity of the Uson Kaldera Based on Infrared and Photographic Aerial Survey, B. V. Shilin, N. A. Gusev, E. I. Vavilov, E. J. Karizhenski 1147

Geological Analysis of Aerial Thermography of the Canary Islands, Spain, R. S. Williams and D. Fernandopulle 1159

Side-Looking Radar Imagery Applied in Seismic-Risk Mapping, E. Y. Kedar and S. Hsu 1195

Research of Space Television Images - A Means of Comparative Planetology, I. I. Bashilova, V. K. Eremin, and G. V. Makhin 1199

Metallogenic Significance of Alaskan Geostructures Seen From Space, E. H. Lathram and G. Gryc 1209

The Use of Satellite Photography in Interpretation of Regional Geology, B. N. Raina 1213

Thermal Inertia Mapping From Nimbus Satellite Data, K. Watson, H. A. Pohn, and T. W. Offield 1237

An ERTS Multispectral Scanner Experiment for Mapping Iron Compounds, R. K. Vincent 1239

Concurrent Session 10

Temporal Analysis of Multispectral Scanner Data, A. J. Richardson, C. L. Wiegand, and R. J. Torline 1249

Multispectral Scanner Imagery for Plant Community Classification, R. S. Driscoll and M. M. Spencer 1259

On Microwave Remote Sensing of Vegetation, F. T. Ulaby, R. K. Moore, R. Moe, and J. Holtzman 1279

A Comparison of Four Remote Sensing Media for Assessing Salt Marsh Primary Productivity, J. L. Gallagher, R. J. Reimold, and D. E. Thompson 1287

Detection of Small Fires and Mapping of Large Forest Fires by Infrared Imagery, K. Ya. Kondratyev, L. N. Dyachenko, V. I. Binenko, and A. P. Chernenko 1297

Photodensity and the Impact of Shifting Agriculture on Subtropical Vegetation: A Case Study in the Bahamas, R. Byrne and J. C. Munday 1311

Remote Sensing of Coconut Plants In Kerala (India), C. Dakshinamurti and A. S. Summanwar . 1327

Plant Canopy Models for Simulating Composite Scene Spectroradiance in the 0.4 to 1.05 Micrometer Region, J. A. Smith and R. E. Oliver 1333

Remote Mapping of Standing Crop Biomass for Estimation of the Productivity of the Shortgrass Prairie, R. L. Pearson and L. D. Miller 1355

Remote Sensing of *Fomes annosus* in Forest Stands, C. E. Olson 1381

Monitoring Levels of Existing Environmental Impact Utilizing Remote Sensing Techniques, M. M. McCarthy 1385

Plenary Session C

ERTS-1 Image Quality, R. Welch 1411

A Computer Based System for Reading and Generalising Remote Sensing Data from ERTS-1, J. R. Tarrant 1425

Interdisciplinary Research on the Application of ERTS-1 Data to the Regional Land Use Planning Process, J. L. Clapp, R. W. Kiefer, M. M. McCarthy, and B. J. Niemann 1429

Satellite Geological and Geophysical Remote Sensing of Iceland, R. S. Williams 1465

Applications of ERTS-1 Imagery to Agricultural Resource Evaluation, W. C. Draeger and A. S. Benson 1467

The Usefulness of ERTS-1 and Supporting Aircraft Data for Monitoring Plant Development in Rangeland Environments, D. M. Carneggie and S. D. DeGloria 1471

ERTS-1 Study of Reservoirs in Kansas, H. L. Yarger, et al 1477

Application of ERTS-1 for Fishery Resource Assessment and Harvest, W. H. Stevenson, B. H. Atwell, and J. M. Maughan 1491

Canada Centre for Remote Sensing ERTS Program, W. M. Strome and E. Shaw 1497

ERTS and Arctic Engineering Geology in Alaska, O. J. Ferrians 1509

Cold Regions Environmental Analysis Based on ERTS-1 Imagery, R. K. Haugen, H. L. McKim, L. W. Gatto, and D. M. Anderson 1511

Expected Results of Hydrologic and Geologic Studies Using ERTS Imagery of the Atacama Desert, Altiplano, and Puna de Atacama, South America, G. E. Stoertz and G. E. Ericksen 1523

REGISTRANTS OF THE EIGHTH SYMPOSIUM

ON REMOTE SENSING OF ENVIRONMENT

ADDRESS, Stanley R.
U. S. Geological Survey
EROS Program
Code 430, NASA
Goddard Space Flight Center
Greenbelt, Maryland 20771

ADEY, A. W.
Communications Research Center
Department of Communications
Shirley Bay
P. O. Box 490
Station A
Ottawa, Ontario, Canada KIN 8T5

AGGARWALA, R. K.
University of Michigan
Remote Sensing/Natural Resources
Room 1534
Ann Arbor, Michigan

AGREN, Carl Hugo
Research Institute of National Defense
Linnegalan 89
Stockholm 80, Sweden

AHL, James G.
Michigan State University
Department of Resource Development
East Lansing, Michigan 48823

AITKENS, David F.
Environment Ontario
Private Waste & Water Management Branch
Ministry of Environment
135 St. Clair Avenue, W.
Toronto, Ontario, Canada

ALAIN, Blanchard
National Space Center
Paris CNES/TOULOUSE
France

ALBERTINI, Peter C.
Honeywell
Earth & Space Observation
2 Forbes Road
Lexington, Massachusetts 02173

ALEXANDER, Robert H.
U. S. Department of Interior
Geological Survey
Room 837, 1717 H Street, NW
Washington, D. C. 20242

ALLCOCK, G.
Physics and Engineering Lab
Department of Science & Industrial Research
Lower Hutt, New Zealand

ALLEN, Peter
University of Michigan
Ann Arbor, Michigan

ALLEN, R.
U. S. Department of Agriculture
Washington, D. C.

ALLEY, Lee R.
University of Nebraska
Computer Science
109 Ferguson
Lincoln, Nebraska 68508

ALLUM, J. A. E.
International Nickel Company
Exploration Department
Toronto-Dominion Centre
Toronto, Ontario, Canada

ALOUGES, A.
CNES
129 rue de l'Universite
Paris, France

ANDERSON, Bill
University of Michigan
School of Natural Resources
Ann Arbor, Michigan

ANDERSON, Delmar E.
University of Kansas
Department of Geography
Lawrence, Kansas 66044

ANIYA, Masamu
Department of Geography
University of Georgia
Athens, Georgia

APEL, John R.
NOAA
Atlantic Oceanographic Meteorological
Laboratories
15 Rickenbacker Causeway
Miami, Florida 33149

ARNETT, Stanley K. II
University of Michigan
School of Library Science
819 E. University #4
Saginaw, Michigan

ATKINS, Gordon R.
U. S. Department of Interior
Bureau of Outdoor Recreation
3853 Research Park Drive
Ann Arbor, Michigan

AXELSSON, R. Sune
SAAB-SCANIA
Aerospace Group
Missile and Electronics Division
Linkoping, Sweden

BAKER, Kenneth
NASA
Manned Spacecraft Center
Houston, Texas 77058

BAKER, Ralph
CCRS/Canada
Department of Energy, Mines & Resources
Booth Street
Ottawa, Ontario, Canada

BAILEY, Walter H.
6611 Georgetown Pike
McLean, Virginia 22101

BALL, David L.
Colorado State University
Watershed Sciences
Ft. Collins, Colorado 80521

BALOGH, Lewis J.
Ministry of Natural Resources
Conservation Authorities Branch
880 Bay Street
Toronto 5, Ontario, Canada

BARNA, George
RCA
Astro-Electronics Division
P. O. Box 800
Princeton, New Jersey 08540

BARNES, Charles M.
NASA
Health Applications Office
Houston, Texas 77058

BARTMAN, F. L.
University of Michigan
Aerospace Engineering
Research Activities Building
2450 Hayward
Ann Arbor, Michigan

BARTOLUCCI, Luis A.
LARS
Purdue University
1220 Potter Drive
West Lafayette, Indiana 47906

BAUER, Marvin
Purdue University
LARS
1220 Potter Drive
West Lafayette, Indiana 47906

BEATTIE, B. S. E.
British Aircraft Corp., Ltd.
Electronic & Space Systems
G.P.O. Box 77 Filton House
Bristol BS99 7AR, England

BEATTY, Frank
Mississippi Test Facility
EROS Support
Building 1100
Bay St. Louis, Mississippi

BEILOCK, M.
Bendix Corporation
Aerospace Systems Division
3300 Plymouth Road
Ann Arbor, Michigan

BENDER, Lee U.
State University of New York
College of Environmental Science & Forestry
Department of Forest Engineering
Syracuse, New York 13210

BENTLEY, Gordon
Bureau of Mines
1414 University Blvd.
P. O. Box 723
Riverside, California 92502

BERG, Mark R.
University of Michigan
Urban & Regional Planning
2036 School of Natural Resources
Ann Arbor, Michigan

BERG, Winifred E.
U. S. Navy
National Academy of Sciences
21st and Pennsylvania Avenue
Joseph Henry Building
Washington, D. C. 20418

BERNATH, Hans J.
University of Washington
Department of Civil Engineering
Seattle, Washington 98195

BESSIS, Jean-Luc H.
C. N. E. S.
Mathematic & Data Processing
BP n° 4
9A. Bretigwy, France

BEST, William
Air Force Office of Scientific Research
Geophysics Division
Arlington, Virginia

BILLINGSLEY, Fred C.
Jet Propulsion Lab
Image Processing Lab
4800 Oak Grove Drive
Pasadena, California 91103

BARTLEY, Willard B.
RESSI
Smith Road
Spring Valley, New York 10977

BLACK, Ken
Philco-Ford Corporation
Earth Resources
1002 Gemini
Houston, Texas 77058

BLACKARD, Jerry J.
U. S. Department of Interior
Bureau of Sport Fisheries & Wildlife
816 Peachtree 7th Building
Atlanta, Georgia 30323

BOETTNER, E. A.
University of Michigan
Environmental & Industrial Health
1530 School of Public Health
Ann Arbor, Michigan

BOHL, Frederick L.
Commonwealth Associates
Architecture & Community Planning
209 East Washington Avenue
Jackson, Michigan 49201

BOHN, Charles G.
NASA - ERTS
USER Support
Code 430
Goddard Space Flight Center
Greenbelt, Maryland 20720

BONN, F.
Universitat de Sherbrooke
Department of Geography
Sherbrooke, Quebec, Canada

BOOTS, Richard A.
Purdue University
LARS
Horticulture Building
Lafayette, Indiana

BOYD, Robert W.
Mississippi State University
Electrical Engineering
Drawer EE
State College, Mississippi

BOYLAN, Myles
Urban Planning & Landscape
Michigan State University
Lansing, Michigan 48906

BRADEN, D. S.
Environmental Engineering
BP Alaska, Inc.
P. O. Box 1379
Anchorage, Alaska 99503

BRADFORD, K. N.
IBM
Department K31 - FSD
150 Sparkman Drive
Huntsville, Alabama 35805

BRADFORD, R.
U. S. Department of Commerce
NOAA
Washington, D. C.

BRADLEY, John S.
Amoco
Research Division
P. O. Box 591
Tulsa, Oklahoma 74102

BRAITHWAITE, John
Environmental Research Institute of Michigan
Willow Run Laboratories
P. O. Box 618
Ann Arbor, Michigan 48107

BRAND, Jim
CCRS/CFASU
CFB Uplands
Ottawa, Ontario, Canada KIA OK5

BRAUNINGER, Buford L.
McDonnell Douglas Astronautics Company
Department E450
P. O. Box 516
St. Louis, Missouri 63166

BRAVO, Sergio A.
University de Chile
N.A.S.A. Department
P. O. Box 2777
Santiago, Chile

BRECHENRIDGE, Roy
University of Wyoming
Department of Geology
Laramie, Wyoming 82070

BRESLAU, Lloyd R.
U. S. Department of Transportation
U. S. Coast Guard
Commandant
Washington, D. C.

BRICKER, Cal D.
Alberta Department of Highways
and Transportation
Planning Branch
106th Street & 97 Avenue
Edmonton, Alberta, Canada

BRIGGS, Darinka
University of Michigan
Geology and Mineral Department
1007 CCL
Ann Arbor, Michigan

BRIGGS, Louis
University of Michigan
Geology and Mineral Department
1007 CCL
Ann Arbor, Michigan

BRISCOE, Frank
Perkin-Elmer
E-O Division
Wilton, Connecticut

BRONSTEIN, Leon
Canada Center for Remote Sensing
Department of Energy, Mines, and Resources
Ottawa, Ontario, Canada

BROWN, Dwight A.
University of Minnesota
Department of Geography
Minneapolis, Minnesota 55455

BROWN, Harold J.
Sperry-Univac
1275 Space Park Drive
P. O. Box 58488
Houston, Texas 77058

BROWN, Ronald J.
Defense Research Board
Remote Sensing
Defense Research Establishment
Ottawa, CFHQ, Ontario, Canada

BROWN, Terry J.
Harvard University
253 Crafts Street
Newton, Massachusetts 02160

BROWN, William L.
Environmental Research Institute of Michigan
Willow Run Laboratories
Building 2041
P. O. Box 618
Ann Arbor, Michigan 48107

BROWN, William M.
Environmental Research Institute of Michigan
Willow Run Laboratories
Building 2202
P. O. Box 618
Ann Arbor, Michigan 48107

BRUNE, Basel H.
University of Maryland
Department of Geography
9111 Contee Road, Apt. 301
Laurel, Maryland 20810

BRUNNSCHWEILER, Dieter
Michigan State University
Geography Department
East Lansing, Michigan

BRUNS, Dennis
Colorado School of Mines
Geology Department
Golden, Colorado 80401

BRYAN, M. Leonard
Environmental Research Institute of Michigan
Willow Run Laboratories
P. O. Box 618
Ann Arbor, Michigan 48107

BURNS, George D.
Office of State Planning
Environmental Planning
Room 506, Finance Building
Main Capitol
Harrisburg, Pennsylvania 17120

BURNS, Kerry
C.S.I.R.O.
Mineral Physics
P. O. Box 136
North Ryde, N.S.W., Australia 2113

CALIO, Anthony J.
NASA/MSC
Director of Science & Applications
Houston, Texas

CAMPBELL, Charles E.
Lockheed Electronics
Earth Observations
16811 El Camino Real
Mail Code B11
Houston, Texas 77058

CAMPBELL, David
University of Michigan
School of Natural Resources
Ann Arbor, Michigan

CAREY, Rex L.
Bureau of Indian Affairs
Department of Interior
820 S. Main
Aberdeen, South Dakota 57401

CARLSON, Walter J. Jr.
University of Minnesota
Space Science Center
103 Space Science Center
Minneapolis, Minnesota 55455

CARMER, Dwayne C.
Environmental Research Institute of Michigan
Willow Run Laboratories
P. O. Box 618
Ann Arbor, Michigan 48107

CARNEGGIE, David
University of California
Forestry Remote Sensing Lab
260 Space Sciences Lab
Berkeley, California 94720

CAROW, John
University of Michigan
2541 Natural Resources Building
Ann Arbor, Michigan

CARTER, Virginia
U. S. Geological Survey
Water Resources Division
USGS/WRD
2100 M Street, N. W.
Washington, D. C. 20242

CARTER, William Douglas
U. S. Geological Survey
EROS Program
1717 H Street, Room 815
Washington, D. C. 20242

CARTWRIGHT, Vern W.
Cartwright Aerial Surveys, Inc.
Executive Airport
Sacramento, California 95822

CASTELLET, Jose Torrent
ETS. Ingenieros Agronomos
Catedra De Edafologia
Madrid 3, Spain

CHANEY, L. W.
University of Michigan
Aerospace Engineering
2450 Hayward
Ann Arbor, Michigan

CHAPMAN, Jack C.
3M Company
Video Tape Duplicating
3M Center
St. Paul, Minnesota 55101

CHASE, Phil
Bendix Aerospace Systems Division
3300 Plymouth Road
Ann Arbor, Michigan

CHEATHAM, Eugene
University of Michigan
Ann Arbor, Michigan

CHEN, Kan
University of Michigan
2517 E. Engineering
Ann Arbor, Michigan

CHILDRESS, Ray
Texas Parks and Wildlife Department
Coastal Fisheries
P. O. Box 808
Seadrift, Texas 77983

CHILDS, Leo F.
NASA/MSC
Earth Observations
Houston, Texas 77058

CINDRICH, Ivan
Environmental Research Institute of Michigan
Willow Run Laboratories
P. O. Box 618
Ann Arbor, Michigan 48107

CIPRA, J. E.
Purdue University
1220 Potter Drive
W. Lafayette, Indiana 47906

CLAPP, James L.
University of Wisconsin
351 Meteorology & Space Sciences Building
Madison, Wisconsin 53706

CLARK, Fitzhugh T.
Department of the Interior
U. S. Geological Survey
EROS Program
1717 H Street, N. W., Room 823
Washington, D. C. 20242

CLEMENT, Pierre
University of Sherbrooke
Department of Geography
Sherbrooke, Quebec, Canada

CLOPTON, Lewis P.
University of Michigan
Ann Arbor, Michigan

CODIK, Andrew
North American Rockwell
Space Division
Downey, California

COFFEEN, D. L.
University of Arizona
Lunar and Planetary Lab
Tucson, Arizona 85721

COKER, A. E.
U. S. Department of Interior
500 Zack Street
Tampa, Florida 33602

COLLINS, W. Gordon
University of Aston
Department of Civil Engineering
Gosta Green
Birmingham B47Et, England

COLWELL, John E.
University of Michigan
School of Natural Resources
Ann Arbor, Michigan

CONITZ, Merrill
University of Idaho
College of Engineering
Moscow, Idaho 83843

CONLEY, Cindy
Environmental Research Institute of Michigan
Willow Run Laboratories
P. O. Box 618
Ann Arbor, Michigan 48107

CONROD, Alfred C.
Bendix Aerospace
3300 Plymouth Road
Ann Arbor, Michigan 48107

COOK, Jerald J.
Environmental Research Institute of Michigan
Willow Run Laboratories
P. O. Box 618
Ann Arbor, Michigan 48107

COOK, Kenneth R.
University of Arkansas
Electrical Engineering
Fayetteville, Arkansas 72701

CORNFORD, E. S.
Department of Transportation
Design and Construction
Tower C Place de Ville
Ottawa, Ontario, Canada

COURTNEY, Howard
Environmental Research Institute of Michigan
Willow Run Laboratories
P. O. Box 618
Ann Arbor, Michigan 48107

COUSIN, S. B.
Lockheed Electronics
HASD
16811 El Camino Real
Houston, Texas 77058

CRAIB, Kenneth B.
Aero Service Corporation
Resources Development
4219 Van Kirk Street
Philadelphia, Pennsylvania 19135

CRANE, Robert
Environmental Research Institute of Michigan
Willow Run Laboratories
P. O. Box 618
Ann Arbor, Michigan 48107

CRICKMAN, Robin
University of Michigan
2036 School of Natural Resources
Ann Arbor, Michigan

CURRIE, G. Dan
Environmental Research Institute of Michigan
Radar & Optics Division
P. O. Box 618
Ann Arbor, Michigan 48107

DAKSHINAMURTI, C.
Water Technology Centre
Indian Agriculture Research Institute
New Delhi-12, India

D'ANNUNZIO, A. M. JR.
The Boeing Company
Wichita Division
3801 South Oliver
Wichita, Kansas 67210

DAVID, A. R.
Environment Canada
IWD
562 Booth Street
Ottawa, Ontario, Canada

DAVIS, J. E.
Lockheed Electronics Company
HASD
16811 El Camino Real
Houston, Texas

DAVIS, William O.
National Oceanic & Atmospheric Administration
6010 Executive Blvd.
Rockville, Maryland 20852

de BOER, Ir. Th. A.
NIWARS
Central Bureau
Kanaalweg 3
Delft, The Netherlands

de DONATO, Gabriel O.
North American Rockwell Corporation
Earth Resources Operations
D/259 Space Division
12214 Lakewood Blvd.
Downey, California 90241

De FIGUEIREDO, Rui J. P.
Rice University
Department of Mathematical Sciences
Houston, Texas 77001

DEGRAFF, Elliott
Ambionics, Inc.
715 Southern Building
Washington, D. C. 20005

DEIBERT, H. Eugene, Jr.
U. S. Army
Corps of Engineers
6500 Brooks Lane
Washington, D. C. 20315

DEL CAMPO, Carlos Acosta
Consejo Recursos Naturales
No Renovables
Ninos Heroes #139
Mexico 7, D. F. Mexico

de MILLE, George
Imperial Oil Ltd.
Minerals Division
500 6th Avenue, S. W.
Calgary 1, Alberta, Canada

DEMLOW, Daniel J.
Michigan Department of Commerce
7 Story State Building
Lansing, Michigan

DENECKE, Mildred
Environmental Research Institute of Michigan
Willow Run Laboratories
P. O. Box 618
Ann Arbor, Michigan 48107

DERBONNE, J. D.
NASA
Earth Resources Lab
Mississippi Test Facility
Bay St. Louis, Mississippi 39520

DEVENY, George R.
Tennessee Valley Authority
Navigation Development & Regional Studies
TVA 210 Mall Building
Knoxville, Tennessee 37902

DEVEZIN, Howard G. Jr.
NASA
Manned Spacecraft Center
Code FM8
Houston, Texas 77058

DEVILLIERS, J. Neil
D.E.M.R.
2464 Sheffield Road
Ottawa, Ontario, KIA OE4, Canada

DILLMAN, Robert
Environmental Research Institute of Michigan
Willow Run Laboratories
P. O. Box 618
Ann Arbor, Michigan 48107

DIMENTO, Joseph
University of Michigan
Ann Arbor, Michigan

DMITRIEFF-KOKLINE, Alexis
Laval University
pav. Pouliot - Ceutreau
Quebec, Canada

DOLEZALEK, Hans
Office of Naval Research
Code 414
Arlington, Virginia 22217

DORIGAN, Charles J.
Coastal Zone Resources Corporation
Air Photo Interpretation-Graphics
4009 Oleander Drive
Wilmington, North Carolina 28401

DORNBACH, John E.
NASA Manned Spacecraft Center
Earth Observation Division
Applications Office
Houston, Texas 77058

DORR, John A. Jr.
University of Michigan
4014 CCL Building
Ann Arbor, Michigan

DOW, William G.
915 Heatherway
Ann Arbor, Michigan

DRAEGER, William C.
University of California
Forestry Remote Sensing Lab
133 Mulford Hall
Berkeley, California

DRAGG, James L.
NASA
Manned Spacecraft Center
NASA Rd. #1
Houston, Texas 77058

DRAKE, Ben
Environmental Research Institute of Michigan
Willow Run Laboratories
P. O. Box 618
Ann Arbor, Michigan 48107

DRAUGHON, Harold M.
NASA
Manned Spacecraft Center
NASA Rd. #1
Houston, Texas 77058

DRAYSON, S. R.
University of Michigan
Research Activities Building
2450 Hayward
Ann Arbor, Michigan

DRISCOLL, R. S.
U. S. Department of Agriculture
240 West Prospect
Fort Collins, Colorado 80521

DUNN, Diana
Temple University
2991 School House Lane L34W
Philadelphia, Pennsylvania

DUNN, Les
EPA
NERC-LV
P. O. Box 15027
Las Vegas, Nevada 89114

DUVALL, William A.
University of Michigan
Landscape Architecture
Ann Arbor, Michigan

DYRING, Eric
FORCKNING OCH FRAMSTEG/AMB 10
Box 23 136; S-104 35
Stockholm, Sweden

ECKHART, David
NIWARS
Central Bureau Kanaalweg 3
Delft, The Netherlands

ECONOMY, Richard
General Electric
Space Division
P. O. Box 8555
Philadelphia, Pennsylvania 19101

EDGERTON, A. T.
Aeroset
1100 W. Hollyvale Street
Azusa, California 91702

EDMOND, James
Bendix Research Labs
Image Data Systems
Bendix Center
Southfield, Michigan 48075

EDMONDS, Robert L.
University of Michigan
3031 Natural Science
Ann Arbor, Michigan

EGAN, Walter
Grumman Aerospace Corporation
Research Department, Plant 35
Bethpage, New York 11714

EICHEN, Leo
RCA
Astro Electronics
P. O. Box 800
Princeton, New Jersey

EICHLER, Rod
Colorado School of Mines
Geology Department
Golden, Colorado

EIKELMAN, John A. Jr.
Stanford Research Institute
Office of Research Operations
333 Ravenswood Avenue
Menlow Park, California

ENGLAND, Anthony W.
U. S. Geological Survey
Denver Federal Center Building 25
Denver, Colorado 80225

ENGLISH, Marianne
Institute of Atmospheric Science
School of Mines
M. I. Building
Rapid City, South Dakota 57701

ENTRES, S. L.
British Embassy
3100 Massachusetts Avenue, N. W.
Washington, D. C. 20008

EPPES, Tom A.
Bendix Research Labs
Image Data Systems
Bendix Center
Southfield, Michigan 48075

EPPLER, Walter G. Jr.
Lockheed Electronic Company
16811 El Camino Real
Houston, Texas 77058

EPPS, James W.
Mississippi State University
Civil Engineering
P. O. Box CE
State College, Mississippi

ERB, Bryan
NASA
Manned Spacecraft Center
Houston, Texas 77058

ERHART, Rainer R.
Western Michigan University
Geography Department
Kalamazoo, Michigan 49001

ERICKSON, Jon D.
Environmental Research Institute of Michigan
Willow Run Laboratories
P. O. Box 618
Ann Arbor, Michigan 48107

ESCHMAN, Donald F.
University of Michigan
4010 CCL Building
Ann Arbor, Michigan

ESTEP, Samuel D.
University of Michigan
964 Legal Research Building
Ann Arbor, Michigan

ESTES, John E.
University of California
Geography Department
Santa Barbara, California 93106

EVANS, Dal
NASA
Manned Spacecraft Center
Houston, Texas 77058

EYER, Jerome A.
Continental Oil Company
Exploration Research
Exploration Research Building
Ponca City, Oklahoma 74601

EZEMENARI, F.R.C.
Atmospheric Environment Service
Environment Canada
4905 Dufferin Street
Downsview, Ontario, Canada

FALBEL, G.
Barnes Engineering Company
Space Instruments Department
30 Commerce Road
Stamford, Connecticut

FALCO, C. U.
Aerojet
Electro Systems
Azusa, California

FALKNER, Edgar
FotoFore
8833 Powell
Brentwood, Missouri 63144

FALLER, Kenneth H.
Tulane University
Radiation Laboratory
6823 St. Charles Avenue
New Orleans, Louisiana 70118

FALLS, Craig
U. S. Department of Transportation
Federal Highway Administration
400 7th Street, S. W.
Washington, D. C.

FALLS, Robert A.
USAMERDC/CM/CI Dept.
Mine Detection Division
Ft. Belvoir, Virginia 22060

FELIX, Michael R.
IBM
1332 Space Park Drive
Houston, Texas 77058

FELSHER, M.
U. S. Environmental Protection Agency
Office of Technical Analysis
Office of Enforcement & General Counsel
Washington, D. C. 20460

FERGUSON, Robert L.
General Electric
P. O. Box 2500
Daytona Beach, Florida 32015

FERRIANS, Oscar J. Jr.
U. S. Geological Survey
Alaskan Mineral Resources Branch
345 Middlefield Road
Menlo Park, California 94025

FINK, W.
c/o South African Scientific Office
C.S.I.R.
South African Embassy
3051 Massachusetts Avenue, N. W.
Washington, D. C. 20015

FIORIO, Franco
Civilta Macchine
2600 N. Nelson Street
Arlington, Virginia 22207

FISCHER, W. A.
U. S. Department of Interior
EROS Program
5213 GSA Building
Washington, D. C. 20242

FONTANEL, Andre
French Institute of Petroleum
Geophysics Division
BP 18
92 Rueil Malmaison
France

FORBES, Clayton D.
NASA
Manned Spacecraft Center
TF6/Principal Investigations
Code TF6
Houston, Texas 77058

FORSTER, S. W.
N.Y.S. Geological Survey
Education Department
969 Education Annex
Albany, New York 12224

FOSTER, Kennith E.
University of Arizona
Ecological Test Site
1201 E. Speedway
Tucson, Arizona

FOX, Lawrence
University of Michigan
Ann Arbor, Michigan

FRAYSSE, Georges
EURATOM
Scientific Directorate
Common Center of Research
Ispra, Italy

FREDEN, Stanley C.
NASA
GSFC
Greenbelt, Maryland 20771

FREDERKING, Ray L.
Purdue University
LARS
W. Lafayette, Indiana

FREY, Thomas
U. S. Department of Agriculture
ERS
Room 425 500 12th Street, S. W.
Washington, D. C. 20250

FRIERSON, Von R.
Lockheed Electronics
HASD
16811 El Camino Real
Houston, Texas 77058

FUENTEALBA, Orlando
University de Chile
Geodetics Department
P. O. Box 2777
Santiago, Chile

GABLE, William L.
Office of Community Affairs & Planning
4901 N. Lincoln
Oklahoma City, Oklahoma 73105

GALLAGHER, James J.
U. S. Navy
Ocean Sciences
New London, Connecticut 06320

GALLAGHER, John L.
University of Georgia
Marine Institute
Sapelo Island, Georgia 31327

GATTO, Lawrence W.
U. S. Army
Cold Regions Research & Engineering Lab
P. O. Box 282
Hanover, New Hampshire

GAWARECKI, Stephen J.
U. S. Geological Survey
Office of International Geology
F and 18th Streets, N. W.
Washington, D. C. 20242

GEERDERS, P. J. F.
Interdepartmental Working Comm. for the
Application & Research of Remote
Sensing Techniques
Delft, The Netherlands

GENZ, Wolfgang
Metallgesellschaft
Aktiengesellschaft
6000 Frankfurt (Main)1
Postfach 2609
Reuterweg 14, Germany

GERBER, Carl Read
Brookings Institution
Foreign Policy Studies
1775 Massachusetts Avenue, N. W.
Washington, D. C. 20036

GERDING, R. Bruce
TRW Systems Group
Space Vehicles Division
Mail Station R5/1091
One Space Park
Rendondo Beach, California 90278

GESELL, Thomas F.
University of Texas
School of Public Health
P. O. Box 20186
Houston, Texas 77025

GINSBERG, I. W.
Sensors, Inc.
303 W. Ann Street
Ann Arbor, Michigan 48103

GIULIANO, David F.
U. S. Navy
Underwater Systems Center
New London, Connecticut

GODBY, E. A.
Energy Mines & Resources
2464 Sheffield Road
Ottawa, Ontario, Canada

GOILLOT, Ch.
Institut National dela Recherche Agronomique
Metrology
I.N.R.A. Route de St. Cyr
78 - Versailles, France

GOLDEN, Michael S.
Alabama A & M University
Natural Resources & Environmental Studies
Box 292
Normal, Alabama 35762

GORANSEN, Rex W.
Gulton
15000 E. Central
Albuquerque, New Mexico 87123

GORDON, K. S.
York University
CRESS
4700 Keele Street
Toronto, Ontario, Canada

GOTTSCHALK, Vincent J.
Corps of Engineers
Military Construction
Office Chief of Engineers
Department of the Army
Washington, D. C. 20314

GOWER, J. F. R.
Marine Science Directorate
Environment Canada
5th Floor
1230 Government Street
Victoria, British Columbia, Canada

GREEN, Andrew A.
Stanford University
Department of Applied Earth Science
Stanford, California 94305

GREENE, William B.
Bureau of Outdoor Recreation
Department of Interior
3853 Research Park Drive
Ann Arbor, Michigan

GREGG, Tim W. D.
Environmental Research Institute of Michigan
Willow Run Laboratories
P. O. Box 618
Ann Arbor, Michigan 48107

GROEN, J. P. P.
Netherlands Agency for Aerospace Programs
Kluyverweg 1
Delft, The Netherlands

GROSS, Harry
Environment Canada
Glaciology
#8 Building
Carling Street
Ottawa, Ontario, Canada

GROSS, H. Gerald
McDonnell Douglas
Space Sciences
5301 Bolsa Avenue
Huntington Beach, California 92647

GROSSMAN, Jack J.
McDonnell Douglas
Space Sciences Department
5301 Bulsa Avenue
Huntington Beach, California 92647

GUENTHER, Gary E.
State of Michigan
Natural Resources
Stevens T. Mason Building
Lansing, Michigan 48926

GUINARD, Norman W.
Naval Research Lab
Electronics
Washington, D. C.

GUSS, Philip
Lockwood, Kessler & Bartlett, Inc.
Photogrammetry
One Aerial Way
Syosset, New York 11791

GUTLOVE, Norman M.
Fairchild Camera
Space & Defense Systems
301 Robbins Lane
Syosset, New York 11791

HAACK, Barry N.
University of Michigan
Geography Department
4518 LSA
Ann Arbor, Michigan

HAAS, Fred C.
U. S. Geological Survey
EROS
Washington, D. C.

HACKER, Carl S.
University of Texas
School of Public Health
Houston, Texas 77025

HAGEMAN, Ir. B. P.
NIWARS
Central Bureau
Kanaalweg 3
Delft, The Netherlands

HALL, Forrest G.
NASA
Manned Spacecraft Center
Earth Observations
Houston, Texas 77058

HALL, William B.
Idaho Bureau of Mines
Department of Geology
University of Idaho
Moscow, Idaho 83843

HALLBERG, George R.
Iowa Geological Survey
16 W. Jefferson
Iowa City, Iowa 52240

HALLOCK, Herbert
Grumman Aerospace Corporation
Department 552, Plant 26
Bethpage, New York 11714

HALLUM, Cecil R.
Loyola University
Department of Mathematics
6363 St. Charles Avenue
New Orleans, Louisiana 70002

HAMILTON, Lynne
U. S. Department of Agriculture
Bureau of Outdoor Recreation
3853 Research Park Drive
Ann Arbor, Michigan

HAMILTON, William
General Research Corporation
P. O. Box 3587
Santa Barbara, California 93105

HANSEN, Robert L.
U. S. Bureau of Reclamation
General Research
Building 56
Denver Federal Center
Denver, Colorado 80225

HANSON, Arnold M.
ONR
536 S. Clark Street
Chicago, Illinois 60605

HARBER, Zane
Department of Interior
Bonneville Power Administration
Power Resources
P. O. Box 3621
Portland, Oregon

HARRIES, J. E.
Prospect House
Department of Trade & Industry
80 New Oxford Street
London WCIA 1HE, England

HASELL, Philip G. Jr.
Environmental Research Institute of Michigan
Willow Run Laboratories
P. O. Box 618
Ann Arbor, Michigan 48107

HAUGEN, Richard
U. S. Army Cold Regions
Research & Engineering Lab
P. O. Box 282
Hanover, New Hampshire

HECKMAN, R. L.
State Board of Agriculture of Colorado
Colorado State University
Ft. Collins, Colorado 80521

HEININGER, H. G.
IBM
Federal Systems
18100 Frederick Pike
Gaithersburg, Maryland 20760

HEINMILLER, Charles
Eastman Kodak Company
Research Labs
Rochester, New York 14650

HELBIG, Horst
Institut fur Satelligeneletronik der DFVLR
Oberpfaffenhofen, Germany

HEMPHILL, William R.
U. S. Geological Survey
EROS Program
Washington, D. C. 20242

HENGEVELD, Henry G.
Government of Canada
Department of Environment
4905 Dufferin Street
Downsview, Ontario, Canada

HENRY, Harold
University of Alabama
College of Engineering
Box 1466
University, Alabama 35486

HEROLD, J. Downs
University of Michigan
412 Maynard Street
Ann Arbor, Michigan

HICKMAN, G. D.
SPARCOM, Inc.
Suite 600/4600 Kenmore Avenue
Alexandria, Virginia 22304

HIGHAM, Anthony D.
Plessey Radar
West Leigh
PRRC/ERL
Havant, Hants, England

HILBORN, W. H.
University of New Brunswick
Faculty of Forestry
Frederkton, New Brunswick, Canada

HILE, Bobby D.
Philco-Ford Corporation
WDL/PHO
Houston Operation
1002 Gemini
Houston, Texas 77058

HODDER, D. T.
North American Rockwell Corporation
Space Division SE68
12214 Lakewood Blvd.
Downey, California 90241

HOLLYDAY, Este F.
U. S. Geological Survey
Water Research Department
144 Federal Office Building
Nashville, Tennessee

HOLMES, R. F.
Environmental Protection Agency
1750 Pennsylvania Avenue, Room 212
Washington, D. C. 20006

HOLMES, R. M.
ERA Instruments
P. O. Box 3444 Station B
Calgary, Alberta, Canada

HOLMES, Quentin A.
NASA
Manned Spacecraft Center
Code FM8
Houston, Texas 77058

HOLTER, M. R.
Environmental Research Institute of Michigan
Willow Run Laboratories
P. O. Box 618
Ann Arbor, Michigan 48107

HOOD, Dennis R.
State Planning Agency
State Capital
Pierre, South Dakota 57501

HORVATH, Robert
Environmental Research Institute of Michigan
Willow Run Laboratories
P. O. Box 618
Ann Arbor, Michigan 48107

HORWITZ, Harold
Environmental Research Institute of Michigan
Willow Run Laboratories
P. O. Box 618
Ann Arbor, Michigan 48107

HOWARD, Gordon E. Jr.
Office of the Governor
Building 1100 MTF
Bay St. Louis, Mississippi

HOYER, Bernard
Iowa Geological Survey
Iowa Remote Sensing Lab
16 W. Jefferson
Iowa City, Iowa 52240

HUBER, John C.
3M Company
Central Research Labs
P. O. Box 33221
St. Paul, Minnesota 55133

HUFFMAN, O. Frank
Gulf Research & Development
P. O. Drawer 2038
Pittsburgh, Pennsylvania 15230

HULET, John
U. S. Government
Bureau of Indian Affairs
Nespelem, Washington

HULSTROM, Roland L.
Martin Marietta Aerospace
P. O. Box 179
Denver, Colorado

HUNTER, Garry T.
Airphoto Analysis Associates Consultants Ltd.
859 College Street
Toronto 173, Ontario, Canada

HYDE, Peter D.
Environmental Research Institute of Michigan
Willow Run Laboratories
P. O. Box 618
Ann Arbor, Michigan 48107

HYDE, William F.
University of Michigan
168 School of Natural Resources
Ann Arbor, Michigan

HYDEN, Rupert
University of Munich
Zentralstelle F. Photogeologie
u. Fernerkundung
Luisenstr. 37
8 Munchen 2, West Germany

HYNEK, Joseph
University of Wisconsin
Madison, Wisconsin

INGELS, Frank M.
Mississippi State University
Electrical Engineering Department
Drawer EE
State College, Mississippi 39762

INOUE, Eiichi
National Institute of Agricultural Sciences
Nishigahara, Kita-ku
Tokyo, Japan 114

IRBE, George J.
Environment Canada
A.E.S.
4905 Dufferin Street
Downsview, Ontario, Canada

ISACHSEN, Y. W.
N.Y.S. Geological Survey
Education Department
969 Education Annex
Albany, New York 12224

JACKSON, Philip
Environmental Research Institute of Michigan
Willow Run Laboratories
P. O. Box 618
Ann Arbor, Michigan 48107

JACKSON, Ross
Scientific Information Section
Research Branch
Agriculture Canada
Ottawa, Ontario K1A 0C6, Canada

JACOBS, George J.
NASA Headquarters
Office of Applications
Code ERR
600 Independence Avenue, SW
Washington, D. C. 20546

JAFFE, Leonard
NASA Headquarters
Office of Applications
Washington, D. C.

JAGER, Ir. Tj.
NIWARS
Central Bureau Kanaalweg 3
Delft, The Netherlands

JANES, Manfred
ESTEC
Noordwijk, Domeinweg
The Netherlands

JEFFERIES, Jonathan
University of Tennessee
Graduate School of Planning
15th and White Avenue Building
Knoxville, Tennessee 37916

JEFFERIS, Lee
Colorado School of Mines
Geology Department
Golden, Colorado

JENNESS, Martin D.
NASA-MSC
MPAD - FM2
NASA RD. 1
Houston, Texas 77586

JOHNSON, Janice L.
State of Kansas
Planning Division
Department of Economic Development
Room 122-S, State Office Building
Topeka, Kansas 66612

JOHNSON, Melvin A.
Corps of Engineers
Environmental Resources Section
601 E. 12 Street, Room 801
Kansas City, Missouri 64106

JOHNSON, Peter
University of Ottawa
Department of Geography
74 Laurier East
Ottawa, Ontario KINGN5, Canada

JOHNSON, R. H.
Bendix Corporation
Aerospace Systems Division
3300 Plymouth Road
Ann Arbor, Michigan

JOHNSTON, John E.
EROS Program
Department of Interior
USGS
1717 H Street, N. W.
Washington, D. C. 20242

JOLLEY, B. E.
United States Air Force
Kirtland AFB, NF
Albuquerque, New Mexico 87117

JONES, Harold G.
The Boeing Company
Life Sciences
2035 Westlake Road
Houston, Texas 77058

JONES, L. M.
University of Michigan
Aerospace Engineering
Research Activities Building
Ann Arbor, Michigan

JONES, Lester L.
University of Michigan
Ann Arbor, Michigan

JONES, W. Linwood
NASA
Langley
M/S 490
Hampton, Virginia 23365

JOYCE, Armond T.
NASA
Earth Resources Laboratory
Mississippi Test Facility
Bay St. Louis, Mississippi 39520

JUODAWLKIS, William
Environmental Research Institute of Michigan
Willow Run Laboratories
P. O. Box 618
Ann Arbor, Michigan 48107

KAREL, Eugene F.
State of Minnesota
Office of Local & Urban Affairs
State Planning Agency
200 Capital Square Building
St. Paul, Minnesota 55101

KAZDA, Louis F.
University of Michigan
2526 E. Engineering
Ann Arbor, Michigan

KEDAR, E. Y.
State University of New York
Department of Geography
Binghamton, New York 13901

KEEBLER, Kathie
University of Michigan
412 Maynard Street
Ann Arbor, Michigan

KELLEY, Charles R.
East Central State College
Department of Geography
Ada, Oklahoma 74820

KELLY, William S.
Commonwealth of Kentucky
Natural Resources
6th Floor Capital Plaza Tower
Frankfort, Kentucky

KENNEDY, Peter D.
Motorola
Government Electronics
8201 E. McDowell Road
Scottsdale, Arizona 85252

KENT, Philippe
IRTA
Via Quintilliano 41
Milano, Italy

KERHIN, Randall
Maryland Geological Survey
Coastal & Estvarine Geol.
The Johns Hopkins University
Baltimore, Maryland 21218

KERSCHBAUM, Richard L.
University of Michigan
Ann Arbor, Michigan

KIHLBLOM, Ulf
VBB
P. O. Box 5038/2
Linnegatan S-102 41
Stockholm 5, Sweden

KILPELA, Einari
Colorado State University
Watershed Sciences
Fort Collins, Colorado 80521

KIRBY, Charles L.
Canadian Forestry Service
Department of Environment
Northern Forest Research Division
Edmonton, Alberta, Canada

KLEINKOPF, M. Dean
U. S. Geological Survey
Building 25, Federal Center
Denver, Colorado 80225

KLEMAS, V.
University of Delaware
College of Marine Studies
Newark, Delaware 19711

KLOOSTER, Steven A.
University of Wisconsin
Remote Sensing
1241 Engineering Building
Madison, Wisconsin

KLOVES, Thomas R.
NASA
Manned Spacecraft Center
TF6
Houston, Texas 77058

KNEPPER, Dan
Colorado School of Mines
Geology Department
Golden, Colorado

KNUTH, William M.
HRB-Singer Inc.
Software & Analysis
P. O. Box 60, Science Park
State College, Pennsylvania

KOHOUT, Francis A.
U. S. Geological Survey
Department of Interior
Water Resources Division
Washington, D. C. 20242

KOLIPINSKI, Milton C.
U. S. National Park Service
Western Regional Office
450 Golden Gate Avenue
Box 36063
San Francisco, California 94102

KONDRATYEV, K. Ya.
University of Leningrad
Leningrad, USSR

KOUTSANDREAS, John
E. P. A.
1750 Pennsylvania Avenue, N. W.
Washington, D. C. 20880

KOVER, Allan N.
U. S. Geological Survey
18th and F Streets, N. W.
Washington, D. C. 20242

KRAL, George J. Jr.
University of Michigan
Urban Planning
Ann Arbor, Michigan

KRAUDELT, Ernest
Environmental Research Institute of Michigan
Willow Run Laboratories
P. O. Box 618
Ann Arbor, Michigan 48107

KRIEGLER, F. J.
Environmental Research Institute of Michigan
Willow Run Laboratories
P. O. Box 618
Ann Arbor, Michigan 48107

KRISHNAN, T. K.
Iron Ore Company
Technical Services
Retty Street
Sept-Iles, Quebec, Canada

KRISHEN, K.
Lockheed Electronics Company
16811 El Camino Real
Houston, Texas 77058

KROESCH, Volkmar
Bundesforschungsanstalt fur Landeskunde u. Raumordnung
Institut fur Landeskunde
Michaelshof, Postfach 130
D-53 Bonn-Bad Godesberg
Federal Republic of Germany

KRUUS, Jaan
Environment Canada
Water Management
Glaciology Division
Ottawa, Ontario, Canada

KUHN, W. R.
University of Michigan
Research Activities Building
2450 Hayward
Ann Arbor, Michigan

KUIPER, Logan K.
Iowa Geological Survey
Remote Sensing Lab
Iowa City, Iowa 52240

LACHOWSKI, Henry
Pennsylvania State University
Agronomy Department
119 Tyson
University Park, Pennsylvania 16802

LADD, Jimmie
Environmental Research Institute of Michigan
Willow Run Laboratories
P. O. Box 618
Ann Arbor, Michigan 48107

LAING, Watson
Hawker Siddeley Dynamics
Space Division
Gunnels Wood Road
Stevenage, Hertfordshire, England

LAIRET, Rafael
Direccion de Cartografia
Department Sensores Remotos
EDF. Camejo 2° Riso C.S.B.
Caracas 101 Venezuela

LAMERS, G. L.
Nationaal Lucht en Ruimtevaart
Sloterweg 145
Amsterdam, The Netherlands

LAND, J. P.
CGG-Geoterrex
Airborne Geophysics
8120 Westglen
Houston, Texas 77042

LANDERS, Robert
Environmental Protection Agency
NERC-LV
P. O. Box 15027
Las Vegas, Nevada 89114

LANDGREBE, David
Lab for Applications of Remote Sensing
1220 Potter Drive
West Lafayette, Indiana

LANDIS, Glenn H.
U. S. Geological Survey
EROS Data Center
Sioux Falls, South Dakota 57198

LaROCCA, A. J.
Environmental Research Institute of Michigan
Willow Run Laboratories
P. O. Box 618
Ann Arbor, Michigan 48107

LARROWE, Vernon
Environmental Research Institute of Michigan
Willow Run Laboratories
P. O. Box 618
Ann Arbor, Michigan 48107

LARSEN, Leo M.
Environmental Research Institute of Michigan
Willow Run Laboratories
P. O. Box 618
Ann Arbor, Michigan 48107

LARSON, Richard W.
Environmental Research Institute of Michigan
Willow Run Laboratories
P. O. Box 618
Ann Arbor, Michigan 48107

LATHRAM, Ernest
U. S. Geological Survey
Alaskan Mineral Resources Branch
345 Middlefield Road
Menlo Park, California

LAYER, Douglas
Imperial Oil
Mineral Exploration
500 6th Avenue, S. W.
Calgary, Alberta, Canada

LeBEAU, Maury
Texas Instruments
Equipment Group
P. O. Box 6015
Dallas, Texas

LEE, Keenan
Colorado School of Mines
Golden, Colorado 80401

LEE, Martin E.
University of Michigan
225 HSRI
Ann Arbor, Michigan

LEE, Patrick
Terra-Scan Limited
2160 Highway #7
Concord, Ontario, Canada

LEESE, John A.
NESS/NOAA
DAPAD
Washington, D. C. 20233

LEGAULT, Richard
Environmental Research Institute of Michigan
Willow Run Laboratories
P. O. Box 618
Ann Arbor, Michigan 48107

LEHR, W. E.
U. S. Coast Guard
Office of Research & Development
Pollution Prevention Projects Branch
Washington, D. C.

LEPLEY, L. K.
University of Arizona
Arid Lands Studies
1201 E. Speedway Blvd.
Tucson, Arizona 85719

LEVEQUE, Paul Ch.
Bordeaux 1 University
Earth Sciences Unite
Lab. de Radiogeologie et Mecanique des Roches
Avenue des Facultes
33405 Talence, France

LEWIS, Anthony J.
Lousiana State University
Department of Geography & Anthropology
Baton Rouge, Louisiana 70803

LIANG, Ta
Cornell University
Hollister Hall
Ithaca, New York 14850

LINS, Harry F. Jr.
U. S. Geological Survey
Geographic Applications Program
1717 H Street, N. W.
Washington, D. C. 20242

LIPPERT, B. O.
Lockheed Electronics Company
Houston Aerospace Division
NASA-MTF
Building 1100, Room A-107
Bay St. Louis, Mississippi 39520

LIPTON, S. Gregory
University of Michigan
Urban Region Planning
Ann Arbor, Michigan

LISKOW, Charles
Environmental Research Institute of Michigan
Willow Run Laboratories
P. O. Box 618
Ann Arbor, Michigan 48107

LITTLE, C. Gordon
Wave Propagation Lab
National Oceanic & Atmospheric Administration
RB#3, Room 467
Boulder, Colorado 80302

LIVISAY, Jackson P. Jr.
Environmental Research Institute of Michigan
Willow Run Laboratories
P. O. Box 618
Ann Arbor, Michigan 48107

LLOYD, Robert A.
Washtenaw County Planning Commission
306 County Building
Ann Arbor, Michigan 48108

LOCKERMAN, Robert C.
NOAA/NODC
Environmental Data Service
Rockville, Maryland

LODGE, R. W.
Voice of America
1459 EMD
219 S. Dearborn
Chicago, Illinois 60604

LOEFFLER, Alf
Gesellschaft fur Weltraumforschung
Programmvorbereitung
Linder Hohe
D-505 Porz-Wahn, Germany

LOVENBURG, Mervin F.
University of Michigan
Department of Geology
2015 CCL Building
Ann Arbor, Michigan

LOW, Bobbi S.
University of Michigan
Ann Arbor, Michigan

LOWE, Donald S.
Bendix Corporation
Aerospace Systems Division
3300 Plymouth Road
Ann Arbor, Michigan 48107

LUNDHOLM, Bengt
Swedish National Research Council
Ecological Research Committee
Wenner-Gren Center
Sveavagen 166-15
Stockholm, Sweden S-113 46

MacDONALD, Robert B.
NASA
Manned Spacecraft Center
Houston, Texas 77058

MACOMBER, Robert T.
University of Michigan
School of Natural Resources
Ann Arbor, Michigan

MADDING, Bob
University of Wisconsin
Marine Studies
1225 W. Dayton
Madison, Wisconsin 53706

MADOLE, Richard
NASA - University of Colorado
Institute of Arctic & Alpine Research
Boulder, Colorado 80302

MALANICK, Charles E.
U. S. Government
818 Harrington Road
Rickville, Maryland 20852

MALILA, William
Environmental Research Institute of Michigan
Willow Run Laboratories
P. O. Box 618
Ann Arbor, Michigan 48107

MALLON, Harry J.
Metropolitan Washington Council of Governments
1225 Connecticut Avenue
Washington, D. C. 20036

MANNEN, M. L.
Lockheed Electronics
HASD
16811 El Camino Real
Houston, Texas

MARCARD, Edward H.
MBB-Ottobrunn
8409 Brimfield Avenue
Panorama City, California 91402

MARK, Herman
NASA
21000 Brookpark Road
Cleveland, Ohio 44135

MARLATT, William E.
Colorado State University
Watershed Sciences
Fort Collins, Colorado 80521

MARSS, Ronald W.
Colorado School of Mines
University of Wyoming
Department of Geology
Laramie, Wyoming 82070

MARSH, William M.
University of Michigan
Flint Campus
Flint, Michigan

MARSHALL, Nichols J.
Australian Selection Pty. Ltd.
Group Exploration Research Coordinator
14 Shirlow Street
Marrickville, Australia 2204

MARSHALL, ROBERT E.
Environmental Research Institute of Michigan
Willow Run Laboratories
P. O. Box 618
Ann Arbor, Michigan 48107

MASSE, Richard
Pennsylvania State University
Agronomy Department
119 Tyson
University Park, Pennsylvania 16802

MATHUR, B. Sen
Ministry of Transportation & Communications
Design Services Branch
1201 Wilson Avenue
Dowsview 464, Ontario, Canada

MAUL, George A.
NOAA/AOML
Physical Oceanography Lab
15 Rickenbacker Causeway
Miami, Florida 33149

MAURIN, Catherine
Bordeaux University
Earth Sciences Unite
Laboratoire de Radiogeologie et
Mecanique des Roches
33405 Talence, France

MAXWELL, J. Robert
Environmental Research Institute of Michigan
Willow Run Laboratories
P. O. Box 618
Ann Arbor, Michigan 48107

McCARTHY, Michael M.
University of Wisconsin
Room 315, Met. & Space Science Building
1225 W. Dayton
Madison, Wisconsin 53706

McCAULEY, James R.
University of Kansas
Center for Research Inc.
Space Technology Center
West Campus
Lawrence, Kansas 66044

McCLAIN, E. Paul
NOAA
National Environmental Satellite Service
Suite 300, 3737 Branch Avenue, S. E.
Washington, D. C. 20031

McCLARY, Michael J.
Environmental Research Institute of Michigan
Willow Run Laboratories
P. O. Box 618
Ann Arbor, Michigan 48107

McCLATCHEY, R. A.
AFCRL
Optical Physics Lab
L. G. Hanscom Field
Bedford, Massachusetts 01731

McDOWELL, David
Eastman Kodak Company
Research Labs
Rochester, New York 14650

McEWEN, Robert B.
U. S. Geological Survey
Topographic
1340 Old Chain Bridge Road
McLean, Virginia 22101

McGINNESS, John W. Jr.
American University
Biology Department
Massachusetts & Nebraska Ave., N. W.
Washington, D. C.

McGINNIS, David F.
National Oceanic & Atmospheric Administration
Environmental Sciences Group S33
3737 Branch Avenue, S. E., Suite 300
Washington, D. C. 20031

McGLADE, William G.
State of Pennsylvania
Department of Environmental Resources
Third & Reily Streets
Harrisburg, Pennsylvania 17102

McHAIL, Rex R.
Bausch & Lomb Inc.
Special Products
635 St. Paul Street
Rochester, New York 14602

McHENRY, J. Roger
U. S. Department of Agriculture
Sedimentation Lab
P. O. Box 30
Oxford, Mississippi 38655

McKIM, Harlan H.
U. S. Army
Cold Regions Research & Engineering Laboratory
P. O. Box 282
Hanover, New Hampshire

McKIMMY, Janice
Environmental Research Institute of Michigan
Willow Run Laboratories
P. O. Box 618
Ann Arbor, Michigan 48107

McMILLAN, R. K.
University of Waterloo
Earth Sciences
Waterloo, Ontario, Canada

McNAIR, Arthur J.
Cornell University
Civil & Environmental Engineering
Hollister Hall
Ithaca, New York 14850

MEALOR, W. T. Jr.
University of Southern Mississippi
Department of Geography
P. O. Box 352
Hattiesburg, Mississippi 39401

MEEKS, David C.
Aerojet Electrosystems Company
Microwave Division
1100 W. Hollyvale
Azusa, California

MELAND, Nils
University of Wisconsin
Geography Department
Oshkosh, Wisconsin 54901

MERRITT, Earl
Earth Satellite Corporation
1771 N Street, N. W.
Washington, D. C. 20036

MEYER, Merle P.
College of Forestry
University of Minnesota
St. Paul, Minnesota 55101

MILAZZO, Valerie A.
U. S. Geological Survey
Geographic Applications Program
1717 H Street, N. W., Room 849
Washington, D. C. 20242

MILLER, Arthur A.
Federal Highway Administration
Highway Design-Aerial Surveys
400 7th Street S. W.
Washington, D. C. 20590

MILLER, Richard C.
Oceanographic Services, Inc.
135 E. Ortega Street
Santa Barbara, California 93101

MILLER, Robert H.
U. S. Department of Agriculture
Room 1667, South Building
Washington, D. C. 20250

MILLER, W. Frank
Mississippi State University
Drawer FD
State College, Mississippi 39762

MILLS, Dana
University of Michigan
School of Public Health
Ann Arbor, Michigan

MIOSGA, Gerhard
DFVLR
Infrared
8031 Oberpfaffenhofen
Wessling, Germany

MITCHEL, Ralph H.
University of Michigan
2023 IST
Ann Arbor, Michigan

MOELLERING, Harold
University of Michigan
4015 LSA Building
Ann Arbor, Michigan

MOHR, Don
Texas Instruments
Equipment Group
P. O. Box 6015
Dallas, Texas 75222

MOKE, Richard A.
NASA
Earth Resources Program
Manned Spacecraft Center
Houston, Texas 77058

MOORE, Gerald K.
U. S. Geological Survey
Gulf Coast Hydroscience Center
Mississippi Test Facility
Bay St. Louis, Mississippi 39520

MOORLAG, Susan
U. S. Department of Interior
Geography Office
Room 835, Matowic Building
1717 H Street, N. W.
Washington, D. C. 20242

MORGAN, Joseph O.
U. S. AID
USOM - Office of Agriculture Development
APO San Francisco, California 96346
Bangkok, Thailand

MORGENSTERN, James
Environmental Research Institute of Michigan
Willow Run Laboratories
P. O. Box 618
Ann Arbor, Michigan 48107

MORRA, R. H. J.
NIWARS
Central Bureau Kanaalweg 3
Delft, The Netherlands

MORRISON, Dennis R.
NASA
Manned Spacecraft Center
Health Applications Office
DD121
Houston, Texas 77058

MOURLON, Jean Claude
Pollution Department
C.N.E.X.O.
39, Avenue d'lena
75 - Paris - 16eme - France

MOWER, Roland D.
Aeronautical Systems Division
Reconnaissance Strike Group
RWS-2
Wright Patterson AFB, Ohio 45433

MUDAR, Joseph
Environmental Research Institute of Michigan
Willow Run Laboratories
P. O. Box 618
Ann Arbor, Michigan 48107

MUNDAY, John C. Jr.
University of Toronto
Erindale College
Clarkson, Ontario, Canada

MURINE, Gerald E.
Actron Industries, Inc.
Engineering
700 Royal Oaks Drive
Monrovia, California 91016

MUSTONEN, Erik
University of Michigan
School of Natural Resources
Ann Arbor, Michigan

NALEPKA, Richard F.
Environmental Research Institute of Michigan
Willow Run Laboratories
P. O. Box 618
Ann Arbor, Michigan 48107

NASH, David B.
University of Michigan
4528 CCL Building
Ann Arbor, Michigan

NAZARE, Charles V.
University of Michigan
Remote Sensing Center
Ann Arbor, Michigan

NELSON, R. M.
Lockheed Electronics
HASD
16811 El Camino Real
Houston, Texas

NICHOLS, H. Janney
Environmental Research Institute of Michigan
Willow Run Laboratories
P. O. Box 618
Ann Arbor, Michigan 48107

NICHOLS, Lester R. II
State of Michigan
State Planning Division
Lansing, Michigan 48913

NICHOLS, Maynard
Virginia Institute of Marine Science
Gloucester Point, Virginia 23062

NIEMANN, Bernard J. Jr.
University of Wisconsin
Landscape Architecture
25 Agriculture Hall
Madison, Wisconsin

NOBLE, Vincent E.
Department of the Navy
U. S. Naval Oceanographic Office
Code 7003
Washington, D. C. 20390

NORWOOD, Virginia T.
NASA Applications Division
Hughes Aircraft Company
P. O. Box 92919, Airport Station
Los Angeles, California 90009

NOYES, J. C.
The Boeing Company
Research & Engineering Division
P. O. Box 3999
Seattle, Washington 98124

OBLANAS, John
Stanford Research Institute
Atmospheric Sciences Lab
333 Ravenswood Avenue
Menlo Park, California 94025

O'HANDLEY, Douglas A.
Jet Propulsion Lab
Image Processing Lab
4800 Oak Grove Drive
Pasadena, California 91103

OLIVER, Robert E.
Colorado State University
Department of Watershed Sciences
Fort Collins, Colorado 80521

OLIVER, Thomas
1907 Buena Vista
P. O. Box 57
Albuquerque, New Mexico 87106

OLIVERSON, Lawrence W.
University of Wisconsin
Remote Sensing Center
1241 Civil Engineering Building
Madison, Wisconsin 53706

OLSON, C. E. Jr.
University of Michigan
School of Natural Resources
Ann Arbor, Michigan

O'MALLEY, James Ross
Department of Geography
University of Tennessee
Knoxville, Tennessee

O'NEAL, James D.
Engineer Agency for Resources Inventories
4701 Sangamore Road
Washington, D. C. 20016

ORY, Thomas R.
Daedalus Enterprises
Data Services
P. O. Box 1869
Ann Arbor, Michigan 48106

OSTERHOUDT, Frank H.
U. S. Department of Agriculture
Economic Research Service
500 12th Street, S. W.
Washington, D. C. 20250

OUELLETTE, Robert J.
Bendix
Research Laboratory
Bendix Center
Southfield, Michigan 48076

OUTCALT, Sam I.
University of Michigan
Department of Geography
Ann Arbor, Michigan

OWEN-JONES, E. S.
Bedford College
Physics Department
Regents Park
London, N.W.I. 4NS, England

PADILLA, Sergio
Space Commission of Mexico
Centro Scop. Ay. Universidad y Xola
Mexico 12, D. F.

PAGE, Carl V.
Michigan State University
Computer Science
Computer Center
East Lansing, Michigan 48823

PALUDAN, Charles T. N.
NASA
George C. Marshall Space Flight Center
Huntsville, Alabama 35812

PARIS, Jack F.
Lockheed Electronics Company
Earth Observation
16811 El Camino Real
Houston, Texas 77058

PARK, A. B.
NASA Headquarters
Earth Resources Survey Program
Washington, D. C. 20242

PARKER, H. D.
Lockheed Electronics
HASD
16811 El Camino Real
Houston, Texas 77058

PARKER, Jonny L.
NASA
Flight Support
Manned Spacecraft Center
Houston, Texas 77058

PARRY, J. T.
McGill University
Department of Geography
Burnside Hall
P. O. Box 6070
Montreal, Quebec, Canada

PASSERELLO, Jack F.
State of California
Office of Planning & Research
1400 Tenth Street
Sacramento, California 95814

PATTESON, Andrew W.
NASA
Manned Spacecraft Center
TF-5
Houston, Texas 77058

PEARSON, Robert L.
Colorado State University
Department of Watershed Sciences
Fort Collins, Colorado 80521

PERELMUTER, Ernest I.
MITRE Corporation
P. O. Box 208
Mail Stop S010
Bedford, Massachusetts 01730

PERLMAN, Ellis
University of Michigan
Flint Campus
Flint, Michigan

PETERSEN, Gary W.
Pennsylvania State University
Agronomy Department
119 Tyson
University Park, Pennsylvania 16802

PETERSON, L.
Department of Interior
3853 Research Park Drive
Ann Arbor, Michigan 48104

PETTYJOHN, Wayne A.
Ohio State University
Geology Department
125 S. Oval Drive
Columbus, Ohio 43210

PHILLIPS, Sheldon
Eastman Kodak
343 State Street
Rochester, New York 14850

PHILLIPS, Terry L.
Purdue University
LARS
1220 Potter Drive
West Lafayette, Indiana 47906

PHILLIPSON, Warren R.
Cornell University
Hollister Hall
Ithaca, New York 14850

PIANTES, A. H.
Aerojet Electro Systems
Washington Operations
1120 Connecticut Avenue
Suite 1050
Washington, D. C. 20036

PIKUS, Irwin M.
General Electric
Space Sciences Lab
Valley Forge, Pennsylvania 19101

PINSON, William
McMaster University
C.A.R.E.D.
c/o Engineering Physics Department
Hamilton, Ontario, Canada

PISHAROTY, P. R.
Indian Space Research Organization
c/o P.R.L.
Ahmedabad, India

PITTS, Alan
U. S. Government
Central Intelligence Agency
Washington, D. C. 20024

PITTS, David E.
NASA
Manned Spacecraft Center
Earth Observations Division
TF3
Houston, Texas 77058

PLEVIN, John
Organization Europeenne
Le Recherches Spatiales
114 Avenue Charles de Gaulle
92200 Neuilly Sur Seine
France

PLITZ, Parker J.
Bay de Noc Community College
Science & Social Science
Escanaba, Michigan 49829

POLCYN, Fabian C.
Environmental Research Institute of Michigan
Willow Run Laboratories
P. O. Box 618
Ann Arbor, Michigan 48107

POLK, Charles B.
Sperry-Univac
1275 Space Park Drive
Houston, Texas 77058

POLLACK, Henry N.
University of Michigan
1006 CCL Building
Ann Arbor, Michigan

POLLARD, Bill
University of Michigan
Ann Arbor, Michigan

PORCELLO, Leonard
Environmental Research Institute of Michigan
Willow Run Laboratories
P. O. Box 618
Ann Arbor, Michigan 48107

POULTON, C. E.
Oregon State University
Rangeland Resources
Corvallis, Oregon

POWER, Eugene B.
2929 Plymouth Road
Ann Arbor, Michigan

PRENTICE, Virginia L.
Environmental Research Institute of Michigan
Willow Run Laboratories
P. O. Box 618
Ann Arbor, Michigan 48107

PRESTIN, Steven
University of Minnesota
Geography Department
414 Social Sciences Tower
Minneapolis, Minnesota 55455

QUERRY, Marvin R.
University of Missouri
Physics Department
1110 E. 48th Street
Kansas City, Missouri 64110

QUIREIN, John
TRW Systems
Software Evaluation Department
1 Space Park Drive
Houston, Texas 77058

RAGLAND, Thomas M.
NASA
Goddard Spaceflight Center
Greenbelt, Maryland

RAINA, B. N.
Indian Photo-Interpretation Institute
Geology Division
Kalidas Road
Dehra Dun, India

RAINES, Gary
Colorado School of Mines
Geology Department
Golden, Colorado 80401

RAJE, Surendra A.
General Electric
Space Division
P. O. Box 8555
Philadelphia, Pennsylvania 19101

RANEY, R. Keith
Environmental Research Institute of Michigan
Willow Run Laboratories
P. O. Box 618
Ann Arbor, Michigan 48107

REBEL, Diana L.
Environmental Research Institute of Michigan
Willow Run Laboratories
P. O. Box 618
Ann Arbor, Michigan 48107

ReVELLE, D. C.
University of Michigan
Aerospace Engineering
Research Activities
Ann Arbor, Michigan

RHUDY, James P.
University of Tennessee Space Institute
Tullahoma, Tennessee 37388

RIB, Harold
U. S. Department of Transportation
Federal Highway Administration
400 7th Street, S. W.
Washington, D. C.

RICHARDSON, A. J.
U. S. Department of Agriculture
P. O. Box 267
Weslaco, Texas 78596

RICHARDSON, Curtis J.
University of Michigan
School of Natural Resources
Ann Arbor, Michigan

RICHARDSON, Wyman
Environmental Research Institute of Michigan
Willow Run Laboratories
P. O. Box 618
Ann Arbor, Michigan 48107

RICHTER, John H.
University of Michigan
Graduate Library
Ann Arbor, Michigan

RIETHOF, Thomas R.
General Electric
Space Sciences Lab
Box 8555
Philadelphia, Pennsylvania 19101

RISLEY, Edward
U. S. Geological Survey
EROS Program
5213 GSA Building
18th and F Streets, N. W.
Washington, D. C. 20242

RITCHIE, Jerry C.
USDA
Sedimentation Lab
P. O. Box 30
Oxford, Mississippi 38655

ROBINOVE, C. J.
U. S. Geological Survey
U. S. Department of Interior
Code 4032 0001
Washington, D. C. 20242

ROGERS, R. H.
Bendix Corporation
Aerospace Systems Division
3300 Plymouth Road
Ann Arbor, Michigan

RHODE, Wayne G.
University of Michigan
Ann Arbor, Michigan

ROLLER, Norman
Environmental Research Institute of Michigan
Willow Run Laboratories
P. O. Box 618
Ann Arbor, Michigan 48107

ROOT, George
Jet Propulsion Laboratory
Space Photography Section
4800 Oak Grove Drive
Pasadena, California 91103

ROSE, Harvey
Environmental Research Institute of Michigan
Willow Run Laboratories
P. O. Box 618
Ann Arbor, Michigan 48107

ROSENHECK, Alma
Wix Library
Weizmann Institute of Science
Rehovot, Israel

ROTTWEILER, K.
Bendix Corporation
Aerospace Systems Division
3300 Plymouth Road
Ann Arbor, Michigan

ROWAN, Lawrence
U. S. Geological Survey
GSA Building, Room 204, 18th & F Streets
Washington, D. C.

RUDD, Stephen
E.R.T.S.
Institute of Arctic & Alpine Research
University of Colorado
Boulder, Colorado 80302

RUDZKI, John E. Jr.
U. S. Air Force
Wright Patterson AFB, Ohio 45433

RUSKEY, Frank
U. S. Bureau of Mines
Denver Mineral Research Center
Building 20, Denver Federal Center
Denver, Colorado 80225

RUTHROFF, David A.
State of Alaska
Department of Administration
P. O. Box 1122
Juneau, Alaska 99801

RUTLAND, David
Spatial Data Systems, Inc.
132 Aero Camino
Coleta, California 93017

RYAN, Irene E.
State of Alaska
Department of Economic Development
Pouch EE
Juneau, Alaska 99801

RYLAND, Dennis
South Dakota State University
Remote Sensing Institute
Brookings, South Dakota 57006

SABATER, Alfredo
Ministerio de Minas
Direccion de Geologia
Photointerpretacion
Centro Simon Bolivar
Piso #19, Torre Norte
Caracas, Venezuela

SABINS, Floyd F.
Chevron Oil Field Research Co.
P. O. Box 446
La Habra, California 90631

SADOWSKI, Frank
Environmental Research Institute of Michigan
Willow Run Laboratories
P. O. Box 618
Ann Arbor, Michigan 48107

SANDLER, Sheldon S.
Geophysical Survey Systems
16 Republic Road
N. Billerica, Massachusetts 01862

SAPP, Barbara S.
Office of the Governor
Kittrel Center, Suite 102
2711 Middleburg Drive
Columbia, South Carolina 29206

SATER, John E.
Arctic Institute of North America
1619 New Hampshire Avenue, N. W.
Washington, D. C. 20009

SATTINGER, Irvin J.
Environmental Research Institute of Michigan
Willow Run Laboratories
P. O. Box 618
Ann Arbor, Michigan 48107

SCARPACE, Frank L.
University of Wisconsin
Marine Studies Center
Madison, Wisconsin 53706

SCHAFER, Robert N.
State of Michigan
Department of Natural Resources
7th Floor, Stevens T. Mason Building
Lansing, Michigan

SCHANDA, E.
Universitat Bern
Institute of Applied Physics
Sidlerstrasse 5
3000 Berne, Switzerland CH-3000

SCHERZ, James
University of Wisconsin
Civil Engineering
Madison, Wisconsin 53706

SCHMER, Fred A.
South Dakota State University
Remote Sensing Institute
Brookings, South Dakota 57006

SCHROEDER, Manfred D.
DFVLR
Sensortechnology
8031 Oberpfaffenhofen, Germany

SCHUBERT, Fred W.
CIBA-Geigy
Saw Mill River Road
Arpsley, New York

SCHUMANN, Herbert H.
U. S. Geological Survey
Water Resources Division
Room 5017, Federal Building
230 N. First Avenue
Phoenix, Arizona 85025

SCHWARZ, David E.
California State University
Geography Department
125 South Seventh Street
San Jose, California 95114

SCOTT, Robert B.
Washington State Department of Natural Resources
Technical Services Division
Olympia, Washington 98504

SELLMAN, A.
Environmental Research Institute of Michigan
Willow Run Laboratories
P. O. Box 618
Ann Arbor, Michigan 48107

SENGER, Leslie W.
University of California
Geography Remote Sensing Unit
Santa Barbara, California 93106

SENNE, Joseph H.
University of Missouri
Civil Engineering
Rolla, Missouri 65401

SETH, Sharad C.
University of Nebraska
Computer Sciences
107 Ferguson
Lincoln, Nebraska 68508

SHAH, G. M.
Atmospheric Environment Science
Department of Environment
4905 Dufferin Street
Downsview, Ontario

SHAPIRO, Sidney
IBM Corporation
FSD
Gaithersburg, Maryland 20761

SHARMA, Ravi Dutta
Department of Science
Indian Institute of Science
Bangalore, India

SHIUE, James C.
NASA
Goddard Space Flight Center
Greenbelt, Maryland 20771

SHULTZ, Harold F.
Emhiser Rand Industries
7721 Convoy Court
San Diego, California 92111

SIERAWSKI, Frank
Bureau of State Services
Treasury Building
Lansing, Michigan 48918

SIMONETT, David S.
Earth Satellite Corporation
1771 N Street, N. W.
Washington, D. C. 20036

SIMPSON, Colin
Commonwealth of Australia
Department of Natural Development
Office of Australian Treasury
636 5th Avenue
New York, New York 10020

SIMPSON, Robert B.
Dartmouth College
Department of Geography
Hanover, New Hampshire 03755

SIPPELL, W. Lloyd
Canada Department of the Environment
Canadian Forestry Service
P. O. Box 490
Sault Ste. Marie, Ontario, Canada

SIZGORIC, Sebastian
York University
C.R.E.S.S.
4700 Keele Street
Toronto, Ontario, Canada

SMEDES, Harry W.
U. S. Geological Survey
Federal Center
Denver, Colorado 80225

SMITH, James A.
Colorado State University
Department of Watershed Sciences
Fort Collins, Colorado

SMITH, O. Glenn
NASA
Manned Spacecraft Center
Houston, Texas 77058

SMITH, William A.
System Planning Corporation
1500 Wilson Blvd., Suite 1500
Arlington, Virginia 22209

SOLLERS, Scott C.
U. S. Army
Policy & Analysis Division
Room 4-G-040, Forrestal Building
Washington, D. C. 20314

SOUSA, Theresa M.
U. S. Geological Survey
EROS Program
19th and F Streets, N. W.
Washington, D. C. 22101

SPANN, George W.
Georgia Technological University
225 North Avenue
Atlanta, Georgia 30332

SPELTZ, L. J.
TRW Systems Group
Control & Sensor Systems Lab
One Space Park, Building R6, Room 1587
Redondo Beach, California 90250

SPENCER, Margaret
Environmental Research Institute of Michigan
Willow Run Laboratories
P. O. Box 618
Ann Arbor, Michigan 48107

STAHL, Robert L.
U. S. Bureau of Mines
Building 20, Denver Federal Center
Denver, Colorado 80225

STAP, John Jr.
Martin Marietta Aerospace
Houston Region
1730 NASA Blvd., Suite 106
Houston, Texas 77058

STEG, Leo
General Electric
P. O. Box 8555
Philadelphia, Pennsylvania

STEINHART, Richard L.
University of Michigan
Department of Geology
Ann Arbor, Michigan

STEINSNYDER, Mike
MDAC/MDC
5301 Bolsa Avenue
Huntington Beach, California 92647

STEINWAY, Daniel
Environmental Research Institute of Michigan
Willow Run Laboratories
P. O. Box 618
Ann Arbor, Michigan 48107

STELLER, David
North American Rockwell
Earth Resources Operation
12214 Lakewood Blvd.
Downey, California 90241

STEPHENSON, Marvin E.
Rockefeller Foundation
Natural & Environmental Sciences
111 W. 50th Street
New York, New York 10023

STERBENZ, John J.
University of Michigan
School of Natural Resources
Ann Arbor, Michigan

STEVENS, Alan R.
Tennessee Valley Authority
Maps & Surveys Branch
216 Haney Building
Chattanooga, Tennessee 37401

STEVENSON, W. H.
National Marine Fisheries Service
Mississippi Test Facility
Bay Saint Louis, Mississippi 39520

STOERTZ, G. E.
U. S. Geological Survey
Water Resources Division
Washington, D. C.

STOHR, Christopher J.
Purdue University
LARS
1220 Potter Drive
West Lafayette, Indiana

STONE, Glenn E.
Martin Marietta Corporation
Manned Space Systems
P. O. Box 179
Denver, Colorado 80201

STONE, Robert M.
Control Data Corporation
16915 El Camino Real, Suite 101
Houston, Texas 77058

STONEY, William E.
NASA
L'Enfant Plaza
Washington, D. C.

STOREMSKI, Janice
Environmental Research Institute of Michigan
Willow Run Laboratories
P. O. Box 618
Ann Arbor, Michigan 48107

STORTZ, Kirby
University of Minnesota
Physics Department
Duluth, Minnesota

STRAIGHT, W. G.
Lockheed Electronics
HASD
16811 El Camino Real
Houston, Texas 77058

STRICKLAND, James
General Electric
ERIS
Betaville, Maryland 20705

STROME, W. M.
Canada Centre for Remote Sensing
2462 Sheffield Road
Ottawa KIA, OE4, Canada

STRONG, Alan E.
U. S. Department of Commerce
3737 Branch Avenue, S. E.
Hillcrest Heights, Maryland

SU, Ming-Yang
Northrop Services, Inc.
6025 Technology Drive, Box 1484
Huntsville, Alabama

SUITS, Gwynn H.
Environmental Research Institute of Michigan
Willow Run Laboratories
P. O. Box 618
Ann Arbor, Michigan 48107

SUMMERS, Robert A.
System Planning Corporation
1500 Wilson Blvd., Suite 1500
Arlington, Virginia 22209

SWANK, Roland P.
Advanced Technology Applications Corporation
P. O. Box 562
Paoli, Pennsylvania

SYDOR, Michael
University of Minnesota
Physics Department
Duluth, Minnesota 55812

SYMEONAKIS, Antonios
University of Guelph
Land Resource Science
Guelph, Ontario, Canada

TANGUAY, Marc G.
Ecole Polytechnique
2500 Marie-Guyard
Montreal, Quebec, Canada

TARANIK, James V.
Iowa Remote Sensing Lab
Iowa Geological Survey
16 West Jefferson
Iowa City, Iowa 52240

TARBET, J. Denton
Philco Ford Corporation
WDL/PHO
1002 Gemini
Houston, Texas 77058

TARDIN, Abilio Cezar
INPE
Remote Sensing Project
Instituto de Pesquisas Espaciais
Sao Jose Dos Campos
Sao Paolo, Brazil

TARR, Earl G.
Knox, Bergman, Shearer Corporation
120 East Lauer Lane
Camp Hill, Pennsylvania 17011

TARRANT, J. R.
University of East Anglia
School of Environmental Sciences
Norwich NOR 88C, England

TAVARES, Harold R.
Honeywell
2 Forbes Road
Lexington, Massachusetts 02173

TAYLOR, M. M.
D.C.I.E.M.
Behavioural Sciences
Box 2000
Downsview, Ontario, Canada

TERASMAE, J.
Brock University
Geological Sciences
Glenridge Avenue
St. Catharines, Ontario, Canada

TERDAL, Linda
University of Michigan
Ann Arbor, Michigan

TERNES, Alan
American Museum of National History
Central Park West at 79th Street
New York, New York 10024

TERROUX, A. C. D.
Environment Canada
Water Management Service
Ottawa, Ontario, Canada

THAMAN, R. R.
University of California
Geography Remote Sensing Unit
Santa Barbara, California 93106

THIE, Jean
Department of Natural Resources
Manitoba Remote Sensing Committee
1301 Ellice Avenue
Winnipeg, Manitoba, Canada

THOMAS, Jean-Claude M.
Catholic University of America
Geography Department
Washington, D. C. 20017

THOMPSON, Donald E.
MAPCOtec Inc.
Thermal Survey Division
P. O. Box 310
Daytona Beach, Florida 32015

THOMSON, F. J.
Environmental Research Institute of Michigan
Willow Run Laboratories
P. O. Box 618
Ann Arbor, Michigan 48107

TIPTON, M. J.
University of South Dakota
South Dakota Geological Survey
Vermillion, South Dakota 57069

TOKERUD, R. E.
Lockheed Electronics Company H
HASD
16811 El Camino Real
Houston, Texas 77058

TONELLI, Arnaldo
Geolab C.N.R.
Geophysics
Via priv. Mario Blanco 9
20131 Milano, Italy

TORBERT, Grover B.
Bureau of Land Management
Department of Interior
Washington, D. C. 20240

TOWLES, Robert W.
General Electric
P. O. Box 2500
Daytona Beach, Florida 32015

TRANTER, William H.
University of Missouri
Electrical Engineering Department
Rolla, Missouri 65401

TRIENDL, Ernest
I. F. Satellitenelektronik
DFVLR
Oberpfaffenhofen, Germany D-8031

TROTT, Warren Calvin
Grumman
S. Oyster Bay Road
Bethpage, New York 11714

TULLOS, Earl J. Jr.
University of Tennessee
Department of Geography
Knoxville, Tennessee 37916

TURNER, Robert E.
Environmental Research Institute of Michigan
Willow Run Laboratories
P. O. Box 618
Ann Arbor, Michigan 48107

TUYAHOV, Alexander J.
State of Texas
Governor's Office of Information Services
P. O. Box 13224, Capital Station
Austin, Texas 78711

ULABY, F. T.
University of Kansas
Irving Hill Road
Campus West
Lawrence, Kansas

URBASSIK, Drew
Environmental Research Institute of Michigan
Willow Run Laboratories
P. O. Box 618
Ann Arbor, Michigan 48107

VACA, Jorge F.
Cetenal
Mexican Government
San Antonio Abad No. 124
Mexico 8, D.F., Mexico

VAN DALL, P.
Bedford Institute of Oceanography
Department of Environment
P. O. Box 1006
Dartmouth, Nova Scotia, Canada

VAN DYKE, Barney
University of Michigan
School of Public Health
Ann Arbor, Michigan

VAN GENDEREN, J. L.
University of Sheffield
UNESCO
Department of Geography
Sheffield 10, England

VAN KONIJNENBURG, Ir. R.
Fokker-VFW NV
Systems Department
Schiphol Oost, P. O. Box 7600
The Netherlands

VAN KUILENBURG, J.
NIWARS
Central Bureau Kanaalweg 3
Delft, The Netherlands

VAN ROOY, D. L.
Rice University
ICSA
Houston, Texas 77001

VAN TRIES, Bill J.
U. S. Department of Interior
Office of the Secretary
Interior Building
Washington, D. C.

VICKERS, R. S.
Colorado State University
Department of Electrical Engineering
Fort Collins, Colorado 80521

VIGLIONE, Sam S.
McDonnell Douglas Corporation
5301 Bolsa Avenue
Huntington Beach, California 92649

VINCENT, Robert
Environmental Research Institute of Michigan
Willow Run Laboratories
P. O. Box 618
Ann Arbor, Michigan 48107

VITALE, Joseph A.
NASA
Office of University Affairs
NASA Headquarters
Washington, D. C. 20546

VOELGER, Klaus
Aero Exploration
605 Offenbach, Ludwigstr. 33
Federal Republic of Germany

VOGEL, Martin
Deutsche Forschungs
und Versuchsanstalt fur Luft
Und Raumfahrt e.V.
Forschungszentrum Oberpfaffenhofen
Germany

VON HESLER, Alexander
Regionale Planungsgemeinschaft
Untermain, Zeil 127
6000 Frankfurt/Main, West Germany

WACKER, A. G.
University of Saskatchewan
Department of Electrical Engineering
Saskatoon, Saskatchewan, Canada

WAGNER, Thomas W.
Environmental Research Institute of Michigan
Willow Run Laboratories
P. O. Box 618
Ann Arbor, Michigan 48107

WALL, Priscilla W.
EROS/USGS
Room 827
1717 H Street, N. W.
Washington, D. C. 20242

WALTERS, Robert L.
University of Kansas
Space Technology Center
2291 Irving Hill Drive
Campus West
Lawrence, Kansas 66044

WALTZ, Fred
South Dakota State University
Remote Sensing Institute
Brookings, South Dakota 57006

WARD, Edward A.
MITRE Corporation
D-22, Westgate Research Park
McLean, Virginia 22101

WARREN, Cliff
AGA Corporation
679 Riverview Lane
St. Charles, Missouri 63301

WASHBURN, A. L.
University of Washington
Quaternary Research Center
Geophysics Building
Seattle, Washington 98195

WASTENSON, Leif
University of Stockholm
Department of Physical Geography
P. O. Box 6801
11386 Stockholm, Sweden

WATERS, Joe
Massachusetts Institute of Technology
Room 26-650
Cambridge, Massachusetts 02139

WATSON, Kenneth
U. S. Geological Survey
Remote Sensing Geophysics
Denver Federal Center
Denver, Colorado 80225

WEBER, Stephen
Tennessee Valley Authority
Division of Forestry, Fisheries & Wildlife
Development
Forestry Building
Norris, Tennessee 37828

WEBSTER, Ronald
State of Michigan
Executive Office
State Planning
Lansing, Michigan 48913

WEIDMAN, Robert M.
University of Montana
Department of Geology
Missoula, Montana 59801

WELCH, Joseph D.
General Electric
Space Division
Room U2432
King of Prussia, Pennsylvania 19401

WELDON, James W.
NASA
Manned Spacecraft Center
Earth Resources Lab
Mississippi Test Facility
Bay St. Louis, Mississippi 39520

WELLS, William C.
Lockheed Research Lab
Building 201
Palo Alto, California 94304

WENGROW, GARY L.
North American Rockwell
Space Division
12214 Lakewood Blvd.
Downey, California 90241

WENTZ, W. Alan
University of Michigan
Ann Arbor, Michigan

WESTBY, R. L.
National Research Council
Radio & Electrical Engineering
Montreal Road
Ottawa, Ontario, Canada

WEZERNAK, Chester
Environmental Research Institute of Michigan
Willow Run Laboratories
P. O. Box 618
Ann Arbor, Michigan 48107

WHISTLER, Chuck
Texas Instruments
Equipment Group
P. O. Box 6015
Dallas, Texas 75222

WHITACRE, Horace E.
NASA Skylab/KM
Houston, Texas

WHITE, Charles
University of Michigan
Ann Arbor, Michigan

WHITE, Owen L.
University of Waterloo
Department of Civil Engineering
Waterloo, Ontario, Canada

WIBERG, Harold J.
Grumman Ecosystems Corporation
Bethpage, New York

WIER, Charles E.
Indiana University
Geological Survey
611 N. Walnut Grove Avenue
Bloomington, Indiana 47401

WIESNET, Donald R.
National Env. Satellite Service
Env. Sciences Group S33
3737 Branch Avenue, S. W., Suite 300
Washington, D. C. 20031

WILKERSON, John C.
U. S. Naval Oceanographic Office
Code 7003
Washington, D. C.

WILLIAMS, Jerome
U. S. Naval Academy
Environmental Sciences Department
Annapolis, Maryland 21402

WILLIAMS, Richard S. Jr.
U. S. Geological Survey
EROS Program Office
1717 H Street, N. W.
Room 819B
Washington, D. C. 20242

WILSON, C.
Bendix Corporation
Aerospace Systems Division
3300 Plymouth Road
Ann Arbor, Michigan

WILSON, J. T.
University of Michigan
6117 IST
Ann Arbor, Michigan

WINIKKA, Carl
State of Arizona
A.R.I.S.
4530 N. Central Avenue
Phoenix, Arizona 35282

WOLF, James M.
Environmental Research Institute of Michigan
Willow Run Laboratories
P. O. Box 618
Ann Arbor, Michigan 48107

WOODRING, Stanley M.
Purdue University
LARS
1220 Potter Drive
West Lafayette, Indiana

WORK, Edgar A. Jr.
Environmental Research Institute of Michigan
Willow Run Laboratories
P. O. Box 618
Ann Arbor, Michigan 48107

WORSFOLD, Richard D.
CCRS/CFASY
CFB Uplands
Ottawa, Ontario, Canada KIV 8R2

WRAY, James R.
U. S. Geological Survey
Geographic Applications Program
1717 H Street, N. W., Room 837
Washington, D. C. 20242

WRIGHT, Donald
E.G.R.G.
P. O. Box 809
Los Alamos, New Mexico 87544

WUKELIC, George
Battelle
Physics Department
505 King Avenue
Columbus, Ohio 43201

WYCHGRAM, Daniel C.
Martin Marietta
P. O. Box 179, Mail Stop 1615
Denver, Colorado 80201

YARGER, H. L.
University of Kansas
State Geological Survey
Lawrence, Kansas 66044

YONKER, Terry
Michigan Department of Commerce
Office of Economic Expansion
7 Story State Building, 4th Floor
Lansing, Michigan 48913

YOST, Edward
Long Island University
Greenvale, New York 11548

YOUNG, Lee A.
Avco Everett Research Laboratory
2385 Revere Beach Parkway
Everett, Massachusetts 02149

YUILL, Robert S.
Central Michigan University
Department of Geography
Mt. Pleasant, Michigan

YUNG, Alfredo A.
Argentine Navy
Hydrographic Office
Moutes de Oce 2124
Capital, Argentina

ZAPUTOWYCZ, Roman Z.
General Electric
Space Division
Box 8555
Philadelphia, Pennsylvania 19101

ZENONE, Chester
U. S. Geological Survey
Water Resources Division
1209 Orca Street
Anchorage, Alaska 99501

ZISSIS, G. J.
Environmental Research Institute of Michigan
Willow Run Laboratories
P. O. Box 618
Ann Arbor, Michigan 48107

ZWALLY, H. Jay
National Science Foundation
Office of Polar Programs
Washington, D. C. 20550

WELCOME AND INTRODUCTION

W. M. Brown
President, Environmental Research
Institute of Michigan
and
Director, Willow Run Laboratories
University of Michigan
Ann Arbor, Michigan

Good morning ladies and gentlemen. On behalf of The University of Michigan and the sponsors of this symposium, it is a pleasure to welcome you here today.

Remote sensing of the environment has been, and no doubt will continue to be, a rapidly expanding area of productive activity. As I recall the beginning over a decade ago, a few people became aware of the possibility of using modern sensor technology in a wide variety of civilian applications. Prior to that time most of the research in sensor technology was sponsored by the Department of Defense, and somewhat inadvertently potential civilian applications were not receiving much emphasis. The initial efforts involved simple demonstrations of capabilities in earth observations from aircraft with breadboard sensor packages and human, non automatic, data processing. Over the past decade we have seen remote sensing become an activity on an international scale with the participation of a large number of government agencies and private companies.

Our last meeting was given extra excitement and significance by the United Nations Workshop that was held just prior to the symposium. This symposium is also held under the influence of a great event. Specifically, in time the earth resources technology satellite was successfully launched. New expanded exciting applications based on the ERTS system are already being demonstrated and some of the capabilities will be presented during this meeting. NASA as an agency and many individuals showed inspiring courage and dedication in advancing the ERTS program. On behalf of you attendees and the entire technical and user community, may I congratulate NASA and the many people who brought us the ERTS program.

On the local scene I would like to mention that the activities of the Willow Run Laboratories are in the process of a major reorganization. Our programs, people, and facilities are being transferred to corporate status separate from The University of Michigan. The new organization is a non profit research institute endorsed and capitalized by the state of Michigan, and our new name is The Environmental Research Institute of Michigan. We may be changing our name, but we are not changing our intense interest and dedication to remote sensing programs.

I hope and trust that your visit to the university and Ann Arbor will be pleasant and professionally rewarding. We certainly take pride in being a part of this symposium.

APPLICATIONS OF REMOTE SENSING IN ARIZONA STATE GOVERNMENT

C. Winikka
State of Arizona
and
H. Schumann
U.S. Geological Survey
Phoenix, Arizona

INTRODUCTION

The mention of Arizona to the average citizen of this country causes him to envision broad expanses of scenery such as the Grand Canyon, hot deserts bristling with cactus, cool Ponderosa pine forests or possibly the cities of Tucson or Phoenix. In any case, Arizona represents a vacationland as do many of the western states. And yet, this doesn't mean Arizona is free of numerous problems of national concern today. Arizona, a state of 114,000 square miles, is feeling the impact of a 50% population increase in the last 12 years, the impact of an ever-increasing number of tourists and the impact of man's activity in resource development, electrical power generation, transportation, and changing land use. What are the results of these impacts? Which are good? Which are bad? How do we define them?

Can we put them in meaningful perspective in order that wise decisions may be made? At this point, I would like to quote the late Dr. William Pecora of the United States Department of the Interior in his remarks at the United States House of Representatives Panel on Science and Technology Meeting in Washington, D.C. on January 26, 1972:

> "If one must call upon the resources of the crust of the earth to supply man in his evolutionary development into the future, one must recognize that certain materials of the crust can be useful to man and decisions must be made, not whether or not to use them, but how to use them."

Many of the impacts requiring identification, definition and measurement in Arizona are directly related to land. They concern vegetation, soils, minerals, water, and other basic resources that are each the proper responsibility of particular Federal and State agencies. Within their area of resource changes taking place; however, relatively little information is exchanged between agencies. They do, however, have a common dedication or purpose, and that is to serve the public in an effective, efficient manner. In order to accomplish this, communication, especially through an effective information exchange, is necessary.

The infinitely complex interactions between man, animals, plants, soil, water, and air are, because of lack of concern or because of prohibitive time and cost requirements, seldom given sufficient attention. Only when they are, can we make the wisest use of our resources.

BACKGROUND

The responsibility for wisely developing resources while adequately protecting the environment is Arizona's concern today. A brief background of our Arizona program may be of interest.

Two separate, significant activities took place in Arizona during 1970, a series of technical meetings were held in Phoenix. At these meetings, the evaluation of remote sensing imagery of Arizona from space was discussed and then field checked on a trip into east central Arizona. Later in 1970, the U.S. Geological Survey, at the request of the National Aeronautics and Space Administration, established the Arizona Regional Ecological Test Site Project (ARETS) to consolidate research efforts and to test and evaluate applications of remote sensor data to earth resources and environmental problems in Arizona.

The first annual ARETS Seminar-Workshop was held in Tucson during October of 1970 at which time the capabilities of remote sensing were more fully discussed. Feasible applications of remote sensing to Arizona were apparent. ARETS activity continued, including the evaluation of National Aeronautics and Space Administration color photography from 60,000 feet with an aerial mapping camera. The

Preceding page blank

potential application of this photography not only to interpretation, but to photogrammetric mapping, became immediately apparent.

In November of 1970, the Arizona Game and Fish Department sponsored a meeting of interested Governmental agencies to discuss the possibility of developing a statewide land use inventory system for Arizona. Representatives from Cornell University were present to describe, as an example, the New York Land Use and Natural Resources Inventory which was based on the use of aerial photography. A high interest developed among the State and Federal agencies present and, as a result, in December of 1970, a Land Use Steering Committee was formed to determine whether such a land use system would be beneficial to Arizona and, if so, to find the most feasible approach for its development.

It is interesting to note that many of the State and Federal agencies represented at the ARETS meeting were also represented on the Land Use Steering Committee; however, the personnel were not the same, since each group was virtually unaware of the other's existence. Early in 1971, a number of State and Federal personnel involved in ARETS were invited to the Land Use Steering Committee meetings, and it became apparent that the goals of each were very similar. For this reason, the application of remote sensing now took on the character of applied research. This in turn resulted in the inclusion of additional State agencies.

Concepts developed at the meetings of both groups merged when the Land Use Steering Committee felt its function could most effectively be coordinated between the various State agencies by the Governor's Office, since this broad subject and its possible solution was greater than the scope of interest of any one agency. The Governor's Office concurred with the Committee's recommendation and thus undertook the coordination of a program to explore the use of remote sensing in State government.

REMOTE SENSING POTENTIAL

As is often the case, the best way to view a problem is to back away from it and view it from a distance. At this point, we literally did this. We studied firsthand, Apollo imagery and underflights of Apollo missions covering large areas of Arizona and thus observed Arizona from a distance never seen before, at least by State agencies.

We also discovered that much work had already been accomplished in Arizona by persons outside Arizona. The results of National Aeronautics and Space Administration funded research in land use, crop identification, and geological studies together with the high altitude photography used for those studies provided an early insight into a possible method for developing a program in Arizona.

Evaluation of NASA photography indicated that this photography was particularly useful to a variety of State agencies, many of which were not related organizationally, i.e., Game and Fish Department, Department of Property Valuation, Highway Department, Oil and Gas Commission, State Land Department and others.

CONCEPT OF PROGRAM

The interest in developing useful applications for remote sensing in Arizona was considerably deeper than just remote sensing. There was also a great need to "pool" all information related to land in a common information system. As a means of accomplishing this information exchange between existing agencies, leadership from the Governor's Office has included the formation of the Arizona Resources Information System, ARIS, the appointment of a Policy Advisory Committee for the Arizona Resources Information System, and the appointment of a Project Director who began this full-time assignment on December 1, 1971. The Policy Advisory Committee consists of the heads of nine State Agencies: Department of Property Valuation, Oil and Gas Conservation Commission, State Land Department, Department of Economic Planning and Development, Water Commission, Highway Department, Health Department, Game and Fish Department, and the Governor's Highway Safety Coordinator. In addition, the Governor's Office, the University of Arizona, the Arizona Regional Ecological Test Site Coordinator and the Project Director for Arizona Resources Information System are on the Committee. A Working Committee consisting of persons representing each of the named agencies and interested additional State agencies has been formed to carry out the necessary coordination in the development of the Arizona Resources Information System.

Early goals in the development of Arizona Resources Information System consist of base aerial photography of Arizona, orthophotoquads of Arizona at 1:24,000, and Arizona Land Use Classification System compatible with a Federal System being developed in the Interior Department, application of remote sensing to problems relating to land management, training in remote sensing for State personnel experienced in their own agency, selection of a series of map scales needed to display base information and early work to evaluate the application of electronic data processing to our information system.

Our approach to the utilization of electronic computers to process information related to land is to develop a system which will store, retrieve, and plot or display any attributes or combination of attributes as they pertain to a particular land area. ARIS user agencies range from those concerned with individual land parcels of irregular shapes and sizes to those agencies responsible for wildlife habitat areas having irregular natural features as boundaries. Incorporating these needs requires the use of polygons, lines and points which define the feature in a form usable to the responsible agency on a common base which will permit a meaningful inter-agency information exchange for planning and management purposes.

ARIZONA LAND USE EXPERIMENT

As further contacts were made with the National Aeronautics and Space Administration and the Department of the Interior, it became apparent that Arizona indeed had a high early interest in the application of remote sensing to State government. This interest extended from the Governor's Office into virtually every State agency concerned with land. It then became desirable to formulate a unique statewide land use experiment to provide a basis for incorporating space and aircraft data sources into ongoing State management programs. This concept was further refined and is now the subject of a joint effort by National Aeronautics and Space Administration, The Department of Interior, and the State of Arizona, to study, in actual applications, the use of remote sensing by operational State agencies. This program is known as "The Arizona Land Use Experiment."

Although much has been accomplished, the program is essentially just beginning in Arizona. Very briefly, high altitude multispectral photo coverage is underway, paneling of existing horizontal control for orthophotoquads is virtually complete and orthophotoquad production is beginning. The orthophotoquads will serve as a base or foundation for a wide range of thematic overlays prepared by those agencies having responsibility for the particular discipline displayed on the overlay. Interrelationship of land ownership, land use and resource development or non-development will then be evaluated as a basis for management decisions in the framework of a realistic perspective.

Arizona has developed a tentative standard land use classification system for use on available high quality base maps of the State.

One of the important products of the Arizona Land Use Experiment will be a manual describing the means by which remote sensing is used in Arizona. This manual, prepared by Arizona, will be for the use of other states in the application of these methods to the solution of management problems.

Timely application of future remotely sensed data from space will be made shortly after acquisition on a specific area basis by comparison with the Arizona base photography. Cross reference from a particular land parcel on the ground to space imagery or from space imagery to a particular ground location will be incorporated in the Arizona Resources Information System.

The development of Arizona Resources Information System and the conduct of the Arizona Land Use Experiment present an exciting challenge to provide for extensive application and evaluation of remote sensing in matters relating to land and resource management.

APPLICATION OF REMOTE SENSING TECHNOLOGY TO RESOURCE MANAGEMENT PROBLEMS OF STATE GOVERNMENT IN CALIFORNIA

John B. Passerello

Governor's Office--Office of Planning and Research
Sacramento, California

David E. Schwarz

Dept. of Geography--California State University
San Jose, California

Remote sensing imagery has been utilized at all levels of government in California. This paper concentrates on those applications of remote sensing that have proven to be of value in solving the problems of managing the State's resources and also those proposed applications from the ERTS program. The State of California requires data which will better enable the clarification of problems, and give resource managers more detailed information upon which to base objective management decisions. Remote sensing technology offers a means of making frequent, rapid and up-dated inventories of California's resources, it makes possible an analysis of the impact of human activity on those resources, and it has helped in setting guidelines for resource use and conservation.

Geographical areas in California for which precision data is needed provide the most varied range of terrain, resources, and population densities to be found anywhere in the United States. The types of areas are similar to others that are put to human use in the Country, but the variation in scale and intensity of use offers a complexity that far exceeds other regions. These areas are urban and rural, desert and mountain, cropland, range land, and forest land, they are geologic formations and natural disasters, and they are covered by air and laced by water.

The State of California recognizing the importance of remote sensing as an important tool to manage the vast natural resources of the State appointed Mr. A. Earl Davis as Remote Sensing Coordinator in July, 1971. His responsibility is to coordinate the total effort of the State's remote sensing program which consists of twelve state departmental coinvestigators. He is also responsible for coordinating with other principal investigators in the State which include the six campus effort of the University of California, Federal Agencies, and local governments. NASA has now approved all portions of the California proposal, "State of California Study Combining Basic Research and Applied Use of ERTS-A, Skylab, and Supporting Aircraft Data for More Effective Resource Management." The State's role is to use the imagery and data from the ERTS program to define user problems and provide more objective solutions to those problems.

The Resources Agency and the Business and Transportation Agency have made good use of aerial photo technology in their projects. The State Division of Highways and the Department of Water Resources, within those two agencies, have been consistently the heaviest users of photography. Currently, the Department of Water Resources is utilizing high-altitude imagery taken by U-2 overflights of certain portions of the State every eighteen days. This has given them the capa-

Preceding page blank

bility of change detection in a variety of land uses that infrequent, low-altitude imagery never gave. Now that the U-2 imagery is available, it is possible to set up a meaningful program concentrating on those categories of land use that will take the greatest advantage of the proposed remote sensing systems. The following table expresses, in summary form, the type of data and projects that are currently being undertaken and the remote sensing application of the ERTS system that will provide more consistently up-dated information. The mapping scale for the various land features would be 1:125,000.

TABLE 1. APPLICATION OF ERTS SYSTEM TO STATE RESOURCES

Land Feature	Remote Sensing Application	Acquisition Frequency	Parcel Size
Urban	-Mapping urban fringe (change detection)	Annually	40 acres
Cropland	-Irrig. vs. nonirrigation	18 days	640 acres
	-Identify trees and vines	Annually	640 acres
	-Salinity detection	Annually	640 acres
Range Land	-Identify grassland and savanna	Annually	640 acres
Forest Land	-Change detection (forest land vs. other uses)	Annually	640 acres
	-Identify shrub-scrub vegetation		
Desert	-As an aid in a detailed evaluation of desert resources by BLM	1-4 times per year	640 acres
Water	-Detection of pollution sources	Annually	640 acres
	-Monitor direction and rate of pollution movement	18 days	40 acres
	-Monitor change in lake and reservoir storage	18 days	40 acres
Geologic Formations	-Identify land forms	Annually	640 acres
	-Evaluate fault lines	Annually	640 acres
	-Identify and map contact zones	One time	640 acres
	-Evaluate beach morphology	Annually	640 acres
	-Evaluate alluvial processes	6 months	640 acres
Natural Disasters	-Delineation of flooded areas	One time	640 acres
	-Mapping burned-over areas	One time	640 acres

The State Department of Water Resources is concentrating remote sensing application on those types of land use that utilize water for survival and those attributes and adverse effects of and on water that will have relevance to its management. Extrapolation of agricultural land use conditions based on point-in-time surveys have already revealed the following results: acreage change detection, delineation of irrigated versus nonirrigated areas, dry-farmed versus native vegetation, determining the change of fallow lands throughout the year, the extent of

double-cropping, and crop planting and harvesting dates. Identification of major crop groups (e.g., tree and vine, forage, row crops) and some individual crops and the evaluation of the rate of expansion of irrigated cropland ground cover throughout the entire drainage basin are also important considerations.

Analysis of the urban landscape by remote sensing has shown results in detecting changes in land use by plotting the expansion of urbanization into prime agricultural land areas. In addition the location and extent of recreational and second-home subdivisions have shown the conflicts between those urban-type uses and needed habitat for cattle grazing and migratory deer winter range. This information has proven to be an asset not only to state resource planning but also to regional, county, and city planning.

Native land analysis includes some of the same identification techniques with the primary goal being to define broad vegetative associations, acreage change detection within and among these associations, and the impact of urban encroachment upon the various associations. Geologic features are also being evaluated (e.g., land forms, fault zones, contact zones, beach morphology, and alluvial processes). Geologic and geomorphic processes and their effects are being monitored with the use of remote sensing, especially in light of their potential for disaster in areas of human habitation and activity.

Air and water pollution are two important areas of environmental analysis that are being greatly enhanced with the aid of advanced remote sensing techniques, which include the periodic surveillance by high-altitude U-2 flights and low-altitude light airplanes along with ground truth observations. In terms of water pollution, the delineation of sediment plumes, the detection of algal blooms, and the evaluation of effluent discharge patterns are being monitored in certain areas.

The technological advancements in remote sensing are already providing State government in California with a greater range of options and capabilities in resource management. Now it is a matter of setting priorities to accomplish those tasks that reflect the State's social, economic, and environmental goals and policies.

REMOTE SENSING, A TOOL FOR STATE PLANNING-MANAGEMENT IN IOWA

Samuel J. Tuthill
State Geologist

James V. Taranik *
Chief of Remote Sensing

Iowa Remote Sensing Laboratory
Iowa Geological Survey
Iowa City, Iowa

ABSTRACT

In September 1971 the State of Iowa established a remote sensing laboratory that coordinates image acquisition and dissemination, supervises ground information collection, and provides data analysis services for 24 state and federal agencies operating in Iowa. The Remote Sensing Laboratory relies on the research output of laboratories that are developing new remote sensing technologies and selects those technologies appearing most applicable at the state level. Remotely sensed data is acquired at scales providing the most information to the maximum number of potential users. Costs, in terms of time and money for data acquisition, are evaluated with respect to work obviated by the remote sensing approach. The Iowa Remote Sensing Program brings together basic researchers from the academic community, analysts of imagery, and those applying the analyses to the practical problems of natural resource management, land utilization planning, and environmental control in the Midwest.

1. INTRODUCTION

There is an increased emphasis on planning in state government because of population shifts and growth, increased urbanization, technological changes in industry and changing patterns in the consumption of goods. The changing relationships between urban-industrial development and rural-agricultural landuse, and the increasing need for natural resources have placed stress on environmental quality and the state economic base. Recognizing the need for meaningful legislative control over resources, land utilization, and the environment, the State of Iowa has developed a remote sensing program capable of inventorying the Iowa landscape and providing knowledge for the technical analysis of problems related to state growth.

The data products from remote sensors imaging the State of Iowa should enable legislators and state agencies to map out state evolutionary trends, regulate economic growth, and maintain orderly state development. Remotely sensed data of

* Speaker

Preceding page blank

Iowa has the potential for application to a broad spectrum of disciplines in the state. The Iowa Remote Sensing Program is organized to identify those useful items of data that come from platforms that range in type from low-altitude aircraft to satellites. State agencies will utilize these analyses in their planning, regulatory, operational, and research functions.

2. ORGANIZATION OF THE IOWA PROGRAM

Since 1892 the Iowa Geological Survey has acted as a research and consulting agency for the State of Iowa in matters related to earth resources and the physical environment. In addition, it is the repository of hydrologic, geologic and physical geographic data for Iowa. The State of Iowa has been using conventional aerial survey methods since 1930 and airborne geophysics since 1952. It has become apparent that remotely sensed imagery is a powerful tool for monitoring aspects of the environment, and the Survey has promoted its use by government agencies having research, regulatory, and/or a ion functions related to or affecting environment, resources, and land usage. The Survey, in September of 1971, developed a staff capable of acquiring, interpreting, and analyzing remote-sensor data and organized a consortium of 24 state and federal agencies operating in Iowa who can employ these data.

There are eight Iowa state agencies that have major regulatory responsibility for aspects of the environment (1). In addition, there are eight action agencies that use spatial and temporal data that characterize phenomena and processes on the earth's surface (2). Supporting these 16 agencies as a significant part of their functions are three state and two federal research agencies (3). In the three state universities there are individuals and groups that are conducting research related to the Iowa environment, the subject of which relates to remotely sensed data.

1. Iowa State Conservation Commission; Iowa Dept. of Agriculture; Iowa Natural Resources Council; Iowa Dept. of Mines and Minerals; Iowa State Dept. of Health, Solid Waste Division; Iowa Water Pollution Control Commission; Iowa Air Pollution Control Commission; and Iowa Chemical Review Board.

2. Iowa Office for Planning and Programming; Iowa Development Commission; Iowa Dept. of Justice; the State Archaeologist; Iowa Highway Commission; Iowa Dept. of Soil Conservation; Iowa Dept. of Revenue; and the Iowa State Dept. of Public Instruction.

3. U.S. Dept. of Agriculture, Soil Conservation Commission; U.S. Geological Survey Water Resources Division; Iowa State Hygienic Laboratory; Iowa Geological Survey and the Iowa State Agricultural Experiment Station.

Iowa Geological Survey has organized these 24 state and federal agencies into a consortium for the purpose of acquiring and applying remotely sensed data to planning and regulatory functions. The Iowa Remote Sensing Laboratory coordinates imagery acquisition projects and information dissemination programs. It is the responsibility of the Laboratory to conduct a monitoring service for specific phenomena and processes that the user-agencies identify as elements of their regulatory, planning, and/or research interests. The Laboratory coordinates acquisition of "ground truth" data by the technical staffs of the various user-agencies, develops analytical advisory services, stimulates research in the field of applications of remotely sensed data to problems in the state, and publishes completed studies in an open-file system that is freely available to the public.

At present it is not possible to describe the full usefulness of remote-sensor data to all of these agencies because it depends upon: imagery limitations, the amount of imagination each agency can bring to the program, and to a small degree the funding available in the individual agencies.

3. MODE OF OPERATION

The Iowa Remote Sensing Program relies on the research output of remote sensing laboratories that are developing new sensors, new data analysis equipment, and new techniques for handling remotely sensed imagery and data. The Iowa program stresses the selection of technologies which appear to be most applicable to problems related to resource management and environmental quality in Iowa, and which best fit the cost-effectiveness relationships defined by the state financial structure. A major

goal of the Laboratory is to determine the unique spectroradiometric properties of the Iowa landscape. Once these properties are understood and directly related to ground phenomena, then hopefully, changes in spectroradiometric character can be related to changes in environmental quality, resources, and land usage. Aerial films have demonstrated their ability to record the geometry and, to some degree, the spectral reflectance of the Iowa landscape. At the present time problems with film emulsions, film aging, and film processing can seriously limit the use of aerial film as a spectroradiometer. Multispectral scanning instruments show promise for mapping spectroradiometric characteristics on a repeatable basis, but at this time the problems with data formats, data processing, and expensive instrumentation limit their use by most state agencies.

The Laboratory relies on local and regional private contractors for their expertise in acquiring imagery. It appears to be more effective, especially in terms of time, to spend money on image acquisition over Iowa than to spend money on aircraft, aerial remote sensing equipment, maintenance, and hangar facilities. The major drawback to this approach is that most major aerial service companies plan weeks, or often months in advance to keep their plane flying. Often, weather and seasonal conditions develop where it suddenly becomes optimal to fly within a matter of days or even hours. Another frequent problem is the acquisition of color or color infrared film on short notice. Small companies may not like to store color films for long periods of time, because of film aging problems and inventory costs. The State of Iowa does own a multispectral camera, primarily because local aerial service companies do not normally fly this system. Expensive metric mapping cameras or multispectral scanners are not planned acquisitions, primarily because, in this time frame, these remote sensing systems are changing rapidly with advancing technology and systems can rapidly become obsolete. Perhaps most important of all, the acquisition of an aircraft, sensors, and aircraft crew, is an extension of government into the free enterprise of aerial contractors, and should be avoided if contractors already have this equipment or are willing to acquire it.

The remote sensing staff generates interest in the application of remote sensing to problems faced by the 24 state and federal agencies operating in Iowa, informs these agencies of the costs for data acquisition, and develops interagency cooperative imagery acquisition programs to achieve the highest cost-effectiveness relationship for remote sensing activities in Iowa.

Remote Sensing Laboratory staff members are currently evaluating costs, in terms of time and money, for remote sensing activities in the state. Mission design, data acquisition, data processing, data analysis, and overhead costs are being evaluated in the light of work obviated by the remote sensing approach. Because remotely sensed data may have many possible uses, this cost analysis evaluates both the primary objectives and those serendipitous opportunities that appear during data analysis.

The goal of the cost-effective approach is to acquire remotely sensed imagery at scales which will have wide application to a variety of state and federal users. The trade-off between information content and number of agencies served is evaluated so that one overflight can serve the needs of as many agencies as possible. It may be possible that any one agency may not receive imagery at scales and resolutions optimal for its individual problem.

The Iowa Geological Survey currently furnishes four Ph.D. level and three M.S. level analysts to the state remote sensing program. One secretary, draftsman, and photointerpreter are furnished to this staff for operational continuity. The Remote Sensing Laboratory currently has a multispectral camera, color-additive multispectral viewer, and an image density-slicing, false-color enhancement, vidicon system. On hand are several high quality image interpretation light tables, and a full complement of stereoscopic analysis equipment. Addition of personnel and equipment was supported by funding through the state legislature as a new program within the Iowa Geological Survey, and with the understanding that the technical expertise of the staff and the equipment would be at the disposal of all agencies operating in Iowa. During the last two years approximately $50,000 has been expended for remote sensing equipment and $50,000 for program personnel salaries. In the future, total expenditures in terms of salary, equipment and operational expense, will probably not exceed $100,000 yearly. Sixty percent of this figure will be used for contracting aircraft, and for acquiring film and film processing in direct support of the 24 state and federal agencies operating in Iowa.

Reports of activities and research results are announced in a newsletter disseminated to user-agencies and the remote sensing community at large. Formal publications of the Investigations of the Laboratory staff are reported in inter-agency open-file reports, and the Iowa Geological Survey Report of Investigations series. Items of general interest to the public are reported in the Iowa Geological Survey Public Information Circulars. Other state and federal agencies are encouraged to publish the results of their investigations using the remote sensing approach either separately or jointly with the Remote Sensing Laboratory staff.

4. PAST ACTIVITIES

Past activities of the Remote Sensing Laboratory include the planning and operation of two thermal mapping missions with the Remote Sensing Institute at Brookings, South Dakota. The purpose of these missions was to determine the present thermal regimen of the Mississippi River, prior to the operation of large nuclear power plants. The thermal mapping missions did not achieve their objectives because an uncalibrated scanner operating in the 3 to 5 micron range was used, mission design required data acquisition at noon, and ground measurements were poor. Additional missions are being planned by Iowa, Nebraska and Missouri for large river systems in the Midwest. Mission design includes data acquisition at 6000 feet with a calibrated scanner and airborne radiometer operating in the 8 to 14 micron range, data acquisition at noon and three hours after sunset, and ground data acquisition with radiometers and thermistor probe strings to sample the entire temperature range in and around the rivers.

The Laboratory has now flown its International Imaging Systems multiband system over several areas in Iowa and has analyzed over 2500 feet of multispectral Kodak type 2424 Infrared Aerographic film. Most missions were flown at altitudes of 4000 and 8000 feet and imagery acquired at both altitudes had acceptable resolution and registration for most applications. Registration problems detected in analysis were related to aircraft roll and pitch, and were caused by the shutter traversing the camera lenses sequentially. The manufacturer is developing a shutter which will eliminate this problem, which is minor at low altitudes. The 6040 I^2S Mini-Addicol Viewer has worked acceptably for the 9½ inch multispectral imagery acquired at low altitudes. Seventy millimeter ERTS-A imagery does not project well in the viewer at a 2.5X magnification. The manufacturer can supply viewers with higher magnifications.

International Imaging Systems recommends processing the Kodak 2424 Infrared Aerographic film so the .7 to .95 micron band (infrared) has a gamma of 1.9. This insures that the developed gammas of the other bands are similar even though film sensitivity of type 2424 varies across the wavelength interval from .4 to .95 microns. The Laboratory has experienced difficulty in achieving the desired film gammas and the problem appears to be related to processing. Kodak is considering the market for a film having more uniform sensitivity than type 2424.

Preliminary investigations by the staff indicate that the use of multiband photography in operational programs is limited by data handling problems, data formats, and by current "off-the-shelf instrumentation". These problems currently prevent the use of the multiband approach for the mapping of earth phenomena on a regional scale. Multiband photography has proved useful in the early stages of remote sensing investigations for defining the films and filters to be used in metric mapping cameras capable of mapping large areas at better resolution and lower costs. Multiband photography has also proved useful for monitoring small areas when ground control is sufficient, mission variables are understood, system variables are held constant, and when film processing is satisfactory.

Some of the most useful camera imagery of Iowa has proved to be the color infrared imagery acquired by NASA during the Corn Blight Watch of 1971. This imagery (Kodak film type 2443, RC-8 camera with .51 micron filter and 6 inch focal length lens, and platform altitude 65,000 AMT) has proved excellent for land-use classification and resource inventory, but poor for crop inventory. The reasons for its poor success in the last category may be related to the mission design problems of sun angle and vignetting, and problems with the film emulsion. These variables introduce problems which severely limit the use of density slicing-false color enhancement devices used in automated analyses. Based on preliminary analyses of this high altitude imagery, the Remote Sensing Laboratory is conducting a pilot study to determine if acquisition of color infrared imagery at altitudes above 45,000 feet might provide Iowa with a badly needed resources and land-use inventory, while at the same time providing 7½ minute orthophoto quadrangles to fill in

gaps in between existing topographic map coverages. Rectified photo quads may be substituted for orthophoto quads in areas of Iowa having low topographic relief.

Imagery from ERTS-A may have already demonstrated some usefulness in Iowa. Analysis of some of the first imagery acquired by ERTS-A has revealed that imagery acquired by the multispectral scanner surpasses that of the Return Beam Videcon. This ERTS-A study of the Midwestern Pleistocene and surficial materials is being managed by Roger B. Morrison of the U.S. Geological Survey in Denver and the Principal Investigator, George R. Hallberg, is employed in the Iowa Remote Sensing Laboratory under a joint contract between the U.S. Geological Survey and Iowa Geological Survey.

5. PROGRAMS IN PROGRESS

Remote Sensing Programs in progress for the State of Iowa include the following:

(1) Development of basic remote sensing techniques for inventorying the Iowa landscape. A six-county area in south-central Iowa is being investigated as a pilot study which proposes to develop methods of presenting the inventoried information in a form that will be meaningful to and usable by legislators, planners, and state agencies who formulate land-use policy.

(2) Development of methods for remote detection of archaeological and historical sites in the Midwest.

(3) Development of remote sensing methods of mapping flood high water and flood damage. Image formats are being evaluated to determine if the same imagery could be used for the making of detailed topographic maps of the floodplain. Joint study with U.S. Geological Survey Water Resources Division.

(4) Development of thermal mapping techniques for locating fish spawning areas with the concurrent locating of ground water discharge in Iowa streams. Joint project with U.S. Geological Survey Water Resources Division and Iowa Conservation Commission.

(5) Development of imagery interpretation keys and optimum remote sensing methods for conducting forest and wildlife inventories in Iowa. Joint study with Landscape Architecture Department, Iowa State University and Iowa Conservation Commission.

(6) Detection and quantitative analysis of thermal effluents in Iowa rivers by thermal mapping techniques. Joint study with the Nebraska Department of Environmental Control, and U.S. Environmental Protection Agency, Kansas City.

(7) Remote detection, mapping, and assessment of the effects of cooling tower discharge on vegetation in the Midwest. Joint study with Iowa Electric Company.

(8) Determination of the relationships between soil moisture content, drainage development, ground water recharge, and surface water flow in the Cedar River drainage basin near Cedar Rapids. Joint study with U.S. Geological Survey Water Resources Division.

6. FUTURE DEVELOPMENTS

The State of Iowa envisions the following development in the Iowa Remote Sensing Program:

(1) One state agency continues to develop the technical expertise for medium- and low-altitude data acquisition, and ground investigations in support of overflights.

(2) Continued integration of the disciplinary expertise of the user agencies with the research design phase of remote sensing missions and utilization of their personnel in ground investigations supporting overflights. Thus, the development of a large, stand-by, specialized and highly trained, multidisciplinary, staff within the Remote Sensing Laboratory is not required for development of the program.

(3) Continued training of the liaison staff members from the user agencies in the engineering limitations of the method and possibilities of the applications of remote sensor data.

(4) Continued identification of operational parameters of remote sensing missions which best define the unique spectral properties of the Iowa landscape.

   a. Selection of optimal seasons of the year, times of day, and conditions for remote sensing investigations.

   b. Selection of optimal sensors and sensor configurations for sampling and mapping the Iowa landscape.

   c. Development of optimal data analysis procedures, and report formats.

(5) Identification and optimization of unpredicted interfaces between various disciplines and applications of remotely sensed data to state planning-management.

(6) Development of a coordinated state system of image acquisition, handling, analysis, storage, information dissemination, and ground-information feedback (both to analysts and data-acquisition systems planners).

(7) Determination of the optimal cost-effectiveness relationships for different remote sensing investigations in Iowa.

The Iowa Remote Sensing Program is truly multidisciplinary and provides an excellent environment for research because it repeatedly brings together basic researchers from the academic community, analysts of imagery, and those applying the analyses to the practical problems of natural resource management, land utilization planning, and environmental control in the Midwest.

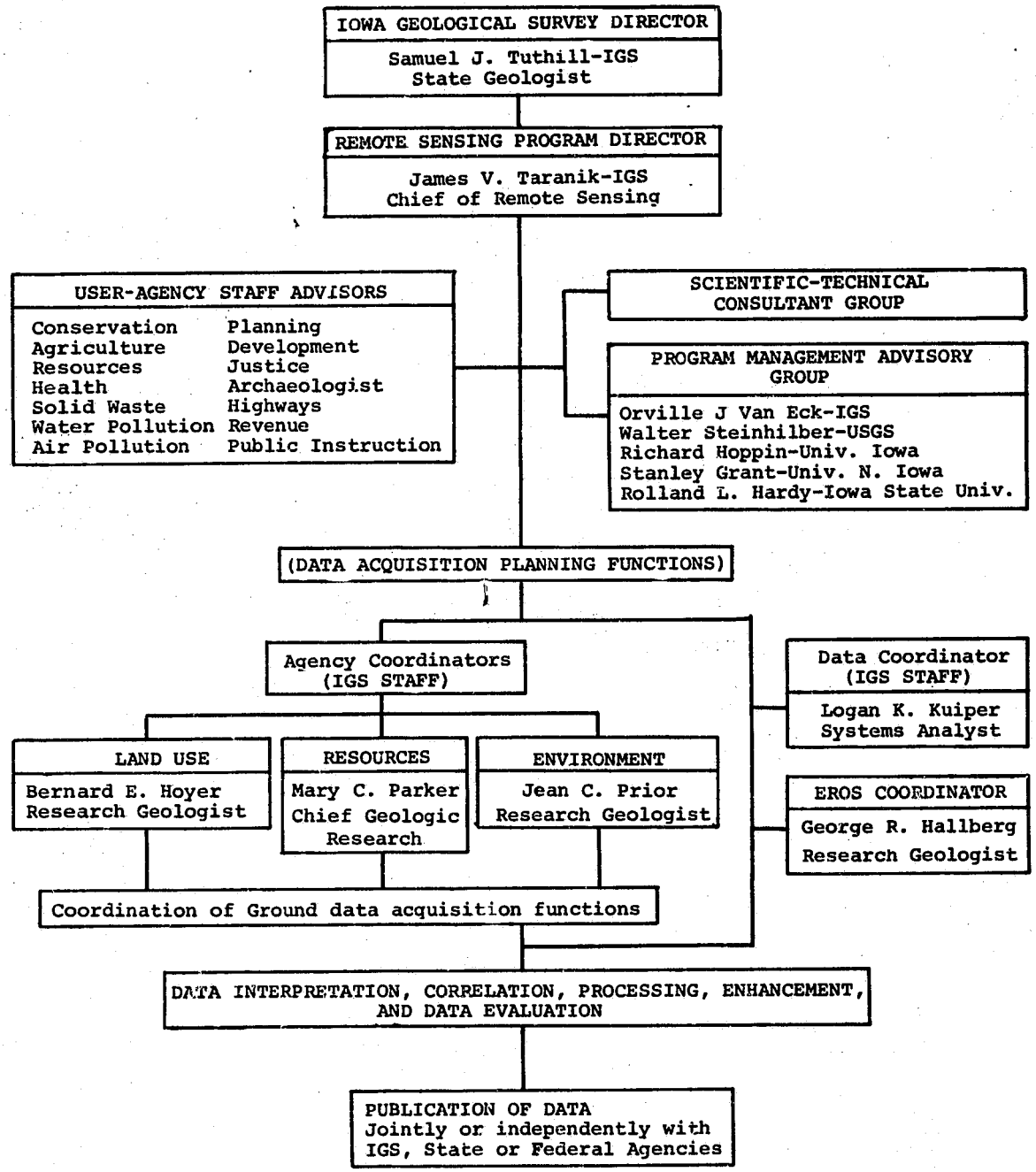
7. REPORTS PUBLISHED OR IN PROGRESS

Tuthill, S.J., Taranik, J.V., and Hoyer, B.E., 1972, Thermal remote sensing on the Mississippi River in Iowa: Available in preprint form from IGS. To be published in Water 1973.

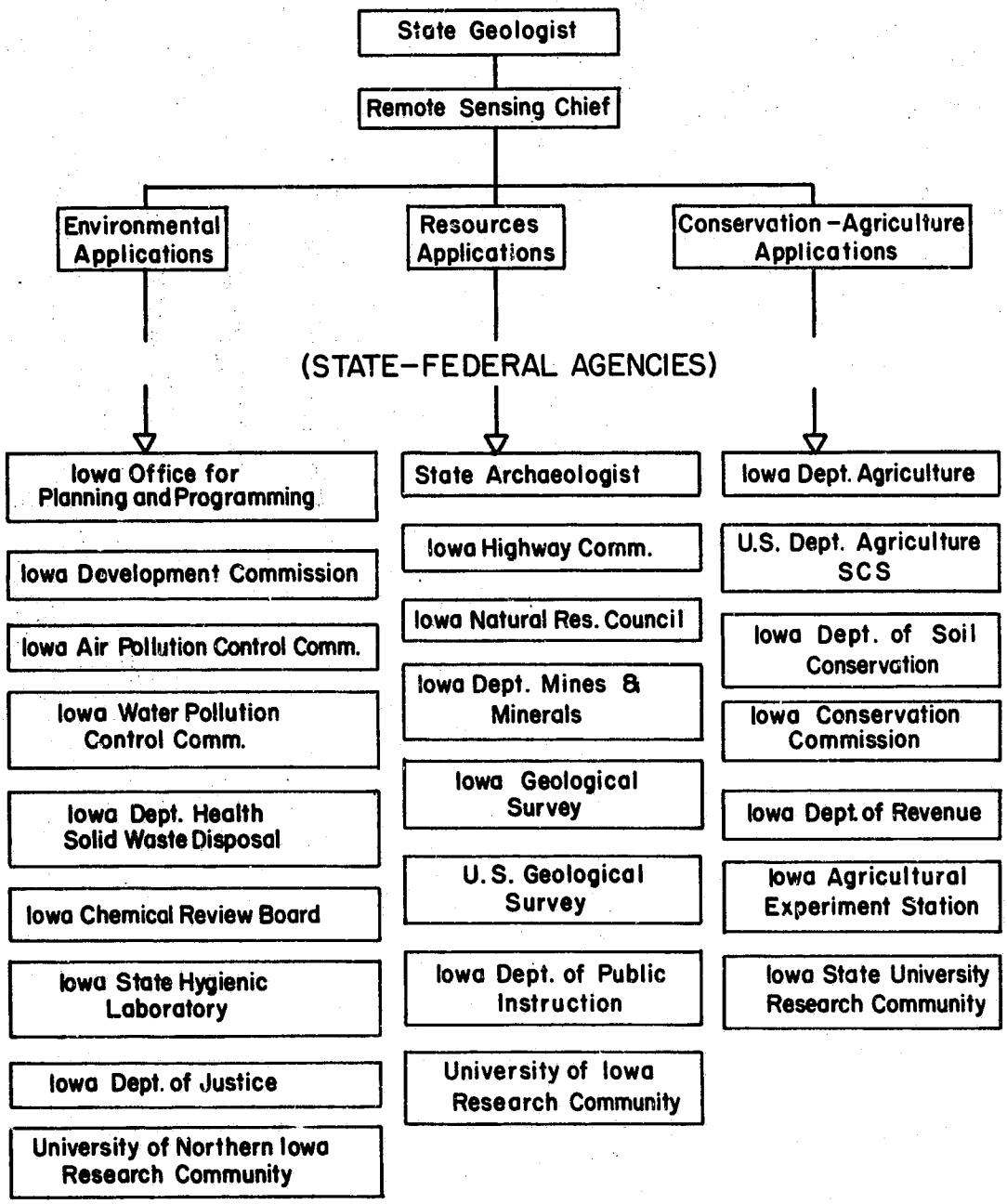
Proceedings of the Seminar in Applied Remote Sensing, Des Moines, Iowa, 1972: Parker, M.C., editor, Public Information Circular No.3, Iowa Geological Survey, In Press.

Tuthill, S.J., et. al., 1972 Thermal Remote Sensing of Hydrologic Systems in the Midwest: Iowa Geological Survey, Report of Investigations, Number 11, in preparation.

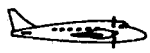
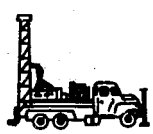
ORGANIZATION OF THE IOWA REMOTE SENSING PROGRAM

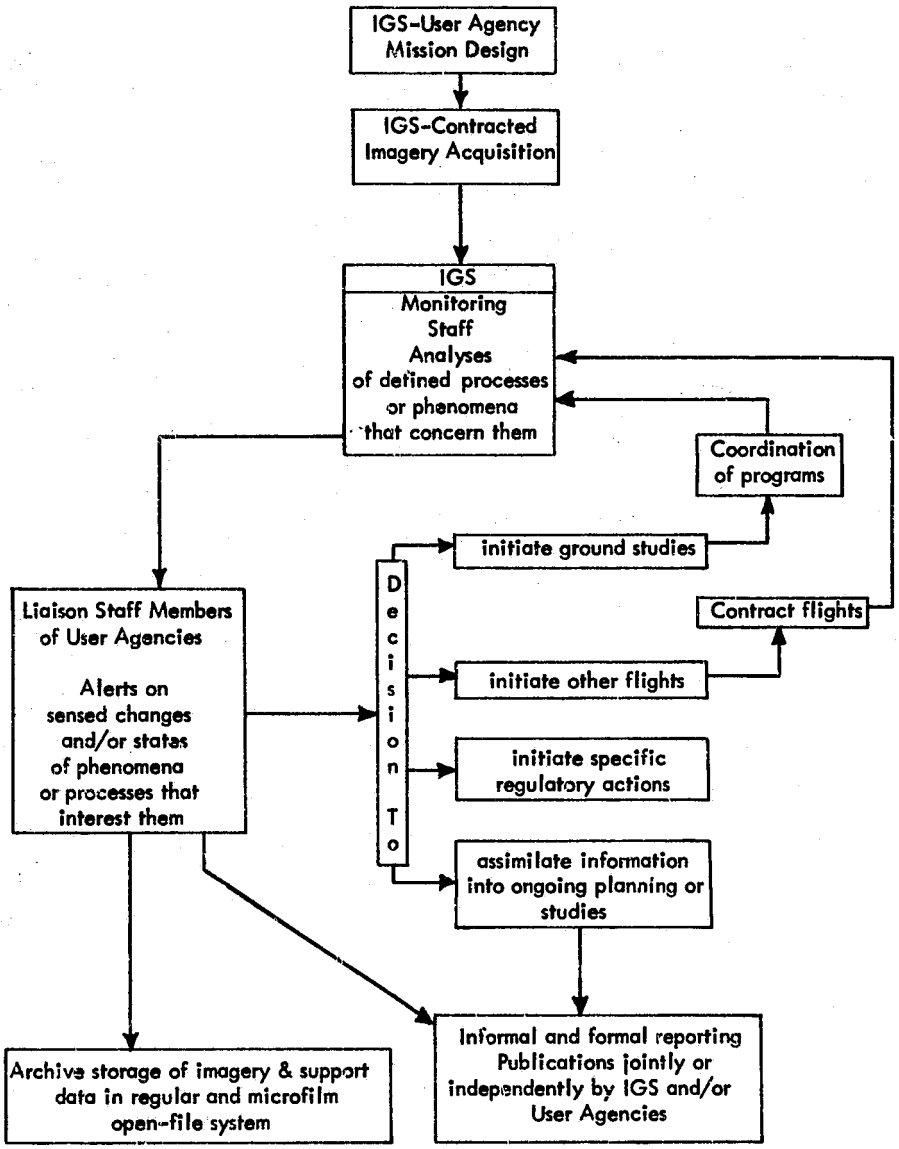


REMOTE SENSING USER AGENCIES IN IOWA



EXPECTED GENERAL CHARACTERISTICS AND EXPECTED APPLICATIONS OF DATA IN IOWA GEOLOGICAL SURVEY REMOTE-SENSING PROGRAM

	Data Characteristics		Expected Applications in Iowa
ERTS and Skylab 	Small scale Low resolution Repetitive	495nm	Synoptic mapping of: Soil groups Surficial geology Karstic terranes (with ERTS "B") Cultural phenomena Crop distributions
		235 nm	Forestry distributions Hydrologic phenomena Identification of temporal aspects of above and changes and patterns of change.
High-Altitude Underflights 	Moderate scale Moderate resolution Seasonal	60,000 ft	Large-systems analysis of all mentioned above at greater resolution and larger scale fundamentally a correlation bridge from satellite data to ground truth.
Medium-Altitude Underflights 	Large scale High resolution Specific missions	30,000 ft	Specific studies and strip monitoring of defined phenomena and processes. Correlation of satellite data with ground truth. Land use and land capability determinations.
Low-Altitude Underflights 	Very large scale Very high resolution Specific missions	15,000 ft 1,000 ft	Scale modification of above where specific problems require higher resolutions.
Surface Studies 	Instrument-acquired data at close range or by contact measurement		Fundamental validation of RS analyses; an organizational format for consolidation of extant and currently acquired earth resources data.
Subsurface Studies 	Remotely-sensed geophysical and drilling data		Fundamental validation of airborne RS analysis for surficial geology, bedrock geology, hydrology, and soils origins.



Data Flow Plan for Iowa

A STUDY OF THE FEASIBILITY OF APPLYING REMOTELY SENSED DATA IN THE MANAGEMENT OF NATURAL RESOURCES AND THE IMPROVEMENT OF ENVIRONMENTAL QUALITY IN ALABAMA

Harold R. Henry

Professor and Head, Department of Civil and Mineral Engineering
The University of Alabama, Tuscaloosa, Alabama

George McDonough

Director of Environmental Applications Office
Marshall Space Flight Center, Huntsville, Alabama

P. E. LaMoreaux

State Geologist, State of Alabama and Professor of Geology
The University of Alabama, Tuscaloosa, Alabama

ABSTRACT

The University of Alabama, the Geological Survey of Alabama and the George C. Marshall Space Flight Center are involved in an interagency, inter-disciplinary effort to use remotely sensed multispectral observations to yield improved and timely assessments of earth resources and environmental quality in Alabama. It is a prime goal of this effort to interpret these data and provide information in a format and schedule which is meaningful to and readily useable by agencies, industries and individuals who are potential users throughout the State. The Alabama Development Office under the Governor's office is providing liaison with user agencies.

In order to assess the full range of potential users of these data in Alabama, three state-wide symposia were held. Before, during and following these symposia several hundred potential users were informed of remote sensing applications in the areas of land use, resource inventory, environmental control, etc., which can make use of observations from NASA's Earth Resources Technology Satellite and associated aircraft flights. Only a few of the people contacted were already familiar with some aspects of remote sensing while the majority had no prior knowledge concerning this tool and its areas of applicability. In spite of this, the responses were enthusiastic and indicated that there would be a large amount of use of remotely sensed data after some degree of interpretation had been accomplished.

Professionals who said they could use the data beneficially included urban planners, regional planners, foresters, geologists, ecologists, hydrologists, agronomists, biologists, physicists, astronomers, chemists, agriculturists, civil engineers, chemical engineers, agricultural engineers, mining engineers, geographers, limnologists, entomologists, architects, archaeologists, demographers, lawyers, and university faculty members.

These same professionals estimated that the data would be useful in the areas of land use, cartography, hydrology, geology, transportation, ecology, forestry, fisheries, minerology, meteorology, morphology, agriculture, oceanography, archaeology, topographical mapping, demography, planning and wildlife studies.

This enthusiastic response from potential users indicated that the planning of varied state-wide applications of remote sensing oriented toward a broad base of grass roots users would be a timely and beneficial effort in Alabama.

Multistage sampling utilizing satellite data, multispectral photography from aircraft flights and ground truth data with emphasis on the data obtained from the DCS platforms will be performed over specific problem areas within the State. Multispectral data from aircraft already exist for certain areas, notably that encompassed by the Top of Alabama Regional Councils of Government as produced under a cooperative agreement with the Marshall Space Flight Center.

In addition, two other areas are planned for multispectral sensing from aircraft. These are a corridor from Tuscaloosa to Gadsden including Birmingham and a corridor from Mobile Bay to the confluence of the Alabama and Tombigbee rivers. Each of these corridors is approximately 120 miles long and 50 miles wide. It is anticipated that a minimum of three and a maximum of six flights over each area will be necessary for application of the multistage sampling techniques. The dates of flights will be scheduled to detect seasonal variations in vegetation and pollution and the number of lines of flight in each corridor will be determined according to the availability of equipment and the sampling requirements. The time of day of the flights will be scheduled so that the aircraft data will provide an optimum supplement to the satellite data.

It has been only recently that the need for better management of the State's resources has been recognized. To a great extent, former policies in regard to resources development have been limited to discovery and advertisement of the assets which provide jobs and wealth; now, greater emphasis is placed upon technical analysis of the problems of economic growth and development and the need for appropriate legislative control over resources, land use and other aspects of an orderly development process. In this connection, the Alabama Development Office and its regional counterparts in the State's twelve multicounty development districts are just beginning to become operational.

The primary need within these planning units, is for useful and current data relevant in managerial decisions. High on this list of data required is information on land use and water quality and quantity. Analysis of existing data is admittedly amenable to the understanding and forecasting necessary for establishing policy on environmental quality, but data useful in the day to day implementation of policy is still a major operational bottleneck in sound regulation. The possibility that ERTS acquired data could eliminate this bottleneck is investigated. Managerial data generated, analyzed or distributed by planning agencies is not limited in usefulness to the public sector. These agencies can provide a useful outlet for dissemination of information from ERTS and other sources to private industries which would support and enhance their operations. These usages of ERTS data will require the closing of the communication gap between the scientific and the resource manager or public policy maker who will use the information digested from the remotely sensed data. A principal objective of this study is to close this gap by developing an effective procedure for processing and interpreting the remotely sensed data and disseminating meaningful information to users.

INVESTIGATION OF LAND RESOURCE USE IN SOUTHEAST MICHIGAN

J.G. Ahl, M.G. Boylan, D.L. Mokma, W.L. Myers, S.W. Schar, R.D. Vlasin

Michigan State University
East Lansing, Michigan

I.J. Sattinger

The University of Michigan
Willow Run Laboratories
Ann Arbor, Michigan

ABSTRACT

Michigan State University and the Willow Run Laboratories of The University of Michigan are collaborating on the investigation and demonstration of operational uses of remote sensing for land and water use planning and policy formulation for Michigan situations. A survey of the information needs of various Michigan-based operating and planning agencies identified a broad variety of applications to which remote sensing could make a contribution. For dealing with the broad issues of land use policy formulation, remote sensing can be used to develop an information base on the state's natural resources and on the use of these resources for urban, agricultural, recreational and other purposes. This information can be used for determining optimum use of land based on land evaluation studies, assessing the environmental impact of proposed developments, measuring broad trends in land use and metropolitan growth, and monitoring conformity of this growth with established land use policies. The survey also identified many applications involving planning and development at localized sites. Such projects as recreation and open site analysis, river channelization and improvement, assessment of the environmental impact of highway extensions and other construction projects, and planning of utilities and services are representative of the variety of problems which can use remote sensing data.

One of the current problems selected for demonstrating the use of remote sensing is that of assessing the environmental impact of the proposed M-14 expressway extension northeast of Ann Arbor, Michigan. The Environmental Quality Act of 1970 and other recent environmental legislation has created the need for "ecological awareness" in any agency concerned with land and water use. Environmental impact statements are now necessary on proposed projects affecting land and water use undertaken by most public agencies. The Michigan Department of State Highways is concerned with developing suitable methods of preparing such statements.

After consultation with the Department, as well as in conjunction with other federal, local, and state agencies, a study was undertaken dealing with the environmental aspects of a proposed alternative expressway extension of M-14 between Ann Arbor and Plymouth, Michigan. This proposed expressway extension will be constructed in an ecologically sensitive wetland and woodland area.

The proposed expressway extension area was analyzed using both remote sensed imagery and various types of ground truth. The area studied contains a section of four lane highway constructed in 1964 and an adjacent area in which a further extension of this highway is planned. Remote sensing included aerial photography and multispectral scanner imagery taken from altitudes of 2,000 and 7,000 feet, and RB-57 photography taken from 60,000 feet. Ground truth included data from existing soil surveys, soil and water samples, vegetation and land use mapping and ground measurements of surface temperatures and spectral characteristics. Remote sensing coverage of areas adjacent to the existing highway were analyzed and compared to aerial photography of the same areas obtained prior to the construction of the highway. Only minor effects on vegetation growth, soils, and land use occured in the existing corridor. In the proposed corridor extensions, analysis indicates that some adverse changes in plant communities and water levels will probably occur, but little change in either soil or land use.

1. INTRODUCTION

In recent years, basic research on the development of new remote sensing techniques has outstripped applied research on the application of remote sensing techniques to practical problems. Michigan State University (MSU) and the Willow Run Laboratories (WRL) are collaborating under a NASA sponsored project working toward making this technology operational. The central objective in this project is to investigate and demonstrate operational uses of remote sensing for land and water use planning and policy formulation in Michigan. Six interrelated efforts are being undertaken to achieve this central objective: (1) survey of resource use problems faced by public and private agencies to which remotely sensed data could make a contribution; (2) correlation of ground truth and remotely sensed data in order to identify reliable indicators of terrain characteristics; (3) testing and perfecting a land classification and reference system suited to the capabilities of remote sensing; (4) evaluation of land and water use inventory and information systems embodying remote sensing as well as other sources of information; (5) presentation and demonstration of results to a broad range of potential Michigan users; (6) application of findings to land use policy formulation in Michigan through cooperation with the agencies responsible.

2. SURVEY OF POTENTIAL USERS AND SELECTION OF PILOT STUDIES

Included in the survey of resource use problems dealing with Michigan-based agencies and groups are federal, state, regional and local governmental agencies; quasi-public corporations and agencies, private corporations, and citizen groups. Included in the kinds of problems, opportunities, and decisions involving resource use were problem areas such as highway expansion, river channelization, recreation and open site reservation, monitoring and analysis of metropolitan growth patterns, and identifications of key natural resource characteristics for improving management.

Resource problems identified in the survey fall into several major categories. A fundamental use for remote sensing which supports many other applications is in the preparation of a resource information base. Depending on the manner in which it is to be used, the form of this resource information base may vary from a series of thematic maps to a completely computerized data base, such as the LUNR inventory developed by the State of New York. A second problem area, closely related to the development of an information base, is land evaluation. Land evaluation is needed for purposes of formulating appropriate land use policy and for more detailed problems of site selection and development. The functional suitability of land for urban development, agriculture, recreation, and other purposes depends on a number of factors which are analyzed and recorded in an inventory of land use and physical characteristics of the terrain.

A related and fundamental problem in land use management is assigning an "optimum use" to land to meet social, economic, and cultural needs, as well as for protection of the environment. Land use assignment involves basic decisions concerning the reservation of lands best suited for their optimum use or uses. For example, some land areas (including water areas) are optimally suited for agriculture, or forests, or recreation--or for other limited human use. The best locations for concentration of continued urban growth and for new communities also need to be selected, as well as suitable sites for commercial and industrial expansion, airports, solid waste disposal, and highways. The implementation of a broad land use plan requires detailed planning at a local level. State Planning and Development Regions in Michigan have been established which provide a suitable

organizational structure for developing regional land use plans. County and municipal planning commissions must also be heavily involved in the planning process, particularly in relating the regional plan to local issues. Mapping of existing land use patterns by means of remote sensing can also provide benchmark data against which conformity of future land use development with the established plan can be monitored.

Aerial photography is already extensively used by all levels of government for such planning considerations as capacity, routes, and delivery points of utilities, transportation, further land development, tax and property records, and public services. The Department of State Highways, for example, makes extensive use of aerial photography for traffic projections and route location studies. Indications are that up-to-date high altitude coverage will find extensive use by many planning and operational units.

Many applications exist for detecting existing or incipient environmental damage. The more permanent forms of such damage are readily detectable, including the effects of erosion and sedimentation, damage to shorelines from wind and wave action, residential development along shorelines, and unplanned, non-systematic urban growth.

One of the current problems selected for demonstrating the use of remote sensing is that of assessing the environmental impact of proposed expressway extensions. Recent environmental legislation, such as the federal Environmental Quality Act of 1969 and the Highway Act of 1970, requires the development of environmental impact statements by state highway commissions prior to the construction of new highways. However, at the present time there is no clearly established, scientifically acceptable method for analyzing the results of highway construction in an "ecologically sensitive" area. Frequent and extended litigation concerning route locations and the ecological effects of the proposed highways testify to the general lack of acceptance of current impact studies by regulating agencies and the public.

The Michigan Department of State Highways (MDSH) is concerned with developing suitable methods of preparing environmental impact statements. After consultation with the Department, as well as with other federal, local, and state agencies, a study was undertaken by WRL and MSU dealing with the environmental aspects of a proposed alternative extension of Michigan Highway 14 (M-14) between Ann Arbor and Plymouth, Michigan. Parts of this proposed expressway extension will be constructed through an ecologically sensitive wetland and woodland area. (Figure 1)

A second resource use problem evolving after consultation with the Michigan Department of Natural Resources, as well as with other federal, state and local agencies, was in the application of remote-sensed imagery to the inventory of land and water resources for management purposes. Research is currently in progress in the Pointe Mouillee game area at the mouth of the Huron River along the lower end of the Detroit River. Analysis of this area will help in the development of management guidelines for multiple use of this critical resource use area in southeastern Michigan.

3. RESEARCH METHODS FOR IMPACT ASSESSMENT

Both an existing expressway segment, built in 1964, as well as the proposed additional segment of M-14 between Ann Arbor and Plymouth, Michigan were analyzed using remote-sensed imagery correlated with ground truth information. The study area, shown in Figure 2, can best be described as a series of three corridors, each displaying individual problems as well as one continuous problem set. The first of these segments or corridors, containing the existing M-14 expressway has been in use since 1964. The second corridor contains a portion of the proposed extension beginning at the existing expressway and running closely parallel to the Ann Arbor-Plymouth Road connecting the expressway with Plymouth, Michigan. The last study corridor sector begins where the proposed new M-14 highway forks north to Plymouth through a relatively natural area. These separate study areas made it possible to examine a completed highway extension as well as a proposed highway extension in one specific area of southeastern Michigan. The location for the proposed extension had already been chosen before the present project was conceived. The major objective of this study became one of helping the MDSH develop an environmental impact assessment in this selected study area. However, the methods developed should be applicable to preparation of impact assessments in similar situations faced by other agencies.

Joint policy sessions between WRL, MSU, and the MDSH produced a schedule of analysis for three major spheres of responsibility, namely: (1) analysis of vegetation; (2) analysis of soil and surface water; (3) and analysis of land use characteristics. Responsibility was then delegated jointly between WRL and MSU to personnel with areas of specialization in these spheres of responsibility, as well as cooperating personnel from the MDSH. After consultation with Highway Department personnel from liaison and planning sections to discuss their needs in terms of environmental impact statements, analysis and evaluation of remote-sensed imagery was undertaken on both existing and proposed corridors of the M-14 highway and correlated with ground truth analysis.

Remote sensing included aerial photography and multispectral scanner imagery taken from altitudes of 2,000 and 7,000 feet, and RB-57 photography supplied by NASA taken from 60,000 feet. Other photographic imagery from 1,500 feet obtained from the MDSH and the ASCS was also used. This photographic imagery had been used for site evaluation prior to the construction of the existing section of expressway. Since conventional aerial cameras are the best known and most readily available sensors, their inclusion into the study forms the basis for assessing the role of more sophisticated types of sensors. Testing efforts for advanced remote sensors were concentrated on the 12-channel M-7 multispectral scanner flown in the NASA-supported C-47 aircraft.

Several major types of photographic imagery were used for site evaluation for the years 1963 through 1972. RB-57 9 in. X 9 in. color infrared imagery was used for vegetative pattern analysis and separating annuals, perennials, brush, and forest cover. It was also used to identify water bodies and in land use analysis. Seventy millimeter color infrared photography was used to determine vegetation types in conjunction with the multispectral scanner output. Black and white infrared 9 in. X 9 in. photos flown by WRL in 1972 were used to identify structures for land use analysis, to check vegetation types, and to update existing RB-57 photography. Black and white panchromatic 1970 photos were also used for the same purpose. Photographic imagery obtained from the ASCS was used in conjunction with soil analysis but only on a limited basis.

Experiments were conducted with multispectral scanner data to determine the extent that it might be possible to replace photo interpretation with computer recognition maps prepared from the scanner data for vegetative analysis. The scanner was also used to map surface water, determine soil drainage on bare soil areas, and land use characteristics. (See Figures 3 and 4.) Training sets were established and ground truth information was correlated with both the multispectral scanner and photographic imagery. Vegetation ground truth involved both a detailed inventory for area vegetation as well as a gross inventory to verify this aerial photographic imagery. Soil samples in selected training sites were also collected for moisture determinations. Land use ground truth involved both verification of photographic and scanner output as well as consultation with agencies to ascertain possible causes of land use change.

4. RESEARCH RESULTS

The M-14 study site as a whole is a rural, agricultural area that lies mostly within the watershed of a small stream named Fleming Creek. This creek empties into the Huron River just south of the study site. The Fleming Creek watershed includes a substantial amount of well and moderately well drained uplands, and some lowlands that are wet and poorly drained. The distribution of vegetation on the area has been controlled by the interaction of moisture conditions and surrounding agricultural land use. Woodlands are limited for the most part to poorly drained areas that are too wet for cultivation. Well drained sites are devoted to row crops, and marginally drained areas are in pasture grass. Aerial photography showed that approximately 10 percent of the area is woodland, 40 percent grasses, 20 percent annuals (small grains and row crops) and 30 percent brushland or mixed types.

The species composition of the woodlands in the area also varies according to the moisture characteristics of the site. Oak-Hickory stands occupy the sites with better drainage. The more moist sites contain mostly maples, although maples constitute a significant component on the drier sites as well. Cottonwoods and willows are prominent in the wet areas. The wet woodlands contain the most sensitive vegetational communities from an ecological standpoint.

Analysis revealed that the potential impact of highways on vegetation can be placed in three categories. The first category comprises the physical injury and exposure that result from the construction work itself. Impacts in this category are virtually unavoidable, since clearing of the right-of-way is essential. Changes in site quality as a result of highway construction make up the second category. The severity of the impacts in this category depends upon the care and ecological insight used in designing and constructing the highway. The third category consists of the effects of highway pollutants such as de-icing chemicals and exhaust emissions on roadside vegetation and species vary considerably in their tolerance to such pollutants.

From an ecological perspective, vegetative communities adjacent to the highway right-of-way should be disturbed as little as possible. Forests, in particular, provide valuable benefits to motorists and residents of the surrounding area. Trees and shrubs are not only aesthetically pleasing but act as sound barriers and windbreaks, as well.

The effects of the construction, maintenance, and use of a major highway on soil are more difficult to determine than the effects different soils within the highway right-of-way may have on road construction or other parts of the environment. There is also a clear correlation detectable between vegetative damage and soil damage in highway construction. Not only may salt used to de-ice highways damage vegetation, it may accumulate in soils near the highway. In other studies, salt

levels in soils have been found to be sufficiently high to cause toxicity to plants growing along the highway as previously mentioned. Some of this salt will also enter streams and lakes as a result of highway runoff. Lead from automobile exhausts has been shown to accumulate in soils near the highway as have accumulations of other metals such as cadmium, nickel and zinc.

Good surface drainage is necessary to maintain a major highway. The ditches constructed along the highway to provide for this drainage may lower the natural water table in some areas of naturally somewhat poorly drained or poorly drained mineral soils and organic soils. In some other areas the highway may act as a barrier to the movement of subsurface water and raise the natural water table or cause more stagnant conditions less favorable for plant growth. The highway may also block some surface water drainage causing intermittent or perennial ponds to form. Bare soil exposed during highway construction is susceptible to erosion. The resulting sediment deposited in a stream channel will reduce the cross-sectional area of the stream causing the banks to be eroded, especially during periods of heavy runoff. Borrow pits extending below ground water level are seasonally full of water and a source of sediment for many years.

Highway construction has both direct and indirect effects on land use. Directly affected is land converted to highway right-of-way. Expressways and their needed interchanges remove a large amount of land acreage from its present use to highway or transportation use only. Expressways built in rural areas remove a large amount of land from agricultural production or simply open space and recreational use. The displacement of both farm and residential families is one adverse effect of highway construction.

In corridor number one, the highway passes along the edges of the wet woodlots on relatively high ground, thus taking advantage of the screening effects of the woodlots without causing noticeable mortality or shifts of species composition within the woodlots. The one exception occurs at the interchange with U.S.-23. The highway passes directly through a woodlot at this point. Some mortality of trees in the woodlot has apparently been caused by interruption of drainage.

The most pronounced effects on plant ecology in corridor number two will take place in the immediate vicinity of the proposed interchange with M-153 at the end of the existing expressway. The proposed site for this interchange is a marsh seepage area with very diffuse drainage. During periods of high water, the interruption of natural drainage will produce localized flooding. In contrast, excessively deep ditches (below the natural water table) would drain the entire marsh area during extended dry periods. Either type of effect would produce marked changes in the vegetative communities.

The proposed location of the highway in corridor three is virtually certain to produce major changes in the ecology of the area. The proposed route runs directly through the largest forested wetland in the corridor. A forested wetland community of this type is very sensitive to the disturbance caused by highway construction. In addition, portions of the area are maintained as a private game preserve. Depending on the design of the ditches, either flooding or drainage of the wetland could result. Either way, changes in species composition will occur through mortality and/or alteration in patterns of regeneration.

To determine the impact the existing portion of M-14 has made on adjoining soils and surface water hydrology, aerial photographs taken in 1970 were compared with those taken in 1958 and in 1963 before construction. The differences between the photographs are very slight. Apparently the highway had little or no lasting visible effect on the soils and surface water resources in the existing M-14 corridor. Five borrow pits and gravel pits have resulted from the construction of this portion. The channel of a creek was relocated to parallel M-14 for about 0.1 mile. This relocation apparently did not significantly affect the soils or surface water hydrology.

Because the existing portion of M-14 does not traverse any large poorly drained areas, it is not possible to accurately predict the impact that the proposed M-14 highway will have on the soils of the large poorly drained area in corridors two and three. The ditches along the highway may become artificial drains and may lower the natural water table in the adjoining area. The somewhat poorly drained and poorly drained, coarse textured soils and organic soils which will be traversed by the proposed M-14 highway may be more susceptible to highway effects than the well drained and moderately well drained, and coarse textured soils along the existing M-14 highway. The highway may have a lesser environmental impact if it does not cross the large area of poorly drained mineral soils and organic soils.

The inevitable relocation of a portion of Fleming Creek may have a more significant effect on the environment than the relocation of the intermittent stream along the existing M-14 highway. The larger volume of water which flows through Fleming Creek may cause greater erosion of the new banks of Fleming Creek with most of the attendent consequences.

The final analysis on land use change requires additional study. However, several generalizations as to the past and current land use situation in the study area can be considered.

The M-14 study site was primarily chosen because it involved expressway extension through an "ecologically sensitive" woodlot and wetlands area. As previously mentioned, this area is rural in character with some agriculture, some open space, and some scattered farmsteads and residential dwelling units. There is only one community on the proposed expressway segment between Ann Arbor and Plymouth (Dixboro) which is a rural-type village.

Table I shows that little change in land use has taken place in the study area in the period from 1964 to 1972, and the potential major effect of the expressway extension is likely to be more of an ecological than an economic change.

In the corridor already constructed, land use has changed since construction in 1964. The major, but limited, change has been a shift from land maintained in agriculture use to unused open space. It can be assumed that land use will change somewhat after the proposed segments of the study area are completed. However, due to the natural and rural characteristics of the area, and the limited access nature of expressways themselves, significant change probably will occur only at the location of proposed interchanges. There are only two of these interchanges planned in the study area and only five in the complete expressway extension from Ann Arbor to Plymouth. The shift in agriculture use to unused open space is most likely to occur when the highway divides the property of individual landowners.

5. SUMMARY AND CONCLUSIONS

The initial phase of the project consisted of a survey of land resource problems in Michigan to which remote sensing could make a contribution. Several problem areas were identified and examined in this survey. The problems of environmental impact analysis and resource inventory were chosen for first year research efforts. Environmental impact analysis was conducted on the M-14 expressway extension and a resource inventory for game management purposes was prepared for the Pointe Mouillee State Game Area at the mouth of the Huron River at Lake Erie.

Analysis on the M-14 expressway extension indicates probable changes in plant communities and water levels, but little change in either soil or land use. Analysis is still in progress at the Pointe Mouillee test site. In these two areas, high altitude color infrared photography has proven useful for categorizing plant communities and land use. The multispectral scanner was used to identify plant species, soil types, and water surfaces.

Based on these collaborative initial research efforts, considerable promise can be discerned for remote sensing as a valuable tool for many facets of land resource use management. As the project proceeds, promising, systematic research endeavors will continue to stress the conversion of remote sensing technology to practical operational uses.

6. ACKNOWLEDGEMENTS

This research effort is being supported by the NASA Office of University Affairs under NASA Prime Contract NSR 23-005-527. Myles G. Boylan, Irvin J. Sattinger, and Raymond D. Vlasin are the principal investigators for this research effort.

TABLE I. TOTAL LAND USE BY ACTIVITY AND ACREAGE IN EXISTING AND PROPOSED EXPRESSWAY EXTENSIONS - 1963 AND 1972

	Year	% of Total Area	Area (Acres)
Agriculture	1963	51.1	4860
	1972	40.1	3894
Forest	1963	11.1	1053
	1972	10.8	1023
Other Open Space	1963	35.8	3414
	1972	45.8	4323
Residential	1963	1.9	181
	1972	2.5	246
Industrial	1963	0.1	12
	1972	0.4	34
TOTAL	1963	100%	9520
	1972	100%	9520



FIGURE 1. STUDY AREA FOR M-14 HIGHWAY EXTENSION

The area studied is shown in this black-and-white reproduction of a color-infrared photograph taken by the NASA RB-57 aircraft during Mission 205, June 11, 1972. The existing section of M-14 is shown in the lower left hand corner. From this four-lane highway, the proposed highway route extends to Plymouth, Michigan, at the right. The interchange with I-96, presently under construction, can be seen in the upper right hand corner.

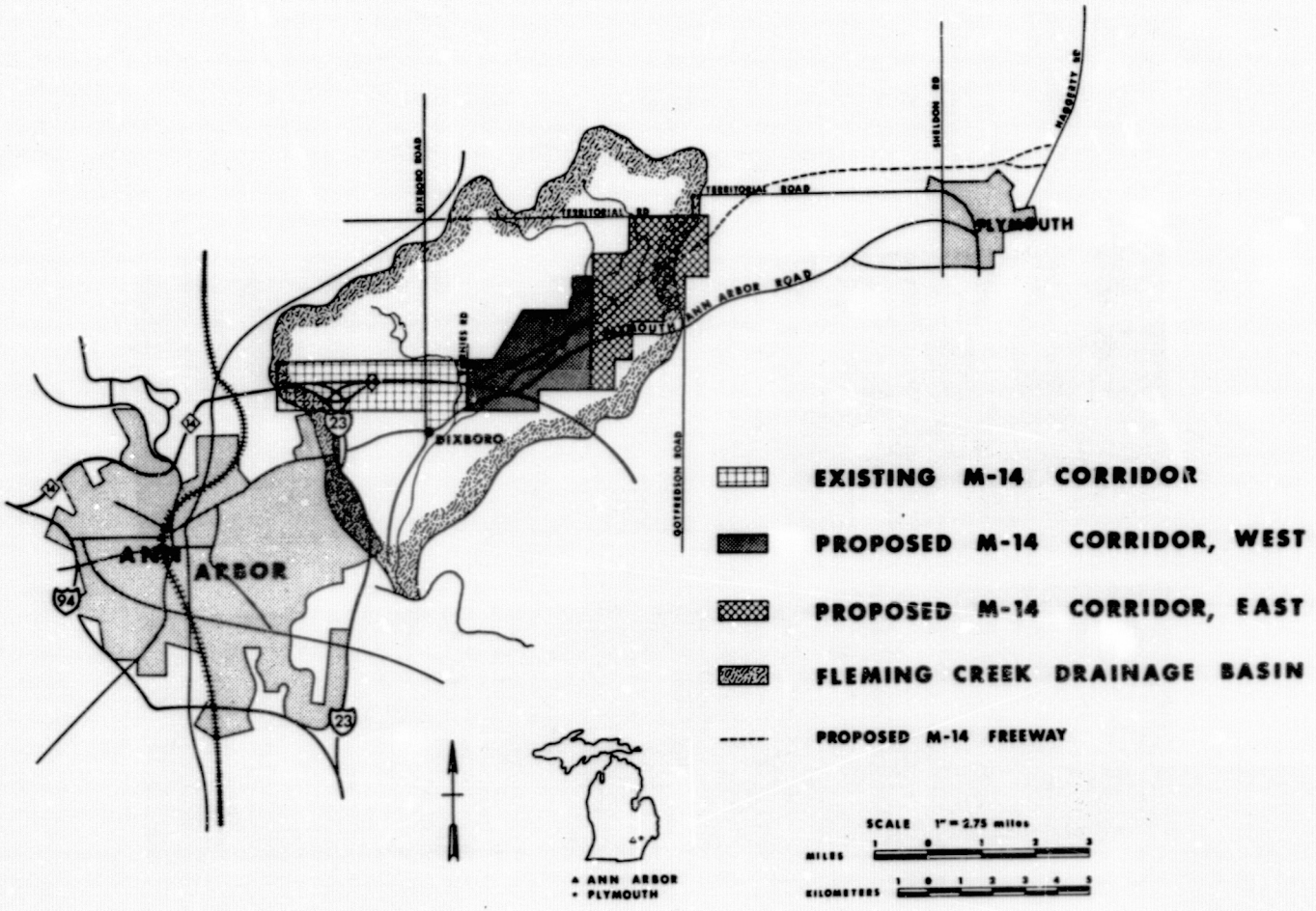
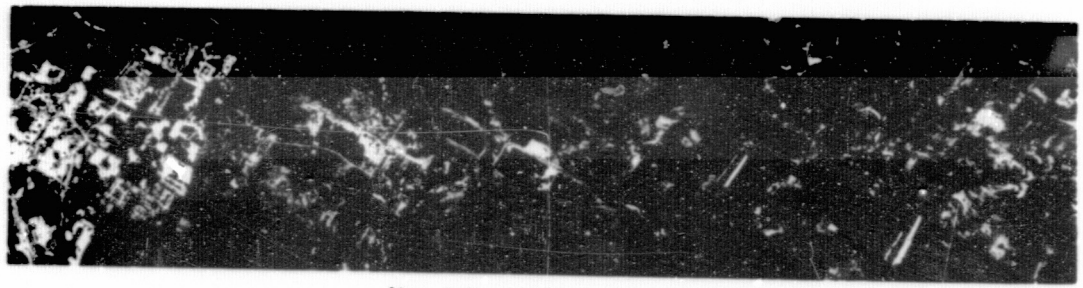
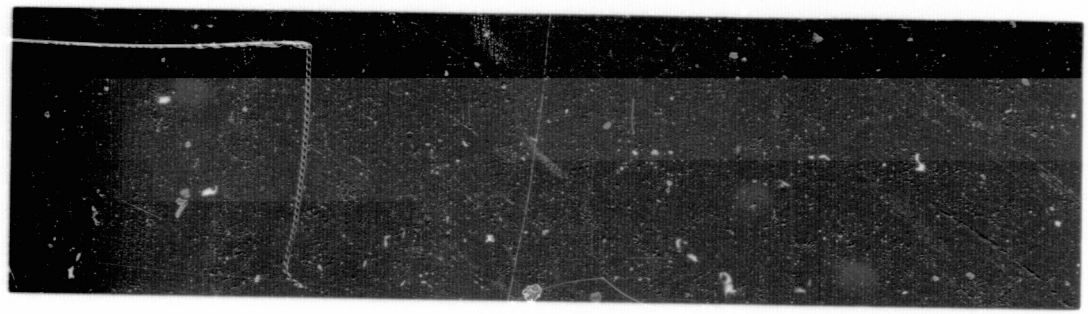


FIGURE 2. EXISTING AND PROPOSED M-14 HIGHWAY EXTENSION CORRIDORS



Near Infrared Video 1.5 - 1.8 μm



Surface Water

FIGURE 3. VIDEO IMAGE AND SURFACE WATER MAP FOR M-14 SITE

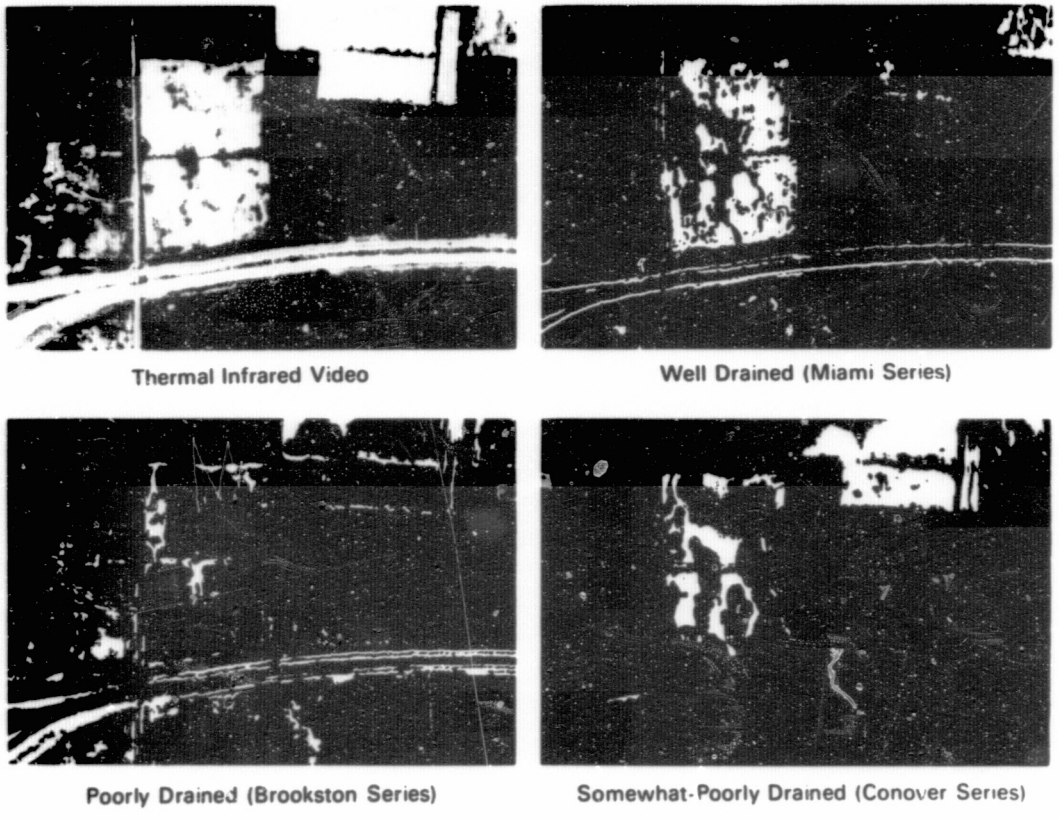


FIGURE 4. DETAILED SOILS RECOGNITION MAP FOR M-14 SITE

DEVELOPMENT OF A PRACTICAL REMOTE SENSING WATER QUALITY MONITORING SYSTEM

James P. Scherz

Department of Civil and Environmental Engineering
and
Institute for Environmental Studies
The University of Wisconsin
Madison, Wisconsin

ABSTRACT

Remote sensing is a promising tool to aid ground enforcement crews in water pollution monitoring in that remote sensing quickly covers vast areas and provides detailed time record images. Thermal scanners showing heated effluent and aerial photography are the most useful types of remote sensing for such monitoring. Photography correlates with the conventional pollution parameter of solids in the water. The best correlation with the aerial image may be with suspended solids, dissolved solids, or total solids, depending on the effluent.

Other factors also show up on the photographic image such as surface phenomena and bottom effects. If present, oil pollution can be detected and monitored as a surface phenomenon and sun glare can be eliminated by proper choice of look angles. Lens and angle of incidence may be significant factors which must be understood before operation correlation can be reliable. Bottom penetration effects can be understood by use of a secchi disc reading and light penetration curves now being refined. Also because depth penetration is wavelength dependent one can analyze the film in the non-penetrating photographic infrared wavelengths if bottom effects are a potential problem.

Correlation of solids with aerial images, correcting for surface and bottom effects, and developing the most practical data gathering, indexing, viewing and analysis system for practical remote sensing monitoring of water pollution is the goal of the Water Quality Remote Sensing effort at the University of Wisconsin.

1. INTRODUCTION

Remote sensing is receiving much attention as a potential tool for many aspects of environmental monitoring. Much effort is being devoted by NASA and other governmental agencies in development of this new tool and the results are indeed impressive. However from the "in-field" operational point of view one often finds a real lag in the practical application of remote sensing. This is especially true of water quality monitoring. In the state of Wisconsin water quality monitoring is done by ground based crews in boats which make a pollution survey of a river basin once in 3 to 7 years, and they check sewage treatment plants about once a year. Needless to say much can happen in a river basin or to a sewage treatment plant in between such surveys.

Preceding page blank

Remote sensing has the capability of covering large areas in a very short period of time and can be potentially used to great advantage in conjunction with the ground surveys thus making ground crews more effective and showing them areas of major concern so their time could be used to best advantage.

Although remote sensing is a promising tool in providing an overall view and a detailed image for time records (3), persons involved in practical monitoring of water quality ask some very important and basic questions about its use. The first question that is asked is what water pollution parameters show up on the image of the water body. They ask how can one be sure it is not bottom or surface glare that one sees. They ask how it can be shown that remote sensing is a reliable, workable tool for water pollution monitoring work and how it can be so used.

The University of Wisconsin began investigating this area in 1965 and excellent relationships have been developed at the request of the Governor of Wisconsin with the state agencies who might effectively use remote sensing. However the basic questions relating to its use must be satisfactorily answered before the state agencies or other agencies can effectively use remote sensing for water pollution monitoring. The primary purpose of the present NASA sponsored interdisciplinary remote sensing program at the University of Wisconsin is toward answering these questions and this paper is devoted to describing the progress being made toward answering them. The primary questions are what it is that remote sensing shows on images of water, and how one can make sure, practical use of remote sensing for water quality monitoring.

2. HARDWARE

Initial work supported by the University of Wisconsin consisted of photographing water pollution with single 35mm cameras and lab reflectance work with a Barnes DU-2 Spectrophotometer (2). Further work requested and supported by the state agencies of Wisconsin utilized 35mm camera banks and 9-inch mapping photography but, like the previous work, it posed more questions than it answered (5).

It was at this time that NASA supported the joint effort at Wisconsin making it possible to launch the program with high quality support to allow investigation of the entire field with sufficient budget support to answer these questions and help solve the problem.

The focus of the NASA sponsored research has been to answer questions of what parameters show up on images of water quality, how can such parameters be effectively measured from the image, and what combination of hardware will provide an economical, workable monitoring system for practical application. The first consideration of such an optimum field system is hardware and its use.

In setting up any remote sensing system, as with one for water quality monitoring, one has a large choice of hardware and techniques. Although other hardware was considered, work on this research was devoted primarily to photography and thermal scanning. Thermal scanning has proven at Wisconsin, as at other places, to be a most practical working tool for monitoring thermal discharges into water (6,7). The level of municipal and industrial pollution, however, seems most practically and best monitored by photography. Most of this report is devoted to research work on photographing water pollution.

2.1. PHOTOGRAPHY

With photography one has the choice of different films and filters to cover the spectral range from about 0.38 to 0.9 microns. One can use multiband black and white photography, or color and color infrared photography. Although work is being done with black and white multiband photography at the University of Wisconsin, because of viewing, economical and time considerations color and color IR film was determined to be much better for the job. Color and color infrared film give a composite picture that is easy to view by laymen and such photos can still be broken into the separate bands by use of a spectrophotometer attached to a microdensitometer which can analyze any color or wavelength on the final photo. This was the photo analysis technique chosen for photo lab analysis (see Figure I).

It was decided that simultaneous color and color infrared photography with a #12 or #15 wratten filter was optimum for the water quality investigation. Various formats were also tested to arrive at the optimum combination for practical monitoring.

2.2. NINE-INCH FORMAT

Nine-inch format and other mapping cameras were tested and proven best where metric resolution and predictable lens falloff is of utmost importance. Such cameras usually have high resolution lenses and between-the-lens shutters so lens falloff is consistent and can be corrected for, which is not necessarily the case with many smaller format focal plane shutters. However, such photography is by far the most expensive, ranging from $5 to $13 a print. Therefore one is hesitant to shoot pictures when there is a question as to whether they will be of use. It has been such numerous chance photos taken with less expensive, smaller format cameras which have often proven most beneficial to the research program. Cost with mapping camera photography is definitely a disadvantage for practical water quality monitoring. An even greater disadvantage than cost is in those cases where simultaneous color and color infrared photography is desired, very few aircraft are available which have mounts and cameras for simultaneous mapping camera coverage for most monitoring agencies.

2.3. 70MM FORMAT

70mm format cameras have resolution which is less than the mapping cameras but is still very good, and many 70mm cameras have between-the-lens shutters which allow reliable correction to be made for lens falloff. Two or more such cameras can be put together to shoot through one camera mount. The film viewing is still done on a light table as with mapping film or on a few special large-format film or microfilm readers. Hand-holding of a 70mm camera bank is possible, but hardly practical, from windows of helicopters or fixed-wing aircraft.

2.4. 35MM FORMAT

35mm format cameras provide a format convenient for either being hand-held or for shooting through vertical camera mounts. Camera banks of up to four cameras are so handled, but a two camera bank is sufficient and is very easy to handle (see Figure II). 35mm format cameras are easily obtained as is the film (except for the bulk color IR film), and the film is quite easy to get processed.* 35mm microfilm viewers are easily used for viewing bulk 35mm film and much library technology has been developed in indexing, retrieving, and viewing 35mm microfilm. Figure III shows 35mm film being indexed and filed as 35mm microfilm and shows a 35mm microfilm viewer.

35mm format cameras can be easily used from either the belly mounts or through the windows of the aircraft. The film can be copied to be viewed as slides or simply viewed as 35mm microfilm. The resolution of 35mm film is about one-fourth as good as with 70mm film. However, for water quality work one is seldom interested in fine metric measurements but instead interested in general size, tone and location of pollution plumes. 35mm format has proven very satisfactory for such work. The economical cost of such size film is a definite advantage.

One such disadvantage of this size format is that most 35mm cameras have focal plane shutters which create somewhat unpredictable focal plane illumination when one is interested in absolute light intensity studies from the film.

2.5. OTHER FORMAT SIZES

Other format sizes such as 16mm and 8mm cameras are used by various people for gathering data on such things as city traffic if resolution is not an important factor. 16mm film can also be handled as microfilm but it has no real advantage over 35mm film for such applications and the decreased resolution is a definite disadvantage.

In the University of Wisconsin's research program various persons have made use of 9-inch photography where metric accuracy is important. For most studies the 35mm bulk film system was used with a supporting microfilm viewing system. 70mm film was also used and was the format of the thermal scanner data.

2.6. THERMAL SCANNERS

Daedalus scanners and Texas Instruments scanners have been flown in twin engine

* A special purchase was made in 1970 of 35mm Kodak bulk color IR film. The minimum purchase in this first case was thirty-six 100-foot rolls.

aircraft on various interdisciplinary research projects and for intensive studies of thermal patterns in Lake Michigan and Lake Superior (6,7). Such scanners are definitely workable and reliable tools for thermal pollution studies and show the skin thermal structure of the water to a very fine resolution. They do not, however, necessarily show the municipal or industrial pollution if the discharge is the same temperature as the receiving water.

2.7. AIRCRAFT

Aircraft platforms include helicopters and small fixed-wing aircraft for window photography. Belly hole aircraft include Cessna 180's, various small twin engine aircraft, and a state owned DC-3. Almost all such aircraft were borrowed, rented or leased.

3. THE UNDERSTANDING TO DATE OF REMOTE SENSING OF WATER POLLUTION

Before remote sensing imagery can be effectively used for water pollution monitoring one must know the pollution parameters it shows and what effects are caused by the water surface, angle of incidence and illumination, and bottom effects.

3.1. WHAT SHOWS UP IN THE WATER

When aerial photography shows plumes of pollution coming from industrial plants or sewage treatment plants it is conclusive that the pollution parameters of solids cause this image. In some cases it may be suspended solids which cause the image; in other cases it may be dissolved solids or total solids. Laboratory analyses with the spectrophotometer have indicated that correlation is possible between reflectance intensity and the pollution parameters of solids (see Figure IV). There is a big gap between the lab and the field, however, because of depth penetration effects and bottom effects both in the lab sample tube and in the field. Absolute correlation curves relating solids with image intensity must be made with actual field water samples taken simultaneously with aerial photographs which are later analyzed with the microdensitometer. Figure IV shows initial results of such correlation from about 40 overflights during the summer of 1971.

When the data from the summer of 1971 was initially analyzed, and an attempt made to ascertain correlation reliability, and to precisely correct for angle effects, it was found that water sample analysis repeatability was far less than the photographic errors which were to be statistically determined. Therefore in the summer of 1972 a very thorough effort was put forth in the mixing zone of a paper mill on the Fox River, and very close control was kept over the water sample analysis so a full correlation can be discerned between the solids being put out by the paper mill and the image intensity on the photograph. The image and water sample analysis for this correlation continues with the goal being to determine the statistical accuracy of determining solids by analyzing aerial photographs and to see which solids parameters, dissolved, total or suspended, give the best correlation.*

3.2. WHAT SHOWS UP ON THE SURFACE OF THE WATER

Surface glare is a problem but proper choice of the look angle by the cameraman will illuminate this troublesome problem. Also oil slicks create a visible and detectable surface phenomenon. Work at the University of Wisconsin by J. Van Domelen (9) and Scherz has shown that the photo response of the oil varies at certain wavelengths in extremely good correlation with the oil thickness. It also appears that the type of oil affects this photographic response as does the cloud cover. Work is in progress in this area as well as a study of effect of the angle of incidence between the water and the camera on the absolute intensity reaching the photograph.

3.3. WHAT SHOWS UP AS TO BOTTOM EFFECTS

Bottom effects at first appear to be a very nasty and troublesome problem, but it can be easily solved if one realizes that such penetration to bottom is wavelength dependent and if one can predict the depth of this penetration. In some cases one wants to look through the water at, for example, the weeds at the bottom. Here the same weeds change tone on the color or color IR photo depending upon their

* Under the direction of T. L. Lillesand and S. Klooster.

depth. This change in tone is also mostly due to the fact that water penetration is wavelength dependent. It most waters maximum penetration occurs in the green part of the spectrum. But a few inches of penetration occur in the photographic infrared part of the spectrum and thermal infrared senses only the skin temperature (3).

Assuming that one wishes to look at the solids discharged in the water by some industry and not at the surface or bottom of the water body, one must be sure that the wavelengths are not penetrating to the bottom and that there is no surface reflection. One can visibly check for glare or oil slicks and one can have a secchi disc set into the receiving water to see the general range of depth penetration in such water. Work in progress (4) indicates that the depth penetration phenomenon can be easily understood by using the secchi disc reading in the water, and derived curves aid in determining the depth of penetration and the amount of energy returning from each layer of water above this depth (see Figure V). For proper correlation of aerial images with water samples the composite water sample should also be gathered in accordance with that proportion of energy returning from each layer as indicated by the curve in Figure V (4).

From the curve one must be sure that the depth to bottom is at least one or two times the secchi disc reading if one is to be free of troublesome bottom effects when analyzing the film. If the depth to bottom is less than the secchi disc reading then it is necessary to analyze the photograph using only the IR energy (i.e. the red layer on the color IR film). Photographic and IR energy penetrate but a few inches into the water.

4. SUMMARY AND OPERATIONAL TECHNIQUES

It is known that the photographic image shows solids in the water. The standard pollution parameter of BOD caused by paper mill waste and municipal sewage is mainly due to organic solids discharged from such sources. Therefore photography can see solids, and solids in many cases are an important pollution parameter. Also sewage treatment plants not working properly put out organic solids. Such solids can show up on the aerial photography and are of interest to the state agencies of Wisconsin. The higher the concentration of solids, the more intense is the image of the plume on the photograph. One should therefore be able to obtain a calibration curve for each particular source by comparing the photo intensity with different outfall loads and if the character of the waste does not change later, determine the solid outfall load merely from the aerial photo.

To make such a calibration curve one must have depth penetration such that bottom effects do not overshadow the image of the desired solids in the water. This depth penetration in the green part of the spectrum can be from 30 feet to less than one foot depending upon the characteristics of the receiving water. Such penetration can be determined by use of a secchi disc and a curve similar to the one in Figure V. Water samples should be taken in accordance with the amount of energy returning from each depth of water as determined by the curve in Figure V.

In order to get a standardization to calculate the absolute reflectance a standard reflectance panel is required in the water. This panel may not be as necessary if one uses the ratio of reflectance at two wavelengths as a function of pollution load rather than absolute reflectance. Work is underway to determine the relative merits of the wavelength ratio method versus the absolute reflectance method.

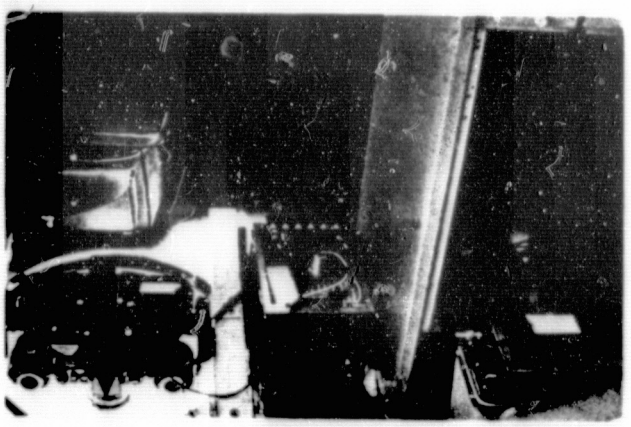
Once these facts about accuracy of correlation of solids with the aerial image are further defined, as well as the depth penetration characteristics, then the question of what does remote sensing imagery of water quality really show and how can it be practically used will be answered. Work at the University of Wisconsin is attempting to finalize the answers to these questions. Close cooperation exists with the state agencies, one of which is presently experimenting with the bulk film 35mm photographic system as a tool for environmental impact statements, and another which is closely involved in answering the above questions on photography of water quality and which is also utilizing thermal scanning in studying thermal discharges from power plants. Once the pertinent questions about photographic monitoring of water pollution are properly answered, past experience with different films, format sizes, and index and viewing systems will allow recommendations of an optimum practical system for immediate application.



FIGURE I. GAMMA SPECTROPHOTOMETER - MICRODENSITOMETER. This device can be used to analyze black and white, color, or color infrared transparencies in 35mm, 70mm, or 9 inch format.



A bank of 2 motor-driven
35mm bulk film camers. Window photography.

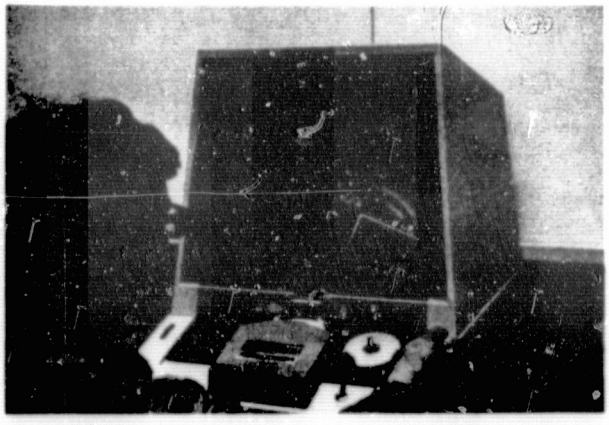


Photography with the 35mm camera bank
through a belly mount. Note the intervolometer
and the self-contained power pack.

FIGURE II. THE 35MM BULK FILM CAMERA BANK.

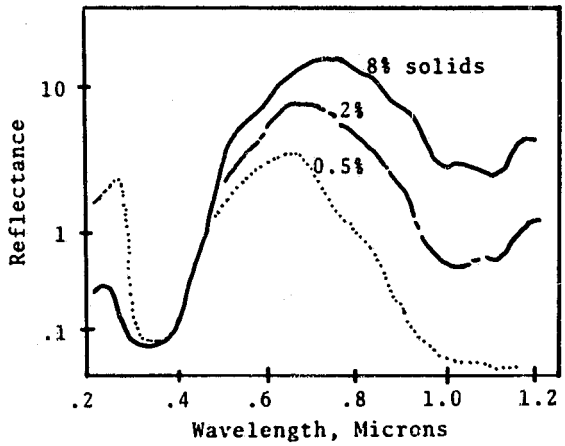


35mm bulk color and color infrared film
being indexed and filed as 35mm microfilm.

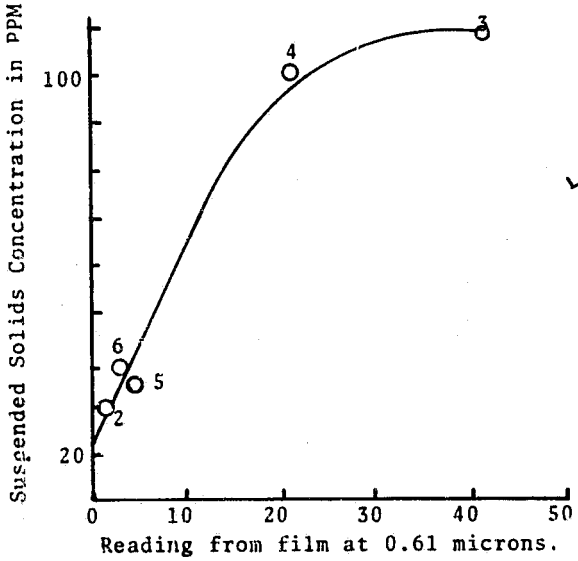


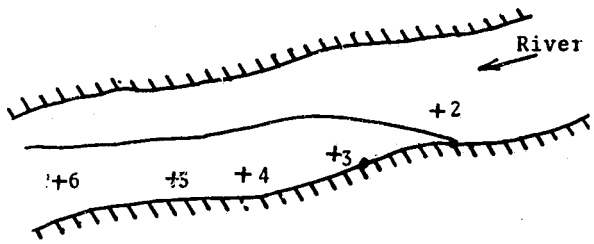
35mm color infrared film being viewed
by use of a 35mm microfilm viewer.

FIGURE III. THE 35MM MICROFILM INDEXING AND VIEWING SYSTEM.



Laboratory analysis with a spectrophotometer on a sample of paper mill waste indicating the change of reflectance as a function of wavelength and solids (2).





Sketch of paper mill plume.
Numbers indicate water sample points.

Preliminary field correlation of solids put out by a paper mill as determined by comparing water samples with simultaneous photography analyzed with a microdensitometer.

FIGURE IV. CORRELATION OF WATER POLLUTION SOLIDS WITH IMAGE INTENSITY.

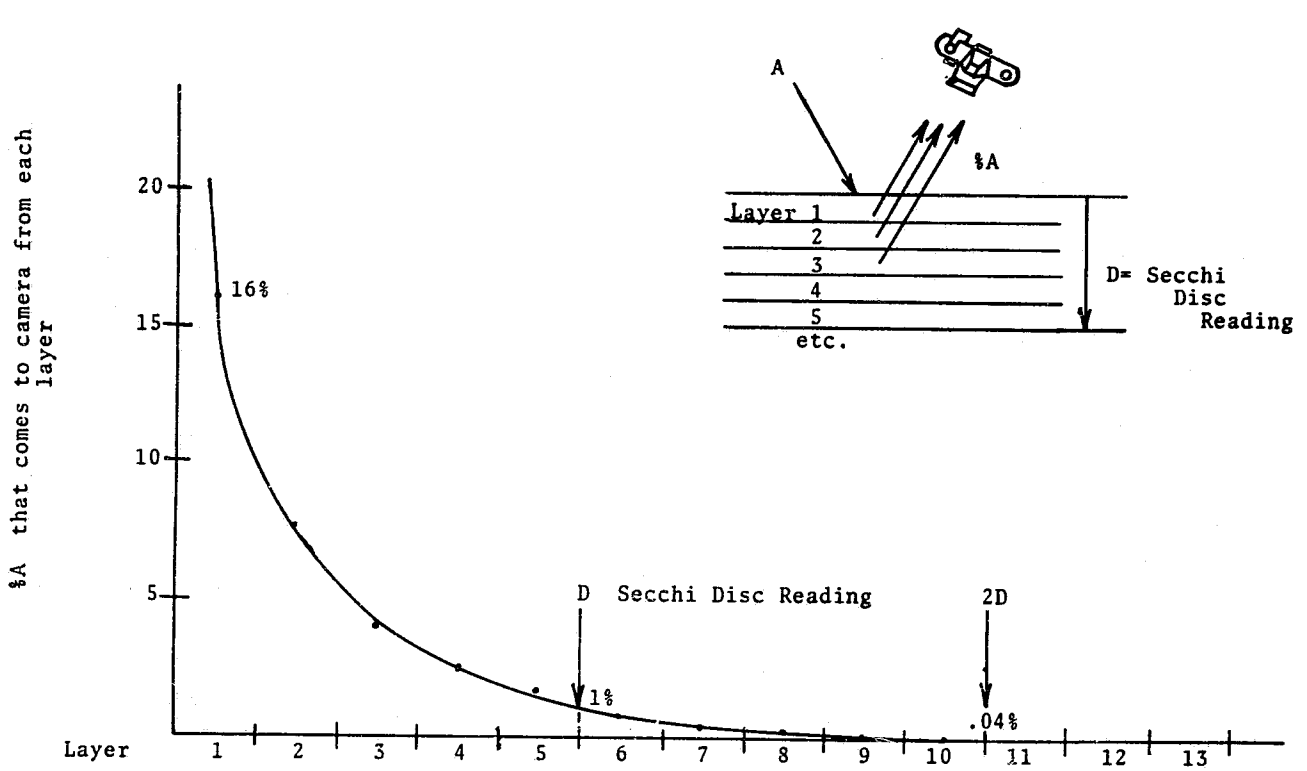


FIGURE V. ENERGY RETURN FROM DEPTH OF WATER. Given a Secchi Disc Reading in the water in question one can determine by use of the above curve how much energy comes to the camera from different depths within the water.

BIBLIOGRAPHY
OF
RELATED CONCURRENT WORKS AT UNIVERSITY OF WISCONSIN.

1. Rinehardt, G.L. and Scherz, J.P. "A 35mm Aerial Photographic System", Proceedings of the 1972 Annual Convention of ASP and ASCM, Washington, D.C., March 1972; also The University of Wisconsin Remote Sensing Program Report Series.

2. Scherz, James P. "Aerial Photographic Techniques in Pollution Detection", thesis presented to the University of Wisconsin, at Madison, Wis., in 1967, in partial fulfillment of the requirements for the degree of Doctor of Philosophy.

3. Scherz, James P. "Monitoring Water Pollution by Remote Sensing", Journal of the Surveying and Mapping Division, Proceedings of the American Society of Civil Engineers, November 1971.

4. Scherz, James P. "Photographing Water Pollution at Chicago", The University of Wisconsin Remote Sensing Program Report Series - Presently in process of being printed.

5. Scherz, James P. "Special Aerial Photography Research Project -- End of Year Report to Water Resources Committee of State Agencies", Madison, Wisconsin, 1968.

6. Scarpace, F.L. and T. Green, III. "The Use of a Thermal Line Scanner in Remote Sensing of Water Pollution", Remote Sensing Paper - University of Wisconsin, 1971.

7. Terrell, R.E. and T. Green, III. "A Method of Investigating the Surface Velocity Structure of Currents and Thermal Plumes." Remote Sensing Paper - University of Wisconsin.

USERS REPORT FOR THE NORTHERN GREAT PLAINS

by

Fred A. Waltz, Victor I. Myers, and Leonard R. Heinemann
Remote Sensing Institute
South Dakota State University
Brookings, South Dakota

ABSTRACT

The application of remote sensing technology on a regional basis involves education, developing data handling techniques, designing data paths, designing information delivery systems, and implementing an action program. The Remote Sensing Institute at South Dakota State University has conducted extensive studies in defining users, data required, format for presentation, frequency of required information, mode of communication required, and types of facilities. A state wide information dissemination plan for South Dakota has been developed and is being implemented.

INTRODUCTION

The applications of remote-sensing techniques offer new and futuristic approaches to many of the present-day problems encountered by various state agencies in South Dakota. The state agencies, however, must be apprized of the potential benefits that could be derived from the interpretational use of remote-sensing data collected by aircraft and satellites. The Remote Sensing Institute at South Dakota State University in Brookings, South Dakota, has pursued the objective of familiarizing state agencies with potential applications and defining data handling systems, information delivery systems and developing a state action plan.

This study has been completed in three phases. The first report presented the information needs of the state agencies and educational efforts. The second report defined the data handling procedures for fulfilling the applications outlined in the first report. The third phase was development of a dynamic information dissemination plan on a state wide basis.

Data handling techniques for research and operations systems for multiple applications were outlined by Waltz in 1970. These principles are still valid and apply to the present day data collection systems.

There are certain data handling principles which are peculiar to remote sensing data.

1. The majority of applications will utilize automatic processing. This appears self-evident when the sheer volume of data (spacecraft and aircraft) to be available is examined. Few organizations will be able to hire the qualified personnel necessary to do extensive manual processing.

2. Methods for handling data must be developed for specific applications. There are a number of standard procedures for extracting pertinent information from data. However, remote sensing applications in the past have not been solved readily with these methods. Therefore, for reasons of economy a method of analysis must be developed for each application and fitted into a larger processing system.

3. A specific application usually requires only a small amount of available data so the problem becomes one of discarding data. A typical remote sensor produces data in film or analog signal form. The complete digitization of this wideband data results in data rates which are excessive for most digital computers. Economics of operation dictate low data rates.

4. Development of data handling methods are more efficient with digital rather than analog data. The flexibility of computer programming when using digital data makes for ease in development of data handling methods. Analyses can be changed by reprogramming the computer rather than by having to build new hardware.

Preceding page blank

5. Operational data handling methods may utilize analog preprocessing with final processing in digital form. The large data rates, and need for real time processing, are compatible with analog equipment. However, the dynamic logic needed for final processing of an application fits digital computers. Thus, hybrid combinations would appear to meet the requirements for most applications.

METHODS

The problem was to define a system to serve EROS-ERTS in the Great Plains environment specifying:

1. users
2. kinds of EROS-ERTS data required
3. format for presentation of information required
4. frequency of information required
5. mode of communication required
6. type of facility required (listing equipment, personnel, plant)

The problem was expanded to use more types of data and provide a step by step analysis of each application.

Efforts were expended in the following areas:

1. Remote sensing educational efforts.
2. Determining potential uses and applications of remote sensing by state and local agencies.
3. Evaluating information exchange and interaction between agencies.
4. Proposing a design for an organization to apply remote sensing systems to support the functioning of state agencies.
5. Obtaining responses from state agencies of their need for remote sensing data.
6. Step by step analysis of each application specified by the state agencies with concomitant information given above.
7. Developing an information dissemination plan for the state considering remote sensing data in the context of the overall information system.

RESULTS

Extensive educational efforts have been carried out by the Remote Sensing Institute staff since January, 1969. These efforts were necessary to promote an understanding of the applications and limitations of remote sensing. Television, news articles and personal contacts were used in this effort. Many of the rapid advances within the state would not have been possible without these educational efforts.

A list of all known potential uses of remote-sensing data was compiled to provide an initial basis for communication with state agencies. State agencies were then listed and cross-referenced to the lists of potential uses. The Remote Sensing Coordinator for State Agencies, who was appointed by the Governor of South Dakota, asked each state agency to indicate its area of interest in remote sensing applications. Their responses were used to lay the groundwork for a series of meetings between data-collection agencies and data users so that the best means of data dissemination could be devised for effective utilization.

The experience of working with the various state agencies and analyzing the interaction model leads to the proposed agency structure which was devised as a dynamic flexible organization which would increase the efficiency of state agencies.

Recommendations are being made by the Remote Sensing Institute to each state agency regarding the type of equipment necessary for their specific purposes. Some equipment will be available to state agencies from the Remote Sensing Institute in Brookings. Signal Analysis and Dissemination

Equipment (SADE), a system for analysis, storage and dissemination of remotely sensed data, is part of this equipment. SADE has the following capabilities:

1. High resolution, high quality digitization (2048 x 2048) of 57 x 57 mm film transparencies
2. Accomodation of 35 mm, 70 mm, and 9½ inch single frame or roll films
3. Multiple frame registration on-line to computer
4. Off-line image registration
5. Digitization of analog magnetic tape information (up to six channels)
6. A solid state memory for the display of processed data on the video monitor and for registration
7. Expandable memory for storage of high resolution imaged data
8. Conversion of processed digital data to hard copy using an output printer (70 mm film) or by photographing video monitor
9. Control of the system's components in communications with the computer via teletype and a system control panel
10. Complete use of a large scale computer with magnetic tape, disk, and core storage along with associated peripherals.

Other possible users of remote sensing data, such as farmers, ranchers, agri-businessmen, and other business establishments, have been familiarized with the availability of remote-sensing data, and its possible applications through printed news media, radio, and television. Feedback from these individuals indicates that they have a good understanding of remote sensing data collection procedures. In addition they indicate a high degree of interest in obtaining and using such data. The proposed state structure is given in Figure I.

The most important segment of remote sensing is the analysis information. A typical sample follows:

Inventory Surface Waters

1. Source of Data

   EROS-ERTS
   State agencies
   RSI aircraft
   USGS quadrangles
   ASCS photographs
   SCS maps
   Ground truth

2. Step-by-Step Analysis

   Correlate data sources
   Color encode density slices of data
   Photograph density slice of surface water
   Apply planimeter to compute area
   Apply correlation correction for areas below ERTS resolutions

3. Format of Data Product

   Photographs
   Transparencies
   Reports
   Thematic maps

4. Equipment and Facilities Needed by User

   Light table
   Projectors

5. Mode of Communication to User

   Mail
   Telephone

6. Frequency of Data Product

   36 days

7. Specialist to Contact for Further Information

   Hydrologist

8. Resolution and Scale of Data Product

   <10 meters ground resolution
   1:50,000

9. Factors Affecting Success

   Weather conditions
   Timeliness of flights
   Accuracy of machine analysis
   Accuracy of correlation correction factor

A very important contribution this symposium or any other could make to remote sensing knowledge and use would be to require that each application reported on provide the above information.

Even if the procedure is wrong it will produce insight to the analysis and provide a starting place for the correct analysis. The method can be used for photo interpretation, automated analysis or any combination of the two.

South Dakota's information needs in agriculture and associated industry as well as in human and natural resources development and conservation are and have been served by the South Dakota State University. Modern concepts and techniques in information dissemination and new sources of data demand that South Dakota take advantage of recently developed facilities available for collection, transmission, analysis and dissemination of a vast amount of useful and needed information.

South Dakota State University is vitally interested in the use of a major new information tool -- remote sensing -- in extending service to agriculture, industry, and to rural and urban living. Therefore, commitments have been made by that organization for additional education of qualified agricultural and engineering personnel in use of remote sensing and related information dissemination systems. The information dissemination plan developed for the state involves all active agencies within the state. Much of the cooperation exists at lower levels rather than being imposed from the top.

The four part information dissemination plan includes: 1) scheduled, specific educational procedures for state agencies through workshops, 2) specific data flow paths have been defined between all agencies involved, 3) monitoring and feedback methods were defined for these paths, and 4) development of an automated pilot dissemination system with a dynamic data bank. The goal is to serve state agencies and the public by using the latest techniques in an organized manner. Funds to implement the information dissemination plan are kept to a minimum by replacing obsolete systems, and utilizing existing personnel and facilities where possible.

The initial establishemnt of data flow paths was begun two years ago with various state agencies which cooperated with Remote Sensing Institute in the collection and use of remotely sensed data. The data paths are of three distinct forms. The first type is computer based with information entered in computer format and disseminated via terminals. This operation is currently being tested by a pilot project. The second path is from data source to analysis, thence to resource specialist to user. The third data path is from source directly to those users with equipment and sophistication to use unanalyzed data.

Recommendations as to realignment of remote sensing tasks with the needs of the state are made yearly. New data paths will be devised as new applications become operational or new data sources are found.

CONCLUSIONS

Significant use of data acquired by airborne and spaceborne remote sensor systems is being made in the Northern Great Plains. Aircraft data, satellite imagery and other remotely sensed information are valuable in the state agencies' decision-making processes. A design for an organization to acquire for the state the advantages of remote sensing systems for resources research and management has been developed.

Education efforts in the Northern Great Plains have produced an informed public. Feedback information indicates a high level of interest in the potential of remote sensing and a need for the applications. A state structure for remote sensing applications was designed and would enhance the use of such data. Implementation is progressing for the use of remote sensing data through a state wide dissemination plan.

Grossling and Johnston related an anecdote about the centipede. The centipede was very tired of walking, and his feet hurt, and he didn't know what to do about it. Somebody told him that the owl could advise him on this problem. So the centipede went to the owl and said "Mr. Owl, you are so wise, will you please tell me what can I do to rest my feet?" The owl, after a brief pause, answered: "Walk for two weeks at one inch above the ground, in that way you will rest your feet." The centipede was very grateful, "Thank you Mr. Owl; that should do it...But, how will I walk at one inch above the ground?" To which the owl gruffly replied "I have solved your conceptual problem. Don't bother me with technical details."

Gentlemen I submit to you the time has come to hit the ground with all one hundred feet running. The time has come to solve the technical problems.

REFERENCES

1. Waltz, F.A. -Multidiscipline Remote Sensing Research for Hydrology and Agriculture. Journal of Remote Sensing, August 1970.

2. Waltz, F.A., Myers, V.I., Heinemann, L.R. -EROS Users Report For The Northern Great Plains, Remote Sensing Institute Report, June 1972.

3. Waltz, F.A., DeVries, M.E., Serreyn, D.V. -EROS Users Report For The Northern Great Plains (Data Handling). Remote Sensing Institute Report, August 1972.

4. _____ Information Dissemination Plan for the State of South Dakota. South Dakota State University document, August 1972.

5. Grossling, F.B., Johnston, J,E. -On Bridging the Gap Between Raw Remote-Sensor Data and Resource and Environmental Information. 15th Annual Technical Symposium of the Society of Photo-Optical Instrumentation Engineers, Anaheim, California, September 1970.

ACKNOWLEDGEMENT

This report was supported by the United States Geological Survey through contracts 14-08-0001-12510 and 14-08-0001-12862; National Aeronautics and Space Administration through Grant 42-003-007; and the state of South Dakota.

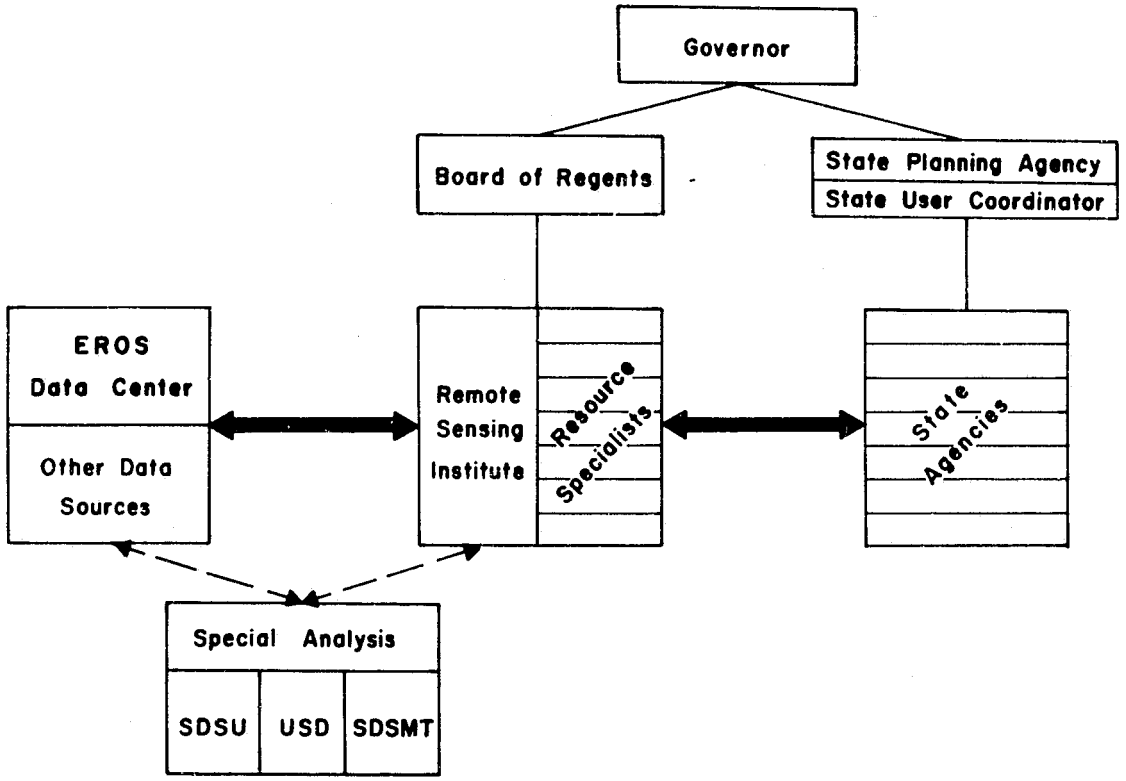


Figure I. Proposed state structure for information processing and dissemination.

REGIONAL LAND INVENTORY SYSTEMS DEVELOPMENT IN THE HOUSTON AREA

Dr. John E. Dornbach

NASA, Manned Spacecraft Center
Houston, Texas

and

Joe B. Harris

Office of the Governor
Austin, Texas

ABSTRACT

It is perhaps axiomatic that accurate and timely information is needed to manage wisely the resources of the Earth and to monitor environmental change as it occurs. Since this use and change may vary greatly from local to regional, national, or international levels, remote sensing from aerospace platforms appears to be one of the most valuable tools for providing quantitative data over extensive geographic areas from which large amounts of needed information can be extracted.

When remote sensing systems are coupled with the use of the computer in automatic data processing and in applications of information and decision making theory, it becomes possible to provide accurate and timely information to the regional planner, manager, or administrator. Only five or ten years ago, it would have been virtually impossible to acquire, analyze, integrate, and correlate all of the required information in the matter of a few weeks or months. Given manual or conventional methods of data acquisition, it is doubtful whether mathematical modelling for predicting change or for choosing alternative management solutions could ever have been optimally utilized on a regional basis.

This paper will discuss how these technologies are being utilized in conjunction with agencies of the Texas State Government and the Houston-Galveston Area Council of Governments to develop initially a regional land inventory and information management system. This is to lead to a better understanding of requirements which could influence development of a regional or national land resources planning and management system.

---

1. INTRODUCTION

In this nation, as in much of the world, there is an increasing concern as to how the land and its resources are being used. There is concern over what is happening to these resources and what can be done to insure an environment of adequate quality for coming generations. Recent and proposed environmental and land use legislation indicates that Federal Agencies and State and Local Governments will be focusing increased attention on the specific area of nation-wide patterns, trends, and impacts of land use.

Many past attempts to inventory an area as large as a State were hampered by the lack of a fast, thorough system for data acquisition and by the lack of a rapid, efficient, and accurate means for synthesizing, analyzing, and displaying the processed information. Today, through data acquisition by remote sensors in high altitude aircraft and spacecraft and through the use of the computer in automatic data processing and in applications of information and decision making theory, it appears that it will soon be possible to provide uniform, accurate, and timely nation-wide

information to the state, regional, or national planner, manager, or administrator.

2. SYNOPSIS OF CAPABILITIES OF LAND INVENTORY SYSTEMS

In order to relate the work being done in the Houston Area Test Site (HATS) to that which has been done in developing "Land Inventory Systems", Figure 1 attempts to categorize the state of systems past, present, and future. The three categories are intended to serve as a type of technology assessment of inventorying systems. The technology has existed for many years to conduct inventories according to the "Yesterday" column. In recent years, technological advances have led to the development and use of systems such as represented in the "Today" column. Many advances in technology will be required to develop the system such as indicated in the "Tomorrow" column. How far into the future is, of course, dependent upon the level of effort expended in order to develop it. The work underway in HATS is being directed toward development, test, and evaluation of this type of system.

2.1 YESTERDAY'S TECHNOLOGY

The type of system used in the 1930's and 1940's in inventorying the area covered by the Tennessee Valley Authority (TVA) is categorized in the "Yesterday" column. Generally speaking, this system required a very large number of large scale photographs and much field and interpretation work to convert them into information. The annotated photographs were keyed to the largest scale topographic maps available. All information was stored in the form of map overlays and much correlative information covering the entire TVA area was presented on smaller scale generalized maps. The methods and techniques used required considerable cost and manpower for what in those days was a large area to receive such a comprehensive survey. Finally, it must be concluded that the planner and manager found it difficult to mentally integrate all the information contained in the maps, in order to evaluate alternative solutions to each environmental or resource problem.

2.2 TODAY'S TECHNOLOGY

Perhaps one of the best examples of a comprehensive land inventory system based on Today's capabilities is the Land Use and Natural Resources (LUNR) Inventory developed by Cornell University for the State of New York, Office of Planning Coordination.

Although this system depended on some of the "Yesterday" techniques in photo interpretation, field checking, and in the use of existing, large-scale topographic maps, it nevertheless converted this information into a form for machine-aided data analysis by the planner or manager. It is perhaps significant to note that many planners and managers in New York are still not using the computer techniques, but are requesting from Cornell the 1:24,000 large scale land-use overlays with which they are most familiar.

2.3 TOMORROW'S TECHNOLOGY

Our efforts in the Houston area along with the Houston-Galveston Area Council of Governments (HGAC) and the State of Texas, Division of Planning Coordination are being directed toward the development of tomorrow's systems. In this system, remote sensor data will be gathered in various parts of the electromagnetic spectrum and at various times. Only a minimal number of training fields or field checks will have to be used. Pattern recognition processing will be done with inter-active systems where the only image forming process need be the screening on a TV display and the selection of training sets. Through improved understanding of the location of each picture element to all others, the classifications can be transformed into any coordinate system. The output classification of land use or other data set will be stored automatically for a certain geographic area along with all types of physical, natural, socio-economic, demographic, and other data. As the planner or manager works with the information management system, he can generate hard copy map overlays if he so desires, but through use of special algorithms, he can by-pass the map overlay-making process and evaluate alternative courses of action by playing certain desired conditions against the information base. It is believed that although a system of this type would be expensive to develop, it could ultimately serve more users, more efficiently and with more cost effectiveness than the systems which have been previously used. Since the development of the experimental system is not an end in itself, a major part of the activity will be based on the test and evaluation of the system by agencies responsible for planning and managing the use of resources and the environment in the Houston area.

Figure 2 indicates the functions of the system which are under investigation. This diagram indicates the various functions which must be considered in a total resource management or monitoring system. We start by assuming that there is a requirement for information about a specific resource or environmental problem. Then, remote sensing plus other methods are used in the data acquisition process. After data processing and data analysis, the information can be used in making

predictions, testing alternative solutions to the problem and in making management decisions. The management decision leads to some action which changes the resource or environmental problem and then, the process begins again as monitoring of the situation continues. Although the time required to complete the circuit is not indicated, it should be apparent that if the data acquisition, processing, and analysis portions consume too much time - in terms of months to years, the decision making process may be seriously affected.

Although remote sensing plays only a part, albeit an important part, no attempt will be made to indicate "who" would perform these functions or "where" they would be performed. In illustration of this, the State of Texas is planning a Natural Resources Information System (NRIS) and HGAC is planning an Environmental Decision Assistance System (EDAS). Since each will have some common systems and will contain similar information for certain cities and counties, it is conceivable that in the future a central data handling facility could exist at the state level with remote interactive terminals in the Councils of Governments, cities, counties, etc.

3. THE HOUSTON AREA TEST SITE (HATS)

Several years ago, the National Aeronautics and Space Administration (NASA) and the U.S. Geological Survey, along with other agencies, states, and local governments established certain regional test sites for the purpose of applying remotely sensed information to what may be termed "real-world" problems. As a result, the Arizona Regional Ecological Test Site (ARETS), the Central Atlantic Regional Ecological Test Site (CARETS), the Houston Area Test Site (HATS) and others, came into being.

The HATS includes the 13-county Houston-Galveston Area Council of Governments (HGAC) which covers about 12,500 square miles and in 1970 contained over 2.3 million inhabitants (See Figure 3). Most of the area is in the Coastal Marshes and Coastal Prairies Regions. The northern portion includes some area in the East Texas Timberlands. In order to provide as much land resource diversity as possible for applications development in the Houston area, an additional four counties were added to the northwest of the HGAC covering the agricultural Blackland Prairie Region and one county was added to the northeast in which the Sam Houston National Forest is located. Therefore, the total HATS area comprises 18-counties covering about 16,000 square miles.

Although many agencies of the Texas State Government have followed the work in HATS, major working relationships are being established through the Division of Planning Coordination and the Office of Information Services, both under the Office of the Governor. The Division of Planning Coordination serves as the focal point for coordination of state agency and regional planning activities and provides staff support to the Governor's Interagency Council on Natural Resources and the Environment. In anticipation of the need to develop proper land resource management policies, Texas has established a Land Resource Management Committee under this Interagency Council. The Office of Information Services is responsible for developing and implementing a Master Plan for using electronic data processing and telecommunications in Texas State Government. This includes the development and implementation of a Master Plan for a Natural Resources Information System in Texas. It is anticipated that HATS will serve as one of several demonstration areas in Texas to assist these and other state agencies in developing a state-wide land inventory and resources management system.

The work in HATS developed several years ago as a result of meetings between representatives of the Manned Spacecraft Center - Earth Observations Applications Office, the State of Texas, the Houston-Galveston Area Council and the Houston Chamber of Commerce. Originally the major thrust was to explore the potentials of remote-sensing technology for use as a tool in the decision-making process dealing with urban and rural environmental studies, programs, and problems. However, it soon became apparent that in addition to remote sensing, much of the technology and experience gained through the spaceflight program in areas such as automatic data processing and information management and utilization was immediately transferable to the information systems problems facing the planner and environmental monitor. As a result, the effort is now aimed toward a demonstration of a total experimental system which effects a linkage of urban physical planning with environmental assessment planning and which provides for an improved effectiveness in urban and regional planning procedures, decision-making, and management of implementation programs.

Figure 4 is a greatly simplified version of the Environmental Decision Assistance System -- An information system for Planning, Development, Management, and Programs-Operations and Up-Dating, which is under development by the Houston-Galveston Area Council. For the past several years, some of the work in HATS has been directed toward developing a Regional Information Management System (RIMS). This system is almost identical to that in the HGAC system. It is basically an automatic storage and retrieval system for technical documents, photographs, base maps, and what may be considered as "static determinants". These are such elements as topography, physiography, soils, geology, and other environmental and ecological information.

In addition, to begin development of a type of "Dynamic Data Base", the land use of HATS was inventoried based on November 1970, 1:120,000 scale RB-57F imagery and manual photo-interpretation techniques. The 18-county area was photographed again by the RB-57F in April 1972. At present the School of Forestry of Stephen F. Austin University is conducting a similar 1972 Land Use Inventory. This will form the basis for studying the systems and techniques necessary to track the changing patterns of land use in this region through the use of a system such as REDRFOS. Two other projects are underway to develop information for use in the static and dynamic data bases. These are projects with:

3.1 The University of Texas-Bureau of Economic Geology in which Maps will be prepared for the 18-counties covering the following environmental geologic, biologic, and other information:

(1) Topography and Bathymetry
(2) Man-made Features & Water Systems
(3) Environments & Biologic Assemblages
(4) Physical Properties
(5) Active Processes
(6) Rainfall, Discharge & Surface Salinity
(7) Mineral and Energy Resources

In addition, Resource Capability Units which have already been developed by the Bureau for the Coastal Zone of Texas will be extended into all of HATS. These units are environmental entities -- land, water, area of active process, or biota defined in terms of the nature, degree of activity, or use it can sustain without losing an acceptable level of environmental quality. Thus, evaluations of present and anticipated resource use activities in terms of intensity, nature, and distribution on each of these units can be used to interpret the use impact on land and water resources.

3.2 The University of Texas-Bureau of Business Research in which data will be provided for each one square kilometer cell in HATS for all major manufacturing, industrial, and other type economic activities.

Finally, the HGAC has obtained 1970 Census Tapes and specialized software which in the future will permit the comparison and correlation of much of the physical, natural, socio-economic, and demographic data to be stored in the static and dynamic data bases for the Houston Area.

4. SUMMARY AND FUTURE ACTIVITIES

An initial, experimental, 1970 Land Use Inventory has been produced for HATS. This information has been published as a research map series for evaluation by user groups in HATS as follows:

1:125,000 scale - 21 sheets (20 land use categories)
1:250,000 scale - 4 sheets (20 land use categories)
1:500,000 scale - 1 sheet (9 land use categories)

Copies of these maps will be available in the near future for purchase through the Denver Distribution Center, U.S. Geological Survey.

An intermediate data base has been established for an experimental RIMS automated storage and retrieval system. At present, 17 attributes concerning location, update date, elevation, land use, transportation features, waterways, and other geographic features have been stored for each of the 44,000 one square kilometer cells in HATS. Information from this data base can be queried, sorted, and retrieved by an experimental information management software system.

In the coming year the following activities will be pursued:

4.1 Begin to incorporate 1970 and 1972 land use, environmental geology, manufacturing and economic, and 1970 census data into the RIMS data base. HGAC plans to identify a comprehensive list of users who require access to this type environmental data bank and information system and who desire to participate in an evaluation program. These users will establish a priority for listing their informational needs. After a familiarization period, they would operate the systems and provide feedback for modifications to the data base and to the design and development of improved system hardware and software.

4.2 Land use classification of the 18-counties will be conducted using data from the Earth Resources Technology Satellite (ERTS-1). ERTS-1 imagery will be interpreted using conventional photo-interpretation techniques and will be compared with data from existing systems. Sequential imagery obtained at 18-day intervals will be investigated for additional information useful in the classification process.

4.3 Using Multi-Spectral Scanner (MSS) data from ERTS and multichannel scanner data from aircraft, automatic data processing techniques will be applied to land use classification in represent-

ative test areas within HATS. A comparison of accuracy, time, and cost effectiveness will be made in relation to conventional manual land use classification techniques.

4.4 With agencies of the State of Texas, a plan will be developed for establishing other demonstration areas in addition to HATS, for the purpose of developing a classification system and data analysis techniques which could be used ultimately in a state-wide Natural Resources Information System.

SYNOPSIS OF CAPABILITIES OF LAND INVENTORY SYSTEMS

Yesterday	Today	Day After Tomorrow
Large scale B&W Imagery	Small scale color and color IR imagery	Multi-sensor data
Much field work	Limited field work and checking	Training Fields
Manual Photo-interpretation	Manual photo-interpretation	Man-assisted computer processing
Large scale topographic maps required	Small scale topographic maps or controlled mosaics required	Pre-existing maps not required
All information stored in form of map compilations	Information stored on magnetic tapes	Advanced memory systems
Output product in the form of generalized maps	Output product in the form of computer generated products	Output products not necessary, but generation unlimited, if required
Regional extent limited due to time, cost and manpower	Regional extent not limited by time, but some limitation by cost and manpower	Extent unlimited, costs and manpower shared by many agencies
Planning and management difficult due to necessity for mental correlation of much information	Planning and management aided by computer generated displays and automated storage and retrieval	Planning and management decision making through use of math modeling and computer generated predictions

FIGURE 1. SYNOPSIS OF CAPABILITIES OF LAND INVENTORY SYSTEMS

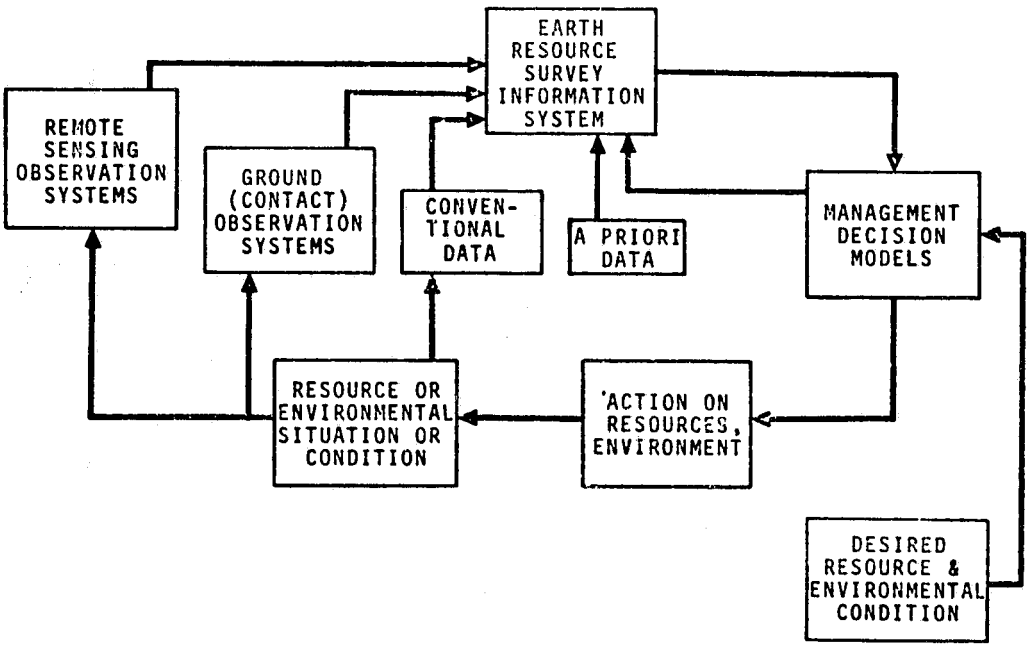


FIGURE 2. FUNCTIONS OF AN EARTH RESOURCES SURVEY AND INFORMATION MANAGEMENT SYSTEM

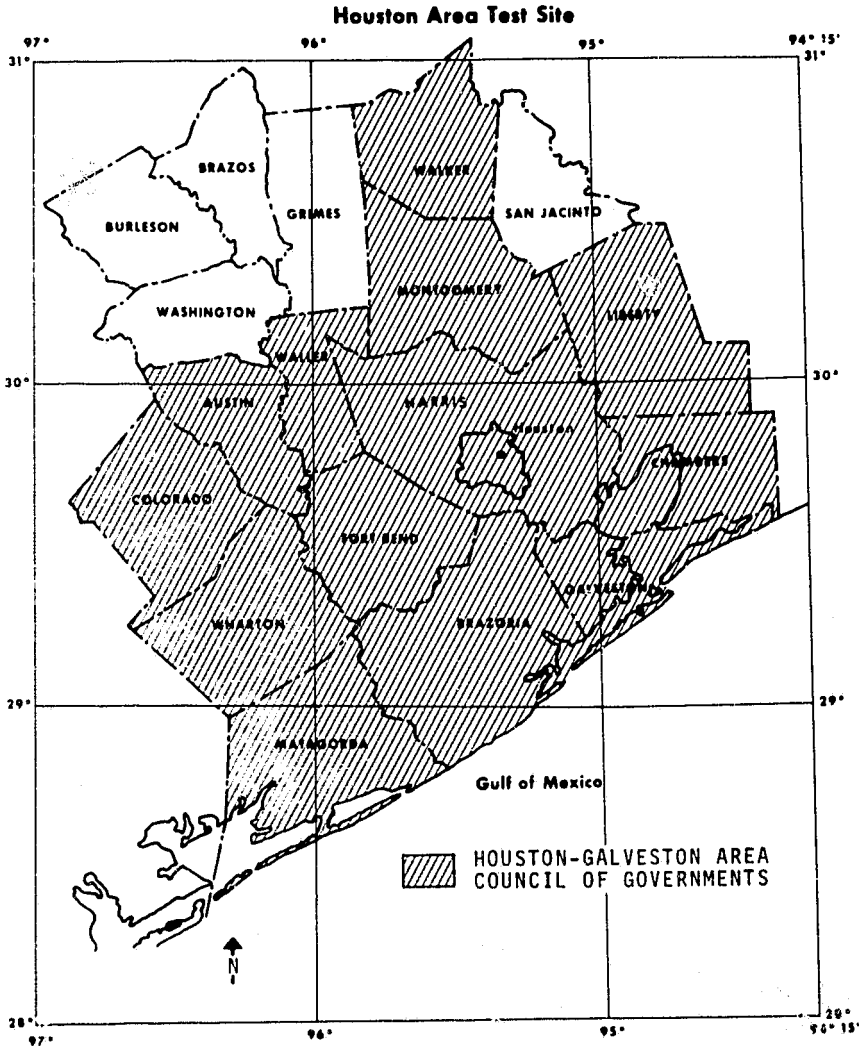


FIGURE 3. THE HOUSTON AREA TEST SITE (HATS)

HOUSTON-GALVESTON AREA COUNCIL OF GOVERMENTS

ENVIRONMENTAL DECISION ASSISTANCE SYSTEM

(EDAS - GENERALIZED DIAGRAM)

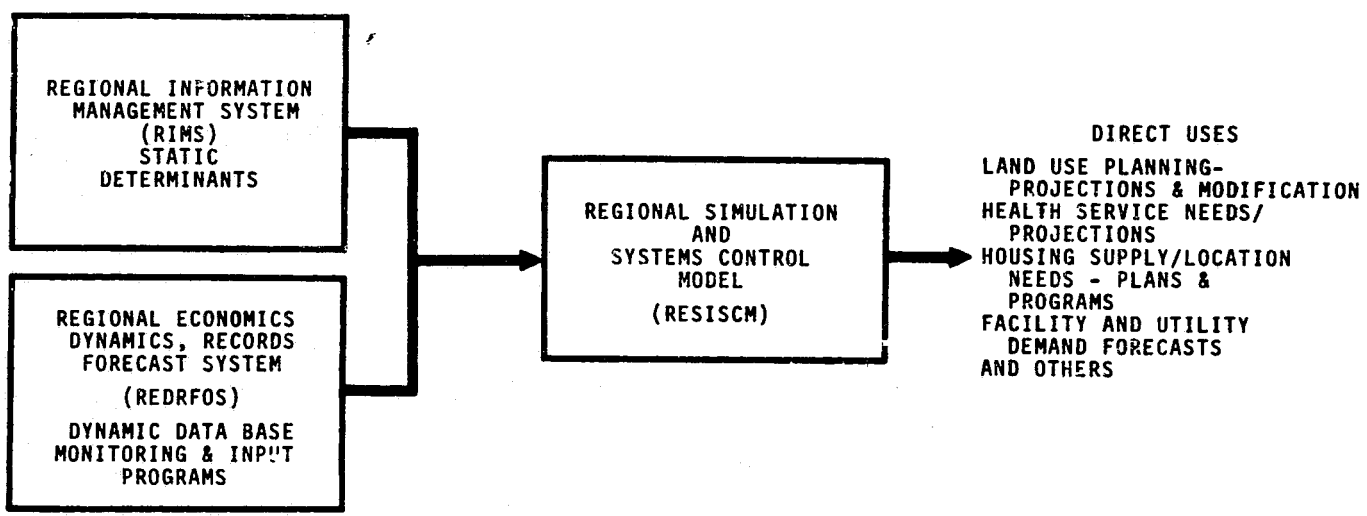


FIGURE 4. ENVIRONMENTAL DECISION ASSISTANCE SYSTEM OF THE HOUSTON-GALVESTON AREA COUNCIL OF GOVERNMENTS

REMOTE SENSING APPLICATIONS IN THE METROPOLITAN WASHINGTON COUNCIL OF GOVERNMENTS

Harry J. Mallon

Director, Remote Sensing Project
Metropolitan Washington Council of Governments
Washington, D.C.

ABSTRACT

In February 1971, a remote sensing project was initiated within the Metropolitan Washington Council of Governments, a regional planning organization for the fifteen major local county and city governments in the metropolitan Washington, D.C. area. The project's work program identified principal areas of application of remote sensing derived data to planning programs and participated in support of several of these. This paper describes the results.

---

1. INTRODUCTION

"The Metropolitan Washington Council of Governments is conducting a major research project to determine if remote sensing imagery and associated data from high-altitude aircraft can be used to monitor land development patterns, housing and neighborhood differences, changes in air and water pollution, and other aspects of local and regional life. If it proves workable, a major benefit of the project would be that these changes could be detected on a regular basis on a monthly or some interval through overflights of high-altitude aircraft or orbiting earth resource satellites", so reads a quotation from the 1971-1972 Annual Report of the Metropolitan Washington Council of Governments.

The Council is the regional planning organization for metropolitan Washington's fifteen major local governments and their officials. (Fig.1) It is a voluntary organization fiscally supported by the participating local governments and by Federal and State grants, and functions under policies and programs established by those officials. The day-to-day work of analysis, planning, and study support are carried out by a full-time professional staff, headed by an Executive Director.

The Council pioneered in framing local air pollution ordnances[1]; developed model plumbing and gas codes;[2,3] developed "fair-share" housing formulae for low and moderate income groups within the area;[4,5] conducted the first comprehensive, regional transportation study since 1955; developed models for regional growth prediction and assessment of growth effects resulting from testing various planning strategies involving local policy implementation programs;[6] developed regional open space retention plans, [7]developed inter-jurisdictional agreements for sanitary land-fill programs;[8] experimented with express-lane bus routes; developed water resource plans and water quality and run-off models;[9] and is the regional clearing house for the A-95 review process, including environmental impact statements where required.

The possibilities of remote sensing applications in support of the Council's planning programs were stimulated by the potential for area and regional data acquisition inherent in the Earth Resources Aircraft and the then pending ERTS-A Programs. In early 1969, planning began with discussions between representatives of the Council of Governments and the U.S. Geological Survey. In July 1970, a research proposal was submitted to the Survey; its acceptance resulted in a contract with work commencing in February 1971. The research objective was designed to investigate, consistent with the research assignments, how remote sensing could be feasibly and effectively utilized in this regional planning "user" environment; i.e., to improve COG's data collection programs; to improve the usefulness of the information base; and to assess time and cost reduction of data collection. The timeliness of this new effort fell in line with the Geological Survey's cooperative NASA/Geographic Applications Program's 1970 Census Cities investigations.

During the initial USGS/COG discussions, certain priority areas of mutual interest, information need and planning concern became evident. These included: land use, urban change, and environmental impact; others were housing and transportation. These information priorities strongly influenced the research phase of investigation and, to some extent, the present work within the project. The importance and appropriateness must be stressed of the need for early development with COG staff elements of some understanding of remote sensing data availability; sources and types of data; strengths and limitations; and an attitude for encouraging internal consideration of remote sensor-derived data use in promising applications.

2. STUDY AREAS

The project's work has fallen into two separate phases: (a) an initial research period devoted to investigating applications potential (the contract phase--February 1971-February 1972) and (b) the application phase (in support of internal departmental work programs--February 1972 to the present.)

During the first phase, a series of seven investigative studies were undertaken. These are described below with comments as to their results.

1. Information on available aerial photographic coverage of the Washington metropolitan region for the period 1951 - 1971 was compiled into a comprehensive photo index.[10] The index consisted of a consolidated listing with accompanying plots of coverage of the region. Photo holdings by Federal agencies as well as of selected private organizations were listed; price schedules, mailing addresses, and telephone contacts were also provided for user convenience (Fig. 2 and Table 1.). This index has received considerable interest within the area and has frequently served as a time-saving reference by MWCOG analysts and by local agencies within the region.

2. A remote sensing land use study of 17 selected census tracts in the northern Virginia area (Fig.3) was undertaken in order to test and compare results with comparable land use data from other local sources. Base date for both sources was 1968 as this was the base date for the acquisition of data from local land records, tax roles, and field surveys. Imagery of the selected areas of the same date was then procured. Tracts were analyzed and measured for land useage and the results delineated on a series of land use maps. Examples of two tracts in Falls Church, Va. and one in Alexandria, Va. are shown in Figs. 4 and 5. The classification system used was the Council of Governments' Generalized Land Use Code (See Appendix). The study results indicated the existence of considerable amounts of incomplete, out-of-date, and in some cases, erroneous land use data in the current COG data base--the principal sources of which, as mentioned above, are the tax roles from the local jurisdictions. The Council of Governments' land use data base, known as the Parcel File, was therefore correspondingly degraded, Within the limitations of success in interpreting the imagery (field-checked as required), the analysis pointed out many jurisdictional variations in land use classification and definition. In one jurisdiction, for example, based upon analysis of several tracts, the rolls do not carry such land use elements as schools, churches, and hospitals, others do not carry highway and railroad rights of ways, power-line and pipe-

line through-ways, airports, and water areas. Some of these land use elements are not tax-bearing; others are (Tables 2 and 3.) As might be expected, the additive values of the measured land use categories from the remote sensing analysis and from the other source data usually were at variance, however, the former were generally in excess of the corresponding values of the latter. (Fig. 6) On the average, this difference amounted to about 20-25%, and is due principally to the inclusion of streets and roads within the generalized outlines of the remote sensor-derived land use delineations.

The principal result of this study, which pointed out the substantial data deficiencies in existing land use records, has been to accelerate high interest within the Council of Government for early implementation of an internal research project in order to develop and maintain an improved land use data base. Land use within the Council of Governments is a basic ingredient for many studies transportation , bed-room to work areas (trip generation) studies, open space planning studies, land use inventories, and others. Since COG's land use data base is already computerized, it is little wonder that the results of this analysis has had many ramifications within the COG with the view of initiating an early data improvement effort.

3. The third investigation consisted of a land use change detection study.[12] This was done by reexamining six of the seventeen census tracts analyzed in the previously described land use study, using photography of 2 to 4 years later vintage. The changes in the use patterns were characterized, measured as before, and compared with the results previously obtained. (Figs. 7 and 8). Types of changes observed included development of open space or undeveloped land into residential or commercial (the most common development pattern) or from an existing useage to one of a more intense but of similar classification,for example, by filling in vacant spaces within residential areas with additional single-family or multi-family units. The study demonstrated that photographic analysis of land use change can provide needed information supporting many other studies. Development of trends may be surveyed, as examples, for estimating the directions and extent of growth or change, estimating areas for which and when public services might be required. Areas of new construction may be located and quantified, encroachment upon open spaces may be detected and recorded, and so forth. A high degree of uniformity was achieved in this analysis since remote sensing sources were utilized for both time periods. Thus the additional bias introduced by use local source and related data were eliminated. Finally, change detection by this method was found to be a relatively rapid and economical analytical process.

4. The fourth research task[13] entailed an investigation of the "art of the possible" in identifying and enumerating, by remote sensing, types of residential units and in describing the quality and condition of housing areas within several census tracts in metropolitan Washington (including the core and surrounding areas). The unique qualities of color infrared imagery made it possible for this study to achieve results which, under the handicaps of scale and urban congestion, would have been less rewarding had ordinary black and white photography been used. Image scale of say, 1:100,000 was satisfactory particularly in suburban areas for identifying and quantifying housing stock by types. However, the distinguishing characteristics of neighborhoods in process of change (conversion of single-family units to multi-family units or rooming houses, damaged structures, boarded up windows and doors, abandoned buildings, etc.(Figs.9 and 10) are just not visible nor reportable at that scale. Additional observable parameters such as street widths, building density, presence or absence of vegetation, curbing, vacant lots between buildings (Fig. 11), off-street parking, etc. are observable only on relatively larger scale imagery, such as say 1:15,000 or 1:20,000 (at the smallest). Color infrared imagery is an absolute requirement for this type of investigation. The detection of trash and litter in alley-ways (Fig. 12), requires, of course even larger scale, of say 1:5000 or better. Finally, architectural design, particularly in newer redeveloped areas of the city, frequently renders the usually distinctive characteristics of multi-family units and single-family row or town house units virtually indistinguishable in the imagery. (Figs. 13 and 14). Serious problems for the image analysts were posed. Close coordination between imagery analysis and ground survey in these areas within city centers was required and is a "must" if the time-saving advantages in area

survey frequently achieved by remote sensing are to be realized. However, even then, such applications in conducting definitive central city housing surveys, have yet, in the opinion of the author, to be fully demonstrated as a better information source in this particular context. In this study, COG found that housing data available from the 1970 census were adequate for many purposes. However, as housing information needs continue to develop during the seventies, area surveys using large scale imagery for spot checking and up-dating may prove sufficiently adequate for certain planning data needs.

5. The fifth study in the series[14] represented an illustrated inventory of some 9 major program areas (Table 4) of data needs to regional planning needs. Against these in the study, were matched a variety of corresponding subject areas, such as observing environmental condition, studying patterns of activity, reporting ecological events, monitoring status of change, etc.- in short, the elements associated with a dynamic urbanizing region--to which remote sensing has applications and can make contributions as a unique or a collateral data source. The illustrations shown in Figures 15-20 indicate some of these subject areas.

The list of applications as indicated in these series of illustrations is varied, as well as lengthly. In some instances, use of remote sensing derived data would, as already pointed out, provide important inputs to the Council of Governments' information and planning programs, and be the principal means of acquiring the data. In other instances, it would provide data essentially supplemental in nature to other sources or even perhaps be relatively minor in its contribution. Applications offering the most appealing promise of immediate and effective utility include, for example, those related to land use analysis, change and growth detection, elements of transportation studies, pollution detection and monitorship, training and photo index research services. For other types of applications such as those dealing with natural features (geology, hydrology, topography, map revision, etc.) in which basic remote sensing analysis is required, reliance by the Council of Governments, because of specialized staff and plant and equipment requirements for this work, must continue to be placed upon those appropriate Federal and State agencies responsible for such analysis and associated end products.

In these other areas involving current research by investigators within the Federal Government and elsewhere who are testing the capabilities of remote sensing data for the determination of specific quantitative relationships in such regional problem areas as air and water pollution and sedimentation processes, COG, presently relying upon conventional data acquisition methods, must contine to maintain contact with and monitor the progress of these research programs, as they appear to have application to this region.

The essence of this study, was, that once having identified areas of feasible and immediate remote sensing data use, it further recommended very early consideration of the establishment within the Metropolitan Washington Council of Governments of an on-going, task-oriented, in-house remote sensing support effort.

6. The sixth study [15] represented a further development and expansion of the previous applications study with respect to specific programs of the Council of Governments. It discussed related technical remote sensing data requirements and offered several examples of economic factors and cost figures justifying such data acquisition and use. The report pointed out that more than cost comparisons alone must be considered in decisions regarding remote sensing data utilization. Reduced costs, though often significant, can only be one way of measuring contributions to the tasks of data acquisition. Other factors and contributions must be considered. In general, there appear to be about five conditions under which remote sensing could make a contribution to data needs of the Council of Governments. These are:

a. More precise data.
b. Easier data update.
c. Verification of current data bases.
d. Source of data otherwise unavailable.
e. Less costly to obtain.

Any one of the first four might outweigh in certain circumstances the cost considerations involved and be of sufficient merit itself to warrant data acquisition by remote sensing techniques. For instance, Montgomery and Fairfax Counties, both within the metropolitan region, have their jurisdictions flown at about two-year intervals in support of general survey needs and for tax-map up-date purposes.

On the other hand, considerations of directness and immediacy of remote sensing data acquisition for single versus multiple program data uses are factors to be reckoned with. For example, the geology and soils of the metropolitan region have previously been mapped. While the underlying geologic structures and features are less subject to change, the surficial characteristics, being more dynamic, are constantly changing. Because of this and the growing urbanization of the region, more detailed analysis of soils, clay formations, sand and gravel deposits, soil erosion, slope surveys, and so on are needed. A variety of remote sensors including side-looking radar supplementing ground surveys could be utilized for data acquisition to produce new information and maps. The question though, is one of cost-effectiveness. Would it be cost-effective for the Council of Governments to plan remote sensing missions soley, to support this kind of information need? It would not. However, as a by-product or as an element in a larger coordinated data acquisition effort, the data obtained might become cost-effective.

This would be the case for many of the applications discussed. By themselves, they ordinarily would not justify the costs required. However, by coordinating the data needs of several analytical programs, the costs to each may be sufficiently reduced to warrant acquisition. This approach reinforces the concept of favorable cost-effectiveness of multi-disciplinary uses of remote sensing data in area-wide applications.

In support of any single dimension of data need, the requirements and priority for the data must be the determining and over-riding factor. In such instances, the data required must not likely to be available from any other source. Examples might be for coverage of an area seriously affected by a damaging natural disaster or for a synoptic overview of an entire metropolitan region, county, or city for a status survey at any one point in time.

Several tables in the study itemized and identified possible, beneficial applications to specific Council of Governments' planning programs and discussed alternate data sources and availability (Table 5); technical requirements of specific sensors (wavelengths, coverage frequencies, scales, etc.) applicable to the data requirements (Table 6); and finally, weighted recommendations for appropriate remote sensing data acquisition and use (Table 7).

7. The seventh, and last substantive study[16] in the series consisted of an enumeration of program planning areas of major concern to the Council of Governments (land use, transportation, water resources, pollution, etc.) and a rationalization of expected data benefits to be achieved in support thereof by the anticipated ERTS-A Program. Data needs related to these programs were translated into observable and measureable parameters to match the expected multi-spectral sensor array of ERTS-A (Table 8), and judgements were provided as to how the collected imagery-derived data would be utilized in the enumerated COG programs. Finally, the study described the anticipated methodology by which the ERTS data would be processed and utilized including tentative thoughts on computerization of results.

During the second or "applications" phase, the project's concern was directed towards providing internal analytical support to specific Council of Governments' planning programs. Several of these are described as follows:

1. The first consisted of providing support to a regional water quality and water run-off investigation. The object of that study was to determine what, if any, relationship existed between the amounts of impervious surface areas (streets, parking areas, roofs, etc.) within certain districts in the region (32 census tracts) and the corresponding population, household, or employment densities within these districts. The population data were available from the Census and other related sources. The information of impervious surface areas was not available in any form; it being necessary therefore to develop it. Available color infrared imagery of the region at 1:50,000 scale and dated

1970, provided the means. Stereoanalysis of the imagery made possible tracings on mylar of the outlines of the census tracts as well as of those areas considered to be of an impervious nature. Then, rather than laboriously measure and total for each tract the areas of the impervious surface areas (total tract area data were available from published sources), recourse was made to use of a digital vidicon image density scanning device.* The impervious surfaces were darkened with opaquing ink, and by contrast against the clear areas within the rest of the census tracts, the scanner distinguished between the two density levels. By means of an electronic planimeter tied into scanner circuit, the ratio (in percentage form) of the areas of impervious surfaces to the total area of each tract was read out and displayed on the console. Considerable time savings were thereby achieved in this analysis. The results, including conclusions as to the sought for relationships and their meaning for water run-off quality analysis, are presently being written up in a paper entitled, Estimation of Imperviousness and Specific Curb Lengths for Forecasting Stormwater Quality and Quantity, by P.H. Graham, L.S. Costello, and H.J. Mallon, being prepared for submission to the Journal of Water Pollution Control Federation, Washington, D.C.

2. The second remote sensing study[17] was conducted in support of the Council of Governments' Open Spaces Planning Program for the region and was concerned with surveying some twenty-two areas comprising about 176,000 acres of open spaces classified by the Council as Areas of Maximum Environmental Quality (MEQA's) (Fig. 21). These areas, generally defined by steep slopes (over 12 %), flood plains, woodlands, and streams, are endangered in many areas by growth pressures and have been recommended by the Council of Governments for protection by local public action. Survey data were required on the extent of urbanizing influences affecting these MEQA's for current status data needs as well as for providing a base for comparison with data from future surveys. The remote sensing project was requested to locate, characterize, and quantify three levels of observed urbanization within these MEQA's: existing, underway, and impending (incipient). The analysis was based upon use of excellent color infrared imagery covering the entire metropolitan region at 1:120,000 scale, dated September 1970, and flown by NASA for the USGS(CARETS Central Atlantic Regional Environmental Test Site) Program. The results clearly demonstrated the unparalled opportunity for such survey work using remote sensing techniques. A sample of the tabulation is shown in Table 9. The study consumed about three to four weeks' time. During discussion in presentation of the results, it was estimated that conducting a similar survey using conventional data acquisition methods might have consumed better than a year's time.

3. The last and most recent study was completed in August 1972 [18] and was undertaken upon request in support of regional growth model input needs. The study applied techniques of imagery analysis for classifying and quantifying land use elements, determining single and multi-family residential unit densities, and developing floor space data on selected industrial, institutional, and commercial livelihood areas, The study covered eight areas within the region representing various levels of urban development: core city, mature developed area, developing area, potential development area, and low density area (Figs. 22 23, 24). At least one district was chosen for each type area. The object of the study was two-fold: (a) to develop data which could be compared with corresponding information from other sources including the Census, the Council of Governments' land use data base, and others (it was felt that such comparisons could fairly rigorously test and measure reliability and consistency of the remote sensing techniques used in this application); (b) to provide data within these districts where none were presently available or were considered unreliable or incomplete. The scope of the study represented a distinct challenge, requiring the application of a variety of techniques involving land use analysis, identification and enumeration of residential units by types, estimating building densities and heights, and measurements of non-residential land use categories and computations of associated floor space areas. For each district analyzed, the cardinal rule of "know the territory" was applied. Windshield surveys buttressed identifications and enumerations. The results, some of which are indicated in Table 10, generally reproduced the comparable and acceptable findings obtained in previous studies where identification and quantification of residential units and land use areas in suburban districts were required. The study also reinforced conclusions obtained in the previous housing study[13] insofar as experiencing limitations in the analysis for identification and quantification of housing units in central city

* Spacial Data Systems, Inc., Data Color Machine, Model 703

or older densely built-up areas (and especially where they contain mixtures of several different land use elements). Definitional problems arose as they related to identifying housing units within areas undergoing or which have undergone material change. The effects of these changes, which have distinctly altered occupancy and housing patterns, will continue to plague the remote sensing analyst in his attempts to develop reliable and definitive housing data within these types of districts. These difficulties were noteably experienced in the analyses of districts in downtown Washington, D.C. and Alexandria, Va. With respect to the determination of the floor space values within the non-residential areas, the comparisons were not always conclusive. There were not sufficient data available from the other sources to allow for many comparisons. In several instances, the analysis revealed data deficiencies in the local source data. In general, however, (except for definitional problems with the analysis encountered in the downtown Alexandria, Va. area), the results were acceptable and are currently being evaluated for model input purposes. As an additional item of interest, it might be noted that during the course of the work, in order to reduce time consumed by interruptions in image viewing to make data notations, frequent use was made of such devices as a manual traffic counter for enumerating building counts and a tape recorder for voice recording of observed density values.

3. CONCLUSIONS

Results to date as to the findings of the project in both the initial investigative and the secondary application phases have shown highly positive results, for the most part, in the study areas, and have demonstrated without any question that regional planning data needs of many kinds (in some instances otherwise unobtainable) can be met from remote sensing analysis functioning in close association with staff planning elements. The "pilot" project at the Council of Governments has developed working relationships in a supporting role with the staff departments, and is presently in position to respond to task requests for needed information support from those departments.

With respect to other priority matters of major concern to the Council of Governments, such as those related to environmental impact (air and water pollution) and area needs for water resource and quality planning, the project must continue to expand its interests, skills, and response capability. Routinization of analytical methodology is required, and most significantly, efforts to develop regional training programs in remote sensing analysis techniques for local planning staffs must be encouraged and implemented.

And finally, the Metropolitan Washington Council of Governments is looking forward with much anticipation to the use of ERTS-1 Program data to extend its investigations of applications in the areas described in the studies and in other related regional planning program areas.

4. ACKNOWLEDGEMENTS

Grateful appreciation is expressed to the Executive Director and all other elements of the Metropolitan Washington Council of Governments whose active and continued interest in this project has made this work and paper possible; and to

The GAP and EROS staffs of the U.S. Geological Survey for their continued interest and support, and for the use of the basic data, without which the work undertaken in this project would not have been possible.

5. REFERENCES

1. Model Local Air Pollution Control Ordinance, Metropolitan Washington Council of Governments (MWCOG), July 1966.

2. Model Plumbing Code for the Washington Metropolitan Area, September 1971.

3. Model Code for the Washington Metropolitan Area, January 1972.

4. Fair-share Housing Formulae, Metropolitan Washington Council of Governments, January 1972.

5. Housing, Policies and Programs for Metropolitan Washington, Metropolitan Washington Council of Governments, 1971.

6. EMPIRIC Activity Allocation Model, prepared for MWCOG by Peat, Marwick, and Livingston and Co., 1969.

7. Preliminary Open Space Plan Program for Metropolitan Washington, MWCOG, 1971.

8. Solid Waste Disposal Study for the Washington Metropolitan Region, prepared by Black and Veatch, Consulting Engineers for the MWCOG, Northern Virginia Regional Planning Commission, and the Maryland - National Capital Parks Planning Commission, 1967.

9. Water Quality Management for Metropolitan Washington - the Northern Virginia Plan (Interim Plan); prepared for the Northern Virginia Planning District by MWCOG, and the Northern Virginia Planning District Commission, April 1972.

10. Mallon, H.J. and Howard, J.Y., 1971, An Inventory of Existing Aerial Photography of the Metropolitan Washington Area, MWCOG, prepared under terms of Contract No. 14-08-0001-12708, Geographic Applications Program, U.S. Geological Survey (unpublished Sept. 1972).

11. Mallon, H.J. and Howard, J.Y., 1971, Land Use Determination by Remote Sensing Analysis, MWCOG, prepared under terms of Contract No. 14-08-001-12708, Geographic Applications Program, U.S. Geological Survey (available as PB 204-246 from N.T.I.S., Dept. of Commerce, Wash., D.C.)

12. Howard, J.Y., 1971, Determination of Land Use Change with the Use of Aerial Photography, MWCOG, prepared under terms of Contract No. 14-08-0001-12708, Geographic Applications Program, U.S. Geological Survey (unpublished Sept. 1972).

13. Mallon, H.J. and Howard, J.Y., 1971, An Assessment of Remote Sensing Imagery in the Determination of Housing Quality Data, MWCOG, prepared under terms of Contract No. 14-08-0001-12708, Geographic Applications Program, U.S. Geological Survey (available as PB 211-380, from N.T.I.S., Dept. of Commerce, Wash., D.C.).

14. Mallon, H.J., Howard, J.Y., and Karch, K.M., 1971, An Examination of Applications of Remote Sensing Data to Metropolitan Washington Council of Governments' Planning Requirements, MWCOG, prepared under terms of Contract No. 14-08-0001-12708, Geographic Applications Program, U.S. Geological Survey, (available as PB 209-684, N.T.I.S., Dept. of Commerce, Wash., D.C.).

15. Mallon, H.J. and Howard, J.Y., 1972, Benefits from Remote Sensing Data Utilization in Urban Planning Processes and System Recommendations, MWCOG, prepared under terms of Contract No. 14-08-0001-12708, Geographic Applications Program, U.S. Geological Survey (available as PP 210-933, N.T.I.S., Dept.of Commerce, Wash., D.C.)

16. Mallon, H.J. and Howard, J.Y., 1972, Proposed Experimental Programs for Testing Remote Sensor Applications in the Metropolitan Washington Area, MWCOG, prepared under terms of Contract No. 14-08-0001-12708, Geographic Applications Program, U.S. Geological Survey (available as PB 207-524, N.T.I.S., Dept.of Commerce, Wash., D.C.).

17. Mallon, H.J. and Howard, J.Y., 1972, Urban Impact on Areas of Maximum Environmental Quality within the Metropolitan Washington Area - A Remote Sensing View, MWCOG, internal report prepared for the Department of Regional Planning (available from MWCOG Library).

18. Mallon, H.J., 1972, Land Use Density Evaluation Study, A Remote Sensing Analytical Methodology, MWCOG, internal report prepared for the Department of Regional Planning (available from MWCOG Library).

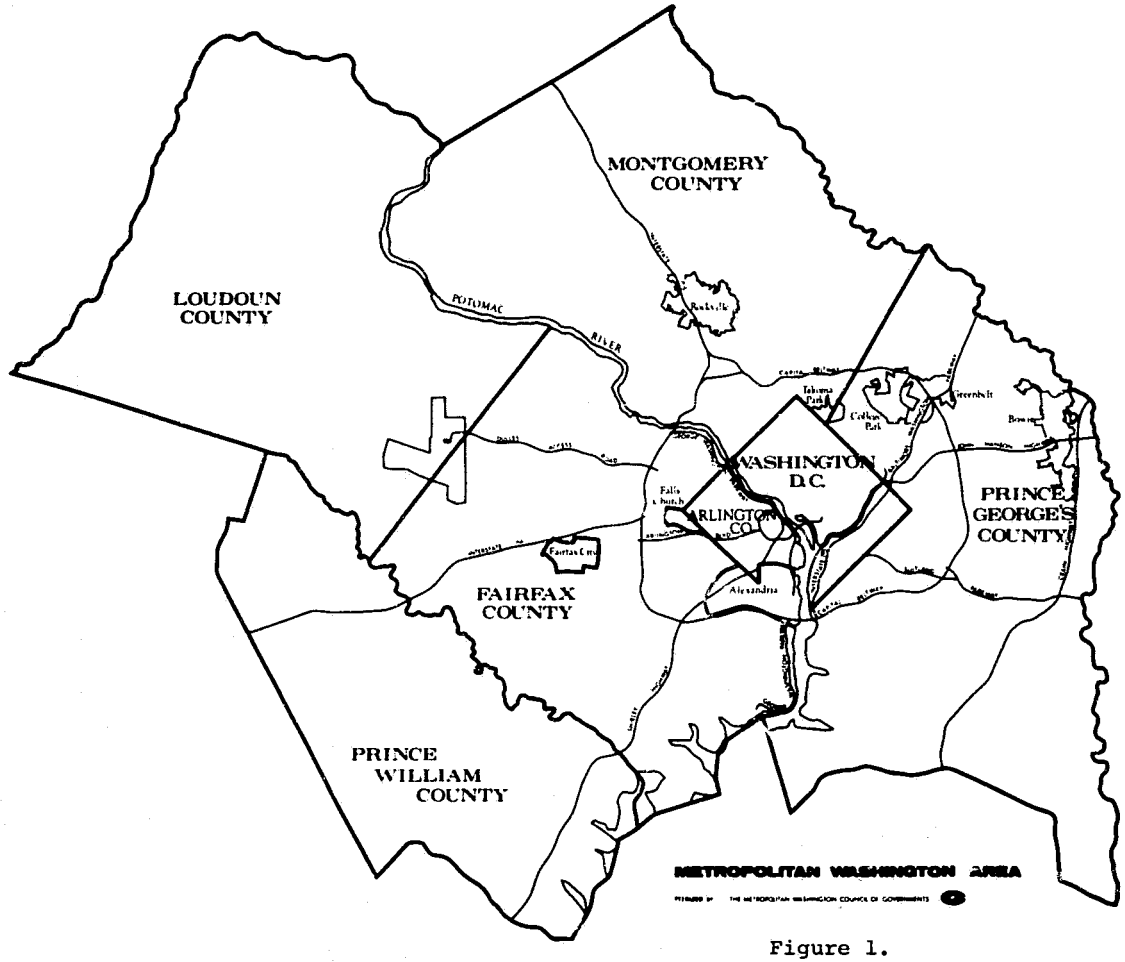

MONTGOMERY
COUNTY
LOUDOUN
COUNTY
POTOMAC
RIVER
WASHINGTON
D.C.
ARLINGTON
CO.
PRINCE
GEORGE'S
COUNTY
FAIRFAX
COUNTY
PRINCE
WILLIAM
COUNTY
METROPOLITAN WASHINGTON AREA

Figure 1.

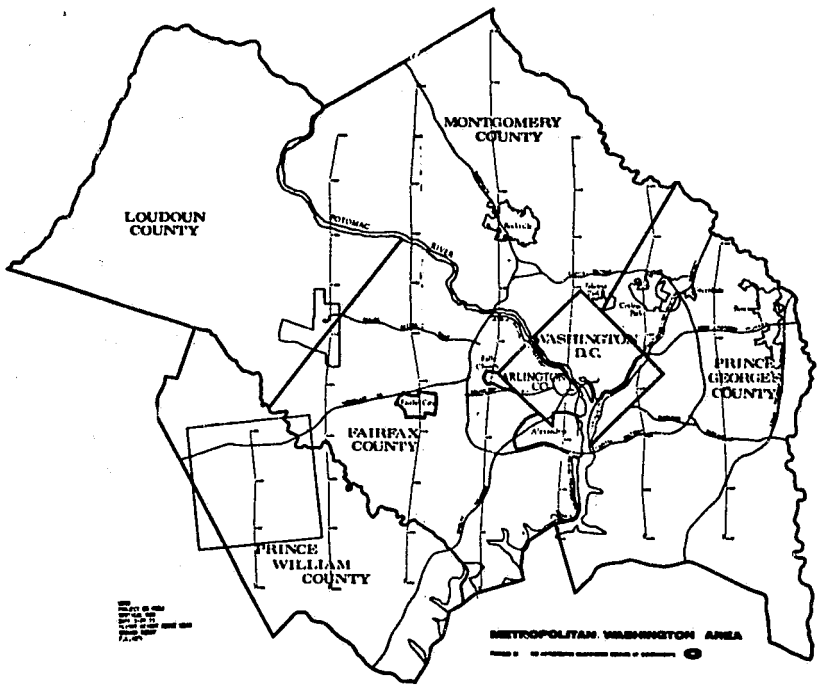


Figure 2. Photo index plot of U.S.G.S. Photo Mission Project GS-VCRJ.

MISSION	DATE	SCALE	FILM TYPE	ALTITUDE (ft.)	CAMERA FOCAL LENGTH (in.)	EXPOSURE (Frame Nos)	REMARKS
GS-VCRJ	3/27/71	1:72,000	Black and White	36,000	6	1/2-1/16, 1/94-1/100, 1/127-1/151, 1/228-1/241 2/231-2/232, 2/287-2/292, 2/351-2/360, 2/368-2/392 2/521-2/524 2/535-2/540 2/A62 3/554, 3/568-3/569, 3/571-3/572, 3/576	Virginia, Maryland, Washington, D.C.

Table 1
COVERAGE DATA, U. S. GEOLOGICAL SURVEY

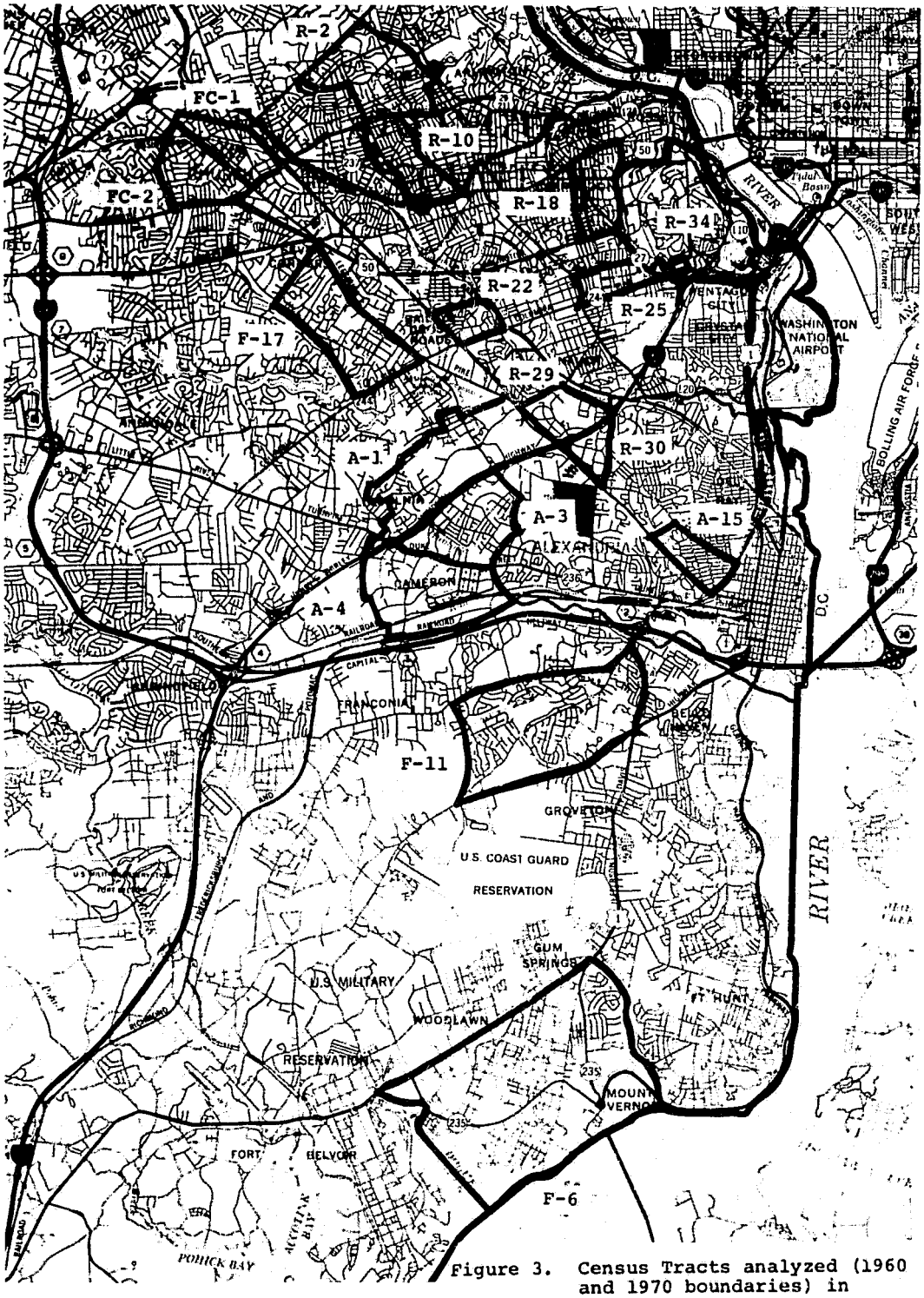


Figure 3. Census Tracts analyzed (1960 and 1970 boundaries) in land use study.

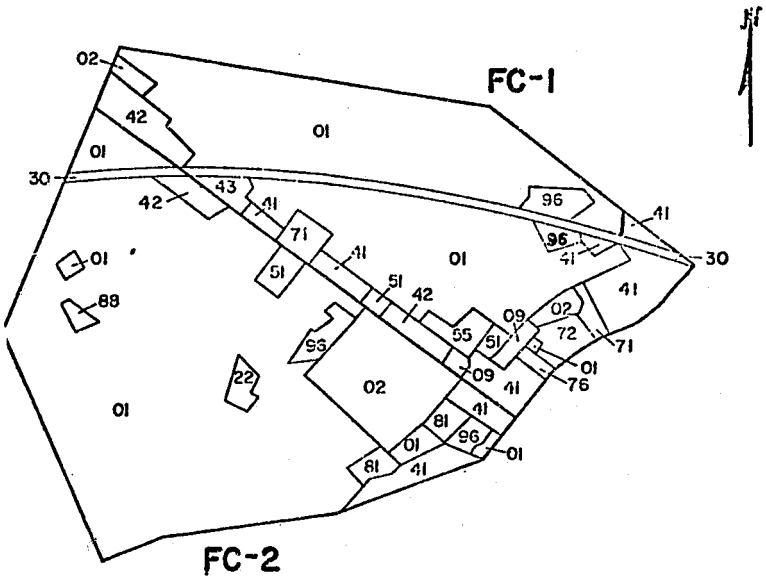


Figure 4. Land use patterns, Census Tracts FC-1 and FC-2, Falls Church, Va.

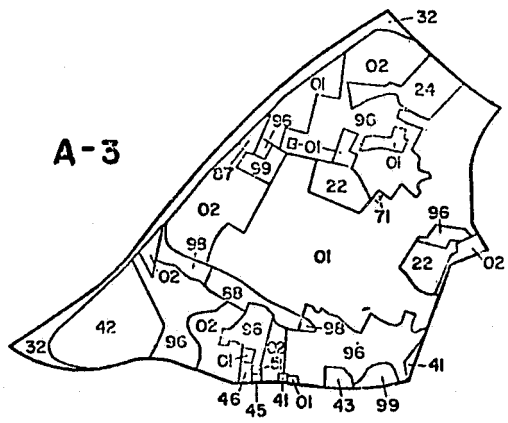


Figure 5. Land use patterns, Census Tract A-3, Alexandria, Va.

Table 2. Land use category data comparisons. Note transportation data.

Land Use Categories*
(Area data expressed in acres)

Census Tract	Data Source	0 Residential	1 Industrial	2 Educational	3 Trans./ Comm./& Utilities	4 Consumer Services	5 Offices	6 Institutional	7 Public Assembly	8 Recreational	9 Undeveloped	Total Tract Acres
A-1	COG[1]	354.9	6.5	0.0	0.0	2.7	0.0	3.1	0.0	0.0	439.2	1006.3
	R.S.[2]	512.8	8.6	22.9	57.1	9.8	3.4	5.7	7.6	0.0	565.3	1193.2
	Diff.	-157.3	-2.1	-22.9	-57.1	-7.1	-3.4	-2.6	-7.6	0.0	-126.1	-186.9
	%Diff.	30.7	24.4	100.0	100.0	72.5	100.0	45.6	100.0	0.0	22.3	15.7
A-3	"	283.4	0.0	0.0	0.0	32.5	0.5	0.0	0.0	5.6	191.1	534.7
		342.1	0.0	49.4	50.3	63.1	1.0	0.0	0.3	14.7	179.2	700.1
		-58.7	0.0	-49.4	-50.3	-30.8	-0.5	0.0	-0.3	-9.1	+11.9	-165.4
		17.2	0.0	100.0	100.0	48.8	50.0	0.0	100.0	61.9	6.6	23.6
A-4	"	139.6	68.5	0.0	1.9	26.0	0.0	0.0	0.0	2.3	671.5	964.1
		115.4	162.2	3.8	29.1	38.4	2.8	104.1	0.0	7.5	551.0	1014.2
		+24.2	-93.7	-3.8	-27.2	-12.4	-2.8	-104.1	0.0	-5.2	+120.5	-50.1
		20.9	57.7	100.0	93.5	32.3	100.0	100.0	0.0	69.3	21.9	4.9
A-15	"	174.9	0.0	0.0	0.0	1.2	0.1	0.0	0.0	0.0	53.9	230.1
		246.3	0.0	4.9	2.8	3.4	1.5	15.3	7.3	1.9	22.5	305.9
		-71.4	0.0	-4.9	-2.8	-2.2	-1.4	-15.3	-7.3	-1.9	+30.4	-75.8
		28.9	0.0	100.0	100.0	64.6	93.3	100.0	100.0	100.0	135.6	24.8

*Metropolitan Washington Council of Governments Land Use Categories

1. COG Land Use Parcel File 2. Remote Sensing

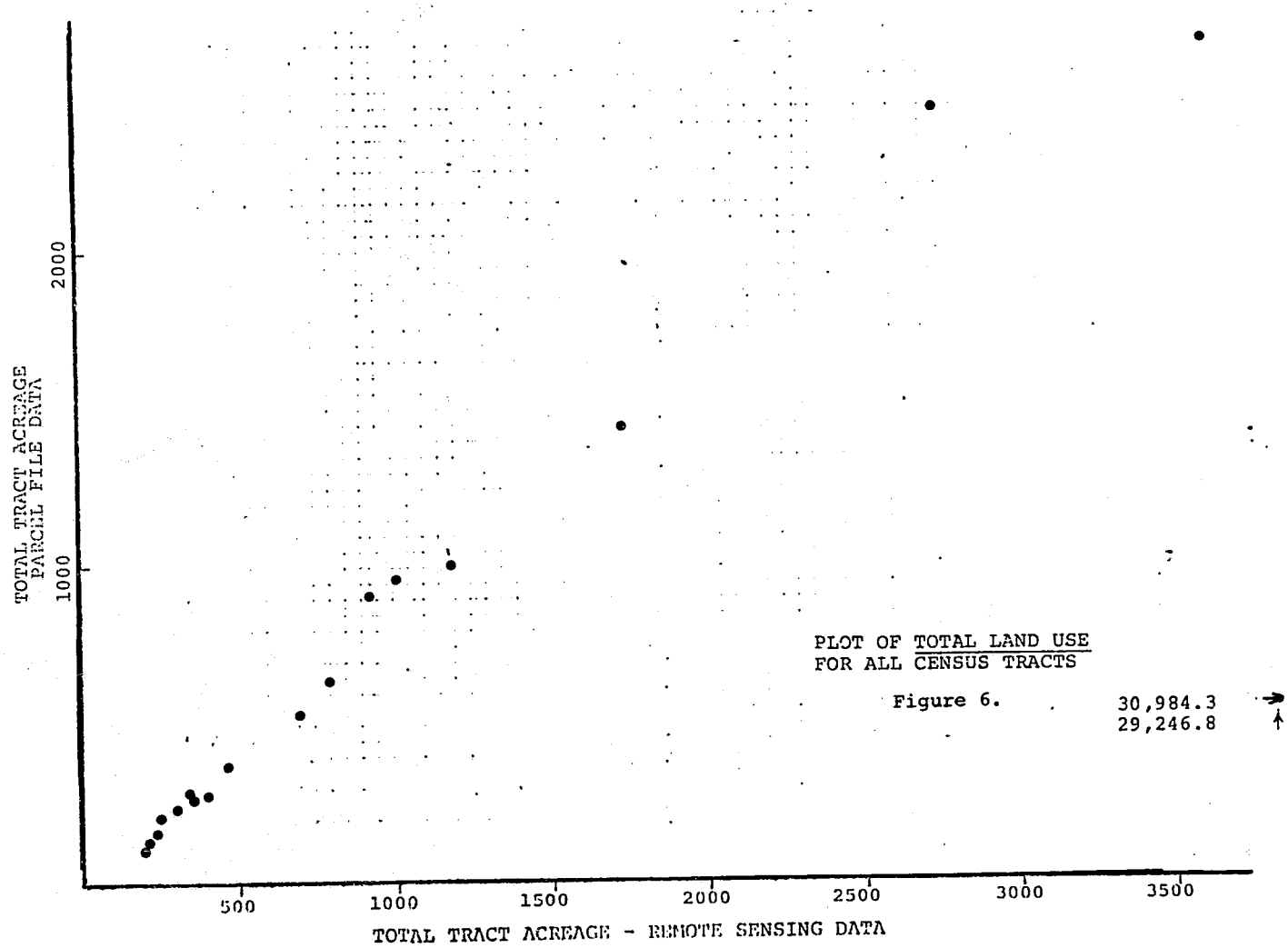
Table 3. Land use category data comparisons. Note educational data.

Land Use Categories*
(Area data expressed in acres)

Census Tract	Data Source	0 Residential	1 Industrial	2 Educational	3 Trans./ Comm./& Utilities	4 Consumer Services	5 Offices	6 Institutional	7 Public Assembly	8 Recreational	9 Undeveloped	Total Tract Acres
R-25	COG[1]	106.3	0.0	12.7	3.8	11.8	1.1	0.0	1.3	1.8	20.1	158.9
	R.S.[2]	143.0	0.0	15.9	10.2	21.3	3.7	39.6	1.4	3.0	9.5	247.6
	Diff.	-36.7	0.0	-3.2	-6.4	-9.5	-2.6	-39.6	-0.1	-1.2	+10.6	-88.7
	%Diff.	25.6	0.0	20.1	62.7	46.8	70.3	100.0	7.1	40.0	111.8	35.8
R-29	"	136.4	49.7	9.8	5.9	26.7	0.9	0.0	2.0	29.9	33.2	288.5
		153.1	43.9	10.2	18.9	58.1	0.0	0.0	2.6	24.6	37.0	348.4
		-16.7	+5.8	-0.4	-13.0	-31.4	+0.9	0.0	-0.6	+0.7	-3.8	-59.9
		10.9	13.2	39.2	68.8	54.0		0.0	23.1	2.8	10.3	17.2
R-30	"	130.6	0.0	8.2	0.0	0.0	0.0	0.0	0.0	0.0	0.0	138.8
		152.6	0.0	8.0	22.3	0.0	0.0	0.0	0.0	10.6	9.5	203.0
		-22.0	0.0	+0.2	-22.3	0.0	0.0	0.0	0.0	-10.6	-9.5	-64.2
		14.4	0.0	2.5	100.0	0.0	0.0	0.0	0.0	100.0	100.0	31.7
R-34	"	19.8	30.4	0.0	0.2	5.5	35.5	2350.0	0.0	0.0	8.2	2499.1
		5.1	107.1	0.0	1190.9	3.4	43.9	811.0	31.1	38.9	511.9	2743.3
		+14.7	-76.7	0.0	-1190.7	+2.1	-8.4	+1539.0	-31.1	-38.9	-503.7	-294.2
		289.0	71.6	0.0	99.9	61.8	19.2	189.5	100.0	100.0	98.5	10.7

*Metropolitan Washington Council of Governments Land Use Categories

1. COG Land Use Parcel File 2. Remote Sensing



PLOT OF TOTAL LAND USE
FOR ALL CENSUS TRACTS

Figure 6.

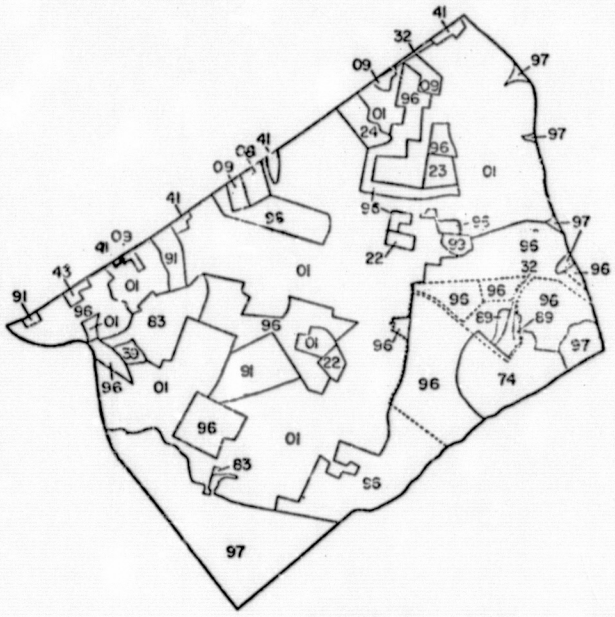


Figure 7. Land use patterns in Census Tract, F-6, Fairfax Co., Va. (based on 1967 imagery).

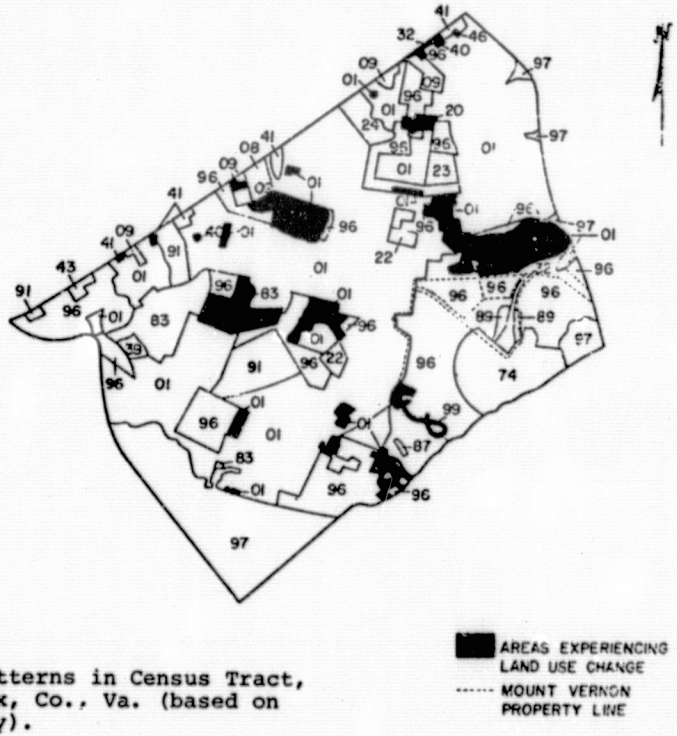


Figure 8. Land use patterns in Census Tract, F-6, Fairfax, Co., Va. (based on 1971 imagery).



Figure 9. Row houses with mixed single and multi-family units (Census Tract 42, Washington, D.C.)



Figure 10. Single-family residential units. Note boarded entry and windows (Census tract 36, Washington, D.C.)



Figure 11. Single-family row house residential units. Note boarded entry and empty lot between buildings. (Census Tract 42, Washington, D.C.)

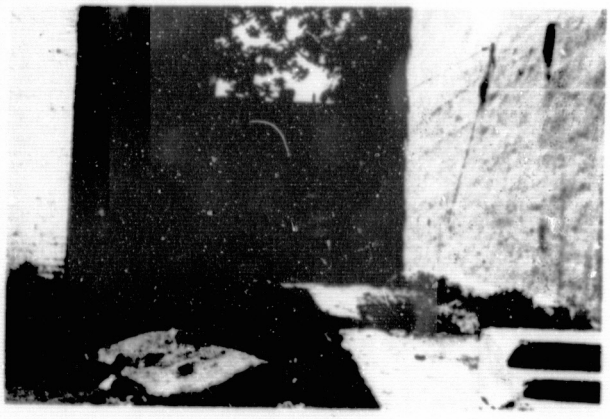


Figure 12. Trash and litter in alley-way, site of removed building (Census Tract 42, Washington, D.C.)

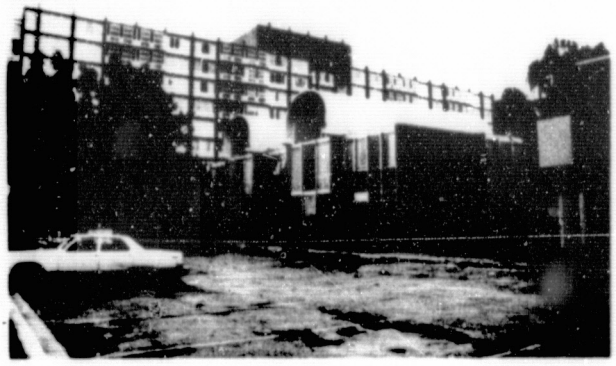


Figure 13. "Dome-type" single-family town houses, SW Redevelopment Area, Washington, D.C. (Census Tract 63).

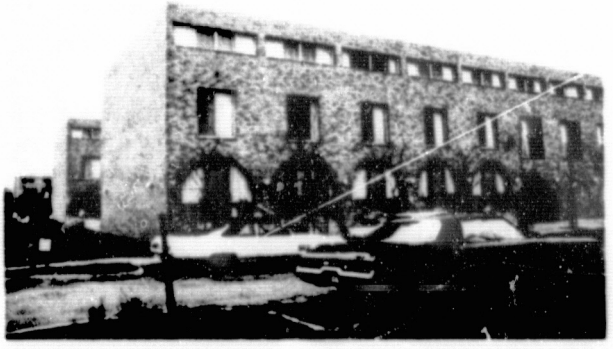


Figure 14. Single-family town house units in SW Redevelopment Area, Washington, D.C. (Census Tract 63).

Table 4.

LIST OF APPLICATIONS OF REMOTE SENSING TO REGIONAL URBAN PLANNING

Areas of Data of Interest to COG	Applications
Natural Features	Geology, soils, slope, flood plains, natural resource deposits, soil mositure.
Transportation	Traffic volume, patterns, movement, and routing, parking and terminal facilities, effect of safety improvements, siting, mapping, synoptic overview.
Land Use	Improvements of land use data in Council of Governments' parcel file, monitoring areas of change and special interest, updating of regional land use maps, historical growth, siting.
Flood	Flood plains, imperviousness, soil moisture, snow cover, runoff retention monitoring, surface water.
Sedimentation	Location and monitoring sources, transport mechanisms, deposition patterns.
Pollution	Monitor water pollution discharges, water temperature and turbidity, oil spills and fish kills, study transport and deposition patterns, locate of air pollution sources, survey air pollution dispersion, study effluent characteristics, monitor treatment plants.
Housing	Identification of housing stock, location, type and structural character. Detection of environmental conditions suggesting quality and condition of housing and neighborhoods.
Miscellaneous	Siting, training, public safety, and aerial photographic availability.



Figure 15. Natural resource status survey. Sand and gravel operations. Note encroachment by residential development. Montgomery Co., Md. (Air Photographics Photo).



Figure 16. Large scale imagery of downtown Washington, D.C. to show use in traffic movement studies. (USGS Photo).



Figure 17. Developing areas in Fairfax Co. and Alexandria, Va. Note variety of land use activities and areas of exposed soils. (NASA/USGS Photo)

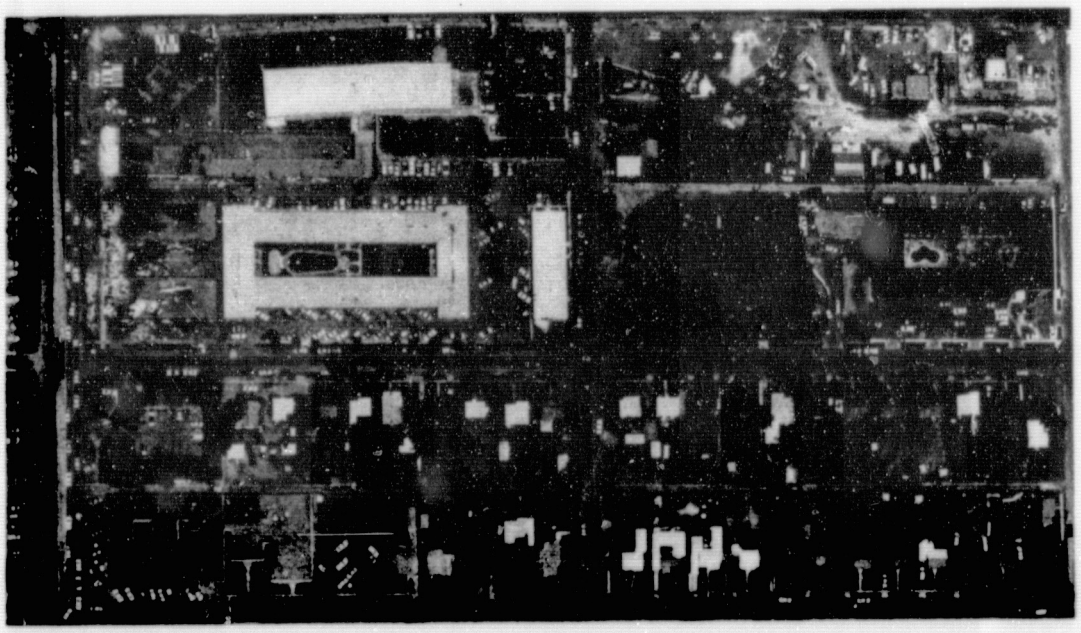


Figure 18. Urban impervious surface areas-streets and parking lots. (NASA Photo).

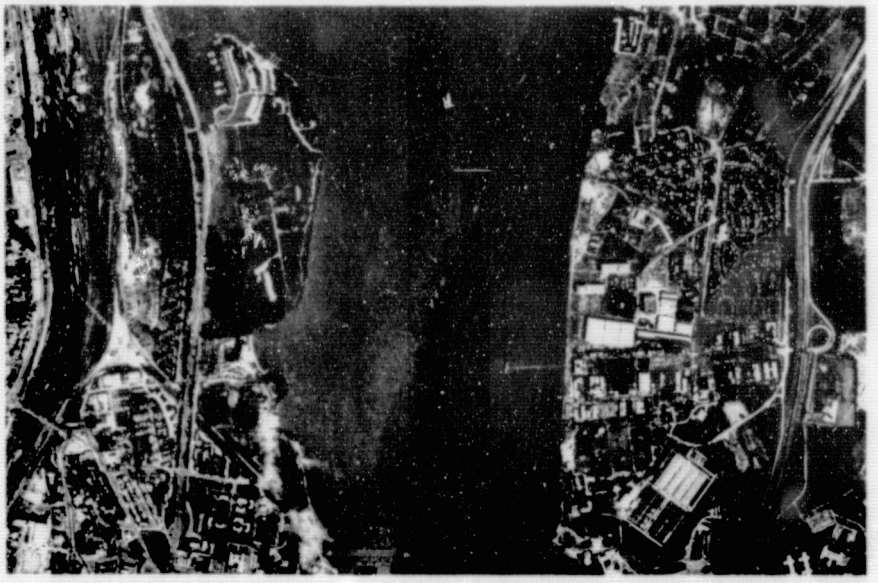


Figure 19. Sewage outfall, smoke and cooling water discharges from thermal power plant, Potomac River, Washington, D.C. Area (USDA Photo).

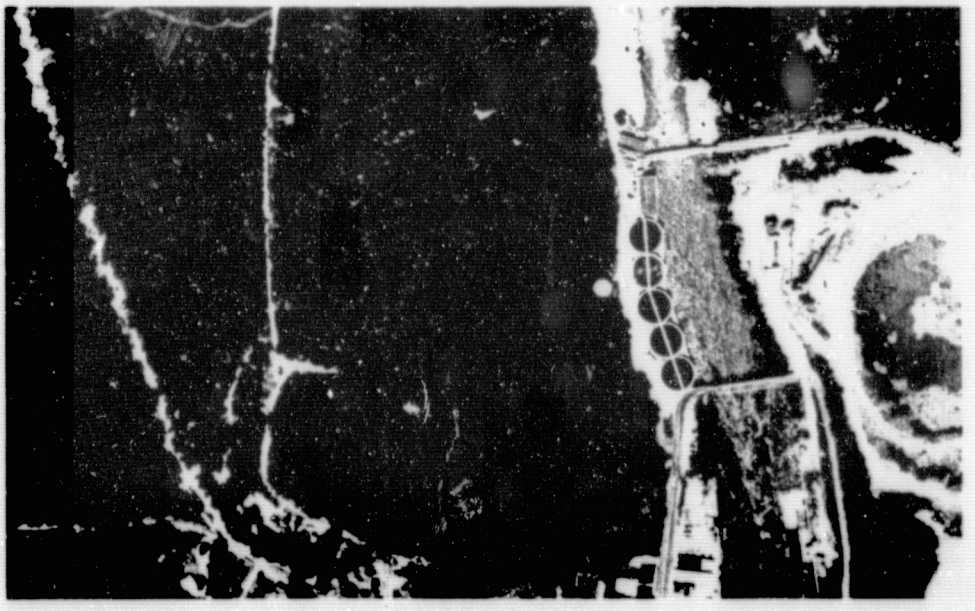


Figure 20. Water treatment plant. Note treatment cells in process of maintenance. Fairfax County Water Authority, Occoquan, Va. (PhotoScience, Inc. Photo).

Table 5.

POSSIBLE BENEFICIAL USES OF REMOTE SENSOR DATA

Application	Program Applicable	Status of the Program	Importance of Data to the Program	Benefits of Using Remote Sensor Data	Current Data Source
1) Improvement of parcel file - locate and assign vacant land.	Improvement of data base	On-going	Would improve base upon which numerous MWCOG programs rest.	Provide improved data base. Verification of current data base.	Local public land records.
2) Regional land use mapping	Regional planning transportation planning	On-going	Basic input to program	Provides easier update. Visual presentation	Parcel file
3) Land use change mapping	Year 2000 Plan	On-going	Proved a visual picture of change and number of acres consumed by development each year. Would demonstrate how area is developing.	A type of data unavailable otherwise.	From local jurisdictions.
4) Update of regional map series	Most of MWCOG's programs	On-going	Provides input and visual display of several categories of data.	Provide easier update and perhaps, therefore, less cost. Synoptic overview.	Aerial photography and field surveys.
5) Monitoring areas of special interest. a. areas of environment quality - designated areas of open space. b. floodplains c. steep slopes d. marshland	Open Space Program Regional Plan	On-going	Provide a means of following encroachment on these areas and possibly indicate need for further controls or action.	Would provide a relatively easy method of following change.	Not gathered as such on these areas.

Table 6. Suggested sensor requirements for data acquisition and use.

Applications	Desireable Sensors	Wavelength ** (microns- μ)	Scale *	Frequency of Coverage	Ease of Attainment and Interpretation
1) Improvement of parcel file	Black and White Color infrared Color	0.4 - 0.7	1:50,000	Annually	Imagery obtainable; interpretation and measurement time consuming.
2) Regional land use mapping	Black and White Color Infrared Color	0.4 - 0.7 0.5 - 1.0	1:300,000	Annually	Imagery obtainable interpretation and measurement time consuming.
3) Land use change mapping	Black and White Color infrared Color	0.4 - 0.7 0.5 - 1.0	1:100,000	Annually	Imagery obtainable; interpretation relatively rapid.
4) Update of regional map series	Black and White Color	0.4 - 0.5 0.4 - 0.7	1:100,000	Annually	Imagery obtainable; interpretation and measurement time consuming.
5) Monitoring areas of special interest			1:25,000 - 1:500,000	Annually	Imagery obtainable; interpretation relatively rapid.
a. open space	Black and White Color infrared	0.4 - 0.7 0.5 - 1.0			
b. flood plains	Black and White Color Infrared	0.4 - 0.7 0.5 - 1.0			
c. steep slopes	Black and White	0.4 - 0.7			
d. marshland	Black and White Color infrared Color Multispectral	0.4 - 0.7 0.5 - 1.0 0.4 - 0.7 0.4 - 1.0			

* Scale values for any imagery analysis are, of course, variable, and are task and experience oriented. Differing scales, larger and smaller, in nearly all cases could be adequate for analysis - image contrast, resolution, and subject activity all considered.

** Wavelengths are given in microns (μ). One micron equals 10^{-4} cm.

Table 7. Summary recommendations for remote sensor use in specific applications.

APPLICATION	CONCLUSIONS and RECOMMENDATIONS	IMPORTANCE INDEX *
1) Improvement of parcel file	Recommended for initiation now. The importance of the data provided outweighs the costs.	1
2) Regional land use mapping	Recommended for now and repeated coverage in future years. Relatively inexpensive. Possibility for use of USGS prepared map should be investigated.	2
3) Land use change mapping	Recommended annually to indicate development of the region, graphic presentation. Could be utilized between available land use maps. Relatively inexpensive.	2
4) Update of regional map series	Merely provide an expansion and improvement of current usage of aerial photography.	2
5) Monitoring areas of special interest	Can be undertaken in conjunction with land use change mapping.	2
6) Location of natural resources	Suggested as a byproduct of any other planned regional flight to provide data otherwise unavailable.	5
7) Mapping additional geologic features	Suggested for incorporation into an existing small scale flight plan.	5
8) Determine average speed over given routes	Not recommended	5

* 1 Highly recommended; 2 Recommended; 3 Suggested

4 Inclusion with existing project; 5 Warranted in special circumstances or rely on other agencies for analysis.

Table 8. Suggested experimental ERTS-A data utilization.

SUBJECT ACTIVITY	WHAT IS TO BE TESTED	PARAMETER TO BE MEASURED	SENSORS	WAVELENGTH microns (μ)	FREQUENCY OF COVERAGE	HOW TO BE USED IN MWCOG PROGRAM
Land Use	Use patterns, change, growth, and associated dynamics	Areas of activity; New development areas: (residential, and others); Open spaces; Livelihood areas; Water areas; Agricultural areas	Multispectral Black and White Color infrared. ERTS-A and pre-ERTS data. (Enlargements and special viewing equipment)	0.4 - 1.0	Quarterly; semi-annually	Regional Planning Studies; Growth prediction studies and models; Impact studies; Land-use delineation maps; Possible parcel-file application. Use of small scale imagery for selective examination of larger scale imagery.
Transportation	Systems spread and layout	Rail routes; highway routes and status of change; Feeder routes; Possibly street patterns Airports, certain facilities	Same	0.4 - 1.0	Same	Transportation route surveys; Use of small scale imagery for selective examination of larger scale imagery
Pollution Water and Air	Detection and location of area and point sources	Discoloration of river and stream courses; Direction and extent of flow, source. Stack gases, haze	Same	0.4 - 1.0	Regularly as feasible	Monitorship, event, detection, followup corrective action programs.

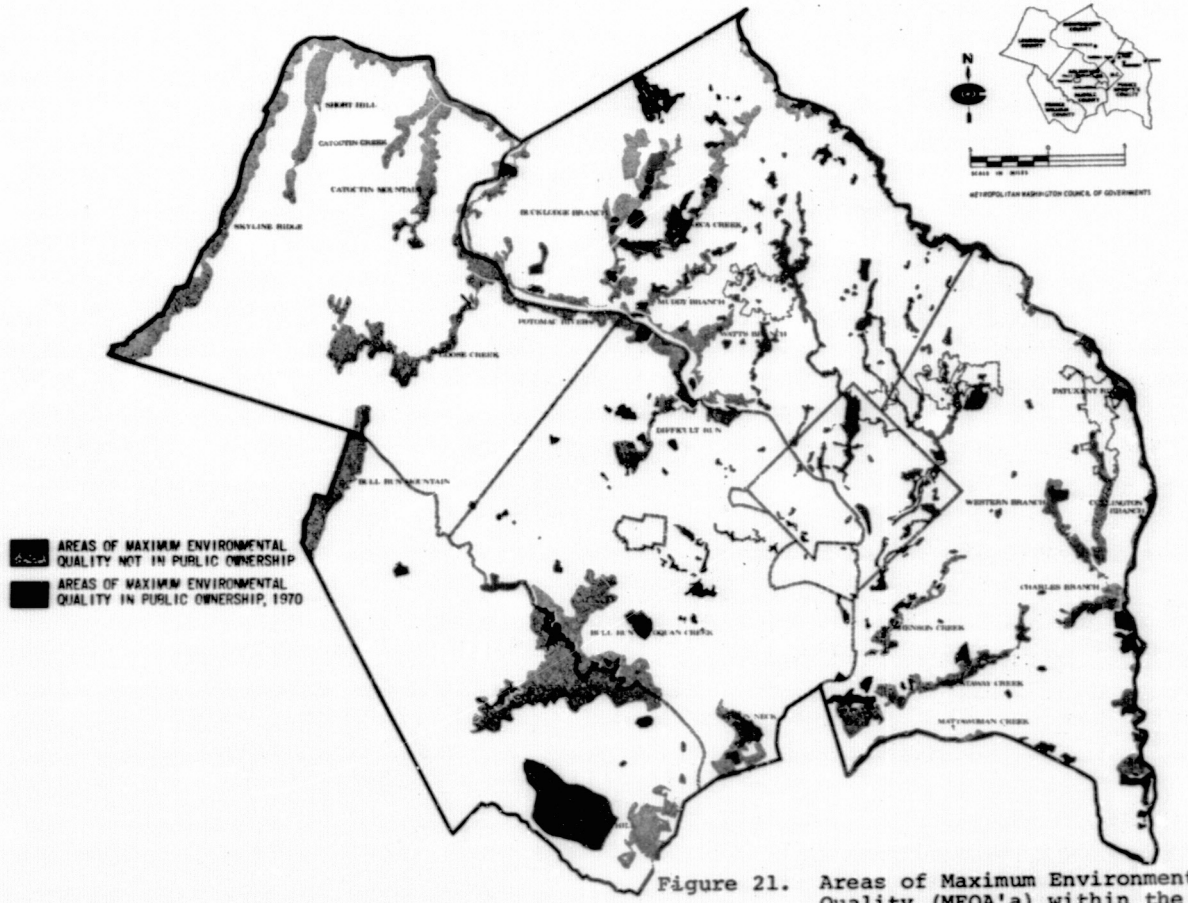


Figure 21. Areas of Maximum Environmental Quality (MEQA'a) within the Washington Metropolitan Region.

Table 9.

EVIDENCE OF URBANIZATION UPON AREAS OF MAXIMUM ENVIRONMENTAL QUALITY WITHIN THE METROPOLITAN WASHINGTON REGION

MAXIMUM ENVIRONMENTAL QUALITY AREA	POLITICAL JURISDICTION	POLICY ANALYSIS DISTRICT*	EVIDENCE OF URBANIZATION FROM REMOTE SENSING
Goose Creek (11,300 acres)	Loudoun Co.	866,867	No evidence. Goose Creek Country Club at N end on Rt. 7.
Bull Run Mountain (7,700 acres)	Loudoun Co.	865	No evidence.
	Pr. William Co.	875	Residential-recreation area (600 acres) along E-central face of MEQA. Roads cut and buildings in area.
Difficult Run (3,900 acres)	Fairfax Co.	656	No evidence along narrow body of Difficult Run. Area (230 acres) of existing roads and low density housing in N portion of MEQA.
		655	Large area (170 acres) of residential development - roads and houses at S tip of MEQA (vicinity of Lake Elsa) - under construction. Evidence of considerable growth pressure on this MEQ Area. From communities between it and the Capital Beltway on the S and E, and also from the Reston developments to the N and W.

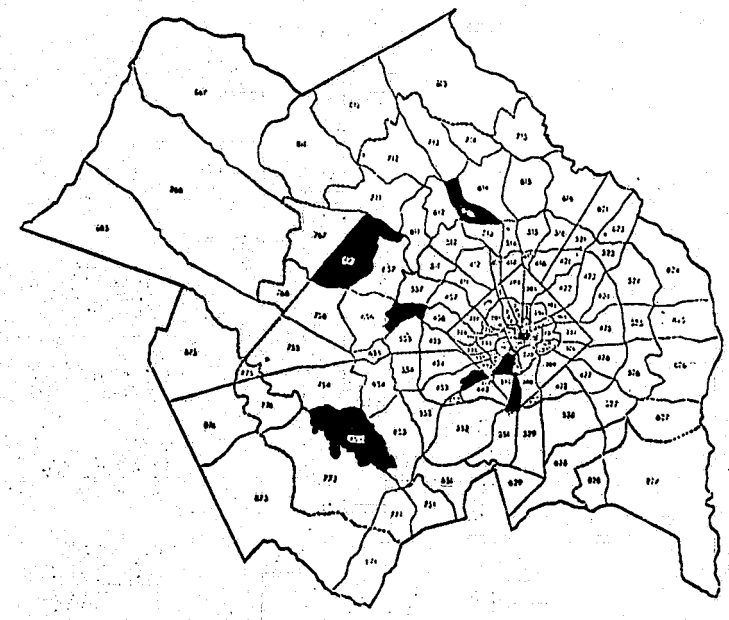


Figure 22. Policy Analysis Districts of the Metropolitan Washington Region. Shaded areas represent those analysed.

REMOTE SENSING DENSITY EVALUATION SURVEY

RESIDENTIAL DATA

PAD[1]	AREA (ft.^{2})	JURISDICTION	RESIDENTIAL UNITS								
			No. Single-family Units (Detached)		No. Single-family Units (Attached)		Multi-family Units				
							Land Use Area (ft.^{2})	Building Area (ft.^{2})	Floor Space (ft.^{2})	No. Equiv Units	No. Units
			R.S.[2]	O.S.[3]	R.S.	O.S.				R.S.	O.S.
006	8,530,000	Washington, DC	5	8	10	No Data					264
232	50,850,000	Arlington Co.	1843	1952	None Visible	"	7,330,000	785,000	5,380,000	6,300	6,147
341	51,350,000	Alexandria	581	2833	1178	"	See	Text	4,130,000	4,900	3,976
443	53,750,000	Alexandria	577	673	150	"	20,000,000	1,700,000	5,600,000	6,600	6,872
556	355,300,000	Fairfax, Co.	1742	1736	35	"	16,800	7,500	22,500	27	85
613	231,000,000	Montgomery Co.	5325	5832	366	"	6,790,000	1,860,000	5,900,00	6,900	5,337
753	721,000,000	Fairfax Co.	442	462	None Visible	"	None	Visible			
737	755,000,000	Fairfax Co.	1395	2217	1202	"	9,080,000	939,000	3,110,000	3,700	975

1. PAD - Policy Analysis District (TPB District, etc.)
2. Remote Sensing Source
3. Other Sources (Census Data, Parcel File, etc.)

Table 10. Remote sensing density evaluation survey--Residential data.



Figure 23. Mature Developed Area.
Policy Analysis District 232,
Arlington Co., Va. and 341,
Alexandria, Va. (USGS Photo).



Figure 24. Developing Area. Policy Analysis District 613, Rockville, Maryland. (NASA/USGS Photo).

APPENDIX

METROPOLITAN WASHINGTON COUNCIL OF GOVERNMENTS

GENERAL LAND USE CATEGORIES

0 - Residential

1 - Industrial/Storage

2 - Educational

3 - Transportation/Communication/Utilities

4 - Consumer Services

5 - Offices

6 - Institutional

7 - Public Assembly

8 - Parks and Recreational

9 - Undeveloped and Resource Use

The COG generalized land use code as proposed by Data Systems has several important new properties:

1. It is hierarchial

2. Education is now a separate category

3. It corresponds closely with URA/BPR and the RMIS Code #1

Use of the most general level of coding (i.e. ending in 0) is permitted for cases when the information is so general as to not allow more specific coding as well as for cases where the information is so specific that no two digit equivalence has been made. An appropriate error message will normally be generated for each assignment to the one digit level of coding.

Blanks will be inserted where a conversion cannot be made to either a one or two digit level.

CODE #1

COG GENERALIZED LAND USE CODE

0 Residential

01 Single Family (including detached, semi-detached, triple-attached and row, plus individual mobile homes)

02 Multi-Family (two or more dwellings in a single building, including apartments and residential hotels)

03 Rooming and Boarding Houses

04 Membership Lodgings

05 Residence Halls and Dormitories

06 Retirement Homes, Orphanages and Religious Quarters

07 Seasonal Housing (including summer cottages and farm labor camps)

08 Mobile Home Parks or Courts

09 Hotels, Motels and Tourist Accommodations

00 Residential, NEC

1 Industrial/Storage

11 Manufacturing and Processing

12 Research and Testing

13 Wholesale, Warehousing and Solid Storage

15 Contract Construction

16 Vehicle Storage - Truck Parking

17 Vehicle Storage - Taxi Parking

18 Vehicle Storage - Bus Parking

19 Refuse Disposal

10 Industrial/Storage, NEC

Educational

21 Nursery Schools

22 Elementary Schools (Grades 1 - 6)

23 Combination of Nursery and Elementary Schools (pre-school through 6)

24 Secondary Schools (Grades 7 - 12)

25 Colleges and Universities

26 Commercial Schools

20 Educational, NEC

3 Transportation/Communication/Utilities

31 Railroad/Rail Rapid Transit Rights of Way (includes terminals)

32 Street and Highway Rights of Way

33 Airports

34 Auto Parking

35 Bus/Taxi Terminals

36 Radio/Television and Telephone/Telegraph Communications

37 Electric Utility

38 Gas Utility

39 Water/Sewer Utility

30 Transportation/Communication/Utilities (includes marinas, pipelines, etc.), NEC

4 Consumer Services

41 Stores

42 Shopping Centers

43 Gas Stations, Auto Repair, Automobile Dealers and Auto and Truck Rentals

44 Repair Services (not auto repair)

45 Personal Services

46 Eating and Drinking

47 Medical and Dental Clinics, Centers, and Laboratory Services

40 Consumer Services, NEC

5 Offices

51 Commercial Offices

52 Professional and Trade Associations

53 Institutional Offices

54 Federal Government Offices

55 State and Local Government Offices

56 Foreign Governments and International Organizations including embassies, chanceries, etc.

50 Offices, NEC

6 Institutional Services

61 Cemeteries

62 Hospitals

63 Nursing Homes

64 Other Health Facilities (except those coded under 47)

65 Police Stations

66 Fire and Rescue Stations

67 Correctional Institutions

68 Military Installations

69 Welfare and Charitable Services

60 Institutional Services, NEC

7 Public Assembly

71 Churches, Synagogues, and other places of worship

72 Civic, social and fraternal associations

73 Libraries

74 Permanent exhibitions, including museums, art galleries, monuments, planetaria, aquariums, and urban historic sites

75 Sports and miscellaneous assembly including stadiums, auditoriums, recreation halls, etc.

76 Entertainment assembly including theaters

70 Public Assembly, NEC

8 Parks and Recreation

81 Indoor recreation, including recreation centers, indoor swimming, gymnasiums, ice and roller skating rinks, bowling, and penny arcades

82 Outdoor amusements, including fairgrounds, race tracks, go cart tracks, miniature golf, golf driving ranges, and amusement parks

83 Private Outdoor Recreation, including tennis, swimming, country clubs, and yachting clubs, limited to members and guests

84 Commercial Outdoor Recreation, including resorts, riding academies, ski runs, organized camps, and marinas

85 Public Golf Courses

86 Play lots, playgrounds and playfields

87 Outdoor Courts and pools open to the public (tennis, basketball, swimming, etc.)

88 Parks - Leisure and ornamental

89 Parks - general recreation, including individual camping and picnicking as well as areas for the enjoyment of nature, including zoos, botanical gardens, arboretums and national parks

80 Parks and Recreation, NEC

9 Undeveloped and Resource Uses

91 Agriculture and Related Activities

92 Forestry Activities and Related Services

93 Mining Activities and Related Services

94 Permanent Conservation Areas

95 Other Resource Production and Extraction

96 Undeveloped and Unused Land Area

97 Water Areas

98 Vacant Floor Areas

99 Under Construction

90 Undeveloped and Resource Uses, NEC

THE ROLE OF EARTH RESOURCES SATELLITE TECHNOLOGY IN ECONOMIC DEVELOPMENT

M. W. Conitz

University of Idaho
Moscow, Idaho

ABSTRACT

While earth resources observation systems employing satellite platforms offer the potential for raising the management of the world's resources to a level of sophistication never before possible, there are many problems of a non-technical nature which must be solved before this dream becomes a reality. Many of these non-technical problems relate to the capacities of the nations of the world, particularly the developing nations, for utilizing the data. An analysis of these capabilities paralleling the development of the hardware may lead to significant improvements in methods of interpreting and distributing data that will have a lasting benefit for mankind.

International interest in satellite systems for the monitoring of resources has centered largely around the needs of the developing countries of the world. Most developing countries are heavily dependent upon resources and at the same time have the poorest facilities for monitoring them. Despite this interest in the possible participation of developing countries, very little is known about their capabilities for utilizing the data. The United Nations World Plan of Action suggests that "In space application systems of the present and foreseeable future, most often the real obstacles that need to be overcome before a country can fully benefit from the system do not lie in the space segment, but in the ground system."

The purpose of the study summarized here is to analyze the potential for the utilization of earth resources observation systems in a typical developing region. It has been hypothesized that there are four chief areas that need to be examined in evaluating this potential. These areas are natural resource potential, human and physical resources, national organizational structures and the potential for regional cooperation. To test this hypothesis, these four indicators have been studied in the East African countries of Ethiopia, Kenya, Somalia and Tanzania. This group of countries appears to contain most of the needs, applications and other variables that might be found in a similar regional grouping elsewhere in the world.

A study of resource potential is a logical first step in evaluating potential participation because resource potential is an important indicator of how seriously a country might wish to pursue the implementation of a resources observation program. As observation systems approach the operational stage, the countries considering participation will demand increasingly refined cost-benefit studies. A knowledge of resource potential is essential in order to eventually quantify the benefits of participation.

Physical and human resources must also be known before intelligent decisions on participation in a program can be made. Unless a country possesses adequate technical skills and facilities, there can be little immediate benefit from participation. Since few developing countries have these skills and facilities, it is also necessary to evaluate their potential for developing or purchasing them.

Regardless of how well endowed a nation might be with natural resources and human technical skills, it must also have the capability of developing the infrastructure necessary to make an earth resources observation system effective. Such a system will require a high degree of interdisciplinary cooperation and the participation of most of the major departments of a government. Many complex interrelationships must be developed in order to speed the flow of data and to interpret them for practical use. While a resources observation system is designed to collect resource data and not to develop resources, there must also be some evidence of capability to carry out resource development to make investment in such a system worthwhile.

Perhaps the greatest challenge to the effective implementation of a system lies in the

Preceding page blank

development of regional cooperation. If a global operational system is designed around a network of regional readout and data processing centers, as has been proposed, the world will be divided into some fifteen to twenty-five regions for data distribution. Unless these regional centers are completely funded and staffed by some aid agency, a prospect which is highly unlikely, a degree of regional participation and cooperation will be required that so far has been unknown anywhere in the world. There must be financial cooperation in developing and operating the centers; there must be relatively free exchanges of skilled personnel; concerns for the sensitivity of the data must be overcome; certain political restrictions on the distribution of data must be overcome or modified; and observation activities must be identified as primarily national or regional in scope, to list only a few of the problems confronting the concept of regional participation. Furthermore, the nature of the technology requires that this cooperation be achieved within geographic rather than political or economic blocks as in the case of economic cooperatives. In other words, successful implementation on a regional basis will require the cooperation of all nations within a given geographic region regardless of whether or not they are politically compatible or at the same level of economic development.

Because of the limited time available for this presentation, I would like to concentrate primarily on regional cooperation as one of the four mentioned indicators of capacity. It has been suggested that among the several ways of distributing data from satellites to the countries of the world, a series of regional readout stations, such as we now have in North America, might be the most feasible. Using this as an assumption and East Africa as a study area, I have examined some of the advantages and potential hazards of this kind of organization.

In addition to the technical details of data handling and the economies of scale, there are many advantages of regional organization for resource surveillance. It has been proposed by FAO and others that the developing countries might profit most from regional centers where the data could be interpreted as well as collected and processed. It is well-known that most developing countries are critically short of the kinds of skills needed to interpret resource data and, in addition to interpreting data, regional centers might be especially effective in training interpreters.

Before these advantages can be realized, however, there must be substantial regional cooperation. In order to assess the potential for regional cooperation, more must be known about the character of surveillance activities and about the needs, attitudes and resources of the participating countries. Generally speaking, surveillance activities can be divided into two categories, those which are intermittent in nature and those for which continuous observation is required. Those surveys which need to be performed only intermittently are usually those which are designed to acquire a data base such as a soil map or a land-use map. As you know, the primary advantage of satellite systems is their ability to provide continuous surveillance economically. Certain types of surveys such as soil moisture studies, analyses of surface water distribution, agricultural crop monitoring, pollution detection and others require continuous surveillance on a daily, weekly, monthly or annual basis.

The significance of classifying surveys as intermittent or continuous is that it helps distinguish which kinds of surveys can be performed successfully at the regional level and which are primarily national in character. Most intermittent surveys are less likely to contain confidential data; they can be reported in such a way that they are useful to persons not versed in remote sensing, as in the case of a land-use map; and they can often be carried out by teams of experts from outside the country when there is little or no national capability in remote sensing. Thus most surveys which are performed intermittently could be conducted successfully through centers serving a multi-national region.

Despite the assertion that an earth resources survey system based on the use of satellites will be a global and regional enterprise which will supersede national boundaries, it must be recognized that there are certain functions which are responsive only to national policies, which produce data that may be confidential in nature, and which can only be performed effectively by local personnel. Most of the surveys which must be performed continuously fall into this category. While most developing countries are willing to accept base data surveys conducted by foreign experts they are becoming increasingly reluctant to depend on foreigners for day to day activities. Thus in proposing the establishment of regional centers with interpretative capabilities it is desirable to first classify all potential remote sensing operations as national or regional in order to determine whether there are a sufficient number of regional applications to justify the expenditure. It is perhaps paradoxical that continuous surveillance activities, which are most suited for satellite systems organized regionally are those which require greater local capabilities, while many of the intermittent type surveys are as well or better suited for aircraft programs which can be implemented on a country by country basis more easily than satellite programs.

Another factor which is likely to influence the success of the development of regional centers is the level of development of the participating countries. An examination of conditions in East Africa has revealed that there are considerable differences in the levels of development of the

various countries and consequently similar differences in their capacities for the use of remotely sensed data. Based on conditions in some of the least developed of these countries, it is not unreasonable to expect that it may be ten to twenty years before their capacities reach the level where the benefits of participation in a regional program will equal the costs. The question then is, if regional centers prove to be the most feasible method of disseminating satellite data, should a region such as East Africa wait until all countries are sufficiently developed to utilize these data effectively before embarking upon the development of a regional center? The answer that first comes to mind, of course, is foreign aid for smoothing out these irregularities in levels of development. While this may be a partial solution, foreign aid experts tell us that countries, like people, tend to appreciate and use things that they have to pay for and perhaps sacrifice for. Thus while aid and technical assistance may make possible the development of regional centers, they will not insure effective participation by all of the nations of a region.

The final question I would like to raise with regard to the implementation of a satellite program on a regional basis is what effect will political differences have on this implementation? East Africa is as politically diverse as perhaps any region of the world, but still there is evidence that a sufficiently receptive climate for cooperation in remote sensing exists. The East African Community, made up of the former British Colonies of Kenya Uganda and Tanganyika administers a variety of common services, many of which are primarily technical in nature. Even during the recent trouble between Tanzania and Uganda the communication and research services of the Community have continued to function. If the Community should be expanded, as expected, to include Somalia, Ethiopia, Zambia and others, the Community could become a model of administrative framework for the introduction of regional remote sensing systems. Even in regions where there are not strong economic ties, it must be remembered that remote sensing is a technical activity which, except for the possible political sensitivity, could probably be carried out effectively among nations having political differences. In East Africa, as well as in other regions, there are examples of international technical activities which can exist in politically diverse climates.

In summarizing, there are economic, social, political and administrative problems which may be more critical to the implementation of world wide remote sensing systems than the technical ones. I have attempted to point out a few of these problems under the assumption that regional cooperation may be necessary for the introduction of this technology into the developing world. The fact that there are no clear-cut answers to these non-technical problems serves to illustrate that a great deal more study is needed to parallel the development of the hardware. The problems of regional cooperation alone suggest that attempts should be made to explore alternatives to regional centers for the distribution of data to the developing nations. The question of whether this distribution of data is accomplished through technical changes or through improved regional cooperation is less important than the fact that resource data are needed urgently to help stimulate economic development.

THE APPLICATION OF REMOTE SENSING TO LOCATING AND MONITORING UNDER-UTILISED LAND IN JAMAICA

W. Gordon Collins
University of Aston
Birmingham, England

ABSTRACT

This project is a pilot study of the existing land use of the parish of St. Catherine, Jamaica, which covers an area of approximately 500 square miles. Apart from three months' field work spent in compiling a key, the land use data was obtained entirely from the interpretation of aerial photographs. Over 30 land use maps were produced at a scale of 1:12,500 showing 21 different crops or land use types.

Use was made of the report and maps of the soil survey produced by the Regional Research Centre, University of West Indies. From this soils information the land capability of every soil/slope combination was determined and mapped, so that direct comparisons could be made with the land use maps which had been compiled. This map comparison of actual and potential land use reveals those regions where the land is not being fully utilised, and a set of 1:12,500 maps was compiled to show the precise extent and location of these under-used areas. These maps show where improvements are most likely to be made, and will, it is hoped, serve as a useful guide to those responsible for the development of land resources on the island.

Preceding page blank

1. INTRODUCTION

"Urban unemployment in the developing countries ..... is a threat greater than hunger in the next decade. The only solution, and even that is but a partial one, lies in agricultural development."[1] This is the theme from one of many reports which emphasises the importance of rural development in the developing countries.

In spite of the substantial financial aid given to the agricultural sector in Jamaica over the past twenty five years, it is still not meeting the agricultural needs of the country, and substantial quantities of food, much of which could be grown locally, are imported - to the detriment of both the employment prospects and balance of trade figures. There are a number of reasons for this; historical, social, economic and political, and the simple fact that much of the essential data required to formulate potentially successful land use policies have not been collected or presented in a suitable form.

One of the main aims of this study was to develop and test a suitable method of acquiring and presenting some of this essential land use information. This paper deals with that part of the study concerned with the use of aerial photography as a source of land use information, and the methodology of using this information to locate and map the extent of under utilised land in the Parish of St. Catherine, an area of about 500 square miles of Jamaica.

2. COMPILATION OF THE AIR PHOTO KEY

In order to map the land utilisation it is necessary to compile a key, using symbols, numbers or colours to represent the various land use types. The International Geographical Union (IGU) in its Report[2] on the Commission on World Land Use Survey has drawn up a classification of land use types which it suggests as a basis for all land use mapping (Figure 1).

In so far as it is applicable this classification has been used but, because the mapping for this project has been carried out at a scale of 1:12,500, considerably larger than that envisaged by the Commission it has been necessary to enlarge and modify the key they suggested.

In the World Land Use (IGU) Classification, cropland is dark brown, but both rice and sugar are included under this heading, so different shades of dark brown were used for these two crops, thus they are distinguishable as far as this study is concerned, and should it be required to abstract this information for mapping at the smaller scales suggested, by the IGU for National Land Use Studies, then the similarity of the two colours makes abstraction a very quick and simple task. A similar procedure was adopted throughout.

Where an area is being used for two or more crops, or where two or more distinct land use types are apparent, the area is classified to show both, and diagonal bands of the appropriate colours are used. No attempt is made to show, or even determine, to what extent one of the crops or land use types is dominant, and the coloured bands are all of equal width.

The very first stage in the production of the land use map was to compile a list of all the main crops and land use types that exist in the parish, and to determine which of these would be readily identifiable on the aerial photographs: e.g., both coffee and cocoa are grown under a variety of shade cover and would most likely be classified as dense woodland, and certain tree crops such as Pimento, Guava, Ackee, Breadfruit, etc., would not easily be recognised as they generally grow as isolated trees in mixed food forest areas.

The key shown in Figure 2 was compiled and used initially, although it was realised that some modification might be necessary as the work proceeded. Indeed, at quite an early stage, it was decided to have a single unqualified item for Grassland. The reasons for this were that, except in some Government agricultural schools and stations, there was virtually no "improved" grassland as defined in the IGU classification, and it was thought that the best way of determining whether the grassland was "used" or "unused" was to indicate whether or not it had reverted to lowland scrub (a speedy process under Jamaican climatic conditions).

Some field work was carried out to annotate selected aerial photographs to show examples of each land use type included in the key. These were subsequently used as references when carrying out the land use mapping of the whole area.

3. COMPILATION OF LAND USE MAPS

The author then returned to England to complete the project. The 1:25,000 vertical black and white aerial photographs were systematically scanned and the land use information was recorded on trace overlays. These were then put into a sketchmaster and the land use information was transferred to a set of thirty two 1:12,500 scale base maps (compiled by radial line methods).

As the work proceeded the completed maps were sent to Jamaica for both random and selective field checking.

The accompanying aerial photograph (Figure 3) shows part of the parish of St. Catherine. The superimposed numbers indicate the existing land use in relation to the key, and it can be seen that some of the land use types can be identified even at this reduced scale. Because the key was compiled on the basis of what crops and land use type were visible on the existing aerial photographs, few problems occurred in their interpretation. In some instances it was necessary to obtain a field check on the photo interpretation, e.g., in one of the coastal areas the air photo showed what looked to be an extensive crop of young sugar cane right in the middle of the salinas! A request was made to field check this apparently odd situation where it was found that one of the sugar plantations had put in this sugar crop to determine whether it would grow under such saline conditions. It is highly unlikely that this plot would have been discovered had the surveys been carried out by ground methods.

Although there were not many interpretation problems, care had to be exercised in carrying out this task. For instance, sugar cane exhibits a very wide tonal range on the aerial photograph; from white when newly cut, going deeper grey with continued growth, and near black when ripe. At certain stages of its growth it could be confused with the banana crop: the main distinguishing factor in this instance is in the subtle texture differences of the photo images of the two crops. In its early stages of growth, rice might be confused with grassland, but there are several distinctive features of a rice area. There is the evidence of irrigation channels and bunds, and the small circular patterns which result from the threshing practices. Also the rice fields are kept clear and clean of any other crops or vegetation.

The aerial photographs used for this study were taken during the month of April, by which time all the tobacco crop had been harvested. This meant it was not possible to locate the tobacco fields by direct identification of the crop. It was still possible however, to map the tobacco areas because almost without exception a drying shed stood in every tobacco field. In those few instances where a field was without a shed, it was generally possible by a process of elimination to restrict the field in question to being one of either tobacco, grassland, or cleared land as it was unlikely to be confused with the other classifications used in the key. In the very few cases where there was any doubt it was mapped as – Cleared Land 70.

Some of the better grasslands in Jamaica have a shade cover of open woodland. Field checks reveal that some areas which were utilised solely as grasslands had been mapped as Open Woodland, 51. It is of course highly likely that most of the areas mapped as open woodland are being utilised as pasturelands, and this should be borne in mind when studying the distribution patterns involved under these headings.

In some areas where horticulture and food forest predominate, there is a tendency for the farm to produce, in addition to the usual range of mixed crops, one or more particular crop as a form of specialisation. Some smallholdings devote a considerable amount of the total area of their farm to, say, sugar or citrus: in such cases a dual classification has been entered on the map. Thus 22/53 indicates a smallholding in which sugar cane occupies a special importance in what otherwise would be a mixed crop farm.

Figure 4 shows, at a reduced scale, one of the completed land use maps. These maps were produced at scales of 1:12,500 and 1:50,000 in both black and white and colour.

3.1 LAND CAPABILITY

There exists a detailed soil survey of each of the thirteen rural parishes which, together with the urban parish of Kingston, cover the entire island. Soil maps were compiled at scales of 1:12,500, 1:25,000, and 1:50,000 of the parish of St. Catherine, and these are accompanied by a Report.[3]

The 1:12,500 soil maps indicate the soil type, degree of slope and the erosion condition. In addition, the soil report contains a list of recommended crops for each soil type, recommended cultivation practices for each soil/slope combination, and a Land Capability classification which takes into account the soil/slope/climate combinations. With this information, it is possible to convert all the soil/slope units (shown on the 1:12,500 soil maps) into Land Capability units.

Trace overlays were drawn of all the original 1:12,500 soil maps; Figure 5 is a simplified map which shows only the soil boundaries. Every soil/slope unit was converted to a Land Capability class unit and the recommended crop for that particular soil unit was also taken into account. Thus, although these trace overlays indicated the soil units, they were used as a basis to show the land potential of these units.

3.2 UNDER UTILISED LAND

As both "existing land use" maps and "land capability" maps were compiled on the same 1:12,500 series of base maps, it was an easy matter to make a direct comparison between them. This comparison of "actual" and "potential" land use revealed areas of both "under" and "over" utilisation, though only the former were mapped.

The 1:12,500 scale "under utilised" land maps (Figure 6) assist in determining the requirements for improvements at local level. In order to study the regional pattern, a map was compiled of the entire parish at a scale of 1:50,000 to show the location, extent and associated soil type of under utilised land. Figure 7 is a reduced-scale copy of this map, and shows the parish divided into four distinctive regions:

(1) The non-limestone uplands

(2) The limestone uplands

(3) The interior basin

(4) The southern plains

3.2.1 The non-limestone uplands

None of the areas comprising this region show any under-utilisation; on the contrary the dominant occupation of these soils is Food Forest and there is evidence of an over-intensive utilisation of the land. These uplands are composed mainly of metamorphosed shales and deeply weathered granodiorites, and the combination of steep slopes, friable soils and unsuitable farming methods result in extensive soil erosion which urgently needs to be checked by the introduction and extension of suitable soil conservation practices.

3.2.2 The limestone uplands

The southern outcrop of this rock occurs in the driest part of the parish and is entirely Limestone Scrub with virtually no opportunity for agricultural development. In the very extensive northern outcrop the situation is slightly better: the rainfall is greater and reasonably fertile soil occurs in isolated pockets. Some of these are capable of improved use, though much of the area is in Food Forest where near subsistence farming occurs over thinly soiled steep slopes giving rise to extensive soil erosion. Here also the emphasis must be primarily on soil conservation.

3.2.3 The interior basins

Most of the "under-used" land in this region is found in the largest interior basin of St. Thomas ye Vale between heights of 250 and 1000 ft. Rainfall is generally adequate throughout, and the under-used areas, which vary considerably in size and location, seem to be mostly on the reasonably fertile Linstead Clay Loam which suffers from drainage and erosion problems.

3.2.4 The southern plains

It is here that most of the under-used land in the parish is found, and this occurs almost entirely on the Old Alluvial soils (4b), though some swamp and salina areas in the extreme east are affected.

The plains can be divided into three zones: (i) eastern, (ii) central and (iii) western, all of which lie below 250 ft., and experience a low rainfall with a long period of drought.

(i) Much of this eastern division is fertile Recent Alluvium (4a) which is served by the waters of the Rio Cobre irrigation system and local wells, hence it is the most intensively cropped part of the parish with little under-used land. Considerable improvements have been carried out during the last few years as is evident when comparing the various sets of aerial photographs taken since 1951: these improvements are particularly striking in the salina and swamp lands.

(ii) The central zone which is served in part by the irrigation system, has more under-used land than the eastern zone, primarily because it consists entirely of Old Alluvium (4b) which tends to be saline, and which has drainage problems.

(iii) The western zone is where most of the under-used land of the southern plains is to be found. This is currently under woodland, grassland, and some lowland scrub. These extensive areas are also composed of Old Alluvium (4b) and here in the extreme south-west of the parish, where the rainfall is less than 50 in. per year, there is between six and eight months of drought each year. Under these conditions irrigation is essential for crop growth.

There is also the problem that many of the soils in this area are naturally wet and create difficulties in drainage. Added to these problems of drought and drainage is that some of the soils tend to be saline. However, the land is very flat, and the soils reasonably deep: conditions which lend themselves to mechanised methods of improvement.

In spite of these conditions there is considerable scope for improving land use, though this is completely dependent on obtaining an adequate supply of irrigation water.

4. CONCLUSION

The field checks revealed that the accuracy with which the land use/crops were identified, from the 1:25,000 scale aerial photographs used in this study was, within the limitations of the classification used, almost equivalent with that of a traditional field survey. However, the air photo based survey had substantial advantages in terms of the speed at which the work could be carried out, and the completeness of the record, i.e. there was much less chance of missing information when scanning the photographs.

An analysis of the information collected shows that, contrary to general belief, there is virtually no "unused" land in St. Catherine which is suitable for agriculture. The little there is occurs mostly as lowland scrub in the southern plains. On the other hand it is found that there are considerable areas in the uplands which are being used far more intensively than the prevailing soil/slope conditions warrant, with the result that soil erosion is both serious and widespread. Whilst no attempt was made to map these "over-used" areas, their extent and location is mentioned in the text of this report. In terms of achieving "optimum" land use these areas of over-utilisation present greater problems than the areas of under utilisation, for improvements in these upland regions depend primarily on a massive reduction of crop farming on steep slopes, and the extension of grassland cultivation, and tree and forest crops. This is not easy to implement because of the dominance of mixed crop small holdings, many of them operating at, or near subsistence levels, with almost all their land on steeply sloping ground.

The map (Figure 7) reveals that a surprisingly large area of the southern plains is being under-used. From the evidence collected in this study it seems most likely that a more intensive utilisation of this land depends upon improvements being made (either singly or collectively) to the drainage conditions, the soil salinity, and the almost permanent water shortage.

4. CONCLUSION (contd.)

However, it will be necessary to undertake detailed local investigations to determine what are the particular requirements of any given area to bring this land into fuller use.

It is hoped that the information presented in this report will be of value to those concerned with the conservation and development of the natural resources of Jamaica, and that similar reports will follow, parish by parish, until the whole island is covered.

When these studies cover the whole of Jamaica, those responsible for the land resources will then be able to draw up a comprehensive "master plan" of land development. Such a plan should contribute substantially to achieving the optimum utilisation of every acre of land in Jamaica.

Follow up studies are now being carried out to utilise earlier sets of air cover, and other imagery which has just become available, including multispectral photography and thermal line scan, to monitor the type, extent, and rate of change of the various land use categories of the whole of Jamaica. This will reveal, among other things, the effectiveness in the agricultural field of Government legislation during the last decade.

It is planned to update and extend the existing 500 sq. miles of Land Use truth site and to use this, and the nearly 5,000 sq. miles of Soil Survey truth site which exists in Jamaica, to evaluate ERTS satellite imagery as an aid to land development in the tropics.

REFERENCES

1. Rural Development
   Ministry of Overseas Development
   London 1969

2. Report of the Commission on inventory of world land use
   International Geographical Union
   New York 1956

3. Soil and Land Use Surveys
   No. 1 - Jamaica. Parish of St. Catherine
   University of West Indies
   Trinidad 1958

Figure 1

KEY COMPILED BY THE INTERNATIONAL GEOGRAPHICAL UNION (IGU)

No.	Description	Colour
1	Settlements and associated non-agricultural lands	Dark and light red
2	Horticulture	Deep purple
3	Tree and other perennial crops	Light purple
4	Cropland:	
	(a) continual and rotation cropping	Dark brown
	(b) land rotation	Light brown
5	Improved permanent pasture (managed or enclosed)	Light green
6	Unimproved grazing land (used)	Orange
	(unused)	Yellow
7	Woodlands:	
	(a) dense	Dark green
	(b) open	Medium green
	(c) scrub	Clive green
	(d) swamp forests	Blue green
	(e) cut over or burnt over forest areas	Green stipple
	(f) forest with subsidiary cultivation	Green and brown dots
8	Swamps and marshes (fresh and salt water - non-forested)	Blue
9	Unproductive land	Grey

Figure 2

KEY COMPILED FOR THE LAND USE OF ST. CATHERINE, JAMAICA

No.	Description	IGU equivalent
19	Settlement	1
12	Mining	1
22	Food Forest	2
24	Coconut	3
27	Citrus	3
25	Banana	3
53	Sugar	4a
56	Rice	4a
58	Other Crops	4a
62	Tobacco	4a
*44	Grassland Improved	5
*	Grassland Unimproved	6
*11	(a) Ured	6a
* 6	(b) Unused	6b
	Woodland	
45	Dense	7a
51	Open	7b
41	Scrub	7c
41'	Scrub Lowland	7c
c/o 41	Cut over forest and scrub	7d
38	Mangrove Swamp	7d
35	Marsh and Swamp	8
30	Salina	9
70	Cleared Land	
71	Unproductive Land	9

*These were subsequently deleted and the term 11, Grassland was used without further subdivision.



Figure 4

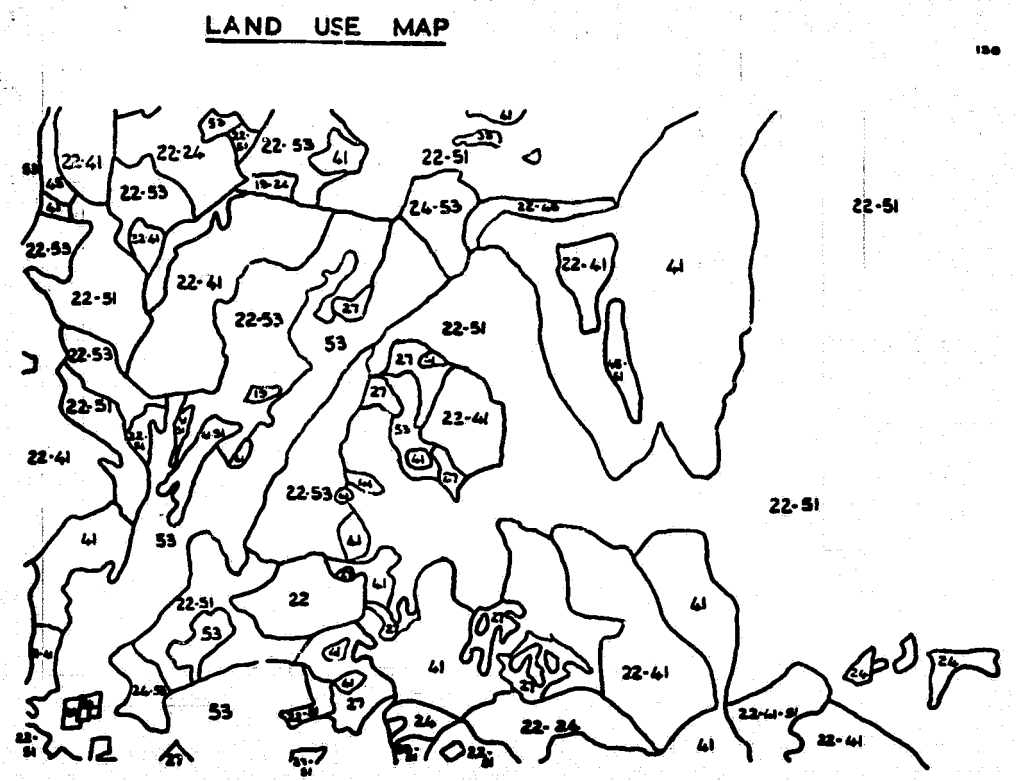

LAND USE MAP
22-41
22-24
22-53
41
22-51
24-53
22-51
22-53
22-41
41
22-51
22-53
53
22-51
22-53
22-51
22-41
22-41
22-53
53
22-51
22
53
41
22-41
24
53
22-24
41
22-41
22-51

Figure 5

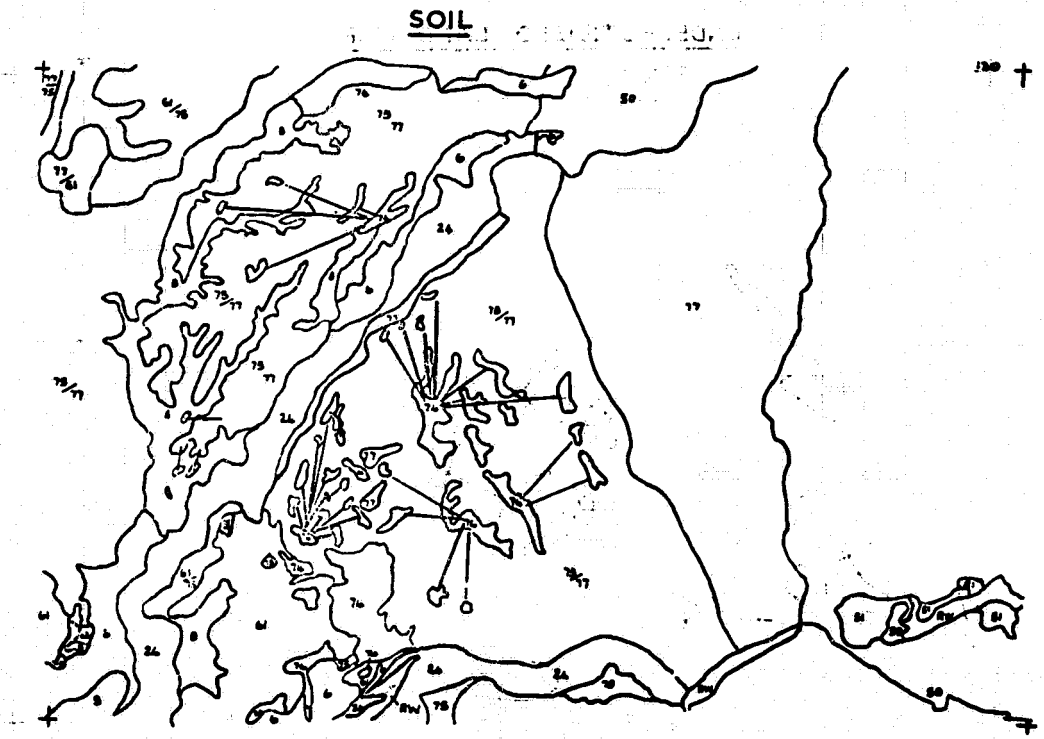


Figure 6

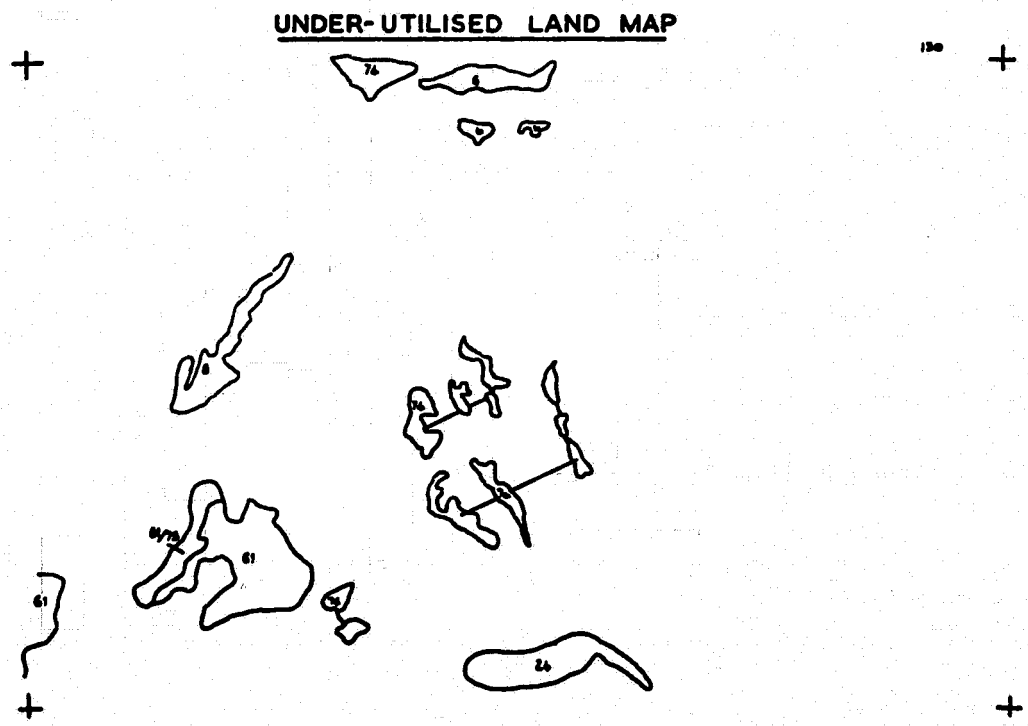
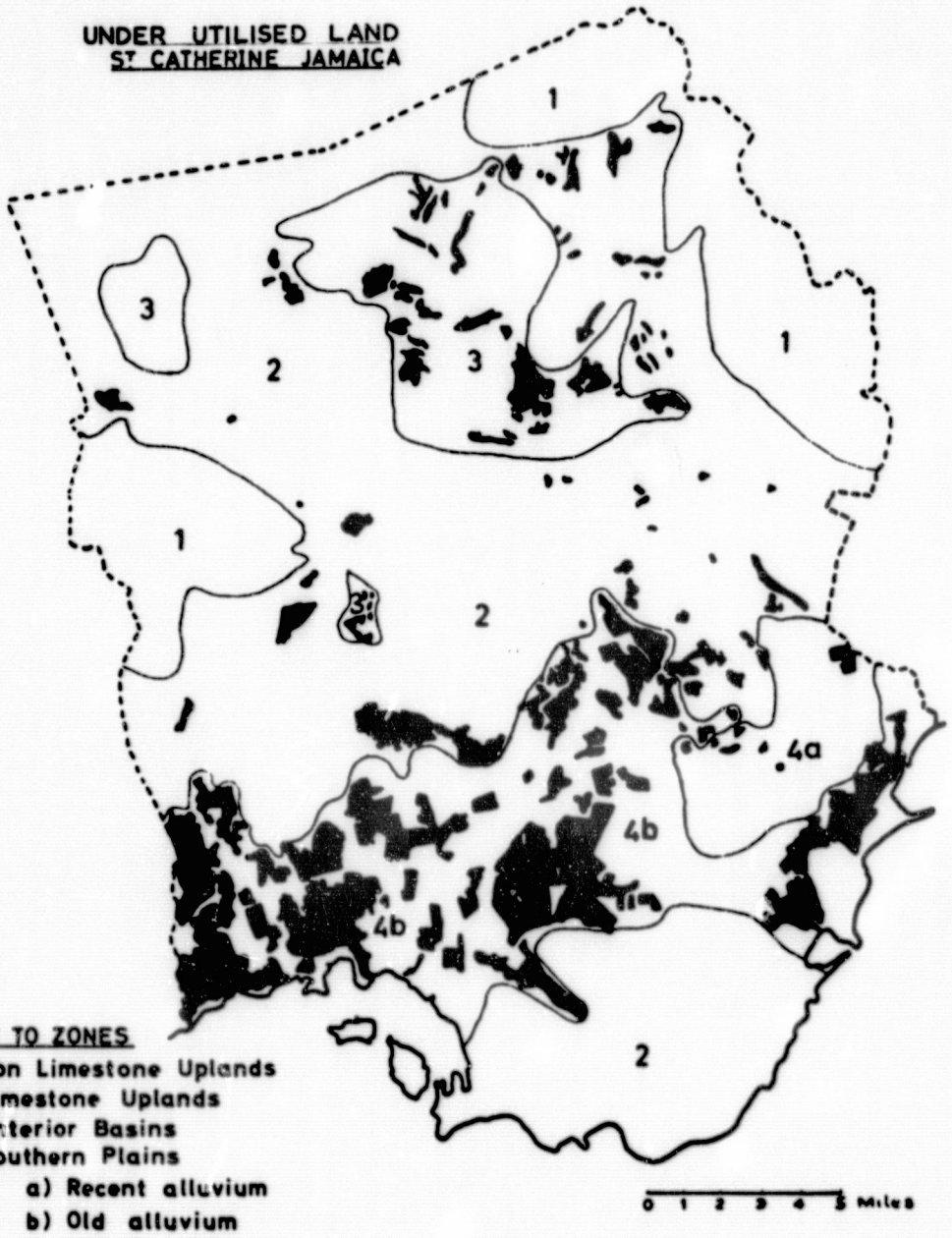


Figure 7


UNDER UTILISED LAND
St CATHERINE JAMAICA
1
2
3
4a
4b
KEY TO ZONES
1 Non Limestone Uplands
2 Limestone Uplands
3 Interior Basins
4 Southern Plains
a) Recent alluvium
b) Old alluvium
0 1 2 3 4 5 Miles

UNDER UTILISED LAND
ST CATHERINE JAMAICA
KEY TO ZONES
1 Non Limestone Uplands
2 Limestone Uplands
3 Interior Basins
4 Southern Plains
a) Recent alluvium
b) Old alluvium

AN INTEGRATED RESOURCE SURVEY USING ORBITAL IMAGERY - AN EXAMPLE FROM SOUTH-EAST SPAIN

J.L. van Genderen

Department of Geography,
University of Sheffield,
Sheffield S10 2TN, United Kingdom

ABSTRACT

Some of the basic aspects of orbital imagery examined in relation to integrated surveys of natural resources are scale, the role of repetitive coverage and types of sensors. An experimental procedure has been devised for natural resource surveys to cope with the problems of data handling and processing of the large quantities of data. Extrapolation away from known ground conditions - a fundamental technique for mapping natural resources, becomes very effective when used on orbital imagery supported by field sampling. Meaningful boundary delimitations can be made on orbital images using various image enhancement techniques only if there is adequate ground truth. As well as semi-automatic and quantitative image enhancement techniques, the Department's work involves understanding the needs of developing countries with regard to the use of orbital imagery for making rapid reconnaissance surveys of natural resources, so that this investigation into the use of satellite imagery for integrated resource surveys involves the analysis of the images by means of standard visual photo interpretation methods.

INTRODUCTION

As a result of the UNESCO sponsored International Postgraduate Course in Applied Geomorphology and Natural Resources Research, an investigation is being carried out by staff members of the Department of Geography, University of Sheffield, on the methodology of integrated surveys of natural resources using orbital imagery in the Murcia province, S.E. Spain. Figure 1 shows the location of the investigation area of approximately 30,000 km^2. The detailed Mula test site within this, has an area of slightly less than 2,000 km^2. The Mula test site has been mapped and classified into 200 'land units', these being characterized by a narrow range of variation in landform, soil and vegetation. These land units are represented by a characteristic appearance on the vertical panchromatic aerial photographs (1:31,000). The land units were subsequently grouped into 40 types of terrain 'land systems' (Christian and Stewart: 1968). The recurrence of a number of units within a land system in a regular pattern gives rise to the distinctive recurring tonal pattern on the aerial photographs. The recognition of these distinctive photo patterns is an integral part of the type of reconnaissance survey carried out. A very extensive literature exists on the subject of aerial photographic interpretation of natural resources (e.g.: Bowden: 1967; Nossin: 1971; UNESCO: 1968; Vink: 1967; Wright: 1971). This paper confines itself to those aspects which are related to orbital image interpretation of integrated resource surveys at a regional reconnaissance level (Badgley and Vest: 1966; Wobber: 1972; van Zuidam: 1971).

SCALE

Scale is a most important element in the recognition of the terrain features used in resource surveys, as the scale of the image determines how large a particular feature will appear on the image and also the number of images required to cover a given area. In many of the vast areas of Africa, Asia, Australia, Central and South America, photography at a scale of 1:40,000 to 1:80,000 has been used effectively for preliminary reconnaissance of the resources of the area. In S.E. Spain, aerial photographs at a scale of 1:31,000 were used. This scale has been found to be less satisfactory, because there are more photographs to handle at all stages, the area covered by each photo-

Preceding page blank

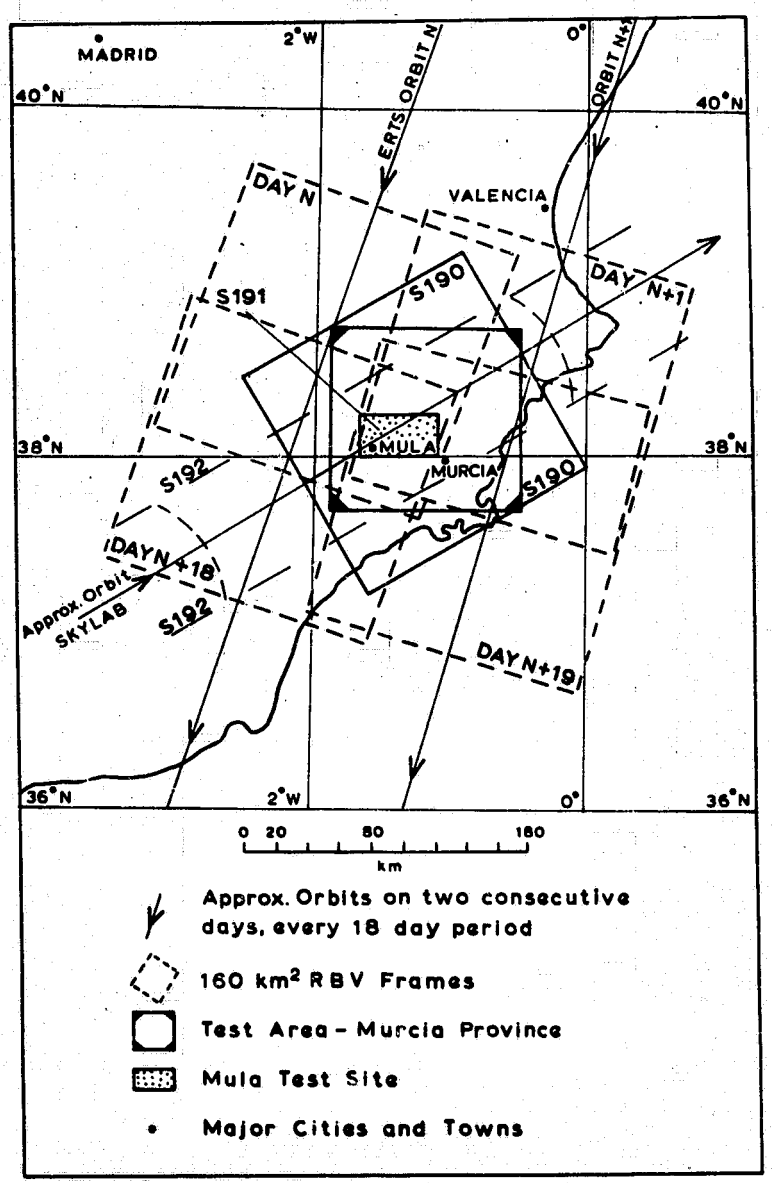


FIGURE 1 : Location of Project Area

graph is relatively small so that deductive interpretation is more difficult, and also, the air photo patterns are diffuse and not easily recognized and mapped. Some of the important advantages of the orbital imagery for mapping earth resources have been found to be, therefore:

1. the synoptic view of large areas. The data provided by ERTS is in the form of images covering an area of 160 x 160 km. Thus one image covers almost the whole study area for which 1,000 aerial photographs would be needed (see Figure 1). This ability to observe large areas under relatively uniform conditions serves to reduce the number of variables that affect the interpretation and use of imagery, such as tonal changes between photographs, thereby facilitating extrapolation away from known ground truth areas - a fundamental technique for mapping natural resources.

2. the reduced volume of data per unit area. A single synoptic image from either EREP (Skylab) or ERTS presents information contained in many hundreds of images from the conventional coverage of the area. Thus the handling and making of mosaics, a major cost factor in resource surveys is greatly reduced.

3. accessibility to remote areas. The satellite images provide a means for the cyclic monitoring of large areas remote from human observation, so that areas which are difficult or impracticable to observe by other means, are brought into view for fuller understanding.

Since the objective of reconnaissance surveys is to make rapid inventories of the resources of large areas, the scale of mapping that was found to be most appropriate in this area was in the range of 1:100,000 to 1:250,000, although for larger areas scales as small as 1:500,000 have been used. The value of mapping earth resources from orbital images is therefore obvious. The average size of a land system mapped in the Murcia area was 50 km^2, so that all the land systems are of a sufficient size to be readily identifiable on orbital imagery, even that with a relatively low ground resolution. Many of the land units are also clearly definable on orbital images. A definite advantage of the method of land systems mapping for resource surveys developed in Sheffield, is that it can be applied to orbital imagery, even though with small scale satellite images the size of the minimum area that can be mapped and recognized as a discrete unit becomes larger. This is so because the basic unit, the 'land unit' is recognized and measured in the field, and subsequently built up into the 'land systems' which may be readily mapped on the orbital images. So, while it becomes almost impossible, for example, to discriminate between small fields - common in many developing countries, it is nevertheless possible to identify the whole complex of fields from the orbital images and map these, since the internal variations and characteristics of the land system (such as the nature, shape and size of individual fields, slope, lithology and soil characteristics, etc.) have been obtained by field checking using standard statistical sampling methods and air photo extrapolation techniques. These methods have been developed because of the prohibitive costs of a complete inventory, as well as the long time that this would involve.

The field work area is located in a semi-arid environment which is, in many respects, similar to the Basin and Range province of south western U.S.A., especially the northern half of the project area. Here, dissected, isolated mountain ranges are girdled by extensive footslopes, with enclosed interior drainage basins, many having salines or playas in their centre. Thus, in preparing for the receipt of the orbital imagery of S.E. Spain, present research has been concentrated on the interpretation and analysis of orbital images of S.W. United States. Because of the similarity of environmental conditions in S.E. Spain and Arizona, it is anticipated that the images will be able to help in the analysis and planning for the extension of existing cultivated land and the opening up of new areas in the Murcia province. On the basis of the results obtained from Gemini and Apollo images, all the new irrigation canals, pipelines, etc. under construction as part of a large development project to increase the irrigation capacity in the area, will be able to be identified and mapped using orbital imagery.

A basic aspect of orbital imagery which needs to be examined in relation to earth resource investigations is the role of repetitive coverage. This is a factor which has seldom been fully appreciated by those bodies concerned with physical resource inventories and management planning. The repetitive coverage which both ERTS and EREP sensors will provide will allow an almost complete record of the changes in agriculture, seasonal run-off, soil moisture conditions, etc. to be accurately monitored. Repetition also makes possible the acquisition of data previously excluded for various reasons. In the Murcia area, the present investigation will trace and examine the developments and changes in the agricultural pattern. This is particularly valuable in semi-arid areas, as the agricultural potential here is limited by water shortage. The effects of the irrigation projects underway to increase the irrigation capacity of the Murcia province, by bringing water into the area over a distance of several hundred kilometres will, in this way, be under constant review.

To compensate for the small scale of the orbital images, emphasis in this project has been placed on those image enhancement techniques which lend themselves to magnification, such as the use of Agfa Contour Equidensity film, the Image Quantizer and the Isodensitracer. Second order Agfa contour pictures are easily magnified, as they consist only of black lines on a white background, so that the picture does not 'break up' as quickly as occurs when enlarging an original orbital image (figure 3). The Image Quantizer recordings, which plot the various tonal densities of orbital images can also be greatly magnified without loss of detail, even though the original recording is made at a scale ratio of 1:1 (figure 4). The Isodensitracer has been found to be particularly useful for small scale orbital images, as this can magnify to the extent of 1,000 to 1 (figure 5).

TYPES OF SENSORS

Such an enormous amount of different image types of the same area will be available from the EREP (Skylab) and ERTS sensors (table 1), that it is claimed that materials such as crops, lithologic types, soils, etc. can be recognized on the basis of characteristic spectra of electromagnetic radiation. Thus present field surveying techniques in the Murcia area include the collection of

SPACECRAFT : EREP (Skylab) - Earth Resources Experiment Package.		
SENSOR : S 190 - Multispectral Photographic Facility.		
Spectral bands:	0.5 - 0.6 μ	(Pan X)
	0.6 - 0.7 μ	(Pan X)
	0.7 - 0.8 μ	(b & w I.R.)
	0.8 - 0.9 μ	(b & w I.R.)
	0.5 - 0.88 μ	(colour I.R.)
	0.4 - 0.7 μ	(Hi Res. Colour)
SENSOR : S 191 - Infrared Spectrometer.		
Spectral bands:	0.4 - 2.4 μ	
	6.2 - 15.5 μ	
SENSOR : S 192 - 13 band multi-spectral scanner.		
Spectral bands:	0.41 - 0.46 μ	0.98 - 1.08 μ
	0.46 - 0.51 μ	1.09 - 1.19 μ
	0.52 - 0.56 μ	1.20 - 1.30 μ
	0.56 - 0.61 μ	1.55 - 1.75 μ
	0.62 - 0.67 μ	2.10 - 2.35 μ
	0.68 - 0.76 μ	10.2 - 12.5 μ
	0.78 - 0.88 μ	
SENSOR : S 193 - Microwave system.		
Spectral band :	13.8 - 14.0	GHz
SPACECRAFT : ERTS - Earth Resources Technology Satellite.		
SENSOR : RBV - multispectral TV camera system.		
Spectral bands:	0.475 - 0.575 μ	
	0.580 - 0.680 μ	
	0.690 - 0.830 μ	
SENSOR : MSS - multispectral scanner system.		
Spectral bands:	0.5 - 0.6 μ	
	0.6 - 0.7 μ	
	0.7 - 0.8 μ	
	0.8 - 1.1 μ	

TABLE 1 : Types of Sensors with their Spectral Bands of EREP and ERTS Satellites.

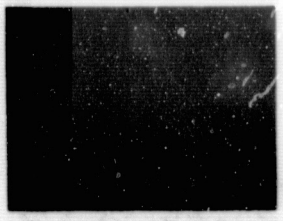


FIGURE 2.1



FIGURE 2.2



FIGURE 2.3

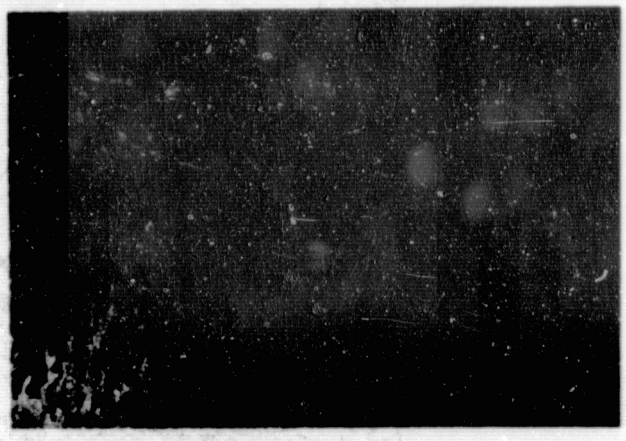


FIGURE 2.4

FIGURE 2.1 : Plunging anticlinal structure near Molina de Segura.

FIGURE 2.2 : The Segura river with its intensively cultivated terraces and the town of Molina de Segura.

FIGURE 2.3 : Alluvial fans at the foot of the Sierra de Santa Ana.

FIGURE 2.4 : Extensive footslopes of the Sierra de Cabeza de Asno.



FIGURE 3.1 : First order Agfa Contour equidensity image of the Segura river with its cultivated terraces and the town of Molina de Segura. (c.f. FIG. 2.2).



FIGURE 3.2 : Second order Agfa Contour equidensity image of alluvial fans of the Sierra de Sant Ana. (c.f. FIG. 2.3).

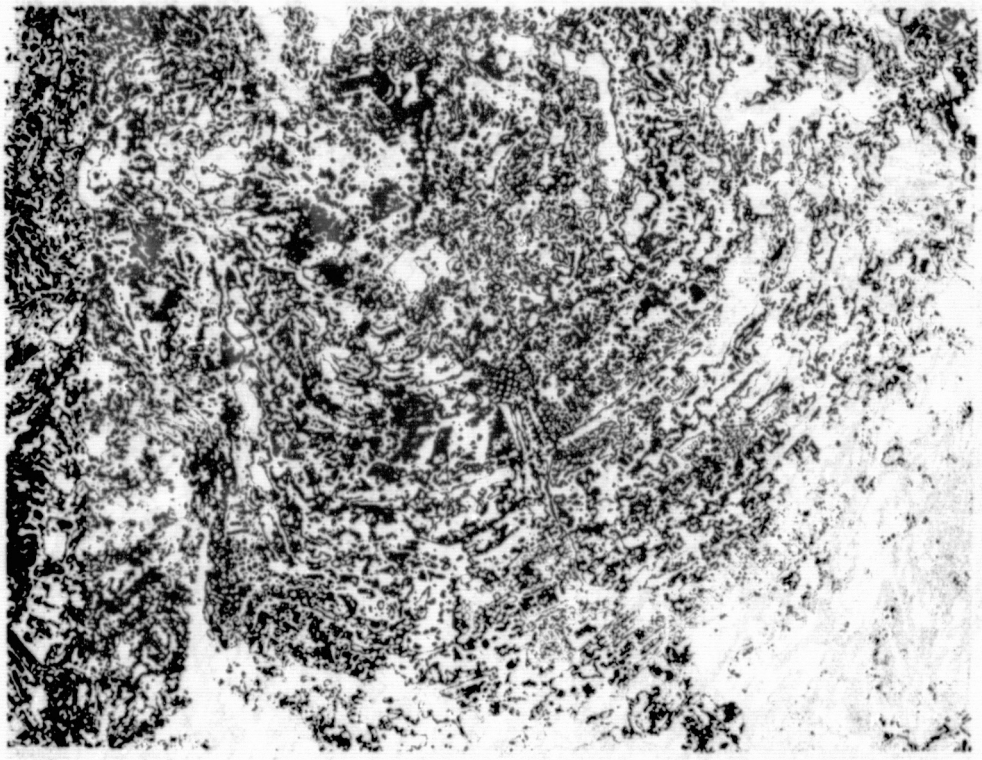


FIGURE 3.3 : Second order Agfa Contour equidensity image of plunging anticlinal structure. (c.f. FIG. 2.1).

FIGURE 4.1 : Image Quantizer Recording

tech/ops

IMAGE QUANTIZER RECORDING

RADIATION PRODUCTS DIVISION BURLINGTON, MASS. 01803



APERTURE	MODE	NOTES:	RECORDING NO.
0.8 mm	✓ Plus / Minus ✓ — d / O — Refl. ✓ / Trans.	Alluvial fans at the foot of the Sierra de Santa Ana. (c.f. FIG. 2.3 and FIG. 3.2).	219 S
0.4 mm			IDENTIFICATION
0.2 mm	THRESHOLD 0-00		DATE 6-8-1972
0.1 mm	INCREMENT 200		OPERATOR

FIGURE 4.3 : Image Quantizer Recording.

tech/ops

IMAGE QUANTIZER RECORDING

RADIATION PRODUCTS DIVISION BURLINGTON, MASS. 01803

APERTURE
0.8 mm
0.4 mm
0.2 mm
√ 0.1 mm

MODE
√ Plus | d | Refl. √
Minus | √Q | Trans.

THRESHOLD 0.00

INCREMENT 100

NOTES: Extensive footslope of the Sierra de Cabeza de Asno. (c.f. FIG. 2.4 and FIG. 5.2).

RECORDING NO. 1055

IDENTIFICATION

DATE 6-8-1972

OPERATOR



FIGURE 5.1 : Three colour Isodensitracer Recording of small part of the town of Molina de Segura (c.f. FIG. 2.2 and FIG. 3.1). Magnification: X 20; Scan width: 100μ^2; Δd Density increment: 0.057).



FIGURE 5.2 : Three colour Isodensitracer Recording of footslopes of Sierra de Cabeza de Asno. (c.f. FIG. 2.4 and FIG. 4.2). Magnification: X 5.

ground truth data (Chapman and Brennan: 1969) which is being incorporated in a data bank system so that computer print-outs can later be obtained separating, for example, wheat from other crops (van Genderen and Hempenius: 1972). The main problem being encountered at present is the difficulty in obtaining compatibility between the orbital image and the ground truth information. One of the reasons for the difficulties being encountered in correlating the imagery with the ground truth information is the problem of interpreting the tonal differences on the images. While these differences may be easily measured and mapped using the techniques discussed below, areas with similar tonal values do not always represent areas with similar ground characteristics, and vice versa, so that appreciable errors in interpretation can arise, once again indicating the need for detailed field information. To overcome this problem to a certain degree, arrangements have been made with several Spanish research organizations in Murcia to record detailed ground data in carefully preselected sample areas on those days that the satellites pass over the area.

A study of several simulated multi-spectral orbital images provided by NASA has shown that for orbital surveying of the earth's resources to be fully utilized, it is necessary to pay special attention to such aspects of spectral resolution as the position and number of bands, width of bands, etc. Another factor to consider is the difference between the RBV and MSS images, for whilst the former has a central projection, the latter uses a line scan technique. On the basis of an examination of a run of several orbital photographs of southwestern U.S.A. and Mexico which had considerable overlap, it is considered that the ERTS' RBV images will allow for the stereoscopic study of the images (figure 1). Although the impression of relief is seldom great, the ability to view the images stereoscopically, or at least to obtain binocular fusion, greatly reduces the signal-to-noise ratio.

DATA HANDLING AND PROCESSING

Despite a reduction in volume of data per unit area, the satellites will generate vast volumes of data of the Murcia area through their repetitive flights and many image types. Such a profusion of data will create new and complex problems of data handling, analysis and use (figure 6), such as problems in sorting the useful data, monitoring changes and the systematic recognition of objects and phenomena.

In order to prepare for this anticipated problem of handling and processing the data, an experimental procedure has been devised and tested for natural resource surveys, in that the new images, together with the need for some form of automation have led to the development of several new techniques to aid in the evaluation and mapping of resources. Of great importance in this respect are the grey and colour tones, which can only be qualitatively assessed by eye. Hence Agfa Contour Equidensity film, an Image Quantizer and a three colour Isodensitracer have been used as well as a microdensitometer, for the quantification of tonal values and the detection of spectral signatures, as these methods allow visual as well as quantitative interpretations to be made.

The fundamental image characteristics which the photo-interpreter uses for identification and analysis are tone, texture, pattern, shape, size, shadow, association and orientation. In photographic terms, variation in tone, or density, is the common factor which constitutes the whole image, thereby making possible the perception of the other image characteristics. Although microdensitometer readings from various targets in a given spectral region imaged on photographic film cannot be compared on an absolute basis with readings in another region, the relative ordering in each spectral region tends to be invariant. Experiments have shown this to hold true for natural targets such as soil, vegetation and rock type. This characteristic relative ordering furnishes a type of spectral signature which can be used as a discriminating functional property of great value to natural resources surveys of large areas from orbital imagery, especially because of the 13 narrow wavelength bands to be used in the MSS scanner of EREP. Experiments of simulated orbital imagery have shown that consistent reflectance differences were obtained only if very narrow wavelength intervals were used. There is still the need for much ground truth against which to establish these results.

The principle, techniques and applications of Agfa Contour Equidensity film have been well described by Ranz and Schneider (1971) in a paper presented at the 7th International Symposium on Remote Sensing of Environment, so that these need not be discussed in this paper. Using Agfa Contour, it is possible to examine the entire density distribution of an original by making several separate equidensities and arranging these subsequently in register to make a family of equidensities. However, it has been found that in many cases the increase in information obtained from a single first order equidensity (by making one copy of an original) is adequate (figure 3.1), especially if a second order equidensity picture is made from the first order equidensity image (figures 3.2 and 3.3).

FIG. 6: FLOW DIAGRAM NASA TO PRINCIPAL INVESTIGATOR, DEPT. OF GEOGRAPHY, UNIVERSITY OF SHEFFIELD, U.K., AND BACK TO NASA

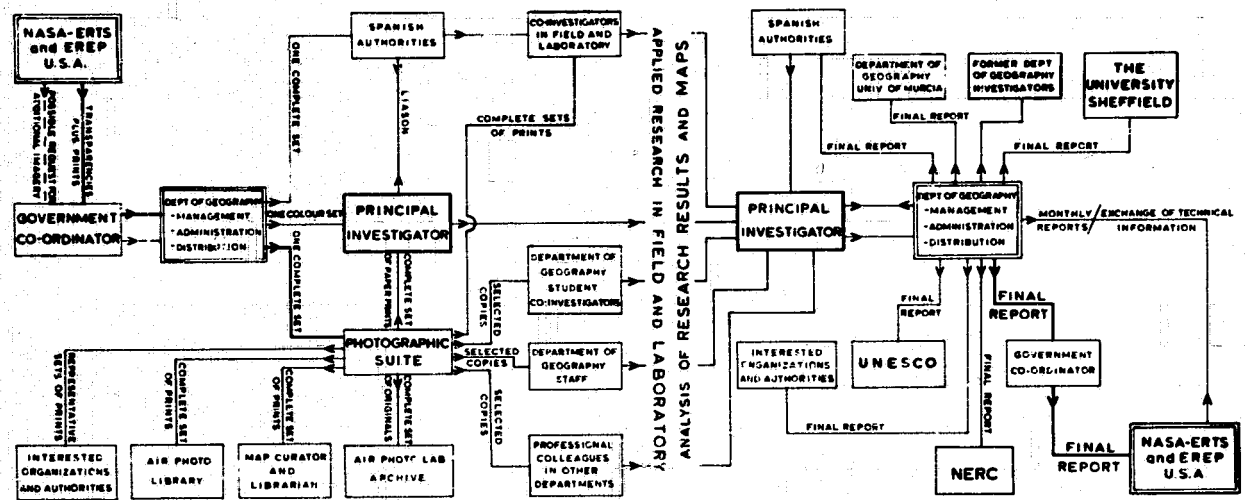


Figure 3.1 is a selected first order equidensity image of an urban and agricultural area along the Segura River in S.E. Spain. The picture shows the ease with which railway lines (A), major roads (B), and even tracks (C) may be plotted. Field boundaries (D) stand out strikingly. Figure 3.2 depicts a single second order equidensity of an area of alluvial fans at the foot of the Sierra de Santa Ana. This picture aids in the analysis and mapping of the major structural features such as faults (A), and bedding planes (B) of the mountain range, and highlights the many shallow drainage lines. Again, most linear features stand out remarkably well such as the fault, tracks, and field boundaries. This single second order equidensity photograph readily distinguishes the olives (C) from the fruit trees (D) and from the vineyards (E). A whole series of equidensities taken with different exposure times therefore, especially when used with all or selected bands of the 13 band multi-spectral scanner in Skylab, will provide identification of various crop types. Figure 3.3 is a single second order equidensity picture of a plunging anticlinal structure. The various exposed beds are clearly depicted by lines in this picture. Thus images such as these are of value for regional geological/geomorphological mapping purposes.

One of the main methods of the approach used in Sheffield for integrated resource surveying is boundary delineation of photo patterns as a precursor to area typing for resource mapping. Boundaries of the land systems are often more easily detected on orbital imagery than on photo mosaics. Most boundaries drawn on orbital imagery have been found to be indicators of real differences in environmental conditions, so that these may be used to select the field sample areas. While some boundaries are diffuse or transitional in terms of tonal density, Agfa Contour Equidensity film highlights these very subtle changes. However, while most boundaries drawn on orbital images no doubt result from changes in one or several terrain features, it has been observed that these boundaries are not always significant, and hence the boundaries should always be checked against the results of the field sampling and the land system boundaries as plotted on the aerial photographs.

The Image Quantizer also provides useful data for reconnaissance surveys, as this instrument will plot the tonal density range of an image - both prints and transparencies up to 23 x 30 cms. in approximately 5 to 7 minutes. Up to 20 isodensity contours can be plotted, with the difference between isodensit contours continuously variable over the range 0.02D - 0.16D. This makes it ideal for rapid, preliminary examination of areas of interest. Figure 4 gives two examples of this instrument. In figure 4.1, approximately the same area as that in figures 2.3 and 3.2 is depicted, while figure 4.2 is of an extensive footslope area, with long, narrow, cultivated drainage floors (c.f. figure 2.4). The density increment setting for figure 4.1 was 200, while that for figure 4.2 was 100. This is explained in figure 7. A similar effect to that obtained by taking single first or second order Agfa Contour Equidensity images as shown in figure 3 can be obtained quickly by this instrument in that the recording threshold may be set to any level. The density range of the isodensity contours can be varied so that only objects of the required density are recorded, those with densities below or above these being eliminated, simplifying the image for subsequent interpretation.

A three-colour Isodensitracer has also been used for detailed examination of tonal differences, as this instrument can plot up to 50 different density contours. A four-colour Isodensitracer also exists which can plot up to 64 density contours for even greater image enhancement so vital for small scale orbital image analysis. The three-colour instrument automatically scans and measures the density of all points in a film transparency and plots the values as a quantitative, three-colour two-dimensional density map of the scanned area. The Isodensitracer uses the 'dropped line' technique, rather similar to that used in the production of orthophotographs. This technique is illustrated in comparison to a conventional pen method in figure 8. This shows that as the density increases, the first coloured pen scribes a sequence of space, then dots, then dash. As the density continues to increase, the second coloured pen is activated and produces space, than dots, then dash and so on. When the density decreases, the above given sequence reverses. As can be seen in figure 5, the pattern produced on the recording paper makes it obvious whether the density is increasing or decreasing as the write-out method changes. The large magnification ratios available make this instrument ideal for studying tonal variations on orbital images, as the visual recording lends itself to easy field checking to determine the significance of the tonal variations.

More information is contained in an image than the normal interpreter is able to detect with accuracy and confidence within a reasonable time. Even though normal objects seldom exhaust the enormous recording capacity of the sensors, reduction of image information into useful, accurate data in a short time is most essential in the case of many earth resource subjects. With the enormous amount of imagery data that will be made available by the EREP and ERTS sensors, the need for quick and reliable processing of the image information, instrumentally if possible, assumes great significance. Hence in the present study, both a Freescan Digitizer and a Particle Size Aanlyzer have been used as well as the techniques outlined above, as these are considered to be most useful for earth resource surveys using orbital imagery. With the digitizer, the location and areas of the various mapping units can be quickly and quite accurately calculated. The digitizer is also

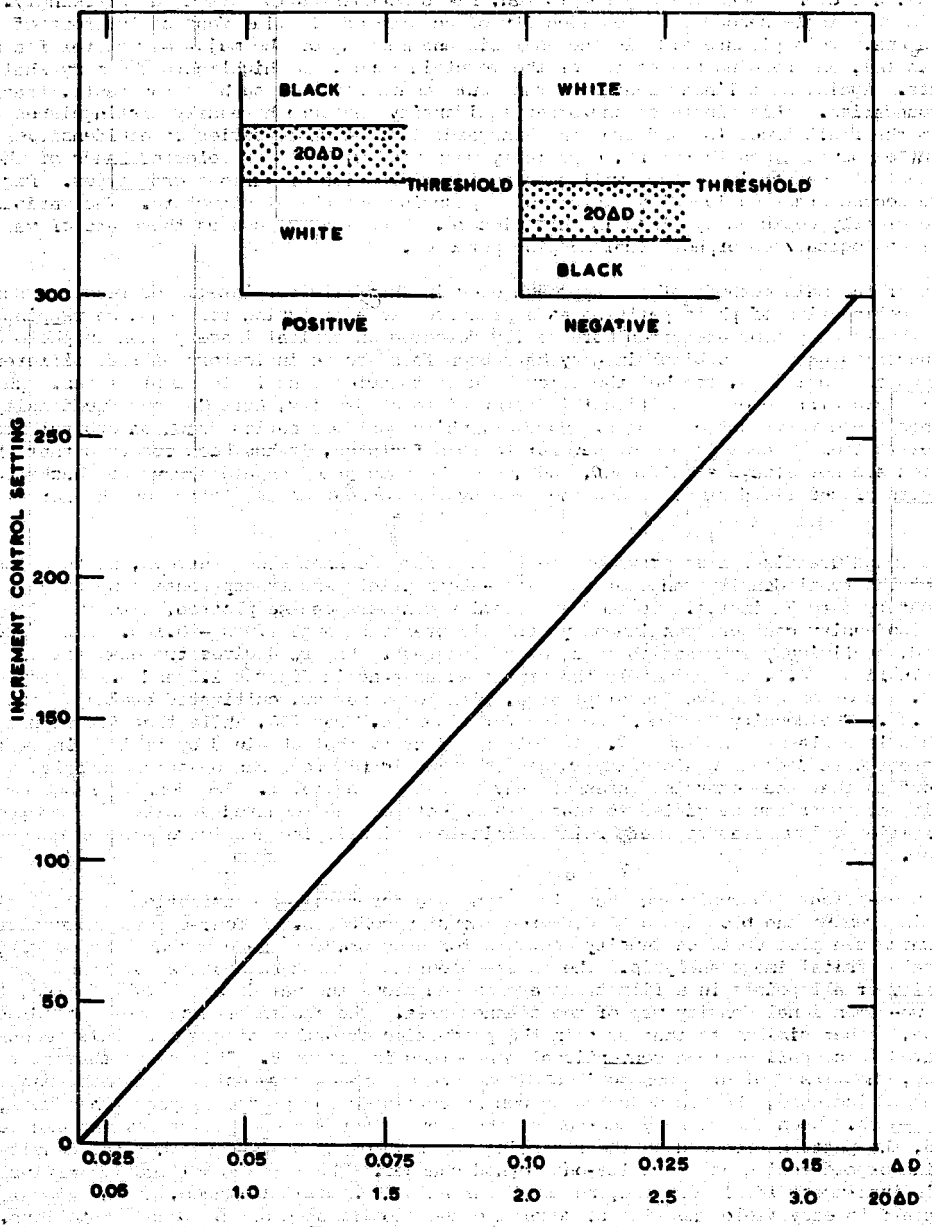


Figure 7: Density Increment Chart for use with Image Quantizer

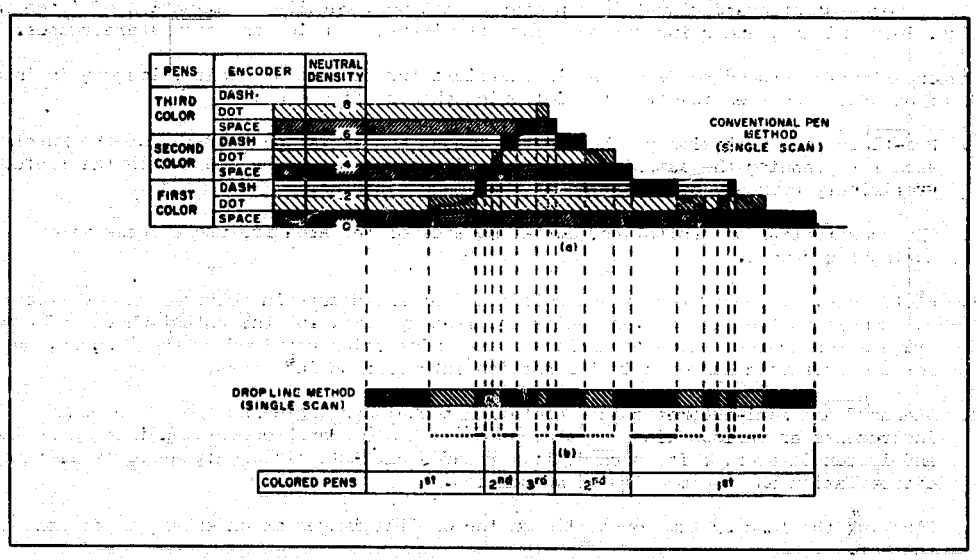


FIG. 8: *Comparison of Conventional and Dropline Write-Outs.*

considered to be invaluable in studying structural features on orbital images such as the gross pattern of structural lineaments of an area, as well as other types of linear features such as roads, irrigation canals, etc. Tests carried out show that the particle size analyzer can be very useful for measuring the individual particle sizes of objects (such as fields, land units, land systems, etc.) and for determining their distribution, as the many images over many spectral bands contain thousands of objects which need to be measured. Using the particle size analyzer, the dimensions and areas of about 500 objects can be measured in half an hour. However, since the eye participates in the measuring process, the diameter of the object to be measured should not be less than 1 mm. The measuring range of 1.0 to 27.7 mm. has been found to be ideal for most objects on orbital images of relevance to natural resource investigations. If the object falls outside these limits, enlargement or reduction of the image has to be made. The rapid recording and monitoring of changes in agriculture, forest clearance, and other aspects of the landscape related to integrated resource surveys can, therefore, be made from orbital images.

As well as the many semi-automatic, quantitative image enhancement techniques, the Department's work involves understanding the needs of developing countries with regard to the use of orbital imagery for natural resource surveys. These countries, due to lack of funds and trained personnel, usually prefer simpler methods. Thus one of the main aspects of this investigation into the use of orbital imagery for integrated resource surveys involves the development of techniques of image analysis by means of standard visual interpretation methods, detailed examination of image characteristics, image mixing, and using various kinds of mirror, scanning and zoom stereoscopes.

The experimental procedure developed in Sheffield for the use of orbital imagery in integrated surveys of natural resources involves the following phases (figure 6):

1. Pre-field interpretation of the orbital images and aerial photographs of the Murcia area for planning the sampling and traversing procedure to be adopted in the field. Preliminary boundary delimitation of the image patterns.

2. The construction of orbital and aerial mosaics of the area for use as base maps during field work.

3. Field work. The measurement and collection of field data in selected sample areas for compiling the list of land units and land systems, for the establishment of ground truth sites against which to calibrate the information provided by the imagery, and for the extrapolation of this information into surrounding areas.

4. Standard and semi-automatic interpretation techniques including the use of such instruments as various kinds of stereoscopes, a microdensitometer, an image quantizer, and isodensitracer, a freescan digitizer and a particle size analyser to facilitate extrapolation and the marking of boundaries.

5. Plotting the land system boundaries on the orbital images or on enlarged sections thereof.

6. Final quantification of results, the compilation of the resource maps, management proposals, reports, etc.

These phases may, of course, be changed or others added as more experience is gained in handling and interpreting the orbital imagery. Using this procedure, orbital images provide a useful synoptic supplement to most of the established applications of aerial photography in the field of natural resource surveys. On the basis of the results obtained to date in experiments, the quantitative and image enhancement techniques, as well as the more elementary methods of stereoscopic or binocular examination of the images, the mixing of different image types, etc., should all be able to provide the earth scientist using orbital imagery for his resource survey, with much useful data.

CONCLUSIONS

Natural resource surveys ultimately require detailed analysis and other types of information that satellites are incapable of providing, so that while the synoptic views of satellites have been shown to provide a major input into the recognition, exploration and management of resources, the demand for detailed data from conventional airborne surveys will increase rather than decrease with the use of space surveys. This is so because the interpretation of the EREP and ERTS data will require detailed knowledge of representative natural and cultural features on the surface of the earth in order to establish spectral signatures. The Mula test site in the Murcia province is one such test area being investigated by conventional field and air survey methods, but many others remain to be identified. As applications to resource surveys for orbital data evolve, the need for

such calibration or ground truth sites, as well as the essential ground and air surveys will increase. Thus future applications of remote sensing to resource development are considered to require a careful blending of space and airborne surveys to realize the goals of resource missions. However, as pointed out, their realization will be dependant upon the solution of the escalating problems of data retrieval, processing dissemination, and the determination of spectral signatures. An increasing number of techniques and procedures, several of which have been discussed in this paper, are now available to meet these problems.

Aerial and ground surveys, therefore, are essential to our understanding of the remote sensors and to the significance of the orbital observations. In the Murcia area, in preparation for the space flights, laboratory tests have been used to select and determine useful parameters for integrated surveys to assess and evaluate certain quantitative as well as qualitative techniques of interpretation and mapping, and to define applications. With this type of framework, it is considered that one will be able, systematically, to use aerial and ground surveys to follow up orbital data in the same way that one now uses field surveys to verify aerial observations.

ACKNOWLEDGEMENTS: The author gratefully acknowledges the financial support of the Royal Geographical Society's 20th I.G.C. Fund and the University of Sheffield Research Grants No. 854 and No. 893 in this project.

SELECTED REFERENCES

BADGLEY, P.C., and VEST, W.L. (1966): "Orbital remote sensing and natural resources" (Photogramm. Eng., vol. 32, pp. 780-790).

BOWDEN, M.G. (1967): "Applications of aerial photography in land systems mapping" (Photogramm. Record, vol. 5, no. 30, pp. 461-464).

CENTRE NATIONAL D'ETUDE SPATIALES (1969): "Remote Sensing Principles and Application to Earth Resources Survey" (Seminar Proceedings, Paris).

CHAPMAN, P., and BRENNAN, P. (1969): "Ground truth acquisition" (Proceedings, 1st Annual I.R.S.I. Symposium, Sacramento, vol. 1, pp. 140-152).

CHRISTIAN, C.S., and STEWART, G.A. (1968): "Methodology of integrated surveys" (in: Aerial Surveys and Integrated Studies, - Proceedings of the Toulouse Conference, UNESCO, Paris, pp. 233-281).

COLWELL, R.N. (1968): "Determining the usefulness of space photography for natural resource inventory" (Proc. of the 5th Int. Symp. on Remote Sensing of Environment, Ann Arbor, Michigan, pp. 249-289).

COLWELL, R.N. (1968): "Aerial and space photographs as aids to land evaluation" (in: Stewart, G.A. (edit.): Land Evaluation, Melbourne).

COLWELL, R.N. et. al. (1969): "A survey of earth resources on Apollo 9 photography" (Forestry Remote Sensing Laboratory, Univ. of California, pp. 68-75).

GENDEREN, J.L. van, and HEMPENIUS, S.A. (1972): "REMOTE SENSING - recording and imaging techniques for unconventional wavelengths and their use in obtaining information for the earth sciences from the air" (I.T.C. Publication, series A, series B. - in print).

KELLER, D.W. (1970): "Earth resources satellite systems" (Jnl. British Interplanetary Soc., vol. 23, no. 4, pp. 257-274).

MOHRMANN, J.C.J. (1966): "Operational planning of integrated surveys in developing countries" (I.T.C. - UNESCO, Publication No. S5).

NATIONAL ACADEMY OF SCIENCE (1966): Spacecraft in Geographic Research (Nat. Res. Council Publ., 1353, 107 pp.).

NOSSIN, J.J. (1969): "Applied geomorphology in integrated surveys" (Scientia, vol. 104, pp. 1-18).

NOSSIN, J.J. (edit.) (1971): "Readings in integrated surveys" (I.T.C. Publication, series B, no. 3).

PETRI, G. (1970): "Some considerations regarding mapping from earth satellites" (Photogramm. Record, vol. 6, no. 36, pp. 590-624).

RANZ, E., and SCHNEIDER, S. (1971): "Progress in the application of Agfa Contour equidensity film for geo-scientific photo interpretation" (Proc. of the 7th Int. Symp. on Remote Sensing of Environment, Ann Arbor, Michigan, pp. 779-786).

STEINER, D. (1971): "Towards earth resources satellites: the American ERTS and SKYLAB programs" (Photogrammetria, vol. 27, no. 6, pp. 211-251).

U.K. DIRECTORATE OF OVERSEAS SURVEYS (1967): "Assistance to developing countries - planning the use of land resources" (Ministry of Overseas Development, London).

UNESCO (1968): "Aerial surveys and integrated studies" (Proceedings of the Toulouse Conference).

UNITED NATIONS (1970): "Natural resources of developing countries: investigation, development and rational utilization" (Report of the Advisory Committee on Science and Technology to Development).

VERSTAPPEN, H.Th., and ZUIDAM, R.A. van (1970): "Orbital photography and the geo-sciences: a geomorphological example from the Central Sahara" (Geoforum, vol. 2, pp. 33-47).

VINK, A.P.A. (1967): "The use of aerial photographs in integrated surveys of resources" (I.T.C. - UNESCO Publication, series P., no. 2).

WOBBER, F.J. (1969): "Environmental studies using earth orbiting photography" (Photogrammetria, vol. 24, (3/4), pp. 107-166).

WOBBER, F.J. (1972): "The use of orbital photography for earth resources satellite mission planning" (Photogrammetria, vol. 28, no. 2, pp. 35-60).

WRIGHT, R.L. (1971): "The role of integrated surveys in developing countries - review and re-appraisal" (Proceedings, International Seminar on Integrated Surveys, Range Ecology and Management, UNESCO, pp. 47-105).

ZUIDAM, R.A. van (1971): "Orbital photography as applied to natural resources survey" (I.T.C. Publication, series B, no. 61).

ENHANCEMENT OF EARTH RESOURCES TECHNOLOGY SATELLITE (ERTS) AND AIRCRAFT IMAGERY USING ATMOSPHERIC CORRECTIONS

Ravi D. Sharma
Department of Space Hq.
Government of India
Bangalore, India
and Willow Run Labs (ERIM)
University of Michigan

ABSTRACT

The major objective of this investigation was to evaluate atmospheric effects in ERTS-1 imagery. Calculations were made using Dr. R. E. Turner's radiative transfer model, which accounts for multiple scattering of radiation for realistic atmospheric conditions. It was necessary to determine vertical aerosol and molecular distribution, using standard atmospheric profiles. Specifically, the horizontal visual range was used for determination of the optical depth. The total downward irradiance, diffuse downward irradiance, path radiance, and transmittance for ERTS-1 multispectral scanner bands were calculated as functions of visibilities.

Calculations for ERTS-1 illumination conditions based upon the model were applied to the Woodworth Study Area, North Dakota, for waterfowl habitat-pond and vegetation mapping. Aircraft coverage of this site is also available for several years. Atmospheric corrections for the Willow Run Laboratories aircraft multispectral scanner data were also calculated for corresponding illumination conditions. Thus, the corrected aerial data can be used for validation or simulation of ERTS-1 imagery. This technique is general in character and can easily be applied to other earth resources oriented problems.

ACKNOWLEDGEMENTS: The author acknowledges Mr. Frederick J. Thomson for his interest and support through NASA Contract NAS9-9784 and Dr. Robert E. Turner for discussions and for use of the radiative transfer model.

INTRODUCTION

The primary motivation for this study has been to estimate the magnitude of atmospheric effects in multispectral earth resources data taken by satellites and aircraft with a view to subsequently compensating such data for atmospheric effects as far as is practically possible. The atmospheric effects are present in all space oriented and aerial data even in the so called atmospheric "windows" through which all sensors observe the ground. This study confines itself to the window regions where absorption of ground radiance is assumed to be small. Nevertheless, the atmosphere is not completely transparent due to scattering of radiation by molecules and particulate matter (aerosols).

As a practical application in the earth resources disciplines, the calculations of atmospheric effects are made for the case of water mapping. Since the background vegetation surrounding water affects the atmospheric corrections, both dry and green vegetation backgrounds are assumed. Specifically, the calculations are made for pond-mapping and waterfowl habitat studies in the Woodworth Study Area - a research site of the Northern Prairies Wildlife Research Center near Jamestown, North Dakota. There has been a continuing study [1] at the Willow Run Laboratories supported by the Bureau of Sport Fisheries and Wildlife of the United States Department of the Interior and by NASA during which considerable aerial scanner data have been collected over this area and recognition studies on water and vegetation have been performed to help wildlife managers develop accurate estimates of waterfowl population. Among other things, these estimates depend upon the area, number, and perimeter of ponds at two times of year, quality and quantity of surrounding vegetation, and surrounding land use. Hopefully, remote sensing techniques will provide useful inputs to a waterfowl productivity model now being developed. Operational use of techniques now under development requires that atmospheric effects be minimized in both the aircraft and the satellite data.

Description of the Atmospheric Model

Atmospheric effects are quite varied and depend on several parameters. One of these parameters is the terrain altitude because the molecular density varies with altitude, and because the amount of particulate matter (aerosols) and its distribution also varies with altitude. Time variation of constituents can also modify the atmospheric effects for a given point in the scene. The spatial variations of these atmospheric constituents in a given scene might make it difficult to apply a uniform atmospheric compensation throughout the scene. When the scene area under observation is large, such as for a single 100 x 100 n mi frame of ERTS data, these spatial variations are probably the rule rather than the exception. This is evident from global meteorological data. If one could therefore measure the vertical distributions of gaseous (including water vapor) and particulate matter as well as their constitution (i. e.,sizes, amounts for each point in a scene), then one could hope to compensate for the atmosphere based on such experimental observations. However, at this stage of remote sensing, simultaneous spectral and spatial observations for determining the atmospheric state at each point in these large scenes are far from routine operations. Thus one tries to model the atmosphere for standard or average atmospheric conditions using realistic vertical distribution profiles for molecular and particulate constituents.

One such physical model has been developed by Turner et al.[2] at the Willow Run Laboratories. In addition to utilizing realistic profiles of constituents, this model adequately treats the radiation field in the framework of Chandrasekhar's radiative transfer theory. The details of the model are available elsewhere [3] and are summarized here only to introduce the quantities which are calculated in this study. The model is intended for use in the visible and near infrared regions of the electromagnetic spectrum in which most of the solar and reflected terrestrial radiation is not absorbed by the molecules and aerosols. The primary mechanism for loss (extinction) of radiation is through scattering by these constituents. Elterman [4] has compiled tables of optical depth, τ, for molecular (Rayleigh) and aerosol (Mie) scattering for realistic atmospheric conditions as functions of the borizontal visual range, V. The optical depth, τ, is a function of the altitude, h and depends upon the size distribution of the particulates and upon the molecular composition, and is defined as:

$$\tau(h) = \int_h^\infty \kappa\,(z)\,dz \qquad (1)$$

where κ is the extinction coefficient, which is reduced to the scattering coefficient in this case. The parameter z denotes vertical position in the atmosphere.

One can define [5] visibility, V, as the distance at which the contrast between a black object (with radiance L) and the sky background with radiance L_B is reduced to two percent, which is assumed to be the limiting (daylight) contrast between objects. The spectral variations in visibility are not accounted for in the present study since V is treated as an input parameter throughout the model. Thus

$$e^{-\kappa V} = \frac{L_B - L}{L_B} = 0.02$$

$$\text{or} \qquad V = \frac{3.912}{\kappa} \qquad (2)$$

Thus, one has a relation by which one can empirically characterize the state of the atmosphere by defining the parameter V. For the case of pure molecular (Rayleigh) scattering, the visibility is 336 km; for a typical clear day bordering haze [3], the visibility is 23 km; and for a dense fog, the visibility is 12 km.

The radiance, L, received by a sensor in an aircraft or a spacecraft can be written as [5]

$$L(\tau,\mu,\phi) = L_I(\mu,\phi)\,T(\tau,\mu) + L_p(\tau,\mu,\phi) \qquad (3)$$

where L_I is the intrinsic radiance of the target, T the transmittance of the atmosphere, and L_p is the path radiance resulting from multiple scattering of radiation in the atmosphere. All above quantities are functions of the wavelength, λ, suppressed here for convenience; μ, is the cosine of the nadir view angle, θ, (also called the scan angle); and ϕ, the azimuthal angle. The transmittance, T, can be simple written as [3]

$$T = e^{-[\tau(0) - (L)]/\mu} \qquad (4)$$

For the case of a perfectly diffuse Lambertian target, (neglecting bidirectional reflectance, for example)

$$L_I = \frac{\rho_T}{\pi} \tilde{E}_- \qquad (5)$$

where ρ_T is the target spectral reflectance, and $\tilde{E}_-$ is the total downward spectral irradiance.

Turner's model is applicable to the case of a plane parallel atmosphere which is homogeneous, i. e., in which the ratio of constituents does not change even though the density is strongly dependent upon the altitude [2, 5]. The radiative transfer theory is simplified to include multiple scattering in a two stream (double-delta) approximation [3] and the resulting expressions are easily computed. The model also allows the calculation of the specular downward irradiance, E_-, and diffuse upward irradiance, E_+, at a given altitude, h, of the sensor. The programs developed to execute Turner's model at WRL were also employed here to calculate T, L_p and other derived quantities for the pond water mapping application under consideration.

Application of the Model to the Test Site (North Dakota)

The Woodworth Study Area in North Dakota has an average altitude of 0.76 km (2500 ft) above mean sea level. The optical depths for Rayleigh (molecular) scattering as tabulated by Eltermann [4] were therefore corrected for this altitude. However, the aerosol distribution was assumed to be the same as that at sea level. June 1 and August 1 dates were chosen for calculations at this site (Latitude = 47°02'; Longitude = 99°15') because the background vegetation is likely to be dry and green respectively on these dates and because these are two flight dates of interest in the pond mapping study. This background surrounding water affects the path radiance, L_p, and, thus, the calculated atmospheric compensations.

Since the sun is not always at nadir, the radiance L and other quantities depend upon the solar zenith and azimuthal angles and are not necessarily symmetric with respect to the nadir. Thus a time of observation of 0900 Central Standard Time was chosen for both available aircraft and ERTS data. The solar apparent time for the site longitude is 0824. This helped determine the solar zenith (θ_o) and azimuthal (ϕ_o) angles utilizing standard spherical trigonometry [6] or tables [7]. The solar azimuthal angle here is measured from the south and one gets $\theta_o = 79.16°$, $\phi_o = 49.25°$ for 1 June; and $\theta_o = 75.50°$, $\phi_o = 52.58°$ for 1 August.

The target and background spectral reflectances were synthesized from the signature library [8] at the Willow Run Laboratories and are shown in Figure 1. For water, a constant 4% reflectance throughout the wavelength range of interest was assumed. The dry and green reflectances were synthesized from typical reflectances of corresponding data available in the wavelength regions of interest.

Based upon the above inputs, values of atmospheric quantities are calculated at specific wavelengths. These were band averaged for the various spectral bands of the scanners aboard ERTS-1 or the aircraft. A definition of the band averaged quantity $\bar{X}$ is as follows:

$$\bar{X} = \frac{\int_0^\infty X(\lambda)\, R(\lambda)\, d\lambda}{\int_0^\infty R(\lambda)\, d\lambda} \qquad (6)$$

where $R(\lambda)$ = spectral responsivity of sensor
$X(\lambda)$ = quantity to be averaged

which reduces to the common definition of the average for the square response function $R(\lambda)$ for the spectral channel under consideration. The band averaged quantities correspond to the aircraft and ERTS sensor observed quantities.

It is also convenient to consider the fraction of surface contrast between two objects

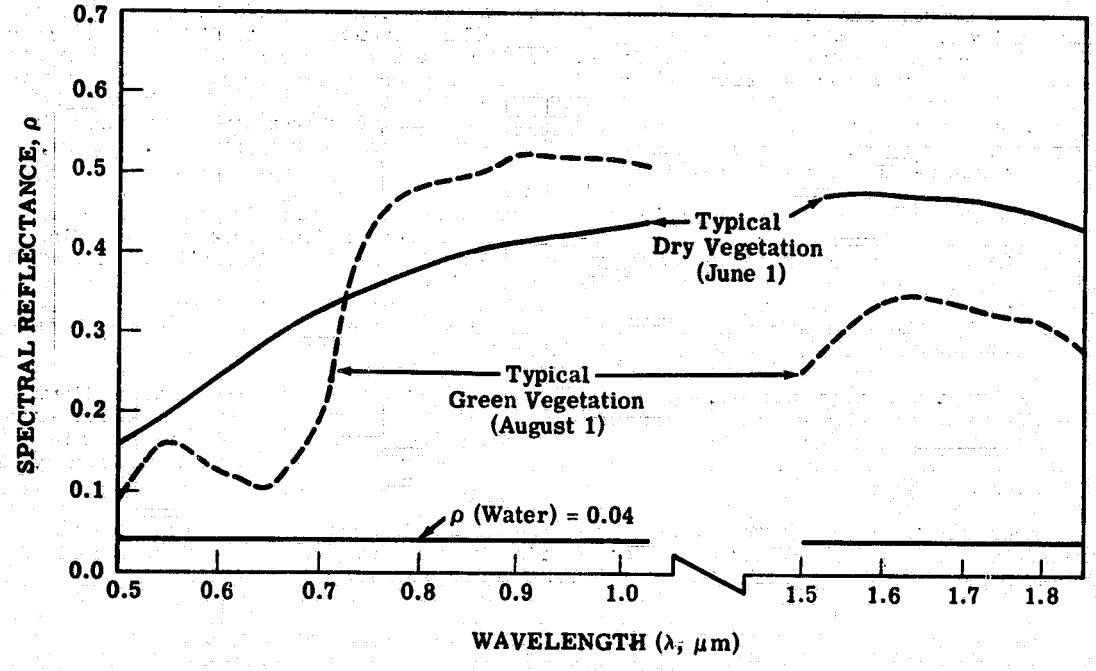


FIGURE 1. SPECTRAL REFLECTANCE FOR WATER AND BACKGROUND VEGETATION

which finally reaches the sensor. The contrast at altitude, h, is defined as

$$C_h = \frac{L_t - L_b}{L_b} = \frac{(L_I T + L_p)_t - (L_I T + L_p)_b}{(L_I T + L_p)_b} \qquad (7)$$

where L_t and L_b are target and background radiances respectively. The contrast at the ground is:

$$C_o = \frac{(L_I)_t - (L_I)_b}{(L_I)_b} \qquad (8)$$

Assuming the target to be small so that L_p is the same for the scene and primarily dependent upon the background reflectance (ρ_b), one gets the contrast transmittance, T_r, as [5]

$$T_r = \frac{C_h}{C_o} = \frac{1}{1 + \frac{L_p}{(L_I)_b}} = \frac{1}{1 + \frac{\pi L_p}{\rho_b \bar{E}_-}} = 1 + \frac{\pi L_p}{\rho_b \bar{E}_-} \qquad (9)$$

where we have used Eq. (5) in the above relation. Thus the contrast transmittance depends only upon the background properties and is independant of the target reflectance.

Atmospheric Corrections for ERTS-1 Scanner Data

The calculated relative spectral response $R(\lambda)$ of the detector filter system for the four channel multispectral scanner (MSS) on ERTS-1 is shown in Figure 2. These channels are designated MSS 4 through 7, and cover the visible and near IR spectral ranges. The band averaged transmittance, T, as calculated for various horizontal visual ranges, V, are shown in Figure 3. As can be seen, the transmittance, T, for the different channels continuously increases from green toward reflective infrared (IR). This is because atmospheric scattering is more prominent in the green than in the IR. Also, only 45% of the radiance originating from the target will reach sensor channel 4 of the ERTS scanner if the ground visibility is 6 km. The exponental dependence of transmission on visual range can be predicted from Eq. (4) which reduces to $T = e^{-\tau(0)}$, since $\mu \tilde{\sim} 1$ for the ERTS scanner, because it looks vertically down from an altitude in excess of 900 km and because the total field of view of the scanner is 11°. All subsequent quantities for ERTS-1 are therefore calculated for a scanner looking vertically downward through atmospheres having various visibilities.

The path radiance, L_p, which is dependent on the background, is shown in Figure 4. For 1 June (dry vegetation background) L_p decreases toward the infrared but the higher reflectance of green vegetation in near infrared wavelengths brings L_p up for MSS-6 relative to MSS-5, even though the solar irradiance is less in MSS-6 than in MSS-5. Finally L_p is greater in MSS-7 for 1 August than for the June case because the green vegetation background has higher reflectance in this band than the dry vegetation background. This clearly shows how L_p depends upon background reflectance. Figure 5 shows the total radiance computed using Eq. (3). In band MSS-4 the atmospheric contribution (from L_p) is more than three quarters of the total radiance received by the scanner for low visibilities. Even for a clear day L_p contributes more than half of the total radiance seen by the detector in that band. Also the total radiance similarly shows strong dependence on background reflectance. Contributions from L_p appear larger because water has a low reflectance.

Figure 6 shows the diffuse downward irradiance, E_-, again a contribution from atmospheric scattering alone, since the downward irradiance above the atmosphere is specular irradiance from the sun [9]. The total downward irradiance E_- is almost constant at all visibilities as shown in Figure 7. This is what the opal glass of the present Michigan M-7 scanner sun sensor measures when exposed to the sky. The present sun sensor is therefore not a very sensitive detector of the atmospheric state. However the ratio (E_-/E_-) is a very good indicator of the atmospheric state as shown in Figure 8. Thus a sun sensor which measured E_-/E_- would be a better device for assessing atmospheric state. This has been also suggested by Nalepka [2] and is being implemented. It can also be seen that E_- depends more strongly upon the background than E_-.

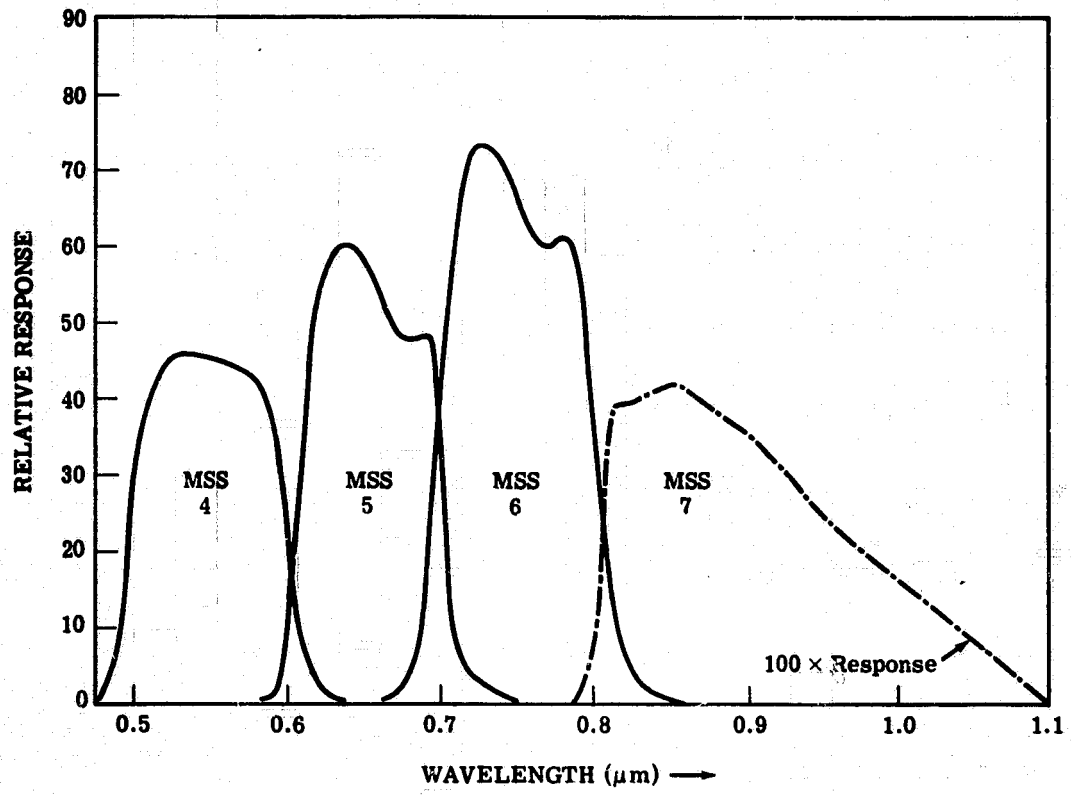


FIGURE 2. CALCULATED SPECTRAL RESPONSE FUNCTIONS FOR ERTS-1 MSS, CHANNELS 4 THROUGH 7.

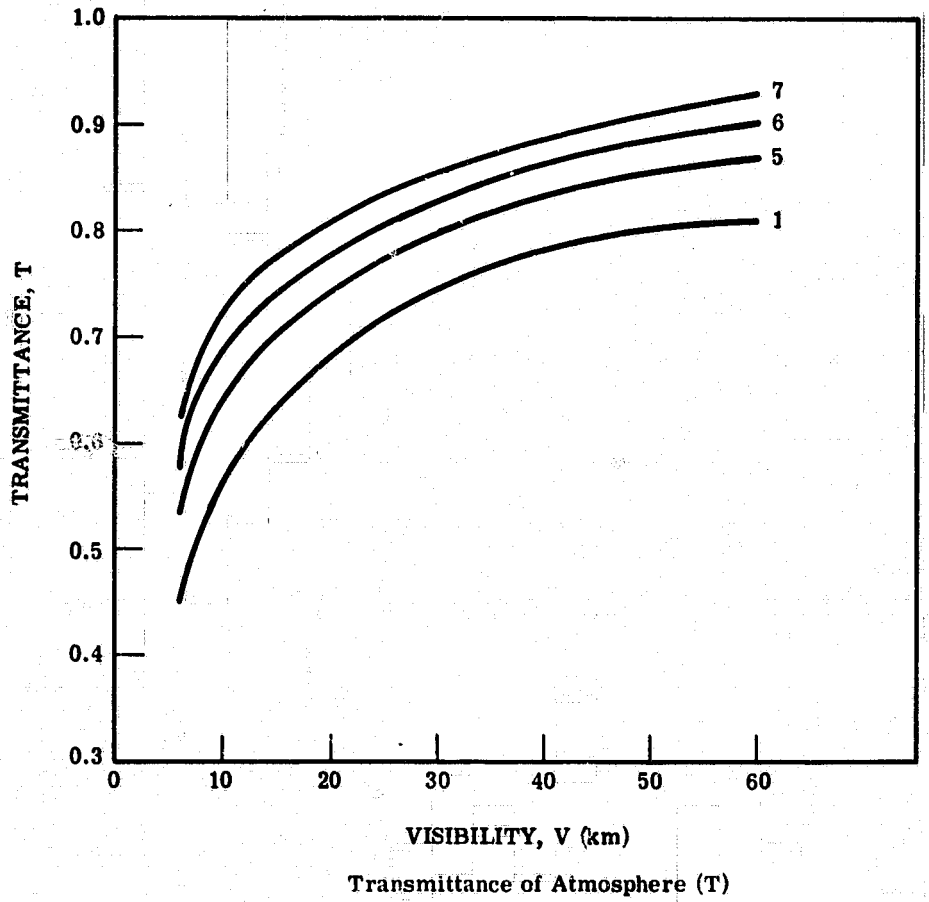
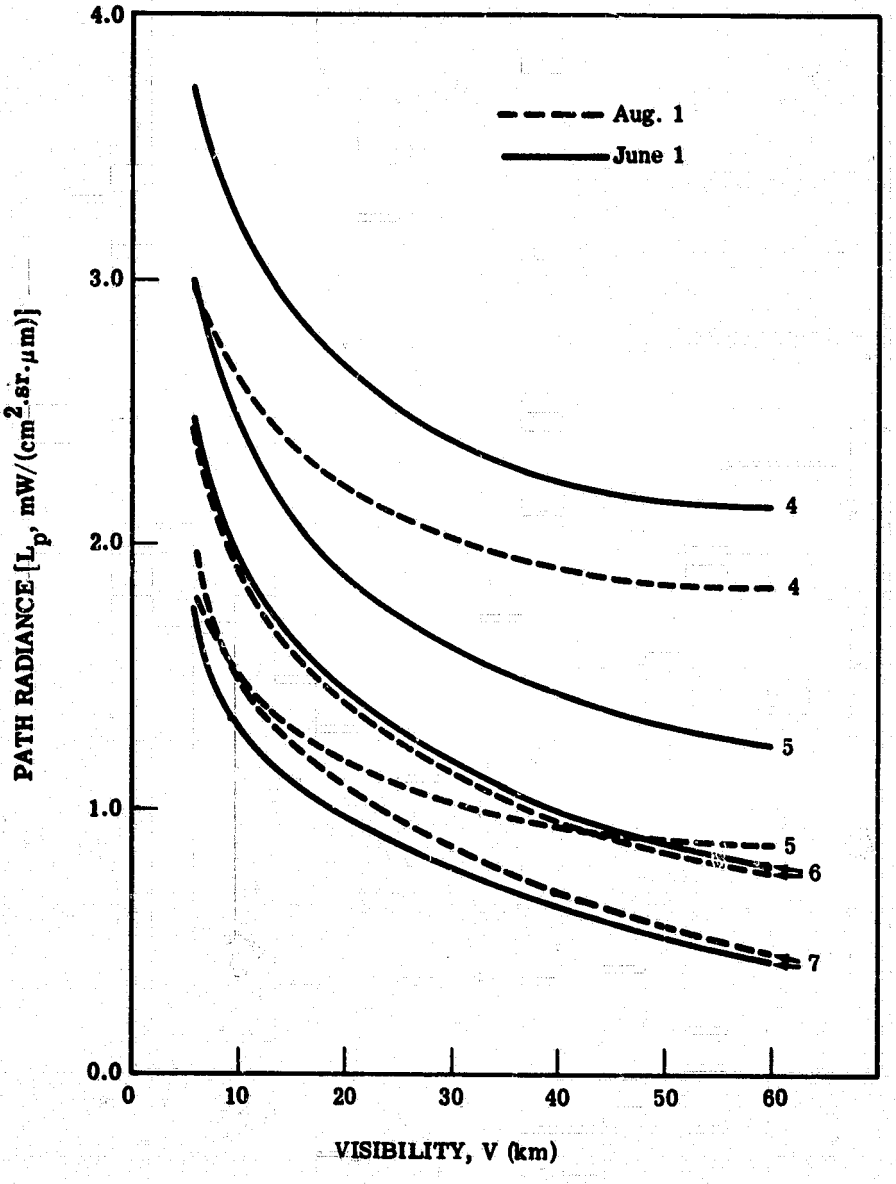
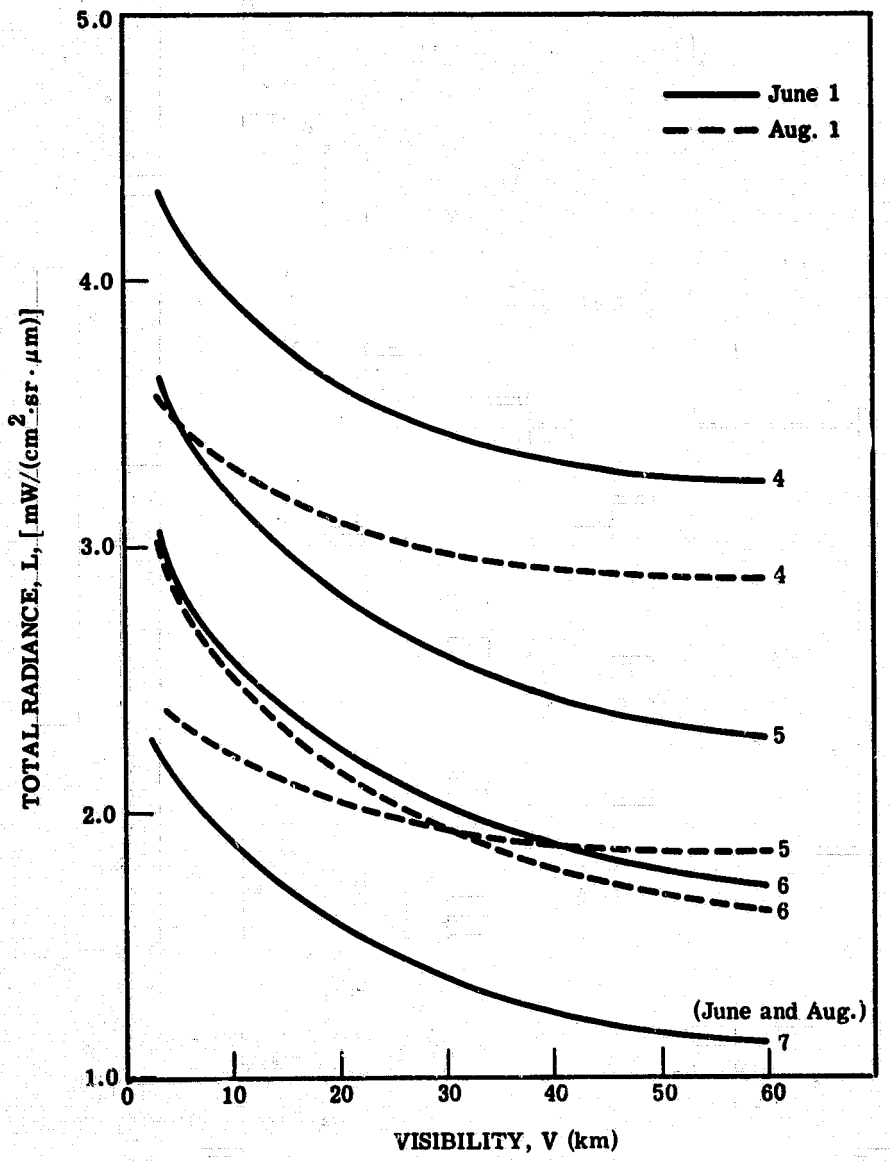


FIGURE 3. ERTS MSS CHANNELS 4 THROUGH 7, NORTH DAKOTA. All quantities are functions of horizontal visual range (Visibility, V).



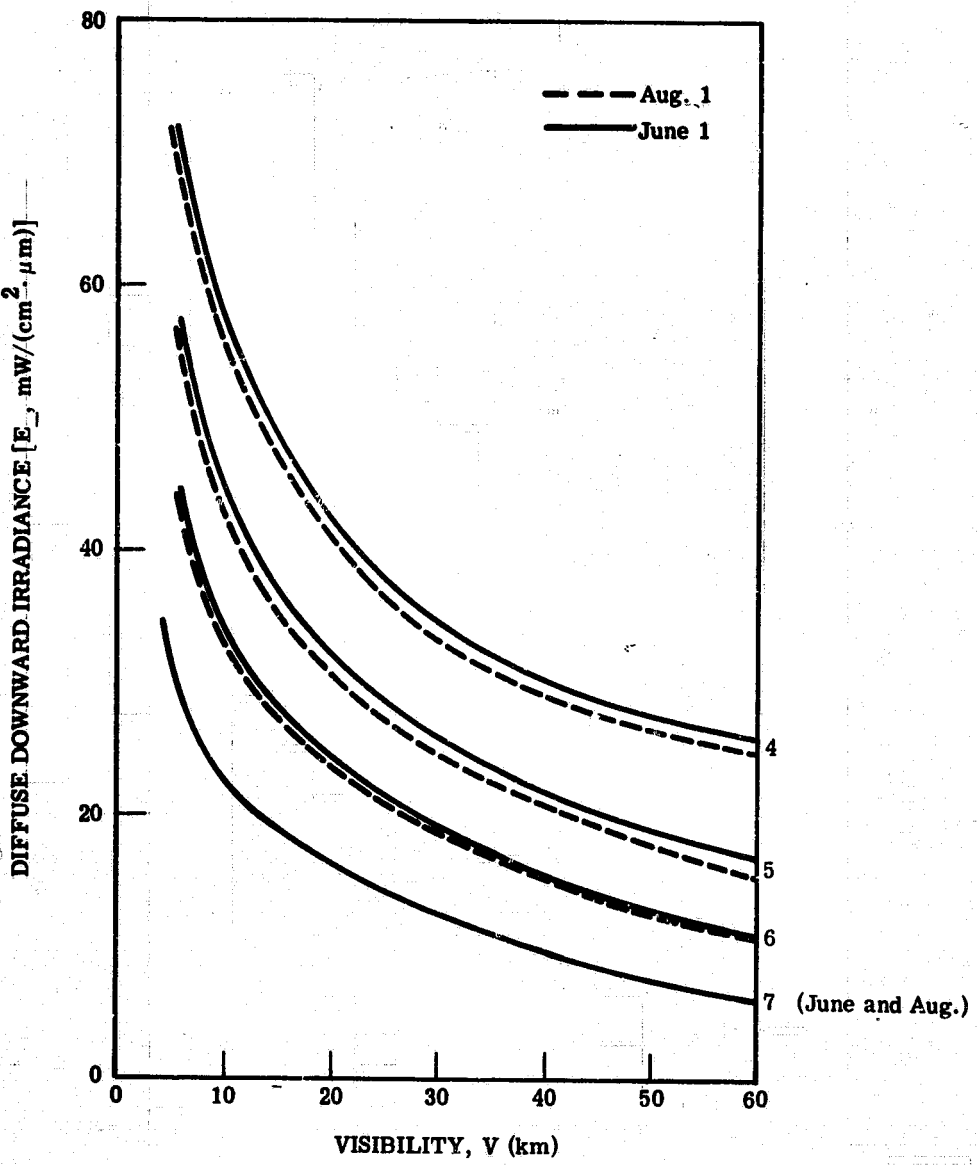
Path Radiance (L_p) for 1 June and 1 August

FIGURE 4. ERTS MSS CHANNELS 4 THROUGH 7, NORTH DAKOTA. All quantities are functions of horizontal visual range (Visibility, V).(Continued)



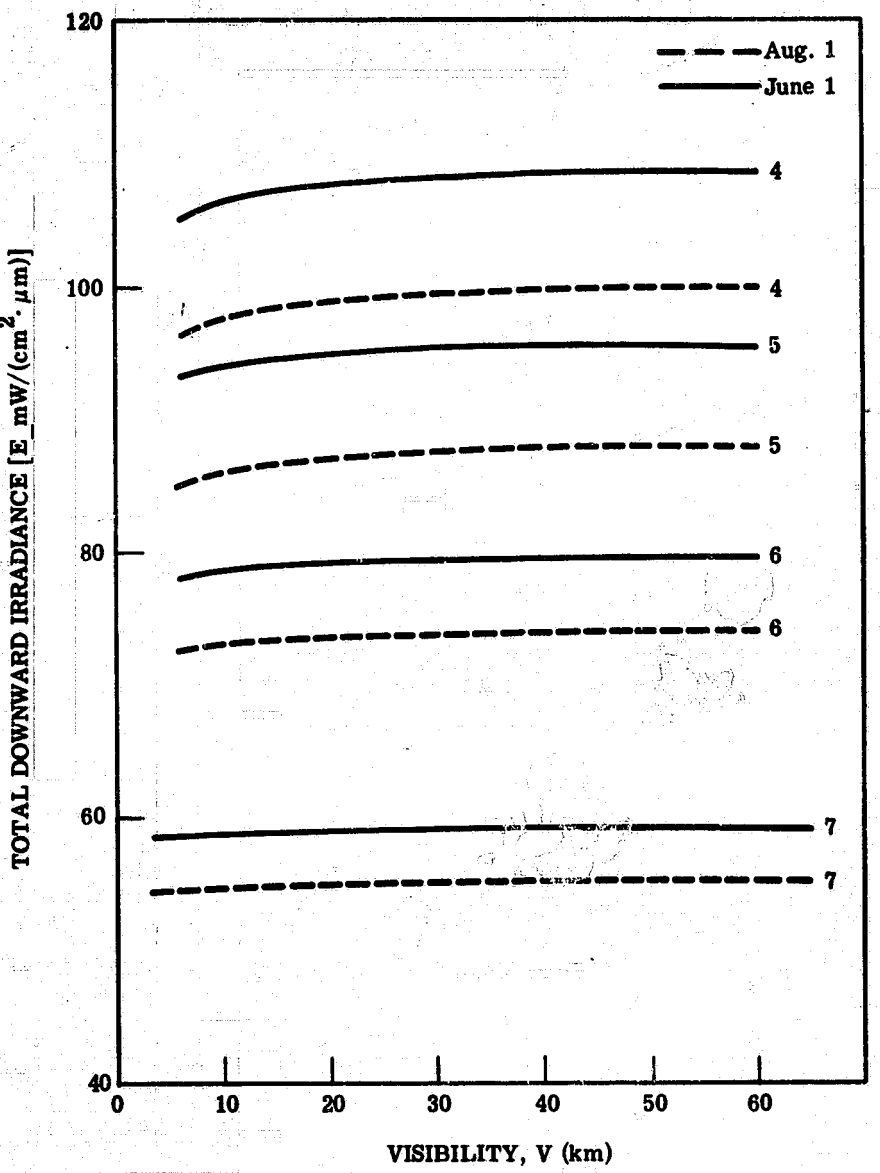
Total Radiance (L) for June 1 and August 1

FIGURE 5. ERTS MSS CHANNELS 4 THROUGH 7, NORTH DAKOTA. All quantities are functions of horizontal visual range (Visibility, V). (Continued)



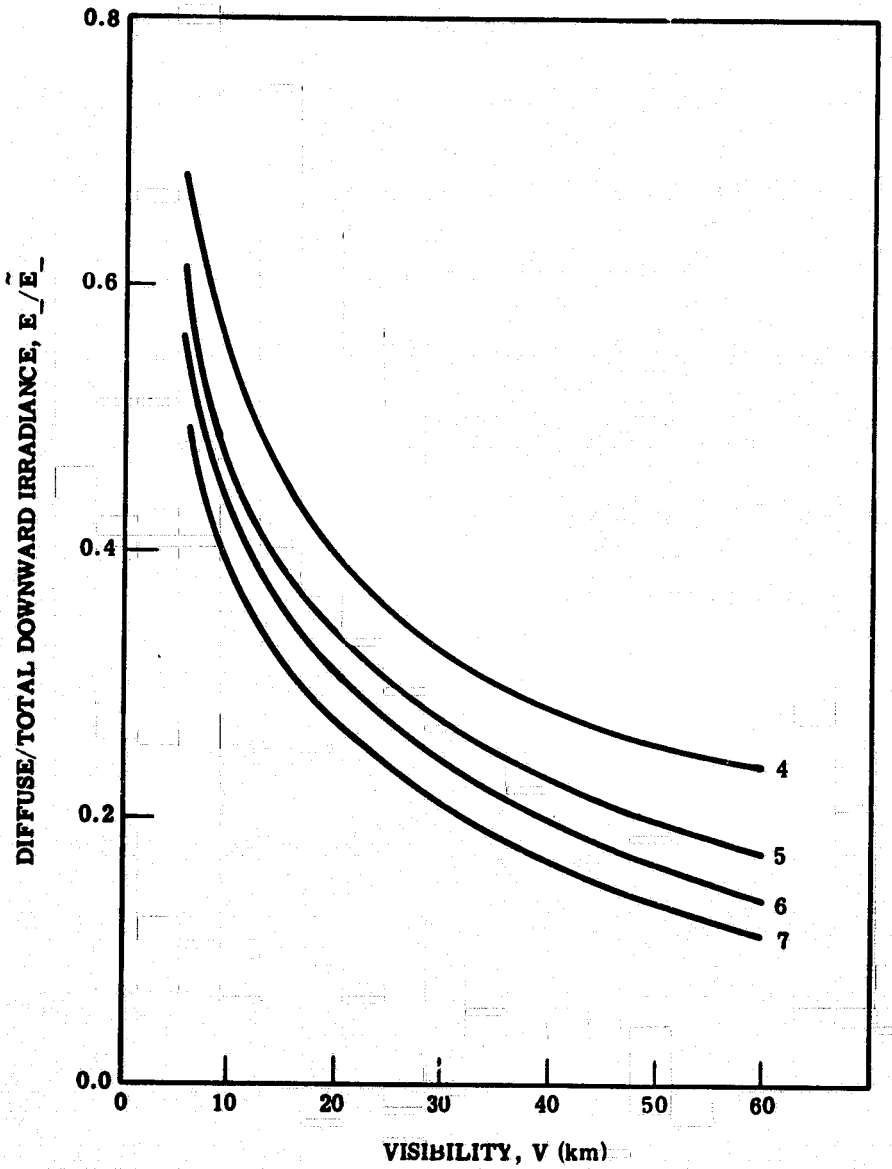
Diffuse Downward Irradiance ($E_{\downarrow}$) for 1 June and 1 August

FIGURE 6. ERTS MSS CHANNELS 4 THROUGH 7, NORTH DAKOTA. All quantities are functions of horizontal visual range (Visibility, V). (Continued)



Total Downward Irradiance ($\tilde{E}_{_}$) for 1 June and 1 August

FIGURE 7. ERTS MSS CHANNELS 4 THROUGH 7, NORTH DAKOTA. All quantities are functions of horizontal visual range (Visibility, V). (Continued)



Ratio of Diffuse ($E_{\downarrow}$) to Total (Specular Plus Diffuse, $\tilde{E}_{\downarrow}$) Downward Irradiance for 1 June

FIGURE 8. ERTS MSS CHANNELS 4 THROUGH 7, NORTH DAKOTA. All quantities are functions of horizontal visual range (Visibility, V). (Continued)

Figure 9 shows the fraction of ground contrast getween two objects that reaches the ERTS sensors; again the effects of background are seen to be strong. The permissible loss of contrast depends on the area under investigation. For similar looking objects such as crops, with small originating contrast, the degradation due to the atmosphere might be sufficient to make them indistinguishable in the data acquired from a remote platform. From a preliminary look at the ERTS bulk imagery of the Woodworth Study Area, it sppears that in MSS-7 there is sufficient contrast between ponds and surrounding vegetation in July so as not to require much atmospheric effect compensation if only pond identification is to be done. However, for perimeter determination and for assessing water depth or quality and vegetation surrounding the ponds, other channels where the contrast is not so high include important information for which these computed compensations might prove very useful.

Corrections for the Aircraft Scanner

Aircraft data for the Michigan multispectral scanner exist for the Woodworth Study Area for several years. These have been used for water mapping using single band gray-level slicing (0.7-0.9 μm and 1.5-1.8 μm channels) as well as using multi-channel data for recognition. The details are described in reference [10]. The atmospheric effects simulation for the aircraft data was for the same dates and time as the ERTS, for a flight altitude of 1.37 km (4500 ft), and for the scanner having a scan angle range of ± 40° from nadir. The scan plane is assumed to be in nearly N-S direction as compared to the E-W direction for the case of the ERTS.

The angular variations of the atmospheric quantities can be best seen in the compensations computed for the aircraft flight discussed above. In Figure 10, the path radiance can be seen to strongly depend upon the scan angle,and its assymetry due to solar illumination effects (off nadir) can also be seen. The effect of increased visibility is, as before, to reduce the path radiance,and a similar effect for longer wavelengths can also be seen.

Conclusions

From this model study of the nature and severity of atmospheric effects in ERTS-1 and aircraft multispectral data over the North Dakota test site, several conclusions may be drawn.

1) For ERTS data, model computed variations with scan angle of atmospheric attenuation and path radiance are very small. This is undoubtedly because of the small total scan angle (11°) of the ERTS-1 sensors. One should not conclude from this that the atmospheric effects on performance of pattern recognition devices used to recognize ponds are negligible. Variations in atmospheric properties across the frame may introduce sizable variations.

2) Aircraft data, even where collected under what were thought to be ideal conditions (i. e. flying into or away from the sun), will have noticable variations in atmospheric effects present for most visibilities. These effects must be compensated for to obtain optimum pond mapping performance.

3) Variations in atmospheric conditions do significantly change the appearance of water from space. The effect is larger in the green than in the near infrared.

4) Background albedo differences influence the magnitude of atmospheric effects. Changes in these effects are greater in spectral regions where albedo differences are greater, and the proportional change in path radiance or transmission with albedo is not a strong function of visibility.

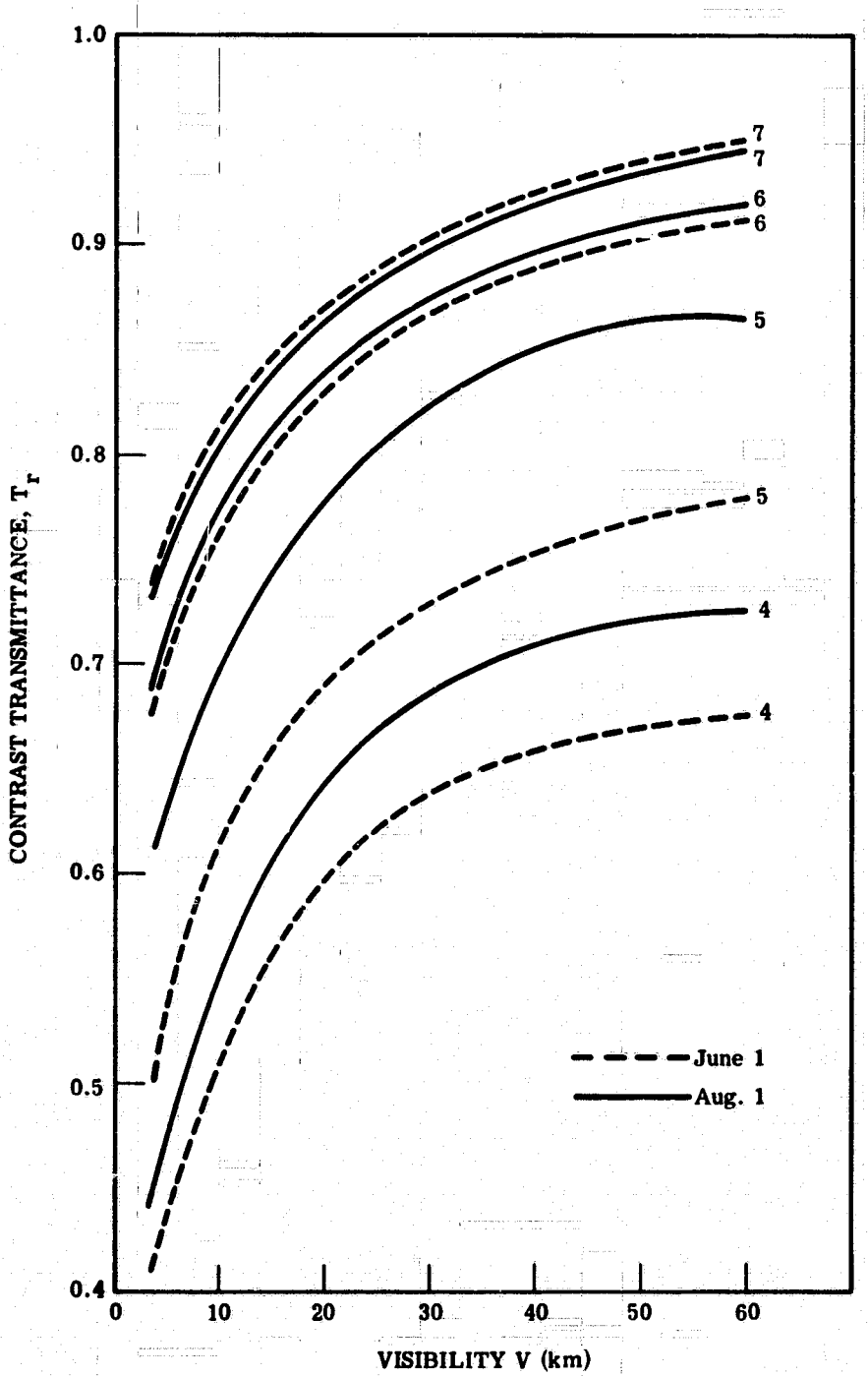
REFERENCES

1. E. A. Work and F. J. Thomson, "Further Studies of North Dakota Wildlife Habitat Mapping," Willow Run Laboratories, The University of Michigan, in publication.

2. R. E. Turner, W. A. Malila, R. F. Nalepka, "Importance of Atmospheric Scattering in Remote Sensing (or everything you have always wanted to know about atmospheric scattering but were afraid to ask)," 10259-1-X, Proc. of the VII International Symposium on Remote Sensing of Environment, 17-21, May 1971, Willow Run Laboratories, The University of Michigan, Ann Arbor.

3. W. A. Malila et al., "Studies of Spectral Discrimination," Willow Run Laboratories, The University of Michigan, Report No. 31650-22-T, May 1971.

4. L. Elterman, "UV, Visible and IR Attenuation for Altitudes to 50 km, 1968," AFCRL-68-0153, Environmental Research Papers, No. 285, Air Force Cambridge Research Labs., Bedford, Mass., April 1968. Also, "Vertical Attenuation Model with Eight Surface Meteorological Ranges 2



Contrast Transmittance (T_r) for 1 June and 1 August

FIGURE 9. ERTS MSS CHANNELS 4 THROUGH 7, NORTH DAKOTA. All quantities are functions of horizontal visual range (Visibility, V). (Concluded)

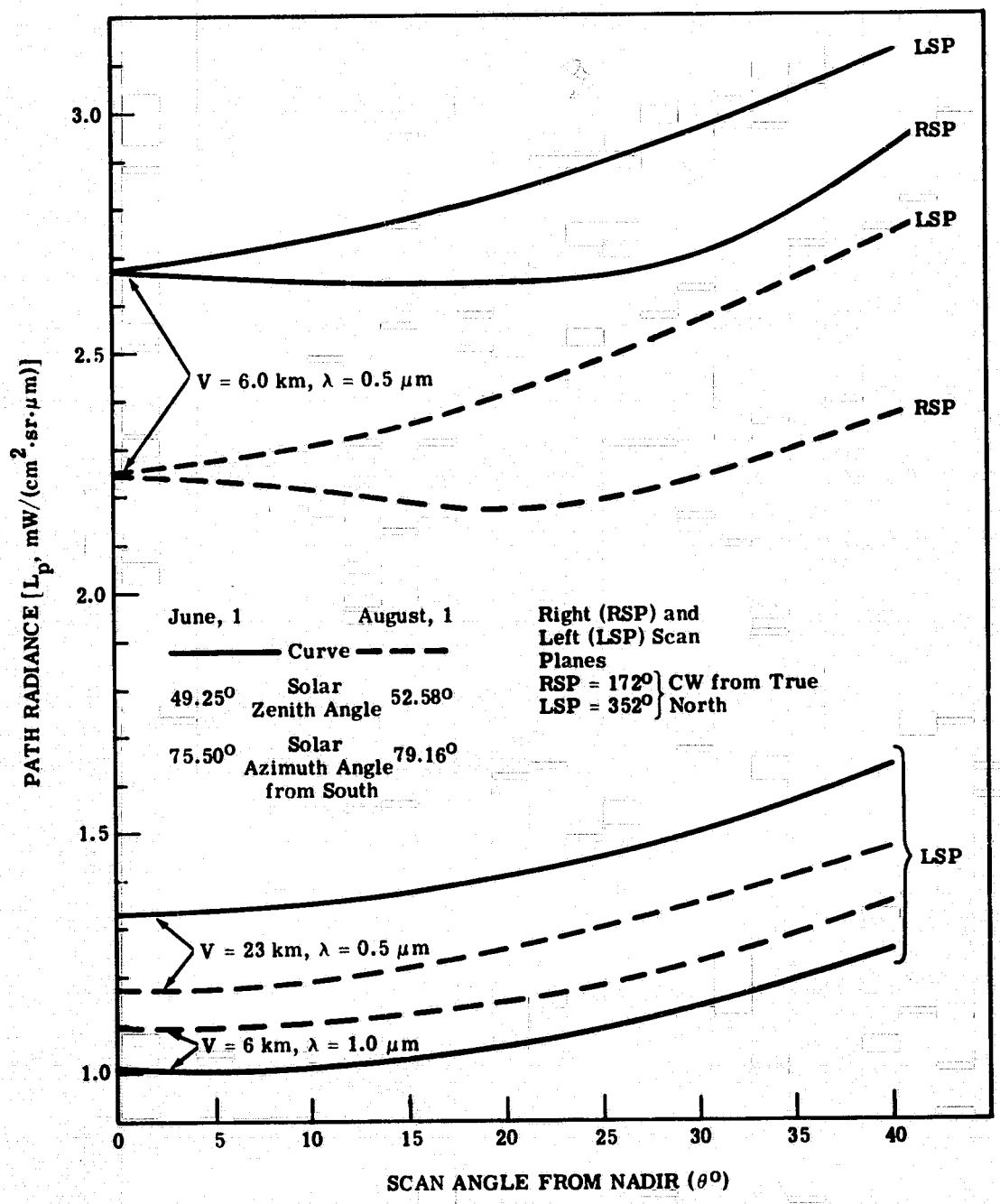


FIGURE 10. VARIATIONS OF ATMOSPHERIC EFFECTS WITH SCAN ANGLE. North Dakota, Woodworth study area [site altitude 0.76 km (2500 ft), latitude 47°02', longitude 99°15']. Simulated aircraft flight at 0900 CST at an altitude of 1.37 km (4500 ft) above terrain.

to 13 Kilometers," AFCRL-70-0200, March 1970. (Same author and address as above).

5. W. A. Malila et al., "Information Extraction Techniques for Multispectral Scanner Data," Willow Run Laboratories, The University of Michigan, Ann Arbor, Report No. 31650-74-T, June 1972.

6. W. D. Sellers, Physical Climatology, pp. 14-16, University of Chicago Press, 1965.

7. Azimuths of the Sun and Other Celestial Bodies of Declination 0° to 23°, U. S. Naval Oceanographic Office, U. S. Government Printing Office, Washington, D. C., H. O. Publ No. 260, 1964.

8. V. Leeman, D. Earing, R. K. Vincent, S. Ladd, "The NASA Earth Resources Spectral Information System: A Data Compilation," Willow Run Laboratories, The University of Michigan, Report 31650-24-T, May 1971.

9. M. P. Thekaekara, "Evaluating the Light From the Sun," Optical Spectra, pp 32, March 1972.

10. W. G. Burge and W. L. Brown, "A Study of Waterfowl Habitat in North Dakota Using Remote Sensing Techniques," Willow Run Laboratories, The University of Michigan, Report 2771-7-F, July 1970.

USE OF REMOTE SENSING IN ENFORCEMENT ACTIVITIES:

PRESENT AND FUTURE

DR. MURRAY FELSHER
ENVIRONMENTAL PROTECTION AGENCY
OFFICE OF ENFORCEMENT AND GENERAL COUNSEL
OFFICE OF TECHNICAL ANALYSIS

Thank you, Mr. Chairman.

Ladies and Gentlemen, the title of my talk is the "Use of Remote Sensing in Enforcement Activities: Present and Future." It is not my intention this morning to present to you a detailed and comprehensive list of subjects, fields, and topics to which may be applied the techniques of remote sensing for enforcement purposes. Indeed, I began to construct such a list, and very soon it became apparent that I was writing a table of contents for a large book on applications of remote sensing of the environment, which resembled very closely the Table of Contents of the Summary volume we received on registering for the symposium yesterday. The point is, of course, that we, in the Environmental Protection Agency, are mandated to specifically undertake what the Agency name says -- protect the environment. And, as we see it, environment is an all-inclusive term. Our concern is with the atmosphere, and the lithosphere, and the hydrosphere, and the biosphere. And remote sensing is concerned with all these. And so we at EPA are concerned with the entire field of remote sensing. Those of us in the enforcement area have special interest in those remote sensing applications and techniques related to the case problem areas we happen to be investigating at the time.

Note also that the title of the talk does not include a reference to the Past. I will speak of the Present and the Future. The reason is, quite frankly, that the gathering of remote sensing intelligence, for use in enforcement-related activities, has been a poor step-child -- shunted aside for reasons that may be too obvious to be stated, but I will state them nonetheless in a few moments. There is no Past. There is a cautious Present. There will be a significant Future. This is my thesis, and this morning I will speak to you on behalf of those of us very much concerned with establishing a means for providing a high quality remote sensing capability to enhance the mission of the operating arms of the Environmental Protection Agency.

The Environmental Protection Agency, under Mr. William D. Ruckleshaus, operates through the offices of five assistant administrators. They oversee: 1) the Office of Planning and Management, 2) The Office of Categorical Programs, such as pesticides and fungicides, 3) the Office of Air and Water Programs, 4) the Office of Research and Monitoring -- OR&M, by the way, you will note is a co-sponsor of this symposium, and 5) the Office of Enforcement and General Counsel.

EPA is a rather small Agency, with a total of about 8000 employees in Washington and our 10 regional offices. The administrative responsibility of remote sensing in EPA resides with the Office of Monitoring, within the Office of Research and Monitoring, under Deputy Assistant Administrator, Willis Foster. A member of the Office of Monitoring, Robert Holmes, is a member of the Program Committee of this symposium and will chair one of the technical sessions tomorrow.

Standard laboratory facilities are available under each of the 10 regional administrators. In addition, four larger National Environmental Research Centers (N-E-R-Cs, or NERCs) have been named, each having smaller satellite laboratories attached to it. These NERCs report directly to the Assistant Administrator for Research and Monitoring, Dr. Stanley Greenfield. NERCs are located in Cincinnati, Ohio; Corvallis, Oregon; Raleigh-Durham, North Carolina; and Las Vegas, Nevada.

Within the past month NERC-Las Vegas has been designated as having particular concern with EPA's monitoring activities. As part of these monitoring activities, NERC-Las Vegas has for some time been gathering a team of specialists and increasing its aircraft capabilities. The facilities are used to support EPA requirements in monitoring atmospheric, terrestrial, and aquatic pollutants, and assessing the effect of the pollutants on the biota. Our air fleet includes 2 Turbo-Beech airplanes, a C-45, a single engine Beech aircraft, a C-123, a Grumman Mohawk, 2 de Havilland Otters, and 2 Huey Helicopters. The aircraft are navigationally well-instrumented, and carry the standard photographic, thermal, and SLAR instruments, besides a full complement of air sampling devices. This effort is the only EPA-operational remote sensing activity. Still, this handful of people and handful of aircraft, have managed, in this calendar year, to undertake and analyze such diverse missions in diverse places as:

- assessment of a San Clemente oil spill,
- assessment of a Gulf of Mexico oil well fire,
-
- investigation of oil shale areas in Colorado, Utah, and Wyoming,
- evaluation of Hurricane Agnes' flood damage to oil tank farms,
- assessment of Newport Bay sedimentation build-up,
- assessment of vegetation damage resulting from air pollution from the plume of a West Virginia power plant,
- survey of New York Harbor dischargers, and
- assessment of paper mill effluent in a Northeast Lake.

The aircraft operation at NERC-Las Vegas is represented here by Leslie Dunn and Robert Landers.

Although the bulk of laboratory operations in EPA fall under the purview of the Office of Research and Monitoring, there are two major laboratory-type facilities that report to the Assistant Administrator for Enforcement and General Counsel, Mr. John Quarles. These are our two National Field Investigation Centers, NFICs, located in Cincinnati, Ohio, and in Denver, Colorado. The mission of the NFICs is to provide for the Office of Enforcement and General Counsel a rapid-response team of field investigators able, at short notice, to acquire evidentiary data for use in case preparation. As part of this team, Denver-NFIC has acquired a capability for analysis of remote sensing photography and imagery. Reports have been submitted for such areas as Houston, Texas; Memphis, Tennessee; and White Wood Creek, South Dakota. By the way, I should note that my reason for pointing out to you the various EPA personnel present today is to ask you, in a not-too-subtle way, to look us up.

Well then -- a budding field operation in Las Vegas, an interest in Denver, and a concern in Washington. That, together with a scattered hopefulness at the regional level, marks the Present in remote sensing in the Environmental Protection Agency. The enforcement-oriented phases of these activities have been, by habit, minor. But they are on the increase.

The reason that there is no enforcement-related Past in remote sensing is due to a philosophical inheritance. There is a reluctance, I am sorry and a little bit afraid to say, on the part of many of you before me today, to engage in enforcement-related activities. There is a fully understandable historical reluctance to GET INVOLVED. (I hope you can hear the capital letters.) It has been difficult for a Federal agency to provide data to an enforcement activity, knowing that these data and those that generated it might one day have to appear as part of a civil or criminal suit in court. It is difficult for a private consulting firm to gather damning remotely-sensed evidence against a major industrial concern, and feel somehow that its name has been placed on a little list somewhere. It is difficult. No doubt. It is easier to direct one's facilities and talents along pure research and developmental lines. It is easier to distinguish from the air healthy foliage from dead foliage without worrying about what killed the trees. It is easier to concern one's self solely with whether or not a thermal sensor is accurate to 0.5 or 0.4 of a degree centrigrade, without worrying if indeed Federal-state thermal standards for effluent discharges are being violated by a power plant. It is easier. The message, for this part of my talk, is "Get Involved." It's as simple -- and as complex -- as that.

There is, fortunately, a growing concern within the highest levels of industry, government, and academe regarding the quality of the environment. This concern, I am certain, will be reflected by all of us, in the way we proceed with our work, and the type of work we elect to do. Regardless of your special training, you meet here as workers in remote sensing. Before you do turn your talents to enforcement-type activities let me caution you on some points. In contact sampling and analyses, some water, let us say, is collected, transported, and analyzed - all the while maintaining a strict record of chain of custody. It is essential that a specific sample be tracked, hand-to-hand, by proper identifying tags, that the sample is locked away carefully under custodial supervision, and so on. In other words, there is maintained specific linkage between sample collection and sample analysis. In remote sensing the same sort of linkage can be established between real-time data and the analyzed information resulting from these data. However, the link between the rock, the water, the soil, per se, and the scan line on the chart -- this link is missing. There is no physical attachment between the material sensed and the sensed data. I tend to think lately of a professor-friend who once told me that remote sensing, to its practitioners, must be likened to girl-watching on campus -- exciting, but inconclusive. One rarely comes to grips with one's subject. The phrase ground truth and validation, then, has nowhere more significance than in a remote sensing exercise undertaken for an enforcement purpose.

The acquisition of data, and their subsequent reduction, do not, of themselves, constitute an adequate response to environmental problems. Technological sophistication in hardware that is not accompanied by an enhancement of interpretative technique will do nothing but assure unacceptance of remote sensing by most of the scientific and legal community. As examples, we have sat through too many aesthetically pleasing slide lectures that have reproduced photography and imagery from aircraft and space platforms, where the speaker is unable to identify, with any assurance, the actual ground features we are observing. In my own work I have concluded that the farther one moves from the ground, the more one must know about it in order to make meaningful interpretations. It becomes crucial, under hospital conditions then, to approach remote sensing from the ground up. This means a team of field scientists (biologists, ecologists, geologists), determining and measuring in situ ground characteristics and parameters at the same time as these characteristics and parameters are imprinting themselves onto mechanical devices in overflight. Only then will we begin to go beyond the pretty-picture syndrome.

That water sample I mentioned earlier -- was collected, transported, and analyzed, all by conventional methods. At this point, allow me to expand on the phrase "conventional methods." These two simple words reflect the whole history of quality control and standardization techniques for collection methods, calibrations, and analyses. These have been built up through generations of trial-and-error, experimentation, and negotiations between national and international laboratories. Yet, as we all know, for many of the most trivial analyses, employing long-used instruments, there remain questions concerning calibration and standardization. For the newer analytical devices, the mass spectrometers, microprobes, NMRs, and the rest, the book is still being written. As for remote sensing devices, we now find ourselves in the unenviable position of looking at things we're unsure of, with instruments whose accuracy is uncertain, but whose reproducibility is definitely questionable!

Let me step backward from my posture of enlightened pessimism. I am indeed certain that there will be commonplace acceptance of remote sensing data in the courtroom. I am speaking now of eventual acceptance of interpretative information based on data acquired by the most sophisticated remote sensing devices. As an example, pursuant to Section 111 of the Clean Air Act, as amended, EPA promulgated in December 1971 New Source Performance Standards for Fossil-Fuel Fired Steam Generators. These standards regulate emission of particulate matter, sulfur dioxides, and nitrogen oxides from new fossil-fuel power plants. We have in-stack samplers. Data derived from these samplers will undoubtedly be acceptable to the court. However, what would the court do if presented with data derived: a) from an in-stack sampler, and b) from a ground-mounted sensor, and c) from an aircraft collecting samples from within the plume, and d) from an aircraft acquiring laser backscatter signatures through the plume, and add on your own e), f), and g) as you will. I believe that the results obtained from sophisticated instrumentation will one day be acceptable in a court of law. However, before moving to the most sophisticated state-of-the-art devices, I urge you to make certain that you can speak with assurance for your most plebian instruments. You don't learn about fiducial marks in law school. And a giga-Herz to a judge will remind him of a rental car -- no more. The message is, go slowly.

Our Assistant Administrator for Enforcement and General Counsel is already on record as having encouraged the development of techniques and expertise in remote sensing within EPA.

There is a willingness on the part of non-technical management to respond positively to the overtures of modern technology. It is essential, then, to proceed with due caution. Those of you considering entering into enforcement-related areas must select your hardware with the thought, in mind, "What will I need to get the job done?" Period. We do not deal in long range developmental programs in our end of the Agency. A case attorney with the Department of Justice will take ground truth plus and 8" x 10" glossy over any number of volumes of questionable printout.

As research and development proceed, various milestones are reached, and various instruments and techniques once classed as "exotic" become standard, off-the-shelf methodology. As such, they become available and acceptable for use in enforcement activities. This presupposes, of course, continual liaison and cooperation between user and research facilities. This means a lot of work. But there is much work to be done. We have identified more than 2700 major industrial dischargers into rivers in priority basins in the conterminous U. S. This is exclusive of municipal dischargers. As a matter of fact, 485 of these reside in EPA Region V of which Michigan is a portion. We have problem areas in:

- temperature differentiation of thermal discharges,
- mapping of suspended sediment distributions,
- delineation of surface and subsurface currents,
- recognition of oil films, toxic and hazardous substances,
- surface recognition of ground water movement in connection with deep-well disposal, and storage,
- ocean outfall delineation and effect,
- effects of dredging operations,
- mapping of salt seeps into navigable waterways,
- and many more.

I began by saying I won't give you a list, and I end by giving you a list.

If you are interested in constructing a rather complete list, look through the program of this Symposium. Each topic, if it is involved in an enforcement conference, or a lawsuit, or a 180-day notice, or a consent decree, or an abatement commitment letter, or any other litigation process, that topic becomes of interest to the Office of Enforcement and General Counsel.

I conclude by reminding you that our office, the Office of Enforcement and General Counsel, is a user office. We will use whatever technical means we have at our disposal to fulfill our mission. The latent present here today could help us fulfill our mission with finesse.

RESULTS OF THE 1971 CORN BLIGHT WATCH EXPERIMENT

Robert B. MacDonald, National Aeronautics and Space Administration
Marvin E. Bauer, Purdue University
Richard D. Allen, U. S. Department of Agriculture
Joseph W. Clifton, U. S. Department of Agriculture
Jon D. Erickson, University of Michigan
David A. Landgrebe, Purdue University

1. INTRODUCTION

A serious and unexpected epiphytotic of southern corn leaf blight reduced the nation's corn crop by 15 percent as a new race of this previously minor disease swept through the Southern and Corn Belt states during July and August, 1970. The disease appeared so suddenly and moved with such speed that accurate information on its extent and severity was not compiled until well after the end of the growing season.

Research by the Laboratory for Applications of Remote Sensing (LARS) in 1970 had shown that three stages of blight infection could be accurately classified from small scale color infrared photography and multispectral scanner data. It therefore appeared that remote sensing could provide valuable information on the incidence and severity of blight as it developed in 1971.

Many advancements in remote sensing technology have been made in recent years, but never before had all the components of an information system utilizing remote sensing measurements been assembled in one package. Thus the Corn Blight Watch Experiment was born out of a need to demonstrate and evaluate remote sensing in a real world situation.

USDA and NASA along with LARS, Willow Run Laboratories, and the Cooperative Extension Services (CES) and Agricultural Experiment Stations (AES) of seven Corn Belt states therefore joined forces to conduct an experiment which included all phases of an information system - remotely-sensed measurements, ground observations, a sampling model, data analysis, and an information dissemination network.

The objective of the experiment was to evaluate the use of advanced remote sensing techniques to:

- Detect the development and spread of SCLB during the growing season across the Corn Belt region;
- Assess the extent and severity of blight infection present in the Corn Belt;
- Assess the impact of blight on corn production;
- Estimate the applicability of these techniques to similar situations occurring in the future.

2. THE CORN BLIGHT PROBLEM

Southern corn leaf blight (SCLB) is caused by the fungus Helminthosporium maydis. The disease has been known for many years and is widespread in corn-growing tropical areas of the world. Until 1969, SCLB was considered a minor disease in the United States since it seldom caused severe leaf damage or loss in yield. At that time, a new race of H. maydis (race T) adapted itself to Texas male-sterile (TMS) cytoplasm corn. Ninety percent of the 1970 crop was the TMS type corn.

The 1970 Corn Blight Epiphytotic - Three factors were responsible for the corn blight epiphytotic of 1970: (1) a susceptible host (in this case Texas male-sterile

cytoplasm corn), (2) a virulent pathogen (in this case a new pathogenic race of the fungus H. maydis), and (3) a favorable environment for the pathogen (in many diseases caused by fungi, of which SCLB is one, warm, damp weather is ideal). The absence of any one of these three factors would have prevented the widespread development of SCLB in 1970. The rapid and widespread development of SCLB in 1970 is shown in Figure 1.

Reduction in 1970 corn yields from SCLB was difficult to estimate. However, blight, combined with severe drought conditions in some areas, is estimated to have reduced 1970 corn production about 700 million bushels from the original forecast total of 4.8 billion bushels. The forecast average yield per acre on July 1, 1970 was 83.1 bushels per acre; in December it was estimated that the harvested yield was an average of 71.7 bushels per acre--a reduction of 15 percent. In some states the average yield loss was greater and in many individual farm fields the crop was nearly a total loss.

Symptoms of SCLB are characterized by tan or light-brown spots or lesions that usually appear first on the lower leaves (Figure 2). Under suitable conditions wind or splashing rain carries spores to upper leaves producing secondary infections. Lesions are oblong and about 1/2 to 1 inch in length and 1/4 to 1/2 inch in width. On susceptible plants the lesions increase rapidly in number. The lesions may merge, severely blighting and killing the leaves. A scale showing the six stages of blight severity which can be identified on the ground is shown in Figure 3.

The lesions on the stalk, leaf sheath, and ear husks may enlarge rapidly to as much as 6 inches in length. The penetration of the silk end of the ear or the shucks takes 7 to 14 days in damp weather, and may lead to a mold of the kernels and cob. The grain is destroyed. With severe leaf-killing, stalk rot by H. maydis and other fungi is increased. As a result there is much lodging where blight is severe.

The Blight Problem in 1971 - The prevalence and severity of only a few crop diseases can be accurately forecast months in advance of their onset. At the present time, SCLB is not one of these. No one could predict with certainty what the extent and severity of SCLB would be in 1971. However, in 1971 the Corn Belt was faced with the very real possibility of more severe and widespread corn blight damage than in 1970. First, there were sufficient supplies of resistant seed to plant only half of the crop. Second, the disease was already omnipresent at the start of the growing season; whereas in 1970 it had developed and spread in the Corn Belt in July and August. Third, normal moisture and temperature conditions in the Corn Belt would be extremely favorable to the development of blight.

Growers planted 5 to 20 percent more resistant, normal cytoplasm seed than had originally been expected. The distribution of the resistant seed played a significant part in the pattern of blight development in 1971. A relatively larger portion of the resistant seed was planted in areas hard hit by blight in 1970. Those areas which escaped serious blight damage in 1970 planted a larger portion of susceptible TMS cytoplasm seed (Figure 4). The most severely-infected areas of the Corn Belt in 1971 were those where there was very little TMS cytoplasm seed planted. In addition, the greatest acreages of corn occurred in those areas which had relatively little blight (Figure 5).

Weather, however, was the single most important factor in determining the severity of SCLB in 1971. A warm, dry spring enabled farmers to plant early. This, combined with favorable growing conditions in May and June, got the crop off to a fast start. In many areas the crop was nearly mature before blight infection reached significant levels.

Cool, dry weather from mid-July to mid-August significantly reduced the build-up of blight which might have otherwise been expected (Figure 6). In many areas across a large portion of the Corn Belt region, blight lesions were present on the lower leaves throughout July and August, but the cool temperatures greatly retarded further development of the disease, and were at the same time favorable for ear development and high yields.

Although widespread the blight was not nearly as severe as in 1970. The 1971 growing season produced the highest corn yields on record, but it should be noted

that about 55 percent of the acreage in the Corn Belt had slight or mild levels of infection. Had the season's weather been warmer and more humid, blight development would have been as much or more than in 1970.

3. SAMPLING PLAN

The sampling plan involved the selection of the study area, determination of the flightline and segment sample design within the study area and determination of a field sample design.

A systems analysis approach was used in designing the Corn Blight Watch sampling model and data acquisition programs. Sampling decisions were not independent of data collection decisions. Decisions on ground data were never divorced from the impacts that those decisions would have on remotely sensed data.

Each decision was made by first defining the objectives for that aspect of the program. What was the goal for that aspect? What information or result was desired? How did each aspect meet the overall objectives of the experiment? How would the data collected be used?

Once the objectives for an aspect of the model had been defined, the resources available were itemized. In general, the resources used in the experiment were manpower, aircraft, and data processing facilities.

Once the objectives, resources and constraints had been defined, alternatives were drawn up and decisions made. In defining alternatives, people with expertise in particular aspects were consulted. Plant pathologists were contacted about the disease itself. People involved in planning large scale interview and field surveys were contacted about data collection forms and techniques. Aircraft people were consulted since the ground data collection had to be consistant with aircraft data gathering capabilities.

The result of this systems approach was an integrated model for sampling and data collection. For example, initial interview data from farmers provided not only the basis for selection of sample test fields, but provided auxiliary information for remote sensing interpretations.

Strict adherence to a sound sampling model enabled results of ground observations and analysis of photography and MSS to be expanded from individual field and segment estimates to estimates of the number of acres of each blight level present in the entire test area. The sampling model has also permitted an analysis of the cost and precision of many different combinations of flightlines, segments and fields to be made. Such information will be valuable in the future for optimizing sampling for remote sensing systems.

Selection of Test Area. The objectives used in selecting the test area in the Corn Belt were to include as much of the nation's corn acreage as possible and provide as wide east-west and north-south coverage as possible.

The main resources were the RB-57F and C-47 aircraft and enough manpower to collect data in approximately 200 segments.

The constraints on the size of the test area were the number of administrative units (states) involved versus the desired precision of estimates from collected data. Manpower and aircraft resources did not limit the size of the test area in themselves, but they did limit the amount of data which could be collected. Given that only so much data could be collected, precision of estimates would depend upon the size of the area sampled.

The test area decided upon included all of Ohio, Indiana, Illinois, and Iowa, the eastern crop reporting districts of Nebraska, the southern crop reporting districts of Minnesota and the northern and eastern crop reporting districts of Missouri. This area included 64 percent of the nation's corn acreage for grain in 1971. The test area provided an east-west magnitude of nearly 900 miles and north-south magnitude of nearly 400 miles.

The test area selected was not a homogeneous area in terms of cropping patterns. The percent of land devoted to corn varies greatly between states and

within states. Field sizes tend to be larger in the major corn producing counties in Iowa, Illinois, Minnesota and Nebraska than in Missouri and Ohio. A large proportion of the corn fields in Ohio and Missouri and in parts of the other states are located close to woods. Some corn fields were located close to or in metropolitan areas. Topography and soil types varied greatly between and within states. Thus, the remote sensing applications of the Experiment involved interpretation of corn against many different backgrounds.

Segment Size Determination - Given a test area for the project, the next necessary step was determination of segment (test site) size and number of segments which could be monitored. Since SCLB affected different cytoplasms or corn to greater or lesser extents, it was desirable to have as many different cytoplasms present within a segment as possible. In order to reduce time and travel costs, a segment had to be no larger than a one-person assignment.

It was necessary to compromise statistical efficiency in order to provide fairly large segments. Adjacent farms tend to be very homogeneous in terms of proportion of land planted to corn, varieties planted and cultural practices. Therefore, the most efficient sampling procedure for estimates from ground data alone would have been to select a large sample of small segments spread throughout the test area. However, this allocation of samples could not be covered in a high altitude aircraft study without going to complete photo coverage of the test area.

Number of segments and size of segment were determined to a great extent by manpower. ASCS indicated a willingness to devote 1,000-1,500 man days to the project for field operations. It was assumed that this input might be matched by the Cooperative Extension Services of the various states. If interviewing took about one week and if 7 to 8 one-day visits were made for field observations, about 200 segments of land could be studied.

A segment size of one mile by eight miles was adopted. This provided a good compromise between ground data collection requirements and expected number of corn fields per segment.

Segment Sampling Design. The objectives in selecting the segment sampling design were to represent the total area and maximize the statistical precision from the number of segments.

With the limitation of having a relatively small number of large segments, a simple random or stratified random sample of segments would have given the most precise estimates. Selecting 200 counties based on the square root of expected corn acres would have given a good distribution across the test area. Establishing one segment in each county would have minimized ground travel time and cost.

Such an allocation of segments was plotted but it could not be covered within the time constraints of two weeks. It was necessary, therefore, to select a sampling plan based on the aircraft limitations. In order to provide photographic coverage within a two-week period, the maximum number of flightline miles was estimated to be about 4,000 if flightlines were 100 miles or longer and about 3,000 if individual lines were to be 50 miles or less.

The sampling plan was re-evaluated in light of the constraints imposed by the aircraft and a two-stage (flightline and segment within flightline) procedure adopted although this would limit the statistical precision of estimates from the experiment. All estimates would contain between-flightline and between-segment within-flightline variations. Since segments within-flightlines should be relatively homogeneous, the between-flightline variance components were expected to be large.

In order to increase the statistical validity of at least part of the Experiment, it was decided to sample a portion of the test area in the more optimum manner. In order to accomplish this, total photo coverage was requested for a portion of the test area.

The three crop reporting districts in western Indiana were selected as the area for the more optimum sampling scheme. Many of the resources available were concentrated in this area. Since the C-47 aircraft could not cover the larger area in a two-week period, all scanner flights were made in what was called the

intensive study area. Thirty segments were designated for the intensive study area.

In the intensive study area three sources of data, ground observations, aerial photography and multispectral measurements, were compared using the more optimum one-stage sampling model.

The rest of the test area was sampled with 30 flightlines of approximately 100 mile lengths, each containing six segments. This gave a total of 210 segments (30 + 180). The total required flightline length was 4,000 miles.

Selection of Segments - Segments in both the intensive study area and the remaining portion of the test area were chosen by accounting for all land on maps and selecting the sample of segments from the total. In the intensive study area, this process involved a process of physically assigning all land to a specific segment. All of the segments were delineated on maps and a systematic sample of 30 segments chosen.

In the portion of the test area outside western Indiana, 1:1,000,000 aeronautical charts were divided into flightlines eight miles wide by approximately 100 miles long. A systematic sample of 30 flightlines was chosen. Each flightline was then divided into segments one mile by eight miles. A sample of six segments was chosen in each flightline.

Sample Field Selection - The goal in selection of fields for visits during the growing season was to represent the different cytoplasms present in each segment. However, the number of fields per segment had to be limited to a number which could be visited in one day.

Eight to ten fields was felt to be a reasonable maximum number of fields for an assignment. Once units were established within a field the field observer returned to the same units each time. Since detailed observations were to be made on only five plants in each of the two units in the field, it would not take long for the observations.

The strata used for sample field selection were (1) normal cytoplasm (resistant to SCLB) only, (2) Texas male sterile (susceptible to SCLB) cytoplasm only, (3) blends of normal and Texas male sterile only, (4) F-2 or open pollinated (non-hybrid) fields and (5) combinations of the other strata planted in a field plus unknown cytoplasms.

Two fields were selected from each stratum present giving a maximum sample size for a segment of ten fields. The maximum in most segments was eight fields since F-2 and open pollinated fields rarely occurred. In the intensive study area the sampling rate was increased to 12 fields per segment.

It was envisioned that nearly all sample corn fields might be needed for training by photo-interpreters and scanner analysts. There would be few, if any, fields with ground data left for testing of classification results. Therefore, an additional sample of fields was selected in 24 segments. These additional fields were worked by ASCS personnel and could be used for testing by individual interpreters and analysts. Also, they would provide insurance that adequate ground data was being collected in at least part of the segments in case more data was needed for training.

4. DATA ACQUISITION

Data acquisition for the CBWE included ground and aerial data. Ground data consisted of baseline data collected during the Initial Interview Survey and blight data collected during the Field Observation Survey. Aerial data consisted of small scale photography and multispectral scanner data.

Ground Data Collection

Initial Interview Survey - The objectives of the initial interview survey were to (1) identify crop or land use in each field within segments, (2) collect information on corn fields for sample selection, and (3) collect information which might be helpful in remote sensing interpretations.

Each farm operator in the segment was identified and interviewed. Each of his fields was delineated on aerial photography prints and numbered. Acreage and crop or land use was recorded for every field. Nonagricultural areas within the segment were delineated, but no information from them was processed.

Additional information was collected for each corn field. Specific questions were asked about the field and its susceptibility to SCLB. These included cytoplasm of corn planted, variety of corn, whether corn was planted in the same field the previous year and if blight was apparent in corn fields the previous year. The remaining questions were intended to provide information for interpreting the appearance of each corn field on remote sensing images. These questions included planting date, row width, plant population, row direction, and whether the field would be irrigated.

The initial interview were conducted by personnel in the county offices of the Agricultural Stabilization and Conservation Service, USDA. These personnel were experienced in contacting farm operators and in the use of aerial photography.

All interviewers attended a one-day training school. All aspects of the survey were covered in these intensive training sessions. Four-man teams from the participating agencies conducted the training schools.

Over 8,000 interviews were conducted by some 300 ASCS personnel during a 10-day period. Information on land use and acreage was obtained for over 56,000 fields.

Field Observation Data - The Field Observation Survey was designed to obtain the following four types of information to describe the conditions in two randomly selected units within the sample fields:

1. The amount of vegetation present.
2. The presence and severity of Southern Corn Leaf Blight.
3. The presence and severity of other crop stresses.
4. Crop maturity and other information which might affect photography and scanner imagery.

To obtain estimates of the amount of vegetation present, the following items were recorded: row width, number of plants in 30 feet of row, number of leaves per plant on five plants in the unit, and length and width of the leaf at the seventh node of each sample plant. From these items plant population and leaf area index could be calculated.

Data for estimating Southern Corn Leaf Blight infection were obtained in two ways: (1) Placing each of the five sample plants in unit 1 and 2 into a blight severity class from zero (none) to five (very severe), and (2) counting the number of lower and upper leaves with lesions and estimating the percentage of lower and upper leaf area covered by lesions. A blight severity rating was then calculated from the information in (2).

Other stresses such as drought, weediness, lodging, hail damage, insect damage, other diseases and nutrient deficiency were identified. Specific comments describing the kind and extent of stress were requested of the field observers to aid in the interpretation of the sample fields on photographs and scanner imagery.

Other information which might aid remote sensing interpretation included information on the stage of maturity and uniformity of the field. The field observer compared the randomly selected units with the portion of the field surrounding the units in determining whether the units were representative of the field.

The basic requirements of the field observation procedures were that data should be repeatable and consistent. If two people were sent to the same field independently, the results should be the same. Thus, variation in observations were due to physiological changes, not sampling variations. In order to have repeatable and sequentially consistent data, certain plants or areas of each field were defined and marked. Procedures were designed so that each observer located and marked the two random sample units in exactly the same manner.

Yield Survey - As the growing season progressed there was increased interest in obtaining yield information from the sample fields. As a result, ears from the sample plants observed during the season were harvested and sent to LARS where they were dried, shelled, weighed and yield estimates calculated.

The information from each field was not expected to be sufficient to accurately estimate the yield of that field; it would take many random samples within a field to arrive at such a figure. However, the data from all similar fields, taken as a group, did give an accurate description of the effect of blight on yield.

Aerial Data Collection

The NASA Manned Spacecraft Center supported the Corn Blight Watch Experiment by acquiring remote sensor data with the dedicated use of the RB-57F and the University of Michigan C-47. The RB-57F collects photography at altitudes of 50,000 to 60,000 feet. The C-47 is equipped with a 12-channel multispectral scanner. The Project was organized into 3 phases based on the mission objectives and imagery required.

The objective of the Phase I, conducted in April, was to acquire current black and white photography to provide enlarged prints of each test segment. These prints were sent to USDA and used for the Initial Interview and Field Observation Surveys, as well as by data analysts.

In May, the RB-57F obtained color infrared photography while the C-47 obtained multispectral scanner data for soils background information. This was termed Phase II.

Finally, the two aircraft collected color infrared photography and multispectral scanner data over their respective flightlines and segments repetitively throughout the growing season. This was known as Phase III and extended from mid-June through September.

RB-57F Mission Requirements - Aerial coverage by the RB-57F included extensive areas of Ohio, Indiana, Illinois, Iowa and portions of Minnesota, Nebraska, and Missouri. Two hundred and ten test segments were defined along 38 flightlines.

Approximately 3800 flightline miles of data were flown during Phase I and Phase II as well as bi-weekly during Phase III. Each flightline was independent except in western Indiana where eight parallel and overlapping flightlines provided contiguous coverage of the intensive study area. Phase I flights were flown at 50,000 feet to provide a convenient scale for subsequent enlargements. Phase II and III were flown at 60,000 feet for optimum aircraft endurance and sensor coverage.

Data acquired by the RB-57F during Phase I was Aerographic Type 2402 black and white photography which was provided to USDA in the form of 24" x 35" paper prints enlarged to a scale of 1:20,000. Aerochrome infrared type 2443 color infrared imagery was acquired by the RB-57F during Phase II and III. Duplicate positive transparencies and color prints were provided to the Data Reduction Center. Delivery of processed imagery to LARS was required with minimum delay to permit analysis of photographic imagery in conjunction with ground observations.

RB-57F Mission Planning and Operations - Planning the RB-57F portion of the project was similar to most previous operations with two major exceptions. These exceptions were data quality and data delivery.

Color infrared imagery obtained from previous RB-57F missions had often been nonuniform in exposure over multiple frames and within frames due to factors such as sun angle and atmospheric effects. Nonuniformity also occurred from frame to frame due to sun angle and scene brightness changes. This made analysis difficult, particularly since the interpreter was looking for subtle tonal differences. To reduce exposure nonuniformity, changes were made in camera operation and processing

techniques. While these efforts did not eliminate the problem, they did result in improved data products. The north-south flightline orientation did permit optimum use of photographic overlap. A single emulsion batch of color infrared film was obtained to reduce the tonal variations anticipated if more than one emulsion batch was used during the Project.

Two problems occurred with the selected infrared film. Early in Phase III, an abnormal spotting condition was detected on the color IR imagery. The defect was termed "cyan spotting" because the mottled appearance of the imagery was caused by a defect in the cyan layer of the emulsion. The cyan spots occurred randomly and made analysis of the imagery difficult. During the Experiment, supplemental film was flown to partially overcome the cyan spotting problem.

In addition to the cyan spotting problem, the selected color IR film lacked adequate range in infrared tonal variations. In other words, the film was too saturated. This problem, also, was partially eliminated by the use of film with a less sensitive infrared emulsion.

Timely delivery of the data to LARS presented a difficult problem. A data management plan was prepared in order to meet the required delivery dates while minimizing the impact to ongoing programs.

Weather is a critical factor in planning aircraft remote sensing missions. The Corn Blight Project made greater use of long range weather planning guides in order to estimate the scope of coverage that should be attempted. Day to day mission operations were conducted with the assistance of an onsite meteorologist who monitored weather conditions and was prepared to advise the aircrew on the most suitable test site areas. While no attempt was made to compare actual versus forecast weather, the success of the data acquisition indicates that both long and short term weather forecasts are essential to mission planning and operations.

A factor that increased the operational flexibility of the RB-57F and directly affected the success of the mission was the use of a standard sensor configuration. This eliminated sensor configuration changes in day to day operations and permitted data acquisition limited only by weather conditions, film capacity, and aircraft endurance.

In summary, the RB-57F efforts resulted in the completion of 85 percent of the required coverage with less than 30 percent cloud coverage affecting the imagery. Fifty-four flights were flown over the Corn Belt. Four hundred hours of flight time were expended on the Corn Blight Watch which is approximately 2/3 of the annual RB-57F flight time allocation. Thirty percent of the available mission time was lost due to unsuitable weather, 20 percent was lost due to unscheduled maintenance, and 5 percent was lost due to scheduled maintenance. A 50 percent utilization factor is probably a good planning figure for future missions under similar conditions.

C-47 Mission Planning and Operations - The University of Michigan C-47 was also dedicated to the 1971 Corn Blight Watch Experiment. The C-47 provided Phase II and Phase III coverage of the 30 test segments within the ISA with the 12 channel multispectral scanner, and supplemental photography. Phase II coverage was coincident with the RB-57F Phase II operations. Phase III operations began in late June and continued bi-weekly until early October. The 30 test segments were flown individually at 5,000 feet.

Operational criteria were established to provide acceptable multispectral scanner data. These criteria specified that visibility at the flight altitude must be at least 6 miles with less than 30 percent cloud cover above the aircraft and less than 15 percent below the aircraft. The minimum acceptable sun angle was 50 degrees although this limit could not be met later in the mission. These criteria proved to be satisfactory; however, an additional constraint was added later in the mission. It was determined that an excessive aircraft drift angle was unacceptable due to excessive image distortion. A limit of 15° drift angle was imposed to reduce the image distortion to acceptable levels.

In summary, 98.4 percent of the sample areas were satisfactorily completed by the C-47. One hundred and fourteen flight hours were expended.

In conclusion, for both the RB-57F and C-47, the project was different than previously planned missions in duration, coverage, and sensor configuration. The wide area coverage and single sensor configuration provided flexibility in mission operations that greatly contributed to mission success.

The project provided a unique opportunity for review of the data on a timely basis permitting sensor corrections to be made and evaluated in the field.

The Experiment was also provided an excellent prelude to future support of complex aircraft and spacecraft missions.

5. DATA HANDLING AND ANALYSIS

Data Flow

The Corn Blight Watch Experiment was conducted in three phases. The data flow is best presented by describing the transfer of data from data acquisition centers to and between the data processing centers for each phase. The data flow plan is graphically shown on diagrams which include each center and each transfer of data between the centers.

Phase I - During Phase I, baseline data for the entire Corn Blight Watch Experiment were collected between April 15 and May 15. Data acquisition for Phase I included the collection of black and white photography. Processing included the reduction of photography to a scale of 1:20,000, the outlining of tracts and fields on the reduced photography, and the reporting of farm operator interviews through SRS to the data reduction center at LARS. Figure 7 shows the data flow for Phase I.

At SRS the segment was outlined on one copy of each print and this was sent with initial interview forms to the Agricultural Stabilization and Conservation Service county enumerators. Each farm operation in the segment was outlined and visited by the ASCS enumerator. During the interviews a field ID was assigned to each field, field boundaries and ID annotations were added to the photograph, and the initial interview forms were filled out for each field in the segment. The annotated photographs and completed initial interview forms were copied onto the other two sets of prints and the data on the forms were coded, punched, edited, and recorded in digital format. One set of baseline photographs and a digital copy of the initial interview data were sent to the Data Reduction Center at LARS. A second set of baseline photographs was sent to the Cooperative Extension Service in each state where segments were located.

Phase II - In Phase II, between May 10 and May 30, color IR photography was collected over the 210 segments and multispectral scanner data were collected over the 30 intensive study area segments. These data were analyzed for soils characteristics to provide soils background information for corn fields in the segments. The flow diagram for Phase II is shown in Figure 8.

Phase III - Eight missions were conducted during Phase III between June 14 and October 13, 1971. During this phase, color IR photography was collected every 14 days over all 210 segments and multispectral measurements were collected every 14 days over the 30 segments in the intensive study area. Early in each 14-day period, ground observations of up to 12 corn fields in each segment were acquired. These data were processed and sent to the data reduction center at LARS. Fifteen segments of multispectral data and ground observations were sent to the data reduction center at WRL. The photographic and multispectral data were analyzed and results were reduced and reported to SRS in Washington and to the other participants in the Corn Blight Watch Experiment. The major data transfers for Phase III are shown in Figure 9.

During Phase III a new mission was started every other Monday, June 14, June 28, July 12, July 26, August 9, August 23, September 6, and September 20. Each mission was completed in 21 days and results were punched, checked, collated, and reported 23 days after the mission began.

The biweekly field observation reports were sent to the SRS state offices during the first week of the period, and, for the 30 segments in the intensive study area, reports were also phoned to the Data Reduction Center. At the SRS state offices data were edited, coded, and punched onto data cards. At SRS in

Washington, they were error checked, copied onto digital data tapes, and listed on ground observation printouts. The biweekly data were delivered to the Data Reduction Center, and Ground Observation Summaries, described later, were distributed to the analysis teams by day 10 of each biweekly period, the same day as photographic data were available.

Analysis Procedures

Each of the data analysis teams was given a Ground Observation Summary for the segments to be analyzed or interpreted. A new summary was distributed each period so that pertinent information required for analysis would always be available. Although the form of the summary was the same each period, parameters listed were added or dropped according to the needs of analysis teams. In the flight information area of the summary, the segment number, film roll number, frame number, date and time of the flight, and flight direction were listed. Next information for the corn fields visited biweekly was listed as well as some information for all other corn fields and non-corn fields in the segment.

Photointerpretation - With the film roll transparencies mounted in the Variscan, a rear projection system, the frame indicated by the Ground Observation Summary could be located by a photographic analysis team as shown in Figure 10. Using the summary and the baseline photograph, the biweekly corn fields were located and studied so the teams could train themselves on the appearances of blight levels in the segment. The number of fields used for training varied during the experiment; not all biweekly field information was used.

Next each corn field in the segment was located and interpreted, and the results recorded on a recording form. These results were coded, punched, edited, and added to the Corn Blight Record for each of the 210 segments. The six teams of photo analysts completed their analysis by day 23 of each period. On the average each segment was analyzed one week after the data collection date.

Multispectral Data Analysis - Fifteen segments out of 30 in the Intensive Study Area were analyzed by LARS. The analog tapes were digitized and displayed on a digital display. Figure 11 shows an analyst locating the biweekly fields using a baseline photograph and lightpen. The data from the biweekly fields were analyzed using a clustering procedure, and the results were used to determine classes for the analysis and data points for generating class statistics. Next the channel selection program was used to pick four optimum channels for classification at Purdue and six optimum channels for classification at WRL. In general all channels of data collected were used during the season. There was no single best set of channels; however, a thermal channel, two reflective IR channels and a visible channel were usually selected for classification of the segment. At WRL a similar procedure was followed using analog techniques on the other 15 segments in the Intensive Study Area.

Results for all 30 segments were reported both on a total segment basis and on a field-by-field basis with LARS and WRL using the same reporting forms. The entire segment was classified into non-corn and corn classes of different blight levels. This is a more complicated classification than interpreting blight levels only in corn fields. The multispectral scanner results were also completed by day 23 of the period and were finished an average of 10 days after the segments had been flown. These results were also recorded on the Corn Blight Record. Detailed descriptions of the LARS and WRL analysis procedures may be found in other reports.

Corn Blight Record

A record of the information obtained for every field in each of the 210 segments was maintained on digital tape. The system designed for accomplishing this task and implemented for the Corn Blight Watch Experiment was called the Corn Blight Record and is shown in Figure 12. The initial interview data and biweekly field observations were merged with flight log information, multispectral analysis results, and photointerpretation results. The resulting tapes, one for the seven state area and one for the intensive study area, were the source of most of the listings and tabulations generated during the experiment.

Data analysis results in the form of tabulations were generated on day 23 of

each period for SRS in Washington. Expansions of results according to the sampling model were also generated for each period for ground observations, photographic analysis, and multispectral data analysis. Breakdowns of blight results by cytoplasm and for many other parameters were made. Yield calculations were also made. In addition, the results were analyzed using standard statistical techniques such as correlation and analysis of variance.

Results Summarization and Dissemination

In Figure 13 the data flow for dissemination of the blight analysis results is summarized. For each biweekly period, color IR photographs were sent to the county enumerators for their particular segments. Questions and training materials were sent with the prints and results were returned for evaluation. The purpose of this aspect of the experiment was to acquaint the enumerators with small-scale photography.

Summarization of ground observations was performed by SRS within one week of data collection. Photographic and multispectral analysis results were sent to SRS within an average of two weeks after data was collected. These results were available to SRS for compiling blight reports to the USDA information center which in turn handled press releases to the news media.

6. EXPERIMENT RESULTS

Blight Detection and Mapping

The development of blight in the Experiment test area is shown in Figures 14 to 16. Through July 30 the average blight severity was only none to slight over the entire area. In T-cytoplasm fields mild levels of infection were developing in Missouri, southern Illinois, and southern and west-central Indiana (Figure 14).

Two weeks later there had been a further increase in the prevalence and severity of blight infection with some areas of severe infection present in Illinois and Indiana (Figure 15). By the last week of August blight infection had become more widespread with at least mild levels present in much of the eastern Corn Belt area. Figure 16 shows the areas in Illinois and Indiana where blight was most severe in T-cytoplasm fields. Although there was some increase in the severity of leaf infection in September, most of the crop was nearly mature and further infection had little or no effect on yields.

The development of blight during the 1971 growing season is summarized in Figure 17. At the end of the growing season less than 20 percent of the acreage had moderate or severe infection levels and only about five percent of the crop was severely infected (Figure 18).

Although the 1971 growing season produced the highest yields on record, it should be noted that about 55 percent of the acreage in the Corn Belt had slight or mild levels of infection. Had the season's weather been warmer and more humid, blight development would have been similar to 1970.

Photointerpretation Results - The photointerpretation results can best be examined by comparing the photointerpretive estimates of blight severity with those made from ground observations. The first level of comparison will be estimates of total number of acres in each blight severity level for the entire experimental area (Figure 19). There is close agreement between the two estimates at all blight levels except 0 and 1. The higher number of acres of blight level 0 estimated by photointerpretation indicates that slightly infected corn could not be distinguished from corn with no infection using photointerpretation techniques; therefore, corn with level 1 infection was probably called blight level 0 (healthy corn) in many cases. The variances for field and photointerpretive estimates are of similar magnitude.

Photointerpretive and field observation results can also be compared at the flightline level. The average blight severity level for each flightline according to ground or photointerpretive estimates was computed from the expanded acreage of corn in each blight level in the flightline. Figures 20 and 21 make these comparisons for the period beginning August 9 and August 23.

During the two-week periods beginning August 9 (Figure 20) and August 23 (Figure 21) the photointerpreters tended to over-estimate the average blight levels relative to ground estimates. This was largely due to the difficulty of distinguishing blight effects from effects caused by other factors which appear similar to blight damage on the infrared film. Some of these factors include other diseases, drought damage, insect damage, and nutrient deficiencies. Work is continuing to further quantify the similarities and differences in appearance of these factors on color infrared film.

Unfavorable weather prevented collection of photography over the eastern half of the area during the period from September 6-19. For those flightlines where comparisons could be made, there was good agreement between ground observations and photointerpretation results.

Although ratings of blight severity were made in many fields across the Corn Belt, an average of only eight fields per segment were checked on the ground. Most of these fields were used for training. To make the best tests of classification accuracies, ratings would be needed from many more fields so that field by field comparisons could be made. However, only a limited number of fields were available for this kind of test. Therefore, other kinds of statistical analysis have been used to evaluate the classification results. One of the procedures used was correlation. Correlation is a quantitative measure of the degree of agreement between the two methods, both of which are known to be subject to experimental error. Close agreement between field observations and photointerpretation (or machine analysis of multispectral scanner data) means that the two methods are estimating the same value for the parameter.

To more quantitatively illustrate the same data shown on the previous maps, plots of field observation estimates versus photointerpretive estimates are presented in Figure 22 for two periods. Segment means are shown in Figure 22 whereas flightline means were shown in the previous figures. Note that there is an increase in the correlation coefficient (r) for the later period when more levels of blight were present. The 1:1 line is shown as an aid in determining when there is good agreement between the two methods; it should not be confused with a regression line. Perfect agreement between the two methods would result in all points falling on the 1:1 line. A consistent bias (either over- or under-estimation) would still result in high correlation.

A major objective of the experiment was to determine if healthy corn could be distinguished from diseased corn by remote sensing methods. The graph of correlations for two classes of blight severity (0-1-2 and 3-4-5) indicates that the corn fields could be accurately separated into the two classes, healthy or slightly blighted and moderately to severely blighted (Figure 23). The data points in Figure 23 represent acres of each blight severity class in a segment. Correlation coefficients of .90 and .64 were obtained for the two classes, respectively. There was a tendancy for photointerpretive results to underestimate the acreages in the healthy corn class and overestimate the acreages in the moderate to severe blight class as compared to ground estimates. Attempts to differentiate the six individual blight classes which can be distinguished on the ground were unsuccessful. This was indicated by low correlation coefficients ($r = .21$ to $.67$), the "scatter" of the data points, and large deviation from the 1:1 line. This is not surprising since differences between individual classes are subtle. The early stages of infection are confined to the lower leaves which are hidden from the view of the sensor.

Several photographic variables may have affected the photointerpretation results and complicated the task of blight assessment by photointerpretation. Changes in illumination conditions, haze, terrain features, and other factors could not be controlled. Problems with oversaturation and cyan spots have already been discussed.

Machine Analysis of Multispectral Scanner Data Results - In the intensive study area multispectral scanner data were collected along with ground observations and color infrared photography. A comparison of three methods of estimating the total acres in each blight class for the entire intensive study area is shown in Figure 24. The ground estimates and machine analysis estimates agree closely and have similar variances. Using photointerpretation techniques blight level 1 was greatly underestimated and blight level 3 overestimated compared to the other two methods.

The correlation of segment average blight levels as estimated by field observations and machine analysis of multispectral scanner data are shown in Figure 25 for two periods. There was much better agreement between the ground observations and machine analysis results as evidenced by higher r values (.86 and .90) and the close fit to the 1:1 line than for the photointerpretation results. As shown earlier for photointerpretation, the two earliest stages of blight infection were difficult to detect remotely.

The separation of fields into either healthy or blighted categories is shown in Figure 26. There is excellent agreement between the field observations and the estimates made from analysis of multispectral scanner data. The data are the number of acres in each blight class for each of the 30 segments in the intensive study area. Correlation coefficients were .94 and .92 for the two classes and the points lie close to the 1:1 line. Attempts to classify the number of acres in each individual blight level were less accurate than for either two or three classes.

There are a number of reasons for what may seem like a poor performance. One is that blight infection is a continuum and does not fall into discreet classes; this can lead to confusion on the ground as to what the true blight class is when, for instance, it is between mild and moderate. Another is that blight, although a dominant factor, was only one of many other factors causing variability in the spectral response of corn fields. These include differences in cultural practices such as plant population, row width and direction, crop maturity, and morphological characteristics of the hybrid, to name only a few. The soil background also often varies considerably from field to field and even within fields. Other factors leading to confusion in blight identification included in some instances the presence of other stresses such as drought damage, nutrient deficiencies, and other diseases which may be spectrally similar to SCLB.

But perhaps more important than the differences introduced by the ground scene are those resulting from variations in the radiation sensed which are not due to changes in the characteristics of the objects being sensed. The primary source of variation is the atmosphere. Other important causes are solar angle and view angle. The effect of these variations is to cause similar objects to exhibit different apparent spectral signatures. The result of this is that training fields are good for only very localized areas. In the Corn Blight Watch there were many instances when there were not sufficient training fields available to describe all of the blight and other conditions known to be present. Data processing techniques need to be developed which allow the extension of spectral signatures over larger areas.

Both LARS and WRL have been conducting research in these critical areas. Both laboratories have used methods whereby the average signal variation as a function of scan angle is computed for each spectral band. Much of the angular variation in the signal can then be eliminated by dividing each scan line of data by the normalized average signal variation. A significant reduction in signal range of corn and other cover types has been accomplished by the application of these relatively simple techniques with the result that crop signatures were more unique and easier to differentiate. Thus far, it has not been possible to determine if the subtle blight level discrimination was affected.

Work has also been underway at both laboratories on other facets of the signature extension problem. At this time it can only be reported that there is reason for cautious optimism that signatures can be successfully extended over time and space, but more effort will be required before these techniques will be operationally useful. More detailed reports of this and other data processing-analysis research can be found in publications by WRL and LARS.

Influence of Blight on Yields

In most of the test area blight did not seriously affect corn yields. In fact, state average yields were the highest ever recorded. There were, however, certain restricted areas where blight did significantly reduce yields. Of the fields for which yield estimates were made, 91 T-cytoplasm fields had blight levels 3, 4, or 5 during the August 23-27 observation period when ear filling was occurring. Twenty-four of these fields had moderate to very severe blight levels on July 26-30; they produced an average yield of 71 bushels per acre. Those that

had none to only mild blight on July 26-30 had an average yield of 97 bushels per acre. The blend fields from the same segments had mild to moderate blight levels and had an average yield of 118 bushels per acre; while the normal cytoplasm fields yielded 130 bushels per acre. It is significant that the blight classes which could be accurately detected remotely were the same as those which significantly affected corn yields.

Crop Identification

An important part of the Experiment was an evaluation over a large area of the accuracy with which crops could be identified by remote sensing techniques. Major crops were accurately identified throughout the season (Table 1) by both photo-interpretive and machine assisted analysis techniques even though this aspect of the Experiment received relatively little emphasis compared to the more difficult blight detection problem. These results give reason for optimism regarding the feasibility of operational remote sensing crop survey systems.

It was also possible in certain instances to identify several key factors affecting corn productivity. These included low population, drought damage, hail damage, extreme weediness. There were other times, however, when these factors undoubtedly could not be differentiated from the effects of blight. Overall blight severity within individual fields was found to be quite uniform; whereas, the factors mentioned above tended to be more irregular in appearance across the field.

7. DISCUSSION

The significant results of the 1971 Corn Blight Watch Experiment can perhaps be best expressed by summarizing how well the application objectives were achieved and by discussing the performance of the key elements of the technology relative to those achievements.

The application objectives required (1) the detection of outbreak, identification of temporal increases in severity levels and the tracking of spread of SCLB over the total study region; (2) an assessment of the impact of SCLB on production; and (3) an estimate of the applicability of remote sensing to other situations which would require surveys on a large scale.

With reference to the first objective, it can be concluded that neither the manual interpretation of small scale photography nor the machine-aided analysis of multispectral measurements adequately provided detection of SCLB during early stages of infection. Analysis of these data did, however, permit the detection of outbreaks of moderate to severe infection levels and mapping of the spread of those levels over the study regions with relatively high accuracy.

Analysis of data acquired in 1971 showed that the variation in the presence and extent of different infection levels increased as the geographic separation between sample areas increased. This leads to a conclusion that a more accurate assessment of conditions due to SCLB could have been realized with a smaller set of data samples had smaller samples been better distributed over the total study region.

As far as the second objective was concerned, investigators were able to associate significant yield reductions with moderate to severe infection levels occurring in August and still greater reductions associated with moderate to severe infection levels occurring in July. The results of the experiment indicate that acreages infected at these levels were identified in the late July and August periods with relatively high confidence.

And finally, results in the area of the third objective clearly indicate that the technology is capable of both reliably identifying and measuring the extent of agricultural crops and land use. Furthermore, it can be concluded that the technology is suitable for detection of crop stress in those instances where the stress changes the radiation characteristics of the crop.

The Corn Blight Watch Experiment provided an excellent opportunity to evaluate all aspects of a system designed to collect, analyze, interpret, and distribute information repeatedly at short intervals throughout a growing season.

While it raised as many questions as it answered, it produced extremely valuable guidelines for future research and development.

An important result of the experiment is the file of photography, multispectral measurements, and field observations collected at biweekly intervals over an entire Corn Belt growing season. This data set is available, and will prove extremely valuable in further studies.

Another important part of the Corn Blight Watch Experiment was the knowledge gained about the costs of a large scale information system using remote sensing. The information on the cost in dollars and time for each part of the experiment will be useful when future experiments or operational systems are planned. These data on labor, computer costs, aircraft, film, processing, etc. expended in the experiment are being used to investigate the relationship between subsampling ratios, costs, and precision of estimates.

The Corn Blight Watch Experiment also demonstrated the value and effectiveness that can be achieved by pooling the resources of a number of cooperating groups. No single organization has at this time the expertise or resources to go it alone in such an effort. Certainly, the Watch provided much valuable data related to the resources required to implement this type of program and insight into the practices and procedures which are most effective in the design and operation of such systems.

Because of the Corn Blight Watch Experiment many agriculturists had an opportunity to work with remote sensing information. The majority of field personnel responded favorably to the aerial color infrared photography sent to them and reported that it could be used to good advantage in their work.

The Corn Blight Watch Experiment demonstrated that a statistical sampling model is a fundamental element of a remote sensing survey system. A general conclusion is that additional effort needs to be expended to develop sampling concepts suited to remote sensing data acquisition systems and automatic data analysis procedures. As a part of the Corn Blight Watch investigators did gain valuable experience developing a capability for setting up survey prediction models utilizing remotely sensed measurements.

The data acquistion elements performed well. The Experiment provided evidence that a fully-committed, high-flying aircraft can effectively acquire data at biweekly intervals for a region as large as the Corn Belt. Furthermore, this was accomplished under the less-than-optimum Corn Belt weather conditions. The University of Michigan C-47 was similarly able to collect multispectral measurements over a 13,000 square-mile area in western Indiana. In contrast, only a comparatively small amount of data was acquired by the large number of ground observers.

Another significant facet of the Experiment was the demonstrated capability to reliably identify crop types over a significantly large area with today's technology. Foreseeable performance improvements over the next several years promise still greater accuracies.

Considerable manpower was required to determine the identification of the crop types and acreages within each of the 210 segments. This was accomplished by ASCS state and county personnel. These data were required as inputs to the sample model. However, considerable savings in manpower can be realized by obtaining these data through remotely sensed measurements. Results of the Corn Blight Watch indicate that crops can be reliably identified by either photointerpretation of small scale infrared photography or through computer processing of multispectral measurements. However, if acreage measurements are to be obtained from scanner data, additional techniques need to be developed. Such efforts need to be undertaken in the near future. It is possible, for instance, that a capability to register different data sets required for temporal analysis would also solve the area determination problem. Multispectral data sets would be registered to a photogrammetrically-corrected data base. Area measurements could then be made from the geometrically-corrected multispectral data classification output. It should be noted that, currently, the acreage in a field is either estimated from the ground or manually measured on black and white photography. Certainly remote sensing presents a more efficient alternative.

Additionally, much was learned about how to acquire information over a large geographic region with manageable data volumes. The use of a statistically sound sampling model was shown to be a key element in accomplishing this.

Other solutions and suggestions include the fact that a helicopter proved to be a valuable aid in acquiring field observation data. Such a system can often permit a more accurate assessment of more fields in shorter periods of time than conventional ground surveys.

Also, results indicate that much more would be gained from the development of techniques which would make possible the acquisition of photography having more consistent exposure from mission to mission. Similarly, improved preprocessing techniques would provide more useful multispectral data over a wider range of conditions (i.e., atmospheric and sun angle effects).

The Corn Blight Watch Experiment resulted in significant improvement of aerial infrared film. The condition which caused the "cyan spots" and hampered the analysis because of their similarity to blight has since been corrected. This deficiency in the film was discovered by the photo-analysts of the Experiment.

The Experiment demonstrated the need for more agriculturists with training in photo-analysis. It is hoped that more schools of agriculture will provide and encourage their students to take course work in remote sensing. If photography is to be utilized in agricultural situations it is imperative to have people trained to work with the data.

Results also lead to a conclusion that machine assisted analysis of multispectral scanner data was more effective in detecting, tracking the spread and assessing the impact of SCLB than was the photo-analysis of the small scale photography. This was expected since the photo-analysts were looking for small tonal color changes in the crop. The multispectral sensor produces a better measurement of these spectral changes and the data are more amenable to machine processing routines.

However, the results indicated that if either remote sensing approach is to offer a decided advantage over ground acquired data, ways must be found which require less ground truth for the initial selection of training samples and techniques developed which permit the use of statistics derived from training samples to a wider range of conditions and over larger geographic distances. In many instances, (especially in those cases involving visual phenomena) it is believed that selected high resolution photography could replace the need for much ground acquired data in the selection of training samples.

There is a need for further work establishing the statistics of the spectral patterns of natural scenes to better determine the causes of variations (including sun angle, observation angle, and atmospheric effects) described by those statistics. It is believed that variations in response not due to the ground scene led to the relatively low accuracies which were achieved over small areas (10's of square miles). The variances were sufficiently large to require samples over relatively large areas before accurate estimates were realized.

Again, results from the Corn Blight Watch indicate that considerable improvement in performance could have been realized had the analysis had the capability to consider temporal variations of spectral patterns. In this light, there continues to be a strong need to be able to automatically make coincident data sets collected at different times. As an example, more is to be gained from eight channels of data collected at three different times than 24 channels collected at one time. It should be noted that data registration is the key to this type of analysis.

An examination of the physical characteristics of SCLB (uniform infection within a field) indicates that improved results could have been obtained with sample classifiers as opposed to the point classifiers currently being used. Before such classifiers can be employed. however, techniques need to be developed to automatically identify the boundaries of data fields.

In the space and time available in a paper of this nature it is impossible to present all of the results of an experiment as large as the Corn Blight Watch

Experiment. It has been possible to present only a brief overview of the more important aspects of the Experiment. A complete description of its implementation and all results will be included in the Final Report of the Experiment.

8. SUMMARY AND CONCLUSIONS

The 1971 Corn Blight Watch Experiment provided a prototype remote sensing system in which techniques of data gathering, storage, retrieval, processing and analysis and information dissemination were successfully used in one integrated system operated in a quasi-operational environment. The experiment effectively focused the efforts of many disciplines and agencies on a common problem and resulted in many people becoming acquainted with remote sensing techniques.

In conclusion, accurate identification of agricultural crops and land use over large geographic areas using remote sensing techniques was clearly demonstrated. The potential utility of these techniques to assess crop stress over large geographic regions was also demonstrated. The 1971 Corn Blight Watch Experiment provided the most quantitative information available on the extent and severity of blight.

But most important, the Experiment was a major milestone in the development of earth resources survey by remote sensing. Existing remote sensing techniques were refined and many new ones implemented as remote sensing moved a step further into the real world.

Finally, the Experiment provided valuable direction for future research and development of remote sensing technology and guidelines for the design of operational information systems utilizing remote sensing.

9. REFERENCES

1. The 1971 Corn Blight Watch Experiment. A series of seven papers presented at the 4th Annual Earth Resources Program Review. Houston, Texas. January 17-21, 1972. Volume V:124-1 to 131-5.

2. 1971 Corn Blight Watch Experiment, Final Report. To be published, January 1973.

10. ACKNOWLEDGEMENTS

The 1971 Corn Blight Watch Experiment was the cooperative effort of many federal, state, and local agencies. The contributions of each of the agencies and of the many individuals who participated in the Experiment is gratefully acknowledged. The agencies which participated in the Experiment included:

United States Department of Agriculture
- Agricultural Stabilization and Conservation Service
- Statistical Reporting Service
- Economic Research Service
- Cooperative State Research Service
- Agricultural Research Service
- Extension Service

National Aeronautics and Space Administration
- Headquarters
- Manned Spacecraft Center
- Ames Research Center

Cooperative Extension Services and Agriculture Experiment Stations of the States of Illinois, Indiana, Iowa, Minnesota, Missouri, Nebraska, and Ohio.

University of Michigan, Willow Run Laboratories

Purdue University, Laboratory for Applications of Remote Sensing

TABLE I. IDENTIFICATION OF CORN AND OTHER CROPS BY PHOTOINTERPRETATION OF SMALL-SCALE INFRARED PHOTOGRAPHY AND MACHINE ASSISTED ANALYSIS OF MULTISPECTRAL SCANNER DATA.

	Analysis Method		
	Photointerpretation		Machine Assisted
Date	Corn	Other[1]	Corn vs. Other[2]
June 14	73	60	-
June 28	85	54	79
July 12	92	50	89
July 26	89	40	91
August 9	93	60	88
August 23	91	60	86
September 6	96	58	88
September 20	96	58	-

[1]Average correct recognition of wheat, soybeans, and hay.

[2]Average correct recognition of corn vs. all other types present including crops, woods, and water.

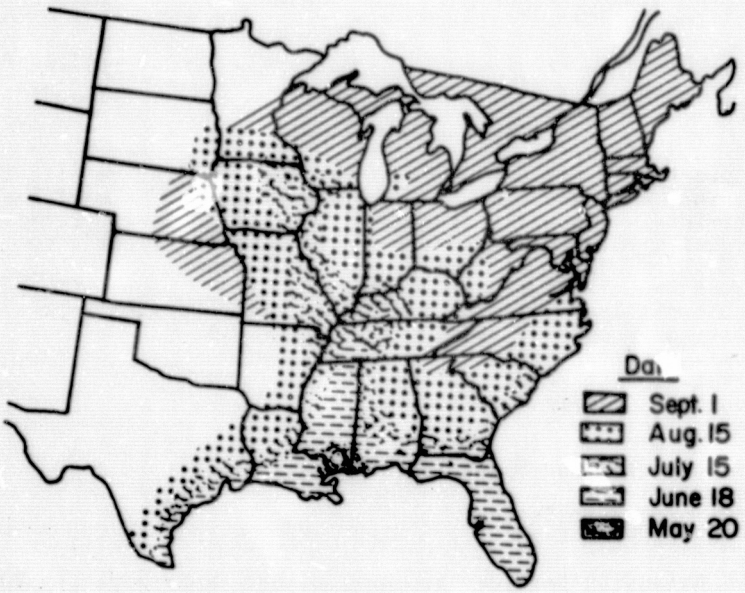


FIGURE 1. IN 1970 SOUTHERN CORN LEAF BLIGHT SPREAD RAPIDLY FROM THE SOUTH TO THE CORN BELT.



FIGURE 2. SOUTHERN CORN LEAF BLIGHT. The disease is characterized by small, brown lesions which increase rapidly in size and number.

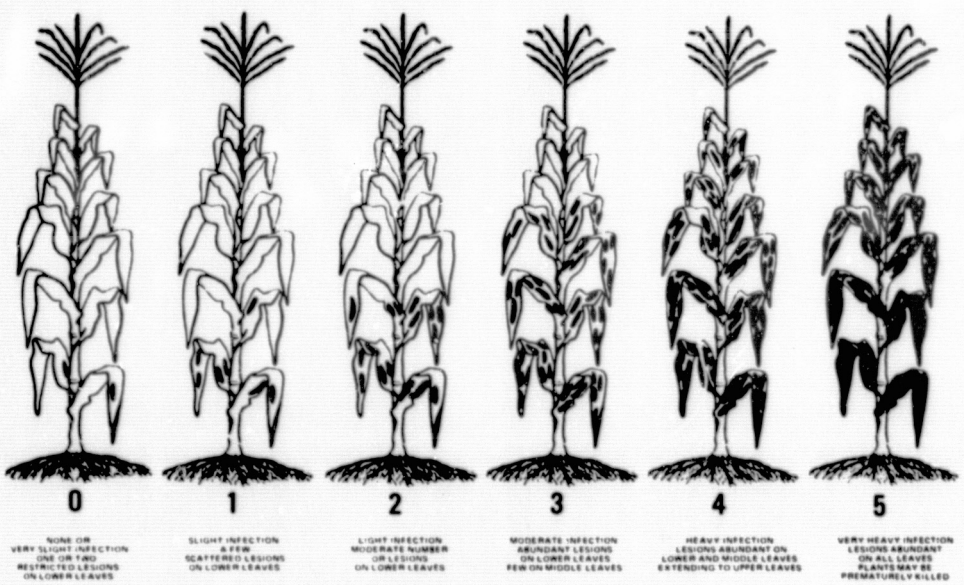


FIGURE 3. SCALE FOR ESTIMATING SOUTHERN CORN LEAF BLIGHT SEVERITY.

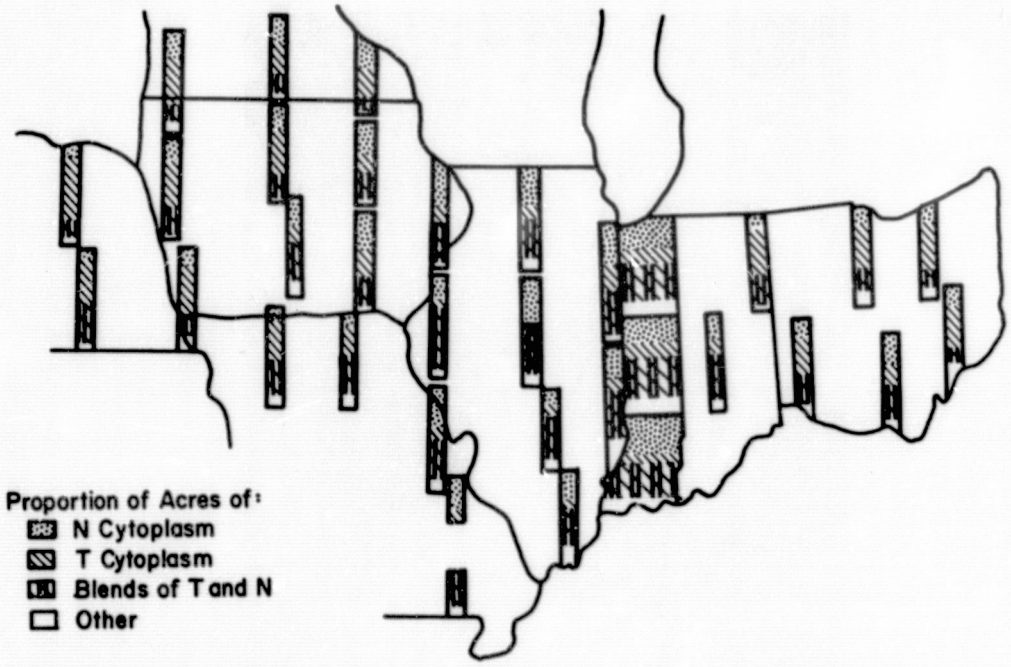


FIGURE 4. DISTRIBUTION OF CORN CYTOPLASM TYPES. The highest propotions of resistant types were planted in the eastern Corn Belt where blight was most severe in 1970.

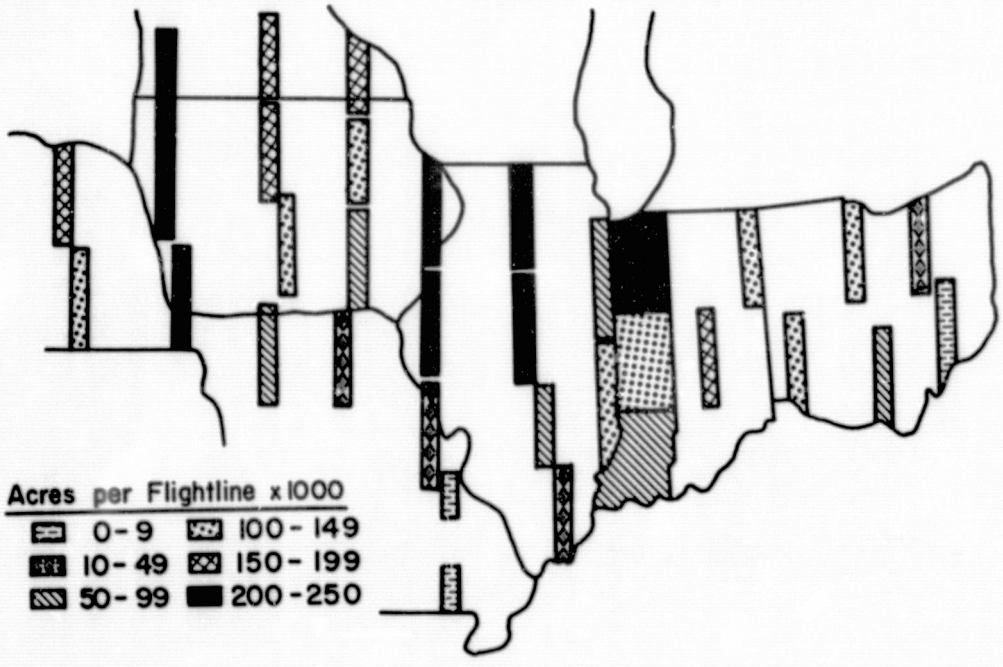


FIGURE 5. DENSITY OF CORN ACRES IN THE EXPERIMENT TEST AREA.

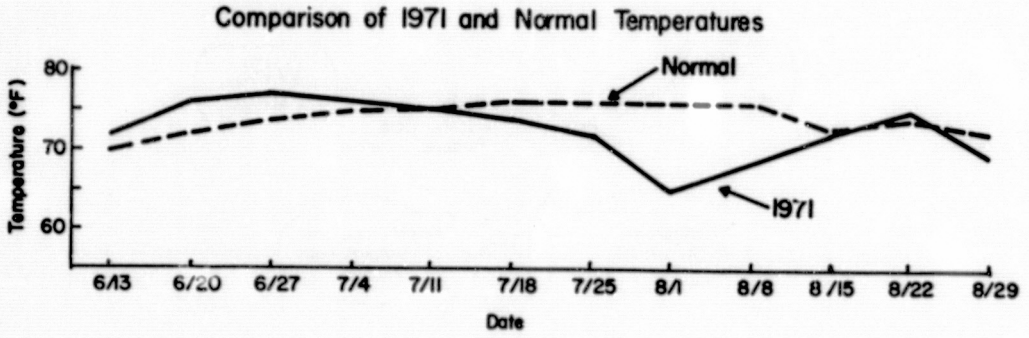


FIGURE 6. COMPARISON OF 1971 AND NORMAL TEMPERATURES. Above-normal temperatures in June and early July were nearly ideal for corn growth. Below-normal temperatures from mid-July to mid-August greatly retarded further blight development and were favorable for high corn yields.

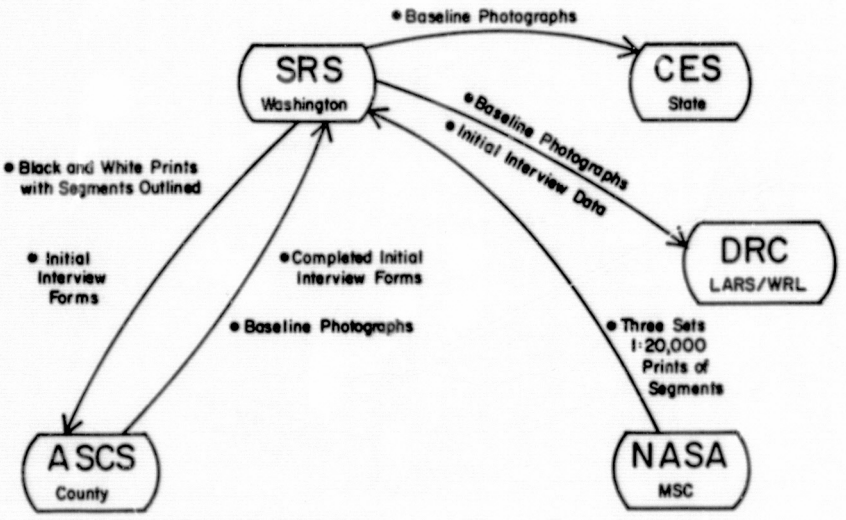


FIGURE 7. PHASE I DATA FLOW. During this phase baseline photography and initial interview data were obtained for use in later phases of the Experiment.

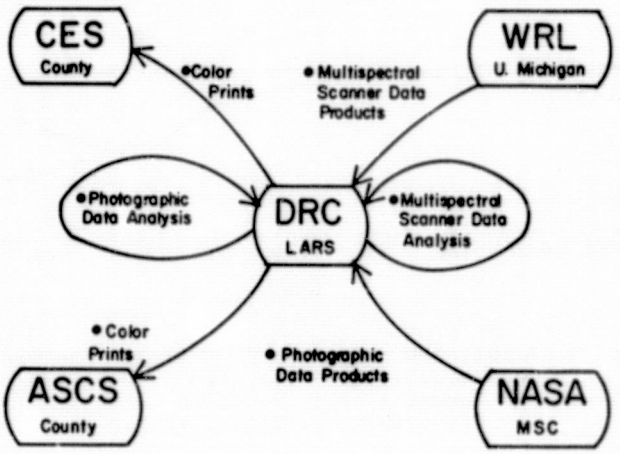


FIGURE 8. PHASE II DATA FLOW. This phase of the Corn Blight Watch was to collect data and perform analyses to determine soils background information for the corn fields.

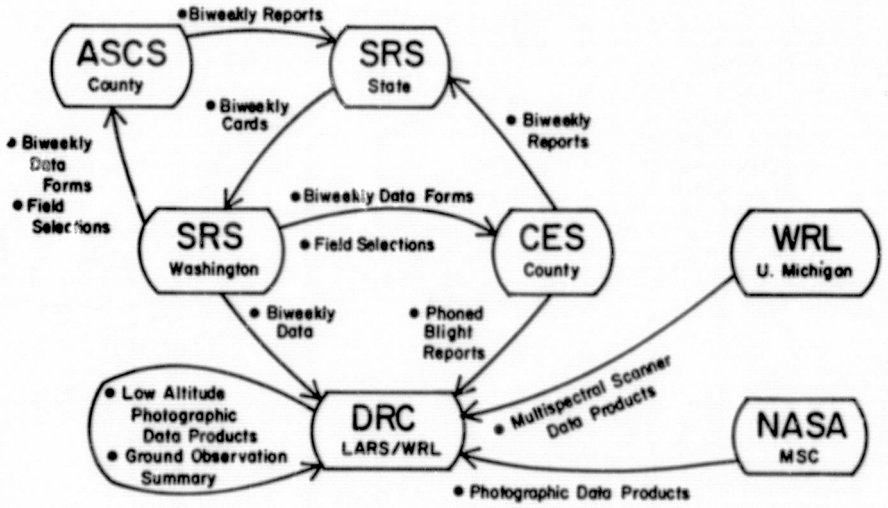


FIGURE 9. DATA ACQUISTION FOR PHASE III. The principal data products were field observation data, photographic data, and multispectral scanner data.

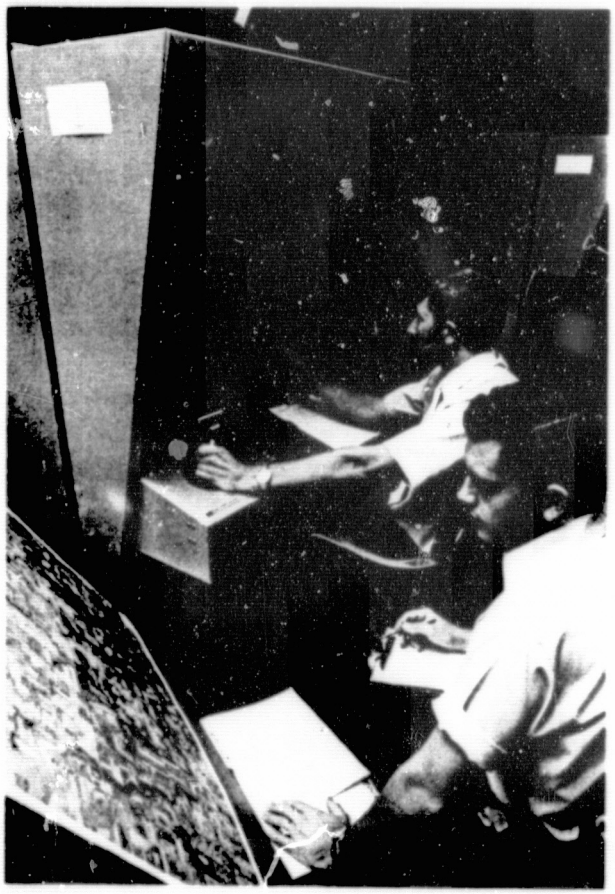


FIGURE 10. INTERPRETATION OF SMALL-SCALE COLOR INFRARED PHOTOGRAPHY USING A VARISCAN REAR-PROJECTION FILM VIEWER.



FIGURE 11. DIGITAL DISPLAY USED AT LARS TO LOCATE AND IDENTIFY TRAINING FIELDS IN THE MULTISPECTRAL SCANNER DATA.

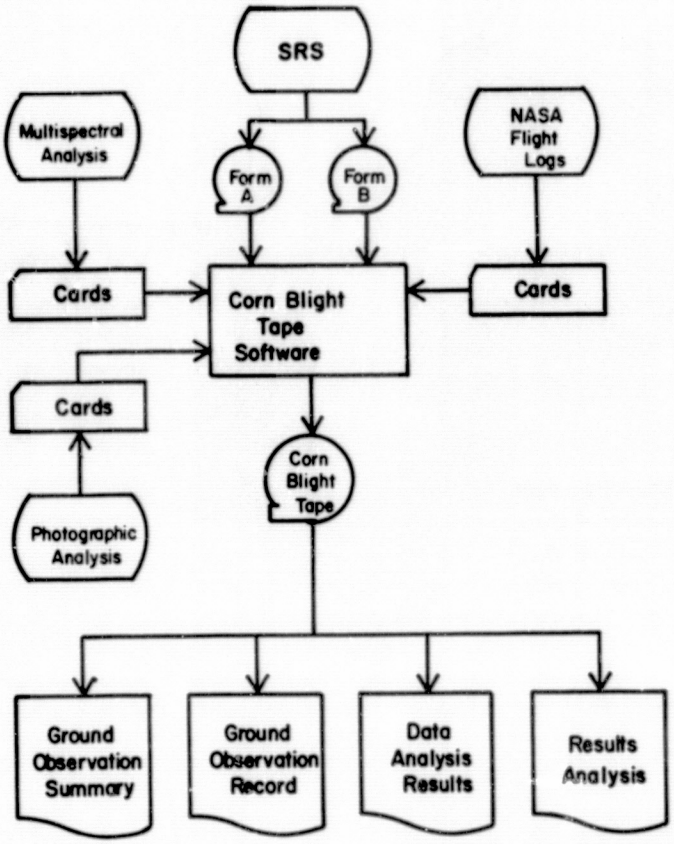


FIGURE 12. ALL GROUND DATA, FLIGHT LOGS, AND ANALYSIS RESULTS WERE STORED ON MAGNETIC TAPE. These merged data were used to analyze and report results of the 1971 Corn Blight Watch Experiment.

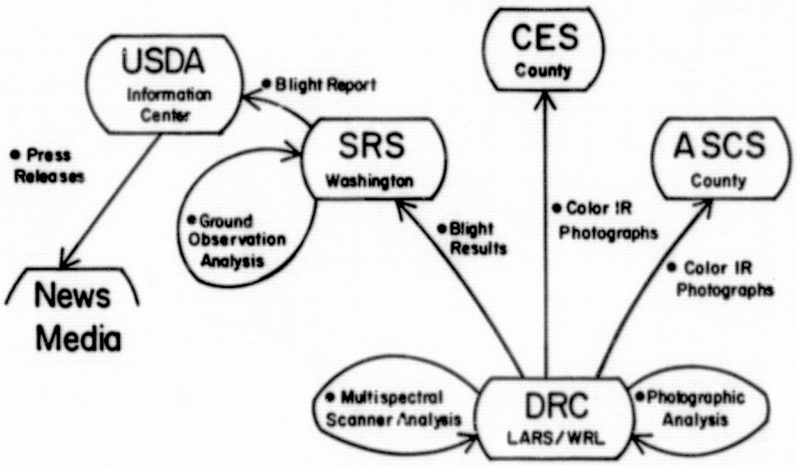


FIGURE 13. RESULTS DISSEMINATION FOR PHASE III. This phase of the Experiment included reporting results to the public.

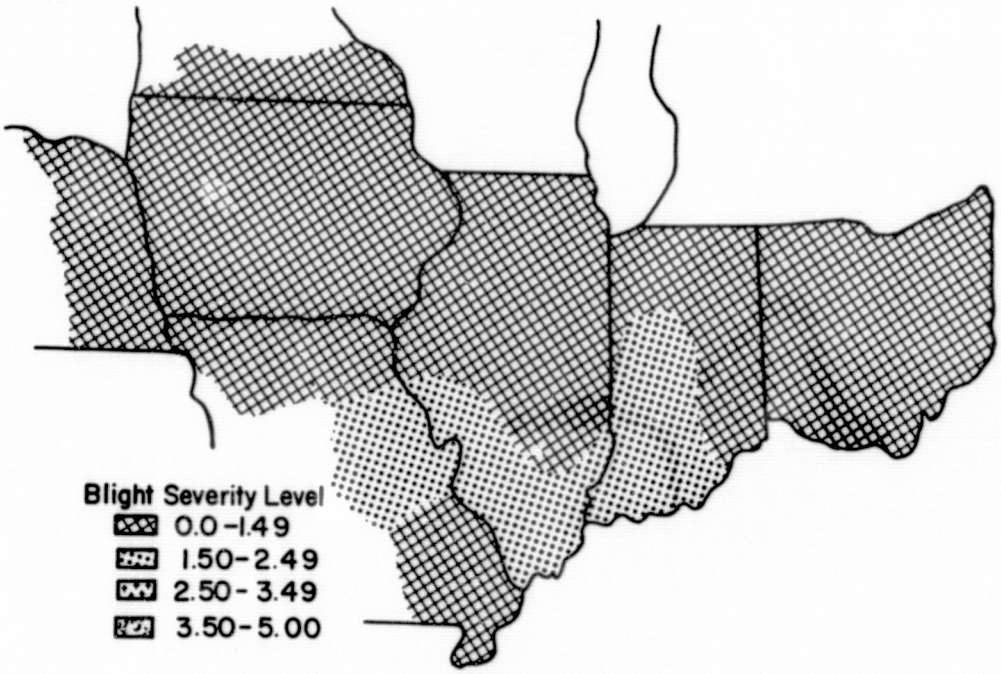


FIGURE 14. · BLIGHT SEVERITY OF TEXAS MALE STERILE CYTOPLASM CORN, JULY 26-30, 1971.

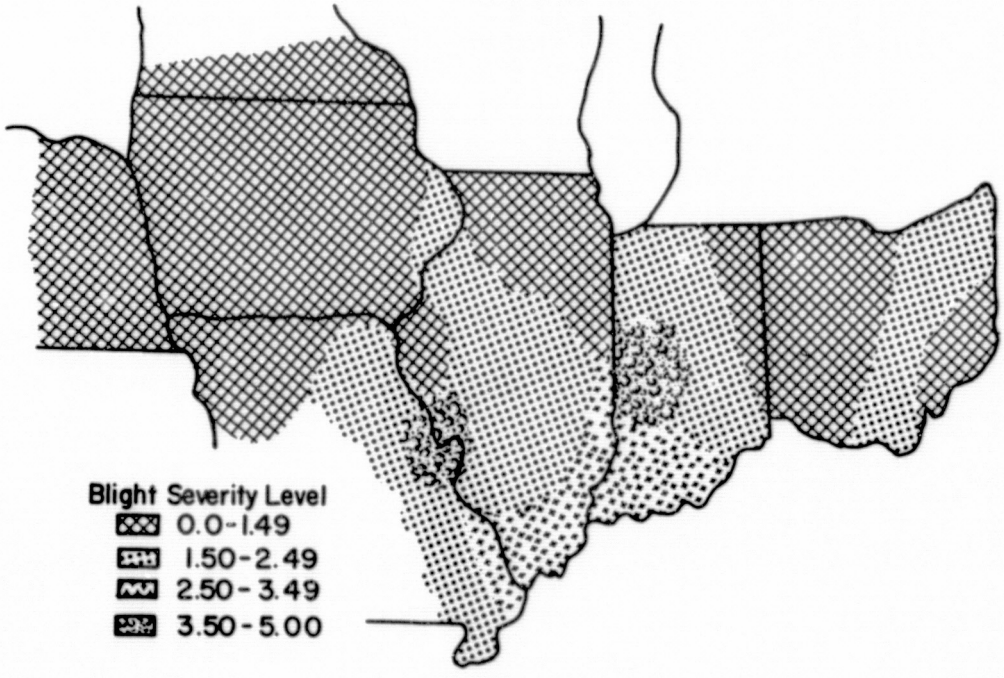


FIGURE 15. BLIGHT SEVERITY OF TEXAS MALE STERILE CYTOPLASM CORN, AUGUST 9-13, 1971.

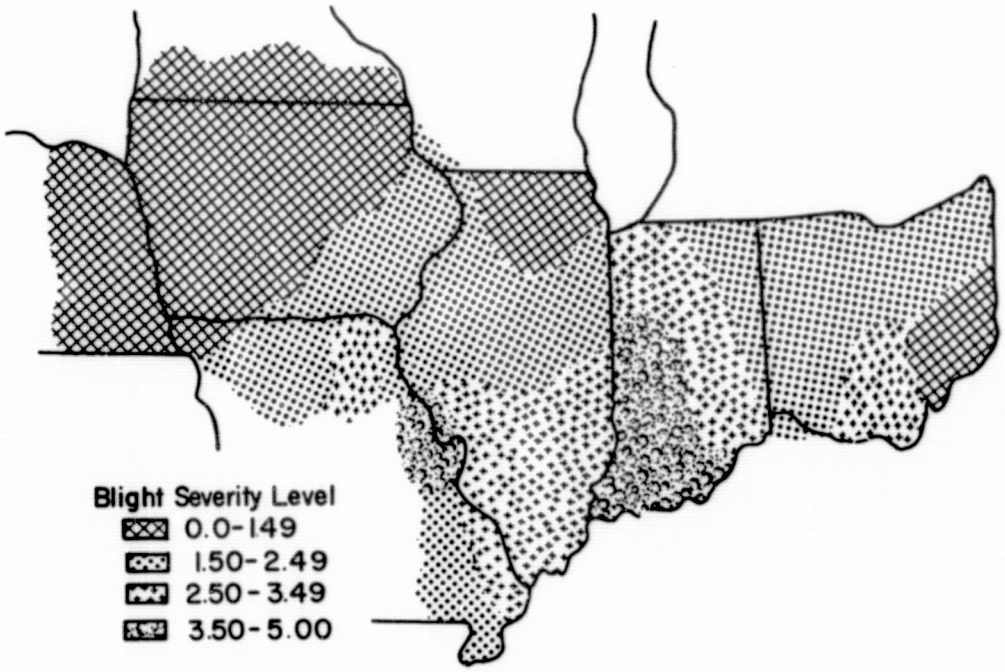


FIGURE 16. BLIGHT SEVERITY OF TEXAS MALE STERILE CYTOPLASM CORN, AUGUST 23-27, 1971.

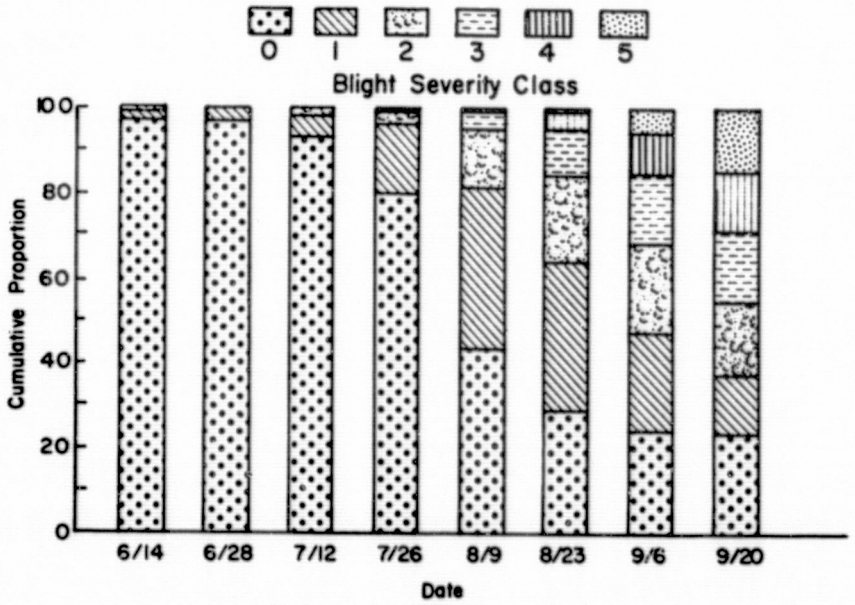


FIGURE 17. DEVELOPMENT OF BLIGHT OVER TIME IN THE CORN BELT AREA.

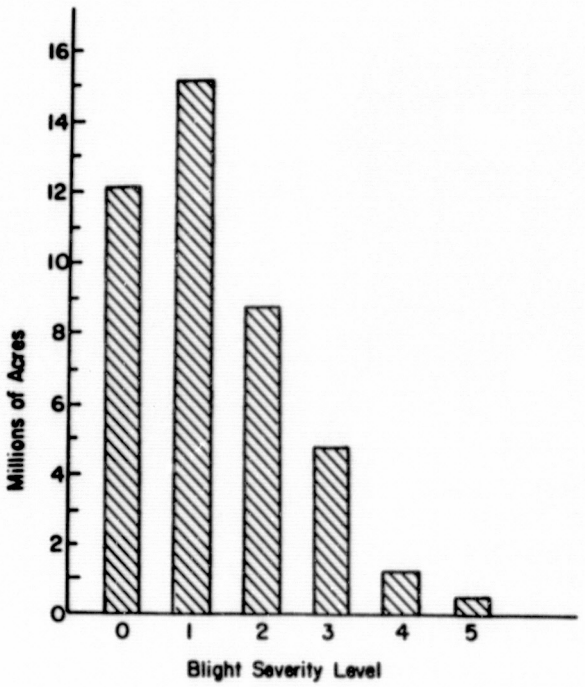


FIGURE 18. NUMBER OF ACRES IN EACH BLIGHT SEVERITY CLASS IN THE CORN BELT, AUGUST 23-27. At this time the crop was nearing maturity and further blight development had little effect on yields

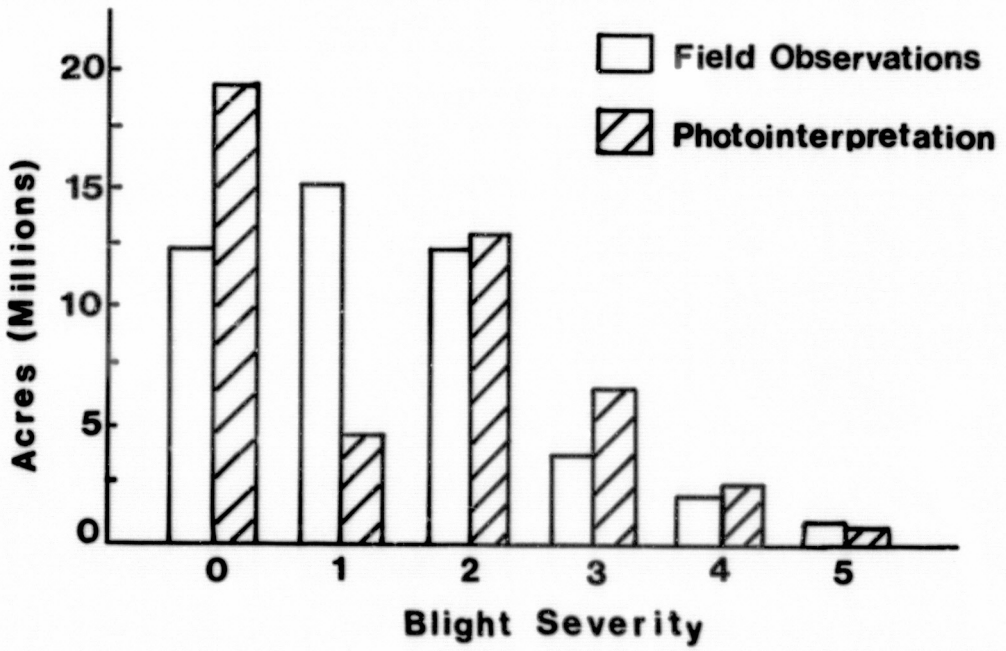


FIGURE 19. COMPARISON OF FIELD OBSERVATION AND PHOTOINTERPRETATION ESTIMATES OF CORN ACREAGES IN INDIVIDUAL BLIGHT CLASSES FOR THE CORN BELT AREA, AUGUST 23 TO SEPTEMBER 5.

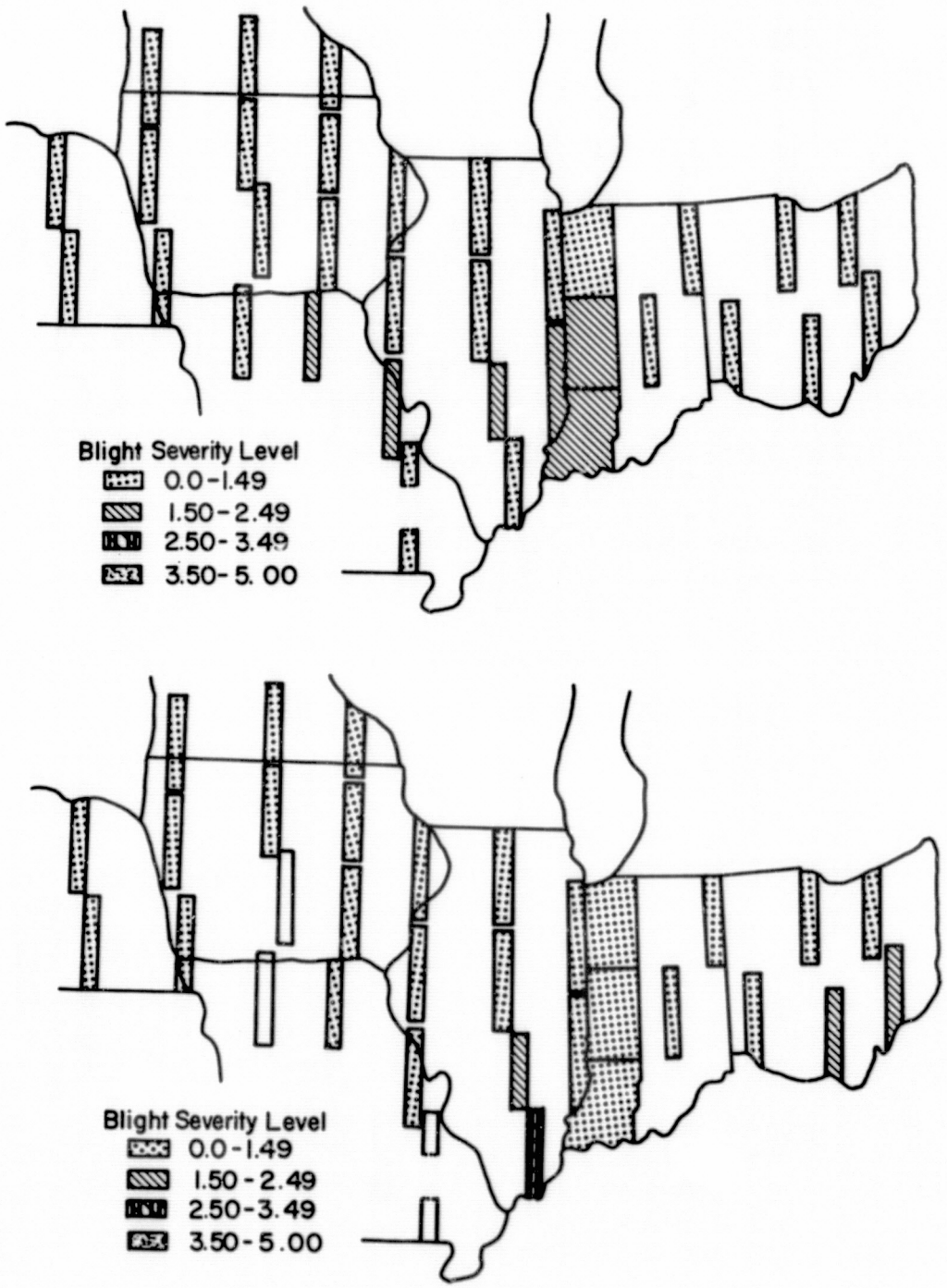


FIGURE 20. AVERAGE BLIGHT SEVERITY LEVELS BY FLIGHTLINE FOR FIELD OBSERVATIONS (TOP) AND PHOTOINTERPRETATION (BOTTOM) FOR THE PERIOD BEGINNING AUGUST 9, 1971.

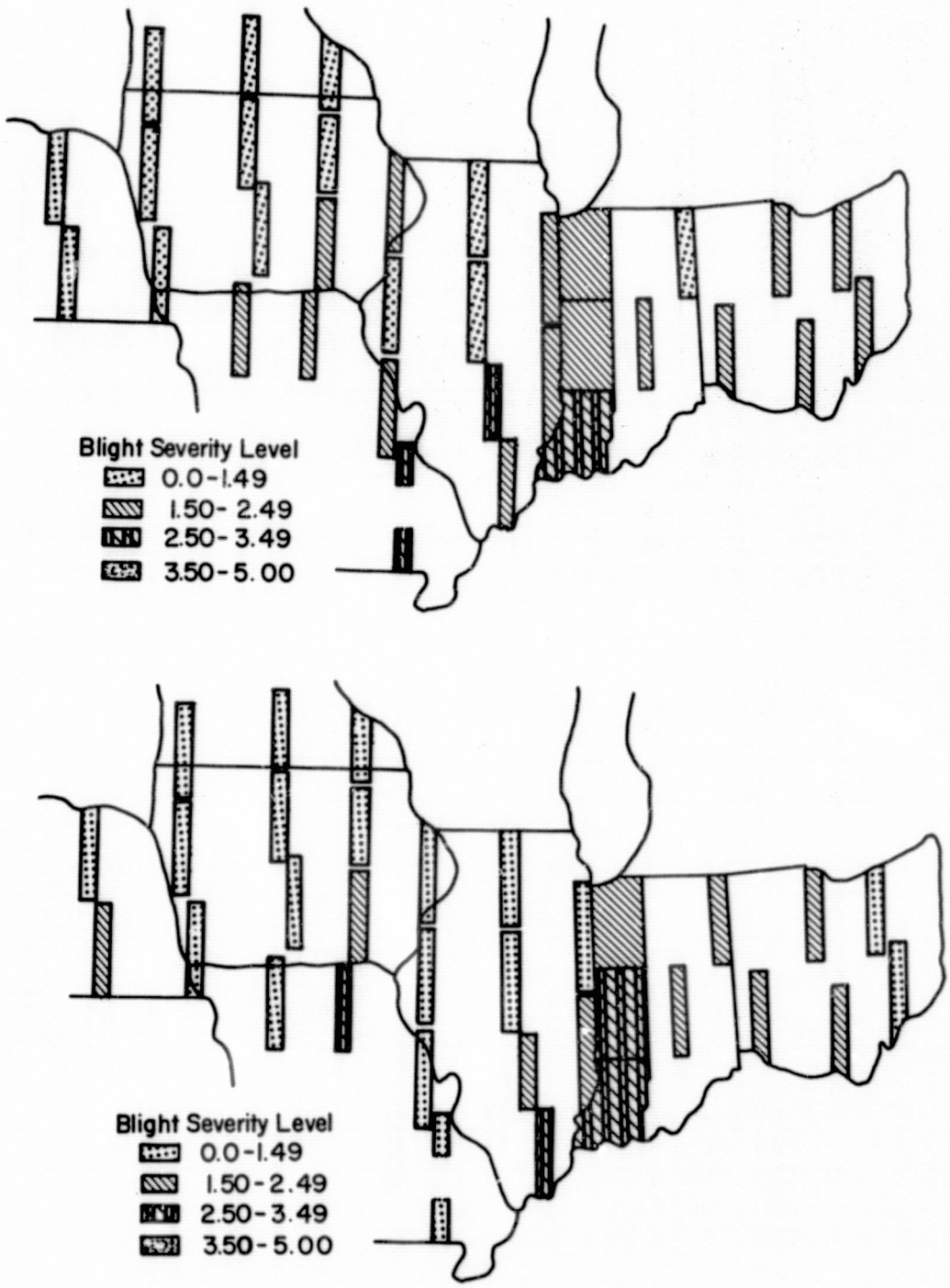


FIGURE 21. AVERAGE BLIGHT SEVERITY LEVELS BY FLIGHTLINE FOR FIELD OBSERVATIONS (TOP) AND PHOTOINTERPRETATION (BOTTOM) FOR THE PERIOD BEGINNING AUGUST 23, 1971.

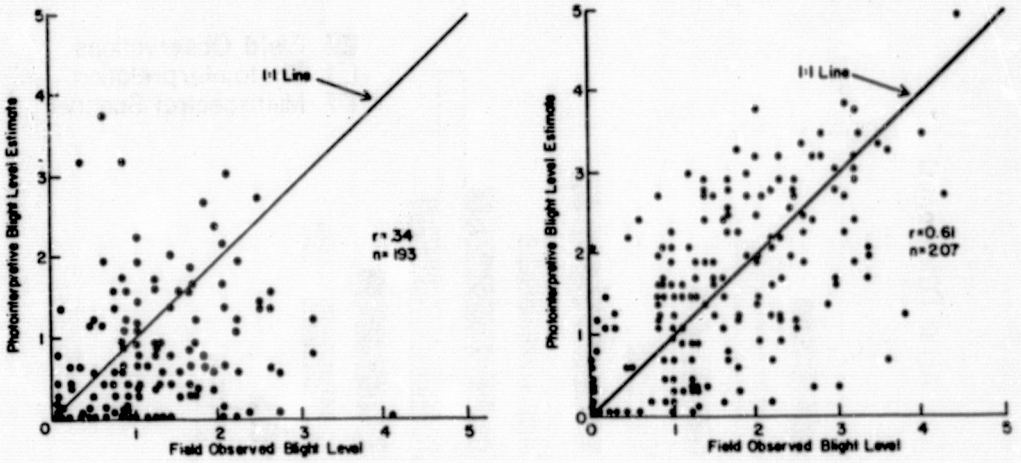


FIGURE 22. CORRELATION OF FIELD OBSERVATION AND PHOTOINTERPRETATION ESTIMATES. The data are segment averages of blight severity for the periods beginning August 9 (left) and August 23 (right), 1971.

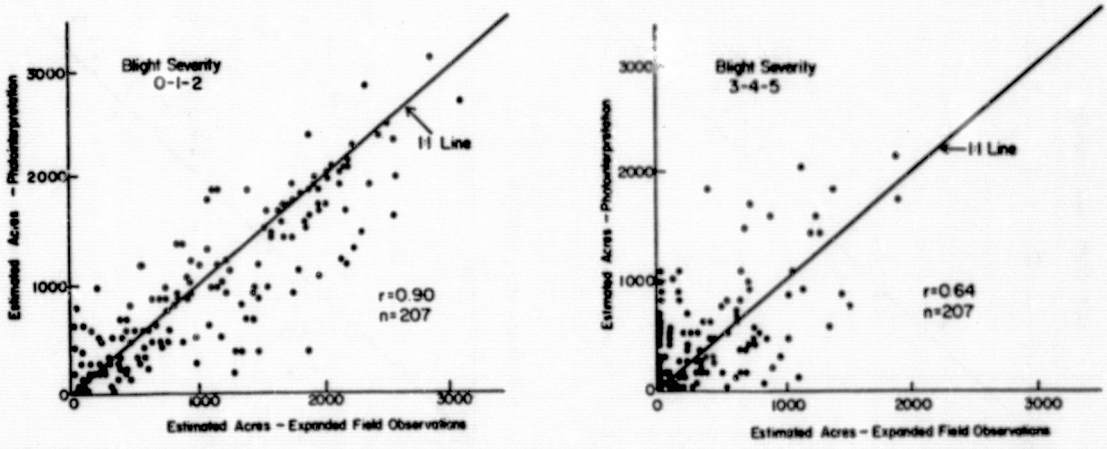


FIGURE 23. CORRELATION OF FIELD OBSERVATION AND PHOTOINTERPRETATION ESTIMATES OF SEGMENT ACREAGES OF HEALTHY (BLIGHT LEVEL 0-1-2) AND BLIGHTED (3-4-5) CORN, AUGUST 23 TO SEPTEMBER 5, 1971.

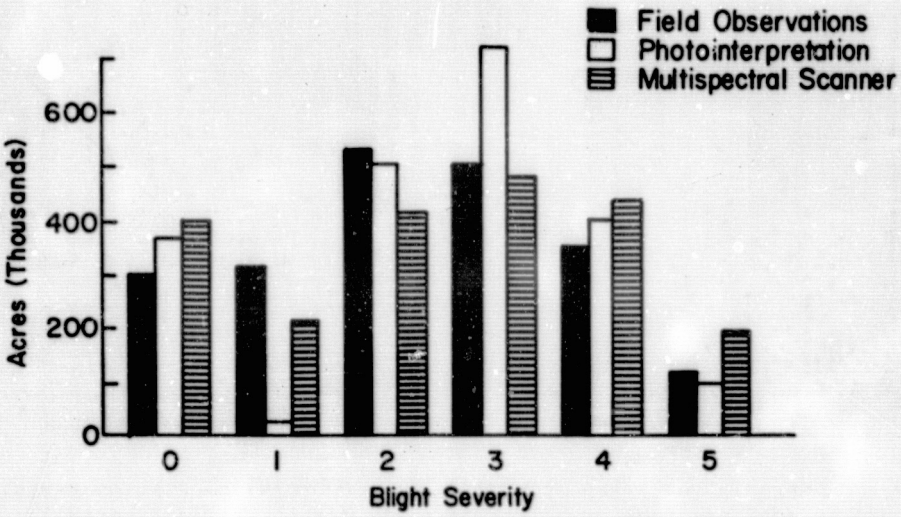


FIGURE 24. COMPARISON OF FIELD OBSERVATION, PHOTOINTERPRETATION AND MACHINE ANALYSIS ESTIMATES OF CORN ACREAGE IN INDIVIDUAL BLIGHT CLASSES FOR THE INTENSIVE STUDY AREA, AUGUST 23 TO SEPTEMBER 5.

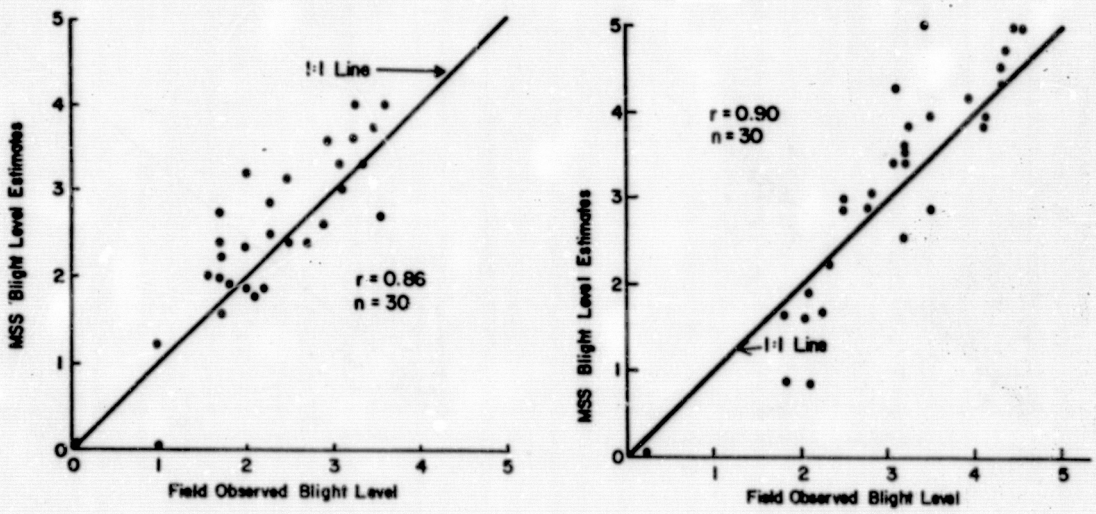


FIGURE 25. CORRELATION OF FIELD OBSERVATION AND MACHINE ASSISTED ANALYSIS OF MULTISPECTRAL SCANNER DATA ESTIMATES OF SEGMENT AVERAGE BLIGHT SEVERITY LEVELS, AUGUST 23 (LEFT) AND SEPTEMBER 6 (RIGHT).

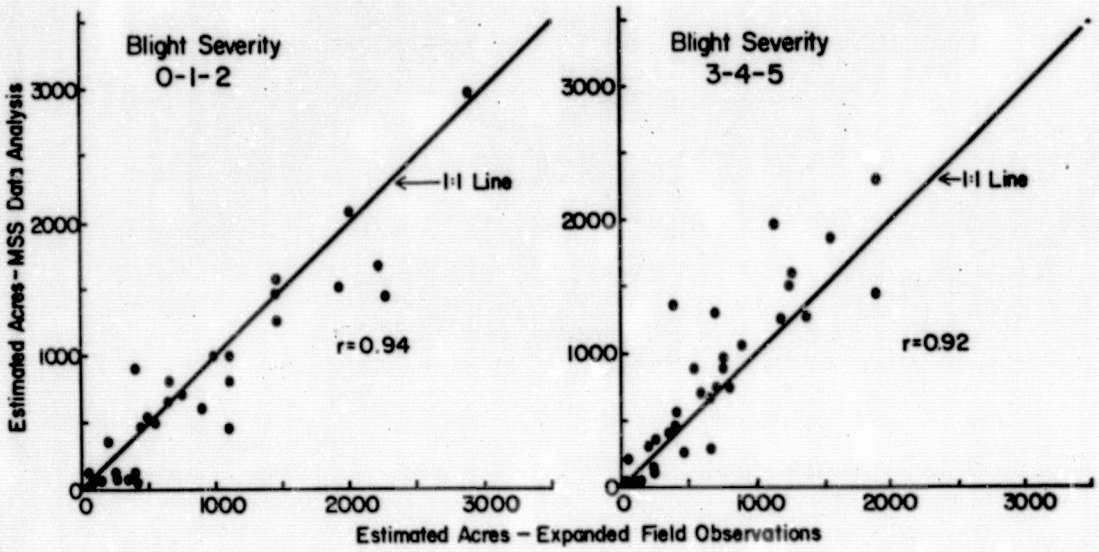


FIGURE 26. CORRELATION OF ESTIMATES FROM MULTISPECTRAL SCANNER DATA AND FIELD OBSERVATIONS OF ACREAGES OF HEALTHY (BLIGHT LEVELS 0-1-2) AND BLIGHTED (3-4-5) CORN IN THE INTENSIVE STUDY AREA SEGMENTS FOR THE PERIOD BEGINNING AUGUST 23, 1971.

KEYNOTE ADDRESS

Remote Sensing and International Affairs

Bengt Lundholm

Swedish Natural Science Research Council
Stockholm, Sweden

When political difficulties were threatening to stop the UN Conference on the Human Environment it was claimed that the preparatory work done for the Conference was so important that the Conference would have to be regarded as a success, even if it never took place.

There was an enormous amount of preparatory work, and it was very skilfully initiated and directed from the Secretariat in Geneva by Mr. Maurice Strong. Contributions came from the participating nations in the form of national reports or special case studies. Intergovernmental organizations such as the specialized agencies of the UN, nongovernmental international organizations, and private persons delivered reports and materials. Everything was done in a spirit of co-operation and readiness. The motivations behind this willingness were very different. In some cases the motivating force was a genuine interest for the environmental problems, in other cases the main concern was for national self-interest.

From the very beginning it was decided that the Conference should be meeting of politicians representing their respective countries. This was not always understood and some expected a Conference of experts.

As a general criticism it might be said that the preparatory information contributed by the experts did not reach the national delegates to the extent it should have. The very valuable reports were hard to get, even for those who really tried. However, even if the information had reached the target - the politicians - it is rather doubtful if they could have digested the material. It is quite clear that there existed a serious information gap between experts and politicians. This does not mean that the careful preparations were in vain, but rather that the effects were delayed and will first appear when the material has been assimilated.

When the Conference terminated, most of the delegates agreed that it had been a great success. In spite of the many political disagreements, it was possible for the delegates to agree on an action program. And what were the results?

A Declaration on the Human Environment was agreed on. It begins with the words, "Having considered the need for a common outlook and for common principles to inspire and guide the peoples of the world in the presentation and enhancement of the human environment:" The declaration ends with 26 principles. The first condemns apartheid and the last condemns "nuclear weapons and all other means of mass destruction."

Looking at principle number 21, it is clear that not the peoples, but the governments are behind these principles.

"States have, in accordance with the Charter of the United Nations and the principles of international law, the sovereign right to exploit their own resources pursuant to their own environmental policies," etc.

More important, however, and more encouraging, the Conference approved 109 recommendations for actions. These recommendations form an action plan that has the following three parts:

1. Environmental Assessment, (or Earth Watch), to identify and determine the extent of environmental problems of international importance and to warn against impending crises. The components of the Earth Watch are research, monitoring, review and evaluation, and information exchange.

2. Environmental management activities to put into practice what is known or will be learned about the environment, with the aim of preserving what is desired and

Preceding page blank

preventing what is feared, but also with the aim of improving the general quality of the environment.

3. Supporting measures, with recommendations dealing with education, training and public information, organizational arrangements, and financial and other assistance.

A special resolution was passed concerning the institutional and financial arrangements for the action plan. The main points in this resolution are:

1. The General Assembly should establish a Governing Council for the environmental programmes composed of 54 members.

2. A small environmental secretariat should be set up to "serve as a focal point for environmental actions and co-ordination within the UN system." Its Executive Direction would be elected by the General Assembly. Among the responsibilities entrusted to this secretariat the following may be mentioned:

   "to secure the effective co-operation of, and contributions from, the relevant scientific and professional communities from all parts of the world."

   and "to administer, under the authority and policy guidance of the Governing Council, the Environment Fund."

3. New money for environmental activities would come from the special Environment Fund, to which Governments would contribute on a voluntary basis. The first goal for this fund is 100 million dollars during five years.

   A ridiculously small amount considering what is at stake. However, the Fund has already got promises from governments corresponding to a sum of between 63 and 75 million. The target of one 100 million $ will probably be reached without any difficulties.

4. In order to cope with very difficult problems of co-ordination, a special Environmental Co-ordinating Board would be set up. This important body would be chaired by the Executive Director.

The Conference also recommended that the Fifth of June should be designated as "World Environment Day". And, in another recommendation, the convening of a Second Conference on the Human Environment was advised.

If we now look at the recommendations in the action plan to determine what consideration was given to remote sensing techniques, we find that this subject was ignored for the most part. We have, however, in recommendation number 67, a general statement:

> "It is recommended that the Secretary General, in co-operation with interested Governments and UN specialized agencies take the necessary steps to encourage further development of remote sensing techniques for resources surveys and the utilization of these techniques on a basis of proper international arrangements."

In recommendation number 25 there is an important suggestion to set up a World Forest Appraisal Programme to "provide basic data, including data on the balance between the world's forest biomass and the prevailing environment, and changes in the forest biomass, considered to have a significant impact on the environment." This is a really important part of the Earth Watch program.

However, in recommendation number 27, remote sensing is again mentioned. FAO should facilitate the transfer of information on "methods for the evaluation of forest resources through sampling techniques, remote sensing and data processing." Here remote sensing is rather a tool for exploitation than for proper management.

This limited interest in, or rather avoidance of, remote sensing is rather remarkable, as the importance of this technique has been strongly emphasized during the preparations. This can be seen in the documentation prepared for and accepted by the Conference. Here I just want to mention a few of the documents of conceptual importance to the Conference. First we can consider the two MIT studies organized by Professor Carroll Wilson. The SCEP study dealt with Man's Impact on the Global Environment, and the SMIC study dealt with Man's Impact on Climate. The first took place in Williamstown, Massachusetts, 1970, and the second in Lidingö, Sweden, 1971.

In both these reports which were widely distributed and were backed by top scientists, not only is it stressed that remote sensing is one of the best tools with which we can understand and follow the global environmental crisis, but also that this technique in some cases is the only possible means of getting the information needed.

The International Astronautical Federation has also pointed out the importance of remote sensing from satellites in a conference report, consisting of ten different papers selected from the 22nd International Astronautical Conference in Brussels, September 1971.

The role of remote sensing in relation to global monitoring was also examined in a report from the Commission on Monitoring, which was set up by SCOPE, The Scientific Committee on the Problems of the Environment. This committee is an ICSU body. ICSU is the International Council for Scientific Unions. This report was especially requested by Mr. Strong, Secretary General of the Stockholm Conference.

The question is now, "Why was remote sensing so neglected?" I will try to answer that question and - I think that the answer is of importance if we want to understand the role of remote sensing in international affairs.

First it is quite clear that there are several reasons for the neglect of remote sensing. I stated in the beginning of my lecture that there was an information gap between the experts and the politicians. I think that a lack of interest is one of the reasons for this gap. During the Conference the Outer Space Affairs Division of the Department of Political and Security Council Affairs at the UN had made special arrangements to inform the delegates about remote sensing technique by means of lectures and a special panel discussion. In the panel were specialists from Brazil, India, Italy, Sweden and the USA.

The situation during this panel meeting is a good example of what it was like in Stockholm. The hour for the panel discussion was changed several times in vain hope of finding a suitable time. The discussion took place in a small room very difficult to find on the top floor in the New Parliament Building. In the same building, one of the main committees was in session, while two of the other main committees met in the old Parliament Building. At the same time there was the on-going general debate at the People's House. On top of that, there were the Environmental Forum and the unofficial People's Forum going on at two other places in the city. It was rather remarkable that even 17 people turned up to listen to the eight panelists who came from all over the world!

Remote sensing, as I understand it, is a child of the space age. It has been developed by the two space powers and only these two powers can, for the moment, make full use of the technique. This aura of "great power" around remote sensing does not make it a popular topic at a UN conference with 113 nations represented. During the preparations, in which representatives of both space powers took part, the two of them were able to agree on and to jointly express a view that was accepted as a balanced view by the representatives from the small nations. In my opinion, based on my experiences as chairman of the Commission on Monitoring, the two space powers were prepared to back remote sensing as a tool to be used in the control of the global environment.

It was, however, from this point of view very unfortunate that the USSR could not take part in the Conference. As a consequence, remote sensing became a technique associated only with the USA. Thus the political climate during the Conference made it impossible to discuss remote sensing without emotional attitudes. Considering the situation, it was better not to discuss remote sensing at all.

The minor role allowed remote sensing during the Conference contrasts sharply with the prospective role this technique could play in connection with international and global problems. I shall elaborate here on this concept taking into account the action plan recommended by the 113 nations at the Stockholm Conference. The first two parts of this plan are "Earth Watch" and "environmental management activities".

One of the main functions of the Earth Watch is monitoring, in order to identify and determine the extent of environmental problems of international importance.

Twenty-three recommendations from the UN Conference deal with some kind of monitoring. These recommendations start with suggestions for monitoring systems covering a wide variety of natural disasters, including tropical cyclones and similar storms, torrential rains, floods, earthquakes and desert locusts. Some of these systems already exist. Some of them need to be improved and coordinated. Of special interest for ecologists is the UN invitation to WMO to promote research on the periodicity and intensity of droughts, with a view to developing improved forecasting techniques. The need for an almost real time recording makes remote sensing from space the only feasible tool for this type of disaster monitoring.

The last recommendation mentioning monitoring suggests that we "consider undertaking to monitor, assess, and regularly report the emergence of tariff and non-tariff barriers to trade as a result of environmental policies". In this case remote sensing is hardly the proper instrument. However, in relation to at least eight of the other 21 recommendations, remote sensing is in my opinion a relevant technique to be considered.

But before further analysis I want to examine the general approach to monitoring in the recommendations. The slogan of the Conference was "Only one Earth" - and in my opinion - this is also very important to keep in mind in relation to monitoring. In the recommendations on monitoring, however, you can hardly trace the concept of the unity of the biosphere. The recommendations reflect, rather, the existing pattern of the UN specialized agencies. Each one has its piece of monitoring. From one point of view this is correct, as the capacity and ability should be used where they are found, and at least some of the specialized agencies have monitoring experience. However, from the other point of view, this might detract from a unified effort. The UN agencies have for practical reasons partly divided the biosphere following the different media, with air to WMO, oceans to IOC, and soils to FAO for example. From the monitoring point of view, this fragmentation into different media is dangerous. A more integrated approach is needed, concentrating on the substances and the interfaces and the transport between the different media. In two recommendations we have this integrated view on monitoring. In recommendation number 73 "It is recommended that Governments actively support, and contribute to, international programmes to acquire knowledge for the assessment of pollutant sources, pathways, exposures and risks...". This is thus a recommendation to the Governments to support rather vague international programmes. Recommendation number 57 recommends the Secretary General "take steps to ensure proper collection, measurement and analysis of data relating to the environmental effects of energy use and production within appropriate monitoring systems". The far-reaching consequences of this recommendation where the following emissions are particularly mentioned: "carbon dioxide, sulphur dioxide, oxidants, nitrogen oxides (NO_x), heat and particulates, as well as those from releases of oil and radioactivity". And the effects to be studied are "on weather, human health, plant and animal life, and amenity values". These two recommendations could really be the basis for a totally integrated global monitoring system.

Considering other recommendations, I think that both the national delegations and the Conference Secretariat were aware of the risks of fragmentation. It will be a difficult task of the new Environmental Secretariat to co-ordinate and streamline all the monitoring activities into an efficient Earth Watch. To aid in this task and to help overcome the difficulties the Environmental Co-ordinating Board will be set up. However, a very effective incentive to cooperation is money. And I hope that the Environment Fund will be the glue that will keep the monitoring activities together and serving "Only one Earth".

During the Conference, attention was mainly focused on the international aspects of the environmental problems, and this also applies to monitoring. For several reasons, very little was said about national monitoring. In this review I will deal neither with local nor national monitoring. I only want to point out that remote sensing and instrumentation developed in this context probably will play an important role in national monitoring. The usefulness of the remote sensing technique depends on which variables one wants to measure. Let us assume that we are interested in recording the SO_2 levels in the air. It is, of course, important to be able to register the levels with proper accuracy, but that is not the main point of monitoring. The important question is whether one can apply this measurement in a useful way. This depends on the frequency with which one needs to measure, and this in turn, depends on the variation in the variable to be measured. If the variable changes quickly in time, you need to have many measurements with short intervals. This is generally the case in the lower atmosphere, where there is extensive turbulence and quick changes occur. In order to get useful information, one must have a stationary, continuous recording. This means that the instrument has to be placed either on the ground or on an earth-stationary platform. A moving satellite would not be useful in this case.

Quite different is the situation in the upper atmosphere, where conditions are much more stable, and there is much less of a need for continuous recording. Here the satellite-borne technique is not only useful, but is the only existing technique. As many of the global environmental problems are affected by the conditions in the upper atmosphere, and as our present knowledge of the conditions in this area is insufficient, it is necessary to promote research so that a monitoring system can be established to follow the conditions in the upper atmosphere. In this connection, the Global Atmospheric Research Program - GARP - is currently in progress. This program is organized by the International Council of Scientific Unions and the World Meteorological Organization.

As I pointed out, the possibilities for using remote sensing techniques for monitoring purposes depend to a high degree on the character of the variables to be measured and their variation patterns.

The variation pattern in the oceans is not very well-known, but remote sensing may be very useful in the study of this variation. In terrestrial areas some of the variables suggested for use in monitoring change extremely slowly. One or a few recordings a year may be sufficient for monitoring purposes. Consider the changes in the gross vegetation pattern, for example. These changes are most critical in marginal, remote and inaccessible areas, such as changes in the timberline, or increases or decreases in desert areas. We frequently hear about man-made deserts and the advance of arid areas into cultivated lands. To record these changes, I think remote sensing from space will be very important -- and as few recordings are needed -- cheap, if there is an operating system such as the ERTS.

There are other variables that can be recorded in the same way and that will be of importance in an Earth Watch. The monitoring of the sea ice in the Arctic areas is an example.

Leaving the more technical aspects of global monitoring and remote sensing, I shall now examine the structure of such activities. I have emphasized earlier the necessity of an integrated approach and have stressed the idea that remote sensing can only be a part of such a system. From the international point of view, however, remote sensing is of importance, as it may be the only means of monitoring the two last "commons", the oceans and the upper atmosphere. Both of these commons are now threatened by the destructive mechanisms so brilliantly analysed by Garrett Harding in his "The Tragedy of the Commons", 1968. In the upper atmosphere the problem is simple - it is to follow changes in the composition and establish trends for different types of pollutants and for the changes in the physical variables. In the oceans the situation is much more complex because there is an interaction between "pollution" and resources. Productivity in the oceans is mostly located to the coastal areas. The primary production is partly dependent upon the outflow of nutrients from the continents. This outflow has been increased by human activities (wastes). This has resulted in higher productivity. However, together with these nutrients resulting from man's activities there has been an outpouring of other biological active substances sometimes toxins, which may make the sea products unfit for human consumption or may cause disturbances in the marine ecosystems. The wide spread dumping of toxic material may also have such effects. In addition we have the very serious oil pollution, which must be regarded as a real global threat. Especially in detecting oil spills remote sensing has unique possibilities.

During the Stockholm Conference the delegates were well aware of the critical situation in the oceans and not less than nine recommendations dealt with marine pollution. There are recommendations for international and national actions, to strengthen the international work in the field, to promote research, and to promote monitoring. I think there is no other area where international monitoring is more needed. Furthermore it seems clear that remote sensing is the best method for rapid surveying of extensive areas. There is only one recommendation missing: an explicit commitment for remote sensing.

Both the oceans and the upper atmosphere are recognized as international areas, even if there are continuous discussions on where the boundaries should be placed. At the same time there is no institutional regime to protect and govern these areas. If Earth Watch is to be of any significance at all, it should start working these areas that do not have protection from any national authority. During the Stockholm Conference the Governments agreed on the principle of "one earth", but stated that the States were given sole responsibility for the protection of the terrestrial areas or the continents. A consequence of this must be that someone else must take the responsibility for the commons. However, we all know that the road to some kind of "ocean regime" or "stratosphere regime" is a long one, but one that we must take.

I want to draw attention to one critical area in this connection and it is the Arctic. The SMIC study has pointed out that we have an important feed-back mechanism in the interrelation between the temperature of the atmosphere and the extent of polar ice. Using present models, only small changes of heat input to the earth's surface may be sufficient to lead to considerable shifts in the limits of polar ice and even removal of the ice. This removal of the Arctic Sea ice-cover might be triggered by natural or human influences. Removal of a sea ice cover would, in turn, presumably have profound influences on the climate of the northern hemisphere. There are, however, conflicting views on this question. A continuous monitoring of the ice situation is recommended, and in this case remote sensing has already been used. Of importance here is the programme AIDJEX, Arctic Ice Dynamics Joint Experiment, sponsored by the National Science Foundation. In this programme different types of remote sensing will be used and the results could be a base for a future monitoring system.

Considering the present situation, it might be possible at this time to establish the first truly international control system without violating the independence of the nations. I am, however, well aware that very strong economic interests will try to stop any development in this direction.

Remote Sensing has also a role to play in environmental management and in the part of the UN action plan dealing with natural resources. In the last two years our attitude toward natural resources has changed. We have heard warnings that the resources of the globe are rather limited and that if present trends continue we are heading for a disaster in the future - and some say a very near future. There are limits to growth and Professor and Mrs. H. Meadows and associates published a book with that very title just a few months before the Stockholm Conference.

If present trends continue, we will be affected in two ways: global resources will be depleted and the upper tolerance level for global mistreatment will soon be reached. Taking a long view of the resource problems, we have to realize that the material resources - the basic compounds iron, copper, oxygen etc. - will never disappear - they will only be scattered or combined in ways, that make their use more difficult or require more energy. More importantly, we now are threatening the life-supporting biological systems. If they are destroyed they will be extremely difficult to rebuild.

The awareness of this situation - overt or covert - was probably the main reason for the split between the developed and the developing nations at the Stockholm Conference. The situation was, of course, also used by other interests. Interests motivated more by personnal economy or political gains than by concern for the human environment.

The complexity of the problems and difficulties in understanding the relationships - together with information problems in the less developed nations - made it easy for these interests to widen the gap between the rich and the poor countries.

The developed countries have tried to help the less developed countries by extensive assistance programmes. Perhaps some of these programmes have had economic and political backgrounds. There has been a transfer of a technology developed in northern countries to tropical and subtropical areas. The results have not always been encouraging. The main reason is that our technology has slowly emerged by trial and error in the very sturdy and tough northern ecosystems, and now the same technology is sent crashing headlong into very fragile tropical ecosystems, about which almost nothing is known. The effects of this can sometimes be disastrous in areas, which have very little strength to withstand disasters. This is not theoretical speculation. Experience has shown how vulnerable the tropical areas are.

Even if there were many activities before and during the Stockholm Conference to overbridge the differences between the rich and the poor nations, it was not possible to conceal the split. From global point of view this is very serious and probably the greatest threat to our environment. I think we now have to approach the problems in a different way and do a lot of rethinking to get out of the present dead-lock. But even with good management of the global resources we are faced with two meta problems. The first is the redistribution of the resources between the "haves" and the "have nots", that is an international problem. The second is to solve the population problem, that is a problem both for the rich and the poor nations, but that has to be done on a national level.

We now must try to give assistance, especially to countries in difficult situations. These are very often situated in the marginal zone, and are very sensitive to technical mistakes. I think that in these areas - often remote and inaccessible - remote sensing can be an extremely useful tool in both planning and management of assistance. Recently we have, in Sweden, formed a special secretariat for international ecology. This secretariat has been jointly set up by the Swedish International Development Authority, SIDA, and the Swedish Natural Science Research Council. This council corresponds to the US National Science Foundation. The Swedish council has, however, also operative functions. This secretariat will have advisory functions in relation to the two parent organizations and will direct its activities toward tropical and subtropical areas. The idea is that this secretariat should act as a catalyst for a more integrated scientific approach to the assistance work. We are well aware of the fact that the scientific knowledge base represented by the Swedish research council is insufficient to cover the tropical and subtropical areas, but we hope that the secretariat will also be able to draw upon and use experts from other countries. Here in the USA the Institute of Ecology has taken a similar approach and is trying now to get an extensive forum of tropical experts in the service of the developing countries.

SIDA has for the present moment many projects in Africa, and the new secretariat will be faced with African problems, especially in arid and semi-arid areas. In these areas the population is poor and the need for aid is shocking. Both SIDA and other national and international assistance organizations are now faced with the very difficult ecological problems of giving aid to the marginal lands of Sahara and Kalahari. The problems are also similar in the arid parts of Latin America and Southeast Asia. Every assistance activity in these areas needs to be very carefully planned. We need methods to assess the primary productivity, not only at a single time, but continuously and over extensive areas. We need information on the irregular rainfall and the water resources. These

are areas which have supported an astonishing amount of mobile game and nomads, but that have been ruined by settlements. The tool for these rapid and repeated surveys over extensive areas, is in my opinion, remote sensing. The technique is available, the methods have only to be worked out and tested.

As the countries where assistance is needed are extremely poor, the methods have to be worked out with some kind of international cooperations. It is, of course, fundamental that the nation in question really wants the assistance. Considered on an individual area basis, the costs would probably be too expensive, but the results from one area can probably be used with slight modifications in other areas. In such a situation, joint international efforts should be worthwhile. For the present moment we have the International Biological Programme and one of its goals is to promote biological productivity on the earth. It may be noted that within this programme remote sensing has been applied with success as a tool for assessing different vegetation types. IBP was launched and is lead by ICSU, International Council of Scientific Unions. The programme, which now is terminating, has in part been a great success, but due to lack of economic resources it has been concentrated on problems in the developed countries. The tropics and subtropics have been rather neglected.

New programmes are now emerging such as UNESCO's Man and Biosphere, MaB-programme and other integrated programmes. They will focus attention on the tropical areas and the impact of man on these areas. As has been indicated during the preparations for the MaB-programme, remote sensing will be important. But also in this context it is quite clear that some nations hesitate to use this technique, which has been developed in connection with space research. This research has been linked with the two space powers, the USA and the USSR.

In order to break down this hesitation, and especially to give help and assistance, where really needed, I suggest that the two space powers jointly offer to contribute to the development of a technique for land-use assessment in arid and semi-arid areas. I also suggest that the ground truth work should be done by international teams organized by a proper international body. I think also, that this work should be funded by national and international development organizations such as United Nations Development Programme and the World Bank. This could be a moderate but important exercise in real international cooperation in order to bridge the gap between the rich and the poor and to promote better global management.

After this review of the rather bright possibilities for remote sensing in a global action plan for the environment, we have once more to look at the institutional arrangements. It has been pointed out, that the glowing technical prospects of remote sensing have earlier obscured the difficult administrative, economic and political problems yet to be solved in the international field. How difficult it is to get international institutions to handle agreements, when national interests are at stake, may be illustrated by two examples from the Stockholm Conference - looking so successful on paper. The Conference condemned very strongly nuclear testing - and the French immediately went home and started to bang their nuclear bombs. The conference recommended a 10-year moratorium on commercial whaling. The recommendation was immediately ignored at a meeting of the International Whaling Commission. Bad omens - indeed - for the global environment and the recommendations from Stockholm.

Unfortunately, we are in relation to remote sensing once more in a situation where the technical development is much more advanced than the political tools with which to handle this development. But as it takes a long time to create proper political instruments, it is very urgent that this work be started, if we want remote sensing to be of service to all mankind.

If we cannot fill the gap between the new technology and the present political incompetence, the impact of remote sensing might be an additional threat to the global environment. Earth-oriented satellites are meant to take regular inventories of earth resources to achieve better management, but they may also be used for harder exploitation. This may be called mis-use, however, the satellites with their instrumentation make this mis-use possible. These objections to remote sensing are very real to an ecologist, and I want to illustrate this with an example. When discussing remote sensing it has been pointed out that it may serve the less developed countries. But it is not enough to give information on existing resources. There is also a need for economic assistance so that these resources can be used in a beneficial way. It has, for instance, even in the recommendations from the Stockholm conference, been pointed out that remote sensing can be a tool for the exploitation of forests. Here the Amazon Basin has been mentioned as a suitable area. This may be correct, but such an exploitation of the Amazon Basin without any knowledge about its ecological effects might be very risky from many points of view. Before we can advise a largely increased utilization of the tropical forests, we must have accurate and detailed predictions concerning all aspects of such an exploitation, including climatological, economic and social consequences. A certain sensivity, to use an understatement, may be felt by nations overflown by satellites making regular inventorial surveys for economic reasons. Information concerning the agricultural aspects of natural resources might be used against the overflown country, especially if this type of

information is not available to everybody. According to the plans for the earth-surveying satellites from the USA, all information should be open and free. In spite of this there is a real danger that this new technology will increase the gap between the developed and the less developed countries. To use the received information it is necessary - as I already have pointed out - to have economic resources. Here the rich nations or rich corporations have an advantage. The consequences of remote sensing without proper control may be more dangerous to the earth than the nuclear bomb, as remote sensing is regarded as a tool for progress and not - as the nuclear bomb an instrument for fear. I have here spoken about remote sensing and international affairs and pointed out how remote sensing can be used in this context. In my closing remarks I want to look at the problems from another angle and pose the question: What can remote sensing do to promote international affairs? Remote sensing, according to M. R. Holter is a technique for rapid surveys of extensive areas, is in itself a boundary - crossing technique. The sensors and the vehicles are air or space borne and may use international space. The targets are mostly located on ground, that is divided by national boundaries or on the international ocean surface. Ground truth is always needed. The synthesis received and computerized must be centralized and managed as a unit. The evaluation of the results may be centralized, or decentralized among different nations. Is it possible that any structure could better illustrate the need for international management? To my opinion this could also be a training ground for international cooperation. The direct results from the sensors may be important, but the real goal is to learn to handle such a system in a truly international way. These experiences could be of immense importance to other types of cooperation.

We are, however, very far from this situation now. If decisions in this direction every will be taken, they have to be taken by politicians and not by technicians or scientists. And the politicians are not yet aware of the possibilities offered by remote sensing. In order to bring about an awareness, we must, on the international level, have an increased information flow to the politicians and the public in general. There is, of course, a lot of information going out all over the world. As this symposium illustrates, the present target groups are, however, rather limited to technical specialists who tend to keep the information to themselves. This is not enough. I think remote sensing at this time is running the risk of losing the wide perspective, and that it should try to broaden its contacts with other sciences and especially with the Public. Not by telling what this marvellous technique can do, but by asking what has to be done and by offering solutions to the problems of others.

MICROWAVE RADIOMETRY AT THE DFVLR, OBERPFAFFENHOFEN, GERMANY

M. Vogel
DFVLR Institut für Flugfunk und Mikrowellen
D 8031 Oberpfaffenhofen, Germany

ABSTRACT

A review of our work in the field of microwave radiometry is given: airborne radiometry and ground mapping with a 35 GHz total power radiometer, development of a self calibrating radiometer for 11 GHz, the use of this instrument for airborne and ground based measurements, and the construction of similar radiometers for the atmospheric windows at 32 GHz and 90 GHz. The information content of passive microwave measurements and possible ways to overcome the basic limitations are discussed.

1. INTRODUCTION

Work in the field of microwave radiometry at this institute was initiated 1962 in the group of Th. Heller and has been continued with varying intensity until now. The motivation was at first the question if passive ground mapping could be used as an aid to aeronautical navigation, but was later generalized to the establishment of knowledge, experience and facilities in the field of passive microwave sensing of environment, including the atmosphere, in the interest of government research authorities financing the DFVLR and others interested in application of this technique to specific questions. Of special importance to us are the complicated relations between radiation intensities measurable as functions of aspect, polarization, frequency, time, and the parameters of smooth and rough materials, terrain, and single objects. These data are needed to design a system for a specific task, or to derive meaningful information from passive microwave observations.

2. EARLY GROUND MAPPING EXPERIMENTS AT 35 GHZ

K. März began 1962 with a study of the basic laws and relations combined with a survey of the low noise sensor technology available for implementation at that time [1, 3]. Following preliminary X-band experiments he constructed a total power superheterodyne radiometer for 35.5 GHz (IF-bandwidth 20 MHz, detectable temperature difference $\Delta T = 3$ K for a time constant of 0.2 s) and used this instrument, with a downward looking fixed paraboloid antenna (320 mm diameter, 3 dB beamwidth 1.9^{o}), for test flights with a small airplane (DO 27) over various terrain. He verified in the limits of available resolution all important properties of terrain: high contrast between water and land

(~ 100 K), medium contrast between "black" wooded areas and ice, snow, roads, buildings (~ 20 K); and very low contrast between different kinds of vegetation (< 10 K) [2].

F. Schlude later added a scanning mechanism to the antenna and a ferrite modulator as a Dicke switch and mapped in meandering flights some bavarian lakes at clear and slightly cloudy weather [4, 5]. No details in land areas were resolvable. He also tested a radiometer with two dishes scanning in antiphase and connected alternately to the receiver [6]. This method, proposed by Th. Heller, scans the ground in parallel lines always in the same direction, thereby improving picture quality. Sky temperature variations observed with the 35 GHz radiometer from the ground [7] were only partly correlated with visible cloud structures; rain showers gave very high contrast in the order of 100 K relative to clear sky.

3. SELF CALIBRATING 11 GHZ RADIOMETER

To achieve higher temperature resolution and the capability for quantitative measurements, P. Hach conceived and built a modified Dicke radiometer for 11 GHz (direct amplification in tunnel diode amplifier, bandwidth 1 GHz) [8, 9]. Two switching circulators and two thermally stabilized reference loads were used. The receiver was connected in turns to antenna, reference load 1, antenna, reference load 2, antenna, reference load 1, and so on. By analog data processing and gain control the receiver calibrated itself continuously and eliminated drift effects. As a price paid for this improvement a small part of the noise fluctuation from the reference channel is modulated into the signal channel by the gain control loop dependent on the signal and control time constants and the receiver noise level. The measured ΔT_{rms} for the 11 GHz radiometer was 0.1 K for τ = 1 s signal time constant and 293 K antenna temperature. The principle of self calibrating was incorporated later as a possible mode of operation also in radiometers with more noisy input stages for 32 GHz and 90 GHz and detailed experience about performance will be collected.

4. MEASUREMENTS WITH 11 GHZ RADIOMETER

The 11 GHz radiometer was used by P Hach for ground observations from an aircraft (Beechcraft "Queenair") equipped with a fixed paraboloid of 1.2 m diameter [12] below the fuselage [10, 11]. Results show not only water areas with very high contrast to land but also many resolvable details in land areas. The radiometer was also used on the ground to obtain "pictures" of the institute building and environment. The importance of using data preprocessing and special display techniques for matching the image display to the human visual system became evident. Work in this direction is done by F. Fischer in close cooperation with the "DFVLR Institut für Satellitenelektronik", Oberpfaffenhofen. Small but clearly resolved contrasts are lost, if one gray scale covers the full dynamic range in a straightforward manner.

J. Preißner later observed from a mobile platform and a 21 m antenna test tower with the X-band radiometer motor vehicles on roads and in various terrain. The effect of metal vehicles can be described by the area of an equivalent mirror reflecting "cold" sky radiation into the antenna's field of view. Based partially on these experiments K. Grüner made a feasibility study about ground based and airborne applications of microwave radiometry related to traffic control.

Flight tests with a combined microwave-infrared system were made by J. Preißner using the 11 GHz radiometer and a 8 - 12 µm infrared radiometer (G. Miosga) simultaneously to measure ground radiation from low altitude. It was tried to follow the same flight path under different weather conditions with the help of an improvised radio interferometer (M. Raab), but irregular movements of the small airplane gave unavoidable deviations. The idea behind this experiment was to reduce ambiguity by combining measurements in frequency bands where reflected background radiation and emitted thermal radiation contribute in a very different way to the signal. In a very rough approximation the infrared measurement gives temperature (most natural surfaces, including water, have a high infrared emissivity) and the microwave measurement temperature times microwave emissivity (the sky radiation is very weak at X-band).

5. AIRBORNE RADIOMETERS FOR 32 GHZ AND 90 GHZ

To make available a set of radiometers operating in the atmospheric "windows" for the measurement of signatures and for other applications we built the already mentioned superheterodyne radiometers for 32 GHz and 90 GHz (B. Aumiller). The 32 GHz radiometers uses a gunn local oscillator. the intermediate frequency band is 10 MHz to 310 MHz, both sidebands are used. At 90 GHz single side band mixing with a 79 GHz klystron to an IF of 11 GHz ± 1 GHz is used. The measured laboratory performance for normal Dicke operations and antenna temperatures around 300 K is ΔT_{rms} = 0,5 K for τ = 1 s (32 GHz) and ΔT_{rms} = 3 K for τ = 1 s (90 GHz). The 32 GHz radiometer was successfully tested in flight. Problems arose with the 90 GHz mixers sensitivity to shock and vibration.

Either millimeter wave radiometer can be mounted with the antenna in a cylindrical extension of the nose of the "Queenair", equipped with optimum thickness (half wavelength) teflon windows looking downward and upward (to measure sky radiation).

A small scanning antenna for the radiometers (1.6^{o} beamwidth for 90 GHz, 5° for 32 GHz) was built and tested by D. Klement as a prototype for larger versions: an excentric cut of a circular paraboloid is rotated about an axis through the feed horn at the focus. Defocussing during scan and aperture blocking is avoided, but linear polarization changes its direction. Measurements were also made at a combination of a fixed paraboloid in combination with a rotating flat deflector plate.

The problem to fly with more than one radiometer and related equipment is not yet completely solved. A "Canberra" is available for DFVLR research flights and the large bomb by will be converted into an equipment compartment. Only a relatively inexpensive solution is financially feasible. The construction of a ladderlike pallet 0.9 m by 4 m with downward looking apertures is in progress.

6. RADIOMETRY OF THE ATMOSPHERE

The investigation of the disturbing effects of clouds and residual ground radiation on satellite borne microwave measurements in the absorption bands around 22 GHz and 60 GHz was requested in 1969 in connection with a planned "Early GARP Experiment". The urgency was reduced after the microwave sensors were considered only supplementary to infrared sensors and not "critical" for the experiment. Work in the field of atmospheric radiometry has been limited to computer similations of measurements from 35 km altitude for different parameters of atmosphere, surface and cloud cover (F. Malota).

Financial and manpower limitations have until now prevented development and construction of radiometers for the atmospheric absorption bands at 22 GHz and 60 GHz. Of special interest would be the experimental answer to the question whether the ground contribution in the absorption bands can be interpolated between window measurements.

7. INFORMATION OBTAINABLE BY MICROWAVE RADIOMETRY

Information obtainable by microwave radiometry alone is rather limited. Spot "temperatures" measurable are related ambiguously to many parameters of the objects, its environment, the background and the radiometer. A priori knowledge and/or additional independent measurements are needed: mapping to obtain topographical relations, size and shape; dual polarization radiometry, use of the radiometer receiver also for active reflectometry, multifrequency observations, combination with high spatial resolution methods in other frequency ranges (photography, line scanner, side looking radar). If "all weather" capability is needed, only active and passive microwave sensors in the atmospheric transmission bands can be combined.

Angular resolution is diffraction limited by the size of realizable antennas, especially in airborne systems. Advance of the theory and technique of imaging antennas is necessary. V. Stein and K. Grüner discussed various types of scanning antennas for radiometry [15]. An optical simulation study of passive high resolution imaging with multilobed (distorting) antennas (e.g. an array of small antennas distributed all over an aircraft) was made by G. Graf, using a deconvolution techniques for the reconstruction of an undistorted image [13].

The data rate of microwave radiometers is severely limited by the statistical properties of the thermal radiation and the absolute bandwidth of the radiometers. The uncertainty ΔT_{rms} of each independent sample of radiometric temperature T obtainable per inverse bandwidth is equal to the mean value $\bar{T}$. Reducing uncertainty by integration over N samples ($\Delta T_{rms} \sim \frac{1}{\sqrt{N}}$) takes time. Very long observation times result in the case of high resolution imaging, impossible in airborne applications. The only way out of the data rate bottle neck appears to be the use of many receivers simultaneously in multibeam systems. This may be feasible in the future after progress in microwave microelectronics has reduced size, weight and price of the receivers sufficiently.

8. OUTLOOK

The still relatively new and unexplored field of microwave radiometry is at present, together with other remote sensing techniques, gaining considerable interest. Work in this field will be continued at DFVLR in the limiting frame of available personnel and financial resources. The microwave group of the institute, where the work is done, consists at present of 9 scientists and engineers and can spend approximately $ 60.000,-- per year for equipment and materiel. The principal activity of the group is divided approximately equally between two directions: microwave radiometry and microwave backscattering from objects. The aims are to gain a better insight into the relations between measurable quantities and physicals parameters of materials and objects, to apply the available sensors to specific problems, and to improve the instrumentation.

9. REFERENCES

[1] K. März, Untersuchungen zur Messung der thermischen Mikrowellenstrahlung. DVL, Oberpfaffenhofen, May 1964.

[2] K. März, Messung der thermischen Mikrowellenstrahlung des Erdbodens vom Flugzeug aus. DLR Forschungsbericht 64-30, DVL, Oberpfaffenhofen, May 1964.

[3] K. März, Der mittlere Fehler von Kurzzeitkorrelationsfunktionen. NTZ 18, 485-487 (H. 8, 1965).

[4] F. Schlude, Some Results of Passive Groundmapping. AGARD Conference Proceedings No. 29, 137-142, 1968.

[5] F. Schlude, Die Verwendung eines 35 GHz-Radiometers zur Kartographie vom Flugzeug aus. DVL-Bericht Nr. 745, DLR Mitteilung 68-10, Oberpfaffenhofen, May 1968.

[6] F. Schlude, Kartographieversuche mit einem Doppelspiegel-Radiometer für 36 GHz. DVL, Oberpfaffenhofen, June 1967.

[7] F. Schlude, Beobachtungen der Himmelstemperatur mit dem 35-GHz-Radiometer. Internal Note, DVL, Oberpfaffenhofen, Februar 1968.

[8] P. Hach, Proposal for a Continuously Calibrated Radiometer. Proceedings IEEE (Letters) 54, 2015 (1966).

[9] P. Hach, A Continuously Calibrated Microwave Radiometer. AGARD Conference Proceedings No. 29, 171-186, 1968.

[10] P. Hach, A Very Sensitive Airborne Microwave Radiometer Using Two Reference Temperatures. IEEE Transactions MTT-16, No. 9, 629-636, September 1968.

[11] P. Hach, Ein selbsteichendes Radiometer zur Messung der thermischen Mikrowellenstrahlung des Erdbodens vom Flugzeug aus. Dissertation, TH München, Dezember 1968.

[12] K. Grüner, V. Stein, Eine X-Band Parabolantenne für radiometrische Messungen vom Flugzeug aus. DVL, Oberpfaffenhofen, Februar 1968.

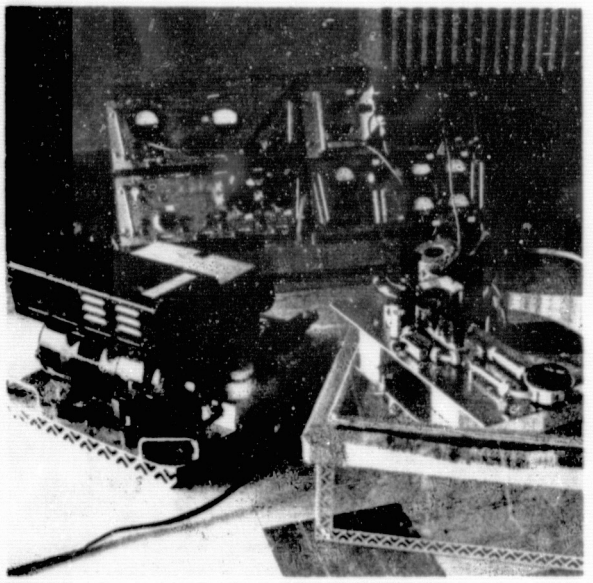
[13] G. Graf, Correction of Microwave Images by Holographic Filtering. AGARD Conference Proceedings No. 50, Ref. 22, 1970.

[14] M. Vogel, Möglichkeiten der Mikrowellen-Radiometrie. DVL Nachrichten, Heft 38, 414-417, Januar 1969.

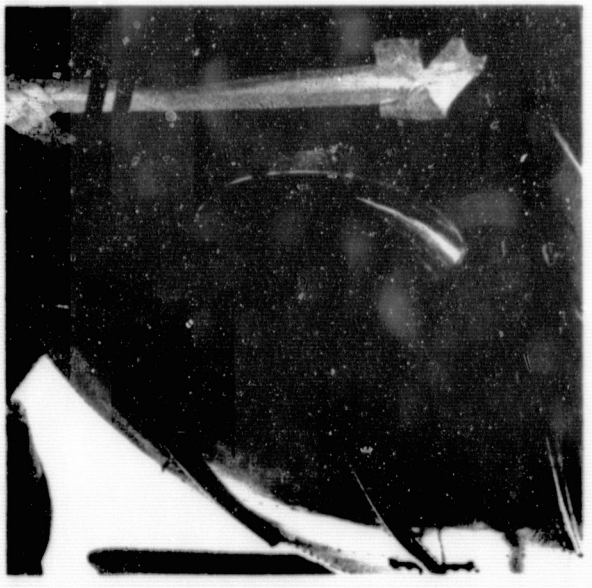
[15] V. Stein, K. Grüner, Antennen mit schwenkbarer Hauptkeule zur Flächenabtastung bei radiometrischen Messungen. DFVLR, Oberpfaffenhofen, Mai 1969.

[16] M. Vogel, Mikrowellenradiometrie und Side Looking Radar. DGLR Symposium, Proceedings: Fernerkundung der Erdoberfläche, DGLR Mitt. 72-10, 1972.

10. FIGURES



Equipment



Antenna below Fuselage

FIGURE 1. AIRBORNE 35 GHZ RADIOMETER. [2].



FIGURE 2. TEST AIRCRAFT DO 27. 35 GHz radiometer installed. [2].

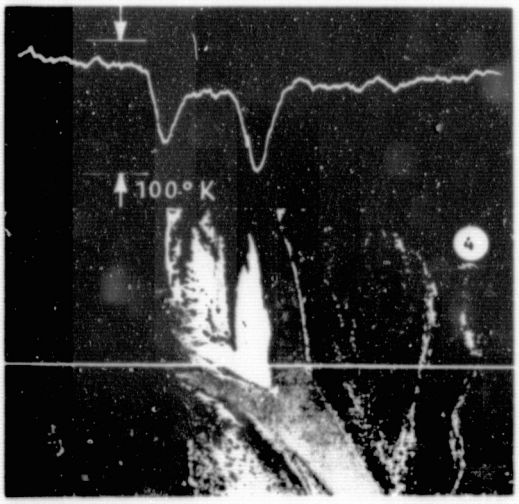


FIGURE 3. EXAMPLE OF TERRAIN RADIOMETRY. Ground track indicated in photograph. Altitude 600 m, 50 m/s, time constant 0.2 s. [2].

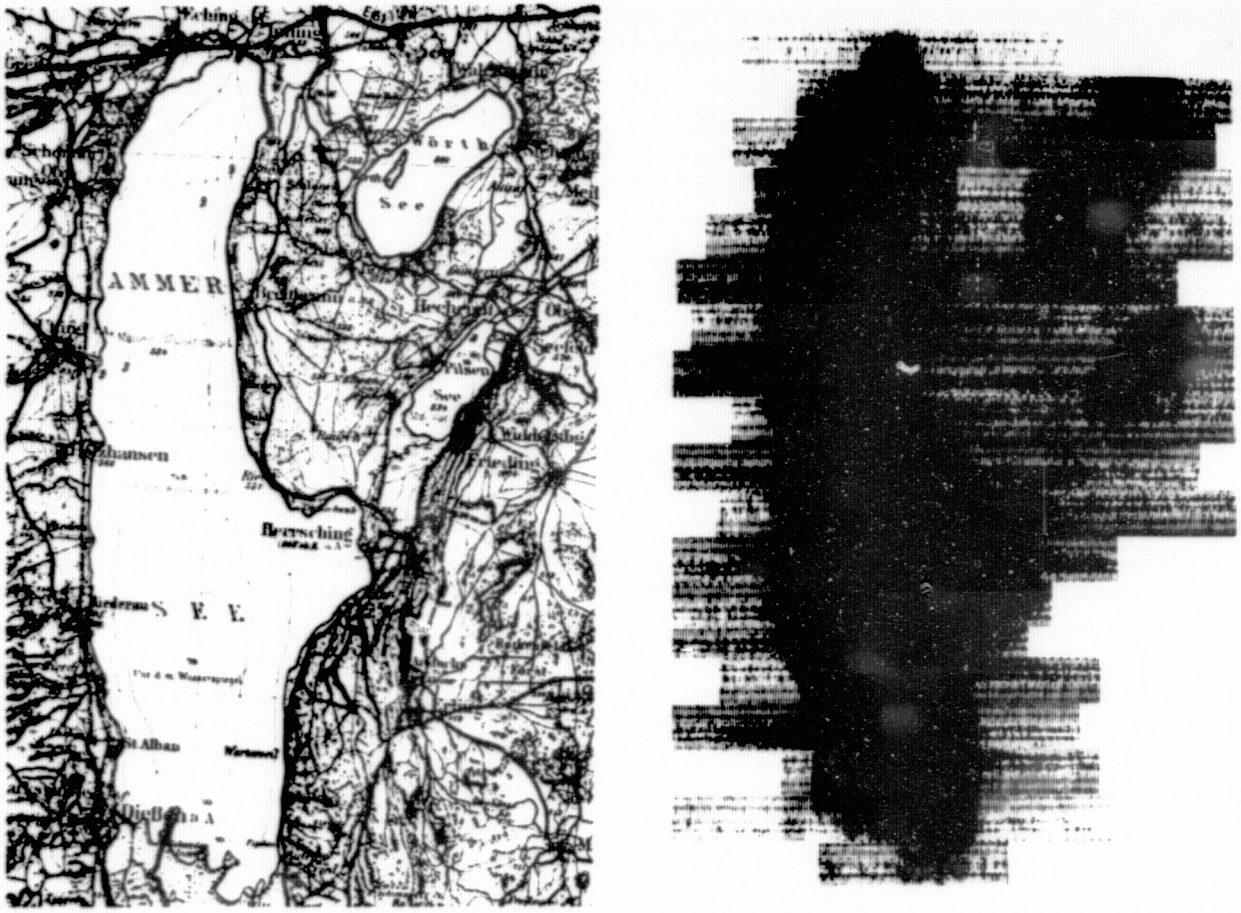
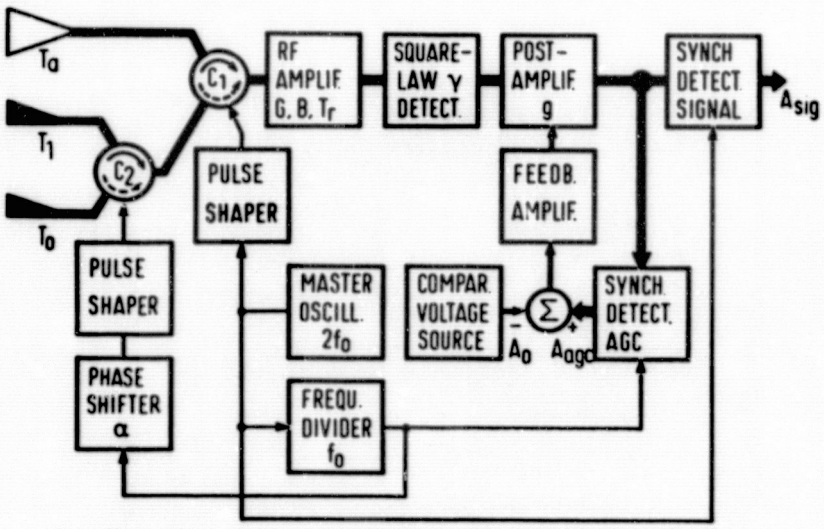


FIGURE 4. THERMAL MICROWAVE MAP OF LAKE AREA.
35 GHz, altitude 2300 m, 1.8^{0} beamwidth. [5].



FIGURE 5. DOUBLE MIRROR SCANNING ANTENNA.
35 GHz, 1.8^{O} beamwidth. [6].



Block diagram of the radiometer.

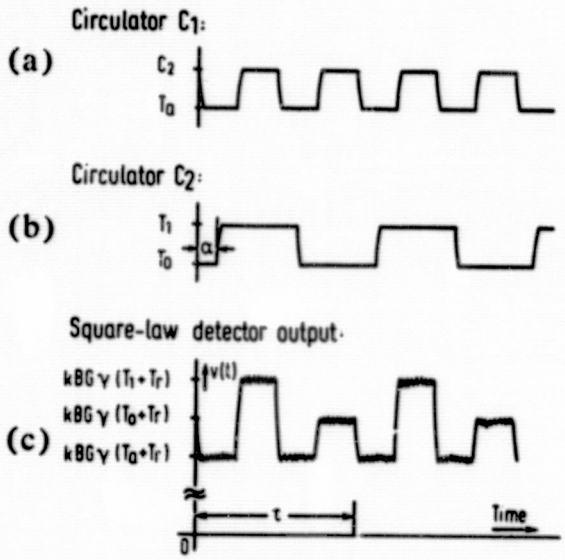
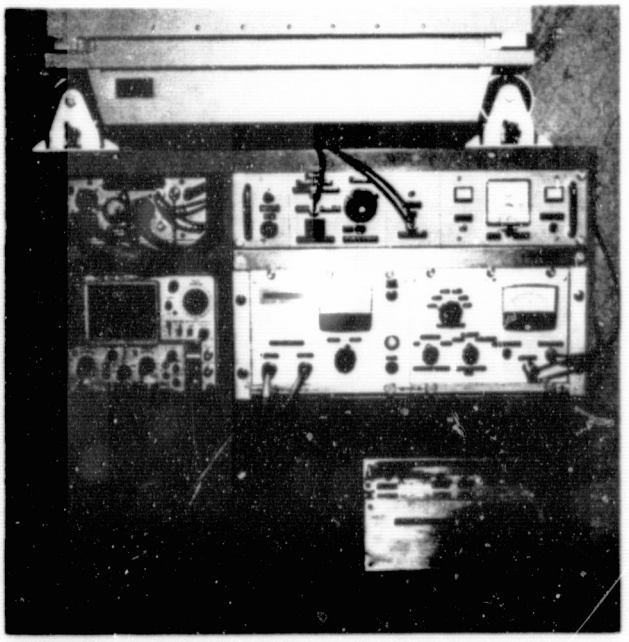
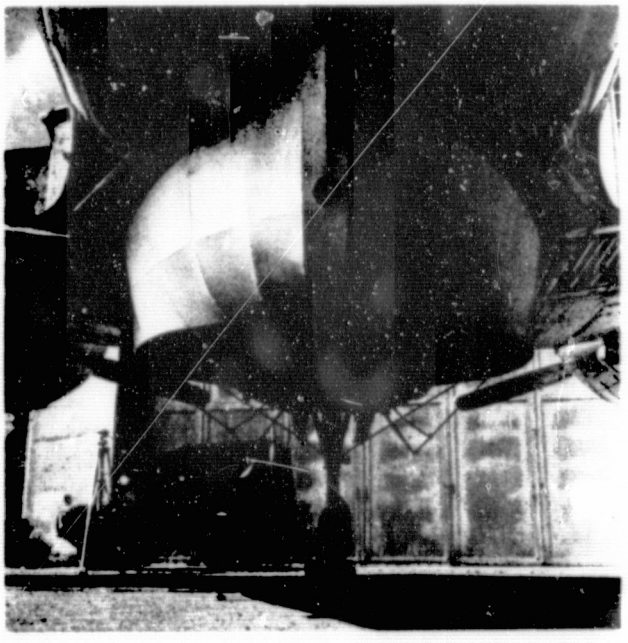


FIGURE 6. SELF CALIBRATING RADIOMETER. [10].



Equipment



Antenna Below Fuselage

FIGURE 7. 11 GHZ RADIOMETER.
[10, 11].

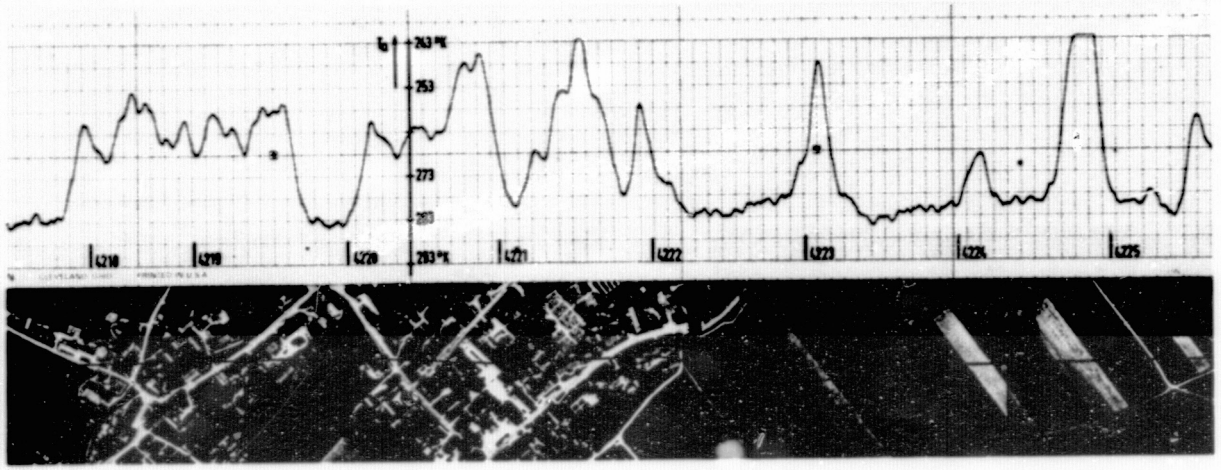


FIGURE 8. 11 GHZ TERRAIN RADIOMETRY. Ground track indicated in photograph. Altitude 300 m, 70 m/s, beamwidth 1.8°, time constant 0.1 s. [11].

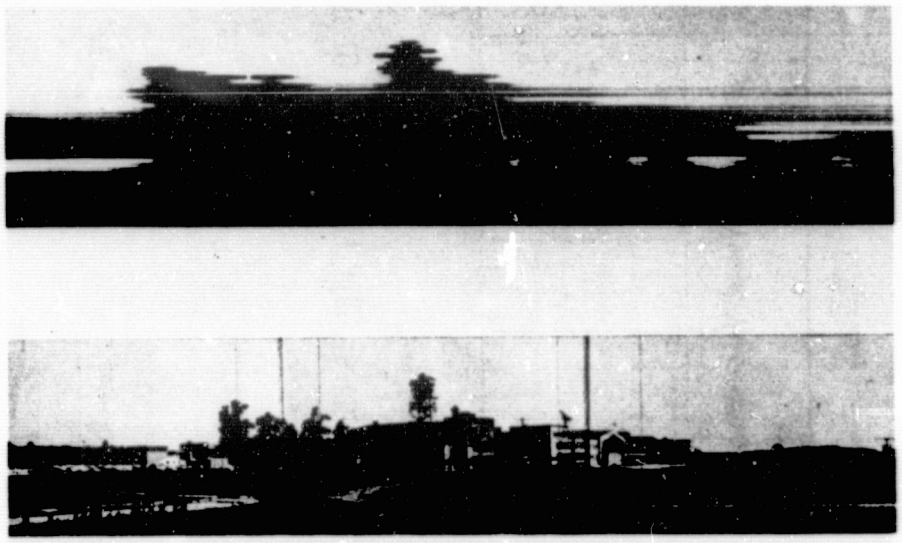
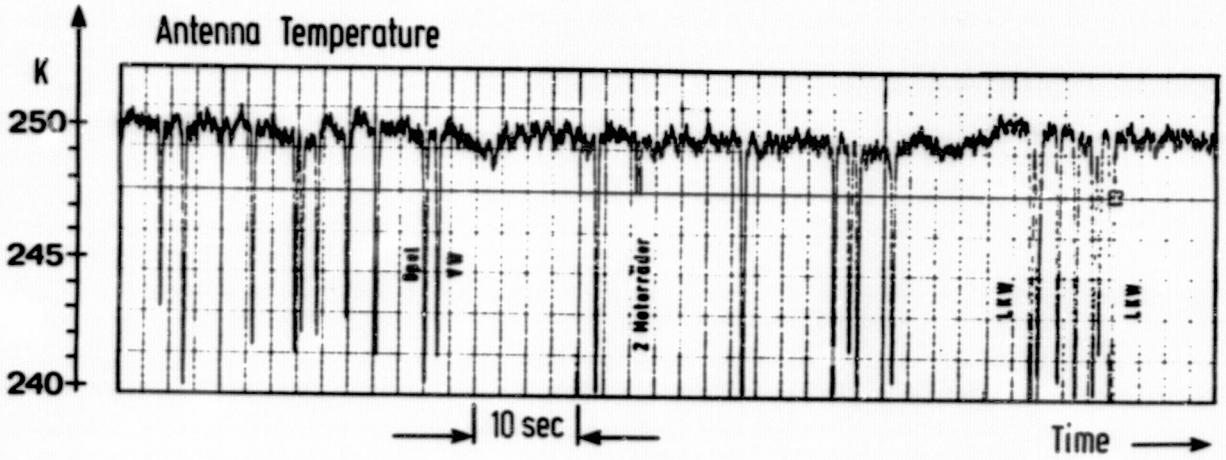


FIGURE 9. MICROWAVE IMAGE OF THE INSTITUTE. 11 GHz, beamwidth 1.8^{o}. Photograph for comparison.



11 GHz 1,2m diameter antenna, distance 180 m, time constant 0,1 sec

FIGURE 10. RADIOMETRY OF ROAD TRAFFIC.

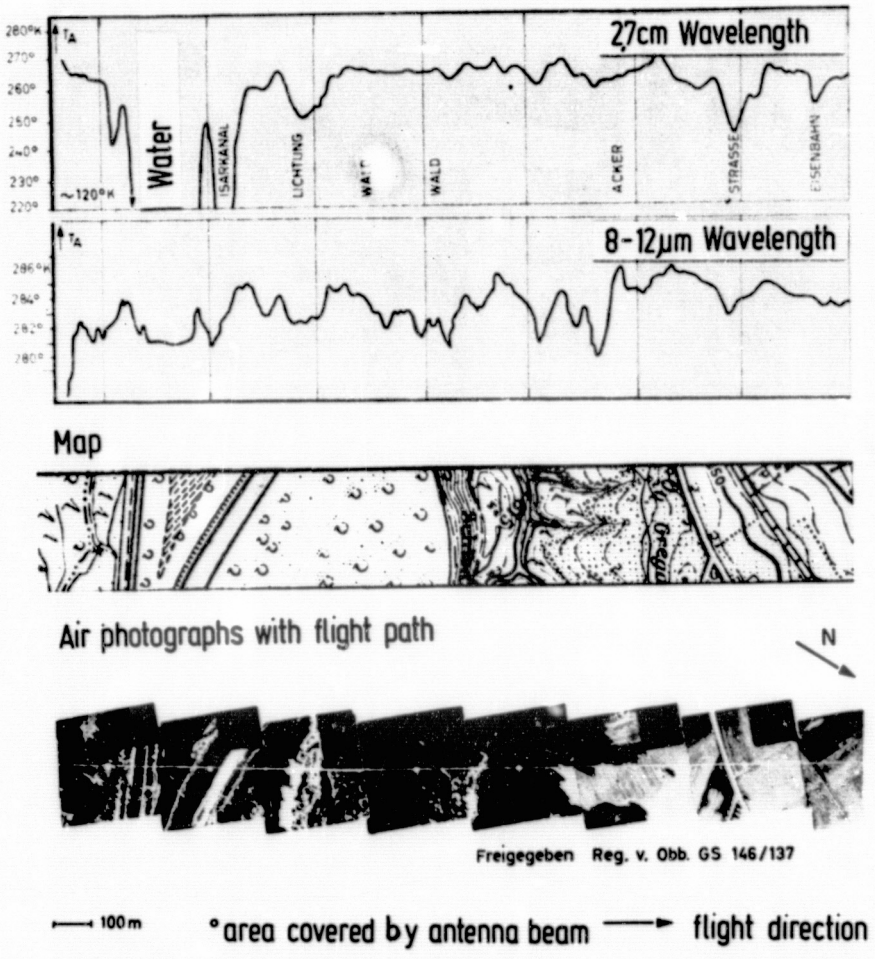


FIGURE 11. SIMULTANEOUS MICROWAVE-INFRARED RADIOMETRY.

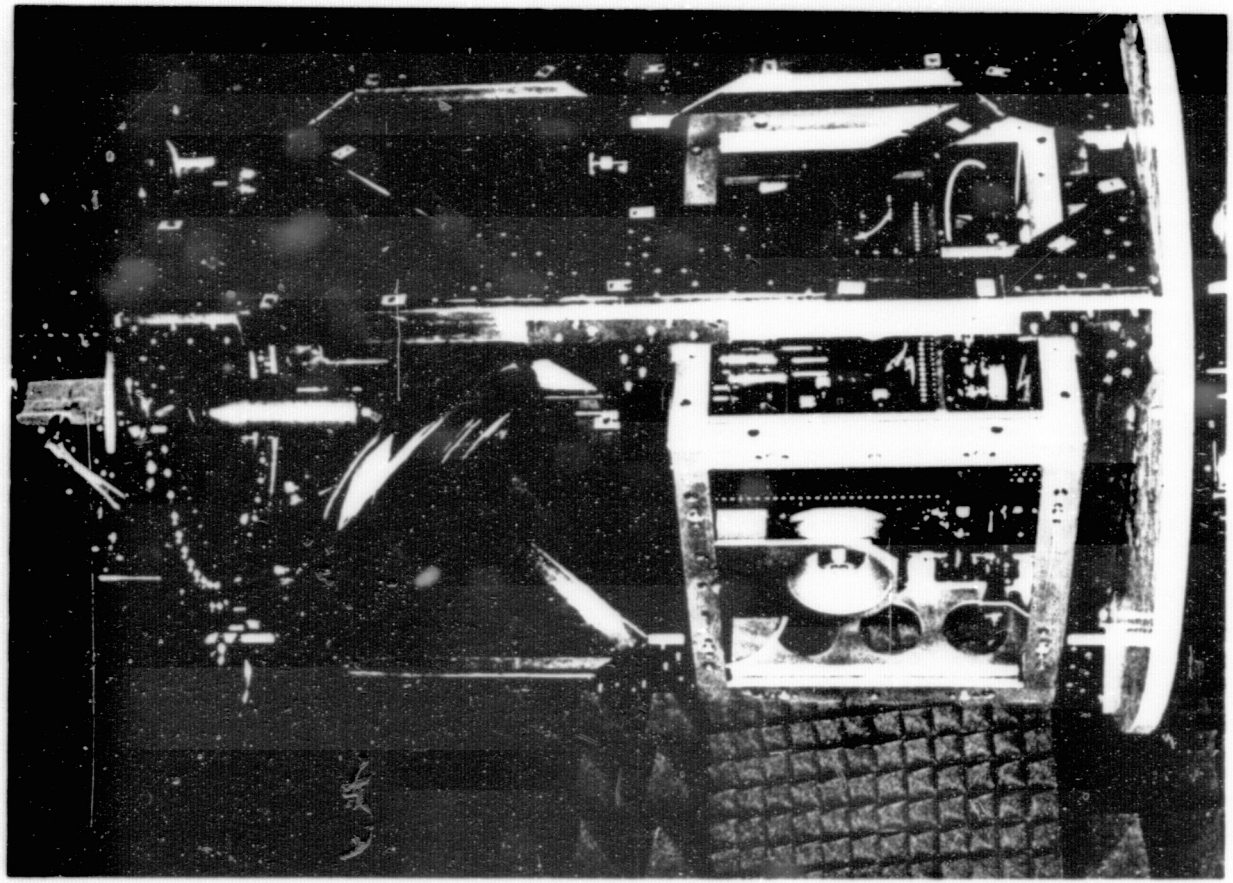


FIGURE 12. AIRBORNE 90 GHZ RADIOMETER.
32 GHz receiver can be substituted.

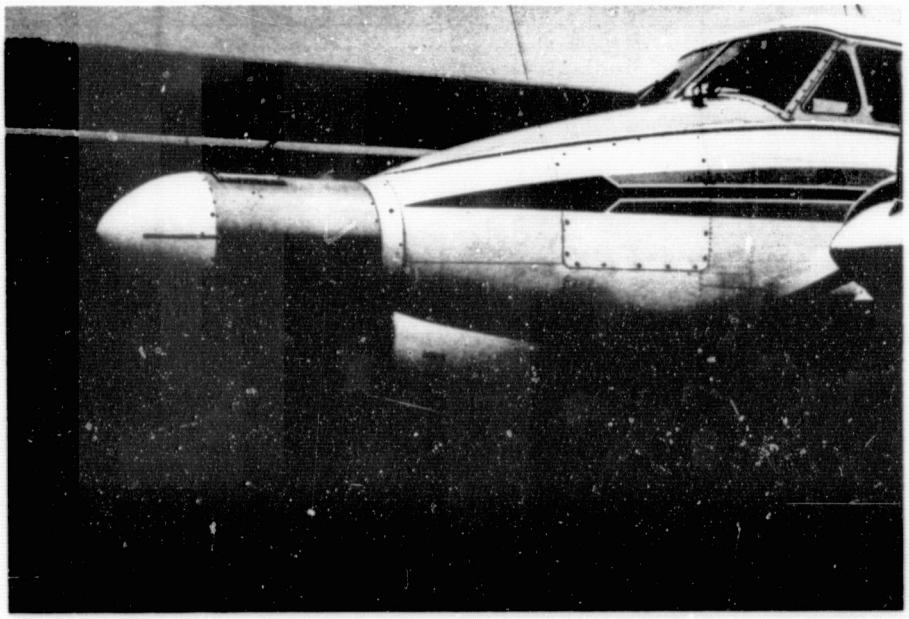


FIGURE 13. RADIOMETER NOSE ON TEST AIRCRAFT.
Teflon windows downward and upward.

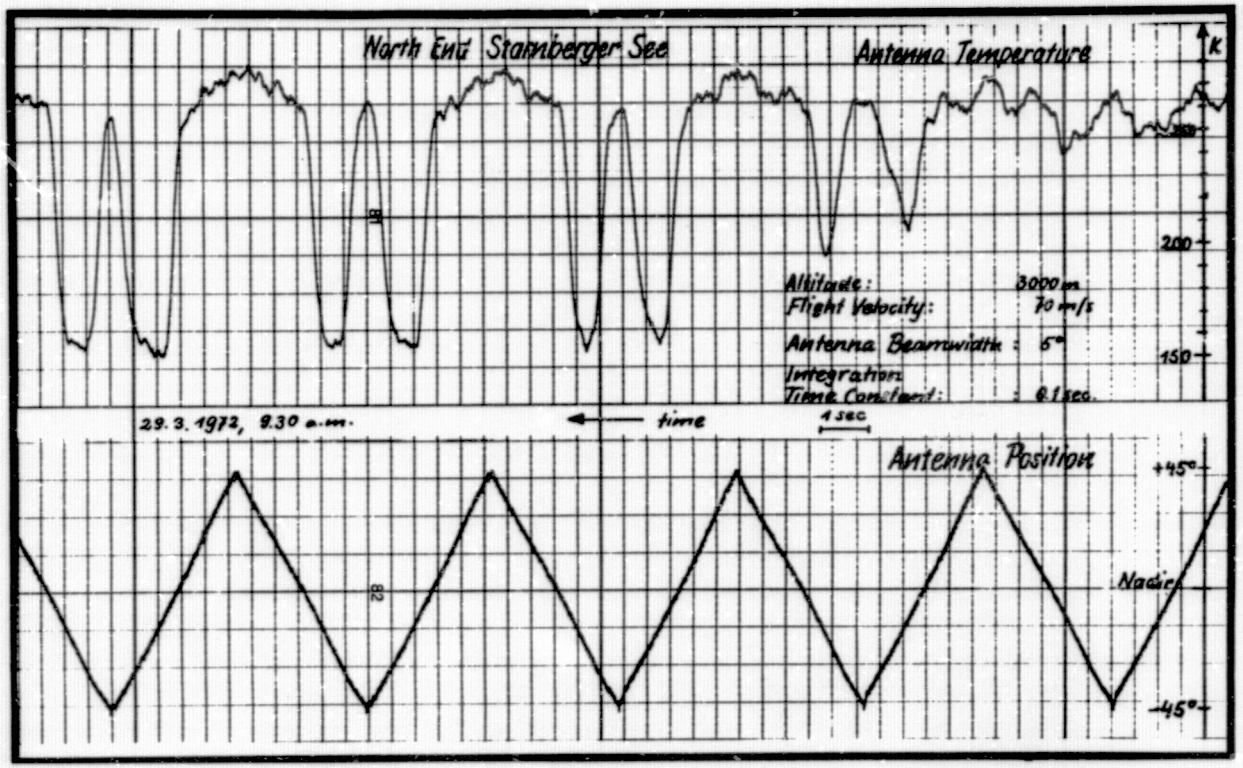


FIGURE 14. OUTPUTS OF 32 GHZ RADIOMETER.

EMISSION PROPERTIES OF NATURAL SURFACES AT MICROWAVE FREQUENCIES

V. V. Melentyev and Yu. I. Rabinovich

Council of Ministers of the USSR
Leningrad, USSR

In order to solve the problem of remote sounding of the underlying surface and atmosphere from flying vehicles, it is important to know exactly the emission properties of different natural surfaces. A knowledge of water-surface emissivity at different temperatures and salinities along with that of different types of soil and vegetation cover is necessary for the interpretation of satellite and aircraft measurements of atmospheric meteorological characterictics. These characteristics are necessary for determination with microwave measurements of underlying surface characteristics such as: surface roughness and wind-speed over the ocean, water temperature, soil humidity, the degree of vegetative cover, ice cohesion, and others. The emission properties of natural surfaces are also of independent interest for the microwave sounding of the surface of Earth and other planets. For this purpose, the detailed calculation of dielectric constants of smooth, fresh, and sea water surfaces at different temperatures and salinities for the centimetre band (0.3 to 8.5 cm) were performed. The calculations showed that the emission of the smooth water surface is mainly influenced by its temperature, whereas the influence of salinity manifests itself only in the longwave part of the region concerned [1,2].

Theoretical and experimental investigations of a number of authors showed the dependence of the sea surface microwave emission on the degree of its roughness - waviness, foam forming, spray, etc. The calculations of the rough sea surface microwave emission for the actually observed characteristics of roughness were performed [3]. The calculation scheme assumes that the rough sea surface may be represented by the sum of an infinite number of elements oriented in different directions. The surface brightness temperature depends on the angle of vision and that elements inclined in different ways produce different inputs to the surface emission. Thus, the dependence of sea surface emission on roughness is reduced to the dependence on inclinations of the infinite number of surface elements, in other words, on the inclination distribution function of the rough sea surface. Here the inclination of the rough sea surface is understood as the gradient of the elevation at this point.

In these calculations, the expression offered by L. M. Martsinkovish [4] for the inclinations distribution function, inferred from the spectrum of elevations described in [5], was used. As a result, the expression for calculating the water surface emissivity was found. This expression for calculating tne water surface emissivity was found. This expression is determined by sea roughness, the inclinations distribution function, the radiation wavelength, the type of polarization, and the dielectric constants of water surface at the given wavelength, hence, by the sea temperature and salinity and the angle of vision:

$$\varepsilon = 1 - A \int_0^{\infty} \int_0^{2\pi} \alpha \cdot \exp \left[- B\alpha^2 \left(1 + C \sin^2 \phi_n\right)\right] \times \left(1 + \alpha \operatorname{tg} \theta_1 \cos \phi_n\right) R(f)\, d\alpha d\phi_n \qquad (1)$$

where

$\alpha = tg\ \theta_n$ the value of inclination

θ_n the inclination angle of the sea surface element

ϕ_n the element asimuth

θ_1 the angle of vision

f the real angle of incidence

R(f) the energetic reflection coefficient for the smooth sea surface

A, B, C coefficients, describing the inclinations distribution function

As the calculations showed, a certain difference appears between the microwave radiation coming from nadir at vertical and horizontal polarization during sea roughness, this difference increasing with the development of roughness. It is known that the smooth surface microwave radiation coming from the normal direction is the same for both polarizations.

Table 1

T = 25°	S = 40°/00,		λ = 3.2 cm					
h^- λ^{-*}	0		0.019		0.028		0.038	
θ°	0	45	0	45	0	45	0	45
Vertical polarization	0.381	0.493	0.390	0.495	0.383	0.492	0.379	0.495
Horizontal polarization	0.381	0.288	0.386	0.296	0.377	0.287	0.368	0.293

The aircraft measurements of the rough sea microwave emission produce the values of brightness temperature close to those calculated by means of the formula for the transfer of the centimetre radiation in the "rough sea surface - cloudless atmosphere" system.

Since the calculations of the natural rough surfaces' emission and reflection properties at microwave wavelengths present considerable difficulties, the laboratory technique for determining the emissivity of natural surfaces was offered. Direct measurements of the emissivities of different natural surfaces were performed in the closed volume in order to eliminate the radiative influence of the sky and surrounding objects [6]. The actual emissivity of the investigated surface can be obtained by two measurements of the volume brightness temperature (Fig. 1), its upper lid alternately presenting a blackbody model and an absolute reflecter at the working wavelength. The technique does not require preliminary measurements of dielectric constants.

The error analysis of the technique showed that the accuracy of determining thermodynamic temperature of the blackbody model and the metallic reflector was 1°K and that of the volume brightness temperature was $\pm$ 1-2°K; the relative error of a single emissivity measurements amounts to 8-10%. But, it is worth noting that the actual accuracy of measurements can be considerably improved, since the accepted technique makes it possible to carry out large measurement series with the following averaging of results.

With the help of this technique, the laboratory measurements of the emissivities for different types of natural surfaces were performed [7] and the dependence of the smooth water surface emissivity coefficients on temperature and salinity at the 3.2; 1.6; 0.8-cm wavelengths was investigated. They appeared to be in good agreement with theoretical calculations [8]. Water temperatures higher than 25-30°C showed the largest deviations of measured from calculated values.

Estimates of the foam and oil or kerosene films influence on water surface emissivity were made (Fig. 2). The increase of brightness temperature for a water surface covered with kerosene and oil films is 11 and 29°K, respectively, compared with the fresh water emission at the same temperature at the 3.2-cm wavelength. For the patterns of egg and soap foam, this increase has the value of 143°K and 152°K respectively. Thus, it appears possible to determine the parameters of sea roughness resulting from wind and the degree of water surface pollution through the value of its input to microwave radiation. Emissivities of various natural surfaces at different wavelengths in relation to humidity, presence of vegetable cover, surface structure, etc. were investigated. The results of measurements are summed up in Table 2. All the values of the emissivity coefficients are obtained by averaging over a great number of single measurements. The emissivity of investigated patterns varies considerable: from 0.961 to 0.655, exceeding the corresponding variations in the infrared. Dependence of emission on the wavelength for damp and dry sand was investigated. It was discovered that the reflection increases with an increase in wavelength. The influence of water upon emission is the same for all the wavelengths investigated, i.e., the soil emissivity decreases with the increase of water content.

The emissivities of two types of dry sand were measured: sand of mild coarseness, consisting of slightly rounded particles (river sand with the roll degree 1-2), and dusty sand of moraine forming. The emissivity of the first sample appeared to be 0.933 $\pm$ 0.005 of the second one - 0.884 $\pm$ 0.004. Thus, some difference was detected between the emissivities of the same material; this could be connected with differences in the structure of the chosen samples, the most probable diameter for the river sand grains being 0.20 mm and for the dusty sand, 0.05 mm.

Investigations of the river sand emissivity dependence on its humidity were performed at the 3.2-cm wavelength. Humidity was controlled at two points of the sample: at the surface and at the 25-cm depth. Emissivity of the sand of 3.4% humidity was found to be 0.927 $\pm$ 0.007, of 10% humidity, 0.703 $\pm$ 0.005, and of 14.5% humidity - 0.655 $\pm$ 0.005. Measured dependences were close to the literature data.

The obtained values of the emissivities are used for interpreting the aircraft measurements of the underlying surface and atmosphere microwave radiation.

Table 2

Surface	Brief Description	Wave-length	Emissivity
Sand	River, dry, middle grains, smooth surface, layer thickness-25 cm	1.6	0.933
		0.8	0.393
Sand	River, damp, smooth surface	3.2	0.749
	layer thickness - 25 cm	1.6	0.769
	River humidity - 3.4%	3.2	0.927
	River humidity - 10%	3.2	0.703
	River humidity - 14.5%	3.2	0.655
Sand	Dry, dusty	3.2	0.884
Detritus	Limestone, large, layer thickness 25-cm	3.2	0.877
Slate	Wavy, several layers, thickness 15-cm	3.2	0.742
Slag	Large, mean size 4-6 cm, layer thickness - 25-cm	3.2	0.787
Grass	Dry, stalk height - 15 to 20-cm	3.2	0.935
Cover	Soil layer thickness - 20-cm	1.6	0.961
Grass	Damp, stalk height -15-20-cm		
Cover	soil layer thickness - 20-cm	3.2	0.890
Wood	Planks, pine, 10-cm thick	3.2	0.878
Foliage	Birchtree branches, layer thickness - 25 cm	3.2	0.882
Concrete	Slab, 20 cm thick	3.2	0.836
Asphalt	Highway	3.2	0.874
Snow	Smooth surface, density 0.58g/cm^3	0.8	0.944

References

1. Rabinovich Yu. I., Melentyev V. V., Trudy GGO, issue 235, 1970.
2. Shifrin K. S., Rabinovich Yu. I., Melentyev V. V., Isvestiya of the USSR Acad. of Sci. Phys. of Atm. and Ocean, v.VII, No. 9, 1971.
3. Martzinkevich L.M., Melentyev V. V., Trudy GGO, issue 291, 1971.
4. Martzinkevich L. M., Meteorol. y Gydrol., No. 10, 1970.
5. Kyrlov Yu. M., Strekalov S. S., Zyplubin V. F., Izvestiya of the USSR Acad. of Sci. Phys. of Atm. and Ocean, v. IV, No. 6, 1968.
6. Rabinovich Yu. I., Melentyev V. V., Trudy GGO, issue 252, 1970.
7. Melentyev, V. V., Rabinovich Yu. I., Trudy GGO, issue 291, 1971.
8. Melentyev V. V., Rabinovich Yu. I., Trudy GGO, issue 291, 1971.

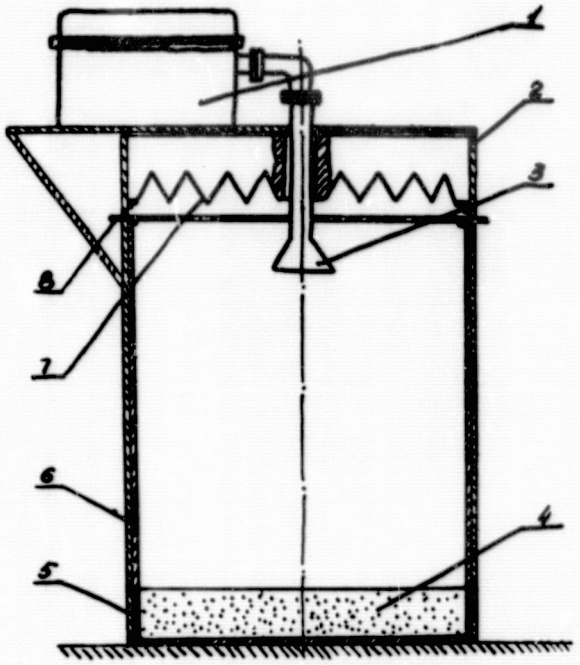


Figure 1

Device for emissivity measurements.

1 - radiometer receivers;
2 - girder - frame
3 - megaphone antenna;
4 - investigated surface;
(absolute reflector).
5 - bath-centainer;
6 - lateral reflecting walls;
7 - blackbody model;
8 - sliding metal screens

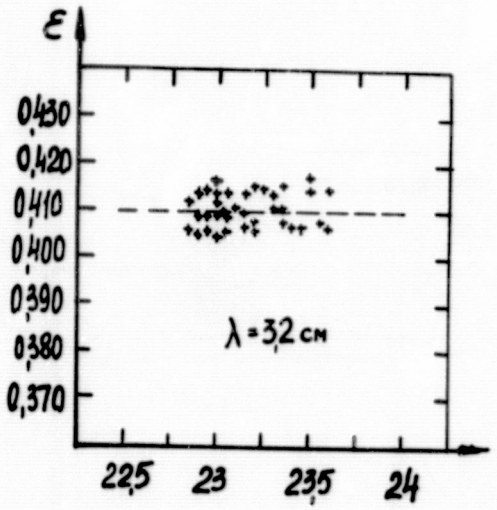


Figure 2a

Emissivity of the film-covered water surface; kerosene

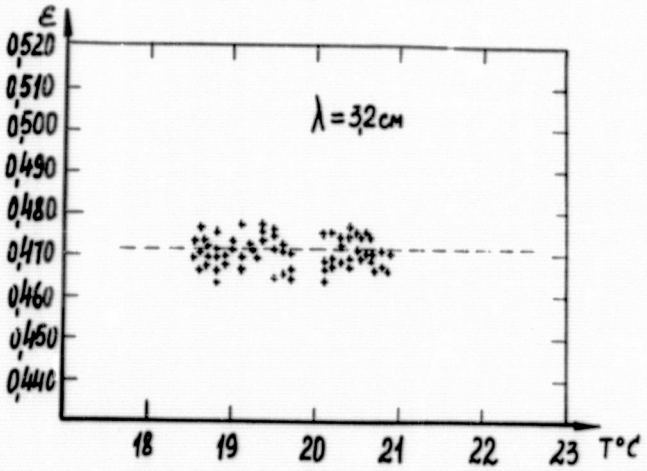


Figure 2b

Emissivity of the film-covered water surface; oil (laboratory measurements)

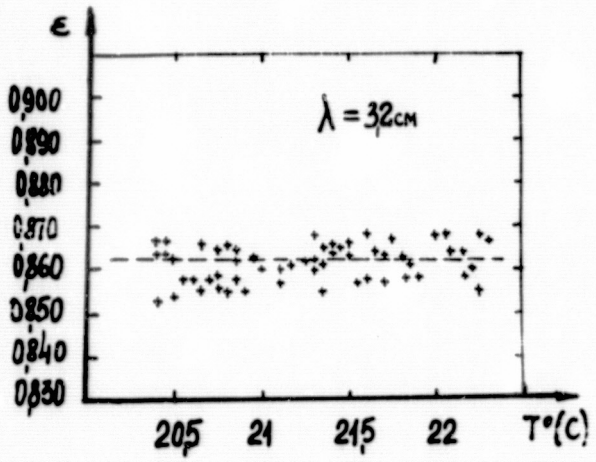


Figure 3a

Emissivity of the water surface covered with; egg foam

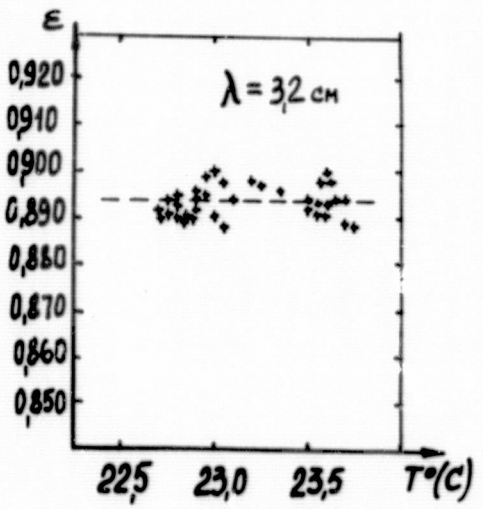


Figure 3b

Emissivity of the water surface covered with; soap foam

DIGITAL DATA PROCESSING FROM SCANNERS

J. L. Bessis
French National Space Research Center
(CNES)
Bretigny, France

I should like to talk this afternoon about digital data processing from scanners.

First of all, I shall briefly explain how since 1970 the French National Space Research Center is taking part in several airborne experiments for a study group in earth resources in which are represented different disciplines interested in remote sensing techniques such as:

- Geology
- Vulcanology
- Hydrology
- Oceanography
- Agronomy
- and of course Pollution

These experiments have been carried out by using two types of platforms;

Firstly - Aircraft for imagery and scanner analysis, up to 30,000 feet, and secondly, stratospheric sounding balloons for small scale photographs between a hundred thousand feet and a hundred and thirty thousand feet.

The sensors used are of two types: - Hasselbad cameras in the visible and near infrared, and - scanners.

This afternoon I shall only be talking about data processing from scanners.

The French National Space Center (CNES) has used two types of scanners on board an aircraft for the earth resources survey.

1. - The Cyclope, manufactured by Sat - the Société Anonyme de Télécommunications. Its characteristics are: - an operating wavelength of 3 to 5μ, a scan rate of 72 scans per second and an instantaneous field of view of 4 mrad, the analog signal is recorded on board the aircraft.

2. - The scanner manufactured by LMD - The Laboratory of Dynamic Meteorology. Its characteristics are: - An operating wavelength of 10.5 to 12.5μ, a scan rate of 1 scan per second and an instantaneous field of view of 10 mrad, the analog signal data is digitized on board the aircraft and recorded on a digital magnetic tape.

In the case of the Cyclope, digitizing of analog data is carried out at the CNES data processing center, in order to enhance a similar program on computer for the two scanners.

Data processing procedure consists of a systematic quick-look, and afterwards a more sophisticated data analysis.

The Systematic Quick Look consists of a geographical representation of the thermal ground image. We are using:

1. A usual high-speed on-line out put printer
2. A micro-film printer plotter (model 1670 Calcomp for example) connected to the computer (which is at the moment a control data corporation 6600).

Every line represents a scan and every point position of a line is edited with one or several characters superimposed according to the signal amplitude. For instance, for a four level system we could use: a dot, then a comma, then a plus sign, and finally, an asterisk.

Preceding page blank

The difficulty lies in a judicious choice of the symbols and their quantitative values.

Each new line represents the progressive horizontal movement of the aircraft.

Several types of quick look are printed on computer printout with numeric and alpha numeric characters used to approximate the original density range.

Column numbers at the top of the printout and line numbers at the left edge of it are used to determine the address of any given data.

The disadvantage of the computer print-out solution is a limitation in the number of horizontal print positions (we have 200 prints per line), which necessitates the juxtaposition of two computer printouts and an excessive computer utilization, which is time-consuming in an operational computer center.

The specialized micro-film printer plotter for the earth resources survey appears to be the best solution.

The systematic quick-look permits the definition of the interesting zones where a deeper analysis is necessary.

It must be noted that picture distortion is inevitable, as no aircraft attitude and speed correction are applied.

SCANNER DATA ANALYSIS

The analysis of raw digital data will provide more or less sophisticated color-coded maps of the measured data, as requested by the experimental team. The analysis is carried out as follows

1. Calibration of the signal in temperature or radiant reflectance.
2. Use of cruising speed of the aircraft (which is as far as possible constant) in order to restitute the observed zone in a coded map which is as geographically exact as possible.
3. tgθ rectification, in other words rescaling of every elementary area observed during one scan, taking account of the distance separating this area from the vertical of the aircraft.
4. Attitude rectification (drift, roll and pitch) and altitude rectification of the aircraft.

A coding device recording these flight parameters was developed as well as a data processing method which makes possible:

Firstly, rectification of the digital image after heading, roll and tilt displacement and secondly, the interpolation between two measurements.

Since two successive lines have a shift in elementary areas, it is necessary, in order to restitute a map of coherent reflectance, to reshift every elementary area on the area of the preceding line.

Then we possess groups of measurements including:

- the reflectance and
- the geographic coordinates of the elementary area of known size.

The graphic representation is produced by a three-color electronic digital plotting system (model 1136 calcomp) and permits, after choosing the interesting area (by the number of the first and the last line), the personalization of every elementary area by means of:

(1) a color (There are three available).
(2) a number or a letter.
(3) physical size of a character.

Every possible gradation is therefore available.

The key of the chosen graphic representation is marked on the paper itself and allows immediate identification of, for example, the measured reflectance level.

The geographical north is also drawn on the chart.

5. Another step consists of choosing the zones within the whole observed area, with reflectance characteristics that remain within given limits.

With this possibility, no information appears on the digital recognition map when we are outside these limits, and a greater degree of accuracy for the information represented is achieved.

6. The next step could be the representation of phenomena by means of "isolevels", for example.

A last representation, directly workable by the users of these experiments consists of curves giving the evolution of the thermal response of the earth versus time in an elementary area.

It is of particular value to agronomists to know the diurnal thermal flux profile of an agricultural field in choosing the type of culture the most appropriate to this field.

In Guadeloupe, for example, results of this type will be helpful for growing lettuces in favourable areas.

Finally, we shall be equipped later this month with a Daedalus 10-channel multiband scanner.

The operating perameters are the following:

Operating wavelength (10 channels from 0.38μ to 1.1μ, scan rate of 80 scans per second, instantaneous field of view of 2.5 mrad, roll correction of $\pm$ 5°.

The scan head is automatically roll stabilized through the use of a small gyro directly on the scan head. Therefore attitude rectification and interpolation will be simplified.

It will then be possible to bring into evidence areas having an identical spectral response i.e. an identical spectral signature, and to represent these areas graphically.

In conclusion, I should like to point out that difficulties in digital data processing lie in the relationship between users and the data processing center. It is not always easy for the users to explain his needs in technical terms to the program analyst, and to understand the volume of data to be processed before arriving at the point where the data is in a workable form from which to begin his scientific study.

A COMPUTER CONTROLLED PRECISION COMPARATOR-DENSITOMETER

P. W. H. Blansjaar, D. Eckhart, P. J. F. Geerders
J. van Kuilenburg, M. E. Seyhan

Netherlands Interdepartmental Working community
for the Application and research of
Remote Sensing techniques (NIWARS)
Delft, Netherlands

SUMMARY

At the NIWARS information processing division a machine was developed and constructed for remote sensing images which automatically measures densities of a photographic plate or film. To be as flexible as possible the points of the plate to be measured are specified by a computer programme. Through this facility it is possible from former measurements to compute the next (optimal) point to be measured. Separate density measurements are performed in 240 µsec, the searching speed on the plates is limited by the allowed maximum speed of the comparator screws. The computer used has a relatively large memory for this use (12 K words), and can be programmed in Algol-60. The basic components are a digital computer of Philips, a modified David-Mann comparator and interfacing logic made by our group. The use of the machine envisaged is high precision measurements of plates and selective measurements of remote sensing images on film. Remote sensing processing tasks for which the instrument is particularly suited are compensation of large image distortions (e.g. in SLAR or IR pictures), reduction of colour images for classification (e.g. in false colour pictures), density-slicing (e.g. in correlation studies of ground truth and image contents) and all further applications where digital picture processing is of use.

Preceding page blank

SATELLITE DETECTION OF MELTING SNOW AND ICE BY SIMULTANEOUS VISIBLE AND NEAR-IR MEASUREMENTS

David F. McGinnis

U.S. Department of Commerce
National Oceanic and Atmospheric Administration
National Environmental Satellite Service
Hillcrest Heights, Maryland 20031

ABSTRACT

Use of near-infrared data in conjunction with reflected visible radiation appears to allow detection of melting snow and ice. Under normal conditions, snow and ice are highly reflective in both the visible and near-infrared areas of the electromagnetic spectrum. Under melting conditions, however, near-infrared radiation is strongly absorbed, whereas visible radiation is strongly reflected. Comparison of simultaneous visible and near-infrared imagery from the Nimbus III satellite provides a method for monitoring the melting of snow and ice that may be applied to snowpack-runoff prediction, flood forecasting, and lake navigation. Several examples, the Sierra Nevada, Lake Winnipeg, the Alps and northwest Canada, are provided to illustrate the use of this spectral difference.

1. INTRODUCTION

Several studies (1, 2, 3) have defined hydrological applications of visible and near-infrared (near-IR) solar reflectance, such as mapping drainage basins, snow cover, plant distribution and flood extent. It now appears possible, through the combined use of both near-IR and visible imagery to detect melting snow and ice. Five examples of apparent snow or ice melt detection are presented in this paper. The areas are the Great Bear Lake-Great Slave Lake-Lake Athabaska region in northwest Canada, Lake Winnipeg in south-central Canada, the Sierra Nevada, and the Alps (two examples).

The National Aeronautics and Space Administration's (NASA's) experimental Nimbus III meteorological satellite, launched on April 14, 1969, provided 24-hour mapping of global cloud cover. During the day, the High Resolution Infrared Radiometer (HRIR) complemented the television coverage (0.5 to 0.7μm) of the Image Dissector Camera System (IDCS) by measuring reflected shortwave radiation in the 0.7 to 1.3μm spectral region. At night, the HRIR provided infrared measurements in the 3.6 to 4.2μm portion of the spectrum to assess earth-surface and cloud-top temperatures. The area instantaneously viewed by the HRIR scanner at nadir is about 8.5 km in diameter, somewhat coarser than the 4.1 km resolution of the IDCS. In addition to the imagery obtained from the two sensors, digital data in the form of computer-printed grids are available for the HRIR scenes. Further information on the Nimbus III satellite system may be obtained from the Nimbus III User's Guide (4).

2. LAKE WINNIPEG AREA

Near 1800 GMT (local noon) on April 25, 1969, the Nimbus III satellite viewed the Plains area of southern Canada and the northern United States. In the IDCS image (Fig. 1a) Lake Winnipeg is clearly visible, lying between two cloud masses. The high reflectance of the lake indicates the presence of ice, likely covered by snow. Small details, such as an island in Lake Winnipeg, are visible.

The corresponding daytime HRIR image (Fig. 1b) exhibits almost identical cloud patterns. In the lower right corner of the image the Mississippi River and part of Lake Michigan appear darker than the surrounding land because vegetation is more reflective than water in the near-IR. The appearance of the frozen Lake Winnipeg would be expected, particularly because of the contrasting snow-free terrain surrounding the lake. However, the dark region between the cloud masses reveals

Preceding page blank

no indication of frozen Lake Winnipeg.

Meteorological data from neighboring ground stations substantiated melting conditions, reporting temperatures between 8 to 15°C.

3. NORTHWEST CANADA

In the area of northwestern Canada viewed by the Nimbus III satellite near 1900 GMT (local noon) the ice- and snow-covered waters of Great Bear Lake, Great Slave Lake, and Lake Athabaska appear uniformly bright against a dark snow-free background in the IDCS image (Fig. 2a). In contrast, the HRIR imagery (Fig. 2b) shows that Great Bear Lake is visible but somewhat darker than the IDCS image, that Great Slave Lake is barely visible, and that Lake Athabaska is not distinguishable. Thus, in one satellite pass a graduated melting condition is detectable from the early stage to complete surface melt.

The north-to-south temperatures in northwestern Canada at local noon on May 23, 1969 averaged -5°C at Great Bear Lake, 3°C at Great Slave Lake, and 9°C at Lake Athabaska. These temperatures are in agreement with the reflectance measurements from the HRIR (Fig. 2b).

4. SIERRA NEVADA AREA

In the area of the western United States covered by simultaneous IDCS and HRIR at 2000 GMT on April 27, 1969, the snow-covered Sierra Nevada appear very bright in the IDCS visible imagery (Fig. 3a). Though not completely absent in the daytime HRIR (Fig. 3b) the bright area over the Sierra Nevada is much smaller and corresponds to the higher elevations.

Temperatures at the 1500-m level were near 8°C, while at elevations above 3000 m there were subfreezing temperatures. Below the 300-m elevation, a thawing snowpack absorbed a sufficient amount of incident radiation to cause it to appear dark in the HRIR image. At higher elevations, the snow surface remained frozen and highly reflective in the near-IR.

5. ALPS AREA

The Alps appear as a very bright band in the IDCS photograph (Fig. 4a) of central Europe, taken near 1100 GMT (local noon) on April 25, 1969. Some clouds exist along the Gulf of Genoa and over the western Alps in Austria. These snow-covered mountains are also visible in the HRIR image (Fig. 4b), but the bright area is more restricted, corresponding to the highest elevations. A satellite pass over the area 17 days later on May 12, 1969, reveals the depletion of snow cover in the Alps as seen in the IDCS picture (Fig. 5a) with only the slightest trace of white appearing in the HRIR image (Fig. 5b); indicating the presence of melting even at the highest elevations.

For both cases in the Alps, all available stations recorded above-freezing temperatures at the time of the satellite's pass. None of the stations was at a sufficient elevation to lie in the area found to be highly reflective in the HRIR image. However, rawinsonde observations indicated the existence of freezing temperatures at levels above 2500 m for the April 25 case and at levels exceeding 3300 m for the May 12 case.

6. DISCUSSION

Supportive field and laboratory information was sought on the reflectance of snow and ice in the visible and near-IR spectra under various conditions. MacLeod (3) noted that fresh snow is light in tone but darker than clouds in the near-IR. However, in 1969 Pouquet (5) attributed the low reflectance of snow to the presence of melted waters on the snow surface. The same conclusions were arrived at independently by Strong *et al.* (6) in 1971.

The extinction coefficient of pure water for wavelengths near 1.2μm, the maximum response of the Nimbus III daytime - HRIR is approximately 1 (7). This value may be interpreted as an optical depth of 1 cm. For a beam of incoming radiation to penetrate a surface water film, reflect from an underlying ice or snow surface, and pass again through the water film, the water film must be significantly less than 1 cm thick; a 1 cm thickness represents nearly total absorption. In fact, considerable absorption would be expected for even a 1 mm layer of water. It therefore appears

that a visible layer of water would not necessarily be needed to cause an appreciable reflectance drop in the near-IR.

Investigations of fresh snow under clear skies (8) revealed an almost constant reflectivity of 90 percent in the visible spectrum. Wet snow produced an invariant, but slightly lower value of reflectance than that indicated for dry snow. Another study (9) found a slight drop in reflectance for dry snow and a more rapid drop for wet snow, particularly at the longer wavelengths (to 0.7μm).

In the lower end of the near-IR spectrum (0.90 to 0.95μm) Kondrat'ev et al. (8) noted a lesser reflectance than in the visible for dry and wet snow. A 16 percent drop in the reflectance was found for wet snow and an 8 percent drop for dry snow. Data (10) shown in Fig. 6 agree with Kondrat'ev's findings and also extend reflectance measurements to 1.5μm. At 1.2μm, where the HRIR response is a maximum, the reflectance of melting snow is only 25 percent. A search is being made for information to describe the reflectance of dry snow beyond 1.0μm. Such information will determine if dry snow retains its high reflectance in the near-IR. The metamorphism of snow and ice must also be examined if the reflectance of melting ice and snow is to be more completely understood.

7. POTENTIAL APPLICATIONS

Although additional information is needed to confirm the hypothesis advanced in this paper, the method for detecting melting ice and snow is of considerable interest to hydrologists. In mountainous areas frequented by deep snowpacks, knowledge of the onset of snowmelt is vital for snowpack-runoff predictions and for flow regulation by downstream reservoirs to control flooding as well as to provide storage to meet water demands during dry periods. On large inland water bodies such as the Great Lakes, where commercial shipping must contend with stoppages due to ice, detecting the beginnings of icemelt could result in improved navigation. TIROS N, planned for launch in 1975 or 1976, with its 1-km resolution will better pinpoint areas of weakened (melting) ice to aid ice breakers in the reopening of shipping channels.

8. CONCLUSION

Although the results of this study are preliminary, a method is put forth for the detection of melting snow or ice through the use of satellite visible and near-IR imagery. The detection procedure uses the strong absorption of incident radiation in the near-IR by a covering film of water. In the visible spectrum the film is essentially transparent. Thus, melting snowpacks or lake ice seen in the visible image become partially or totally absent in the near-IR image. Surface temperatures for the five cases were above 0°C substantiating melting conditions. Measurements made of the reflectance of melting and non-melting snow partially explain the phenomenon, however, additional laboratory and field information is needed on the response of dry snow in the near-IR spectral region before final conclusions can be reached.

REFERENCES

(1) Barnes, J.C., and Bowley, C.J. (1970), "The Use of Environmental Satellite Data for Mapping Annual Snow-Extent Decrease in the Western United States," Final Report, Contract No. E-252-69(N), Allied Research Associates, Inc., Concord, Mass., 105 pp.

(2) MacLeod, N.H. (1970), "Observations of the Inland Delta of the Niger River by Nimbus 3 High-Resolution Infrared Radiometer (HRIR)," Report No. X-652-70-315, Goddard Space Flight Center, National Aeronautics and Space Administration, Greenbelt, Md., 12 pp.

(3) MacLeod, N.H. (1970), "Ecological Interpretation of Nimbus 3 High-Resolution Infrared Radiometer," Journal of Geophysical Research, Vol. 76, No. 6, pp. 1588-1594.

(4) Goddard Space Flight Center, NASA (1969), Nimbus III User's Guide, National Aeronautics and Space Administration, Greenbelt, Md., 238 pp.

(5) Pouquet, J. (1969), "Near-Infrared Daytime Surface Characteristics from Nimbus III High Resolution Infrared Radiometer Data, Geological Aspects," Paper presented at the Fall Meeting at American Geophysical Union, San Francisco, Calif.

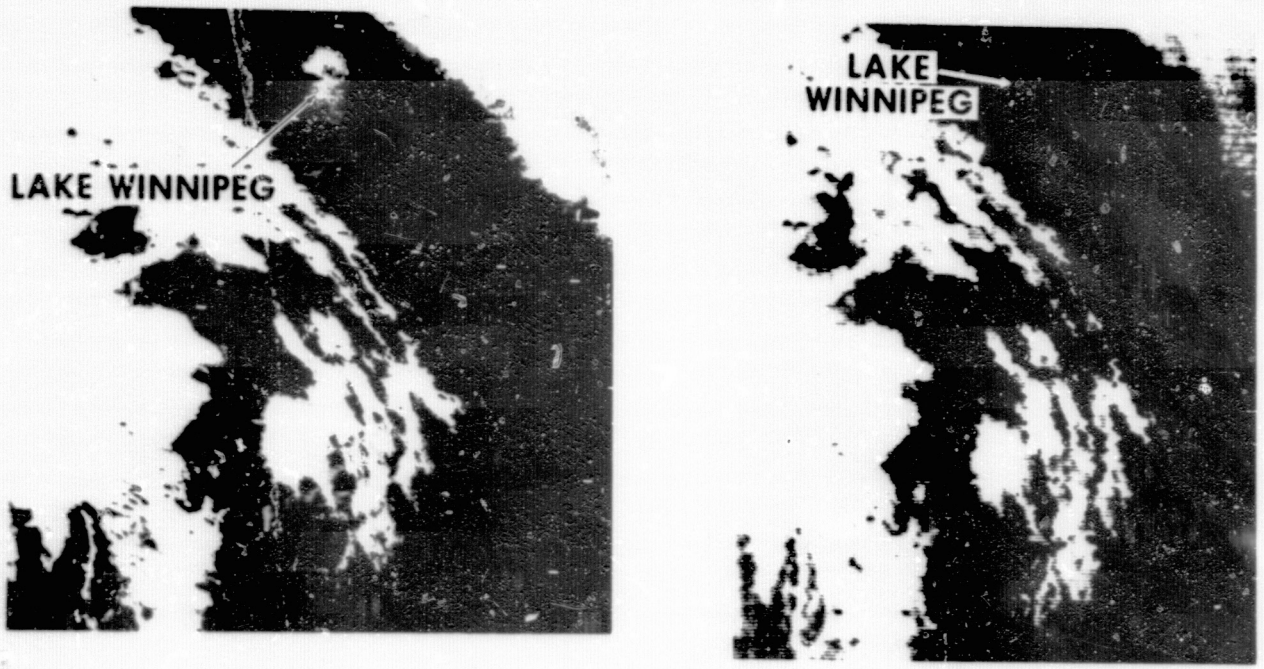
(6) Strong, A.E., McClain, E.P., McGinnis, D.F. (1971), "Detection of Thawing Snow and Ice Packs through the Combined Use of Visible and Near-Infrared Measurements from Earth Satellites," Monthly Weather Review, Vol. 99, No. 11, pp. 828-830.

(7) Neumann, G. and Pierson, W.J., Jr. (1966), Principles of Physical Oceanography, Prentice-Hall, Inc., Englewood Cliffs, N.J., 545 pp.

(8) Kondrat'ev, K.Y., Mironova, Z.F., and Otto, A.N. (1964), "Spectral Albedo of Natural Surfaces," Pure and Applied Geophysics, Vol. 59, No. 3, Basel, Switzerland, pp. 207-216.

(9) Mellor, M. (1964), "Properties of Snow," Cold Regions Science and Engineering, Part III, Sec. A, U.S. Cold Regions Research and Engineering Laboratory, Hanover, N.H., 105 pp. (see p. 84.)

(10) Mancis, H. (1951), "Review of the Properties of Snow and Ice," available from U.S. Cold Regions Research and Engineering Laboratory, Hanover, N.H., p. 62.



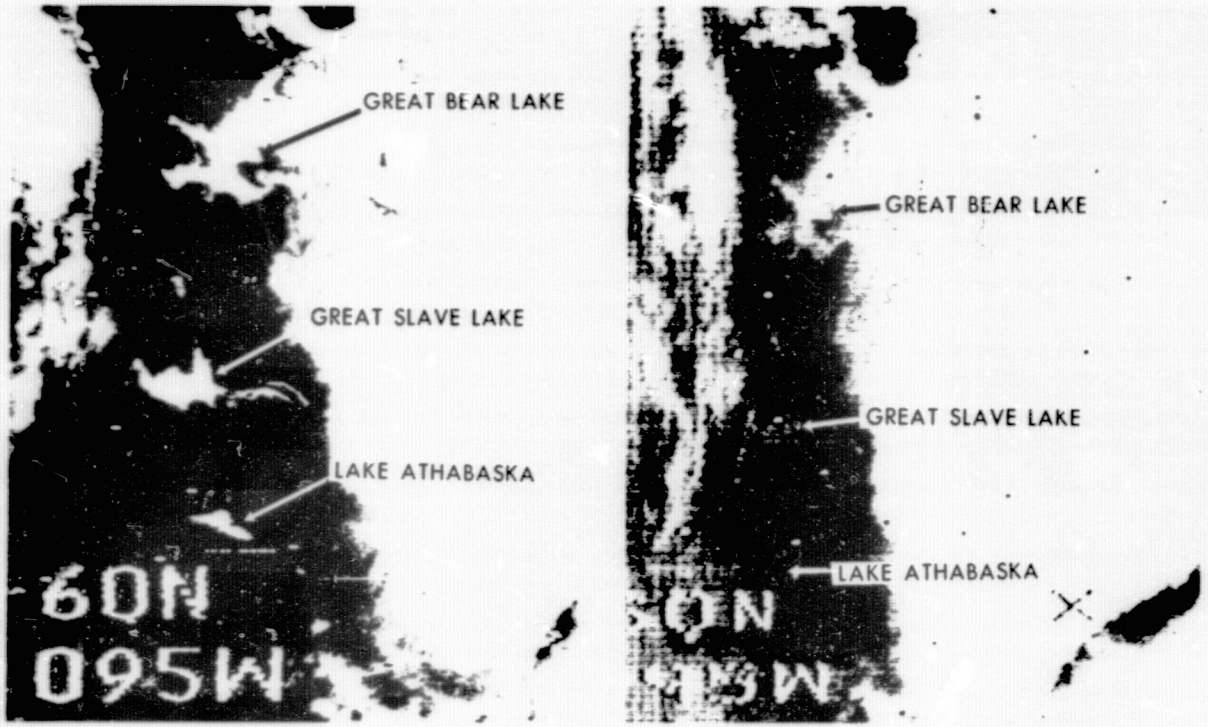
(a) IDCS
λ = 0.5 to 0.7 μm

(b) HRIR
λ = 0.7 to 1.3 μm

NIMBUS III ORBIT NO 153

APRIL 25, 1969

FIGURE 1. 1800 GMT 25 APRIL 1969. Visible (a) and near-infrared (b) images over Lake Winnipeg, Canada, from Nimbus III.



NIMBUS III ORBIT NO. 528

MAY 23, 1969

FIGURE 2. 1900 GMT 23 MAY 1969. Visible (a) and near-infrared (b) images over northwestern Canada, from Nimbus III.

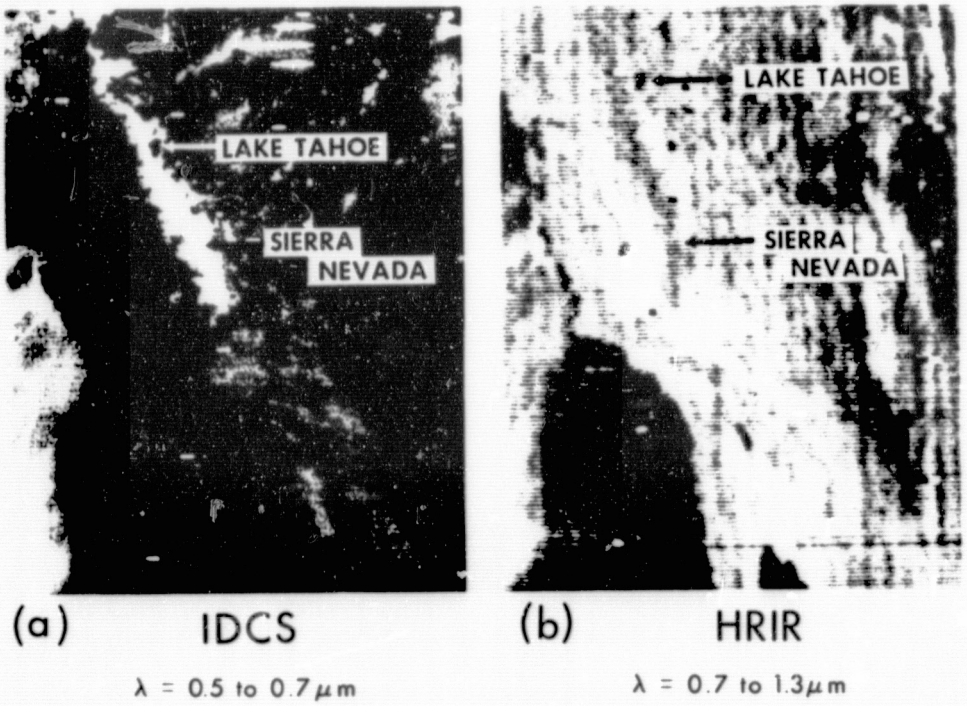
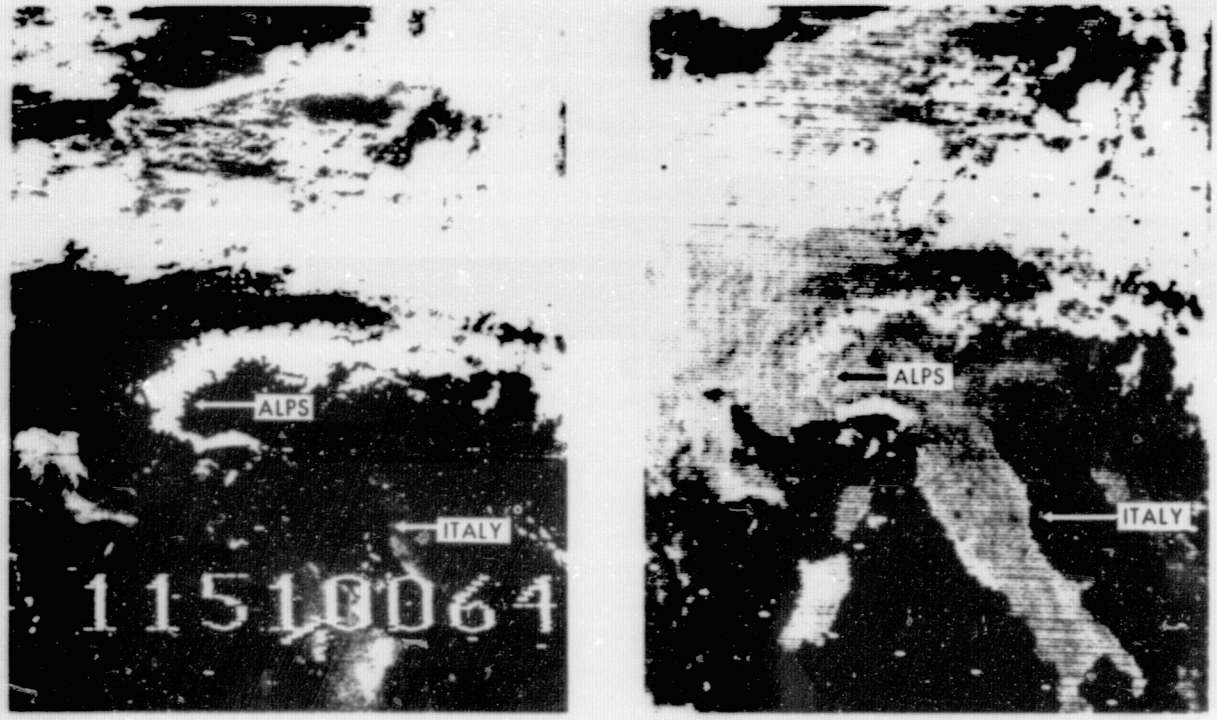


FIGURE 3. 200 GMT 27 APRIL 1969. Visible (a) and near-infrared (b) images over the Sierra Nevada, from Nimbus III.



(a) IDCS

λ = 0.5 to 0.7μm

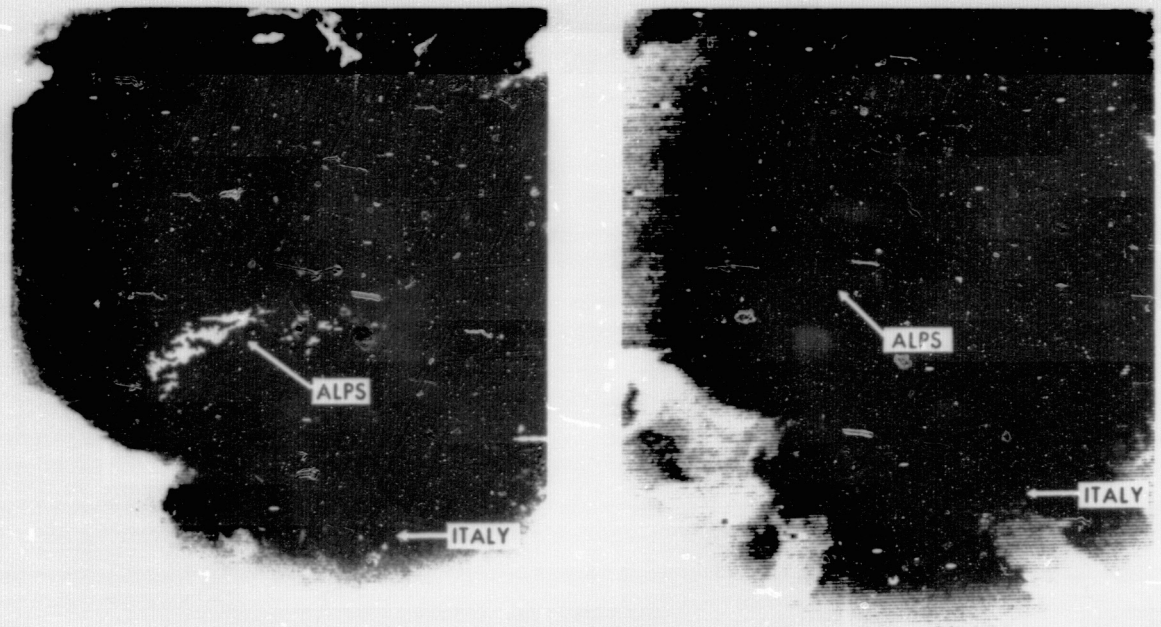
(b) HRIR

λ = 0.7 to 1.3μm

NIMBUS III ORBIT NO. 149

APRIL 25, 1969

FIGURE 4. 1100 GMT 25 APRIL 1969. Visible (a) and near-infrared (b) images over the Alps, from Nimbus III.



(a) IDCS

λ = 0.5 to 0.7μm

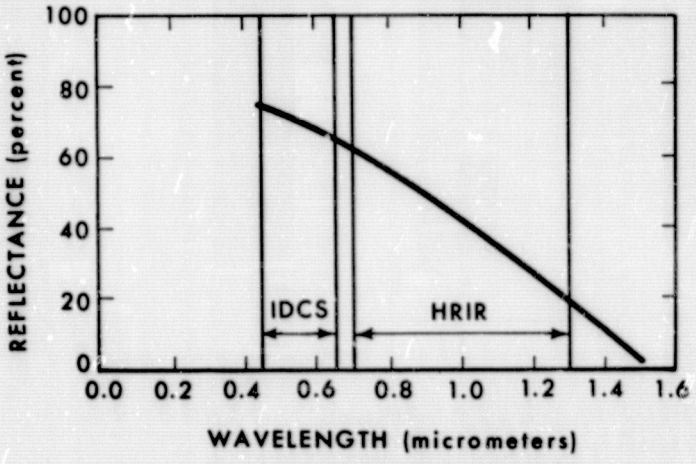
(b) HRIR

λ = 0.7 to 1.3μm

NIMBUS III ORBIT NO. 377

MAY 12, 1969

FIGURE 5. 1100 GMT 12 MAY 1969. Visible (a) and near-infrared (b) images over the Alps, from Nimbus III.



GURE 6. Spectral reflectance of melting snow (10).

LOCATING LARGE MASSES OF GROUND ICE WITH AN IMPULSE RADAR SYSTEM*

C. L. Bertram, K. J. Campbell, and
S. S. Sandler

Geophysical Survey Systems, Inc.
16 Republic Road
No. Billerica, Massachusetts 01862

ABSTRACT

An impulse radar system has been developed to perform shallow subsurface investigations. The technique is known as Electromagnetic Subsurface Profiling (ESP) and is the electrical analog of the seismic sub-bottom profiling method used in marine geology. The system operates by detecting the interface between two materials having different electrical properties. Large masses of artificially-emplaced and of naturally-occurring ground ice have been located with the system. Theoretical considerations indicate that the system also should be able to determine the approximate volume of interstitial ice in frozen soils. Additional research is necessary to define limitations of this geophysical tool when used to investigate the various types of permafrost.

1. INTRODUCTION

An impulse radar system has been developed to perform shallow subsurface investigations. The system detects and graphically displays subsurface interfaces to depths of as much as 100 feet. The technique is known as Electromagnetic Subsurface Profiling (ESP) and is the electrical analog of the seismic sub-bottom profiling method used in marine geology. Subsurface profile data is collected by slowly traversing the area of interest with the system. A small truck or boat is normally used as a survey vehicle and houses the electronic gear (Figure 1). A sled-mounted antenna is towed behind the vehicle (Figure 2). The antenna can also be handpulled over an area as much as 200 feet from the vehicle or towed behind an all-terrain vehicle in areas where the standard vehicle is unsuitable. The data is stored on magnetic tape and may be printed out graphically in the field for immediate interpretation or sent back to the laboratory for computer processing and data enhancement when necessary. The printout displays a close approximation to the interfaces seen in the vertical wall of a trench dug below the corresponding traverse line.

The system operates by detecting the differences in the electrical properties of materials. Broad-band, time-limited pulses of electromagnetic energy are continuously radiated into the earth from the antenna moving along the surface. Each pulse is partially reflected back to the antenna from the first electrical interface. The remainder of the pulse travels downward to the next interface where the process is repeated. The reflected pulses are separated on a time basis and are printed out graphically as a continuous profile. Each electrical interface generally corresponds with a physical interface such as the contact between materials of different grain size or to the soil/bedrock contact.

*This project was sponsored by the Office of Naval Research (Contract No. 00014-71-C-0392). Logistic support for the experimental work performed in the Barrow, Alaska area was provided by the Naval Arctic Research Laboratory.

Interfaces between discrete objects such as boulders or metal pipes and the surrounding soil are also displayed. A block diagram is shown in Figure 3.

The shape of each reflected pulse depends only on the transfer function of the material from which it is reflected. This transfer function in turn is dependent on the dielectric constant and conductivity of the material. If these parameters are known, and an incident pulse with a Gaussian distribution in time and space is assumed, the reflected pulse shape can be calculated. This implies that materials can be identified within broad limits based on the shape of the reflected pulse.

The impulse radar system had been used successfully to measure fresh-water and sea-ice thickness, map bottom topography through ice on fresh-water lakes, locate buried objects such as pipes, tunnels, barrels, and synthetic foam, profile the bedrock surface buried beneath unconsolidated materials, and display the geologic structure of several deposits of unconsolidated materials. For example, the typical structure of a glacial delta is displayed in the electromagnetic subsurface profile shown in Figure 4. Theoretical work suggested that the impulse radar system should also be capable of detecting large masses of ground ice. Subsequent experimental work showed that large ice wedges in the Barrow, Alaska area as well as artificially-emplaced block ice could be detected and located accurately with the impulse radar system.

2. THEORY

The impulse radar system utilizes a time-domain method for finding the dielectric constant and conductivity of a medium probed by the system. These parameters, which are affected by the physical and chemical properties of the medium, give rise to a reflected pulse unique to the medium by influencing pulse shape and propagation. The dielectric constant determines the velocity at which the pulse travels through the medium. If the velocity and time of travel are known, the distance, or thickness of the medium, can be determined. The conductivity of a medium causes loss of energy in the form of heat in the impulse and must also be considered. The theory can be used to calculate the shape of a reflected pulse from different media, assuming that a Gaussian pulse is transmitted (Figure 5).

It is possible to express this time-domain impulse through its Fourier transform as a frequency spectrum of components (Sokolnikoff and Redheffer, 1958; Adler, Chu, and Fano, 1960). The reflection of each of the spectral components and hence the reflected pulse is determined by the dielectric constant and conductivity of the medium from which it is reflected. This is because the reflected pulse must satisfy the boundary conditions at each interface. These boundary conditions are derived from Maxwell's Equations (Adler, Chu, and Fano, 1960). When the impulse travels through multiple media it is partially reflected and partially transmitted at each interface (Figure 6). It is the reflected pulse that the radar system detects, analyzes and records.

The mathematical derivations of the transmitted and reflected pulses for a single-layer medium, assuming that the impulse radar system transmits a Gaussian pulse, follows:

The incident pulse transmitted by the impulse radar system is

$$e_x^i(z,t) = e_x^i(o,o) \exp\left[-(t-z/c)^2/2t_1^2\right] \qquad (1)$$

where

t_1 = a constant parameter that is a measure of the pulse width in time

z = ct_1 is the corresponding pulse width in space

c = velocity of light in space

t = time

z = direction in which the pulse is travelling

$e_z^i(o,o)$ = the amplitude of the Gaussian pulse at t = o and z = o

The spectrum contained in the impulse is given by its Fourier transform:

$$E_x^i(z,\omega) = \int_{-\infty}^{\infty} e_x^i(z,t)\ \exp\ [-j\omega t]\ dt$$
$$= e_x^i(o,o)\int_{-\infty}^{\infty} \exp\ \left[-(t-z/c)^2/2t_1\right]\ e^{-j\omega t}dt \qquad (2)$$

where

ω = the angular radian frequency.

This is readily integrated to give

$$E_x^i(z,\omega) = e_x^i(o,o)\ \exp(-j\omega z/c)t_1(2\pi)^{\frac{1}{2}}\exp(-\omega^2 t_1^2/2) \qquad (3)$$

At z = o, i.e., the boundary between air and the dissipative medium (earth),

$$E_x^i(o,\omega) = e_x^i(o,o)t_1(2\pi)^{\frac{1}{2}}\exp(-\omega^2 t_1^2/2) \qquad (4)$$

The field transmitted into the dissipative medium to a distance z = d at the particular frequency ω is

$$E_x^t(d,\omega) = E_x^i(o,\omega)G(d,\omega) \qquad (5)$$

where $G(d,\omega)$ = the steady-state transfer function of the medium. The instantaneous field at the depth d due to all the spectral components of the Gaussian pulse is obtained by using an inverse Fourier Transform:

$$e_x^t(d,t) = (2\pi)^{-1}\int_{-\infty}^{\infty} E_x^t(d,\omega)e^{j\omega t}d\omega$$
$$= (2\pi)^{-1}\int_{-\infty}^{\infty} E_x^i(o,\omega)G(d,\omega)e^{j\omega t}d\omega \qquad (6)$$

The expression cannot be evaluated numerically with the infinite upper limit. However, it has been shown (King, 1968) that for the Gaussian impulse a negligible error is made if the upper frequency limit is taken at $2.6/t_1$ instead of infinity. The integral to be evaluated numerically, is therefore,

$$e_x^t(d,t) = \frac{2t_1}{(2\pi)^{\frac{1}{2}}}\ e_x^i(o,o)\int_o^{2.6/t_1} \left[G_R(d,\omega)\cos\omega t -\right.$$
$$\left. G_I(d,\omega)\sin\omega t\right]\ \exp\ \left[-\omega^2 t_1^2/2\right]\ d\omega \qquad (7)$$

Using equations (1) and (7), the reflected pulse can be calculated from the boundary conditions:

$$e_x^r(z,t) = e_x^t(z,t) - e_x^i(z,t)\ \Big|_{z=o} \qquad (8)$$

where

$e_x^r(z,t)$ = the reflected pulse.

To summarize the results so far we have:

The incident pulse:

$$e_x^i(z,t) = e_x^i(o,o) \exp\left[-(t-z/c)^2/2t_1^2\right] \tag{9}$$

The pulse transmitted through the medium:

$$e_x^t(z,t) = \frac{2e_x^i(o,o)t_1}{(2\pi)^{\frac{1}{2}}} \int_o^{2.6/t_1} \left[G_R(z,\omega)\cos\omega t - G_I(z,\omega)\sin\omega t\right] \exp(-\omega^2 t_1^2/2)\,d\omega \tag{10}$$

and the reflected pulse

$$e_x^r(z,t) = \frac{2e_x^i(o,o)t_1}{(2\pi)^{\frac{1}{2}}} \int_o^{2.6/t_1} \left[G_R(z,\omega)\cos\omega t - G_I(z,\omega)\sin\omega t\right] \exp(-\omega^2 t_1^2/2)\,d\omega - e_x^i(o,o) \exp\left[-(t-z/c)^2/2t_1^2\right] \tag{11}$$

It can be seen that the reflected pulse depends on G_R and G_I, the transfer function of the medium. King (1968) has shown that the transfer function depends only on dielectric constant and conductivity.

The multilayer theory is obtained from the single-layer theory when it is understood that the impulse transmitted in the first layer becomes the incident pulse for the second layer. By solving the boundary conditions at the second interface (see equation 8), the reflected pulse from the second interface is obtained. This process is continued for the next layer and so on.

The starting point for the solution to the single-layer theory is an expression for the difference between the theoretical and the measured reflected pulses at two different times: ta and tb (Figure 7).

At time t = ta and distance z = o,

$$f(\sigma,\varepsilon) = e^r_{theo}(o,t_a) - e^r_{meas}(o,t_a) \tag{12}$$

and at time t = tb and distance z = o,

$$g(\sigma,\varepsilon) = e^r_{theo}(o,t_b) - e^r_{meas}(o,t_b) \tag{13}$$

where

$e^r_{theo}(o,t_a)$ = the value of the calculated reflected impulse at $t = t_a$ and $z = o$.

$e^r_{meas}(o,t_a)$ = the value of the reflected pulse as measured using the long-wire experiment at $t = t_a$ and $z = o$.

$e^r_{theo}(o,t_b)$ = the value of the calculated reflected impulse at $t = t_b$ and $z = o$.

$e^r_{meas}(o,t_b)$ = the value of the reflected pulse as measured by the long-wire antenna.

The theoretical pulse is calculated using values of dielectric constant and conductivity found in the literature. The idea is to adjust the values of dielectric constant and conductivity until the theoretical impulse is identical with the measured impulse at times $t = t_a$ and $t = t_b$. Since the pulses are assumed approximately Gaussian in shape, only two points are needed to construct them. When the theoretical pulse is equal to the measured pulse, equations (12) and (13) are zero. They can, therefore, be expressed by a Taylor expansion about zero. The first terms of the expansion for (12) and (13) are

$$f(\sigma,\varepsilon) = f(\sigma_k,\varepsilon_k) + \Delta\sigma\, f\sigma\Big|_{\sigma_k,\varepsilon_k} + \Delta\varepsilon\, f\varepsilon\Big|_{\sigma_k,\varepsilon_k} \tag{14}$$

and

$$g(\sigma,\varepsilon) = g(\sigma_k,\varepsilon_k) + \Delta\sigma\, g\sigma\Big|_{\sigma_k,\varepsilon_k} + \Delta\varepsilon\, g\varepsilon\Big|_{\sigma_k,\varepsilon_k} \tag{15}$$

where

σ_k = the initial guess for conductivity

ε_k = the initial guess for dielectric constant

$\Delta\sigma$ = the difference between the theoretical value and initial guess for the conductivity

$\Delta\varepsilon$ = the difference between the theoretical value and the initial guess for dielectric constant

$f\sigma\Big|_{\sigma_k,\varepsilon_k}$ = the partial derivative of $f(\sigma,\varepsilon)$ with respect to conductivity evaluated at σ_k and ε_k

$f\varepsilon\Big|_{\sigma_k,\varepsilon_k}$ = the partial derivative of $f(\sigma,\varepsilon)$ with respect to dielectric constant, ε, evaluated at σ_k and ε_k

$g\sigma\Big|_{\sigma_k,\varepsilon_k}$ = the partial derivative of $g(\sigma,\varepsilon)$ with respect to conductivity σ, evaluated at σ_k and ε_k

$g\varepsilon\Big|_{\sigma_k,\varepsilon_k}$ = the partial derivative of $g(\sigma,\varepsilon)$ with respect to dielectric constant ε, evaluated at σ_k amd ε_k

Equations (14) and (15) are solved simultaneously for new values of σ and ε. These values are now called σ_{k+1} and ε_{k+1} where

$$\begin{bmatrix}\sigma_{k+1}\\ \varepsilon_{k+1}\end{bmatrix} = \begin{bmatrix}\sigma_k\\ \varepsilon_k\end{bmatrix} - \begin{bmatrix}f_\sigma f_\varepsilon\\ g_\sigma g_\varepsilon\end{bmatrix}^{-1} \begin{bmatrix}f(\sigma_k,\varepsilon_k)\\ g(\sigma_k,\varepsilon_k)\end{bmatrix} \tag{16}$$

The multilayer problem is solved by considering the layers individually using the single-layer theory.

The theory predicts that the electrical parameters of a medium can be determined if the incident and reflected pulses are known. Conversely, if the incident pulse and electrical parameters are known, it is possible to calculate the reflected pulse shape. By using a Gaussian impulse in the time domain as the incident pulse, and by taking values of dielectric constant and conductivity from the literature, it was possible to calculate the reflected pulses for various media (Figure 8). It can also be shown that the reflected pulse varies for varying moisture conditions occurring in the same medium. This implies that from the shape of the reflected pulse it is possible to determine the type of medium and its moisture (or ice) content.

3. EXPERIMENTAL WORK

Experiments were performed with both artificially-emplaced and naturally-occurring ground ice to determine if ground ice could be detected and located accurately using the impulse radar system.

3.1. Artificially-Emplaced Ground Ice

An ice "wedge" and an ice "lens" were constructed by burying six tons of block ice in two holes excavated in interbedded sand and silt. The "wedge" was twelve feet long, five feet thick and, four feet wide. The "lens" was ten feet long, eight feet wide, and one foot thick. Both masses of ice were detected by the impulse radar system. The electromagnetic subsurface profile of the traverse made directly over and parallel to the long axis of the "wedge" is shown in Figure 9.

3.2. Naturally-Occurring Ground Ice

Traverses were made over naturally-occurring ground ice near Barrow, Alaska during March 1972. Ice wedges were detected with the system and their presence was confirmed by inspecting large holes augered in the permafrost. Several subsurface features which may have been ice lenses were also detected by the system. No augering was done to determine the true nature of these features.

A detailed study was made in an area of high-center, ice-wedge polygons between Middle Salt Lagoon and South Salt Lagoon. This area was chosen because of its accessibility and because relatively large ice wedges are associated with the polygons in this area. The troughs and the center of a polygon were staked out by visual inspection of the area and by probing with a crowbar where snow masked the microrelief. An electromagnetic subsurface profile was then taken parallel to the line of stakes. A map of the area showing the polygon and the position and direction of the traverse is given in Figure 10. As anticipated, strong signals were received when the antenna passed over a trough. These signals were presumably from an ice/soil interface associated with an underlying ice wedge. The subsurface profile for this traverse is shown in Figure 11. After the traverse was made, the stakes over the troughs were moved two to five feet to positions directly over the ice wedges as indicated by the subsurface profile. Three large holes, about twelve feet deep and two feet in diameter, were then augered in the permafrost to determine the presence or absence of an ice wedge beneath each stake. Each hole was inspected by a geologist who used a rope ladder to gain access. A geologic cross section of the polygon was constructed from the data obtained (Figure 12). A limited number of samples was taken for salinity and moisture content determinations.

A comparison of the electromagnetic subsurface profile (Figure 11) with the cross section (Figure 12) shows the close correlation between the signals on the profile and the positions of the ice wedges determined from the augered holes. The abrupt change in media caused the signal recorded on the profile. The depth scale shown on the profile was then determined by assuming that the signature on the profile associated with each ice wedge represented the interface between the base of the ice wedge and the underlying frozen soil. This depth scale approximates a theoretical depth scale calculated from dielectric constants of ice and frozen soil.

The peculiar geometry of the signature of the signal returned from the base of the ice wedge is a function of the beam width of the antenna pattern. The beam width of the antenna pattern is relatively broad, which permits energy to preceed and trail the antenna. The apparent depth to the base of an ice wedge continuously changes as the antenna, moving along the ground surface, approaches, passes over, and moves away from a wedge. For example, when the antenna is approaching or moving away from a wedge (Positions 1 and 3, Figure 13) some of the transmitted pulses intersect and are reflected from the interface at the base of the wedge. These reflected pulses require more time to reach the antenna than the reflected pulses that will be received when the antenna is directly above the base of the wedge (Position 2). Since time is translated directly into depth on an electromagnetic subsurface profile, the base of the wedge appears to be at a greater depth when the antenna is in Positions 1 and 3 than in Position 2. The result is the typical convex-upward signature. In terms of shape and width, it is not a true representation of the interface between the base of the ice wedge and the frozen soil.

Near-surface details can not be seen in the subsurface profile of the traverse made over the polygon. In an attempt to obtain near-surface details of other polygons, another traverse was made on a nearby gravel-fill road. The road was apparently constructed by dumping several feet of gravel directly on polygons. The original ground surface as well as "near-surface" details associated with the buried polygons are shown in the subsurface profile (Figure 14). Preliminary interpretation indicates that both tops and bottoms of several ice wedges are also shown on the profile. Because of the location of this traverse, it was not possible to auger holes for confirmation.

4. CONCLUSIONS

The impulse radar system is capable of accurately locating large masses of artificially-emplaced or naturally-occurring ground ice. Theoretical considerations indicate that the system can identify within broad limits the materials from which pulses are reflected by analyzing the frequency content of these pulses. This implies that the approximate volume of interstitial ice in frozen soil can be determined by the system since the reflection characteristics vary with ice content. Additional research is necessary to define limitations of this geophysical tool when used to investigate the various types of permafrost.

5. REFERENCES

Adler, R.B., Chu, L.J., and Fano, R.M., 1960, Electromagnetic Energy Transmission and Radiation: New York, John Wiley, p. 6-24 and 189-194.

Sokolnikoff, I.S., and Redheffer, R.M., 1958, Mathematics of Physics and Modern Engineering: New York, McGraw-Hill, p. 175-195 and 482-488.

King, R.W.P., 1968, The Transmission of Electromagnetic Waves and Pulses into the Earth: Jour. of Applied Physics, v. 39, No. 9, p. 4444-4452.

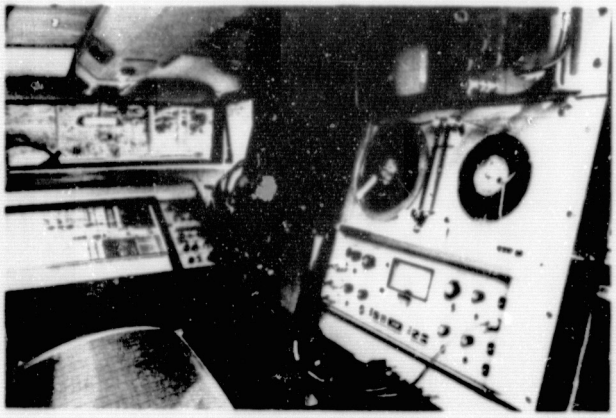


FIGURE 1. IMPULSE RADAR SYSTEM. Electronic Gear mounted in survey truck.

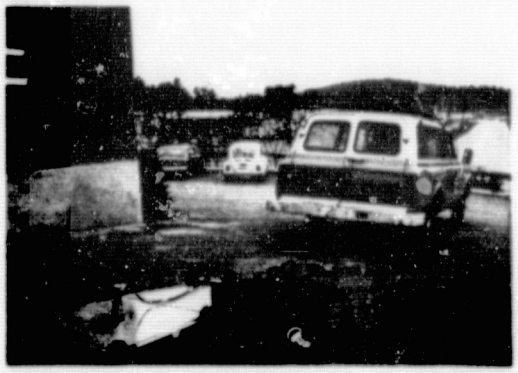


FIGURE 2. SURVEY TRUCK AND SLED-MOUNTED ANTENNA.

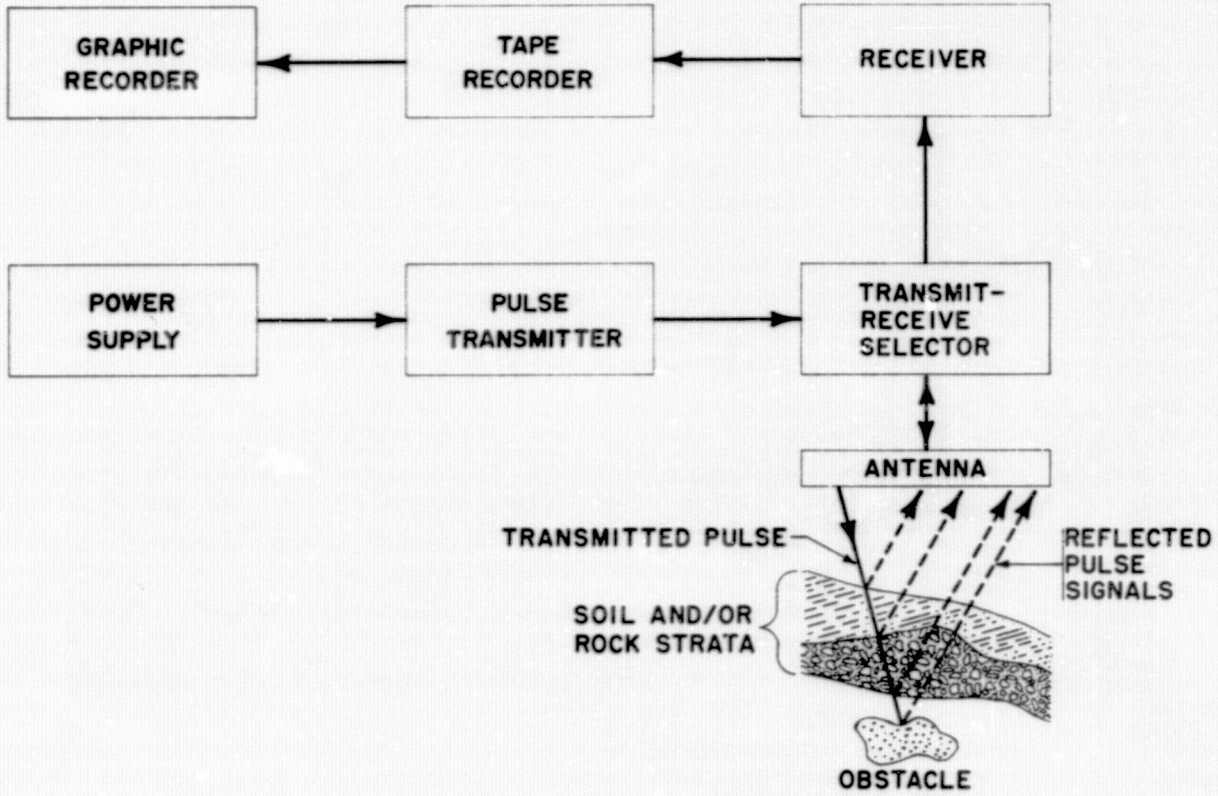


FIGURE 3. BLOCK DIAGRAM OF IMPULSE RADAR SYSTEM.

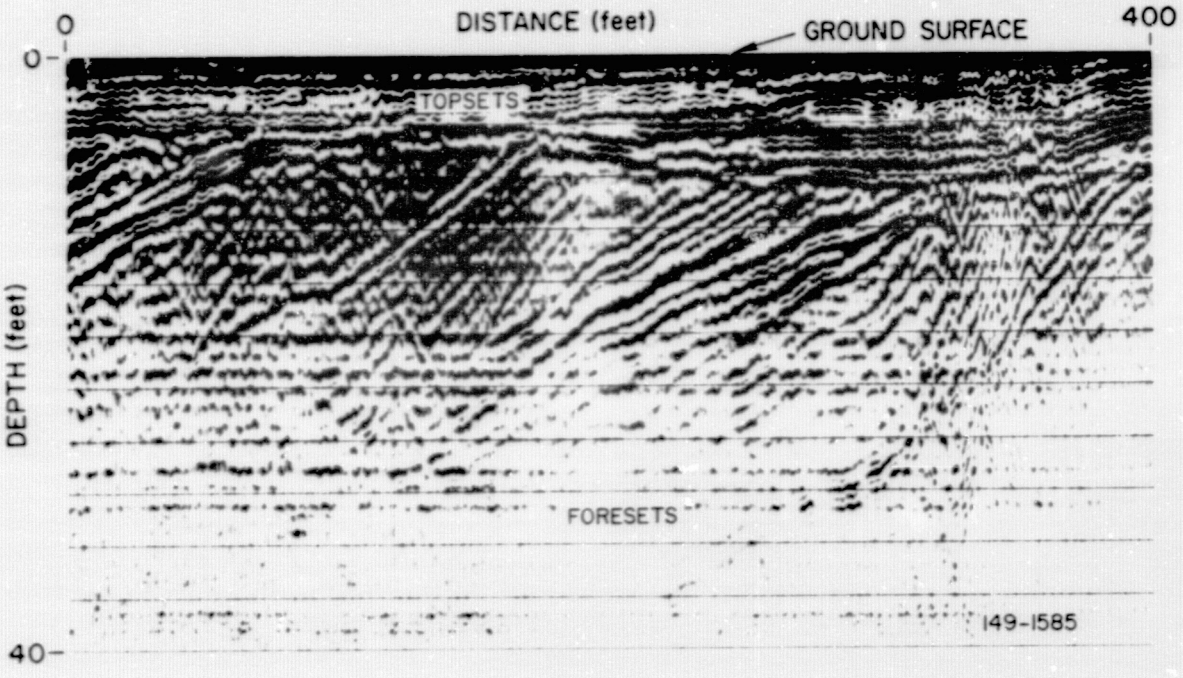


FIGURE 4. ELECTROMAGNETIC SUBSURFACE PROFILE. The typical structure of a glacial delta is clearly shown.

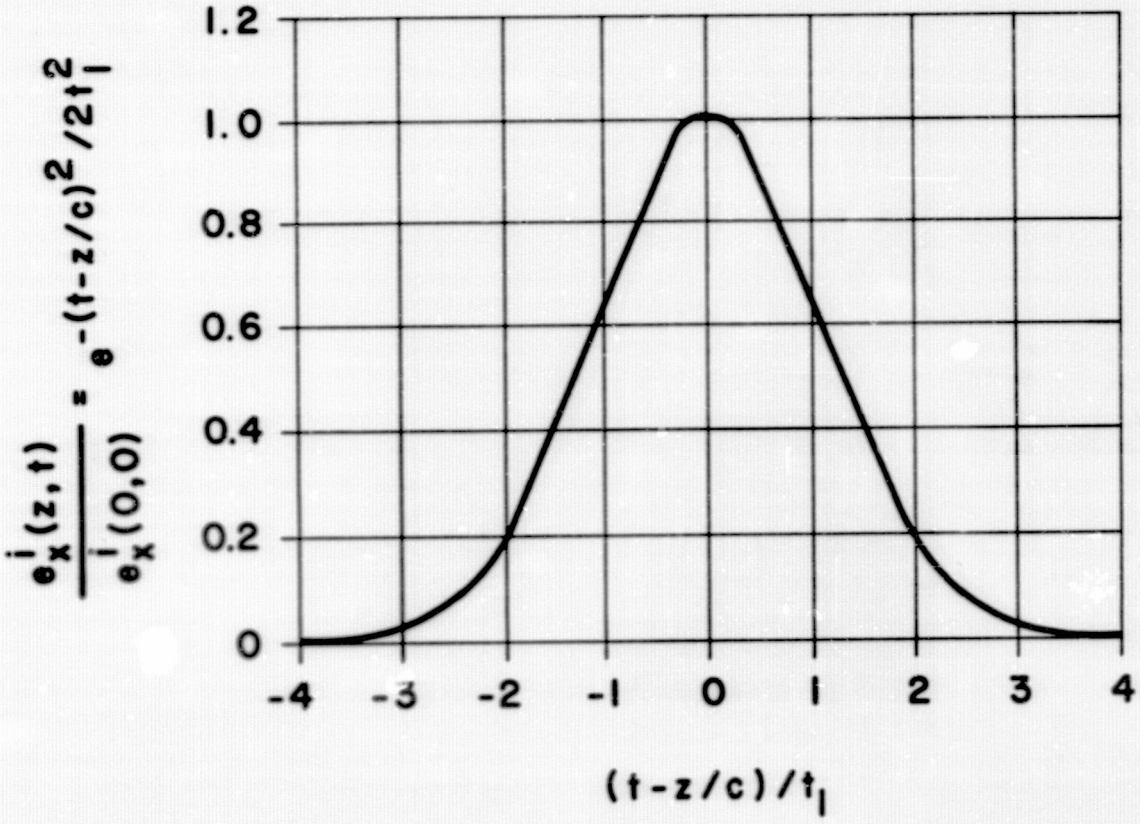
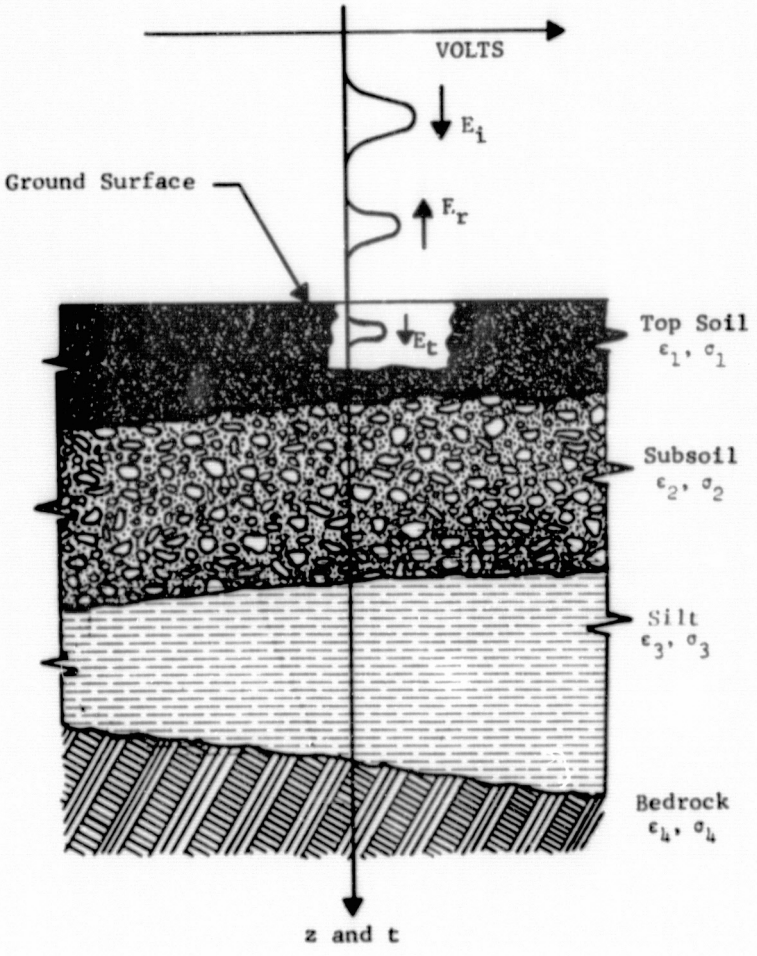


FIGURE 5. A GAUSSIAN PULSE.



LEGEND

E_i = Incident Pulse (Pulse Transmitted by Radar)
E_r = Reflected Pulse From Interface (Ground Surface)
E_t = Transmitted Pulse Into Ground
z = Distance
t = Time
ϵ = Dielectric Constant
σ = Conductivity

FIGURE 6. MULTIPLE MEDIA

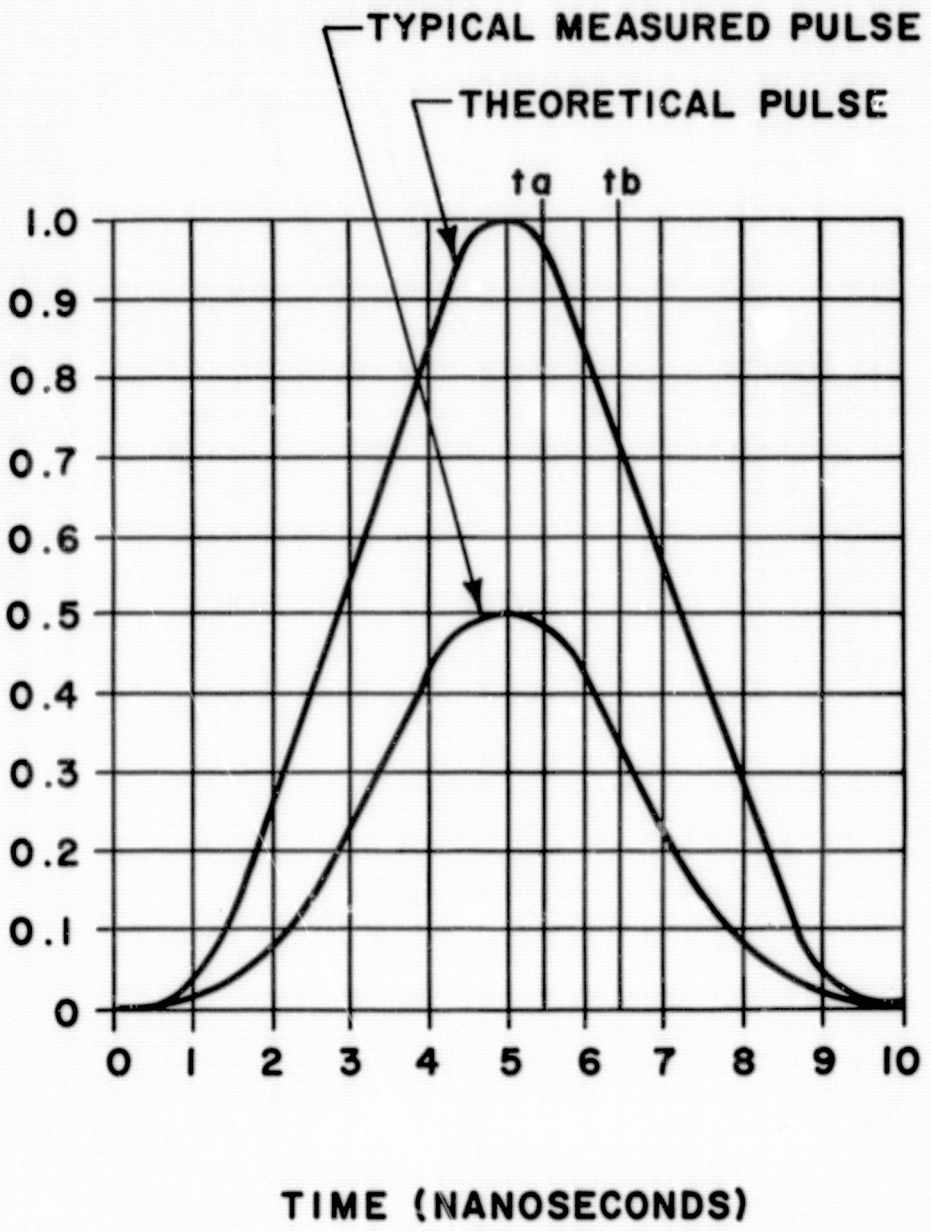


FIGURE 7. THEORETICAL AND MEASURED REFLECTED PULSES.

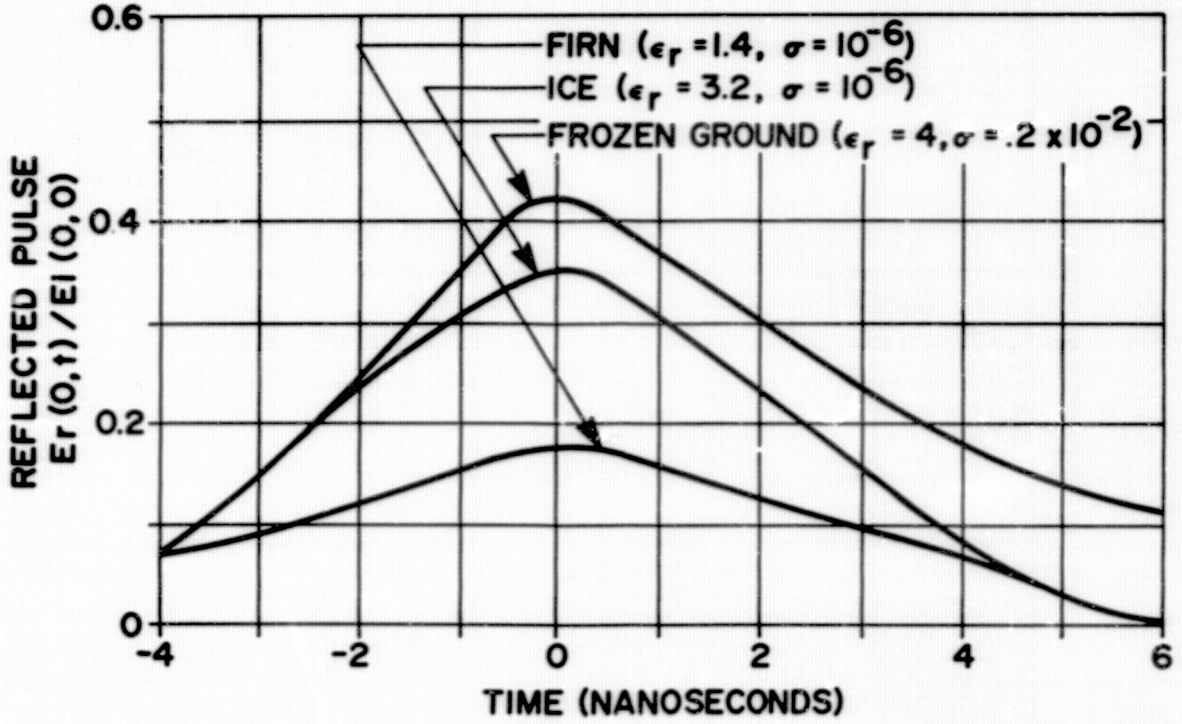


FIGURE 8. THEORETICAL REFLECTED PULSES. Firn, Ice and frozen ground.

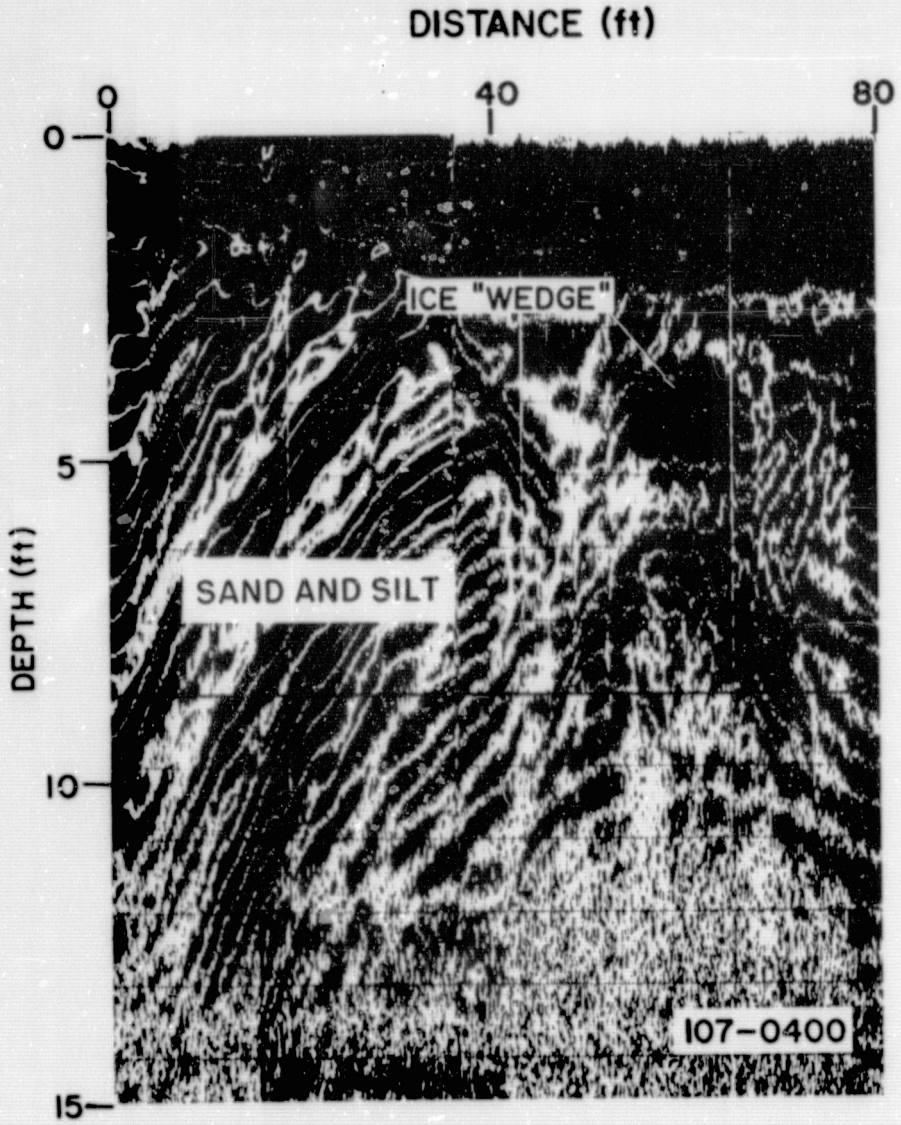


FIGURE 9. ELECTROMAGNETIC SUBSURFACE PROFILE. Artificially-emplaced ice "wedge". Note the truncated bedding caused by excavation.

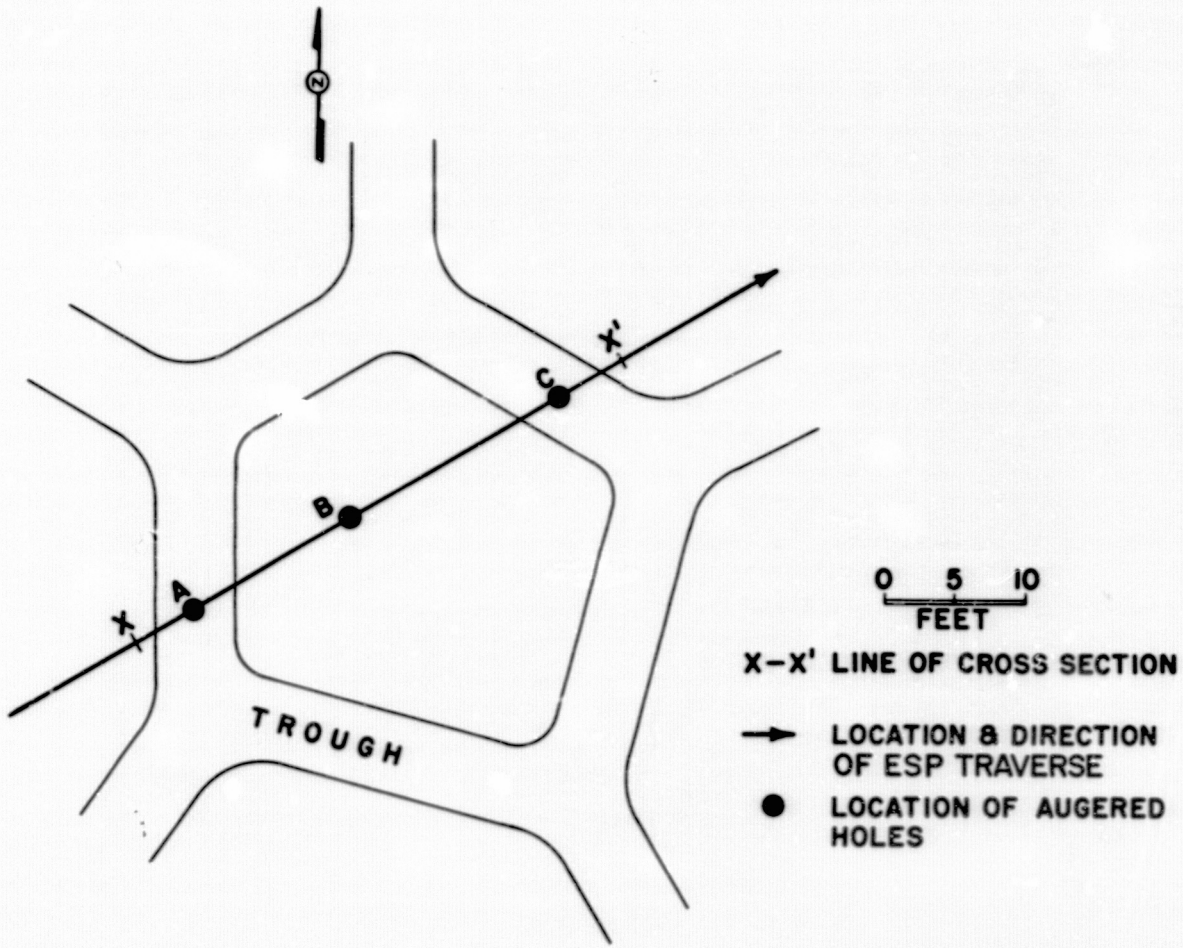


FIGURE 10. MAP OF ICE-WEDGE POLYGON.

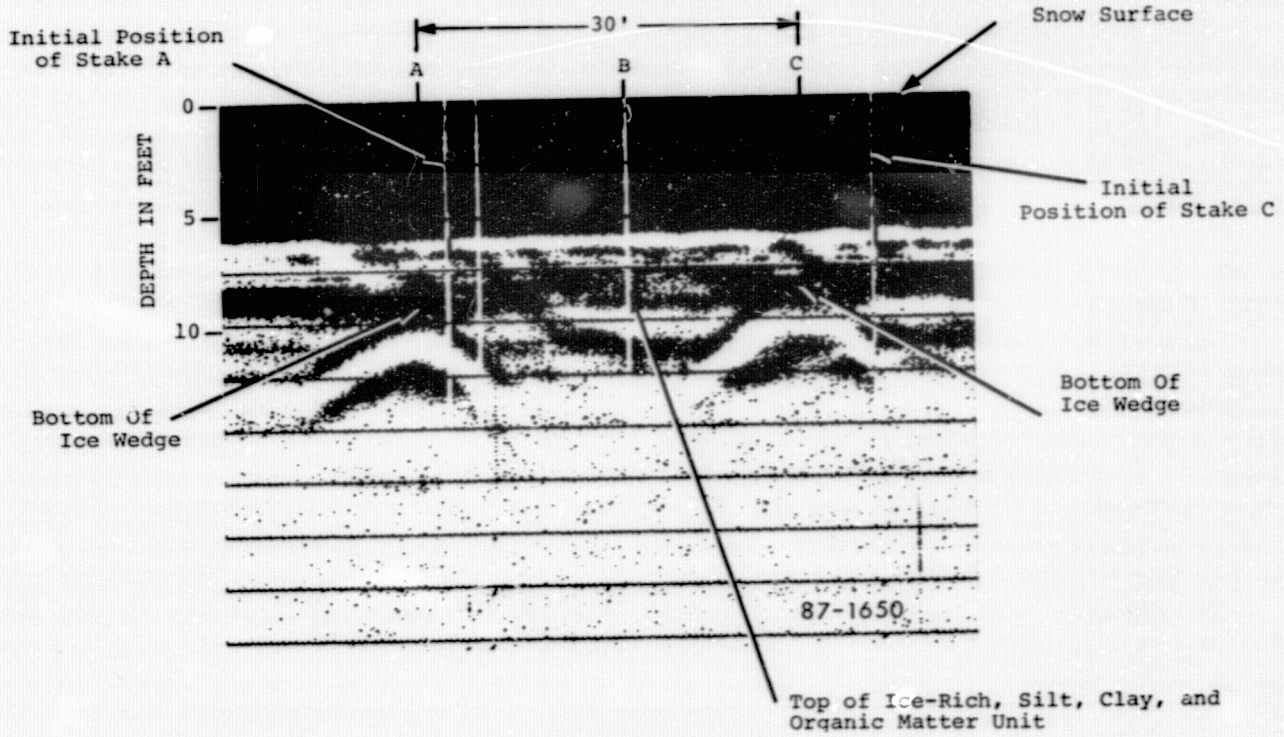


FIGURE 11. ELECTROMAGNETIC SUBSURFACE PROFILE. Ice-Wedge Polygon.

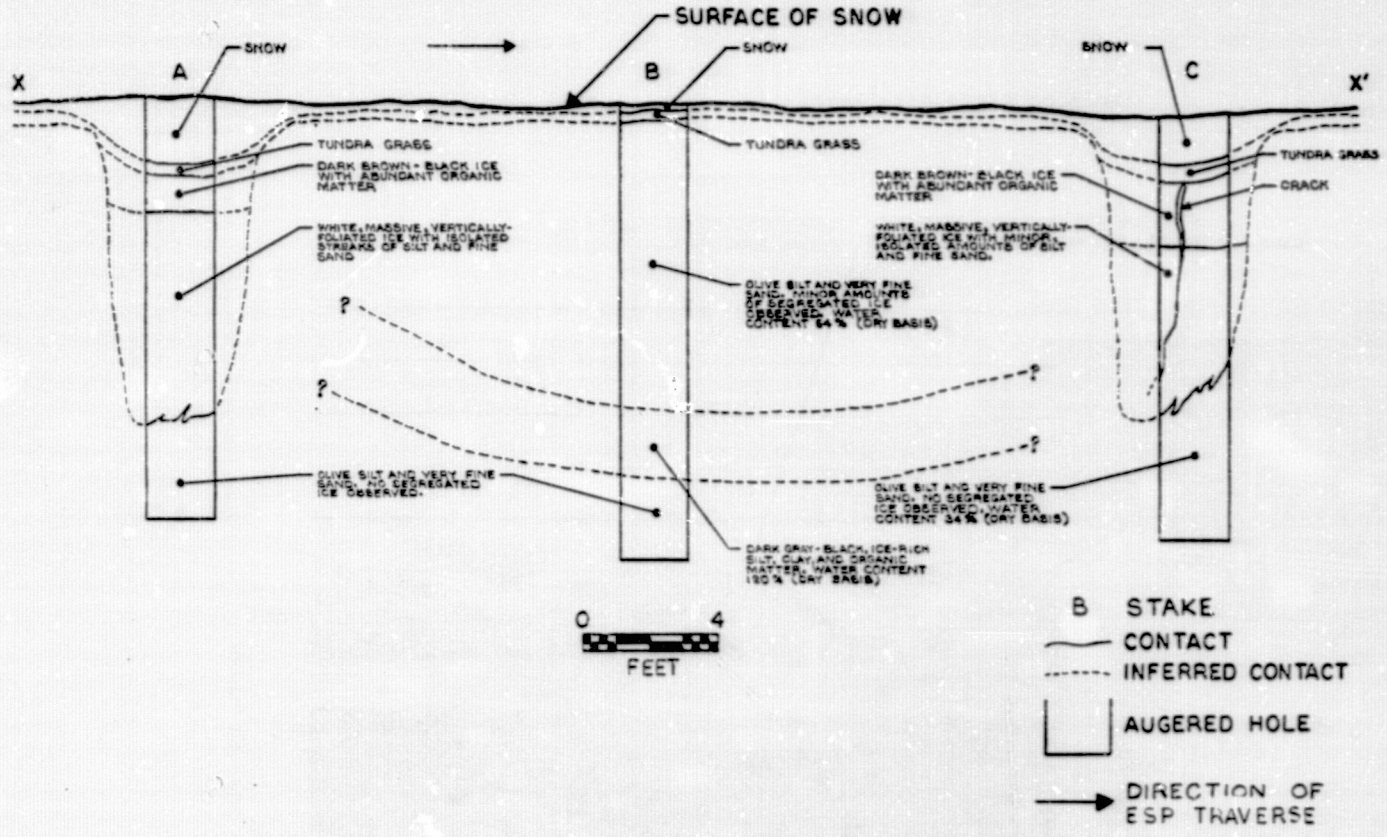


FIGURE 12. CROSS SECTION OF ICE-WEDGE POLYGON.

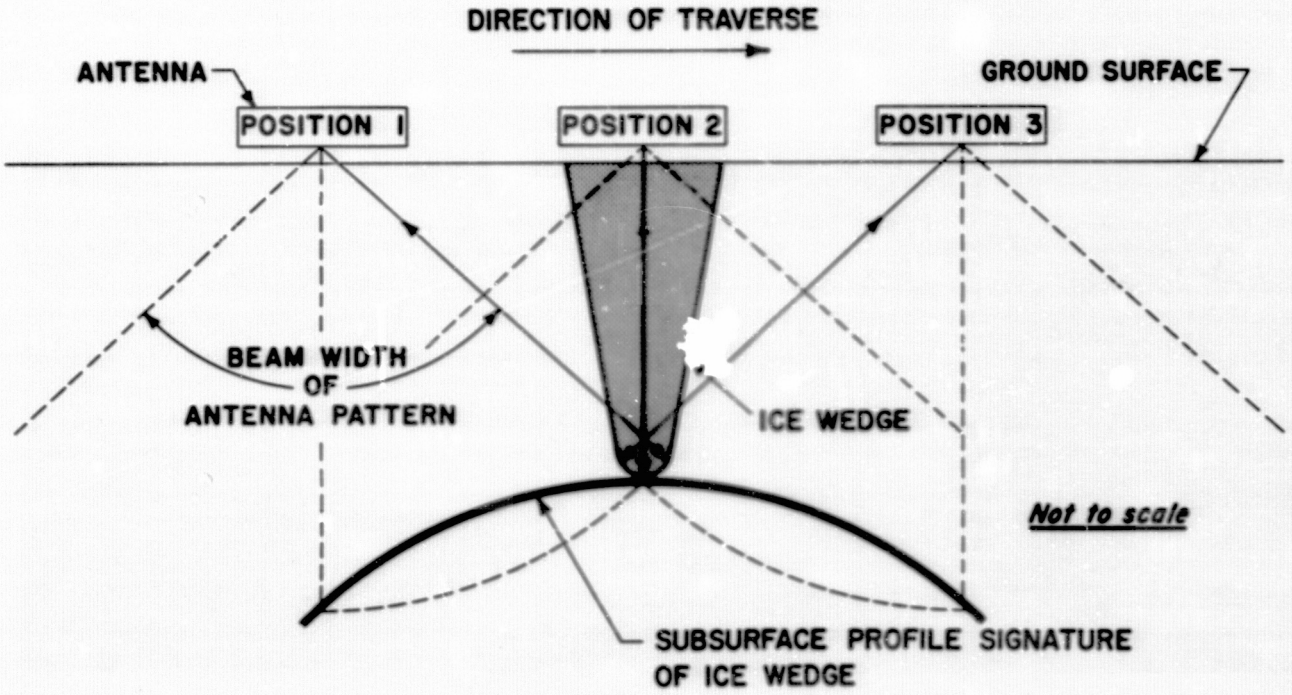


FIGURE 13. SIGNATURE OF AN ICE WEDGE.

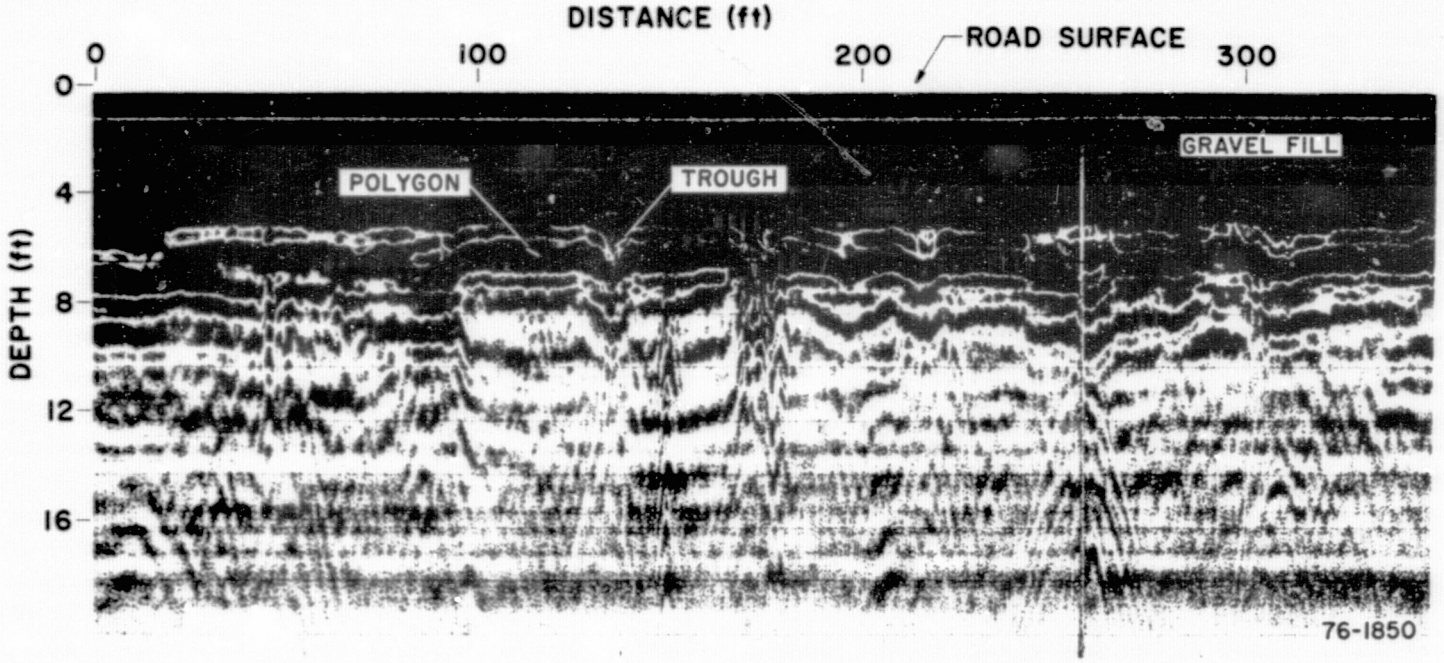


FIGURE 14. ELECTROMAGNETIC SUBSURFACE PROFILE. Ice-Wedge polygons.

HIGH RESOLUTION MEASUREMENTS OF SNOWPACK STRATIGRAPHY USING A SHORT PULSE RADAR

R. S. Vickers and G. C. Rose

Colorado State University
Department of Electrical Engineering
Fort Collins, Colorado

SUMMARY

The measurement of snowpack thickness, density and stratigraphy has been the subject of many remote sensing papers in recent symposia. In this paper, as system is described which can be used to derive either the snow thickness, or the average snow density by measurement of the transit time of one nanosecond radar pulse. Data is given which shows that the radar system is capable of providing an accuracy of better than 10% when used to measure the density of the snowpack. Operations in the Rocky Mountain Watershed are reported in which the system was used in both static and mobile configurations to measure snow depth.

The use of the radar system to detect horizontal layering within the snowpack is also reported and the radar data for this application is compared with that from simultaneous measurements with gamma ray density profiling equipment. The limitations of the method are presented.

1. INTRODUCTION AND BACKGROUND

Techniques for the remote measurement of snow and ice thickness have been studied for a number of years. They range from infrared and microwave multichannel radiometers (1,2) and gamma ray absorption spectrometers (3) to a wide variety of active radar techniques (4,5,6). All the methods except those involving radar signals rely on the natural absorption and emission from the ice or snow subsurface, and are hence subject to natural variables such as snow temperature, surface roughness and ground temperatures. Radar techniques, while not totally independent of these parameters, provide the most direct approach to the measurement of layer thickness in ice and snow, and in some circumstances can also provide data on the water equivalent of the snow, as will be shown later.

In this paper, the development of a high resolution system for the remote measurement of layer thickness is described. The system has been designed for eventual incorporation into a light aircraft, although the study reported here only includes measurements taken a few feet off the ground. The system presently has a vertical resolution of less than 3" in free space.

The work described in this paper was supported by the USBR Contract No. 14-06-D-7159.

2. MICROWAVE PROPERTIES OF SNOW AND ICE

The attenuation of a microwave signal propagating through frozen water in its various forms is well reported in the literature (7,8). Using the data shown in figure 1, it can be seen that there exists a range of frequencies between 1 GHz and 3 GHz for which the attenuation is less than 0.1 db/metre, and does not change drastically with frequency. Within this range, the wavelengths are sufficiently short to allow a theoretical resolution (half a wavelength) of a few centimeters. Figure 2 shows the variation in the dielectric constant of snow as a function of snow density for 3.2 cm radiation. It has been noted by Cumming (8) that the dielectric constant of snow does not vary appreciably between 0°C and -20°C, and this parameter will therefore be considered as a constant for a given frequency in this paper.

The data shown in figures 1 and 2 indicate that radiation in the 2 to 4 GHz band should be able to penetrate layers of ice and snow with acceptable losses. The penetration depth can be calculated from the dielectric approximation to the skin depth formula:

$$\text{Skin Depth} \quad \delta = \frac{2}{\sigma}\sqrt{\frac{\epsilon}{\mu}} \quad \text{meters} \qquad \text{(I)}$$

where σ = conductivity (mhos/m)

ϵ = permittivity of the medium

μ = permeability of the medium

For a loss tangent of 2×10^{-3} and f = 2 GHz; δ = 40 m.

The velocity of propagation of an E-M wave in a dielectric is given by

$$v = c \left(\frac{1}{\sqrt{\epsilon}}\right) \qquad \text{(II)}$$

and the time for a pulse to propagate through a layer 'h' meters thick is

$$t = \frac{h\sqrt{\epsilon_r}}{c} \quad \text{secs.} \qquad \text{(III)}$$

where $c = 3 \times 10^{8}$ m/sec

h = thickness in meters

ϵ_r = relative dielectric constant

Since the dielectric constant is a function of density only, for dry snow, τ can be plotted for a fixed value of h as a function of ρ (density in gms/cc). This plot is given in figure 3. Although this graph could be used in the form shown to calculate snow depth, it is more convenient to use a linear approximation to an appropriate part of the graph. Referring to the graph in figure 4, it can be seen that the average snow density fluctuated during the measurement season from 0.31 gms/cc to 0.40 gms/cc, with maxima (taken from the individual profiles) up to 0.5 gms/cc. Therefore, it is justifiable to use a linear approximation between the limits $0.25 < \rho < 0.5$ gms/cc. The approximation has the equation (found graphically)

$$\tau = [6.8 + 4.33\rho]\ h \quad \text{(nanoseconds)} \qquad \text{(IV)}$$

This expression was used in reducing the data reported in this paper.

Reflection Coefficients - Assuming that the snow is a dielectric, the reflection coefficient between two layers of permittivity ε_1 and ε_2 is given by

$$R = \frac{\sqrt{\varepsilon_2} - \sqrt{\varepsilon_1}}{\sqrt{\varepsilon_2} + \sqrt{\varepsilon_1}} \qquad \text{(V)}$$

Table I shows the range of values in ε_r which can be expected for ice and snow layers.

Consider now a layer of snow ($\varepsilon_r = 1.4$) with the lower surface in contact with the ground which is not frozen ($\varepsilon_r = 81$). The reflection coefficient from the upper surface will be 0 = .084 and from the lower surface will be approximately 0.7 (as seen by the radar antenna). Even a snow/ice interface would have an effective coefficient of 0.13, thereby indicating that the most difficult boundary to observe will not be the snow/ground interface as might first be expected, but the snow/air interface. This prediction is verified in practice. Measurements on fresh snowfall at -1°C indicated a surface reflection coefficient of 0.04 to 0.06 at the time of settling, and a lower boundary reflection of approximately 0.6. Reflections can also be expected from stratification within the snowpack (if any) due to changes in the dielectric constant.

In summary, the microwave properties of dry snow are compatible with the short pulse radar approach to snow thickness measurements. The case where the snowpack contains quantities of distributed free water is also of interest, however. Water in the liquid phase has a dielectric constant of approximately 81 at 2 GHz. The effect of this high value of ε_r would be to increase the pulse travel time dramatically and make interpretation more difficult. On the other hand, the effect offers the possibility of measuring the free water content of the pack by radar, a parameter which is difficult to measure even by direct sampling. The other property of liquid water which is less desirable is the higher conductivity resulting in reduced penetration of the snowpack.

3. SYSTEM DESIGN

A diagram of the system design appears in figure 5. The S-Band source for the research instrument is a klystron capable of being tuned over a narrow range centered at 2-7 GHz.

The CW signal from the source is modulated by a double balanced mixer to produce a pulse of approximately 1 nsec duration. The signal strength at this point is only a few milliwatts, and it is therefore passed to a Traveling Wave Tube (TWT) amplifier to produce a peak output power of 1 watt into the transmitting antenna. The return signal is again amplified and then fed to an envelope detector and displayed on a sampling oscilloscope. Experiments with this configuration indicate a usable range of 40-50 feet.

4. EXPERIMENTAL RESULTS

Static Measurements - A prototype radar system was installed at the University of Colorado's High Altitude Test Site at Red Mountain Pass, Colorado on March 3, 1972. This site is operated by the Institute of Arctic and Alpine Research under contract to the U. S. Bureau of Reclamation. The site was chosen because of its regular scheduled operation during the winter months and because of the

nature and quantity of reliable supporting data that was available at the same site. Of particular importance to this study was the presence of a Gamma Ray Density Profiler operated by the Aerojet Nuclear Corporation. This instrument provided detailed density profiles of the snowpack on a five day/week basis. the profiler was situated in an 'intensive study' area some 100 feet from the radar system.

At the time of installation there were approximately 170 cms of snow at the site. It was not possible, therefore, to prepare the site to ensure undisturbed snow, or to pick a measurement area that was flat. The choice of the site for the radar measurement was dictated somewhat by the maximum permissible length of cable to the antennas, which was about 30 feet, the main electronics being housed in a nearby heated shed at the study plot. Data was recorded on a daily basis by taking polaroid photographs of the oscilloscope trace.

An example of the raw data is given in figure 6, where the profiles from the γ ray profiler, a ram resistance gauge, and the radar system (not drawn to scale) are compared. It will be noted that the solar ice crusts shown by the increased density at A, B, and C, are well-defined in the radar signature. The disparity in relative placement of these features that can be detected by close examination of the figure is most likely due to the differences in the structure of the snowpack at the radar and γ ray sites. It is clear from figure 6 that the variations in density shown in the gamma ray profile also affect the radar return. The close visual agreement between these two data presentations may be to some extent fortuitous however, since if the radar had possessed better resolution it would have recorded two pulses for each ice crust, corresponding to a reflection from each side of the crust. If the crusts on these three days did not possess sharp boundaries, then the radar return is accurate, but it should be remembered that with the system used in these studies, the peaks in the reflected signal correspond to a high density gradient, and are not necessarily indicative of a high absolute value of density. A system that would respond to both, however, would not be hard to conceive. An alternate method of data presentation, with the radar system in a mobile configuration is shown in figure 7. Here, the high reflectivity regions appear as dark bands and zero reflectively as white. This method presents some promise for large scale surveys of snowpack where the stratification as well as the water equivalent is of interest.

Ancilliary information including air temperature, snow temperature and time since last snowfall were also recorded. Table II summarizes the quantity of data that was taken until early April when the installation was disassembled for use in mobile tests.

In some cases, where the snow density was not recorded an interpolated value from figure 4 was used to complete the radar calculation, and the result compared with the snow depth as given by a stake adjacent to the γ ray profiler.

5. ERRORS IN THE STATIC MEASUREMENTS

Taking the γ ray measurements as a standard, the errors in depth as measured by the radar system are tabulated in the righthand column of Table II. It can be seen that the majority of readings are well under the 10% error bar, and that the mean square error is 8.7% if the days on which γ ray data was not available are excluded. If the remainder of the data is included, using density value interpolated from figure 4, the error is 9.4%.

The calculated values of snow depth are plotted against the values given by the nuclear profiler in figure 8. It will be noticed that all the high error points are clustered on the high estimate side of the +10% bar, suggesting a possible common source of error. The uncorrected presence of free water for example would account for such errors.

The sources of these errors are quite numerous and can mostly be traced to the hasty installation of the system, too late in the season to be properly integrated into the experimental complex at the High Altitude Site. The major causes of error are:

1) Separation between the γ ray and radar sites causing disparities between the two depth estimates. The separation between the two instruments was over 100 feet, and discrepancies of 10 cm or so would be quite reasonable due to local geography.

2) Errors present in the γ ray calibration: These are of an unknown nature and readings from this instrument were taken as true, since no other data was available with such frequency.

3) Interpretation of the polaroid photographs undoubtedly caused some errors, especially late in the season when the radar gain was turned high to compensate for conductive losses in the snow. This source of error could be removed completely by some redesign in the radar system.

6. MEASUREMENTS FROM A MOBILE PLATFORM

On the 13th April 1972 the radar system was assembled on the back of a 'Snow Cat' (track laying snow vehicle). The antennas were mounted on a boom off to one side of the vehicle as shown in figure 9. The power supply was a 2KW gasoline generator, mounted next to the radar set.

The timing of these tests was not optimal in that being late in the season, the snow had mostly gone into an isothermal state some days before, and was hence liable to contain free water. The particular snow course selected had a surface temperature of -2.5° C., and at 20 cms. depth the temperature was -0.5° C. Two cameras were used to record the data, the second being a polaroid back-up system should the main 35mm framing camera fail. Weather conditions during the tests were adverse, with moderate winds, cold temperatures, and snowfall making camera operation difficult. Three traverses were made, with data being photographed approximately every 5 ft. on the first traverse and every 10 ft. on the second and third.

The most dramatic phenomenon noticed during the first run was the sensitivity of the system to the relative antenna/snow surface orientation. As the snow surface (or subsurface layer) became normal to the antenna beam, the signal strength would increase by as much as 10 db over the non-specular case. This phenomenon could have been avoided by using a different antenna design, but the problem although anticipated, could not be fully appreciated until tests such as these were conducted. Raw data from one of these tests is shown in figure 10, where the returns from a number of points approximately 15 ft. apart are shown. The first reflection (on the left hand side of each photograph) is from the snow/air boundary, and the bottom of the snowpack appears in approximately the middle of the photographs. Much structure within the pack is visible on these returns, and by spacing the measurements closer together, a map of the interior of the snowpack could have been constructed.

Several points are worth noting from this data. Firstly, the small reflection coefficient of fresh snow (falling during these tests) can be seen as a small precursor return just prior to the main pulse (e.g. C6, C7, D1 in figure 10). In some cases this return is not resolvable from the first large pulse, and merely makes the pulse assymmetrical (e.g., C5, C8 in figure 10). The path taken by the Snow Cat encompassed areas with tree shading, and large surface slope angles, thus accounting for the wide variability in the response to the new snow

surface. In all calculations, the pulse travel time was measured from this first and sometimes very small return, in order to compare the data with snowstake or snowpit data.

7. FURTHER APPLICATIONS OF SHORT PULSE RADAR

It is not difficult to conceive other stratified features in the area of Earth Resources which would lend themselves to study by the short pulse radar techniques. Studies are being pursued presently in this laboratory on measuring the depth to water table in semi-arid regions, and other near-surface phenomena. The data presentation for this work is similar to that shown in figure 11, from which it can be seen that a qualitative interpretation is considerably easier than in the case of a single radar return.

It is anticipated that a system similar to that described herein will be tested in an airborne configuration during the coming year. The peak power of the system is presently only 1 watt, and the receiver gain approximately 30 db. At least five orders of magnitude increase in signal to noise ratio are therefore available for the airborne system (100 watts and 70 db) before limitations in off-the-shelf hardware are encountered.

8. CONCLUSIONS

The most significant conclusion that can be drawn from this study is that it has been proven that a short pulse radar technique can be used to remotely sense the depth or density of a given snowpack, and that given a suitable calibration point, the water equivalent of the pack is also a measurable quantity. The main limitation at present is that the pack must not contain significant quantities of free water. It is possible that this limitation could be removed by the use of more sophisticated equipment.

The horizontal stratification within the snowpack, and its time history are clearly displayed on the radar returns, although absolute calibration of a density profile is not possible with the existing system.

The presence of free water in the pack causes two effects to take place, the radar signal is elongated in time and at the same time highly attenuated. If the attenuation problem can be solved by using higher power equipment and range dependent gain, then it should be possible to estimate the 'ripeness' (free water content) of the pack by remote means.

Finally, no fundamental problems have been encountered during this study that, assuming some equipment redesign, would prevent the technique from being used operationally as a means of monitoring snowpack hydrology, from either a surface or airborne platform.

REFERENCES

1) Meier, M. F. and Edgerton, A. T., "Microwave Emission from Snow," Proc. 7th Symp. on Remote Sensing, University of Michigan, 1971.

2) Kennedy, J. M. and Sokamoto, R. T., "Passive Microwave Determinations of Snow Wetness," Proc. 4th Symp. on Remote Sensing, University of Michigan, 1966.

3) Deal, L. J., et al., "Environmental Radiation Surveys and Snow Mass Predictions from Aircraft," Proc. 7th Symp. on Remote Sensing, University of Michigan, 1971.

4) Cook, J. C., "Proposed Monocycle - Pulse V.H.F. Radar for Airborne Ice and Snow Measurements," Trans. A.I.E.E., November 1960.

5) Meyer, M. F., "Remote Sensing of Ice and Snow Thickness," Proc. 4th Symp. of Remote Sensing, University of Michigan Press, April 1966.

6) Barringer, A. R., "Recent Progress in Remote Sensing with Audio and Radio Frequency Pulses," Proc. 3rd Symp. of Remote Sensing, November 1965.

7) Evans, S., "Dielectric Properties of Ice and Snow," J. Glaciology 5, 42, 773-792, 1965.

8) Cumming, W. A., "The Dielectric Properties of Ice and Snow at 3.2 cms.," J. App. Phys. 23, 7, July 1952.

TABLE I. ELECTROMAGNETIC WAVE ATTENUATION BY SNOW AND ICE

	Frequency (cps)	Dielectric-Loss Tangent	Relative Dielectric Constant (ϵ'/ϵ_0)	Attenuation (db/meter)
	10^3	0.4920	3.33	$7.9414(10^{-5})$
	10^4	0.3420	1.82	$4.1378(10^{-4})$
Freshly	10^5	0.1400	1.24	$1.4144(10^{-3})$
Fallen	10^6	0.0215	1.20	$2.422(10^{-3})$
Snow	10^7	0.0040	1.20	$3.9856(10^{-3})$
($-20^{\circ}C$)	$3(10^8)$	0.0012	1.20	$3.5870(10^{-2})$
	$3(10^9)$	0.00029	1.20	$6.6688(10^{-2})$
	$*10^{10}$	0.00042	1.26	4.2882
	10^5	1.5300	1.90	$1.6130(10^{-2})$
Hard	10^6	0.2900	1.55	$3.2503(10^{-2})$
Packed	$3(10^9)$	0.0009	1.50	$3.0078(10^{-1})$
Snow	$3(10^5)$	0.8000	4.80	$1.4927(10^{-2})$
($-6^{\circ}C$)	$3(10^6)$	0.1200	4.15	$2.2193(10^{-2})$
	10^8	0.0180	3.70	$3.1493(10^{-1})$
Ice	$3(10^9)$	0.0009	3.20	$4.3932(10^{-1})$
($-12^{\circ}C$)	10^{10}	0.0007	3.17	1.1336

*At $-6^{\circ}C$.

TABLE II

Date		Radar Data	Ray Data	Radar Estimate of Snowpack Water Content (cms) Depth	W.E.	Estimate of Water Content using γ Ray or Snowstake Data (cms) Depth	W.E.	Radar Error
March	3	x	x	178	56.3	172	53.4	+ 3.5%
	4	x						
	5							
	6	x	x	158.5	50.3	163.5	52.1	- 3.1%
	7	x						
	8	x						
	9							
	10		x			150		
	11							
	12							
	13		x			145		
	14		x			141		
	15		x			143.5		
	16							
	17	x	0	161.5	58	139**	50.1	+16%
	18							
	19	x	0	126	45.6	135**	48.8	- 6.7%
	20	x	x	141	51.4	135	49.2	+ 4.4%
	21	x	x	128.5	46.5	132	47.8	- 2.6%
	22							
	23	x	x	137	47.8	147	51.4	- 6.7%
	24	x	0	132	46	140	48.8	- 5.7%
	25							
	26	x	0	152	56.3	133**	42.3	+14%
	27	x	x	154	58.5	131	49.6	+17.5%
	28	x	x	162	55.5	149	50.8	+ 8.7%
	29	x	x	140.5	48	148	50.6	- 4.4%
	30							
	31	x	0	135	46.8	146**	50.5	- 7.5%
April	1							
	2							
	3	x	x	162	57.8	145	51.8	+11.7%
	4							
	5							
	6							
	7	x	x	147	58.6	132	52.6	+11.3%
	8							
	9							
	10	x						

**Using interpolated value of density from figure 4 and depth data from a snowstake adjacent to the γ ray profiler.

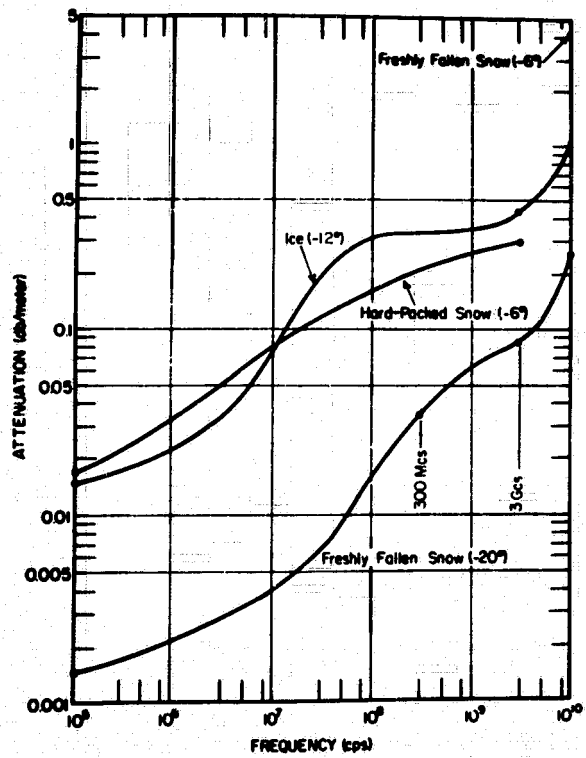


FIGURE 1. ATTENUATION OF AN ELECTROMAGNETIC WAVE BY ICE AND SNOW
(Temperatures in degrees Centigrade)

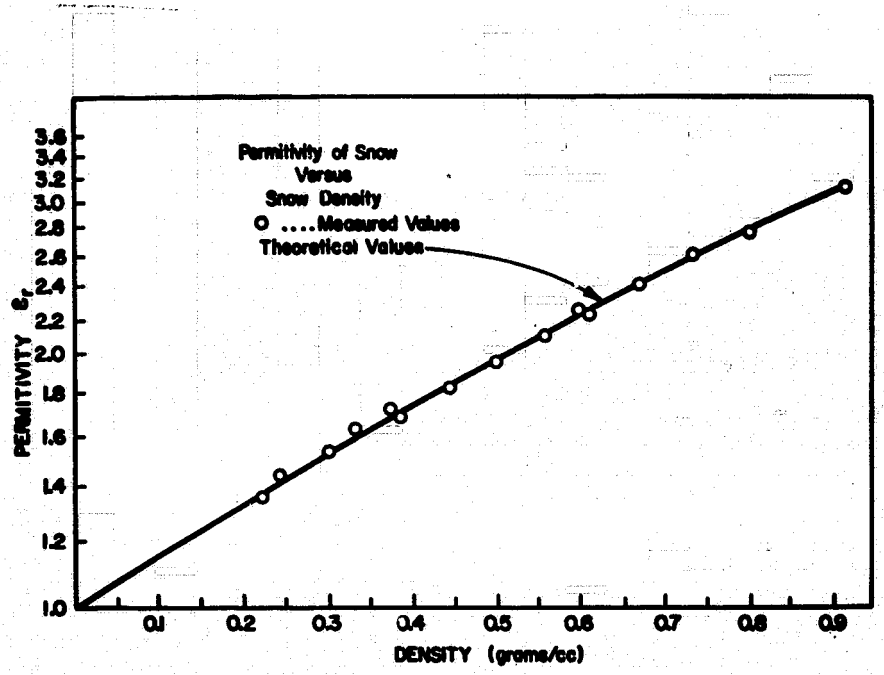


FIGURE 2. THE DIELECTRIC CONSTANT OF SNOW AS A FUNCTION OF DENSITY

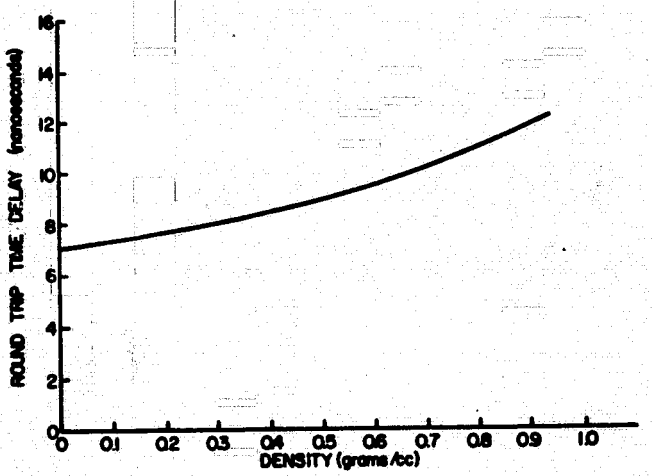


FIGURE 3. TRAVEL TIME OF AN ELECTROMAGNETIC PULSE THROUGH 1 METRE OF SNOW AS A FUNCTION OF SNOW DENSITY

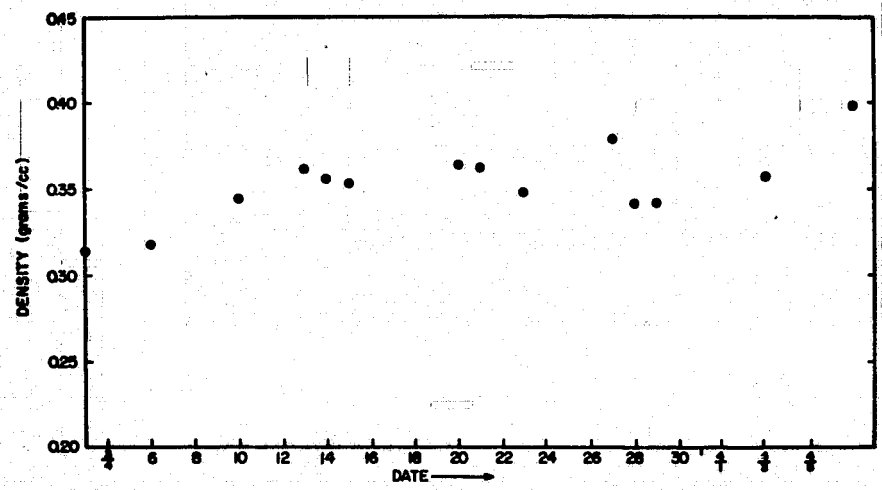


FIGURE 4. AVERAGE SNOW DENSITY AS GIVEN BY A NUCLEAR PROFILER FOR RED MOUNTAIN PASS TEST SITE

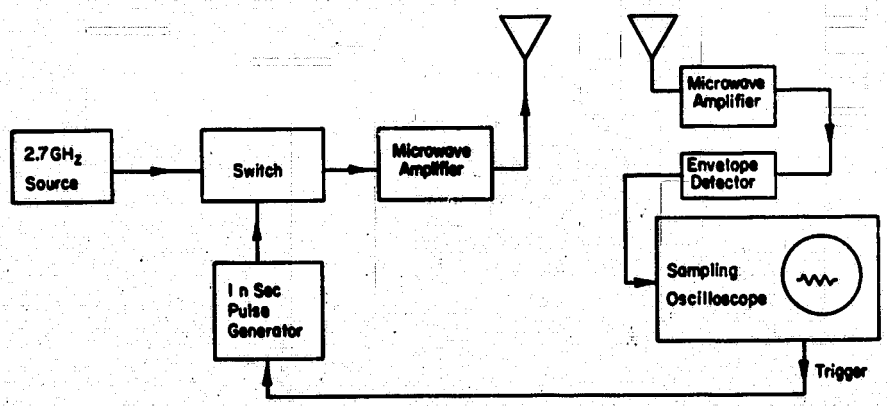


FIGURE 5. THE SHORT PULSE RADAR SYSTEM

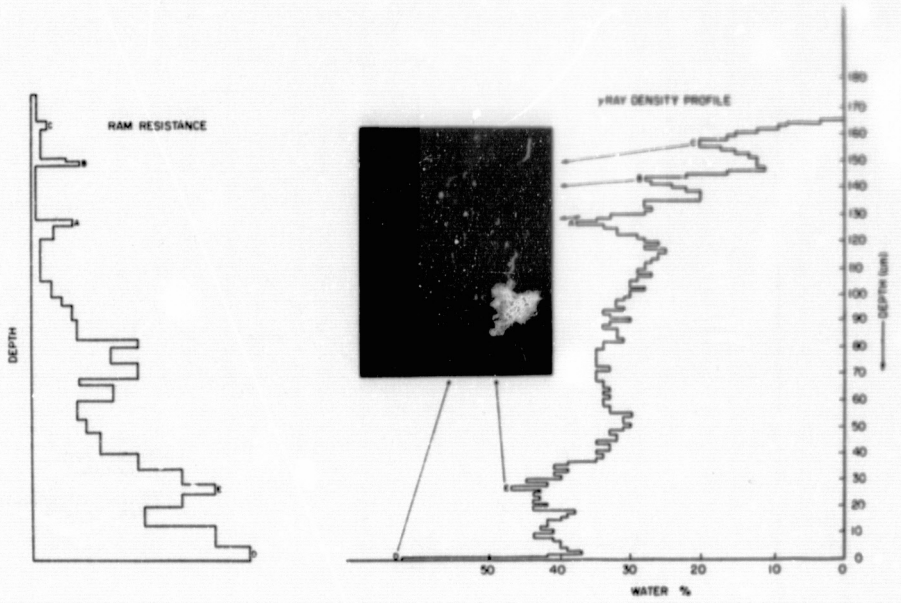


FIGURE 6. A COMPARISON OF RADAR, GAMMA RAY, AND RAM RESISTANCE PROFILES OF SNOWPACK STRATIGRAPHY

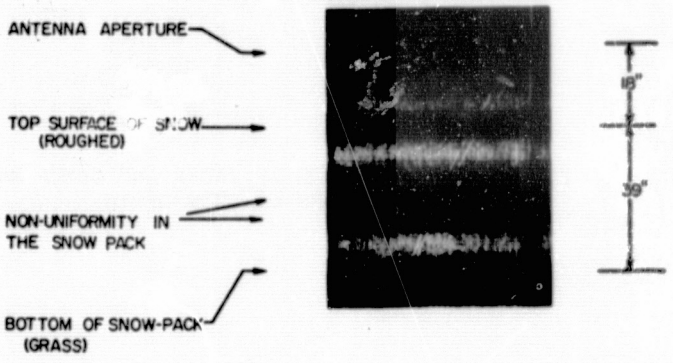


FIGURE 7. DATA FROM A TRAVERSE OVER SNOW 39 INCHES DEEP AT -½°C USING A SHORT PULSE RADAR OPERATING AT 2 GHz

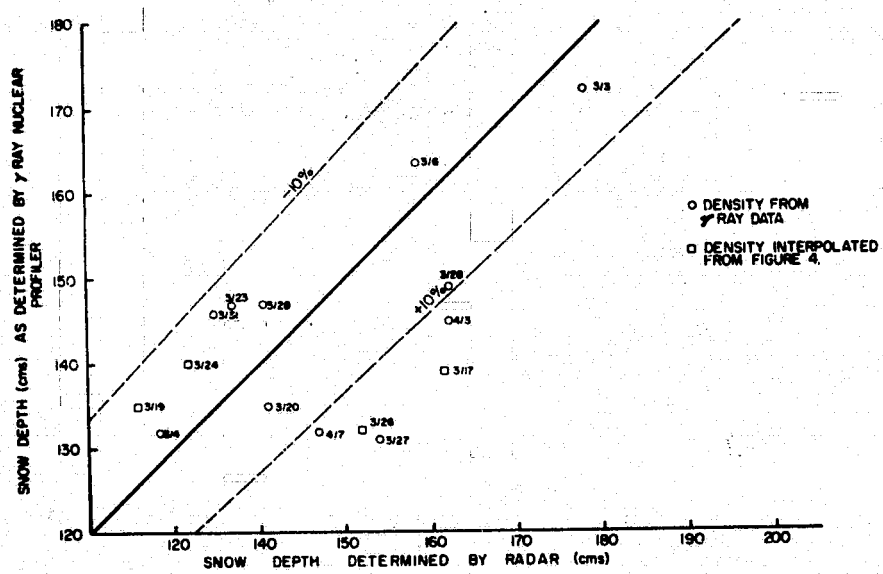
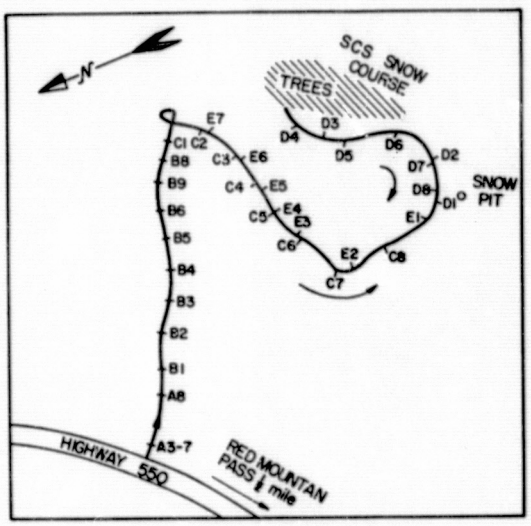


FIGURE 8. A COMPARISON OF RADAR AND GAMMA RAY DETERMINATIONS OF SNOW DEPTH



DATA SAMPLE FROM RUN 3

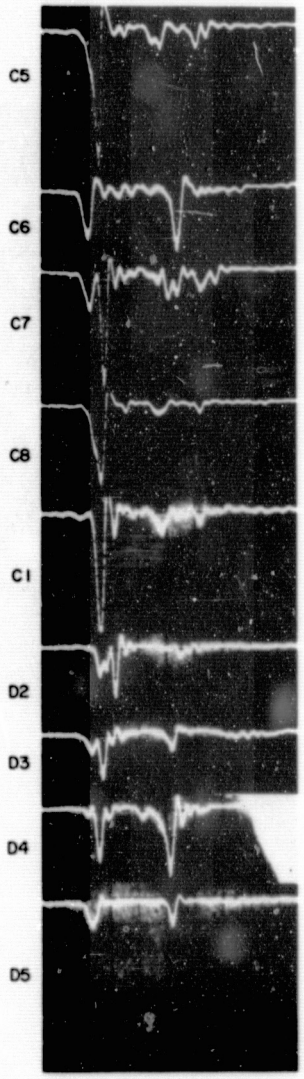


FIGURE 10. A SAMPLE OF RAW DATA FROM THE MOBILE RADAR TESTS SHOWING INTERNAL STRUCTURE WITHIN THE SNOWPACK

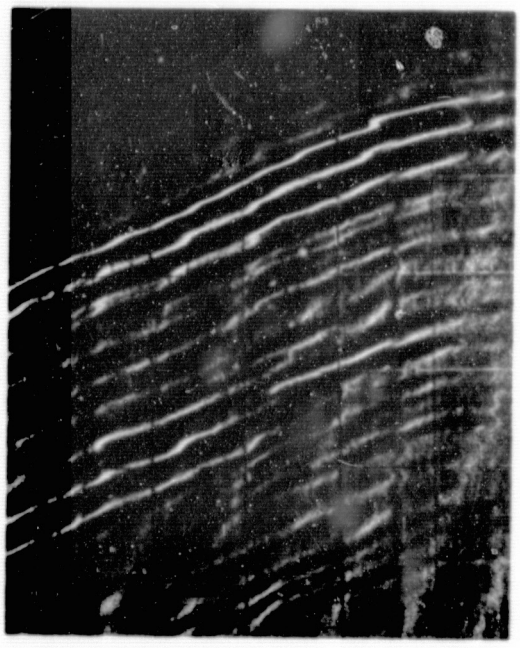


FIGURE 11. ALTERNATIVE DATA DISPLAY FROM A SHORT PULSE RADAR TO PROVIDE SUBSURFACE IMAGES

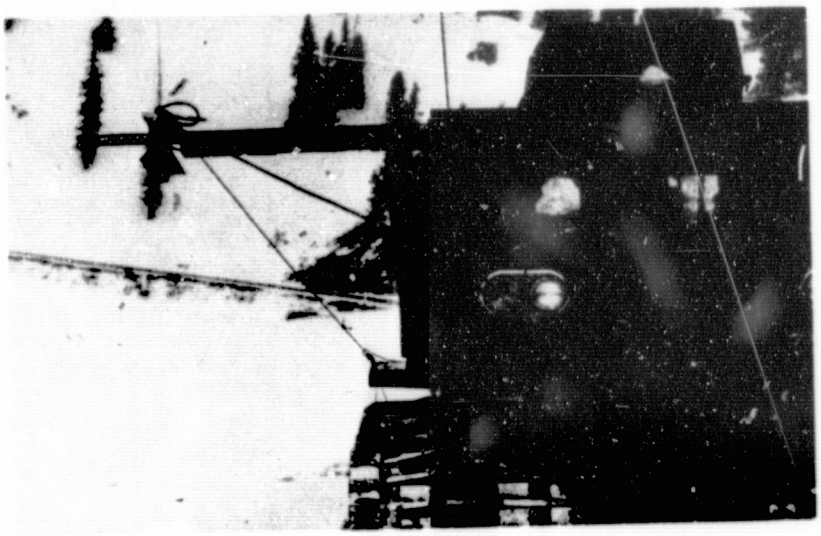


FIGURE 9. MOBILE TESTS OF THE SHORT PULSE RADAR

TWO-DIMENSIONAL STATISTIC ANALYSIS OF RADAR IMAGERY OF SEA ICE

Zagorodnikov A.A., Loshchilov V.S., Chelyshev K.B.
The Arctic and Antarctic Research Institute,
Leningrad, USSR

ABSTRACT

Theoretical assumptions and operational technique for obtaining morphpmetric characteristics of sea ice cover using airborne remote sensing SLAR) data are discussed. The technique is based on two-dimensional Fourier transformation of small-scale SLAR images of the ice cover by means of optical image filtering.

Examples of optical image filtering and spectral analysis of images of different areas of ice cover are given. It is shown that the optical method is apparently the most appropriate for operational statistic analysis of ice images, obtaines by a side-looking airborne radar "TOROS".

The aerial reconnaissance of the arctic sea ice from the aircraft equipped with remote sensors, such as a side-looking airborne radar (SLAR) has been extensively used lately (1,4/. SLAR imagery of ice cover seems in a number of cases much more informative than aerial photography. By means of an airborne sidelooking radar it is possible to survey vast sea ice cover areas and accumulate a large quantity of data. This equipment installed at the satellites is even more promising.

The interpretation of the imagery obtained from scanning remote sensors, SLAR in particular, is still under investigation. Visual interpretation of SLAR imagery is neither strictly objective nor fully informative. Photometry of images by individual cross-sections with their subsequent statistic processing is also a time consuming procedure, which requires a sophisticated equipment.

Two-dimensional optical interpretation technique seems to be the most promising for a statistic analysis of radar images /5/. The procedure is as follows: small-scale radar image and its microcopy represent a complex diffraction grating for the coherent light. According to Fourier theory an image is a superposition infinite number of waves, each wave being characterized by a certain orientation frequency and amplitude. Diffraction pattern in the focal plane of the optical system is a two-dimensional spectrum of the frequency and wave

Preceding page blank

number. Further analysis of the spectrum results in statistic parameters of ice cover imagery.

The relationship between radar imagery and ice objects

Reflectivity of the ice cover in the radio wave range like that of other irregular surfaces depends on its roughness /2/. We can distinguish three types of ice surface irregularities with their different roughness parameters (and hence reflectivity is different). The reflectivity is characterized by the energy amount, radiated from the surface towards SLAR. (Figure 1a). Figure 1b shows the brightness changes at the cross-section. Signal maxima, marked by T corresponds to hummocks, signal minima P corresponds to leads, while medium intensity corresponds to separate ice floes.

Distinct variations of brightness of the images of ice floe surfaces, leads and hummocks allows us to use two-dimensional spectral analysis for the study of the distribution of ice floes of different sizes. Gradual brightness changes make the analysis more complicated, therefore it is recommended to pass the signal which records the image through a threshold device, which filters out intermittent grades and provides well-marked boundaries between major ice formations. For the analysis of lead distribution it is desirable to use two thresholds : lower (I) and medium (II). The resulted ice imagery will appear as a two-dimensional s rabdom signal /6/, (Figure 1-c shows a portion of its cross-section). Minimum signal level corresponds to leads (I), while the peaks show the compact sea ice.

To evaluate the distribution of ice floes by their size in the area without leads it is expedient to use medium (II) and high levels of restriction. Figure 1-c shows a cross-section potion at which lower level (II) indicates smooth surface of the ice floe and upper level (III) ice cake and hummocked zones.

Thresholds allow us to work only with two gradations of brightness instead of three; more over, typical ice formations are distinctly outlined on the imagery.

At present SLAR "TOROS" is used for aerial sea ice reconnaissance, this system has only visual channel for evaluation of ice cover characteristics all signal gradations are passed through this channel. It is, however, not difficult to add one more channel with adjustable threshold levels. When the ice cover is very compacted, no leads (or only a few) are present it is more convenient to distinguish only two brightness gradations. In this case the restriction is not required for the statistic analysis.

The relationships between the ice floe size and two-dimensional energy spectrum of the imagery.

Brightness gradations of SLAR imagery of the ice cover can be described by a random function of two variables, frequently referred to as a random field. $Z(x,y)$ function can be in any coordinate system, polar coordinates $Z(\rho,\theta)$ including. By correlation theory a homogenious random field of its two-dimensional correlation function /7/

$$K_Z(\Delta x, \Delta y) = \frac{1}{XY} \int_{-\frac{X}{2}}^{\frac{X}{2}} \int_{-\frac{Y}{2}}^{\frac{Y}{2}} Z(x,y)\, Z(x+\Delta x, y+\Delta y)\, dx\, dy, \qquad (1)$$

where $X\,Y$ square area of averaging, the field may be described also by two-dimensional energy spectrum

$$S_Z(u,v) = \int_{-\infty}^{\infty} \int_{-\infty}^{\infty} K_Z(\Delta x, \Delta y)\, e^{-j(u\Delta x + v\Delta y)}\, d(\Delta x)\, d(\Delta y), \qquad (2)$$

Where u and v the components of K wave number in orthogonal coordinates. If a given field is in orthogonal coordinates, it is convenient to express its correlation function and its spectrum as $K_Z(\Delta\rho, \Delta\theta)$, $S_Z(K,\theta)$,

when the field is isotropic its correlation function and spectrum are independent of direction, that is

$$K_Z(\Delta\rho, \Delta\theta) = K_Z(\Delta\rho); \quad S_Z(\theta) = \int_0^{\infty} S_Z(K,\theta)\, dK = const. \qquad (3)$$

If the field is anisotropic, S_Z is the function of θ angle. The degree of anisotropy can be evaluated by assuming angular $S_Z(\theta)$ spectrum constant $S_{Z0}(\theta)$ and $S_Z(\theta) - S_{Z0}(\theta)$ components variable, θ angle changes only in the range $0 \div 2\pi$, then

$$S_{Z0}(\theta) = \frac{1}{2\pi} \int_0^{2\pi} S_Z(\theta)\, d\theta, \qquad (4)$$

and a variable component is determined by its root-mean-square value

$$\sigma[S_Z(\theta)] = \frac{1}{2\pi} \left\{ \int_0^{2\pi} [S_Z(\theta) - S_{Z0}(\theta)]^{1/2}\, d\theta \right\}; \qquad (5)$$

$$A = \frac{\sigma[S_Z(\theta)]}{S_{Z0}(\theta)}. \qquad (6)$$

Ratio (6) might be taken as an anisotropy measure of a homogenious random field. From (6) it follows that for isotropic field $\sigma[S_Z(\theta)] = 0$ and anisotropic measure $A = 0$

Data on spatial spectrum allow us to evaluate medium ice floe sizes. Figure 2-a shows contours of ice floes bounded by pressure ridges or ice cakes. If we consider a cross-section l at angle α to axis x, then brightness variations in that direction $B(l)$ indicates ice floes and space between them. This function is shown in Figure 2-b. The points of intersection of function

with an average level (zero-functions) can be assumed field boundaries. By the theory of random functions /3/ averagelength $\bar{L}$ of spatial periods of a given realization is equal to

$$\bar{L}(\alpha) = 2\pi \left[\int_0^\infty S_z(K,\alpha)\, dK \Big/ \int_0^\infty K^2 S_z(K,\alpha)\, dK \right]^{1/2}, \qquad (7)$$

where $S_z(K,\alpha)$ - one-dimensional energy spectrum of the function which describes brightness distribution in direction α .

This spectrum can be obtained from two-dimensional one

$$S_z(K,\alpha) = \int_{-\frac{\pi}{2}}^{\frac{\pi}{2}} S_z\left(K/\left|\cos(\theta-\alpha)\right|, \theta\right) \left|\cos(\theta-\alpha)\right|^{-1} d\theta . \qquad (8)$$

In orthogonal coordinates one-dimensional spectrum in α direction equals to

$$S_z'(u',\alpha) = \int_{-\infty}^{\infty} S\left[u'(u,v); v'(u,v)\right] dv' . \qquad (9)$$

The transiti n from (u,v) coordinate system to (u', v') is accomplished on the basis of the known dependencies

$$u = u'\cos\alpha + v'\sin\alpha ; \qquad v' = -u'\sin\alpha + v'\cos\alpha . \qquad (10)$$

As follows from the geometry mean spatial periods of function is lineary related to average sizes of ice floes

$$\bar{D} = \alpha \bar{L} . \qquad (11)$$

For fairly compacted ice cover we can assume $\alpha = 1$.

Thus, determining two-dimensional and one-dimensional energy spectra of ice cover by SLAR imagery it is possible to evaluate floe sizes. To use these characteristics extensively it is nevessary to know statistic characteristics of the dimensions of ice cover features. For this purpose let us introduce a linear dimension l determined by

$$l = \sqrt{l_{max} \cdot l_{min}} \qquad (12)$$

where l_{max} the masimum floe size

l_{min} the size taken from mid point of l_{max} and normal to it.

Assuming ice floe shape as an ellipse l becomes the radius of the equivalent circle. l has the following statistic characteristics: $W(l)$ -probability density, $\bar{l}$ - average value, σ_l^2 - dispersion, K_l - correlation function. It should be noted that the transition to linear dimension by (12) allows us to deal with a more simple one-dimensional statistic analysis.

Histogram of l distribution (Figure 3) is obtained by means of a special processing of the area of realization of ice cover (See figure 6-b). It is seen that the distribution is a monotonically decreasing function, which means that the larger is ice floe size, the less is their probabilty. An average ice flow size $\bar{l}$ for the outlined realization is 708 meters, root-mean-square error σ_l = 1478 meters.

Two-dimensional statistic processing of radar images.

Radar images were processed by means of an optic scheme (Fig. 4) of two-dimensional Fourier transformation. The signal $Z(x,y)$ in the form of transparency (negative) is put in P_I plane. Photographic plate is erected in plate P_2 which register the distribution of light, corresponding to two-dimensional spectrum $S(u,v)$. To obtain one-dimensional spectrum from $S(u,v)$ we should integrate $S(u,v)$ by one of the variables. Figure 4-b shows the scheme which allows us to make this. The integration is realized by a moving fissure diaphragm mounted in plane P_2. The one-dimensional spectrum is registered by a photographic detector mounted in the focal place P_3 of lens L_3. The integration should be made by all possible values of the variables, which means that fissure length of the diaphragm should be larger than the transparency with $S(u,v)$ spectrum. If the diaphragm length is limited by Δl value, we obtain spectrum cross-section in a given direction.

To obtain one-dimensional spectrum in wave numbers K (polar coordinates) the integration should be made by means of a circular diaphragm (Figure 5-a). To reduce spectrum $S(u,v)$ to angular one the integration should be made by means of a radial diaphragm (Figure 5-b). To obtain angular spectrum in the required frequency band the radial diaphragm length should be restricted as necessary (Figure 5-c). Thus, simple and readily operated optic schemes result in two-dimensional spectra of the ice cover areas and their frequency characteristics. If necessary this simple technique may be used to obtain two-dimensional correlation function and its components.

Results of the spectral analysis

Ice imagery, covering area of 30 x 30 km, shown in Figure 6 was statistically processed. Two-dimensional energy spectra of these images are given in the right-hand corner of Fig.6. Angular spectra of Figures 6-b,c,d, are shown in Fig.7.

Angular ypectrum analysis has shown that anisotropy coefficient is very small ($A = 0.04 - 0.05$) that is the ice cover and its radar image can be assumed a locally isotropic random field, at least in the 30 x 30 km area. This makes the statistical analysis much easier, since spectrum cross-sections and one-dimensional linear spectra of the cross-sections are actually independent of the observational directions.

Cross-sections of $S_z(u,0)$ spectra of ice images (Figures 6-b-f) are shown in Figure 8. Figures 6-b, 6-d, 6-c indicate spectrum cross-sections of compact pack ice (without leads). Figures 6-e and 6-f indicate cross-sections of spectra of ice floes, separated by leads. The wider is the spectrum of the image the less is the average size of ice floes.

To determine analytical functions which describe spectrum cross-sections Gauss functions (marked by small circles) are shown, they are superimposed at

level 0.5 for images of Figures 6-c and 6-e. Small crosses indicate a function expressed by

$$S_z(u,0) = \frac{b^2}{a^2 + u^2}, \qquad (13)$$

where b and a are constant.
Function (13) is also superimposed along 0.5 level on spectrum cross-sections of Figures 6-e and 6-f.

The comparison has shown that experimentally obtained spectra of compacted sea ice cover images are in extremely good agreement with two-dimensional circular Gauss function

$$S_z(u,v) = \exp(-u^2/2\sigma_u^2 - v^2/2\sigma_v^2);$$
$$\sigma_u = \sigma_v = \sigma_r; \qquad S_z(K,\theta) = \exp(-K^2/2\sigma_r^2). \qquad (14)$$

Average size of typical ice formations in all directions is the same and by expressions (7) and (11) is equal to

$$\bar{L} = 2\pi/\sigma_r. \qquad (15)$$

For instance, for ice cover areas (Fig. 6 b-d) it is 670 m, 750 m, 785 m, respectively. Experimentally obtained spectrum of SLAR imagery of ice floes, surrounded by leads lies somewhere between the Gauss function and the one, expressed by (13). Image spectrum resulted from the processing of the aerial photography of the same area corresponds to the function expressed by (13). And this is not surprising, since aerial photography has essentially only two brightness gradations, corresponding to leads and sea ice. The photography is a two-dimensional random pulse with the same amplitudes for all two-dimensional pulses.

Summing up we can draw the following conclusions:

1. Two-dimensional spectra of ice cover imagery are actually isotropic. Sea ice cover comprised of complex monolythic ice formations of different sizes can be also regarded locally isotropic, at least in the range of 30x30 km.

2. Two-dimensional energy spectrum of SLAR imagery of compacted pack ice is described by the circular Gauss function. The spectrum width at the fixed level is inversely proportional to the average ice floe size.

3. Two-dimensional energy spectra of SLAR imagery of open sea ice with upper signal restriction as well as spectra of equivalent aerial photo pictures are described by a circular function (13) (spatial correlation function is expressed by an exponent). The spectrum width is proportional to an average size of ice floes.

4. The relationship between average ice floe dimensions and width of spatial spectrum of SLAR imagery allows us to make use of two-dimensional statistic analysis, realized by optical method, for operational interpretation of ice imagery. Ice imagery is obtained by side-looking airborne radar "TOROS".

Acknowledgements

The authors are deeply indebted to I. M. Bondarenko and P. S. Belousov for their valuable assistance in the study.

REFERENCES

1. V. M. Glvshkov, S. E. Kontorov, V. S. Loshchilov, S. S. Nikolski, K. N. Chubakov, M. I. Shevelev, 1970, New Methods of Obtaining Information on Ice. Journal "Ocean Fleet", No. 9.

2. S. G. Zubkovich, 1968, The Statistical Characteristics of Radio Signals Reflected From the Earth's Surface. Publishing House "Soviet Radio".

3. M. S. Longe-Higgins 1962, The Statistical Analysis of the Random Motion of Surfaces. Buttetin "Wind Driven Waves", Publishing House I. L.

4. Rose, 1969, The Identification of the Types of Arctic Ice Through the Use of Radar. Proceedings of the Institute of Electronic and Radiotechnicological Engineering, Volume 57, No. 4 (April, 1969).

5. L. M. Soroko, 1971, The Fundamentals of Holography and Coherent Optics. Publishing House, "Science".

6. V. I. Tikhonov, 1966, Statistical Radiotechnology. Publishing House "Soviet Radio".

7. A. M. Yaglom, 1957, Several Classes of Random Fields in a Two-Dimensional Surface, Arising From Stationery Random Processes, Monogram "Theory of Probability and its Applications", Volume 2, issue 3.

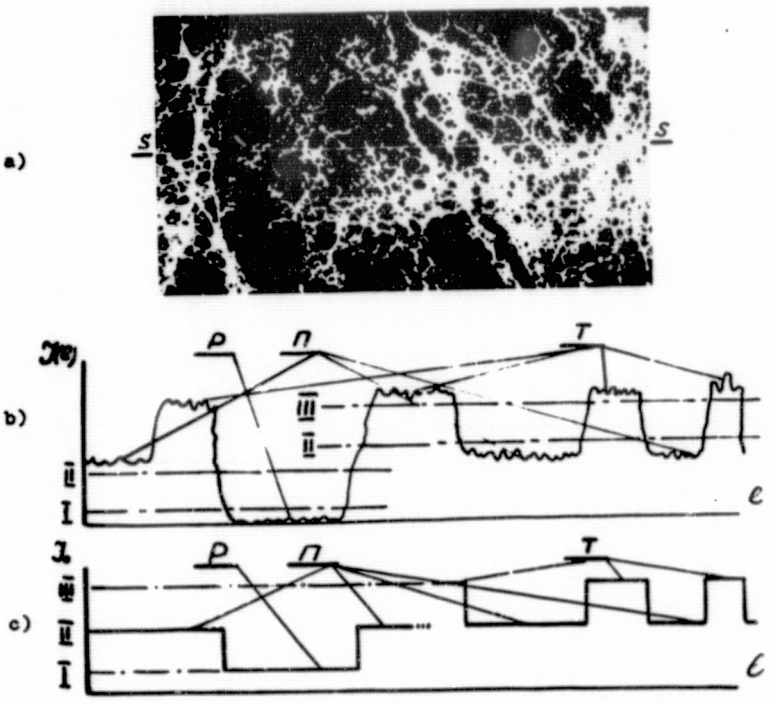


FIGURE 1. RADAR IMAGES OF FIRST-YEAR SEA ICE AND GRAPHS OF SIGNAL INTENSITY IN THE CROSS-SECTION S-S : a. radar image, b. graph of signal intensity at the cross section portion S-S, c. graph of signal intensity at the cross-section portion (S-S) after its filtering through a threshold device.

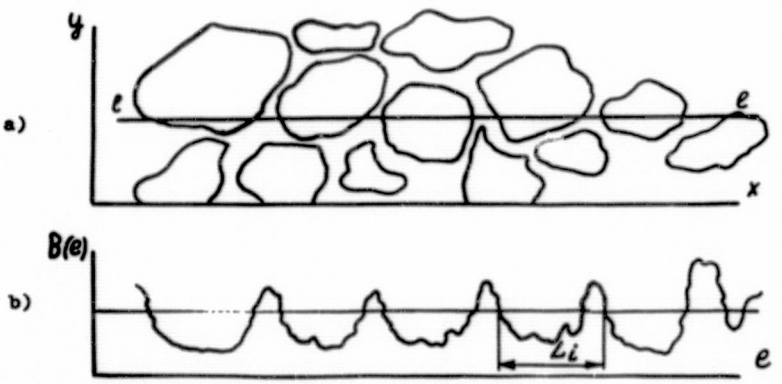


FIGURE 2. SCHEME OF THE ANALYSIS OF ICE FLOE SIZE: a. arbitrary cross-section of image contours, b. brightness change along this cross-section.

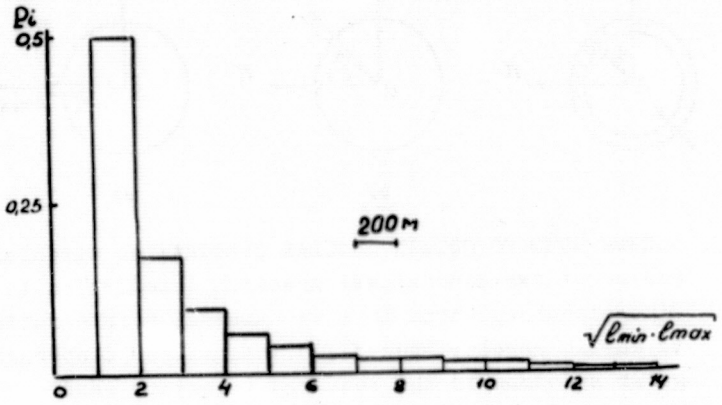


FIGURE 3. HISTOGRAM OF THE ICE FLOE DISTRIBUTION BY THE DIMENSION OF AN EQUIVALENT DIAMETER.

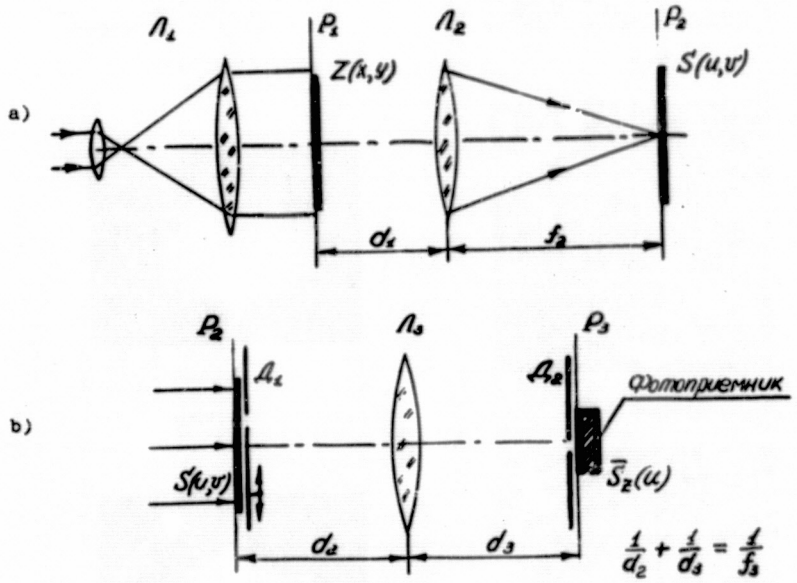
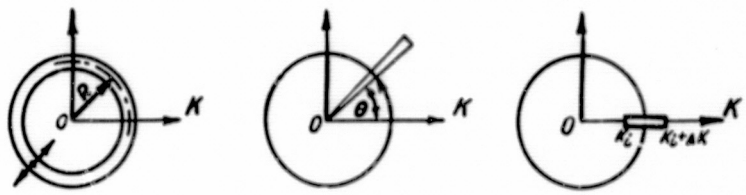
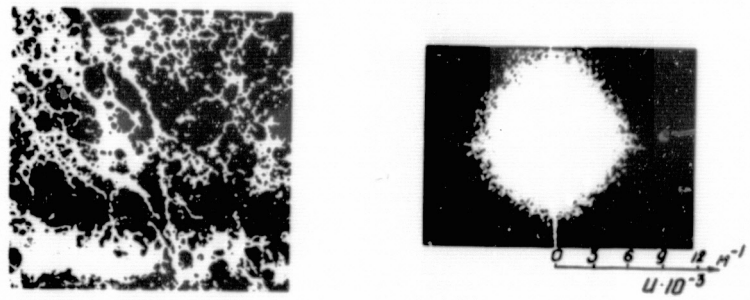


FIGURE 4. SCHEMES OF OPTICAL DEVICES: a. to obtain two-dimensional spectra; b. to obtain cross-sections and one-dimensional linear spectra.



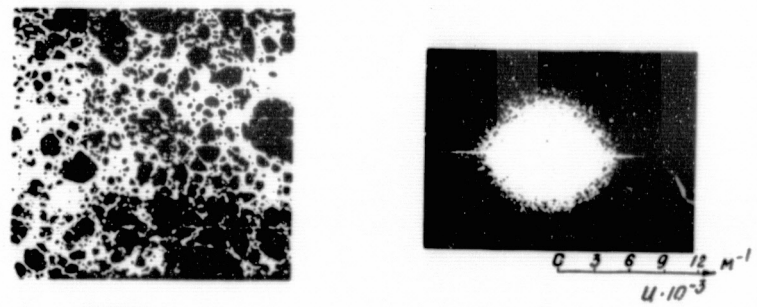
a) b) c)

FIGURE 5. SCHEME USED TO OBTAIN ANGULAR SPECTRA: a. circular diaphragm of two-dimensional spectrum integration to obtain one-dimensional spectrum in wave numbers; b. integration diaphragm to obtain angular spectra; c. integration diaphragm for angular spectrum in the required frequency band.



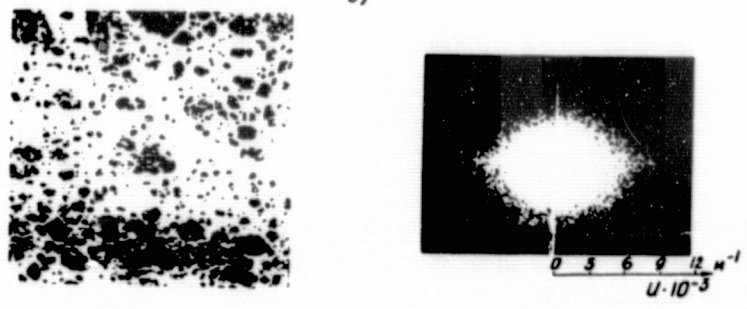
images spectrum

a)



images spectrum

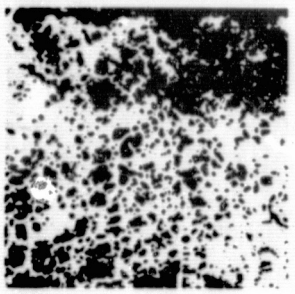
b)



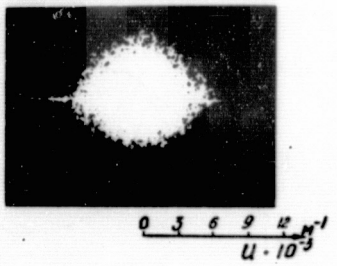
images spectrum

c)

Fig. 6 a, b, c

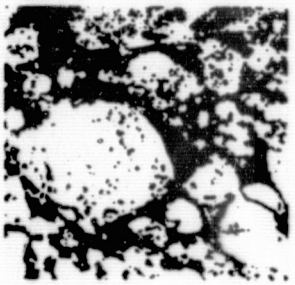


images

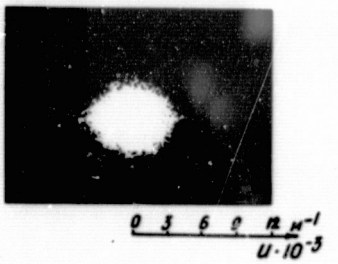


spectrum

d)

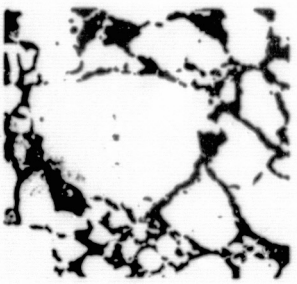


images

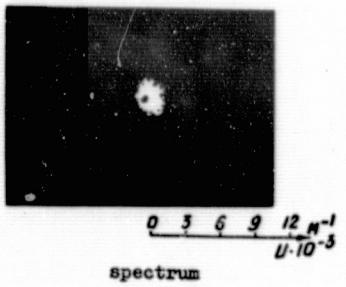


spectrum

e)



images



spectrum

f)

Fig. 6 d, e, f

FIGURE 6. RADAR IMAGES (SIGNALS) OF DIFFERENT ICE COVER AREAS AND THEIR TWO-DIMENSIONAL SPECTRA.

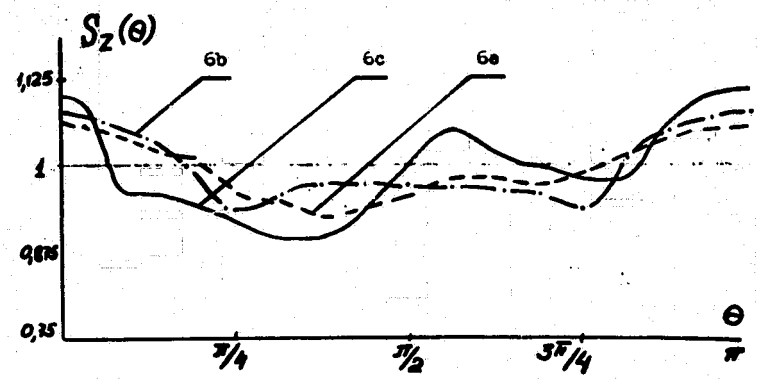


FIGURE 7. ANGULAR SPECTRA OF RADAR ICE COVER IMAGES (SEE FIG.6.)

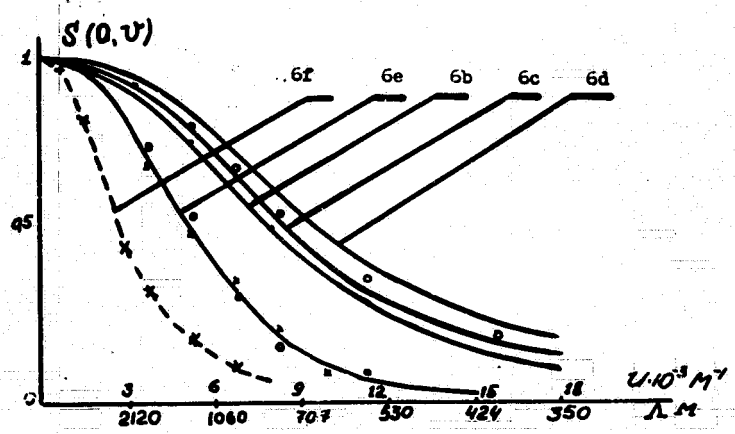


FIGURE 8. SPECTRUM CROSS-SECTION OF RADAR ICE COVER AREAS (See Fig.6).

SATELLITE MEASUREMENTS OF MICROWAVE AND INFRARED RADIOBRIGHTNESS TEMPERATURE OF THE EARTH'S COVER AND CLOUDS

A. E. Basharinov, A. S. Gurvitch, A. K. Gorodezky, S. T. Egorov, B. G. Kutuza,

A. A. Kurskaya, D. T. Matveev, A. P. Orlov, A. M. Shutko

Inst. of Atmospheric Physics Acad. Sci.

USSR

Inst. of Radioeng. and Electronics

Acad. Sci. USSR

ABSTRACT

Radiometric investigations of the Earth were started in the USSR in 1968 [1, 2] by launching the satellite "Cosmos 243" equipped with microwave and infrared radiometers aboard.

This experiment was conducted over the Southern hemisphere during the spring season.

The data obtained during this experiment allowed us to estimate the ocean-surface temperature, the boundary of floating ice around the Antarctic continent, the temperature and the state of continental ice covers, atmospheric water vapor content, the liquid water content of clouds, characteristics of rains and some other geophysical data [1-4].

These radiometric microwave and infrared investigations of the Earth were conducted from the "Cosmos 384" satellite which was launched in December 1970.

The "Cosmos 384" satellite had a declination of the orbit of 72,9° and an altitude from 212 up to 314 km.

The season during which this experiment took place corresponded to summer for the Southern hemisphere.

Some results of the data obtained at 8.5 cm, 0.8 cm, and 10-12 mkm wavelengths during this experiment are discussed.

Figure 1 indicates the boundary of the floating sea ice near Antarctic Continent obtained from radiometric data. A comparison of these data with those obtained from the "[illegible]or" satellite TV observations shows good agreement.

The brightness temperature variations due to the floating ice have been observe.

During the flight over the Antarctic Continent the synchronous latitudinal brightness temperature variations detected by microwave and infrared radiometers have been observed. The value of these variations for some regions was 10-15°K greater as compared with the latitudinal variations

of the mean climatic temperatures of the ice cover (see Figure 2).

During flights over land, the latitudinal brightness temperature variations and the variations caused by local thermal processes have been observed. For example see the brightness temperature profile obtained over West Africa at 8.5 cm wavelength which is presented in Figure 3. The brightness temperature variations observed in Figure 3 are caused by the latitudinal variations of the air temperature. Here are observed: region 1 with a slow reduction of temperature from the sea coast (8° N. L.); region 2 which corresponds to the northern part of the Sahara where the temperature variations are small; and region 3 which corresponds to the montane area near the Mediterranean Sea coast.

The brightness temperature variations at 0.8 cm wavelength over the oceans are explained first of all by the presence of water droplets in the atmosphere in the form of clouds and rains [1].

The data presented in Figure 4 illustrate the latitudinal brightness temperature variations between 20° N.L. and 60° S.L. over the Pacific Ocean, where as seen from TV data the large area is covered with clouds.

Large values of these variations indicate the large range of the water content variations in clouds. Some estimations of the water content values in clouds obtained by means of the microwave radiation measurements are presented in Figure 4.

As indicated by data obtained at 0.8 cm wavelength an increase in brightness temperature is observed in the case of flying over the atmospheric fronts.

Figure 5 illustrates the brightness temperature profile at 0.8 cm wavelength over the central part of the Pacific Ocean between 30° N.L. and 40° N.L. where the presence of a cold front was indicated.

As has been obtained from ITOS-I and synoptical data the observed area has been characterized with the presence of clouds and rains. The greatest value of the brightness temperature indicates the presence of rains.

The infrared data with the aid of the procedure described in [5] were used for the estimation of the upper boundary height of clouds.

Figure 6 illustrates the brightness temperature data over the equatorial part of the Pacific Ocean and the scale of the upper boundary heights of clouds. The estimations obtained indicate that the uppermost height of the boundary of the clouds is about 15 km.

The concurrent analysis of the microwave and infrared radiation data has been applied to determine the macrostructure of the precipitation field.

Figure 7 illustrates the synchronous microwave and infrared brightness temperature variations which indicate some dependence between the height and the liquid water content in clouds.

REFERENCES

1. A. E. Basharinov, A. S. Gurvitch, S. T. Egorov, Dokl. AN SSSR, v. 188, N 6, 1969.

2. A. K. Gorodetzky, M. S. Malkevith, A. O. Orlov a.o. Izvest. AN SSSR. Physica Oceanai Atmosphery, v. 6, N. 5, 477, 1970.

3. A. M. Obukhov, A. E. Basharinov, Yu. W. Wasiliev, A. S. Gurvitch a.o. Kosmicheskie issledovaniya. IX, 1, 66, 1971.

4. A. E. Basharinov, A. S. Gurvith, S. T. Egorov, W. I. Zsukov, A. A. Kurskaya, a.o. Kosmicheskie issledovaniya IX, 2, 268, 1971.

5. A. K. Gorodetzky, M. S. Malkevith, W. I. Sachinov, Dokl. AN SSSR v. 200, 3, 588, 1971.

6. A. E. Basharinov, A. S. Gurvith, S. T. Egorov, Proc. of VII International Symposium on Remote Sensing of Environment p. 199, 1971.

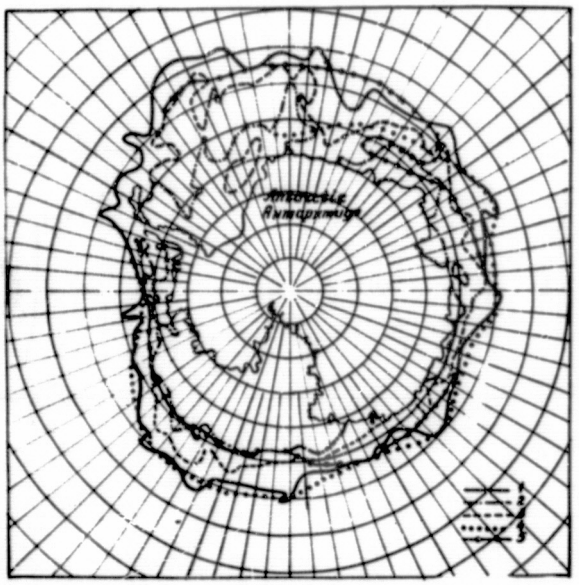


FIGURE 1. THE MAP OF ICE DISTRIBUTION AROUND THE ANTARCTIC CONTINENT IN DECEMBER 1970 OBTAINED FROM RADIOMETRIC DATA FROM THE "COSMOS 384" SATELLITE 1 - the boundary of floating ice derived from the "Cosmos 384" data; 2 - the boundary of 30% ice compaction; 3 - the boundary of 70% ice compaction; 4 - the boundary of ice from the "Meteor" satellite TV data; 5 - the boundary of ice devoted to mean climatic data.

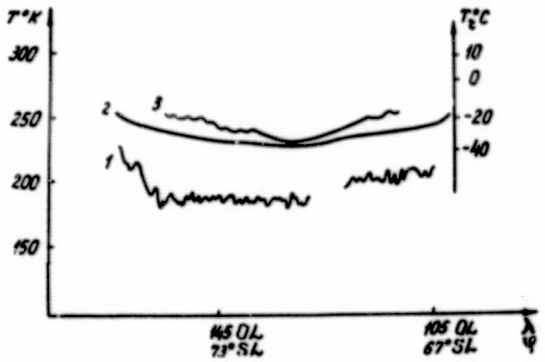


FIGURE 2. THE LATITUDINAL MICROWAVE AND INFRARED BRIGHTNESS TEMPERATURE VARIATIONS OVER ANTARCTIC CONTINENTAL ICE COVER
1 - the microwave brightness temperature data; 2 - the averaged monthly data along the subsatellite track; 3 - the infrared temperature data

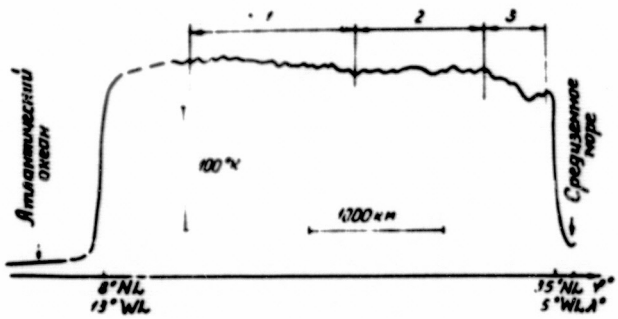


FIGURE 3. THE BRIGHTNESS TEMPERATURE DATA OVER NORTH-WESTERN AREA OF THE AFRICA OBTAINED AT THE 8.5 CM WAVELENGTH 10 DECEMBER 1970
1 - The sea coast region; 2 - The northern part of Sahara region; 3 - The coast of the Mediterranean sea region.

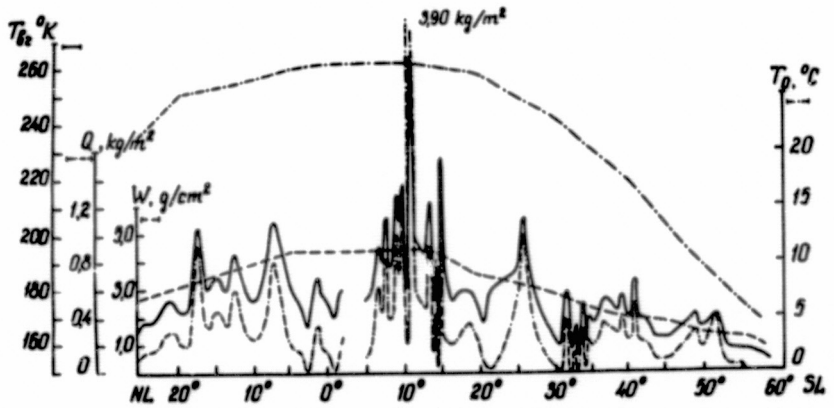


FIGURE 4. THE BRIGHTNESS TEMPERATURE (-) DATA AT 0.8 CM WAVELENGTH

(--.--) the liquid water content data in clouds,
(------) the averaged monthly data of atmospheric water vapor content
(-.-.-) the surface temperature T of the Pacific Ocean

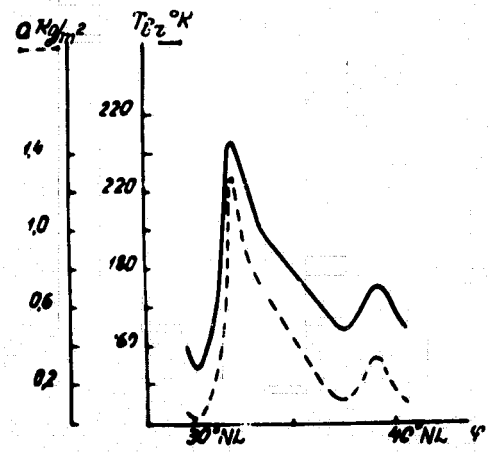


FIGURE 5. BRIGHTNESS TEMPERATURE (——) AND WATER CONTENT (---) DATA IN CLOUDS OF THE COLD FRONT OVER THE CENTRAL AREA OF THE PACIFIC OCEAN 11 December 1970.

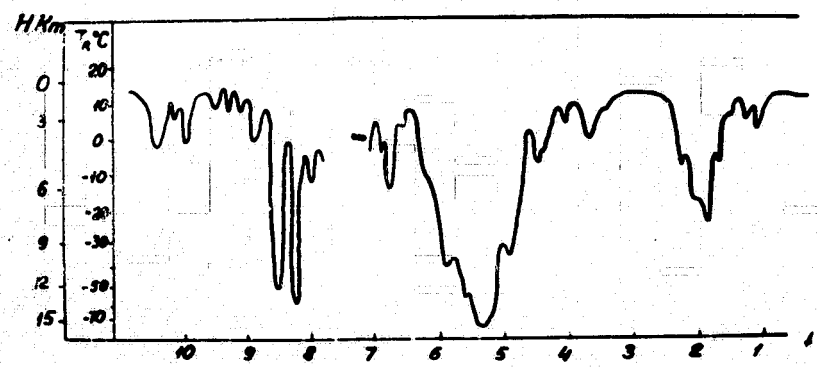


FIGURE 6. THE UPPER BOUNDARY HEIGHTS OF THE CLOUDS OBTAINED FROM INFRARED TEMPERATURE DATA OVER THE PACIFIC OCEAN 10 December 1970.

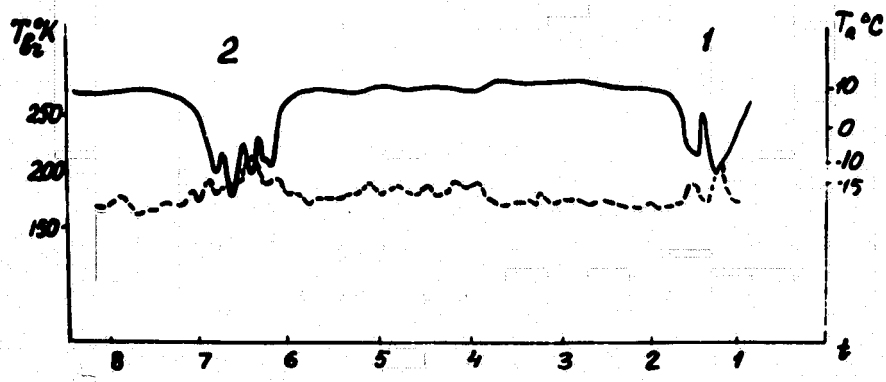


FIGURE 7. CONCURRENT MICROWAVE AND INFRARED DATA OVER THE PACIFIC OCEAN 10 DECEMBER 1970.
(——) microwave brightness temperature
(——) infrared temperature

A DATA BASE FOR COMPARISONS BETWEEN PLANNED AND UNPLANNED URBAN GROWTH*

Frank H. Osterhoudt**

Natural Resource Economics Division
Economic Research Service
U.S. Department of Agriculture

ABSTRACT

Comparative land use maps drawn from air photos provide a means for professionals, local government officials, and laymen alike to visualize land use situations and explore planning problems. Such maps and data base can be relatively uncomplicated and inexpensive to prepare.

There has been much land use planning in our nation in the past, and it will probably continue. Despite this interest and experience, many land use plans have not been implemented or have otherwise failed. Why do they fail? Land use maps drawn from air photos provide a means for professionals, local government officials, and laymen alike to visualize land use situations and explore planning problems. Maps showing the actual growth of an area, juxtaposed with maps showing what the growth would have been under specified planning criteria, provide an easily manipulated data base for comparisons, evaluations, and re-evaluation of development patterns and their implications.

Development of Data Base

A data base for land use planning was developed for Las Cruces, New Mexico, to help analyze local problems and provide a more general understanding of land use planning. The principal components used to develop the data base were air photos and the current city plan.

Air photos were readily available because--as with amny other small cities located in agricultural regions--Las Cruces is included in the periodic photo coverage carried out by the Agricultural Stabilization and Conservation Service (ASCS). Enlargements of the 1967 photo coverage were mosaicked to form the base map for the study. The 1967 land use pattern of the city and the adjacent planning and platting jurisdiction was identified, primarily through stereo viewing of contact prints. Ground truth was incorporated to facilitate the training of the photo interpreter and to increase precision. The land uses were classified into eleven categories and color-coded onto a mat acetate overlay superimposed over the photo mosaic. The resulting map described the 1967 land use of Las Cruces and the surrounding area.

A map of Las Cruces, showing land use patterns in 1947 was then constructed. Through interpretation of 1947 ASCS stereo photo imagery, differences between 1947 and 1967 land uses were colored onto a second overlay covering the original mosaic and overlay. Since the 1947 land use differences of the second overlay hid the underlying colors of the 1967 overlay, the combination formed a 1947 land use map. Stereo coverage of the area was available for 1955 and 1960, as well as 1947 and 1967; this intermediate information assisted in determining 1947 land use. The acreage for each land use in 1947 and 1967 was measured by dot grid. All tabulations were kept according to subsectors delimited by the 1967 elementary school districts within the 1967 city limits.

---

* The author wishes to acknowledge the work of Jake C. Brooks, former graduate assistant, who developed the maps and made the step-by-step land use decisions. Mr. Brooks is now Regional Planner of the Southern Rio Grande Council of Governments.

** Paper prepared when Assistant Professor of Agricultural Economics, New Mexico State University.

To gain insights as to the effects and problems of land use planning, a "planned 1967" map of Las Cruces was developed to compare with "actual 1967." How would Las Cruces have looked in 1967 if the current city plan had been initiated in 1947 and followed since then? The "planned 1967" map was constructed from three elements: the map of actual 1947 land use, the measurements by category of the city's actual acreage increase between 1947 and 1967, and the criteria of the current city plan. 1/ The city's growth in each land use category was added to the 1947 map according to the criteria of the current city plan.

The data base was relatively inexpensive. Total costs of the research, including professional salary and other overhead, amounted to $12,156. The direct cost was $3,705; this included $2,850 for a graduate student half-time for ten months, $470 for hourly help, $321 for the air photos, $56 for other materials, and an $8 pocket stereoscope. Now that the method has been established, it would take about six months at half-time to make similar maps for other dates or other cities.

Use of Data Base

The maps and area tabulations form an easily understood, common base for various comparisons of development with and without land use planning. Among the economic impacts that can be evaluated are differences in tax revenues and their incidence with and without the plan. Another economic impact is the differences in costs of utilities and services. The relative suitability of the soils used for urban development or agriculture can be ascertained. Attractiveness or community appearance, including dust and erosion problems, can be studied. Various institutional and regulatory situations, such as the effect of the personal income tax, property taxes, subdivision regulations, zoning regulations and guidelines for the extension of utilities, may be compared. The sociological implications of the city with and without the plan may be ascertained.

In addition to "with plan" and "without plan" comparisons, individual situations or problems stand out. When applying the city planning criteria, a number of problems become apparent. In older areas of the city, where development is scattered, criteria requiring compact development are difficult to apply: who wants to put a new house into a declining area? At least one residential development of 1967 would have been eliminated by the city plan. The development occurred because the land was cheap, and because the developer's clientele wanted certain amenities and wished to avoid some conditions built into the central city. The need to reassess various laws, wants, and the criteria themselves were highlighted.

Some preliminary findings are apparent from the study. Las Cruces would have been more compact if land use planning had been imposed in 1947; the maps show the actual city of 1967 was 20 percent larger than the "planned" one. Only an additional 198 acres of agricultural land would have been preserved; the differences in agricultural production and its multiplier effect on the community would have been relatively small. By recording all tabulations according to elementary school districts, neighborhood boundaries have been approximated; some schools are clearly not centrally located. The desirability of relocating some industry, parks, and streets, is brought to the viewers' immediate attention.

Air photos offer a relatively easy and inexpensive method of developing a land use data base for comparative studies. The photo mosaic map and the land use overlays form a common starting place by which the interested layman and professional alike can approach the physical, economic, social and institutional problems of land use.

1/ Harland Bartholemew and Associates. Comprehensive Plan, Las Cruces, New Mexico, St. Louis, Missouri, November 1968, 94 p.

URBAN LAND USE FROM RB-57 PHOTOGRAPHY: COMPUTER GRAPHICS OF THE BOSTON AREA*

Robert B. Simpson
Dartmouth College
Hanover, New Hampshire

Robert S. Yuill
Central Michigan University
Mt. Pleasant, Michigan

David T. Lindgren
Dartmouth College
Hanover, New Hampshire

ABSTRACT

A machine retrievable set of data for the Boston Metropolitan Area was derived from a conventional land use map interpreted from RB-57 imagery. The 93,000 point data set was obtained by superimposing a dot grid (U.T.M. coordinate system) over the conventional map. A series of computer maps from that data set illustrate the advantages (selectivity, flexibility, etc.) of information in this form.

The city of Boston was one of the prototype investigation areas of the "Census Cities" project. This program of the United States Geological Survey, Geographic Applications Program, was designed to provide a basis for the examination of urban growth and change by remote sensing. An important aspect of this project was the production of land use maps to serve as bases of comparison for detection of urban change by ERTS imagery, and to evaluate the utility of the high altitude photography (scale 1:120,000) taken on the NASA RB-57 missions.

The present paper extends the investigation by converting the information on the land use map to a machine retrievable form. It becomes therefore possible to produce computer maps from these data ranging from the distribution of a single land use to a composite pattern. Single item distributions can be examined in more detail without the distracting complexities of standard land use maps. The advantages of this mapping flexibility are illustrated in the following series of maps generated for the Boston Metropolitan Area.

The initial map was a full-colored manuscript interpreted from color-infrared imagery. The areal extent of the map includes most definitions of the Boston Metropolitan Area (central city, suburbs, and satellites), and extends to Brockton, Lowell, and Worcester (south, north, and west respectively). The proportions of the various land uses were calculated using this base area.

A computer base of alphanumeric information was derived from the manuscript map. This base of approximately 93,000 data points was created by superimposing a dot grid over the manuscript. The grid was oriented to the U.T.M. coordinate system by the use of U.S.G.S. topographic quadrangles. Each datum point represents the land use at the center of a four hectare cell (a ground spacing of 200 meters).

---

*The data and original land use map for this paper were produced under G.A.P. contract No. 14-08-0001-12958. Acknowledgement is also made of the source of the RB-57 photography from which the land use map was interpreted: NASA-MSC Earth Observation Program Mission No. 103, September 13, 1969.

Although this spacing obviously generalizes the information contained in the manuscript map, the spatial resolution of the computer data is of the same order as the ERTS optical resolution so the computer data also serve as a basis for future comparison.

The following maps generated from the computer data show some of the land use patterns which characterize the Boston area today. Each map consists of three panels fitted together to form a single map three and one-half by four and one-half feet in size. The graphics betray their origin in machines invented by mathematicians rather than by cartographers (e.g. the square data matrix must be portrayed in a rectangular format so that the East-West scale does not equal the North-South scale). The distortion is evident in the one-kilometer grid ticks on the borders of the maps.

Figure 1. Transportation (1.1% of the Land Area): "Filtering" the Boston transportation pattern through a 200 meter grid suppresses much of the familiar web-like pattern of individual railway lines, highways, streets, and roads. In its place emerges a Burgess-type pattern of concentric zones, made up of the area-demanding nodes of the transportation systems: airports, highway interchanges, and railway yards. It is apparent that a kind of time filter as well as space filter has been placed on the system, for with the exception of the railway yards the features shown are of recent origin. The hub of the system is Logan International Airport while the first ring out contains the railyards. Next are the closely spaced interchanges of Massachusetts Route 128 and finally there appear the interchanges of the new Interstate 495.

Figure 2. Commerce (1.7% of the Land Area): The 200 meter grid is fairly selective in its representation, filtering out many small areas of commercial land use. The remaining areas show a pattern to be expected by accessibility considerations: Boston's Central Business District, the smaller spatial concentrations of the satellites and regional shopping centers, plus the conspicuous ribbon development along the radials of the metropolitan area.

Figure 3. Industry (2.3% of the Land Area): Dominating the industrial pattern is the sprawling zone which spreads around the waterways and railyards of the inner city. Over the entire area there is a rough inverse relationship between the size of the industrial nodes and distance from the central city. Proximity to a railroad has been the prime locational factor, but the growing importance of Highway Routes 128 and I-495 is apparent.

Figure 4. Multifamily and Mixed Residences (3.7% of the Land Area): The pattern of distribution of the traditional Boston "three-decker" and other multifamily residences is seen to be compact and central both in Boston and to a lesser extent in the satellites. Multifamily housing constitutes a kind of "squeeze zone" imploded between the hard internal core of livelihood-producing and public-owned land use categories on the one hand, and the stable single family residential areas which lie to the outside on the other.

One scarcely expects an urbanized area of 3.2 million people on a low-featured glacial plain to exhibit more than the most rudimentary physical-cultural relationships. However, there is a remarkable correspondence between the boundaries of the central multifamily residential area and those of the sedimentary rock formations of the Boston Lowland geomorphic region.[1] Possibly physical environmental differences, subtle but significant during the settlement period, have been reinforced through subsequent generations by the imposition of economic, social, and legal restrictions.

Figure 5. Single Family Residences (22.6% of the Land Area): This represents the second largest land use of the study area. The predominant element in the pattern is the flocculation of residential areas both in the suburbs around central Boston and in lobate radial extensions of those areas. An important secondary aspect is

1. La Forge, Lawrence. Geology of the Boston Area, Massachusetts. U.S. Geological Survey. Bulletin No. 839. Washington D. C., 1932.

the scatter of this land use over the entire study area, representing the phenomenon of modern metropolitan sprawl.

Figure 6. Woodland (41.6% of the Land Area): The distribution of woodlands marks the land areas which have not yet been completely subjugated to urban usage. It is therefore not surprising that no woodland as such was mapped in the central city or on the Boston Lowland. A few parcels exist in the adjacent Needham Upland, and larger blocks of forest are associated with the rocky hillmounts of the Fells Upland and the Blue Hills, where they have been preserved against the development pressures of the past century by early inclusion in the public domain.

Figure 7. Vacant (17.3% of the Land Area): The composite category of vacant land occurs almost uniformly over the entire area with the exception of Boston and its immediate suburbs. Much of the land in the outlying areas is diced into uniformly small parcels of pastures and hayfields. The exceptions to this pattern of small parcels are the areas of marshland and the linear pattern associated with the Massachusetts Turnpike.

Figure 8. Built-Up Area (37.6% of the Land Area): The last map shows a composite of the following land uses: Single and multifamily residences, commercial, industrial, institutional, recreation, and transportation. The overall pattern shows an almost solid urban development westward from Boston and along the coastline. A much less concentrated pattern extends toward the northwest.

An important consideration is that this composite land use map derived from remote sensing imagery is quite similar to the "Urbanized Area" defined by the Bureau of the Census (1970 enumeration districts with more than 1,000 people per square mile). This correspondence indicates that remote sensing imagery as processed here can accurately depict urbanization and concomitantly urban change. In addition, the land use map is considerably more detailed since the data points represent much smaller areal units than enumeration districts.

The computer graphics illustrate some of the advantages of machine retrievable forms of data - selectivity and flexibility. This form is also suitable for direct further manipulation such as aggregation into different areal units. Of equal importance is the fact that the data matrix was recorded on a general coordinate system (U.T.M.). The data points themselves are thus relocatable and it is relatively easy to compare the land use information with other types of spatial distributions.

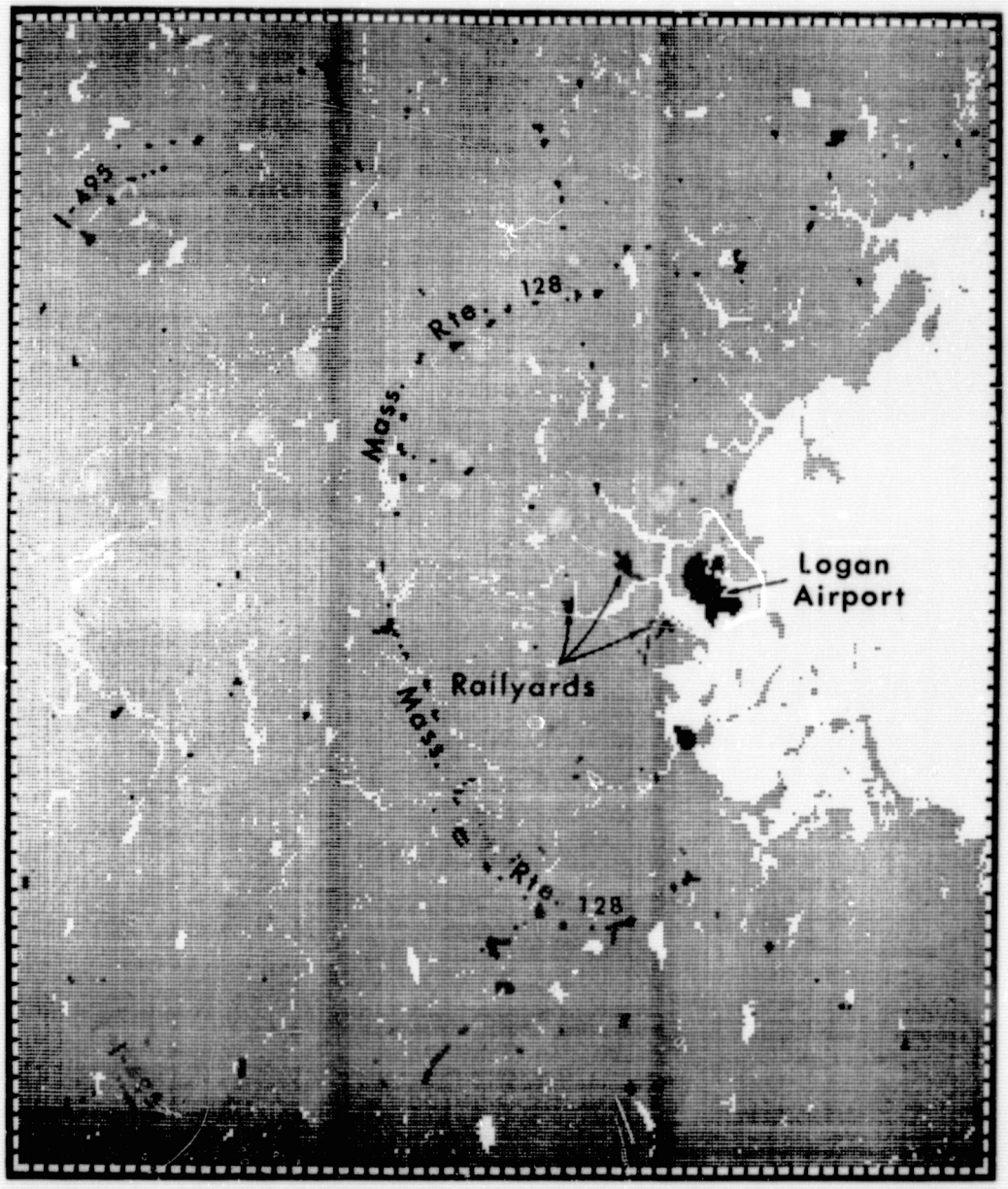


Figure 1. Transportation

(Note: In all the figures, the featured land use is in black, all others are in gray, and water areas are white.)

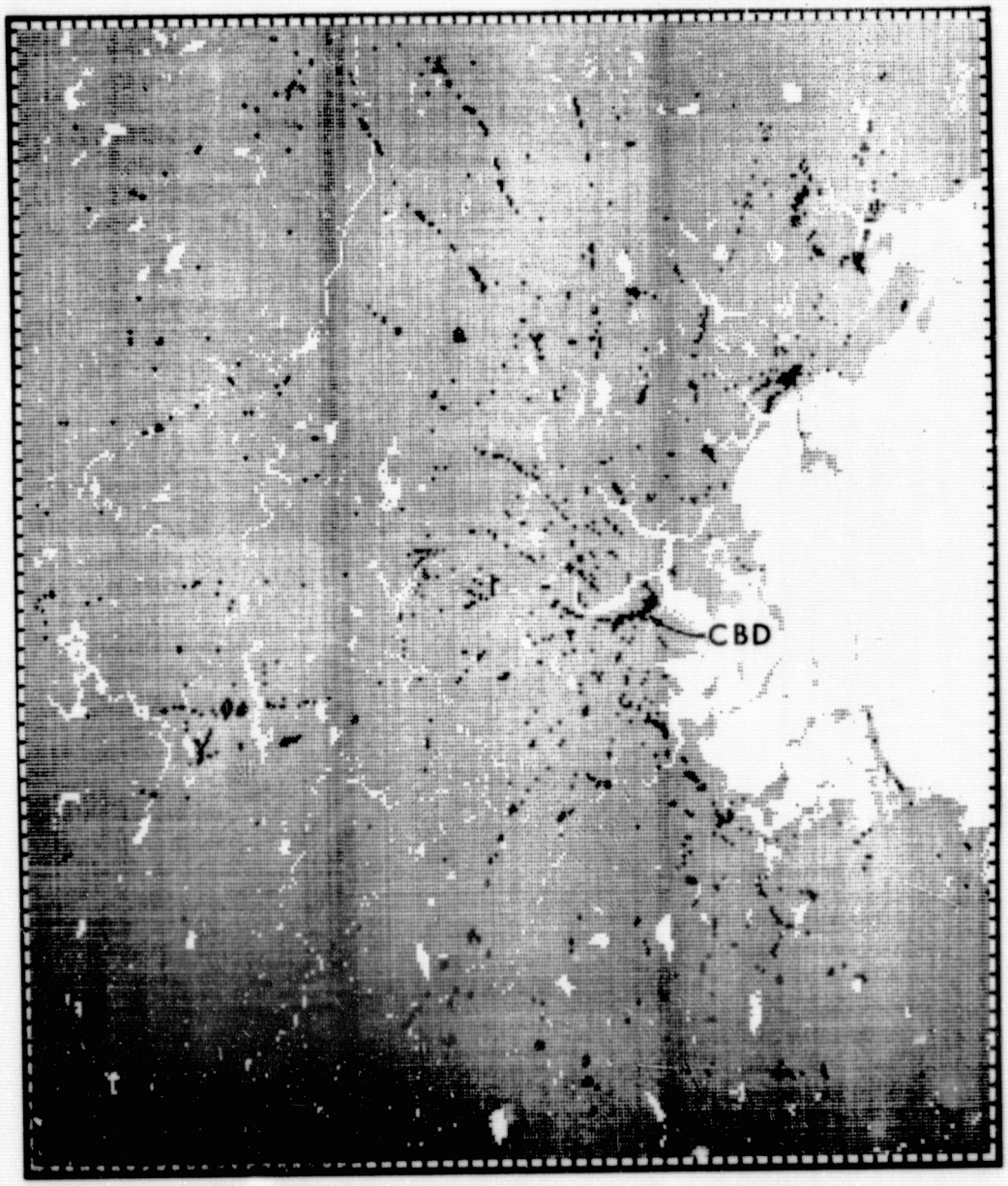


Figure 2. Commerce

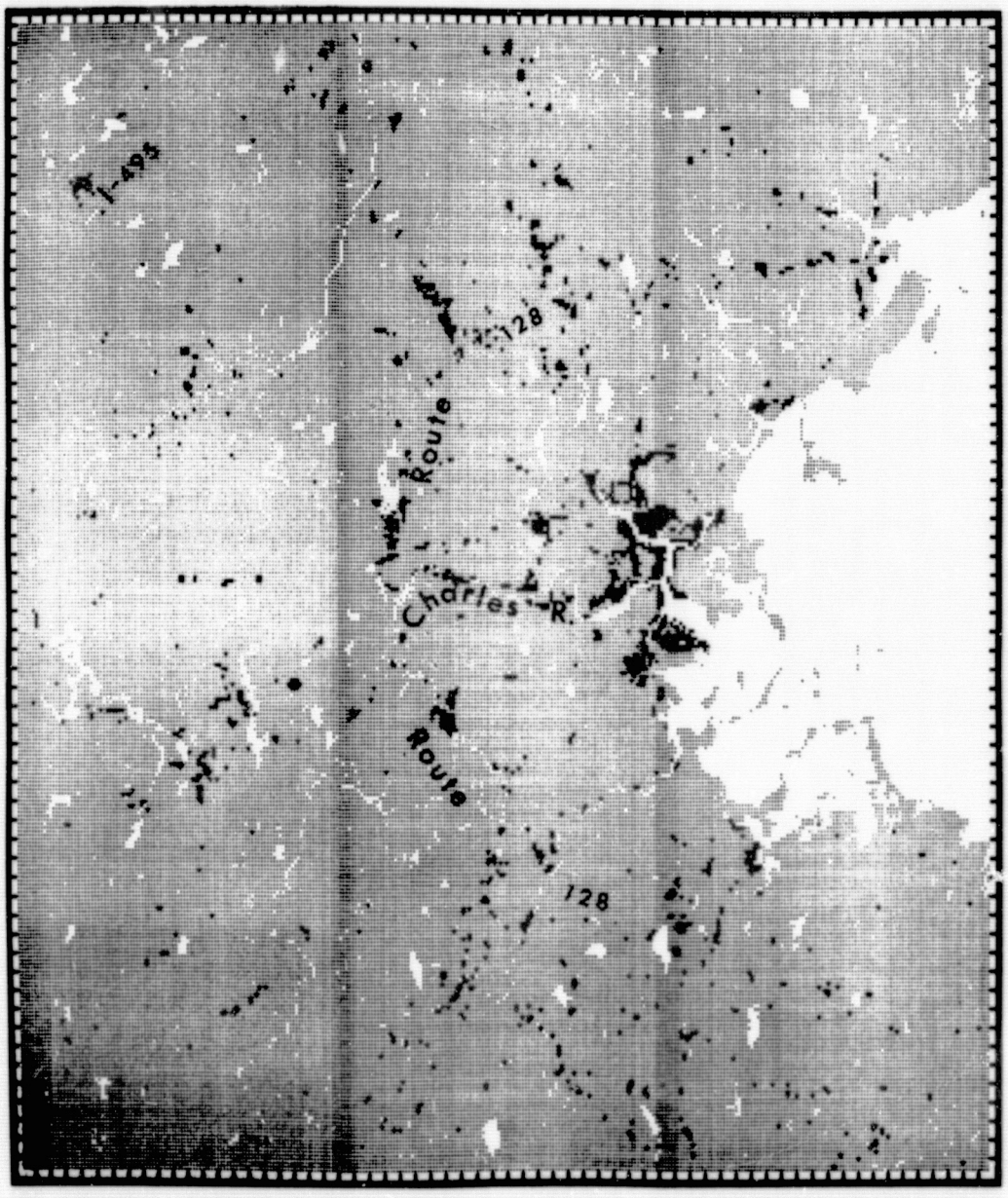


Figure 3. Industry

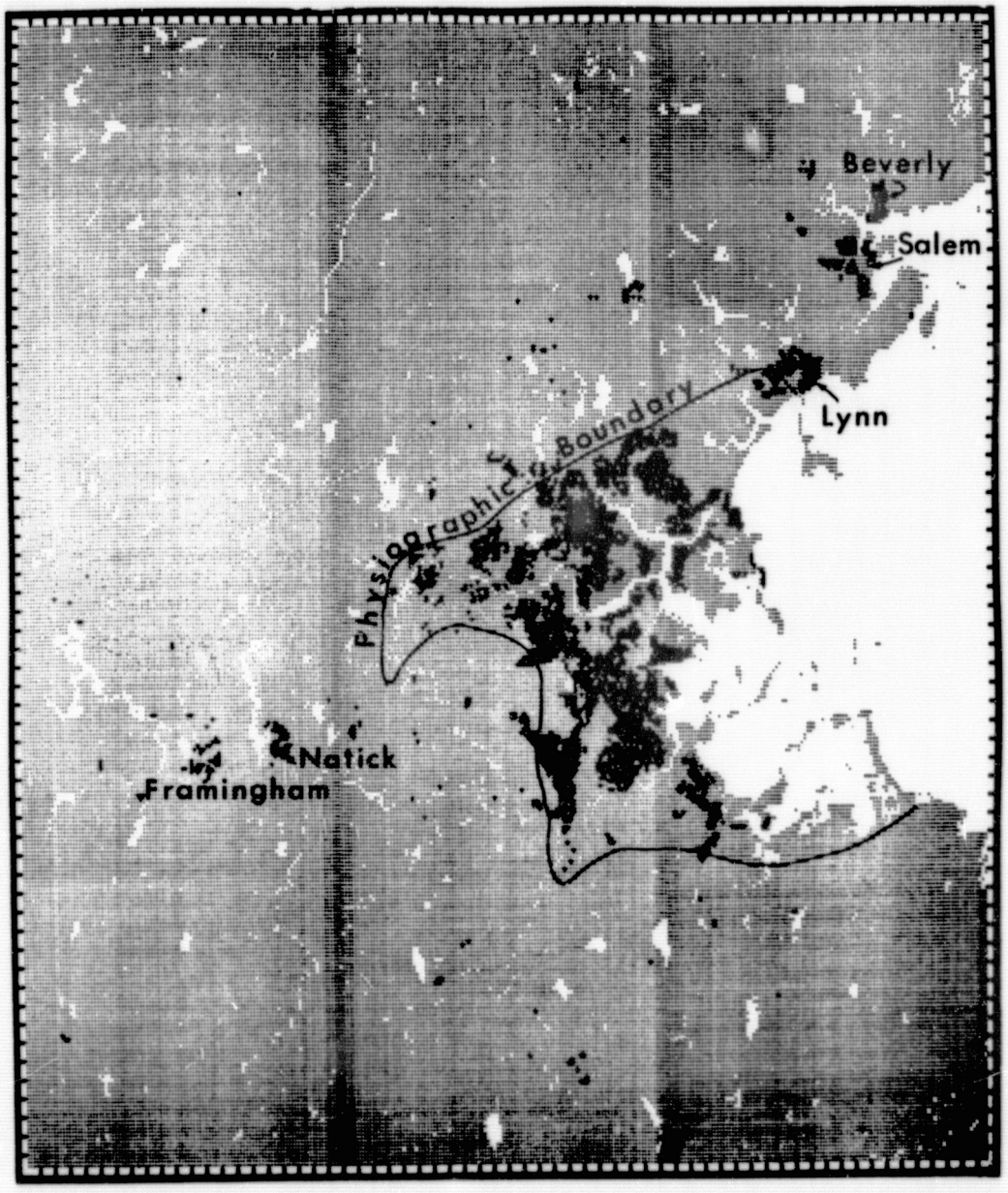


Figure 4. Multifamily Residential

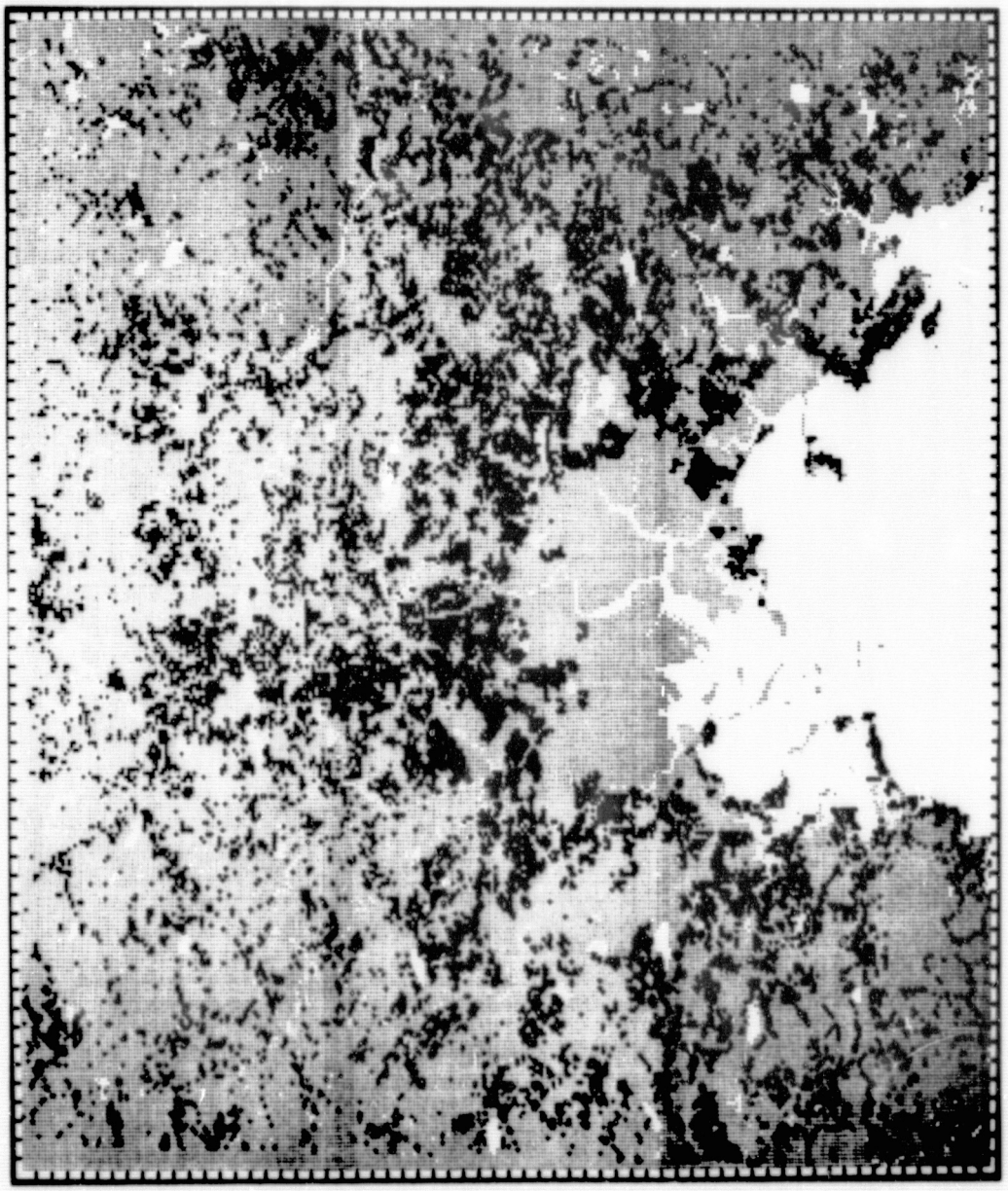


Figure 5. Single Family Residential

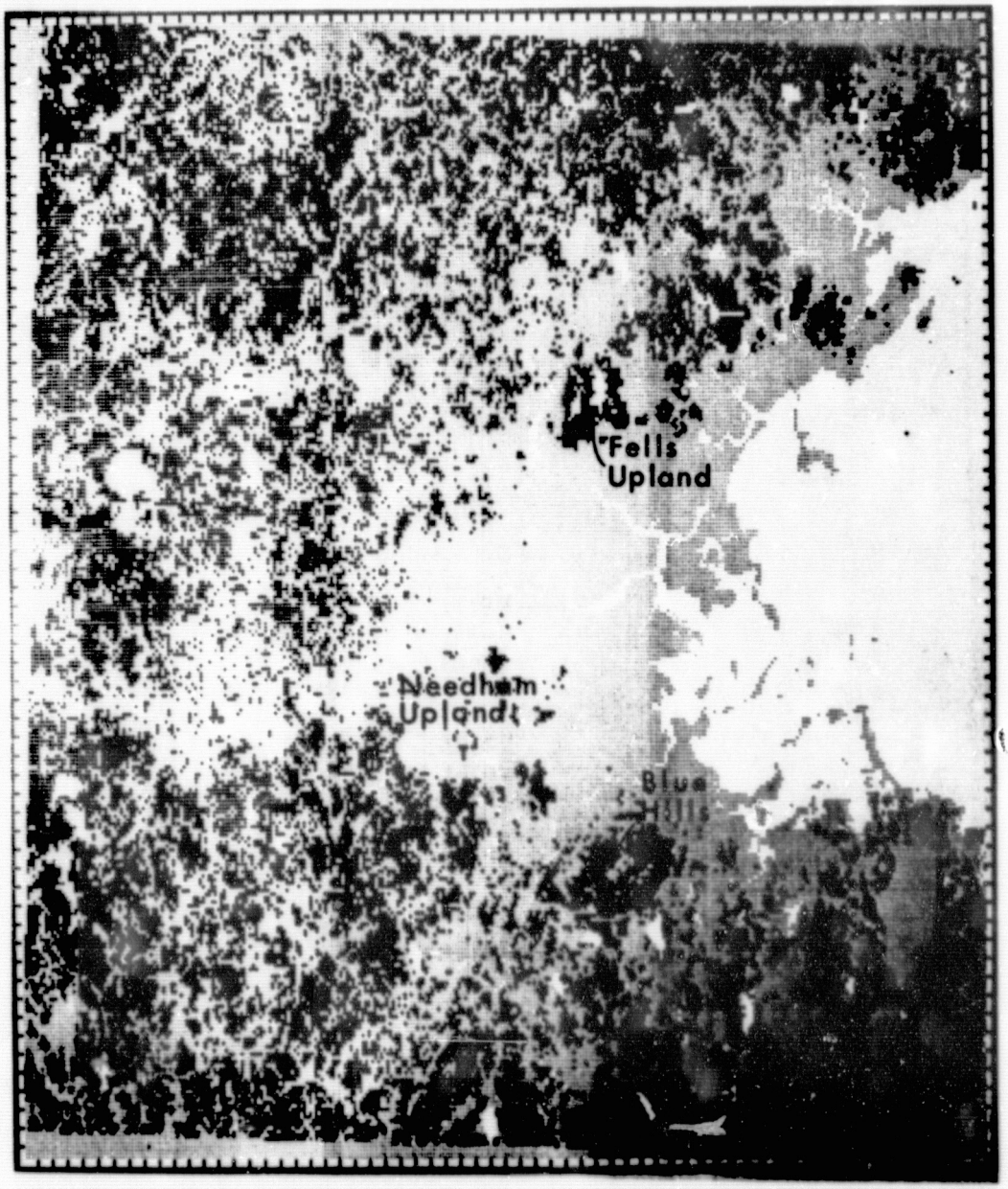


Figure 6. Woodland

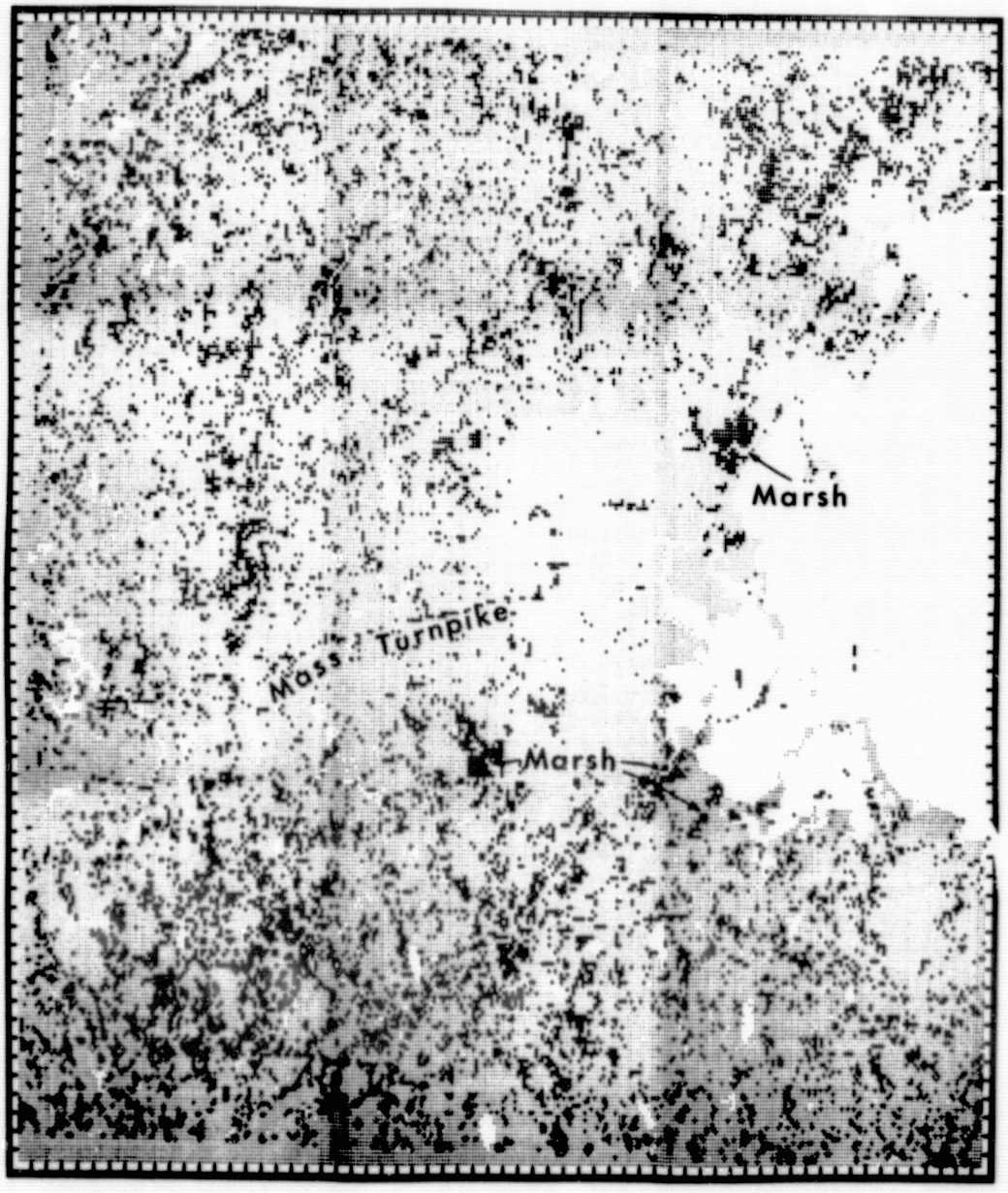


Figure 7. Vacant

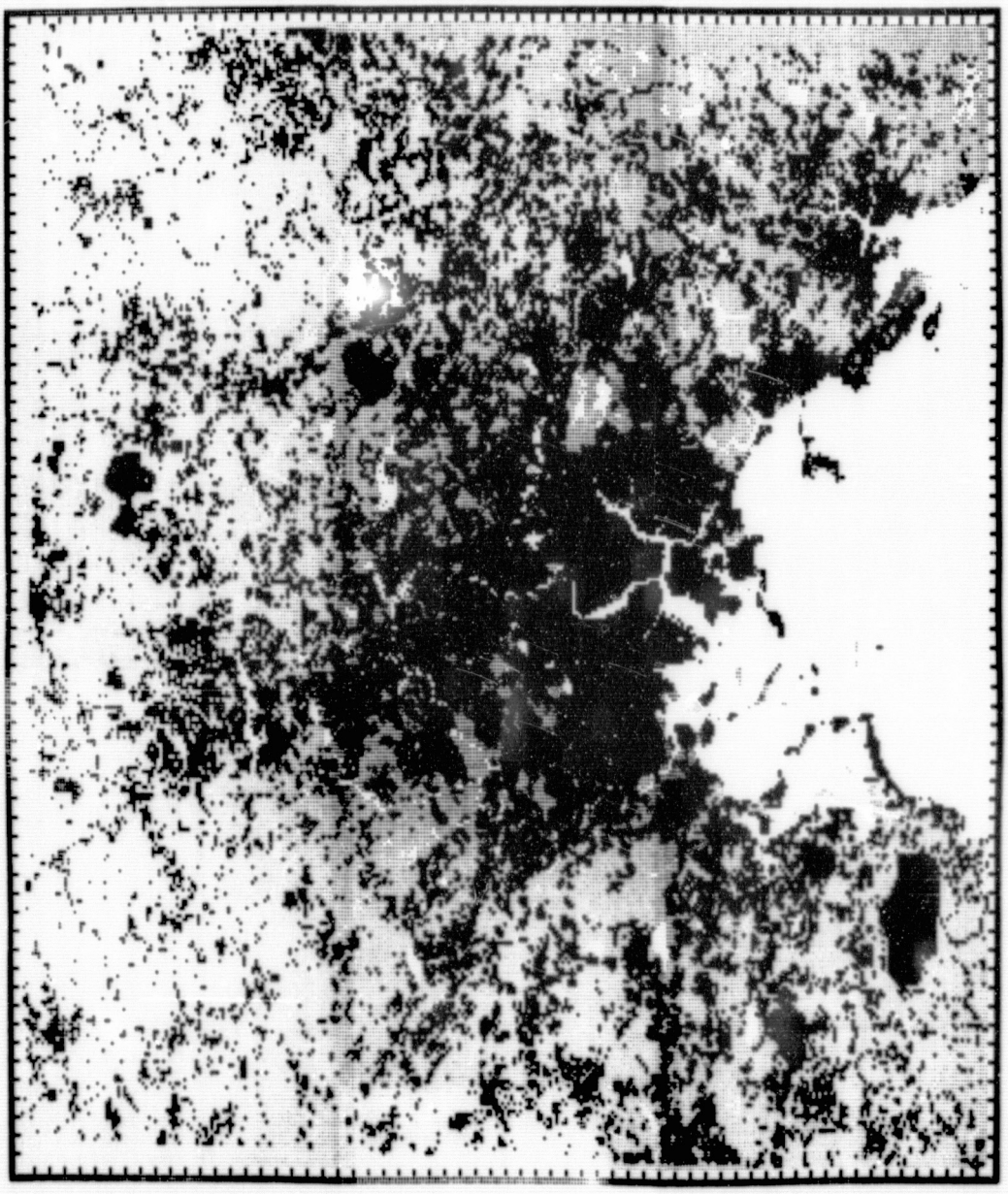


Figure 8. Built-Up Area

APPLICATIONS OF REMOTE SENSING TO URBAN RECREATION PLANNING

Diana R. Dunn
Associate Professor

College of Education
Temple University
Philadelphia, Pennsylvania

ABSTRACT

Remote Sensing has been recognized as a promising source of data for rural (outdoor) recreation planning and for general urban planning. However, its application to urban recreation planning has not yet been adequately explored. This paper identifies remote sensing application opportunities in urban recreation planning, examines several factors likely to impede collaboration between the two fields and describes work in progress in selected major U.S. cities.

1. URBAN RECREATION

The U.S. Department of the Interior has reported that "over 75 percent of all recreation occurs close to home after work and school . . . and on short outings." Further, "in urban America, where 75 percent of our population is concentrated, only 25 percent of the recreation facilities and only 3 percent of public recreation lands are reasonably accessible." Clearly, the best possible use must be made of inadequate urban recreation resources.

1.1 DATA INSUFFICIENCY

Unfortunately, there has always been insufficient data for urban recreation planning purposes, for they have never been comprehensively and periodically collected. This is due in part to the heterogeneity of governmental units, private and voluntary agencies and commercial establishments which own and operate recreation resources in urban areas. Data deficiency may also be traced to sporadic, crisis-provoked studies which have not provided the synoptic base necessary to assure systematic data for local, state and national planning. A more fundamental reason for the deficit has been the nation's traditional aggressive commitment to satisfying rural data requirements and concomitant passivity with respect to meeting urban data needs.

While the lack of sufficient planning information has always been regretable, the dramatic acceleration of the rate of change in urban social and physical environments has made the condition progressively intolerable. The increasing pace of contemporary policy and managerial decision making, and the widening scope and lengthening impact of its effect, mandates that new technologies replace old myopic methods and that they be integrated rapidly into the information gathering and analyzing phase of the planning process.

1.2 REMOTE SENSING POTENTIAL AND PROBLEMS

Remote sensing imagery can effect urban recreation planning as profoundly as Apollo 8 photographs changed man's perception of the Earth. Visual imagery is comprehensive and transcends legal, political and sectorial boundaries. Its importance is magnified by the fact that the data is periodic and systematic. Despite what appears to be unlimited opportunity in theory, optimism must be tempered with an awareness of the limitations which attend the transfer of any new technology from the milieu in which it was developed to a new area of application.

Human obstacles need to be anticipated. It is reasonable to expect resistance from some planners who may perceive remote sensing to be either an intellectual or professional threat. They may be quite comfortable dealing with seldom changing information and data specific only to the political province of their employer, yet be overwhelmed when confronted by dynamic and comprehensive interdisciplinary data beaming regularly from space. They will require sensitive guidance and

Preceding page blank

training by remote sensing specialists and probably a cadre of mediators or translators to efficiently assimilate and utilize this new source of data. Conversely, enthusiastic and enterprising remote sensing experts must control any premature inclinations to promote remote sensing as a panacea and to prescribe indiscriminately its applications. Recalcitrant planners and zealous space application buffs could thwart the best of potentials.

Technical hazards also exist and must be surmounted before the application of remote sensing to urban recreation planning will become painless and routine. There is little likelihood that current remote sensing output formats will be isomorphic to present planning input requirements. Disputes relating to scale, resolution, reliability, standardization, coordination, uniformity and system compatibility still must be identified and resolved. Present gross land use classification, identification and change monitoring is not enough; if remote sensing is to be a useful tool for urban recreation planners, more discriminative interpretation capabilities must be developed. Only then will the gross and fine data needs of both policy and management levels be met. One further caveat must be introduced. Full realization of the potential of remote sensing to the urban recreation planning process assumes that urban recreation planners have a complete understanding of their own informational needs and are able to articulate fully these requirements. There is no basis for such a sweeping supposition.

Neither remote sensing specialists nor urban recreation planners can achieve functional success in a vacuum; foresight, coordination and cooperation are essential. Recognition of possible human and technical difficulties encourages early attention to the development of an interface whose purpose is to hasten the day when remote sensing can fulfill its theoretical promise to ameliorate some of the data insufficiencies plaguing urban recreation planning. This linkage mechanism must permit prudent and continuing mediation so human and technical problems can be kept in perspective and dealt with reasonably.

2. APPLICATIONS

The application of remote sensing to urban recreation planning can be both direct and indirect.

2.1 DIRECT APPLICATIONS

Remote sensing can be used to inventory present indoor and outdoor recreation resources and to assess their condition with respect to development and maintenance. It can also assist in keeping inventories current, particularly as enumeration efforts in the public, private and voluntary and commercial sectors are seldom simultaneous and are nearly always anachronous.

Remote sensing can monitor the change in the use or function of open space and recreation facilities due to development, demographic change, accessibility improvement, weather or seasonal variation, difference in time of day or day of week, holiday occurrence, modification of school or work patterns, or other social, cultural or technical evolution.

Discernment of disease in urban biological systems is an important potential application of remote sensing. The monitoring of a wide variety of environmental insults to these systems in urban areas may permit timely interventions to save or replace endangered species.

Perception of pollutants and their sources both inside and outside urban recreation resources is within the capability of remote sensing. Such pollutants have subtle and/or outrageous impacts on the use or users of facilities, and improved knowledge about them can be expected to have a direct influence on policy and managerial decisions. This is particularly true with respect to water and air pollutants.

Periodic observation of visitor attendance and use patterns at urban and suburban recreation resources will enhance the management of existing facilities and planning for future acquisition and development. Also, remote sensing can monitor environmental impact of recreation use upon recreation facilities and upon the wide variety of support systems necessary to their existence.

Many additional tactical applications of remote sensing to urban recreation planning will undoubtedly be identified as the technique is introduced into the planning process.

2.2 INDIRECT APPLICATIONS

Remote sensing can be used in the identification and monitoring of natural systems which affect urban recreation resources and their users, including geophysical, hydrological, biological and climatological. Similar applications may be anticipated with respect to man-made systems which affect urban recreation, including transportation, communications, commercial and industrial trends, agricultural development, residential patterns, demographic changes and social and economic trends.

The most important potential benefits to urban recreation planning appear to be in this indirect sphere of application, for it will enable planners to consider alternative actions in light of enormous quantities of strategic information never previously available. It will also place a new responsibility on the planners, for they will be accountable for the wide ranging and long term effects of their selected actions.

3. 1970 URBAN RECREATION BENCH MARK DATA SOURCES

Four independent studies conducted in 1970 now provide simultaneous data and information for urban recreation planning.

- The U.S. Department of Commerce Bureau of the Census conducted the 1970 decennial census which provides housing and population data for cities and for census tracts within them.
- The U.S. Department of the Interior's Earth Resources Observation Systems (EROS) program, in cooperation with the National Aeronautics and Space Administration (NASA), photographed 26 U.S. cities from aircraft at altitudes exceeding 50,000 feet to test the feasibility of detecting and monitoring urban land use changes from earth-orbiting observation satellites.
- The National Recreation and Park Association (NRPA) gathered national data for its quinquennial statistics report on local public park and recreation space, facilities, finance, personnel, programs and management.
- NRPA conducted a ground inventory and analysis of public and private open space and recreation resources in selected core area census tracts in 25 of the country's largest cities under contract to the U.S. Department of Housing and Urban Development.

Table I presents the relationship of the four studies with regard to five possible units of analysis. Table II shows the potential data interrelationships of the 1970 data obtained from the four independent studies, as well as the respective emphasis of the four studies with regard to sphere and level.

TABLE I. RELATIONSHIP OF THE UNITS OF ANALYSIS

Unit of Analysis	Study			
	U.S. Census of Population	EROS Photos	Yearbook Survey	Recreation Needs in 25 Cities
U.S. Total	X		X	
Individual States	X		X	
Selected Cities	X	X	X	X
Census Tracts (in selected cities)	X	X		X
Individual Open Space and Recreation Units		X		X

TABLE II. RELATIONSHIP OF THE LEVEL AND SPHERE OF DATA

Level	Data Sphere	Study			
		U.S. Census of Population	EROS Photos	Yearbook Survey	Recreation Needs in 25 Cities
MICRO	Social	X			X
	Physical				X
	Professional				X
MACRO	Social	X			X
	Physical		X	X	X
	Professional			X	X

4. PRELIMINARY REMOTE SENSING APPLICATION EFFORTS

The EROS flights included remote sensing of eight of the cities selected for NRPA's 25-city study: Atlanta, Boston, Denver, Houston, New Orleans, Phoenix, Seattle and Tampa. Visual inspection of color infrared enlargements was revealing.

In New Orleans, for example, a projection enlargement from an intermediate color negative of an area of approximately 50 square miles was scrutinized, the scale being about 1/50,000 (frame 025 from the Zeiss camera used on Mission 238, May 3-4, 1970, using color infrared modified by a "D" filter). When compared with field data, or with a street map or topographic map, open space and recreational land use was readily identifiable. Mini-parks in model cities areas were located, and the presence or absence of tree plantings in them and along streets and in block interiors was apparent. Closely spaced, above ground burial vaults and the inner courtyards in the Old French Quarter were observable features unique to the city. In addition to census tract boundaries, it was easy to locate Tulane University and stadium (Sugar Bowl), public and private golf courses (including fairways, sand traps and water hazards), swimming pools, playgrounds, marinas, fairground, municipal auditorium, zoo and other recreation resources.

"Ground truth" was similarly verified in Denver, Colorado, where infrared color photos of an area of about 250 square miles revealed lake and river configurations, as well as transportation linkages and residential developments influencing recreation patterns. Other infrared photos permitted the detection of Dutch Elm Disease in trees at the east entrance of Denver's City Park which were confirmed subsequently by laboratory examination. Golf courses, playing fields, and a wide variety of indoor and outdoor recreation facilities were easily perceived in this and other Denver parks. Attendance, as reflected in parking lot utilization and by groups of visitors visable in open park areas, could be roughly computed.

Main irrigation canals, streets and highways, and Sky Harbor Airport were clearly identifiable in EROS photos of Phoenix, as was the city's unique mountain park system. Small and large urban parks and golf courses and the Braves stadium were among recreation and open space resources which could be analyzed from Atlanta photos. Imagery of sprawling Houston also confirmed ground enumeration efforts with respect to the 1970 status of inner city open space and recreation opportunities.

5. FUTURE APPLICATIONS

While many photographs are now available from the 1970 flights, trends obviously will not be apparent until photos are obtained from several subsequent missions. Satellite deployment will provide important periodic monitoring of the urban areas. The prospect for urban change detection by satellite has been examined, and in a few instances, recreation facilities were study objects. Wray (17) reported on successive missions over an Arizona golf course complex:

> Preliminary work at the Phoenix urban test site analyzed gross urban land use by interpreting color infrared imagery from the Apollo IX mission in March 1969. Detectable in the space photo is a circular golf course, 1.5 miles in diameter at Sun City, a retirement community on the growing edge of metropolitan Phoenix. In the months before and after the Apollo mission, geographers . . . documented some land use change . . . In the vicinity of the initial circular golf course at Sun City the very rapid expansion of residential land use is shown in a series of conventional black and white air photos taken six months apart. The expansion is providing a second circular golf course tangent to the east of the first one where a common clubhouse will serve both . . . We anticipate that such changes in the growing edge of urban areas may be monitored from ERTS-type imagery, and that changes in the rural-urban interface are indicative of other changes.

With respect to status assessment, the EROS photographs confirmed ground observation and enumeration conducted by project field research leaders two months after the flights, and verified and updated available maps of the cities for study purposes. It is reasonable to speculate that the inventory of urban recreation resources by remote sensing will replace ground observation altogether. This prophesy is prompted not by infatuation with remote sensing, but by simple recognition that ground observation, because of its enormous cost and theoretical complexity, has never been a feasible or conventional means of acquiring urban recreation data; the 1970 HUD-NRPA study was atypical. Therefore, remote sensing is not so much a way to complement, supplement or extend old techniques as it is a means to obtain information long needed but never available.

6. CONCLUSION

Presently both high altitude aircraft photography and satellite imagery consistently confirm optimistic preliminary forcasts regarding the potential of remote sensing for urban recreation planning. Even with the caveats introduced, there appears to be justification for further development and the encouragement of studies and planning efforts which seek to bring articulation between the teachnology and the planning process.

7. SELECTED REFERENCES

1. Berlin, G.L., Application of Aerial Photographs and Remote Sensing Imagery to Urban Research and Studies, exchange bibliography 222, Council of Planning Librarians, Monticello, Illinois, September 1971.

2. Bigler, Richard A., "Infrared: New Tool for Park Planners," Parks and Recreation, February 1972.

3. Bowden, L.W., "Sensing Land Pollution," paper presented at Joint Conference on Sensing of Environmental Pollutants, Palo Alto, California, November 8-10, 1971.

4. Branch, Melville C., City Planning and Aerial Information, Harvard University Press, Cambridge, Massachusetts, 1971.

5. Colwell, Robert N., "Uses of Aerial Photographs in Forest Recreation," Photogrammetric Engineering, March 1950.

6. Conference Papers, Conference on Land Use Information and Classification, cosponsored by U.S. Department of the Interior Geological Survey and the National Aeronautics and Space Administration, Washington, D.C., June 28-30, 1971.

7. Douglass, Robert W., Application of Remote Sensing Techniques to Water Oriented Outdoor Recreation Planning, U.S. Department of the Interior Geological Survey Interagency Report USGS-191 (Technical Report 69-2), Washington, D.C., January 1970.

8. Dunn, Diana R., "1970: Urban Recreation and Park Data Bench Mark Year," Parks & Recreation, February 1971.

9. Griffiths, Thomas B., et al., Developing Remote Sensing Display Modes to Satisfy Urban Planning Data Input Needs, U.S. Department of the Interior Geological Survey, Interagency Report USGS-207, Washington, D.C., January 1971.

10. Harker, George R. (ed.), Proceedings: Remote Sensing Conference for Recreation and Resource Administrators, sponsored by Department of Recreation and Remote Sensing Center, Texas A&M University, College Station, Texas, December 9-10, 1969.

11. Howard, William A., "Infrared: Battles Dutch Elm Disease," Parks & Recreation, February 1972.

12. Kracht, James B., and Howard, William A., Bibliography: Applications of Remote Sensing, Aerial Photography, and Instrumental Imagery Interpretation to Urban Area Studies, U.S. Department of the Interior Geological Survey, Interagency Report USGS-199, Washington, D.C., August 1970.

13. Latham, James P., "Urban Applications of Remote Sensing," The Geographical Review, No. 1, 1971.

14. Reed, Wallace E., et al., Remote Sensing as a Source of Data for Outdoor Recreation Planning, prepared for the Department of the Interior Bureau of Outdoor Recreation by the University of Virginia, January 1972.

15. Sattinger, Irvin J., "Satellites to Monitor Earth Resources," Parks & Recreation, December 1971.

16. Wray, James J., "A Remote Sensing System for Detecting Gross Land Changes in Metropolitan Areas," paper presented at the Conference on Land Use Information and Classification, cosponsored by USGS and NASA, Washington, D.C., June 28-30, 1971.

17. _____, "The Census Cities Project: A Status Report for 1971," paper presented at the NASA Fourth Annual Earth Resources Program Review, Manned Spacecraft Center, Houston, Texas, January 17-21, 1972.

REMOTE SENSING IN THE DETECTION OF REGIONAL CHANGE[1]

J. E. Estes and L. W. Senger

Geography Remote Sensing Unit
University of California
Santa Barbara, California

ABSTRACT

A major indicator of the regional transformation processes which take place in an area are the changes in general land use characteristics. Land use changes were investigated in the West Side of the San Joaquin Valley, an area presently undergoing regional transformation, utilizing United States Department of Agriculture airphoto mosaics and high altitude NASA photography for the dates 1957 and 1971. Attention was focused on land use characteristics for the two dates, changes which had taken place, and the sequence of land use category change. Research indicated overall regional change trending from an oil-producing and grazing area into a cropping region. Furthermore, the general pattern was moving in the direction of higher economic intensity land use succession. Findings indicate satellite data, e.g. ERTS-type, should be capable of providing similar information. Satellite imagery acquired over short time intervals, in conjunction with automated display techniques, could then make significant contributions to theory concerning regional transformation processes and land use change detection.

1. INTRODUCTION

Pressure from increasing population is intensifying demands upon the environment. Both the use and quality of environmental resources are undergoing rapid and constant change. If the utilization and quality of environmental phenomena are to be maintained and/or improved, earth scientists must be able to understand, monitor, and predict patterns of change. Since change in any given area may have both internal and external effects, there is a need to view the phenomena within a broad synoptic context. City and county planning agencies are already in the process of joining, combining, and developing into regional planning groups. Basic information is important at all levels, and, as these small area groups combine, problems of compilation and assimilation of regional data are compounded.

The Geography Remote Sensing Unit at the University of California, Santa Barbara is presently conducting an investigation of the impact of the California State Water Project on the West Side of the San Joaquin Valley of California. The West Side is an arid area, where lack of an adequate water supply has inhibited any intensification of the development of the region. The availability of water from the California Aqueduct has altered the situation, and the area is currently undergoing a process of regional transformation. One of the significant indicators of the nature and degree of this transformation is general land use. The major objectives of the land use investigation currently being conducted in the West Side include: 1) the compilation of sequential land use maps to determine gross land use change; 2) detailed examination of particular land use categories to detect specific patterns of development emerging; 3) as an outgrowth of these objectives, to interface West Side land use data with classification systems generated in other areas in order to develop a workable system for automated mapping of regional change; and 4) using

[1]This work was supported by the National Aeronautics and Space Administration Grant Number NGL 05-003-404.

Preceding page blank

data generated by remote sensing, to evaluate a theoretical model of the development of agricultural regions as formulated by Spencer and Horvath.

At the present stage of investigation, the latter two objectives have not yet been achieved. Emphasis in this paper has therefore been placed on the first two objectives, gross land use change and the patterns of that change. The remainder of the paper is divided into four sections which concern these objectives. A brief historical background to West Side land use is provided to indicate developmental trends within the study area. The next section explains the methodology utilized in the land use investigation. The following section considers the results of the investigation, in terms of the data generated and the analysis that was performed. Finally, conclusions are presented with respect to the study area and its wider implications.

2. BACKGROUND TO STUDY AREA

The West Side is fairly typical of arid environments where the lack of water has placed severe constraints on the pattern of human occupance. The earliest known inhabitants of the West Side were Indians who possessed a relatively low level of technology. They were able to exploit the area's environmental potential in a limited fashion, basically through hunting and gathering activities. Population densities were low and stress on the environment was minimal. The Spanish arrived in the late 1700's. Despite their limited technological capacities, they turned the area into an extensive rangeland and, as is done today, grazed sheep and cattle. A limited amount of irrigation agriculture was practiced, primarily for subsistence purposes. Population densities, although still low, increased and greater stress was placed on the area's limited resources.

The change over to American dominance of the West Side, after California became a state, led to further intensification of land utilization. Grazing continued to be the principal land use, but more acreage was now put into crops (particularly wheat). Pump water irrigation systems began to be employed to provide water for the wheat crop.

By 1900, oil had acquired value owing to extraregional technological advances (a changing energy base orientation within the United States as a whole). The mineral had been known to exist in the West Side, but there had been no extensive use of it. When the national situation changed, the hills of the West Side were drilled for the now valuable product. Oil wells dotted the landscape and became the dominant economic land use. Grazing, which can be compatible with oil extraction, continued as an important land use (in terms of area utilized rather than dollar value), while crop acreages stabilized or declined owing to lower water tables (due to extraction from aquifers above the levels of their ability to replenish themselves for agricultural purposes) as well as the increased costs of pump irrigation.

This was essentially the situation up to the 1960's. Patterns of land use continued to intensify, while population densities increased at a slower rate. Pressure on limited environmental resources increased with concurrent changes in the composition of natural vegetation associations and marked lowering of water tables. Conditions had reached the stage where further growth of the area was inhibited by the lack of a sufficient water resource.

In 1960, the California State Water Project was financially authorized to direct excess waters from the northern third of the state to southern portions. This introduced a new factor into West Side development, a substantial, although limited, new source of water supplies. An additional factor which could enhance expansion was provided by the proposal, and now actual, construction of a segment of Interstate Highway 5, connecting San Francisco and Los Angeles. The new freeway passes along the eastern portion of the West Side, providing the area access to major urban centers on a here-to-for unknown scale. By 1968, water was being delivered in limited quantities to the area and considerable sections of Interstate 5 were in the process of being constructed. New lands were being brought under cultivation and formerly abandoned acreages were once more being cropped. The process of regional transformation of the West Side had begun.

3. METHODOLOGY

In order to evaluate Aqueduct-related changes on the West Side, land use maps were constructed for the dates 1957 and 1971. USDA air photos were available for 1957, and this time period represented a relatively stable situation in the development of West Side land use. Agricultural land use had expanded as far as practical with pump well irrigation, and other land use patterns were similarly well-established and essentially stabilized. The area had also been imaged on photography flown by the NASA RB-57 in 1971. By 1971, the boom in new agricultural land had slowed and the rate of change had begun to level off. The 1971 photography, therefore, permitted an analysis of Aqueduct-induced changes in the pattern of land use. Although USDA photographic coverage of the area existed for 1967, it was decided not to use the photos because some changes were already occurring at that time in anticipation of Aqueduct water.

For mapping purposes, general land use categories were chosen which were considered compatible with satellite resolutions. Further considerations in their selection were to simplify identification, reduce interpretation errors, and provide a format amenable to modification in order to make it compatible with land use classification systems being tested elsewhere. The categories included transportation networks, settlements, oil extraction, cropland, grazing, and non-productive.

Two types of maps were produced to obtain measures of the nature and degree of gross general land use change. The first type involved a set of maps for the 1957 and 1971 dates illustrating the total land use picture for each date. This provided an overall view of the land use situation for each of the selected years. The second type consisted of a set of maps showing the areas which had changed between the two dates. The first map delimits the areas that changed and what the land use categorizations were for those areas in 1957. The second map of the set shows the same areas and what the land use had changed into by 1971. The two types of land use maps generated were then overlain with a square grid to derive a quantitative estimate of the acreage in each land use category found on the West Side at the two base times. Using the maps and the quantitative measures, it was possible to describe the land use characteristics of the region at the two dates, locate areas and categories of change, and identify the sequence and degree of change which took place between the two base times.

4. RESULTS

The status and distribution of land use in 1957 and 1971 is illustrated graphically by the two maps in Figure 1. A quantitative estimate of land acreages in the non-urban land use categories was obtained from the maps using a square grid overlay. The results of this estimation procedure are displayed in Table I. The 1957 period is characterized primarily by grazing and cropland. Grazing, some 51% (1,440,000 acres) of the total area, dominates cropland, 38% (1,095,000 acres), in terms of areal extent. Oil extraction, 4% (116,000 acres), and non-productive land, 7% (205,000 acres), occupy significantly less area. By 1971, the pattern showed definite indications of change. Cropland, with 43% (1,233,000 acres) of the total areal extent, appears on its way to achieving parity with grazing, now at 47% (1,330,000 acres) of the total acreage. Oil extraction has expanded significantly to 6% (174,000 acres), and non-productive land is on the decline at 4% (109,000 acres).

In terms of an overall pattern of change in the 14-year period, cropland has increased in areal extent by almost 13% (138,138 acres), while grazing has decreased by some 7% (100,454 acres). Oil extraction has expanded in area by a dramatic 51% (58,778 acres), while non-productive land declined by some 47% (96,461 acres). About 19% (519,885 acres) of the total area of 2,855,425 acres underwent a change from one land use category to another.

A more detailed breakdown of the nature of the change can be seen in Figure 2. The two maps portray the various categories that changed and the distributional pattern of the changes. More than twice as much grazing land was converted into cropland than vice versa, while non-productive land was changed into both cropland and grazing land in about equal amounts. Oil extraction expanded mainly into those areas adjoining regions producing in 1957, at the expense of both cropland and grazing land. The non-productive category appears to have absorbed minor acreages from the other three categories, while suffering major losses. Of the more than one-half million acres of land that changed, the majority went into cropland, 46% (238,899 acres), or grazing, 30% (158,618 acres). Negligible amounts changed to the other categories.

The above changes may also be examined as a function of the economic intensity of the land use. In this scheme, oil extraction represents the highest economic intensity, cropland second, grazing third, and non-productive land as the least economically intensive. Using these criteria, 86% (86,733 acres) of cropland changed to a lesser economic intensity, while 14% (14,029 acres) converted to a higher usage. With respect to grazing land, 92% (239,002 acres) went to a higher intensity, while 8% (20,070 acres) changed to a lesser usage. Areas of oil extraction which changed (26,931 acres) converted to lesser economic intensity, while non-productive land (133,120 acres) all changed into higher land usage. Of the total area that changed, 26% (133,734 acres) was converted to lesser economic uses, and 74% (386,150 acres) went to higher economic intensity.

5. CONCLUSIONS

Information derived from the mapping and tabulating of data acquired in this study indicates a definite trend towards the development of an agricultural landscape and increasing intensification of land use on the West Side of the San Joaquin Valley, California. The introduction of water into this arid region is resulting in large acreages of land being brought under cultivation. Consequently, cropland is assuming a more dominant position with respect to areal extent. At the same time, there is a trend towards increasing intensification of all land uses. The sequence of change is predominantly in the direction of higher economic intensity land use succession. There is some retreat to less intensive usage, but this appears to be a relatively minor component of the overall pattern.

The most significant implication of the study, based on the general nature of land use categories mapped, is the potential capability of satellite data to document the changes discussed above. As more data are collected over shorter intervals of time from ERTS-type satellites, it may be possible to refine assumptions concerning the nature and character of regional change. As technological developments permit large tracts of presently non-productive land to be brought into production and urban areas encroach on already productive land, the ability to monitor and predict the areas and rates of these changes becomes quite important. By putting the base maps of this study into computer format, periodically updating them, and automatically printing areas of change and non-change, a detailed assessment of the processes affecting, and actually producing, change in an area might be made.

Table 1. NON-URBAN LAND USE 1957 AND 1971 WEST SIDE SAN JOAQUIN VALLEY

LAND USE CATEGORY	1957 (ACRES)	1971 (ACRES)	NET CHANGE (ACRES)
Cropland	1,094,926.3	1,233,063.9	+ 138,137.6
Grazing	1,439,843.3	1,339,388.9	- 100,454.4
Oil Extraction	115,575.0	174,352.6	+ 58,777.6
Non-Productive	205,080.6	108,619.8	- 96,460.8
Total	2,855,425.2	2,855,425.2	

Table II. LAND USE CHANGES 1957 - 1971

1957	1971 Land Use Changes In Acres				
	Cropland	Grazing	Oil Extraction	Non-Productive	Total
Cropland		71,475.2	14,028.8	15,257.6	100,761.6
Grazing	167,321.6		71,680.0	20,070.4	259,072.0
Oil Extraction	6,758.4	18,841.6		1,331.2	26,931.2
Non-Productive	64,819.2	68,300.8			133,120.0
Total Change in Land Use Acreage	238,899.2	158,617.6	85,708.8	36,659.2	519,884.8

Net Change In Land Use Categories (Acres)

Cropland

Loss: 100,761.6
Gain: 238,899.2
Change: +138,137.6

Grazing

Loss: 259,072.0
Gain: 158,617.6
Change: -100,454.4

Oil Extraction

Loss: 26,931.2
Gain: 85,708.8
Change: +58,777.6

Non-Productive

Loss: 133,120.0
Gain: 36,659.2
Change: -96,460.8

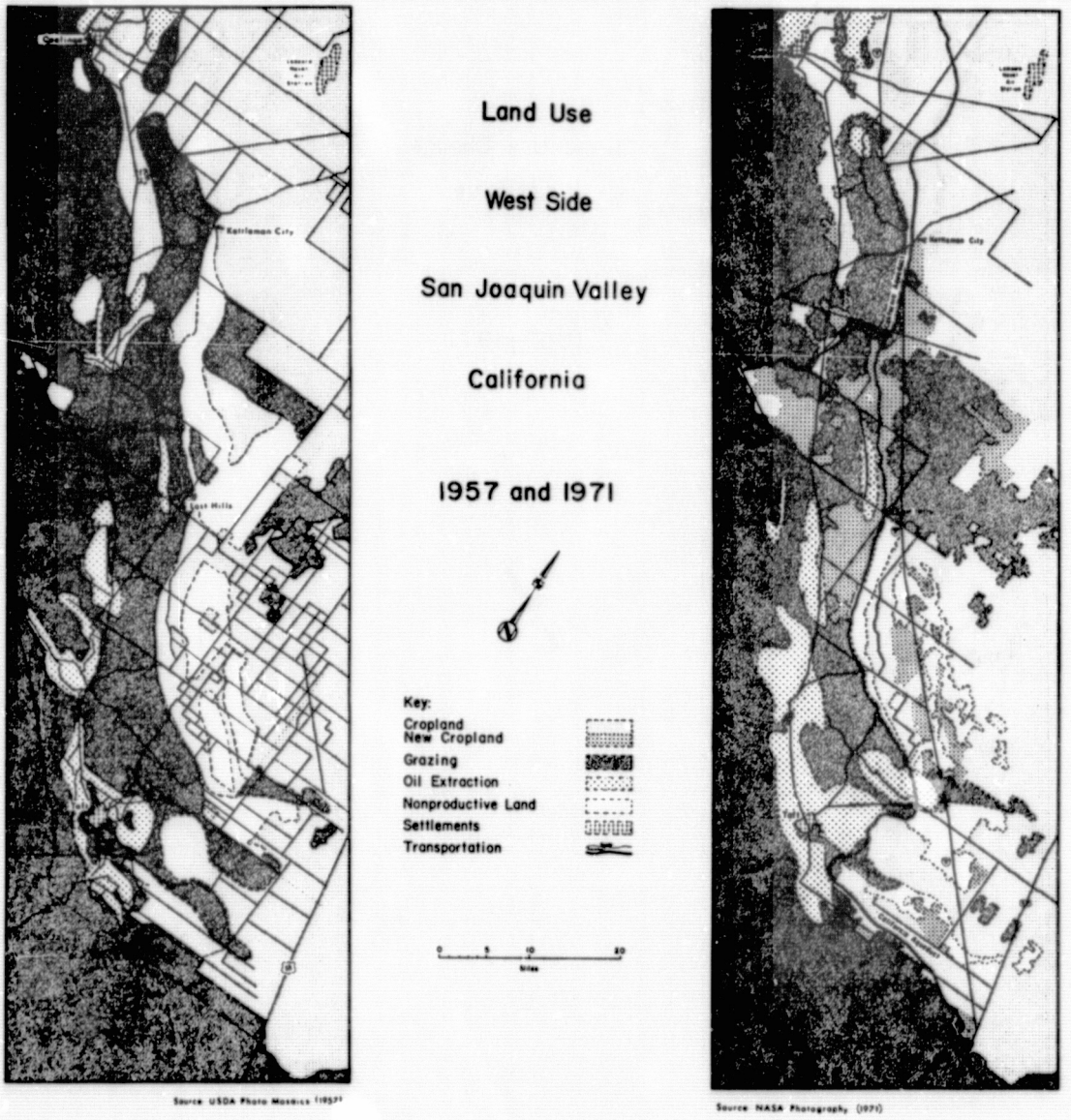


Figure 1. Land Use 1957 and 1971.

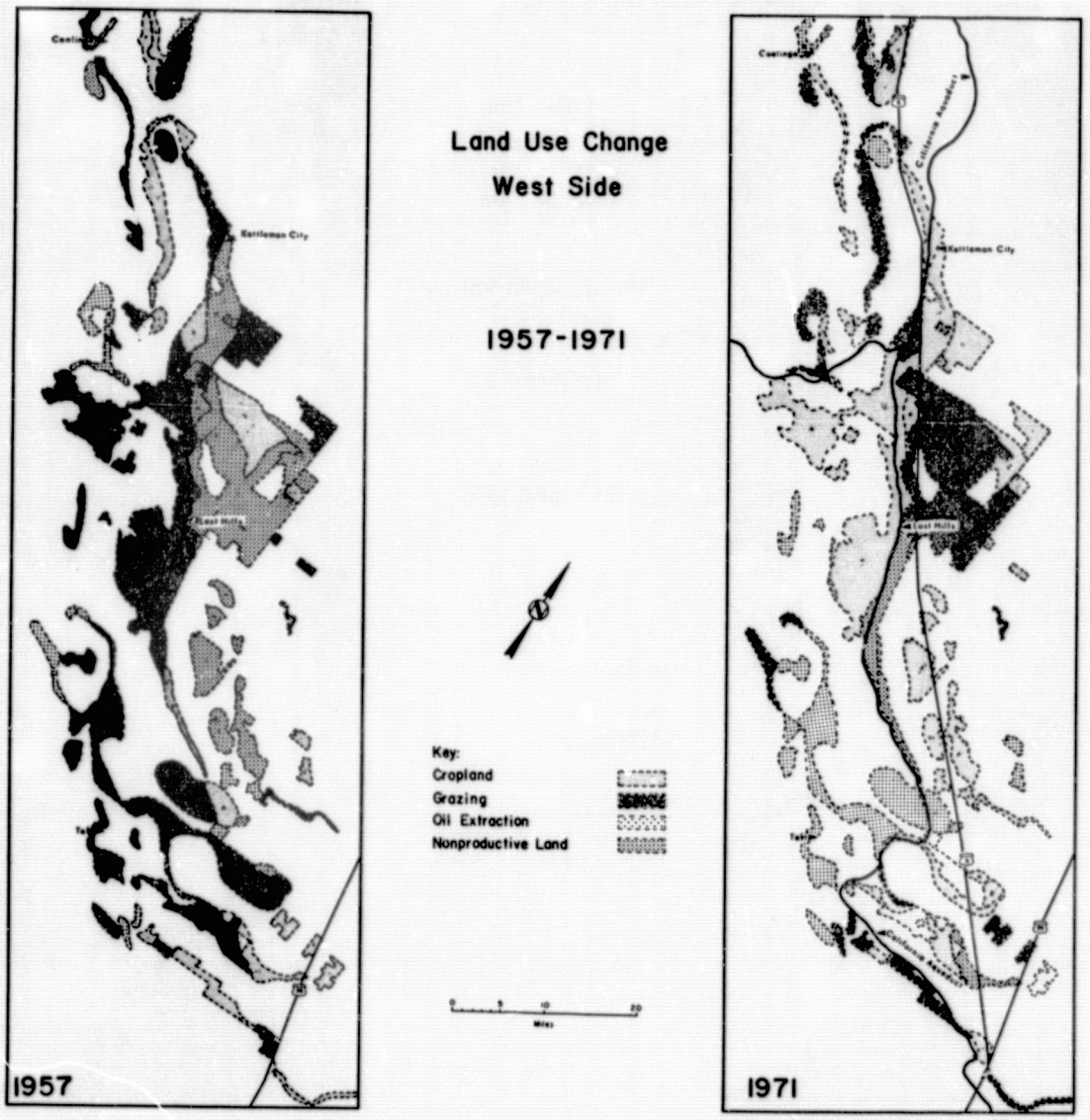


Figure 2. Land Use Change From 1957 to 1971.

THE USE OF SMALL-SCALE MULTI-BAND PHOTOGRAPHY FOR DETECTING LAND-USE CHANGE[1]

Harry F. Lins, Jr. and Valerie A. Milazzo

Geographic Applications Program
U.S. Geological Survey
Washington, D.C. 20242

ABSTRACT

Recent small-scale photography from two separate high-altitude NASA aircraft missions was used to map land use and detect land use change for both an urban and rural study area. Photographic frames in three spectral bands from each mission were combined on the I²S additive color viewer from which land use for both time periods was mapped using a high altitude compatible land use classification scheme. Resultant land use and land use change maps were produced which indicated that authentic changes in land use could be detected. In addition, the change maps showed strikingly a number of apparent land use changes at points where, in reality, no change occurred. The detection of these "false change areas" can be attributed, in part, to inherent inconsistencies that arise when analyzing photography from two separate systems on a comparative basis. These inconsistencies also illustrate the need for control in the photo processing stage.

1. INTRODUCTION

With the recent advent of repetitive high-altitude flights over selected test sites within the United States, a large quantity of small scale imagery has become available for study. Until now, little has been done to implement small scale imagery in land use mapping and change detection. This paper documents a study in which small scale photography is used to determine to what level land use and land use change can be detected between two time periods for two environmentally different areas, one urban and one rural (Figure 1).

The urban area occupies approximately 250 square miles just east of Washington, D.C. It borders the 1970 census defined limit of the Washington, D.C. urbanized area and as such is an area experiencing dynamic growth as evidenced by the rapid conversion of farmland to urban use. The rural test site covers about 100 square miles on the Eastern Shore of Maryland stretching from the town of Easton, south to Cambridge. This region is primarily agricultural with most of the land being devoted to crops and pasture. As might intuitively be inferred, it is an area of little change both temporally and spatially.

For each test area, photographic frames in three spectral bands were selected from two sensor systems, the 40 mm Hasselblad 500 EL and the 44.3 mm Vinten System A (Figures 2 and 3). Each produces imagery in the green, red, and near infrared spectral bands on a 70 mm format. The Hasselblad photography was acquired for the USGS Geographic Applications Program by an RB-57 aircraft during NASA Aircraft Mission 144 on September 22, 1970, from an altitude of 60,000 ft. at an image scale of 1:450,000. The Vinten photography was obtained from a U-2 aircraft during NASA ERAP (Earth Resources Aircraft Project) Flight 71-032, flown on September 15, 1971 at an altitude of 65,000 feet and at an image scale of 1:470,000.

[1]Publication authorized by Director, U.S. Geological Survey.

2. LAND USE MAPPING

Land use mapping was performed with the aid of the I^2S Mini-Addcol additive color viewer. Each of the three frames in the green, red, and infrared bands were combined and registered to form a false color infrared composite at a 2.6 times magnification. Stable-base frosted Herculine drafting film was placed over the projection screen and land use interpretations were traced directly onto it. Only the land use boundaries were outlined and categories were number coded for identification. Land use was interpreted according to a prototype classification scheme developed by the U.S. Government Inter-Agency Steering Committee on Land Use Information and Classification (Figure 4). For the scale of the analysis (approximately 1:200,000), the minimum mapping size was a use pattern of 20 acres. Land use was mapped at the Level II category. It was found that land uses corresponding to Level II discrimination could be identified and, for the most part, extracted from the imagery for both the urban and rural test areas with an acceptable degree of accuracy (Figures 5, 6, 7, 8).

Land use was first mapped using the Hasselblad photography (1970). The photographic quality and resolution, for the discrimination level of the land use classification used, permitted the interpretation of both urban and non-urban land use to proceed with relative speed and ease. One problem that was encountered in the land use analysis for the urban area was that full coverage of the test area required two frames for the 1970 mission and three frames for the 1971 mission. A further complication arose in getting identical coverage of the area for both periods because of the different flight azimuths between the two missions. This increased registration difficulties (beyond normal rotational shifts) not only between photos for one time period but among photos, and interpretations thereupon, between the two time periods. Since the images were unrectified and boundaries were not plotted onto a rectified base, differences in photo orientation and consequently of land use boundaries between photos due to minor differences in rotation, tip, tilt, shift, etc. in the adjustment of the viewer occurred among the images and interpretations. This necessitated a certain amount of cartographic correction and editing to place the land use boundaries in their proper positions on the final land use map.

In some cases, interpretation difficulties were encountered concerning identification of certain land uses. This resulted not only from mis-interpretation on the part of the analyst but also from resolution and scale constraints imposed by the photography being used. In land use interpretations for both time periods, as might be expected, most change areas (bare ground) and cultural features showed up strikingly well due to lighter tonal contrast with the remaining features. However, even though bare ground areas could be distinguished easily from the rest of the scene, some difficulty arose as to their classification as either "open land" or "extractive industry" namely sand and gravel pits. In some instances it was apparent that the feature was a sand and gravel operation as inferred from such surrogates as road pattern, presence of industrial ponds, etc., but in other cases, lack of such detail precluded definite identification of the use as extractive. Familiarity with the area, however, indicated that there is an abundance of sand and gravel extraction operations. Thus, for most bare ground areas where there was some question as to the land use present, "extractive industry" was the category applied.

To help overcome some of the interpretation difficulties encountered in the analysis and to corroborate land use interpretations, larger scale photographs and topographic maps were used as supplemental reference sources when needed. In addition, some experimentation with different filter and intensity combinations was performed on the additive color viewer to investigate possible enhancement of certain land use features. There was no magical response or signature appearance that popped up for any one land use feature. As Don Ross of International Imaging Systems has pointed out: "Some (users) have been led to expect the image information related to their specialties to be presented in clear, unmistakable form as

the knobs are turned. Alas there are few if any unique spectral signatures in nature" (Ross, 1972). One interesting combination, however, which seemed to enhance the forest/agriculture contrast quite well was achieved by projecting the green band through a clear filter, the red band through a blue filter, and the IR band through a red filter. By varying the intensities of each of the bands until contrast was at a maximum, discrimination of forest and agricultural lands was facilitated. Other than this combination, time constraints precluded any further experimentation to determine any optimum film/filter/light intensity combinations for the discrimination of land use types.

Apart from combining the three spectral bands to form the false color infrared image from which the majority of the interpretation was taken, each spectral band was viewed singly on the viewer through a clear filter. This technique did indicate that for both urban and rural areas, certain land use features appeared differently in each band. For example, on the photography used in this study, the green band alone appeared to show a slightly sharper contrast between forest and agricultural land than did the other two spectral bands. On the other hand, the red band enhanced the contrast between heavily vegetated areas and extensive cultural features, such as suburban residential subdivisions. In addition to the massed cultural features, bare ground areas and sand and gravel operations showed up vividly on the photo due to a lighter and brighter tonal appearance.

The black-and-white infrared band from the Hasselblad set was fair in that different land use features could be seen by tonal variations, although the overall appearance of the IR image was washed out. In contrast, the IR image taken by the Vinten system was of very poor quality. Most features were almost completely washed out and thus, indistinguishable. In addition, bright streaks of static electricity appeared across several of the frames which obscured parts of the photograph. This may have been responsible, in part, for the poorer image quality and subsequent interpretation difficulty of the Vinten photography when this band was combined with the others on the I^2S Viewer. For both camera systems, the IR was of sufficient quality to show marked land/water contrasts and was useful for delineating the land/water interface.

3. CHANGE DETECTION

Following the mapping of land use for both time periods, the change detection phase of the analysis was begun. Before changes in land use could be mapped, some cartographic steps had to be taken to eliminate unnecessary discrepancies in the two interpretations and to prepare for the subsequent comparison of land use change.

For both the 1970 and 1971 missions, interpretations taken from the separate photos had to be reregistered and combined onto one overlay. These steps involving the redrawing of the land use boundaries were necessary due to slight rotational shifts between the photos causing misregistration and orientation differences of the same land use areas taken from different photos, and scale differences between the interpretations taken from the Hasselblad and Vinten photography. Thus, on the new tracing of the land use areas, the boundary lines were edited, i.e., homogeneous use areas were consolidated, areas were checked for proper number identification, and categories of use were examined for consistency of identification and coding.

When redrafting the boundaries for the 1971 data, the interpretations from the 1970 data served as a reference base. To eliminate excessive and unnecessary variations in land use boundary interpretations for the 1971 material, land use boundaries that looked as though they were the same as those for 1970 (even though they were not drawn identically) were adjusted on the new overlay. This was strictly a judgment decision. In cases where the boundary line deviated significantly from the same land use for the two time periods, or where the land use changed from one category to another, larger scale photography and maps were checked to confirm whether or not this was a legitimate change.

After rectifying the land use boundaries for both years, the overlays were superimposed and land use areas compared. Another overlay was drawn identifying only those land use areas that changed from one use (Figures 9 and 11) to another (Figures 10 and 12) over the one year time span. Changes that occurred that were smaller than the minimum mapping size and thus absorbed in the more dominant use were not mapped but in some instances were visible.

3.1 URBAN

For the urban area at the Level II classification, selected areas of land use change could be detected and mapped using the small scale Vinten photography. Figure 10 shows the areas of land use change that occured within the one year time period. As can be seen, most of the change occured in the croplands and pasture and residential categories. The increase in agricultural land, however, seems dubious (for several reasons which will be pointed out later). However, the increase in residential land use at the urban fringe shows strikingly the outward growth of the urbanized area. Another noteworthy feature of the land use change map is indicative in most instances of increased clearing of land to make way for further residential subdivisions, many of which were already under various stages of development. Figure 9 shows clearly that the dominant transition in land use was from forest to agriculture, and agricultural land, in turn, to open and residential land use. This conversion reflects again the apparent growth of the urbanized area fringe.

The two overlays reflect not only the actual changes in land use that occurred in the one year interval, but also indicate apparent changes in use at points where, in actuality, there may have been no change at all. This detection of change at points of no change can be attributed to differences in the two sets of photography from which the land use information was extracted. Because the Vinten photography had an overall poorer resolution than that of the Hasselblad, there was a loss of detail in the mapping of land use categories. As a result, for the 1971 analysis there was more homogeniety of land use since the smaller land use areas were grouped and classified along with the larger use areas which gave the impression that a change in land use had occurred. It is probably safe to say that a large percentage of the change portrayed on the change detection map is due to this factor. Unlikely change conversions showing on the overlay, such as residential to crops and pasture and other more intensive uses to those less intense are, in all probability, not actual instances of change but rather "false change areas" mapped at points where no change occured. From analyzing both land use maps, this loss in more intensive land use is readily apparent especially in the area just north of Route 50 and west of Bowie, Md. (center top third of Figures 9 and 10) where a predominantly residential area changed to agricultural usage. Even with these difficulties encountered in land use change assessment, the ability to detect authentic changes in land use from high-altitude, small scale photography has been demonstrated.

3.2 RURAL

The detection of land use change at the Eastern Shore test site turned out to be something less than what had been expected. Due to the incompatibility of the two sensor systems used in this study, accurate determinations of land use change were not easily made.

From field observations it appeared that very little change had occured since the flight in September, 1970, although on the photography obtained in September, 1971 this would not be the case. The interpretation made from the latter photography showed a number of small areas which changed, mainly from forest to cropland and from cropland to wetland, which in reality have not changed at all. Another apparent change which turned out to be a misnomer was the declining size of the residential area of Easton, Maryland. There were other areas which exhibited minor change but due to the incongruencies which appeared in some larger, more

easily identifiable areas, i.e., Easton and some forest tracts, remarks on the validity of such apparent land use changes whould be made reluctantly. All of this explanation is based on interpretations made using the additive color viewer at a 2.6X enlargment.

4. PROBLEMS ENCOUNTERED

Although the two sensor systems exhibit, superficially at least, many similar characteristics, the sets of photography from each were markedly different. In an attempt to discover the reason or reasons for this unexpected difference a survey was made of the variables involved in photo acquisition (Figure 13). The time of year was very nearly the same (51 weeks apart); there was less than an hour's difference in the time of day; the spectral bands, except for the infrared were very close; the film types were identical; lens focal lengths were nearly the same, flight altitudes were close (the differences in lenses and altitudes cancelled each other).

With all these variables so closely matched it seemed apparent that the difference in photography was arising from something else. Having seen Vinten photography of the Phoenix, Arizona area which was equal to the quality of the Hasselblad photography of Mission 144, it was apparent that the systems were in fact quite similar. The obvious alternative was then to assume that there were inconsistencies in the photo processing. The two systems match so closely in all other respects that it would appear that given a well controlled, consistent photo processing stage, the photo sets would be close enough (in terms of tone, contrast, etc.) to make reliable land use and land use change determinations.

5. SUMMARY

Based on the work completed to date it would appear that land use mapping and change detection operations can be effectively performed using small-scale photography. The degree of accuracy to which these operations can be accomplished is a function of two major factors, these being 1) classification scheme used - there is a need for using a classification which is detailed enough to encompass small area features, but one that is also broad enough to maintain an acceptable level of interpretation accuracy. The classification used in this study conforms quite well to both of these criteria: 2) quality of photography - in order to perform reliable land use interpretations it is necessary to have good quality photography. When photographs from two time periods are being analyzed for change it is imperative that the photography for both periods be consistent with regards to contrast, scale, ground resolution, and spectral bands. This particular problem has two control areas, image acquisition and image processing. The need for consistency in the operation of aircraft and instrumentation is apparent but of equal importance is the need for consistency in the method and performance of photo processing. Special care should be given to maintaining equality in spectral density and film gamma. It seems apparent at this time that given stricter and more consistent control at these two critical points photography obtained at high-altitude and at small scale can effectively and efficiently be used to map land use and denote land use change.

6. REFERENCES

Colvocoresses, A. P., 1970, "ERTS-A Satellite Imagery," Photogrammetric Engineering, v. 36, no. 6, pp. 555-560.

Doyle, F. J., 1967, Mapping from Satellite Photography, American Society of Photogrammetry, National Science Foundation, Visiting Scientist Program.

Eyre, L. Allan, 1971, "High-Altitude Color Photos," Photogrammetric Engineering. v. 36, no. 11, pp. 1149-1153.

International Imaging Systems, 1971, Maintenance and Operating Manual for the I²S MINI-ADDCOL Additive Color Viewer, Mountain View, California.

Lent, J. D., and Thorley, G. A., 1969, "Some Observations on the Use of Multiband Spectral Reconnaissance for the Inventory of Wildland Resources," Remote Sensing of Environment, v. 1, pp. 31- 45.

Poulton, C. E., Faulkner, D. P., and Martin, N. L., 1971, A Procedural Manual for Resource Analysis with Supporting Appendices, Application of Ecology and Remote Sensing in the Analysis of Range Watersheds, Final Project Report, Range Management Program Agricultural Experiment Station, Oregon State University, Corvallis in cooperation with U.S. Department of the Interior, Bureau of Land Management.

Ross, D. S., 1972, Simple Multispectral Photography and Additive Color Viewing, Paper presented at the 38th Annual Meeting of the American Society of Photogrammetry, Washington, D.C., March 12-17.

Rudd, R. D., 1971, "Macro Land-Use Mapping with Simulated Space Photos," Photogrammetric Engineering, v. 37. no. 4, pp. 365-372.

Short, N. M., and MacLeod, N. H., Analysis of Multispectral Images Simulating ERTS Observations, NASA, Goddard Space Flight Center Report, Number X-430-72-118, 1972, pp. 1-22.

Simonett, D. S., and Coiner, J. C., 1970, The Susceptibility of Environments to Low Resolution Imaging, Appendix 6 of Third Annual Report, University of Kansas, under Contract USGS 14-08-0001-12077.

Waltz, D. M., 1968, Technological Base for Planning of Spaceflight Missions to Obtain Data on the Earth's Resources," Paper presented at the Fifth Annual AIAA Meeting, Earth Resources Session, Philadelphia, Pennsylvania, October 21-25.

Welch, R., 1972, "Quality and Applications of Aerospace Imagery," Photogrammetric Engineering, v. 38, no. 4, pp. 379-398.

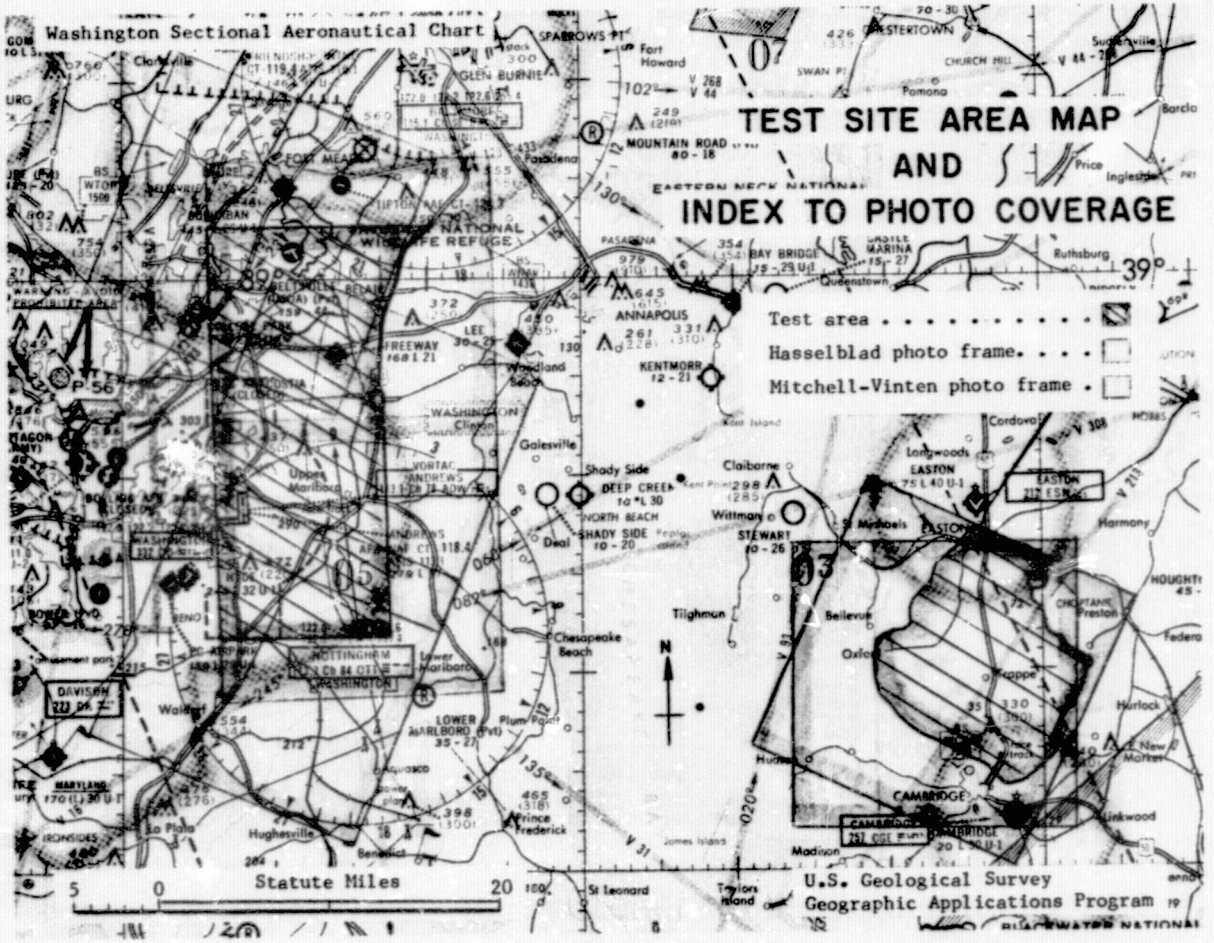
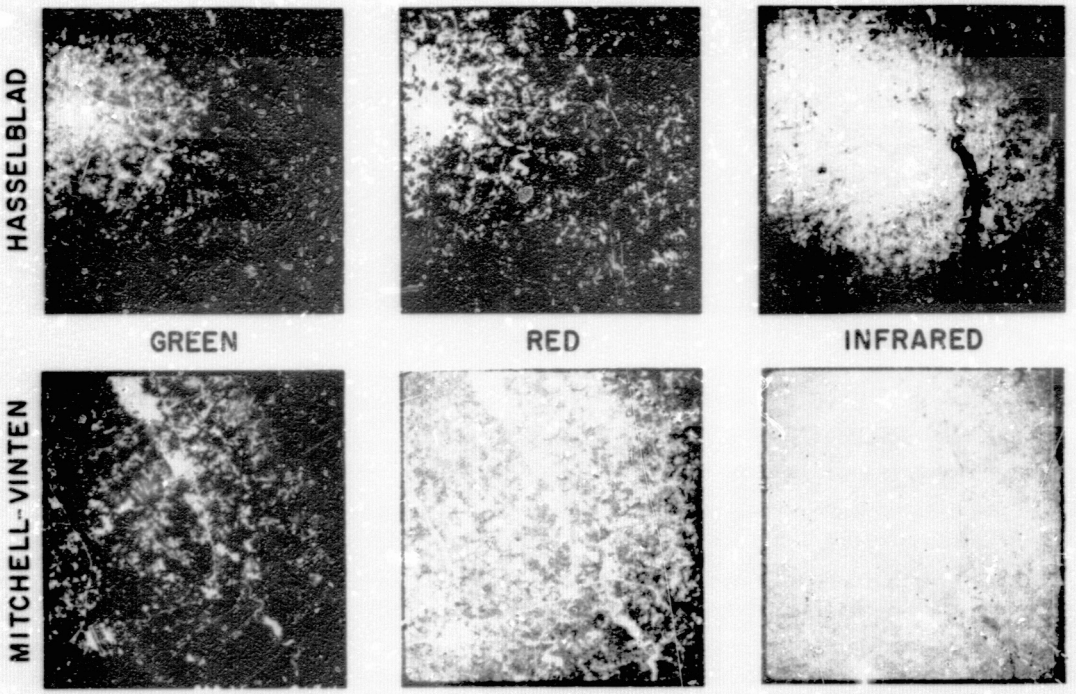

Washington Sectional Aeronautical Chart
TEST SITE AREA MAP
AND
INDEX TO PHOTO COVERAGE
Test area . . . . . .
Hasselblad photo frame. . . .
Mitchell-Vinten photo frame .
Statute Miles
5 0 20
U.S. Geological Survey
Geographic Applications Program
ANNAPOLIS
EASTON
CAMBRIDGE
Chesapeake Beach
Shady Side
Galesville
Tilghman
Bellevue
Oxford
Hurlock
Hughesville
Prince Frederick
Waldorf
Lower Marlboro
Deal
Claiborne
Wittman
STEWART
Madison
Taylors Island
St Leonard
Fort Howard
Pasadena
Woodland
Queenstown
Ruthsburg
Harmony
Federalsburg
Linkwood
New Market

FIGURE 1

Urban Area

SAMPLE HASSELBLAD AND MITCHELL-VINTEN PHOTO FRAMES



U.S. Geological Survey

Geographic Applications Program

FIGURE 2

Rural Area

SAMPLE HASSELBLAD AND MITCHELL-VINTEN PHOTO FRAMES

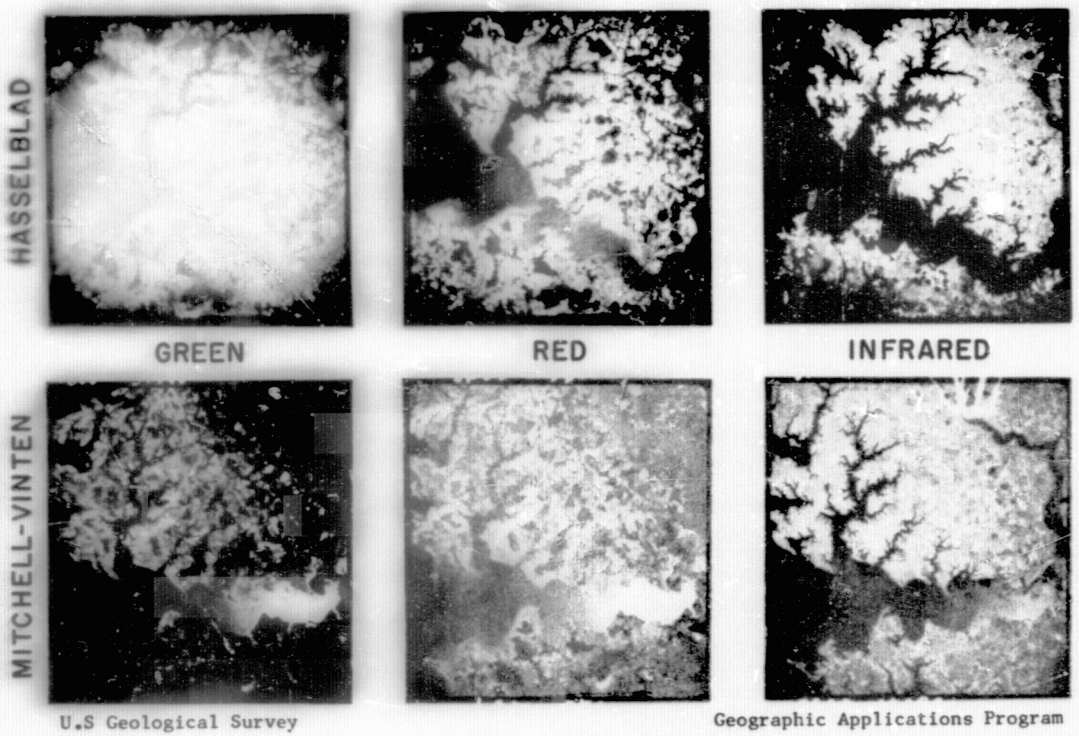


FIGURE 3

A LAND USE CLASSIFICATION SYSTEM FOR USE WITH REMOTE SENSOR DATA

Level I	Level II	Level I (Digit)	Level II (Digit)
Urban & Built-up		01	
	Residential		01
	Commercial & Services		02
	Industrial		03
	Extractive		04
	Major Transport Routes & Areas		05
	Institutional		06
	Strip & Clustered Settlement		07
	Mixed		08
	Open & Other		09
Agricultural		02	
	Cropland & Pasture		01
	Orchards, Groves, Bush Fruits, Vineyards & Horticultural Areas		02
	Feeding Operations		03
	Other		04
Rangeland		03	
	Grass		01
	Savannas (Palmetto Prairies)		02
	Chaparral		03
	Desert Shrub		04
Forestland		04	
	Deciduous		01
	Evergreen (Coniferous & Other)		02
	Mixed		03
Water		05	
	Streams & Waterways		01
	Lakes		02
	Reservoirs		03
	Bays & Estuaries		04
	Other		05
Non-Forested Wetland		06	
	Vegetated		01
	Bare		02
Barren Land		07	
	Salt Flats		01
	Sand (other than beaches)		02
	Bare Exposed Rock		03
	Beaches		04
	Other		05
Tundra		08	
	Tundra		01
Permanent Snow & Ice Fields		09	
	Permanent Snow & Ice Fields		01

FIGURE 4

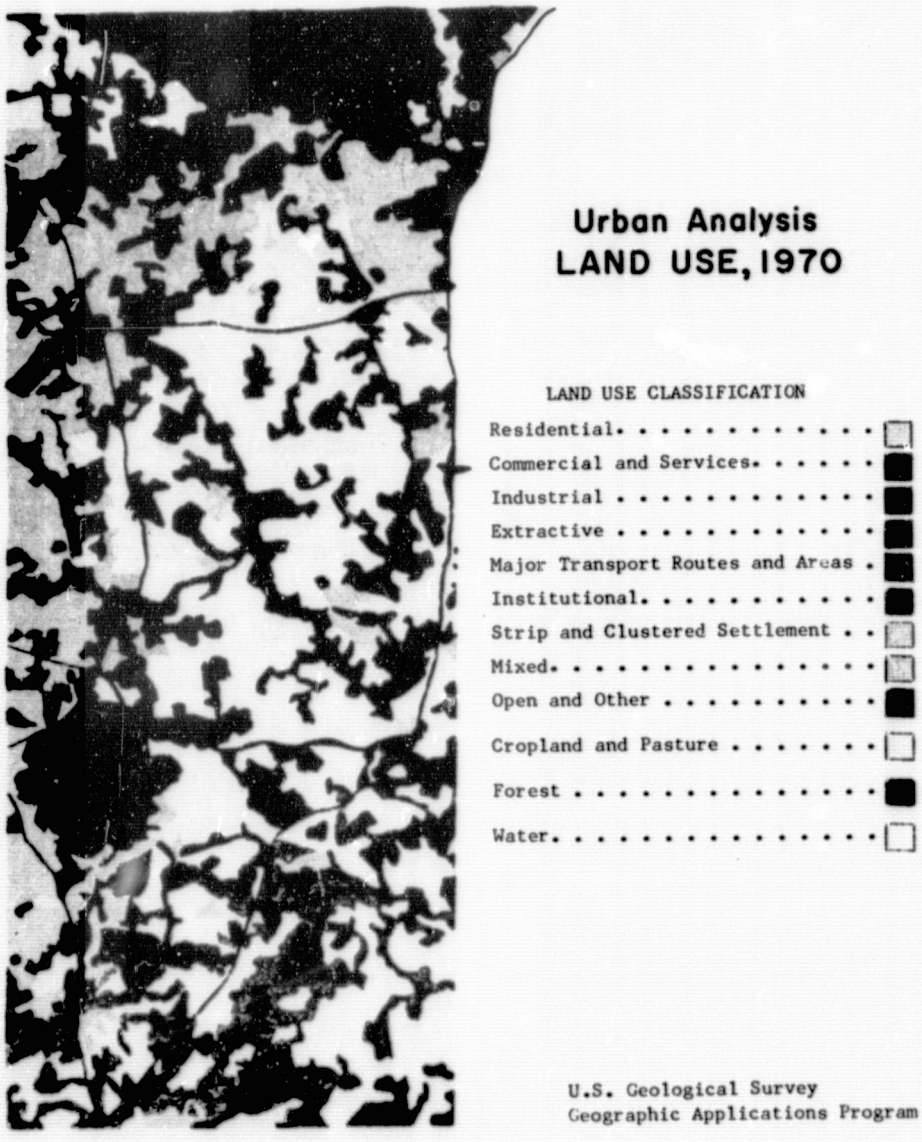

Urban Analysis
LAND USE, 1970
LAND USE CLASSIFICATION
Residential
Commercial and Services
Industrial
Extractive
Major Transport Routes and Areas
Institutional
Strip and Clustered Settlement
Mixed
Open and Other
Cropland and Pasture
Forest
Water
U.S. Geological Survey
Geographic Applications Program

FIGURE 5

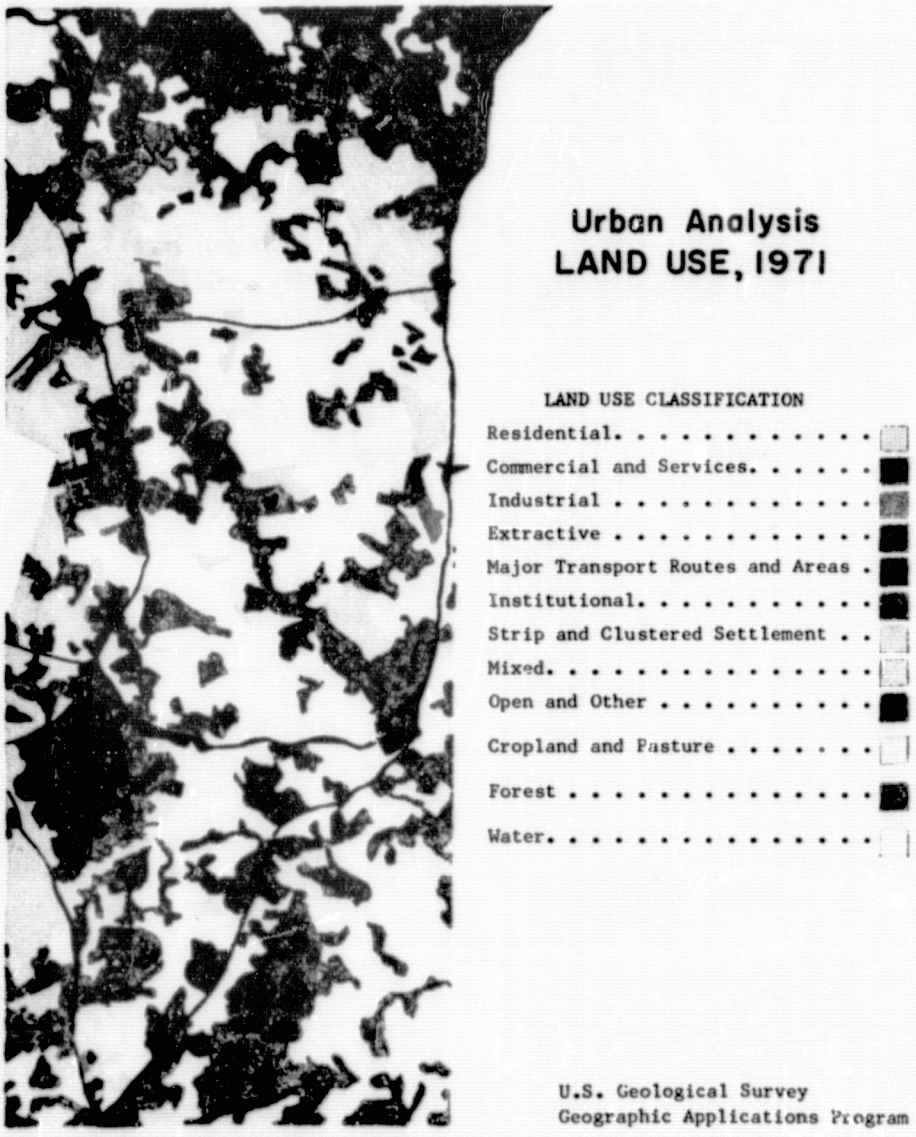

Urban Analysis
LAND USE, 1971
LAND USE CLASSIFICATION
Residential. . . . . .
Commercial and Services. . . . . .
Industrial . . . . . .
Extractive . . . . . .
Major Transport Routes and Areas .
Institutional. . . . . .
Strip and Clustered Settlement . .
Mixed. . . . . .
Open and Other . . . . . .
Cropland and Pasture . . . . . .
Forest . . . . . .
Water. . . . . .
U.S. Geological Survey
Geographic Applications Program

FIGURE 6

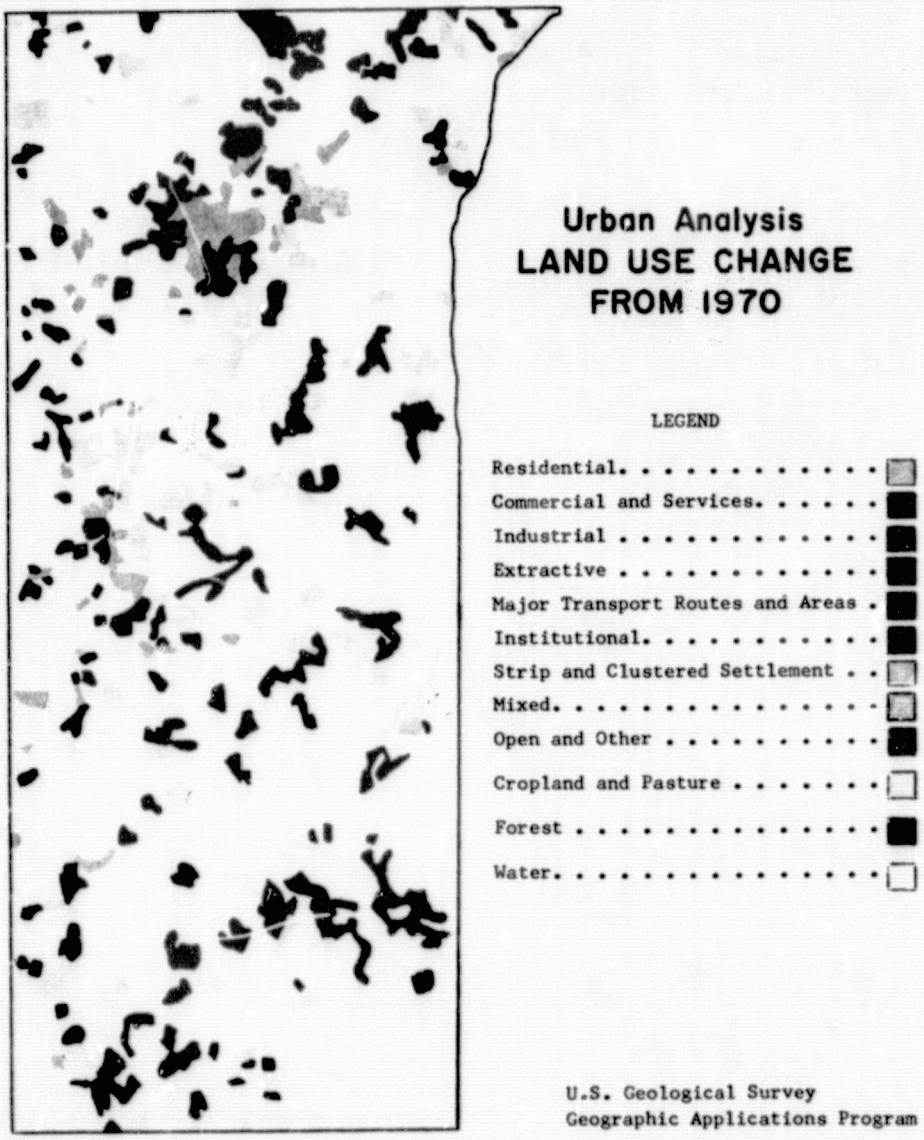
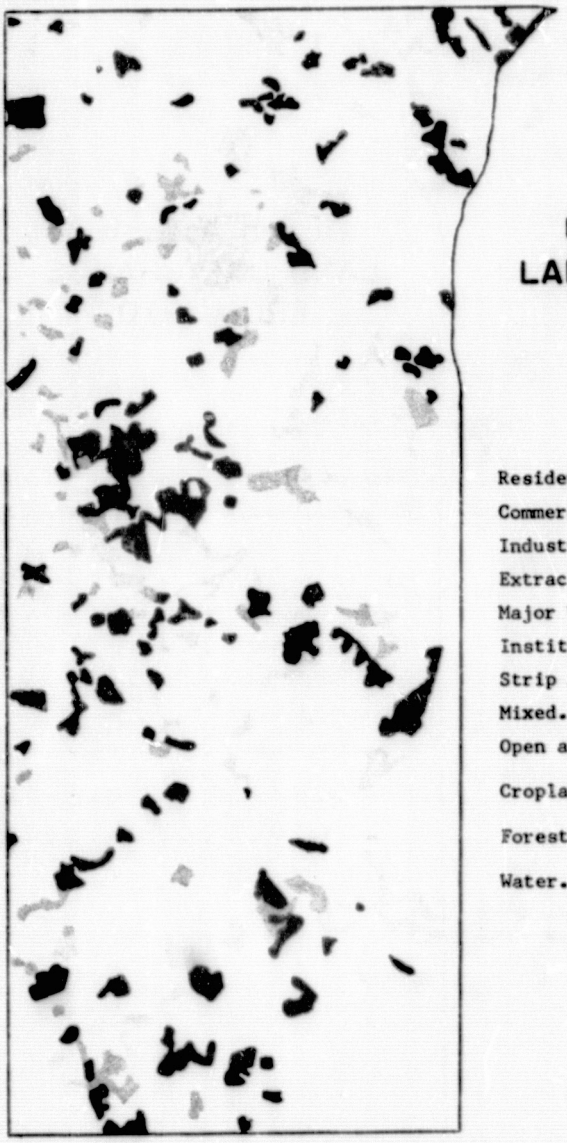

Urban Analysis
LAND USE CHANGE
FROM 1970
LEGEND
Residential
Commercial and Services
Industrial
Extractive
Major Transport Routes and Areas
Institutional
Strip and Clustered Settlement
Mixed
Open and Other
Cropland and Pasture
Forest
Water
U.S. Geological Survey
Geographic Applications Program

FIGURE 7



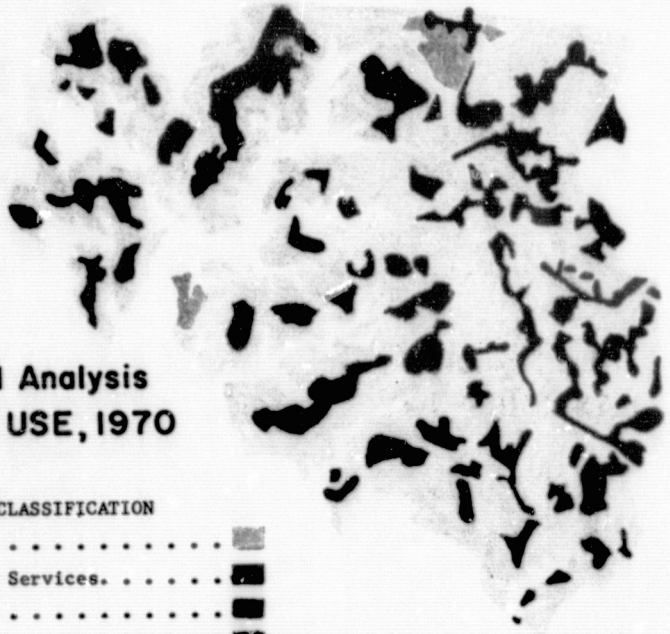
Urban Analysis
LAND USE CHANGE
TO 1971

LEGEND

- Residential
- Commercial and Services
- Industrial
- Extractive
- Major Transport Routes and Areas
- Institutional
- Strip and Clustered Settlement
- Mixed
- Open and Other
- Cropland and Pasture
- Forest
- Water

U.S. Geological Survey
Geographic Applications Program

FIGURE 8



Rural Analysis
LAND USE, 1970

LAND USE CLASSIFICATION

- Residential
- Commercial and Services
- Industrial
- Extractive
- Major Transport Routes and Areas
- Institutional
- Strip and Clustered Settlement
- Mixed
- Open and Other
- Cropland and Pasture
- Forest
- Wetland
- Water

U.S. Geological Survey
Geographic Applications Program

FIGURE 9

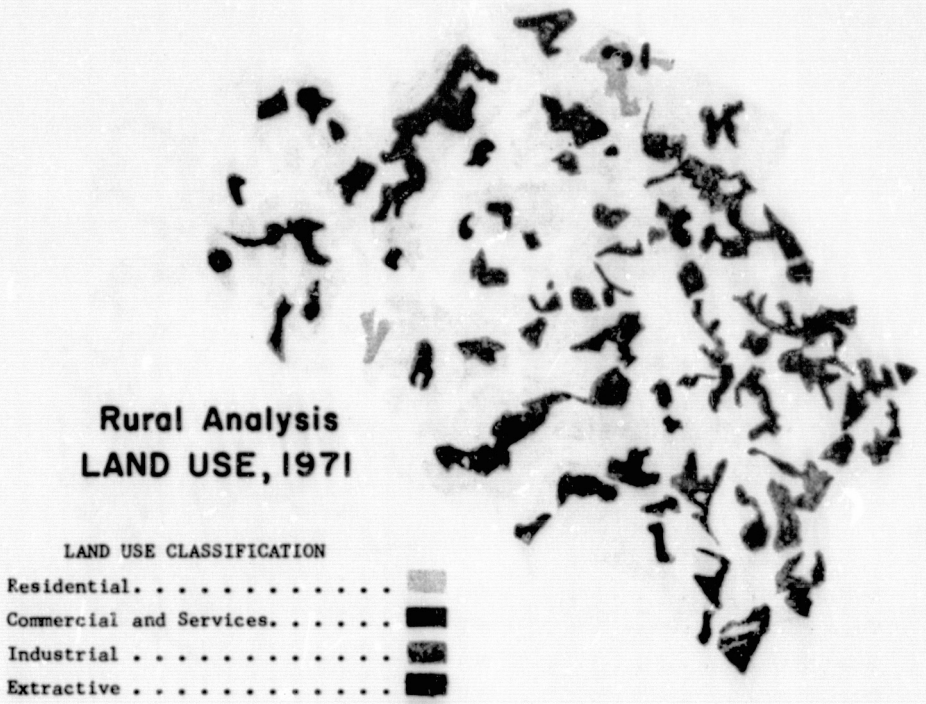
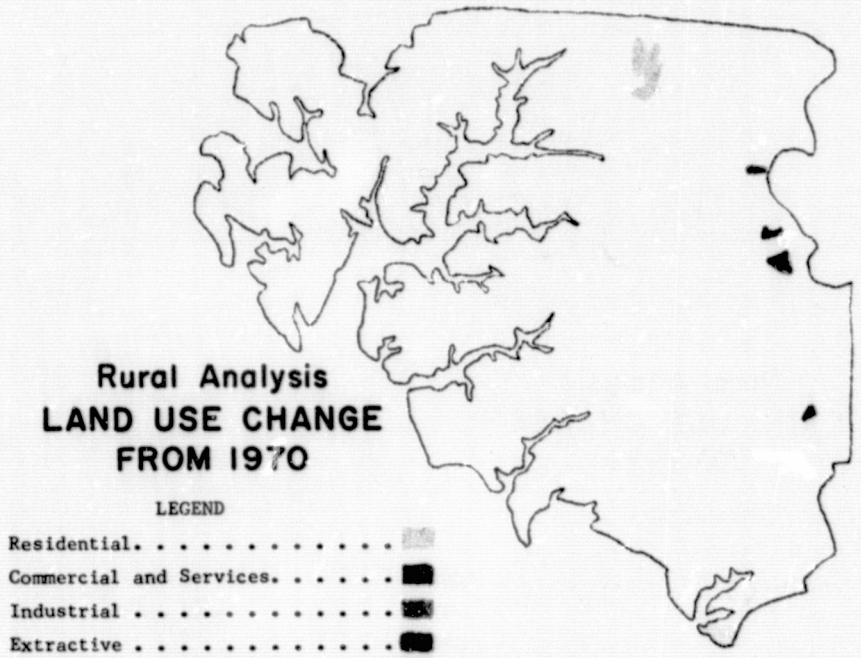

Rural Analysis
LAND USE, 1971
LAND USE CLASSIFICATION
Residential. . . . . .
Commercial and Services. . . . . .
Industrial . . . . . .
Extractive . . . . . .
Major Transport Routes and Areas .
Institutional. . . . . .
Strip and Clustered Settlement . .
Mixed. . . . . .
Open and Other . . . . . .
Cropland and Pasture . . . . . .
Forest . . . . . .
Wetland. . . . . .
Water. . . . . .
U.S. Geological Survey
Geographic Applications Program

FIGURE 10



Rural Analysis
LAND USE CHANGE
FROM 1970

LEGEND

Residential. . . . . .
Commercial and Services. . . . . .
Industrial . . . . . .
Extractive . . . . . .
Major Transport Routes and Areas . .
Institutional. . . . . .
Strip and Clustered Settlement . .
Mixed. . . . . .
Open and Other . . . . . .
Cropland and Pasture . . . . . .
Forest . . . . . .
Wetland. . . . . .
Water. . . . . .

U.S. Geological Survey
Geographic Applications Program

FIGURE 11

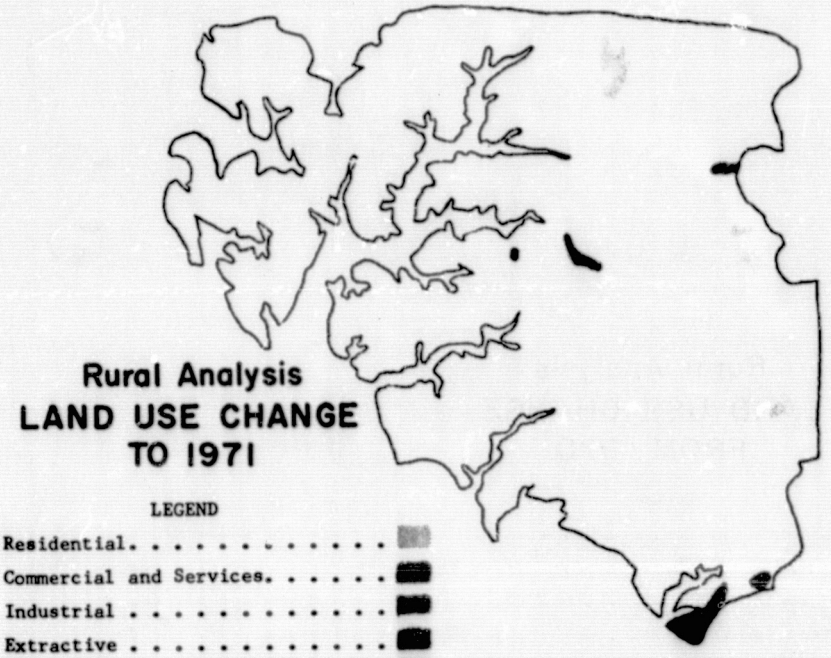

Rural Analysis
LAND USE CHANGE
TO 1971
LEGEND
Residential
Commercial and Services
Industrial
Extractive
Major Transport Routes and Areas
Institutional
Strip and Clustered Settlement
Mixed
Open and Other
Cropland and Pasture
Forest
Wetland
Water
U.S. Geological Survey
Geographic Applications Program

FIGURE 12

HASSELBLAD AND MITCHELL-VINTEN SYSTEMS COMPARISON

PARAMETER	HASSELBLAD	VINTEN
Time of year	22 Sep 70	15 Sep 71
Time of Day G.M.T. Local	 16:41:30 11:41 a.m.	 15:50:00 10:50 a.m.
Spectral Bands (nanometers)	480-580 580-720 710-900	475-575 580-680 690-760
Film Types	2402 2402 2424	2402 2402 2424
Lens Focal Length (millimeters)	40.0	44.3
Altitude (MSL)	60,000	65,000
Area of Coverage (nautical miles)	14.0 x 14.0	14.0 x 14.0
Scale of Original Photography	1:450,000	1:470,000
Ground Resolution (feet)	42	46

FIGURE 13

NASA ENVIRONMENTAL APPLICATIONS DEMONSTRATIONS IN SOUTHEASTERN UNITED STATES

C. T. N. Paludan

National Aeronautics and Space Administration
Marshall Space Flight Center, Alabama

ABSTRACT

Field Centers of the National Aeronautics and Space Administration have engaged in preliminary activities with potential data users in the Earth Resources Survey Program. An example of its demonstration projects in this field is Marshall Space Flight Center's research in land-use study. The methodology of a land-use study is described.

1. INTRODUCTION

The approach of the flight dates of the first orbital missions dedicated to earth resources surveys focused attention toward the outstanding gap in the program: lack of involvement by a broad spectrum of potential local, regional and state data users. The Announcements of Flight Opportunity (AFO) for the Earth Resources Technology Satellites, Missions A and B, and the Skylab Earth Resources Experiment Package, resulted in proposed participation by many of these potential data users. In an effort to further close the gaps, the NASA Field Centers have been working with their near-by communities on projects designed to demonstrate the utility of application of aerospace technology to pressing environmental problems.

Typical of the NASA Field Center activity are the "Demonstration Projects" of the Environmental Applications Office of the George C. Marshall Space Flight Center (MSFC). These projects bring NASA personnel into close contact with state and local government officials, local universities, and individuals such as county agents, farmers, and business men. Demonstration Projects include the following: (1) solicitation of participation by local users in the Earth Resources Survey Program, (2) demonstration of applications of aerospace technology to community problems, (3) definition of the problems by the potential users--not by NASA personnel, (4) utilization of the extensive in-house capability of MSFC's employees, (5) application of NASA's broad background in data handling and analysis, (6) coverage of a wide spectrum of disciplines, and inclusion of a geographic area encompassing a significant region of the nation, and (7) full consideration of the activities of other federal and state agencies.

Typical demonstration projects have included activities in hydrology, land-use survey, agricultural stress, new community site survey, transportation studies, and urban environmental quality. To illustrate the scope of NASA-Community involvement, this paper outlines the procedures and results of a typical demonstration project: the study of land-use.

2. GENERAL LAND-USE PROBLEMS FACING THE U. S. SPECIFICALLY ALABAMA

Land-use studies have never had their importance under-estimated in the United States but difficulty in obtaining or updating has severely limited data availability. Some of the history and difficulties were reported in a report by the Resources for the Future, Inc. (Clawson, 1965). On the nation wide level, the 1:7,500,000 scale map in the National Atlas of the United States, by

Preceding page blank

Anderson, is based primarily on Marschner's study of the 1940's (National Atlas, 1970, pp. 157-159). Of the 50 states, only New York state has an up-to-date comprehensive land-use data base (Shelton and Hardy, 1971, pp. 1571-1575).

Several factors focus attention on larger scale land-use studies at the present moment in U. S. history. First, there is the national public concern over the condition of the environment-to a large degree touched off by the rearward observations of the 1968 Apollo lunar flight; second, Federal legislation has forced each of the 50 states into immediate action on land-use planning; third, federal judicial rulings have forced some states to revise and equalize property tax assessment which may result in taxation according to land use; and fourth, the remote sensing technology and the National Aeronautics and Space Administration's (NASA) Earth Observations Program has made the needed data available comprehensively and cheaply for the first time.

The state of Alabama has been particularly affected by all the factors mentioned. NASA's largest field center, the George C. Marshall Space Flight Center (MSFC), is located there, giving the entire state an unusually receptive attitude toward space acquired observations. Alabama has many untapped resources. For that reason, the state government has been very active in attempts to encourage new industry. It is recognized, however, that Alabama's relatively unspoiled environment (Birmingham excepted) is fragile and state and local officials charged with development are anxious to develop a rational approach to land use. There has been some historical experience in the state with this approach. The great land development project of the 30's, the creation of the Tennessee Valley Authority, was greatly aided by land use studies conducted using aerial photography (Hudson, 1936).

3. DIRECT RELATIONSHIP OF ALABAMA TO SPACE ACQUIRED DATA.

In the spring of 1971, in response to the Announcement of Flight Opportunities, the University of Alabama supported by a number of state agencies including, especially, the Geological Survey of Alabama, the Alabama Development Office, and the Governor, submitted a proposal on the use of data acquired by the Earth Resources Technology Satellite for natural resource planning within the state. Considerable state resources were pledged to support the proposal, which was accepted by NASA and is presently an on-going project. MSFC is also a contributor to the overall proposal, especially in the field of computer-aided data analysis. A statewide land-use study is an important part of the overall proposal (Henry, McDonough, and LaMoreaux, 1972).

In an effort to acquaint state and local officials with the advanced technology techniques NASA has learned to apply, MSFC has been working with these officials since early 1971 in a number of demonstration projects, one of the most important of which is a land-use study. Prior to the flight of the Earth Resources Technology Satellite, data acquired by aircraft have been used in this demonstration project.

In northeast Alabama, a five county, 10,000 km^2 region known as the "Top of Alabama" constituted MSFC's initial demonstration area.

4. TECHNIQUES

Resources were not available for extensive use of traditional field study. In fact, resources were judged to be inadequate for manual photo interpretation of conventional aerial photography. Advanced remote sensing techniques were clearly indicated. But MSFC was only partially equipped for this, e.g., no in-house experience with side looking airborne radar was available. Some experience with multispectral photography and a considerable experience with automated data analysis dictated our approach (Paludan, 1970, pp. 373-382).

A methodology was developed which permitted rapid translation of data from four-band photography into land-use information. The goal of this demonstration project was to develop techniques that could be applied to data returning from the Earth Resources Technology Satellite.

5. LAND-USE

Of the many small scale land-use studies conducted within the United States it is very difficult to find any two that use the same classification system. Certainly it is difficult to find any that adhere to the classification system proposed by the International Geographical Union in 1949 for the World Land-Use Survey. The most comprehensive standard is the Standard Land-Use Coding Manual published by the Urban Renewal Administration and Bureau of Public Roads in 1965. In recognition of the peculiar problems involved in use of a classification system with the data primarily coming from orbital altitudes the National Aeronautics and Space Administration and the Department of Interior jointly sponsored a conference in the summer of 1971 to consider what a new national classification system should entail (Inter-Agency Steering Committee, 1972). Several well-known systems were put forward as candidates for adoption. These included the Canada Land Inventory, the Land Use and National Resources Inventory of the State of New York, and a system developed by the Commission on Geographic Applications of Remote Sensing of the Association of American Geographers (Department of Regional Economic Expansion, 1970) (Center for Aerial Photographic Studies 1970) (Anderson, 1971, pp. 379-387). Potential users of the data from a broad cross section of the United States were given the opportunity to contribute to the final recommendations which are still being developed by the steering committee. The preliminary indications are that the classification scheme will be as shown in Table I. The colors indicated are not a part of the present scheme, but are adapted from the World Land Use Survey. The system is a multi-level hierarchy with the nine first level categories being those that can primarily be determined solely by remote sensing with little need for ground truth. The second level categories would require some ground truth in many cases. The third and fourth level categories would contain information not available by the remote sensing techniques which are the concern of this paper. It is this classification system that MSFC has applied to its preliminary studies in the state of Alabama.

Another general problem considered early in the demonstration project was that of a locational grid. Of several systems considered, the Universal Transverse Mercator (UTM) grid was chosen. One reason for its selection is that NASA has made a choice that the Earth Resources Technology Satellite data will have the UTM grid super-imposed upon the data that is being sent out to the various investigators. A metric grid was readily acceptable in the state of Alabama where some speed limit signs already appear in metric units.

6. AUTOMATED DATA ANALYSIS

The earlier study of land-use in the Top of Alabama Region was based solely upon four-band multispectral photography - a relatively sophisticated, rapid, but non-automated technique was used for data analysis. Resulting maps are being published by the Tennessee Valley Authority in the scale of 1:24,000. Several approaches to truly automated data analysis are being pursued at MSFC.

Data management activities at MSFC run the gamut from the remote sensing of data through data processing and data analysis to the design of a computerized multi-purpose information system (Su and Cummings, 1972).

For the past few years, MSFC has developed a repertory of computer aided data analysis techniques. Automatic pattern recognition techniques using both electronic (analog and digital) and optical methods were developed to analyze the geometric properties of images. Automatic signature recognition techniques were developed to perform feature classification of species separation, using spectral characteristics.

Contrast enhancement had background removal algorithms using classification decision logic based solely on contrast differences were successful in several cases where the distinctive categories were partially obscured by background. However, the limitations incurred by this technique necessitated the development of decision logic based on pattern recognition techniques as a means for accounting for the correlation between different features in the classification algorithms. The vector representation of spectral signatures in Hilbert space is particularly useful since the highly sophisticated algorithms of feature classification can be applied directly (Bond and Atkinson, 1972). This technique has been applied to the interpretation of

multispectral photography with spectacular results. For example, in one case involving a Chandler Mountain farm in Alabama, ground tomatoes were successfully distinguished from staked tomatoes.

7. AUTOMATED DATA RETRIEVAL FOR RESOURCE MANAGEMENT

In addition to maps, an essential element of the demonstration project has been adaptation of an existing, space-related, data retrieval system to meet user needs in Southeastern U. S. The system has the capability to accept and manipulate analytic data based on lab and field research and archival data such as census information and courthouse records (Auburn University, 1972).

TABLE I. LAND-USE CLASSIFICATION

	SYMBOL	COLOR
URBAN & BUILT-UP	U	Red
RESIDENTIAL	Ur	
COMMERCIAL & SERVICES	Uc	
INDUSTRIAL	Ui	
EXTRACTIVE	Ue	
MAJOR TRANSPORT ROUTES & AREAS	Ut	
INSTITUTIONAL	Up	
STRIP & CLUSTERED SETTLEMENT	Us	
MIXED	Um	
OPEN & OTHER	Uo	
AGRICULTURAL	A	Light Brown
CROPLAND & PASTURE	Ac	
ORCHARDS, GROVES, BUSHFRUIT, VINEYARDS & HORTICULTURAL AREAS	Ah	
FEEDING OPERATIONS	Af	
OTHER	Ao	
RANGELAND	R	Orange
GRASS	Rg	
SAVANNAS (PALMETTO PRAIRIES)	Rs	
CHAPARRAL	Rc	
DESERT SHRUB	Rd	
FORESTLAND	F	Green
DECIDUOUS	Fd	
EVERGREEN (CONIFEROUS & OTHER)	Fe	
MIXED	Fm	
WATER	W	Light Blue
STREAMS & WATERWAYS	Ws	
LAKES	Wl	
RESERVOIRS	Wr	
BAYS & ESTUARIES	Wb	
OTHER	Wo	
NON-FORESTED WETLAND	M	Dark Blue
VEGETATED	Mv	
BARE	Mb	
BARREN LAND	B	Yellow
SALT FLATS	Bh	
SAND (OTHER THAN BEACHES)	Bs	
BARE EXPOSED ROCK	Br	
BEACHES	Bb	
OTHER	Bo	
TUNDRA	T	Grey
TUNDRA	T	
PERMANENT SNOW & ICE FIELDS	S	White
PERMANENT SNOW & ICE FIELDS	S	

REFERENCES

Anderson, James R., 1971, "A Tentative Land Use Classification Scheme for Use with Remote Sensing Complemented by Other Information Sources," Photogrammetric Engineering, Vol. XXXVII, No. 4, pp. 379-387.

Auburn University Engineering Systems Design Summer Faculty Fellows, 1972, ERISTAR; Earth Resources Information Storage, Transformation, Analysis, and Retrieval, NASA Grant NGT-01-003-044, Rpt. No. CR-61392.

Bond, A. D., and Atkinson, R. J., 1972, "An Integrated Feature Selection and Supervised Learning Scheme for Fast Computer Classification of Multi-Spectral Data," in Shahrokhi, F., (ed.), Remote Sensing of Earth Resources, University of Tennessee Space Institute, Tullahoma, Tennessee, pp. 645-672.

Center for Aerial Photographic Studies, 1970, "A Review of the New York State Land Use and Natural Resources Inventory," Cornell University, Ithaca.

Department of Interior, 1970, The National Atlas of the United States of America, U. S. Government Printing Office, Washington, D. C., pp. 157-159.

Department of Regional Economic Expansion, 1970, "A Guide to the Classification of Land Use," The Canada Land Inventory, Report No. 1, 2nd Edition, Ottawa.

Henry, H. R., McDonough, G. F., and LaMoreaux, P. E., 1972, "A Study of the Feasibility of Applying Remotely Sensed Data in the Management of Natural Resources and the Improvement of Environmental Quality in Alabama," Proc. of the Eighth International Symposium on Remote Sensing of Environment, Ann Arbor.

Hudson, G. D., 1936, "The Unit Area Method of Land Classification," Annals of AAG 26, pp. 99-112.

Inter-Agency Steering Committee on Land Use Information and Classification, 1972, A Land Use Classification Scheme for Use with Remote Sensor Data, Department of the Interior, Washington.

Paludan, C. T. N., 1970, "Potential Contributions of Orbital Earth Resources Data to Urban Planning," Planning Challenges of the 70's in Space, Morgenthaler, C. W. and Morra, R., (eds.), Tarzana, Calif., American Astronautical Society, pp. 373-382.

Shelton, R. L. and Hardy, E. E., 1971, "The New York State Land Use and Natural Resources Inventory," Proc. Seventh International Symposium on Remote Sensing of Environment, Ann Arbor, pp. 1571 - 1575.

Su, M. Y. and Cummings, R. E., 1972, "An Unsupervised Classification Technique for Multispectral Remote Sensing," Proc. Eighth International Symposium on Remote Sensing of Environment, Ann Arbor.

LAND USE CLASSIFICATION IN THE SOUTHEASTERN FOREST REGION BY MULTISPECTRAL SCANNING AND COMPUTERIZED MAPPING

F. P. Weber and R. C. Aldrich

Pacific Southwest Forest and Range Experiment Station
Forest Service, U. S. Department of Agriculture
Berkeley, California

and

F. G. Sadowski and F. J. Thomson

Environmental Research Institute of Michigan
(Formerly Willow Run Laboratories)
The University of Michigan
Ann Arbor, Michigan

ABSTRACT

The feasibility of mapping land use categories by airborne multispectral scanning was tested over two 42-square-kilometer sites in the Southeastern United States. New techniques were applied in preprocessing the data collected to compensate for effects of atmosphere and changing solar irradiance. The capabilities of extending spectral signatures from one training flight line to three additional lines for both test sites were analyzed. The data processed by the SPectral Analysis Recognition Computer system were compared to those obtained from color infrared photographs and ground surveys. The effects of time-of-day and selection of optimum channel on accuracy of mapping classification were investigated.

1. INTRODUCTION

A twofold challenge faces natural resource inventory specialists in the 1970's: (1) to develop a rapid classification system for following the dynamic changes affecting our Nation's resources and (2) to make that system accurate and efficient enough to be cost-effective. Some scientists believe, as we do, that such a system may well be an airborne multispectral scanner (MSS) for collecting data coupled with a hybrid analog/digital computer for analyzing and displaying the information gathered.

Past studies have shown that air photo interpretation used in combination with ground examinations can result in land use and forest classification accuracies of well over 80 percent--even at photographic scales as small as 1:420,000 (Aldrich, 1953; Aldrich and Greentree, 1972). But current national standards require an accuracy of better than 95 percent in the estimation of forest area on extensive forest inventories. Interpretation of aerial photographs can provide inventory estimates of this accuracy, but not without expending large amounts of time in photo preparations, tedious photo interpretation, and data handling.

Since the early 1960's there has been extensive research on the development of spectral signatures and pattern recognition theory in processing multispectral data. Some of this work focused on forest resource problems and has been conducted cooperatively by the U. S. Forest Service, U. S. National Aeronautics and Space Administration (NASA), and the Willow Run Laboratories (WRL) of the University of Michigan (Weber, 1971). The goal of this research has been to analyze more quickly and accurately than a human photo interpreter the large volume of airborne data generated by a multispectral scanner.

Several investigators have studied the feasibility of mapping classes of terrain objects by using the spectral signature as representative of the object (Burge and Brown, 1970; Erickson and Thomson, 1971; Kolipinski et al., 1969). Further studies in pattern recognition using maximum likelihood ratio processing have been accomplished on both analog and digital computers (Marshall et al., 1969; Nalepka et al., 1971). Weber and Polcyn (1972) report application of these methods in a forest stress classification study.

Our study is similar to previous multispectral processing feasibility studies, with one important exception: Attention was centered on the ability to process economically data sets of a useful size (i.e., 42 square kilometers) by using the same procedure used on smaller data sets (i.e., 10 square kilometers). When we began to study large data sets, some of the variables which were ignored in the smaller sets used for feasibility studies could no longer be ignored. Most important of these variables are solar irradiance and atmospheric path radiance and transmission. Furthermore, we considered whether the signature from a single training set was truly representative of all of that material in a large block of data. Solutions to these and other problems were crucial to the success of pattern recognition techniques applied to multispectral data. If the performance obtained in feasibility studies cannot be extended to large data sets, the technique is not practical.

The University of Michigan's Willow Run Laboratories have done a large amount of theoretical work to determine the nature of, and to attempt to compensate for, changes in solar irradiance and atmospheric conditions. Because such changes directly affect the data, techniques have been devised to correct raw MSS data before processing (Nalepka et al., 1971; Malila et al., 1971). Theoretical study of these effects is being pursued with models (Suits et al., 1972; Turner et al., 1971).

In this study we applied preprocessing theory to compensate for effects of atmosphere and changing solar irradiance. We used signatures from one of four parallel, overlapping flight lines to classify data on all four lines. Compensation for solar irradiance changes in the morning data was made by dividing all data by the sun sensor signal level. Thus, this study was not only a feasibility study of mapping important land use categories but also tested the ability to extend the utility of spectral signatures collected from one run to three additional runs made shortly before or after the first.

This paper reports a test of multispectral scanning of two 42-square-kilometer sites near Atlanta, Georgia. The purposes of the test were: (1) to prepare land use (forest and nonforest) maps with estimates of use, by terrain classes, and (2) to determine the accuracy of class signatures developed on a single training flight for classifying data on four adjacent flight lines (signature extension).

2. DATA COLLECTION

Within each test block a small area with features representative of the block was selected for ground instrumentation. Two sets of data were to be collected within each block--one in the early morning and one at midday.

Data collection began about 1330 hours (local sun time) November 3, 1971, at Block 2 (Figure 1). The University of Michigan's scanner-equipped C-47 aircraft flew four parallel flight lines at an altitude of 3,450 meters.

A second flight was made over Block 2 the next morning, starting at about 0900 hours. After successfully completing the work in Block 2, we moved to Block 4. The first data set in Block 4 was completed on the afternoon of November 4. The next morning, commencing at about 0930 hours, we collected the last of the four ground and aircraft multispectral data sets. On November 7, the U. S. Forest Service's Aero Commander photographed Blocks 2 and 4 with color infrared film at a photo scale of 1:35,000.

While the Michigan aircraft was collecting data, men on the ground, who had two-way radio contact with the plane, were also collecting data. Solar radiation was measured by a portable pyrheliograph at the ground site. Two men in a "cherry picker" collected data on spectral irradiance of several landscape targets, such as conifers, hardwoods, pastures, transitional fields, and water. They also measured target net radiation and reflected solar radiation. During the period November 3 to 5, a two-man ground crew inspected about 50 percent of both blocks and recorded ground classification data.

2.1. MICHIGAN MULTISPECTRAL SCANNER SYSTEM

Hasell (1972) has described the construction details of the Michigan M-7 scanner used in this study. In the past we had used earlier versions of it which were double-ended and multipathed to achieve multispectral sensing in forest resource problems. Analysis of that data strongly indicated the requirement for a multispectral scanner to produce simultaneously registered data covering the

bandwidth 0.4 to 13.5 micrometers (μm) in select narrowband increments (Weber and Polcyn, 1972). Our study in the Southeastern United States provided the first opportunity to test the merits of multispectral data collected with a truly single line-of-sight scanner.

3. DATA PROCESSING

In this study we used both the digital and analog computing facilities. To produce the land use maps, a pattern classification technique known as the maximum likelihood ratio was applied to the spectral signature data we obtained. And to insure the fairest test of signature extension, careful preparation of the raw MSS taped data was required (Nalepka and Thomson, 1972). In particular, we had to compensate for variations in spectral signatures that depended on observed scan angle. The four optimum channels for classifying land use classes were identified by digital computer analysis. This analysis was done before preparation of recognition maps on a hybrid digital/analog computer. Additional digital analysis was conducted after the recognition maps were prepared to identify causes of some misclassifications in data collected in early morning.

3.1. DATA PROCESSING HARDWARE

The digital computer we used was a CDC 1604B with 15k-48bit words of storage. Associated with the computer are eight 7-track, 200 bpi digital tape drives and a special-purpose analog/digital and digital/analog interface. A multispectral analysis computer program was developed to convert analog scanner data to digital, display them, quantify variations in spectral signatures, compensate for these variations, and prepare recognition maps using the supervised-learning, maximum-likelihood-ratio classifier (Erickson and Thomson, 1971).

The SPectral Analysis Recognition Computer (SPARC) system is a parallel-organized system designed to implement likelihood ratio classification of multispectral data at real-time rates. The system consists of an analog tape recorder, suitable interface gear, a preprocessor, the computer itself, 70 mm film printing, and CRT display equipment. It can classify data at about 80,000 decisions per second and prepare 70 mm filmstrip recognition maps at the same time.

Because of its parallel organization, SPARC can use only a limited number of channels and training sets. Any combination of channels and land use classes whose product is 48 or less can be used. In this study we used four channels and 12 training sets.

SPARC operates in two modes--training and operational. The machine is programmed to recognize land use classes in the training mode. An operator enters samples of data from training sets and a statistical description of each training set. Thus, each class to be recognized must be represented by at least one training set within SPARC. Once training has been completed, the operational phase begins. Unknown data are classified by using the likelihood ratio as a measure of similarity of scenepoint spectral signatures to those of the training sets. Recognition maps of each class are printed on 70 mm film. To depict an entire scene, the number of filmstrips must equal the number of training sets.

The 70 mm recognition maps may be individually analyzed by overlaying each map with conventional video filmstrips. The individual maps can also be color coded and combined into a mosaic by means of the color ozalid process. The color ozalid approach was used for this study.

3.2. PROCESSING EFFORT

3.2.1. EXPERIMENT PLAN

Two data sets were defined by the principal investigator for processing--the 1200 hours flight of Block 2 on November 3 and the 0900 hours flight of Block 4 on November 4 (Figure 1).

Each of the two 42-square-kilometer blocks was processed separately. One of the four parallel flight lines from each block was digitized initially. The lines selected were line 43 from Block 2 and line 14 from Block 4. These lines provided the best selection of training areas for the land use recognition classes desired. The objective of the digital work was to identify angle correction functions and determine optimum spectral channels for use in the analog processing. Once determined, the results were applied to the remaining three flight lines in each respective block.

Signatures of representative areas for each land use category were programmed into the SPARC and recognition obtained. Signatures trained on line 43 and line 14 then were played on the three remaining flight lines in each respective block as a test of signature extension capabilities. We hypothesized that uniform color coding of results and the mosaicking of adjacent flight lines for each block would result in reliable area-recognition maps of good geometric fidelity.

3.2.2. PROCESSING EFFORT - BLOCK 2

A. DIGITAL WORK

Data from line 43 were digitized by using a computer program called A2F3 that reads analog data in an analog/digital converter and "smooths" the data by averaging from 3 to 15 consecutive scan lines into a single composite scan line. Program A2F3 also repacks the data into the standard digital tape format and writes the resulting scan lines as records on digital tape. Thus, it produces finished ready-to-process digital data from analog data in a single step.

The data were digitized at the rate of 2.5 milliradians per resolution element, and eight consecutive scan lines were "smoothed." Each resultant digital element, therefore, represented an effective ground resolution patch size of 7.6 m x 7.6 m which closely approximates the minimum scanner resolution capability at an altitude of 3,048 m.

All 12 MSS channels were digitized simultaneously, except for the near IR channel of 2.0 to 2.6 μm which was rendered unusable owing to cross-coupling of signals from the adjacent thermal channel.

A program called GRAYMAP produced a digital printout of a red channel (0.62 to 0.70 μm). It divides the signal range of a selected channel into seven intervals and assigns a unique typewriter symbol of decreasing density to six of the intervals, with the seventh left blank. The digital elements on the tape are then scanned consecutively point by point and line by line. The value of each element is classified into the appropriate interval, and the corresponding symbol is assigned. A printout of the results yields a maplike presentation in which tone gradations are represented by symbols of varying density so that light-toned areas appear white and dark-toned areas appear black. Numbers printed along the top and down one side allow for a coordinate reference system useful for locating specific points. Such a map provides a visual display with which to check the merits of the digitization process and to locate training areas for signature extraction.

Before processing can continue, the digitized data must be calibrated to some reference, all channels brought into registration, and the dynamic range scaled. These three steps are taken by using the programs AUTOCAL and CSD which: (1) clamp the voltage levels from inside the scanner housing to zero. (This enables all radiation inputs from the scene and calibration sources to be referenced to a uniform minimum voltage level.); (2) deskew signals from adjacent wavelength intervals. (Owing to slight misalignments of tape recorder and playback heads, signals from adjacent channels may not be properly registered. As such, signals in two widely separated channels on the tape may appear to come from the same data point although actually arising from two different data points. Such misregistration is termed "skew" and must be corrected.); and (3) scale the voltage levels in each channel to make optimum use of the dynamic range available and prevent loss of signal due to overshoot.

Once the data were corrected, the variations in observed radiance were identified by the program ACORN4. These variations occur because the angle of observation changes as each scan line is traced across the scene. The result is varying magnitudes of scene radiance due to varying path lengths or variations in bi-directional reflectance of the scene components or both. Compensations for such variations are made by averaging the variation of scene radiance with scan angle over the length of the flight line and by generating second-degree functions which define the variation with scan angle for each channel.

The program NORMTA then normalizes the digital data by subtracting or multiplying the data by the coefficients of the functions calculated in ACORN4. The coefficients were also later used on the preprocessor of the SPARC system.

After the data were normalized, the analysis to determine the performance of the spectral channels in separating the land uses of interest was begun. Training areas, originally designated on 1:35,000 scale color infrared (CIR) photography, were located on the digital graymap. Rectangles were drawn within the bounds of each training area, and the line and point numbers of the four corners then identified the area for signature extraction by the program IMPROVE. IMPROVE was used to average the voltage levels within a training area for each channel and print out the resulting mean and standard deviation for each MSS channel along with a covariance matrix for all channels. The training signatures were computed from either individual area or from a combination of several separate areas.

Eight land use classes--four forest and four nonforest--had originally been designated for recognition and classification. These classes are as follows:

Forest	Nonforest
Conifers	Agriculture
Upland hardwood	Pasture
Bottomland hardwood	Water
Undecided	Transitional

Analysis of the resulting spectral signatures indicated significant variability within two of the nonforest categories--agriculture and pasture. Therefore, we decided that additional land use categories would have to be designated to obtain significant recognition results. Agriculture and pasture were each divided into three subcategories, and the resulting classification scheme became:

Forest	Nonforest
Conifers	Row crops
Upland hardwood	Bare soil
Bottomland hardwood	Orchard
Undecided	Improved pasture
	Old pasture
	Pasture
	Water
	Transitional

The signatures computed by IMPROVE were used to determine the optimum channels for use on the SPARC system. Optimum channels are those spectral regions which are most useful in discriminating the training areas. Since 12 land use classes were now selected for recognition on the SPARC, only the four best channels could be used (the product of land use classes and channels cannot exceed 48).

The program STEPLIN computes the Average Pairwise Probability of Misclassification (APPM) for each channel for all possible pairs of signatures. The channel having the lowest APPM is selected as the best one. Next, the program computes the APPM for all possible pairs of channels given the best channel. Again, the channel with the lowest APPM is selected and becomes the second best channel. Then the program computes the APPM for all triples of channels given the best pair. This process is repeated until all channels are classified.

The first four channels selected were 1.5 to 1.8 μm, 9.3 to 11.5 μm, 1.0 to 1.4 μm, and 0.41 to 0.49 μm. The fifth channel selected--the red region of 0.62 to 0.70 μm--had an average probability of misclassification for all 12 categories that was only 0.3 percent higher than that of the fourth channel selected, given the previous selection of the three best channels (Table 1). However, the red spectral region enhanced discrimination between varying pasture conditions (which constitute a significant portion of the scene) and was ultimately used in place of the blue channel.

It seemed useful at this point to create a digital recognition map to determine the adequacy of the 12-category/4-channel setup in recognizing the scene. The program EXPLIN performed a linear approximation to the maximum likelihood ratio decision rule in classifying the digital data points. The resultant signal levels on the output tape represented the recognition of various categories with an additional level for an unrecognized category to avoid numerous false classifications. Typewriter symbols were assigned to each signal level with a blank designated for the unrecognized category. A computer printout of signal levels resulted in the digital recognition map. Color coding of various groups of categories was achieved by printing only a subset of signal levels for a particular color of printer ribbon. Each time the data were processed the computer/printer ribbons were changed, and another subset of levels was printed. The resulting land classification map therefore depicted the scene in four different colors.

B. ANALOG WORK

For analog processing the preprocessor unit was programmed with the ACORN4-derived angle-correction coefficients. A single representative area for each land use class was identified on line 43 of Block 2. In the digital program, it was possible to lump several training areas together and obtain a composite signature for a land use class. But the analog program does not have this capability. Each area must be "trained" separately; therefore, it was important to pick areas which were most representative of the category.

SPARC training required that a duplicate analog tape (which had been deskewed) be cut into sections, each section containing all of the data from one or more training areas. Each tape section was made into a continuous loop, and the loops then played on a conventional tape recorder with a loop adaptor. The SPARC operator viewed the loop on a real-time, C-scan display. Each time the loop recycled, the scene was repeated on the C-scan. This repetitive display of the tape data containing the training areas permitted bracketing each training set with horizontal and vertical electronic gating mechanisms so that only signals from the training area were sent to the SPARC. The mean, standard deviation, and covariance for each of the digitally selected optimum channels were entered into SPARC. When all channels had been trained on the first set, the next training set was gated in and the channels trained in like manner. When all training sets had been programmed, the training phase of SPARC recognition was completed.

In an effort to guarantee that all 12 land use classes were programmed accurately, a Euclidean-distance decision rule (Nalepka et al., 1971) was used to recognize training sets. The criterion for acceptable training of each set involved recognition of at least 90% of the area within the set. In applying the Euclidean distance rule, we specified a threshold and identified all points whose probability density function (pdf) values exceeded it. All points whose pdf values fell below the threshold were not identified. Recognition results were quantified with a high-speed digital counter which tallied the number of points (resolution elements) identified as the target of interest. Percent recognition was the number of points counted as recognition for the target compared to the total number of points in the gated training set.

The operational phase of the SPARC recognition process involved playing another copy of the original analog tape through the tape recorder in standard fashion. Each time the tape was played, one of the land use classes was selected for recognition. As each scene point on the tape was reached, a likelihood ratio was computed, and a decision was made as to whether the point resembled the target. If so, SPARC put out a recognition signal, and the high-speed counter recorded the tally. The recognition signal was printed on 70 mm film moving past a rapid line-scanning cathode ray tube. This process continued on a real-time basis until all scene points were classified.

When all 12 recognition strips for line 43 were complete, the operational phase of the SPARC work was repeated for each of the three remaining flight lines in Block 2 as a test of "signature extension." Preprocessing coefficients and signature settings remained unchanged from line 43. Geometric corrections were made to all flight lines to insure as uniform an aspect ratio as possible. Scanner angular distortion was corrected with the use of a tangent function, and forward scale was standardized for all lines within each block.

Each set of recognition strips for a particular flight line was color coded by using an ozalid process. The individual color separations were then overlaid and registered to form an ozalid "sandwich." Each sandwich was photographed to create a color-coded recognition map of each flight line. The resulting four photographs were finally mosaicked to create a color-coded recognition map for the entire block (Figure 2).

3.2.3. PROCESSING EFFORT - BLOCK 4

A. DIGITAL WORK

Data from Block 4 were processed much the same way as those from Block 2. Line 14 was processed digitally to obtain optimum channels and preprocessing coefficients for use on the SPARC. The reflective IR channel of 1.5 to 1.8 μm was not available for this data set since it had been assigned to the same malfunctioning preamplifier that rendered the 2.0 to 2.6 μm channel unusable for Block 2. This was unfortunate since it was the 1.5 to 1.8 μm channel which had been the best channel for discriminating the various categories in Block 2.

Angle correction functions were again identified and used to normalize both the digitized data and the analog data of all four flight lines. Eleven signatures were derived from the digitized data to correspond with like land use categories recognized in Block 2. (An "orchards" category does not appear in Block 4.)

For this data set, optimum channels were determined for each of three postulated classification problems in an attempt to identify channels most useful in discriminating the more dominant scene components from each other (i.e., forests and pastures). The cases considered were: (1) all 11 land use categories, (2) the four forest categories, and (3) the four forest and three pasture categories (Table 2). The thermal channel (9.3 to 11.5 μm) was not used in the selection process. We judged that the use of thermal data collected in the morning would result in poor signature extension because of the rapid change in terrain feature temperature. Channel selection for the SPARC work was based on an ability to discriminate well in all three classification problems. The four channels selected were 0.52 to 0.57 μm, 0.58 to 0.64 μm, 0.62 to 0.70 μm, and 2.0 to 2.6 μm.

Although the channel 0.41 to 0.48 μm performed well in discriminating the various forest and pasture categories, it was rejected on the basis of inordinate noise on duplicated tape for SPARC. The 1.0 to 1.4 μm channel also had to be rejected due to excessive signal overshoot caused by a malfunctioning preamplifier during the flight.

B. ANALOG WORK

The use of a different set of channels and data collected at a different time of day necessitated some changes in the classification scheme developed for Block 2 during the training phase of the SPARC work. For example, differentiating between upland and bottomland hardwoods was not possible in Block 2 although it was attempted. Areas typed on the 1:35,000 scale CIR photography as mixed conifer/hardwood had a multispectral signature so similar to that of pure conifers that the two had to be combined for effective recognition. Areas designated as row crops on the photography were indistinguishable from pastures. We decided that two signatures were required for acceptable water recognition--one for clear deep water and a second for the muddier, shallow ponds. An additional signature was used for each of the transitional and improved pasture categories to minimize the variability within these categories.

Thus, in all, eight categories were programmed into the SPARC computer representing these land uses in Block 4:

Forest	Nonforest
Conifers	Improved pasture
Hardwoods	Old pasture
	Pasture
	Bare soil
	Water
	Transitional

Recognition strips were then printed for each of the eight categories in line 14. Signature extension, color coding of recognition strips, and mosaicking of the flight lines were done similarly to Block 2.

C. FURTHER DIGITAL ANALYSIS - BLOCK 4

Additional processing of Block 4 was necessary to investigate the reasons for variable recognition results obtained during the signature extension work. As initially processed, angle correction functions derived during the digital processing of line 14 (the last line flown) were applied to all the flight lines for the SPARC recognition procedure. Although the application of uniform correction functions to successive lines of data may be acceptable for midday periods, whether such corrections are reliable in early morning situations when illumination level and sun angle are changing rapidly was not certain. (Block 4 was flown at 0912 hours local time, with the time interval between the start of line 11 and the end of line 14 being 31 minutes.)

Flight lines 11, 12, and 13 were digitized, clamped, scaled, and deskewed for the optimum channels used to process line 14. Average scan lines for each flight line in each channel were then plotted. Examination of the curves suggested two possible causes for the slight change in recognition that was shown from line 14 to each of the earlier lines--change in illumination level and change in angle effects.

Owing to limited time and funding, additional SPARC processing was restricted to line 12. Illumination change was assessed by noting the signal level at the peak of the aircraft sun sensor pulse in each channel in lines 12 and 14. Such a pulse appears in every reflective channel on every scan line of the data. It is the result of incident illumination on the top of the aircraft being transmitted through a flat opal glass port about 8 inches in diameter. The radiation is directed into the scanner housing where it is recorded on each successive revolution of the scanner collecting optics. The resultant signal pulse is available for use as some measure of incident illumination level during the flight. Signal levels for line 12 were lower than for line 14 as follows:

	Spectral Channel			
	0.52 to 0.57 μm	0.58 to 0.64 μm	0.62 to 0.70 μm	2.0 to 2.6 μm
$\frac{SS_{(line\ 12)}}{SS_{(line\ 14)}}$	$\frac{1.3}{1.4} = 92.8\%$	$\frac{1.3}{1.5} = 86.6\%$	$\frac{0.8}{0.9} = 88.8\%$	$\frac{1.5}{1.6} = 93.7\%$

in which SS is the peak voltage of the sun sensor for the line indicated.

We decided to increase the gain in each of the channels for line 12 as a means of compensating for the lower illumination level present at the time the data were recorded. Gains were increased by elevating the peaks of the sun sensor by these amounts:

Spectral Channel	% Increase
0.52 to 0.57 μm	7.2
0.58 to 0.64 μm	13.4
0.62 to 0.70 μm	11.2
2.0 to 2.6 μm	6.3

Recognition strips of line 12 were then printed and area counts obtained for each of the signatures as trained on line 14.

A change in angle effects was also deemed important as a potential source of error. The nonuniformity of signal on either side of nadir seemed to increase as zenith angle increased (i.e., with decreasing line number). The calculation of zenith angle for each of the two lines on the date of the flight indicates a difference in sun angle of 3.18°. Such a difference could account for some variations in angle effects across the scene, considering the magnitude of the zenith angles (65.62° for line 14 and 68.80° for line 12).

Coefficients for use in normalizing the average scan lines were derived digitally with the program ACORN4 for line 12 as had been done for line 14. The preprocessor of the SPARC was then configured with the coefficients, and recognition strips for line 12 were again printed.

Finally, a set of recognition strips was printed and area counts obtained employing both of the corrections.

3.3. COMPARISON OF SPARC MOSAIC WITH CIR PHOTOS AND GROUND TRUTH

A technique was developed to compare SPARC-produced color-coded mosaics made from multispectral scanner data with maps made by interpretation of 1:35,000 scale color infrared photographs and ground checks of over 50 percent of the classifications. A systematic dot grid (10 dots per square inch) was placed over the land use map of each of the two blocks drawn to a scale of 1:35,000 and the number of points listed by the classification within which they fell. There were 490 of these points that fell within the boundaries of Block 2 and 458 points that fell within the boundaries of Block 4 (Tables 3 and 4). Each photographic sample point in Block 2 represents about 7 hectares (17.5 acres), whereas in Block 4 each point represents 8 hectares (20.5 acres).

Next, we selected 20 points at random from each land class (except orchards and water) recorded in each test block--a total of 171 points. These sample points were used to check the MSS imagery as displayed on the SPARC mosaics. In Block 2 we could identify only 16 orchard samples on the photo points, and only seven points fell in water. We found an additional eight points to represent water and finished with a total of 15 samples. Block 4 had no orchards; thus, this class was not a factor in this block. Only 12 points were in the water class, but eight additional samples were found to supplement these.

Templates were made to show the location of 171 points in Block 2 and 160 points in Block 4. The color-coded film transparency of each multispectral scanner mosaic was placed in an enlarging projector-viewer and scaled to the 1:35,000 scale of the photo/ground survey map. Since there was geometric distortion throughout the MSS mosaics, the scale was adjusted for best fit while we checked sections of the mosaic. The template of point locations was placed over the projected image and keyed to the 1:35,000 photo/ground survey map. With the images coinciding as nearly as possible, each point was examined and the MSS classification recorded.

4. RESULTS

4.1. BLOCK 2 - MIDDAY FLIGHT

4.1.1. TWELVE-CATEGORY RECOGNITION OF LINE 43

As originally designed, the eight-category recognition scheme for Block 2 would have allowed for the use of six waveband channels on the SPARC. However, the great amount of variability noted in the signatures of two of the categories (pasture and agriculture) necessitated the creation of six categories to replace the intended two. The effect was to reduce the number of channels for use in the recognition effort. This limitation was not considered to be significant because of some previous experiences in multispectral recognition studies. The APPM decreased rapidly as the first few channels were selected for use (Table 1). The APPM associated with the use of a fifth channel after the four most optimum have been selected was already less than 1% for all cases. The reduction in classification error from the four- to the six-channel case was not more than 0.35%. Thus, the increase in APPM is minimal especially when more training sets are used on SPARC with fewer channels.

A qualitative comparison of the SPARC color-coded recognition for line 43 with the type-mapped color infrared photograph revealed generally good recognition. Areas typed on the photo as being row crops, bare soil, and water seemed to be accurately identified. Forested areas are well differentiated from nonforested areas. Within forested areas, large dense conifer plantations are solidly recognized. Some confusion exists around edges of plantations and with small clumps of conifers in that bottomland hardwoods and mixed conifer/hardwood forest categories seem to mask the conifer's signature. Within hardwood areas, the predominant recognition seems to be of upland hardwoods, with bottomland hardwoods and mixed conifer/hardwood categories being somewhat more selective. Whether this situation portrays the actual site conditions or is the result of slightly different signature settings on the SPARC is difficult to say.

Pastures show the extreme variability that necessitated the creation of three subcategories during the digital processing. With few exceptions, pasture recognition is characterized by all three of the pasture signatures within the same field boundary. Several sizable fields in the center of the southern half of the flight line have little or no recognition. Although no significant difference between these fields and others in the area can be detected on the photography, they seem to be very unique spectrally. During the training phase of SPARC work, training was attempted in this area, but the resulting signature was very poor in recognizing other areas in the scene, so the training area was moved. A few smaller pastures are recognized as row crops. This is not surprising, considering the time of year and the similarity between mowed hay fields and "browned-out" pastures.

Orchards vary widely in appearance on the photography, ranging from peach and pecan seedlings with bare soil backgrounds to mature trees with pasture-like backgrounds. The training area for the orchards category was placed in a young orchard (not the seedling stage) with a predominantly bare soil background. Other similar orchards were recognized, but mature orchards were understandably classified as upland hardwoods and very young orchards as bare soil.

Transitional areas are spotty in recognition, with much competition between them and upland hardwoods. Water areas were recognized accurately except for one unrecognizable small pond in the center of the line. The very light tone of this pond on the photograph is probably indicative of heavy sediment content to the extent that the spectral signature is significantly different from the "water" signature trained on the SPARC.

In several areas on the SPARC map, low-lying regions of pastures, row crops, and orchards illustrate changes in recognition from the immediate surrounding regions. Many of the same areas show tone changes on the photography but no changes in texture or pattern, indicating spectral variation as a possible consequence of soil moisture conditions. Thus, in the case of automated classification of many land use categories, some of which are only slightly different from each other, it appears that soil moisture conditions adversely affect the accuracy of correct identification.

4.1.2. SIGNATURE EXTENSION OF BLOCK 2

Recognition for signatures trained on line 43 was extended to line 44 flown after line 43 and the two lines, 42 and 41, flown before 43. From a qualitative viewpoint, recognition of land use categories showed only slight change in comparison to line 43. Transitional areas seemed to be more solidly recognized--both east and west of line 43--although we do not know why. Recognition within hardwood areas appears to decline somewhat on the two earlier flight lines, with bottomland hardwood recognition noticeably lacking on line 41. On the signature extension, pastures seemed to be classified into only the "improved" or "old" categories on lines 42 and 41. Very little

"pasture" appears on these two lines.

In comparing results from SPARC and from the photo/ground survey for Block 2, we found that 75 of the sample points or 44 percent were correctly classified (Table 5). The class with the greatest accuracy was pasture--85 percent of the points in pasture were correctly classified, but 18 points were called pasture when they were actually something else. The misclassifications were commission errors. The class that showed the poorest result was transitional agriculture--abandoned agriculture returning to forest. In this case only one point was correct. There were no commission errors. Of the forest classes, pine (conifer) was correctly classified on 29 percent of the point samples, with one commission error. Bottomland and upland hardwoods were classified correctly 50 and 55 percent of the time, respectively, but with a high number of commission errors.

These results suggest the need to reconcile the additional SPARC classification of mixed conifer/hardwood. SPARC was trained to classify only the pure pine plantations as conifer, whereas pines growing in association with hardwoods were recognized as a mixed conifer/hardwood category. If we combined the conifer category with the conifer/hardwood category, we would total 19.1 percent (SPARC) as compared to 20.4 percent (photo point analysis).

As indicated previously, SPARC area counts for each category were tabulated with the high-speed digital counter as recognition strips were printed. Recognition was therefore expressed on a quantitative basis as well as illustrated graphically. Table 3 indicates the scene composition of Block 2 on a percent basis, comparing SPARC classification with photographic point classification. Due to the extensive overlap between MSS flight lines, most of the scene was included more than once when totaling recognition for each category over all four flight lines. However, since total area was also included more than once, percentages for the entire block would not be far off if it is assumed that recognition in any one flight line is uniform over that line and objects recognized are uniformly distributed.

4.1.3. DIGITAL AND SPARC MAP COMPARISONS

A brief comparison of the digital recognition results for line 43 was made with the SPARC results. Their differences were:

	Program EXPLIN	SPARC
WATER:	Excellent recognition	Good recognition -- 1 pond missed. Some perimeters of smaller ponds missed.
CONIFERS, BOTTOMLAND HARDWOODS, MIXED:	Good job separating conifers from hardwoods.	Some conifer areas classified as bottomland hardwoods or undecided forest.
UPLAND HARDWOODS, TRANSITION:	Proper classification of transitional areas.	Too much classification of transitional areas as upland hardwoods.
ORCHARDS:	Seems to be a broader signature. Young orchards are well recognized and portions of bare soil, row crops, and sparse pasture areas are also classified as orchards. Old orchards classified as hardwoods.	Seems to be a more stringent signature. Young orchards are spotty in recognition while not many other areas are classified as orchards. Old orchards classified as hardwoods.
ROW CROPS:	Most row crop areas have some indication of proper recognition, but entire areas are not solidly recognized. Rather much row crop area is classified as orchard, transition, bare soil, and unrecognized categories.	Good recognition.
BARE SOIL:	Many bare soil areas classified as orchards.	Good recognition.

Program EXPLIN	SPARC
PASTURES: Much less improved pasture recognition. "Pasture" category increases. Some portions of fields which were recognized by SPARC are not recognized by EXPLIN.	Considerably more improved pasture recognition.

Overall it appears that EXPLIN was best at classifying the water, transition, and four forest categories. SPARC did better with the orchards, row crops, and bare soil categories. A judgment concerning pasture recognition must be withheld because subcategories of pastures were not typed on the 1:35,000 scale color infrared photograph used for ground truth information.

4.2. BLOCK 4 - MORNING FLIGHT

4.2.1. EIGHT-CATEGORY RECOGNITION OF LINE 14

The absence of the 1.5 to 1.8 μm waveband channel made it difficult to differentiate between upland and bottomland forest or between mixed conifer/hardwood forest and conifers during the SPARC training phase of Block 4. Not only had this channel been the best for discriminating all land use categories in Block 2, but it had been particularly effective in separating the four forest categories from each other. The fact that the channels 0.41 to 0.48 μm and 1.0 to 1.4 μm were unavailable for use also contributed to the recognition difficulties and the resultant decrease in number of categories.

A qualitative comparison of the SPARC color-coded recognition for line 14 was again made with the type-mapped color infrared photograph. Areas of conifers, hardwoods, bare soil, water, and transition seemed to be accurately recognized. Shadows along tree lines were prominent due to the low sun angle. Many of them were recognized as water. Such recognition may be related to the existence of early morning frost which was known to have been present.

Many pasture areas in line 14 are not well recognized, again pointing out the extreme variability of these areas. Increased pasture recognition could probably have been obtained in both blocks with the addition of more training areas.

A different type of quantitative assessment of recognition reliability on line 14 was made as an additional experiment to test an objective method for reporting recognition results. Line 14 provided a good opportunity to make such a test since the various categories of land use are fairly well distributed throughout the scene. Moreover, the frequency of each category permitted the selection of several test areas.

Using the typed color infrared photograph, we selected areas which appeared similar to the eight land use classes for which SPARC was trained. Three areas per class were defined, approximately 2,500 square meters in size. Areas used for training signatures were not selected. A gate was placed in each of the selected areas, and the appropriate signature was played on the SPARC. Recognition of the area within the gate was recorded in terms of the area count registered on the high-speed digital counter. Percent recognition was obtained by dividing the number of correctly recognized points by the total area count of the training area (Table 6).

Good performance in this test requires that the test areas be accurately typed on the photograph. And areas selected within each category should be spectrally representative of the class. Areas of conifers and bare soil show high recognition because they satisfy both of these requirements. Hardwoods and water show slightly less recognition because of some inherent spectral variability between test areas and the trained areas. Ponds have obvious tone differences on the photograph owing to depth and sediment content. And deciduous forest areas do not manifest the smooth, continuous canopy that conifers do.

The mediocre performance for the three pasture categories can be attributed to the spectral variability inherent in pasture areas in November and the failure of the photographic type map to recognize three separate categories of pasture. Test areas were selected from the photo solely on the basis of tone similarity to the trained areas.

Low performance for "transitional" areas is mostly due to the great spectral variability from one area to the next. A difficulty encountered in testing transitional areas was finding areas large enough in which to place a gate. Aside from the two large areas trained during initial recognition work, other transitional areas are spotty in appearance. This difference made it difficult to get a high percentage of recognition in any gated area.

4.2.2. SIGNATURE EXTENSION FOR BLOCK 4 - MORNING FLIGHT

Table 4 indicates the scene composition of Block 4 on a percent basis. Several noticeable deviations from proper recognition were manifested on each of the three earlier flight lines in Block 4. The water, transitional, and pasture categories showed changes, with the others showing little or no changes.

Water recognition faded slightly on each earlier line; that is, ponds began to display less solid recognition. Small ponds on the earliest flight line were identified, but most were only 50 percent recognized. There was a significant increase in the recognition of shadows as water on each earlier flight line--a development which dramatizes the rapidly changing sun angle.

Transitional areas actually became more and more misclassified as hardwoods on each earlier flight line. Most of these areas were small fringe areas. However, large areas of transition continued to be correctly identified--even on the earliest flight line.

The recognition of pastures appeared to improve greatly on the three earlier flight lines.

A comparison of the SPARC results with the ground survey showed that there were fewer errors in Block 4 than in Block 2 (Table 5). For instance, pasture again was classified with the greatest accuracy but with a high number of commission errors--90 percent were correct, and there were 18 commission errors. The transitional class was correct 45 percent of the time, with two commission errors. Of the forest types, pine was correct 80 percent of the time but with a high number of commission errors. Combined hardwood types were correct at 60 percent of the point samples, with moderately high commission errors.

The accuracies for water and urban areas seem to be rather consistent between the two test blocks according to the point sample analysis. For instance, water was correct in 60 percent of the cases on both blocks. For the purpose of the point sample analysis, the urban class (towns, highways, and other manmade features) was considered the same as the SPARC unclassified area. Using this criterion, we found 60 and 75 percent agreement on the urban classification for the two blocks. A large number of commission errors were found in Block 2 but only a few in Block 4.

4.2.3. ADDITIONAL PROCESSING OF LINE 12, BLOCK 4

Our attempts to correct for changes in illumination and angle effects on line 12 were inconclusive. In general, water recognition increased for each successive correction. However, the variation in recognition was not uniform; that is, some ponds increased while others decreased in recognition for each correction applied. The variation seemed to be independent of pond location in the flight line.

A slight increase in the proper recognition of transitional areas was noted with the correction for illumination level. However, the improvement did not account sufficiently for all the transitional areas typed on the photograph.

For most categories, the correction for illumination level (both by itself and in combination with the correction for angle effects) resulted in large, inordinate changes in recognition. However, the application of new preprocessing coefficients as a correction for varying angle effects yielded relatively small changes. In some cases the changes were barely detectable; in others they seemed to increase recognition accuracy slightly. Exceptions included the water and transition categories; water recognition increased greatly to an acceptable level of accuracy, and transition recognition declined instead of increasing.

These results suggest that the correction for angle effects owing to sun angle change is a more important consideration than the correction for illumination level, but some cautions must be borne in mind.

First, the adjustment for angle effects on line 12 was done correctly in that new coefficients were computed from the data itself. However, the observation that prompted the correction was based on a comparison of data collected over two flight lines of nonidentical terrain. The change in angle effect suggested by the average scan lines may have been a consequence of the terrain itself--the slight change in sun angle may have had little or no effect at all.

Second, the assessment of, and adjustment for, change in illumination level may not have been correct. That the sun sensor accounted for illumination change in the low sun angles is doubtful for two reasons:

1. The projected area of the flat opal glass surface exposed to the sun varies as the cosine of the illumination angle. At low sun angles, slight attitude changes caused by aircraft roll will have considerable effects on the exposed surface area of the sun sensor.

2. The transmission of opal glass varies with angles of incidence (Wiseman, 1969).

A more accurate method of assessing illumination change would have involved the use of a pyrheliograph and other ground-based data collected at the time of the flight.

4.3. MOSAIC QUALITY

Each block mosaic was assembled by standard photo-mosaicking procedures. Sufficient sidelap between flight lines was insured during the planning phase of data collection. All flight lines were flown in the same direction so that crab angles, if any, would be constant for all runs. A standard processing function involved correcting the data for roll to prevent displacement of features along the scan line.

The length of recognition strips for successive flight lines was adjusted by using the first flight line processed for that block as a standard. This effort to insure uniform aspect ratio corrected for slight changes in aircraft speed (averaged over the run) that occur from one run to the next. Any residual mismatch of terrain features must be attributed to random pitch and crab motions or speed variations of the aircraft during the flight. The effect of these slight changes in aircraft attitude on data collected from 10,000 ft is considerable. Witness the mismatch of terrain features at the northern end of lines 41 and 41 in Block 2. SPARC mosaics show obvious geometric distortions when compared to the 1:35,000 scale color infrared photography. This fact makes point comparisons difficult at best. However, errors introduced from mosaic distortions are clearly the type which can be improved on in future missions.

5. CONCLUSIONS AND RECOMMENDATIONS

At first glance the results of this feasibility test may appear to be discouraging, but they do afford some promising leads. This study marked the first time multispectral scanner data were used to classify forest type and land use on an area basis. And we did not expect to solve all problems in one test. On the whole, the study demonstrated an advancement in making terrain class maps by automatic data processing methods. Signature extension from one flight line to the remaining three was deemed reasonably successful. But it was not as successful for the morning data as for the noon data.

On the basis of the results, we concluded that:

1. Recognition of 12 categories (four forest, three pasture, bare soil, water, row crop, orchard, and transition) was possible by using data collected near noon from Block 2. On Block-4 data collected in early morning, eight-category recognition seemed reasonable (two forest, three pasture, water, bare soil, and transition). The drop in the number of discriminable classes can be attributed in part to the nonavailability of the 1.5 to 1.8 μm channel. This channel was found best for discrimination of hardwood forest categories.

2. Some deficiency in signature extension existed even after attempts to correct data for changes in irradiance (using sun sensor) and for effects of scan angle for each line. This deficiency may be caused by imperfect estimates of scan angle variations, which in turn are caused by scene nonhomogeneity and by the poor diffusion provided by the sun sensor at the low sun angles encountered in the morning data. More work is required to extend adequately signatures in morning data. Specific areas for study would include: (a) a better algorithm for applying sun sensor and other ancillary information, (b) an improved sun sensor design, and (c) the use of atmospheric model results to correct preprocessing data.

3. The quality of the mosaic of recognition maps is compromised by uncertainties of aircraft altitude and velocity change. Uncertainty in these parameters directly affects both map quality and accuracy of point location. Better geometric fidelity is required before forest managers can accept classification data, by location. Improvements in knowledge of aircraft parameters is required and should be immediately studied.

4. Optimum channels for the noon data include a visible red, two near infrared, and a thermal channel. This combination demonstrates the utility of the single-aperture M-7 scanner which brought these bands together for the first time in an operational airborne multispectral scanner.

5. Electronic classification using multispectral scanner data is new to forestry classification, and we recognize that the forest and nonforest classes used in the processing may not be the best for multispectral recognition. For this reason, our classifications should be

reexamined and redefined, if necessary, to improve recognition accuracy.

Additional research is needed at all seasons to test and improve techniques and classifications. But the potential for automatic data processing of airborne data is more promising than other systems tried to date.

REFERENCES

1. Aldrich, Robert C. 1953. Accuracy of land-use classification and area estimates using aerial photographs. J. Forestry 51(1):12-15.

2. Aldrich, R. C., and W. J. Greentree. 1972. Microscale photo interpretation of forest and nonforest land classes. Fourth Annual Earth Resources Program Review, Manned Spacecraft Center, Houston, Texas. 1972: 121-1 through 121-21.

3. Burge, W. G., and W. L. Brown. 1970. A study of waterfowl habitat in North Dakota using remote sensing techniques. Report No. 2771-7-F, Willow Run Laboratories, Institute of Science and Technology, University of Michigan.

4. Erickson, J. D., and F. J. Thomson. 1971. Investigations related to multispectral imaging systems for earth-resources surveys. Report No. 31650-17-P, Willow Run Laboratories, Institute of Science and Technology, University of Michigan.

5. Hasell, Philip G., Jr. 1972. Michigan experimental multispectral scanner system. Fourth Annual Earth Resources Program Review, Manned Spacecraft Center, Houston, Texas. 1972: 34-1 through 34-13.

6. Kolipinski, M. C., A. L. Higer, N. S. Thomson, and F. J. Thomson. 1969. Inventory of hydrobiological features using automatically processed multispectral data. Proc. Sixth International Symposium on Remote Sensing of Environment, Institute of Science and Technology, University of Michigan. 1969: 79-95.

7. Malila, W. A., R. B. Crane, C. A. Omarzu, and R. E. Turner. 1971. Studies of spectral discrimination. Report No. 31650-22-T, Willow Run Laboratories, Institute of Science and Technology, University of Michigan.

8. Marshall, R. E., N. S. Thomson, F. J. Thomson, and F. J. Kriegler. 1969. Use of multispectral recognition techniques for conducting rapid, wide wheat surveys. Proc. Sixth International Symposium on Remote Sensing of Environment, Institute of Science and Technology, University of Michigan. 1969: 3-20.

9. Nalepka, R. F., H. M. Horwitz, and N. S. Thomson. 1971. Investigations of multispectral sensing of crops. Report No. 31650-30-T, Willow Run Laboratories, Institute of Science and Technology, University of Michigan.

10. Nalepka, R. F., and F. J. Thomson. 1972. Contribution to the corn blight watch final report. Report No. 31650-104-L, Willow Run Laboratories, Institute of Science and Technology, University of Michigan.

11. Suits, G. H., G. Safir, and A. Ellingboe. 1972. Prediction of directional reflectance of a corn field under stress. Fourth Annual Earth Resources Program Review, Manned Spacecraft Center, Houston, Texas. 1972: 31-1 through 31-11.

12. Turner, R. E., W. A. Malila, and R. F. Nalepka. 1971. Importance of atmospheric scattering in remote sensing or everything you've always wanted to know about atmospheric scattering but were afraid to ask. Proc. Seventh International Symposium on Remote Sensing of Environment, Institute of Science and Technology, University of Michigan. 1971: 1651-1698.

13. Weber, F. P. 1971. The use of airborne spectrometers and multispectral scanners for previsual detection of ponderosa pine trees under stress from insects and disease. In: Monitoring Forest Land From High Altitude and From Space. Annual Progress Report for Earth Resources Survey Program, OSSA/NASA, by the Pacific Southwest Forest and Range Experiment Station. 24 p.

14. Weber, F. P., and F. C. Polcyn. 1972. Remote sensing to detect stress in forests. Photogramm. Eng. 38(2):163-175.

TABLE 1. OPTIMUM CHANNEL SELECTION SEQUENCE FOR ALL 12 CATEGORIES OF BLOCK 2

Spectral Channel	ITERATION NUMBER										
	1	2	3	4	5	6	7	8	9	10	11
0.41-0.48 μm	0.1130	0.0297	0.0151	0.0093*							
0.46-0.49 μm	0.1324	0.0398	0.0185	0.0118	0.0086	0.0065	0.0056	0.0051	0.0049	0.0045	0.0042*
0.50-0.54 μm	0.1198	0.0389	0.0179	0.0109	0.0083	0.0063	0.0055	0.0050*			
0.52-0.57 μm	0.1165	0.0340	0.0167	0.0105	0.0080	0.0059*					
0.55-0.60 μm	0.0987	0.0331	0.0189	0.0122	0.0087	0.0067	0.0056	0.0052	0.0046*		
0.58-0.64 μm	0.0959	0.0329	0.0197	0.0127	0.0081	0.0068	0.0055	0.0051	0.0047	0.0044*	
0.62-0.70 μm	0.1004	0.0324	0.0197	0.0126	0.0073*						
0.67-0.94 μm	0.2026	0.0323	0.0178	0.0129	0.0089	0.0067	0.0054*				
1.0 -1.4 μm	0.1575	0.0325	0.0140*								
1.5 -1.8 μm	0.0514*										
9.3-11.5 μm	0.1389	0.0226*									

* indicates the lowest average pairwise probability of misclassification for each iteration. Thus, the 1.5 to 1.8 was first, 9.3 to 11.5 second, 1.0 to 1.4 third, etc.

TABLE 2. OPTIMUM CHANNEL SELECTION SEQUENCE FOR EACH OF THREE POSTULATED CLASSIFICATION PROBLEMS FOR BLOCK 4

	ITERATION NUMBER									
	1	2	3	4	5	6	7	8	9	10
	ALL 11 LAND USE CATEGORIES									
Spectral Channel (μm)	0.58-0.64	2.0-2.6	0.67-0.94	0.62-0.70	0.41-0.48	1.0-1.4	0.52-0.57	0.55-0.60	0.46-0.49	0.50-0.54
APPM*	0.1238	0.0711	0.0444	0.0326	0.0251	0.0210	0.0185	0.0179	0.0172	0.0166
	FOUR FOREST CATEGORIES									
Spectral Channel (μm)	0.41-0.48	0.58-0.64	1.0-1.4	2.0-2.6	0.62-0.70	0.67-0.94	0.52-0.57	0.46-0.49	0.55-0.60	0.50-0.54
APPM*	0.2056	0.1620	0.1383	0.1277	0.1081	0.1007	0.0955	0.0921	0.0896	0.0877
	FOUR FOREST AND THREE PASTURE CATEGORIES									
Spectral Channel (μm)	0.52-0.57	0.41-0.48	0.58-0.64	2.0-2.6	0.62-0.70	1.0-1.4	0.67-0.94	0.46-0.49	0.50-0.54	0.55-0.60
APPM*	0.1408	0.0919	0.0710	0.0574	0.0463	0.0390	0.0355	0.0343	0.0332	0.0323

* APPM is average pairwise probability of misclassification

TABLE 3. SCENE COMPOSITION IN BLOCK 2
BY PHOTO INTERPRETATION/GROUND SURVEY AND SPARC

Land Classification	Number of Photo Points	Area, by Land Use	
		CIR Photo/Ground Survey	SPARC
		Percent	
Pine	100	20.4	3.7
Pine/hardwood mixture	--	--	15.4
Upland hardwood	20	4.1	27.8
Bottomland hardwood	89	18.2	6.0
Agriculture	70	14.3	7.8
Pasture	118	24.1	28.0
Transitional	20	4.0	3.5
Orchard	16	3.3	1.6
Urban	50	10.2	5.3
Water	7	1.4	0.9
TOTAL	490	100.0	100.0

TABLE 4. SCENE COMPOSITION IN BLOCK 4
BY PHOTO INTERPRETATION/GROUND SURVEY AND SPARC

Land Classification	Number of Photo Points	Area, by Land Use	
		CIR Photo/Ground Survey	SPARC
		Percent	
Pine	135	29.5	37.8
Hardwood	96	21.0	28.5
Agriculture	36	7.9	2.2
Pasture	106	23.1	19.7
Transitional	28	6.1	5.9
Urban	45	9.8	4.3
Water	12	2.6	1.6
TOTAL	458	100.0	100.0

TABLE 5. ACCURACY OF SPARC CLASSIFICATION
AS DETERMINED BY PHOTOGRAPHIC SAMPLE POINT ANALYSIS

Land Classification	Classification Accuracy		Commission Errors
	Number of Points	Percent	Number of Points
	BLOCK 2		
Pine[1]	4	29	1
Bottomland hardwood	10	50	20
Upland hardwood	11	55	35
Agriculture	10	50	3
Pasture[2]	17	85	18
Transitional	1	0	0
Orchard[3]	2	14	0
Urban[4]	12	60	14
Water[5]	9	60	4
ALL CLASSES	75	44	96
	BLOCK 4		
Pine	16	80	20
Hardwood	24	60	19
Agriculture	3	15	2
Pasture[6]	18	90	18
Transitional	9	45	2
Urban	15	75	1
Water	12	60	1
ALL CLASSES	97	61	63

[1] Fourth forest category, "mixed pine/hardwood" was not considered in analysis

[2] Includes all three categories of pastures

[3] Insufficient number of points to obtain 20 samples; 16 used

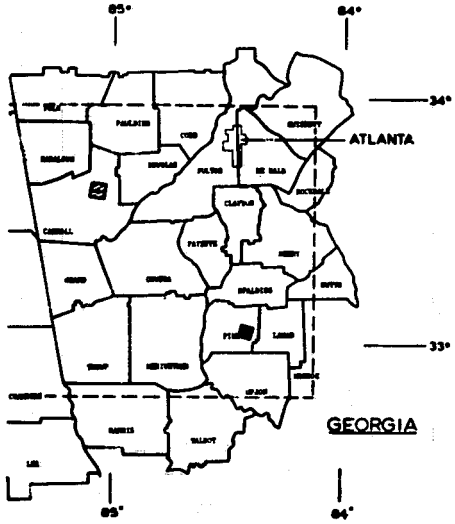
[4] Unclassified areas considered urban

[5] Insufficient number of points to obtain 20 samples; 15 used

[6] Includes both categories of pasture

TABLE 6. QUANTITATIVE ANALYSIS OF SPARC RECOGNITION ACCURACY FOR TEST AREAS IN LINE 14, BLOCK 4, BY COMPARISON TO PHOTOGRAPHIC INSPECTION

TEST AREA	PERCENT RECOGNITION
Conifers (1)	98.0
Conifers (2)	98.7
Conifers (3)	87.4
Mean	94.7
Hardwoods (1)	86.3
Hardwoods (2)	78.3
Hardwoods (3)	68.9
Mean	77.8
Improved pasture (1)	77.6
Improved pasture (2)	59.8
Improved pasture (3)	95.6
Mean	77.7
Old pasture (1)	72.3
Old pasture (2)	88.5
Old pasture (3)	35.4
Mean	65.4
Pasture (1)	87.1
Pasture (2)	90.6
Pasture (3)	8.9
Mean	62.2
Bare soil (1)	97.4
Bare soil (2)	85.3
Bare soil (3)	87.9
Mean	90.2
Water (1)	79.7
Water (2)	74.2
Water (3)	93.7
Mean	82.5
Transition (1)	56.4
Transition (2)	0.6
Transition (3)	14.1
Mean	23.7



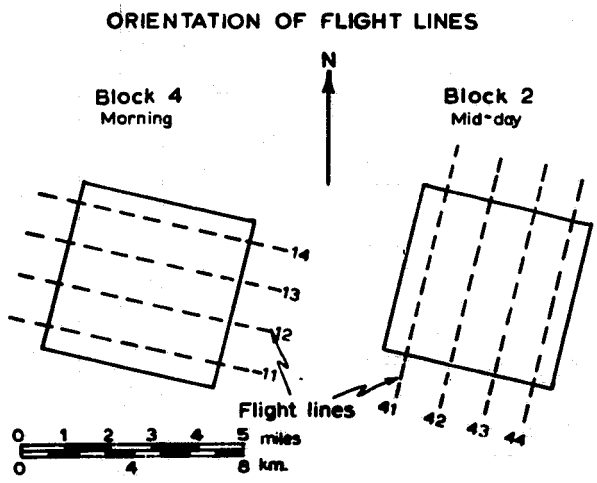


FIGURE 1. UPPER PHOTO. These two 42-square-kilometer test sites were used in the study. Block 2 is 96 kilometers south of Atlanta, and Block 4 is 73 kilometers west of Atlanta.

LOWER PHOTO. Flight lines were oriented as shown for early morning, 0900 hours (Block 4), and midday, 1200 hours (Block 2), flights.

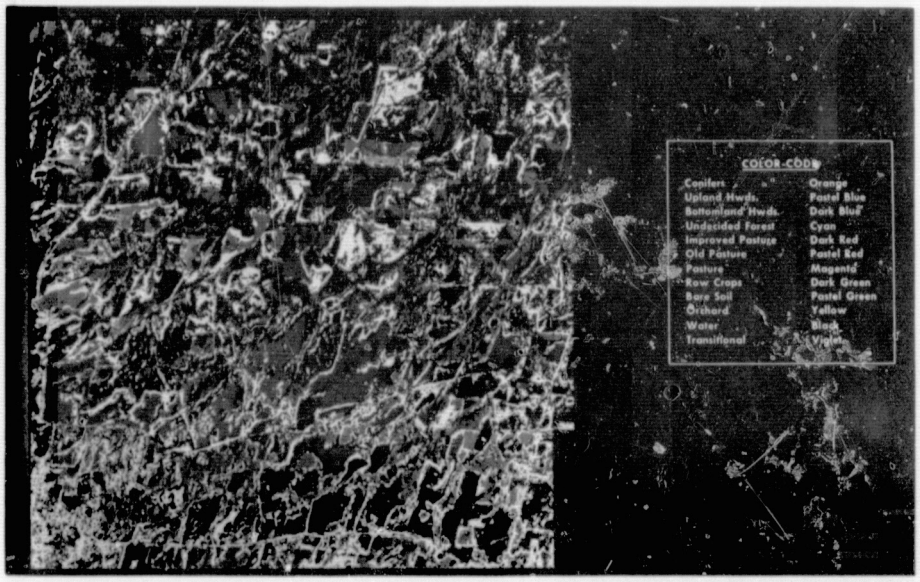


FIGURE 2. a. Study Block 2 is Shown by the SPARC System-Produced Recognition Map with 12 Color Coded Land Use Classifications.

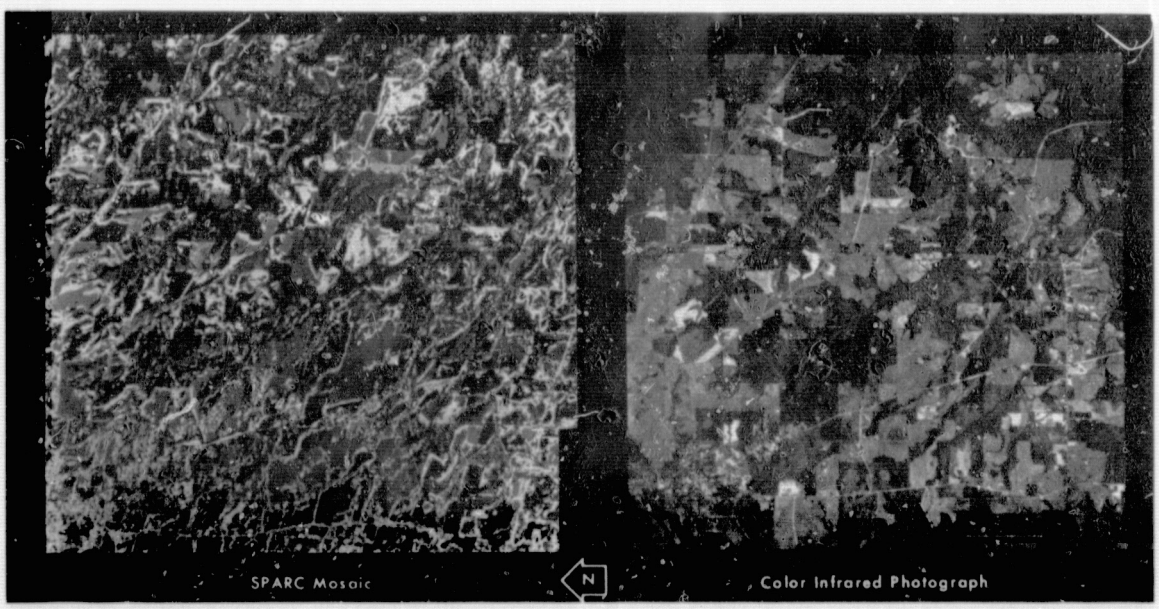


FIGURE 2. b. The SPARC Classification Map for Block 2 (Left) is Shown With the 1:35,000 Scale Color Infrared Ground Truth Photograph (Right).



FIGURE 3. a. Study Block 4 is Shown by the SPARC System-Produced Recognition Map With 8 Color Coded Land Use Classifications.

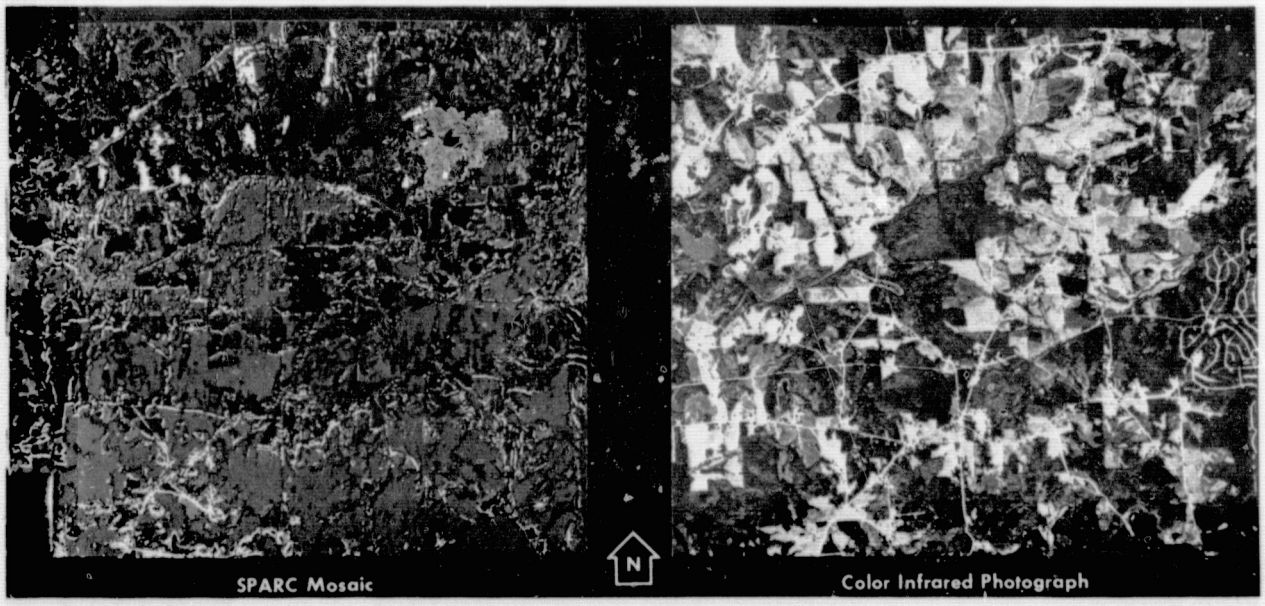


FIGURE 3. b. The SPARC Classification Map for Block 4 (Left) is Shown With the 1:35,000 Scale Color Infrared Ground Truth Photograph(right).

UTILIZING REMOTE SENSING DATA FOR LAND USE DECISIONS FOR INDIAN LANDS IN SOUTH DAKOTA[1]

by

C. J. Frazee, R. L. Carey, and F. C. Westin[2]
Remote Sensing Institute and
Plant Science Department
South Dakota State University
Brookings, South Dakota
and
Branch of Land Operations
Bureau of Indian Affairs
Aberdeen, South Dakota

ABSTRACT

Research was initiated on the Pine Ridge Reservation in southwestern South Dakota to determine the usefulness of remote sensing techniques for making, updating, and revising soil and range inventories. Photographic and thermal-infrared imagery were acquired at an altitude of 11,500 feet above ground level on October 15, 1970; June 30, 1971; and August 2, 1971. A density slicing system was used by experienced soil and range scientists to enhance film optical density differences associated with range sites and soils. Prints enlarged from 35 mm slides of the density slicing analyses were used in the field to compare soil and range boundaries, as delineated by density slicing, to actual soil and range conditions.

The range site boundaries in native rangeland areas were delineated best by the density slicing analysis of color infrared film obtained in August 1971. The range site maps produced by density slicing were superior to existing range inventory maps. The density slicing analysis of color infrared film from the August 1971 flight was best for locating soil boundaries in rangeland areas. Data based upon density slicing, used in conjunction with slope gradient information derived from stereoscopic analysis, were needed to adequately map soils in rangeland areas. These soil maps produced by density slicing and stereoscopic analyses provided more detailed and accurate information than is presently available from existing maps of the area.

Examples of interpretive groupings of soil and range inventory data for uses which currently are of interest to resource managers on the reservations in South Dakota are shown. The soil units were rated according to their suitability for cropland, recreational development, and irrigation. Range sites were used to determine land value, potential grass production, and suitability for range improvement practices.

INTRODUCTION

The increasing demand for food and fiber dictates that soil and range resources of agricultural and wildland areas be accurately identified and located. The soils and their limitations for various land uses must be known to make wise land-use and management decisions. Knowledge of range resources, how much and where, is essential for determining the potential of an area for producing beef.

Presently this information is available in reports similar to the soil and range inventory of the Pine Ridge Reservation which was completed in 1961 (BIA, 1963). The soil inventory describes the kinds of soils, their location, and their limitations to various types of land use. Soil inventory data are used to indicate: areas where soil conservation practices are necessary, soils suitable for cultivation, soils suitable for irrigation, and areas suitable for non-agricultural

---

1 [1]Approved for publication by the Director of the South Dakota Agr. Exp. Sta. as Journal Series No. 1138. SDSU-RSI-72-18. Work performed under Bureau of Indian Affairs contract A00C14201232 and NASA contract NGL 42-003-007.

[2]Assistant Professor, Plant Science Department, South Dakota State University, Brookings, S. D. 57006; Area Soil Scientist, Bureau of Indian Affairs, Aberdeen, S. D. 57401; and Professor, Plant Science Department, South Dakota State University, Brookings, S. D. 57006.

Preceding page blank

uses such as recreation development. The range inventory, which lists the kinds of range and its suitability for grazing, is one of the tools used to determine the number of cows which can be grazed on a range unit. The condition of the range changes with time primarily according to intensity of grazing. Therefore, range inventories rapidly become outdated and need updating almost annually. Also, the soil inventory needs to be revised as more is learned about the soil and as land use becomes more intensive.

The soil and range inventory of the Pine Ridge Reservation (BIA, 1963) is over ten years old and the range inventory is rapidly becoming outdated. Many changes in the condition of the range have occurred which need to be considered in determining stocking rates. These changes can not be physically monitored with present techniques and resources. With present techniques, 20 to 30 man-years would be required to update the soil and range inventory of the Pine Ridge Reservation. Hopefully, remote sensing will provide the tools to accomplish the updating and revising in less time. Considerable research is necessary to determine the exact role of remote sensing for updating soil and range inventories.

The objectives of this initial research effort are:

1. To determine the validity of remote sensing for making and updating soil and range inventories.

2. To demonstrate the use of soil and range inventory data for typical land-use decisions facing resource managers on Indian reservations.

DESCRIPTION OF STUDY AREA

Bennett County lies in the Missouri Plateau subdivision of the Great Plains physiographic province which is covered by Tertiary sediments (Fenneman, 1931). This area was selected because a large amount of ground data is available for reference (Collins, 1959, 1960; Chamberlin and Radeke, 1971). The study area is part of the Pine Ridge Reservation in southwestern South Dakota (Figure 1). Approximately 300,000 of 761,000 acres of land in the county are Indian owned. Nearly three-fourths of the county is covered with native mid- to short-range grasses which are used for grazing. The other major land use of the county is winter wheat farming (20%). The three major soil associations of the study area are the rolling to hilly sandy soils of the Nebraska Sandhills in the south, the nearly level to gently sloping silty soils in the central area, and the rolling to hilly loamy soils in the northern part of the county. The major soil limitations are:

1. erosion of sloping upland soils

2. wetness of depressional or alluvial areas

3. soil rooting zone limitations

   a. claypans of varying depths and thickness

   b. shallow depth to bedrock

   c. shallow sandy and silty soils

   d. shallow depth to gravel.

Additional data and information about Bennett County and the study areas may be found in Chamberlin and Radeke (1971) and Collins (1959, 1960)

MATERIALS AND METHODS

Photographic and thermal-infrared data were acquired for the study area using the South Dakota State University Remote Sensing Institute's aircraft at an altitude of 11,500 feet above ground level on October 15, 1970; June 30, 1971; and August 2, 1971.[3] The flight line is two miles wide and 28 miles long (Figure 1). The following sensors were flown: (1) 70 mm Hasselblad camera with black and white film filtered to study the green portion of the visible spectrum (Kodak 2402 with Wratten filter no. 58), (2) 70 mm Hasselblad camera with black and white film filtered to study the red portion of the visible spectrum (Kodak 2402 with Wratten filter no. 25A), (3) 70 mm

[3]All photographic and thermal scanner data used during this project were collected for NASA contract NGL 42-003-007.

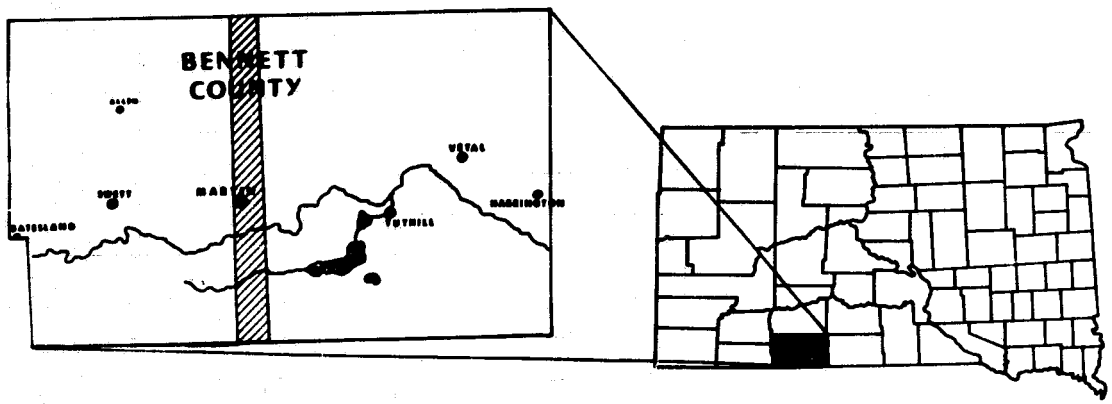


Figure 1. - LOCATION OF FLIGHT LINES IN BENNETT COUNTY, SOUTH DAKOTA

Hasselblad camera with color infrared film (Kodak 2443 with Wratten filter no. 15G and Kodak filter no. 30M), (4) 70 mm Hasselblad camera with black and white infrared film (Kodak 2424 with Wratten filter no. 89B), and (5) a thermal-infrared scanner, 4.5-5.5μ wavelength. In addition, night time flights were made with the thermal-infrared scanner. These data were obtained to evaluate the importance of season and sensor type for collecting remote sensing data for soil and range site mapping. Ground data on the various land-use and soil conditions were recorded at the time of overflight.

To assist the visual interpretations of the imagery, a density slicing system was used by experienced soil and range scientists to enhance optical density differences associated with soils and range sites (Frazee et al, 1972). Density slicing analyses were made of all available imagery from each flight for several cropland and rangeland areas. The resultant color encoded representations were photographed and enlarged prints were made for field checking. The enlarged prints were used in the field to compare soil and range boundaries as delineated by density slicing to the actual soil and range conditions. The density slicing analysis which best represented the actual field situation was selected and the other density slicing analyses were visually compared to that analysis. The slope gradients of the areas separated by the density slicing analysis were estimated using a mirror stereoscope.

This research is related and largely dependent on the project, "Remote Sensing of Soils, Land Forms, and Land Use in the Northern Great Plains in Preparation for ERTS Applications", which is funded by NASA contract NGL 42-003-007 under the direction of the Earth Observation Office and Office of University Affairs. A portion of the imagery collected for the above NASA contract was interpreted for specific uses that the Bureau of Indian Affairs have for remote sensing data. This research was cooperative with Bureau of Indian Affairs personnel working closely with scientists from the Remote Sensing Institute and the Plant Science Department on all aspects of the project.

RESULTS AND DISCUSSION

TIME FOR ACQUIRING IMAGERY

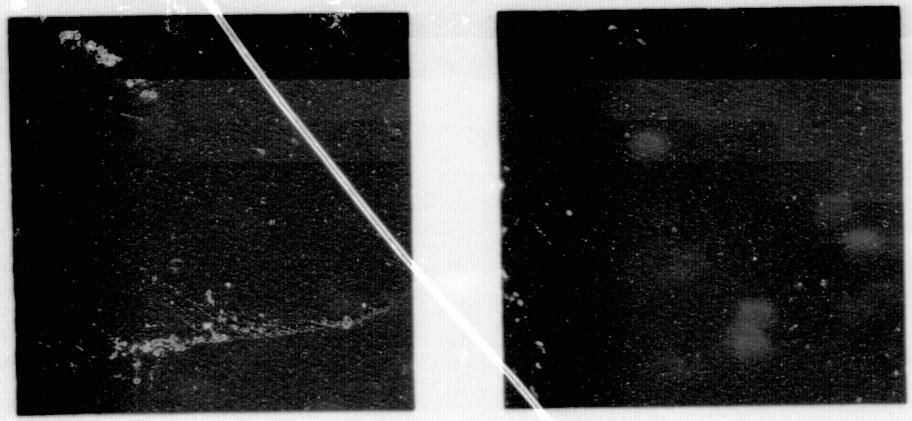
The time or season for collecting remote sensing data is important primarily because the vegetative cover on the soil surface changes seasonally. The photographic characteristics associated with soils, primarily tone and pattern, usually are significantly affected by seasonal changes in vegetation and frequently to the extent that the photograph or image is not suitable for making inferences about soils. If remote sensing techniques are to be effectively utilized, the images or photographs to be interpreted must be acquired at the time when the recognition features associated with soils or range sites are optimized. Presently, most soil and range inventories are prepared using available photography rather than optimum photography.

The vegetative cover on the soils of the native rangelands changes seasonally (Figure 2). In October the range grasses were matured and the contrast in photographic tones was small (Figure 2). The reflectance patterns from the June and August, 1971, imagery were similar and had more contrast than the October imagery (Figure 2). The differences in native vegetation are greatest and soil conditions are indicated more clearly on either the June or August imagery than on the October imagery.

EVALUATION OF IMAGERY

The photographic tone pattern shown in Figure 3 is typical of the silty rangeland areas in Bennett County. The lighter tones depict areas with shallow or thin soils with severe erosion hazards. The intermediate tones delineate the normal uplands soils which have moderate erosion problems. The darker tones portray soils with deep dark-colored surface horizons which have occasional wetness limitations. In addition to the above, small barren rock outcrops are represented by the lightest tones. These general relationships of tone and soils are displayed on all of the imagery except the black and white infrared film and the midday thermal infrared imagery (Figure 3). There is little contrast on the black and white infrared film except for the drainageways and upland depressions which appear as the lighter tones. These areas have substantial infrared reflectance because of the vegetation growing in these areas. The tone and soil relationships were reversed on the midday thermal infrared imagery when compared to the other imagery.

The density slicing analyses were used to visually rank the various imagery for delineating soil and range site boundaries in rangeland areas. The color encoded density slicing analyses of the midday and pre-dawn thermal infrared imagery did not correspond with soil and range site boundaries observed during the field checking. The poor resolution of thermal infrared imagery is probably the main reason for this observation. The black and white infrared film also was not suitable except for depicting above normal range sites like overflow or closed depression. The delineations which are shown on the density slicing analyses of the black and white films and the



October August

Figure 2. - Seasonal changes of native grasses. T39N, R37W, Sec. 12, NE¼.
Scale = 1:10,560. Kodak 2402 with 25A filter.

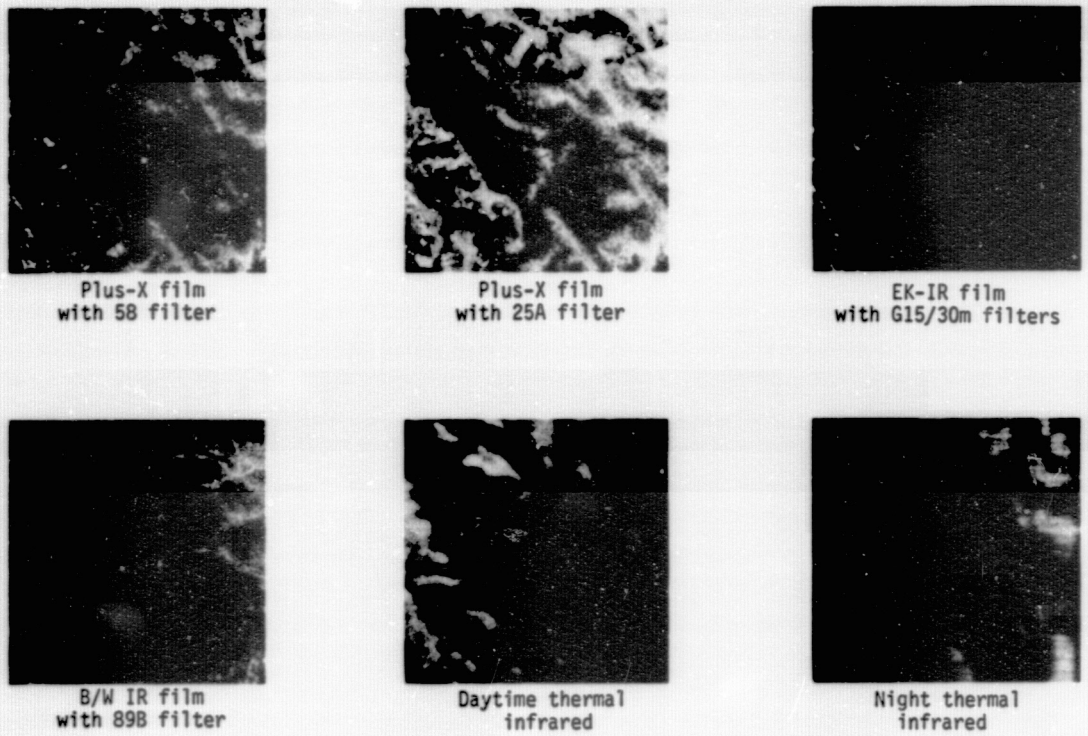


Figure 3. - Photographic and thermal infrared imagery of a representative rangeland area in Bennett County. T39N, R37W, Sec. 32, NE¼. Scale = 1:15,840.

color infrared film are similar and coincide with the actual range site boundaries satisfactorily. For mapping soils, the results were similar to the above except the patterns exhibited on the density slicing analysis of the color infrared film correlated best with the actual soil boundaries.

Based upon the above observations concerning the proper season and the best type of imagery for studying soils and range sites, if one flight is to be flown, the color infrared film would be flown in August to obtain optimum imagery for delineating soil and range site boundaries.

COMPARISON OF DENSITY SLICING ANALYSES WITH EXISTING SOIL AND RANGE SITE MAPS

The density slicing analysis of the color infrared film from the August 1971 flight which best represented actual field conditions was compared to the existing range site and soil maps. Comparison of the map produced by the density slicing analysis with the existing soil map (Chamberlin and Radeke, 1971) reveals little similarity in map units (Figure 4). The individual soils are mapped on the density slicing analysis whereas soil complexes are indicated on the existing map. None of the five color encoded density levels were related to one soil. However, after field checking the color encoded density analysis could be interpreted for soils (Table 1). Two soils were found in the areas color encoded yellow. In order to adequately map these soils, information about the slope gradients of the areas is needed. This information can readily be derived using a stereoscope. The areas color encoded light and dark green represent the L6R-R soil unit. The areas color encoded light green in general, are more sloping. The M6-2 soil unit, which is represented by red and blue colors, is delineated more accurately than on existing maps by the density slicing analysis. Figure 4 illustrates an improved soil map of the area based upon data obtained from the density slicing analysis and slope information derived from stereoscopic analysis. Interpretation of the soil units may be found in Table 1. This map illustrates the use of remote sensing techniques to update soil surveys or inventories. The density slicing analysis of the color infrared film for the rangeland area and the existing range site map (BIA, 1963) are illustrated in Figure 5. The explanation of the range sites mapped by the density slicing analyses is listed in Table 2. The only similarity between the areas illustrated on the density slicing analysis and the existing range site map are in the southwest corner (Figure 5). The shallow or thin upland sites are mapped separately from the silty range sites. The thin upland areas in the northeast corner were not mapped properly on the existing map. The shallow and thin upland range sites which have similar yields appear similar on the imagery and cannot be separated. The areas color encoded black on the density slicing analysis are not shown on the existing map because they are too small. Field checking revealed that the range site map based upon the density slicing analysis is superior and provided more accurate information than the existing map. The delineation on the density slicing analysis more accurately displays the individual range sites than the existing map because the areas shown on the existing map consist of more than one range site (complexes).

TABLE 1. Interpretation of soils mapped by density slicing analysis of T39N, R37W, Sec 32, NE¼.

Color	Area	BIA Soil Unit	Interpretation
	%		
black and yellow	13	L6R-25 and L6R-15	Deep, medium textured, moderately steep and strongly sloping, moderately permeable soils with thin topsoils. Severe water erosion.
light green	66	L6R-6	Deep, medium textured, gently sloping, moderately permeable soils with thin surface layers. Moderate erosion problem.
red and blue	21	M6-2	Deep, medium textured, nearly level, moderately permeable soils with thick surface layers.

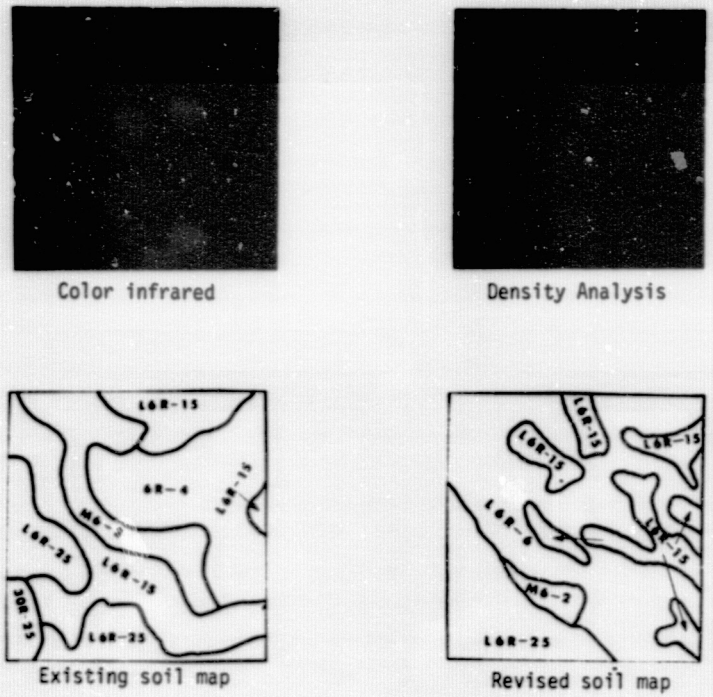
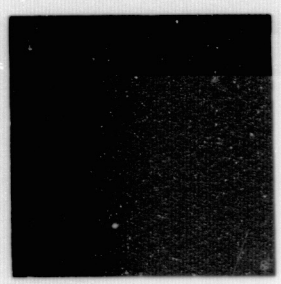
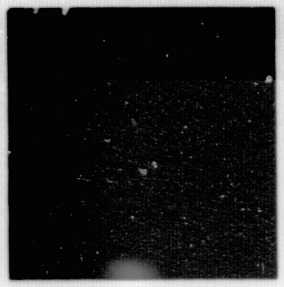


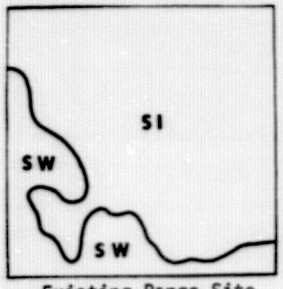
Figure 4. - Use of Remote Sensing techniques to revise soil map. T39N, R37W, Sec. 32, NE¼. Scale = 1:15,840.



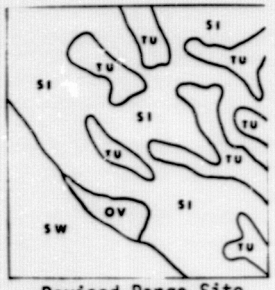
Color infrared



Density Analysis



Existing Range Site Map



Revised Range Site Map

Figure 5. - Use of Remote Sensing techniques to improve range site map. T39N, R37W, Sec. 32, NE¼. Scale = 1:15,840

TABLE 2. Interpretation of range sites mapped by density slicing analysis of T39N, R37W, Sec 32, NE¼.

Color	Area	Range Site	Yield*
	%		lbs/A
yellow	27	thin upland (TU) or shallow (SW)	800
red	59	silty (SI)	1500
black	14	overflow (OV)	2300

*Yield is an air-dry weight obtained from clipping studies within these areas.

USE OF SOIL AND RANGE INVENTORY DATA

Aerial photographs commonly are used as the base map for publishing soil and range inventories (Chamberlin and Radeke, 1971; BIA, 1969). On the maps, alphabetic and numeric symbols indicate not only the soil and range mapping units but also prominent physical and cultural features. Examples of the types of physical features shown are rock outcrops, streams, drainageways, lakes, ponds, and wet spots. Cultural features such as highways, roads, railroads, bridges, cemeteries, buildings, etc. are also shown. To most people these maps and symbols are often confusing. In order to make the detailed soil and range inventory easier to understand and use, the map units are grouped and interpreted for particular uses or needs of users. The agencies who are members of the National Cooperative Soil Survey have worked together to develop interpretive criteria and groups for various soil uses. In South Dakota the agencies involved are: Soil Conservation Service, South Dakota Agricultural Experiment Station, Bureau of Indian Affairs, Bureau of Reclamation, and Forest Service. The following examples illustrate interpretive groups of soil and range units for uses or problems which currently are of interest to resource managers on the reservations in South Dakota.

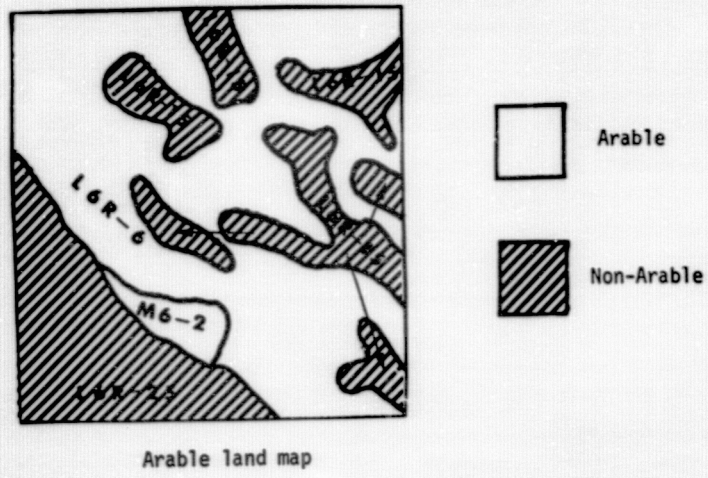
LAND SUITABLE FOR CULTIVATION

The Land Capability Classification System (Klingebiel, A. A. and Montgomery, P.H., 1961) places limitations of soils for crop production into four groups: erosion, climatic, soil rooting zone, and wetness. The kind and degree of limitation is indicated for each soil. The L6R-15 and L6R-25 soils are not suited for cultivation because they occur on moderately steep and steep slopes and have a severe erosion hazard (Figure 6). The last two numbers of the above symbols (15 and 25) indicate the percent slope of these mapping units. The L6R-6 soil units are suited for cultivation. However, these soils are located on strongly sloping areas and have moderate erosion hazards. Special tillage practices are required to control erosion. The M6-2 soil unit has no limitation to crop production except climate. Rainfall is insufficient for most cultivated crops. Figure 6 illustrates the suitability for cultivation of the soils in the study area. Other non-soil factors must be evaluated in order to decide whether to recommend cultivation for this tract of land.

RECREATIONAL DEVELOPMENT

One of the initial steps in determining the suitability of an area for recreational development is to evaluate the soils. Interpretive maps showing the suitability of the soils for playgrounds, camp areas, picnic areas, paths and trails will be discussed (Figure 7). Criteria used for evaluating soils for recreational development include: wetness, flooding, permeability, slope, texture, stoniness, and rockiness (Montgomery, P. H. and F. C. Edminster, 1966).

Rating these soils for suitability for playground development, the L6R-25 area has severe limitations because of steep slopes and shallow depth to bedrock (Figure 7). The L6R-15 soils have severe limitations because of moderately steep slopes. The L6R-6 soils could be used but have moderate limitations because of sloping topography. The M6-2 soils have a moderate limitation due to occasional periods of wetness. The ratings for suitability of the soil areas for picnic areas are the same as for playground development (Figure 7).



Arable land map

Figure 6. - Suitability of soils for cultivation.

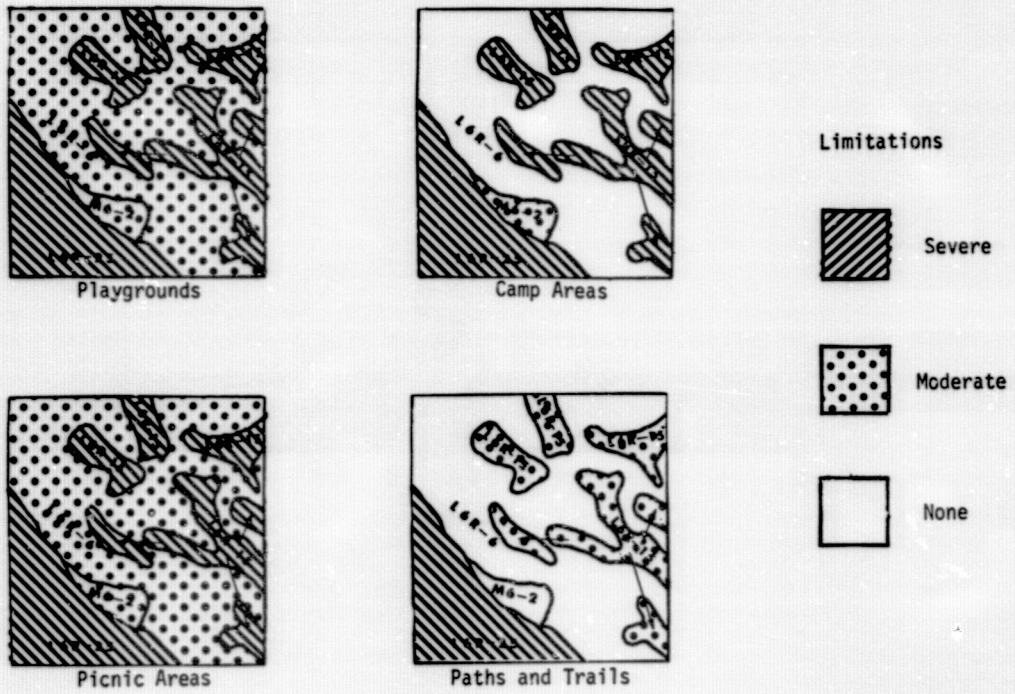


Figure 7. - Suitability of soils for recreational development.

A plan to develop this site for a camp area would have to exclude the L6R-15 and L6R-25 areas because of severe slope limitations. The L6R-6 areas are suitable for camp areas. The M6-2 areas could be used but occasional periods of wetness cause moderate limitations that would have to be considered in planning.

When this area is considered for development of paths and trails, the L6R-25 soils have a severe limitation due to steep slopes (Figure 7). The L6R-15 soils have a moderate limitation due to moderately steep slopes. The L6R-6 and M6-2 soils are suited to this use.

SUITABILITY FOR IRRIGATION

The criteria used to determine the suitability of soil for irrigation have been developed primarily by the Bureau of Reclamation. Although soils are rated for topography, drainage, and soil deficiencies, only soil and topographic limitations will be considered in this presentation. The L6R-25 and L6R-15 soils would be eliminated from an irrigation project because of steep and moderately steep slopes and the shallow depth of the L6R-25 soils (Figure 8). The L6R-6 soils are irrigable but have slope limitations that would be an important factor in determining the type of system to use. The M6-2 soils are also irrigable. These soils have a fine textured subsoil which reduces the permeability slightly.

POTENTIAL FOR PRODUCING GRASS

Rangeland is divided into range sites which are distinct because of local differences in climate, soil, and/or topography. These distinct range sites produce different kinds and amounts of vegetation. The range site boundaries are based upon the soil inventory of the area. The annual yield of herbage produced on the different range sites varies considerably (Chamberlin and Radeke, 1971). The factor most responsible for the differences in grass production within a pasture is usually topography, probably because of its effect on moisture distribution. The potential of an area for producing grass is determined by taking into account the acres of each range site present and the average yield of each range site. The potential for the study area is illustrated in Table 3. The range conservationist uses this information along with observations on condition of the range to estimate stocking rates.

TABLE 3. Potential for producing grass. T39N, R37W, Sec. 32, NE¼.

Range Site	%	Yield*	
		lbs/A	
SW	17.6	1800	
TU	23.8	1850	
SI	55.3	2200	
OV	3.3	3200	
			2079 lbs/A

*Chamberlin, E. and R. E. Radeke, 1971.

RANGE IMPROVEMENT PRACTICES

Range sites differ not only in their potential to produce forage but also in their suitability for various use and management practices. Range improvement practices can or cannot be applied. The practice of reseeding range sites in poor condition cannot be used on the Shallow range sites because the slopes are too steep for the machinery needed and the erosion hazard is severe (BIA, 1963). This practice can be used on Thin Upland and Silty range sites, but conservation practices must be used to control erosion. The Overflow range site can be reseeded if necessary. (Figure 9)

LAND VALUE

A guide to the value of land is valuable to many people; buyers, sellers or appraisers. Consolidation of small tracts on the reservation into larger tracts is necessary to provide areas of suitable size for farming, ranching, or recreational development. The value of the tract shown

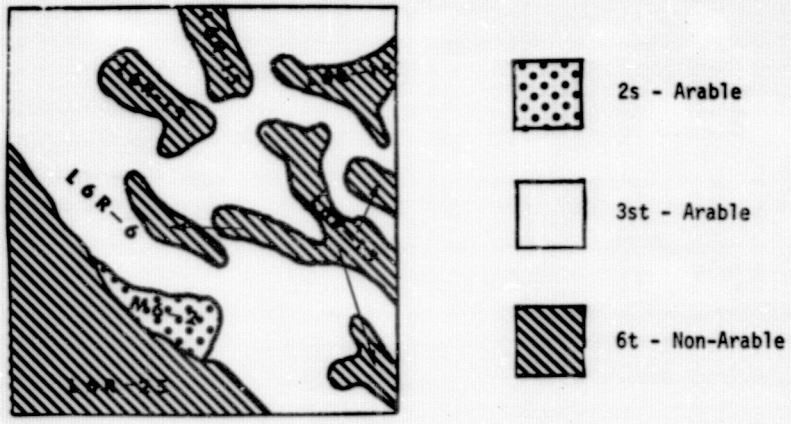


Figure 8. - Suitability of soils for irrigation

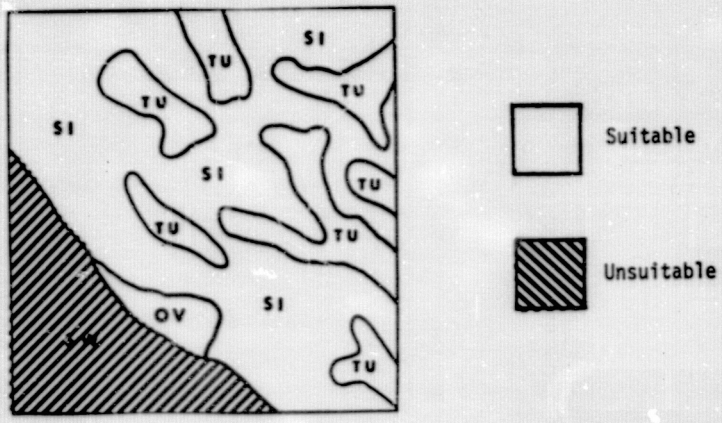


Figure 9. - Suitability for range improvement practices.

in Figure 5 can be calculated using a land evaluation guide developed for western South Dakota (Westin, 1972) (Table 4). The acreages of each range site are multiplied by the CDV (conceptional dollar value) for that range site.

TABLE 4. Value of land in T39N, R37W, Sec. 32, NE¼.

Range Site	%	CDV*	
SW	17.6	$39.06	
TU	23.8	39.06	
SI	55.3	52.08	
OV	3.3	75.22	
			$47.45/A

*F. D. Westin, 1972.

Summary and Conclusions

Photographic and thermal-infrared imagery from three different times were evaluated for use in mapping range sites and soils. Density slicing was used by experienced soil and range scientists to enhance the visual interpretation of soils and range sites of representative cropland and rangeland areas.

The range site boundaries in native rangeland areas were delineated best by the density slicing analysis of the color infrared film obtained in August 1971. The range site maps produced by density slicing were superior to existing range inventory maps.

Density slicing analysis of color infrared film from the August 1971 flight was best for locating soil boundaries in rangeland areas. To adequately map soils in rangeland areas, data based upon density slicing used in conjunction with slope gradient information derived from stereoscopic analyses provided more detailed and accurate information than is presently available from range site and soil maps of the area.

The results of this first year study suggest remote sensing techniques can be applied to making, updating, and revising soil and range inventories. Improved soil and range site maps were produced utilizing film optical density and slope gradient data which were remotely sensed. The utilization of soil and range inventory data for current problems or uses by resource managers on Indian reservations in South Dakota was illustrated.

LIST OF REFERENCES

1. Bureau of Indian Affairs. 1963. The Land of Red Cloud Today. Part II: Its Soil and Range, Present and Potential Use. Aberdeen Area, Branch of Land Operations.

2. Bureau of Indian Affairs. 1969. Soil and Range Resources Inventory, Garvin Basin, Crow Indian Reservation, Montana. Missouri River Basin Investigations Report 193.

3. Chamberlin, E. and R. E. Radeke. 1971. Soil Survey of Bennett County, South Dakota. USDA Soil Conservation Service.

4. Collins, S. G. 1959. Geology of the Martin quadrangle. S. Dak. Geo. Survey map and text.

5. Collins, S. G. 1960. Geology of the Patricia quadrangle. S. Dak. Geo. Survey map and text.

6. Fennemen, N. M. 1931. Physiography of western United States. McGraw-Hill, New York.

7. Frazee, J. J., V. I. Myers, and F. C. Westin. 1972. Density Slicing Techniques for Soil Survey. Soil Sci. Soc. Amer. Proc. 36: 693-695.

8. Klingebiel, A. A. and Montgomery, P. H. 1961. Land Capability Classification. USDA Handbook 210.

9. Montgomery, P. H. and F. C. Edminster. 1966. Use of soil surveys in planning for recreation. In Soil Surveys and Land Use Planning. pp. 104-112. American Society of Agronomy, Madison, Wisconsin.

10. Westin, F. C. 1972. Personal communication.

A COMPREHENSIVE REMOTE SENSING LEGEND SYSTEM FOR THE ECOLOGICAL CHARACTERIZATION AND ANNOTATION OF NATURAL AND ALTERED LANDSCAPES [1]

Charles E. Poulton, Director

Environmental Remote Sensing Applications Laboratory
Professor of Range Ecology
Rangeland Resources Program

Oregon State University
Corvallis, Oregon
97331

ABSTRACT

An integrated legend system is presented for use in multistage inventory of earth resources and land use. Provision is made for symbolic, descriptive and interpretive legend components. The symbolic legend follows a computer-compatible, decimal system and the logic is devisive-hierarchical. The legend has been extensively tested with space, highflight and conventional aircraft photography as well as by note taking on low-level flight and ground reconnaissance. The broader hierarchical classes are especially suited to interpretation of space and highflight imagery. The system provides for treatment of natural vegetation, land uses that have changed the natural landscape, macrorelief, landforms, surficial geological material and soils. The land use legend adapts the classes in the Standard Land Use Coding Manual to this more comprehensive, ecological approach to resource and land use inventory.

INTRODUCTION

Geographers have synoptically portrayed almost every kind of earth resources subject. To do this, they have devised many kinds of classifications and legends for expressing resource, land use, and cultural features of the Earth's surface. The individual natural resource disciplines have also contributed to legend concepts, but generally at a much more refined level of detail. In almost all cases the contributions from both these groups have tended to be single-discipline oriented, although some notable exceptions in team analysis have evolved in recent years (Hills, 1961; Perry, 1962; Lacate, 1966; California State Office, Bureau of Land Management, 1971; U.S. Forest Service, 1972; Bureau of Land Management Manual, Section 1605).

Traditionally, in the United States, resource inventory and analysis have also been single-problem oriented. The product has been the limited sets of data required for solution of a specified problem or to meet the specific information needs of the sponsoring discipline. These kinds of inventory maps and the information they provide have played an important role in the business, industry, politics, planning and development of many regions. Their importance and role in resource development and management are not discounted by the new, emerging requirements of resource planning and allocation in the space age.

PROBLEM STATEMENT

Three changes have taken place in the last decade that require modification of the way we approach the analysis of earth resources and of man's impact on the land, rivers, and oceans we use and presume to manage. The first change is the upsurge of ecological awareness by man himself--what is his total relationship to his environment. This has stimulated a holistic or integrative approach

[1] Technical Paper Number 3435, Oregon Agricultural Experiment Station, Oregon State University, Corvallis, Oregon, 97331.

Preceding page blank

to resource surveys and management rather than the single-discipline resource analysis that has been dominant in the United States through the 1960's and the early 70's. The second change is a quickening of the pace at which resource professionals are picking up and using remote sensing as an information technique in preference to a larger amount of direct ground contact. The shift to stronger reliance on remote sensing technology has drawn attention to the particular characteristics of mapping legends required for imagery interpretation. The third change is the availability to the civilian sector of small-scale, earth-looking remote sensing systems from both high flying aircraft and space platforms. These permit synoptic coverage of extremely large areas. Because these single scenes provide coverage beyond the bounds of individual land ownerships, beyond state and county boundaries and areas of agency jurisdiction, it has become imperative that a common system be developed for the characterization and annotation of both the natural and the altered features of landscapes--including the oceans and seas. This paper presents a contribution to this need. The proposed legend has been designed for compatibility with remote sensing technology. We have strived to maintain a consistent logic in all legend components. What we are now presenting has been developed and tested through numerous revisions over nearly a ten year period and proven useful across a broad spectrum of information needs in resource and land use problem solving and decision making. While we do not claim that the job is necessarily complete or the result perfect, it is our intention to give you a sufficiently clear picture of the approach and the result so that you can evaluate it, hopefully incorporate its strong points into your own work, and help further to refine and improve on the details of the system as we all strive to give man the tools and knowledge required for a more compatible relationship with the Earth that supports him.

PHILOSOPHY OF APPROACH

We in the United States now appear more amenable to guiding resource and land use development through the mechanism of advanced planning with control by social or political action. To be right in these actions, in turn, requires a high level of integrated information derived by multi-discipline teams rather than by individual specialists working in isolation. The emphasis on modeling as an aid to the decision process further implies an integration or meaningful synthesis of information. While one might argue that separate disciplinary surveys can be combined by a system of overlays, from computerized data banks, or by interpretation and redrafting, the problems of cartographic generalization and the "impurity" of mapping units generated by independent disciplines create some time-consuming, if not impossible, difficulties for the person who must interpret and overcome the cartographic anomalies that will forever result when the resource disciplines work in relative isolation. One important question is, "How much of this synthesis can be accomplished or facilitated because of the way inventories are made?" The key objective is to simplify or make more effective the physical inputs to a model or to the human decision. All this means that the basic information system needs to be cast more in a holistic, ecological context. Information synthesis is the keynote! To the extent the resource analyst doesn't accomplish the synthesis, the planner or the management decision maker must. It has proven much more efficient to work from a consolidated legend concept and in a team effort than by later drawing together the separate disciplinary analyses. The end result is ecologically more valid and usually provides information more relevant and meaningful to the solution of individual as well as multiple-use problems. One of the key objectives of resource analysts is to effect easy transfer and efficient use of resource information by the decision maker--the ultimate user of our product.

The ecological context in which present land use and resource management problems are being viewed also requires that a consolidated legend system or philosophy be developed so that the ecology of the natural vegetation, the landforms, soils, water resources, and man's modification of these natural systems can be portrayed in a meaningful and consistent way. While we quickly admit that all information and cartographic detail required for each of the separate disciplines cannot be met with a combined legend system, our experience shows that we can go part way toward this goal with beneficial results to the information user. Admittedly, each discipline may need its own specialized legend system, especially at detailed levels of analysis.

With platforms available for remote sensing of earth resources from conventional to very high altitude aircraft and orbiting satellites, it is essential that legend systems be hierarchical, allowing for both broad levels of generalization and highly specific levels without changing the logic of the system. Subordinate classes should be subsets of a higher hierarchical level in the scheme. National, regional, state and county planning requires broader levels of information generalization that does resource management. At the broader planning levels the detail to which the average resource manager is accustomed may be irrelevant or even confusing to the land use

planner. A generalization of information is essential to put the problem in the perspective of the planning area or region, its people, economy, and politics. Resource managers, on the other hand, require high levels of detail with minimal generalization. The concept of multistage imaging and interpretation has been given increasing attention as a resource inventory technique since the Apollo IX and the S-065 experiment. Thus, the need for a multistage legend scheme is very real.

Furthermore, the acquisition of increasing proportions of resource information by direct image interpretation (by both man and machine) makes it important that the hierarchical classes used in the legend system also be compatible with the image identification needs at each level of scale and resolution in the imagery available to the analyst. This presents some problems and requirements not encountered when devising a legend for conventional planimetric mapping at a single specified scale. Here the legend is only a mechanism for information transfer. Where the legend is to be used in image interpretation, on the other hand, one must ask the additional question, "Can each legend class be discriminated and identified through image analysis at the specified scales?" In legend development for remote sensing, one works toward an affirmative answer to both parts of this question. This requirement is probably new to those who have merely been accustomed to cartographic summarization of results on planimetric or topographic maps. It may also be new to those who may have only used the photo mosaic as a base for data summarization without major reliance on image interpretation to develop the map and related statistical information.

In addition, a multi-discipline legend system cannot be allowed to change with each political subdivision, land ownership or agency responsibility if it is to be meaningful in the context of county, state and regional planning. Those of you who have had experience putting together a meaningful, composite map of a large region from the myriad of systems, mapping intensities, and specialized considerations of separate agencies can probably attest to the relevance and importance of this statement.

Since man has modified natural resource systems in numerous instances, it is important that the legend also accommodate the impact of those land uses that eliminate and replace the natural vegetation. It is not enough merely to have a uniform land use legend or an interpretive land use capability legend. An adequate legend system must permit characterization of the inherent biological and physical features of the landscape together with land use patterns that have altered the surface of the Earth. Such an integrated legend system is called for by the nature of the information needs in resource problem solving that confront us today. One of the most critical needs in land use planning and resource management is for an information base that will provide an accurate picture of the inherent ecological characteristics of the land and that will help us to understand the criteria by which each kind of land can be recognized. This kind of working base also provides three very important side benefits from resource inventory and analysis--namely, (1) by enabling the accurate interpretation of the allowable potentials of each kind of land for use, development, improvement and management, (2) by developing an awareness of the limitations or constraints that the ecological characteristics of each kind of land place on the decisions and actions of man, and (3) by providing an accurate and biologically sound basis for generalizing to new areas what we have learned from experience in resource development and management, and from designed experimentation. This kind of working base permits us to realize greater returns from research on natural resource and land use problems as we seek to guide planning, zoning and the structuring of legislation designed to improve man's relationship to the land.

Most existing land use legends present high levels of detail in agriculture, urban and industrial categories, but range, forestry, recreation and watershed generally are grouped under a very limited number of classes. Inadequate allowance is, therefore, made for the differing levels of use or land use suitability within these latter categories. In areas suitable for these latter extractive but renewable resource uses, the potential for each is generally self-evident when the natural, ecological characteristics of the range or forest area are made known. In addition, a land use legend that uses the categories of "range" and "forestry" or "grazing" and "lumbering or timber industry" confuses land use with a kind of land and produces an unreal exclusiveness in the resource inventory decision. This restricted approach does not allow for the almost universal fact of dual- and multiple-use in naturally vegetated landscapes. In addition, such use-biased classes preclude the opportunity to express the natural vegetational and soil characteristics that are the key to allowable kinds and combinations of land use, current or potential, on each natural landscape.

An explanation of what we mean by a natural resources and land use legend is appropriate before presenting the details. We view the legend much as does the soil scientist. In its complete form,

a working legend for resource inventory and analysis consists of three parts. Each has a unique function. The Symbolic Legend is a kind of shorthand mainly for the cartographic representation of what the analyst learns about the landscape. The Descriptive Legend, as the name implies, describes and characterizes each legend unit. It may consist only of an organized characterization in narrative or of a combination of tables, charts, and photographs plus narrative. In many respects a good descriptive legend consists of two parts, a technical descriptor that may be written in scientific or technical terms and intended mainly for the analyst and resource management professionals and a narrative prepared to inform the lay reader or ultimate user. The third component, Interpretive Legend, is often combined into the descriptive legend; but we prefer to separate all interpretive, applications, or significance and relevance statements into a separate component of the legend. This part of the legend treats what we know from experience and research or hypothesis, about the relevance of each legend unit (kind of land) to various decision alternatives. The interpretive legend summarizes land use suitability, management potentials and limitations, natural ecological potential, etc., for each legend unit. This section may be in narrative, tabular or combined form. The strongest justification for separation of the Descriptive and the Interpretive Legends is that the former should present only the facts. If one does not emphasize this distinction, there is a strong tendency to incorporate supposition into the description in a way that tends to perpetuate erroneous interpretations made in good faith as a "best guess." If our best current judgment and knowledge about each legend unit as it relates to use and application is presented in a specific interpretations section, the "educated guesses" are not likely to be misinterpreted and can easily be updated or corrected as we gain knowledge. It should be obvious that we view the legend as something far more comprehensive than a symbology with a few keyword descriptors and that a functioning legend is in certain respects dynamic--continually being kept up to date with advances in both knowledge and applications experience.

DEVELOPMENT OF THE LEGEND SYSTEM

With special emphasis since 1968, a group of scientists in the Rangeland Resources Program at Oregon State University has been developing a system that meets the above conditions as closely as possible. The problem of legend development had been casually considered earlier, but our first involvement with vegetational and land use interpretations from space photography in 1966 made the urgency of a solution to the legend problem apparent (Poulton, Roberts, and Carneggie, 1967). Prior to this we had developed and used a nonconnotative, alphanumerical map annotation system that was computer compatible. As the new legend developed, we decided to restrict symbolization to a decimal system in keeping with the hierarchical classes that the problem required.

Since one of the key problems in resource analysis is to identify areas having analogous environments, the plant sociological approach obviously held many outstanding advantages. A plant community orientation in legend development had another distinct advantage in that vegetation is, with the exception of some desert environments, a strong determinant of image characteristics. It is generally the vegetational and landform images that we must interpret. Secondly, vegetational changes are often well correlated with those of landform, geology, and soils so that these latter features, not always directly or clearly imaged by remote sensing systems operating in the visible and near infrared regions, can be accurately inferred from vegetational identifications, once the vegetation is properly classified and the relationships are established through research. Thirdly, an ecological orientation to resource analysis (1) establishes a biological basis for understanding the resource as a foundation for action and (2) provides a reference base for monitoring change in vegetational resources.

PROCEDURE

The procedure used in legend development has been to prepare an hierarchical classification and test it by application in the operational interpretation of imagery. Following this we have repeatedly reexamined the legend classes and revised them to solve the problems encountered and improve the consistency and logic with which each class could be applied. For these reasons, the details of the system are now quite different than when originally presented (Poulton, Driscoll, and Schrumpf, 1969) although the logic and format have remained unchanged. We have, of necessity, worked from the broad or highly generalized units to the more specific and refined. We have, in addition, tested the vegetational categories by application to classes developed or proposed by plant geographers and ecologists. In the broad vegetational classes the criteria have been physiognomic and structural

whereas floristic criteria have determined the intermediate classes and phytosociological criteria have produced the most refined classes.

In the land use areas we have incorporated, essentially without change, classes of the highly compatible system already developed by the Department of Transportation (1969) plus the agricultural section as revised by Professor Claude W. Johnson (1969). The landform legend has been developed by combining reasonably standard classes into a hierarchical system of macrorelief in the highest order and ecologically relevant groups of landforms in the lower or more detailed levels. Surficial geology is handled on a rock-type classification that is relevant to the process of soil formation (Poulton, Fosberg, and Pyott, 1968; California State Office, Bureau of Land Management, 1971). The soils legend can be handled on the basis of groups of ecologically meaningful soils characteristics or by the classified soils taxa according to any one of a number of soil classification systems. We have taken responsibility for development of the vegetational classification system, but we have tried to use accepted classes developed by the other disciplines wherever they give results relevant to the ecology of the landscape and its development and management.

THE LEGEND

THE LEGEND FORMAT

The legend format has remained unchanged since it was first proposed (Poulton, et al., 1969). The generalized form of the symbolic legend is shown in Figure 1. We believe this to be a highly logical and practical format because it treats earth subjects in a numerator/denominator form that is analogous to the concept of phenomena taking place on a supporting surface and permits characterization of both. The numerator symbolization depicts either the natural vegetational features or the cultural modifications that have replaced the natural vegetation. The denominator depicts selected characteristics of the physical environment. Because we need a hierarchical system that permits broad as well as refined levels of differentiation, the concept of moving through a series of numerical indices from general on the left to specific on the right is consistent with this need and with the decimal system of numerical notation.

The specific legend components are shown in their relative relationship in Figure 2. While all components of the legend, in their ultimate detail, may not be needed for all applications, this figure shows how the complete symbol would look if expressed cartographically. To the extent feasible, these can be combined into one notation; or they can be separated into logical groups on separate maps or overlays. If stored in a computer data file, the components would be similarly addressed and could be called out in any combination or at any specified level of detail up to the most intricate level entered in the record. For highly generalized needs, a symbol might, for example, read:

$\frac{320.}{2.2}$ (= natural vegetation, shrub-scrub or chaparral, on a dissected, undulating to rolling land), or

$\frac{510.}{3\ 6.33}$ (= an urban residential area in a hilly macrorelief but built on a complex of exposed and protected sloping lands, generally within the range of 15 to 35 percent slope)

For an intermediate level of detail, one might see the symbol:

$\frac{344.69}{1.1\ 2.2}$ (= natural vegetation, forest or woodland, mixed needleleaf, broadleaf hardwood, prominently such bottomland species as Bald cypress-Tupelo-Oak forest, on an undissected flat macrorelief, in a broad river bottom)

For a highly refined level of resource analysis such as one might do for intensive management, a symbol might read:

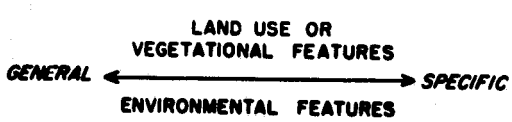


FIGURE 1. THE GENERALIZED LEGEND FORMAT

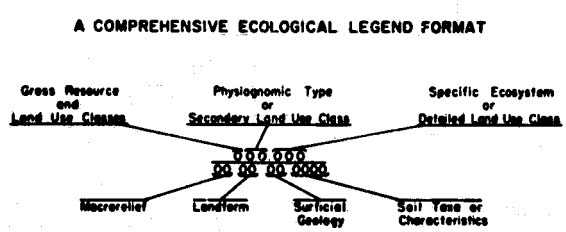


FIGURE 2. THE DETAILED FORMAT FOR A COMPREHENSIVE ECOLOGICAL LEGEND. The legend is designed to treat multiple natural features of the landscape as well as land use and to be computer compatible.

324.113
2.1 3.12 11 1963

(= a natural vegetation community, shrub-scrub, salt tolerant species, with the character and differential species Atriplex confertifolia-Artemisia spinescens/Oryzopsis hymenoides-Sitanion hystrix on an undissected gently rolling land, fan or bajada, sloping between 5 and 15%, mostly acid igneous rock, grey-desert or Zerollic Durargids soils, medium textured, less than 16" deep, > 60% gravel cover on soil surface with little gravel in the profile)

Now let us see how these symbols are derived.

NATURAL VEGETATION AND LAND USE LEGEND

Explanation of these classes can best be handled as we work through the legend categories starting with the first left-hand digit in the numerator. In at least the first two digits of the numerator and the first two classes in the denominator, we were striving to define features that could be discriminated and identified from both space and highflight aerial photography. These broad classes have been developed to this point by use in mapping from Apollo and highflight photography over southern Arizona (Poulton, et al., 1969, 1970, 1971) and by operational use in rangeland resource inventory and landscape characterization during commercial and private aircraft flights at moderately high and low altitude.

The following classes seemed to fit the highest possible level in the useful generalization of images that we should be able to delineate and/or identify from space:

PRIMARY SURFACE FEATURE CLASSES

100 - BARREN LANDS (other than crop fallow)
200 - WATER RESOURCES (free water surfaces)
300 - NATURAL VEGETATION
400 - AGRICULTURAL CROP AND IDLE LAND
500 - URBAN AND INDUSTRIAL LAND (including transportation features)
600 - OBSCURED SURFACE (not visible, atmospheric obstruction)

Notice that the logical arrangement is from nonvegetated, to naturally vegetated, to altered landscapes. Subsequent experience in the use of these classes over an extremely wide scope of ecological conditions and with a wide variety of imagery confirms their workability and usefulness.

In the space available, we obviously cannot include the entire legend, but illustrations of key subclasses will demonstrate how the detail is structured. Following are the secondary legend classes for Barren Land.

SECONDARY BARREN LAND CLASSES

100 - BARREN LAND
- 110 - Playas (dry or intermittent lake basins)
- 120 - Aeolian Barrens (dunes, sandplains, exclusive of beaches)
- 130 - Rocklands
- 140 - Shore-lines (beaches, tidal mud flats, sand and gravel banks)
- 150 - Badlands (barren silts, clays, and related easily weathered rock types)
- 160 - Slicks (saline, alkaline, soil structural non-playa barrens)
- 170 - Mass Movement (barrens associated with slumps and mud flows)
- 180 - Man-made Barrens (mine dumps, excavations, fills and settling ponds)
- 190 - Undifferentiated complexes of barren lands

In most cases this is as far as is appropriate to break down barren land types. If one goes beyond this point, the subclasses become particularly redundant with landform with is reserved for characterization in the denominator. One important exception may be the 130, Rockland, class which can be meaningfully broken down as follows without redundancy:

TERTIARY BARREN LAND CLASSES

100 - BARREN LAND
  130 - Rocklands
    131 - Bedrock outcrops (intrusive & erosion or tectonically bared strata)
    132 - Extrusive igneous (lava flows, pumice, cinder & ash)
    133 - Gravels, stones, cobbles and boulders (usually transported)
    134 - Scarps or cliffs and associated talus (systems of outcropping strata)
    135 - Patterned rockland complexes (nets/stripes)
    139 - Undifferentiated complexes of rockland

If these classes are broken down more finely as a characterization of the surface, they become redundant with the classes of surficial geology or soil-forming material, also reserved for the denominator. Note that wherever possible we have strived to retain the "9" digit for an undifferentiated subclass.

Water resources have been effectively handled by the following classes:

SECONDARY WATER RESOURCE CLASSES

200 - WATER RESOURCES
  210 - Ponds, lakes and reservoirs
  220 - Water courses, permanent flowing
  230 - Springs, seeps, and wells
  240 - Bays, coves, and estuaries
  250 - Lagoons and bayous
  260 - Oceans, seas and gulfs
  270 - (Unused Class)
  280 - Snow and ice
  290 - Undifferentiated complexes of water resources

Each of these classes can be subdivided and a little imagination will suggest many of the tertiary classes we have used. It has been somewhat traditional to treat "Snow and ice" as a separate primary class. Since ice is merely a physical form of water, we believe the logic of inclusion in major category 200, Water Resources, is superior to a separate class at the primary level.

The secondary vegetational classes are based on three sets of criteria--physiognomic, structural, and growth form. The tertiary classes are floristically determined and the most highly refined classes are derived by careful phytosociological study under the plant community concept. The well-proven methods of leading European and North American plant ecologists have been found entirely adequate and highly appropriate to these objectives (Ellenberg, 1956; Braun-Blanquet, 1964; Küchler, 1967; Daubenmire, 1968; Blackburn, Eckert, and Tueller, 1971). In developing the broader physiognomic classes we consulted a cross section of the literature on plant geography (Fosberg, 1961; Küchler, 1967). We found no one system adequate for defining vegetation in terms that were compatible with the objectives of remote sensing imagery interpretation. It was necessary to depart from much of the excellent classification work done in plant geography and devise our own descriptors under the primary resource class 300, Natural vegetation. We started with seven subclasses and, with experience, narrowed to the following four secondary classes.

SECONDARY VEGETATION CLASSES

300 - NATURAL VEGETATION
  310 - Herbaceous types
  320 - Shrub-scrub types
  330 - Savanna types
  340 - Forest and woodland types
  390 - Undifferentiated natural vegetation

Of these, 330, Savanna, gives us the most difficulty in application. Down to and including the units position in the vegetation legend, we have been able to base classes exclusively on structural and physiognomic characteristics of the vegetation. In most instances we have used eight classes in the tertiary level. The digit "9" is again reserved for an "Undifferentiated" class. Following are two representative classes from each of the four sets to illustrate how the tertiary classes are structured:

TERTIARY NATURAL VEGETATION CLASSES

310 - Herbaceous types
  312 - Prominently annuals
  314 - Bunchgrass steppe
320 - Shrub-scrub types
  322 - Microphyllous thorn scrub
  326 - Evergreen sclerophyll shrub
330 - Savanna types
  332 - Tall, deciduous shrub savanna
  333 - Broadleaved, evergreen tree savanna
340 - Forest and Woodland types
  341 - Needleleaf
  343 - Broadleaf, evergreen

The quaternary level is based on floristic criteria. I shall illustrate this first floristic level with only three examples as follows:

QUATERNARY, FIRST FLORISTIC VEGETATION LEVEL

324 - Microphyllous salt tolerant shrub types
  324.1 - Saltsage (Atriplex) prominent types

326 - Evergreen sclerophyll scrub
  326.2 - Manzanita (Arctostaphylos) scrub

341 - Needleleaf forest and woodland types
  341.01 - Juniper and pinyon-juniper (Pinus-Juniperus) types

Notice that the identification of specific botanical taxa, usually at generic level, comes into play at this point. Image identification at this level requires, therefore, that certain taxonomic discriminations be possible--either directly or accurately by inference and a knowledge of what to expect in the area imaged. Thus we are now working at a level appropriate to the interpretation of intermediate- and large-scale imagery.

Below the quaternary level, it is necessary to classify the highly specific vegetational systems that are appropriate to the needs of intensive resource management and to interpretation from large-scale imagery. To characterize the vegetational community indicative of each ecosystem, additional digits are appended to the above. Perhaps one illustration will suffice. The following legend units were developed from detailed phytosociological studies and vegetation-soil relationship investigations in Oregon and used operationally in a resource inventory made from 1:20,000 and 1:12,000 scale aerial photography (Martin, 1970; Poulton, Faulkner, and Martin, 1971):

VEGETATION CLASSIFICATION TO ECOSYSTEM LEVEL

300 - NATURAL VEGETATION
  320 - Shrub-scrub vegetation
    324 - Microphyllous salt tolerant vegetation
      324.1 - Saltsage (Atriplex) prominent vegetation
        324.11 - Shadscale/Budsage (Atco/Arsp) communities

(Continued)

324.111 - Atco(4-5)-Arsp(3-4/Sihy(3-5)-Brte(0-3)[2]
324.112 - Atco(4-5)-Arsp(3-5)-Grsp(2-3)/Sihy (1-5)-Brte(0-5)
324.113 - Atco(4-5)-Arsp(3-4)-Save(2), Chvi, Chna(2)/Sihy(3-5)-Pose(2-3)-Brte(0-5)

It is our present opinion that legends developed at the above intensive level will have to be regionalized. It seems that only the upper levels, primary possibly through quaternary, are adaptable to interregional and global use.

In developing legends for the classes 400, Agricultural, and 500, Urban and Industrial, we have relied on the work of experts in these areas. In approaching the task we examined quite a number of legend systems and it appeared that the Standard Land Use Coding Manual (U. S. Department of Transportation, 1969) contained a workable format and was sufficiently comprehensive to meet nearly all foreseeable needs. This Manual uses a numerical system for its symbolic legend thus establishing conceptual compatibility between our approaches.

To compile a 400, Agricultural, legend, Claude Johnson's horticultural/agricultural classification, which in turn was based on the Standard Land Use Coding Manual, was adapted to our primary classes by merely replacing the Manual's "81" designator with a "4" and adding a decimal between the tertiary and quaternary levels (Pettinger, 1970).

A single example from Draeger's modification will enable others to immediately adapt Johnson's modified agricultural classification into this system by reference to the original work (Johnson, 1969).

ADAPTATION OF EXISTING AGRICULTURAL CLASSIFICATION

400 - AGRICULTURAL LANDS
  410 - Field and seed crops
    412 - Legumes for seed
      412.2 - Peas, field

The urban, industrial, and extractive land use legend was created simply by adding a "5" ahead of appropriate code numbers in the Standard Land Use Coding Manual. Following is an example:

ADAPTATION OF EXISTING URBAN-INDUSTRIAL CLASSIFICATION

500 - URBAN AND INDUSTRIAL (Including transportation)
  510 - Residential housing
    511 - Household units
    512 - Group quarters
      512.3 - Residence halls and dormitories
  540 - Transportation, communication and utilities
    543 - Aircraft transportation
      543.1 - Airports and flying fields

While both of these legends (Agricultural and Urban and Industrial) include many categories that cannot be photo identified, their main advantage is the comprehensive treatment of practically all necessary classes. Since each is a hierarchical system, a level can generally be identified that is compatible with the image interpretation. These two simple revisions of the Agricultural and Urban, Industrial, and Extractive Industry land use legends have enabled us to incorporate these important features of the Earth's surface into our unified legend system.

---

[2] These symbols are derived from the scientific plant name, and the numerals express relative prominence of the species in the community.

PHYSICAL ENVIRONMENT LEGEND

The most obvious feature and highest level of generalization of the physical environment is macrorelief. It is, in fact, best and most easily interpreted from space and high altitude photography. Following are the four classes of macrorelief we have used successfully and consistently for twenty years in both ecological research and remote sensing interpretation:

PRIMARY PHYSICAL ENVIRONMENT CLASSES

1.0 - Flat lands (slopes < 10 percent)
  1.1 - Nondissected
  1.2 - Dissected
2.0 - Moderately undulating to rolling lands (slopes 10-25 percent)
  2.1 - Nondissected
  2.2 - Dissected
3.0 - Hilly lands
4.0 - Mountainous lands

These classes define the gross macroscale relief and contour features of the Earth's surface in a way that is ecologically relevant. Consistency in their use is high. As with any classification, one can correctly imagine difficulty with questions such as, "Where do the hills stop and the mountain begin?" The answer is found in the judgment of the analyst plus a few ground rules and carefully worded descriptions we have prepared for these and other categories (Pettinger, 1970).

The secondary level in the physical environment descriptor (denominator) is landform. This category has been most difficult to develop, and it has gone through a greater evolution than any other legend component. We tried and discarded a rather complete listing of landforms as used in the geomorphological and soils literature (Fosberg and Chugg, 1967) because they were not hierarchically arranged and many of the classes were not particularly relevant to either the ecology of the landscape or to the use and management of surface resources.

We are, at present, using a set of six broad classes as follows:

SECONDARY PHYSICAL FEATURE CLASSES

1.0 - Depressional or wet lands, non-riparian
2.0 - Bottomlands, riparian
3.0 - Planar surfaces
4.0 - Aeolian featured landscapes
5.0 - Slope systems
6.0 - Gravity and mass movement landscapes

These represent a consolidation of a larger number of primary classes formerly used. For each class we are incorporating conventionally named subclasses and where appropriate adding a slope class to the symbology, as the last digit to the right.

TERTIARY PHYSICAL FEATURE (LANDFORM) CLASSES

3.0 - Planar surface
  3.1 - Fans and bajadas
  3.2 - Terraces
  3.3 - Pediments

These classes or close approximations have been tested in many kinds of environments and geomorphic conditions. They work reasonably well if one can live with not being a geomorphological purist, and they do result in a characterization of the land surface that is relevant to the ecology and geography of the vegetation and to the management and use activities of man. In addition, most of the classes are readily photo identifiable.

To develop an information base for land use and multiple resource management decisions, the inventory and analysis of the Earth's surface must include a treatment of surficial geology and soils.

Some would say that the former is inherently taken into account by a thorough treatment of the latter, but we think surficial geology should be included in the inventory as a unique disciplinary product. In our judgment, minimum annotation of surficial geology should characterize soil forming or parent materials. Rock type may be the best criterion for legend classes. We have done some work with such a system (Poulton, Fosberg, and Pyott, 1968); and, building on our work in southern Arizona, the Bureau of Land Management independently developed an almost identical approach which they used in a pilot inventory of part of the California Desert (California State Office, Bureau of Land Management, 1971). Both systems used the following major or primary classes:

PHYSICAL ENVIRONMENT CLASSES
SURFICIAL GEOLOGY

10 - Coarse grained igneous
20 - Fine grained igneous
30 - Sedimentary
40 - Metamorphic
50 - Unconsolidated material
90 - Undifferentiated soil forming material

Secondary classes indicate specific rock types. Amplification from this beginning is probably the way we shall treat future work.

A resource inventory is not complete until it includes a critical treatment of soil as well as vegetation and the other physical features just discussed. Soil notation can be handled in either of two ways with satisfactory results. One is to symbolize meaningful soils characteristics and the other is to treat the subject by identified and correlated soils taxa. The latter is preferred except that soils have not been classified in sufficient detail for many of the range and forest areas of the world and the taxa are changing because of the dynamic evolution of improved soils classifications systems.

There are numerous excellent examples of taxonomic classification of soils in the various standard soil survey reports and maps available in the United States and throughout the world. These soils classification schemes are hierarchical and thus compatible with the needs of multiscale image interpretation. Whether at series, association of, or other higher level, soils data helps to complete the reservoir of information critical to the land use and resource allocation decision.

The alternative approach where soils are not classified is to display or summarize those soils characteristics that are most relevant to land use or resource management decisions--that is, to the ecology of the landscape. These will vary somewhat among ecological provinces and geological regions; but such features as solum depth, texture, stoniness, degree of development, presence of restrictive layers or pans, etc., are examples of the kinds of notations required. In most instances, these can also be translated into a numerical symbology that is computer compatible (Poulton, Fosberg and Pyott, 1968). In our current program to evaluate the ERTS-1 imagery, we may well be using both systems and will work out the details in the months ahead.

SUMMARY AND CONCLUSIONS

This paper presents an integrated legend system that treats resource and land use analysis in an ecological context. Descriptive classss and a logical symbology are provided for the following features: Natural vegetation, land uses that have changed the cover or nature of the land surface, macrorelief, and landforms. Suggestions are made as to how some features of surficial geology can be handled in a parallel manner, and two alternatives are discussed for the cartographic and symbolic treatment of soils information. We believe there are significant advantages to the land use planner from a common legend system that follows the same philosophy and symbolization concepts in all aspects of inventory. It is highly beneficial to view land use in the perspective of an ecologically analyzed landscape. Regardless of how results from the separate categories are combined, expressed, or stored and retrieved, this holistic approach provides a picture of land use and human activity in an ecological perspective that is superior to any other system presently in use. When this legend approach is combined with the synoptic view from space or high altitude, the total power of the new space-age capability in land use planning and resource allocation becomes apparent.

Some may fault this legend system in that it does not provide for direct assessment of such land uses as grazing, forestry, watershed, wildlife production and harvest, and aesthetics and other recreational oriented uses. These particular uses are generally self-evident in the biological and physical nature of each ecosystem. Each use can be inferred from the basic resource data provided by this ecological approach. If these kinds of uses are directly assessed, the all-important documentation of the relationship of each use to the natural ecosystems from which it is derived is lost. With our approach, one is better able to put land use in the perspective of the ecological conditions which permit or constrain each kind of use and with which the activities of man must be in harmony.

The total legend has been put together in a working outline form. Descriptions of many of the classes have been prepared in an accompanying narrative to help the image interpreter consistently apply the classes. These operational aids have reasonably stabilized and are about ready for description and illustration in a final narrative.

We are depending on other experts (Inter-Agency Steering Committee on Land Use Information and Classification, 1972) to come up with improvements in the Land Use, Extractive Industries, and Agricultural Legends, but with the hope they will make their classes compatible so that they can be similarly incorporated into this more comprehensive system. We would welcome the opportunity to interact with those concerned with new land use classification schemes and legends.

While the above legend has been presented in the context of a symbolization technique, let us keep in mind that this is mainly for convenience of discussion and illustration. What may seem to have evolved into unreasonably long and complicated symbolization is merely the components of a data system that can be applied in an integrated set of maps, through an overlay system, or stored in a data bank. In the latter format, especially, it can be recalled at whatever generalization level and in only those data components that are appropriate to a specified problem or information need.

This legend system and most of the classes have been tested in a wide range of conditions from arid deserts to coastal marshes and tropical forests. Although the available classifications are imperfect for many of these kinds of vegetation, the concepts, logic and applicability seemed encouragingly fitting for each of these diverse environments. The legend is particularly appropriate to the concept of multistage (multiscale) sampling with various kinds of remote sensing imagery and does appear to provide most of the categories needed for an initial stratification from space imagery. Vegetational and land use classification to the secondary level and the macrorelief classes are most easily assigned from space imagery. Many of the landform classes are easily detectable from space and highflight imagery, especially when stereo viewing is possible.

While the primary, secondary, and some of the tertiary classes have widespread applicability, we are becoming quite confident that natural vegetation legends at detailed plant community or specific ecosystem levels will have to be regionalized for maximum effectiveness. The concept of basing a vegetational legend on physiognomic and structural characteristics at the higher levels, on floristics at intermediate levels, and on phytosociological principles of classification at the more refined levels seems ideally appropriate to the development of legend classes for multistage remote sensing interpretation (Daubenmire and Daubenmire, 1968; Blackburn, Tueller, and Eckert, 1969; Daubenmire, 1970; and Martin, 1970). The concept is also compatible with the differing levels of information need in land use planning and resource management.

We have used this legend system in an inventory from both Apollo IX and NASA highflight photography in Maricopa County, Arizona (Poulton, et al., 1969, 1970, 1971; Pettinger, 1970), and are now embarking on parallel undertakings in Oregon as a part of our ERTS-1 evaluation and in a highflight resource analysis project of the Environmental Remote Sensing Applications Laboratory. The broader vegetation legend classes have been used by our colleagues at the Forestry Remote Sensing Laboratory, Berkeley (Lauer, et al., 1971), and the complete system was successfully tested with high and intermediate altitude aerial photography by the Bureau of Land Management in preliminary studies relating to their California Desert Program (California State Office, Bureau of Land Management, 1971). In addition, the author has found the broader legend components particularly useful on low-elevation reconnaissance flights across a very wide diversity of ecological conditions in western and southern United States. With this amount of testing, it appears that the system would merit careful evaluation and use by others who may, in turn, contribute to its improvement

In conclusion, this legend system embodies an ecological approach to resource analysis. It draws together and helps to clarify the interrelationships of vegetation, soils, geology, and geomorphology so that one is able to read environmental potentials and limitations through the vegetation as a mirror of effective environment. The approach also related man-imposed modifications of the natural landscape to the basic ecosystem units so that land and resource suitability can be judged and extrapolated in an ecological framework. The natural ecological unit of the landscape then becomes the common denominator through which management practices, research results, and knowledge can best be generalized to new locations as we guide man's future activities to achieve compatibility with the potentials and limitations of his environment.

ACKNOWLEDGEMENTS

The research on which this paper is based was performed by the Rangeland Resources Program over a period of years under two Western Regional Projects on Rangeland Ecology, W-25 and W-89, and under Research Contracts from the Oregon State Land Board and the U.S. Department of Interior, Bureau of Land Management. The most recent work in the refinement and adaptation of the legend system to space application and multistage inventory has been done under funding from the National Aeronautics and Space Administration through the U.S. Department of Agriculture, Forest Service in cooperation with the Forestry Remote Sensing Laboratory, University of California, Berkeley.

Especially significant contributions of the following Rangeland Resources personnel at Oregon State University are gratefully acknowledged: David P. Faulkner, Edmundo Garcia-Moya, Arleigh G. Isley, James R. Johnson, Niels L. Martin, David A. Mouat, William T. Pyott, and Barry J. Schrumpf. In the early development of the concepts, E. William Anderson, Soil Conservation Service, Portland, Oregon, assisted with a University resource inventory project and helped to formulate the ideas that evolved into the present legend system.

In collaboration with William C. Draeger, Forestry Remote Sensing Laboratory, University of California, Berkeley, we were successful in combining our system with two others to produce a combined Vegetational and Land Use Legend. The Agricultural Legend component was adapted from the work of Claude W. Johnson, University of California, Riverside (Johnson, 1969). The Urban-Industrial-Transportation Legend was adapted from the U.S. Department of Transportation Standard Land Use Coding Manual (1969).

LITERATURE CITED

Blackburn, Wilbert H., Paul T. Tueller, and Richard E. Eckert, Jr. 1969. Vegetation and soils of the Pine and Mathews Canyon Watersheds. Agric. Expt. Sta. Max C. Fleischmann College of Agriculture, Univ. of Nevada Report R-46 (April 1969). 109 pp. illus., map.

_____, Richard E. Eckert, Jr., and Paul T. Tueller. 1971. Vegetation and soils of the Rock Springs Watershed. Agric. Expt. Sta. Max C. Fleischmann College of Agriculture, Univ. of Nevada. Report 83. 116 pp. map, tabs.

Braun-Blanquet, J. 1964. Pflanzensociologie, Grundzüge der Vegetationskunde. Dvitte Auflage. Springer-Verlag, Wein-New York. XIV and 865 pp.

Bureau of Land Management. Unit Resource Analysis. BLM Manual 1605.

California State Office, Bureau of Land Management. 1971. Appendix B, Pilot Resource Inventory Report. In Development and Resources Corporation. 1971. Planning Guidelines for California Desert Program. Prepared for Bureau of Land Management, U.S. Dept. of Interior, Sacramento, Calif. In 2 Vols. 72 pp. illus., tabs.

Daubenmire, R and Jean B. Daubenmire. 1968. Forest vegetation of eastern Washington and northern Idaho. Washington Agric. Expt. Sta Technical Bulletin 60. 104 pp. illus.

_____ 1970. Steppe vegetation of Washington. Washington Agric. Expt. Sta. Technical Bulletin 62. 131 pp. illus.

Daubenmire, Rexford. 1968. Plant Communities: a textbook of plant synecology. Harper and Rowe, New York. 300 pp.

Fosberg, F. Raymond. 1961. A classification of vegetation for general purposes. Tropical Ecology. 2:1-28.

Fosberg, M. A. and J. C. Chugg. 1967. Landform definitions for soil survey and IBM data code processing. Univ of Idaho, College of Agric., Dept. of Agric. Biochem. & Soils. Moscow, Idaho. May 1967. Mimeo. 13 pp.

Ellenberg, Heinz. 1956. Grundlagen der Vegetationsgliederung. I. TEIL, Aufgaben und Methoden der Vegetationskunde. Einführung in Die Phytologie, IV. Stuttgart.

Hills, G. A. 1961. The ecological bases for land-use planning. Ont. Dept. of Lands and Forests, Technical Series. Res. Report No. 46.

Inter-Agency Steering Committee on Land Use Information and Classification. 1972. A land use classification scheme for use with remote sensor data. A. Proceedings of the conference on land use information and classification, June 28-30, 1971; and B. Land use classification scheme, Levels I and II, with definitions of categories (preliminary version). U.S. Dept. Interior, Geological Survey. Washington, D.C. 205 pp. (Processed).

Johnson, C. W. 1969. A system of regional agricultural land use mapping tested against small scale Apollo 9 color infrared photography of the Imperial Valley, University of California, Riverside. USDI Status Report III, Tech. Report V, Contract Number 14-08-0001-10674.

Küchler, A. W. 1967. Vegetation Mapping. The Roland Press Co., New York. 472 pp.

Lacate, D. S. 1966. Wildland inventory and mapping. The Forestry Chronicle 42:184-194.

Lauer, Donald T., et al. 1971. Image interpretation and enhancement. In Forestry Remote Sensing Laboratory. 1971. Analysis of remote sensing data for evaluating vegetation resources. Univ. of Calif., Berkeley. Annual Progress Report, 30 Sept. 1971. For Earth Resources Program, OSSA/NASA. pp. 56-113.

Martin, Niels Leroy. 1970. Development of a legend and key for ecological resource analysis in the 15-mile administrative unit, Malheur County, Oregon. Master's Degree Thesis. Oregon State University, Corvallis, Oregon 97331. 231 pp. Illus.

Perry, R. A. 1962. General report on lands of the Alice Springs Area, northern territory, 1956-57. Commonwealth Scientific and Industrial Research Organization, Australia. Land Research Series No. 6.

Pettinger, Lawrence R. 1970. The application of high altitude photography for vegetation resource inventories in southeastern Arizona. Final Report, 31 Dec. 1970. For Earth Observations Division, Manned Spacecraft Center, NASA, Contract No. NAS 9-9577, with contributions by Charles E. Poulton, et al., Oregon State University. 147 pp. Illus., map.

Poulton, C. E., E. H. Roberts, and D. M. Carneggie. 1967. The feasibility of analyzing range and related resources from Gemini color photography. In Carneggie, David. M. et al., 1967. Remote sensing applications in forestry. The evaluation of rangeland resources by means of multispectral imagery. Forestry Remote Sensing Laboratory, Univ. of Calif., Berkeley. Annual Progress Report, 30 Sept. 1967. For Natural Resources Program, OSSA/NASA. pp. 47-57. Illus.

_____, et al. 1969. Inventory of native vegetation and related resources from space photography. Annual Report. For Earth Resources Program, OSSA/NASA, by Range Management Staff, Oregon State University, Corvallis, Oregon. 66 pp.

_____, J. R. Johnson, D. A. Mouat, and B. J. Schrumpf. 1970. Inventory of native vegetation and related resources from space photography. Annual Report. For Earth Resources Program, OSSA/NASA, by Range Management Staff, Oregon State University, Corvallis, Oregon. 32 pp.

Poulton, Charles E., Maynard A. Fosberg and William T. Pyott. 1968. Electronic data processing in range ecology research. Physiography and soils data codes, punch-card and tape format. Unpublished manuscript, Research Files, Rangeland Resources Program, Oregon State University, Corvallis. 53 pp.

_____, Richard S. Driscoll, and Barry J. Schrumpf. 1969. Range resource inventory from space and supporting aircraft photography. In National Aeronautics and Space Administration, Second Annual Earth Resources Aircraft Program Review. Vol. II, Agriculture/Forestry and Sensor Studies. Sept. 16-18, 1969. Manned Spacecraft Center, Houston, Texas. pp. 20-1 to 20-28.

_____, David P. Faulkner, James R. Johnson, David A. Mouat, and Barry J. Schrumpf. 1971. Inventory and analysis of natural vegetation and related resources from space and high altitude photography. Annual Report. For Earth Resources Program, OSSA/NASA, by Range Management Staff, Oregon State University, Corvallis, Oregon. 59 pp.

_____, David P. Faulkner, and Niels Leroy Martin. 1971. A Procedural Manual for Resource Analysis. With Supporting Appendices. Application of ecology and remote sensing in the analysis of range watersheds. Final Project Report. April 1971. For U.S. Department of Interior - Bureau of Land Management.

_____, Barry J. Schrumpf, and James R. Johnson. 1971. Ecological resource analysis from highflight photography for land use planning. In Applied Remote Sensing of Earth Resources in Arizona. Proceedings, 2nd ARETS Symposium, University of Arizona, Tucson. Nov. 2-4, 1971. pp. 35-57.

U.S. Department of Transportation. 1969. Standard land use coding manual. Govt. Printing Office. (Reprint of 1965 ed.). 111 pp.

U.S. Forest Service. 1972. Personal communication re Multidiscipline Team analysis and planning.

DESIGN AND PERFORMANCE CHARACTERISTICS OF THE VERTICAL TEMPERATURE PROFILE RADIOMETER (VTPR) FOR ATMOSPHERIC TEMPERATURE SOUNDINGS

Gerald Falbel

Barnes Engineering Company
Stamford, Connecticut

1. SUMMARY

This paper describes the design and performance characteristics of the Vertical Temperature Profile Radiometer (VTPR) used in the ITOS Spacecraft. This radiometer obtains spectral measurements in eight optical filter channels, six in the wings of the 15-micron atmospheric CO_2 absorption band, one in the 8-12 micron "window," and one in the 18.7 micron H_2O absorption band. The CO_2 and the H_2O corrected window channels radiometrically probe the temperature of various altitude strata in the atmosphere. By operating on these radiometric measurements with a mathematical inversion program, scientists at the National Oceanic and Atmospheric Administration can derive a vertical temperature profile of the atmosphere for each set of 8 measurements.

This atmospheric temperature profile derivation capability has been demonstrated using data from the SIRS multi-channel grating spectrometer on NIMBUS 344. Since the SIRS was developed, advances in the state-of-the-art of bandpass optical filters have permitted equivalent spectral resolutions to be achieved through the use of discrete optical filters. Much higher optical gain can be achieved with filters than gratings for equivalent field of view and instrument sizes. This is known as the "throughput advantage" and arises from the elimination of the entrance slit required by dispersive spectral instruments. This is shown by the fact that the VTPR provides a radiometric sensitivity approximately equal with an angular field of view solid angle approximately 1/30th that of the SIRS. The weight and power consumption of the VTPR is 30 lbs. and 19 watts, respectively.

In operation, the VTPR scans across the Earth's surface over angles of ±32° from the nadir on each side of the orbit ground track in a "step-scan" motion and has the capability of generating 23 vertical temperature profiles per scan line, or 12,600 profiles per orbit. However, data reduction considerations, cloud coverage and weather forecasting requirements result in the generation of only 3 profiles per 8 scan lines, or 570 profiles per orbit. In addition to providing greatly increased geographic coverage compared to SIRS, this scanning technique allows the generation of accurate vertical profiles in the presence of partly cloudy conditions by comparing in the data reduction process the radiances obtained in adjacent fields of view. In order to provide the required accuracy of the vertical temperature profiles, a noise equivalent radiance difference equivalent to <0.1% of the signal range is provided by the instrument.

When the data from a 24-hour period are processed on the ground, they will result in a continuous series of world-wide "real-time" isotherm maps at altitudes up to 100,000 feet. Such a real-time map has never been achieved in the history of meteorology.

The crosstrack scanning of the VTPR is achieved through the use of a stepper motor driving a cam and roller follower, this entire assembly operating in the

space vacuum.

The VTPR achieves its 8-channel capability by sequentially viewing the eight optical filters mounted in a rotating filter wheel, with a single IR detector and electronic amplification channel processing the signal for all the filters. The advantages and disadvantages of this sequential approach as compared to eight "parallel" radiometric channels (each comprising a telescope and detector) are discussed. The parallel system provides advantages in "spatial simultaneity" (discussed below) and in facility of optical filter temperature control (which is necessary to maintain the center wavelengths of the filters within the tight tolerances required for generating an accurate temperature profile).

The sequential system has the critical advantage of providing 38% better sensitivity for equivalent size and weight instruments. A design problem which had to be resolved in order for this sequential approached to be used, involved the requirement that each optical filter must see the same spatial area on the ground. If this were not accomplished, a variation in cloud cover seen by each filter would cause significant errors in the vertical temperature profile calculated from this data. This spatial simultaneity is achieved by using a spiral mask in the filter wheel which automatically indexes the system field stop as each filter is viewed by the detector so as to "track" the angular rate of a spot on the Earth surface and thus compensate for the orbital motion of the satellite.

In order to maintain the required spectral tolerances on the filter channels, the rotating filter wheel must be thermally controlled. The means by which this is accomplished and the system error implications of this thermal control loop are discussed, and measured performance data is presented.

This is the first space instrument to use a pyroelectric infrared detector. This detector is uncooled and provides the same spectral response as a thermistor detector, but three times better sensitivity.

This paper also presents the measured results of the radiometric sensitivity long term calibration accuracy and environmental performance obtained with the Engineering and Flight Models of the VTPR. These test results show that the radiometric errors introduced by thermal rates of change in the instrument temperature of up to 2°C/30 minutes can be almost completely compensated for during data reduction so as to result in a residual rms calibration error of $<0.1\%$ of the signal range.

2. OVER-ALL FUNCTION AND PERFORMANCE REQUIREMENTS OF THE VTPR

The VTPR is the latest in a series of multispectral radiometers and spectrometers designed to measure the vertical temperature profile of the atmosphere using the basic techniques originally generated by Dr. L. Kaplan (Ref. 1). Briefly, this technique involves looking through the earth atmosphere from space in various narrow spectral regions in the wings of the atmospheric CO_2 band at 15 microns. As the spectral region gets further away from the peak absorption region, the amount that the radiometer's field of view penetrates the atmosphere increases until finally it penetrates to the earth's surface. From this radiometric data, a temperature profile of the earth's atmosphere can be obtained through the use of weighting functions dependent upon known properties of the atmosphere (see Figure 1), and matrix inversion techniques (Ref. 2). As can be seen in Figures 2 and 3, the VTPR generates a grid of scanned spots, dwelling at each spot for 0.5 sec., in which time radiometric readings are obtained for all 8 filter channels. As shown in Figure 3, as many as 64 scanned spots are combined in order to generate one atmospheric temperature profile. This is done to compensate for the effects of clouds (see Section 2.4), as well as minimize the effects of random noise. Figure 4 shows the geographic coverage of the VTPR as compared to SIRS.

The VTPR instrument performance requirements which came out of this over-all function requirements are itemized as follows:

2.1 SPECTRAL BANDWIDTHS OF THE FILTER CHANNELS

The spectral bandwidths of the filter channels vary from 10 cm^{-1} to 18 cm^{-1} wide at their half power points for seven of the eight channels. (See Figure 5 and Table 1.) The eighth channel is only 3.5 cm^{-1} wide, since it is centered at 668.5 cm^{-1} near the maximum absorption point of the CO_2 band (or the Q-branch). The center wavelengths of all the filters are tightly controlled, since the altitude stratum equivalent to each filter channel is a strong function of its center wavelength. The tightest tolerance of ±0.5 cm^{-1} is applied to the Q-branch channel which provides the highest altitude temperature stratum. Optical filters meeting these Q-branch requirements have been developed by Dr.S. D. Smith in Great Britain (Ref. 3) and Spectrum Systems, Inc. in the United States. The other filters have been obtained from OCLI. Furthermore, since the center wavelength of these filters is also a function of their ambient temperature, the tight tolerances on the Q-branch channel have required that the filter wheel be temperature controlled. The thermal control of this filter wheel represents one of the major design areas of the VTPR and is covered in Section 4.6.

2.2 RADIOMETRIC SENSITIVITY

In order to obtain accurate atmospheric profiles with the use of the weighting function-matrix inversion process, the rms uncorrelated (random) errors between radiometric channels must be minimized so that the rms spectral radiance error between any two channels is less than 0.25 mw/m^2-ster-cm^{-1}. This is equivalent to a temperature change in a 300°K blackbody of 0.15°K.

2.3 ABSOLUTE ERRORS OF THE VTPR

In order to define the atmospheric profile in absolute temperature terms, there is an absolute radiometric accuracy of 1 mw/m^2-ster-cm^{-1} required for the VTPR (which is equivalent to 0.6°K for a 300°K blackbody). This accuracy refers to a correlated error for all the channels. Since the signal dynamic range of the channels goes from the zero radiance of cold space to the 220 mw/m^2-ster-cm^{-1} of the hottest Sahara Desert, this absolute accuracy represents 0.5% of the dynamic range. This absolute accuracy is achievable through the use of periodic in-flight calibration in which the VTPR views cold space and an in-flight calibration source whose temperature is the same as the VTPR housing and is telemetered down on the main data stream.

2.4 SCANNING REQUIREMENTS

A scanning requirement is incorporated in the VTPR for two reasons:

1) With step spatial scanning in which a vertical profile could be generated from each spatial step, there is a much higher probability that a cloud-free area would be viewed. Cloud-free areas provide the optimum data for obtaining the best vertical temperature profile.

2) Through the use of a correlation process developed by Dr. W. L. Smith of NOAA (Ref. 4), the amount of cloud cover in each VTPR scanned spot can be determined by comparing it to its adjacent spots, without the need for any auxiliary cloud picture data.

3. EVALUATION OF ALTERNATE SYSTEM APPROACHES

The performance requirements discussed above can be achieved by using several design approaches. Some of these include: dispersive instruments, which separate the filter channels by using a diffraction grating (as in the SIRS Instrument), and multiple filter instruments such as the VTPR. A further sub-division in the design choice relates to whether the N spectral channels are simultaneously viewed by N optical telescopes and N detectors (i.e., "parallel channels"), or time-shared in one telescope by viewing the filters sequentially with one detector.

As mentioned in Section 1, a multiple filter system provides a major sensitivity improvement over a spectrally dispersive system due to the elimination of the entrance slit, so the system design choice for the VTPR involved a comparative evaluation between a configuration having N "parallel" vs. N sequential channels.

3.1 PARALLEL-CHANNEL SYSTEM ADVANTAGES

The parallel system configuration consists of N optical telescopes chopped by a single chopper, with each optical telescope defining one filter channel. Such a system has two advantages:

1) Since the filter channels are viewed simultaneously, the spatial simultaneity requirement discussed in Section 1 can be achieved by using precise alignment of the N telescopes, whereas in the sequential filter configuration, image motion compensation must be introduced to insure spatial simultaneity in the presence of orbital motion.

2) In a parallel system the filters are stationary and thereby do not introduce dynamic radiometric signals into the electronic processing. Furthermore, their temperature can be controlled by quite straightforward conductive means, whereas in the sequential filter configuration the filter wheel must be temperature controlled by a non-contact radiometric thermal coupling.

3.2 SEQUENTIAL FILTER SYSTEM ADVANTAGES

In the critical area of instrument sensitivity versus total size and weight, the sequential filter configuration is clearly superior to the parallel telescope configuration. This advantage is shown in the following analysis:

Let us define:

$NE\Delta N_s$ = Noise equivalent radiance difference for a sequential filter system.

$NE\Delta N_p$ = Noise equivalent radiance difference for a parallel telescope system.

System comparisons can be made using the well-known formula

$$NE\Delta N = \frac{\sqrt{A_d \ \Delta f}}{(\pi/4)\ D_o^{\,2}\ \eta\ D^*\ \Omega} \qquad (1)$$

where:

A_d = Detector area

Δf = Noise bandwidth

D_o = Optical entrance aperture diameter

η = Optical efficiency (including obscuration and filter transmission)

D^* = Detector specific detectivity

Ω = Radiometer solid angle field of view

In comparing systems of like optical configurations but different sizes, we hold Ω, f/no. (effective optical speed), η, and detector D^* constant, so that equation (1) is not directly usable for comparison purposes in its given form. This difficulty may be circumvented using the relationships:

$$\text{f/no.} = (\text{effective focal length})/D_o \qquad (2)$$

and

$$\Omega = A_d/(\text{effective focal length})^2 \qquad (3)$$

Using the above substitutions, equation (1) may be reduced to:

$$NE\Delta N = \frac{K\sqrt{\Delta f}}{D_o} \tag{4}$$

where the factor K is independent of the size of the instrument.

Using equation (4), the two basic optical configurations may readily be compared on an equal size basis. At this point, detail instrument considerations enter the picture, with chopping considerations precluding the possibility of close-packing a multitude of telescopes. Since it is highly desirable or even necessary to chop the radiance entering all telescopes of a parallel system with a single chopper, a circumferential arrangement such as shown in Figure 6 is necessary. From this figure, the following relationships may be derived:

where: $1.1\, r_p = (r_o - r_p) \sin(180°/N)$ (5)

N = Number of parallel telescopes

1.1 = Factor to allow adequate clearance between telescopes for optical baffling, mounting structure, etc.

Hence: $$r_p = \frac{r_o \sin (180°/N)}{1.1 + \sin (180°/N)} \tag{6}$$

or, $$D_{op} = \frac{D_{os} \sin (180°/N)}{1.1 + \sin (180°/N)} \tag{7}$$

In a like straightforward manner, noise bandwidths of sequential and parallel systems may be compared. For the sequential system, the allowable integration time per optical filter "look" for the same spatial dwell time is multiplied by 1/N, so that the noise bandwidth correspondingly increases. This relationship may be expressed by the formula:

$$\Delta f_s = N\,(\Delta f_p) \tag{8}$$

where the subscripts are used to denote the respective systems being compared. Equations (7) and (8) may now be substituted in equation (4) for each system, and the ratio of the noise equivalent radiance difference for the two systems obtained as follows:

$$\frac{NE\Delta N_p}{NE\Delta N_s} = \frac{K\sqrt{\Delta f_p}\,(D_{op})^{-1}}{K\sqrt{N\,\Delta f_p}\,(D_{os})^{-1}}$$

Substituting equation (7) for D_{op} yields:

$$\frac{NE\Delta N_p}{NE\Delta N_s} = \frac{1}{\sqrt{N}\left[\frac{\sin (180°/N)}{1.1 + \sin (180°/N)}\right]} \tag{9}$$

Equation (9) is easily evaluated for any numerical value of "N" filter channels and yields ratios of 1.28, 1.38, and 1.66 for 4, 8 and 16 channel systems respectively.

Other pertinent considerations which apply to the general area of sensitivity versus weight are:

1) The above analysis does not consider the additional weight (and power) required for N detectors and their preamplifiers.

2) It is practical to select and maximize the D* of the single detector in a sequential system and thus achieve a better over-all sensitivity, but this becomes impractical for large values of N in a parallel system.

In view of this, the actual sensitivity advantage for equal size and weight systems may approach a factor of 2 for the sequential system.

4. DETAIL DESCRIPTION OF THE VTPR

4.1 OPTICAL CONFIGURATION

The over-all optical and scan parameters are summarized in Table 2. The optical parameters are implemented as shown in Figures 7, 8, and 9.

Radiant energy is collected from the 2.2° x 2.1° field of view by a Cassegrain type optical system using spherical surfaces on the primary and secondary mirrors. These two elements produce an f/3 converging optical beam onto the rotating filter wheel at which point the field defining stops are situated. After passing through this field stop, the energy is focused onto a pyroelectric detector cell by a field optical system comprised of an IRTRAN-4 field lens and a reflective pyramid optic. The detector is situated at the truncated opening of the reflective pyramid which produces an essentially circular image polyhedron. This image polyhedron effectively magnifies the detector area and results in an effective optical speed for the instrument of f/0.6.

The image polyhedron is imaged onto the secondary optic by the field lens so that in essence the entrance aperture is defined by the edge of the image polyhedron. This was done to eliminate any black aperture stops in the primary or secondary mirror, since these aperture stops would produce radiometric error signals.

Under the same considerations, instead of blackening the obscured area in the secondary mirror, a concave radius equivalent to the back focal length from the secondary mirror has been incorporated. With this configuration, the temperature-controlled detector either sees itself or the temperature-controlled filter wheel, thereby minimizing the error associated with the temperature variance of the optics.

The filter wheel and chopper are geared together and driven by a 2000 rpm synchronous motor. The chopper is two-bladed and is phased to the filter wheel so that as the bar between two adjacent filters just enters the field stop, the chopper closes and stays closed until the bar just leaves the field stop. In this way, the time that would normally be "wasted" when the bar is situated within the field stop is used to obtain a radiometric reference as defined by the chopper.

The image motion compensation requirement mentioned in Section 1. is implemented by using a spiral mask in the filter wheel as is shown in Figure 10. The two edges of the spiral mask define the field stop in the orbit plane direction. (The field stop in the orthogonal direction is defined just behind the filter wheel by a fixed stop in front of the detector.) As the filter wheel rotates through one revolution, the VTPR field of view is caused to "track" the motion of the earth surface relative to the satellite. Since the ITOS Satellite has a circular orbit, this ground rate is quite constant.

4.2 SCAN MECHANISM

The method of image motion compensation discussed above has a significant impact on the technique used to achieve the scanning requirement for the VTPR. As can be seen in Figures 7, 9, and 11, crosstrack scanning is achieved through the use of a stepper motor and cam, which in turn causes the scan mirror to move about an axis normal to the optical axis of the VTPR telescope. For in-flight calibration, it is necessary to move the scan mirror about the optical axis of the telescope.

One might ask why both crosstrack scanning and periodic in-flight calibration could not have been accomplished with a more conventional 45 degree flat mirror rotating about the optical axis of the VTPR telescope. The basic problem with this approach was that this method of scanning would have rotated the field of view of the VTPR relative to the orbital plane through an angle proportional to the angle of the scan beam on either side of nadir. This would have destroyed the effectiveness of image motion compensation as is indicated in Figure 12, and was thus not acceptable.

In contrast, the method of scanning used in the VTPR does not rotate the field of view relative to the orbit plane.

Another requirement for scanning is that the movement of the mirror from one position to the next be accomplished in less than 90 milliseconds, which is equivalent to a (chopper closed time)-(Q-branch filter look)-(chopper closed time). At the end of this 90 milliseconds, the scan mirror oscillations must be essentially zero, so as not to spatially smear the field of view while it is being viewed through the other filters. This requirement is related to the requirement that all filters see the same area on the earth. In the case of the Q-branch, since it operates above the highest clouds, some spatial smearing is allowed. This scan stepping speed requirement is accomplished successfully through a combination of the geometry of each cam step and a retro-torque damping configuration for the stepper motor.

4.3 IN-FLIGHT CALIBRATION MECHANISM

In-flight calibration is achieved either by command or periodically by a timer in the VTPR which causes an in-flight calibration sequence every 6 minutes.

In-flight calibration consists of a 3.5 second electrical calibration sequence function, thus calibrating the linearity of all of the signal processing electronics except the detector. Then there is a 15 second view of cold space (at 60° from the nadir) (see Figure 9), and a 16 second view of an in-flight calibration source whose temperature is telemetered on the main data channel during the 2.5 second mirror retrace period from the in-flight calibration sequence.

The radiometric views of cold space and the in-flight calibration source provide periodic corrections to the gain of the VTPR. They also eliminate any bias errors or offsets applicable to the filters which may have occurred due to thermal variations of the VTPR. The calibration sequence takes 37.5 seconds, which amounts to a data interruption of this time period. It is therefore desirable to maximize the time between in-flight calibrations. Ideally, the in-flight calibrations should be accomplished once every orbit when the VTPR is over the earth's pole, and is thus providing redundant vertical temperature profile information to that obtained on previous orbits. In order to achieve this capability, the command logic of the VTPR provides the capability of eliminating all in-flight calibrations except on command, in which case the command would be given when the ITOS vehicle is situated over the pole.

A Life Test Model of the scan and calibration assembly described above was subjected to a 10 month life test in a vacuum of better than 10^{-6} Torr. Extrapolation of the results of this test indicate successful operation of the mechanism for over one year in space. No indication of any "cold welding" of the follower to the cam was noted in this test. All the bearings in the scan assembly are of the Barden "Bartemp" variety, which include impregnated teflon ball separators that continually wipe a dry lubricant onto the ball and races in each bearing.

4.4 IR DETECTOR

The IR detector used in the VTPR is a pyroelectric thermal detector. Although this detector can operate satisfactorily at any temperature below its Curie point of +47°C, considerations discussed in Section 4.6 require that it be controlled at

+35°C in the VTPR.

A thermistor-bolometer IR detector was utilized in the early phases of the VTPR design. However, side-by-side comparison tests of equivalent thermistor bolometer and pyroelectric detectors showed a sensitivity improvement factor of at least 3:1 for the pyroelectric detector. Furthermore, the pyroelectric detector requires no high-voltage filtered bias supply, thus eliminating both a possible corona arc problem and the bias supply.

For the above reasons, the pyroelectric detector was incorporated into the VTPR design.

4.5 ELECTRONIC PROCESSING OF THE VTPR

The electronic processing of the VTPR is discussed in detail by D. Zink (Ref. 5). In this paper we will cover only the over-all signal processing concept.

The chopper and filter wheel rotation rates are such that all eight filters are viewed by the detector in 0.5 second for each spatial spot, with a chopper closed period occurring between each filter "look" time (see Figure 13). Therefore, the output signal equivalent to the radiometric input would consist of a 16 Hz pulse train having variable amplitudes for each pulse. In order to retrieve this pulse train signal, the preamplifier compensates for the 6 db/octave fall-off signal response of the detector above 0.08 Hz. Fortunately, the detector generated noise drops off at approximately 5 db/octave, so that no great penalty in signal to noise ratio is paid for this "treble pre-emphasis" preamplifier compensation. The output of the preamplifier and postamplifier is fed into a synchronous clamp (or dc restoring circuit) which clamps during the chopper closed period, and thus establishes the radiometric reference at the chopper temperature. During the filter look time, the clamp opens and the output pulse (equivalent to the radiance coming through the filter being viewed) is then integrated in a RC integrator circuit which also performs a sample and hold function. This circuit serves to minimize the noise bandwidth of the VTPR, and the output signal-to-noise ratio is established at this circuit's output. This output is then digitized into a 10-bit word, combined with a 5-bit word which identifies the scan step and mode of operation of the VTPR, and sent into the ITOS telemetry chain.

4.6 THERMAL DESIGN

The thermal design of the VTPR hinges on the requirement to maximize the time between in-flight calibrations, and thus minimize the data loss periods. It is desirable to achieve the capability of having an in-flight calibration only every two hours or one orbit period. This is accomplished by minimizing the optics' emissivity so that the radiometric errors introduced are minimized. Furthermore, as stated earlier, we must control the temperature of the filter wheel to stabilize the central wavelengths of all the filters. The temperature control circuitry was designed to operate successfully in the presence of a 5°C change in temperature of the ITOS Spacecraft for orbits which go from full sun to full shadow.

The filter wheel and chopper are controlled by mounting them on thermally insulating hubs and surrounding the chopper and filter wheel assembly with a black housing called a shroud (see Figure 14). The shroud is heated to a temperature above that desired for the filter wheel. Heat from the shroud is then radiated into the filter wheel and chopper so as to compensate for the heat flow out through their insulated shafts to the heat sink of the mounting plate on which everything is mounted. Thus, we can maintain the filter wheel and chopper at a temperature which is a linear function of the shroud temperature.

The detector, which is directly behind the filter wheel, views adjacent filters as they pass by. Although these filters are not chopped by the chopper, this filter movement relative to the detector will create a false radiometric signal if there is any temperature difference between the filter wheel and detector, and if

there is any emissivity difference between adjacent filters. Furthermore, while the radiance coming through the filters has a spectral bandwidth of only 0.1 micron, the radiance coming from the rear side of the filters has a bandwidth of approximately 10 microns. This is necessary because the detector must have a wide enough spectral bandwidth to accept all the filter regions. Therefore, if the emissivity of adjacent filters were 1 and 0 respectively, then a 0.1°C difference between the filter wheel and detector would produce as much signal as a 10°C difference in target temperature (which at 300°K would be equivalent to a target radiance change of 17 mw/m^2-ster-cm^{-1}), or 70 times the desired relative calibration accuracy. These errors have been reduced to insignificant levels by minimizing the out of band emissivity of the optical filters and tightly controlling the temperatures of the filter wheel and detector.

Two controllers are utilized to maintain the filter wheel in close temperature proximity to that of the detector over the ambient temperature range of the VTPR. One controls the detector temperature at an absolute level of +35°C. The shroud controller uses four thermocouples to measure the differences between shroud temperature, detector temperature and ambient temperature. The thermocouples are so arranged that the shroud controller equation is as follows:

$$(T_d - T_a) - k\,(T_s - T_d) = S_c$$

where:

T_s = Shroud temperature

T_d = Detector temperature

T_a = Temperature of the heat sink or mounting plate

S_c = Controller input to shroud heater

The value of k in the above equation is empirically established for each unit by inserting a "black" filter into one sector on the filter wheel whose channel will directly measure the difference between filter wheel and detector and allow the value of k to be experimentally established with high accuracy.

5. PERFORMANCE OBTAINED WITH THE VTPR ENGINEERING AND FLIGHT MODELS

The VTPR Engineering Model is essentially identical to the Flight Models that are used on the ITOS Spacecraft. It has been tested in a thermal vacuum simulation fixture which closely simulates the radiometric and thermal characteristics of the ITOS Spacecraft and the 790 nautical mile orbit. This thermal vacuum simulation fixture (shown in Figure 15) contains cooled plates which provide the radiance and solid angle equivalent to space and earth in a 790 nautical mile orbit. A quartz-halogen lamp is used to simulate the varying earth albedo as a function of orbit position. The VTPR is mounted inside a box which simulates the ITOS Spacecraft. The box temperature can be separately controlled through the use of a recirculating ethylene glycol temperature controller.

At either end of the VTPR scan are situated two precision blackbody sources fabricated by Eppley Labs. By stopping the VTPR scan, either in Step 1 or Step 23, the VTPR continuously views one of these precision sources. The output of the VTPR and the output of the source are recorded versus time. The overall stability of the VTPR output for a fixed radiance input can thus be established in the presence of the various input stimuli, such as changing ITOS temperatures and varying albedo.

Figure 16 is a typical recording of the input stimuli to the VTPR and outputs of one of the filter channels. The test was conducted over a four-hour period to simulate two full orbits and to allow the oscillatory temperatures to reach steady state. As can be seen in this figure, the errors are highly correlated and

are therefore absolute errors as defined in Section 2.3. It can be further noted that by calibrating every twenty minutes or less, these absolute errors can to a large extent be removed. Alternatively, if it is desired to calibrate every two hours, by using a correlation process on the temperature of the optics (which are telemetered down every 12.5 seconds on the main data channel during the scan retrace period) the absolute errors, which are predominantly due to the variation in optic temperatures, can also be taken out by this means. These results show that by using the above mentioned calibration or correlation techniques, the VTPR can provide a corrected absolute stability over a two hour period of better than 0.25 mw/m^2-ster-cm^{-1} rms, or better than 0.15% of the full scale reading on all the channels.

Insofar as relative calibration error is concerned, this is predominantly determined by the noise of the pyroelectric detector. The results of the sensitivity measurement conducted with a typical Flight Model of the VTPR, are presented in Table 3. These results indicate that the relative error on all channels, except the very narrow band Q-branch channel, provide a relative calibration accuracy of better than 0.2 mw/m^2-ster-cm^{-1}, which is less than 0.1% of the full dynamic range.

Another performance parameter which has been evaluated, is the correlation of the in-flight calibration of the VTPR to the calibration obtained using the reference standard Eppley blackbodies. This was done by comparing the radiometric output obtained when viewing the in-flight calibration source in the VTPR to that obtained when viewing the Eppley blackbody at the same temperature. The histogram shown in Figure 17 is the distribution of measurement points taken for all filter channels in two VTPR Flight Units, where each measurement point represents the radiance difference at the VTPR output between the Eppley blackbody standard and the in-flight calibration source at the same indicated temperature. These data were taken over an ambient temperature range of the VTPR from 0°C to +30°C. As can be seen in this figure, the rms or 1 sigma error is 0.5 to 0.7 mw/m^2-ster-cm^{-1}.

It had been hoped that flight data for the two VTPR units on ITOS-D would be available in time for publication in this paper. Unfortunately, schedule delays have shifted the launch date just past the publication date. However, to indicate the efficacy of the atmospheric temperature profile inversion technique, Figure 18 shows a series of retrieved temperature profiles abstracted from Ref. (6). These profiles were generated by data from SIRS (which has filter channels closely similar to those of VTPR) and are compared to radiosonde data in the same geographic location. We trust the VTPR will provide equal or better performance.

6. CONCLUSIONS

This paper has discussed various design characteristics and performance achievements of the Vertical Temperature Profile Radiometer.

On the basis of the measurements taken with the VTPR Engineering and Flight Models, it can be concluded that:

1) The VTPR provides a relative calibration accuracy between seven of the eight channels of better than 0.1% rms of the full dynamic range, and on the very narrow band Q-branch filter it provides a relative calibration accuracy of better than 0.2% rms of the full dynamic range.

2) The absolute accuracy achievable between in-flight calibrations of 6 minutes, or between 2-hour calibrations using optical temperature correction factors, is better than an rms value of 0.15% of full scale.

3) The radiometric correlation between the VTPR in-flight calibration source and a reference standard blackbody is better than an rms value of 0.5% of full scale.

ACKNOWLEDGEMENT

The author would like to express his appreciation to NASA Goddard Space Flight Center, Operational Satellite Branch, for their sponsorship in developing the instrument described in this paper, and to Messrs. H. Ruddy, R. Grudee, D. Zink and S. Kaminsky of Barnes Engineering Company, who were respectively responsible for instrument mechanical design and mechanical analysis, electronic design and system analysis.

REFERENCES

1. L. D. Kaplan, "Inference of Atmospheric Structure from Remote Radiation Measurements," Journal of the Optical Society of America, 49, 10, pp.1004-1007, October 1959.

2. D. Q. Wark and H. E. Fleming, "Indirect Measurements of Atmospheric Temperature Profiles from Satellites," Monthly Weather Review, 94, 6, pp. 351-352, June 1966.

3. S. D. Smith, J. S. Seeley and F. S. Ritchie, "Final Scientific Report Multilayer Filters for the Region 0.8 to 100 Microns." (University of Reading, Reading, England, 1968) Contract AF61(052)-833.

4. W. L. Smith, "An Improved Method for Calculating Tropospheric Temperature and Moisture from Satellite Radiometer Measurements," Monthly Weather Review, 96, 6, pp. 387-396, June 1968.

5. D. Zink, "Electronic Processing in the Vertical Temperature Profile Radiometer," pp. 194-202, NTC '71-Record of the National Telemetering Conference, Washington, D.C., April 12-15, 1971. (Institute of Electrical and Electronic Engineers, New York, N.Y., 1971) Publication No. 71 C10-NTC.

6. D. Q. Wark, "SIRS: An Experiment to Measure the Free Air Temperature from a Satellite," Applied Optics, Vol. 9, No. 8, August 1970.

TABLE 1. RADIOMETER FILTER CHARACTERISTICS AT 35°C

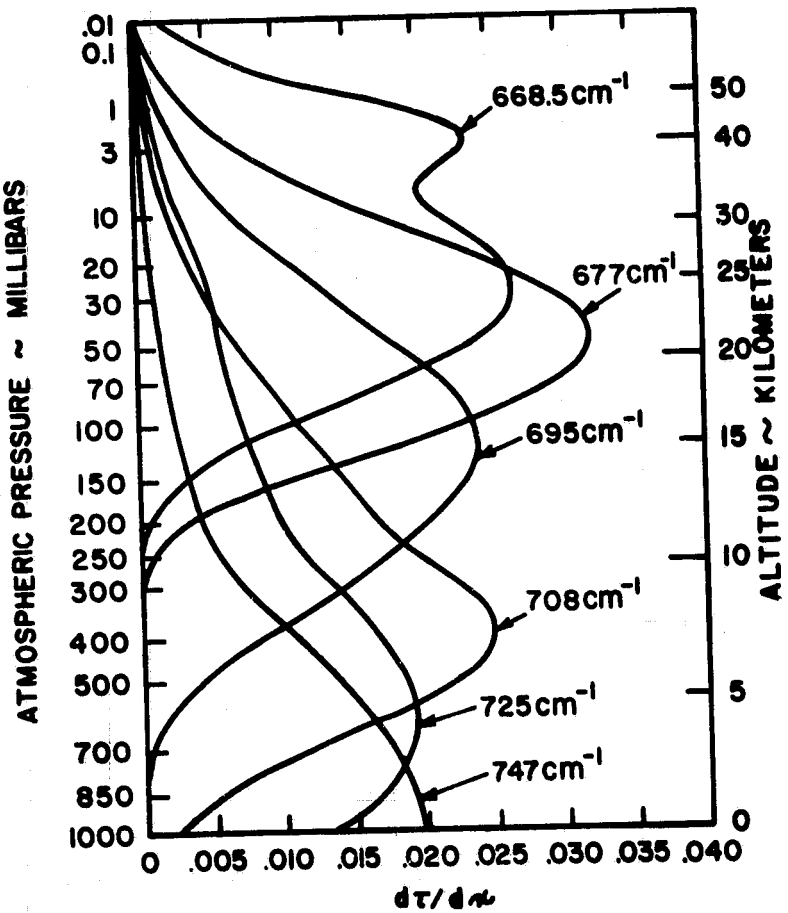
Filter No.	Center of Spectral Response Wave No. (cm^{-1})	Bandwidth and Tolerance 50% Response (cm^{-1})	10% Response (cm^{-1})
1 (Q-Branch)	668.5 ± 0.5	3.5 ± 0.5	10.5 ± 1.5
2	695 ± 1	10.0 ± 2.5	20 ± 5
3	725 ± 1	$10.0^{+1.0}_{-2.0}$	20^{+2}_{-4}
4	535 ± 1	$10.0^{+1.0}_{-2.0}$	20^{+2}_{-4}
5	835 ± 1	$8.0^{+1.0}_{-2.0}$	16 ± 2
6	747^{+2}_{-1}	10.0 ± 2.5	20 ± 5
7	708 ± 1	10.0 ± 2.5	20 ± 5
8	677^{+2}_{-1}	10.0 ± 2.5	20 ± 5

TABLE 2. OPTICAL AND SCAN PARAMETERS OF THE VTPR

Optical Parameters	
Primary Mirror Diameter	73.5 mm
Secondary Mirror Diameter	28.6 mm
Entrance Aperture Diameter (D_o)	66 mm
Focal Length of Cassegrain Optics	197 mm
Field of View (FOV)	2.235° x 2.135°
Detector Area (A_d)	1.5 x 1.5 mm^2
Effective Focal Length (e.f.l) = $\frac{\sqrt{A_d}}{\sqrt{FOV}}$	38.5 mm
Effective System f/no. = $\frac{efl}{D_o}$	0.584
Scan Parameters	
Cross Track Scan Angle	63.4°
No. of Steps per Scan	23
Time per 23 Steps	11.5 sec
Scan Retrace Time	1.0 sec.

TABLE 3. VTPR RADIOMETRIC PERFORMANCE

Filter No.	Channel (cm^{-1})	Required RMS NEΔN (mw/m^2-ster-cm^{-1})	Typical Measured RMS NEΔN (mw/m^2-ster-cm^{-1})
1	668.5	0.75	.46
2	695	0.25	.12
3	725	0.25	.13
4	535	0.25	.17
5	835	0.25	.13
6	747	0.25	.11
7	708	0.25	.10
8	677	0.25	.12



NOTES

τ = ATMOSPHERIC SPECTRAL TRANSMISSION

ν = (ATMOSPHERIC PRESSURE)$^{2/7}$

THESE DATA OBTAINED FROM DR. D.Q.WARK OF NOAA.

FIGURE 1. TYPICAL WEIGHTING FUNCTIONS OF THE VTPR (UNCORRECTED FOR ATMOSPHERIC H_2O AND OZONE)

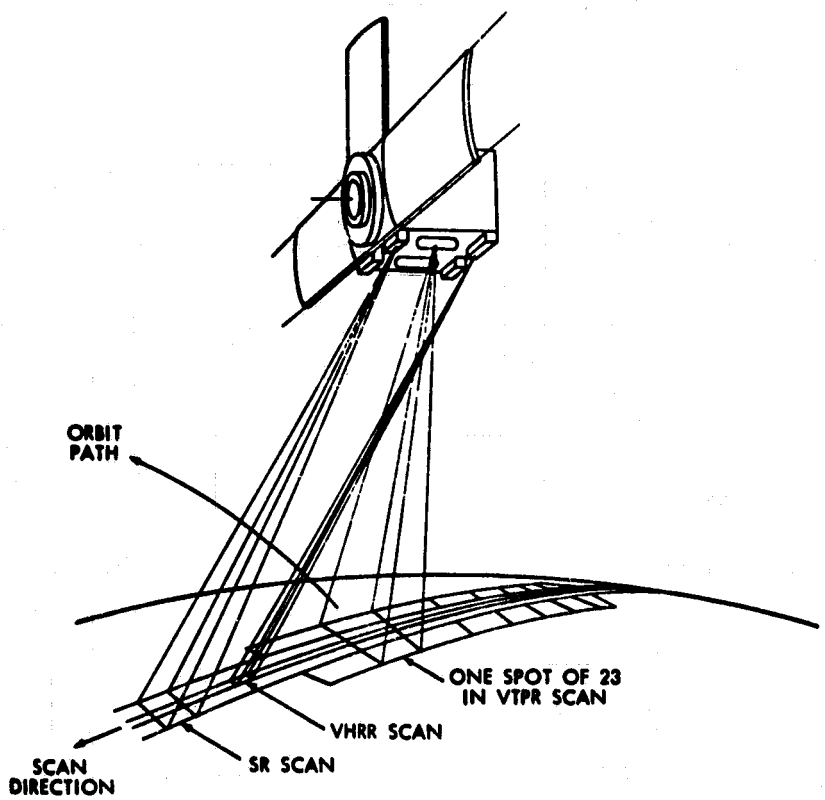


FIGURE 2. ITOS-D THRU G SATELLITE IN OPERATIONAL MODE SHOWING SENSOR FIELDS OF VIEW

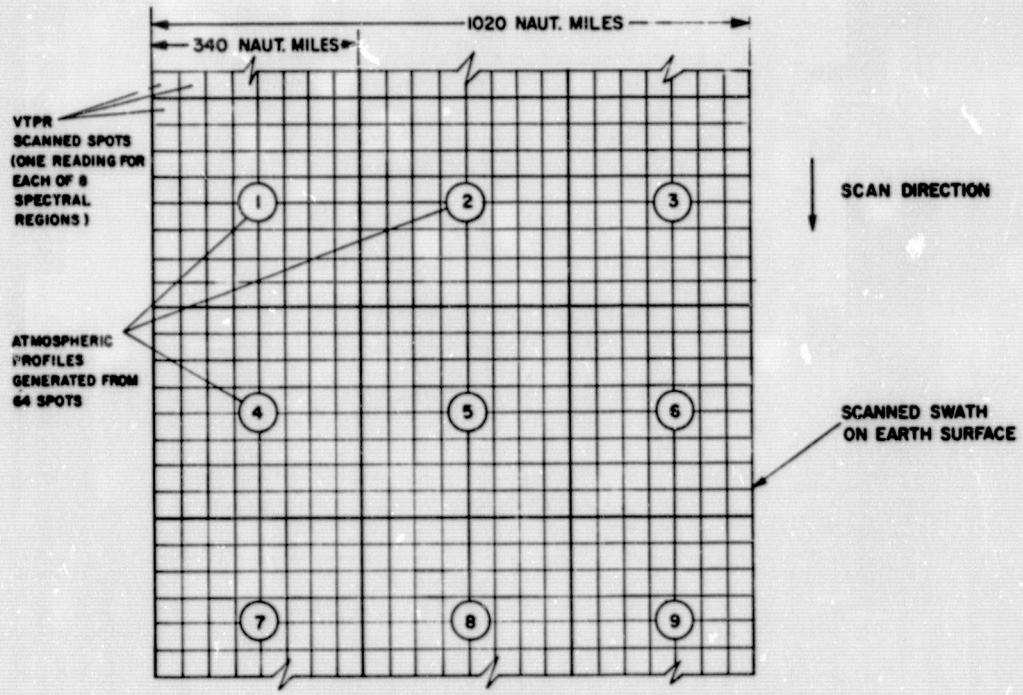


FIGURE 3. ATMOSPHERIC TEMPERATURE PROFILE GENERATION FROM VTPR DATA BY NOAA

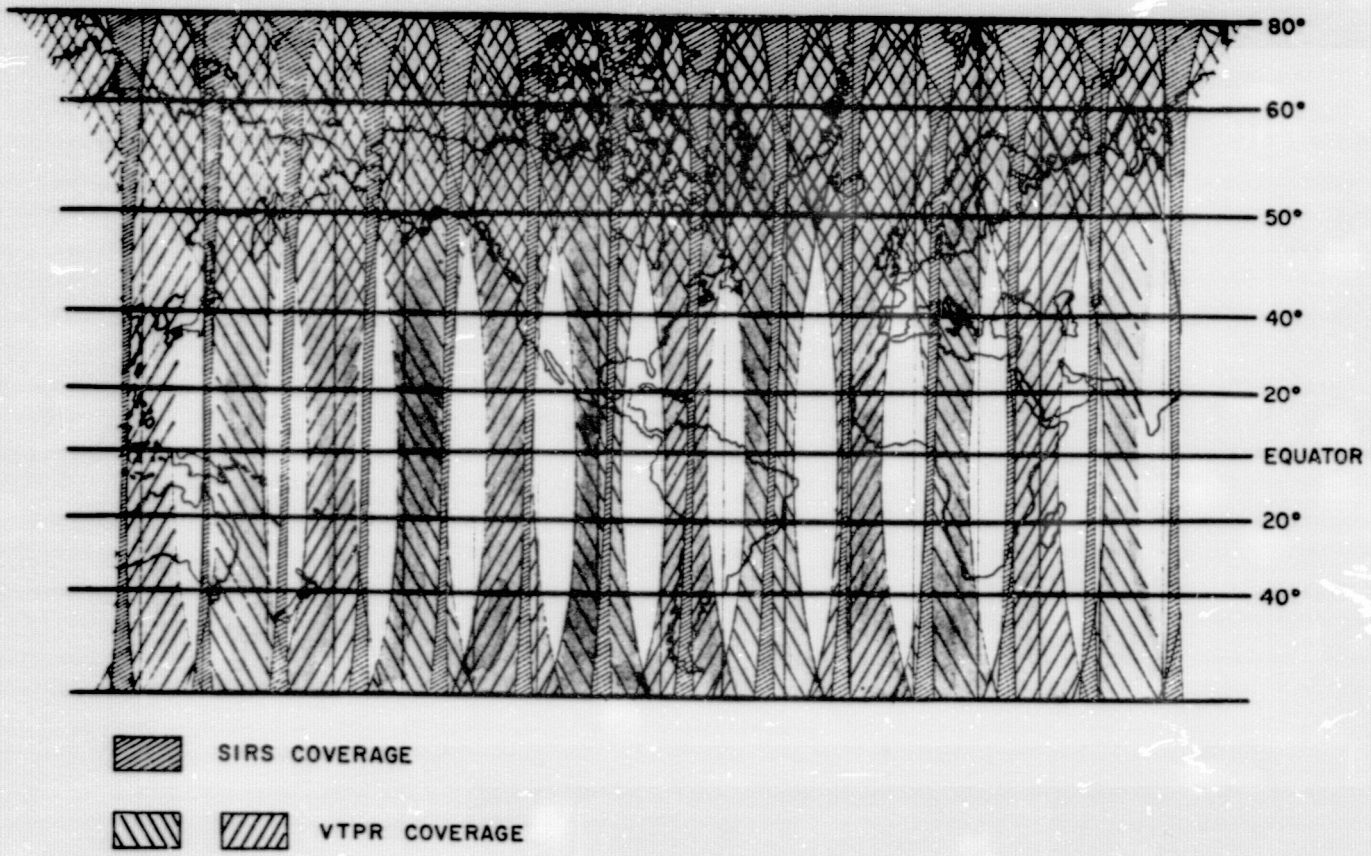


FIGURE 4. GEOGRAPHIC COVERAGE OF SIRS SUPERIMPOSED ON VTPR COVERAGE

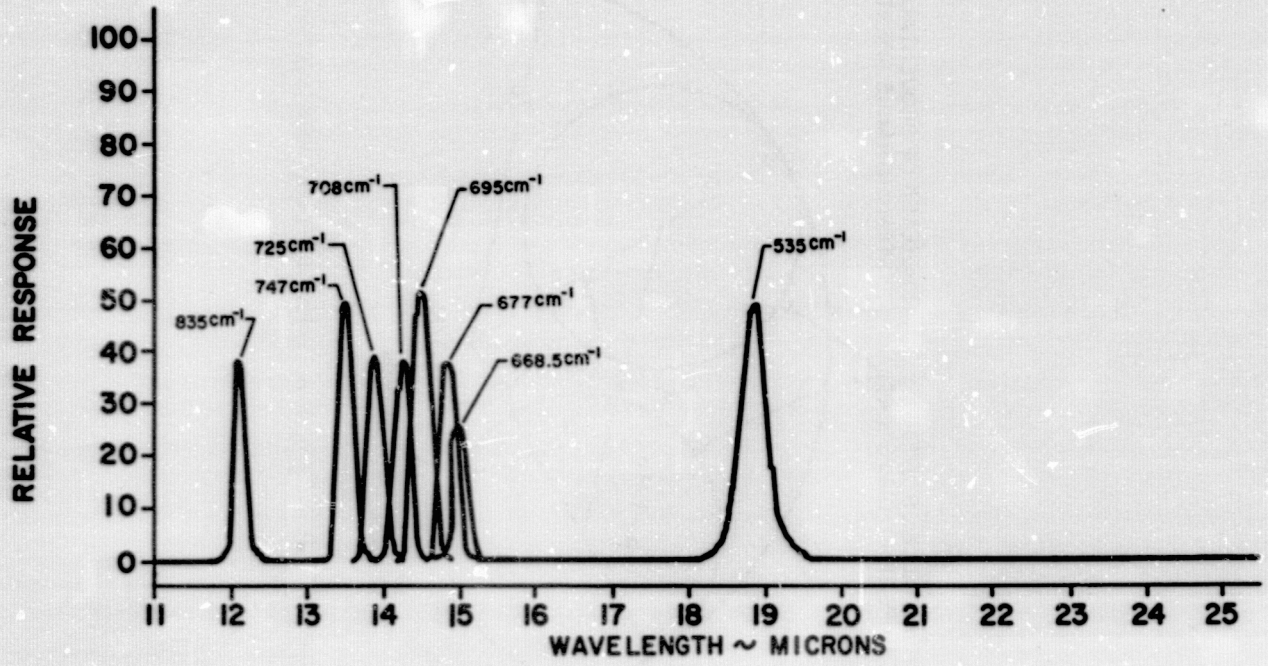


FIGURE 5. SPECTRAL TRANSMISSION & DISTRIBUTION CHARACTERISTICS OF VTPR OPTICAL FILTERS

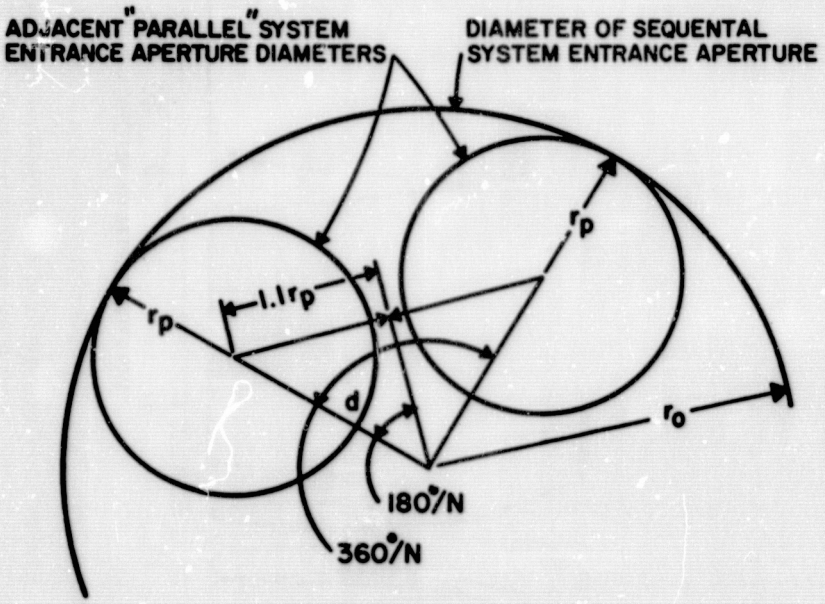


FIGURE 6. GEOMETRY OF A "PARALLEL" TELESCOPE SYSTEM

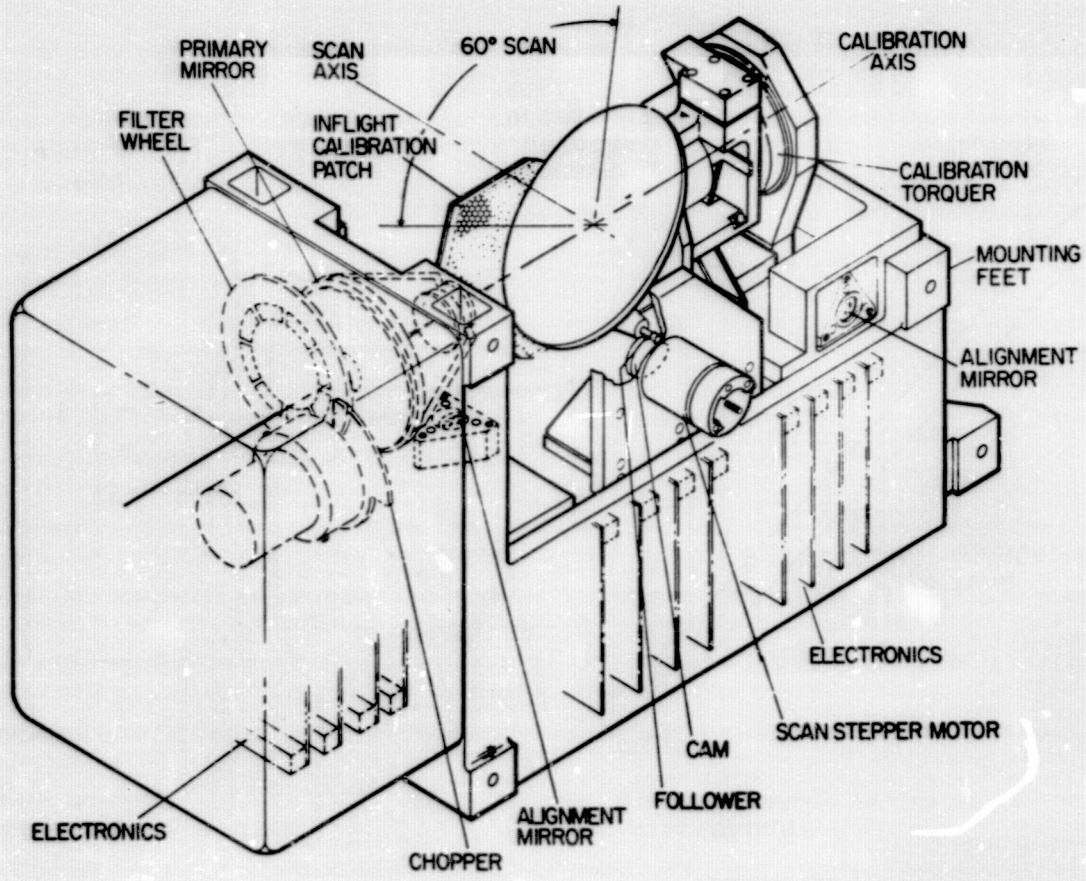


FIGURE 7. ISOMETRIC VIEW OF VTPR

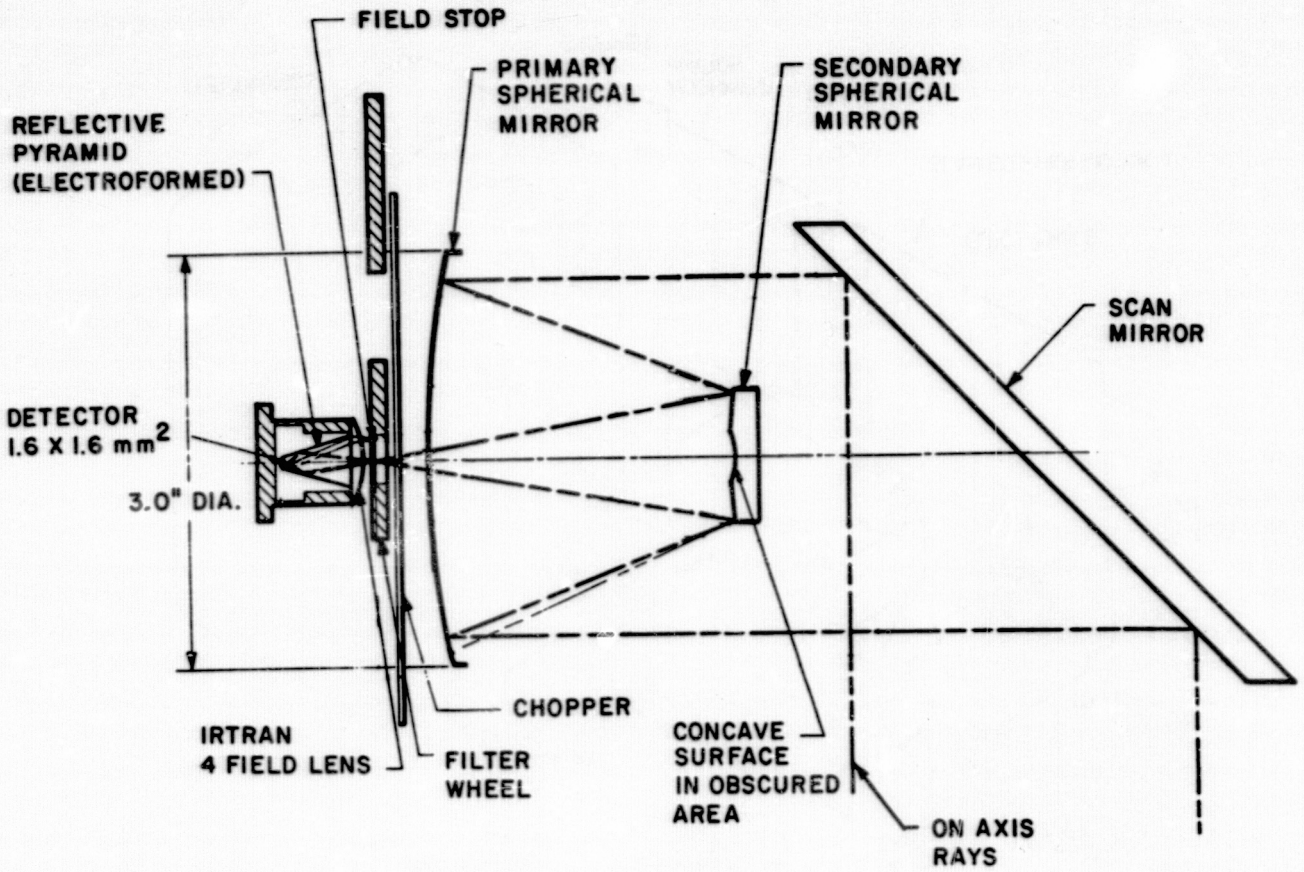


FIGURE 8. OPTICAL SCHEMATIC

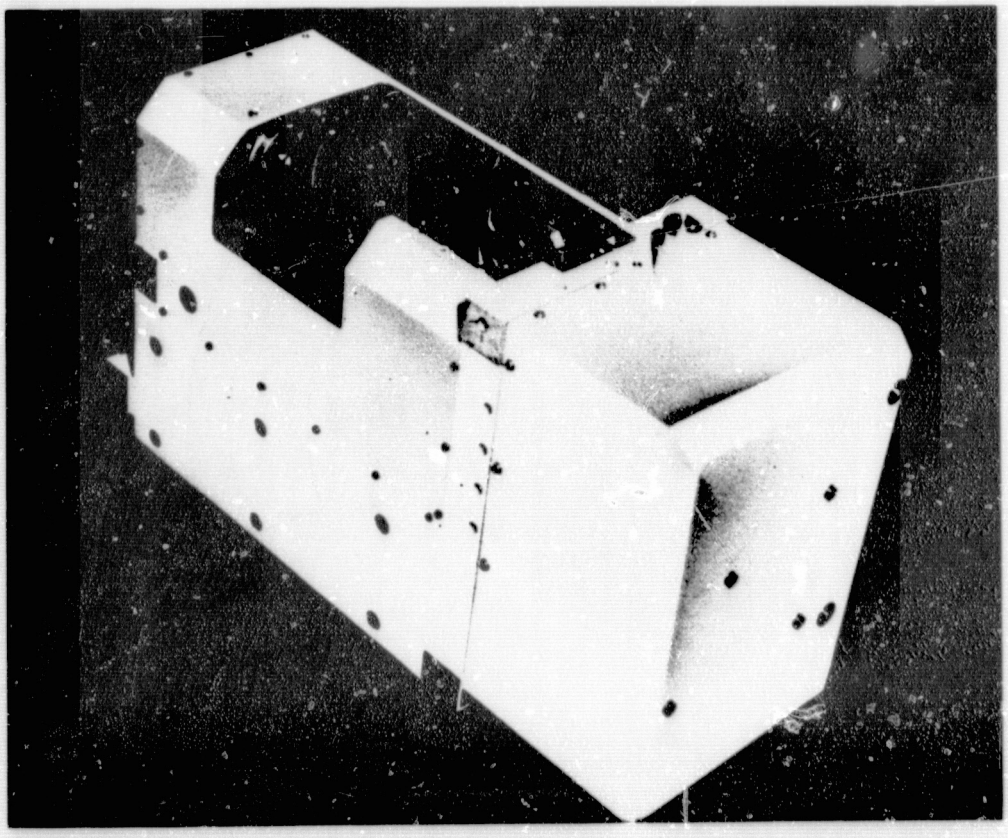


FIGURE 9. PHOTO OF VTPR

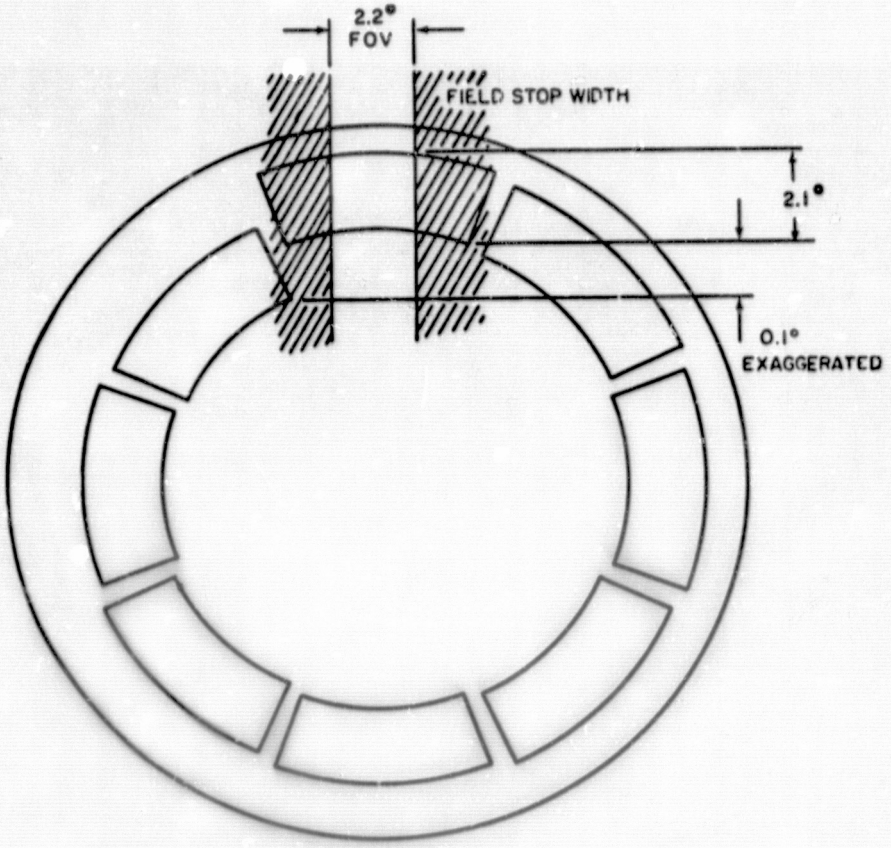


FIGURE 10. IMAGE MOTION COMPENSATION MASK

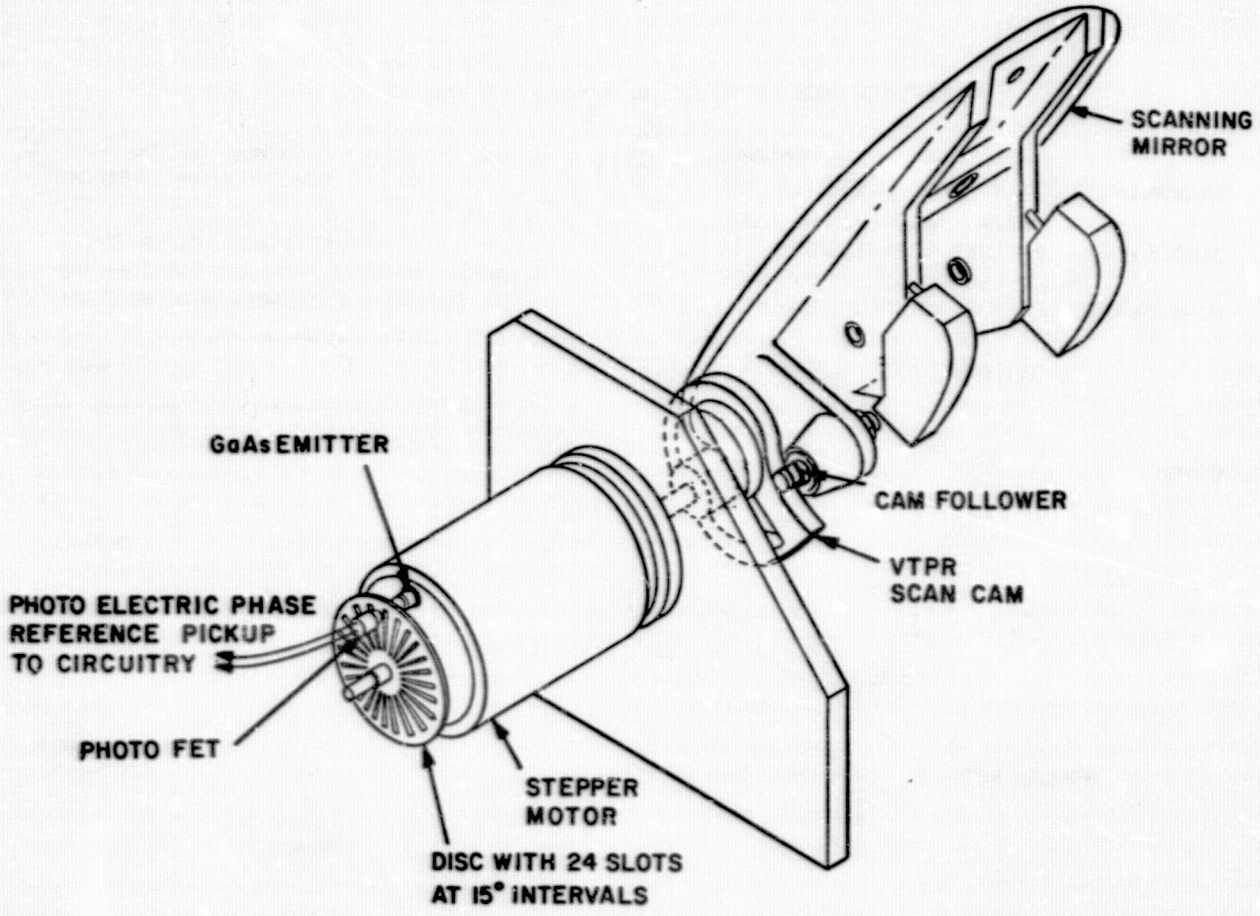
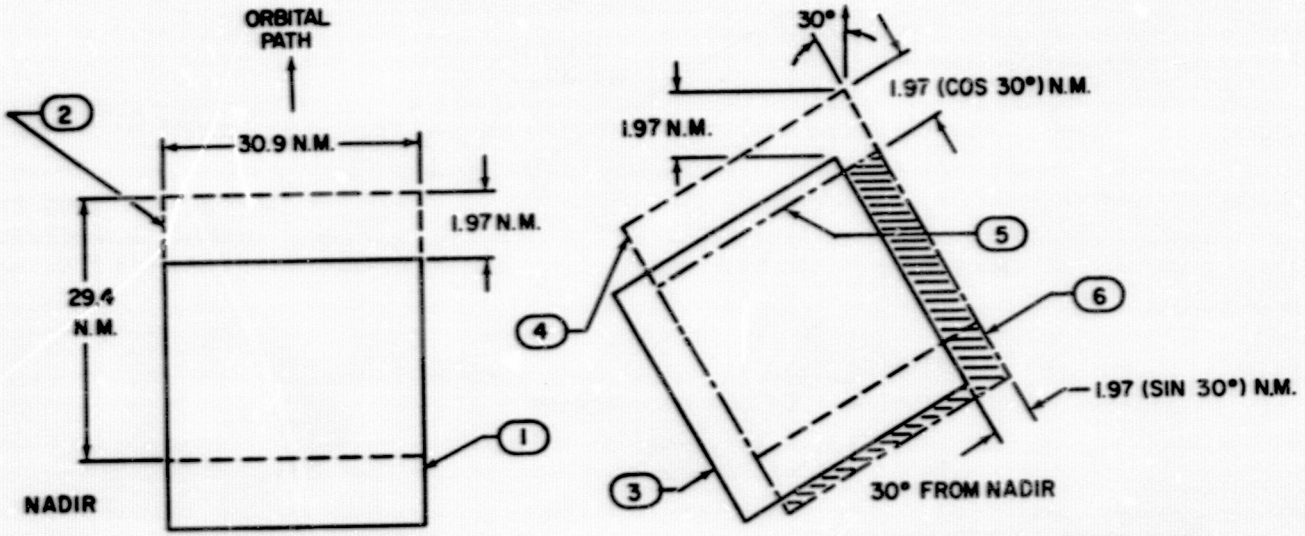


FIGURE 11. SCAN MECHANISM



1. FIELD OF VIEW PROJECTION ON EARTH AT FILTER 1 AND FOR ALL OTHER FILTERS WITH IMAGE MOTION COMPENSATION.
2. F O V PROJECTION ON EARTH AT FILTER 8 WITH NO IMAGE MOTION COMPENSATION.
3. F O V PROJECTION ON EARTH AT FILTER 1.
4. F O V PROJECTION ON EARTH AT FILTER 8 WITH NO IMAGE MOTION COMPENSATION.
5. F O V PROJECTION ON EARTH AT FILTER 8 WITH IMAGE MOTION COMPENSATION.
6. SHADED AREA IS IMAGE MOTION COMPENSATION ERROR.

FIGURE 12. FIELD ROTATION AT SCAN EXTREMES

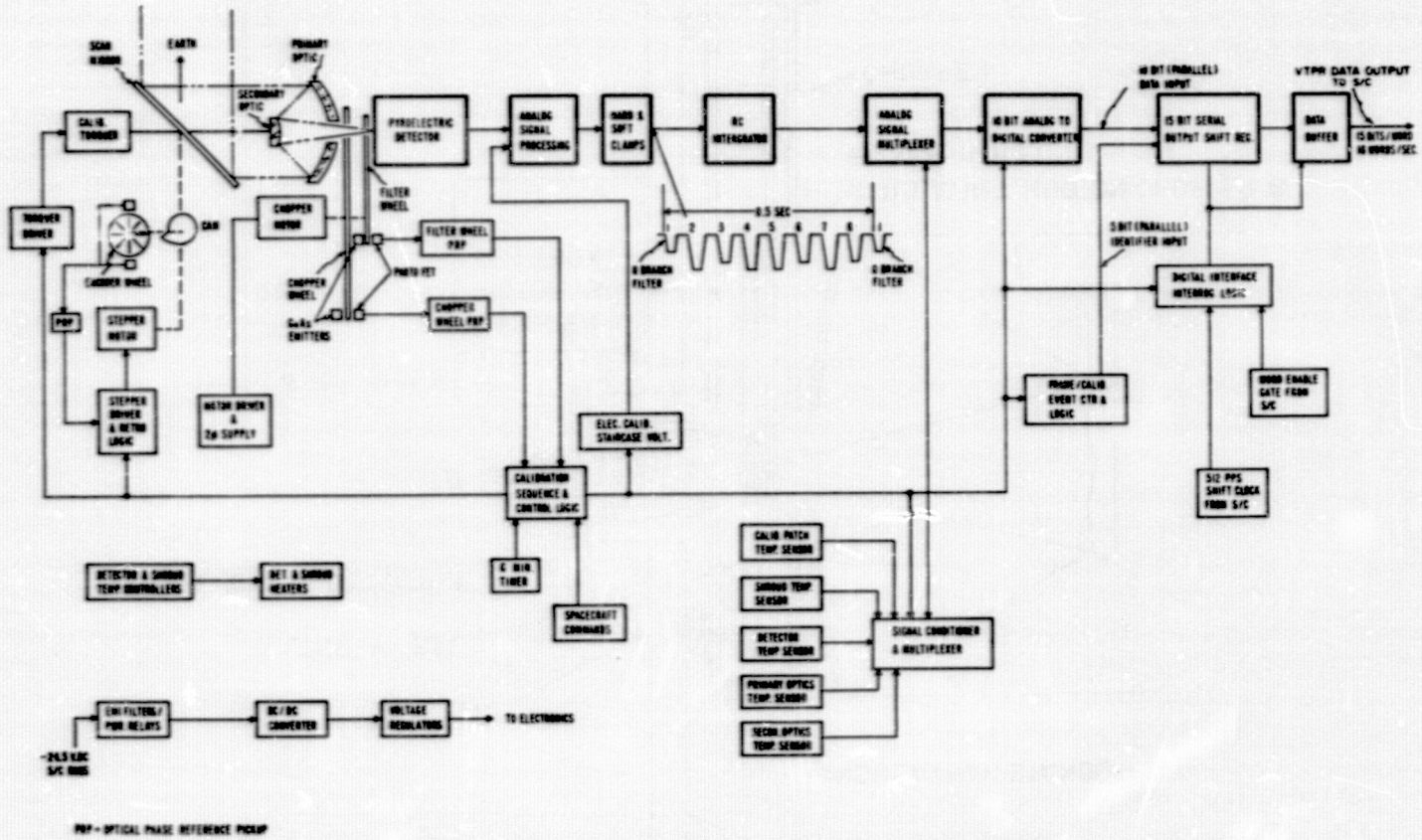


FIGURE 13. SIMPLIFIED ELECTRONIC BLOCK DIAGRAM

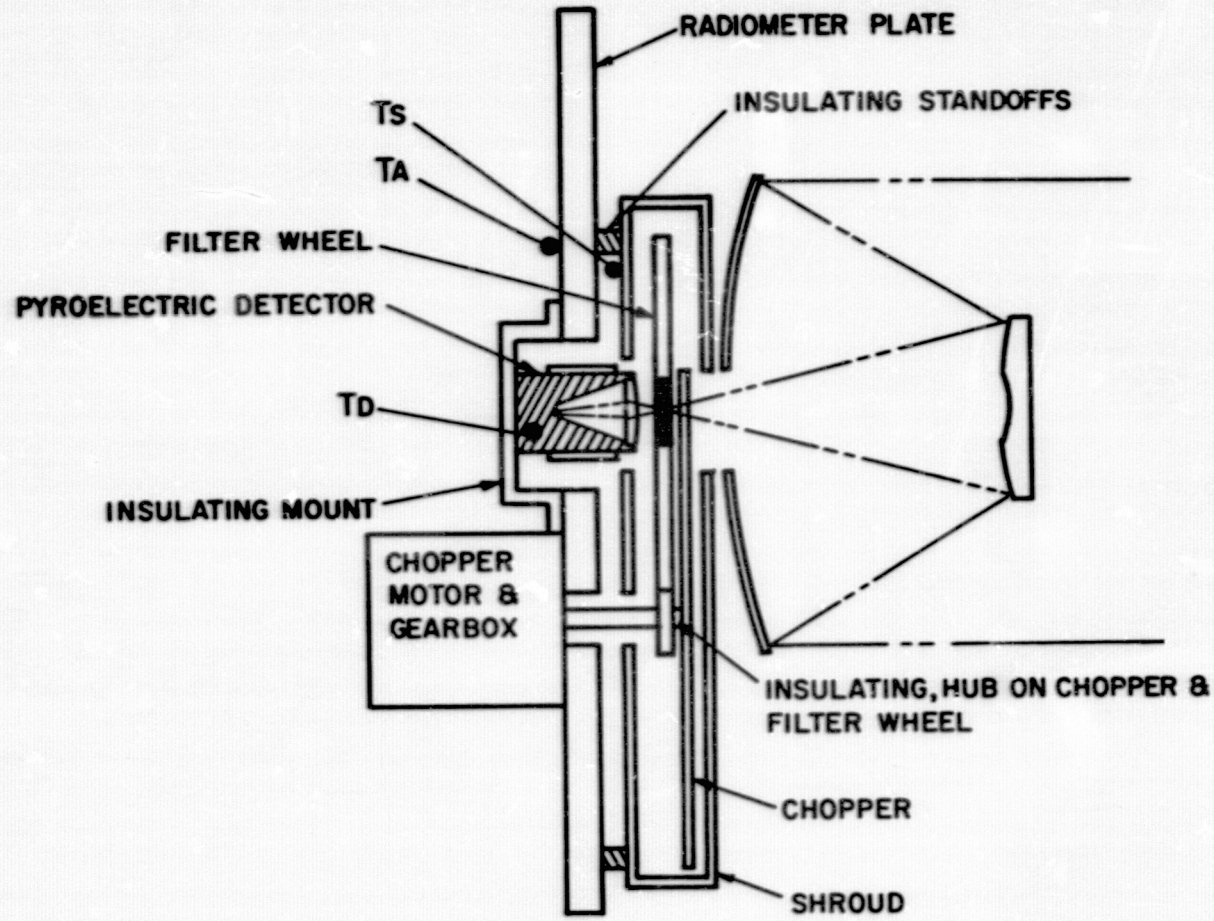


FIGURE 14. THERMAL CONTROL MECHANICAL SCHEMATIC

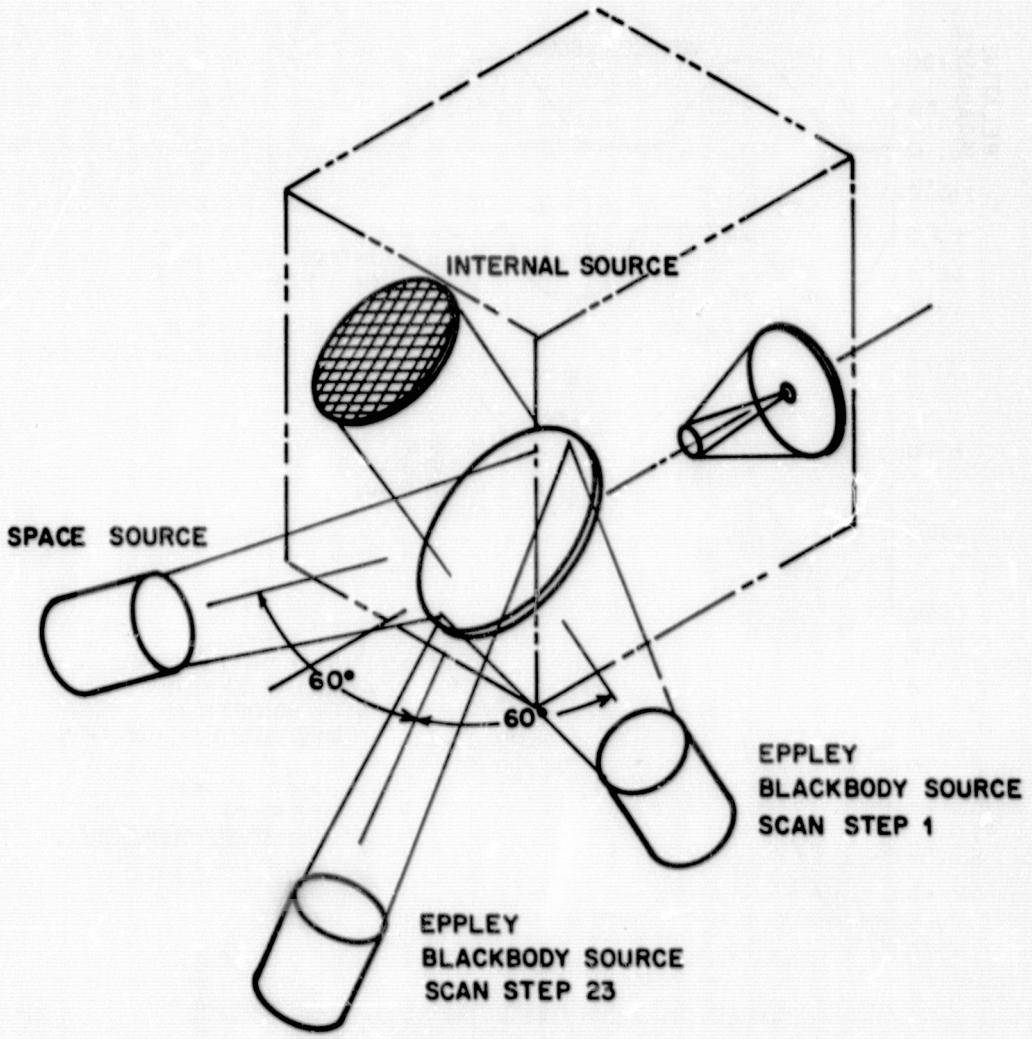


FIGURE 15. THERMAL VACUUM RADIOMETRIC CALIBRATION SET UP

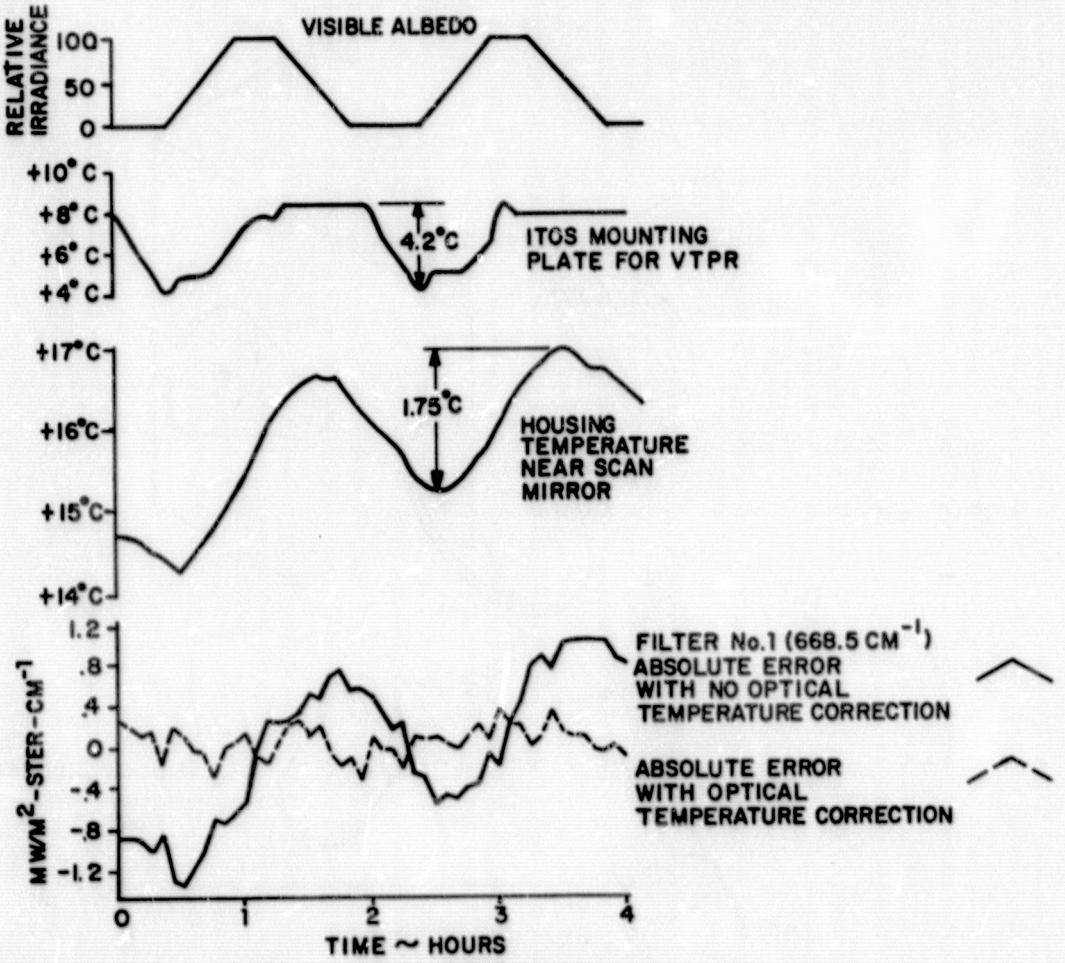


FIGURE 16. ENGINEERING MODEL THERMAL VACUUM TYPICAL TEST RESULTS

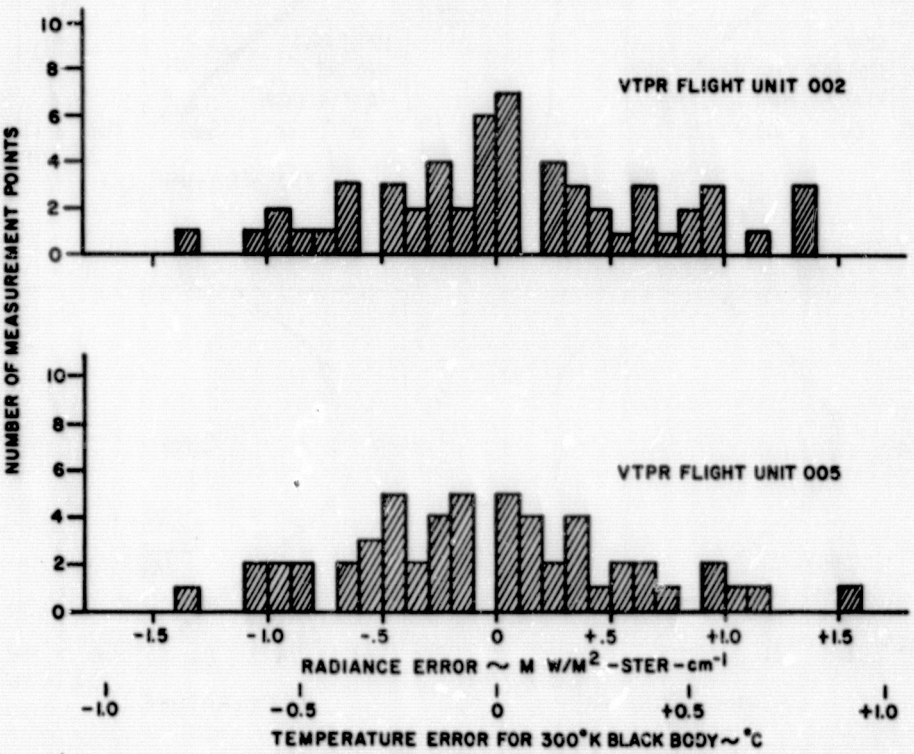
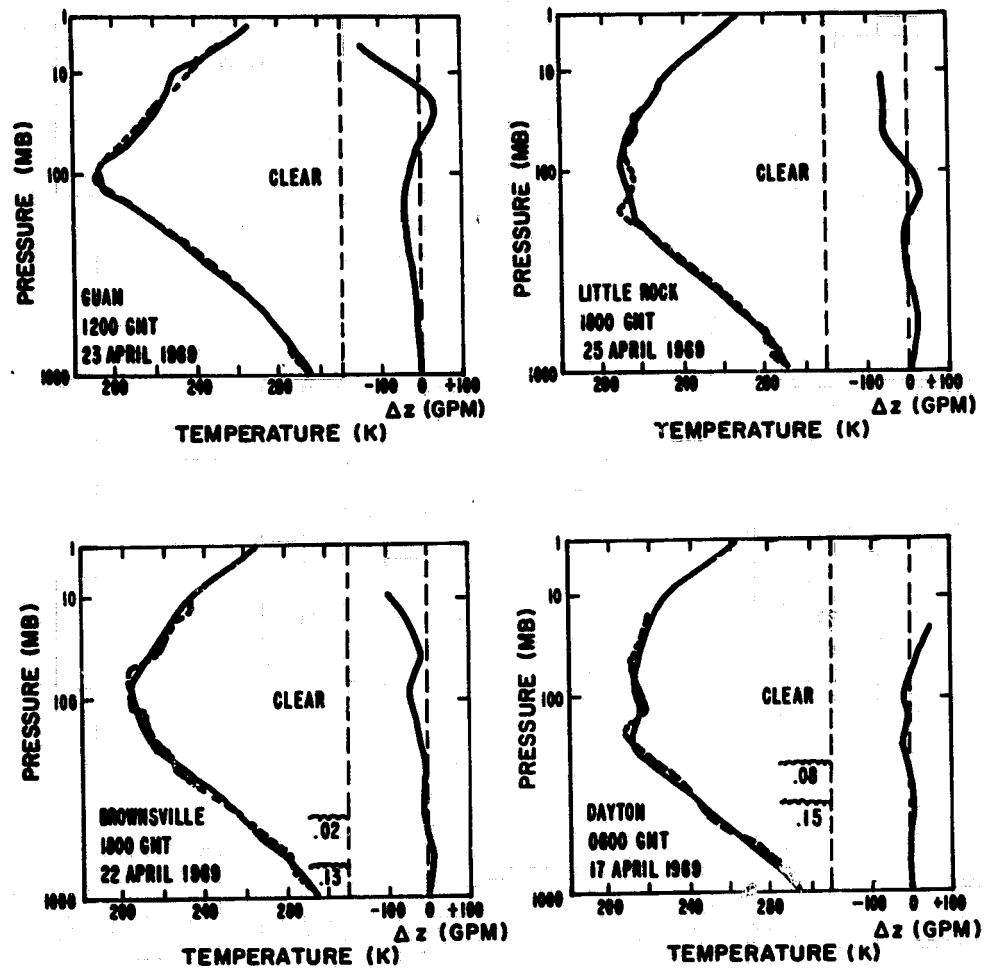


FIGURE 17. CORRELATION OF INTERNAL CALIBRATION SOURCE RADIOMETRIC SIGNAL WITH THAT OF THE STANDARD BLACKBODY



NOTES:

1. Δz = DIFFERENCE IN GEOPOTENTIAL HEIGHTS OF THE PRESSURE LEVELS FOR THE SIRS VS. RADIOSONDE PROFILE ~ METERS.
2. THIS DATA ABSTRACTED FROM REF. 6.

FIGURE 18. FOUR TYPICAL ATMOSPHERIC TEMPERATURE PROFILES OBTAINED FROM SIRS DATA COMPARED TO RADIOSONDE DATA

AN EXPERIMENTAL MODEL FOR THE AUTOMATED DETECTION, MEASUREMENT, AND QUALITY CONTROL OF LOW-LEVEL CLOUD MOTION VECTORS FROM GEOSYNCHRONOUS SATELLITE DATA

R. Bradford, J. Leese and C. Novak

National Environmental Satellite Service
Washington, D. C. 20233

ABSTRACT

A computer model developed for obtaining cloud motion vectors from geosynchronous satellite data contains all the components of an automated operational procedure. This model was run for a four-month operational test period to determine the ability of the different software components to perform detection, measurement and quality control functions in the automated processing of raw data into low level cloud motion vectors. An evaluation of the computed vectors showed that 83% were operationally useful. Image data from the Applications Technology Satellites (ATS) were processed on 56% of the days from ATS-1 and 88% of the days from ATS-3. The low success rate achieved with ATS-1 is not indicative of the model's ability to produce, but is a function of weaknesses found in the ATS-1 processing system. The 88% success rate is indicative of the performance level that can be achieved after some of the system weaknesses are eliminated. Comparisons between manual and computer vectors yielded an RMS difference of about 30 degrees in direction and seven knots in speed. This difference varied with latitude, a factor which is most probably related to picture registration accuracy.

The model is now in use operationally to obtain a significant portion of the low-level cloud motion vectors from ATS-1 and ATS-3 data.

1. INTRODUCTION

The advent of the spin-scan cloud camera on board the Applications Technology Satellite (ATS) made possible sequential viewing of the same geographical scene at relatively short time intervals. Shortly after the launch of ATS-1 in 1966, Dr. Fujita of the University of Chicago demonstrated the feasibility of measuring cloud displacements by viewing a sequence of images from the spin scan camera in a "closed loop" projection. Cloud motion vectors have been derived in daily operations since 1969 by subjectively viewing an animated sequence of cloud pictures and manually fixing the positions of cloud elements at the beginning and end of the picture sequence. The details of the current procedures have been described by Young, Doolittle, and Mace (1972). These vectors provide information about wind speed and direction, the most important parameters used in numerical weather prediction. The tedious nature of the manual process for deriving cloud motion vectors makes highly desirable the automation of as much of the process as possible. The feasibility of measuring cloud motion vectors with computer methods has been demonstrated for a number of cases (Bristor et. al. 1967, and Leese et. al. 1970). An automated operational procedure requires, in addition to a valid measurement

technique, the ability to register the pictures to a high degree of precision and to detect valid areas for making measurements, and the exercise of quality control procedures over the numerical values obtained from the measurement process. The model described in this paper contains all of the components for an automated operational procedure. An on-line test in an operational environment was used to determine the ability of the components to perform the detection, measurement, and quality control functions in automated processing of raw data into low-level cloud motion vectors.

2. DESCRIPTION OF THE SYSTEM FOR ACQUIRING ATS CLOUD PICTURES

There are two ATS satellites now functioning; ATS-1 at about 150° W and ATS-3 at about 70° W. This provides data coverage sufficient for the determination of cloud motion vectors from about 40°N to 40°S and 30°W to 170°E. Figure 1 shows the flow used to obtain a single picture on digital tape. To obtain additional pictures the process is repeated.

The sensors, operating in the visible range of the spectrum, are of the spin scan type, i.e., a scan line is swept out, the viewing angle is incremented, and the next scan sweep is performed. The direction of the forward scan cycle is from north to south with respect to the earth. When the forward scan cycle is completed, the scanner is stepped back to its start position at a rate ten times that of the forward scan advance. The total cycle is composed of the forward scan image and the subsequent retrace. The picture start time interval is measured from beginning of forward scan to beginning of forward scan. For ATS-1, this cycle is 24 minutes (about 22 minutes forward scan and 2 minutes retrace); for ATS-3, it is 27 minutes (24.5 minutes forward scan and 2.5 minutes retrace).

The forward scan data contains the Earth disc which is centered horizontally but the vertical orientation varies according to the orbital position and attitude of the spacecraft. The nominal raster for ATS-1 is 2017 lines and 4096 samples per line. The horizontal width of the disc is about 3800 samples at the equator. The nominal raster for ATS-3 is 2408 lines and 4096 samples per line. The horizontal width of the disc is about 3850 samples at the equator. The vertical size is affected by the attitude or tilt of the spacecraft. Very often the attitude is such that either the northern or southern portion is outside the angular limits of the scanner. The nominal spot resolution at the straight down view is about two miles in the horizontal (E-W) direction and about three miles in the vertical (N-S).

3. MODEL FOR COMPUTER DERIVED LOW LEVEL CLOUD MOTION VECTORS

A generalized flow diagram of the model is shown in figure 2. It consists of three major units - Preprocessing, Selection and Measurement, and Quality Control. Although the model is applicable to either ATS-1 or ATS-3 data, discussion in this section will be limited to ATS-1 data only.

3.1 PREPROCESSING UNIT

3.1.1 DATA INGEST. The ATS data ingested at Suitland are received in the form of a serial bit stream. Marker bits implanted in the data stream denote frame start and line synchronizing signals. The bit stream is reformatted into individual six bit samples (64 gray shades) and is passed to a small computer to be stored on a magnetic tape. Data representing one picture of the full Earth disk (fig. 3) contains approximately 8,000,000 six bit bytes all of which can be stored on one tape.

Although the model uses only two pictures as input, three successive pictures (24 minutes apart) are ingested to provide a backup in case one of the first two pictures is bad. Picture pairs having 24 or 48 minute intervals are suitable for input to the model. The 48 minute interval is preferred for reasons of accuracy.

3.1.2 PICTURE DATA PREPROCESSING. Earth location, in terms of latitude or longitude, is done by the procedures described by Doolittle et.al. (1970) and so will not be described in detail here. Horizontal and vertical centering of the Earth's disc is done to achieve a "normalized" frame, i.e. to locate the Earth's disc in a pre-specified raster frame. The relationship between

latitude and longitude, and picture sample and scan line number are computed for a "normalized" frame based on camera attitude and orbital parameters. These values are translated to the raw picture coordinates. Each picture of the pair is preprocessed individually and stored on disk.

3.1.3 PICTURE PAIR REGISTRATION. Precise registration of the two images is required to measure cloud motion vectors accurately. We have found that given the preprocessing information, the orbital elements, and the satellite attitude, the registration of one picture with respect to the second is insufficiently accurate for measuring vectors. Figure 4 shows the map coordinates of the island of Tahiti. A unique point was picked off the island at latitude 17.6°S and longitude 149.5°W. Given this latitude and longitude, the corresponding sample and scan line values were computed for the August 29, 1972 picture pair at 2154 and 2218Z times. Figure 5 shows a 64 x 64 array, taken from the 2154Z picture, centered at the computed sample and scan line corresponding to the unique latitude and longitude position. Figure 6 shows the array taken from the 2218Z picture. Both arrays are displayed in alphanumeric characters to enhance the island landmark feature. The landmarks are also outlined. These arrays show evidence of the following.

a) A geographical error exists since the point picked on the landmark is left of the array center.

b) The geographical error is not the same for the 2154 and 2218Z pictures. A relative registration error exists between the landmark images.

Evidence indicates that the geographical error is related to two factors. First, thresholding logic is used to determine the east or west horizons of the Earth's disc. Considering changes in illumination and noise in the data, the thresholding logic gives an approximate solution at best. Secondly, the location of unique sample and scan line numbers also is a geometric function of the satellite's orbital elements and attitude. If these parameters are not known precisely, geographical error can exist. The conclusion was that the image data for independent pictures can be located with approximate accuracy but that the relative registration was not sufficiently precise for cloud motion computations.

Investigation has shown that the relative registration error for different cloud free landmarks extracted from ATS picture pair data is nearly constant (within $\pm$ 1 sample and scan line). This is also true of stationary clouds such as those caused by island orographic effects (Hawaii) and some stratus fog banks (off the California coast). Once registration error can be distinguished from spurious cloud motions, it can be used as a correction factor.

The procedures used to determine registration error are demonstrated using the ATS-1 picture pair data for 2154 and 2218Z August 29, 1972. The procedures follow:

a) Sixteen pre-determined landmarks were chosen from the ATS-1 field of view.

b) Using preprocessing information, orbital elements, and attitude for each location, a 64 x 64 area is extracted from each picture of the pair.

c) Cross-correlation matrices are computed forward ($t_o > t_1$) and backward ($t_1 > t_o$) in time for each landmark location in the following manner.

1. A 32 x 32 subset centered in the middle of the 64 x 64 at t_o is correlated with the 64 x 64 at t_1.
2. A 32 x 32 subset centered in the middle of the 64 x 64 at t_1 is correlated with the 64 x 64 at t_o.

d) For each correlation matrix, the lag values of all relative peaks and neighbor coefficients within 0.005 of the peaks (chosen empirically) are determined. The lag value position(s) from the largest maxima are accumulated in a primary frequency distribution. The lag value positions associated with all other maxima are accumulated in a secondary frequency distribution. The lag values for primary and secondary peaks for each landmark are given in table 1. The distributions shown in figures 7 and 8 contain the final results for the primary and secondary frequency distributions after all cross-correlation matrices have been processed.

e) The primary distribution is searched for the maximum frequency of occurrence which in this case is located at lag value 7, 2. This is used as a first guess.

f) The fields of primary and secondary distributions are added. From a 3 x 3 array centered about the first guess position, (7, 2) the center of mass is determined. This value is the refined registration error.

The unique peak found in the primary distribution shows the consistency of the relative registration error. Secondary peaks are beneficial when landmarks are partially cloud covered since either peak may represent the displacement depending upon the extent of the cloud cover. The computation of the cross-correlation matrices forward ($t_o > t_1$) and backward ($t_1 > t_o$) in time for each landmark is beneficial in the case of large mislocations in one of the pictures. For example, it is possible that the landmark may be located in the 32 x 32 subset at t_1 and in the 64 x 64 array in t_o but not in the 32 x 32 subset at t_o. A valid registration error would be determined from $t_1 > t_o$ but not from $t_o > t_1$. Lag values having coefficients which are within 0.005 of the peak are considered as if they were true peaks. The reason for this is that noise may dampen the true peak in areas of flat gradients and possibly may displace it by a lag value. The cumulation of lag values having the above criteria from matrices computed forward and backward in time will reinforce the true peak.

The final result of this procedure is an accurate vector slightly mislocated since no attempt is made to correct any remaining geographical error.

3.2 SELECTION AND MEASUREMENT

3.2.1 TARGET SELECTION. Cloud motion computations are made at intersections determined by a fixed geographical grid. The target area consists of a 32 x 32 array centered at each five degree latitude-longitude intersection. A target selector developed from multiple discriminant analysis procedures (Booth, 1972) was used to determine whether the satellite imagery located at a particular grid intersection could produce a valid low-level motion vector. Initial experiments showed this could be accomplished 70% of the time. Significant improvements in this accuracy would require normalizing the pattern parameters for signal variations and solar zenith angles. Simple post-editing procedures produced results equal to and sometimes better than the results obtained by using the target selector. It was decided at the beginning of the test period to delete the target selector from the model and rely on post editing to delete measurements from invalid target areas.

3.2.2 DISPLACEMENT MEASUREMENT. The measurement algorithm used to compute landmark and cloud displacements is cross-correlation. The fast Fourier Transform method is used to increase the efficiency of computing correlation coefficients. These procedures are described by Leese et. al. (1971) and Leese and Novak (1972).

In terms of the cloud displacements, the cross-correlation matrix is computed backwards in time ($t_1 > t_o$) with the 32 x 32 subset being in t_1 and correlated with the 64 x 64 array at t_o. No advantage was seen to going both forward and backward in time. The backward direction was arbitrarily chosen.

3.2.3 MOTION CALCULATION. The location of the maximum correlation coefficient is proportional to the vector displacement of the cloud patterns in the time interval between the picture pairs. Let p' and q' be the lag values that yield the maximum correlation coefficient, i.e.:

$$R(p', q') = \max [R(p, q)]$$

The speed and direction of the cloud motion is given by

$$|\vec{c}| = \frac{[(p' \cdot \Delta x)^2 + (q' \cdot \Delta y)^2]^{\frac{1}{2}}}{t}$$

$$\theta = \text{Arctan} \left(\frac{p' \cdot \Delta x}{q' \cdot \Delta y} \right)$$

where:

$|\vec{C}|$ is the speed of motion,
θ is the direction, and
Δx and Δy are the sampling intervals of the input picture matrix in the east-west and north-south directions, respectively.
Δt is the time interval between the two pictures.

3.3 QUALITY CONTROL

3.3.1 POST-EDITOR. The validity of each vector is determined through a simple post-editing procedure based upon climatology. A vector is considered to be invalid if:

a) its magnitude is greater than 40kts,

b) it has a westerly component and is located between 20°N and 20°S.

In a climatological sense, these criteria are valid for low level vectors. However, on a day-to-day basis, valid vectors may be discarded or invalid vectors accepted since the editor is climatological and not meteorological in nature. We realize the need for a meteorological post-editor, and work has begun on its development. The rejected vectors are flagged for future study toward improving the editing procedures.

It should be pointed out that the final results are not pure climatology since variations take place from day to day, but not to the extent of having westerly winds.

3.3.2 MAPPED VECTORS. The valid vectors are mapped on a mercator map base (fig. 9). The figure shows mapped vectors derived from ATS-1 picture pair data for September 12, 1972. The vectors are also available in the form of punched card output.

3.3.3 MANUAL EDITING. A meteorologist uses the facsimile display of the mapped vectors to perform additional editing. The criteria for the manual editing are:

a) analysis and forecasts based upon conventional meteorology, and

b) subjective experience in the selection and measurement of vectors from "loop movies". These procedures are described in a paper by Young et. al. (1972). The manually rejected vectors also are flagged for future study.

3.3.4 PRODUCT TO USER. After the manual editing of the facsimile display, the rejected computer vectors are sorted from the punched cards. Vectors that have survived the manual editing are combined with cloud motion vectors determined from "loop movie" procedures. The combined punched card product is then used as input to the numerical weather prediction model at the National Meteorological Center.

4. EVALUATION OF MODEL AND ATS SYSTEM

4.1 TEST PERIOD

The model was put into experimental operational use, using ATS-1 data, on May 1, 1972. Data from ATS-3 were introduced on June 18, 1972. The ATS-1 data for 2200 to 2300 GMT and ATS-3 data for 1400 to 1500 GMT were used each day as input. The results of this "real world" test are reported in this section.

4.2 SYSTEM PERFORMANCE

The model was the most reliable part of the ATS processing system during the four month test period. The inability of the model to produce vectors on a given day was not the fault of the model but of weaknesses in the ATS-1 processing system This is reflected in table 2 which

shows the major causes of the failure. Figure 10 is a time plot of ATS-1 (solid lines), and ATS-3 (dashed lines) system performance for the four month period. The graph shows the number of successes plotted against time over 10 day units from May 1 through September 2. The performance level for ATS-3 is more reliable than that for ATS-1. The striking difference in the performances of ATS-1 and ATS-3 may be attributed to three main causes: (1) ATS-1 was used as the forerunner and encountered most of the problems first; (2) ATS-1 data is processed during an evening shift (eastern time) with a reduced staff and during the high volume 0000 GMT observation time so that the entire processing facility is under high strain and more subject to error than at other times; (3) ingest computer problems causing mislocated tape documentation affecting ATS-1 only. The 88% success rate on ATS-3 is indicative of the performance level that can be achieved with the present system structure.

4.3 EVALUATION OF COMPUTER DERIVED VECTORS

The vectors from the computer model were mapped onto a Mercator projection. Using the latest available tropical surface analyses from the National Meteorological Center (NMC), meteorologists evaluated these vectors. The general rule was that if the vector direction was within 40° of the analysis direction and within 5 kts of the analysis speed then the vector was acceptable. Other judgement was added. Film-loop movies showing flow aided in assuring that the general direction was correct. Also, the general flow of the vectors had to be consistent, e.g., according to the 40° rule, two adjacent vectors could be 80° different in direction; in such a case one would be discarded because it did not agree with the general flow.

During the test period the average daily production was computed (table 3). These data were compiled for 30°N to 30°S across the longitudinal range of coverage. The 23 days of ATS-1 data during the period July 10 to August 31 and the 40 days of ATS-3 data during the period June 26 to August 31 were used to compute average daily production. Column 1 shows the number of vectors computed on the fixed grid; column 2 the number that passed the computer post-editor test, and column 3 the number that were considered acceptable by the meteorologists. In table 3 it is shown that 75% of the computed vectors are, in a crude sense, climatologically sound and that 83% of these are operationally useful. On the other hand, only 63% of the total number of vectors computed appear useful. This latter figure is a measure of production efficiency.

4.4 COMPUTER-MANUAL COMPARISONS

Manual wind estimates from "loop movies" are derived daily for ATS-1 and ATS-3 using procedures described by Young, et.al. (1972). Computer wind estimates were derived at the same geographical locations and compared with the manual wind estimates. This was done daily whenever possible during the period July 15 through August 28, 1972.

A brief analyses of the computer model and manual procedures, in terms of their differences, may give some insight to the interpretation of the comparison statistics.

1. Registration - Both techniques use Baja, California and Hawaii as primary landmarks for registration. The computer model uses objective procedures to register the picture pair. The registration of the individual frames comprising the loop movie is accomplished by a photo-technician. The registration correction is determined by the motion of landmarks and the ability of the analyst to determine the position of a unique point in the first and last frame in the loop movie. This correction is used to refine the satellite attitude. In the computer model, the registration correction is applied to adjust for the translational error found between the picture pair. Considering the registration approaches and the manner in which the corrections are applied, one would expect to find the minimum differences in the comparisons in the region containing the primary landmarks, assuming no variability among people in registering pictures visually and in selecting and detecting unique landmark points.

2. Time Interval - The computer model uses two pictures 24 or 48 minutes apart. The interval between the first and last frame in the loop movie is 2 to 2 1/2 hours. The life cycle of clouds, especially in tropical areas, can vary greatly in a given time interval. The differences in the comparisons should be a minimum in regions where cloud growth and decay are also a minimum.

If the satellite attitude is not precisely known, error can be introduced into the vector computation because earth locating the vector end points is dependent upon the time interval. Unfortunately, this may have been the case because attitude determinations were based upon marginal orbital information during this period.

3. Displacement measurement - Measurements determined by manual procedures can be subject to large variability depending upon the individual making the measurements. The displacement measurement obtained by the computer is objective and measures integrated pattern motion. The individual selects cloud elements which appear to the eye as being "passive tracers". The objective measurement of the motion of the full gray scale topography which falls into a 32 x 32 array may be somewhat different than what the individual visualizes.

4. Geographical Error - If geographical error is present because of poor attitude determination, the image being measured by the computer model may not be the same as that followed by the individual.

5. Contamination - The 32 x 32 array centered at the geographical location where the manual estimate was made can be contaminated by clouds not at the low levels.

Figure 11 (a and b) shows the cumulative frequency distributions for the absolute directional and speed differences (in solid lines) for the manual-computer comparisons from July 15 to August 28. Results from a previous "controlled experiment" are also presented (broken lines). The purpose of this experiment, based upon ATS-1 data for August 15, 1971, was to minimize as much as possible the differences between the manual and computer approaches, by using only different displacement measurement techniques. The dotted curve is the cummulative differences for all vectors above 15°N latitude from July 15 to August 28.

The curves from the total sample (summer of 1972) and the "controlled experiment" show divergence especially in the speed difference comparisons. The comparisons from the controlled experiment show what can be done when the differences in procedures between manual and computer methods are minimized. Also, the vectors derived manually for the controlled experiment were produced in a relaxed environment without the pressures of operational deadlines. The results from the summer comparisons show greater differences since the differences in the computer and manual operating procedures were not minimized. The manual vectors produced operationally do not have the accuracy of those computed for the controlled experiment. The comparisons taken for the region north of 15°N (dotted curve) show better agreement. This result was expected, as mentioned in the discussion of the analysis of the differences between computer model and manual procedures. The computer and manual registration methods are closely related in this region since it contains the primary landmarks. Also, cloud stability and well defined elements characterize this region.

The comparisons from the summer of 1972 were broken up by latitude bands, and the cumulative frequency distributions for directional and speed differences were computed for each band. Figure 12 shows the results for the individual bands. The dotted curve contains the results from north of 15°N, the dashed curve 15°N to 15°S, and the solid curve south of 15°S. A comparison of the curves show the results becoming progressively worse as the bands proceed southward or away from the region of primary landmarks. Also, the meteorological regimes associated with each band are different. The band above 15°N is probably the most stable. The tropical band is subject to the most fluctuations in terms of cloud growth and decay. The band south of 15°S is in its winter season which is marked by rapidly moving meteorological systems. In terms of the time interval used by either approach, greater differences in the comparisons should be found in the tropical and southernmost bands.

Figure 13 (a and b) shows a plot of the modal directional and speed difference with respect to time from the summer of 1972 comparisons. The modal values were determined from the daily directional and speed difference frequency distributions. This value was taken since it seemed most representative of the low level clouds not affected by contamination. Figure 13 shows most of the modes for the directional differences are between $\pm$ 10°. The speed difference modes shown in Figure 13b vary from -2 kts to +5 kts, with a mean speed difference of about 3 kts. The direction and speed plots reflect several interesting aspects. First, they

indicate the variability among individuals in terms of picture registration and end point selection for the manual vectors. This is shown by the extremes of some of the points plotted. The cyclic nature of the plotted points in the speed differences indicates a possible problem concerning accurate knowledge of satellite orbital and attitude parameters.

The statistics are based on preliminary investigation, so many of the results should be considered as indications. A detailed study of the differences between the computer model and manual procedures is planned for the near future.

5. CONCLUSIONS

The experimental model performed very well during the period of this test. It demonstrated the operational feasibility of using an automated preprocessing, selection and measurement, and quality control system for processing raw ATS data into low-level cloud motion vectors.

The Preprocessing, and Selection and Measurement Units performed their functions, when not hindered by weaknesses in the ATS processing system, with a high degree of reliability (as shown with ATS-3 data). Although the selection and quality control procedures are not optimum, they can function in an operational environment. It would be very desirable to have a target selector which would identify valid target areas for measurement. A post-editor based upon meteorological constraints is another desirable feature.

Although the model is now in use as an operational procedure, the results of the evaluation of the test phase are being used by the authors to design a more efficient operational model.

ACKNOWLEDGMENT

The operational test of the model described in this paper owes its success to the cooperative efforts of several score persons involved in the acquisition and processing of ATS satellite data. The enthusiasm and perseverance of this group in tracking down system problems and achieving solutions made a significant contribution to the success rate achieved with a system which has practically no backup or redundancy for achieving reliability.

This project was partially supported by the National Aeronautics and Space Administration under Contract No. NASA S-70245-AG. Mrs. Shaw typed the manuscript.

REFERENCES

Booth, A. L., 1972: "Cloud Classification of Mapped Satellite Imagery by Discriminant Analysis and Perceptron Methods", Unpublished Manuscript.

Bristor, C. L., Frankel, M., and Kendall, E., 1967: "Some Advances in Automatic Determination of Cloud Motion and Growth from Digitized ATS-1 Picture Pairs", Unpublished Manuscript.

Doolittle, R. C., Bristor, C. L., and Lauritson, L., 1970: "Mapping of Geostationary Satellite Pictures, An Operational Experiment", ESSA Technical Memorandum NESCTM-20, NOAA, 28 pp.

Leese, J. A., Novak, C. S., and Taylor, V. R., 1970: "The Determination of Cloud Pattern Motions from Geosynchronous Satellite Image Data", Pattern Recognition, Pergamon Press, Vol. 2, pp 279-292.

Leese, J. A., Novak, C. S., and Clark, B. B., 1971: "An Automated Technique for Obtaining Cloud Motion from Geostationary Satellite Data Using Cross Correlation", Journal of Applied Meteorology, American Meteorological Society, Vol. 10, No. 1, pp 118-132.

Leese, J. A., and Novak, C. S., 1972: "Reply", Journal of Applied Meteorology, American Meteorological Society, Vol. 11, No. 4, pp 754-755.

Young, M. T., Doolittle, R. C., and Mace, L. M., 1972: "Operational Procedures for Estimating Wind Vectors from Geostationary Satellite Data", NOAA Technical Memorandum NESS-39, NOAA, 19 pp.

LAT/LON	DESCRIPTION	$t_o \rightarrow t_1$ Primary	$t_o \rightarrow t_1$ Secondary	$t_1 \rightarrow t_o$ Primary	$t_1 \rightarrow t_o$ Secondary
28.7-114.7	Baja California - North of most western tip	6,3	-8,14	7,3	-11,14
22.7-109.7	Baja California - Southern most tip area	7,2	-	8,1	-
27.5-114.7	Baja California - Along western coast	7,2	-	7,2	-
28.8-112.5	Baja California - Point on Isla tiburon	7,2	-9,14	7,2	-
26.2-109.5	Baja California - Along west coast of Mexico	7,2	10,-2	7,2	-11,12
34.5-120.5	Calif - Vandenburg AFB	7,3	11,-7	7,3	12,-5
36.7-122.3	Calif - West of Monterey Bay	7,1	10,-11	9,0	6,13
37.5-118.5	Calif/Nev - Mt Bishop	8,2	-15,13	9,2	9,-12
191.5-155.5	Hawaiian Islands - Island of Hawaii	6,1	-9,-13	6,2	-4,4
21.0-156.7	Hawaiian Islands - between Molokai and Maui	6,-1	-9,6	6,-1	-
21.5-158.0	Hawaiian Islands - Oahu	5,-1	-10,1	4,0	-3,8
22.2-159.5	Hawaiian Islands - Kauai	6,2	13,11	7,2	-5,4
15.6-146.7	Vicinity Rangirou Island - South Pacific	3,1	-5,3	3,1	15,-1
9.1-.39.8	Marquesas Islands	4,2	7,1	4,2	8,1
1.9-157.2	Christmas Island	5,2	-	6,2	-10,2
17.6-149.5	Tahiti	7,1	10,15	8,1	0,4

TABLE I. LANDMARK LOCATIONS AND LAG VALUE SHIFTS

	ATS-1 (May 1-Aug 31)	ATS-3 (Jun 18-Aug 31)	TOTAL
SUCCESSES	69 (56%)	66 (88%)	135 (68%)
FAILURES	54	9	63
Mislocated Tape Documentation	17	1	18
Hardware	12	6	18
Bad Ingest Data	10		10
No Data Available	8		8
Human Error	6	2	8
Poor Attitude	1		1
Model	0	0	0

TABLE II. SUMMARY OF SYSTEM FAILURES

Average Daily Production

	Computed (30N-30S)	Survived Post-Editor	Survived Manual Edit	
ATS-1	203	157	132	(23 days)
ATS-111	197	143	119	(40 days)
TOTALS	400	300 75%	251 63% of total 83% of delivered	

TABLE III. AVERAGE DAILY PRODUCTION

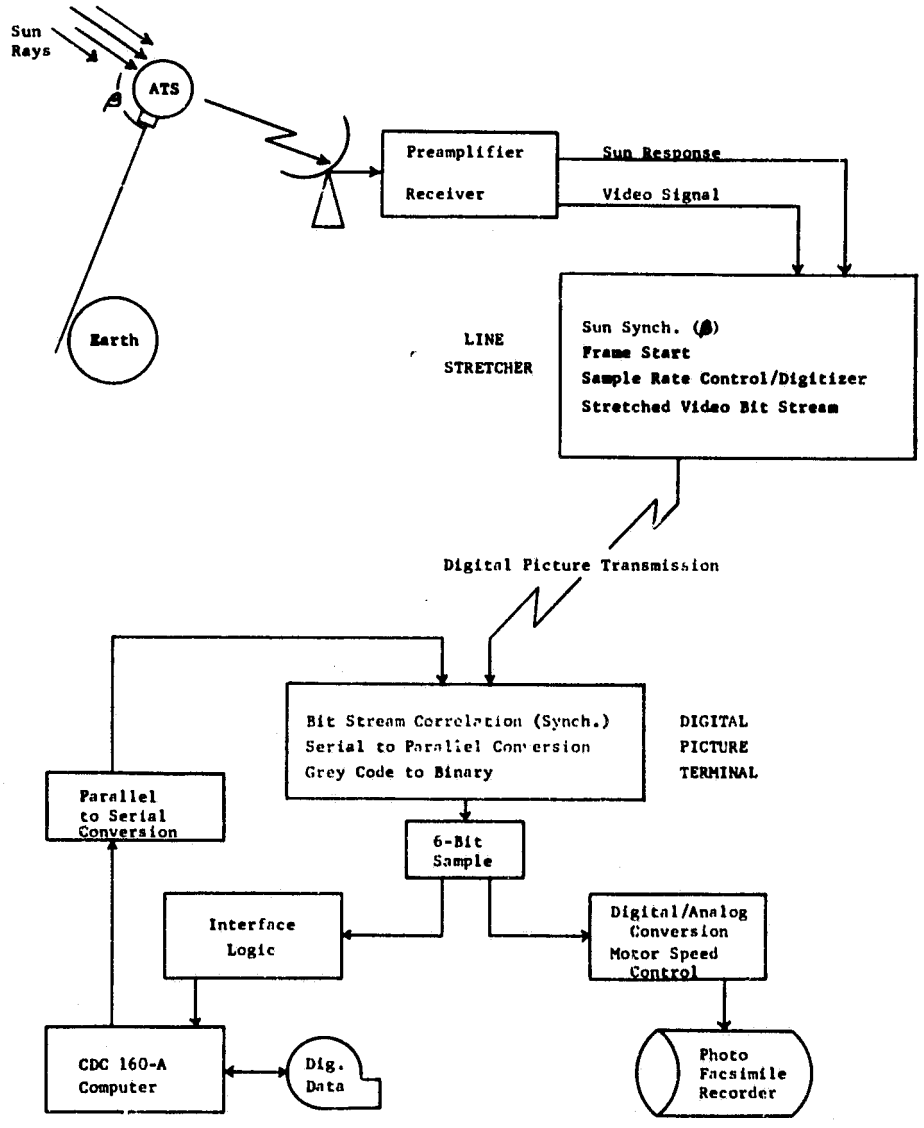


FIGURE 1. Flow diagram illustrating the acquisition of ATS cloud pictures.

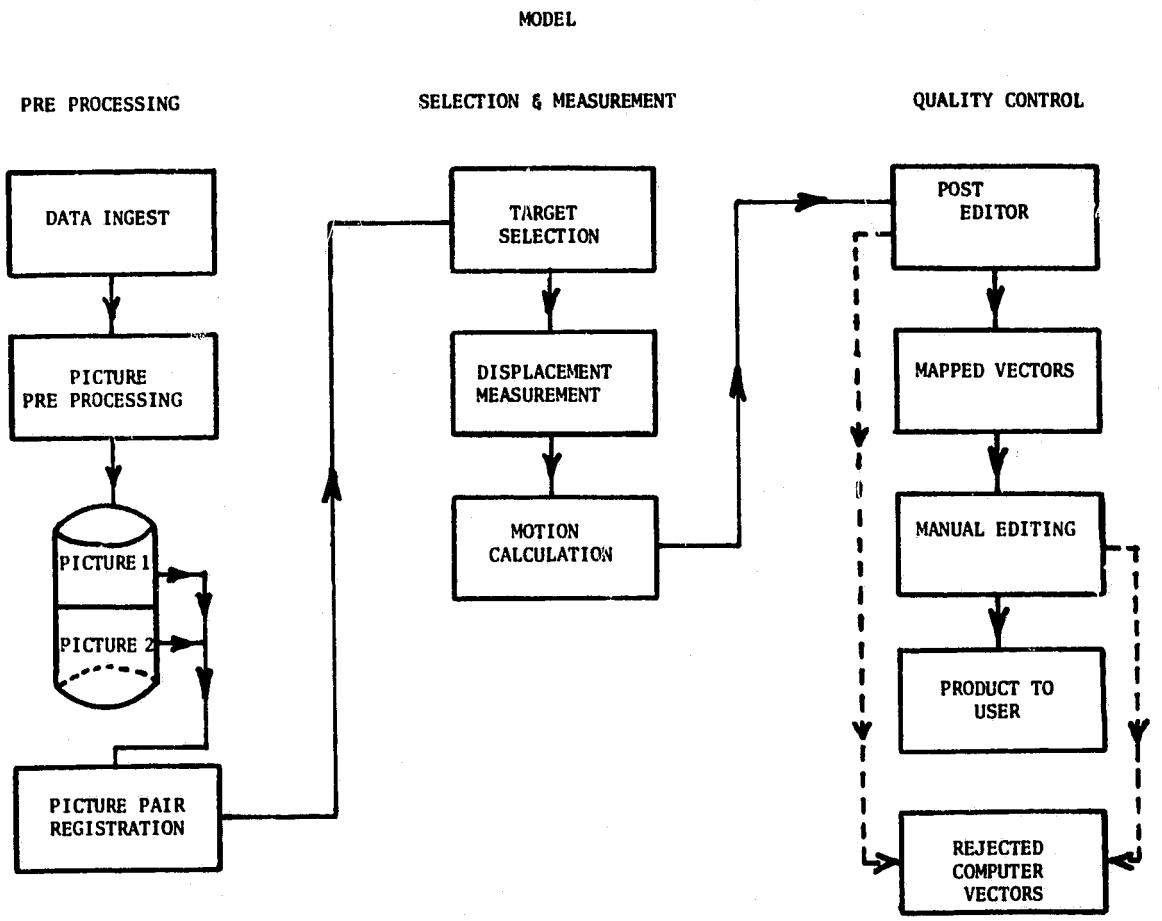


FIGURE 2. The cloud motion model data flow.



FIGURE 3. The ATS-1 raw picture for 2154Z on August 29, 1972.

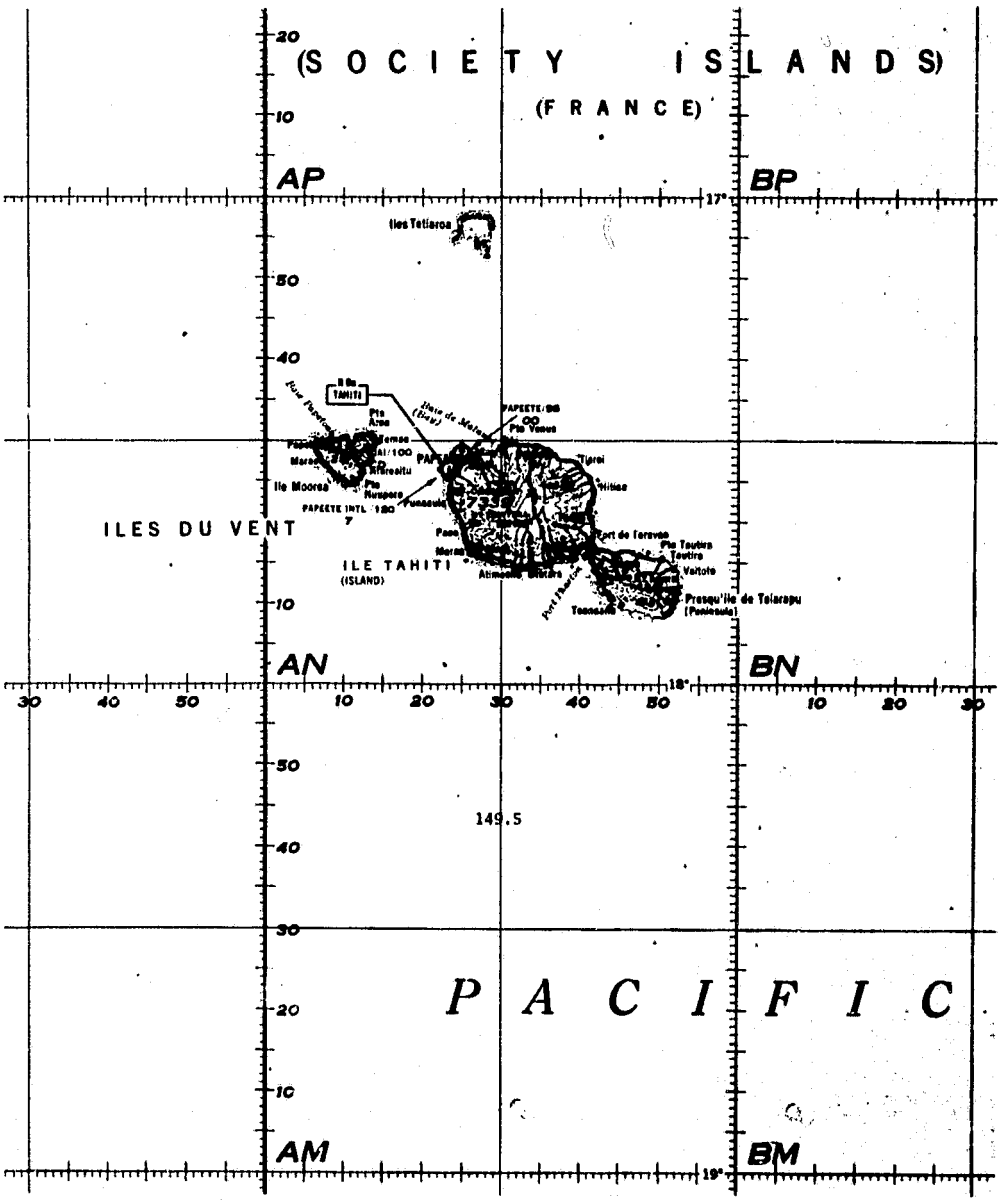


FIGURE 4. Atlas depiction of the Island of Tahiti. The cross at 17.6°S, 149.5°W indicates the center of this landmark for registration purposes.

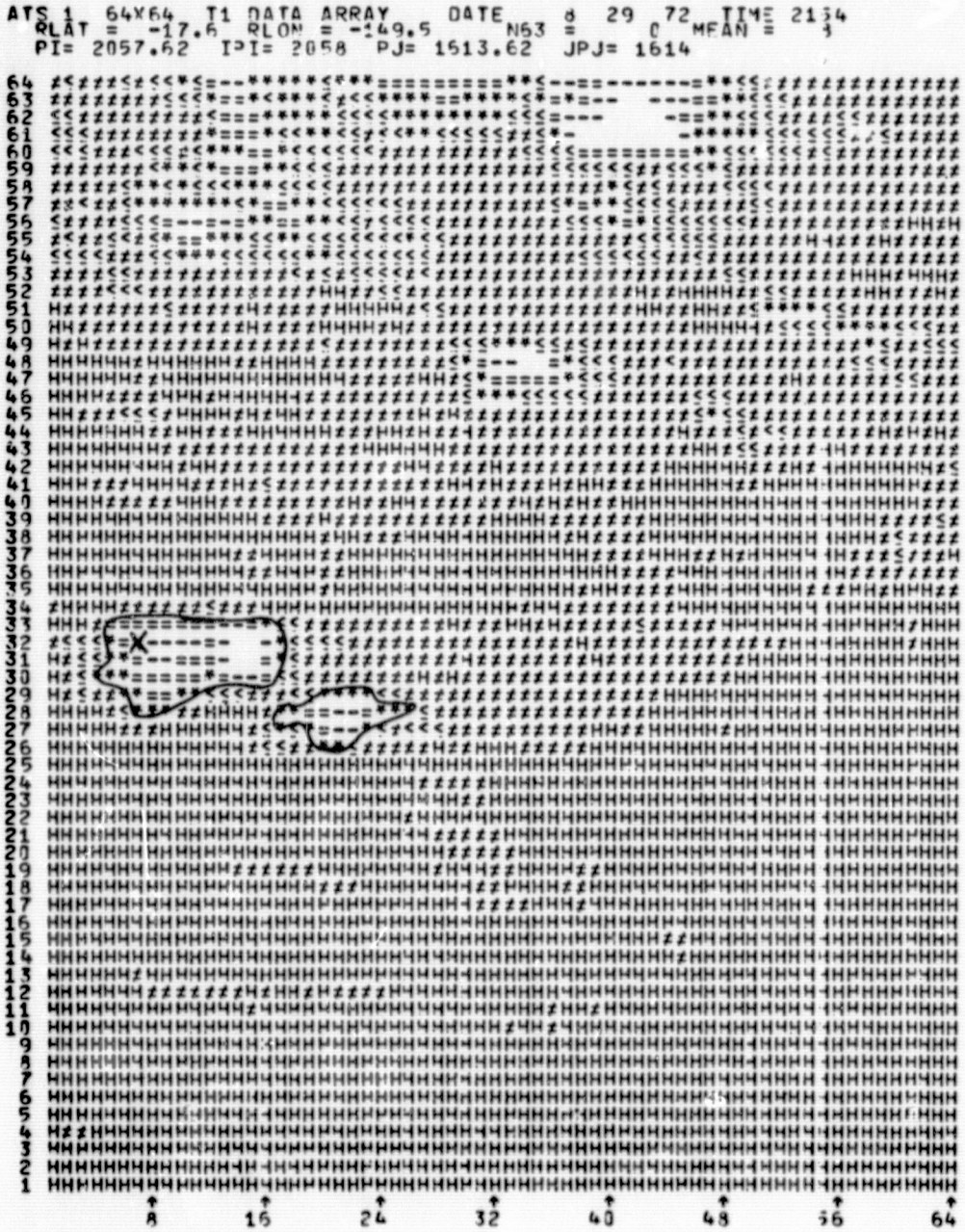


FIGURE 5. The gray scale depiction, using alphanumeric characters, of the Island of Tahiti as observed by ATS-1 at 2154Z on August 29, 1972. The "X" at 7, 32 corresponds to the position of the cross in Figure 4.

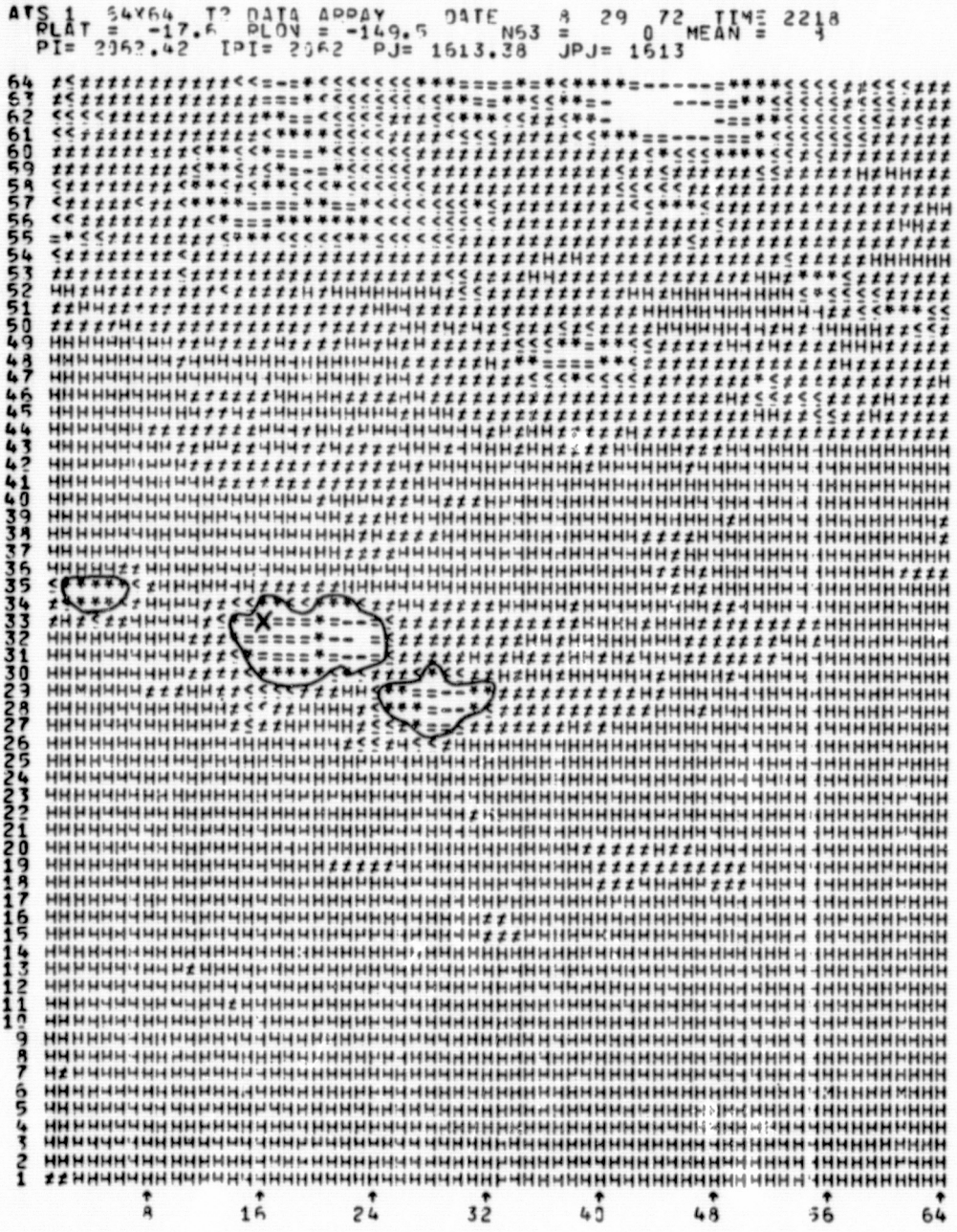


FIGURE 6. The gray scale depiction, using alphanumeric characters, of the Island of Tahiti as observed by ATS-1 at 2218Z on August 29, 1972. The "X" at 16, 33 corresponds to the position of the cross in Figure 4.

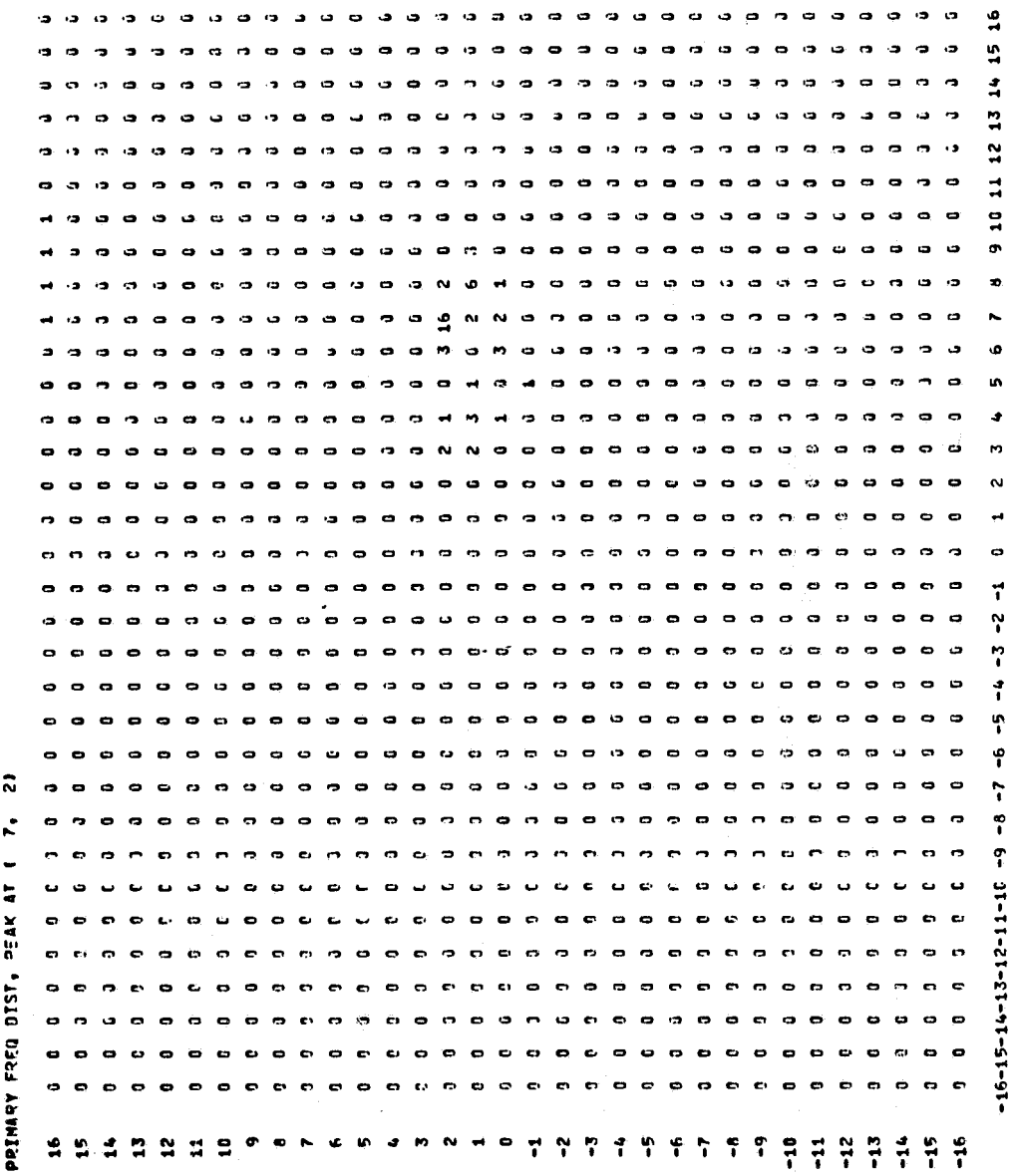


FIGURE 7. Frequency distribution of the positions of the cross-correlation peak values for the landmark to register the 2154 and 2218Z pictures of ATS-1 on August 29, 1972. The peak occurs at 7, 2.

FIGURE 8. Frequency distribution of the positions of the secondary peak values corresponding to figure 7. The dispersion of apparent motions is obvious. There is only a minor influence in the 3 x 3 area around the point 7, 2.

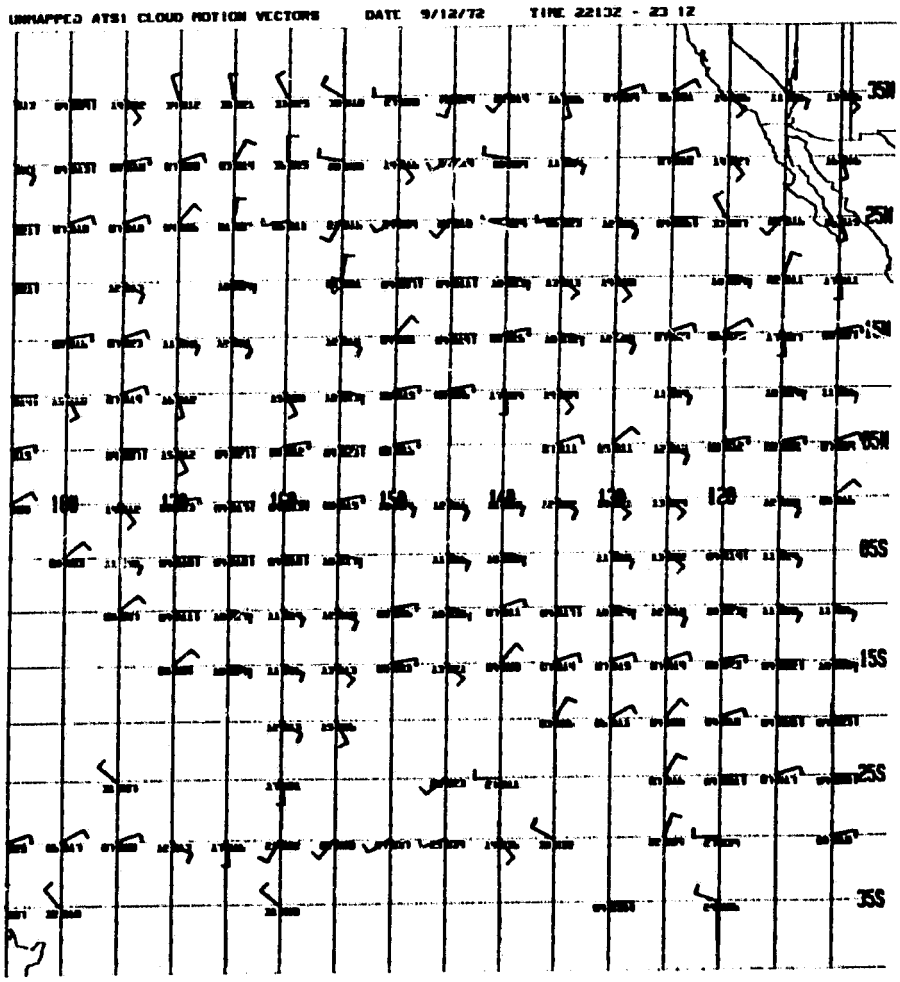


FIGURE 9. This illustrates the mapped vector field in the ATS-1 area for the picture pair time 2213-2301Z on September 12, 1972 as presented to the Meteorological Analyst. The barb indicates the approximate wind direction (16 point compass). The direction in tens of degrees and speed in knots is printed below each point.

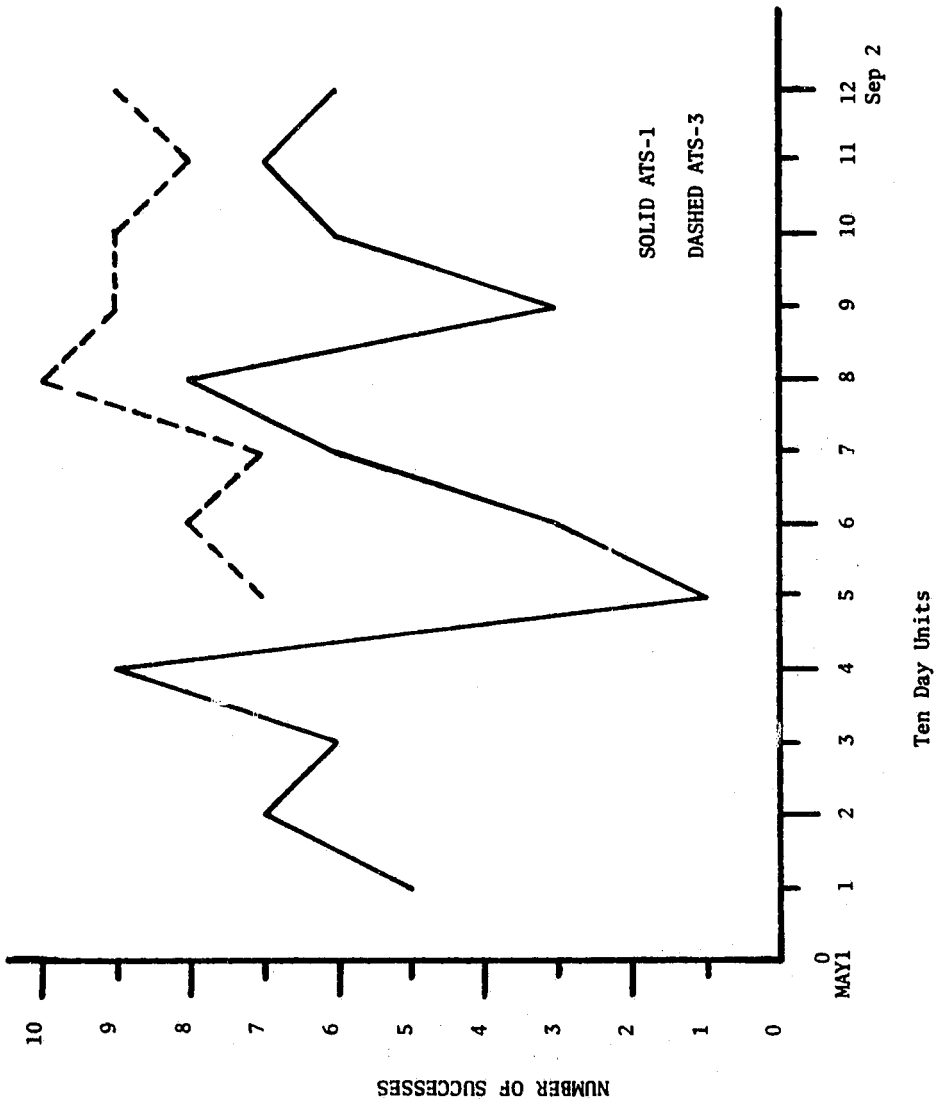


FIGURE 10. The system performance is shown in contiguous ten day increments from May 1 to September 2, 1972. The number of successes is equivalent to percent successful. The erratic behavior with ATS-1 is apparent, as is the consistent high performance level of ATS-3.

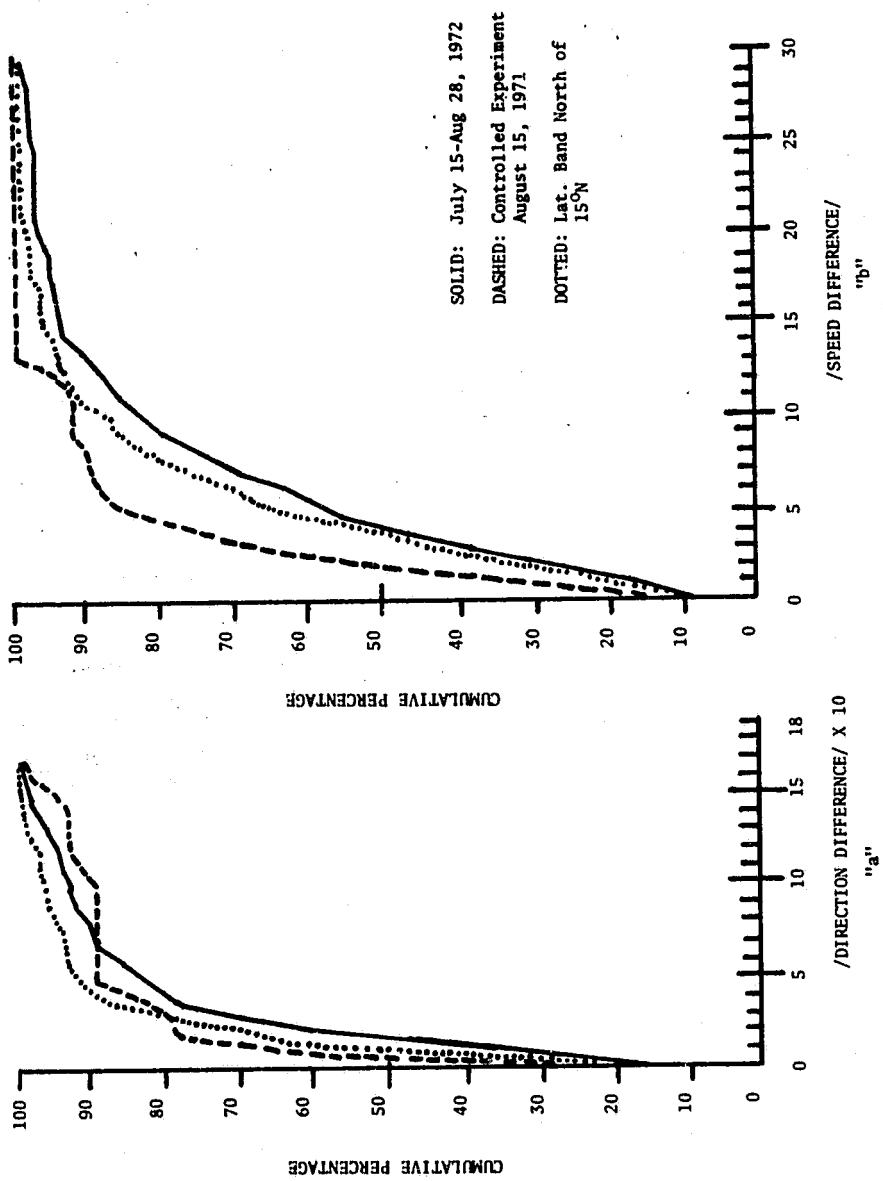


FIGURE 11. The cumulative frequency distributions of the absolute differences in direction (a) and speed (b) between manually measured motions and computer measured motions at manually selected points. The operationally derived data (solid line) shows generally a poorer comparison than the "controlled" experimentally derived data (dashed line). The data from the latitudinal band from 15°N to 35°N from the operational data shows better agreement thus implying a problem in other latitudinal bands.

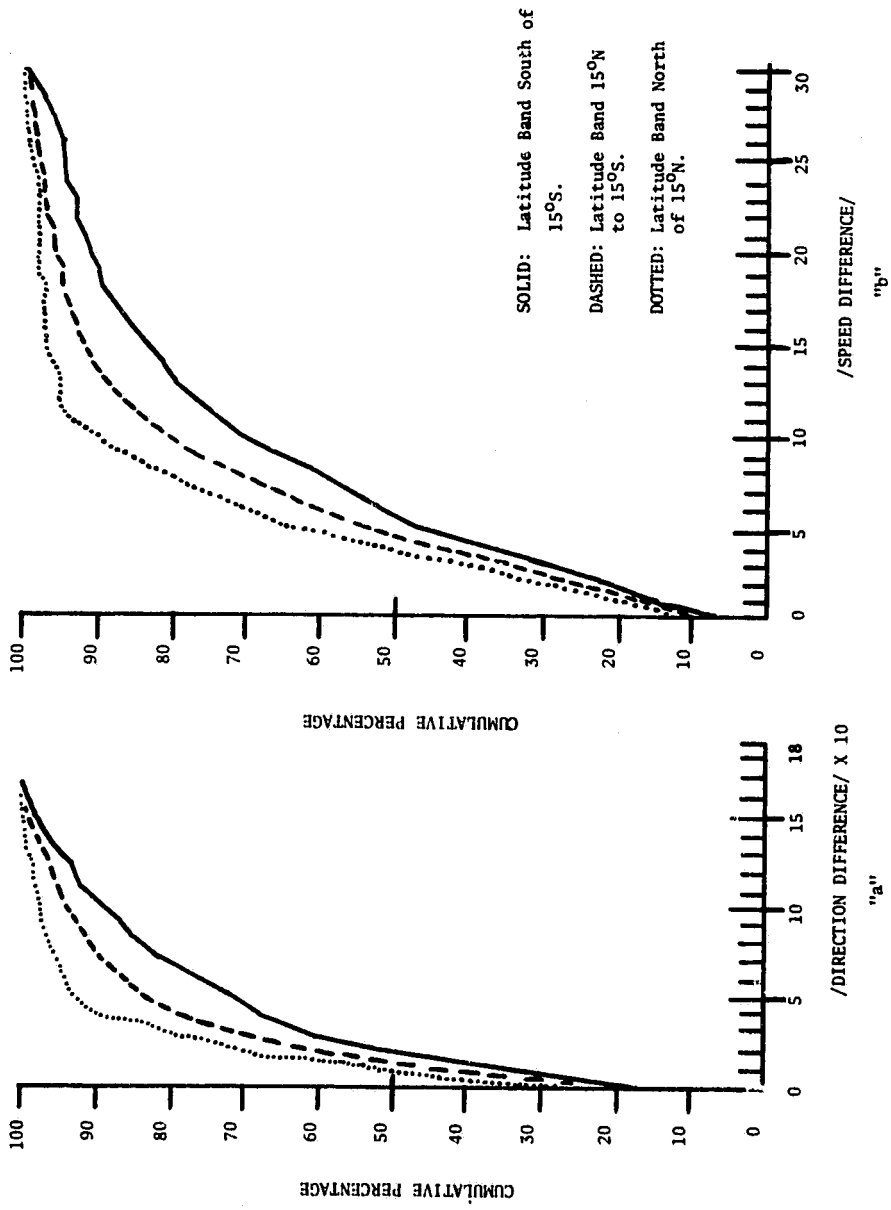


FIGURE 12. The cumulative frequency distributions of the absolute differences in direction (a) and speed (b) between manually measured motions and computer measured motions at manually selected points. These data are based upon the operationally derived data. The increase in disagreement is evident as the latitudinal bands move southward into areas not having common landmarks and where the atmosphere is more dynamic.

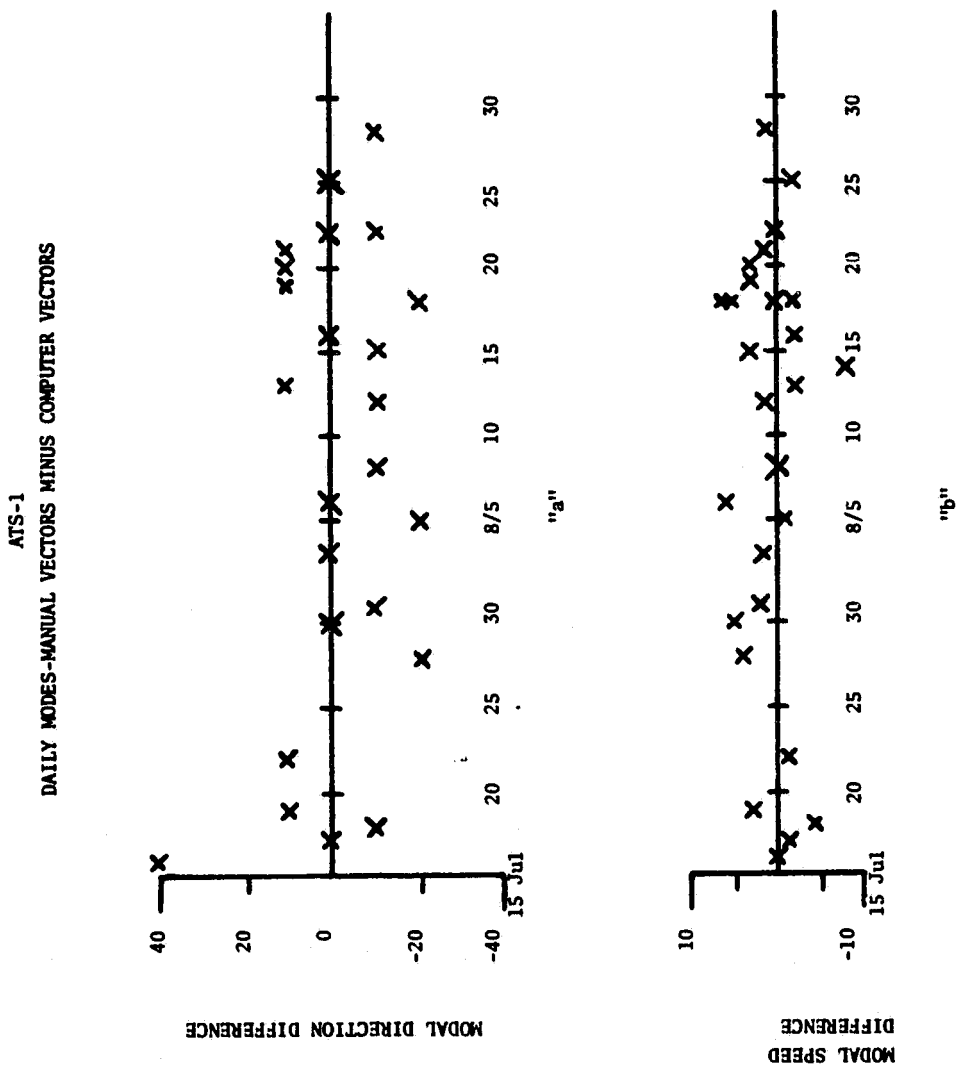


FIGURE 13. Plot as a function of time of the modes from daily distribution of differences in direction)a) and speed (b) between manually measured motions and computer measured motions.

STRUCTURE OF DUST STORMS FROM ITOS-I T.V. IMAGES OBTAINED OVER IRAQ AND THE GULF OF PERSIA

B. V. Vinogradov
Moscow Institute
Aerospace Methods
Moscow, USSR

A. A. Grigoryev and V. B. Lipatov
University of Leningrad
Institute of Physics
Leningrad, USSR

The atmospheric dust storms and dust-sand flows and high altitude dust transfer are characteristic of arid and subarid regions [1]. Yet the distribution and structure of the dust-wind formations are insufficiently studied due to a small number of meteorological stations and difficulties of observations during the dust storms. Recently, large dust storms have been detected in space photos over the Near East (from "Zond -7" photos.) [2], over southern Sahara (from "Zond-5") [3], over the equator along the west African coast (from the ESSA-5 T.V. images) [4], and over southern Iran (from the manned spacecraft Gemini-12). None of the above observations describes the structure of dust storms.

The present paper offers the first results of the analysis of the dust storm structure from space imagery. In the T.V. image (Fig. 1), the dust storms and dust-sand flows are distinctly seen over Mesopotamia lowland and the northern part of the Persian gulf in the form of four subparallel strips. Being lighter than the surface of the sea and the lowland they mask the nonuniformities of the underlying surface.

The value of the dust atmospheric turbidity is found from the comparison with the T.V. image of the same area obtained on July 29, 1970 for the case of transparent atmosphere.

The analysis of the meteorological data on the network of local stations derived on July 17, 1970 at 15 hr., Moscow time and synchronized with the T.V. ITOS-1 survey showed the prevalence of the SW wind related to the trades in the western periphery of the south Iran baric depression. The strongest winds (more than 20 m/sec) were observed over Mesopotamia. A strong NW wind with the maximum velocity at a height of 1 - 1.5 km (to 40 m/sec) was constant up to 3-5 km. The visibility decreased to 1-15 km. The local name of this dust storm is Great Shemal.

A densitometric analysis of the negative images permitted the classification of natural formations (the sea, oases, stone and sand deserts, clouds) and the dust turbidity zones in the atmosphere from the gradations of the intensity of the T.V. signal and the density of the ITOS-1 negative image. This in turn allowed, from the objective criteria, the representation of the dust storm linear structure using the semi-instrumental method (Fig. 2).

We have distinguished four gradations of the atmospheric dust turbidity. A weak dust turbidity slightly affects the density of the background image: it increases the density of its negative image less than by 0.1 (with the image ($\alpha = 2$). The moderate turbidity essentially masks the nonuniformities of the surface structure showing only the high contrast details with higher than 0.7 and increases the density values by 0.12 - 0.25. The mean turbidity almost completely masks the landscape details though the influence of the underlying surface brightness on the integral image tone of the dust-sand flow is still preserved and increases the image density by 0.25 - 0.45. A heavy dust turbidity completely masks all the details of the underlying surface increasing the image density by more than 0.45 - 0.50 thus leveling them with the image density of the surrounding sand-loam deserts.

For an objective analysis of the TV signal measurements, we have used values at the points where the underlying surfaces, with known values of the integral brightness coefficients, have been recognized. The correlation between the densities of the negative TV image (or the intensive TV signal) and spectral brightness turned out to be so high that the use of the densitometric data as a criterion of the classification of natural objects proved reliable. However, the integral brightness even of the heaviest dust turbidity is slightly higher than the brightness of the sand-loam desert

(R = 0.25 - 0.50). Therefore, the atmospheric dust turbidity can be measured from TV images only against the background of the surfaces whose brightness is below 0.20 - 0.25, i.e., against the background of the sea, oases, luxuriant vegetation, humus and moistened soils, the outcrops of dark-colour rocks and stone deserts.

Analysis of the photoimage, the consideration of all meteorological data densitometric measurements of the negative image, the study of relief and the investigation of the composition of loose deposits and soils of the dust-storm region permitted the detection of a number of details of its structure.

The dust storm originates in Mesopotamia lowland south of lake El-Milh and Milet Tartar where a series of dust vortices are observed in the form of shapeless dust-sand formations with slightly visible isometric elements. Here the wind velocity sharply increases which leads to the abundant capture by wind flows of the dust particles from the loess-like loam alluvial and irrigation deposits as well as from the mantle of rock debris. The deserts attached to the lowland do not produce such a large quantity of the suspended dust material, and it is only the bottoms of temporary lakes at the lowland edges that serve, though to a lesser degree, as a source of the dust turbidity.

The main part of the dust-wind structure is occupied by the system of subparallel dust-sand streams over the Persian gulf where there is no dust material to feed the flow. The stream lying farthest west is not very pronounced in the photo. This stream, about 20 km in width and about 400 km in length, goes over the right-bank deserts. The second stream (as counted from the west), about 25-40 km in width and 600 km in length, is most pronounced and exhibits the largest brightnesses of the dust turbidity. It moves over the dry land and the strip of the unfixed sands attached to oasis Az. Rahib, its extension over the gulf of Persia being 150-200 km. The third and the fourth streams (as counted from the west), about 500 km long and 20-25 km wide, have a smaller brightness since they contain a much smaller amount of the suspended material and spread mainly over the lakes, swamps, and the irrigated areas.

To conclude, judging from the space image, the dust turbidity zone consists of two elements: the local dust-sand storms or vortices of isometric form; and the dust-sand streams, more than 500-600 km long and 20-40 km wide, extending along the prevailing winds.

Comparison of space TV images with the meteorological data from the local stations show that the ground-based observations can only fix the region of dust storms but do not permit the determination of their morphology and of accurate distribution in space and time. The space image analysis detects the relationship between the dust storms and the underlying surfaces: dust storms fade over the stone deserts and moistened areas, go along the depressions and around the elevations. The data of space survey confirm the concept of a great geological role of the dust storms and dust-sand flows in the formation of relief and loose deposits.

References

1. Nalivkin D. V. Hurricanes, storms and whirlwinds. Izd. Nauka L., 1969.

2. Grigoryev A. A., Lipatov V. B., Vinogradov B. V. Study of the Connection between the characteristics of the Earth's surface and some meteorological elements from the global pictures from the automated interplanetary station Zond-7. Space Research 11, Akademie Verlag, Berlin, 1971.

3. Vinogradov B. V. Global Photography of the earth. Global Photography. Earth and Universe No. 1, 1970.

4. Prospero J. M., Bonattie E. et. al. Dust in the Carribean atmosphere traced to an African dust storm. Earth and Planetary sciences Letters. v. 9, No. 3, 1970.

5. Wobber F. J. Orbital photos applied to the environment. Photogramm. Engng., v. 34, No. 9, 1970.



Fig. 1 The fragment of the regional ITOS-1 TV image of the dust storm over Mesopotamia lowland and the Persian gulf as obtained on 17, June, 1970 by the receiving station APT, Leningrad University.

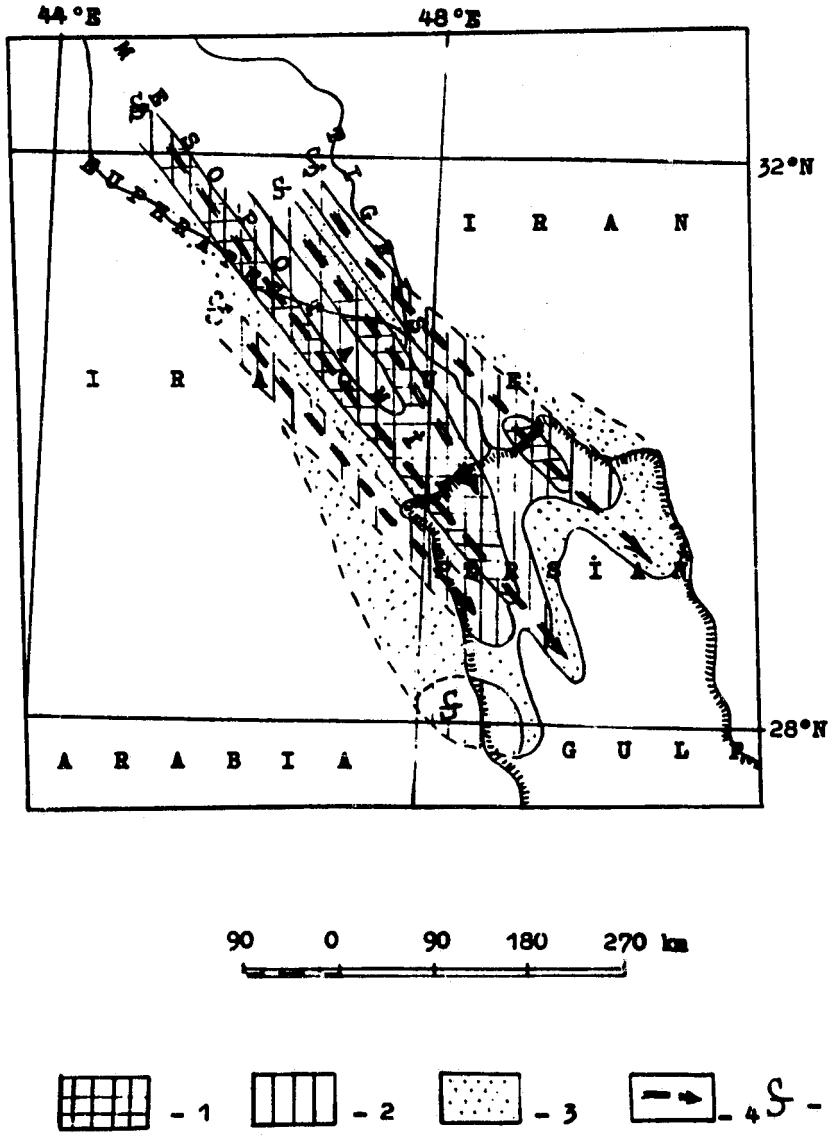


Fig. 2. Results of the TV interpretation of the dust storm structure over Mesopotamia lowland and the Persian gulf (Fig. 1) 1 - a heavy dust turbidity, 2 - the mean dust turbidity, 3 - the moderate dust turbidity, 4 - the direction of the dust-sand streams, 5 - dust storms and vortices.

REMOTE SENSING OF ATMOSPHERIC O_3 AND H_2O TO 70 km BY AIRCRAFT MEASUREMENTS OF RADIATION AT 1.64 mm WAVELENGTH

Joe W. Waters

Massachusetts Institute of Technology
Department of Electrical Engineering and
Research Laboratory of Electronics
Cambridge, Massachusetts 02139

ABSTRACT

Calculations are given of atmospheric emission from the 183.3 GHz H_2O line and the 184.4 GHz O_3 line for observations from 12 km. Present state-of-the-art radiometers can observe both lines simultaneously and should allow average mixing ratios up to 70 km to be measured with rms accuracies of $2 \cdot 10^{-8} \frac{\text{gm } H_2O}{\text{gm air}}$ and $8 \cdot 10^{-8} \frac{\text{gm } O_3}{\text{gm air}}$ for 30-minute integration time.

Ozone (O_3) has many relatively strong spectral lines in the millimeter wavelength region, [Gora (1959), Lichtenstein and Gallagher (1971)] and as millimeter receiver technology advances it becomes feasible to sense ozone remotely by measurements of thermal emission from these lines. Stratospheric emission by many of the submillimeter wavelength O_3 lines has been observed recently by Fourier-transform spectroscopy techniques from aircraft [Harries, et al. (1972)]. With the best resolution attainable at present, however, Fourier-transform spectroscopy measurements do not resolve the narrow O_3 lines and the measurements give only the total amount in the line of sight with little information about the distribution. The purpose of this paper is to point out that an O_3 line exists at 184.378 GHz (1.6 mm wavelength), conveniently near the 183.310 GHz water-vapor line, and that a single microwave radiometer can sense both O_3 and H_2O up to altitudes of ~70 km from aircraft measurements of thermal emission. An aircraft (or other) platform at ~10 km or higher altitudes is required because of strong water-vapor absorption in the troposphere. Remote sensing of stratospheric water vapor by balloon and satellite measurements of 183-GHz emission has already been considered theoretically [Gaut (1967, 1968)]. Remote sensing of ozone with the 184-GHz line has not been considered before, although lower frequency O_3 lines for remote-sensing purposes have been examined theoretically [Waters (1970)] and experimentally [Caton (1968), Rudzki (1971)].

A nominal atmospheric O_3 distribution up to 60-km altitude and a water-vapor mixing ratio of $2 \cdot 10^{-6} \frac{\text{gm } H_2O}{\text{gm air}}$ was used to compute the atmospheric emission spectrum as observed at 12-km altitude and the results are shown in Figure 1. For these distributions the 183-GHz H_2O line and 184 GHz O_3 line are computed to be of approximately equal intensity. A matrix element $\phi^2 = 5.7$, inferred from Gora [Gora (1959)], and lower state energy $E_\ell = 0.81 \cdot 10^{-14}$ erg, calculated from the slightly asymmetric prolate rotor energy level formula [Townes and Schawlow (1959)] (appropriate for O_3) was used to calculate the $J_K = 10_0 - 9_1$ 184-GHz O_3 rotational transition. Other parameters in the expression for the O_3 absorption coefficient have been discussed elsewhere

[Waters (1970)]. The expression of Gaut and Reifenstein [Gaut and Reifenstein (1971)] was used for the H_2O absorption coefficient. Oxygen absorption at these frequencies was computed to be negligible. The O_3 distribution used for the calculation of Figure 1 is indicated by a heavy line in Figure 2. Atmospheric ozone below ~30 km has been studied routinely and measurements of ozone up to ~50 km, with few exceptions, are in substantial agreement. Most recent stratospheric water-vapor measurements give mixing ratios of $\sim 2 \cdot 10^{-6} \frac{\text{gm } H_2O}{\text{gm air}}$ up to ~30 km altitude. Above ~30 km, water-vapor concentrations have not been accurately measured, but observations of atmospheric emission at the 22-GHz H_2O line [Waters (1970)] indicate that the average H_2O mixing ratio in the 30-60 km region does not exceed $2 \cdot 10^{-6}$. It is interesting to note that if the water-vapor mixing ratio at this altitude range is significantly less, the stratospheric emission spectrum at $\lambda \cong 1.6$ mm is dominated by the O_3 line, not the H_2O line, as is usually believed. The spectral lines in Figure 1 are shown in Figure 3 on an expanded frequency scale for 3 elevation angles of observation.

Resolved measurements of emission from these lines allow remote sensing of O_3 and H_2O with ~16-km altitude resolution up to the altitude at which Doppler broadening dominates the linewidth [Waters (1970)]. This occurs at altitude ~70 km for both lines. Above 50 km only a few measurements of O_3 distribution have been made, and these measurements are not in general agreement. This altitude region is also marked by photochemical reactions involving ozone which predict a nocturnal increase, and the O_3 distribution can be calculated if certain assumptions are made about reaction rates. Certain reported O_3 profiles above 50 km are shown in Figure 2, and Figure 4 gives the spectra computed for them. Also shown is the water-vapor line computed for $2 \cdot 10^{-6}$ H_2O mixing ratios extending to 60-km and 80-km altitudes. Note that the frequency scale has again been expanded for Figure 4 and that the center of the lines for 15° elevation in Figure 3 is shown again in Figure 4. Figure 5 gives the calculated zenith transmissivity of the atmosphere at the line frequencies as a function of height for three different model atmospheres and indicates the expected tropospheric attenuation of the lines. Table I gives the strengths of the lines calculated for 12-km zenith observations, a constant $2 \cdot 10^{-6}$ mixing ratio for both O_3 and H_2O, and for different atmospheric temperature profiles [Valley (1965)]. The line strengths vary by less than 10% for the extremes of the model temperature profiles.

The radiometer sensitivity required for use of these lines as meaningful atmospheric remote sensing tools is ~1°K rms. (Less sensitivity is required, of course, for simply detecting the lines.) A frequency resolution of 1 MHz is required for sensing to 50 km and 0.1 MHz for sensing up to 70 km. A reasonable integration time is $\sim \frac{1}{2}$ hour which, with the resolution and sensitivity just mentioned, dictates maximum single sideband receiver noise temperature of 18,000°K and 6,000°K for meaningful remote sensing to 50 km and 70 km, respectively. These receiver noise temperatures are well within state-of-the-art technology. Room-temperature 170-GHz mixer-receivers with ~2,000°K noise temperatures have recently been constructed by radio astronomy groups which should allow average mixing ratios to 70-km altitude to be measured with rms accuracies of $2 \cdot 10^{-8}$ for H_2O and $8 \cdot 10^{-8}$ for O_3 using 1/2 hour integration time. It may also be possible to increase the receiver sensitivity an order of magnitude by using cryogenically cooled mixers or maser amplifiers. Both lines can be observed simultaneously with the same radiometer simply by making the bandwidth sufficiently large (1.1 GHz) that both lines are covered and by arranging the frequency down-conversion so that the two lines appear in the output at different IF frequencies.

It should be pointed out that temperature to ~50 km can also be inferred from radiometric measurements of 5-mm wavelength thermal emission of high angular momentum O_2 transitions, as has been discussed for ground-based measurements [Waters (1970)]. The strongest O_2 line appropriate for stratospheric temperature sensing from 12-km zenith observations is calculated to be the 25_ line at 53.596 GHz with 128°K amplitude (for the 1962 U.S. Standard Atmosphere) over ±100 MHz, although less intense lines are more sensitive to atmospheric temperature variations. One can envision developing radiometers at 1.6 mm and 5 mm wavelength for aircraft which can sense temperature, water vapor, and ozone in the stratosphere and mesosphere. Such an instrument can be built compactly and automated so that measurements of these quantities would be routine. Mounting this instrument as a permanently installed sensing device on an atmospheric research aircraft would supply, as a matter of routine, stratospheric and mesospheric data for scientists studying upper atmospheric processes. Global coverage would be quite limited, of course, but the measurements would be valuable in designing a similar experiment for a satellite platform.

Acknowledgments

This work was supported in part by the National Aeronautics and Space Administration Contract NAS1-10693 and by the California Institute of Technology Contract 95268.

References

Caton, W. M., et al. 1968, "Radio Measurements of the Atmospheric Ozone Transition at 101.7 GHz," Astrophys. J., 151, L153.

Gaut, N. E. 1967, 1968, "Studies of Atmospheric Water Vapor by Means of Passive Microwave Techniques," Ph. D. Thesis, Department of Meteorology, M. I. T., July 1967; Technical Report 467, Research Laboratory of Electronics, M. I. T., December 1968.

Gaut, N. E., and E. C. Reifenstein III 1971, "Interaction Model of Microwave Energy and Atmospheric Variables," Technical Report No. 13, Environmental Research and Technology, Lexington, Massachusetts.

Gora, E. K. 1959, "The Rotational Spectrum of Ozone," J. Mol. Spectry., 3, 78.

Harries, J. E., N. R. W. Swann, J. E. Beckman, and P. A. R. Ade 1972, "High Resolution Observations of the Submillimetre Stratospheric Emission Spectrum," Nature, 236, 159.

Hays, P. B., et al. 1972, "Terrestial Atmospheric Composition from Stellar Occultations," Science, 176, 793.

Hunt, B. G. 1965, "A Non-equilibrium Investigation into the Diurnal Photochemical Atomic and Ozone Variations in the Mesosphere," J. Atmos. Terrest. Phys., 27, 133.

Lichtenstein, M., and J. J. Gallagher 1971, "Millimeter Wave Spectrum of Ozone," J. Mol. Spectry., 40, 10.

Reed, E. I. 1968, "A Night Measurement of Mesospheric Ozone by Observations of Ultraviolet Airglow," J. Geophys. Res., 73, 2951.

Rudzki, J. E. 1971, "Remote Sensing of Mesospheric Ozone," Ph. D. Thesis, Department of Electrical Engineering, M. I. T.

Townes, C. H., and A. L. Schawlow 1955, Microwave Spectroscopy (McGraw-Hill Book Company, Inc., New York).

U. S. Standard Atmosphere Supplements, 1966 (U. S. Government Printing Office, Washington, D. C., 1967).

Waters, J. W. 1970, "Ground-Based Microwave Spectroscopic Sensing of the Stratosphere and Mesosphere," Ph. D. Thesis, Department of Electrical Engineering, M. I. T.

Valley, S. L. (Ed.) 1965, Handbook of Geophysics and Space Environments (McGraw-Hill Book Company, Inc., New York).

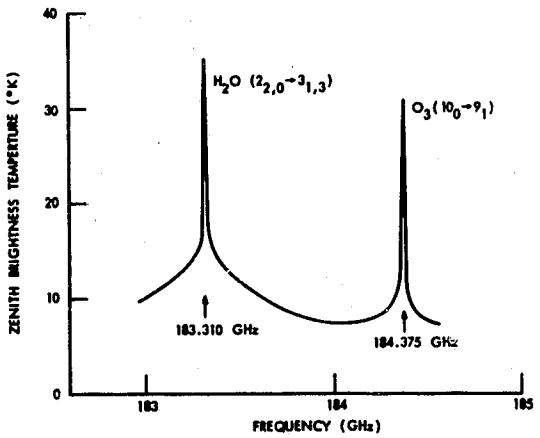


FIGURE 1. COMPUTED ATMOSPHERIC EMISSION SPECTRUM FOR NOMINAL DISTRIBUTION OF H_2O AND O_3 UP TO 60 km, AND 1962 U.S. STANDARD ATMOSPHERE TEMPERATURE PROFILE. Calculations are for zenith observations made from 12-km altitude.

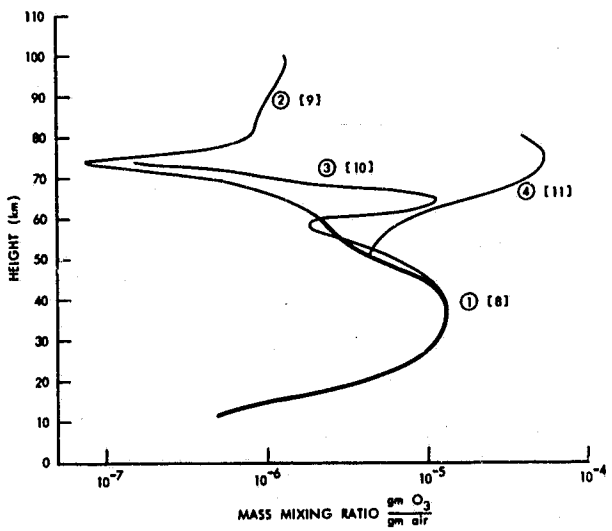


FIGURE 2. OZONE PROFILES USED FOR COMPUTATIONS. Circled numbers refer to profiles used for respective calculations in FIGURE 4 and to references as follows: 1. U.S. Standard Atmosphere Supplements, 1966 (1967). 2. Hayes et al. (1972). 3. Reed (1968). 4. Hunt (1965). The original data from the references were converted to mixing ratios by use of densities from the 1962 U.S. Standard Atmosphere.

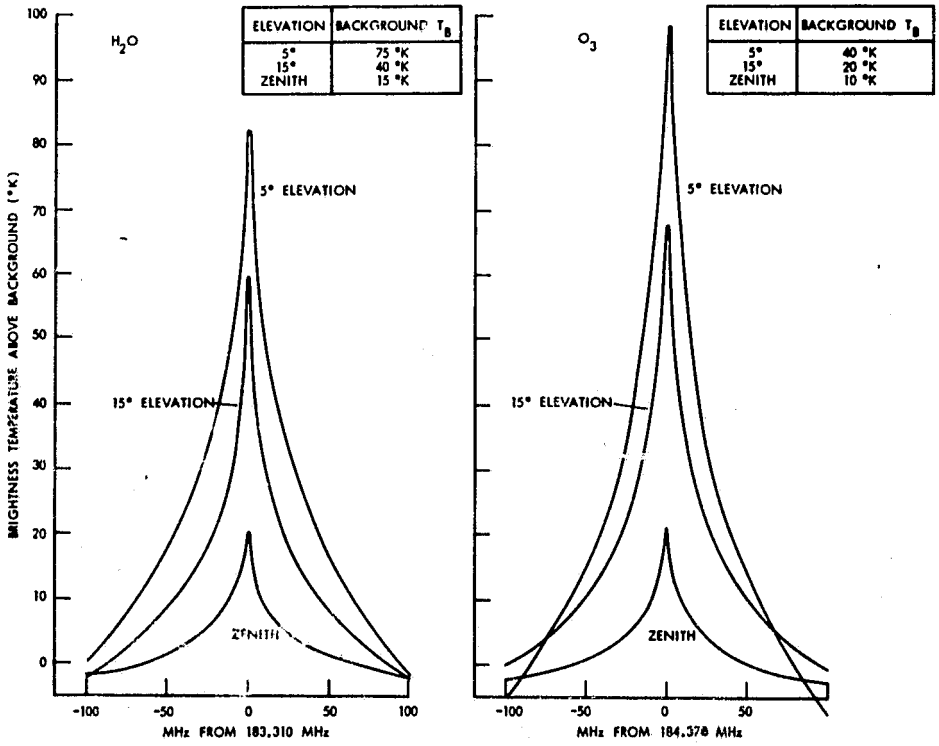


FIGURE 3. SPECTRAL LINES OF FIGURE 1 ON EXPANDED SCALE AND FOR DIFFERENT ELEVATION ANGLES OF OBSERVATION.

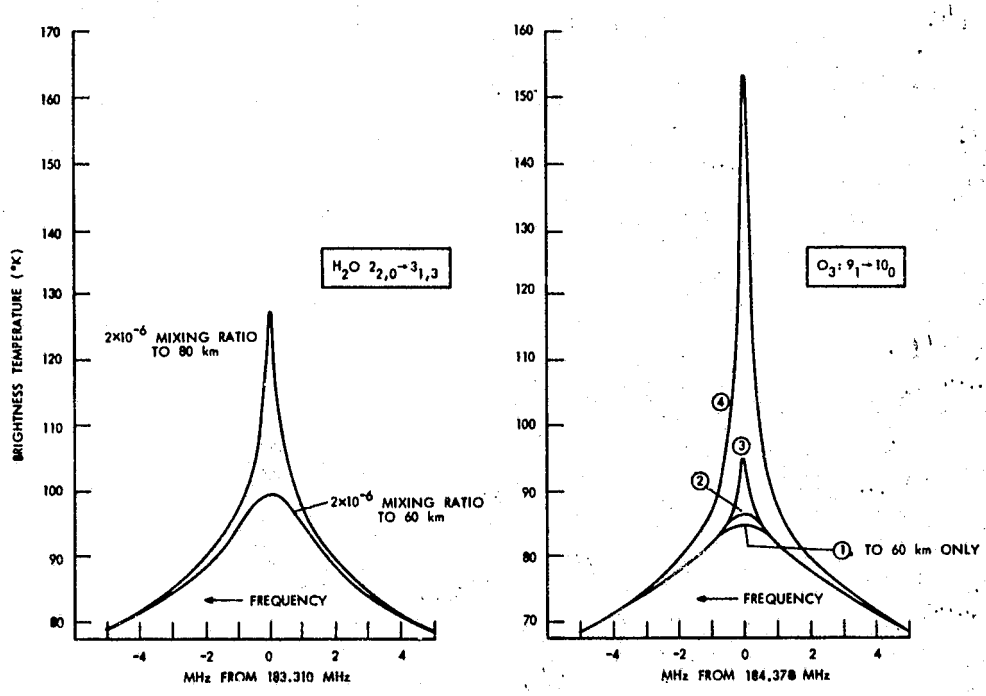


FIGURE 4. CALCULATIONS OF SPECTRAL LINE EMISSION FOR DIFFERENT PROFILES ABOVE 60 km. The frequency scale has again been expanded. Observation altitude, 12 km. Elevation angle 15°.

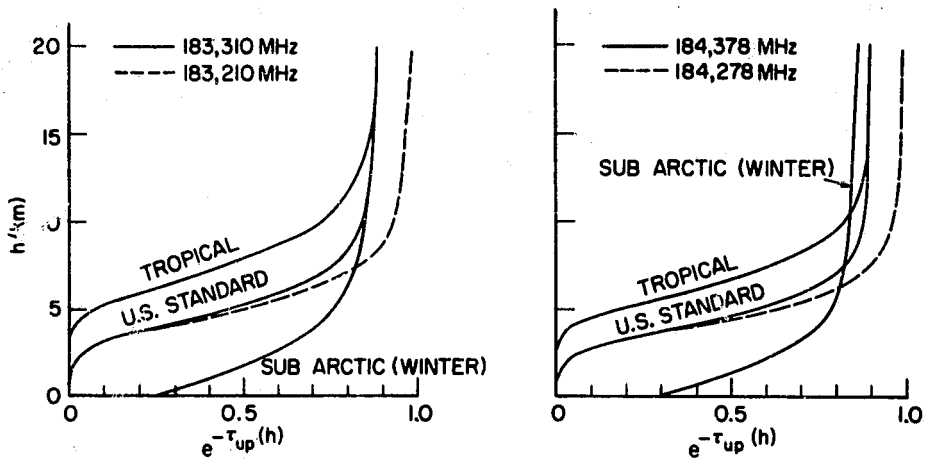


FIGURE 5. CALCULATED ZENITH ATMOSPHERIC TRANSMISSIVITY AS A FUNCTION OF HEIGHT FOR DIFFERENT ATMOSPHERIC CONDITIONS. Temperature profiles were obtained from Valley [1965] with ozone profile (1) in Figure 2 and $2 \cdot 10^{-6}$ stratospheric H_2O mixing ratio above a breakpoint H_B with an exponential tropospheric water-vapor distribution decreasing from a surface value ρ_o to height H_B. The values used for H_B and ρ_o are: tropical, $\rho_o = 20$ gm/m^3, $H_B = 16$ km; U.S. Standard, $\rho_o = 5$ gm/m^3, $H_B = 12$ km; subarctic winter, $\rho_o = 0.5$ gm/m^3, $H_B = 10$ km.

TABLE I. CALCULATED LINE STRENGTH FOR $2 \cdot 10^{-6}$ MASS MIXING RATIOS FOR BOTH H_2O AND O_3 AND FOR DIFFERENT ATMOSPHERIC TEMPERATURE PROFILES. The calculations were made for zenith observations from 12 km and the temperatures in the table are the difference in emission between line center and −100 MHz from line center.

Temperature Profile	183.3 GHz H_2O line (°K)	184.4 GHz O_3 line (°K)
60°N January	30.5	7.4
60°N July	31.2	7.5
U.S. Standard	31.3	7.6
15°N Annual average	29.7	7.0

REMOTE SENSING OF STRATOSPHERIC GASES USING SUBMILLIMETRE RADIATION

J E Harries

Division of Electrical Science
National Physical Laboratory
Teddington
Middlesex
UK

ABSTRACT

This paper summarises extensive studies which have been made of the submillimetre (far infrared) spectrum of the stratosphere. Using first a Golay cell detector, then a more sensitive cooled InSb bolometer, with a Michelson interferometric spectrometer, high altitude spectra have been obtained at resolutions of up to 0.06 cm^{-1}. From these, measurements of H_2O, O_3, HNO_3, N_2O and NO_2 have been made, from several aircraft and a balloon.

The techniques used, results obtained, and the future developments of this work are discussed.

1. INTRODUCTION

The presence of pure rotation lines from nearly all polar atmospheric gases in the submillimetre (far infrared) region makes possible quantitative measurements of these gases from spectroscopic observations. Our group at the NPL has been studying the properties of the atmosphere at these long infrared wavelengths (typically 100 μm to 5000 μm) in order to develop submillimetre techniques for atmospheric measurements.

Use of the submillimetre region had previously been limited by low source power levels and poor detectors, but we have been able to show that using Fourier spectrometric techniques[1], (with their inherent advantages of energy-gathering efficiency), phase modulation[2], and improved detectors, including ones cooled with liquid helium these problems may be overcome. Such long infrared wavelengths may be satisfactorily measured with equipment designed to much more relaxed optical and mechanical tolerances than, for example, corresponding near infrared devices, and may, therefore, be considerably more robust, an important advantage in the sometimes rigorous environments encountered in atmospheric studies. In addition, a number of very important gases have intense lines in this region, including H_2O and O_3, and others such as HNO_3, N_2O, NO, NO_2, atomic O and several others. These facts, together with others, such as low cloud scattering cross sections, combine to produce a potentially very powerful tool for atmospheric measurements.

As a result of the high line intensities of the dominant spectral species, H_2O, tropospheric studies are usually limited to quite short distances of less than a few hundred metres, unless millimetre wavelengths are used[3] ($\lambda > 1000$ μm). It is, therefore, the stratosphere which is particularly suitable for submillimetre measurements, with the relatively high transmission at these altitudes due to the low densities.

2. EARLY WORK

Following the measurements by Gebbie et al.[4], over the USA, our first measurements in Britain were made in 1969 in a Comet 2E aircraft which reached an altitude of up to 42,000 feet[5,6] Measurements of the emission spectrum of the stratosphere were made at a zenith angle of 80°, using a Michelson interferometer, incorporating phase modulation[2] for the first time, and a Golay detector. Sky emission (rather than solar absorption) observations were chosen so that the complication of a sun-seeking heliostat was not necessary: the disadvantage in emission measurements, of course, is that the inversion analysis is often more difficult; although, by using the concept of weighting functions this can be adequately solved. The spectral range covered in these flights was 10 cm^{-1} to 90 cm^{-1} (1000 μm to 110 μm) and spectral resolutions of between 0.5 cm^{-1} and

Preceding page blank

0.25 cm^{-1} were achieved. Since 1969 five series of flights have been made[5,12].

The results obtained immediately indicated the power of these techniques: a large number of H_2O, O_2 and O_3 lines were visible, many for the first time[5]. The presence of several pairs of H_2O and O_2 lines in close proximity suggested the use of the O_2 lines as a means of calibrating the quantity of stratospheric H_2O in the atmospheric path[7]: a technique was then developed which allowed the mixing ratio of H_2O (to air) to be derived from the ratio of H_2O and O_2 equivalent widths[5,6]. Figure 1 shows one of these H_2O/O_2 pairs at 60 cm^{-1}, and gives the expression used for deriving the mixing ratio. Plotting our results over the period November 1969 to June 1972 shows some very interesting trends (see Figure 2*); we observe a linear increase superimposed on an annual cycle. An approximate equation describing these trends is given by

$$\mu_{H_2O}(t) = 2.1 + 0.02\,t + 0.6\,\sin\left(\frac{2\,t}{12} + \phi\right)$$

where u is in mg kg^{-1}, t is in months (with t = 0 at November 1969) and ϕ is an arbitrary phase term. The linear term indicates an increase in the humidity of the lower stratosphere by about 0.24 mg kg^{-1} yr^{-1}, or about +10% per year. The oscillatory term is thought to be related to the annual cycle in tropical tropopause temperature, which 'throttles' the input of the H_2O to the stratosphere during the Hadley cell circulation process. Thus, if this is the case, observations made at one position as a function of time, will indicate 'waves' of H_2O. Similar phenomena have been observed by McKinnon and Morewood[8] and in the extensive measurements by Mastenbrook[9], both over North America. Further, more frequent, measurements are planned using our system to monitor this behaviour.

In October 1971 for the first time we flew a balloon-borne experiment[10], consisting of a phase-modulated 0.5 cm^{-1} resolution interferometer with a Golay cell detector. Using an elevation angle of 4°, the humidity of the stratosphere above 31 km was determined to be (1.7 ± 0.8) mg kg^{-1}, ie again very dry, and quite consistent with our other measurements. More flights are planned, and will include measurements with a simple band-pass radiometer, which will be calibrated for H_2O measurement against the accurate but more complex interferometric system.

3. HIGH RESOLUTION WORK

Since November 1971 we have used a helium cooled Rollin InSb electron bolometer[11], at first in collaboration with the Physics Department of Queen Mary College, who supplied the detector[12]. The high sensitivity of this detector has been utilised to increase the resolution to 0.06 cm^{-1}: higher resolutions are currently limited by the available mirror traverse, which will be increased to allow up to 0.020 cm^{-1} to be reached in suitable conditions.

A typical interferogram, obtained in about 30 min, is shown in Figure 3: the phase sensitive detector output was smoothed with a 300 ms time constant.

At a resolution of 0.06 cm^{-1} a signal-to-noise ratio of about 50 : 1 per resolution interval has been achieved, and this allows the identification of a very large number of new atmospheric lines. The majority of these, as Figure 4 shows, are due to O_3. Figure 4 shows the average of two sky spectra (resolution 0.0625 cm^{-1}) compared with a theoretical spectrum of O_3 calculated from the data of Gora[13]. The excellent agreement is an indication of the quality of these experimental results.

Other lines which occur in this region are due to HNO_3, N_2O, NO and NO_2[14,15]. Because of the many intense O_3 lines, however, several lines are blended and are difficult or impossible to measure. However, at present resolutions, in addition to H_2O and O_3, accurate measurements are possible for HNO_3 and N_2O, with lower accuracy possible for NO_2 and NO. Higher resolution will produce more accurate determinations (see below). Some results for these species will be published in the near future.

The weak lines of the minor species are not suitable for comparison with the much stronger O_2 lines, and so we are using both laboratory measurements and theoretical calculations to obtain strengths and frequencies with which to assign lines and calculate concentrations. This obviously places an emphasis on laboratory measurements and we are undertaking a programme at the NPL to produce the required data to sufficient accuracy in both intensity and frequency.

One of our instruments has been fitted to the British Concorde 002 and emission observations have been made from this aircraft up to 52 000 feet, in a number of regions of the world (mainly

---

* The frost point measurements mentioned in the caption to Figure 2 were made for use, for comparison purposes, by the British Meteorological Office.

during the far eastern tour of Concorde 002 in June 1972). The experimental installation is shown in Figure 5. The data obtained are still being analysed, and so a full discussion of them cannot at this time be presented. However Figure 6 shows a raw spectrum directly output from our computer, as an example. On this spectrum (which is an average of two runs, each taking 11 mins, obtained using a 200 ms time constant), the positions of weak lines due to the various minor species mentioned above are indicated by asterisks and may be identified by reference to Table 1. Other lines are due to H_2O, O_2 and O_3, as indicated in Fig 4[12]. A full analysis of the total concentrations derived from this series of spectra will be published elsewhere in the near future. Accuracies achieved vary from about $\pm 5\%$ for H_2O, to $\pm 25\%$ for HNO_3 and $\pm 40\%$ for NO_2.

TABLE 1. PARTIAL LIST OF ASSIGNMENTS

Line Number	Measured Wavenumber (cm^{-1})	Predicted Wavenumber	Species
7	10.181	10.25	HNO_3
10	10.650	10.65	HNO_3
		10.72	N_2O
12	11.064	11.08	HNO_3
23	12.963	12.96	HNO_3
25	13.200	13.14	HNO_3
29	14.10 (sh)	13.94	HNO_3
36	15.094	15.05	NO
		15.06	N_2O
51	17.593	17.58	N_2O
52	17.70 (sh)	17.75	HNO_3
62	19.566	19.566	SO_2
65	19.988	20.09	N_2O
66	20.172	20.26	NO_2
		20.26	HNO_3
71	20.944	21.01	NO_2
81	22.578	22.59	N_2O
		22.62	HNO_3
87	23.59 (sh)	23.45	N_2O
88	23.71 (sh)	23.67	HNO_3
92	24.262	24.18	NO_2
		24.26	N_2O
93	24.375	24.45	HNO_3
		24.51	NO_2
97	25.381	25.43	SO_2
		25.44	NO_2
101	26.287	26.14	HNO_3
103	26.609	26.54	HNO_3
104	26.766	26.73	NO_2
		26.76	N_2O
107	27.325	27.39	HNO_3
		27.339	O_3 (weak)
111b	28.47	28.44	NO
		28.50	SO_2
115	29.050	29.05	HNO_3
116	29.180	29.20	NO

4. FUTURE WORK

In order to improve the accuracy of the remote measurement of the minor stratospheric species such as O_3, nitrogen oxides and HNO_3, an increase in resolution is being attempted, by increasing the length of scan of the moving mirror of the interferometer.

As well as an improvement in resolution and therewith concentration measurement, however, we require to determine the distribution profile of the emitting gases with height. This is best achieved using a satellite, and studies of an orbiting experiment are in progress. The chief technical problem is that of cooling the detector to 4K: at present this would require a very massive refrigeration plant to be flown.

In the meantime, however, we are considering various ways of estimating, albeit approximately, the vertical distributions using aircraft and balloon equipment. This should be possible at altitudes of interest to the participants in the SST pollution debate, ie up to about 30-35 km. However, it is unlikely that, without the use of orbital spacecraft, concentrations can reliably be determined above these heights. Methods by which (non-orbital) profile estimations can be made are by zenith angle variations, and flight altitude variations.

CONCLUSION

A considerable amount of work has shown that the far infrared/submillimetre region has considerable potential for atmospheric sounding. This is a relatively new region to atmospheric studies and, while it is not claimed that all atmospheric measurements are best done here (eg temperature sounding is probably best done in the 15 μm CO_2 band), it is evident that there are a number of problems which can most profitably be studied using submillimetre techniques. The far infrared holds the compromise position between the high optical and mechanical precision required in near infrared spectrometers, and the large scale complex configurations required at micro-wavelengths, and so is eminently suitable to be applied to atmospheric studies, where often complexity, fragility and size are undesirable quantities.

REFERENCES

1. Vanasse, G. and Sakai, H., (1967), Fourier Spectroscopy; Prof. in Optics, 6, 261-330.

2. Chamberlain, J., (1971), Phase Modulation in far infrared (submillimetre-wave) interferometers, I, Infrared Phys., 11, 25-55.

3. Harries, J.E. and Ade, P.A.R., (1972), The high resolution millimetre wavelength spectrum of the atmosphere, Infrared Phys. 12, 81-94.

4. Gebbie, H.A., Burroughs, W.J., Harries, J.E. and Cameron, R.M., (1968), Astrophys. J., 154, 405-408.

5. Harries, J.E. and Burroughs, W.J. (1971), Measurements of submillimetre wavelength radiation emitted by the stratosphere, Q.J.Roy.Met.Soc., 97, 519-536.

6. Harries, J.E. and Burroughs, W.J. (1971), NPL Division Report DES 7, 83pp.

7. Burroughs, W.J. and Harries, J.E. (1970), Direct method of measuring stratospheric water vapour mixing ratios, Nature, 227, 824-825.

8. McKinnon, D. and Morewood, H.N. (1970), Water vapour distribution in the lower stratosphere over North and South America, J.Atmos.Sci., 27, 483-493.

9. Mastenbrook, H.J. (1968), Water vapour distribution in the stratosphere and high troposphere, J.Atmos.Sci., 25, 299-311.

10. Harries, J.E., Swann, N.R., Carruthers, G.P. and Robinson, G.A. To be published.

11. Kinch, M.A. and Rollin, B.V. (1963), Brit.J.Appl.Phys., 14, 672-675.

12. Harries, J.E., Swann, N.R., Beckman, J.E. and Ade, P.A.R. (1972), High resolution observations of the submillimetre stratospheric emission spectrum, Nature, 236, 159-161.

13. Gora, E.K. (1959), The rotational spectrum of ozone, J.Mol.Spec., 3, 78-99.

14. Stone, N.W.B. (1963), PhD Thesis, University of London.

15. Harries, J.E., Burroughs, W.J. and Duxbury, G. Pure rotation spectrum of HNO_3 vapour, Nature Phys.Sci., 232, 171-173.

16. Burroughs, W.J. and Harries, J.E. (1971), On the use of apodisation in submillimetre Fourier transform spectroscopy, Infrared Phys., 11, 99-108.

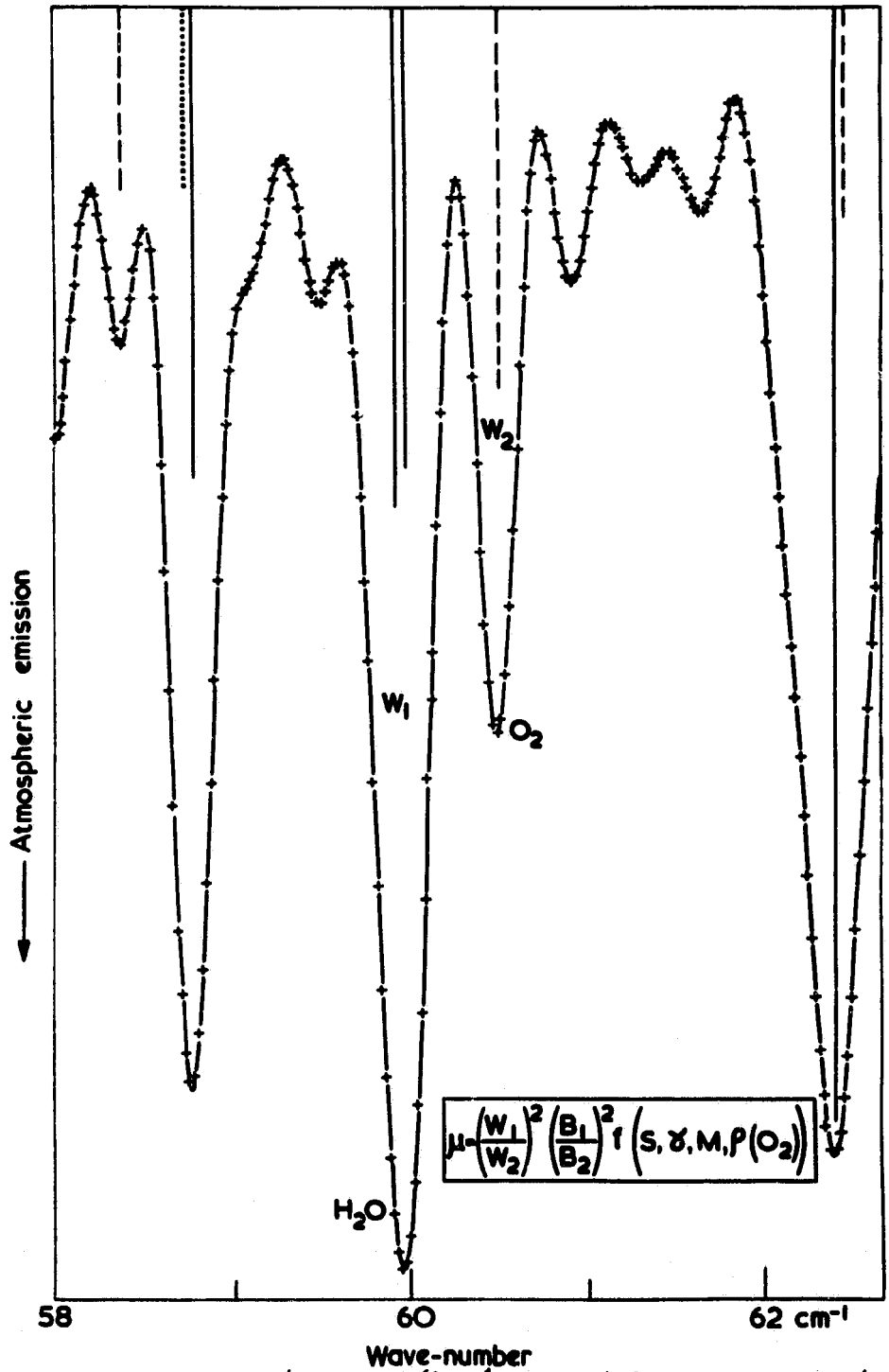


FIGURE 1. A typical pair of H_2O/O_2 lines at 60 cm^{-1}. Theoretical assignments to H_2O (solid lines) O_2 (broken lines) and O_3 (dotted lines) are given at the top of the diagram. The resolution is 0.33 cm^{-1}, altitude 40 000 feet, elevation angle 10°. The expression for mixing ratio μ is shown: the function f contains terms describing line strengths and widths.

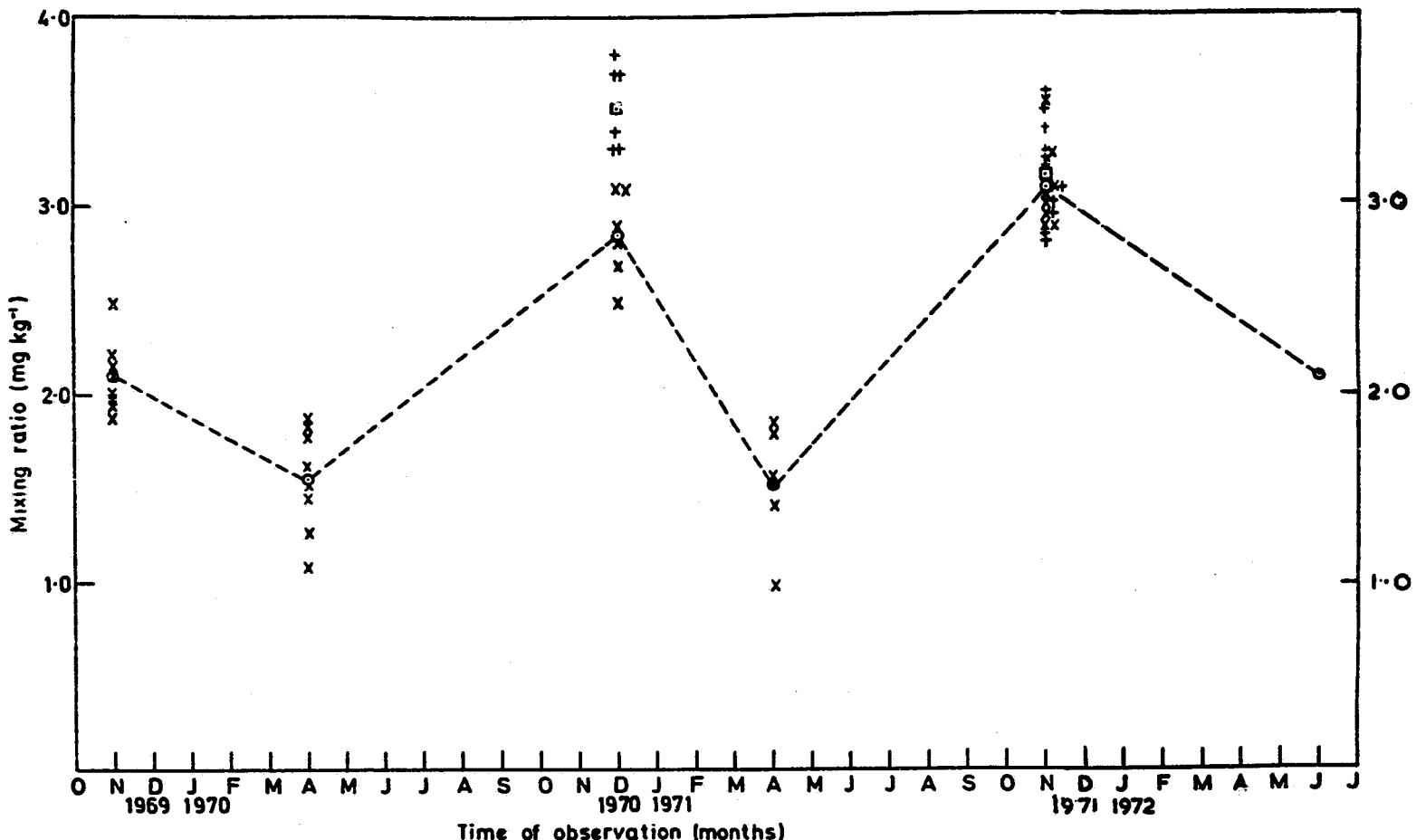


FIGURE 2. The humidity mixing ratio u derived from our results, as a function of time. The symbols have the following meaning:-

X single NPL observations
0 averaged NPL observations
+ single frost point hygrometer measurements
⊡ averaged frost point hygrometer measurements

A discussion of the apparent variation in μ is given in the text.

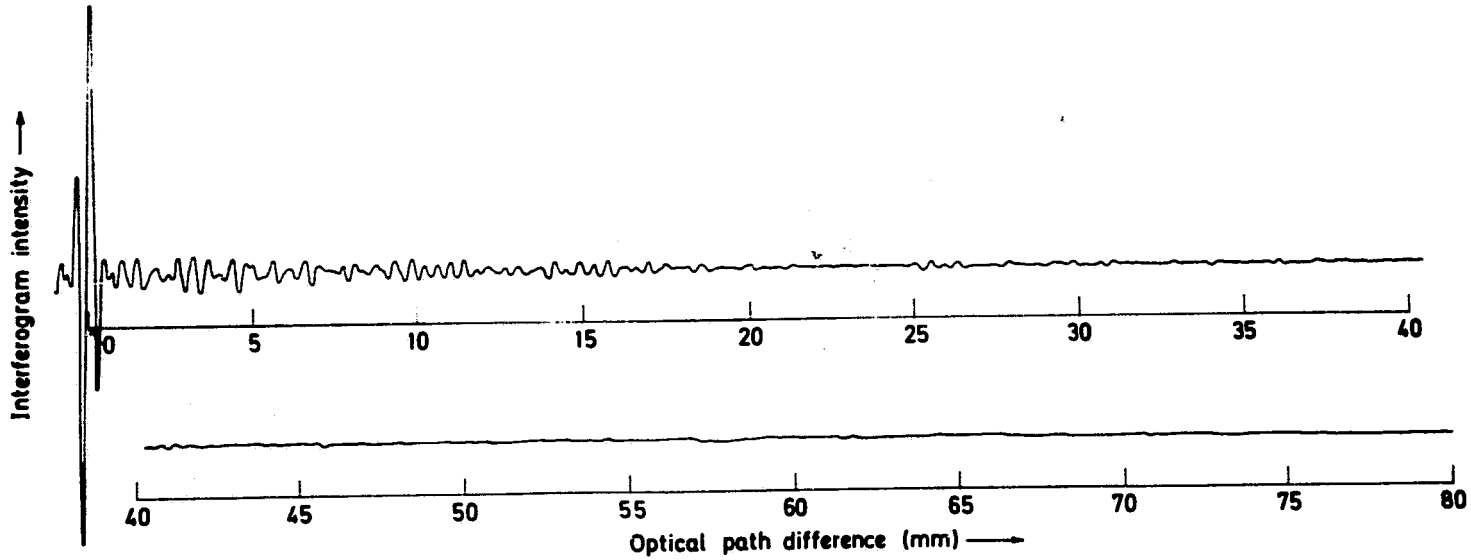


FIGURE 3. A high resolution interferogram obtained in the Comet at 40 000 feet, and + 15° elevation. The output was smoothed with a 300 ms time constant and the run was obtained in 32 min.

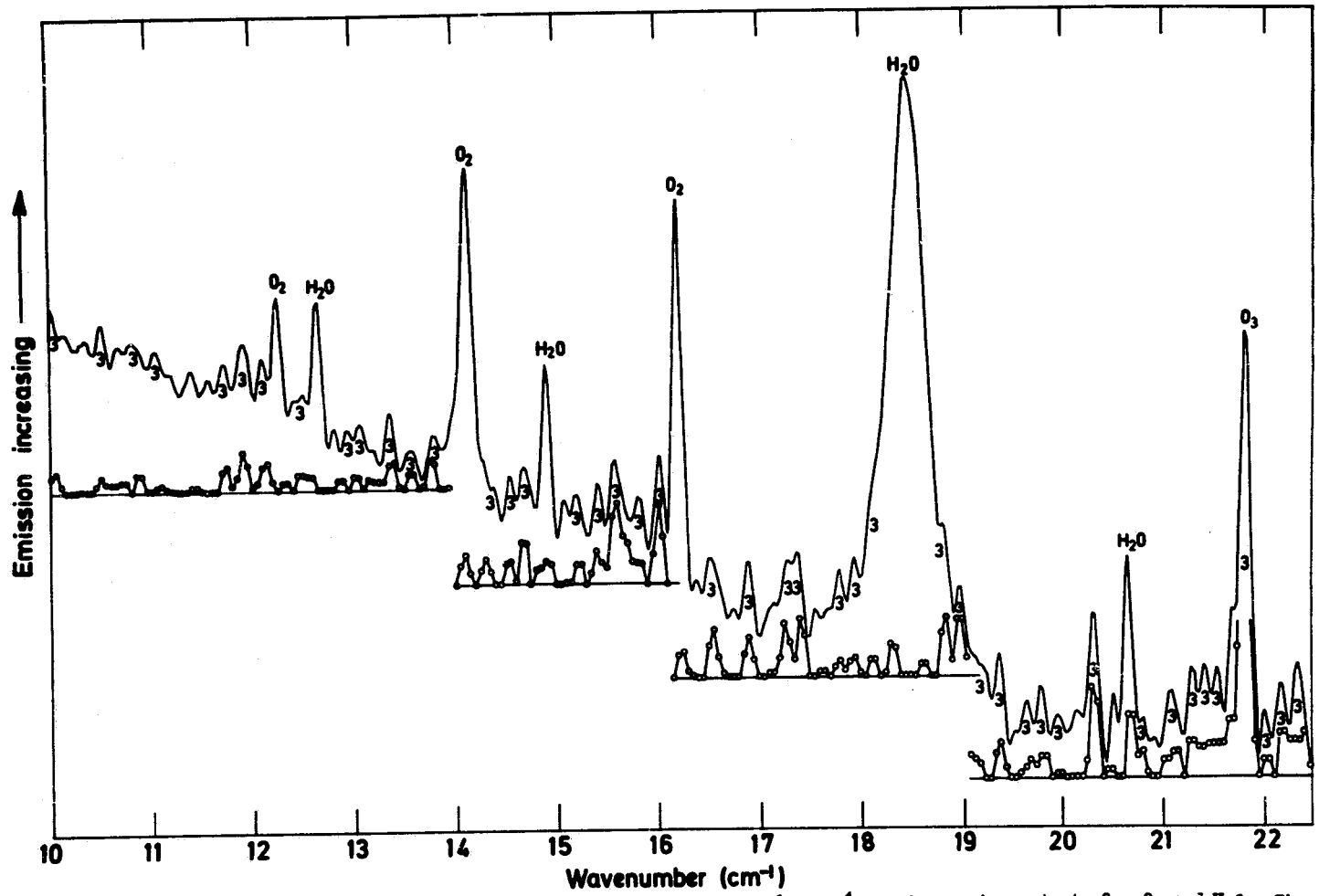


FIGURE 4(a) An average of two Comet runs, at a resolution of 0.0625 cm^{-1} showing assignments to O_3, O_2 and H_2O. The lower sections are theoretical, calculated from Gora's data.

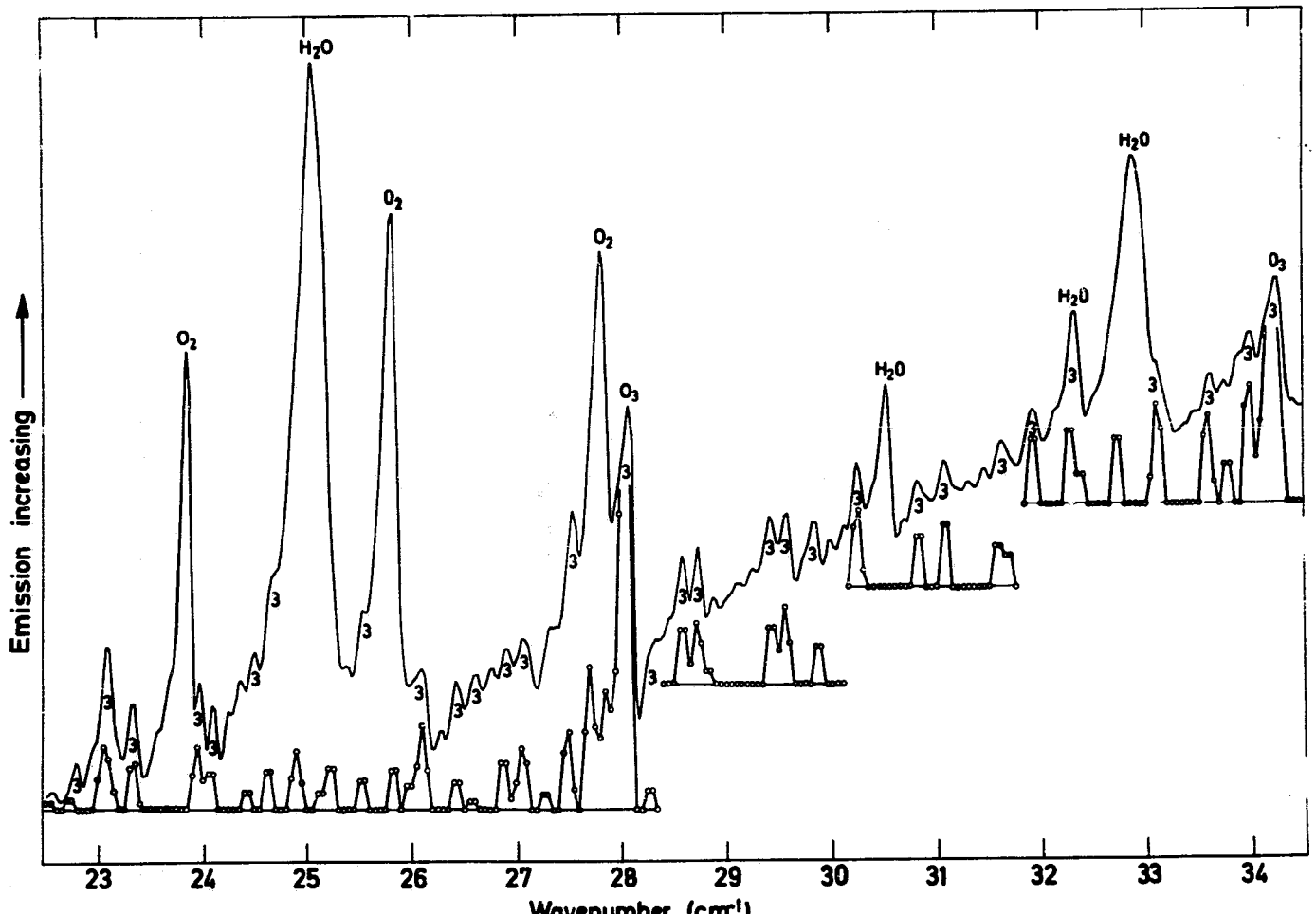


FIGURE 4(b). An average of two Comet runs, at a resolution of 0.0625 cm^{-1} showing assignments to O_3, O_2 and H_2O. The lower sections are theoretical, calculated from Gora's data.

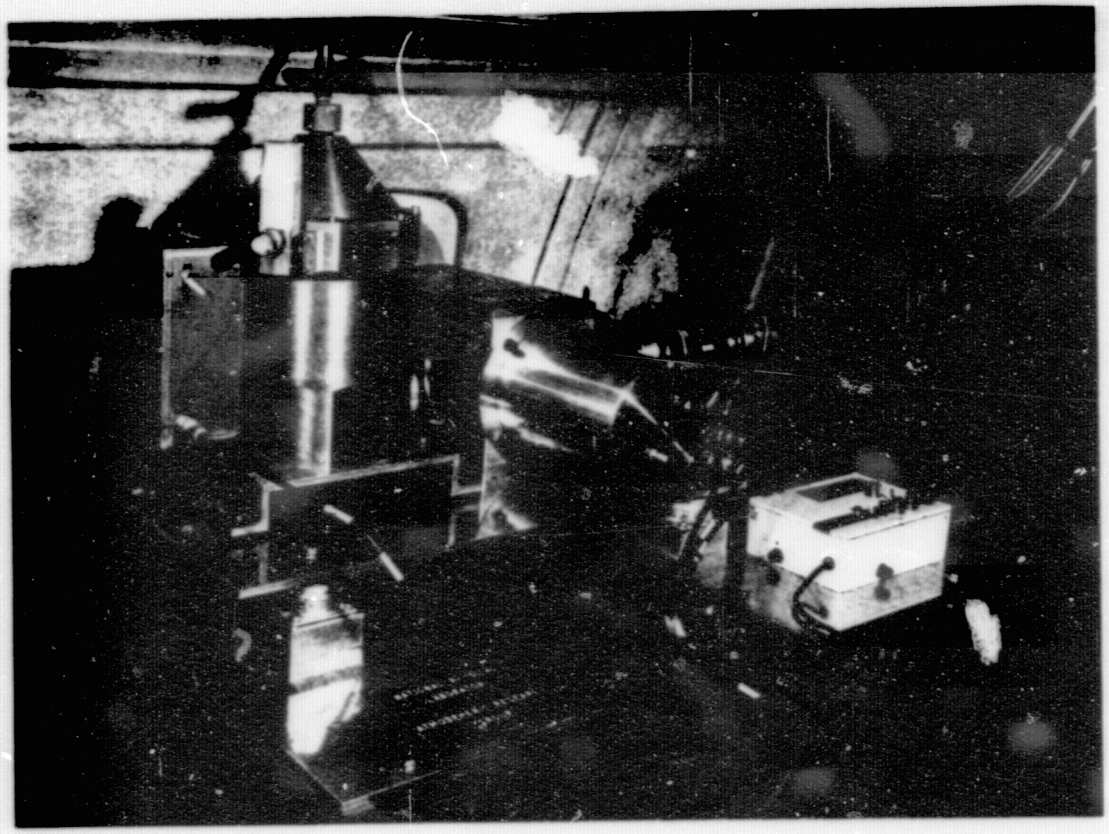


FIGURE 5. A picture of the NPL installation in the British prototype Concorde 002. The cylindrical vessel to the left is the detector cryostat. The moving arm of the interferometer may be seen to the right. The phase modulation unit is contained in the cylindrical extension projecting from the interferometer. A window of 3.5 in aperture consisting of two 0.5 in panes separated by 0.5 in gap is placed in the fuselage.

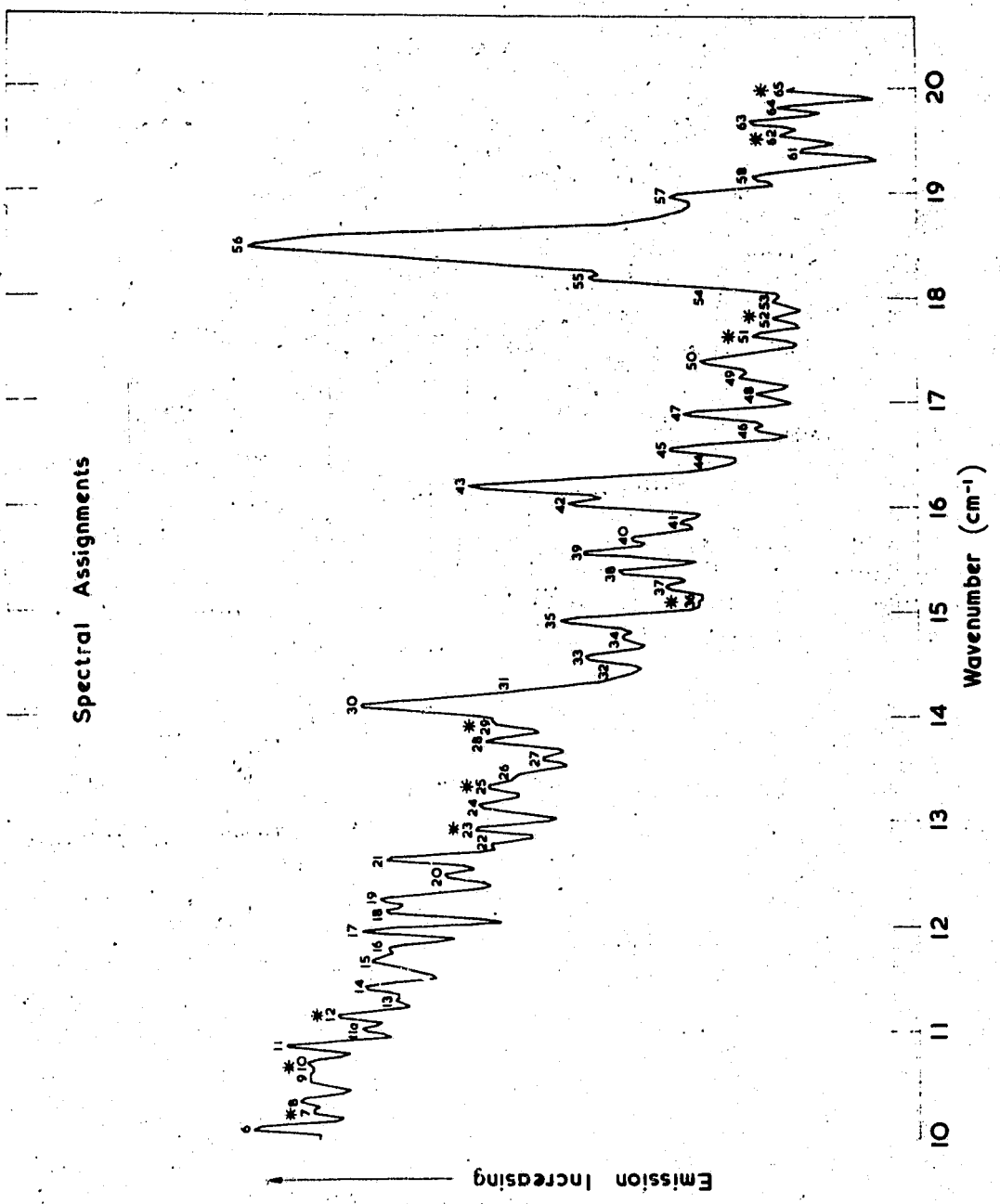


FIGURE 6.(4) An example of a spectrum obtained during the Concorde 002 tour of the Far East. This is an average of two at 0.067 cm^{-1} each obtained in 11 min, over South Australia, above 50 000 feet. Assignments are indicated in Table 1 for the asterisked lines. Others are due to H_2O, O_2 and O_3 (see ref 12 and Fig 4).

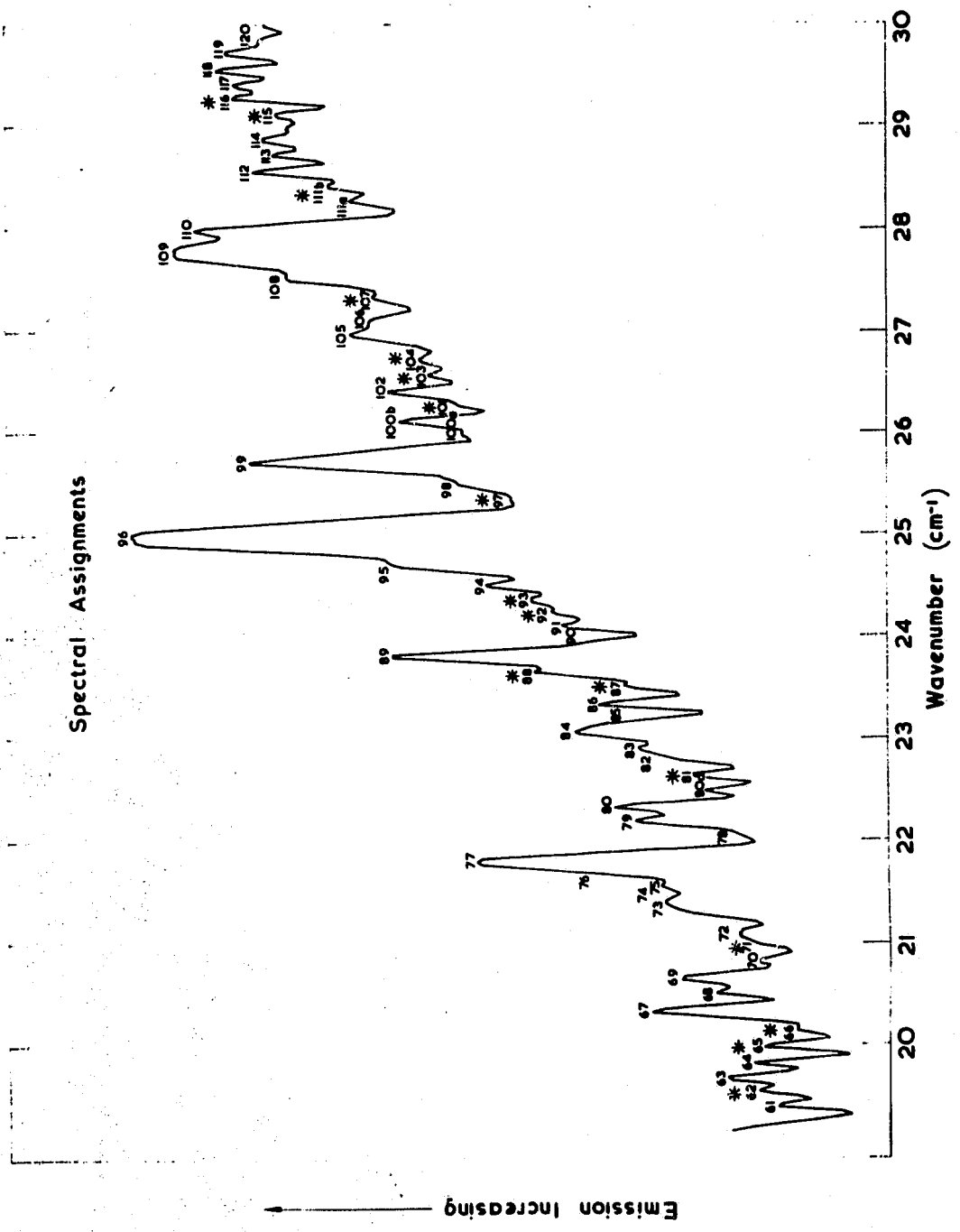


FIGURE 6(b). As Fig.6(a), continued.

REMOTE SENSING OF MESOSPHERIC OZONE

J. E. Rudzki, Jr.

Air Force Avionics Laboratory
Dayton, Ohio

ABSTRACT

Photochemical ozone theory and microwave spectroscopy suggest that microwave radiometry can be used to verify remotely the existence of the mesospheric ozone diurnal variation. A description of the theory and a radiometer built to test the theory is described. Experimental results are given which place an upper limit on the nighttime mesospheric ozone concentration of 5×10^{10} cm^{-3} at 50 km dropping exponentially to 10^{9} cm^{-3} at 80 km.

1. INTRODUCTION

Ozone is a trace constituent of the atmosphere with concentrations of a few parts per million. It is a strong absorber of ultraviolet radiation, and it is very active chemically. It plays an important part in the earth's radiation budget as it absorbs solar ultraviolet radiation, and absorbs and reradiates the infrared radiation from the earth. A measure of its importance is the fact that it is believed to be responsible for the increase with altitude of the temperature of the stratosphere.

Few ozone concentration measurements have been made over 35 km. Photochemical theories describe some of the gross features of the ozone concentration profile satisfactorily. One key point of the theory is that the concentration of mesospheric ozone should vary diurnally, increasing at night and decreasing during the day. This has never been verified experimentally. A major objective of this work was to measure with microwave techniques, the extent to which mesospheric ozone does vary diurnally.

2. PHOTOCHEMICAL THEORIES OF THE DIURNAL VARIATION OF OZONE

In the early 1900's observations of stellar spectra, including that of the sun, were cut off sharply in the vicinity of 3000 Å. As this coincided with the absorption bands of ozone measured in the laboratory, the presence of ozone in the atmosphere was suspected. Fabry and Buisson (1913) studied the absorption of the solar spectrum between 3000 and 3340 Å at different zenith angles and showed conclusively that absorption spectra coincided with the absorption bands of ozone.

Dobson (1930) concluded a long and extensive series of absorption measurements of the total amount of ozone in the atmosphere and showed the extent of the seasonal and latitudinal variations of the total amount of ozone above the observation stations. Concurrently, Gotz and Dobson (1928) began their attempts to determine the mean height of the ozone. Their tentative conclusion at that time was that the main part of the ozone was to be found at a height of about 50 km. Gotz then developed the Umkehr method of determining the height with much greater precision and Gotz, Meetham, and Dobson (1934) showed that the ozone concentration reached a maximum around 25 to 30 km, with a rapid decrease above it, and a less rapid decrease below it. This finding was then confirmed by balloon flights by Regener and Regener (1934), and by many measurements afterwards.

The first attempt to explain the presence of ozone in the atmosphere was made by Chapman (1930c), using photochemical reactions.

2.1. CHAPMAN PHOTOCHEMICAL THEORY

About the time that Dobson and Gotz were conducting their ozone measurement program, Chapman (1930a, b, c) proposed several photochemical reactions to explain why the ozone concentration above the ozone maximum should vary diurnally. He assumed that the ozone layer was about 10 km thick at an altitude of 45 km. The green line in the spectrum of the aurora was evidence that atomic oxygen existed in the upper atmosphere. So, he reasoned, the molecular oxygen must be dissociated into atomic oxygen, the atomic oxygen then combines with molecular oxygen to form ozone or with itself to form molecular oxygen again, and the ozone had to disappear by combining with itself or atomic oxygen to form molecular oxygen, or by dissociating to produce molecular and atomic oxygen. These reactions are summarized below:

$$O_2 + h\upsilon \ (\lambda < 2423\text{Å}) \rightarrow O + O \qquad 2.1.1$$

$$O + O_2 + M \rightarrow O_3 + M, \ M = O_2, N_2 \qquad 2.1.2$$

$$O + O + M \rightarrow O_2 + M \qquad 2.1.3$$

$$O_3 + O \rightarrow 2\ O_2 \qquad 2.1.4$$

$$O_3 + O_3 \rightarrow 3\ O_2 \qquad 2.1.5$$

$$O_3 + h\upsilon \rightarrow O + O_2, \ \lambda < 3100\ \text{Å}, \ 3100\ \text{Å} < \lambda < 11{,}800\ \text{Å} \qquad 2.1.6$$

The presence of ozone was definitely established by observation. If atomic oxygen were produced only by ozone, the ozone would slowly disappear. So, the formation of atomic ozygen from O_2 had to be the more fundamental.

During the night, the two dissociating reactions, 2.1.1 and 2.1.6, producing O stopped, but the combination reactions, 2.1.2 and 2.1.4, continued. Therefore, the O concentration had to decrease, but the ozone concentration could either increase or decrease. Chapman assumed that the concentrations of O and O_3 were unaffected by convection or diffusion. He also estimated the reaction rates and dissociation rates as shown in Table I. On the basis of a cosinusoidal dissociation function during the day, he estimated that the O_3 concentration just above the ozone maximum would increase as all the O was combined. Progressively higher, less and less of the O would combine to form O_3, until at around 80 km, there would not be much change in the atomic oxygen at all, and ozone concentration would remain about 10^5 cm^{-3}.

2.2. COMPARISON OF THEORETICAL OZONE CONCENTRATIONS

Following Chapman, up to the present time, refinements to the photochemical theory were attempted. The results of the various calculations are shown in Figure 1. Included are the water-vapor atmosphere of Bates and Nicolet (1950), the effects of nitrogen as computed by Paetzold (1961), the variable temperature model of Leovy (1964), and finally the three models used by Hunt (1965, 1966). All of the models predict a substantial change in the mesospheric ozone concentration during the night.

2.3. OBSERVATIONS OF THE DIURNAL OZONE PROFILE

The results of the observations of Randhawa and Hilsenrath are plotted in Figure 2. They represent the only known attempts to measure the diurnal variation in a reasonable time interval. Randhawa's measurements were made over a 24 hour period, but did not reach above 50 km. Because of a rocket failure, Hilsenrath's measurements were more than a day apart. The profiles predicted by Hunt in a moist atmosphere are shown for comparison.

3. MICROWAVE MEASUREMENT OF MESOSPHERIC OZONE

When the ozone concentration profiles predicted by the theories are compared with the limited observations, it is evident that the diurnal variation of ozone concentration was neither verified nor disproved. The objective of this experiment was to determine if the diurnal variation existed using a microwave sensor.

3.1. MICROWAVE SPECTROSCOPY OF OZONE

Microwave spectroscopy is a well established technique to study the physics of molecular structures. Townes and Schawlow (1955) and Gordy, et. al. (1953) are representative texts on the subject. Under carefully controlled conditions in the laboratory, well defined spectra are obtained. Microwave spectroscopy of gases in the atmosphere is much more difficult, and there are only a few successful observations. Among the reported observations of the ozone molecule are 1.) Mouw and Silver (1960) at 36.025 GHz in absorption against the sun, 2.) Caton, et. al. (1967) at 37.836 GHz in absorption and 30.056 GHz in emission, 3.) Barrett, et. al. (1967) at 23.861 GHz in emission, and 4.) Caton, et. al. (1968) at 101.737 GHz in absorption.

Gora (1959) has compiled an extensive listing of the molecular resonances of ozone and compared them with the observed frequencies. The frequency of the $4_{0,4} \rightarrow 4_{1,3}$ Q_r[(4_0) in Gora's notation] line was listed by Gora to be 100.7367 GHz, but it may have been a typographical error. Trambarulo, et. al. (1953) reported the measured frequency to be 101736.83 .14 MHz. This resonance was selected for the experiment because the equipment used by Caton was available, the frequency was measured accurately, and it was a moderately strong line.

3.2. THEORY

The spectra, both absorption and emission, are caused by the interaction of microwave energy with the ozone molecule. Following Townes and Schawlow, molecules can be broadly categorized as diatomic, linear polyatomic, symmetric tops, or asymmetric tops. Ozone is closely approximated by a symmetric top. That is, of the three principal moments of inertia, two are nearly equal.

In the microwave frequency range, the Rayleigh-Jeans approximation to the Planck black-body law applies. The intensity of electromagnetic radiation from a substance is proportional to a brightness temperature, T_B. If a gas has a temperature T (ℓ) and an absorption coefficient $\alpha(\ell)$ as a function of position, ℓ, then the brightness temperature is given by the equation of radiative transfer.

$$T_B(\ell) = T_{B_0} e^{-\tau(\ell)} + \int_0^L T(\ell) e^{-[\tau(L)-\tau(\ell)]} d\tau(\ell) \qquad 3.2.1$$

where $\tau(\ell) = \int_0^{\ell} \alpha(\ell') d\ell'$

and L = total path length.

The absorption coefficient, $\alpha(\ell)$, computed from the Van Vleck-Weisskopf (1945) equation, is assumed to be the sum of the absorption coefficients of all nearby molecular resonances. In the atmosphere, the water vapor resonances at 22.235 GHz and 183.3 GHz, the oxygen complex around 60 GHz, the single oxygen line at 118 GHz, and the individual ozone lines all contribute to the absorption coefficient around 101.7 GHz.

The computer program used to compute the absorption coefficient and brightness temperature is a modified version of the Microwave Emission Spectrum program described by Waters (1970). The 1962 U.S. Standard Atmosphere model was used for the temperature and pressure values vs. heights. Fifteen ozone lines were used in the calculations, in the frequency range 93-119 GHz.

The model ozone profiles used were the ones given by Hunt (1966b) shown in Figure 2. The result of the calculations for a day profile is given in Figure 3. The effect of the change in mesospheric ozone concentrations would be a sharp spike on top of the line. This is illustrated in Figure 4, where both the day and night spectrum are plotted. The change from day to night in the spectrum is very substantial, almost a 20% change in absolute temperature.

The temperature measured by the radiometer is the brightness temperature integrated over the antenna pattern which is designated the antenna temperature $T_A(f)$.

$$T_A(f) = \frac{1}{4\pi}\int_{4\pi} G(f,\theta,\phi)\, T_B(f,\theta,\phi)\, d\Omega \qquad 3.2.2$$

$G(f,\theta,\phi)$ = Antenna Gain Function $\int_{4\pi} G(f,\theta,\phi)\, d\Omega = 4\pi$

If the antenna has a high gain and narrow beam width, then the gain can be assumed constant over the beam width. Similarly, if the brightness temperature is a slowly varying function over the beam solid angle, it too can be assumed constant. The line strength was multiplied by 0.8 to account for the efficiency of the antenna. The line strength was estimated to be (20°) 0.8 = 17° high, in a bandwidth or "window" of 4 MHz.

3.3. RADIOMETER SPECIFICATIONS

With the predicted line strength and shape known, the bandwidth, resolution, sensitivity, and frequency stability of the radiometer could be specified. The line is about 300 kHz wide at half-height, so a resolution of about 100 kHz would be required over the 4 MHz bandwidth. This established the pre-detection bandwidth to be 100 kHz.

The time required for the mesospheric ozone to reach its maximum value is predicted to be on the order of minutes, and it maintains its value over several hours (Maeda and Aikin, 1968; Hunt, 1966b). A post-detection bandwidth equivalent integration time of 4000 seconds would be reasonable.

The receiver sensitivity can be expressed in terms of the rms fluctuations of the noise at the output. This is given by:

$$\Delta T_{rms} = \frac{\alpha(T_A+T_R)}{\sqrt{B\tau}} = \frac{\alpha(T_{sys})}{\sqrt{B\tau}} \ ^\circ K \qquad 3.3.1$$

where ΔT_{rms} = rms value of the output noise (°K)

T_A = antenna temperature (°K)

T_R = noise contributed by the receiver (°K)

T_{sys} = system temperature = $T_A + T_R$ (°K)

B = pre-detection bandwidth (Hz)

τ = integration time (sec)

α = a constant between 1 and 3

$\alpha \approx 2$ for the Dicke-type receiver

A ΔT_{rms} = 1°K would give a 16:1 ratio of the line strength to the rms noise. With these parameters fixed, a T_{sys} = 10,000°K would be required. This is also expressed as a system noise figure, F, by:

$$T_{sys} = (F-1)\ 290^\circ K$$

and $F_{dB} = 10 \log_{10} F$. The receiver noise figure would have to be less than 15.5 dB.

The frequency stability of the receiver should be such that the signal remains within the 100 kHz channel resolution for more than one hour. Using a margin of ten, the frequency stability would have to be 10 kHz in 101×10^6 kHz, or a stability of a part in 10^7 over a period of one hour.

The instrument required would have to operate at 101.736 GHz with at least a 4 MHz bandwidth, 100 kHz resolution, 10^{-7} frequency stability, and a 10,000°K single side band system temperature. Spectra produced by observations made at various times during the day and night would be analyzed. The appearance of the narrow spectral feature at night as opposed to a flat spectrum expected from the day distribution would confirm the diurnal variation of mesospheric ozone. The width and height of the feature would be a measure of the altitude and concentration of the mesospheric ozone.

4. RADIOMETER DESCRIPTION

The radiometer built and used in this experiment met the design specifications. It included an accurate temperature calibration circuit, a noise balance circuit, and a precise frequency calibration circuit. It was a Dicke switched receiver with a system temperature between 4,000 and 5,000°K. Rough checks of the radiometer's frequency response indicated that the image band may be attenuated by approximately 20 dB by the ferrite switch, but these tests were hampered by the lack of test equipment in this frequency band. So the system temperature is assumed to be double side band, which is still within the required sensitivity specification.

4.1. RADIOMETER CIRCUIT

Figure 5 is a schematic of the radiometer. The noise tube balance circuit also served as the frequency calibration circuit. The tenth harmonic of an independently phase-locked signal at X-band (10.173683 GHz) was fed into the signal port of the waveguide switch through a 10 dB coupler. The second port of the switch connected to the calibration leg.

The first traveling wave tube amplifier had a noise figure of 5 dB measured by both a H. P. noise figure meter and an AIL hot-cold noise source. The second converter stage L.O. was at 3.255 GHz, temperature stabilized to less than 500 Hz drift over 0°C. to 60°C. The stability of the oscillator was measured to be less than 10^{-7} over one hour as measured by a frequency counter and digital recorder. The first local oscillator was phase locked against a stable X-band reference generated by another phase lock loop that was stable to 10^{-8} in one hour.

The second I.F. could be selected by the choice of the first L.O. frequency. For use at the Haystack Observatory, the second I.F. was 30 MHz, and a 10 MHz filter was used before the second converter as an image filter. When the MIT 20 channel synchronous detector was used, either 60 MHz or 105 MHz was used as the second I.F. An image filter covering 3065 to 3235 MHz was used before the second converter in those circumstances.

4.2. OBSERVATION PRODEDURES

Absorption and emission measurements were made at the Haystack Field Station of Lincoln Laboratory, Westford, Massachusetts. Broadband emission measurements were made at M.I.T., Cambridge, Massachusetts, from the Compton Laboratory roof, and at Lincoln Laboratory, Lexington, Massachusetts, from the D building roof.

4.2.1. OBSERVATIONS AT HAYSTACK FIELD STATION. The Haystack spectral line analysis is described in detail in Conant and Meeks (1968). The "1-bit autocorrelator", described by Weinreb (1963), is the hardware portion of the system. It is a 100-channel data processor which has an effective resolution of 1/40th the input bandwidth. The input bandwidths available are 20, 4, 1.2, 0.4, 0.12 and 0.04 MHz. The 4 MHz bandwidth was normally used for the night emission spectra, so the frequency resolution was 100 kHz. All the bandwidths below 4 MHz are part of the same processor and are routinely used by radio astronomers to study spectral lines from space.

A Univac U-490 computer coupled to a high speed printer produces almost "real-time" plotting of the spectra. Within 5 seconds after the end of the integration period the data is Fourier transformed, but the high speed printer takes 20 seconds to print the output data format consisting of the bandpass characteristic, the numerical data, and the spectrum, along with numerical subsidiary calculations.

The integration periods are selected in 30 second increments, with periods up to 999x(1/2 minute), or about 500 minutes, possible. In addition, the data is recorded on magnetic tape for post real time processing, so that extremely long equivalent integration times can be accumulated. Several integrations in the 18,000 to 22,000 second range have been made using this technique.

With the post real time processing, different spectra were compared by subtraction. Since the emission line was to increase at night, a 4,000 sec. load switched run, taken before sunset, was subtracted from an equal run after sunset; a run taken before sunrise was subtracted from an equal run after sunrise; and an hour run after mesospheric sunset was compared to an hour run ending before sunrise in the mesosphere to detect any spectral change between those times.

4.2.2. BROAD BAND EMISSION MEASUREMENTS. The broad band emission measurements made at MIT and Lincoln Laboratory used the processor described in detail by Waters (1970). The I.F. band centered at either 60 MHz (48 MHz wide) or 105 MHz (160 MHz wide) was power split into the corresponding number of channels. Following amplification and detection, the signal was converted to a digital signal by a voltage to frequency converter, up-down counted in synchronism with the Dicke switch, and the accumulated counts punched out on paper tape. The paper tape data was punched onto cards, which were then read into a computer and processed.

5. EXPERIMENTAL RESULTS

Observations were conducted from March to December 1970 concurrently with the radiometer development program. Meaningful data was received, however, only from the last radiometer configuration which was built at the end of August. The effects of both ozone and water vapor were observed.

5.1. EXPERIMENTAL SPECTRA

5.1.1. NARROW-BAND MESOSPHERIC SPECTRA. The presence of a sharp line in the night emission spectra was sought as evidence of the nocturnal increase in mesospheric ozone. A line was never detected despite measurements under many different conditions. The results of the observations considered significant are given in Table I. Observations during periods when the surface water vapor content was greater than 15 gr/m^3 were rejected as the sky was too opaque.

A representative observation is shown in Figure 6. This was taken in the one hour period after mesospheric sunset, when the diurnal variation should occur. It is significant that at the time of the observation the ground water vapor content was low, around 3.5 gr/m^3, so the atmospheric water vapor attenuation is less than that used to predict the emission line. The predicted line, reduced by a factor of two to account for the assumed double sideband response of the radiometer, is that computed. The peak-to-peak variation of the noise is assumed to be $6\Delta T_{rms}$, so the minimum detectable signal, ΔT_{rms}, is about 0.5°K. The 0.2°K/MHz slope is assumed to be instrumental but may be caused by water vapor attenuation. The spectra have not been edited and are extracts of the processor output. The integration periods were accumulated normally in ten minute periods with a calibration performed between integrations. The base line was stable, and the system temperature would change about 500°K over one hour. This represents a gain change of less than 1/2 dB. Since this was a gradual change, much slower than the 5 Hz switch rate, it is felt that the Dicke switching was effective.

5.1.2. BROAD BAND STRATOSPHERIC SPECTRA. In addition to the search for the mesospheric emission line, a search for the stratospheric ozone emission line was also made. If successful, detection of the line would confirm both the operation of the radiometer and the frequency of the ozone line. The width at half height of the stratospheric ozone line is about 50 MHz, so a broad band system was required.

The radiometer was used to make broad band emission measurements using the MIT Digital Synchronous Detector System designed by Waters (1970). The emission spectrum taken on the night of September 2, 1970 is shown in Figure 7. The predicted spectrum is the day emission spectrum and it has been reduced by a factor of 2. The temperature scale is marked with respect to the balanced antenna temperature.

6. CONCLUSIONS AND DISCUSSION

6.1. CONCLUSIONS

Our experiments do not support the analysis of Hunt which predicts that the mesospheric ozone near 70 km altitude increases diurnally to around 5×10^{10} cm^{-3} at night from a daytime concentration of about 10^9 cm^{-3}.

We have considered the effect of the tropospheric and lower stratospheric ozone changes. Ozonesondes are launched from L.G. Hanscom Field each Friday afternoon. The ozone profiles from these probes were used in the model and the expected line calculated. The predicted night mesospheric line is insensitive to the changes in ozone profile below 30 km that occur in the vicinity of Bedford, Massachusetts.

To check the possibility that the ozone distribution at night was different from Hunt's calculated one, several ozone profiles were modeled as shown in Figure 8. The profile of Reed, a sharp peak distribution at 76 km, and exponential decreases from the concentration at 50 km with different slopes were used. Most observations and theories agree to about 50 km, so that is the breakpoint chosen.

The anticipated line strengths in a 4 MHz bandwidth are shown in Figure 9. The sensitivity of our instrument is adequate to detect a 2°K line strength in this bandwidth.

We conclude, therefore, that if the mesospheric ozone increases at night, it does not exceed an exponential distribution with a concentration of 10^9 cm^{-3} at 80 km. Our observations indicate that the night concentration is similar to the concentration observed by Johnson, et. al. and Hilsenrath's daylight probe.

6.2. DISCUSSION

The question of why the mesospheric ozone concentration does not increase at night might better be phrased as should the ozone concentration increase at night in the mesosphere. The answer lies in the equations of the photochemical theory which predicts it. In short, the reaction rates are so poorly known that a positive statement based on these equations is unjustified.

Another weakness in the photochemical theory is that dynamical equilibrium is assumed. Neither molecular and eddy diffusion, nor the large scale transport of ozone from the tropics is considered in the theory. It is a crude theory from this point of view.

The water vapor concentration in the mesosphere affects the ozone concentration appreciably. See Waters (1970) for an extensive bibliography on atmospheric water vapor. When Hunt added water vapor to his model (1966a in contrast with 1966b) the computed night concentration of ozone at 80 km dropped by a factor of 30. It may be significant that at 70 km Bates and Nicolet used slightly higher water vapor concentrations than did Hunt (1966b). The night ozone concentration predicted by Bates and Nicolet is within the upper limit observed in this experiment. It is of further interest to note that Hesstvedt (1964) concluded that the water vapor mixing ratio begins to drop off from 2×10^{-4} at 68 km to about 5×10^{-6} at 80 km. This is much higher than that used by either Bates and Nicolet or Hunt, but the ozone concentration computed by Hesstvedt is correspondingly much lower. Hesstvedt found that the ozone number density at 70 km was 2×10^6 and that there was no diurnal change in the ozone concentration. Since so few measurements of either water vapor or ozone have been made above 50 km, it would only be speculation to say that water vapor mixing ratios around 10^{-5} at 70 km account for the low mesospheric ozone concentration.

To state that the ozone concentration increases at night implies that the concentration can be measured both before the event occurs and after the event occurs. Of all the techniques used, only a microwave radiometric observation can readily make that kind of an observation. The result shows that the ozone concentration does not increase above an exponential distribution reaching 10^9 cm^{-3} at 80 km.

TABLE I. MESOSPHERIC OZONE OBSERVATIONS

Date	Time	PH_2O(8r/m^3)	Integration Time (sec)	ΔT_{rms}(°K)	Experiment
22 Oct	1800-1900	13	4,000	0.3	Post sunset (20 MHz)
20 Oct	1800-1900	4	4,000	0.2	Post sunset (4 MHz)
17 Oct	1800-1900	3.5	4,000	0.5	Post sunset (4 MHz)
18 Oct	2300-0400	5.5(Avg)	22,000	0.15	Night emission (4 MHz)
	0630-0730	8.5	4,000	0.3	Post sunrise (4 MHz)
14 Oct	2200-2300	9.9	2,400	0.3	Night emission (4 MHz)
	2400-0100	9.9	3,000	0.25	Night emission (20 MHz)
	0400-0800	9.9	3,600	0.4	Night emission -Post sunrise (4 MHz)
6 Oct	2300-0600	12	19,279	0.2	Night emission (4 MHz)
5 Oct	2200-0230	8	4,000	0.4	Night emission E-plane Vertical (4 MHz)
		8	4,000	0.4	Night emission E-plane Horizontal (4 MHz)
24 Sep	2300-0400	10.5	4,000	0.6	Night emission, High resolution (0.4 MHz BW)

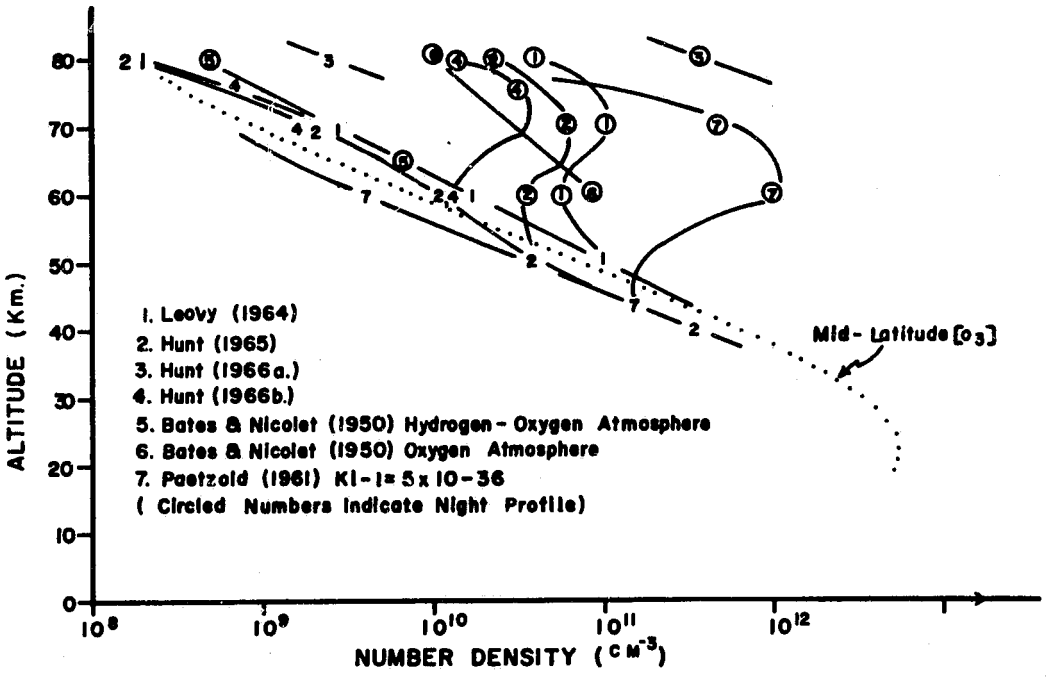


FIGURE 1. COMPARISON OF PREDICTED OZONE CONCENTRATION PROFILES.

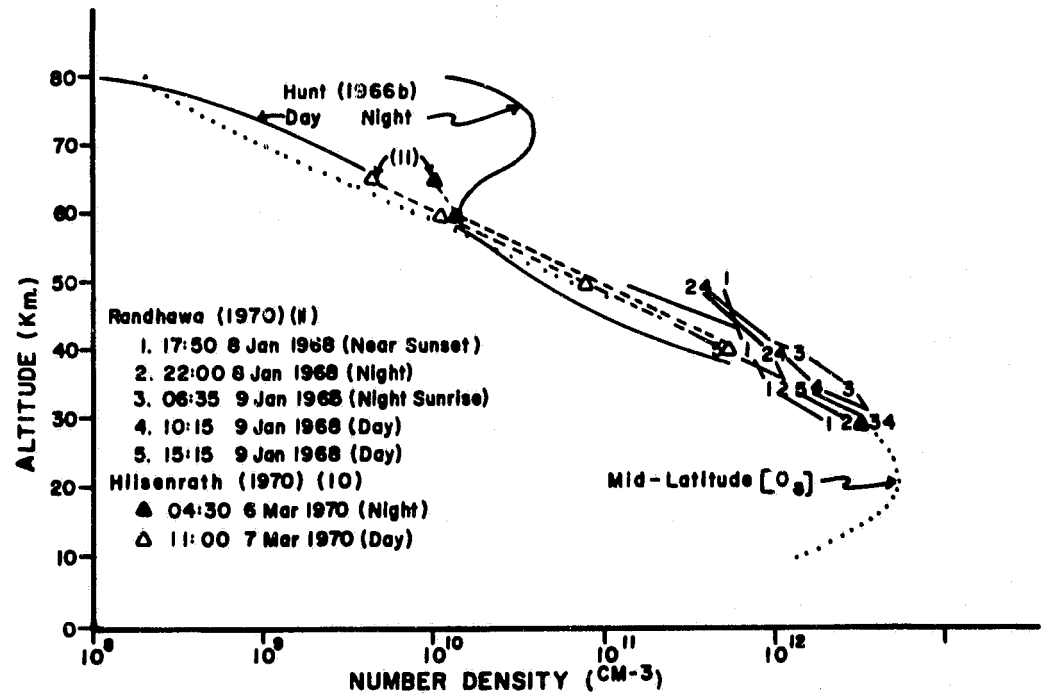


FIGURE 2. OZONE CONCENTRATION PROFILES MEASURED DIURNALLY

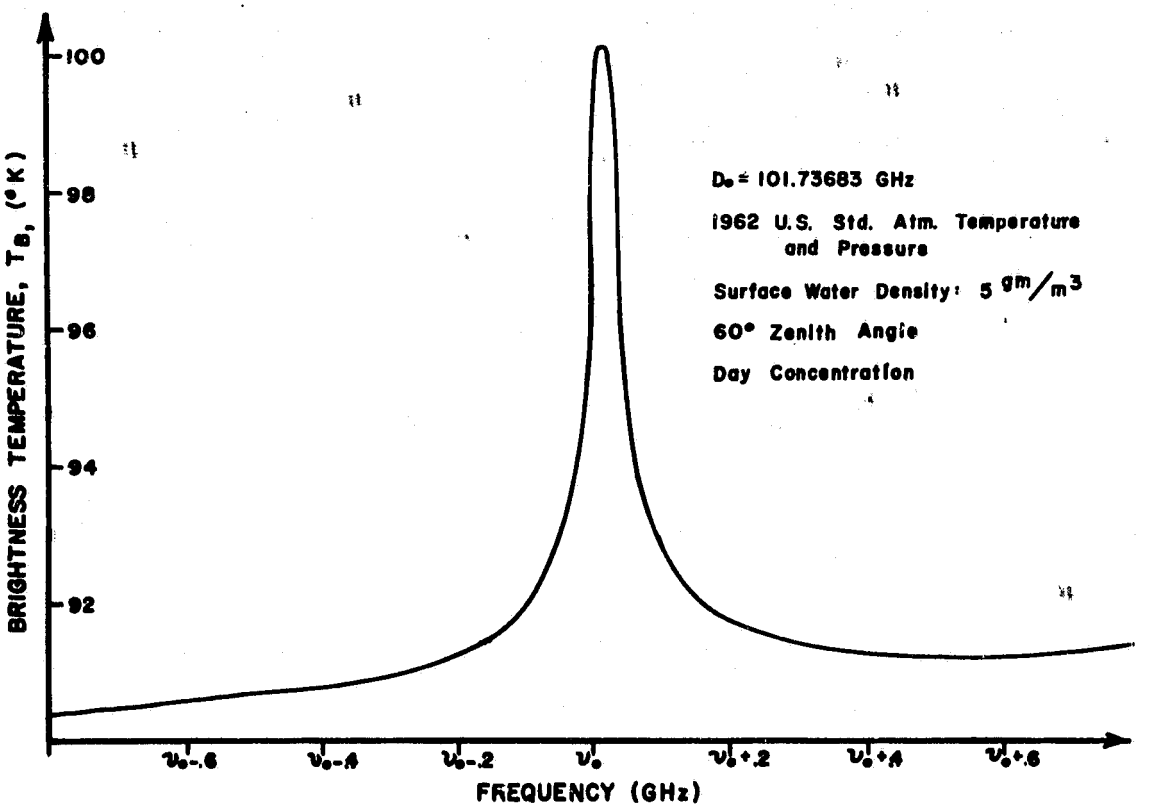


FIGURE 3. COMPUTED BRIGHTNESS TEMPERATURE FOR THE ASSUMED DAY OZONE CONCENTRATION PROFILE.

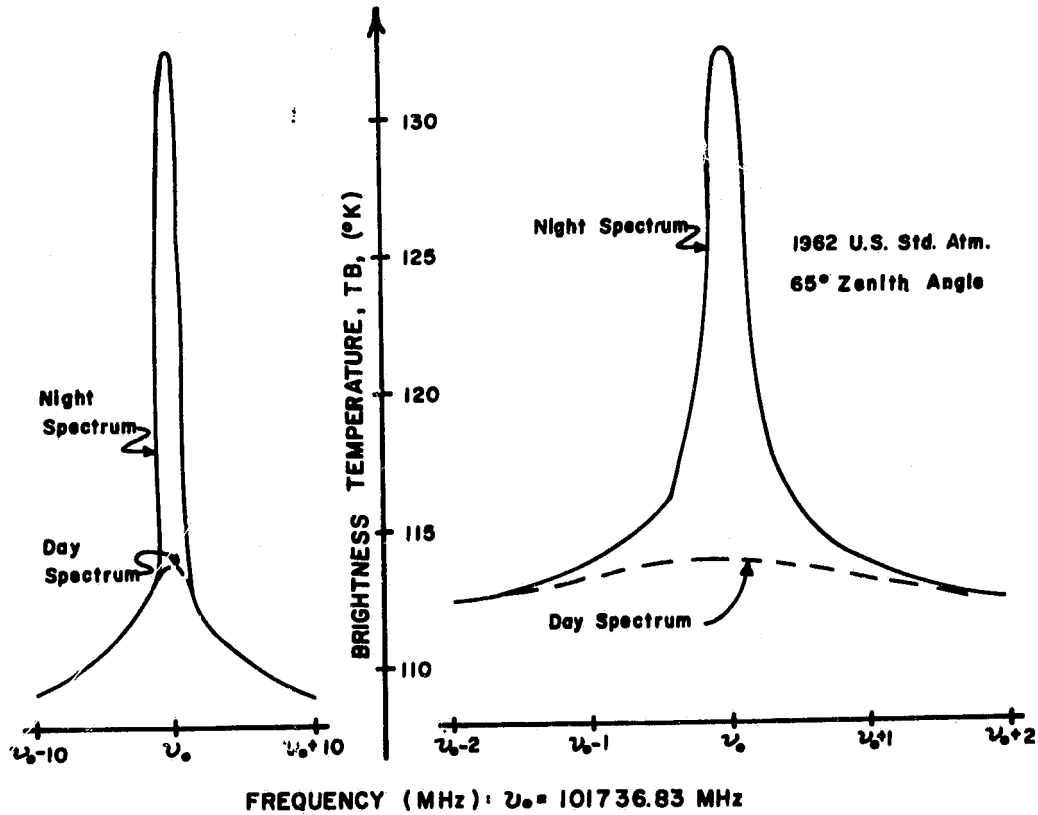


FIGURE 4. COMPARISON OF DAY AND NIGHT SPECTRA.

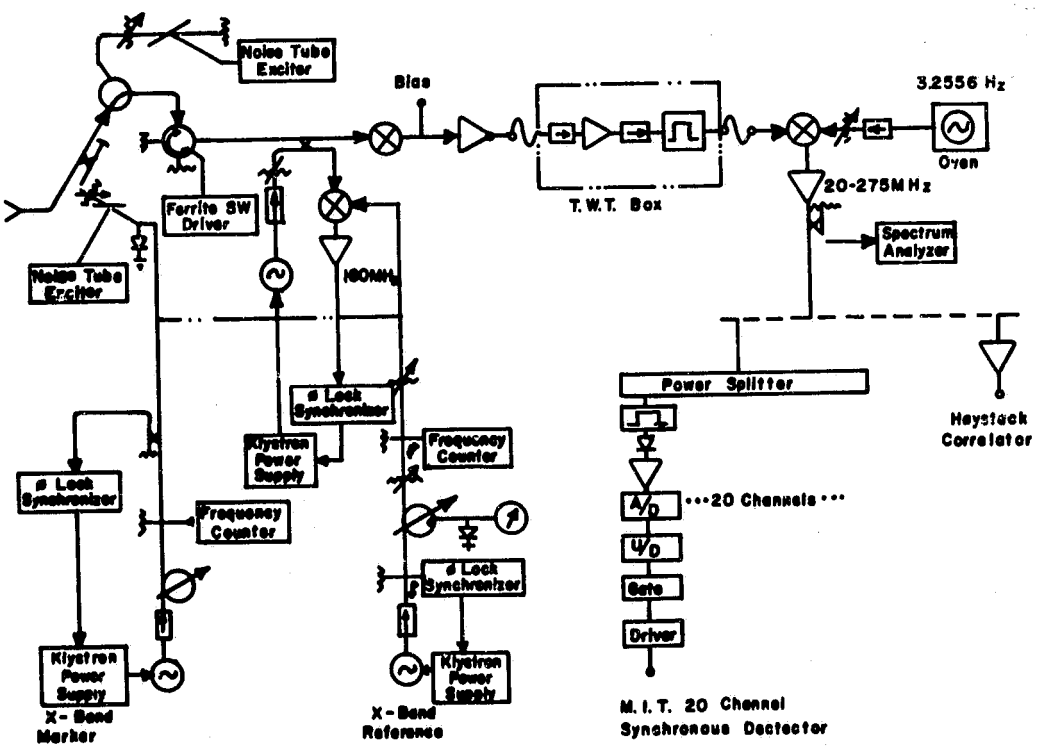


FIGURE 5. RADIOMETER CIRCUIT.

STAELIN 1 OZONE SEARCH, 101 GHZ RUDZKI
SUNSET EMISSION MSMT, HORN NORTH, 30 DEG ELEV
TREF= 9C, TANT=-106.8, NT BAL 8.1DB, TEMP=41F
WX: BOS1700, T=43, RH=49, ALT29.92R, N WIND 25, SKY CLEAR.
T(21-181)

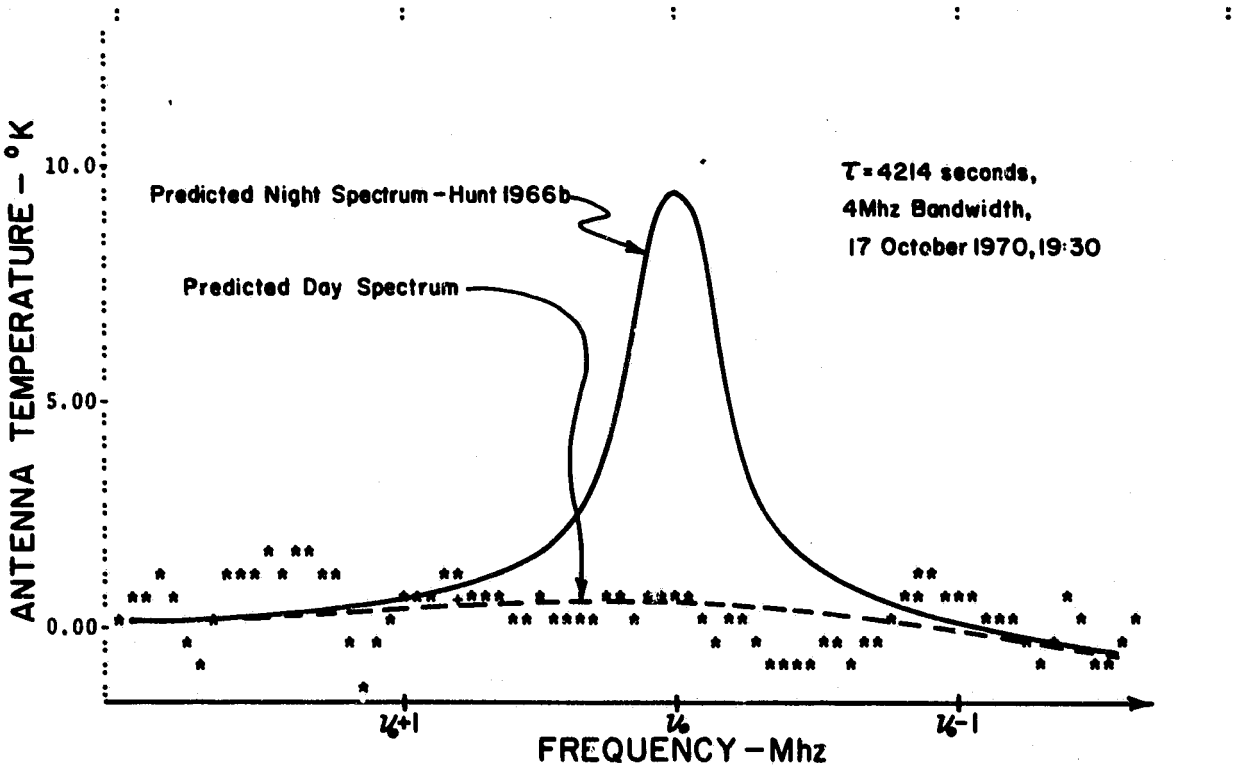


FIGURE 6. NIGHT EMISSION SPECTRA.

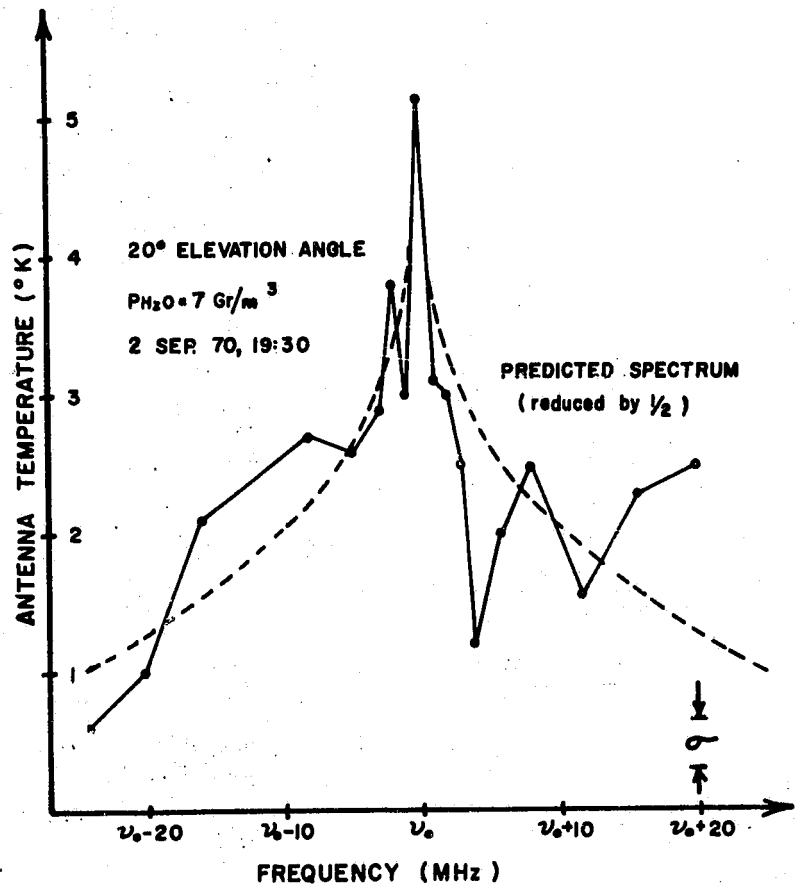


FIGURE 7. BROADBAND EMISSION LINE, 20° ELEVATION ANGLE.

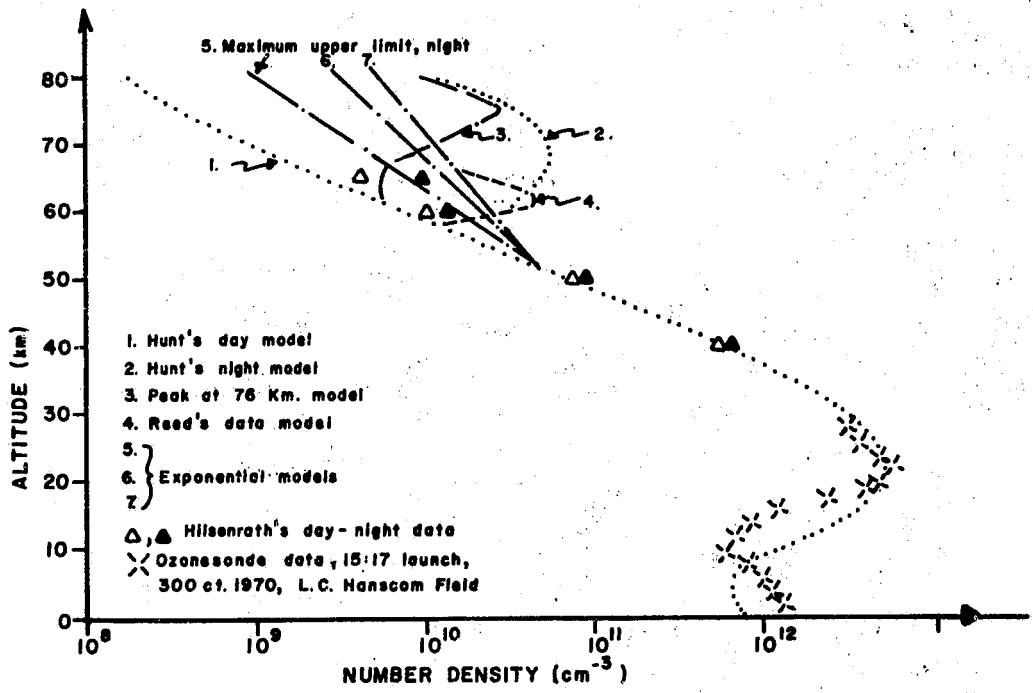


FIGURE 8. MODEL OZONE CONCENTRATION PROFILES AND OZONESONDE DATA.

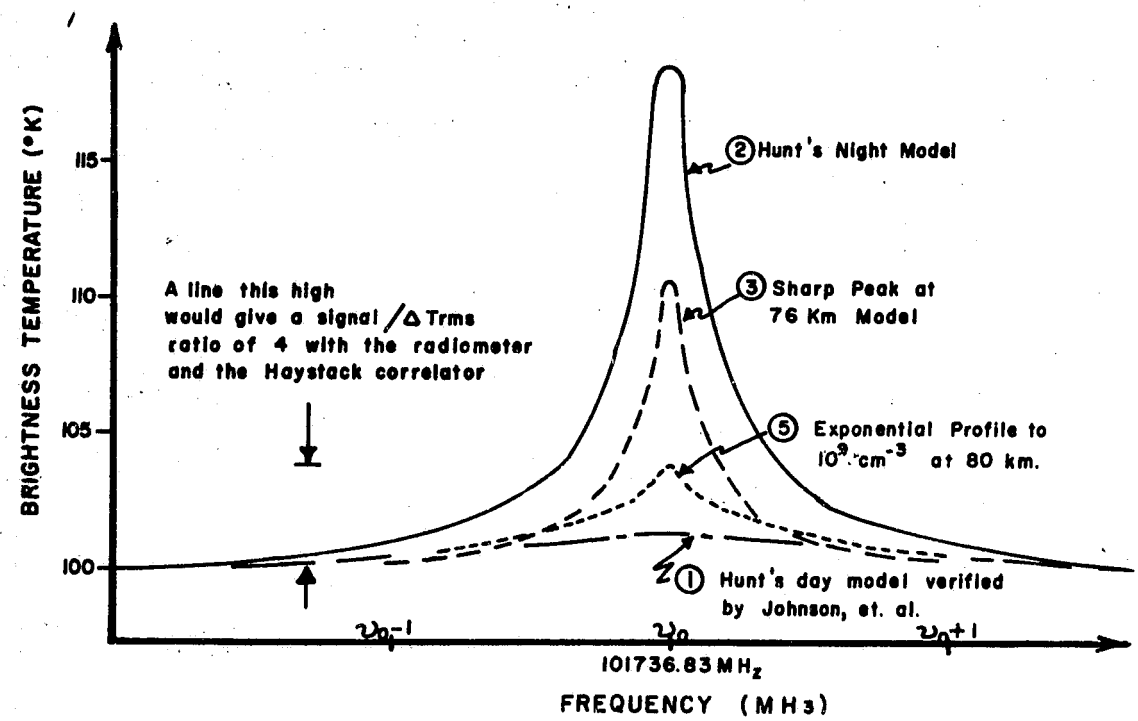


FIGURE 9. COMPARISON OF CALCULATED BRIGHTNESS TEMPERATURES AND SYSTEM SENSITIVITY.

BIBLIOGRAPHY

Barrett, A. H., R. W. Neal, D. H. Staelin, and R. M. Weigand, 1967, "Radiometric Detection of Atmospheric Ozone," Quart. Prog. Report #86, Res. Lab. of Electronics, MIT, p. 26.

Bates, D. R. and M. Nicolet, 1950, "The Photochemistry of Atmospheric Water Vapor," J. Geophys. Res., 55, p. 301.

Caton, W. M., G. C. Mannella, P. M. Kalaghan, A. E. Barrington, and H. I. Ewen, 1968, "The Radio Measurement of the Atmosphrric Ozone Transition at 101.7 GHz," Astrophys. J., 151, L153.

Caton, W. M., W. J. Welch, and S. Silver, 1967, "Absorption and Emission in the 8-mm Region by Ozone in the Upper Atmosphere," Space Sci. Lab., U. C. Berkeley, ser. 8, issue 42.

Chapman, S., 1930a, "A Theory of Upper Atmospheric Ozone," Quart. J. Roy. Met Soc., 3, p. 103.

Chapman, S., 1930b, "On the Annual Variation of Upper Atmospheric Ozone," Phil. Mag., 10, p. 345.

Conant, G. H., Jr. and M. L. Meeks, 1968, "Radiometer Spectral-Line Processing in the Haystack Antenna Pointing System," MIT Lincoln Lab. Tech. Note 1968-1.

Dobson, G. M. B., 1930, "Observations of the Amount of Ozone in the Earth's Atmosphere and Its Relation to Other Geophysical Conditions," part IV, Proc. Roy. Soc. London, A129, p. 411.

Fabry, C. and M. Buisson, 1933, "L'absorption de l'ultraviolet par l'ozone et la limite du spectre solaire," J. Phys. Rad., Ser. 5, 3, p. 196.

Gora, E. K., 1959, "The Rotational Spectrum of Ozone," J. Molecular Spectroscopy, 3, p. 78.

Gordy, W., W. V. Smith, and R. F. Tranbarulo, 1953, Microwave Spectroscopy, Wiley, N.Y.

Gotz, F. W. P. and G. M. B. Dobson, 1928, "Observations of the Height of the Ozone in the Upper Atmosphere," Proc. Roy. Soc. London, A120, p. 251.

Gotz, F. W. P., A. R. Meetham and G. M. B. Dobson, 1934, "The Vertical Distribution of Ozone in the Atmosphere," Proc. Roy. Soc. London, A145, p. 416.

Hesstvedt, E., 1964, "On the Water Vapor Content in the High Atmosphere," Geofysiske Publikasjoner, Geophysica Norvegica, 25, No. 3, p. 1.

Hunt, B. G., 1965, "A Non-equilibrium Investigation into Diurnal Photochemical Atomic Oxygen and Ozone Variations in the Mesosphere," J. of Atmos. and Ter. Phys., 27, p. 133.

Hunt, B. G., 1966a, "The Need for a Modified Photochemical Theory of the Ozonesphere," J. Atmos. Sci., 23, p. 88.

Hunt, B. G., 1966b, "Photochemictry of Ozone in a Moist Atmosphere," J. Geophys. Res., 71, No. 5, p. 1385.

Leovy, C. B., 1964, "Radiative Equilibrium of the Mesosphere," J. Atmos. Sci., 21, p. 238.

Maeda, K. and A. C. Aikin, 1968, "Variations of Polar Mesospheric Oxygen and Ozone During Auroral Events," Planet. Space Sci., 16, p. 371.

Mouw, R. B. and S. Silver, 1960, "Solar Radiation and Atmospheric Absorption for the Ozone Line at 8.3 Millimeters," Insti. Eng. Res., U. C. Berkeley, ser. 60, issue 277.

Paetzold, H. K., 1961, "The Photochemistry of the Atmospheric Ozone Layer, Chemical Reactions in the Lower and Upper Atmosphere," Proc. Int. Sym., Stanford Res. Insti., Interscience, 181.

Regener, E. and V. H. Regnner, 1934, "Aufnahmen des ultravioletten Sonnenspektrums in der Stratosphare und die vertikale Ozonverteilung," Phys. Z., 35, p. 788.

Townes, C. H. and A. L. Schawlaw, 1955, Microwave Spectroscopy, McGraw-Hill, N.Y.

Trambarulo, R., S. N. Ghosh, C. A. Burrus, Jr., and W. Gordy, 1953, "The Molecular Structure, Dipole Moment, and a g Factor of Ozone from its Microwave Spectrum," J. Chem. Phys., 21, p. 851.

VanVleck, J. H. and V. F. Weisskopf, 1945, "On the Shape of Collision-Broadened Lines," Rev. Mod. Phys., 17, No. 2&3, p. 230.

Waters, J. W., 1970, "Ground-Based Microwave Spectroscopic Sensing of the Stratosphere and Mesosphere," Ph.D. Thesis, MIT Dept. of Elec. Eng.

Weinreb, S., 1963, "A Digital Spectral Analysis Technique and its Application to Radio Astronomy," Res. Lab. of Electronics, Tech. Report #412, MIT.

SOME RESULTS OF SPECTROPHOTOMETRIC STUDIES OF NATURAL FORMATIONS FROM THE MANNED SPACECRAFT "SOYUZ-9"

K. Ya. Kondratyev
A. A. Buznikov
O. B. Vasilyev
B. V. Vinogradov
V. M. Orlov
V. I. Sevastyanov
O. I. Smokty

Leningrad University
Institute of Physics
Leningrad
USSR

Results are given of spectrophotometric measurements of natural formations performed with the help of the handheld spectrograph RSS-2 installed on the "Soyuz-9" spacecraft. Comparison is made with the data of the surface spectrophotometric measurements.

Manned space flights and interplanetary missions of automated stations open up great opportunities for the study of the earth's surface including investigations of its resources using optical, radar, and other methods of observation [1, 2, 3].

Currently, the largest amount of information from space on the state of the environment is obtained by investigation methods connected with the interpretation of photographic or television images of the objects observed. These serve as a basis for a complex analysis of space-time variability of various characteristics of natural formations [2]. However, the data on the spatial distribution of brightness in a spectral region determined by the sensitivity of a photographic film are not sufficient for a unique description of the properties of the objects observed. For studying the characteristics of natural objects, quantitative methods are needed. From this point of view, the spectra of the solar radiation reflected by natural formations have significant informational content.

The first spectra of solar radiation reflected by natural objects were obtained during the "Soyuz-7" space flight [4, 7]. The spectra both of the cloud cover and of the desert surface have been studied. Yet, the sparse data obtained showed only the possibilities of the solution of some problems of space spectrophotometry.

The eighteen-day "Soyuz-9" flight permitted one to extend the programme of spectral investigations and to perform spectrophotometric measurements of natural formations in different areas of the globe.

1. TECHNIQUE FOR OBTAINING SPECTRA

Spectrophotometric measurements of the earth's surface from the manned spacecraft "Soyuz-7" and "Soyuz-9" were made with the help of the spectrograph RSS-2 [5 - 8]. An autocollimation scheme is used in this instrument. The diffraction grating has 600 lines/mm. The focal distance of the

collimator is 110 mm, its aperture ratio being 1:4. The height of the entrance slit is 6 mm; its width is 0.3 mm. The linear dispersion of the spectrograph is 16 nm/mm; the spectral resolution is about 5 nm. The measured radiation flux is recorded on photofilm sensitive in the region of 400 + 700 nm. The entrance objective has a focal distance of 135 mm.

Photos of the spectra obtained were processed on the microphotometer MF-4. Values proportional to the density of the blackening of the exposed film were recorded on microphotograms. Simultaneously a calibration grid was printed. To obtain spectral brightnesses of the objects investigated, the film was calibrated (the transition was made from the optical densities to the amount of illumination of the photofilm).

In the "Soyuz-9" experiments, with the purpose of calibrating photoemulsion, thirteen pictures of a standard radiation source spectrum were taken on the same film using different neutral filters. Thus, the densities of blackening were obtained for the known energies and characteristic curves were drawn. For obtaining absolute values of energy, characteristic curves for all the wavelengths were standardized with respect to the sun. Brightness of the diffusely transmitting milk glass illuminated by the sun was taken as a standard source. The brightness coefficients of the glass were measured in the laboratory. Standardization of measurements with respect to the sun and spectrophotometric measurements of the underlying surface were performed through the same porthole of the spacecraft, therefore the transmission coefficient of the latter was excluded from measurements.

All the computations including the construction of the graphs of characteristic curves and a calculation of brightness of underlying surfaces from the negatives of spectra were made on the computer "Minsk-22".

2. SPECTRA OF NATURAL FORMATIONS

From the "Soyuz-9" RSS-2 measurements, spectral brightness coefficients of different types of underlying surfaces were obtained. Account was taken of a sun elevation above the horizon at the subsatellite point. The sun's elevation was found from the moment of photography and the coordinates of this point which, in turn, were determined from the parameters of the orbit.

Table 1 presents the spectral brightness coefficients measured. Figures preceded by a dash denote the number of the frames and profiles (all the area covered by the slit was separated into 19 equal portions, 0.45 x 0.45 km^2 in size).

The spectral brightness coefficients derived are in good quantitative agreement with the theoretically expected picture which takes into account the influence of the atmospheric transfer function [6]. In the shortwave spectral region, the spectral brightness coefficients are considerably higher as compared to those derived in the ground-based measurements, which is particularly noticeable for the underlying surfaces having, in this spectral region, a small reflection coefficient. In the longwave region, the difference between the spectral brightness coefficients measured at the level of the earth's surface and from space is small. Let us dwell, in greater detail, upon the spectral peculiarities of the individual natural formations observed according to their classes.

Vegetation. A marked increase of spectral brightness coefficients in the "green" ($\lambda \approx 550 + 560$ nm) and the decrease in the "red" ($\lambda > 600$ nm) and "blue" ($\lambda < 500$ nm) regions are characteristic of the vegetation spectra shown in Fig. 1, the values of the spectral brightness coefficients for vegetation ranging from 0.12 to 0.35. The "green" maximum is small:

$$K_1 = \frac{\tau_{490}}{\tau_{550}} \quad \text{and} \quad K_2 = \frac{\tau_{640}}{\tau_{550}}$$

reaching the values of 0.74 - 0.85 and 0.57 - 0.84 respectively. Variations in spectral brightnesses of these surfaces are related to the changes occurring in the atmospheric transparency, in the optical properties of the visible soil surface, and in the density and type of vegetation. So, the dense gygrophyle vegetation of the swamps (curves 2.92 - 10 and 2.50 - 12) is characterized by a decrease in the spectral brightness coefficients at the wavelengths of 550 nm to 640 nm, which is evidently associated with the distinctness of the vegetation absorption band and the integration of the vegetation image with the image of the moist dark soil. The mesophyle vegetation of smaller density and lighter color (Fig. 1a, profile 2.97 - 10) produces the sharpest "green" maximum. Spectral brightness coefficients are about 0.33 - 0.34 at λ = 550 nm and about 0.28 at λ = 640 nm. Xercmesophyle vegetation (Fig. 1a, profile 2.93 - 04) has slightly smaller values for the spectral brightness coefficients (as compared to the mesophyle vegetation) with the pronounced maximum at λ = 550 nm ($r_{550} = 0.30$ and $r_{640} = 0.23$).

Finally, the area with the xerophyle semidesert vegetation (Fig. 1, profile 2.50 - 10) whose density is lower than 60% has a more pronounced spectral variation of the spectral brightness coefficient with the values of about 0.18 to 0.22 (which may be due to the soil seen through the vegetation).

The "red" spectral region is raised (as compared to the spectra of vegetation). This may be explained by a small vegetation coverage of the soil - the soils are visible and raise the curve in the minimum of the chlorophyle absorption.

Outcrops, soils. The larger portion of the land spectra free of clouds belongs to the class of soils, soil-eluvium formations, quaternary deposits and outcrops since the desert and semi-desert vegetation of the Near East and Middle Asia is sparse and xerophyle. As a rule, it does not noticeably affect the spectral reflectances of the landscape; the surface of the soil in these areas during the flight was dry. Spectral brightness curves of the desert and semi-desert surface mostly covered by soil-elvium formations have the smoothest spectral variation with weakly pronounced increases in the red specgrum. Rather high values for spectral brightness coefficients, about 0.2 - 0.3, prevail over the whole spectrum. Their variations depend on the lithological composition of the soil-eluvium formations. Stone and stone-rubble deserts produce spectral brightness coefficients of 0.19 - 0.26, sand and loam soils give 0.22 - 0.32 (Fig. 1b, profiles 2.50 - 0.2, 2.50 - 0.4 and 2.51 - 10). The brightness of the surface particularly increases when the suspended dust and sand are present in the atmosphere. Sand-clay deposits have a more distinct increase, up to 0.30, in spectral brightness coefficients in the "red" spectral region (λ = 610 - 670 nm). All t curves have small maxima near λ = 550 + 560 nm, which is evidently explained by the presence of a small amount of vegetation on the soils.

Water, snow and cloud surfaces. The water surface is characterized by the lowest values for spectral brightness coefficients, in particular, in the "red" region (λ > 610 - 630 nm) and by the most monotonous variation in brightness with a gradual increase in the spectral brightness coefficient in the "light blue" region. The minimum values of the spectral brightness coefficients (0.07 - 0.08) are observed at λ > 630 nm, the increased values ($\sim$ 0.14 - 0.19) being observed in the "green-blue" region at λ = 490 - 570 nm (Fig. 1c, profiles 2.50 - 15, 2.93 - 14, 2.92 - 03). The water reflection spectra just as the spectra of other surfaces are characterized by the influence of atmospheric haze. Spatial variations of spectral brightness coefficients of the water surface are slight. The water reservoir spectra obtained are characterized by small maxima at λ = 550 - 560 nm, which indicates shallows and to the presence of vegetation in the water. A gradual transition from the water spectra to those of water vegetation can be observed.

In the photographs obtained, snow surfaces do not form continuous fields and are included in the field of spectrophotometric measurements together with the vegetation, outcrops and clouds. In a region of 610 nm they are characterized by high spectral brightness coefficients ($\tau_\lambda \geq 0.6$) with a marked decrease in the "red" region (λ > 610 nm).

As seen in the photographs, a large area is covered by clouds. Its spectral brightness coefficients strongly vary depending on the density, thickness and type of cloudiness and the composition of the underlying surface. In general, cloudiness has mean values for spectral brightness coefficients > 0.6 at λ = 460 - 600 nm, their decrease is observed in the "red" region at λ = 610 - 630 nm. Brightness variations associated with the appearance of semiopaque cloudiness of Ci and Ac types as well as with the breaks in cloudiness and the amount of clouds less than 0.9 lead to the decrease in spectral brightness coefficients at λ = 460 - 610 nm. Drop in spectral brightness coefficients is particularly seen in the region at λ > 610 ÷ 630 nm.

The spectra of snow surfaces and cloudiness are rather similar.

3. COMPARISON WITH THE GROUND-BASED MEASUREMENTS, THE ATMOSPHERIC TRANSFER OPERATOR AND IDENTIFICATION OF THE SPECTRA OBTAINED

Investigations of the spectral brightness coefficients and the albedo of natural formations measured at the earth's surface and from the aircraft have been performed for a number of years (see e. g.,9[9, 10]). Compare the results of "Soyuz-9" and ground-based spectrophotometric measurements of the same objects.

"Space" curves for spectral brightness coefficients of soils and outcrops have a less pronounced spectral dependence as compared to the ground spectra. For example, $K_{640/550}$ of soils under the ground conditions is 1.3 - 1.5, whereas, from space it is equal to 1.1 - 12. The total brightness of the soil and geological formations observed from space increases, which is particularly pronounced: (1) in the blue-green region (λ = 450 + 500 nm) where the atmospheric

haze brightness increases the brightness coefficients by 0.10 - 0.15 and (2) in the green-orange region (λ = 500 + 600 nm) where the brightness coefficients are increased by 0.05 - 0.10. In some cases, spectral brightness coefficients are increased in the "red" region at λ > 600 nm (Fig. 2).

The fact that the ecological types of vegetation were clearly differentiated from space spectra was quite unexpected since the vegetation spectra obtained from space are considerably distorted as compared to the ground spectra.

Distinctness of the "green" maximum of brightness sharply falls from K $\sim$ 0.4 (under the ground conditions) to K $\sim$ 0.75 - .85 (in space). This is explained by the superposition of the brightness of the atmospheric haze, which being over a surface with more or less dense vegetation always increases the brightness coefficients by $\sim$ 0.10 - 0.12 at λ = 490 nm.

Water surfaces measured from space produce higher brightness coefficients as compared to the ground conditions. Quantitative characteristics of spectra are also changed. The maximum of the brightness coefficient at λ = 530 nm is not pronounced - it is completely overlapped by the superposition of the atmospheric haze whose brightness at λ < 500 nm increases the coefficient by 0.10 - 0.15.

Spectral brightness coefficients of snow surfaces measured from space have a spectral variation with a stronger decrease in the "red" region (as compared to the ground measurements). On an average, brightness coefficients measured from space are by about 0.2 lower than those obtained under ground conditions. A marked decrease in brightness coefficients in space spectra at λ = 600 nm is evidently due to breaks in cloudiness and to the influence of the light-to-shade structure of the cloud-field surface.

The atmospheric influence on the spectra of natural surfaces obtained from space, as compared to the ground measurements, can be described by the "transfer function" or the "atmospheric transfer operator" [6]:

$$\tau_x^{\infty} = \tau_x^{o} \; t_x + \tau_\lambda^{h},$$

where τ_λ are spectral brightness coefficients at the earth's surface, τ_λ^{∞} are spectral brightness coefficients measured from space, t_x is the spectral factor of the atmospheric attenuation and τ_λ^{h} is the spectral brightness coefficient of the atmospheric haze. Using the published data on τ_λ^{o} for the types of surfaces considered [10] the values for t_λ and τ_λ^{h} have been calculated for the conditions of the experiment considered (Table 2).

The parameters of the atmospheric transfer operator given in Table 2 can be used for the reductions to the earth's surface of the natural formation spectra obtained from space.

To use the reflection spectra of natural formations for the identification of the latter, it is necessary to work out a spectral parameterization technique allowing the quantitative approach to the solution of the identification problem. To check a smiliar approach, the natural formation spectra were coded according to the one-dimensional system of coding proposed in work [11]. From the codes obtained, the identification of spectra was made. Table 3 presents the results of coding and of identification of the "Soyuz-9" spectra which indicate an efficiency of the technique applied.

λ, nm	400	450	500	550	600	650	700
τ_λ^{h}	0.17	0.14	0.12	0.10	0.08	0.07	0.06
t_x	0.65	0.74	0.80	0.84	0.88	0.91	0.94

TABLE 2

Hence, the processing of the spectrograms obtained showed a real possibility of the identification of underlying surfaces and of the study of their characteristics from the reflection spectra measured from the spacecraft or a long-duration orbital station.

REFERENCES

1. K. Ya. Kondratyev, Satellites and the Problem of Earth's Resources. "Znanie", Moscow, 1971.

2. B. V. Vinogradov, K. Ya. Kondratyev, Space Methods of Terrestrial Studies. Gidrometeoizdat, 1971.

3. B. V. Vinogradov, K. Ya. Kondratyev, V. D. Stepanenko. Kosmich. Issled. Vol. 6, No. 6, 904, 1968.

4. K. Ya. Kondratyev, A. A. Buznikov, B. V. Vinogradov, V. N. Volkov, V. V. Gorbatko, O. I. Smokty, V. M. Orlov. Dokl. Acad. Sci. USSR, Vol. 195, No. 5, 1084, 1970.

5. K. Ya. Kondratyev, A. A.BBuznikov, B. V. Vinogradov, V. N. Volkov, V. V. Gorbatko and O. I. Smokty. Spectrophotometry of the Earth from Manned Spacecraft. Space Research XI, Vol. 1, Akademie-Verlag, Berlin, 619, 1971.

6. K. Ya. Kondratyev, A. A. Buznikov, O. B. Vasilyev, B. V. Vinogradov, V. M. Orlov, O. I. Smokty. Problems of Atmospheric Physics, iss. 10, Leningrad University, 3, 1972.

7. K. Ya. Kondratyev, A. A. Buznikov, O. B. Vasilyev, B. V. Vinogradov, A. A. Grigoryev, Yu. I. Rabinovich, L. I. Chapursky. Dokl. Acad. Sci. USSR, Vol. 196, No. 6, 1333, 1971.

8. A. P. Galtsev, V. V. Michailov, M. N. Sokolsky, Ya. M. Kruger, Yu. I. Brainin, L. B. Alekseev. Problems of Atmospheric Physics, iss. 7, Leningrad University, 171, 1969.

9. E. L. Krinov. Spectral Reflectance of Natural Formations. Acad. of Sciences, USSR, Moscow-Leningrad, 1947.

10. Investigations of Optical Properties of Natural Formations and Their Aerophotographic Image. Collected papers, "Nauka", Moscow, 1970.

11. K. Ya. Kondratyev, O. B. Vasilyev, Z. F. Mironova. Problems of Atmospheric Physics, iss. 10, Leningrad University, 1972.

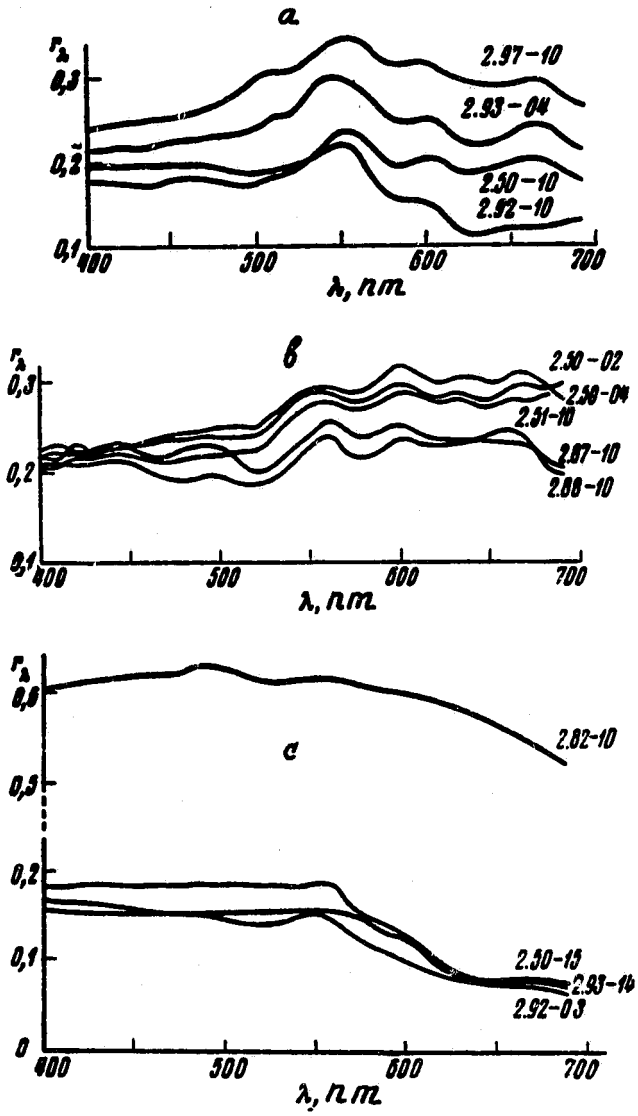


FIGURE 1. Spectral brightness coefficients for the underlying surfaces covered by vegetation - (a) for outcrops and soils; (b) and for water surfaces and cloudiness; (c) according to the data of the "Soyuz-9" spacecraft; a) 2.92 - dense gygrophyle vegetation of swamps and of the banks of lakes of the Mesopotamia lowland, 2.97 - 10 - mesophyle meadow vegetation of small density, southern Azerbaijan, 2.93 - 04 - xeromesophyle steppe vegetation on the edge of the Mesopotamia lowland, 2.50 - 10 - xerophyle sparse semidesert vegetation in the south-west Afganistan; b) 2.87 - 1- and 2.88 - 10 - stone and stone-rubble deposits and soils on the plains of southern Syria, 2.50 - 02, 2.50 - 04 and 2.50 - 10 - sand and loam deposits and soils on the plains of south-west Afganistan; 2.50 - 15 - the lake surface in the south-west Afganistan, 2.93 - 14 and 2.92 - 03 - the lake surface in the Mesopotamia lowland, 2.82 - 10 - cloudiness.

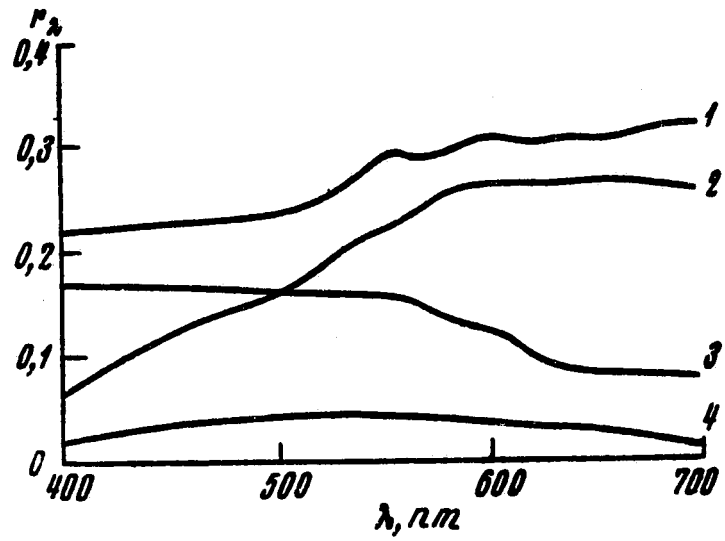


FIGURE 2. Spectral brightness coefficients for two types of the underlying surface as measured from space

(H = 250 km) and the earth's surface (H = 0).

1 - sand (H = 250 km), 2 - sand (H = 0),
3 - water (H = 250 km), 4 - water (H = 0).

λ, nm	Frame, profile														
	2.50-0.2	2.50-0.4	2.50-0.8	2.50-10	2.50-12	2.50-15	2.51-10	2.82-10	2.87-10	2.88-10	2.92-03	2.92-10	2.93-04	2.93-14	2.97-10
1	2	3	4	5	6	7	8	9	10	11	12	13	14	15	16
400	0,222	0,218	0,183	0,181	0,171	0,172	0,208	0,606	0,218	0,209	0,159	0,196	0,215	0,184	0,243
405	0,222	0,220	0,190	0,174	0,170	0,169	0,210	0,608	0,218	0,211	0,157	0,196	0,215	0,181	0,246
410	0,229	0,220	0,193	0,178	0,170	0,165	0,210	0,610	0,217	0,209	0,157	0,196	0,218	0,184	0,243
415	0,221	0,222	0,196	0,178	0,168	0,169	0,215	0,610	0,217	0,206	0,157	0,196	0,218	0,186	0,246
420	0,223	0,221	0,193	0,175	0,170	0,166	0,220	0,612	0,229	0,209	0,157	0,196	0,222	0,184	0,248
425	0,226	0,222	0,194	0,173	0,170	0,165	0,217	0,614	0,229	0,211	0,156	0,196	0,219	0,185	0,247
430	0,225	0,224	0,195	0,174	0,168	0,162	0,220	0,615	0,225	0,211	0,155	0,196	0,219	0,185	0,249
435	0,228	0,226	0,193	0,170	0,164	0,161	0,215	0,617	0,229	0,214	0,155	0,196	0,219	0,186	0,252
440	0,230	0,228	0,195	0,172	0,167	0,160	0,219	0,616	0,230	0,215	0,155	0,196	0,220	0,186	0,254
445	0,229	0,225	0,195	0,173	0,167	0,156	0,220	0,617	0,229	0,214	0,155	0,196	0,224	0,185	0,255
450	0,231	0,228	0,197	0,178	0,165	0,159	0,220	0,619	0,227	0,211	0,154	0,194	0,226	0,184	0,254
455	0,234	0,233	0,197	0,181	0,167	0,156	0,217	0,621	0,222	0,206	0,153	0,193	0,228	0,184	0,257
460	0,233	0,235	0,200	0,180	0,165	0,154	0,215	0,621	0,218	0,201	0,152	0,191	0,228	0,185	0,258
465	0,231	0,238	0,203	0,180	0,164	0,155	0,217	0,621	0,218	0,200	0,150	0,194	0,228	0,185	0,261
470	0,237	0,237	0,204	0,178	0,163	0,152	0,214	0,621	0,218	0,195	0,154	0,195	0,229	0,185	0,264
475	0,236	0,241	0,202	0,175	0,167	0,150	0,212	0,621	0,222	0,192	0,154	0,193	0,231	0,185	0,268
480	0,239	0,244	0,202	0,176	0,162	0,150	0,215	0,621	0,227	0,191	0,154	0,191	0,232	0,186	0,273
485	0,238	0,245	0,205	0,176	0,159	0,146	0,218	0,621	0,227	0,191	0,153	0,187	0,236	0,185	0,278
490	0,240	0,247	0,204	0,173	0,160	0,150	0,219	0,637	0,228	0,197	0,156	0,187	0,237	0,185	0,284
495	0,237	0,247	0,205	0,174	0,161	0,140	0,220	0,645	0,224	0,198	0,155	0,186	0,237	0,185	0,299
500	0,239	0,248	0,207	0,176	0,158	0,146	0,221	0,635	0,219	0,194	0,153	0,186	0,241	0,184	0,303
505	0,242	0,250	0,208	0,180	0,161	0,144	0,218	0,627	0,214	0,189	0,152	0,188	0,250	0,184	0,307
510	0,240	0,251	0,210	0,185	0,163	0,140	0,225	0,624	0,210	0,188	0,153	0,191	0,256	0,184	0,310
515	0,242	0,250	0,212	0,190	0,164	0,138	0,226	0,622	0,206	0,188	0,155	0,193	0,258	0,181	0,310
520	0,240	0,248	0,209	0,189	0,163	0,137	0,223	0,611	0,202	0,187	0,154	0,191	0,256	0,183	0,308
525	0,248	0,256	0,216	0,198	0,167	0,140	0,230	0,612	0,206	0,192	0,156	0,196	0,268	0,183	0,312
530	0,268	0,264	0,223	0,204	0,172	0,142	0,238	0,613	0,212	0,197	0,157	0,200	0,281	0,183	0,319
535	0,272	0,276	0,234	0,214	0,180	0,147	0,251	0,624	0,223	0,206	0,159	0,208	0,300	0,182	0,332
540	0,279	0,278	0,237	0,219	0,182	0,149	0,258	0,617	0,220	0,211	0,156	0,210	0,300	0,182	0,336
545	0,286	0,284	0,243	0,227	0,187	0,152	0,268	0,614	0,238	0,221	0,154	0,215	0,301	0,183	0,342
550	0,290	0,289	0,248	0,233	0,195	0,156	0,276	0,610	0,246	0,231	0,153	0,218	0,300	0,187	0,346
555	0,289	0,290	0,252	0,235	0,199	0,159	0,279	0,607	0,252	0,238	0,151	0,217	0,298	0,187	0,344
560	0,290	0,294	0,256	0,236	0,200	0,162	0,282	0,621	0,257	0,241	0,149	0,213	0,295	0,187	0,346

TABLE 1. Spectral brightness coefficients (τ_λ) of natural formations

λ, nm	Frame, profile															
	2.50-0.2	2.50-0.4	2.50-08	2.50-10	2.50-12	2.50-15	2.51-10	2.82-10	2.87-10	2.88-10	2.92-03	2.92-10	2.93-04	2.93-14	2.97-10	
1	2	3	4	5	6	7	8	9	10	11	12	13	14	15	16	
565	0,279	0,284	0,245	0,222	0,187	0,155	0,272	0,618	0,247	0,229	0,138	0,194	0,277	0,173	0,332	
570	0,281	0,299	0,238	0,214	0,177	0,149	0,272	0,613	0,245	0,223	0,131	0,180	0,268	0,164	0,331	
575	0,281	0,291	0,229	0,204	0,170	0,141	0,273	0,612	0,242	0,219	0,125	0,167	0,260	0,154	0,324	
580	0,292	0,294	0,223	0,196	0,165	0,134	0,274	0,610	0,242	0,219	0,119	0,158	0,252	0,147	0,317	
585	0,285	0,299	0,224	0,194	0,162	0,130	0,277	0,608	0,245	0,224	0,115	0,154	0,247	0,143	0,313	
590	0,290	0,306	0,230	0,197	0,159	0,128	0,281	0,606	0,248	0,229	0,110	0,151	0,245	0,140	0,313	
595	0,295	0,313	0,236	0,202	0,156	0,127	0,285	0,605	0,250	0,233	0,105	0,151	0,247	0,136	0,314	
600	0,300	0,320	0,242	0,207	0,157	0,126	0,292	0,600	0,253	0,238	0,101	0,151	0,252	0,130	0,318	
605	0,297	0,316	0,239	0,206	0,154	0,121	0,291	0,598	0,249	0,236	0,096	0,146	0,249	0,119	0,313	
610	0,291	0,310	0,233	0,201	0,148	0,113	0,289	0,595	0,244	0,233	0,092	0,138	0,242	0,107	0,307	
615	0,285	0,302	0,227	0,194	0,139	0,103	0,286	0,593	0,239	0,230	0,086	0,126	0,232	0,097	0,299	
620	0,283	0,299	0,225	0,189	0,133	0,095	0,285	0,590	0,236	0,229	0,082	0,119	0,225	0,090	0,295	
625	0,286	0,301	0,227	0,189	0,130	0,091	0 285	0,585	0,236	0,230	0,079	0,116	0,223	0,086	0,293	
630	0,288	0,306	0,229	0,190	0,129	0,090	0,285	0,585	0,236	0,232	0,079	0,116	0,224	0,084	0,294	
635	0,288	0,309	0,232	0,192	0,130	0,090	0,283	0,580	0,236	0,235	0,079	0,116	0,225	0,082	0,293	
640	0,284	0,308	0,233	0,193	0,130	0,088	0,280	0,576	0,235	0,238	0,077	0,116	0,226	0,080	0,293	
645	0,282	0,304	0,236	0,196	0,132	0,085	0,278	0,573	0,237	0,243	0,075	0,118	0,230	0,078	0,293	
650	0,282	0,300	0,238	0,199	0,134	0,080	0,277	0,567	0,236	0,245	0,072	0,119	0,234	0,075	0,293	
655	0,287	0,304	0,239	0,201	0,135	0,078	0,280	0,563	0,235	0,247	0,072	0,121	0,240	0,075	0,294	
660	0,292	0,308	0,238	0,201	0,134	0,077	0,285	0,558	0,234	0,246	0,072	0,121	0,243	0,075	0,296	
665	0,298	0,313	0,239	0,199	0,130	0,078	0,287	0,554	0,234	0,243	0,074	0,123	0,245	0,076	0,298	
670	0,299	0,311	0,235	0,195	0,126	0,079	0,282	0,546	0,231	0,234	0,073	0,123	0,239	0,075	0,296	
675	0,298	0,306	0,228	0,189	0,13	0 077	0,282	0,541	0,222	0,219	0,072	0,121	0,231	0,075	0,287	
680	0,296	0,296	0,232	0,185	0,124	0,073	0,287	0,534	0,214	0,208	0,071	0,126	0,222	0,078	0,277	
685	0,296	0,288	0,230	0,187	0,120	0,078	0,287	0,526	0,208	0,199	0 069	0,129	0,219	0,083	0,271	
690	0,300	0,281	0,231	0,198	0,125	0,078	0,200	0,520	0,206	0,2 0	0 064	0,130	0,219	0,090	0,268	

TABLE 1. (Continued) Spectral brightness coefficients (τ_λ) of natural formations

Frame profile	H = 250 km			H = 0			K_1	K_2	Code	Identification
	400 nm	550 nm	680 nm	400 nm	550 nm	680 nm				
1	2	3	4	5	6	7	8	9	10	11
2.50 -02	0.222	0.290	0.300	0.079	0.241	0.271	1.12	0.33	1132	Sand
2.50 -04	0.218	0.289	0.281	0.074	0.240	0.251	1.05	0.31	1032	Sand
2.50 -08	0.198	0.248	0,231	0.037	0.190	0.197	1.04	0.19	1011	Soils
2.50-10	0.179	0.233	0.198	0.016	0.185	0.161	0.87	0.09	0801	Vegetation with the visible soil
2.50 -12	0.171	0.195	0.125	0.004	0.127	0.082	0.65	0.03	0601	Vegetation
2.50 -15	0.170	0.156	0.078	0.003	0.080	0.030	0.38	0.04	0.300	Water surface with vegetation
2,51 -10	0.209	0.276	0.287	0.060	0.224	0.257	1.15	0.27	1122	Sand
2.82 -10	0.605	0.610	0.520	0.642	0.625	0.510	0.82	1.03	0806	Snow, clouds
2.87 -10	0.218	0.246	0.224	0.074	0.188	0.189	1.01	0.39	1031	Soil
2.88- 10	0.210	0.231	0.200	0.062	0.170	0.171	1.01	0.36	1031	Soil
2.92 -03	0.158	0.153	0.064	0.002	0.075	0.015	0.20	0.03	0200	Water surface with vegetation
2.92 -10	0.196	0.218	0.130	0.042	0.154	0.087	0.56	0.27	0521	Vegetation
2.93 -04	0.215	0.300	0.219	0.069	0.253	0.184	0.73	0.27	0722	Vegetation with visible soils
2.93 -14	0.183	0.187	0.090	0.022	0.095	0.044	0.46	0.23	0420	Water surface with vegetation
2.97 -10	0.244	0.346	0.268	0.109	0.308	0.237	0.77	0.35	0733	Vegetation with visible soils

TABLE 3. Spectral coding and identification of natural formations.

AIRBORNE INFRARED POLARIMETRY

D. L. Coffeen
Lunar and Planetary Laboratory
University of Arizona 85721

and

J. E. Hansen
Goddard Institute for Space Studies
New York 10025

ABSTRACT

An infrared polarimeter (AEROPOL) was developed for an airborne remote sensing study of terrestrial cloud particle sizes and shapes. The instrument is capable of ±0.1% accuracy for linear polarization, over the range 1.1-3.5μ, with a 1°5 field of view. It uses a rotating wire-grid polarization analyzer, PbS detector cooled with Freon-13, and operates under minicomputer control, giving a polarization least-squares solution each 2.5 seconds. The AEROPOL instrument was flown on the NASA CV-990 aircraft, over a variety of continental and maritime cloud forms.

Linear polarization was measured as a function of phase angle, for a given wavelength. Liquid water clouds exhibit considerable detail in their polarization curves, including a positive cloudbow near 40° phase angle, and negative polarization at phase angles less than 20° and greater than about 100°. Theoretical polarization computations have been made for single and multiple scattering by water spheres, as a function of wavelength, particle size, and cloud thickness. Many features are size-dependent; in particular the exact phase angle of the polarization inversion point is directly correlated with the mean size in the cloud tops. Cloud systems were found with mean particle radii as small as 5μ, and as large as 30μ.

A remarkable curve of polarization versus phase angle was obtained for thick tropical cirrus clouds. Polarization is negative at the large and small phase angles; it is positive from 20° to 145°. There is no indication of a cloudbow or other detailed structure. Theoretical calculations are not yet possible for these crystalline shapes. However it is very easy to differentiate between water and ice clouds based on the observed polarizations.

---

1. INTRODUCTION

The remote determination of cloud particle characteristics is important for terrestrial meteorological studies and predictions, and for planetary atmosphere understanding. The scattering by a single particle contains information on the particle size, shape, and complex refractive index. Our problem is one of inversion

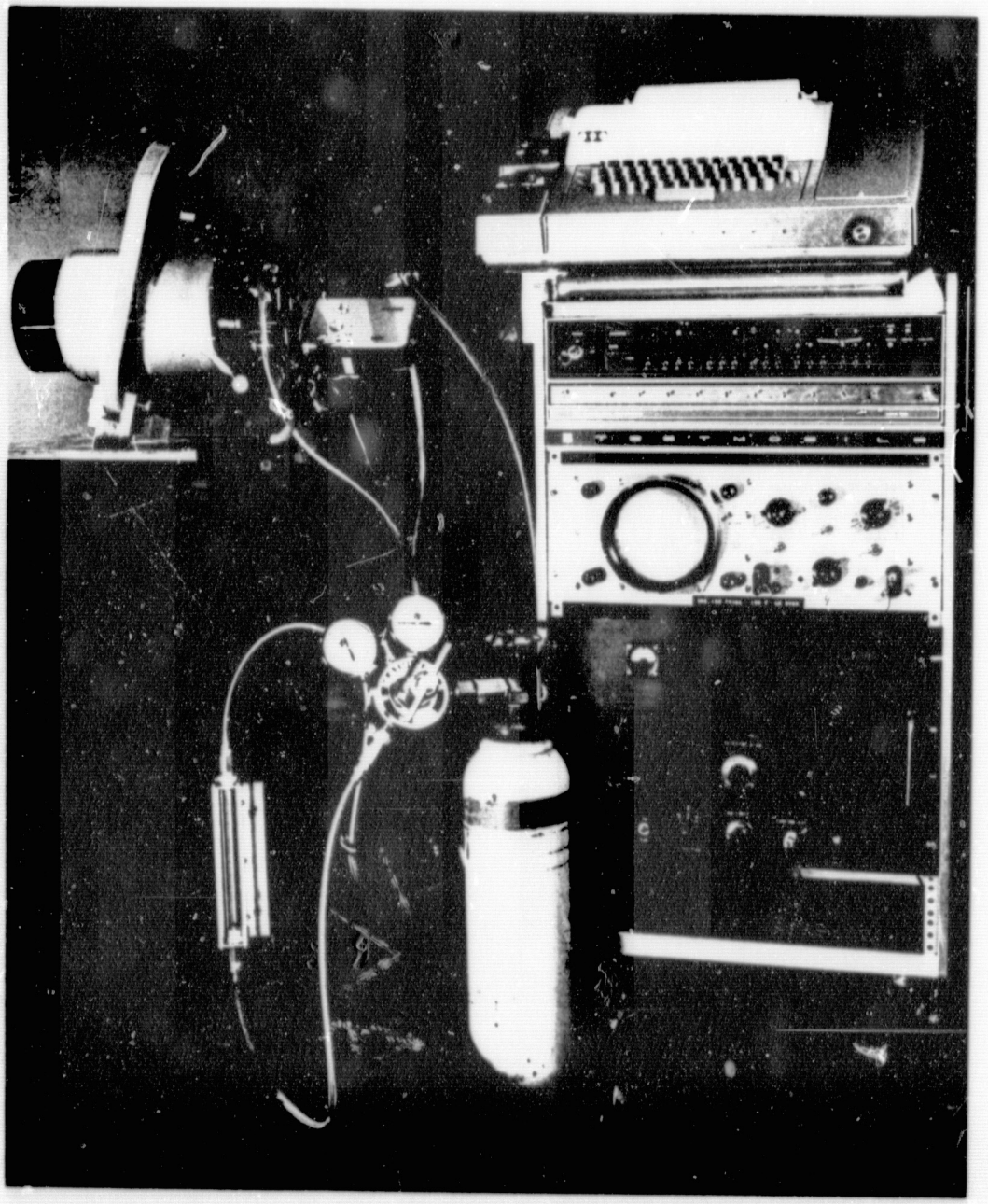


Figure 1. AEROPOL system, including infrared polarimeter, Freon-13 coolant, power supplies, oscilloscope, Nova minicomputer, and teletypewriter.

to determine these particle characteristics having measured the scattered radiation as a function of wavelength and phase angle (sun-cloud-observer angle) for a given target. The single most important measurable parameter appears to be the percentage linear polarization. In spite of multiple scattering in a thick cloud layer, the net polarization retains most features present in the scattering by single particles.

An airborne polarimeter was built to test these inversion techniques in the case of terrestrial water and ice clouds. The infrared domain (1-4μ) was dictated by contamination from molecular scattering at short wavelengths and thermal emission at long wavelengths, and by desire that wavelengths be comparable to particle sizes, and that measurements be made in wavelength regions of differing amounts of particle absorption.

In the following sections we present a description of the instrument, flight results, theoretical calculations and interpretations. Complete details will be published elsewhere (see References).

2. INSTRUMENT

Figure 1 shows the AEROPOL system, consisting of infrared polarimeter unit mounted on an aircraft side window plate, Freon-13 coolant supply for detector, power supplies, oscilloscope, Nova minicomputer, and teletypewriter. The polarimeter can be rotated manually about a horizontal axis, to scan or to track a cloud form, over the range ±70° from the nadir. The instrument field-of-view is 1°.5. A parallel viewfinder with a 10° field permits target identification and tracking; a single-lens-reflex super-8 movie camera is used to record the target field during data-taking. Sequential passbands are centered on 1.24, 1.60, 2.22, 3.08, and 3.38μ.

The instrument uses standard infrared radiometer techniques combined with a rotary polarization analyzer. Light from below passes through a pressure window, past three insertable calibration slides (dark shutter, standard lamp array, and polarizer), and through a rotating (2.1 rps) module consisting of wire grid analyzer followed by a MgF_2 objective lens which depolarizes the transmitted beam. The converging beam then falls on a reflective chopper blade (83 chops per second), through a six-position filter wheel, through the focal plane aperture, and into a cold dewar containing a Si Fabry lens and 0.5 x 0.5mm PbS detector. Cooling is by Freon-13 gas running through an open-loop Joule-Thompson cryostat, at 225 psi and approximately 1 liter/minute.

The AC (chopped) component of the voltage drop across the detector, using several volts bias, is preamplified and then amplified with a gain switched separately for each optical filter. The output is sampled once each dark and light chop, or 80 times per rotation of the polarization analyzer.

Instrument operation is fully automatic under control of a Nova 1200 minicomputer. Flexibility is achieved by manual entry of program parameters. The computer controls chopper motor frequency, filter wheel stepper motor pulses, camera exposure pulses, and output sampling. It monitors and outputs filter wheel position, instrument pointing angle, instrument temperature, and synchronization of the polarization analyzer. Real-time least-squares solutions are made for the percentage linear polarization, position angle of polarization, and mean intensity every 2.5 seconds. These results are printed on the teletypewriter and punched on paper tape for later plotting and analysis. The computer solution uses integer arithmetic and table look-ups for sine and cosine functions. The system can yield absolute accuracies of ±0.1% polarization.

In addition to the real time calibrations, the instrument has undergone extensive laboratory test and calibration. Instrumental polarization (measured with unpolarized light incident) is at all wavelengths less than 1% and is determined to 0.1% polarization.

3. FLIGHT RESULTS

In January 1972 the polarimeter was flown on the NASA CV-990 jet on ten flights over the northwest U.S. coast, the central U.S., the Caribbean, and the equatorial western Atlantic. Typical flight altitude was 12 km. The polarization

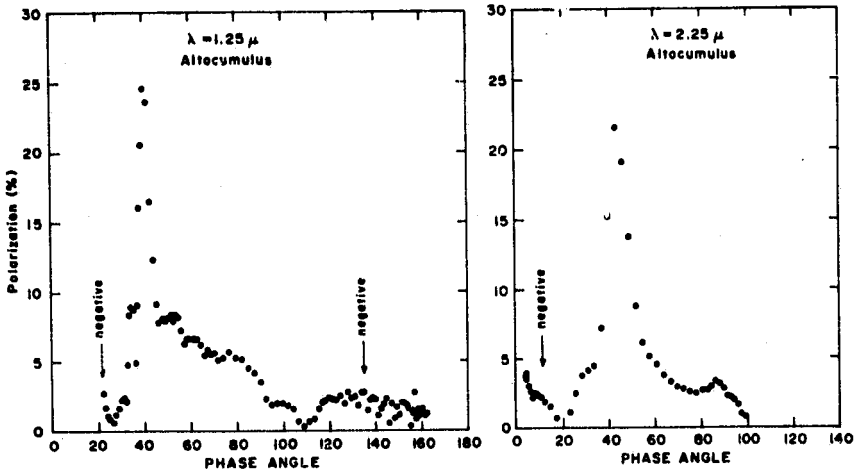


Figure 2. Percent polarization of reflected sunlight observed at 1.25μ and 2.25μ over two different cloud systems. The highly polarized cloudbow occurs near 40° phase angle. "Negative" refers to branches of the curves where the direction of polarization is predominately parallel to the plane of scattering.

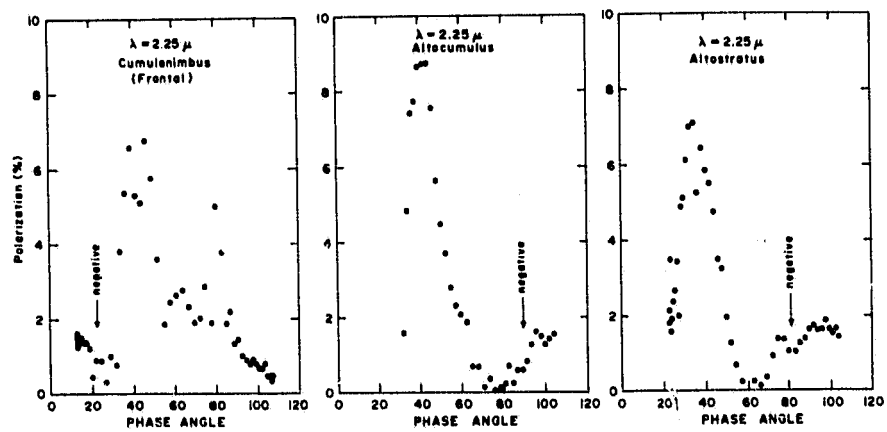


Figure 3. Percentage polarization of reflected sunlight observed at 2.25μ over three different cloud systems. The observations on the left were taken over a narrow front of raining clouds over Florida. The other two sets of data were taken on successive cloud systems behind the front. Mean particle radii are deduced by comparison with cloud model calculations, giving for the three cases 30μ, 10μ, and 5μ respectively.

of reflected or scattered sunlight depends primarily on the phase angle (sun-cloud-instrument angle); our goal was to measure the polarization of a cloud system as a function of phase angle, by tracking a given cloud as we flew over, and to do this at several wavelengths. To get the maximum range of phase angle (0°-180°) requires that the sun be near the horizon, and that the aircraft fly in the sun's vertical plane. This condition was approximated for some data runs reported here; we have measured partial phase curves for several dozen cloud systems.

Instrument problems arose on the first flights. These were all traced to excess cooling in the air stream, which caused overloading of the synchronous chopper motor, and oscillation of the signal amplifier. Both problems were cured with localized heating elements. In addition an amplifier nonlinearity was present, such that measured polarization was too low at high light levels. The effect was consistent, and has been removed by calibrating the instrument as a function of incident flux, and correcting the data accordingly. Accurate measurements were obtained at 1.2, 1.6, and 2.2μ. Results at 3.1 and 3.4μ were of low quality due to low signal-to-noise, and complicated by thermal emission in the instrument.

Figure 2 shows polarizations measured on two different cloud systems, at different wavelengths. For each of these a cloudbow (i.e,a rainbow feature for intermediate-size cloud particles) was visible to the eye. This is seen in the polarization as a strong positive peak (i.e., electric vector perpendicular to scattering plane) near 40° phase angle, and is diagnostic of spherical (and therefore liquid) particles. Several features are found to be indicators of mean particle size, including the position of the cloudbow and the position of the two zero points of polarization (see next section). Figure 3 shows a series of three consecutive cloud systems encountered on a flight north over Florida. First was a front of raining cumulus clouds, several kilometers long and several hundred meters wide. These clouds were turbulent and nonuniform, accounting for the irregularity of the polarization curve. Next were encountered layers of altocumulus and altostratus, showing well-defined polarization curves.

Figure 4 shows observations of a thick tropical cirrus system. The curves are uniform, with no indication of a cloudbow, with a broad branch of positive polarization, and with negative polarization at phase angles less than 20° and

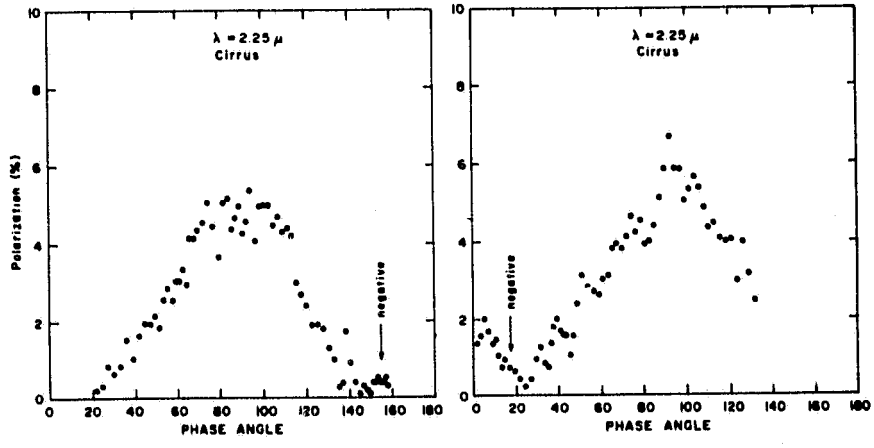


Figure 4. Percent polarization of reflected sunlight observed at 2.25μ over a thick tropical cirrus system in the intertropical convergence zone. The two sets of observations were taken on the same cloud system several miles apart.

greater than 145°. These results may be representative for thick cirrus, but must eventually be compared with many more measurements, because of the wide variety of ice crystalline forms, their preferential alignments during fall, and our lack of theoretical results for nonspherical particle scattering.

4. INTERPRETATION

For spherical particles it is possible to compute the scattered intensity and polarization exactly, for any refractive index, particle size, and phase angle. This can be extended to an integration over a size distribution. Furthermore, with recent developments in multiple scattering we can compute the polarization scattered by a particulate layer of arbitrary optical depth.

Figure 5 shows the polarization for single scattering by a size distribution of water spheres, $n(r) \sim r^2 e^{-r/2}$, with a mean effective radius of 10μ and effective variance of 1/5. Percentage linear polarization is plotted as contour levels over the wavelength/phase angle domain. The strong positive polarization running horizontally across the diagram for wavelengths near 3μ is due to Fresnel reflection from the outside of the particles. In this wavelength region water is strongly absorbing, so there is practically no penetration of the particles by light. For wavelengths less than 2.5μ the narrow positive feature near phase angle 0° is the glory. The large positive polarization with its maximum near 40° phase angle is the primary rainbow, while the second rainbow is just apparent near 60°. For phase angles between 80° and 160° and wavelengths $\lesssim$ 2.5μ most of the light is from rays refracted through the spheres with no internal reflections; this is negatively polarized. For wavelengths between 3.25 and 4μ these concepts of geometrical optics are less applicable, since the wavelength is approaching the particle size; this is the transition region between Rayleigh scattering and large particle scattering.

These diagrams have been prepared for several particle size distributions. At the longest wavelengths the polarization features of geometrical optics develop more and more distinctly as the particle size increases. The positive polarization near 3μ is rather independent of size, in the range of particle radii studied, viz., 5μ-30μ. For wavelengths less than 2.5μ the polarization at 80° phase angle is strongly dependent on particle size. At 2.25μ it is -14% for 5μ mean radius, -5% for 10μ, and +10% for 20μ. This is understood as an increasing predominance of Fresnel reflection from the surface of the particles (positively polarized), with the negatively-polarized twice-refracted rays becoming more localized to the geometric-optics limit, as size increases.

The above results were for pure single scattering. Calculations have been made for full multiple-scattering in plane-parallel layers; it is found that the primary effect of multiple scattering on the degree of polarization is to reduce its value without changing its form. Figure 6 is presented as an example of this; it shows the computed intensity and polarization at 2.25μ for the reflection of sunlight from a plane-parallel water cloud for different optical thicknesses. The mean particle radius is 6μ and the variance 1/9. The polarization retains more of the features of single scattering than does the intensity, especially for large optical thicknesses. This is expected, since the multiply scattered photons in general have little net polarization regardless of their net intensity.

With this brief background of the theoretical results we can do a simple analysis of the observed polarizations. The polarization dilution by multiple-scattering appears to range from about 3 to 8, depending on phase angle and cloud system. The well-defined polarization inversion point at 110° phase angle in Figure 2 indicates a mean particle radius of ~25μ. Comparing Figure 3 with a sequence of theoretical models, we find mean particle radii of ~30μ for the irregular cumulonimbus frontal system, ~10μ for the altocumulus, and ~5μ for the altostratus farthest behind the front. The unique correlation of the position of this inversion point with particle size gives a simple, straightforward procedure for droplet size determination by remote sensing.

5. ACKNOWLEDGEMENTS

The AEROPOL program is supported by Goddard Space Flight Center. The instrument was built by the Polariscope Group at the University of Arizona. We thank the personnel of the Ames Research Center Airborne Science Office for their cooperation.

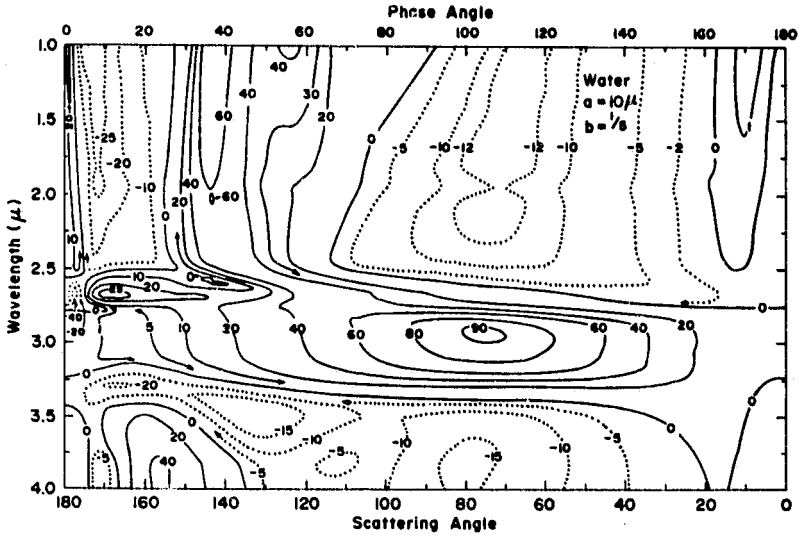


Figure 5. Computed contour diagram of percent polarization as a function of wavelength and phase angle, for single scattering by a size distribution of water particles. The mean particle radius is 10μ and the variance 1/5. Solid curves are used for positive polarization and dotted curves for negative polarization.

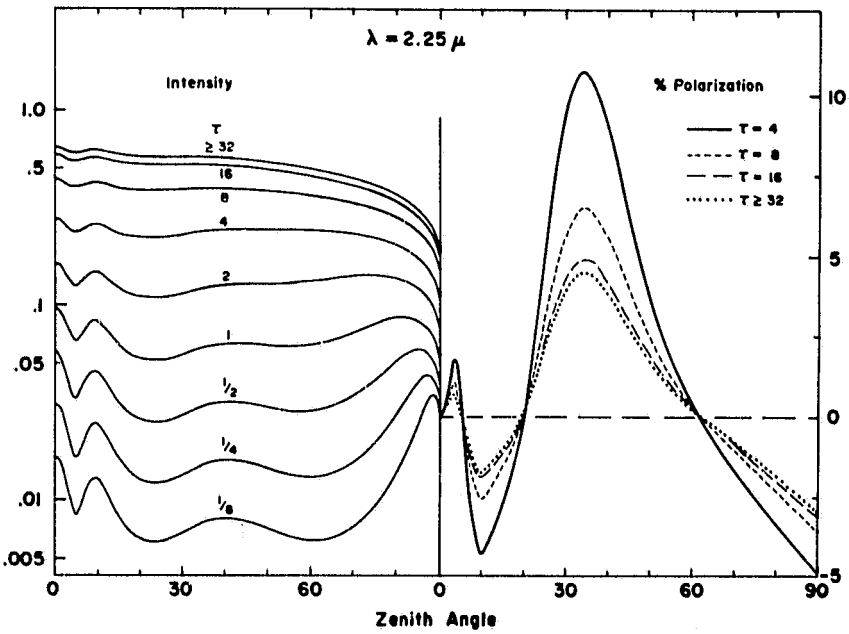


Figure 6. Computed intensity and polarization for multiple scattering by a plane-parallel water cloud with the sun overhead. The wavelength is 2.25μ and results are given for several optical thicknesses, τ. The abscissa is the zenith angle of the reflected light. The calculations are for a size distribution with mean radius 6μ and variance 1/9.

REFERENCES

More complete details may be found as follows.

Instrument:

Coffeen, D. L., J. Hämeen-Anttila, and R. H. Toubhans 1973 "Airborne Infrared Polarimeter", Space Science Instrumentation 1 (in press).

Flight Results:

Coffeen, D. L. and J. Hansen 1973, J. Atmos. Sci. (in preparation)

Single scattering calculations:

Hansen, J. E. and D. L. Coffeen 1972 "Polarization of Near-Infrared Sunlight Reflected by Terrestrial Clouds", Preprint Volume of the Conference on Atmospheric Radiation, 55-60.

Multiple scattering calculations:

Hansen, J. E. 1971 "Multiple Scattering of Polarized Light in Planetary Atmospheres. Part II. Sunlight Reflected by Terrestrial Water Clouds" J. Atmos. Sci. 28, 1400-1426.

PRINCIPLES AND TECHNIQUES OF POLARIMETRIC MAPPING

John Halajian
Herbert Hallock

Grumman Aerospace Corporation
Bethpage, N.Y.

ABSTRACT

This paper introduces the concept and potential value of polarimetric maps and the techniques for generating these maps in operational remote sensing.

The application-oriented polarimetric signature analyses in the literature are compiled, and several optical models are illustrated to bring out requirements of a sensor system for polarimetric mapping. By use of the concepts of Stokes parameters the descriptive specification of one sensor system is refined.

The descriptive specification for a Multichannel Digital Photometric-Polarimetric Mapper is based upon our experience with the present single channel device which includes the generation of polarimetric maps and pictures. High photometric accuracy and stability coupled with fast, accurate digital output has enabled us to overcome the handicap of taking sequential data from the same terrain.

Polarimetric maps and pictures of a portion of the moon at quadrature, and a polarimetric picture of Long Island Sound waters are shown. The remote sensing application over water is the mapping of turbidity in the top layers.

1. GENERAL BACKGROUND

For aerial reconnaissance and remote sensing in the optical spectrum there has been warranted emphasis on spectral reflectance values in the interpretation of photographic and similar data, but only occasional reference to the importance of considering polarization as a factor (1). It has been shown that polarization bias in laboratory instrumentation can lead to errors in the measurement of reflectances, and in colorimetry,(2) but little attention has been paid to polarization bias effects in remote sensing optical systems which may, in some cases, be quite pronounced. Similarly, in spite of number of reports suggesting the benefits which can be derived from remotely sensing optical polarimetric properties, very little serious effort seems to have been devoted to putting these suggestions to routine practical use, as with photography, multispectral scanning, etc.

The principal reason for not making effective use of polarimetric properties is lack of polarimetric mapping instrumentation which compares with the practicality of photography, for example, in map-making and in interpretation. Polarization has to do with the vectorial, as contrasted with the scalar quantities in light measurement,

and the geometric factors are naturally more pronounced, not only in terms of the internal parts of the sensor (i.e., analyzer orientations), but also with respect to the external frame of reference.

An example of the importance of external geometric factors is shown in Fig. 1, which is laboratory data taken with a directional polarimeter under conditions where the viewing direction could be continuously varied while the direction of incidence of the source light remained fixed. The phase angle is the angle between the light incidence and the viewing directions which, together with the normal to the surface, lie in what we define here as the principal plane. Likewise the plane containing the normal and the viewing axis of the sensor will be defined as the measurement plane for discussion of cases where sunlight strikes the measurement plane at an angle. Percent polarization, defined in terms of light vectors perpendicular and parallel to the principal plane, is markedly dependent upon the phase angle. One implication of the data is that the surface water content of the topsoil could be measured remotely by polarimetric analysis, as was suggested previously by Stockhoff and Frost of the General Electric Co.(3). Obviously only by taking careful account of geometry would it be possible to make a measurement.

Another example of the finesse which might be expected for practical applications is shown in Fig. 2 which follows the approach suggested by Millard and Arvesen(4) for the use of polarimetry in the airborne optical surveillance of oil slicks, but poses a more difficult problem to examine an oil of relatively low index of refraction (1.46) on water of index equal to 1.33.

These examples typify most of presently available polarimetric signature data in that a principal plane reference for the vectorial analysis is used, and only linear polarization is considered. There is a tendency also to borrow the "s-component" and "p-component" terminology commonly applied in Fresnel reflection equations, and apply them with reference to the measurement plane(2). The choice of two mutually orthogonal polarization analyzer orientations, using the measurement plane for reference, has the advantage of consistency. This choice leads to the concept of "positive" and "negative" polarization, positive meaning an excess of "s" over "p" values, and negative an excess of "p" over "s".

A number of references are cited in Table 1 pertaining to the remote sensing of other significant physical conditions by polarimetry. Included are references on the de-polarization signature which applies to the use of an active (laser) plane polarized source.

2. IMPLICATIONS OF STOKES PARAMETERS FOR SENSOR DESIGN AND MAPPING OUTPUT

Stokes parameters are generally accepted as complete characterization of the polarimetric properties of light. Using the terminology of Born and Wolf(22) the four parameters of the quasi-monochromatic plane wave may be specified as follows:

$$\text{First} \qquad S_0 = I\,(0°, 0) + I\,(90°, 0) \tag{1}$$

$$\text{Second} \qquad S_1 = I\,(0°, 0) - I\,(90°, 0) \tag{2}$$

$$\text{Third} \qquad S_2 = I\,(45°, 0) - I\,(135°, 0) \tag{3}$$

$$\text{Fourth} \qquad S_3 = I\,(45°, \tfrac{\pi}{2}) - I\,(135°, \tfrac{\pi}{2}) \tag{4}$$

The I-values represent intensity of the light vibrations in the direction with respect to any arbitrary axis, transverse to the direction of propagation, signified by the angle in degrees within the bracket, and subjected to the phase retardation indicated by the number of radians following the axis designation within the bracket. Also the percent polarization of the wave is defined in terms of Stokes parameters as:

$$P = \frac{\left(S_1^2 + S_2^2 + S_3^2\right)^{1/2}}{S_0} \times 100 \tag{5}$$

and the angle, ω, which defines the orientation of the major axis of the polarization ellipse may be computed as follows:

$$\tan 2\omega = \frac{S_2}{S_1}. \tag{6}$$

The fourth Stokes parameter is concerned with the excess of right hand circular polarization over left, and implies the use of a quarter-wave plate in the sensor. For the most part experimenters in polarimetry of remote surfaces have concerned themselves only with an assumed predominance of linear polarization. In one report which is concerned specifically with polarimetry for atmospheric turbidity analysis (18), measurements of circular polarization confirmed the validity of this assumption. There are probably exceptions related to the detection of unusual materials, or surfaces, but let it be assumed for the present purposes that the bulk of practical applications can be pursued without use of the fourth parameter. Under this assumption the percent polarization may be expressed as:

$$P = \frac{\left(S_1^2 + S_2^2\right)^{1/2}}{S_0} \times 100 \tag{7}$$

Again as pointed out by Herman, et al,(18) it is not essential to measure I (135°, 0) in addition to I (45°, 0) for computations involving the third parameter since the following relationships hold:

$$I\ (135°,\ 0) = I\ (0°\ 0) + I\ (90°,\ 0) - I\ (45°,\ 0) \tag{8}$$

and, therefore

$$S_3 = 2\ I\ (45°,\ 0) - I\ (0°\ 0) - I\ (90°,\ 0). \tag{9}$$

On these premises complete characterization of linear polarization can be made by recording three channels of data; namely two at mutually orthogonal analyzer orientations and one at an intermediate 45° orientation. Thus it is seen that proper use of Stokes parameters may make it feasible by the use of three real-time recorded channels to examine the polarization of practical-size areas of remote sensing interest.

For airborne investigative work we have found that it is practical to limit the number of channels to two by reason of previous knowledge of polarization vector orientation. As previously pointed out most laboratory investigations have been confined to a principal plane. It is possible to conduct field operations in a principal plane by flying "down-sun" for the most part, although there are strong reasons at times for flying "toward" the sun. In order to show the implications more clearly Figures 3 and 4 show the polarization vector changes resulting from not flying in the principal plane mode. Both figures show the vectors as they would appear to an observer looking down the sensor axis toward the remote surface. In the great majority of cases the vectors will look like those in Fig. 3 when flying "principal plane" whereas if the sun seems to be coming "from the right" the vectors may appear as shown in Fig. 4(10). In experimental investigation it is possible to rotate the analyzer to mutually orthogonal axes suggested in Fig. 4. Two channels will still suffice, but the implication of "positive" and "negative" polarization will no longer be clear cut.

It is probably true that in routine operational mapping three (or possibly more) channels would be required. Thus the requirements upon sensor and operator versatility would be relieved.

3. INTERPRETATION FACTORS IN CHOICE OF POLARIMETRIC MAPPING FORM

The I-values of the Stokes parameters will be represented in the practical sensor output as radiance values based upon an instantaneous field of view defined sharply by a field stop. Thus the "principal plane" vectorial radiances could be designated N_s and N_p, and equations (1) and (2) could be expressed respectively as equations (10) and (11):

$$S_0 = N_s + N_p \tag{10}$$

$$S_1 = N_s - N_p \tag{11}$$

A mapping portrayal of the first parameter is obviously an ordinary picture if the numerical values are linearly converted to gray tones. A portrayal of the second parameter will not appear "normal", but will still carry information related to the light fluctuations in the field (i.e., highlights and shadows, light source fluctuations, spectral reflectance variations). While, in general, difficult to interpret this mapping of the second parameter might be ideal for the oil slick case (Fig. 2) if cloud shadows and other extraneous factors did not interfere too much.

To interpret multispectral remote mapping in terms of identifying and measuring important physical conditions it is necessary to extract reflectance values, which means it is necessary to take account of the spectral irradiance of the source and the spectral transmission losses. Dividing these measured and computed quantities produces a quotient which can represent the spectral reflectance of each elemental area, independent of highlight and shadow situations. A "picture" of color or gray tone values corresponding to each quotient would not look "normal", but would convey exact meaning.

Similarly in the polarimetric regime one could obtain quotients in accordance with the following relationship:

$$\rho_s = \frac{\pi N_s}{t_s H} \tag{12}$$

and

$$\rho_p = \frac{\pi N_p}{t_p H}, \tag{13}$$

in which ρs and ρp are polarimetric diffuse reflectance factors; t_s and t_p are the transmission loss factors and H is the source irradiance. These reflectance factors can be likened to spectral reflectances in the colorimetry regime, and mapping in these quotients would have the shadow-less attributes of the spectral reflectance map. As a matter of fact, however, spectral reflectance would continue to be a dominant influence in these quotients and it might be difficult to extract unique polarimetric interpretation.

When the percent polarization is computed, as in the simplified case under discussion by means of the equation,

$$P = \frac{N_s - N_p}{N_s + N_p} \times 100 \quad , \tag{14}$$

it is apparent that the values become more uniquely polarimetric, and divorced to a greater extent from spectral reflectances. Separation can never be complete, and it would be more appropriate to call the operation spectro-polarimetric mapping. Another interesting consequence is the influence of the irradiance, H, disappears providing N_s and N_p values are taken simultaneously. For example, light cloud shadows do not constitute a serious disruptive influence. A somewhat analogous quantity in the color regime is the chromaticity coordinate.

4. EXPERIMENTAL POLARIMETRIC MAPS AND PICTURES

A two-dimensional matrix of numerical values of Stokes parameters, or of percent polarization, arranged in map-like form to a definite scale, is defined as a polarimetric map. An example is shown in Fig. 5 with percent polarization chosen as the numerical value to be presented. Contour lines can be drawn as with elevation or other numerical map data. The orthogonal vectorial component magnitudes entering into the computation are shown in similar form in Fig. 6. These data were recorded in digital form at an observatory telescope* directed at the lunar surface. The "H"

*61 inch telescope, Catalina Station, University of Arizona Lunar and Planetary Laboratory, December 3, 1969.

and "V" designations refer to the right ascension and declination planes of the telescope, and do not correspond exactly to "s" and "p", but are close enough to warrant analogous mathematical treatment.

Obviously these data could be prepared in the form of a transparent overlay to be superimposed upon a suitably scaled photographic print for interpretation. Another way in which the data could be used for ready interpretation is to change the digital values to a gray-tone picture by use of digital tape-to-film conversion. Fig. 7 shows an example of this conversion, resulting in what we define here as a polarimetric picture. This picture can be used as an aid to interpretation of the comparably scaled conventional picture by noting variations in gray tone polarimetric values and associating them with the terrain areas they represent. The picture is confined to "plus" polarization only and the gray tones proceeding from dark to light indicate increasing positive values of percent polarization.

The observation upon which this picture was based was made at the last quarter of the moon and, as can be seen from the more conventional appearing tape-to-film converted picture in Fig. 7, the distinctive crater features are brought out by shadowing. These features do not appear in the polarimetric picture for reasons explained previously. Without entering into detail as to all the seleno-physical interpretations which may be based upon the polarization properties, it may be pointed out that high reflectance (not radiance) is usually associated with low polarization (dark).(10) The lunar highlands are more highly reflective than the lowlands. Consequently the highland area near the limb, for example, looks dark polarimetrically, whereas the mid-lunar lowland area appears light polarimetrically, indicating high plus polarization. Some of the crater floors, and some of the rims appear polarimetrically dark, indicating probably high reflectance values.

A similar polarimetric picture of negative polarization values may be made in which the gray tones would become progressively lighter with increasing negative arithmetic values. The lunar surface at quadrature is not a good medium with which to illustrate negative polarization. We do not at this time have a "picture" which is a good illustration of negative trends. However, Fig. 8 shows data in line trace form which was acquired with the same sensor. The negative excursions of the percent polarization data reveal the presence of moist, or vegetated areas adjacent to dry "cultural" surfaces such as roads, sand banks and buildings, which are "plus". It should be noted that the observation geometry is close to 0° phase angle in contrast to the lunar data taken at a rather large phase angle.

When the two or three channels of data are taken for polarimetric purposes various forms of data presentation (pictures or maps) are possible which provide the visual clues necessary to locate and identify the features with unusual polarization; or to merely retrieve from the stored information the polarimetric properties of any one feature. Portrayal of the first Stokes parameter, or either of its two components, looks quite conventional as shown in the upper picture of Fig. 7. A picture showing the second Stokes parameter, or the third could be valuable.

We have another example of the preparation of a polarimetric picture, the purpose of which is to depict the surface turbidity in natural bodies of water. We have previously shown that there is a definite relationship between the polarization of sunlight scattered by the water and the particulate content of the top layers (14) (15) (16). Observation at rather large phase angles maximizes the signature as shown in Fig. 9(14). It has been recognized recently(23) (24) that photometric measurements of water can be correlated with turbidity. The advantage of polarimetry over straight photometry lies in the ultimate ability to disentangle from the photometric data the extraneous sunlight fluctuations, sensor drift and water surface phenomena. The gray tone rendition of percent polarization shown in Fig. 10 shows a gradual improvement in the surface clarity of Long Island Sound waters as the middle of the Sound is approached from the Throg's Neck Bridge area. Again it shows increase in turbidity as the plane approaches the still-distant Connecticut Shore*. We believe it would readily be admitted that consistent portrayal of this effect with conventional photography would be next to impossible. The data were taken in the red end of the visual spectrum (0.6μm to 0.7μm).

*These pictures were prepared under NASA, MSC, Houston Contract NAS9-12963 (Earth Observation Division, Applied Physics Branch)

5. THE POLARIMETRIC MAPPING SENSOR

The sensor used for the data presented in this paper is the Grumman Digital Photometric Mapper (DPM) which is an electronic line scanning device based upon the image dissector camera tube[25]. As a line scanner it requires relative motion perpendicular to the scan to generate a map, or picture, Used as a focal plane scanner in a large observatory telescope this relative motion was provided by constant earth rotation. In aircraft the forward motion relative to earth serves this function and the DPM carries its own objective lens. Strip mapping works within a restricted viewing angle range compared to a frame-by-frame approach and thus fulfills an important requirement for polarimetric mapping.

Figure 11 illustrates a typical geometry of airborne strip mapping. Obviously some transverse deviation from the principal plane is necessary in order to scan, but the compromise is minimal. By use of pivoted support bracketry the obliquity of the viewing angle can be changed to suit geometric requirements which can be seen in Fig. 1 and 2 to be very important. The use of one optical head for each channel of data would be ideal if it were not for the bulk and cost. An alternative believed to be attractive in practice is shown in Fig. 11. Two channels (or more) are extracted from one head (a single objective lens) by pointing one channel axis slightly ahead of the other. This appears preferable to time sharing, or to the use of beam-splitters. Since plastic polarization analyzers and the absorption-type spectral filters will work well near the focal plane it is possible to devote narrow strip filters to each channel's line scan. A common digitally controlled staircase-type scan makes temporal registration of the resolution elements very accurate from one channel to the others, and allows for a "staring" type measurement at each scan "step". This type of scan is characteristic of our present DPM which has only one scanning channel.

Basically, it is our favorable experience with airborne sensing using the present DPM which has led us to make this suggestion. Consecutive overflights are necessary presently to generate the equivalent of multi-channel data, and post-flight registration of common points is a problem even with computer assistance. A second non-scanning optical photometer feeding digital tape has been added for centerline two-channel data, however.

Figure 12 is a schematic of the suggested Multichannel Digital Photometric Mapper. The image dissector in our present DPM is the ITT Fort Wayne, Indiana Vidissector Type F4011. A multi-channel version of the image dissector tube was developed by ITT for the Mitre Corp. and called the DI-SCAN tube[26]. A refined version was more recently developed by ITT for NASA Goddard[27]. Under reasonable optical and mechanical assumptions this type of multi-channel sensor could provide angular channel separation in the order of two to four degrees. Use of the charge-coupled silicon photodiode linear arrays[28] would enable the separation to be decreased to a fraction of one degree.

The electronic requirements for the precisely regulated staircase scans are shown in block diagram form in the illustration. Our present DPM digitizes to eight bits (255 levels), but ten bits (1023 levels) are more in line with presently improved technology. An adequate signal-to-noise ratio to justify all these levels can only be provided by precise signal integration which is accomplished electronically in our present device. While the present DPM can make about 3000 measurements per second (to within 1% error at adequate light level) multiplexing for several channels can facilitate 12,000 points per second without straining the electronic capability. By use of a high speed objective lens (Super-Farron f/0.87) enough light can be collected, even over water, to provide an information rate suitable for mapping at reasonable spatial resolution and coverage.

6. CONCLUSION

Evidence has been presented in this paper for the value and practicality of polarimetric mapping as an adjunct to multi-spectral techniques in the remote sensing of important physical properties.

ACKNOWLEDGEMENTS. This effort was supported by Grumman Aerospace Corporation Advanced Development Programs. Sensor installation in the aircraft and flight operations were performed by Grumman Ecosystems Corporation. The polarimetric picture of Long Island Sound waters was produced by Grumman Data Systems Corporation under NASA Contract NAS 9-12963.

TABLE I REFERENCES FOR SPECIFIC APPLICATIONS OF REMOTE SENSING BY OPTICAL POLARIMETRY

Physical Property	Reference (see List of References)
Surface microstructure	(5),(6),(7),(8),(9),(10)
Surface diffuse reflectance	(6),(9),(10)
Degree of specularity of surface	(11),(12)
Water content (e.g., soil, foliage)	(3),(11),(13)
Water surface roughness	(17)
Index of refraction (e.g., oil slick)	(4)
Turbidity of water	(14),(15),(16)
Turbidity of atmosphere	(18),(19)
Vegetative cover characteristics	(20),(21)

REFERENCES

1. K.L. Coulson, "Effects of Reflection Properties of Natural Surfaces in Aerial Reconnaissance", Applied Optics Vol. 5, No. 6, June 1966

2. A.R. Robertson, "Effects of Polarization on Reflectance Factor Measurements", Applied Optics Vol. 11, No. 9, Sept., 1972

3. E.H. Stockhoff and R.T. Frost, "Polarization of Light Scattered by Moist Soils", Proc. of the Seventh International Symposium on Remote Sensing of Environment, Vol. 1, 345-364

4. J.P. Millard and J.C. Arvesen, "Airborne Optical Detection of Oil on Water", Applied Optics Vol. 11, No. 1, Jan., 1972

5. B. Lyot and A. Dollfus, Compt. Rend. 228, 1949

6. B. Hapke, Report No. 169, Cornell University Center for Radiophysics and Space Research, 1964

7. T. Gehrels, and T.M. Teska, "The Wavelength Dependence of Polarization", Applied Optics Vol. 2, No. 1, Jan., 1963

8. D.L. Cofeen, "Wavelength Dependence of Polarization", Astron J 70, August 1965

9. W.G. Egan, L.L. Smith and G.C. McCoyd, "Polarimetric Measurements of Simulated Lunar Surfaces", Final Report on Contract NAS9-4942, Grumman Research Report RE-250, May 1966

10. C.A. Pearse, "Photometry and Polarimetry of the Moon and Their Relationship To Physical Properties of the Lunar Surface", Bellcomm, Inc., Aug., 1963

11. J. Halajian and H.B. Hallock, "Uses of Temporal Data in Remote Sensing", NASA SP 177 Proc. Sixth Annual Meeting of Working Group on Extraterrestrial Resources, Brooks AFB, Feb., 1968

12. W.G. Egan and H.B. Hallock, "Coherence-Polarization Phenomena in Remote Sensing", Proc. IEEE 57, April 1969

13. W.G. Egan, J. Grusauskes, and H.B. Hallock, "Optical Depolarization Properties of Surfaces Illuminated by Coherent Light", Applied Optics Vol. 7, No. 8, Aug. 1968

14. H.B. Hallock and J. Grusauskes, "The Polarimetric Signature of Natural Water Surfaces", JOSA Vol. 57 No. 4, Paper FE12

15. H.B. Hallock and J. Halajian, "Correlation of Optical Models and Aircraft Data of Water Turbidity" JOSA Vol. 61, No. 11, Paper ThJ16

16. NASA SP 285, "Remote Measurement of Pollution, Langley Research Center, NASA, Aug. 1971

17. J. Halajian and H.B. Hallock, "Digital Photometric and Polarimetric Surveys of Water and Land Areas" Grumman Aerospace Corp. Report ADR 03-02-71.1, August 1971

18. B.M. Herman, S.R. Browning, and R. Guiran, "The Effect of Atmospheric Aerosols on Scattered Sunlight", J. Atmos. Sci. Vol. 28, 1971

19. Z. Sekera, "Determination of Atmospheric Parameters from Measurement of Polarization of Upward Radiation by Satellite or Space Probe", Icarus Vol. 16, 1967

20. W.G. Egan, and H.B. Hallock, "Polarimetry Signature of Terrestrial and Planetary Materials" Proc. of Fourth International Symposium on Remote Sensing of the Environment, Univ. Mich. April 13, 1966

21. W.G. Egan, "Optical Stokes Parameters Farm Crop Identification" Remote Sensing of Environment 1, 1970 165-180

REFERENCES (Cont.)

22. M. Born and E. Wolf, Principles of Optics, Macmillan 1964, 554, 555

23. G.N. Plass and G.W. Kattawar, "Radiative Transfer in the Earth's Atmosphere-Ocean System" 1972 Spring Meeting Optical Soc. Amer. Paper TuIl1

24. V.L. Granatstein, M. Rhinewine, A.M. Levine, D.L. Feinstein, M.J. Mazurowski, and K.R. Piech, "Multiple Scattering of Laser Light From a Turbid Medium", Applied Optics Vol. 11, No. 5, May 1972

25. H.B. Hallock, J. Halajian and S. Skeels, "A Digital Electro-Optical Photometric Mapper", JOSA Vol. 60, No. 5 Paper FE15

26. R.S. Nielsen and M.A. Ford, "DI-SCAN, Versatile Image Sensor", Optical and Electro-Optical Information Processing MIT Press 1965

27. P.N. Slater, "Multi Band Cameras" Photogrammetric Engineering V. XXXVIII, No. 6, June 1972 543-548

28. W.S. Boyle and G.E. Smith, "Charge-Coupled Semiconductor Devices" BSTJ, 49, No. 4, April 1970

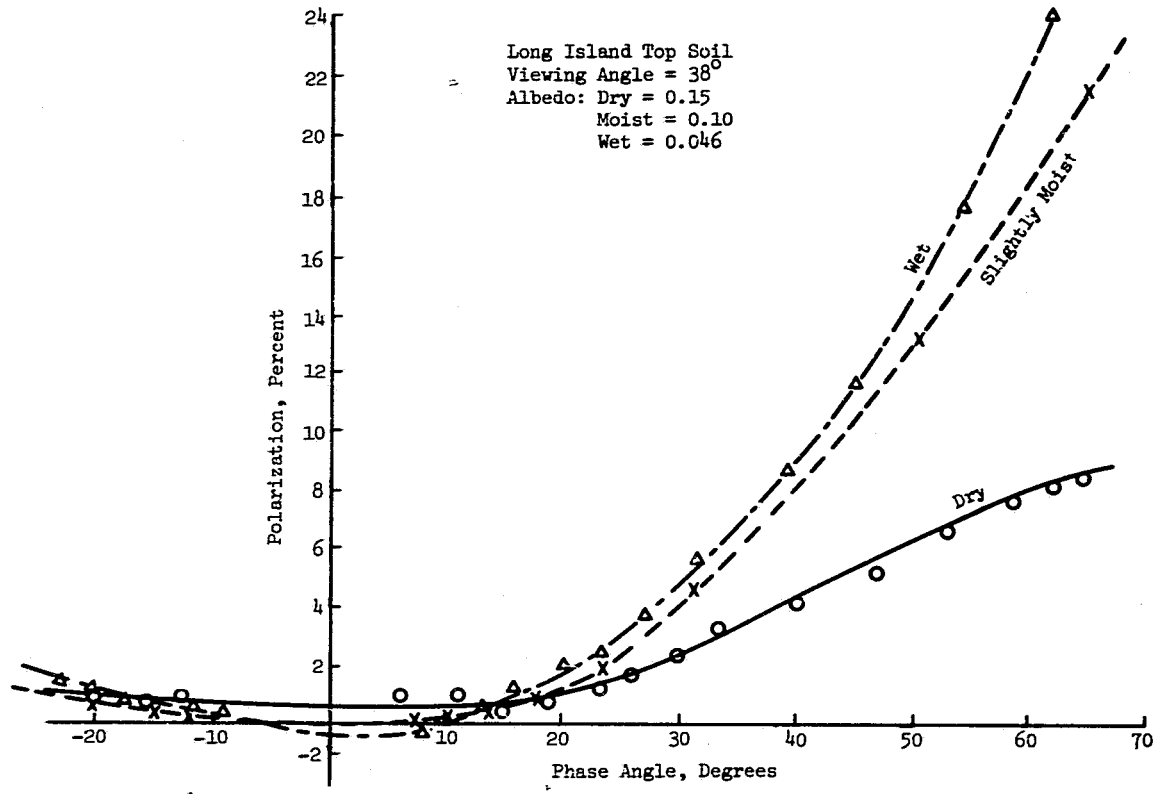
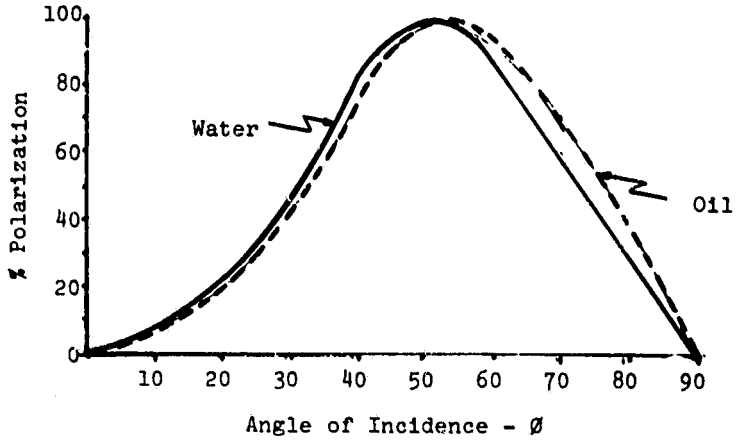


Figure 1. LABORATORY POLARIMETRIC ANALYSIS OF TYPICAL LONG ISLAND TOP SOIL



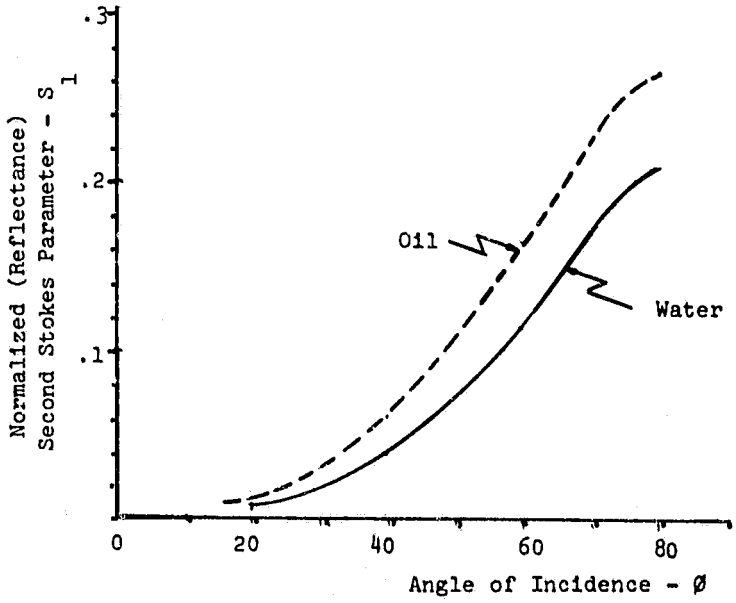


Figure 2. POLARIZATION OF OIL AND WATER

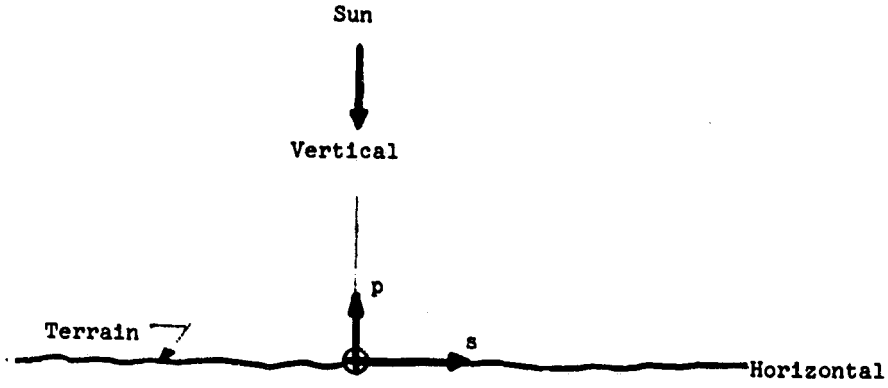


Figure 3. PRINCIPAL PLANE POLARIZATION VECTORS

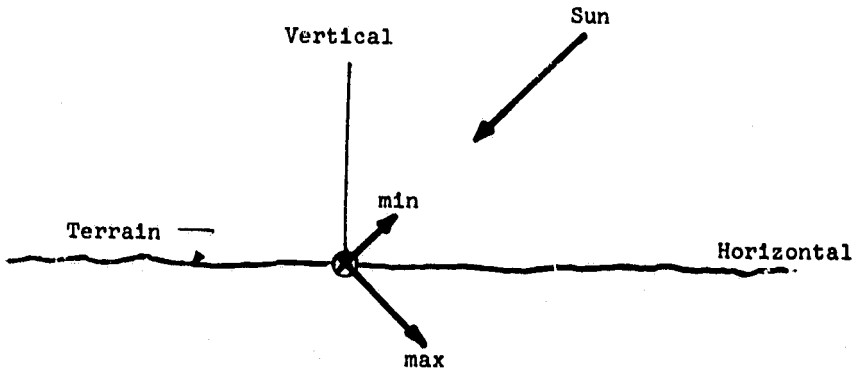


Figure 4. NON-PRINCIPAL PLANE POLARIZATION VECTORS

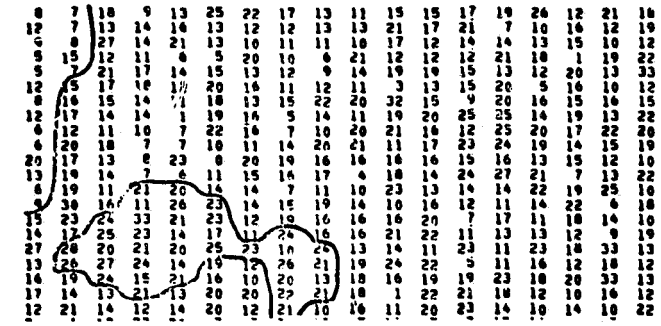


Figure 5. PERCENT POLARIMETRIC MAP OF MOON, (TOBIAS MAYER REGION) AT QUADRATURE

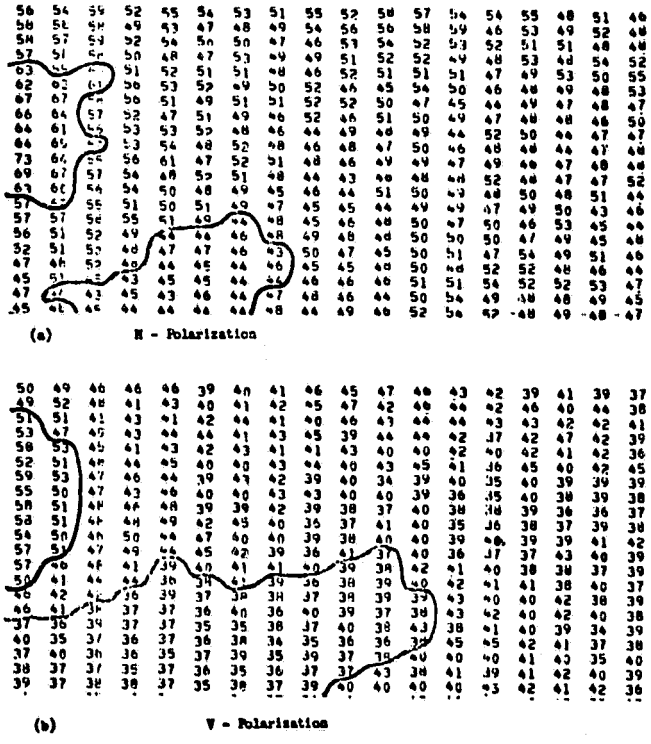


Figure 6. POLARIMETRIC COMPONENTS OF MAP IN FIGURE 5
(Resolution Element = 2 Km x 2.6 Km)

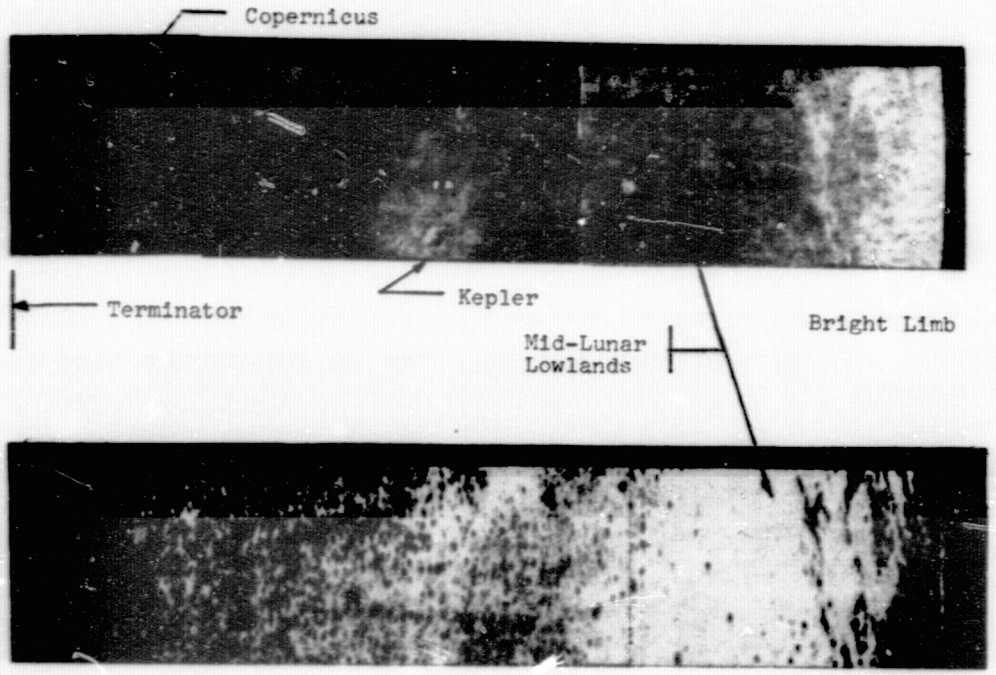


Figure 7. PERCENT POLARIZATION PICTURE (BOTTOM) COMPARED TO CONVENTIONAL TAPE-TO-FILM CONVERTED PICTURE (TOP). THE MOON AT LAST QUARTER

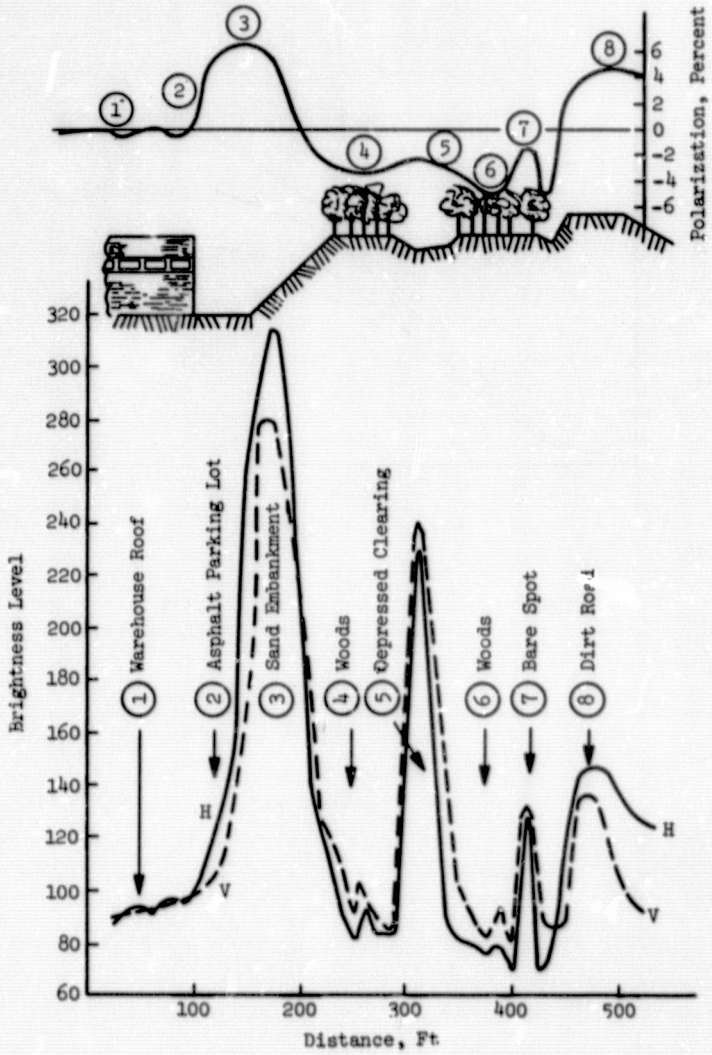


Figure 8. PHOTOMETRIC AND POLARIMETRIC ANALYSIS OF SOILS AND VEGETATION

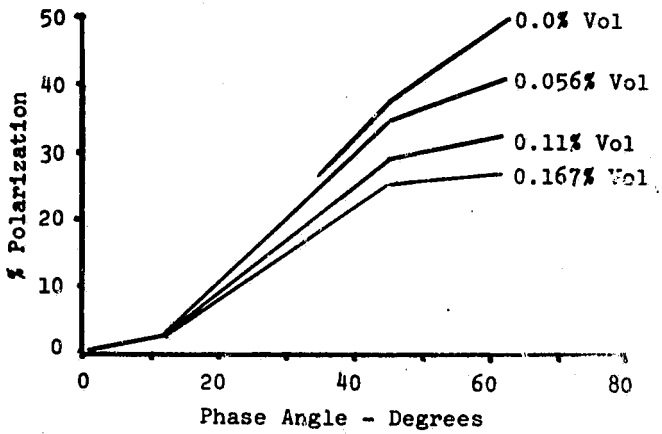
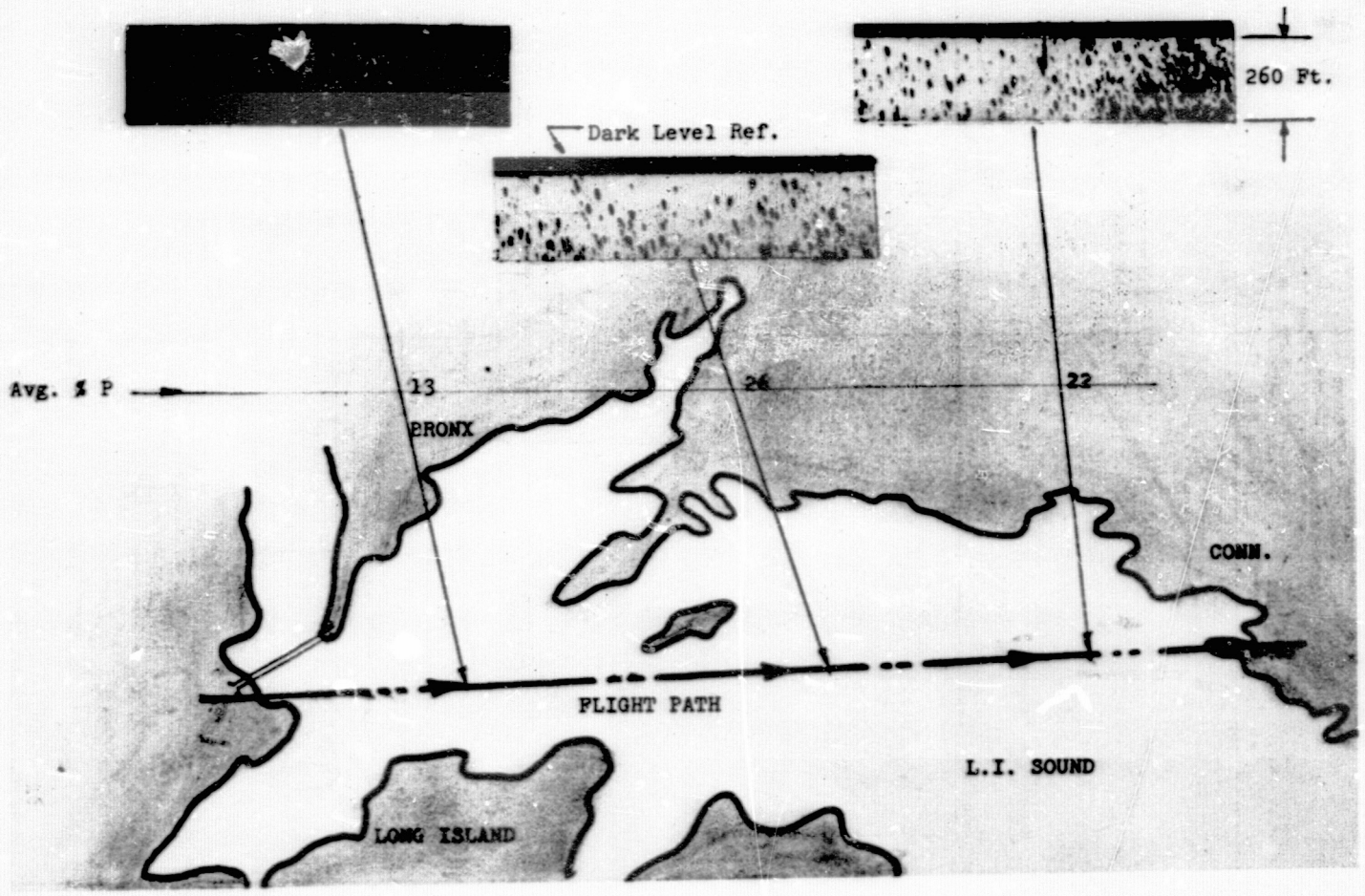


Figure 9. LABORATORY POLARIMETRIC SIGNATURE OF TURBID WATER

Figure 10. PERCENT POLARIZATION PICTURE OF LONG ISLAND SOUND



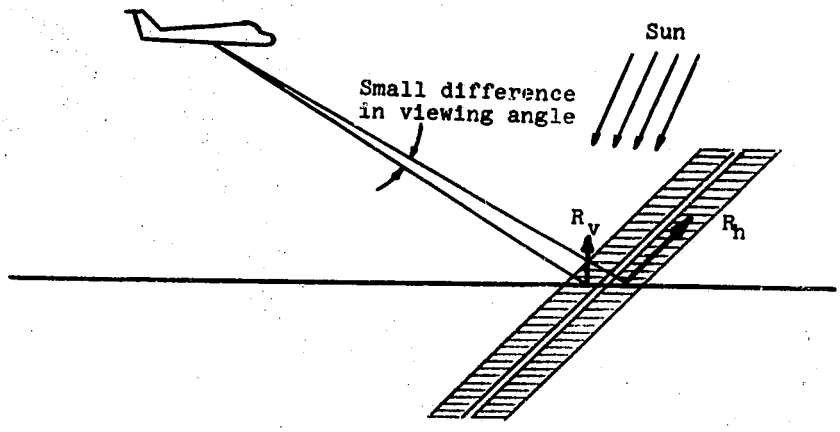


Figure 11. SCANNING GEOMETRY FOR MULTICHANNEL POLARIMETRIC MAPPING

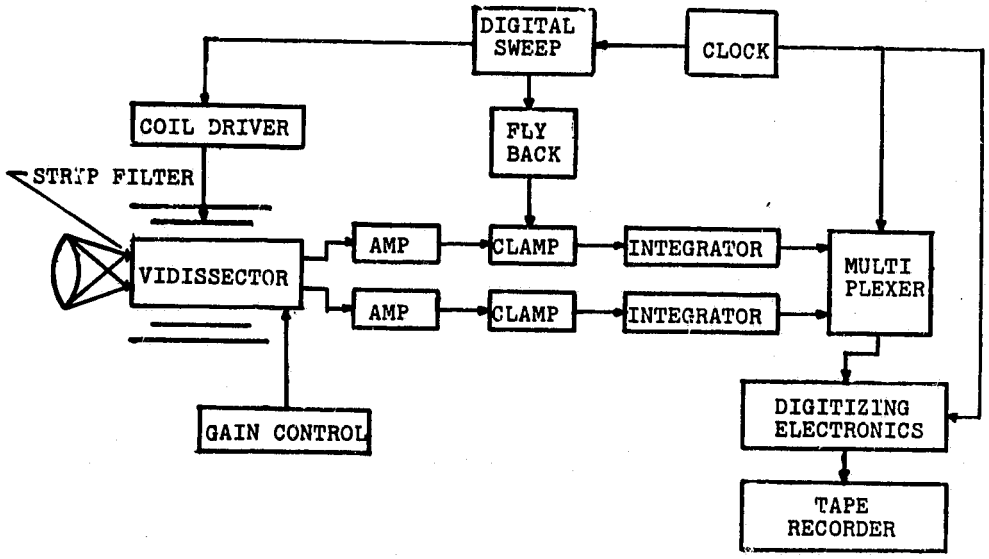


Figure 12. MULTICHANNEL DIGITAL PHOTOMETRIC MAPPER FOR POLARIMETRIC MAPPING

EUTROPHICATION ASSESSMENT USING REMOTE SENSING TECHNIQUES

by

C. T. Wezernak and F. C. Polcyn

Environmental Research Institute of Michigan
(Formerly Willow Run Laboratories
The University of Michigan)
Ann Arbor, Michigan

ABSTRACT

An important element in present and future programs for controlling eutrophication is the requirement for; (1) data which defines the existing trophic state of surface waters, (2) information which identifies cultural activities which contribute to the nutrient load entering a body of water, and (3) a mechanism for assessing eutrophication trends. Viewing these requirements in terms of the present situation in the U. S. and elsewhere, it is clear that consideration must be given to exploiting the capabilities of remote sensing technology. The sheer magnitude of the task indicates that current methods of data acquisition must be supplemented.

Reviews of the problem of eutrophication assessment indicate that over the years numerous parameters have been and are being used to measure eutrophication. The majority of these are closely interrelated and generally represent an attempt to measure directly or indirectly the major manifestation of the "enrichment of natural waters", which of course, is an increase in concentration of algae and higher plants. This paper discusses the potential use of remote sensing for the measurement of chlorophyll, suspended solids, "colored water masses", and aquatic vegetation.

INTRODUCTION

The literature dealing with eutrophication measurement indicates that over the years various investigators have relied on one or more of the following parameters to measure eutrophication [1,2,3].

1. Standing crop of algae and aquatic plants
2. Amount of suspended solids
3. Volume of algae
4. Chlorophyll levels
5. Number of algal blooms
6. Transparency
7. Plant regression
8. Photosynthesis
9. Primary production
10. Aquatic plant nutrient content
11. Hypolimnetic oxygen concentrations
12. Sediment composition
13. Dissolved solids
14. Conductivity
15. Nutrient concentrations
16. Cation ratio, $\frac{(N_a + K)}{(Mg + Ca)}$

The above list reflects the fact that no single parameter can serve as the measure of the trophic state, and also that certain parameters and combinations thereof appear to be most suitable in a particular geographic area. Additionally the list reflects the conceptual difficulty associated with the term trophic state. In the absence of a precise scientific definition, the term has been used to describe either productivity and/or nutrient status. In general, however, many of the parameters listed are closely interrelated and represent an attempt to measure directly or indirectly the major manifestation of the "enrichment of natural waters", which of course, is an increase in concentration of algae and higher plants. Concurrent with the above, attempts are normally made to document the nutrient status to some extent.

Examining the above list from the standpoint of current remote sensing technology; chlorophyll, colored water masses, suspended solids, transparency, and aquatic vegetation are regarded as being in the operational or near-operational state of development. In the case of eutrophic bodies of water the above measurements can be supplemented by documentation of algal blooms. All of the above parameters and manifestations are universally used and are regarded as basic indicators.

COLORED WATER MASSES

In addition to color originating from pollution sources, decaying vegetation, or other natural sources, color changes may occur as a result of changes in phytoplankton ecology and frequently are indicative of environmental changes in a body of water. Therefore, the occurrence of colored water deserves to be delineated and documented even if the observed phenomenon are not immediately interpretable. A case in point is the development and frequency of occurrence of colored water masses in southern Lake Michigan.

Development of "milky water" in Lake Michigan has been widespread during the last six years. The explanation for this phenomena is still lacking. It may be related to a new alga in the lake such as the Hypnodinium-like alga reported from Georgia by Ahearn, Hall, and Reinhardt [4], or to the synergistic action of a group of organisms. In Georgia, algal blooms which produce a milky color have been observed during 1968, 1969, and 1970. Disagreeable odors and thick surface flocs are other characteristics of the bloom. Ahearn, et al., report that the alga grossly resembles Hypnodinium sphaericum Klebs, a species which was reported only once previously from the United States.

The foregoing observations underscore the fact that the appearance of color anomalies or even subtle color changes may have important ecological implications. Hence color analysis must be included in a total eutrophication assessment program.

Frequently, color anomalies are subtle and hence difficult to identify and delineate without the use of remote sensing and computer-implemented processing of data. One processing system available at the Willow Run Laboratories for separating or identifying water masses is the SPARC (Spectral Analysis and Recognition Computer). Given a spectral signature as defined by the signals received from the various channels in the scanner, the SPARC maps all areas in the scene which have similar spectral characteristics. The output from the processor is normally in the form of color-coded recognition maps. An example is presented in Figure 1.

Data collected at water level along a transect through the scene are shown in Table 1.

The data shows that six distinctly different water masses were identified using the SPARC, whereas the observer at water level distinguished only three. Secondly, the data indicates that one important difference between the various water areas shown is Secchi disc transparency. Undoubtedly the differences are due not only to variations in total suspended solids but also variations in algal concentrations.

AQUATIC VEGETATION

An inventory of the standing crop of attached algae and/or higher aquatics constitutes yet another important data product in any lake assessment program. Information regarding changes in either the dominant species or total standing crop at a given geographic location normally contributes in a significant way towards characterizing a given water body and judging the effectiveness of control measures.

Delineation of the distribution of attached algae and/or higher aquatic plans is feasible by remote sensing using either photographic or multispectral scanner techniques. Simply documenting the growth of emergent vegetation or plants floating on the water is a relatively trivial task. Whereas identifying the species and calculating the areal distribution of each species in a scene

is a more complex undertaking, which in the majority of cases requires the application of spectral-signature recognition techniques.

In principle, the areal distribution of submerged aquatic vegetation can be determined using one of several computer-implemented recognition techniques. Although a considerable amount of experience has been gained in applying the above techniques in a number of fields, use of these techniques for the purpose of identification of submerged aquatic vegetation has not been attempted to any great extent. The efforts to date have been largely confined to very shallow waters. An example of the latter is seen in Figure 2.

Shown in Figure 2 is a portion of a river with heavy growths of Potamogeton and Cladophora in the study section. In this case, species identification using spectral recognition techniques was successful and area calculations were made. With ground-truth support, estimates of biomass also appear to be feasible.

A second example of the use of remote sensing for large scale mapping of the standing crop of attached algae is shown in Figure 3. In this particular situation Cladophora is the dominant attached species, hence identification of a mixture of species does not enter into the problem. In Lake Ontario, the growth of Cladophora normally reaches nuisance proportions and affects a number of beneficial water uses.

In this situation, maximum water penetration using the WRL scanner was obtained in the 0.52 - 0.57 μm band. Photography using a polarizer to minimize surface reflection was also found to be useful.

CHLOROPHYLL AND SUSPENDED SOLIDS

Chlorophyll has frequently been used as a measure of eutrophication. The relationship of the chlorophylls to phytoplankton production, phytoplankton activity, photosynthetic oxygen production, and state of eutrophication has been examined and reported by numerous investigators over the years [5,6,7,8,9,10].

The substances responsible for the absorption of light are the chlorophyll pigments, carotenoids, and special accessory pigments (see Table 2).

Two approaches are currently being exploited for the determination of chlorophyll by remote sensing. These are; (1) analysis of backscattered light in the chlorophyll absorption bands, and (2) fluorescence measurement. With respect to the former, Clarke, et al., [11] showed good correlation between shipboard measurement of chlorophyll and the spectra of backscattered light obtained from aircraft. Examining the spectral ratios 540 nm/460 nm, the authors found a decrease in reflectance at 460 nm and an increase in reflectance at 540 nm with increasing chlorophyll concentrations. Recent work by Arvensen, et al., [12] serves to further document the potential of the above ratioing technique. Using a differential radiometer operating at 443 nm and 525 nm, the authors were successful in measuring chlorophyll concentrations in the range 0.03 mg/m^3 - 10 mg/m^3. Others are investigating the use of fluorescence techniques [13,14].

The concentration of chlorophyll has been used as an index of phytoplankton concentration. Although the practice of using chlorophyll for the determination of phytoplankton concentrations has frequently been criticized, the technique remains popular, due in part to the speed and simplicity of analysis. In using chlorophyll as an index of phytoplankton concentration it must be recognized that a number of environmental and physiological factors will affect the chlorophyll-phytoplankton ratio. Light intensity, nutrients, species of organism, cell size and age will influence the amount of chlorophyll present. However, once the environmental-chlorophyll relationships are defined, quantitative estimates of phytoplankton present and their activity, can be made on the basis of chlorophyll analysis.

The fact that suspended solids have a bearing on the optical properties of a water mass and are a factor in other measurements, requires that any proposed remote sensing monitoring program include a provision for measurement of this parameter. For example in applying the ratioing technique for chlorophyll measurement, the effect of suspended solids cannot be completely ignored. For a given body of water, where particle size distribution and suspended solids concentration do not vary greatly, differential scattering will not produce significant errors in the reflectance ratios. However, failure to provide a procedure for normalizing the data may make comparisons between vastly different bodies of water difficult.

The problem of relating airborne scanner data to suspended solids concentration has been investigated at the Willow Run Laboratories. Prewett [16,17,18] has developed two general

equations for this purpose. The first is based on single scatter approximation and therefore, is suitable only for relatively clear waters; whereas the second equation attempts to take into account multiple scattering and can be used in any situation where bottom reflectance is not a factor. Results from a study of a series of ponds which receive treated effluent are shown in Table 3. The relative concentrations of suspended solids were found to be in good agreement with ground truth data. Chlorophyll "a" data were not available in this case, however, the variations in chlorophyll ratios are in general agreement with suspended solids data and the nutrient data which were available.

CONCLUSIONS

In addition to surface chlorophyll data, suspended solids, aquatic vegetation, etc., it should also be noted that remote sensing can provide a considerable amount of morphological and land use data which has a direct bearing on the trophic state of a body of water. Included in this last category is information dealing with shoreline development, watershed land use, lake surface area, and other cultural and physical features. From a water quality management standpoint this information is vital and equal in importance to the chemical and biological data normally collected.

With respect to the water mass, remote sensing techniques can provide data in terms of the major manifestations of eutrophication. However, characterization of the water mass with regard to nutrient status is outside the scope of current remote sensing technology. This last fact in no way detracts from the usefulness of remote sensing. The data needs of a statewide or nationwide lake assessment program and a lakes management program are very extensive. Meeting these needs will require the use of remote sensing together with conventional chemical and biological analytical procedures.

ACKNOWLEDGEMENTS

Data which forms the basis for this paper is derived in part from studies supported by the Environmental Protection Agency, Project Number 16020FOY and Project Number R-800778.

REFERENCES

1. Shannon, E.E. and Brezonik, P.L., 1972. "Eutrophication Analysis: A Multivariate Approach." Journal of the San. Eng. Div., ASCE., Vol. 98, No. SA1, pp. 37-57, February 1972.

2. Fruh, E.G., Stewart, K.M., Lee, G.F., and Rohlich, G.A. 1966. "Measurements of Eutrophication and Trends." Journal Water Pollution Control Federation, Vol. 38, No. 8, pp. 1237-1258, August 1966.

3. Lee, C.F. 1970. "Eutrophication." The University of Wisconsin, Water Resources Center, Eutrophication Information Program, Occasional Paper No. 2, University of Wisconsin, Madison, Wisconsin.

4. Ahearn, D.G., Hall, E.J. Jr., and Reinhardt, D.J. 1971. "Hypnodinium-like Algal Blooms in Georgia Lakes," BioScience, Vol. 21, No. 3, p. 18, February 1, 1971.

5. Ryther, J.H. and C.S. Yentsch. 1957. "The Estimation of Phytoplankton Production in the Ocean from Chlorophyll and Light Data." Limnology and Oceanography, Vol. 2, No. 3, pp. 281-286, July 1957.

6. Copeland, B.J., Minter, K.W., and Dorris, T.C. 1964. "Chlorophyll a and Suspended Organic Matter in Oil Refinery Effluent Holding Ponds." Limnology and Oceanography, Vol. 9, No. 4, pp. 500-506, October 1964.

7. Bailey, T.E. 1967. "Measurement and Detection of Eutrophication." Journal of the Sanitary Engineering Div., ASCE, Vol. 93, No. SA6, pp. 121-132, December 1967.

8. Strickland, J.D.H. 1960. "Measuring the Production of Marine Phytoplankton." Bulletin No. 122, Fisheries Research Board of Canada, Ottawa 1960.

9. Aruga, Y. and Monsi, M. 1963. "Chlorophyll Amount as an Indicator of Matter Productivity in Bio-Communities." Plant and Cell Physiol., Vol. 4, pp. 29-39.

10. Lorenzen, C.J. 1970. "Surface Chlorophyll as an Index of the Depth, Chlorophyll Content, and Primary Productivity of the Euphotic Layer," Limnology and Oceanography, Vol. 15, pp. 479-480, 1970.

11. Clarke, G.L., Ewing, G.C., and Lorenzen, C.J. 1970. "Spectra of Backscattered Light from the Sea Obtained from Aircraft as a Measure of Chlorophyll Concentration." Science, Vol. 167, pp. 1119-1121, February 20, 1970.

12. Arvensen, J.C., Weaver, E.C., and Millard, J.P. 1971. "Rapid Assessment of Water Pollution by Airborne Measurement of Chlorophyll." Proceedings Joint Conference on Sensing of Environmental Pollutants, Am. Inst. of Aeronautics and Astronautics, Palo Alto, California, November 1971.

13. Hickman, G.D. and Moore, R.B. 1970. "Laser Induced Fluorescence in Rhodamine B and Algae." presented at the 13th Conference on Great Lakes Research, Buffalo, New York, April 1970.

14. Stoertz, G.E., Hemphill, W.R., and Markle, D.A. 1969. "Airborne Fluorometer Applicable to Marine and Estuarine Studies." Marine Technology Society Journal, Vol. 3, No. 6, pp. 11-26, November-December, 1969.

15. Seliger, H.H. and McElroy, W.D. 1965. "Light: Physical and Biological Action." Academic Press, New York, New York.

16. Prewett, O. 1971. "A Model for Determining the Relative Concentration of Suspended Solids in Infinitely Deep Bodies of Water." Unpublished report, Willow Run Laboratories, Ann Arbor, Michigan.

17. Prewett, O. 1972. "Determination of Contour Lines of Constant Suspended Solids Concentration for Water of Infinite Depth." Unpublished report Willow Run Laboratories, Ann Arbor, Michigan.

18. Brown, W.L. et al., 1972. "Calculating Water Quality Parameters using Remotely Sensed Scanner Data." Proceedings, Eighth International Symposium on Remote Sensing of Environment, The University of Michigan, Ann Arbor, Michigan.



FIGURE 1

DIFFERENTIATION OF WATER MASSES USING SPARC PROCESSING
LAKE MICHIGAN AT ST. JOSEPH, MICHIGAN
Area = 8 x 1.3 miles

COLOR CODE: Green = emergent vegetation
Red = Potamogeton
Blue = Filamentous algae attached to hard surfaces

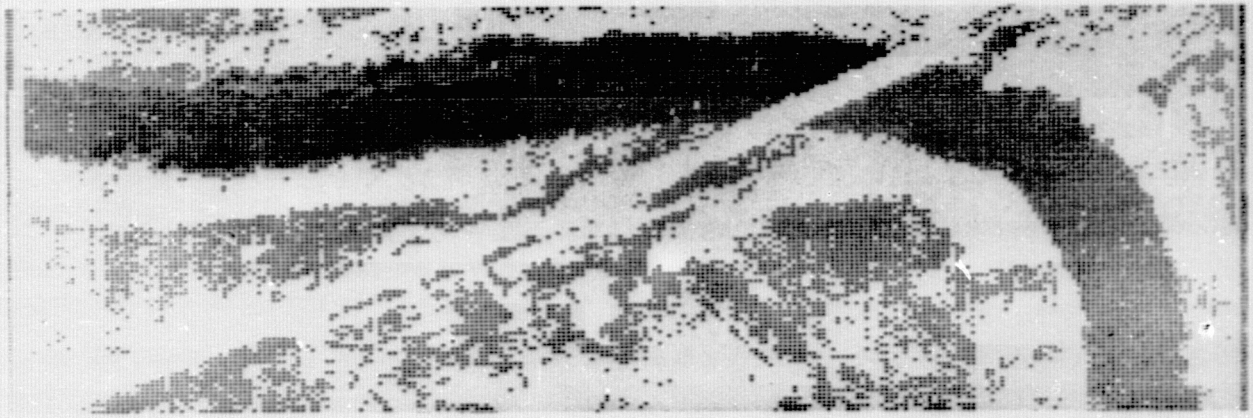
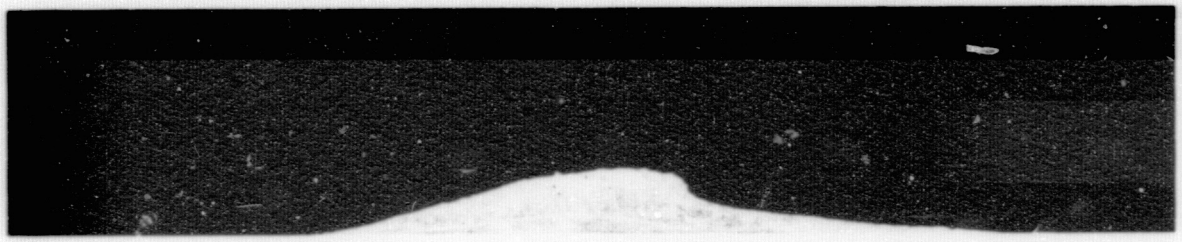
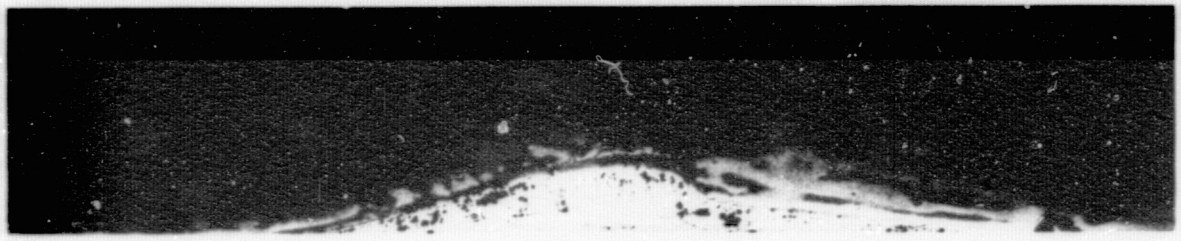


FIGURE 2. DIGITAL MAP OF AQUATIC VEGETATION
FLINT RIVER, GENESEE COUNTY, MICHIGAN



9.3-11.7 μm



0.52-0.57 μm

MULTISPECTRAL IMAGERY—LAKE ONTARIO NEAR NORTH HAMLIN, N. Y.
20 JUNE 1972

Sheet 1 of 2 Sheets

FIGURE 3

TABLE 1

TRANSPARENCY AND OBSERVED WATER COLOR LAKE MICHIGAN AT ST. JOSEPH, MICHIGAN

Station	SPARC Color Code	Secchi Disc Transparency (meters)	Observed Water Color
1	tan	0.8	milky light brown
2	light tan	1.5	milky light brown
3	green	1.8	milky brown green
4	green	1.9	milky brown green
5	green	2.1	milky brown green
6	green	2.3	milky brown green
7	light blue	2.9	milky brown green
8	light blue	2.9	milky brown green
9	medium blue	2.5	milky brown green
10	medium blue	2.5	milky brown green
11	medium blue	2.5	milky brown green
12	dark blue	5.6	milky light green
13	dark blue	3.7	milky light green

ERIM

TABLE 2

SPECTRAL CHARACTERISTICS OF PIGMENTS

"In vivo"

Wavelength (Peak Absorption)	Pigment
6750-6950 Å ca. 4400 Å	Chlorophyll a
ca. 6500 Å ca. 4650 Å	Chlorophyll b
ca. 6400 Å ca. 5850 Å	Chlorophyll c
ca. 4700 Å	fucoxanthin
ca. 5650 Å	phycoerythrin
ca. 6200 Å	phycocyanin

Source: Strickland [8]
Seliger and McElroy [15]

TABLE 3

RELATIVE CONCENTRATION OF SUSPENDED SOLIDS AND CHLOROPHYLL RATIOS SUMPTER TOWNSHIP, MICHIGAN

Location	Apparent Reflectance $\lambda = 0.41\text{-}0.48\ \mu$	Apparent Reflectance $\lambda = 0.52\text{-}0.57\ \mu$	Chlorophyll Ratio $\frac{R_{0.52-0.57}}{R_{0.41-0.48}}$	Suspended Solids Relative Conc. $c(r)/c(r_o)$
Pond #1	0.36	1.23	3.42	2.84
Pond #2	0.42	0.97	2.31	2.67
Pond #3	0.41	0.96	2.34	2.48
Pond #4	0.30	0.85	2.83	1.32
Control	0.34	0.62	1.82	1.00

ERIM

INVESTIGATION OF LAKE WATER QUALITY IN EASTERN SOUTH DAKOTA WITH REMOTE SENSING TECHNIQUES*

by

Fred A. Schmer, Merlin J. Tipton, Dennis W. Ryland

James Hayden, and George Beaver**

ABSTRACT

This study was directed toward hydrologic research with special emphasis on geology and its relationship to lake water quality. The applicability of remote sensing techniques for the evaluation and monitoring of lake water quality and as an aid for geological mapping was investigated. Ten lakes and their surrounding area (approximately 128 square kilometers) in northeastern South Dakota were selected for the study. These lakes were selected because of the diversity they represent in terms of water quality and fluctuation.

Visual interpretation of the imagery has resulted in a better understanding of the hydrology and geology of the study area. Improved geologic maps have been produced. The analysis of the remote sensing imagery and the water quality data was accomplished with linear correlation. Results of the correlations between the water quality parameters and the imagery were inconsistant and basically unsuccessful.

INTRODUCTION

This study is directed towards hydrologic research of 10 lakes in northeastern South Dakota in an area of approximately 128 square kilometers (50 square miles) (Figure 1). The specific objective is to determine the applicability of available remote sensing techniques for evaluation and monitoring the quality of the lake water with special emphasis on the geology and biology of the area and their relationship to lake water quality. Photographic and thermal remote sensing imagery aided in the interpretation of chemical, geological, and biological features and events, but water quality-imagery correlations were largely unsuccessful.

Eastern South Dakota has thousands of relatively small lakes and is covered by an uneven mantel of glacial drift. Most of the lakes owe their existence to depressions in this drift. Generally the depressions are due to uneven deposition of till, to melting of large chunks of ice buried within freshly deposited drift, or to depressions in the bedrock surface beneath the drift.

The 10 lakes studied in this report range in size from a fraction of a hectare to several square kilometers. All of the lakes are 1.5 to 6 meters (5 to 20 feet) deep with the exception of Medicine Lake which is 10 meters (35 feet) deep at the south end. Many are intermittent, or nearly so, within a few months following spring runoff. Some are semi-permanent, drying only in years of severe drought, and a few are permanent. Large differences in seasonal and yearly quality of these lakes has been observed. For example, the total solids in Medicine Lake near Watertown, South Dakota, varies from about 39,000 to over 80,000 ppm. Included within the 10 lakes is a range from Cooley Lake with 200,000 ppm total solids to Grass and Kampeska Lakes with total solids of 500 ppm.

DATA COLLECTION AND PROCEDURE

Remote sensing aerial flights were conducted during all seasons of the year to provide data

*The research work on which this paper is based was funded in part by the United States Department of Interior, Office of Water Resources Research Project B-022-SDAK.

** Hydrologist, Remote Sensing Institute, South Dakota State University; Associate State Geologist, South Dakota Geological Survey; Assistant Hydrologist, Remote Sensing Institute, South Dakota State University; Research Assistant, Biology Department, University of South Dakota; Research Assistant, Department of Geology, University of South Dakota

Preceding page blank

over varying water and ground conditions. Sixteen aerial flights were flown from May 26, 1970 to May 15, 1972. Aerial data collection was accomplished with a twin engine Beechcraft, RC45J, at altitudes of 1220 meters (4,000 feet) and 3050 meters (10,000 feet) above ground level. Fifty-two kilometers (32 miles) were covered on each flight over selected transects across the lakes and surrounding area. The variables, spectral ranges, and sensors used to collect the aerial data are listed in Table I. Data for all variables were not obtained for every aerial mission because of sensor limitations.

TABLE I. AERIAL DATA COLLECTION

Variables	Spectral Range	Method of Collection
Photography - Four Cameras		70mm Hasselblads
Black and White Film-Filtered		
Blue - 47B	0.37μm → 0.50μm	2402 Film
Green - 58	0.47μm → 0.61μm	2402 Film
Red - 25A	0.59μm → 0.70μm	2402 Film
Near Infrared - 89B	0.68μm → 0.90μm	2424 Film
Color Film - Filtered		
Color Reversal Infrared 15G/30M	0.51μm → 0.90μm	2443 Film
Color Film - HF 3/4	0.39μm → 0.70μm	2448 Film
Incoming Radiation	0.35μm → 1.15μm	Solameter
Outgoing Radiation-Filtered		Solameters
Blue - 47B	0.37μm → 0.50μm	
Green - 58	0.47μm → 0.61μm	
Red - 25A	0.59μm → 0.70μm	
Near Infrared - 89B	0.68μm → 0.90μm	
Thermal Infrared Radiation	4.5 μm → 5.5 μm 8.7 μm →11.5 μm	Daedalus Line Scanner
Surface Temperature	8.0 μm →14.0 μm	Precision Radiation Thermometer
Haze Condition		Evaluate
Cloud Type and Condition		Evaluate
Cloud Cover		Evaluate

Ground truth data consisting of lake surface temperatures and water samples for laboratory analysis were collected simultaneously with the remote sensing flights. A four liter Van Dorn sampler was used for the water samples, and a Model FT3 hydrographic thermistor thermometer (Applied Research Austin, Austin, Texas) was employed for the thermal measurements.

One liter water samples were collected at various selected sites (Figure 1) on each lake until it was determined by chemical analysis that mixing was sufficient to allow one, or at most, three samples from each lake. Water samples were analyzed for the following parameters: chloride, total hardness, sulfate, calcium, alkalinity, iron, magnesium, total solids, manganese, nitrogen, fluoride, ortho and poly phosphate, and pH. The water temperatures from various depths in the lakes were also recorded. In addition vertical control data were collected to gain an understanding of topographic and geologic relationships of hills, outwash, lake levels, and moraines.

Medicine Lake, around which the entire study revolved, was given priority during data collection, and hence, up to two hours delay occurred between collection of the aerial data and the ground truth for the last lake on the flightline (Kings Lake). However, since it is well known that water temperature changes occur very slowly, little if any error was thought to have occurred from this delay.

Collection of data proceeded as follows in all but the 5/15/72 flight: Medicine Lake, McKillicans Lake, Round Lake, Horseshoe Lake, Long Lake, Stink Lake, Nicholson Lake, Cooley Lake, Grass Lake, and Kings Lake. During the 5/15/72 flight, two boats were used resulting in much less delay between ground truth data and aerial data collection.

The majority of the lakes may be considered magnesium-sulfate lakes with sodium becoming the more dominant cation in the more senescence lakes.

Poor aquifer flushing, characteristic of closed drainage systems resulted in an accumulation of dissolved solids in the ground water. The ground water averaged 2153 mg/liter dissolved solids with an accumulation of sulfate which averaged 40% of the dissolved solids by weight. With the exception of Grass Lake, the study lakes all occupy closed depressions with little or no ground water movement between, and exist in various stages of senescence depending upon local climate and edaphic conditions. All lakes except Grass Lake are also similar in chemical composition with sulfate again the dominant ion averaging between 63% and 70% by weight of the dissolved solids. Evaporation appears to be the principal cause of water loss and consequent mineralization.

Medicine Lake is a permanently stratified lake with a dissolved solids concentration increasing from about 5% to 17% with depth. In a narrow zone at a depth of 3.2 - 3.7 meters, intense photobacterial activity existed during the ice-free season. This bacterial plate was found at 4.3 meters in the late fall and winter. Surface water carbon-fixation rates usually were below 25 mg C/m^3/day, but an early July rate of 200 mg C/m^3/day was recorded. Bluegreen algal production in the upper-chemocline resulted in rates in excess of 300 mg C/m^3/day. Photobacterial production rates between 1000-2000 mg C/m^3/day were common in the summer months with the photobacteria accounting for approximately 43% of the recorded pelagic production. Total summer square meter pelagic production rates were below 700 mg C/m^2/day which would put Medicine Lake in the mesotrophic lake category. However, CHARA production rates were not assessed, and had the rates of these littoral producers been averaged with the pelagic production rates, a higher estimate or productivity and lake trophy may have resulted.

IMAGERY ANALYSIS

Remote sensing imagery analysis was accomplished by visual interpretation, color encoding analysis, and statistical analysis aided by ground truth data obtained at the time of the aerial flights.

Geology

The geology of the study area can be found in either of two previous studies; Flint (1955) for a broad overview of eastern South Dakota, and Tipton and Stockdale (1971) for a more detailed report. It was not the purpose of this study to repeat former work, but to expand and improve the mapped areas using remote sensing imagery as a tool.

A mosaic of the color-infrared imagery was prepared. From this mosaic, ground surveys carried out by the authors, aerial photography done for the South Dakota Geological Survey in 1953, and mapping done by Richard Stockdale (1971), overlays were drawn showing the geology of the study area.

As a direct result of remote sensing imagery, several topographic features were identified, clarified, and mapped which were not previously known or else simply overlooked. However, it cannot be stated with any certainty whether or not these features would have been found had the mosaics not been made. Once the features were located they were very obvious in the 1953 aerial photographs.

Figure 2 is a well developed disintegration ridge that is approximately 4.8 kilometers (3 miles) long, 18 meters (60 feet) wide, and 9 meters (30 feet) high. At the south end, the ridge turns from a positive topographic feature to a negative one as it becomes an intermittent stream in the direction of Lake Kampeska. This evidence would suggest a subsurface stream at the base of a disintegrating ice block or, it would indicate where the sub-ice river exited the ice block and began cutting a channel in the till. It is difficult to say why the authors and two previous investigators missed such a well-developed ridge during their surveys, but it is certain that the infrared mosaic was responsible for its discovery.

The thermal imagery was especially effective in improving the mapping of three previously mapped disintegration ridges near Medicine Lake. This was most notable on the east-west trending ridges during the day when differential heating of the north and south slopes provided striking contrasts on the imagery.

Figure 3 shows a topographic feature called a doughnut. These structure are circular, raised

mounds of varying sizes characterized by a depressed center, thus resembling a large doughnut. Formation of these doughnuts is still highly speculative, but it is generally agreed that they are characteristic of stagnation drift. This particular doughnut is several hundred meters across, somewhat less than circular, and about 6 meters (20 feet) high. The surrounding topography is uneven enough to mask the presence of the doughnut from observation on the ground, but the aerial photography picks it out quite well, as the figure plainly shows.

Figures 4 and 5 show strand lines as much as 9 meters (30 feet) above the present shores on McKillicans Lake and Medicine Lake respectively. The peninsula jutting into Medicine Lake in Figure 5 shows the best markings left by old lake levels. Here it is interesting to note that only the infrared imagery shows such clearly contoured strand lines. Neither the 1953 black and white photographs nor the regular color photos from this study show such clear details.

Lake Anomalies

Visual interpretation aided by ground truth information was utilized to explain anomalies that appeared on the aerial imagery. Such an anomaly was observed in Medicine Lake shown in the color infrared photograph of Figure 6 taken on April 20, 1972. The light circular patterns in the lake had not been observed at any previous time and were believed to be a white sulfur bacterium such as Beggiota sp. layered at a temporary oxidation-reduction transition zone approximately 1.5 meters below the water surface. The phenomena did not last for an appreciable period of time as Figure 7 taken on May 4, 1972 illustrates. The white layer of sulfur bacteria and the chemical gradient responsible for the redox transition zone were partially dissipated by subsequent stronger winds and forced down to a greater depth of approximately 2.5 meters.

Color Encoding Analysis

The interpretation of imagery, particularly thermal infrared imagery, was aided by the use of a color encoding film density analysis system. Figure 8 shows the results of the color encoded density analysis of the thermal infrared imagery of Medicine Lake for four aerial flights conducted in 1971. Nine density levels were used in the analysis where light areas represent cooler surface temperatures than dark areas. One of the factors which can affect the collection of accurate thermal infrared data is surface wind. Figure 8(a) shows the possible effect of surface wind by the change from warm on the windward side to cool on the leeward side of the lake.

Another interesting phenomenon observed from Figure 8 is the complete reversal of the surface temperature from one end of Medicine Lake to the other between the June 13 and August 11 aerial flight. Medicine Lake is unique in that one end is deep (10 meters at the deepest point) and the other end is shallow (1.5 meters at the deepest point). The June 13 flight shows the surface temperature of the deep end to be the coolest and the August 11 flight shows the shallow end to be the coolest.

Statistical Analysis

Determination of the relationship between the water quality parameters and the remote sensing aerial photography was accomplished with the use of the statistical method of linear correlation which is a measure of the degree to which variables change together. Spot film densities were measured on the 1220 meter and 3050 meter imagery at the location where the water samples were taken. Densities were measured with a transmission densitometer. All four filters were used for color and color infrared film. The red, green, and blue filters allow measurement of film density for each of the three layers of color and color infrared film.

Correlation coefficients were computed for eight of the aerial missions flown in conjunction with the collection of water samples. The significance of each correlation coefficient at the five and one percent level was then determined. Table II shows the correlation coefficients, aerial mission date, and altitude for color infrared film using the infrared layer of the film. The water quality parameters and film-filter combinations presented in Table II were selected because of the significance shown by the correlation coefficients over all the aerial mission dates and altitudes. The lack of consistent correlation between aerial missions may be caused by variations of weather conditions, and date and time of day of the flight which would affect the sun angle and the amount of radiation reflected from the surface being photographed.

Although turbidity was only included in the water analysis for two sampling dates it is interesting to note the significance of the correlation coefficients obtained. The results would seem to show that the correlation of turbidity and film density is possible but because of the limited data available additional study would provide more conclusive results.

SUMMARY AND CONCLUSIONS

Research was begun to determine the applicability of remote sensing techniques for evaluating and monitoring lake water quality, as an aid for geological mapping and in locating and explaining temperature variations and anomalies in the lakes. Aerial flights provided photography and thermal scanner imagery of selected lakes and their surrounding area in northeastern South Dakota. During the aerial flights extensive ground truth data was collected to aid in the analysis and interpretation of the aerial imagery.

The correlation of film density with the water quality parameters showed good results for specific aerial missions but considerable variability was noted between aerial missions. The correlation coefficients for the infrared layer of the color infrared film showed the best results over all the aerial missions. Significant correlation coefficients were obtained for turbidity, total solids, chloride, and iron for more than one aerial mission. With the analysis techniques utilized the photographic and thermal remote sensing imagery aided in the interpretation of chemical, geological, and biological features and events, but water quality-imagery correlations were basically unsuccessful.

REFERENCES

1. "Climatological Summary", U. S. Department of Commerce, National Oceanic and Atmospheric Administration, Environmental Data Service, Asheville, North Carolina, 1971.

2. Flint, R. F., 1955, Pleistocene Geology of Eastern South Dakota: U.S.G.S. Prof. Paper 262, 172 p.

3. Gates, David M., "Characteristics of Soil and Vegatated Surface to Reflected and Emitted Radiation", Proceedings of the Third Symposium on Remote Sensing of Environment, University of Michigan, Ann Arbor, Michigan, pp. 573-600, 1966.

4. Helgeson, Gaylord A., and Ross, Donald S., "Remote Sensor Imaging for Oceanography", Oceanology Vol. 5, No. 9, pp. 20-25, September, 1970.

5. Ross, Donald S., "Enhanced Oceanographic Imagery", Proceedings of the Sixth International Symposium on Remote Sensing of Environment, University of Michigan, Ann Arbor, Michigan, pp. 1029-1044, 1969.

6. Standard Methods of the Examination of Water and Wastewater, 13th Ed. New York: American Public Health Assoc. A., Water Works Assoc., and Water Pollution Control Federation.

7. Steele, Robert G. D., and Torrie, James H., Principles and Procedures of Statistics, McGraw-Hill Book Company, Inc., New York, NY, pp. 183-193, 453, 1960.

8. Tipton, M. J., and Stockdale, R. G., 1971, A geologic study of the chemical quality of Medicine Lake: Office of Water Resources Research, Brookings, South Dakota, 46 p.

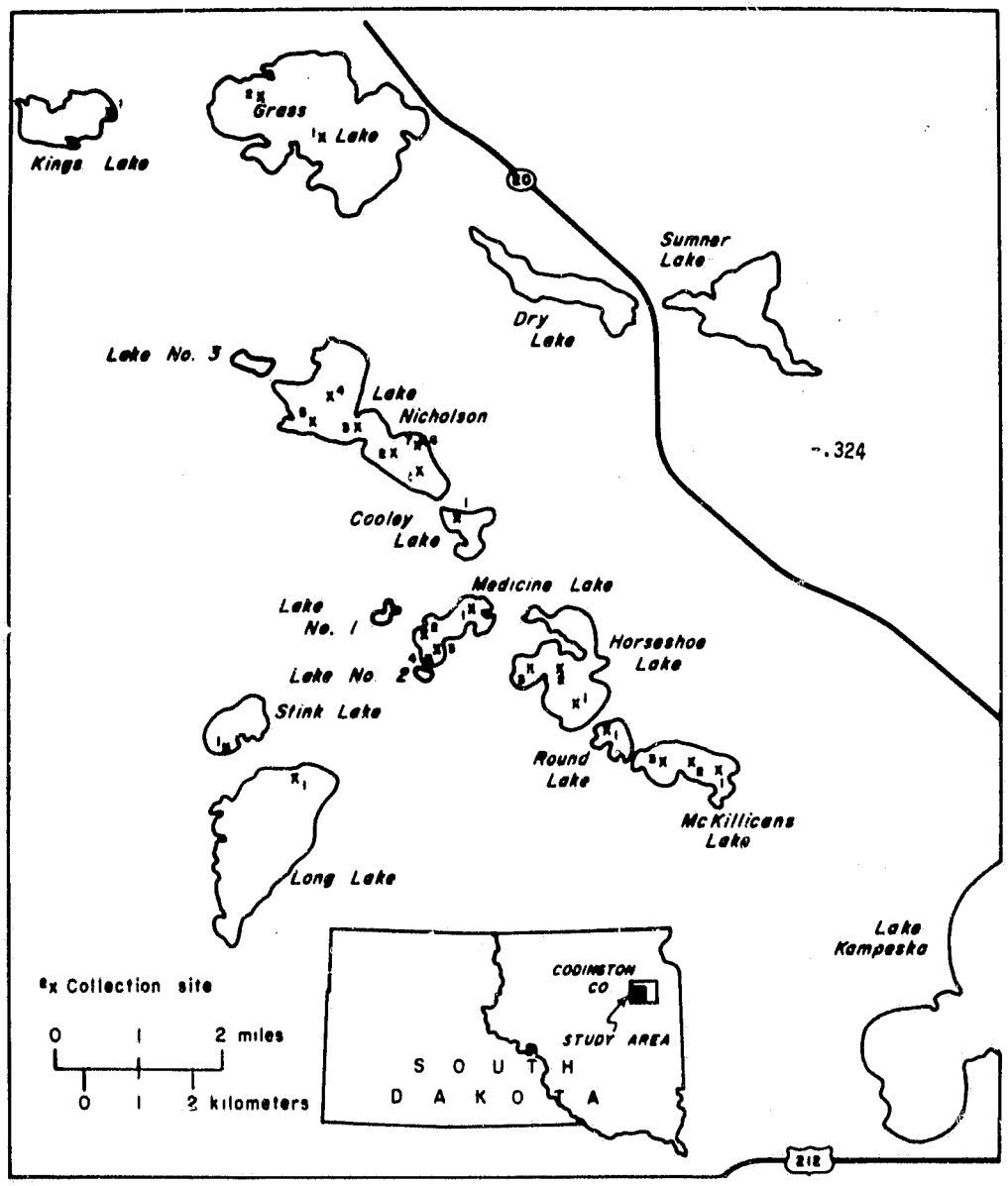


Figure 1. Index map of study area, Codington County, South Dakota, showing collection sites.

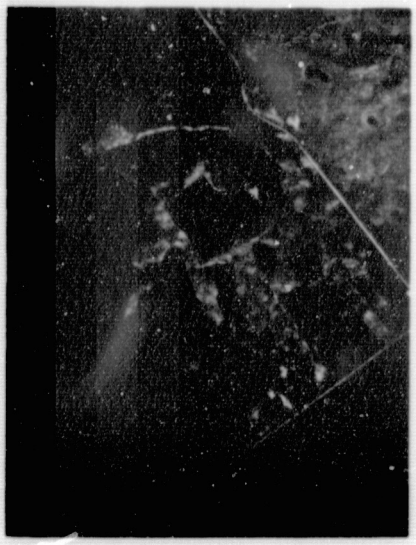


Figure 2. Altitude 3050m (10,000 ft)

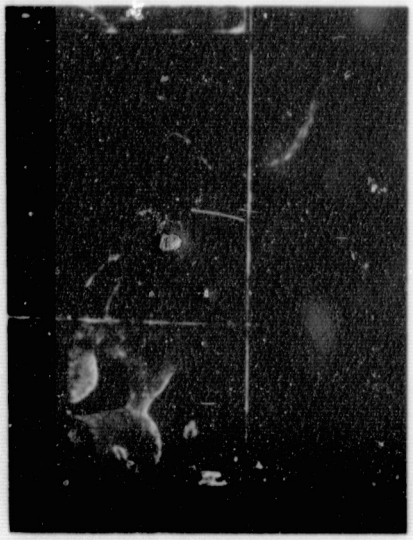


Figure 3. Altitude 3050m (10,000 ft)

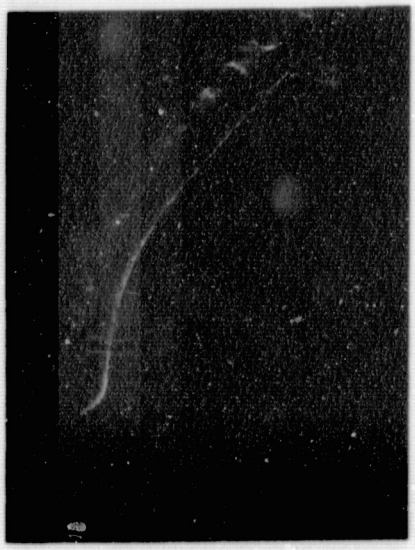


Figure 4. Altitude 1220m (4,000 ft)



Figure 5. Altitude 1220m (4,000 ft)

Figures 2,3,4,5. Color infrared imagery showing topographic features discovered in the study area.



Figure 6. Print from color infrared film, #8443 with G15/30M filter, showing Medicine Lake on April 20, 1972, 1220m (4,000 ft) agl, 3X enlargement, scale: 1 cm = 85m.



Figure 7. Print from color infrared film #8443 with G15/30M filter showing Medicine Lake on May 4, 1972, 3050m (10,000 ft) agl, 5X enlargement, scale: 1cm=120m.



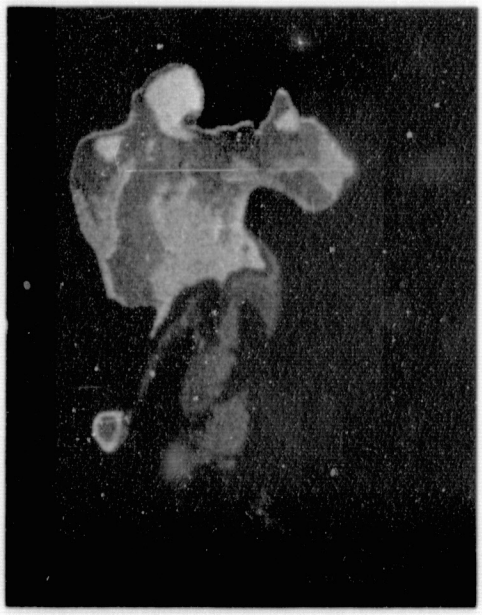
(a) April 14, 1971



(b) June 13, 1971



(c) July 26, 1971



(d) August 11, 1971

Figure 8. Color encoded density analysis of thermal infrared imagery showing Medicine Lake for the four 1971 aerial flights.

TABLE II. CORRELATION COEFFICIENTS FOR COLOR IR (RED FILTER) AND SELECTED WATER QUALITY PARAMETERS

Date / Altitude (Meters)	Water Quality Parameters					
	Total Solids	Calcium	Chloride	Iron	Nitrate	Turbidity
05 26 70						
4420	-.756	.186	-.784	-.968**	-.936**	
07 29 70						
1220	.145	.143	-.688	.110	.058	
08 25 70						
3050	-.191	-.192	-.693	-.381	-.422	
1220	-.177	.036	-.850*	-.519	.089	
04 14 71						
3050	-.590*	-738**	-.614**	-.682**	.089	
06 13 71						
3050	-.237	-.084	-.212	-.690**	.049	-.847**
08 11 71						
3050	.098	-.053	.062	.032	.102	-.621**
1220	.224	.062	.241	.298	.100	-.538**
05 04 72						
3050	-.506*	-.393	-.464*	-.410	.174	
1220	-.520*	-.393	-.489*	-.550*	-.001	

** Significant at the one-percent level
* Significant at the five-percent level

CALCULATING WATER QUALITY PARAMETERS USING REMOTELY SENSED SCANNER DATA

by

W. L. Brown, F. C. Polcyn, J. R. McKimmy, and O. E. Prewett

Willow Run Laboratories
The University of Michigan
Ann Arbor, Michigan

ABSTRACT

The method for calculating relative concentration gradients in shallow bodies of water is demonstrated, and the model for extending the method to very deep and/or very turbid water is presented. The information obtained from the wide-area application of these techniques will assist greatly in assessing water quality and in analyzing the eutrophication of major bodies of water.

The shallow-water case which was analyzed was along the shoreline of Lake Michigan. The data used in the analysis were obtained under contract with the Indiana and Michigan Electric Company as part of a study of power plant cooling-water discharges in the vicinity of Bridgeman, Michigan. The deep, turbid-water case is part of a study of Lake Ontario, sponsored by U. S. Army Corps of Engineers. The general modeling formulation was sponsored by Space Oceanography Group formerly under NRL and now under NOAA.

1. INTRODUCTION

When a body of water in direct sunlight is viewed by a multispectral scanner, it receives electromagnetic radiation which has been reflected from the air/water interface, from particles in the air and particles in the water, and from the ocean floor. Previous work by the authors (Ref. 1) showed how the spectrally variant attenuation coefficients of the water and the reflectance of the ocean floor could be determined directly from the multispectral data. The present work has extended these results to the calculation of relative concentrations of bodies (sand, algae, etc.) suspended in the water.

2. MATHEMATICAL BASIS AND PROCEDURE

Consider the radiation incident upon the aperture of the multispectral scanner. This radiation can be separated into (a) radiation reflected from the ocean floor and (b) radiation from other sources. In the case of very "cloudy" water, the "ocean floor" may in fact be a pseudo-floor which is actually comprised of a myriad of light-reflecting particles suspended in the water. One striking example of the latter condition was reported by the authors in an earlier work (Ref. 2), where the Caesar Creek ship channel in Miami was being studied. A ship had passed through the channel, churning up sand from the bottom, just prior to the overflight of the multispectral scanner. Subsequent analysis of the data indicated that the channel was about 12 ft deep, compared with its actual depth of 20 to 30 ft. Visual inspection of the channel, under similar conditions, indicated that the depth as determined by a "secchi disk" measurement would have been very close to the calculated figure of 12 ft.

2.1 SHALLOW-WATER CASE

It has been shown (Ref. 1) that the magnitude of the illumination from the ocean floor can be estimated from the following:

$$\ell n \left[\frac{\Delta V_i}{(V_i)_{ss}} \rho_{ss}(\lambda_i)\right]$$

$$= \ell n [\rho_b(\lambda_i) - \rho_s(\lambda_i)] - (a_i + s_i) f(\theta, \phi) z$$

where ΔV_i = signal in spectral band λ_i induced by incident radiation from ocean floor;

$(V_i)_{ss}$ = signal from solar reference in band λ_i;

$\rho_{ss}(\lambda_i)$ = throughput of the solar reference in band λ_i;

$\rho_b(\lambda_i)$ = bottom reflectance;

$$\rho_s(\lambda_i) = \frac{s_i}{a_i + s_i} \quad \frac{1}{4\pi(1 + \sec\theta/\sec\phi)}$$

a_i = absorption coefficient of water;

s_i = scattering coefficient;

θ = look angle (from nadir);

ϕ = solar declination;

$f(\theta, \phi)$ = $\sec\theta + \sec\phi$

z = water depth

Note that, if $z \to 0$, the result is:

$$\frac{\Delta V_i(z = 0)}{(V_i)_{ss}} \rho_{ss}(\lambda_i) = \rho_b(\lambda_i) - \rho_s(\lambda_i)$$

Also, the slope of the function is:

$$(a_i + s_i) f(\theta, \phi)$$

It is instructive to look at these values as θ and ϕ approach zero, i.e., for normal viewing and illumination. In such case, we obtain:

$$\frac{\Delta V_i(z = 0)}{(V_i)_{ss}/\rho_{ss}(\lambda_i)} \doteq \rho_b(\lambda_i) - \frac{1}{8\pi} \quad \frac{s_i}{a_i + s_i}$$

$$\text{SLOPE} \doteq 2(a_i + s_i)$$

The parameter $\frac{s_i}{a_i + s_i}$ is given the name $(w_o)_i$, for simplicity. Thus,

$$(w_o)_i \doteq 8\pi \left[\rho_b(\lambda_i) - \frac{\Delta V_i(z = 0)}{(V_i)_{ss}/\rho_{ss}(\lambda_i)}\right]$$

$$s_i = (1/2 \text{ slope}) \cdot (w_o)_i$$

$$a_i = 1/2 \text{ slope} \cdot [1 - (w_o)_i]$$

The relative concentration is given by the following formula (Ref. 3):

$$\frac{c}{c_{REF}} = \frac{(w_o)_1 \; a_1}{g_{1,2} - (w_o)_1 \; h_{1,2}}$$

where $g_{1,2} = \dfrac{(w_o)_1 \; (w_o)_2 \; (a_2 - a_1)}{(w_o)_1 - (w_o)_2}$

and $h_{1,2} = \dfrac{(w_o)_2 \; a_2 - (w_o)_1 \; a_1}{(w_o)_1 - (w_o)_2}$

The steps which are taken to compute the ratio of the local concentration to the reference concentration are:

(a) Obtain values for $(w_o)_1$ by plotting ΔV_1 versus z;

(b) Obtain values for a_1;

(c) Compute the ratio.

The values of λ_1 and λ_2 must be chosen carefully. It is important that they be chosen in a region of the spectrum where the value of a_1 is varying rapidly. Also, c_{REF} must be measured from the point of maximum concentration so that $(c/c_{REF}) \leq 1.0$ everywhere.

The Lake Michigan shoreline provided an ideal test site for the method, since the properties of the bottom (sand) are well known, the depth profile was measured on the day of the flight, and the variations were relatively slow and smooth. A computer program was developed which computed a + s (total attenuation) from the slope of the ΔV_1 curve. The results of this process are presented in Figure . Note that the total attenuation at 0.42 μm and 0.48 μm appears to be constant with depth. Also, note that the rate of change of attenuation with depth is apparently identical for wavelengths greater than 0.51 μm.

2.2 DEEP WATER CASE

In the case of deep water, or water which is so cloudy that the bottom cannot be seen, the determination of the relative concentrations of suspended solids proceeds in two steps. The first is the determination of the parameter w_o and the second the determination of the concentration using the parameter w_o.

The parameter w_o is the ratio of the total scattering coefficient s to the extinction coefficient a + s. This parameter is determined implicitly, for waters of infinite depth, by the equation

$$V_s(\mu') = \frac{w_o}{4} H(\mu)H(\mu_o)N(\mu)T(2,1,\mu)T(1,2,\mu_o')\left(\frac{n_1}{n_2}\right)^2 \frac{V_{ss}}{\mu_o \rho_{ss}} + V_\infty(\mu')$$

The symbols used above are grouped into classes and defined below.

(1) Observables - These quantities are data taken by or in conjunction with the scanner.

$V_s(\mu')$ = the observed scanner voltage

V_{ss} = the voltage of the sun sensor

μ' = the cosine of the "look" angle in air of the scanner. This angle is measured from the downward vertical direction.

ρ_{ss} = the reflectance of the sun sensor. This quantity is determined by direct measurement when the scanner is calibrated

μ_o' = the cosine of the zenith angle in air of the sun at the time of the flight

$V_\infty(\mu')$ = the contribution of background light and haze to the observed voltage $V_s(\mu')$. This

contribution is equal to the scanner voltage $V_s(\mu')$ over an infinitely deep body of pure water. For practical purposes, clean lake water of depth greater than 50 feet will suffice.

(2) Tabulated Quantities

n_1 is the index of refraction of air. This number may be taken to be 1.000

n_2 is the index of refraction of water. This number may be taken to be 1.33

$H(\mu)$ is the Chankasakhar H function. It is given in tables supplied by Prewett.

(3) Calculated Quantities

μ_o is the cosine of the zenith angle, in water, of the sun. This quantity is calculated from μ_o' by the equation

$$\mu_o \cos\left[\sin^{-1}\left\{\left(\frac{n_1}{n_2}\right)\sin(\cos^{-1}\mu_o')\right\}\right]$$

which is just a transformation of Snell's Law.

μ is the cosine of the zenith angle, in water, of the scanner look angle. It is found by substituting μ' in the formula above for μ_o'. In general, the primed quantities refer to the air side of the air-water interface; and the unprimed quantities refer to the water side of the interface.

$N(\mu)$ is calculated by means of a computer program developed by Dr. Omer E. Prewett and Mr. Dave Zuk.

$T(2,1,\mu)$ is the quantity $1-\rho(2,1,\mu)$, where $\rho(2,1,\mu)$ is the reflectance and the air-water interface of a ray traveling from the water to the air. This is calculated from the Fresnel equations using n_1, n_2, and μ.

$T(1,2,\mu_o')$ is the quantity $1-\rho(1,2,\mu_o')$ where $\rho(2,1,\mu_o')$ is the reflectance at the air-water interface of a ray traveling from the air to the water. This quantity is calculated from the Fresnel equations using n_1, n_2, and μ_o'.

w_o is the ratio of $s/(a+s)$. The determination of this quantity is the object of this section.

The parameter w_o is determined from the observed data in the following way:

(1) Using the data determine $\Delta V \equiv V_s(\mu') - V_\infty(\mu')$

(2) Then find the quantity

$$G(w_o) \equiv \left(\frac{\rho_{ss}\,\mu_o}{V_{ss}}\right)\left(\frac{n_2}{n_1}\right)^2 \frac{\mu}{[T(2,1,\mu)][T(1,2,\mu_o')]}\,\Delta V(\mu')$$

This quantity $G(w_o)$ equals

$$G(w_o) = w_o\, H(\mu)\, H(\mu_o)\, N(\mu)$$

each factor of which depends either explicitly or implicitly on w_o.

(3) Solve the equation

$G(w_o) = w_o\, H(\mu)\, H(\mu_o)\, N(\mu)$ for w_o by numerical or graphical means.

The quantity $w_o\, H(\mu)\, H(\mu_o)\, N(\mu)$ is a monotonic single-valued function of w_o. Hence, since $G(w_o)$ is known, a unique solution exists for w_o. The simplest way, conceptually, to determine w_o is by graphing $G(w_o)$ as a function of w_o and picking the w_o corresponding to the value of $G(w_o)$ determined from the data. For numerical solution by computer an iterative procedure will probably be necessary.

The relative concentration of suspended solids in water is determined using the values of w_o found at a particular point in the body of water. The location of this point will be denoted by the vector r. Because of the multispectral nature of the data, for each point r, there are as many

values of w_o as there are wavelength bands in the scanner. These wavelengths bands are denoted by λ_1. The dependence of w_o on both r and λ_1 is indicated by writing $w_o = w_o(r,\lambda_1)$.

The relative concentration is found upon 4 imput parameters. These are $w_o(r, \lambda_1)$, $w_o(r, \lambda_2)$, $w_o(r_o, \lambda_1)$, $w_o(r_o, \lambda_2)$. The variable r_o refers to the location of the reference concentration $c(r_o)$ and the variable r refers to the location of the concentration being measured, c(r). It is necessary also to know the absorption coefficients a_{H_2O} of lake water without suspended solids, at wavelengths λ_1 and λ_2.

The relative concentration is given by the following formula:

$$\frac{c(r)}{c(r_o)} = \frac{w_o(r, \lambda_1)\, a_{H_2O}(\lambda_1)}{g(r_o,\lambda_1,\lambda_2) - w_o(r,\lambda_1)h(r_o,\lambda_1,\lambda_2}$$

where

$$g(r_o,\lambda_1,\lambda_2) \quad \frac{w_o(r_o,\lambda_1)\, w_o(r_o,\lambda_2)[a_{H_2O}(\lambda_2) - a_{H_2O}(\lambda_1)]}{[w_o(r,\lambda_1) - w_o(r,\lambda_2)]}$$

$$h(r_o,\lambda_1,\lambda_2) = \frac{[w_o(r_o,\lambda_2)a_{H_2O}(\lambda_2) - w_o(r_o,\lambda_1)\, a_{H_2O}(\lambda_1)]}{w_o(r_o,\lambda_1) - w_o(r_o,\lambda_2)}$$

The next phase of the work will involve applying the foregoing algorithms to data collected over a particularly interesting portion of the Niagara River Plume.

3. CONCLUSIONS

We have shown that it is practical to compute relative concentrations of suspended particulate matter over wide areas of water. The techniques, with refinement of computer implementation and data handling methods, should prove useful in environmental studies.

REFERENCES

1. W. L. Brown, F. C. Polcyn, and S. R. Stewart, "A Method for Calculating Water Depth, Attenuation Coefficients and Bottom Reflectance Characteristics," Proc. Seventh International Symposium on Remote Sensing of Environment, 17-21 May 1971, pp. 663-682.

2. F. C. Polcyn, W. L. Brown, and I. J. Sattinger, "The Measurement of Water Depth by Remote Sensing Techniques," The University of Michigan, Institute of Science and Technology, Willow Run Laboratories, Report 8973-26-F (October 1970).

3. O. E. Prewett, "Determination of Contour Lines of Constant Suspended Solids Concentration for Water of Infinite Depth," (unpublished paper), March 3, 1972.

LOCATION OF SAWDUST IN THE PENOBCOT RIVER

BY A MULTISPECTRAL SCANNER

Phil Chase and Al Conrod
Bendix Aerospace Systems Division
Ann Arbor, Michigan

Edward Imhoff
University of Maine
Orono, Maine

ABSTRACT

An airborne multispectral scanner was employed in locating sawdust in the Penobscot River estuary at low tide. Airborne color photography was used as a remote means of selecting classification areas for training the computer to automatically produce imagery displaying the sawdust only, mud (and muddy water) only, and sawdust and mud simultaneously. The statistical analysis and processing techniques are briefly described and the imagery presented.

A ground team using the automatically produced imagery searched the river with a Ponar Grab for the sawdust deposits. The location of the sawdust by a ground team has been placed on the imagery. The imagery was accurate.

Having now developed and established this use of the airborne multispectral scanner, it is compared to other methods of location in terms of cost per river mile, accuracy, and safety. The advantages of the multispectral scanner technique are its ability to cover large stretches of river in a short time and produce selective imagery.

The importance of locating and removing sawdust is brought out: Sawdust prevents shellfish growth. It also would serve as a BOD source after the river water quality has been improved.

A gross estimate of the negative economic impact of sawdust on the reclamation of the estuarine rivers in Maine is given. Then, a gross estimate is given of the cost of sawdust removal and finally the savings incurred by the use of remote sensing.

INTRODUCTION

Sawdust and wood chips have been settling in the tidal rivers of Maine for at least 100 years. These deposits are costly in both an economic and an ecological sense. On the other hand removal of the deposits is expensive. These costs in removal of the sawdust beds derive from their location, the estimate of their areal extent and depth and in the dredging. The benefits of the removal are greater than the cost.

Preceding page blank

Even though dredging is the greater portion of the cost, savings can be obtained by locating and estimating the areal extent of the sawdust beds by remote sensing. The combined role of remote and in situ sensing is necessary to obtain an estimate of the depth of the beds. Because the rivers are hydraulically active, the in situ techniques are in some measure dangerous and certainly quite time consuming. And, as was determined, the sawdust beds form generally along the banks. These banks are exposed at low tide. Remote sensing from aircraft is able to sense these banks. Once the sawdust beds are located, in situ methods, such as probing (coring), are used to obtain the depth of the beds. From these data the dredging operation can be planned.

The airborne sensors were a 70 mm framing camera (color film) and an eight channel multispectral scanner (MSS). The color film was used to select an area of sawdust (and wood chips) to train the computer to recognize other sawdust areas in the MSS tape recorded data. A thematic map is automatically produced for the river and its banks. A similar routine is used for mud (and muddy water). Surface location of the beds was conducted independently at first using a Ponar grab. Later in the project the thematic maps were used to select areas for surface exploration. This latter procedure was more successful.

The discussion that follows presents a brief description of the remote sensing technique employed and the thematic maps obtained automatically. These maps are compared to a map prepared by surface techniques. The comparison is favorable in that the sawdust locations are almost the same. The value of this remote sensing application is placed in the context of dollars saved by remote sensing in sawdust removal and in turn the economic return for the removal of the sawdust.

THE REMOTE SENSING MISSION

The Penobscot River was flown at 1000-ft altitude from north of Old Town to the southern tip of Verona Island. Both the Eastern Channel and the river at Verona Island are included. Adjacent land for at least 250-ft back from each bank is included. The time of flight was 16 August 1971 from 11:30 a.m. at Old Town to 12:45 p.m. at Verona Island. Low tide occurred at approximately 1:15 p.m. The weather conditions were generally sunny and clear with scattered high cirrus clouds. Ground temperature was 24°C at Bangor. The section of the river is shown on the map following Figure 8 in the paper. A Maine road map will locate the area.

The mission instrumentation included a Hulcher 70 mm framing camera and an 8 channel Bendix multispectral scanner (MSS) with wavelength band widths as shown in Figure 1. Color film (Aero Neg. #2445) was used. The framing camera imagery is used as a guide to selecting portions of the scene that are thought to be the targets of interest. These portions are used to train the computer to combine the data from each MSS channel as recorded on magnetic tape. Magnetic tape data is automatically corrected for aircraft roll.

The second phase of the mission was the statistical processing of a selected portion of the Penobscot River—from Oak Point to the South Branch Marsh River. This is a section of the river that was reported to contain old sawdust deposits on river bank mud flats. The river is tidal at this point and the banks and flats were exposed at the time of aircraft flights.

AUTOMATED STATISTICAL ANALYSIS OF PENOBSCOT RIVER FROM OAK POINT TO SOUTH BRANCH MARSH RIVER

The first task of the statistical analysis was to locate the sawdust deposits and the second task to automatically sort sawdust, from mud, muddy water, marsh vegetation, undifferentiated vegetation, and other types of scene content.

The first step is to provide the statistical analysis programs with spectral signatures of the categories of interest. This yields spectra representative of sawdust. In the case of the Penobscot River, aerial color photography was used as a guide in the selection of multispectral signatures describing the characteristics of a stated category (sawdust) at a given location.

The second step is to use the above representative spectra in special computer programs that generate sets of weighting coefficients to be used to form linear combinations of the scanner channels. This is a linear transformation which maps the original data channels into a new coordinate system

in which the axes are called canonical variables. The coefficients are chosen to maximize the separation between the category (sawdust) and all other categories in the transformed space obtained by applying weighting coefficients. Figure 2 is a representation of the transformed data showing typical separation. Previous to the transformation, the scatter diagrams are quite complicated with much overlap present. Figure 3 demonstrates the selection of a circular representation of the transformed scatter. Points Q_1 and Q_2 represent transformed density values in the imagery after application of the linear combination coefficients. Figure 4 is an attempt to depict the probability density in the two transformed axes, the location of the points Q_1 and Q_2 and a simple schematic showing the separation of points within the circular bivariate normal distribution. The coordinate values are used for deflection voltage on a cathode ray tube (CRT), and Q_1 is recorded at a grey level corresponding to its point on the bivariate normal density transparency. Q_2 is not recorded at all. Figure 5 is a more complete schematic of the hardware. (The term Factor Score is sometimes used instead of variable or canonical variable. The mathematics which specify the transformation are different in such cases.)

When the data are transformed and the flying spot scanner applied as discussed, a signal corresponding to the conditional probability density for each category or target type of interest is produced. Separate film images corresponding to the probability density of each target (mud, sawdust, muddy water) are generated. When the probability densities for these categories have little overlap, the film images could be called "decision imagery." Under such conditions, only one of the categories of interest produces a large signal at any given time. This imagery does not produce a simple "yes" or "no" type decision, because the film-recorded signal has a continuous range of values allowed. The variation is nonlinear, because it is determined by the transparency function. This type of imagery is called Probability Density Imagery.

Two categories of Probability Density Imagery are presented in Figure 6. These are probability density for:

1. Mud and muddy water - Figure 6 (C)
2. Old sawdust - Figure 6 (D).

The second techniques of separating targets is called Probability Imagery (see Figure 7 A). It is performed by normalizing the probability density at each point:

$$P_1 = \frac{P_1}{P_1 + P_2 + P_n + C}$$

where the constant C prevents the denominator from approaching zero if $P_1 + \ldots + P_n$ is quite small. In some instances this step, which requires probability density, further sorts out categories. Sawdust in Probability Imagery is shown in Figure 7 (A) and can be compared to sawdust in Probability Density Imagery. The west bank is much lighter, indicating that mud is also present. If P_1 is sawdust and P_2 mud, then for $P_1 = P_2$, $P_1 = 0.5$ and for $P_1 \gg P_2$, $P_1 \rightarrow 1.0$, assuming $P_i \ll P_1$ for $i = 3, \ldots$.

One simple way to force a decision is to select a value of probability density such that for values greater than the preselected value a decision is made to classify the area under consideration as arising from the category of interest. Imagery resulting from the above technique will possess only two distinct colors representing a "yes" decision and a "no" decision. Imagery of this type is called Binary Imagery.

A threshold technique of this kind, when applied to probability density, cannot be expected to produce the best possible decisions. A maximum likelihood decision can be obtained only by comparison of all allowed conditional probabilities. Two kinds of errors are introduced by a threshold operation on a single probability density:

1. The probability density tested may fall below the threshold even though it is the largest of the allowed probability densities.
2. The probability density tested may fall above the threshold even though it is not largest of the allowed probability densities. This is overlap.

If the probability densities have overlap, the above techniques will contain misclassification in the overlap regions.

To reduce the frequency of misclassification, the probability densities are processed to compute a probability for each category in the following manner: The probability densities for all categories are summed and the ratio of probability density for each category to the summation is computed. These quantities are a measure of the probability that the area under consideration has arisen from the category of interest. Probability signals occupy a continuous range of values. As with the probability density signals, a threshold value may be chosen so that values greater than the threshold result in a decision to classify the observation as arising from the target category. When this signal is used without a threshold to modulate the film grey scale, the result is called Probability Imagery as before. When the decision has been forced for pairs of categories and all others, it is called Three State Imagery. The decision rule and a plot of the levels are given in Figure 8.

A Three State Imagery strip was obtained for sawdust, mud (and muddy water) and all other categories. It is shown in Figure 7B. The density levels are now discrete. Grey is always "all other" targets while white is sawdust and black is mud or muddy water. The Three State Imagery is annotated.

SURFACE VALIDATION OF THE REMOTE SENSING

The long-established method of bottom sampling with a Ponar grab sampler was used in June and July of 1971. The sampler was used because measurements were taken at times other than low tide. The results of the surface validation are presented on MAP I. Substantial sawdust and wood chips were found at Oak Point Cove (W-6), south of Oak Point Cove on the east side at E-12 and south of Winterport on the east side E-15 and E-16. The observer noted that traces of sawdust appeared everywhere.

The automatic thematic imagery identifies substantial deposits at Oak Point Cove (W-6), E-15 (and in part E-16), E-12 and E-13. The automatic imagery identifies sawdust in the northern part of W-12 and north of W-12 but not in W-11. A sample was not taken between W-11 and W-12 where the remote sensing indicates sawdust. The presence of sawdust along both banks is indicated in all three types of processed imagery. However, probability imagery tends to represent somewhat more closely the surface validation from just south of Oak Point Cove to just north of E-15. The surface validation was obtained one to two months previous to the aircraft flight. It was noted by the observer that the upper portion of the sawdust and wood chips shifted to some extent as a function of the position of the tide and the shift of the river. In places where the sawdust and wood chip beds are not deep, the shift is likely to cause a change in their position: Substantial beds will not move in the remote sensing imagery. The remote sensing technique identified the substantial beds at W-6, E-12, and E-15. It located additional areas of sawdust which are not as substantial. The area between W-11 and W-12 appears to have sawdust in extent if not in depth. No substantial beds were missed by remote sensing. It is possible (not probable) that a false identification might exist between W-11 and W-12.

COMBINATION OF TECHNIQUES

The remote sensing technique is the first technique to be applied. It locates all substantial beds that are exposed at low tide. The Ponar grab sampler is then used for verification: Although the remote sensing may flag areas with little actual volume of sawdust, large areas would not require surface sampling. The Ponar grab sampler is also used to show the areal extent of the bed not exposed by low tide. Depth of the ancestral sawdust beds are not determined through these two techniques.

A geophysical method, the bottom profiler, offers promise of three dimensional classification. In application in the Penobscot, many operational problems were encountered which were never fully overcome. First, the extreme tidal activity presented navigation problems for the instrument vessel. Secondly, the method was generally insenstivie, in the short range used, to delineation of the vertical boundary between marine muds and sawdust. It was possible to pick-up the bed-rock river bottom, but not possible to discriminate accurately between layers of the saturated overlying

sediment, with the instrument. The bottom profiler can be operated, in a river the width of the Penobscot, at a cost of about $300/river mile.

Used on a limited basis, Ponar grab sampling is complementary to the aerial survey method, in that it provided the essential ground truth. Used extensively, it is a tedious and occasionally hazardous enterprise in an active tidal river, such as the Penobscot. Successful operation requires two experienced boatsmen, a sturdy, rough-water boat, a high powered engine, a Ponar grab sampler, and a considerable amount of time. Converting these factors into costs, we find that delineation of the horizontal extent of ancestral sawdust deposits in the Penobscot River estuary would cost about $400/river mile.

Remote sensing costs about $30/river mile for data collection. This includes aircraft (including ferry costs and standby time), instrumentation, expendables and miscellaneous expenses (mission planning, crew field expenses, etc.). A rule of the thumb is that data processing, interpretation and documentation for feasibility demonstration costs about twice data collection costs. A conservative cost estimate for an established application as this is $30 + $60 or $90 per line mile*. This compares favorably with $300/river mile for the bottom profiler and $400/river mile for Ponar grab sampling.

Actual and projected costs for data collection are shown below. The section of the Penobscot River that served as a test site was seven miles long. Surface sampling methods were applied over three miles of the river, from Oak Cove to the South Branch Marsh River. (Map, Figure 9).

The actual costs of the survey work reported here, and based on the costs/mile just given, were:

Remote sensing from Oak Cove to South Branch Marsh River:
$90 x 7 river miles = $630.

Ponar Grab Sampling W-6, E-12, E-15 and between W-11 and W-12:
$400 x 3 river miles = $1200.

Bottom Profiler W-6, E-12, E-15 and between W-11 and W-12:
$300 x 3 river miles = $900.

The total cost from Oak Point to South Branch Marsh River is $2730.

Had the entire seven miles been surveyed with the Ponar grab sampler alone, the survey would have cost $400 mile x 7 miles = $2800. If grab sampling were the only ground truth method used, the cost saving when using remote sensing is ($400 - $90) x (7 - 3)** = $1240 of an original cost of $2800 for the Ponar grab alone. This is an approximate saving of 44% when the two are combined. If Ponar grab sampling is not used as verification of the remote sensing, the saving is ($400 - $90) x 7 or $2170 of a Ponar grab cost $2800. The remote sensing cost is 77% less than the Ponar grab cost when each is used by itself as a technique.

---

* For rivers in Maine a line mile is very nearly equivalent to a river mile, since rivers are generally straight. In meandering, geologically old, streams, a line mile might represent well over a river mile.

** Three (3) miles are subtracted from the seven (7) because the Ponar grab is used as verification over the three miles identified by remote sensing. Its costs is entered into the calculation for a combined technique.

The saving derived from remote sensing is obvious. It would be sizeable if it was required to locate sawdust banks for all the tidal rivers in the region. For example, for 1000 river miles the competitive costs would be approximately:

$90,000	Remote Sensing
$400,000	Ponar Grab Sampling
$300,000	Bottom Profiler

For the combined techniques, and assuming that 20% of the river miles require follow-up surface validation:

(1) $90,000 + $60,000 or $150,000 for Remote Sensing plus bottom profiling, respectively.

(2) $90,000 + $80,000 + $60,000 or $230,000 for Remote Sensing, Ponar Grab Sampling, and bottom profiling, respectively.

Having established the application of remote sensing, its combination with surface validation and depth measurement, and its cost saving, it is well to analyze the overall cost benefit of locating and removing the sawdust and wood chip beds.

NEGATIVE IMPACT OF SAWDUST DEPOSITS IN THE ESTUARY

Biological sampling by ecologists at the University of Maine has demonstrated the general unsuitability of sawdust deposits as a substrate for such benthic organisms as clams. Horizontal shifting and vertical "flexing" of the deposit (with the tide), and pollutional effects contribute to the essential sterility of sawdust as a life medium. To a reasonable extent, a tangible economic measure can be ascribed to this sterility. In a geographical area extending from, roughly, Drachm Point to Islesboro[1] in a zone clearly suitable for clam production—there are about 600 acres of sawdust deposits covering areas which might well produce clams. If we apply a minimum production factor of only 100 bu./per acre/per year, the resultant annual value at $8.0/bu. is $480,000[2].

If a value added factor of 10 is applied to this account, very conservatively, for the price of clams sold in local dineries, a potential value of $5 million emerges.

Certainly this is the minimum annual cost of the sawdust deposit. Such an estimate does not include: The possible deleterious effect of sawdust on such important recreational species as the Atlantic salmon and such important commercial species as the flounder—a bottom species, reportedly damaged by sawdust deposition.

Because of difficulties in determining vertical extent of sawdust deposits, it has not been possible to develop reliable estimates of the volume of sawdust in the zone suitable for clams. If we assume a mean depth of 10 feet (which seems extreme), 10 million yards of sawdust-like materials are to be found as an interference agent in the productive zone of the estuary. Dredging and deep water disposal of this volume of material would cost $30,000,000[3].

An equivalency comparison is in order:

Present worth benefit of clams

i = 6%
n = 50 years[4]
p = $5 million (15.76)
= $80 million

---

1 This is not in the test site for the remote sensing. However, the calculations that follow readily apply to the test site and other areas in the State of Maine. Isleboro is on Long Island in Penobscot Bay.

2 Note. Sources of Cost data on clam value: Maine Department of Sea and Shore Fisheries.

3 Note: Source of costs on dredging: U.S. Army Corps of Engineers.

4 For n = 25 years, p = $5 million (12.78) = $64 million.

Present worth of dredging costs

p = $30 million

Thus it is seen that location and removal of the sawdust deposits might, conservatively, be worth some $50 million over a 50 year period, or $34 million over 25 years.

The above calculation is for one site of clam production. The dredging cost of $30,000,000 is much greater than the remote sensing and surface validation costs. However, the savings in money, effort, and time of remote sensing is still sizeable on a yearly basis. Several surveys for monitoring would be required over a 50 year period and remote sensing would offer a savings with each survey.

ACKNOWLEDGEMENTS

The long-established method of bottom sampling with a Ponar grab sampler was demonstrated by graduate students John H. Moroney and Gary White, working under the direction of Dr. Malcolm Coulter, Professor of Wildlife Resources. Tests with a seismic instrument, a Bottom Profiler, were performed by Dr. Harold Borns and Mr. Frederick Bragdon, of the Department of Geological Science, University of Maine at Orono.

Mr. Charles Wilson of Bendix and his staff, Mr. David Hanson, Mr. Harry Neindorf, Mr. Karl Melow, Mr. William Haeske collected and processed the remote sensing (aircraft) data (MSS and Color Camera). Mr. Wilson is acknowledged for his direction during the program and his thoughtful review of the paper.

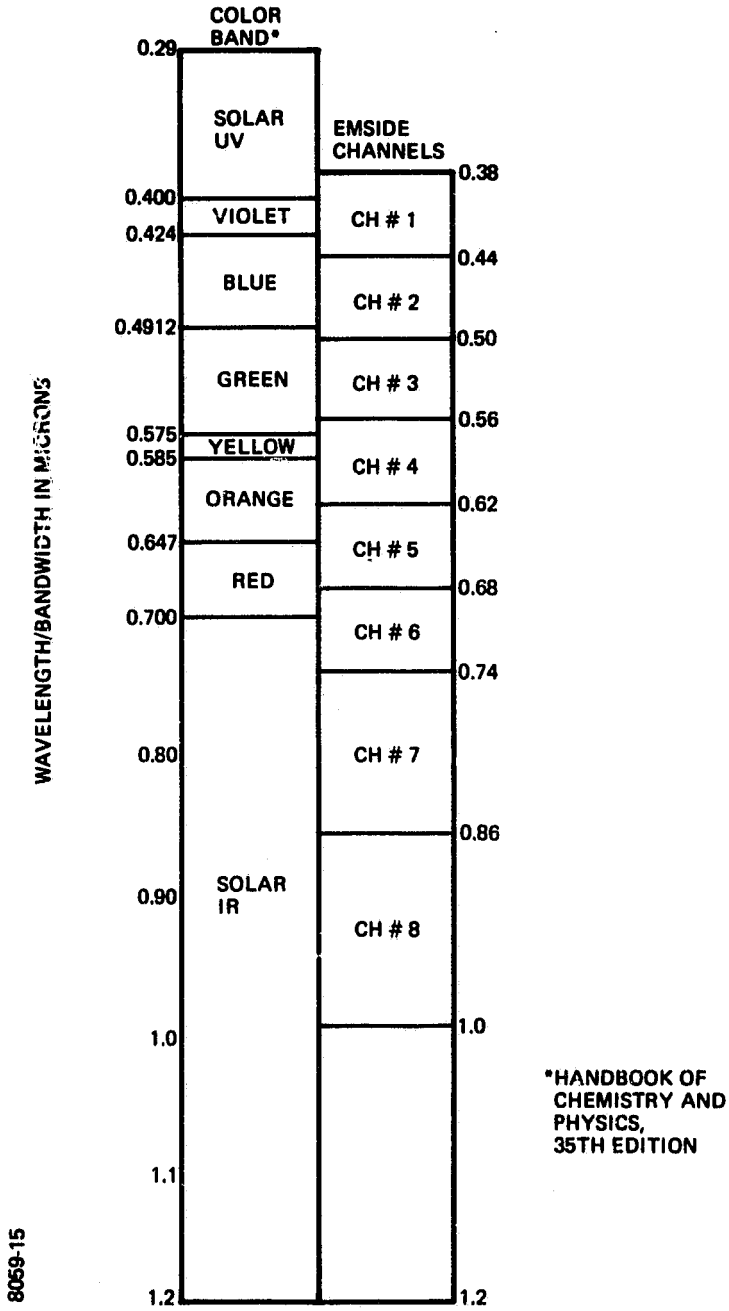


FIGURE 1. EMSIDE CHANNEL LOCATIONS

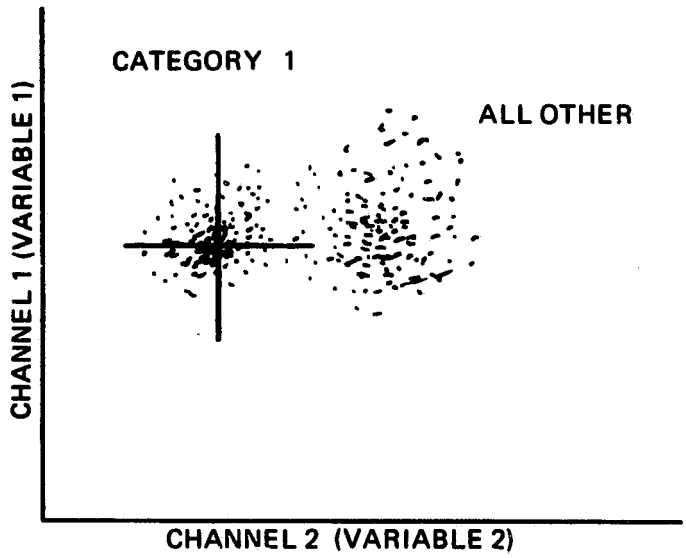


FIGURE 2. CLUSTERING OF POINTS FROM "KNOWN" TARGET AREA AND ALL OTHER AREAS AFTER TRANSFORMATION

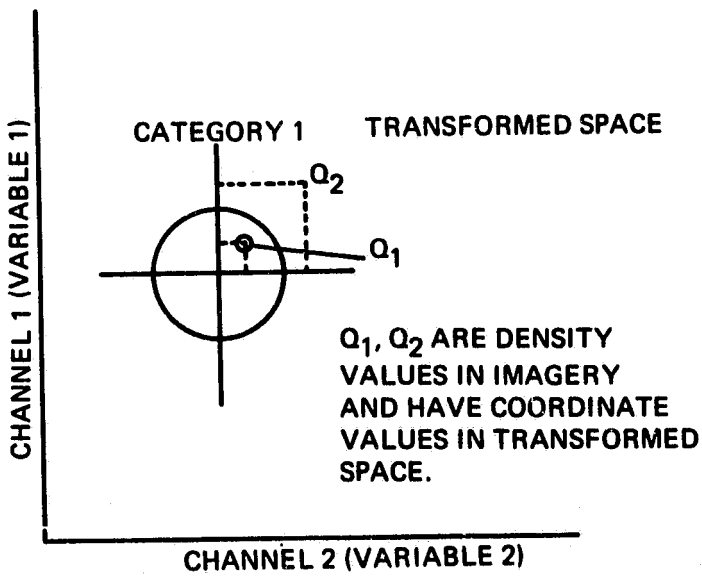


FIGURE 3. CIRCULAR REPRESENTATION IN TRANSFORMED SPACE

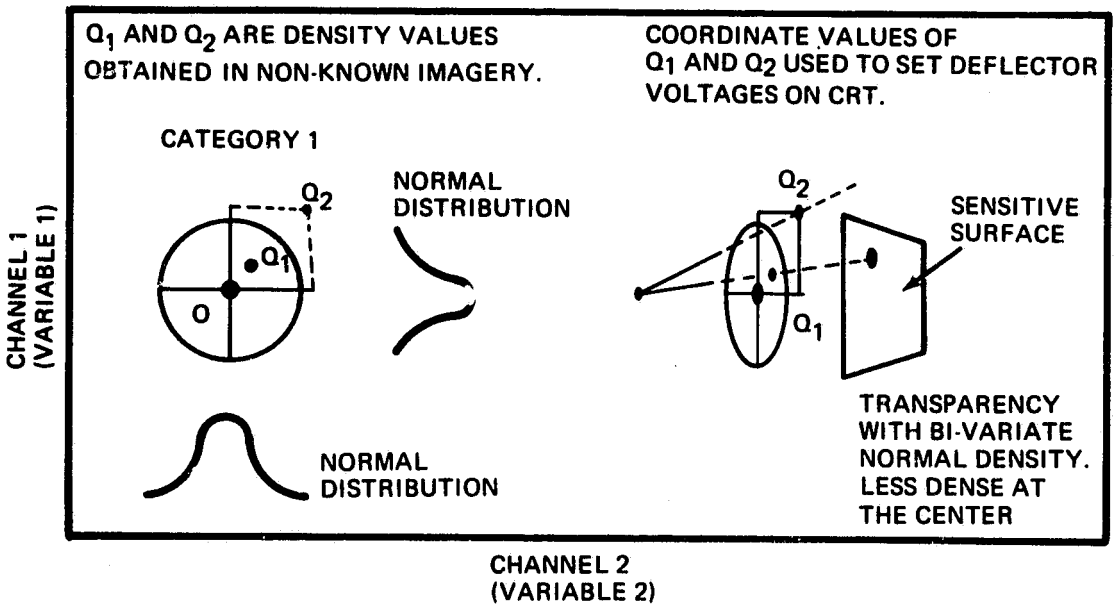


FIGURE 4. DISTRIBUTIONS AND THE SCHEME FOR SEPARATING FLYING SPOT SCANNER READINGS OF CATEGORY 1 FROM ALL OTHERS

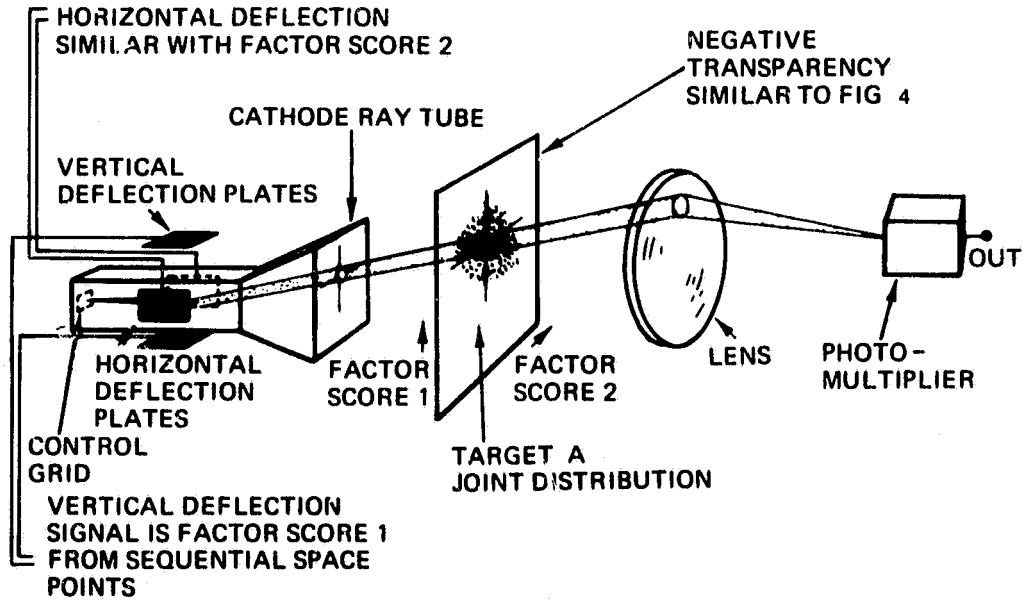
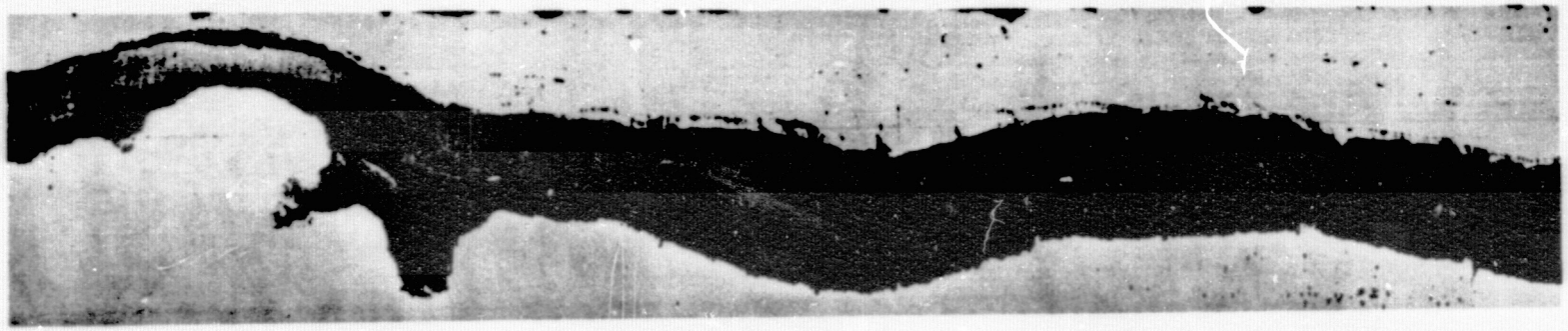
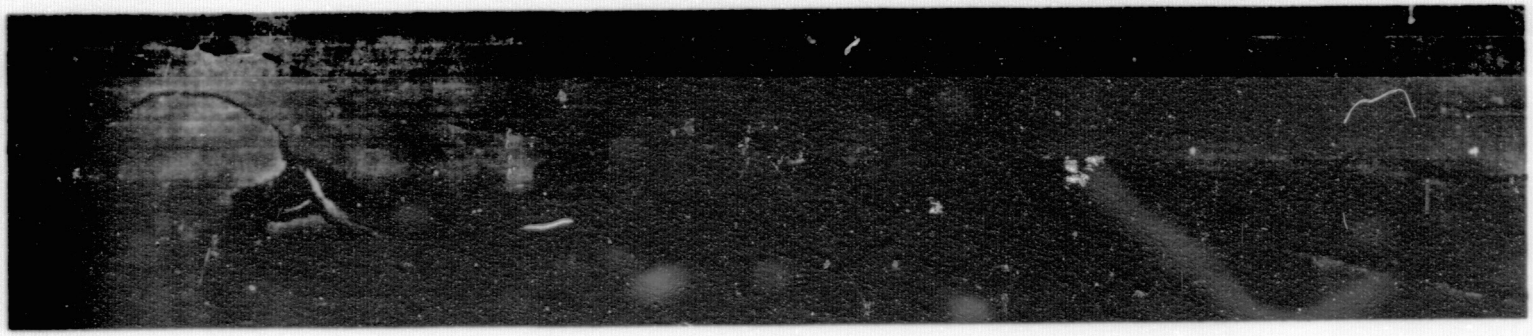


FIGURE 5. FLYING SPOT SCANNER OPERATION



MUD AND MUDDY WATER

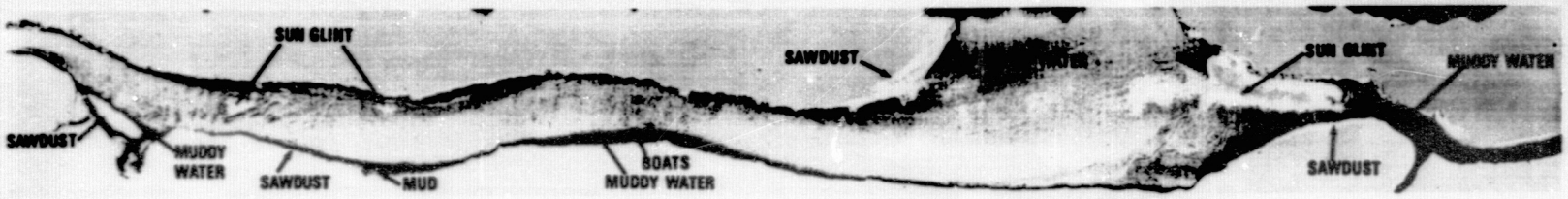


OLD SAWDUST

FIGURE 6. PROBABILITY DENSITY IMAGERY OF PENOBSCOT RIVER: OAK POINT AND WINTERPORT.



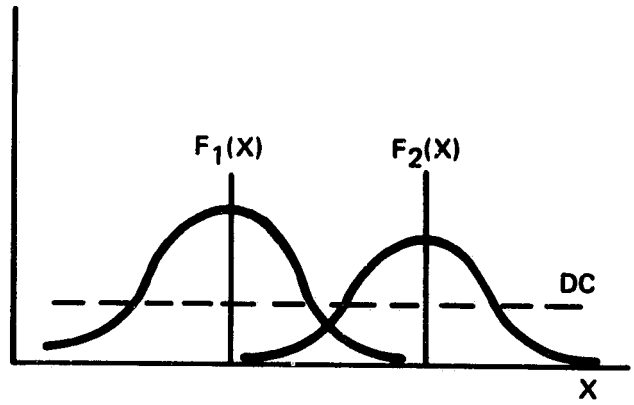
(A) PROBABILITY IMAGERY: OLD SAWDUST



(B) THREE-STATE IMAGERY: OLD SAWDUST AND MUD (AND MUDDY WATER)

580

FIGURE 7. PROBABILITY AND THREE STATE IMAGERY OF PENOBSCOT RIVER: OAK POINTTO SOUTH BRANCH MARSH RIVER.



DECISION RULE

IF $F_1 > F_2$

AND $F_1 > DC$

DECIDE D_1 IN FAVOR OF F_1

IF $F_2 > F_1$

AND $F_2 > DC$

DECIDE D_2 IN FAVOR OF F_2

IF $F_1 < DC$

AND $F_2 < DC$

THERE IS NO DECISION

FIGURE 8. DECISION ALGORITHM FOR THREE-STATE CIRCUITRY

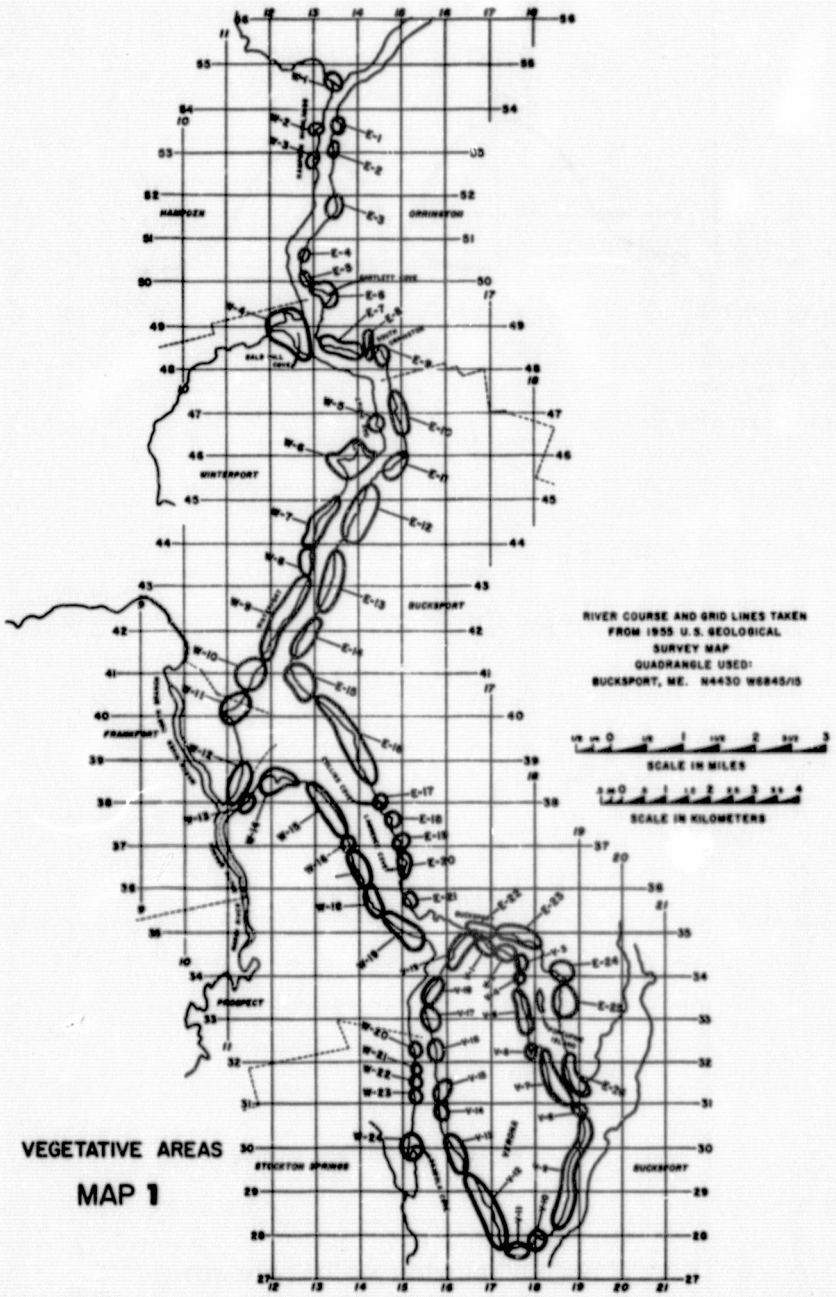


FIGURE 9. VEGETATIVE AREAS

MULTISPECTRAL SURVEY OF POWER PLANT THERMAL EFFLUENTS IN LAKE MICHIGAN

by

F. C. Polcyn, W. L. Brown, and S. R. Stewart

Environmental Research Institute of Michigan
(Formerly Willow Run Laboratories
University of Michigan)
Ann Arbor, Michigan

ABSTRACT

As a result of the study on the 3 sites and 12 plumes covered by this report, we are able to draw several important conclusions concerning power plant discharges into Lake Michigan. First, it appears from the digital analysis of the multispectral scanner data, that a direct relationship exists between the critical area of the plume, power load on the plant, and wind velocity. This relationship, although observed from an empirical analysis, is so sensitive to the wind velocity that more accurate measurement of these velocities is critical to future analysis. Another result, again derived independent of any theoretical analysis, is that the maximum temperature rise in the plume as measured by an airborne scanner can be calculated from the intake and discharge ΔT, the power load on the plant, and the flow rate of coolant. Very careful monitoring of these variables is crucial to eliminate variance between the calculated plume temperatures and the measured values. The empirical model derived herein does not cover the case where significant cooling occurs in the flume leading from the plant to the point of entry into the lake. More data on cooling rates in the flume would be needed in order to draw reliable conclusions.

INTRODUCTION

This paper concerns the study of selected thermal effluents discharged into Lake Michigan during the period April to May 1971. The investigation was sponsored by three companies, The Indiana Michigan Electric Power Company, The Consumers Power Company, and The Northern Indiana Public Service Company.

The study was conducted using data collected with the WRL multispectral scanner which obtains registered data in 12 bands covering the ultra-violet, visible and thermal infrared regions of the electromagnetic spectrum. Because this system has two temperature references, as well as solar and reference lamp signals, and the data is stored on magnetic tape, computers are used in the analysis of the data to provide quantitative measurements on both temperature gradients and the area extent of each temperature zone. In addition, a special analog computer developed at WRL was used to study water color relationships that occur at this time of the year during the formation of the "thermal bar".

A number of flights were made throughout several diurnal cycles over a two month period in order to observe the thermal discharges under a variety of conditions especially different wind histories. The investigation collected data before and after the onset of a distinct thermal boundary at 4°C in the nearshore waters which has become known as the "thermal bar". The flightlines used are shown in Figure 1.

In Figure 2 we illustrate the results obtained for the times indicated at the Campbell Plant which discharges into Lake Michigan south of the Grand River. As one can see from the figure, the discharge pattern is critically related to both the wind direction and wind velocity. On 22 April, 1971, a strong northwesterly wind restricts the mixing pattern to a region that closely follows the shoreline. The next day with a more westerly wind the discharge plume

reverses direction. A week later on the 30 April we can see the transition between 11:00 AM and 2:00 PM as the wind increases in velocity. And, finally on the 28th of May under calmer conditions we see again the mixing pattern of the discharge plume.

Because of the thermal references aboard the aircraft and the tape recording of the signals each temperature level can be isolated electronically from the data and displayed separately. Figure 3 shows the area covered for different temperature ranges for data collected on April 30. By use of color coding of each of the temperature levels, color composite displays, as shown in Figure 4 are feasible and thus temperature area maps are readily generated. Figure 4 is a quantified color coded temperature map of the discharge plume for the Campbell Plant on the 30th of April 1971.

Alternatively, the area data for each temperature level can be measured and displayed through the use of a digital computer as shown in Figure 5. In this case symbol selections and color of symbols are used to display the temperature zones. The computer counts each symbol occurrence and by the appropriate multiplication of an area constant, the area of each temperature contour for a particular plume is easily calculated. Since standards for thermal discharges have been suggested such as limitations of discharge plumes to 3°F above ambient within a 1000 ft of the point of discharge, this technique lends itself useful as a monitoring tool and for testing the suitability of different criteria. It also serves to reduce speculation on what really happens when thermal discharges are released into large bodies of water. This measurement technique was also applied at two plant sites and to two river discharges in addition to the Campbell site. The Michigan City Plant is shown in Figure 6 and the Bailley Plant at Burns Ditch shown in Figure 7. Discharge patterns of the St. Joseph River and Grand River were also mapped.

The geometry for the discharge is different in each of the three power plant cases so that a study of the pattern of distribution and areas was considered useful. The discharge plumes were measured by the computer and a table of areas was constructed for 12 different combinations of plants and dates. A mean radius of the 3°F contour from the point of discharge was computed and results are shown in Table 1. From the empirical information of acreage and a knowledge of different temperature zones, the winds, and the quantity of water being discharged it was possible to construct a simple model relating the observed ΔT across the plume and receiving waters with those temperature values measured across the intake and discharge points reported from the company. The goal of this approach was to be able to predict conditions at future installations, that is, what will the area of the plume be and what will be the maximum temperature gradients, one might expect, given a certain cooling capacity and a certain power generation capability.

This predictive model has the form

$$\Delta T_{scanner}(°F) = 4.13 \times \frac{load(MW)}{flow_{(KGPM)}} + 4.5 \text{ or approximately } 4\ [\frac{load}{flow} + 1]$$

where $\Delta T_{scanner}$ is the maximum temperature gradient in °F measured by the airborne scanner.

load is the power generating load of the plant in megawatts

flow is the water cooling capacity of the plant in 1000 gal per min

This simple model was used to predict temperature gradients for the above mentioned twelve conditions. It showed a remarkable correlation, on the average, but has a root mean square variance between temperature estimates of about 5°F. See Table 2.

Further analysis of the relationship of plume area to wind velocity suggested a decreasing relationship to the inverse square of the wind velocity. It was found, however, that better accuracy of wind velocity and direction measurement at the sites were needed to improve the model. Nevertheless the degree of correlation was significant and further study is deemed fruitful [1].

NATURAL THERMAL VARIATIONS

As indicated earlier, for part of the experimental plan, a section of shoreline about 15 miles in length was flown at 10,000 ft between Port Sheldon and Grand Haven for each of the dates, April 22, 23, 30 and May 7 and 27, 1971. These flights were designed to map the temperature changes expected nearshore as the land heated the water and produced the spring time phenomenon called the "thermal bar". They also permitted a mapping of the temperature regimes of

the Campbell Plant and the Grand River discharges into Lake Michigan. Figure 8 shows the infrared thermal image of the area for four dates covering the before-and-after look at the formation of the thermal bar.

On the 22 and 23 April imagery in Figure 8, the thermal bar is not present although a significant amount of warm water masses are noticed nearshore. This water mass is not the thermal bar since a much sharper discontinuity exists when the thermal bar is present as will be shown shortly. However, it is entirely possible that there is some relationship between this water mass and the thermal bar since only one week later the bar had indeed formed in this area. It is interesting to note the influence of the Grand River outfall on this water mass as shown in the April 22, 6:55 PM strip. It appears that the river itself is the cause of a large portion of the thermal water mass seen nearshore.

On the 30 April, imagery in Figure 8, the thermal bar is quite evident by the sharp jagged line between the fairly uniform warm water nearshore and the colder water on the other side of the bar. Here it is about 1-1/2 to 2 miles offshore. Off the Campbell Plant there appears to be a double bar separated by about 1 mile which had not been observed before. On 7 May in Figure 8, the bar has moved about 4 miles offshore. The jagged edge is barely visible on the upper quarter of the imagery. The effect of wind on both the plant discharge plume and the Grand River outfall is quite noticeable in this figure.

In Figure 9, there are approximately 3°F steps between both demarcation of the thermal bar, i.e., there appears a boundary between 34.6°F and 37.7°F as well as 37.7°F and 40.9°F. It is at this latter boundary that the increased density of water produces the sinking which is part of the mechanism for warming the lake naturally each year. There is a large heat input from the Grand River (47.2°F) for this time of the year which appears to increase the boundary of the 40.9°F zone farther from shore. The heat input to the lake from the Campbell Plant appears to influence a much smaller surface area which decreases even more at the higher temperatures. The outfall here may serve to force outward the warm water due to land heating as seen by the 44°F and 47.7°F temperature contours.

One of the more interesting questions which has arisen lately, on the subject of lake eutrophication, is the interaction between the thermal bar and a warm water discharge plume such as at the Campbell Plant. Much of the physics for the appearance of the thermal bar phenomenon has been explained although relatively little is known in detail about its behavior. Figures 10 and 11 are the result of a recognition process with the SPARC wherein, water masses of the same spectral characteristics are enhanced and can be displayed by an arbitrary color code. Shown in Figure 10 is a SPARC color overlay (the colors are arbitrary and are used only for coding separate zones) of the shoreline between the Campbell Plant and the Grand River discharge at Grand Haven taken on April 30, 1971. Each color in the figure represents a body of water of approximately the same "color" and same apparent water quality. A thermal image of the temperature gradients of this same area taken on the same day can be seen in Figure 8 for comparative purposes. The sharp demarcation between the blue and white regions of Figure 10 shows quite clearly the edge of the thermal bar. This edge coincides with the boundary of a distinct temperature gradient.

A second boundary not observed before is shown in purple (Figure 10). It is interesting to note that this second bar is nearer the shoreline at the Campbell Plant (indicated at the bottom of the picture by an arrow). It is also apparent that the water mass boundary is not as sharply defined at the Campbell Plant site. In general, though, there is very little mixing of water masses on the shore side of the bar. Since the wind on this particular day was less than 5 mph, this is not surprising.

Figure 11 shows the same shoreline as above only on May 7 and under a somewhat stronger wind condition (5-8 mph). Here, a considerable amount of mixing appears to be taking place on the shore side of the thermal bar boundary. The bar edge is indicated by the purple and dark blue colors. The plume from the Grand River is seen to be longer than before and again does not appear to be interacting with the thermal bar. A smaller plume also is seen at the discharge point of the Campbell Plant but it too does not have an apparent connection with the thermal bar. Note that the bar has moved about 2 miles further offshore in this picture. Observing the results from the two dates selected we note that there is not a characteristic water mass traceable solely to the existence of the power plant plume while the plume of the Grand River is distinctly outlined and the boundary of the thermal bar is also evident.

There is a noticeable difference in the color patterns for the two dates for which data was processed. The existence of shore currents, upwellings, nutrient differences and changing wind conditions make it very difficult to make general conclusions about what biological conditions are prevalent. The map of different water masses along shore for the May 7 date emphasizes the

complex environment in Lake Michigan and the danger of drawing a conclusion from only a small number of samples. It also suggests, the conditions at one location can be the result of processes originating elsewhere and brought along-shore by wind action and shore currents.

Airborne data collection and analysis were undertaken offshore the mouth of the St. Joseph River as part of the program to document existing lake conditions prior to the operation of the Donald C. Cook Plant. The outfall of the river represented a natural "input of heat and nutrients" to the lake, the characteristics of which should be documented.

Figure 12 shows the infrared thermal images for this area for the five dates indicated. The wind variations are evident and a particular offshore barrier is noted in the data taken on 30 April 1971 when a marked thermal bar structure was observed further north near Grand Haven (see Figure 8).

The data for 30 April was temperature coded and is displayed in Figure 13. A sharp temperature boundary at 44°F is clearly seen. In fact the outfall of the river is observed to be trapped by this line. This phenomena has been observed at other times on this side of Lake Michigan and is related to along-the-shore currents generated by strong winds. Temperatures observed aboard ship confirmed the airborne results reported here.

Water color measurements were made at the same time and correlation with changes in secchi disk depths were found to correspond to changes in water mass boundaries [2]. The structure of water masses near the St. Joseph River appeared more complicated than those near the power plants and hence more indicative of changes in sediment loading, nutrients and algae communities. Warmer water alone does not seem to bring about changes in water color characteristics. The St. Joseph River outfall at this time of year contains both warmer water than the lake as well as nutrients and high sediment transport.

In summary, the results of the multispectral surveys demonstrated the usefulness of new technology to map large areas repetitively in short times to produce quantitative thermal measurements and to measure their areal extent which delineates the dynamic water mass mixing, and thus contributes to the understanding of the complex phenomena involved in discharges into large water bodies.

REFERENCES

1. Stewart, S. R., W. L. Brown, and F. C. Polcyn, April 1972. "Multispectral Survey of Power Plant Thermal Effluents in Lake Michigan", Annual Report, Willow Run Laboratories, University of Michigan, Ann Arbor, Michigan.

2. Wezernak, C. T. and F. C. Polcyn, October 1972. "Eutrophication Assessment Using Remote Sensing Techniques, Presented at the Eighth International Symposium on Remote Sensing of Environment, The University of Michigan, Ann Arbor, Michigan.

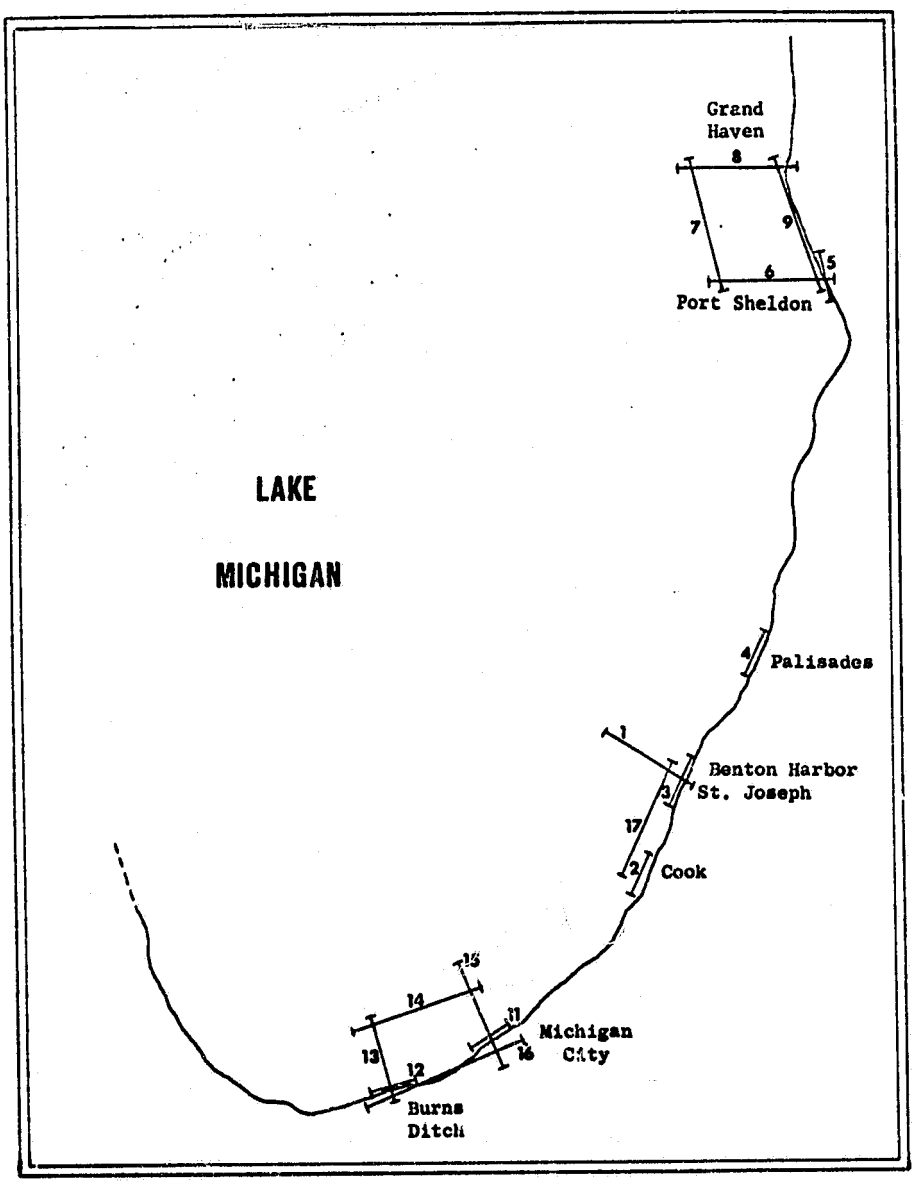
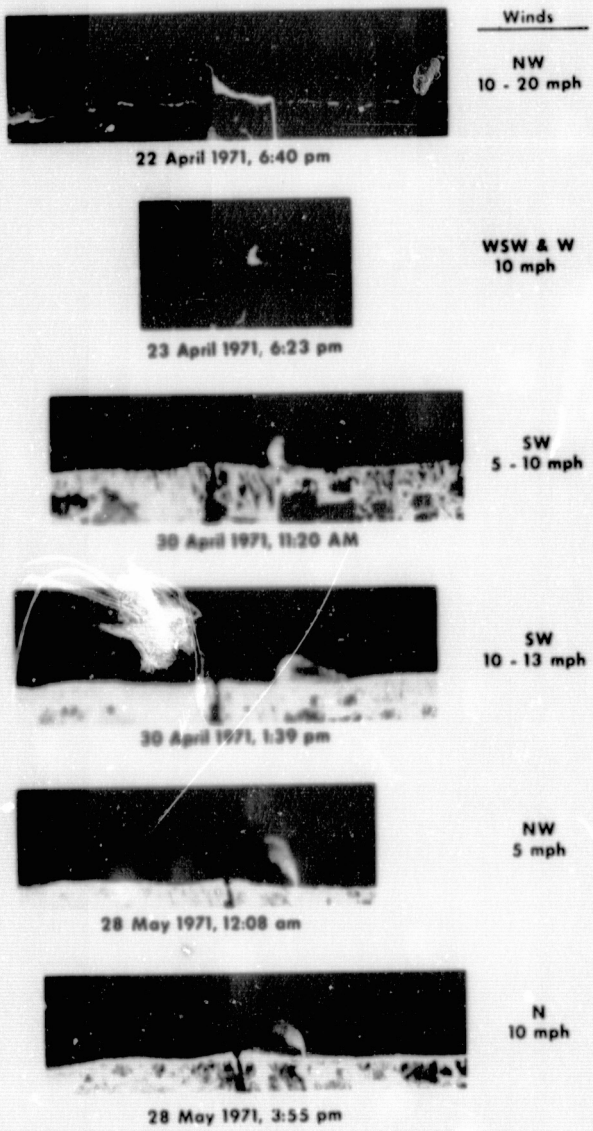


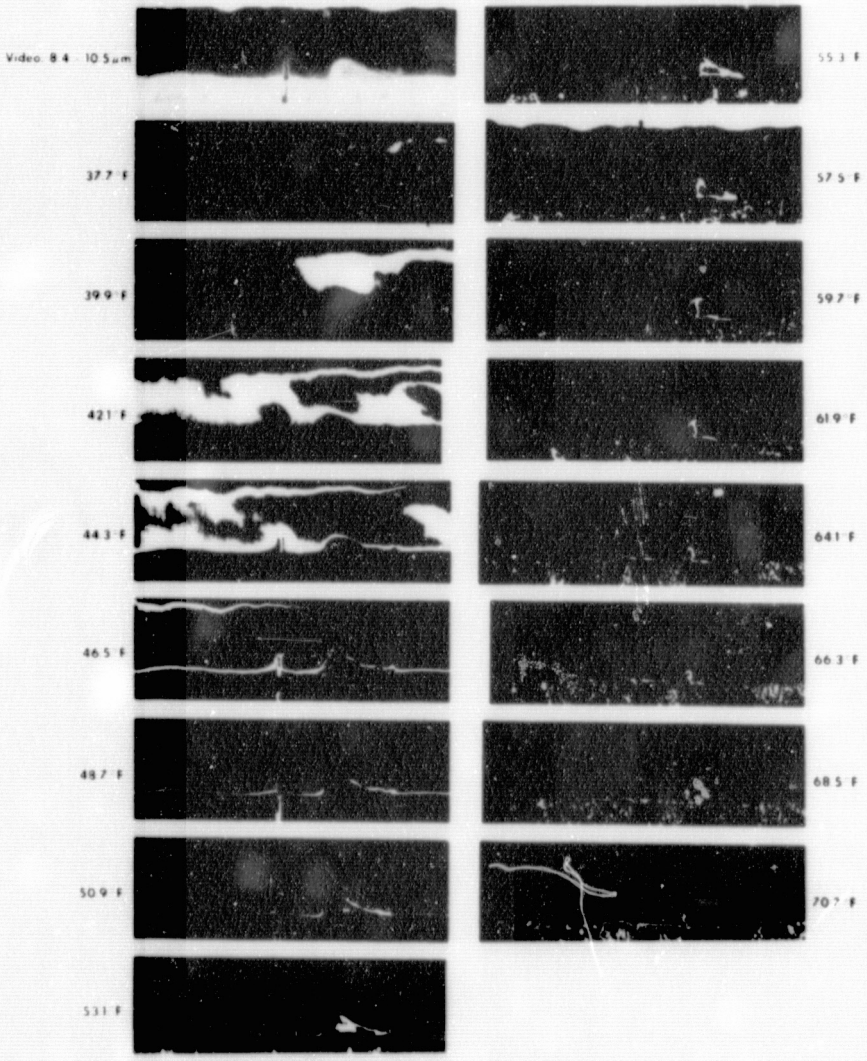
FIGURE 1

LOCATION OF FLIGHT LINE COVERAGE
FOR POWER PLANT EFFLUENT STUDY



WIND EFFECT ON CAMPBELL PLANT DISCHARGE PLUME
Area: 1.3 x 5 miles

FIGURE 2



TEMPERATURE CONTOUR MAP
J. H. CAMPBELL PLANT, PORT SHELDON, MICHIGAN
30 April 1971, 1339 hrs. Area: 1.3 x 5.5 Miles

FIGURE 3



FIGURE 4

COLOR CODED TEMPERATURE CONTOUR MAP
J. H. CAMPBELL PLANT, PORT SHELDON, MICHIGAN
30 April 1971, 1339 hrs. Area: 1.3 x 5 miles

Color Temperature Key (Degrees Fahrenheit)

Light Brown	- 70.7°	Pink	- 53.1°
Cyan	- 68.5°	Yellow Orange	- 50.9°
Purple	- 66.3°	Dark Brown	- 48.7°
Light Blue	- 64.1°	Yellow	- 46.5°
Green	- 61.9°	Blue	- 44.3°
Brown	- 59.7°	Magenta	- 42.1°
Black	- 57.5°	Dark Blue	- 39.9°
Orange	- 55.3°		



FIGURE 5

DIGITAL COMPUTER PRINTOUT OF TEMPERATURE CONTOURS
J. H. CAMPBELL PLANT, PORT SHELDON, MICHIGAN
30 April 1971, 1339 hrs. Area: 3 x 1.3 miles

Color Temperature Key (Degrees Fahrenheit)

Blue	M$	43.25° & Colder	Black	M$	62.40°
	X-	45.40°		X=	66.30°
	=	47.50°		0-	68.40°
Red	M$	49.60°		*	70.50°
	X-	51.70°		=	72.70°
	=	53.90°		=	74.80°
Green	M$	56.00°			76.90 & Hotter
	X-	58.10°			
	=	60.20°			

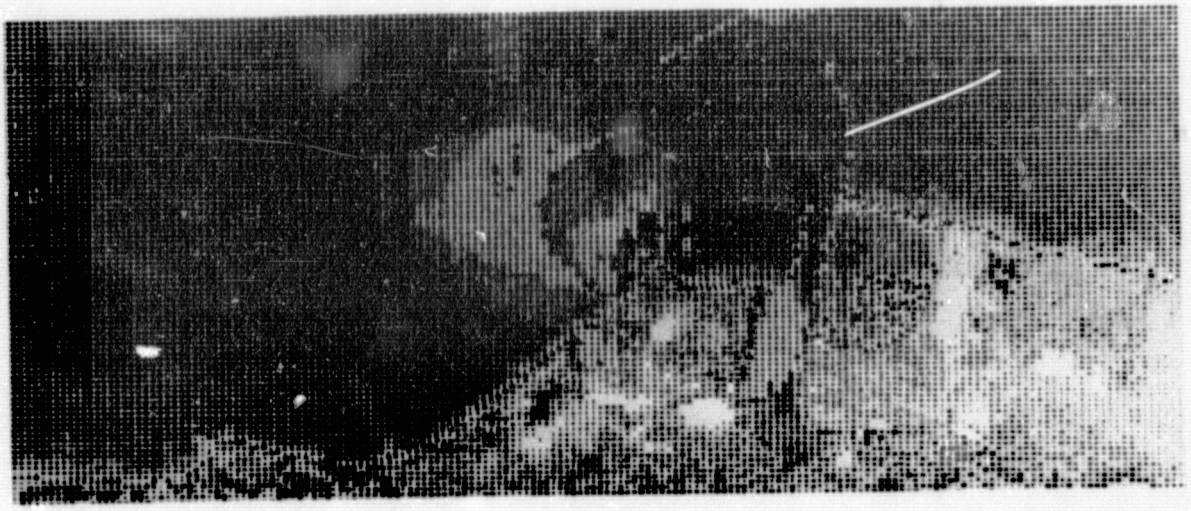


FIGURE 6

DIGITAL COMPUTER PRINTOUT OF TEMPERATURE CONTOURS
MICHIGAN CITY PLANT, MICHIGAN CITY, INDIANA
7 May 1971, 1002 hrs. Area: 2.5 x 1.0 miles

Color Temperature Key (Degrees Fahrenheit)

Blue	M$	50.7° & Colder	Black	M$	60.2°
	X-	51.6°		X=	61.3°
	=	52.7°		0-	62.4°
Red	M$	53.8°		*	63.5°
	X-	54.9°		=	64.5°
	=	55.9°		-	65.6°
Green	M$	57.0°			66.7° & Hotter
	X-	58.1°			
	=	59.1°			

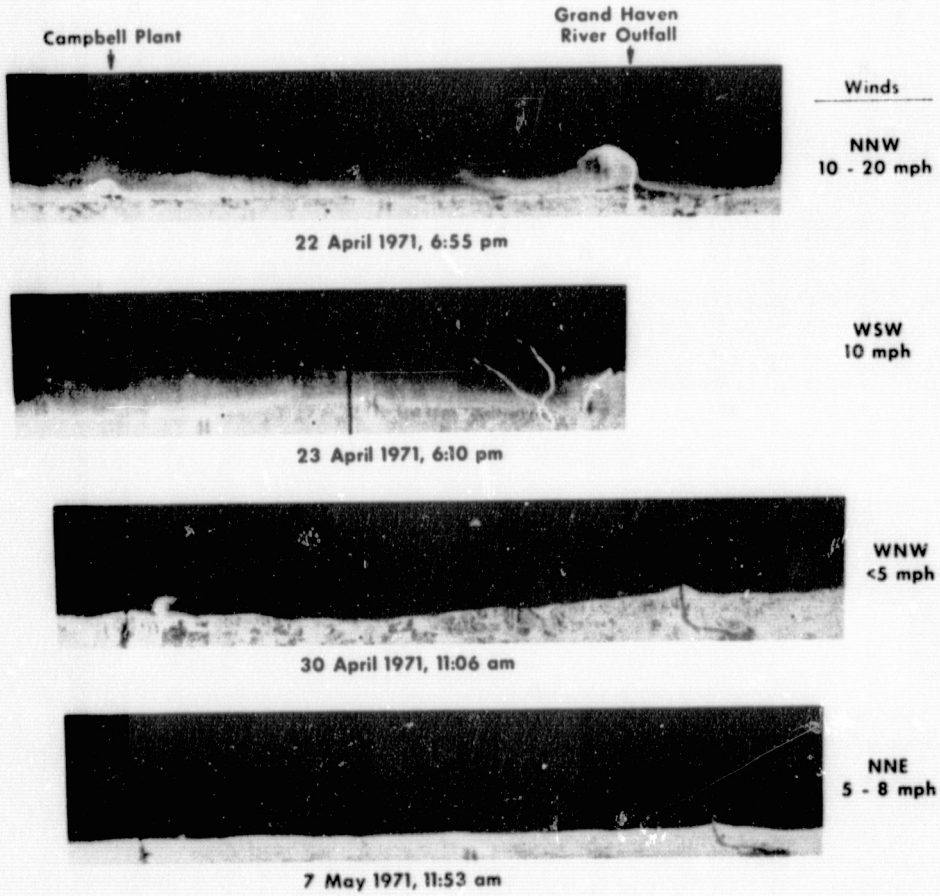


FIGURE 7

DIGITAL COMPUTER PRINTOUT OF TEMPERATURE CONTOURS
BAILLEY GENERATING STATION, BURNS DITCH, INDIANA
7 May 1971, 1007 hrs. Area: 3.0 x 1.3 miles

Color Temperature Key (Degrees Fahrenheit)

Blue	M$	50.7° & Colder	Black	M$	60.2°
	X-	51.6°		X=	61.3°
	=	52.7°		0-	62.4°
Red	M$	53.8°		*	63.5°
	X-	54.9°		=	64.5°
	=	55.9°		-	65.6°
Green	M$	57.0°			66.7° & Hotter
	X-	58.1°			
	=	59.1°			



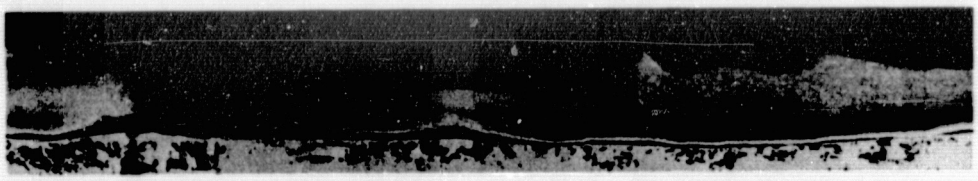
FORMATION AND MOVEMENT OF THERMAL BAR ALONG SHORELINE FROM CAMPBELL PLANT TO GRAND HAVEN
Area: 14.5 x 2.7 miles

FIGURE 8



TEMPERATURE CONTOUR MAP
SHORELINE FROM GRAND HAVEN TO J.H. CAMPBELL PLANT
30 April 1971, 1110 hrs. Area: 2.7 x 19 Miles

FIGURE 9



Campbell Plant



Grand River Outfall

FIGURE 10. SPARC PROCESSING FOR WATER MASS DIFFERENCES ACROSS THE THERMAL BAR AND NEAR THE SHORELINE BETWEEN CAMPBELL PLANT AND GRAND HAVEN

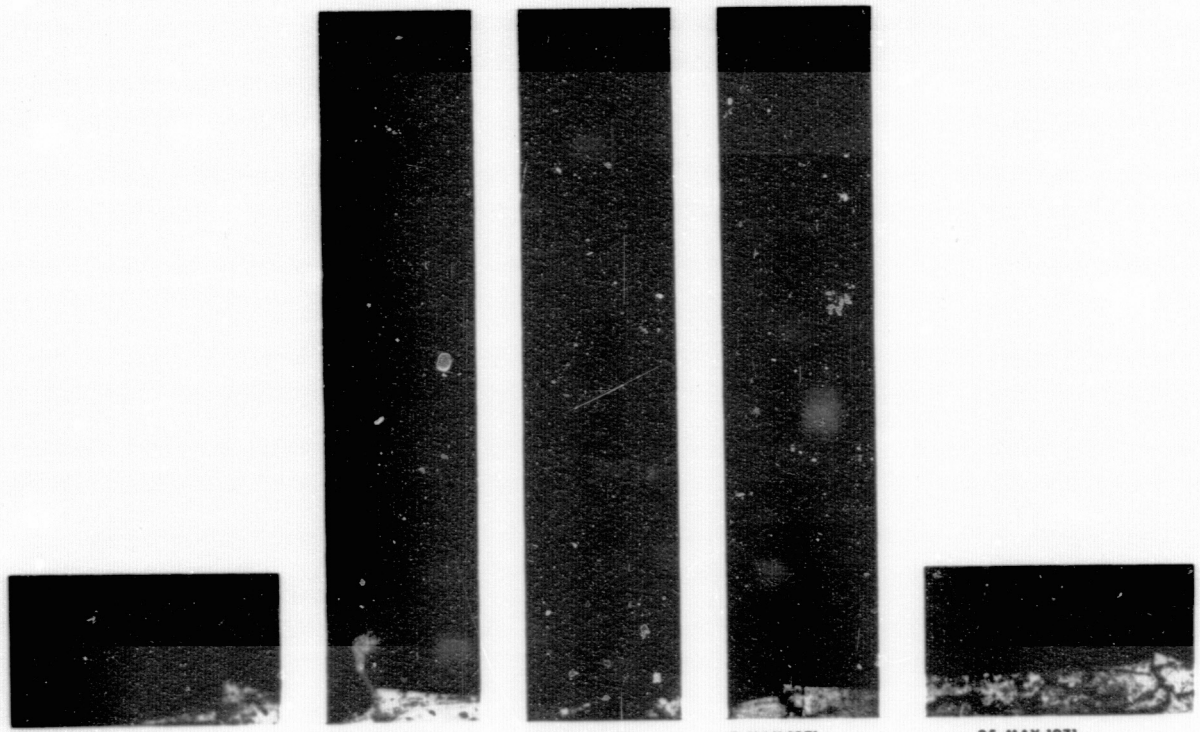
30 April 1971, 1106 hrs. Area: 14.5 x 2.5 miles



Grand River Outfall

FIGURE 11. SPARC PHOCESSING FOR WATER MASS DIFFERENCES ACROSS THE THERMAL BAR AND NEAR THE SHORELINE BETWEEN CAMPBELL PLANT AND GRAND HAVEN

7 May 1971, 1153 hrs. Area: 14.5 x 2.7 miles



22 APRIL 1971
TIME: 9:35 AM
ALT: 5000 ft
AREA: 3 × 1.3 mi
WIND: NW 10-20 mph

23 APRIL 1971
TIME: 9:36 AM
ALT: 5000 ft
AREA: 1.3 × 8 mi
WIND: WSW 5 mph

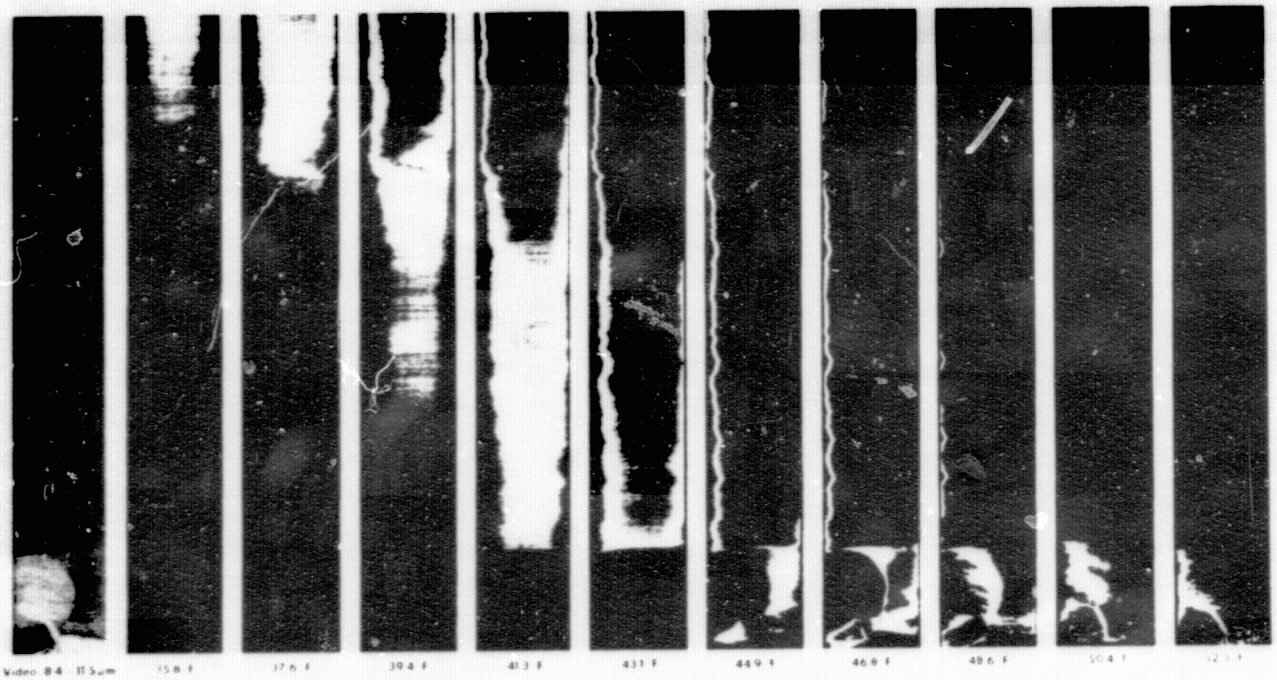
30 APRIL 1971
TIME: 9:32 AM
ALT: 5000 ft
AREA: 1.3 × 8 mi
WIND: SW-W 0-5 mph

7 MAY 1971
TIME: 10:43 AM
ALT: 10,000 ft
AREA: 2.6 × 15.5 mi
WIND: SE 9 mph

25 MAY 1971
TIME: 10:57 AM
ALT: 10,000 ft
AREA: 6 × 2.6 mi
WIND: NW 4 mph

EFFECTS OF WIND AND THERMAL BAR FORMATION ON OUTFALL OF THE ST. JOSEPH RIVER DURING MONTHS OF APRIL - MAY

FIGURE 12



TEMPERATURE CONTOUR MAP
ST. JOSEPH RIVER OUTFALL, ST. JOSEPH, MICHIGAN
30 April 1971, 0935 hrs. Area: 1.3 × 12 miles

FIGURE 13

TABLE 1

AVERAGE RADIUS OF 3°F CONTOUR FOR POWER PLANT COOLING WATER DISCHARGES

Plant	Date	Time	Power Load (MW)	Radius (Ft)
Campbell (avg. Radius = 1256 ft.)	22 April	1839	605	673
	23 April	1823	605	2020
	30 April	1337	618	1575
	28 May	1208	606	755
Michigan City (avg. Radius = 767 ft.)	23 April	0954	127	740
	23 April	1714	122	760
	7 May	1002	174	655
	28 May	1010	128	913
Burns Ditch (avg. Radius = 612 ft.)	23 April	1000	367	1020
	23 April	1720	367	220
	30 April	0955	498	449
	7 May	1007	386	759

TABLE 2

ESTIMATED TEMPERATURE RISE VS. MEASURED RISE AT SOURCE OF PLUME

Plant	Date	Time	$4 \times [(\frac{load}{flow}) + 1]$	$\Delta T_{scanner}$
Campbell	22 April	1829	20.	13.
	23 April	1823	12.	14.
	30 April	1337	20.	17.
	28 May	1208	12.	7.
Michigan City	23 April	0954	9.	18.
	23 April	1714	9.	10.
	7 May	1002	11.	9.
	28 May	1010	9.	10.
Burns Ditch	23 April	1000	10.	17.
	23 April	1720	13.	15.
	30 April	0955	10.	11.
	7 May	1007	10.	14.
		MEAN:	12.1	12.9

INVESTIGATION OF REMOTE SENSING TECHNIQUES FOR AGRICULTURAL FEEDLOT POLLUTION DETECTION*

BY

Fred A. Schmer, Dennis W. Ryland and Fred A. Waltz
Remote Sensing Institute
South Dakota State University
Brookings, South Dakota

ABSTRACT

This research effort was directed toward the application of remote sensing techniques for the detection and monitoring of pollution from cattle feeding operations. Five livestock feeding operations were selected for the study along the James River from Huron to Redfield, South Dakota. Thirteen aerial missions providing aerial photography and thermal infrared data under various conditions such as snow and ice cover and runoff from rainfall were flown from January 1, 1971 through June 30, 1972. Water samples were collected during nine of the aerial flights at fourteen locations selected above, at and below the five feedlots. Regular water sampling at scheduled intervals provided continuity of water quality data. Water samples were collected a minimum of every three weeks regardless of whether an aerial mission was scheduled.

Data analysis consisted of visual interpretation of aerial photography and statistical analysis of film densities and water quality parameters. Film densities were read at the location of the fourteen water sampling sites and correlated with the water quality parameters. Analysis of variance and linear regression techniques were also utilized. Results indicate that remote sensing techniques, utilizing low and high altitude aircraft photography, can be used to locate potential feedlot pollution sources. The statistical analysis showed good results for specific aerial missions but considerable variability was noted between aerial flights indicating that additional study is warranted.

INTRODUCTION

Pollution and its effect on our environment is of upmost concern. Agriculture is receiving its share of attention with runoff from livestock feeding operations as one of the most obvious agricultural forms of pollution affecting our water supplies. Laws and regulations to control runoff and discharges into our water resources have been passed, but before they can be effectively enforced improved techniques are needed to locate and monitor pollution sources.

This research effort was concerned with techniques of detecting and monitoring agricultural feedlot pollution. Feedlots along a river in east central South Dakota were selected for study using remote sensing techniques such as aerial photography and thermal infrared sensing during all seasons of the year. In addition, water samples were collected to provide an indication of the water quality of the river and the presence of pollution from the feedlots. The use of high altitude photography was also investigated. Remote sensing with its advantage of synoptic view versus present day point sampling and its potential of rapid coverage offers a useful tool for detecting and monitoring the movement of wastes from cattle feeding operations to our water supplies.

DATA COLLECTION

Project Area

The James River, located in central South Dakota and flowing from north to south across the state, was selected as the primary project site. Figure 1 shows the location of the river in South Dakota. Potential feedlot pollution sources were selected along the James River

*This paper is a condensation of a Remote Sensing Institute, South Dakota State University Technical Report, SDSU-RSI-72-14 and entitled "Investigation of Remote Sensing Techniques For Agricultural Feedlot Pollution Detection". This research was funded in part by Environmental Protection Agency research grant No. 16020 FPH.

Preceding page blank

based upon a preliminary remote sensing aerial mission in April, 1970. This flight was made in cooperation with the Federal Water Pollution Control Administration, the South Dakota Department of Health and the Remote Sensing Institute.

The climate of the area can be considered semi-arid. Average annual precipitation is 48 cm (19 inches) with 65 percent of the total moisture falling during the growing season from April through August. The terrain of the area is extremely level and flat. The slope of the James River is 6.3 to 9.5 centimeters per kilometer (4 to 6 inches per mile) causing an average stream flow of approximately seven cubic meters per second (250 cfs) during the peak runoff periods of April and May.

From the preliminary aerial photographs and ground observations five feeding operations were selected for sequential aerial and ground truth data collection. These sites were selected on the basis of potential pollution hazard, accessibility to sampling sites, size of feeding operation and cooperation of the operators involved. Figures 2 and 3 show the location of the five feedlots. Feedlot sites were lettered from A through E moving in a south to north direction along the James River.

Site A is a 200 head confined dairy feeding operation located 200 meters from the James River. Prior to August 1, 1971, all runoff from the feedlot flowed directly to the river. During August settling ponds were constructed between the feedlots and the river to alleviate the runoff problem.

Site B is a 250 beef cow and calf feeding unit located next to a stream flowing into the James River. The cattle are fed in the lots during the winter and pastured in the summer. Feedlots located farther upstream from Site B may also be potential polluters.

Site C is a beef feeding operation of approximately 100 feeders. All runoff from the feedyard flows into a drainage way and directly to the James River. No attempt has been made to divert the runoff from the feedlot.

Site D is a 150 feeder calf unit located next to the James River and next to a stream flowing into the James. Although runoff from the feedlot does not seem to drain directly to the river in any observable way, the close proximity of the feedlot to the river makes it a potential pollution problem.

Site E is a relatively small beef feeding operation of 40 cows and feeder calves. Drainage from the feeding area is toward the river but, because of the relative small size of the operation, pollution may not be a problem. The site was selected to possibly illustrate that not all feedlots are polluters, even though located near a water source.

Aerial Data Collection

Aerial data collection was conducted during all seasons of the year. Aerial missions flown during the winter were for the purpose of locating feedlots and potential pollution with snow-cover conditions. Aerial missions flown in the spring, summer and fall were for detecting and monitoring the movement of feedlot pollutants to water supplies following the spring thaw and rainfall producing runoff.

Aerial data collection was accomplished with a twin engine Beechcraft, RC45J. Weather permitting, the flight altitudes were 3050 meters (10,000 feet) above ground level over the complete flight line of 129 kilometers (80 miles) and 1067 meters (3500 feet) above ground level over the selected study areas. Sensors used to collect the aerial data included four 70mm format, Hasselblad cameras; Daedalus thermal infrared scanner; Barnes precision radiation thermometer; and solameters. Table I lists the sensors, spectral ranges and film types for the project. It should be noted that not all sensors or film-filter combinations were used for each mission.

Aerial missions were scheduled as soon as possible after rainfall producing runoff. Due to the unfavorable flying and aerial photographic conditions often encountered following a rainfall it was difficult to obtain timely data; therefore some aerial flights were scheduled with adverse conditions such as partial or complete cloud cover. Another problem encountered was sunglint or the reflection of direct sunlight off the surface of the water. To avoid this problem aerial flights were scheduled two hours before or after the sun reached its highest solar angle and cameras were tripped at an interval providing 60 percent stereo overlap.

TABLE I. REMOTE SENSING AERIAL DATA COLLECTION

Variables	Spectral Range	Method of Collection
Photography		70 mm Hasselblads
Black and White Film - Filtered		
Red - #25A	0.59μm → 0.70μm	2402 film
Green - #58	0.47μm → 0.61μm	2402 film
Blue - #47B	0.37μm → 0.50μm	2402 film
Color Film - Filtered		
Color reversal infrared #15G + 30M	0.51μm → 0.90μm	2443 film
Color film - #HF3 + 4	0.39μm → 0.70μm	2448 film
Incoming Radiation		Solameter
Outgoing Radiation - Filtered		
Green - #58	0.47μm → 0.61μm	Solameter
Blue - #47B	0.37μm → 0.50μm	
Thermal Infrared Radiation	4.5 μm → 5.5 μm	Daedalus Line Scanner
Surface Temperature	8.0 μm → 14.0μm	Barnes PRT
Haze Condition		Evaluate
Cloud Type and Condition		Evaluate
Cloud Cover (%)		Evaluate

Ground Truth Data Collection

Ground truth data collection consisted of securing water samples at 14 sites selected to provide samples upstream from the feedlots, at the feedlots and downstream from the feedlots. Figures 2 and 3 show the location of the water sampling sites in relation to the five feedlots. Water samples were collected a minimum of every three weeks from April 7 through November 3 regardless of whether an aerial mission was scheduled. The three week minimum between sample collection was used to provide a regular schedule enabling the water quality data to be analyzed on a continuous time base.

When aerial data collection was made the water samples were collected as close to the time of the overflight as possible. Samples were taken at mid-stream by lowering a one quart weighted plastic container one foot below the water surface. The water temperature at each sample site was also recorded. Samples were kept in coolers and delivered to the laboratory within six hours after collection to keep deterioration to a minimum.

Two types of analysis were performed on the water samples-- bacteriological and analytical. The bacteriological analysis determined numbers of total coliform bacteria, fecal coliform bacteria, and fecal streptococcus bacteria. The analytical procedure determined dissolved oxygen, chemical and biochemical oxygen demand, kjeldahl nitrogen, nitrates, total phosphate, total solids, total volatile solids, suspended solids, volatile suspended solids, pH, conductivity and turbidity. All analyses were conducted according to methods outlined in the 13th edition of Standard Methods for the Examination of Water and Wastewater.

ANALYSIS AND RESULTS

Water Quality Analysis

The analysis of the water quality data, independent of the aerial data, was conducted to provide indications of trends over the complete sampling period from April 7 through November 3, 1971. Statistical analysis of variance was used with F-tests indicating which sources of variation were significant at the one and five percent levels. The analysis of variance which was used consisted of the 12 water sampling dates from April 29 through November 14; feedlot sites A, B, C and D; the above, at and below water sampling sites; and all combinations of the above. Feedlot E was not used in the analysis because water samples were collected only above and below the feedlot. Table II presents a summary of the results of the F-tests. The results indicate that significant differences did exist between the sampling dates, feedlots and sampling sites for a number of

water quality parameters.

TABLE II. SUMMARY OF SIGNIFICANCE TESTS FOR ANALYSIS OF VARIANCE OF WATER QUALITY PARAMETERS

Water Quality Parameters	Source of Variation					
	Dates	Feedlots	Sites	DF	DS	FS
Temperature	**	**			**	**
Kjeldahl Nitrogen	**	**		**		**
Biochem. Oxygen Dem.	**	*				**
Chemical Oxygen Dem.	**					
Dissolved Oxygen	**		**		*	**
Nitrate Nitrogen						**
Total Phosphates	**	**		**		**
pH	**	*	**	**	*	**
Conductivity	**			**		
Total Solids	**	*		**		
Total Vol. Solids	**			*		
Susp. Solids	**	*	**			*
Vol. Susp. Solids	**	**				
Turbidity	**	**	*			
Total Coliform						
Fecal Coliform						
Fecal Streptococcus			*			

** Significant at the one percent level
* Significant at the five percent level

The averages of the 14 water sampling sites indicate that biochemical oxygen demand, chemical oxygen demand and nitrate nitrogen were highest for the first sampling date, April 7, 1971. This is a possible indication that spring runoff caused the greatest amount of pollution during the sampling period. Biochemical oxygen demand is a common term used to indicate the concentration or pollutional strength of organic wastes in terms of the oxygen demand exerted by the waste on a body of water. It measures the quantity of free oxygen required by bacteria for biological decomposition under aerobic conditions, at a specified temperature and a specific time period.

The means indicate that sample site six showed the most variability. This could be attributed to the fact that the site was located on an intermittent stream which did not flow except under heavy runoff conditions. When the stream was not flowing, samples were taken from the stagnant water backed up from the James River. Concentrations of biochemical oxygen demand, chemical oxygen demand, and kjeldahl nitrogen were the lowest for site six but the concentrations of nitrate nitrogen and total phosphates were the highest. Concentrations of total coliform, fecal coliform and fecal streptococcus were also among the highest for site six.

Sample site 12 was a situation similar to site six as it was located on a stream flowing into the James River with the stream flowing only during periods of heavy rainfall and runoff conditions. Biochemical oxygen demand and kjeldahl nitrogen were highest for site 12 and concentrations of chemical oxygen demand and nitrate nitrogen were also among the highest of the sample sites. No other sample sites exhibited any marked trends or differences over the period which samples were obtained.

Film Density-Water Quality Analysis

The analysis of the film density and water quality parameter data consisted of statistical analysis of variance, linear correlation and linear regression. Film densities were measured on the 1067m altitude (3500 ft) imagery at the location of each of the 14 water sampling sites. Because the imagery was taken with 60 percent overlap per frame it was possible to obtain more than one film density for each sampling site. Two sets of film density data were obtained. One set consisted of taking the average of all valid film densities for each sampling site or, in other words, all densities not appearing to be affected by sunglint or cloud cover. The second set of film densities was obtained by taking the density closest to the center of the frame and not affected by sunglint or cloud cover. From the linear correlation analysis of both sets of film density data with the water quality data it was apparent there was no advantage to reading all the valid film densities and obtaining an average film density. Therefore all analyses presented in this report will utilize only the "center of the frame" film density data.

The analysis of variance of film densities obtained using the total density for all films is presented in Table III. The sources of variation consisted of the four film-filter combinations, seven aerial flight dates, 14 sampling sites and all combinations of the above. Only seven of the nine flight dates could be used in the analysis. Results of the F-tests in Table III show that there was a significant difference between film densities for the flight dates, the four film-filter combinations, and the flight dates by film-filter interaction.

TABLE III. ANALYSIS OF VARIANCE OF FILM DENSITIES

Source of Variation	Degrees of Freedom	Sum of Squares	Mean Squares	F
Films (F)	3	22.25	7.42	247.5 **
Dates (D)	6	1.15	0.19	6.3 **
Sites (S)	13	0.42	0.03	1.0
FD	18	14.17	0.79	27.4 **
FS	39	0.90	0.02	0.7
DS	78	0.96	0.01	0.3
FDS	234	7.80	0.03	
Total	391	47.66		

** Significant at the one percent level.

The analysis of variance of film densities for color and color infrared film is presented in Table IV. The sources of variation consisted of the two film-filter combinations (color and color infrared), the four densitometer filters (total, red, green, blue), seven aerial flight dates, fourteen sampling sites and all combinations of the above. Results of the F-tests indicate a significant difference existed between film densities for film types, densitometer filters, aerial flight dates and sampling sites.

The comparison between film densities and the water quality parameter analysis was accomplished with the statistical method of linear correlation. Correlation coefficients were computed for each of the nine aerial flights and for all the aerial missions combined. The significance of each correlation coefficient at the five and one percent level was then determined. Table V presents the correlation coefficients for film densities versus water quality parameters for the nine aerial missions combined. Significant correlation coefficients were obtained for temperature, dissolved oxygen, suspended solids, turbidity and total coliform for most of the film-filter combinations. The highest correlation coefficients were obtained for the black and white film with green filter #58. Significant correlation coefficients were also obtained for the infrared layer of color infrared film.

TABLE IV. ANALYSIS OF VARIANCE OF COLOR AND COLOR INFRARED FILM DENSITIES

Source of Variation	Degrees of Freedom	Sum of Squares	Mean Squares	F
Films (C)	1	41.29	41.285	13,760**
Filters (F)	3	50.53	16.876	5,630**
Dates (D)	6	30.94	5.157	1,720**
Sites (S)	13	3.57	0.274	90**
CF	3	15.38	5.126	1,710**
CD	6	10.03	1.671	556**
CS	13	1.22	0.094	30**
FD	18	2.76	0.153	50**
FS	39	0.14	0.004	1
DS	78	18.28	0.234	77**
CFD	18	2.86	0.159	53**
CFS	39	0.16	0.004	1
CDS	78	5.15	0.066	23**
FDS	234	0.63	0.003	1
CFDS	234	0.80	0.003	
TOTAL	783	183.83		

** Significant at the one percent level.

Visual Analysis

One of the objectives of the project was to investigate the applicability of remote sensing techniques for locating potential feedlot pollution sources. To accomplish this objective aerial flights were scheduled during periods of snow and ice conditions when feedlots are easily discernible due to snow compaction and waste deposits by the livestock. It was also found that following periods of thawing the movement of runoff from feedlots onto the ice of rivers and streams was easily detected on aerial photographs. These areas were particularly evident during the spring before the breakup of the ice in the river.

The aerial mission flown on March 8, 1972, illustrated very well the potential of remote sensing for locating feedlot pollution. Figure 4 is an aerial photograph of a 40 cow dairy operation located next to the James River. Figures 5 and 6 are ground photographs of the feedlot area showing the runoff draining directly into the river. No attempt has been made to divert the runoff or correct the pollution situation.

Figure 7 is an aerial photograph of feedlot site A taken on March 8, 1972. Settling ponds were constructed in August, 1971, to collect the runoff from the feedlot of the 200 cow dairy operation. The settling ponds are pointed out in the photograph. It appears from the photograph that runoff is still reaching the river possibly from another operation on the farm. Figure 8 is an aerial photograph of another feeding operation located on the banks of the James River. The area pointed out on the river ice may not be caused entirely by runoff from the feeding area, but by looking at Figures 9 and 10 taken on the ground the potential for runoff from the feedlot reaching the river certainly does exist.

Figure 11 is an aerial photograph of feedlot site C. Examination of the aerial photograph does not reveal any runoff reaching the river at the time of the flight. However, the ground photographs in Figures 12 and 13 taken five days after the aerial flight show that runoff from the feedlot does flow directly to the James River and that a definite pollution problem does exist. This illustrates the necessity for very timely data collection during the spring thaw period.

Another area of remote sensing that deserves consideration for use in locating potential feedlot pollution sources is high altitude imagery. Figure 14 is a print from National Aeronautics and Space Administration Mission #146 flown at 18,300 meters (60,000 feet) above ground level on November 5, 1970. An advantage noted in this print is the partial snow cover conditions which make it easier to locate the feedlots against the white of the surrounding terrain. Figure 15 is a 16X enlargement of the feedlot pointed out in Figure 14. The sharp contrast between the snow covered areas and the feedlot area makes it possible to determine the actual size of the feedlot from the photograph.

The examples shown in this section have illustrated the potential of aerial photography for locating feedlot pollution sources. It is evident that once the potential pollution sources are located observation of the sites on the ground is required. It should be pointed out that the visual interpretation discussed in this section can be accomplished with a light table and very inexperienced photo interpreters. However, automatic analysis techniques may be developed which could produce the same results without any visual photo interpretation.

CONCLUSIONS

Remote sensing techniques can be used to locate potential feedlot pollution sources and monitor the movement of the pollution to water supplies. Visual interpretation of aerial photography and thermal infrared imagery conclusively illustrated its usefulness in delineating potential pollution sources, provided the imagery was taken at the right time with the proper conditions. The best results were obtained when aerial flights were made with ice and snow cover conditions following a period of thawing causing runoff from the feedlots. The period during the spring thaw before the breakup of the river ice was found to be an ideal time to obtain imagery showing potential pollution conditions. High altitude (18,300m) photography was also found to be applicable for locating feedlots and therefore potential pollution sources.

The statistical analysis of variance of the water quality parameters and film densities revealed that significant differences were present in the data. The linear correlation analysis of film densities versus the water quality parameters showed good results for specific aerial missions but considerable variability was noted between missions. The correlation coefficients for the black and white film with a green filter showed the best results for the nine aerial missions combined. Significant correlation coefficients were obtained for temperature, suspended solids and turbidity.

The variation in correlation coefficients obtained between aerial missions can be attributed to several factors. Variations in wind conditions from one flight day to another and from one location on the river to another for the same day would cause varying wave action on the river and therefore affect the reflected radiation. The time of day and season of the year of the aerial flight causes variations in the amount of reflected radiation. Varying cloud and haze conditions cause the attenuation of incoming radiation and therefore vary the amount of reflected radiation. The instability of photographic films and changes in film processing from one data collection to another affects the resultant film densities. Additional research attempting to consider these factors in a more comprehensive analysis is indicated by the results of this research effort.

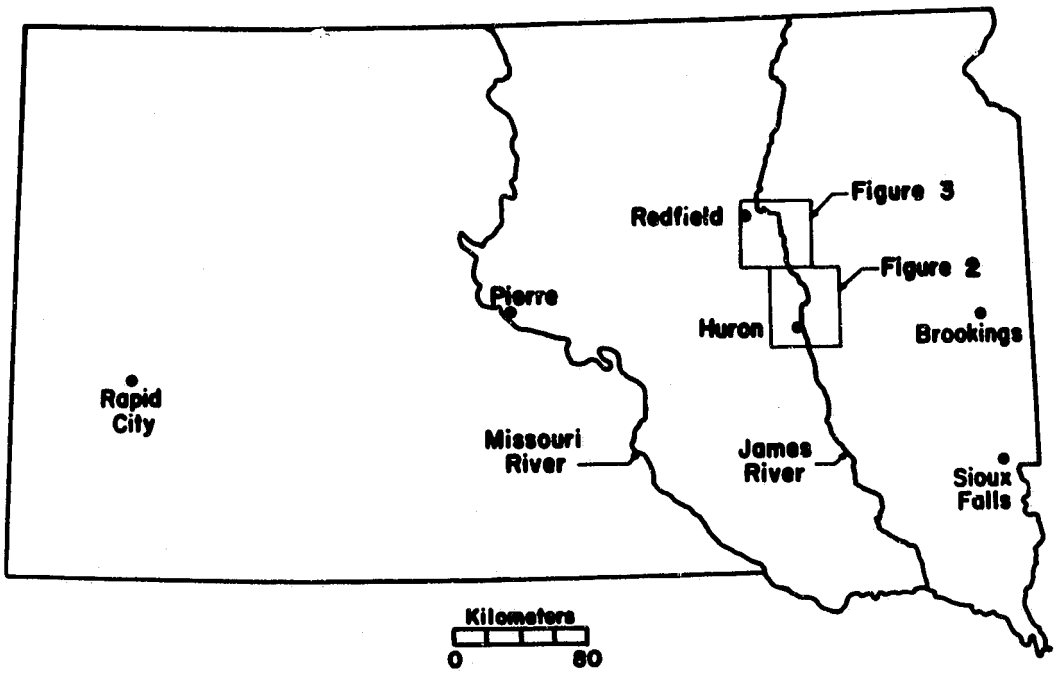


Figure 1. Location of James River and project area in South Dakota.

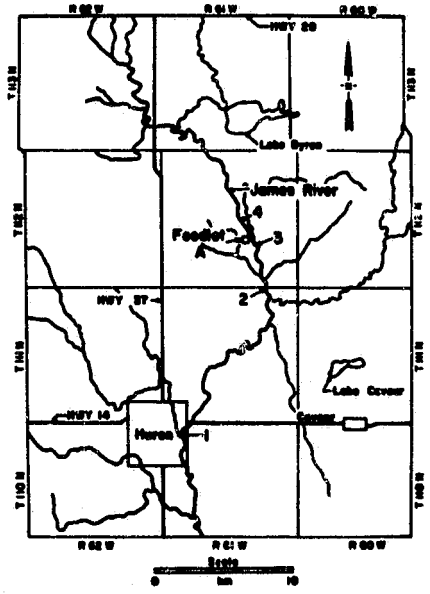


Figure 2. Location of feedlots (designated by letters) and sampling sites (designated by numbers) in southern half of project area.

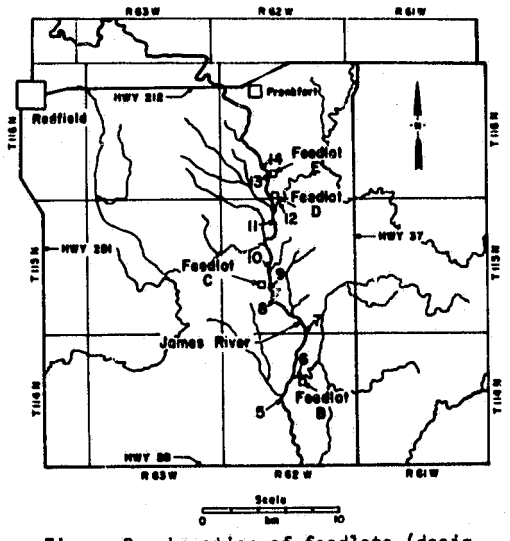


Figure 3. Location of feedlots (designated by letters) and sampling sites (designated by numbers) in northern half of project area.



Figure 4. Print from 70mm color film, #2448 with HF3 filter, taken March 8, 1972, 1067m agl, 3X enlargement, scale 1cm = 70.5m.



Figure 5. Ground truth photograph of feedlot shown in Figure 4 March 13, 1972.



Figure 6. Ground truth photograph of feedlot shown in Figure 4 March 13, 1972.

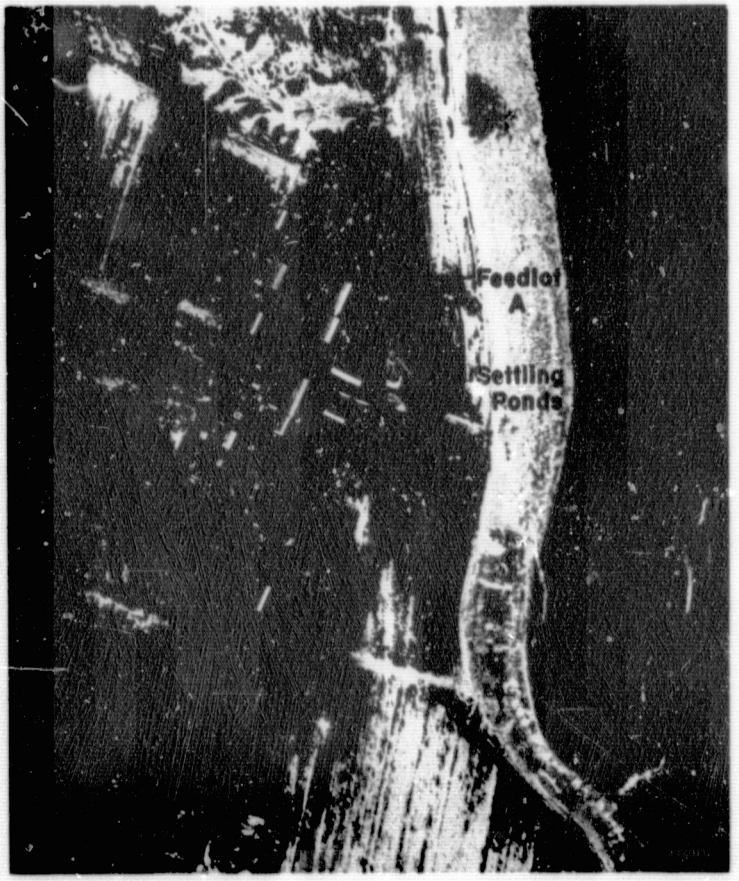


Figure 7. Print from 70mm color film, #2448 with HF3 filter, taken March 8, 1972, 1067m agl, 3X enlargement, scale: 1cm=70.5m.

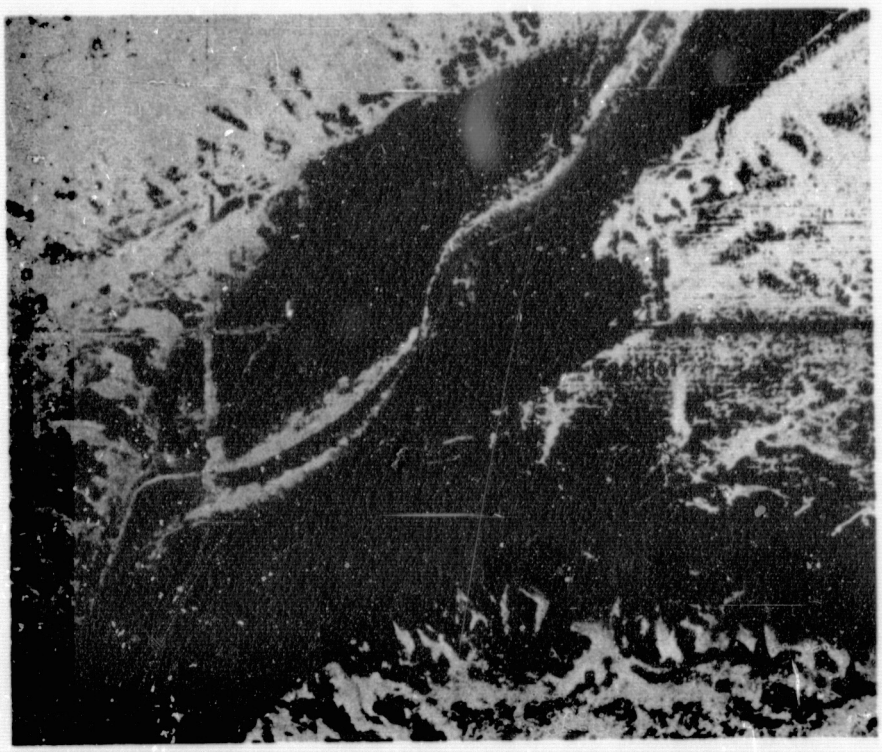


Figure 8. Print from 70mm color film, #2448 with HF3 filter, taken March 8, 1972, 1067m agl, 5X enlargement, scale: 1cm=42.2m.



Figure 9. Ground truth photograph of area shown in Figure 8 March 13, 1972.

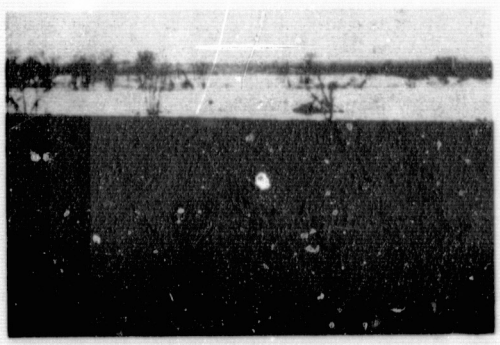


Figure 10. Ground truth photograph of area shown in Figure 8 March 13, 1972.

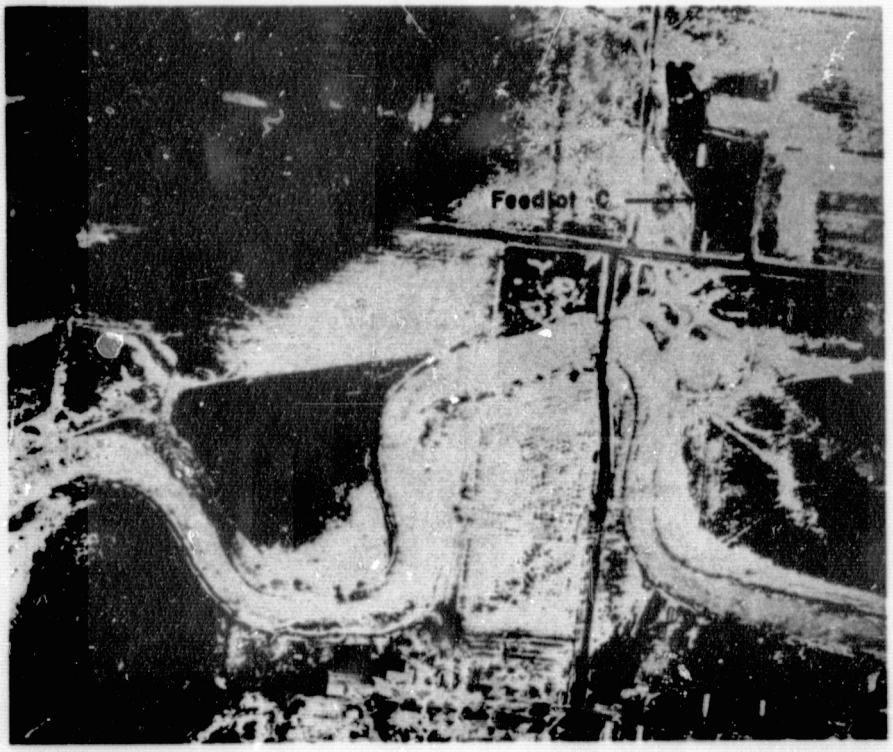


Figure 11. Print from 70mm color film, #2448 with HF3 filter, taken March 8, 1972, 1067m agl, 3X enlargement, scale: 1cm=70.5m.

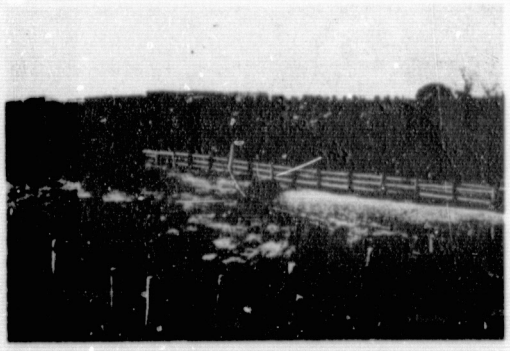


Figure 12. Ground truth photograph of feedlot shown in Figure 11 March 13, 1972.



Figure 13. Ground truth photograph of feedlot shown in Figure 11 March 13, 1972.

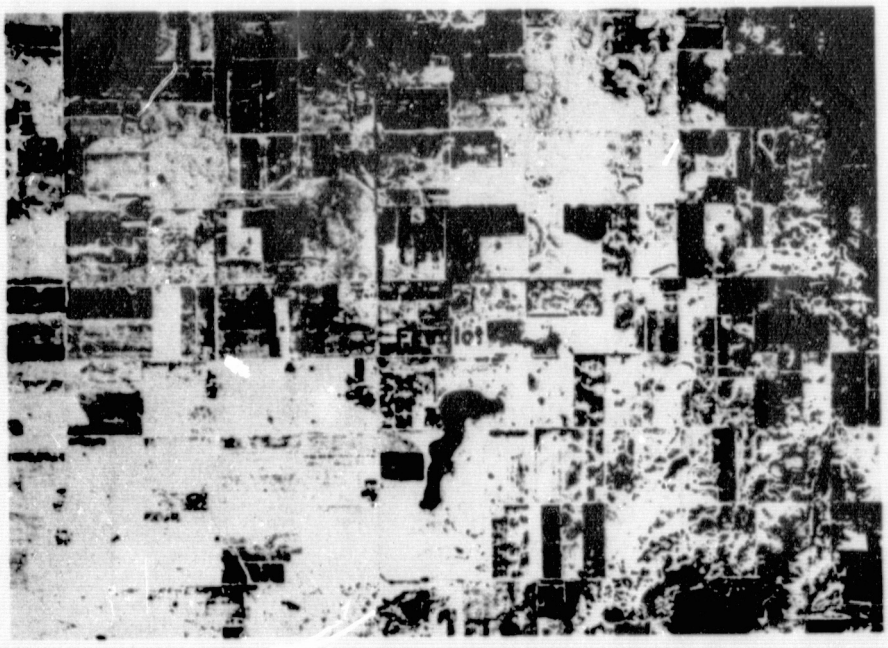


Figure 14. Print from NASA RB-57 Mission #146 taken on November 5, 1970, with color infrared film #2443, 18,300m (60,000 ft) agl, 1X enlargement, scale: 1cm=1118m.

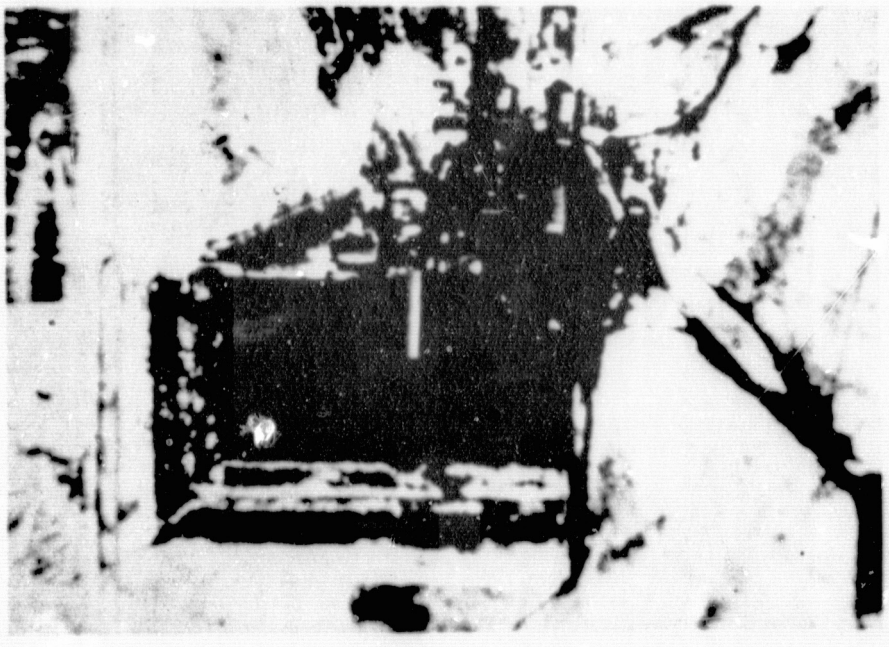


Figure 15. Print from NASA RB-57 Mission #146 taken on November 5, 1970, with color infrared film #2443, 18,300m (60,000 ft) agl, 16X enlargement, scale: 1cm=70m.

TABLE V. CORRELATION COEFFICIENTS FOR FILM DENSITIES AND SELECTED WATER QUALITY PARAMETERS FOR NINE DATA COLLECTION MISSIONS

Water Quality Parameters	B&W Grn Fltr #58	B&W Blue Fltr #47B	Color IR Total	Color IR Infrared Layer	Color IR Red Layer	Color IR Green Layer	Color Total	Color Red Layer	Color Green Layer	Color Blue Layer
Temperature	.735**	-.259**	-.407**	-.492**	-.376**	-.338**	-.276**	-.368**	-.239*	-.206*
Dissolved Oxygen	-.500**	.194*	.328**	.410**	.300**	.256**	.250**	.311**	.204*	.155
pH	-.236**	.141	.356**	.270**	.345**	.338**	-.099	-.020	-.141	-.195*
Total Solids	.103	-.275**	-.109	-.115	-.087	-.100	.165	.115	.203*	.252**
Susp Solids	.323**	-.006	-.224*	-.298**	-.209*	-.188*	-.262**	-.277**	-.255*	-.235*
Vol Susp Solids	.304**	.053	-.230**	-.264**	-.225*	-.198*	-.281**	-.287**	-.287**	-.211*
Turbidity	.541**	-.109	-.324**	-.484**	-.301**	-.254**	-.425**	-.465**	-.404**	-.349**
Total Coliform	-.330**	-.196**	.333**	.175	.390**	.357**	.267**	.275**	.258**	.204*

* Significant at the five percent level.
** Significant at the one percent level.
In comparison of negative type black and white films and positive type color films the correlation coefficient sign must be changed for one of the films.

APPLICATION OF A PULSED LASER FOR MEASUREMENTS OF BATHYMETRY AND ALGAL FLUORESCENCE[1]

G. D. Hickman
J. E. Hogg
E. J. Friedman
A. H. Ghovanlou

Sparcom, Inc.
Alexandria, Virginia

ABSTRACT

A number of applications using a pulsed N_2/Ne tunable dye laser as a remote sensor are currently being investigated at Sparcom. Two programs which have been extensively studied are 1) laser bathymetry and 2) laser stimulated fluorescence of algae. Laser transmission measurements were performed in turbid water made from resuspended bottom sediment and water taken in situ from eastern U. S. coastal and bay sites. The results indicate it should be possible to measure bathymetry in the coastal zone to depths corresponding to 15 attenuation lengths from an altitude of 500 meters. The upper limit on the capability of the bathymetry system has been determined for a spot size (at the bottom) of $\leq$ 40% of the actual depth and for a detector field of view of 5 milliradians. Laser excitation spectra for various types of algae ranged from 4200 to 6750 Å, while their fluorescent spectra ranged from 5800 to 6850 Å. Since the results of these experiments show a wide variation in both the excitation and fluorescent wavelengths, the possibility exists that this technique could be used for detecting and identifying various algal classes. Extrapolation of measurements which were made of laser stimulated fluorescence as a function of both the algal cell concentration and distance between the algae and the laser/receiver indicate that a laser system operating from an altitude of 500 meters should be capable of detecting chlorophyll concentrations as low as 1.0mg/m^3.

1. LASER BATHYMETRY

Although the feasibility of obtaining water depth information from an airborne pulsed laser has been demonstrated (Hickman and Hogg, 1969; Hickman et al, 1969) the constraints imposed upon such a system have not been investigated. The capability of this system depends upon a number of environmental and operational parameters. Our present program is designed to measure, in the laboratory, the degredation effect of these parameters on the transmitted and reflected laser signals. The data presented in this work can be used for the design of an optimal real time laser bathymetry system for shallow waters.

[1]The research is jointly sponsored by the Office of Naval Research, Geography Programs, the National Ocean Survey Engineering Development Laboratory, the U.S. Geological Survey, and NASA, Wallops Island.

The parameters which are being investigated during the current program include the following: (1) maximum turbidity of the water as defined by the absorption and scattering coefficients (2) reflectivity of the bottom sediment, (3) altitude of the laser/receiver system, (4) speed of the aircraft, (5) pulse rate of the laser, and (6) scan angle of the laser beam with respect to the surface of the water.

The technique of deploying a pulsed laser to remotely measure water depths is shown pictorially in Figure 1 while a diagram showing the various pulses involved is given in Figure 2. A short (nanosecond) pulse of light is emitted from a laser which is located on a platform r meters above the surface of the water. For the present application, this platform is considered to be either a ship, a fixed wing, or a rotary wing aircraft. The pulse of energy travels at the velocity of light and impinges upon the surface of the water. A portion of this energy (approximately 2%) is specularly reflected from the air/water interface. The receiver located on the remote platform intercepts a portion of this reflected signal. The remaining 98% of the laser energy is transmitted into water, wherein its velocity is decreased to about three-quarters of its velocity in air. In addition, the signal experiences extreme absorption and scattering which are characteristic of highly turbid shallow waters. If the signal is of sufficient intensity it will be reflected from the water/sediment interface and eventually be detected at the receiver. The time difference between the initial laser pulse and first reflection (the surface reflection), divided by two, yields the height of the remote platform above the water surface. The time difference between the first and second reflection (the bottom sediment reflection), again divided by two, results in an accurate determination of the water depth.

Measurement Program

The application of a laser to measure bathymetry requires knowledge of the optical properties of the medium which in turn determines: (1) the spatial distribution of the laser power on the water/sediment interface, (2) the percentage of laser power and its angular distribution reflected from the sediment and (3) the energy received by the detector. Knowing the total incident power on the target, and a value for the target reflectivity, one can calculate the signal reflected back to a detector co-located with the laser transmitter. These results are then used to extrapolate expected signal levels at a remote (airborne) platform. It should be noted that various sea-state conditions affecting the turbidity of the water may modify the results presented in this report.

The majority of basic data on light scattering in turbid water has, in the past, been obtained either by using small laboratory test cells or measured in the real environment. Since the process of multiple scattering and absorption is complicated, it has been impossible to predict the transmission properties of light in a given environment from the results obtained in another environment. Preliminary measurements (Hickman, et al, 1970) showed that the basic behavior of light in water could be investigated in the laboratory by simulating turbidity conditions found in the real environment. Using this procedure, it was found that a multitude of environments could be easily investigated. A mechanism is therefore provided for determining the independent signal loss from the suspended sediment, air/water interface, bottom, etc.

The turbidity conditions of the water in the laboratory are adjusted in small increments by controlling the concentration of various marine sediments, which are added to the water. These sediments are collected from selected shallow waters. Water samples are also collected from each site where sediment is taken. The particles which make up these sediments are those that have most recently been in suspension and those that will be resuspended by bottom currents, storms, etc. Values of the attenuation coefficient, α, obtained in the test tank for the equivalent sediment loading, using the sediment to simulate turbidity conditions are compared. If indeed it can be shown that a good correlation does exist between α and sediment loading in the two cases, the basic behavior of a laser beam in the simulated environment should be very similar to that expected for the beam when operated in the real environment.

Experimental Facilities

The following basic equipment was used in the laboratory to measure the transmission of light in water of varying turbidity.

Laser

The laser was a pulsed gas laser (AVCO-C950). When the cavity is filled with neon gas the output is at 5401 nm. This laser line is used for the basic transmission measurements. With nitrogen in the cavity and a dye cell attached, the output of the laser is tunable over the range of approximately 4000-7000 Å by deployment of 10 different dyes. This tunability was used in the algal fluorescent measurements described in Section 2. The short pulse width (5-10 nsec) combined with its high pulse repetition rate (100-1000 pps), make this laser the best candidate for a high resolution, shallow water reconnaissance system.

Controlled Environmental Water Test Tank

The test tank measures 30 x 10 x 7 feet and has two 4 x 4 plexiglass windows (1 inch thick) at each end and twelve, six inch diameter portholes on the sides. Initially the water in the tank is filtered by circulating the water through a high rate sand filter to yield clarity conditions approximating deep ocean water (α=0.07m^{-1}). The laser beam is introduced into the tank at one end of the tank and rotated, in milliradian steps, across an underwater photomultiplier tube detector. Figure 3 is a schematic diagram showing the laser beam, tank, and underwater detector.

Absorption and Attenuation Instruments

As the turbidity of the water was changed in the test tank, measurements were made of both the attenuation coefficient alpha (α) and the absorption coefficient (a). The attenuation coefficient of the water was measured with a Marine Advisor Transmissometer, while the absorption coefficient was measured with an absorption meter built on the original design of Sorenson and Honey (1968).

Delaware Bay Measurements

On August 24, 1971, five samples of sediment and three water samples were obtained from Delaware Bay from Lewis to Cape May. The bottom sediment samples were taken from depths averaging approximately 40 feet, while the water samples were taken at the same stations from mid depth. Measurements on the water samples showed the alpha of the water to be less than 1.0m^{-1} while the sediment loadings were determined to be < 4mg/liter. One water sample showed extremely high values for both α and sediment loading, thereby indicating that the sample was taken in a region of a sediment plume. Using the bottom sediment to mock up the turbidity of Delaware Bay in our test tank a curve of alpha vs sediment loading was constructed. These results showed a value for α of 2=$\overline{3m}^{-1}$ to correspond to a sediment load of approximately 4 mg/liter. A good correlation of α is therefore seen to exist between the values of α and sediment loading obtained for the water samples and those obtained for the water which was made to simulate Delaware Bay. Secci disc measurements in Delaware Bay ranged from 1.3-1.8m which is equivalent to α meter readings of < 3m^{-1}, although no simultaneous measurements of α, Secci discs and sediment loading is available. From aerial photographs it has been estimated that approximately 70 percent of the Bay falls within this range of turbidity (Klemas, 1972).

Angular power distributions for the laser beam were measured in the tank at distances of 2, 4, 6, and 8 meters. In these measurements the water turbidity ranged from α=0.07-2.0m^{-1}. The values of a/α were measured to be 0.20 ± 0.02. Figure 4 shows a typical dependence of the measured angular power distribution for various values of α. As to be expected, not only does an increase in turbidity reduce the central intensity (several orders of magnitude) but causes a flattening of the angular scattering distribution of the laser beam in the range 0-200 milliradians. This reduction is due to the combined effects of scattering and absorption.

Having obtained the angular power distributions of the laser light, one can now calculate the total power contained in the solid angle incident on a given target plane, i.e., 2, 4, 6, or 8 meters. The integrated power distribution in a cone whose half angle is θ is given by the expression

$$P_{\alpha a}(h,\theta) = \frac{2\pi h^2}{A} \int_0^{\theta} f_{\alpha a}(h,\theta')\theta' d\theta' \qquad (1)$$

where

$f_{\alpha a}(h,\theta')$ is the measured power angular distribution
α = total attenuation coefficient
a = absorption coefficient
A = detector area
h = depth of water

A typical set of integrated power distributions is shown in Figure 5. For clear water (α=0.07m^{-1}) the integrated power distribution reaches its maximum value in the interval of 0-3 milliradians. However, as the turbidity is increased the maximum power is reached at much larger angles. Extrapolation of the curves for angles > 200 milliradians is indicated by the dotted portion of the curves. For the case α=1.97m^{-1} the spot size is 3.2 meters at a depth of 8 meters for a half cone angle (θ) of 200 milliradians.

Reflectivity measurements which were made for each of the sediments showed an average value of approximately 10%.

Extrapolation of Results to Airborne Operation

The strength of the laser signal which is received by an airborne laser/detector system is a function of the following parameters.

1) altitude of the aircraft, r
2) input power of the laser, P_o
3) depth of the water, h
4) attenuation (α) and absorption (a) coefficients of the water
5) bottom reflectivity, R
6) field of view of the detector, ϕ

It has been shown that the received power can be written as

$$P_{rec}(r) = [P_o \cdot (A/4\pi)\tan^2(\phi/2)][RN_{\alpha a}(h,\theta)\frac{e^{-h'a}.e^{-ha_o}}{h'^2} \qquad (2)$$

where A = area of detector
a_o = absorption coefficient for clear water
$N_{\alpha a}$ = normalized measured power angular distributions
and

$$h' = \sqrt{h^2 + h^2\tan^2\theta + r^2\tan^2(\phi/2) + 2hr\tan\theta\tan(\phi/2)} \qquad (3)$$

This calculation has only considered the loss of energy due to the attenuation by water.

It should be noted that the received power is a function of the absorption coefficient and not the attenuation coefficient. This fact has been proven experimentaly and results in greater penetration depths that would be obtainable if the received power were a function of α. Figure 6 shows the calculated received power as a function of depth for various values of α. This figure

shows that the maximum depth of penetration for an airborne laser/receiver system from an altitude of 500 meters is limited to approximately 15 attenuation lengths ($\alpha h=15$). For example, in water having a value of alpha equal to $1.0m^{-1}$, the depth of penetration would be 15 meters. For a water depth of 8 meters and a value of α equal to $2.0m^{-1}$, the spot size at the bottom corresponding to a value of θ equal to 200 milliradians, is 3.2 meters. In this case the field of view of the detector (ϕ) is 5 milliradians.

2. LASER STIMULATED FLUORESCENCE OF ALGAE

Fluorescence Spectra of Algal Pigments

Of the fluorescent pigments in algae, the most common is chlorophyll. Chlorophyll is a major factor in the ability of plants to utilize light for energy by photosynthesis. Although the various types of algal species contain varying concentrations of different types of chlorophyll, chlorophyll a is the main factor which is important in the conversion of light into energy for plants. In addition to chlorophyll, there are several other phytosynthetic pigments whose absorption and fluorescence spectra are of interest.

Measurement Program

The fluorescence of the photosynthetic pigments of algae can be excited by conventional light sources as well as laser light. Preliminary measurements (Hickman and Moore, 1970) using a laser to stimulate fluorescence showed that it might be feasible to use this technique for the purpose of remotely sensing algae. Kim and Mumola (1972) detected algae via helo mounted laser.

The present research program has been oriented toward examing the problems, capabilities and limitations of a laser detection system which is based on measuring the fluorescence of algae. The major emphasis of the program has been concerned with the measurement of the absorption and fluorescence spectra of various species of algae along with a determination of their fluorescence quantum efficiencies.

Using this data, an extrapolation has been made to a remote airborne laser transmitter/detector system. A mathematical model for calculating the signal/noise ratio of a detector has been formulated. This model includes such parameters as background noise provided by the sun and skylight, geometric effects and laser power and detector field of view considerations.

Fluorescence Spectra

The fluorescence spectra of various selected algae were made under a variety of conditions including various excitation wavelengths, concentrations, etc. These spectra were obtained using both a spectrophotofluorometer (SPF-xenon-arc lamp excitation) and a laser-scanning spectrometer system (LSS).

Using both of these systems, the fluorescence spectrum of a particular sample was measured over the entire optical spectrum for a given excitation wavelength. Following this procedure, the fluorescence spectrum was measured for a variety of excitation wavelengths. All spectra were corrected for system parameters such as phototube response, laser power, and spectrometer grating efficiency.

The spectra generated by the laser system are presented in Figure 7 as points superimposed on the continuous spectra obtained from the spectrophotofluorometer. Spectra were obtained for four different algal species, Chlorella pyrenoidosa, Porphyridium cruentum, Agmenellum quadruplicatum, and Chlamydomonas reinhardt.

Excitation and Absorption Spectra

Measurements of both the excitation and absorption spectra were made for the various algal species for a variety of concentrations. The excitation spectra were made on the spectrophotofluorometer (SPF) and the laser-scanning spectrometer(LSS), while the absorption spectra were obtained using a dual beam spectrometer.

Figure 8 shows the excitation and absorption spectra for the four algal species described above. These spectra were obtained by setting the output of the spectrometers to pass only the 685 nm fluorescence line, which is characteristic of chlorophyll a, and scan the excitation wavelength. Some distinction should be made between the excitation and absorption spectra. Excitation spectra illustrates the effectiveness of various wavelengths for generating a particular fluorescence wavelength, in this case the 685 nm peak. The absorption spectra on the other hand show the total absorption at various wavelengths, regardless of whether the absorbed light generates a fluorescent signal. The difference between the two curves represents the amount of energy which is absorbed and not transferred to the generation of chlorophyll a fluorescence. In general, the two curves overlap at longer wavelengths but show a discrepancy in the near uv. In addition to identifying the various absorption pigments in algae, these measurements provided the optical density data necessary for determination of the algal quantum efficiencies.

Quantum Efficiency

The quantum efficiency q is defined as the number of quanta emitted at the fluorescence wavelength divided by the total number of quanta absorbed by the sample. This parameter is important in the mathematical analysis for the fluorescence of the photosynthetic pigments in the plankton because it allows a direct comparison between them. In order to calibrate the quantum efficiency of the algae, quantum efficiency measurements have also been made for several organic dyes.

The technique which was used for the measurement of q is the same as that used by Parker and Rees (1960). A measurement of the fluorescent spectrum for both the known and the unknown samples is made on the same instrument so that a direct comparison can be made. The unknown quantum efficiency is then given by

$$q_u = q_r \frac{f_u}{f_r} \frac{O.D._r}{O.D._u} \frac{I_r}{I_u} \frac{\lambda_{re}}{\lambda_{ue}} \left(\frac{\lambda_{uf}}{\lambda_{rf}}\right)^2 \qquad (4)$$

where

u = unknown sample
r = reference sample
f = fluorescence generated-it is equal to the area under the curve, corrected for phototube response and grating efficiency
O.D. = optical density of the solution
I = intensity of the exciting radiation
λ_e = excitation wavelength
λ_f = peak fluorescence wavelength

Table I presents the q values which were obtained during this study along with values measured by other investigators. In addition q values for various dyes are also given in Table I. Included in Table I are the q values for a 10 nm band centered at 685 nm. This 10 nm band simulates the optical filtering of an operational laser fluorescence system. This filter is chosen to coincide with the maximum algal fluorescence (produced by chlorophyll a) which peaks at 685 nm. The significance of this q value is that it represents the actual quantum efficiency for the generation of the portion of the fluorescence spectra that will be detected by an operational system.

It should be noted in Table I that the q values vary from specie to specie. A specie like Agmenellum quadruplicatum, which has a predominant phycocyanin fluorescence, has a fairly low fluorescence output at 685 nm. Hence it will have a low quantum efficiency. However, those species whose fluorescence is mostly from Chlorophyll a will have a relatively high q value at 685 nm.

TABLE I: Quantum Efficiencies for Various Algae Normalized to that Obtained for Rhodamine B Dye

Species	Excitation	q(%)	q of 10 nm band at 685(%)	Ref.
Algae				
Agmenellum	337	.6	.03	1
Chlorella	337	.291	.06	1
Chlorella	436	1.7-2.7		2
Chlorella	436	.15-.3		3
Porphyridium	337	.26	.01	1
Chlamydomonas	337	.7	.15	
Dyes				
Rhodamine B	366	.68		1
Rhodamine B	366	.73		4
Acridine Orange	366	.53		1
Acridine Orange	366	.46		4

1 - Friedman and Hickman (1972)
2 - Latimer Bannister Rabinowitch (1957).
3 - Vermeulen, Wassink and Reman (1937)
4 - C. A. Parker (1968)

Fluorescence Lifetimes

Measurements were made of the fluorescence lifetimes of the various algae. This was accomplished by observing the pulse width from a phototube having a 2 nsec rise time with a 150 Mhz oscilloscope (2 nsec rise time). The pulse width was found to be 8 $\pm$ 2 nsec. This spread in signal is expected since it is the minimum pulse resolution allowed by the detection system. Observation of the fluorescence pulse width resulted in values of 10 $\pm$ 2 nsecs, thereby indicating a fluorescence signal having a duration of 1-2 nsecs. These values agree well with published data (Brody and Rabinowitch, 1957) which showed chlorophyll a to have a lifetime of 5.1-7.8 nsecs in solvents and about 1/4 that value in live cells i.e., 1-2 nsecs.

Simulated Remote Sensing

In an effort to make simple tests of the basic assumptions about an operational system, simulated remote sensing experiments were performed using the laser to activate the algae. A spectrally filtered photomultiplier (10 nm interference filter, centered at 680 nm) was used as the detector.

Two basic measurements were made to determine the fluorescent siganl as a function of (1) algal concentration and (2) distance. The configuration of the experiment which was used to determine the functional dependence of the algal concentration is shown in Figure 9, along with the results which were obtained for the specie Agmenellum. In this experiment the detector was located one meter above the surface of the water. For low concentrations the fluorescent signal is directly proportional to the algal concentration. In the second experiment the algal concentration was fixed and the fluorescent signal measured as a function of the distance (R) between the laser/receiver and the algae. The results of this experiment as R was varied from one to 12 meters showed the fluorescent signal to fall off approximately as $1/R^2$.

Mathematical Analysis of a Laser/Detector System

This section deals with a number of salient environmental and system parameters which must be considered in assessing the feasibility of a remote laser system for the detection and identification of algae. The equations which are given below are used for estimating the signal-to-noise ratio for remote detection of the fluorescent signal.

Fluorescent Signal

Figure 10 is a schematic diagram of a remote laser/detection system for the activation and detection of algae. It can be shown that the laser induced algae fluorescence incident on a remote detector co-located with the laser transmitter is given by

$$P_S = P_L \, \epsilon_T \, e^{-(\alpha_A^{\lambda} + \alpha_A^{\lambda'})} \, (1-\rho)^2 \, \frac{\epsilon_A \epsilon_c A_c}{4\pi R^2} \, \frac{\alpha_W^{\lambda}}{\alpha_W^{\lambda} + \alpha_W^{\lambda'}} \, [1-e^{-(\alpha_W^{\lambda} + \alpha_W^{\lambda'})h}] \qquad (5)$$

where

P_L = primary laser power
ϵ_T = transmitter optics efficiency
ϵ_A = coefficient for producing algal fluorescence
ϵ_c = collector optics efficiency
A_c = area of the receiver
ρ = reflectivity of the water surface
$\alpha_W^{\lambda'}\alpha_A^{\lambda'}$ = absorption of the fluorescent signal in the water/algae medium and the atmosphere respectively
$\alpha_W^{\lambda}\alpha_A^{\lambda}$ = absorption of the laser signal in the water/algae medium and the atmosphere respectively
R = distance from laser/receiver to water/algae surface
h = depth of algae in water

Signal to Noise

There are many sources of background signals which must be considered when calculating the signal/noise of a laser/receiver system. They are due to sun and skylight generated algal fluorescence, reflections, and air and water backscattered signals. Each of these potential sources of background must be calculated and their sum compared to the noise equivalent power of the photodetector. A nominal value of NEP for the photomultiplier is roughly 7×10^{-10} watts for a 150 Mhz bandwidth. Computation of the power of the various background signals as a function of altitude were made and the sum set equal to P_B.

The signal to noise ratio is given by

$$\frac{S}{N} = \frac{\rho P_S^2 (R)}{2h\nu B P_B} = \frac{P_S^2 (R)}{NEP \cdot P_B} \qquad (6)$$

where ρ is the photomultiplier quantum efficiency
P_S = signal power
h = Plank's constant
ν = optical frequency
P_B = background power
R = aircraft altitude in kilometers
B = post detection bandwith

Substituting the expression for P_S (equation 5) into equation (6) and inserting appropriate values for the various parameters result in the following expressions for the signal to noise ratios for excitation wavelengths of 600 and 337 nm

respectively.

Excitation at 600 nm

$$\frac{S}{N} = \frac{68}{R^4} \quad \frac{e^{-0.192R}}{11.73-10.13\, e^{-0.064R}} \qquad (7)$$

Excitation at 337 nm

$$\frac{S}{N} = \frac{12.5}{R^4} \quad \frac{e^{-0.544R}}{11.73-10.13\, e^{-0.064R}} \qquad (8)$$

A plot of P_S (equation 5) and S/N (equation 7 and 8) for the two excitation wavelengths are given in Figure 11. Excitation at 600 nm is seen to yield both signals and signal to noise values which are substantially larger than those obtained for excitation at 337 nm. These results, along with the data generated on the fluorescence, absorption and excitation spectra for the various algae, clearly indicate that the optimum laser wavelength for remotely detecting chlorophyll a in the environment is approximately 600 nm.

3. CONCLUSIONS

The results of laser bathymetry program showed that to a good approximation, the turbidity of natural bay waters can be simulated to a high degree in the laboratory for making laser transmission/scattering measurements. This is accomplished by adding known amounts of sediment to the water in our controlled water tank test facility. The sediment is taken from the environment which is under investigation. Using the measured angular power distributions and the sediment reflectivities, the strength of the laser signal which is received by an airborne laser/receiver system can be calculated. Such calculations can be made as a function of aircraft altitude, laser input power, water depth, attenuation and absorption coefficients, sediment reflectivity and detector field of view. For the results obtained for Delaware Bay it has been shown that the maximum water depth measuring capability for an airborne laser system, at an altitude of 500 meters, is 15 attenuation lengths. It is estimated that a well designed airborne system could map approximately 70% of the bathymetry of Delaware Bay.

The results of the laser stimulated fluorescence experiments on algae showed that the various species had different fluorescence spectra depending on their pigments. It therefore appears possible, especially using a tunable laser for excitation, to identify various algal species from an analysis of their fluorescent spectra. However, if one is concerned only with chlorophyll a, the optimum excitation is 600 nm while the detector should monitor the fluorescence at 685 nm. From an analysis of both the laboratory results and a calculation of the signal to noise ratio at the receiver, it appears feasible to measure chlorophyll a in concentrations as low as 1.0mg/m^3 using a 100 kw peak power laser from an altitude of 500 meters.

In addition to the potential applications of using the laser from a remote platform to map bathymetry in the shallow waters and to detect algae, especially chlorophyll a, a number of other airborne laser applications appear to be feasible. These include (1) synoptic tracking of surface/subsurface water currents by measuring laser-induced fluorescence of various organic dyes, (2) detection, identification and mapping of oils by observing laser-induced fluorescence signatures, and (3) determination of water turbidity (suspended detrites, organic pollutants, etc.) by observation of laser backscattering from the water.

REFERENCES

Brody, S. and E. Rabinowitch, 1957 Science 1-2 , p. 555.

Friedman, E. J. and G. D. Hickman, 1972, Laser Induced Fluorescence of Algae, Sparcom, Inc., report, Alexandria, Virginia.

Hickman, G. D., and J. E. Hogg, 1969, Application of an Airborne Pulsed Laser for Near Shore Bathymetric Measurements Remote Sensing of Environment 1, 47-48.

Hickman, G. D., Hogg, J. E., Spadaro, A. R. and Murray Felsher, 1969, The Airborne Pulsed Neon Laser: A New Oceanographic Remote Sensing Device, presented at the Sixth International Symposium on Remote Sensing, Ann Arbor, Michigan, Oct 14-16.

Hickman, G. D., Hogg, J. E. and A. R. Spadaro, 1970, Optical Attenuation Measurements of a Pulsed Ne Laser in Turbid Waters. Syracuse University Research Corporation, report, ASD TR-69-33.

Hickman, G. D., and R. B. Moore, 1970, Laser Induced Fluorescence in Rhodamine B and Algae presented at the 13th Conference on Great Lakes Research, Buffalo, New York, March 31-April 3.

Kim, H.H. and Mumola, P. B., Laser Induced Fluorescence for Rapid Mapping of Phytoplankton Distribution in the Sea, Annual Meeting of Optical Society of America, N. Y., April 12, 1972.

Klemas, Vic, 1972, University of Delaware, private communication.

Latimer, P., Bannister, T. T. and E. I. Rabinowitch, 1957, Research in Photosynthesis, Interscience, N. Y., p. 107.

Parker, C. A., 1968, Photoluminescence of Solutions, Elsevier, N. Y.

Parker, C. A. and W. T. Rees, 1960, Analyst, 85 p. 587.

Sorenson, G. P., Gilbert, G. D., Honey, R. C., and R. E. Meyers, Optical Absorption Meter, SRI, Contract N630530-68C-1423, 1969.

Vermuelen, D., Wassink, E. C., and G. H. Reman, 1937, Enzymologia 4, p. 254.

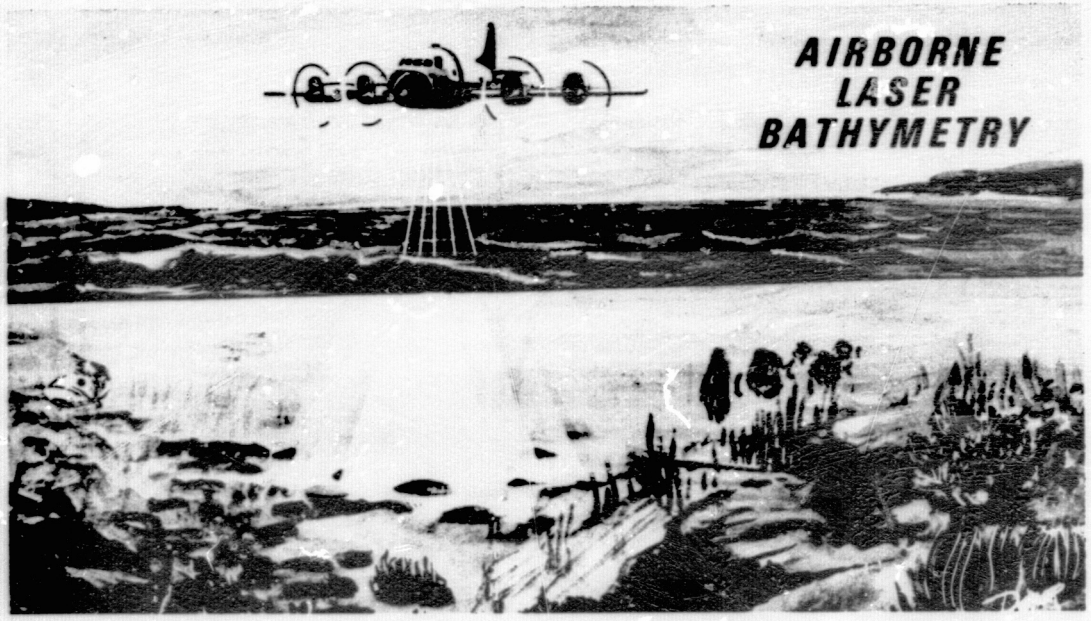


Figure 1: Airborne Laser Bathymetry

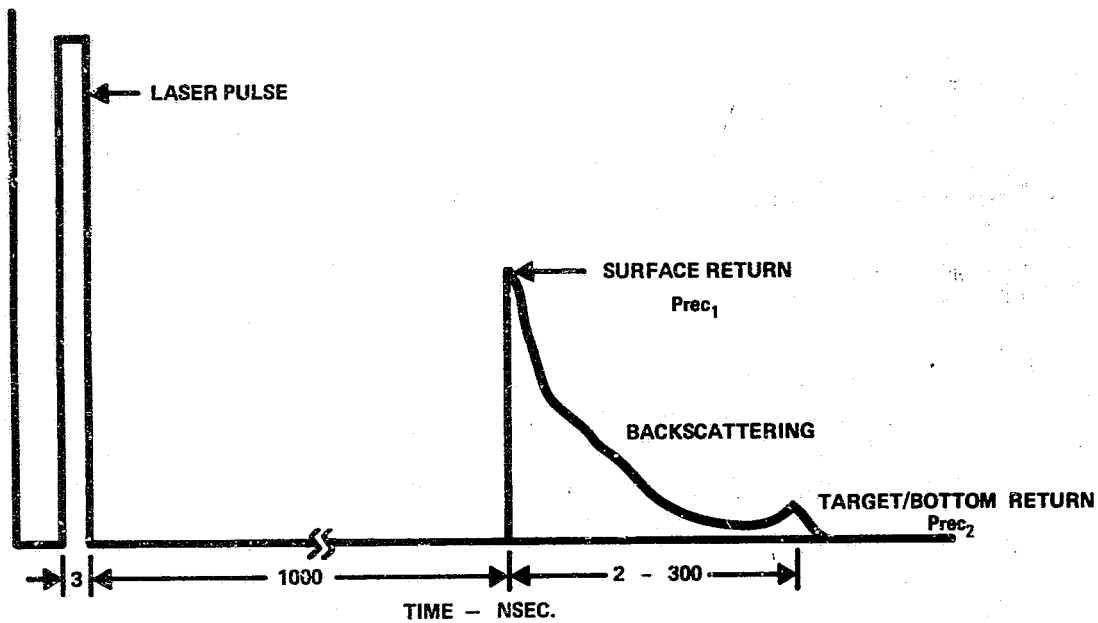


Figure 2: Schematic Timing Diagram Showing Laser Pulse and Various Return Signals

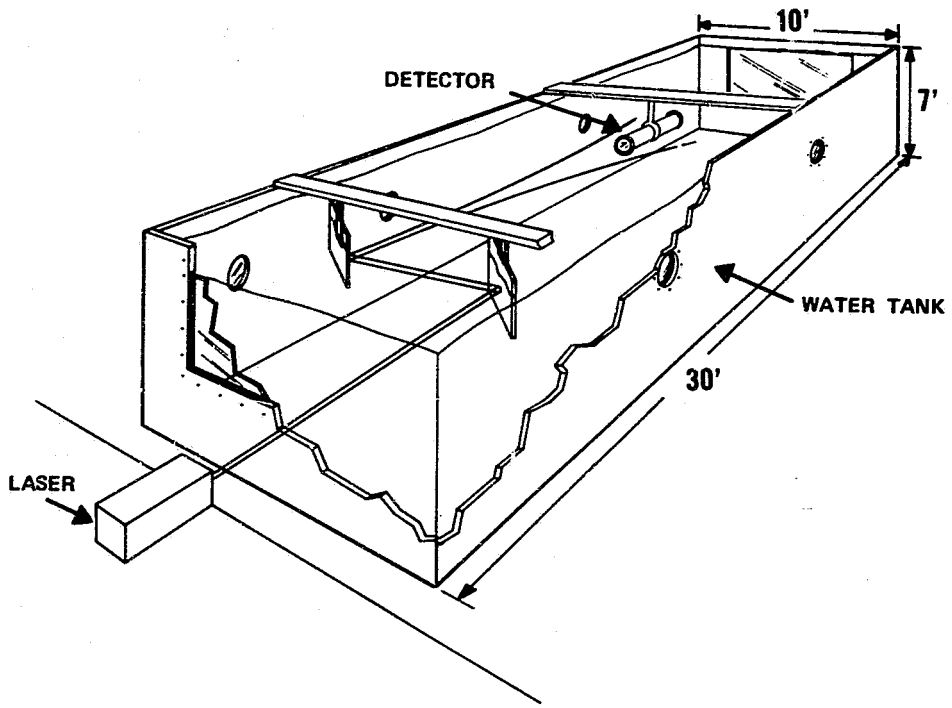


Figure 3: Environmental Test Tank Facility

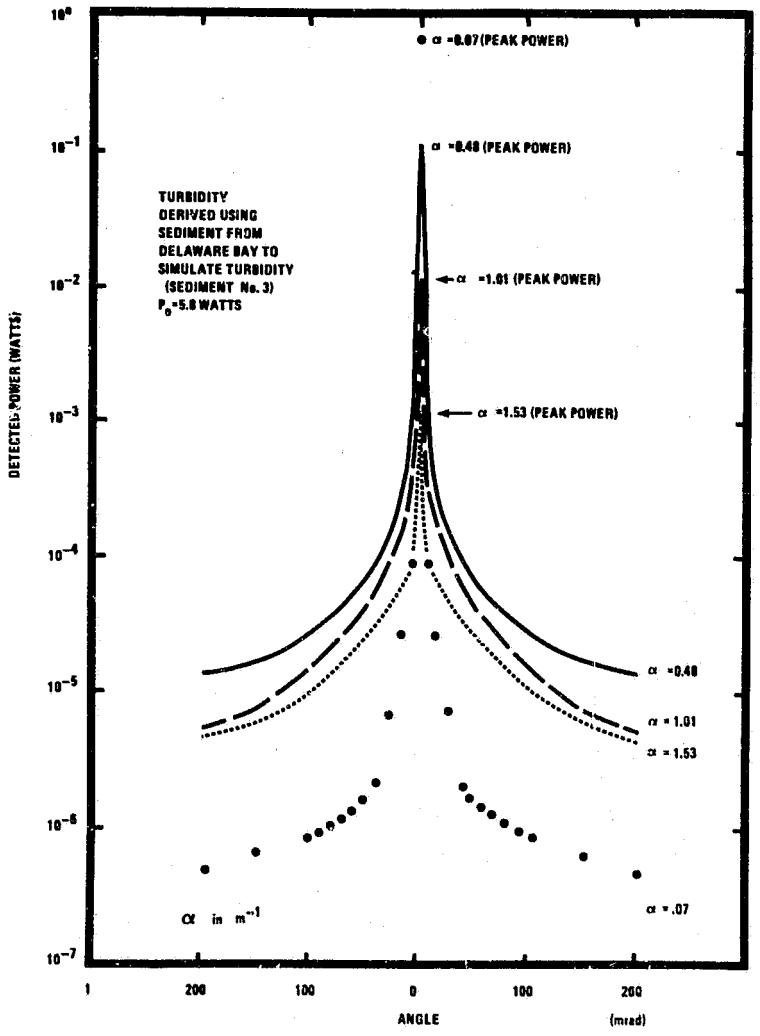


Figure 4: Angular Power Distributions for Large Angles as a Function of α

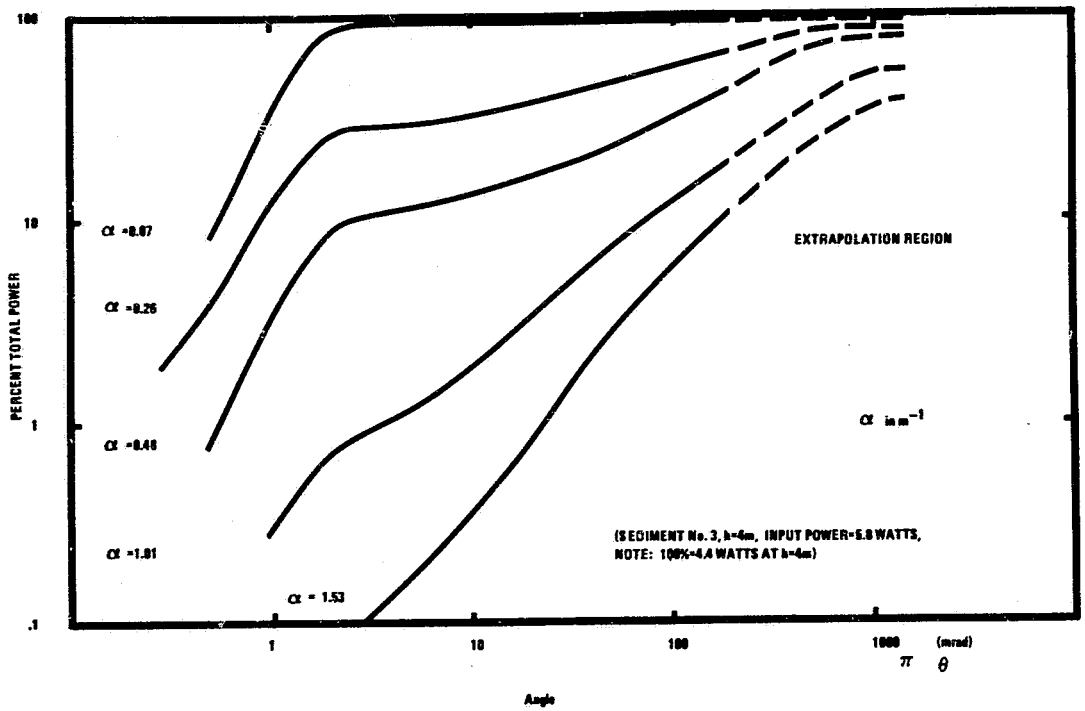


Figure 5: Integrated Power Distributions Derived
Using Sediment from Delaware Bay to Simulate Turbidity

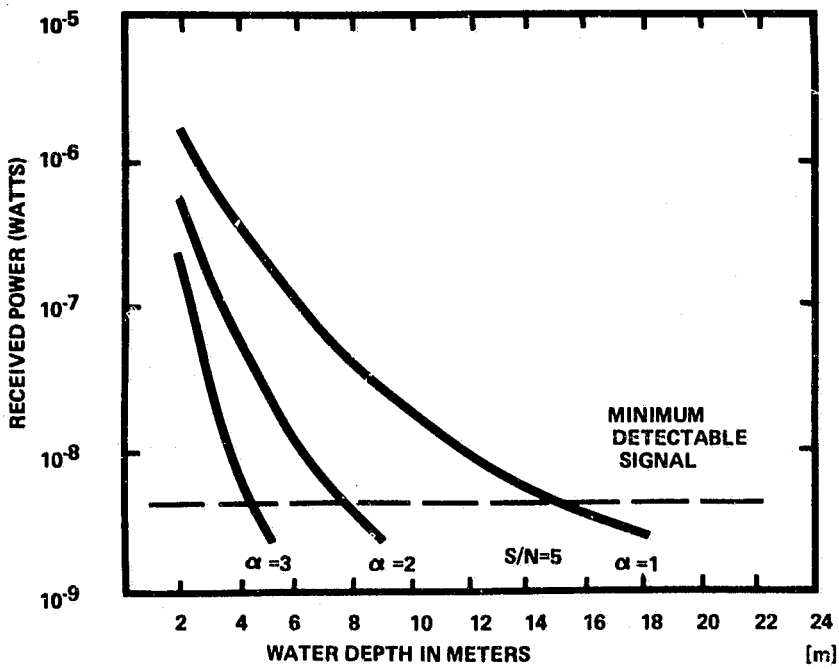


Figure 6: Calculated Power Incident on an Airborne Receiver (Po=30 kw/pulse; R = 500 meters)

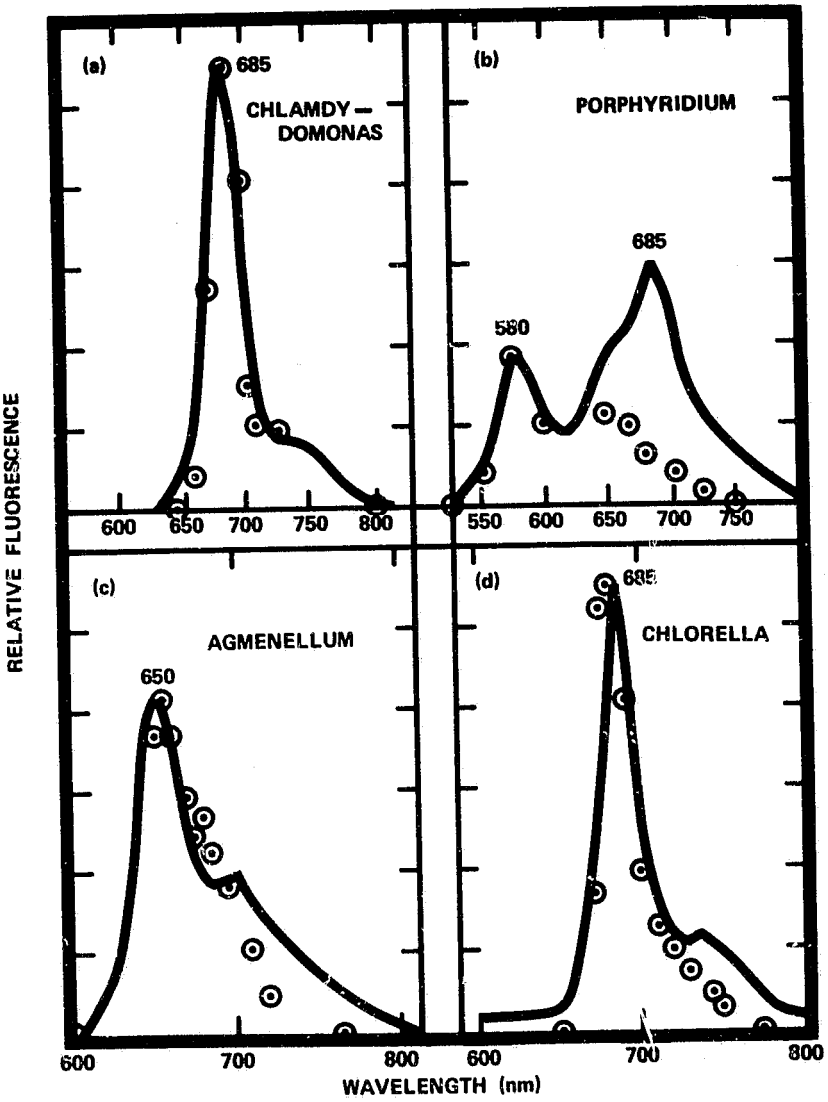


Figure 7: Fluorescent Spectra of Various Species of Algae (Circles are laser generated data, while the solid lines were obtained from the SPF).

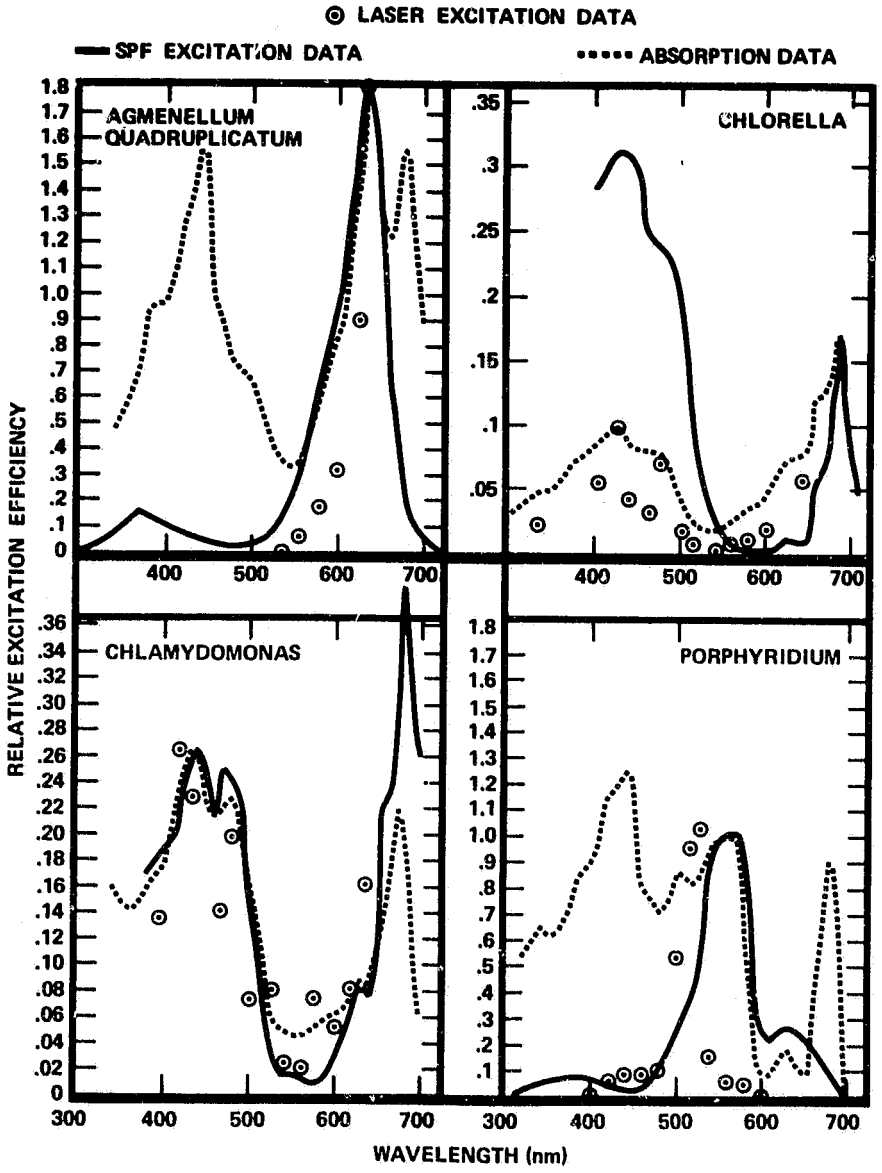


Figure 8: Excitation and Absorption Spectra for Various Algal Species

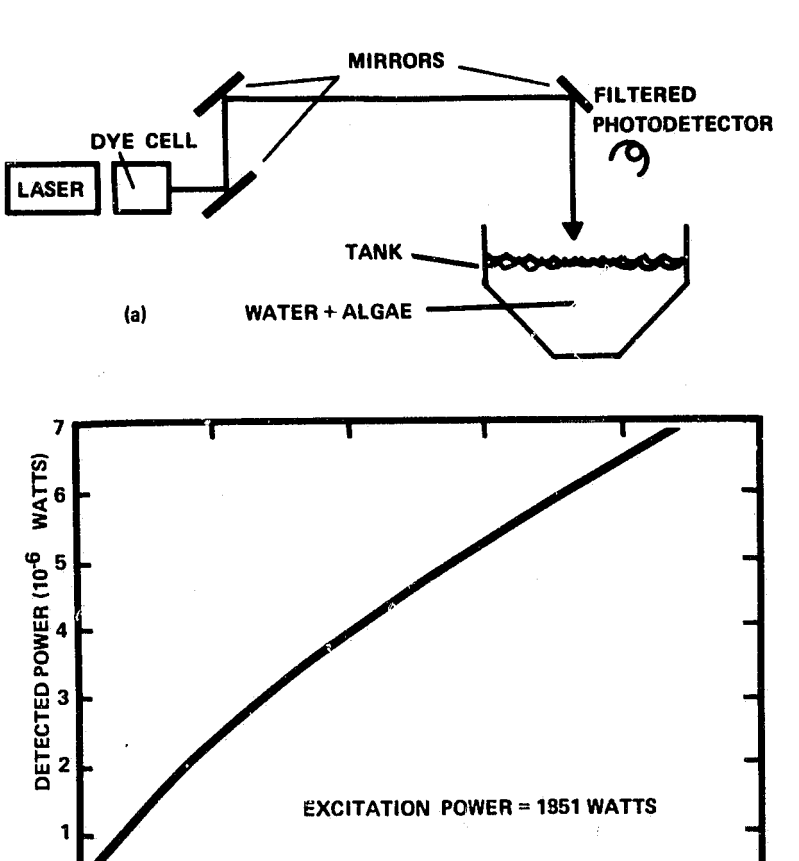


Figure 9: Signal vs. Algal Cell Concentration with the Detector 1 Meter Above the Water

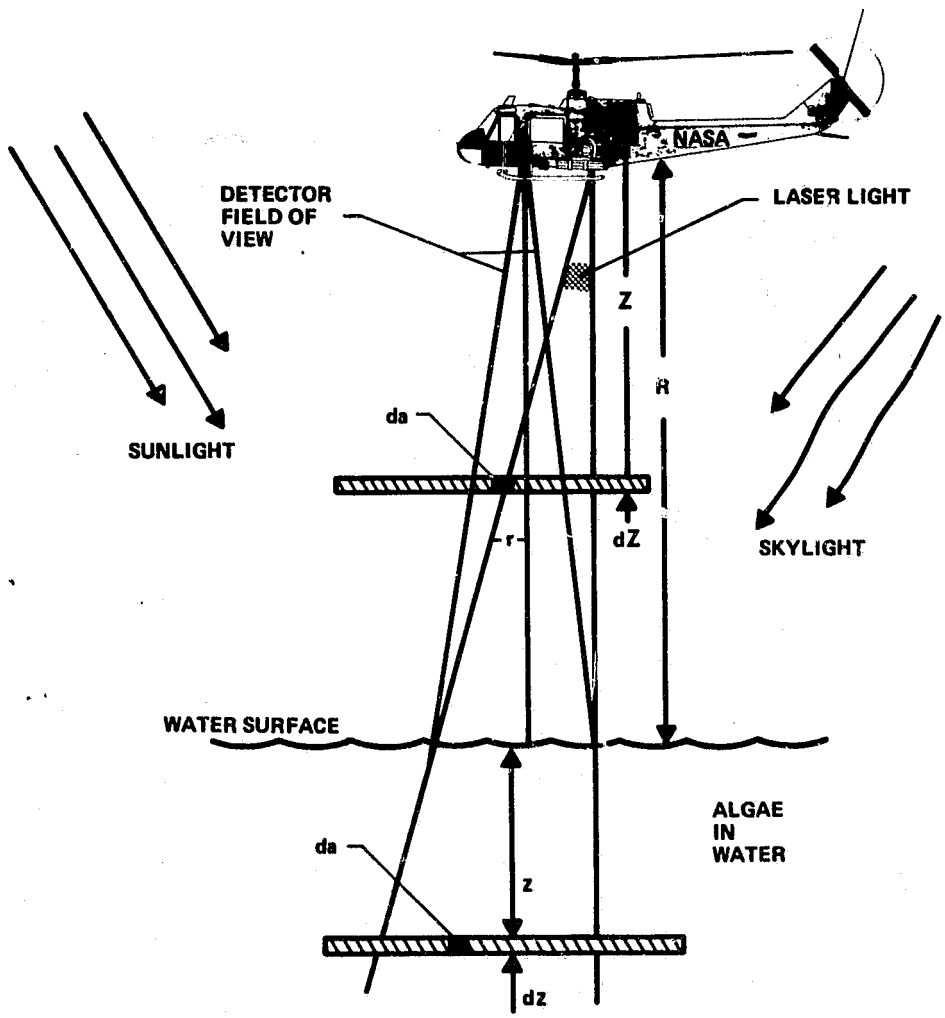


Figure 10: Geometry Used to Calculate Signals at an Airborne Receiver

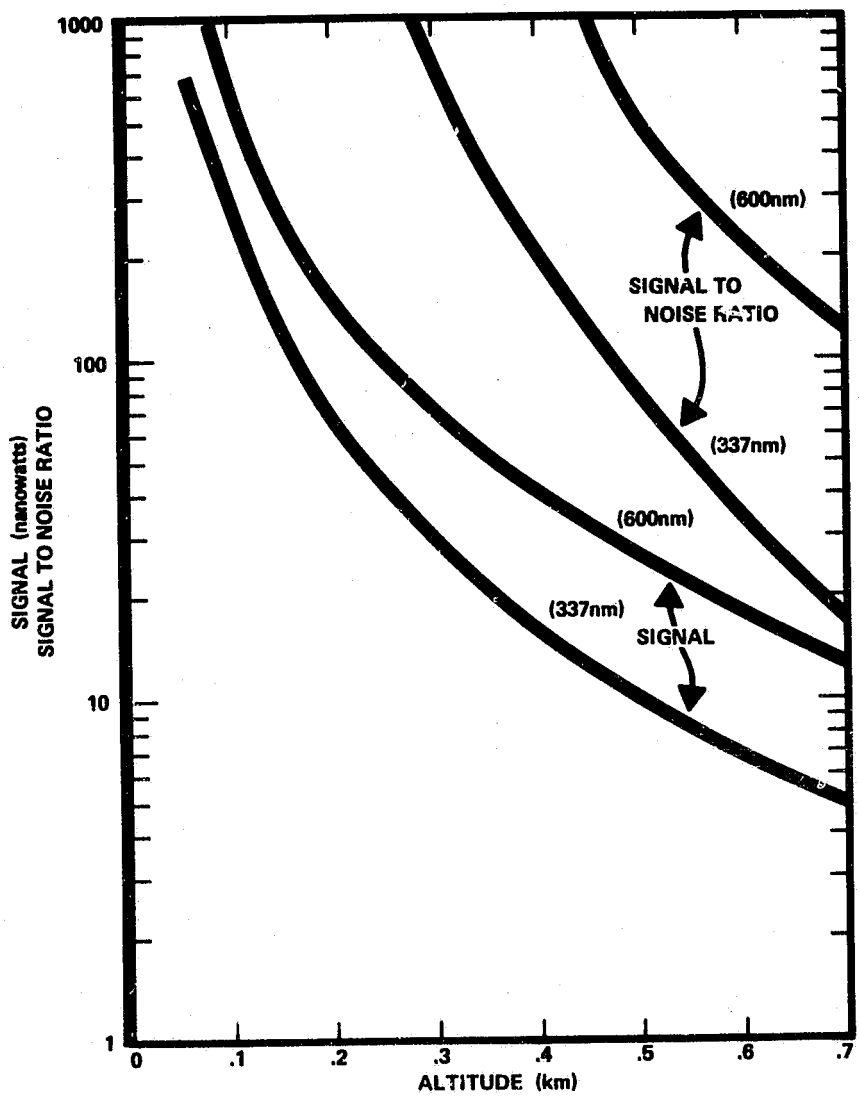


Figure 11: Signals and Signal-to-Noise Ratios for Detection of Algae (C=60 mg/m^3)as a Function of Altitude - P_o=100 kw/pulse

MULTISPECTRAL REMOTE SENSING OF ELEMENTS OF WATER AND RADIATION BALANCES

W. A. Malila
T. W. Wagner

Environmental Research Institute of Michigan
(Formerly, Willow Run Laboratories
of The University of Michigan)
Post Office Box 618
Ann Arbor, Michigan

ABSTRACT

Methods for extracting a diversity of useful information from multispectral scanner data are illustrated for evaluating elements of the terrestrial water balance equation. Radiation balance and water balance relationships are linked by the energy budget equation, and scene attributes are derived from scanner signals for detailed scene radiation mapping. The synoptic coverage and quantitative extrapolation capabilities of multispectral systems are discussed.

1. INTRODUCTION

Drainage basins, urban and rural watersheds, and stands of natural and cultivated vegetation are open physical systems in their utilization of both water and radiant energy. Variability of system inputs of precipitation and radiation and outputs of water runoff, evaporation, and re-radiation make it difficult to accurately assess utilization rates for large areas. However, knowledge of the amounts of water and radiant energy used by these systems is important to decisions in irrigation, agriculture, forestry, and regional or urban water supply. Remote (airborne or orbital) sensor systems provide a new capability for observing and monitoring these quantities.

Two equations express the fundamental relationships of the water and radiation environments within ecosystems — the terrestrial water balance equation and the radiation balance equation. A third equation, the so-called energy budget, provides the inter-connection between these two balances. On a large scale, when applied to the earth as a whole, these three equations characterize that great heat engine of weather and climate — the hydrologic cycle [1]. When applied to areas of local or regional size, knowledge gained from solution of these equations can be applied to decisions of foresters, agriculturalists, and hydrologists [2,3,4]. It is the purpose of this paper to examine each of these equations in terms of the capability of multispectral remote sensors in supplying information useful to their solution. Essentially we are concerned with the methodologies whereby multispectral data may be processed to yield results applicable to these equations.

2. BACKGROUND

Remote sensing is related to water and radiation balances by the fact that radiant energy arriving at the earth's surface is differentially reflected, absorbed, and reemitted by the physical features of the terrain [5]. A careful sampling by a remote sensor of this natural outgoing radiation, coupled with a knowledge of the incoming radiation, provides a basis for making quantitative radiation estimates and image maps of hydrologically significant features for large and diverse areas. Currently, multispectral scanners are the only systems which provide such a broad spectral sample in a synoptic and spectrally coincident format. In particular, reference is made in this paper to the multispectral scanner system developed by the

Preceding page blank

Willow Run Laboratories (WRL) of The University of Michigan [6]. This system collects data in twelve bands over the 0.32 to 13.5 μm wavelength range. This wavelength range, comprising visible, ultraviolet, and infrared portions of the electromagnetic spectrum, is most significant for sensing terrestrial biological [7] and hydrological characteristics of the terrain surface.

3. TERRESTRIAL WATER BALANCE

The erosional drainage basin has long been recognized as the basic unit of terrestrial hydrology. A drainage basin may be of any size and is characterized by the channeling of surface runoff into a single stream. The terrestrial water balance equation expresses the relation between hydrologic processes within a basin and is the object of intensive regional and global study during the current International Hydrological Decade - 1965 through 1974 [8]. In generalized form, this equation is:

$$P = \Delta S + R + E \tag{1}$$

where P is precipitation
ΔS is change in water storage
R is runoff (discharge)
E is evaporation

Precipitation is the input to the balance; runoff and evaporation are outputs; and changes in water storage represent internal adjustments of the basin to temporary differences in input and output.

3.1 WATER IN STORAGE

To obtain a knowledge of changes in water storage (ΔS) using remote sensing, we would like to be able to accurately assess storage at two or more points in time. The difference between two observations represents the change in storage. Storage is actually a composite term as shown in the following equation:

$$S = L + M + V + I + G \tag{2}$$

where S is storage (total),
L is surface water (lakes, rivers, etc.),
M is soil moisture
V is water in vegetation,
I is ice and snow,
and G is ground water.

At present, it appears feasible to monitor, or partially monitor, four of the five major components of basin storage - surface water, soil moisture, water in vegetation, and snow and ice. The fifth component, ground water storage, is not amenable to recording by current optical imaging sensor systems. To date much of our work has been directed at detecting and mapping surface water.

3.1.1. SURFACE WATER. Surface water, such as lakes, ponds, reservoirs, and streams, may be reliably identified using remote sensor data collected in the near infrared range of the spectrum. Liquid water absorbs most of the incident solar radiation in the 0.7 to 2.6 μm wavelength range — in contrast to the normally high reflectances for most terrain features (soils, vegetation, rock outcrops) [9]. Of four spectral bands routinely recorded by the Michigan multispectral scanner (0.67 - 0.91 μm, 1.0 - 1.4 μm, 1.5 - 1.8 μm, and 2.0 - 2.6 μm), the 1.5 to 1.8 μm band repeatedly has been found to be most effective in discriminating surface water areas [10]. In some situations, specular reflectance from the water surface in the near-infrared leads to the use of the thermal infrared band (9.3 - 11.7 μm) but, in general, this thermal band is less reliable than the near-infrared channel for daytime data collection due to variations which frequently occur in surface water and terrain temperatures.

Quantitative assessment of surface water is accomplished by thresholding the signals recorded by the multispectral scanner in the 1.5 to 1.8 μm band. Thresholding is accomplished in such a way that all recorded signals below an empirically determined threshold value are automatically tallied and printed as surface water areas. The threshold can be automatically adjusted for scene illumination changes caused by clouds or haze.

Two methods have been developed for continuously adjusting threshold levels to correct for changing scene illumination. One is to link the threshold level to signals that measure the sun and sky radiation incident on a diffusing plate built into the roof of the aircraft.

Thus, this "sun sensor" records changes in illumination reaching the aircraft. The use of this technique requires the assumption that changes in solar illumination at the aircraft altitude are correlated with changes in illumination reaching the terrain underneath the aircraft — that is, all atmospheric effects which reduce illumination occur above the aircraft and affect the aircraft sun sensor and the terrain simultaneously and proportionally. The alternative technique uses an adaptive threshold level. In this method, the threshold level is automatically varied as the signals from areas of standing water increase or decrease with illumination changes. This is accomplished by feeding back into the threshold circuitry a running mean of the signals classified as being from surface water and allowing this mean to modify the threshold level as the processor plays back the data at a real time rate. This latter technique is most useful where changes in illumination occur gradually over the scene. Figure 1 shows the better overall performance obtained with such a self-adapting technique as compared to results with two different constant threshold levels on the same data set.

Figure 2 presents a recognition map of surface water in an 81-sq.-mi. drainage basin along with a high-altitude photograph of the same area. This area is the Oakville Representative Basin — a watershed which is being studied as part of the Terrestrial Water Balance Program of the International Field Year for the Great Lakes (IFYGL). It contains numerous small farm ponds and several reservoirs. Areal statistics obtained from the thresholding operation show that only 0.61 sq. mile (less than 0.8%) of the basin are surface water.

To estimate the amount of water held in surface storage, some knowledge of average depth is required in addition to pond surface areas. For the present, statistical analyses of past measurements allow one to correlate pond depth with pond area and perimeter, both of which are determinable from recognition maps of pond surfaces. Several techniques that use multispectral data for directly determining water depths have been reported [10,11]. Future work at Michigan will combine depth determinations with surface area and perimeter determinations. Seasonal changes in surface water storage, as detected by the processing of multispectral scanner data, are illustrated in Figure 3.

3.1.2. SOIL MOISTURE. For a number of years, it has been suggested that thermal infrared remote sensor data might be used to determine soil moisture status. Moisture has the effect of increasing the thermal inertia (heat capacity) of a soil body. As a result, soil that contains a relatively great amount of water shows less surface temperature variation over a diurnal period than does the same type of soil containing less moisture. A moist soil normally will be warmer at night and cooler during the day than a dry soil. If a quantitative relationship could be established between soil moisture and surface temperature, it would be possible to use remotely sensed terrain temperatures to predict soil moisture status.

One-dimensional heat flow models, developed at WRL [12], have been used to predict surface temperatures under different soil moisture regimes. These models have the capability of predicting temperatures over diurnal periods when the thermal properties of the soil and climatic data are available. Examples of the changes in temperature, which are predicted to occur over a given diurnal period, is shown in Figure 4. These temperatures are for soils which are bare of vegetation. Note that the largest temperature differences occur during mid-day and predawn hours. These represent optimal times for recording surface temperature differences related to soil moisture. Also note that two soils of the same moisture content but different textures will have different thermal regimes. Figure 5 shows how temperatures change for a single soil with soil moisture for the two optimal times of day. The method, then, is to measure apparent temperature differences with an infrared scanner and use model calculations to estimate soil moisture content. The extraction of apparent surface temperatures from calibrated thermal scanner data is well documented in the remote sensing literature [13] and will not be discussed here. The problem with this technique is that the thermal model calculations require knowledge of soil textural and structural characteristics and a considerable amount of meteorological data for up to five days prior to the temperature-sensing flights. Also the relation between surface moisture and subsoil moisture is not straightforward [14].

Where vegetation obscurs the soil surface, this technique is not applicable. However, methods of detecting water stress in vegetation are being developed [15] and may provide an indirect measure of soil moisture in cropped or forested areas in the future.

3.1.3. WATER IN VEGETATION. All living organisms are comprised principally of water; the amount of water in transit through vegetation, after uptake by roots and prior to transpiration by leaves, can be considerable for vegetated basins. Roughly up to 80% of the fresh weight of a standing crop is water. Thus a grassland may contain some 50 metric tons of water per hectare and a mature northern hardwood forest over 300 metric tons of water per hectare. This amount of water remains fairly constant with respect to vegetation type during the growing season, but harvesting or senescence of the standing crop may represent a loss to the system.

One of the most significant contributions of multispectral remote sensing to date has been its demonstrated ability to map and quantitatively assess areas of diverse vegetation types [16,17]. Where detailed discrimination of different vegetative communities or crops is required, multichannel statistical correlation techniques usually are needed. However, for hydrologic purposes, a simple classification of forest vegetation, crop or grassland vegetation and bare soil may be adequate, and this might be accomplished by using the thermal inertia approach and temperature slicing of scanner data described in the previous section. Figure 6 shows the level-slicing of daytime thermal infrared data for discrimination of areas of heavy vegetation (forest and woodlot), light (crop) vegetation, and bare soil. If areas are computed for the vegetation classes, reasonably good estimates of the water stored in vegetation may be obtained.

3.1.4. SNOW AND ICE. Little attention has been directed to the use of multispectral data for recording and measuring snow and ice conditions for drainage basins. Certainly multispectral data may be used in the same way that aerial photography is used to record the areal extent of snow or ice cover (Figure 7), but a hydrologically significant parameter of snow and ice is their water equivalent. An equal volume of wet snow may contain several times as much water as so-called "dry snow". It is doubtful whether quantitative information on snow pack can be obtained from multispectral data, but recent studies have shown that several different categories of sea ice can be recorded and mapped [18]. This area needs further research for terrestrial application.

3.1.5. GROUND WATER STORAGE. The accurate measurement of ground water constitutes a formidable problem for hydrologists. Variations in ground water storage are estimated by fluctuations of the water table and measurement of the water yield coefficients of aquifers. Aquifers are water-bearing sediments, often at some depth, composed of either unconsolidated or consolidated, but fractured, geologic materials. Faults and fracture zones and sediment trends detected on remote sensor imagery may provide indications of the location of ground water supplies, but the precise location and areal variation of most aquifers is a problem to which multispectral sensors are not likely to contribute significantly in the near future.

3.2 RUNOFF

Runoff is one of the two major output components of the terrestrial water balance. In humid temperate climates, runoff normally accounts for anywhere from 20 to 80% of the total precipitation [19]. Variations in runoff are related to seasonal precipitation and single storm events, topography and cover type, and surface permeability. Hydrologists have experimented for years with models of the runoff process in an effort to better understand and predict the effects of storms of different intensities on a watershed and the impact of man-induced changes to the physical system. At present it is the areal extent and variability of a basin which makes unrealistic the development of complete model structures in terms of differential equations describing runoff and runoff related processes. While remote sensors are not well suited to measuring runoff directly, a great deal of information can be obtained concerning landforms and land use, both of which affect surface and subsurface (groundwater) runoff. Surface runoff from natural vegetation (forests and grasslands) is several orders of magnitude less than it is from cultivated fields, and urbanization has the effect of water proofing major portions of the terrain with concomitant rapid surface runoff rates. These differences in runoff rates for terrain surfaces have been documented [20], and Figure 8 demonstrates the ability of processed multispectral data to delineate a variety of surfaces. Automatic spectrum-matching techniques were used for this task with the following channels.

TABLE I.

SIX SPECTRAL CHANNELS USED FOR RECOGNITION OF TERRAIN CLASSES

CHANNEL	SPECTRAL RANGE	COLOR
1	0.43 - 0.48 μm	violet
2	0.46 - 0.49	blue
3	0.54 - 0.60	yellow-orange
4	0.58 - 0.65	red
5	0.66 - 0.76	dark red
6	0.72 - 0.92	reflective IR

3.3. EVAPOTRANSPIRATION

Evapotranspiration is the other major output component of the terrestrial water balance relationship. Both evaporation rates from soil and other surfaces and transpiration rates from vegetation are controlled by the prevailing meteorological conditions — radiation, wind, temperature, and relative humidity. Since the physical process of evaporation requires an input

equations for this purpose. The first is based on single scatter approximation and therefore, is suitable only for relatively clear waters; whereas the second equation attempts to take into account multiple scattering and can be used in any situation where bottom reflectance is not a factor. Results from a study of a series of ponds which receive treated effluent are shown in Table 3. The relative concentrations of suspended solids were found to be in good agreement with ground truth data. Chlorophyll "a" data were not available in this case, however, the variations in chlorophyll ratios are in general agreement with suspended solids data and the nutrient data which were available.

CONCLUSIONS

In addition to surface chlorophyll data, suspended solids, aquatic vegetation, etc., it should also be noted that remote sensing can provide a considerable amount of morphological and land use data which has a direct bearing on the trophic state of a body of water. Included in this last category is information dealing with shoreline development, watershed land use, lake surface area, and other cultural and physical features. From a water quality management standpoint this information is vital and equal in importance to the chemical and biological data normally collected.

With respect to the water mass, remote sensing techniques can provide data in terms of the major manifestations of eutrophication. However, characterization of the water mass with regard to nutrient status is outside the scope of current remote sensing technology. This last fact in no way detracts from the usefulness of remote sensing. The data needs of a statewide or nationwide lake assessment program and a lakes management program are very extensive. Meeting these needs will require the use of remote sensing together with conventional chemical and biological analytical procedures.

ACKNOWLEDGEMENTS

Data which forms the basis for this paper is derived in part from studies supported by the Environmental Protection Agency, Project Number 16020FOY and Project Number R-800778.

REFERENCES

1. Shannon, E.E. and Brezonik, P.L., 1972. "Eutrophication Analysis: A Multivariate Approach." Journal of the San. Eng. Div., ASCE., Vol. 98, No. SA1, pp. 37-57, February 1972.

2. Fruh, E.G., Stewart, K.M., Lee, G.F., and Rohlich, G.A. 1966. "Measurements of Eutrophication and Trends." Journal Water Pollution Control Federation, Vol. 38, No. 8, pp. 1237-1258, August 1966.

3. Lee, C.F. 1970. "Eutrophication." The University of Wisconsin, Water Resources Center, Eutrophication Information Program, Occasional Paper No. 2, University of Wisconsin, Madison, Wisconsin.

4. Ahearn, D.G., Hall, E.J. Jr., and Reinhardt, D.J. 1971. "Hypnodinium-like Algal Blooms in Georgia Lakes," BioScience, Vol. 21, No. 3, p. 18, February 1, 1971.

5. Ryther, J.H. and C.S. Yentsch. 1957. "The Estimation of Phytoplankton Production in the Ocean from Chlorophyll and Light Data." Limnology and Oceanography, Vol. 2, No. 3, pp. 281-286, July 1957.

6. Copeland, B.J., Minter, K.W., and Dorris, T.C. 1964. "Chlorophyll a and Suspended Organic Matter in Oil Refinery Effluent Holding Ponds." Limnology and Oceanography, Vol. 9, No. 4, pp. 500-506, October 1964.

7. Bailey, T.E. 1967. "Measurement and Detection of Eutrophication." Journal of the Sanitary Engineering Div., ASCE, Vol. 93, No. SA6, pp. 121-132, December 1967.

8. Strickland, J.D.H. 1960. "Measuring the Production of Marine Phytoplankton." Bulletin No. 122, Fisheries Research Board of Canada, Ottawa 1960.

9. Aruga, Y. and Monsi, M. 1963. "Chlorophyll Amount as an Indicator of Matter Productivity in Bio-Communities." Plant and Cell Physiol., Vol. 4, pp. 29-39.

Sample site 12 was a situation similar to site six as it was located on a stream flowing into the James River with the stream flowing only during periods of heavy rainfall and runoff conditions. Biochemical oxygen demand and kjeldahl nitrogen were highest for site 12 and concentrations of chemical oxygen demand and nitrate nitrogen were also among the highest of the sample sites. No other sample sites exhibited any marked trends or differences over the period which samples were obtained.

Film Dens ty-Water Quality Analysis

The analysis of the film density and water quality parameter data consisted of statistical analysis of variance, linear correlation and linear regression. Film densities were measured on the 1067m altitude (3500 ft) imagery at the location of each of the 14 water sampling sites. Because the imagery was taken with 60 percent overlap per frame it was possible to obtain more than one film density for each sampling site. Two sets of film density data were obtained. One set consisted of taking the average of all valid film densities for each sampling site or, in other words, all densities not appea ing to be affected by sunglint or cloud cover. The second set of film densities was obtained by taking the density closest to the center of the frame and not affected by sunglint or cloud cover. From the linear correlation analysis of both sets of film density data with the water quality data it was apparent there was no advantage to reading all the valid film densities and obtaining an average film density. Therefore all analyses presented in this report will utilize only the "center of the frame" film density data.

The analysis of variance of film densities obtained using the total density for all films is presented in Table III. The sources of variation consisted of the four film-filter combinations, seven aerial flight dates, 14 sampling sites and all combinations of the above. Only seven of the nine flight dates could be used in the analysis. Results of the F-tests in Table III show that there was a significant difference between film densities for the flight dates, the four film-filter combinations, and the flight dates by film-filter interaction.

TABLE III. ANALYSIS OF VARIANCE OF FILM DENSITIES

Source of Variation	Degrees of Freedom	Sum of Squares	Mean Squares	F
Films (F)	3	22.25	7.42	247.5 **
Dates (D)	6	1.15	0.19	6.3 **
Sites (S)	13	0.42	0.03	1.0
FD	18	14.17	0.79	27.4 **
FS	39	0.90	0.02	0.7
DS	78	0.96	0.01	0.3
FDS	234	7.80	0.03	
Total	391	47.66		

** Significant at the one percent level.

The analysis of variance of film densities for color and color infrared film is presented in Table IV. The sources of variation consisted of the two film-filter combinations (color and color infrared), the four densitometer filters (total, red, green, blue), seven aerial flight dates, fourteen sampling sites and all combinations of the above. Results of the F-tests indicate a significant difference existed between film densities for film types, densitometer filters, aerial flight dates and sampling sites.

The comparison between film densities and the water quality parameter analysis was accomplished with the statistical method of linear correlation. Correlation coefficients were computed for each of the nine aerial flights and for all the aerial missions combined. The significance of each correlation coefficient at the five and one percent level was then determined. Table V presents the correlation coefficients for film densities versus water quality parameters for the nine aerial missions combined. Significant correlation coefficients were obtained for temperature, dissolved oxygen, suspended solids, turbidity and total coliform for most of the film-filter combinations. The highest correlation coefficients were obtained for the black and white film with green filter #58. Significant correlation coefficients were also obtained for the infrared layer of color infrared film.

of energy (in particular, heat energy), evapotranspiration represents a loss of energy from an ecosystem. Therefore, we turn to the energy balance relationship to determine ways in which multispectral remote sensing might contribute to the assessment of evapotranspiration over large areas — a problem common to hydrology, agriculture, and meteorology.

Every ecosystem must maintain, on the average, a balance between the energy it receives and that which it gives up. (See Figure 9 [21]). Of the several physical processes by which energy is exchanged, radiation is the one that has the most influence on the energy balance (or heat budget) relationship of a system. The energy balance equation equates net energy received in the form of radiation (over all wavelengths) to the sum of the various sinks into which this energy is dissipated or distributed:

$$Q_{Net} = Q_E + Q_H + Q_G + Q_V + Q_P \tag{3}$$

where Q_{Net} is the net all-wave incoming radiant energy

Q_E is the latent heat energy loss by evapotranspiration,

Q_H is turbulent sensible heat transfer to the atmosphere,

Q_G is vertical heat transfer to the ground,

Q_V is horizontal heat transfer, or advection,

and Q_P is the net energy used in natural processes such as photosynthesis.

Typical units are joules and calories.

In Eq. (3), Q_p is a minimal quantity and can be neglected for our purposes. Q_V is not significant for conditions of little wind or for large areas. Thus, more simply and for most practical purposes, we can say

$$Q_{Net} = Q_E + Q_H + Q_G \tag{4}$$

or rearranging,

$$Q_E = Q_{Net} - Q_G - Q_H \tag{5}$$

Note that these energies are usually evaluated during a fixed interval, e.g., a year, a month, a day, or an hour. The importance of the terms depends in part on the time interval and the type of ground cover. For example, the net heat transferred to the ground, Q_G, is negligible over a 24-hour period because upward flux at night approximately balances downward flux during the daytime. However, during daylight hours, Q_G might be as much as 25 to 30% of Q_{Net} for bare soil [1], but generally would be a smaller fraction of Q_{Net} for vegetated surfaces, with the canopy structure and density determining the overall transfer of heat to the soil. It is possible to measure Q_G at selected points in a scene.

A multispectral remote sensor measures instantaneous energy rates (i.e., power in watts or cal.min^{-1}) but can be used to estimate the time-integrated quantitites of Eq. (5) over an entire scene.

Ground investigators frequently measure or estimate the Bowen ratio, the ratio of sensible to latent heat energies, $\beta = Q_H/Q_E$, or energy densities, $\beta = H_H/H_E$ [22]. In terms of β, Eq. (5) becomes

$$Q_E = \frac{Q_{Net} - Q_G}{1 + \beta} \quad \text{(joules or calories)} \tag{6}$$

or, in energy density units,

$$H_E = \frac{H_{Net} - H_G}{1 + \beta} \quad (\text{joules.m}^{-2} \text{ or cal.cm}^{-2}) \tag{7}$$

One then can solve for the amount of water evaporated by use of the latent heat of vaporization for water (energy per unit weight) and the energy used for evaporation, Q_E or H_E.

Current methods of estimating evapotranspiration (e.g., with lysimeters or evaporation pans, eddy correlation, aero-dynamic profile, energy balance, or combination methods [1,23] are accurate for their locations but are of questionable value for application to diverse areas of

large size. Accurate values are important as inputs to hydrologic models because bias errors in potential evapotranspiration have been shown to result in considerable errors in predictions [24].

Combination of continuous point samples and periodic spatial measurements of net radiation with multispectral remote sensors will lead to more acceptable values for large basins than are presently obtainable. The solving of the areal variability problem associated with estimates of E will be significant for other applications outside the discipline of hydrology. In agriculture, for example, problems of crop selection, irrigation, and growth and vigor are related to rates of evapotranspiration.

4. RADIATION BALANCE

The instantaneous radiation balance is the only component of an energy budget that is measurable by a remote sensor. However, radiation balances, like energy budgets, are definable for a variety of time intervals and conditions. For example, the average annual temperature of the Earth, as a planet, is constant because the all-wavelength average outgoing radiation at the top of the atmosphere just equals, or balances, with incoming radiation. In general, this is not the case at the Earth's surface, for any given latitude, for periods shorter than a year, or for specific wavelength regions. Total outgoing surface radiation and net (incoming minus outgoing) surface radiation are of principle interest here.

Traditional approaches discuss two categories of radiation for radiation balance and energy budget relationships [1,25]. These are: (1) short-wavelength solar radiation from 0.3 to about 3 μm and (2) long-wavelength thermal radiation from about 3 to 30 μm. Briefly consider the radiant flux (energy/unit time) on a horizontal unit area just above a vegetation canopy or other surface feature. This quantity is the incidance, E, measured in units of watts$\cdot$m^{-2}.* The corresponding outgoing radiation is called the exitance, M.

Solar radiation reaching the Earth's surface has both direct and indirect, or diffuse, components. The direct component is reduced by transmission losses as it passes through the atmosphere. The diffuse component occurs because of scattering by aerosols and molecules in the atmosphere and by clouds. Also, a substantial amount of thermal radiation reaches the Earth's surface as a consequence of thermal emission by these same air molecules, aerosols, and clouds.

Radiation leaves the Earth's surface at short wavelengths by reflection and at long wavelengths primarily by thermal self emission. For an opaque diffusely reflecting surface, there is a simple equation for the balance of radiant flux on a surface of unit area (i.e., for the net incoming radiant flux density):

$$E_{Net} = (E_S + E_s) - \rho(E_S + E_s) + \varepsilon E_T - M_T \qquad (8)$$

where

E_{Net} is the net radiant incidance,

E_S is the direct solar incidance,

E_s is the indirect, or diffuse, solar incidance,

ρ is the diffuse hemispherical reflectance (sometimes called albedo) of the surface (typical values are between 0.1 and 0.2 in the absence of snow),

E_T is the thermal incidance (i.e., incoming thermal radiation),

ε is the thermal absorptance (emissivity) of the surface (a number between 0.90 and 0.96 for most natural objects),

and M_T is the thermal exitance of the surface (i.e., self-emitted thermal radiation which depends on both the temperature, T_S, and the emissivity of the surface; $M_T(T_S) = \varepsilon \sigma T_S^4$, where σ is the Stefan-Boltzmann constant).

All quantities except ρ and ε, which are dimensionless, have units W$\cdot$m^{-2}(or ly$\cdot$min^{-1}).

---

*These units are gaining acceptance in the scientific community over other units such as cal$\cdot$cm$^{-2}\cdot$min^{-1} or langleys$\cdot$min^{-1}; note that 1 ly$\cdot$min^{-1} = 698 W$\cdot$m^{-2}.

Eq. (8) can be rewritten as follows:

$$E_{Net} = [E_S + E_s + \varepsilon E_T] - [\rho(E_S + E_s) + M_T] \tag{9}$$

$$E_{Net} = [\text{Incoming Radiant Flux Density}] - [\text{Outgoing Radiant Flux Density}]$$

$$E_{Net} = E_{Total} - M_{Total} \tag{10}$$

In Eq. (10), E_{Total} is the total incidance, while M_{Total} is the total exitance. If the surface is not a diffuse reflector and emitter, Eqs. (8) and (9) become more complex. For example, the reflected radiation from a non-diffuse surface depends on the spatial distribution of the incoming radiation such that the same reflectance term is not always applicable to both direct and indirect components of solar radiation in these equations.

4.1. MEASUREMENT CONSIDERATIONS

Exitance, a measure of the radiation leaving a surface, is one of many attributes that can be derived from multispectral scanner measurements. However, airborne and spaceborne multispectral scanners cannot completely measure surface exitance. They sample the radiation from the surface - spectrally, spatially, and temporally - through the atmosphere which both attenuates the surface radiation and adds extraneous radiation.

4.1.1. SENSOR CHARACTERISTICS. Spectral sampling is partly a result of atmospheric absorption. The self-emitted spectral radiance from a 300°K surface is maximum at about 10 μm, and is significant over the spectral region from 4 to 30 μm. However, the atmosphere absorbs radiation extensively throughout much of this spectral region. Measurements made at those wavelengths for which the atmosphere is relatively transparent (so-called windows) can be used to estimate the total thermal radiance of the surface.

The near-infrared region of the spectrum also has atmospheric windows between several prominent absorption bands, and the visible region is in an atmospheric window region. Multispectral scanners are designed to synoptically sense and record radiation in several spectral intervals in most of these window regions [6].

Two spatial sampling characteristics of multispectral scanners are important. First, a scanner measures the surface radiance ($W \cdot m^{-2} \cdot ster^{-1}$) within a narrow solid angle, while exitance ($W \cdot m^{-2}$) is radiated into a hemisphere by each point on the ground. Second, the angular field of view and the limits of the scan angle lead to definitions of scanner ground resolution element size and area of coverage, respectively, when coupled to the sensor altitude.

Because a remote sensor measures instantaneous radiation values, time-integrated effects must be determined from multiple passes, appropriate continuous ground-based measurements, and/or model calculations.

4.1.2. ATMOSPHERIC CHARACTERISTICS. In meteorological satellite studies of radiation balance, the atmosphere is part of the system being measured. Estimation of actual surface radiation balances from satellite or aircraft data is more complex because the atmosphere becomes an intermediate and interfering medium. Airborne measured radiance consists of two parts: (1) radiance of the surface after transmission losses through the atmosphere to the scanner and (2) extraneous path radiance produced by the atmosphere.

Atmospheric transmittance and path radiance are spatially and spectrally dependent. The spatial dependence at short wavelengths is related to the direction of view relative to the sun's position. The atmosphere also modifies the spectrum of radiation that reaches the surface. At visible and ultraviolet wavelengths, the absorption of radiation is low but scattering from atmospheric particles becomes more severe as the wavelength decreases. Consequently, spatial contrasts and the proportions of useful radiation are low in the blue and ultraviolet wavelengths.

Radiative transfer models can be used to estimate these atmospheric effects for both solar [26] and thermal [27] radiation to improve the accuracy of exitance and radiation balance estimates based on remotely sensed data.

4.2. ESTIMATION AND MAPPING OF EXITANCE

To estimate total surface exitance from multispectral scanner data, one should account for the sensor's spectral sampling characteristics, spatial reflectance and emittance characteristics

of the observed surface, and atmospheric effects. Equations 8 and 9 assume that observed surfaces have Lambertian (diffuse) reflectance and emittance characteristics, i.e., that the spatial distribution of the outgoing radiance obeys a cosine law and, for reflection, is independent of the spatial distribution of incoming radiation. Natural surfaces depart from these idealized properties--introducing errors if this departure is not properly incorporated into the estimation procedure. Both the angles of view and illumination [28] and the overall spatial distribution of exitance are important.

For thermal radiation, the spectral shape of the emitted radiation from vegetation is essentially that of a blackbody radiator. If the sensor response function is known and the atmospheric effects in the spectral window are calculated, all the necessary information is available for estimating the total thermal radiance of the surface. The remaining problem is that of accounting for the spatial emission characteristics of the surface so as to convert radiance ($W \cdot m^{-2} \cdot ster^{-1}$) to exitance ($W \cdot m^{-2}$). For a Lambertian surface, exitance is $1/\pi$ times the radiance. Non-Lambertian thermal emission characteristics have not been investigated widely; however, in at least one study, empirical corrections have been extracted and applied to meteorological satellite data [29].

For short-wavelength radiation, the spectral reflectance function differs with material so one cannot assume a standard spectral shape. However, if wavelength intervals are chosen to match the atmospheric windows, most of the exitance is measured, owing to the fact that atmospheric absorption reduces the incidance on the surface at the non-window wavelengths. Summation of corrected radiance values from several channels then represents an integration over the spectrum of interest; weighted summation can be used to adjust for sampling.

The spatial conversion from narrow-angle radiance to hemispherical exitance is complicated by the fact that short-wavelength exitance depends on illumination geometry in addition to view angle. In other words, the bidirectional reflectance properties of the surface are involved. For improvement on the Lambertian assumption, mathematical models of the bidirectional reflectance of vegetation canopies recently have been formulated [30] and can be used to correct exitance calculations for spatial effects.

For scenes of interest, the short- and long-wavelength exitances can be computed and mapped separately [18]. Summation of the two components provides the desired estimate of the total exitance which also can be mapped [31,32]. Exitance maps provide the opportunity to examine scene differences on a gross level for major cover types or on a detailed level within a cover type. An example total exitance map of a golf course is presented in Figure 10b. Lambertian surfaces were assumed and the gray scale used for the map presents the greater exitances in the lighter tones. Exitance differences for various grasses on the greens, fairways, and rough are evident. A black-and-white infrared photograph is presented for comparison in Figure 10a.

A different illustration of exitance mapping is presented in Figure 11. This figure contains a total exitance map for an apartment complex, together with a black-and-white infrared photograph. (Investigators have begun to study the radiation environment of urban areas as an important aspect of human living conditions.)

4.3. ESTIMATION OF INCIDANCE, AND RADIATION BALANCE MAPPING

An estimate of total incidance is required to calculate a radiation balance from multispectral scanner data. There are various ways of obtaining this estimate. First, ground instrumentation might be located strategically along the flight path. Second, weather station data (including meteorological soundings) might be used as inputs to radiative transfer models for computing both the solar and thermal inputs. Third, auxiliary sensors on airborne platforms might provide additional information for estimating incidance and atmospheric effects. For example, a sun sensor coupled with the Michigan scanner provides a measure of solar incidance at the sensor altitude. If flown at several different altitudes, the sun sensor data can help characterize the atmospheric state. Also, up-looking and down-looking pyranometers mounted on aircraft have been used to measure spectrally integrated solar radiation fluxes [33] and similarly thermal pyrgeometers used to measure thermal fluxes.

Exitance determined from multispectral scanner data can be subtracted from estimates of incidance from model calculations and/or auxiliary sensor measurements to obtain radiation balance estimates [18,32] that is, estimates of the net radiant flux density input to the surface systems observed. Then, maps of net radiation can be produced [31,32].

Figure 12 presents a relative net radiation map of an agricultural test plot at Michigan State University. Observed differences in net radiation values can be related to known differences between the crops and soils. On this map, the lightest tone represents the greatest amount of net radiation absorbed by the surface. On a gross level, one can identify the small light spots in the

lower left hand corner which are individual trees in a young orchard. The light semicircular area above them is wet bare soil with dry bare soil to the right; the net radiation of the wet soil is greater than that of the dry soil because it reflects less radiation and is cooler owing to evaporation. On the right are two corn fields; the lower, more mature one appears to have slightly greater net radiation, perhaps because it reflected less near-IR radiation and was cooler due to greater evapotranspiration than the upper field.

On a detailed level, uniformity of the energy dissipation pattern within individual fields can be assessed. Some of the irregularities in the lower corn field are due to plant differences caused by a southern corn leaf blight. On the other hand, the upper field exhibits a broad pattern that is an artifact caused by the particular scanning geometry employed and should be discounted. Differences in moisture availability or drainage patterns should be readily seen when they occur and edge effects due to prevailing winds should be discernible. One can use such a map to assess the extent to which ground instrumentation sites are representative of the fields and areas in which they are located.

For hydrology, the main use of radiation balance maps would be in determining more realistic estimates of evaporation rates.

5. CONCLUSIONS

There is real potential for extracting a diversity of useful information from multispectral scanner data. Two important capabilities of multispectral systems are for (1) large-area synoptic coverage over a broad spectrum of wavelengths and (2) quantitative extrapolation of point measurements to watersheds or other types of ecosystems.

The application of multispectral processing techniques to the elements of the terrestrial water balance has been discussed and demonstrated, including the development of attributes for detailed scene radiation mapping. If the approach here, to complex water balance and energy balance relationships, was simplified, it was done so as to focus on current capabilities of multispectral systems. The results encourage continued research in this effort.

Full potential of information obtained from multispectral systems will be attained when coordinated with selected ground-based measurements and observations. It would seem timely to carry out a test of the array of techniques for water balance analysis of a selected watershed.

6. REFERENCES

1. Sellers, W. D. 1965. Physical Climatology, University of Chicago Press, Chicago.

2. Scientific American, (special issue: The Biosphere) September 1970, Vol. 223, No. 3.

3. Eckardt, F. E. (ed.) 1968. Functioning of Terrestrial Ecosystems at the Primary Production Level - Copenhagen Symposium, UNESCO, Belgium.

4. More, R. J. 1969. "The Basin Hydrological Cycle" in Water, Earth and Man (ed R. J. Chorley), Methuen and Co., Suffolk, pp. 66-76.

5. Colwell, R. N. (ed.) 1963. "Basic Matter and Energy Relationships Involved in Remote Reconnaissance," Photogrammetric Engineering, Vol. 29(5), pp. 761-799.

6. Hasell, P. G. 1972. "Michigan Experimental Multispectral Scanner System" in 4th Annual Earth Resources Program Review, Vol. II, MSC-05937, Manned Spacecraft Center, Houston, Texas, January 17-21, 1972, pp. 34-1 thru 34-13.

7. Gates, D. M. 1967. "Remote Sensing for the Biologist," BioScience, Vol. 17, No. 5, pp. 303-307.

8. Heindl, L. A., 1971. "Hydrological Mapping and the IHD," Nature and Resources, Vol. VII No. 1, pp. 15-19.

9. Leeman, V., D. Earing, R. Vincent, and S. Ladd, 1971. The NASA Earth Resources Spectral Information System: A Data Compilation. Willow Run Laboratories, Report 31650-24-T.

10. Burge, W. G. and W. L. Brown, 1970. "A Study of Waterfowl Habitat in North Dakota Using Remote Sensing Techniques," Willow Run Laboratories Report 2771-7-F.

11. Brown, W. L., F. C. Polcyn, and S. R. Stewart. 1971. "A Method for Calculating Water Depth, Attenuation, Coefficient and Bottom Reflectance Characteristics", Proceedings of the 6th Symposium on Remote Sensing of Environment, pp. 663-682.

12. Horvath, R. 1971. "Thermal Modeling for Mission Planning and Data Analysis", in Remote-Sensing-Analysis-Projects-NASA, Willow Run Laboratories Report 3165-26-T.

13. Nalepka, R. F. (ed.) 1970. "Investigation of Multispectral Discrimination Techniques" Willow Run Laboratories Report 2264-12-F.

14. Childs, E. C. 1969. The Physical Basis of Soil Water Phenomena, J. Wiley and Sons, New York.

15. Weber, F. P. and F. C. Polcyn, 1972. "Remote Sensing to Detect Stress in Forests," Photogrammetric Engineering, Vol. 38, No. 2, pp. 163-175.

16. Driscoll, R. S. and M. M. Spencer. 1972. "Multispectral Scanner Data for Plant Community Classification", Eighth International Symposium on Remote Sensing of Environment, Ann Arbor.

17. Weber, F. P., R. C. Aldrich, F. G. Sadowski, and F. J. Thomson, 1972. "Computer-Generated Land-Use Maps of a Southeastern Forest Region," Eighth International Symposium on Remote Sensing of Environment, Ann Arbor.

18. Horvath, R. and W. L. Brown, 1971. "Multispectral Radiative Characteristics of Arctic Sea Ice and Tundra", Willow Run Laboratories Report 27980-2-F.

19. Bormann, F. H. and G. E. Likens, 1969. "The Watershed-Ecosystem Concept and Studies of Nutrient Cycles" in The Ecosystem Concept in Natural Resource Management (Van Dyne, ed.) Academic Press, New York.

20. Morgan, M. A. 1969. "Overland Flow and Man", in Water, Earth and Man (ed. R. J. Chorley), Methuen & Co., Suffolk, pp. 239-255.

21. King, K. M. 1961. "Evaporation from Land Surfaces, in Proceedings of Hydrology Symposium No. 2. Evaporation Department of Northern Affairs and Nat. Resources (Ottawa).

22. Storr, D., H. L. Ferguson, and H. F. Cook, 1970. "A Graphical Aid for Bowen Ratio Calculations*." in Journal of Applied Meteorology, Vol. 16, No. 9, pp. 940-942.

23. Tanner, C. B., 1968. Evaporation of Water From Plants and Soil. Water Deficits and Plant Growth, Vol. I, edited by T. T. Kozlowski, Academic Press, New York.

24. Parmele, L. H. 1972. "Errors in Output of Hydrologic Models Due to Errors in Input Potential Evapotranspiration." Water Resources Research, Vol. 8, No. 2., pp. 348-359.

25. Gates, David M., 1962. Energy Exchange in the Biosphere, Harper and Row, New York.

26. Turner, R. E., and W. A. Malila, and R. F. Nalepka, 1971. Importance of Atmospheric Scattering in Remote Sensing. Proceedings of Seventh International Symposium on Remote Sensing of Environment, May 17-21, 1971, Willow Run Laboratories, The University of Michigan, Ann Arbor, Michigan.

27. Rose, H. M., D. C. Anding, and J. Walker, 1971. Computation of Atmospheric Effects on Remote Sensing, Proceedings of Seventh International Symposium on Remote Sensing of Environment, May 17-21, 1971, Willow Run Laboratories, The University of Michigan, Ann Arbor, Michigan.

28. Malila, W. A., 1968. Multispectral Techniques for Image Enhancement and Discrimination, Photogrammetric Engineering, Vol. XXXIV: 566-575.

29. Raschke, E. and W. R. Bandeen, 1970. The Radiation Balance of the Planet Earth from Radiation Measurements of the Satellite Nimbus II, J. Appl. Meteor., 9:215-237.

30. Suits, G. H., 1972. Calculation of the Directional Reflectance of a Vegetative Canopy, Remote Sensing of Environment, Vol. 2, No. 2, American Elsevier, New York.

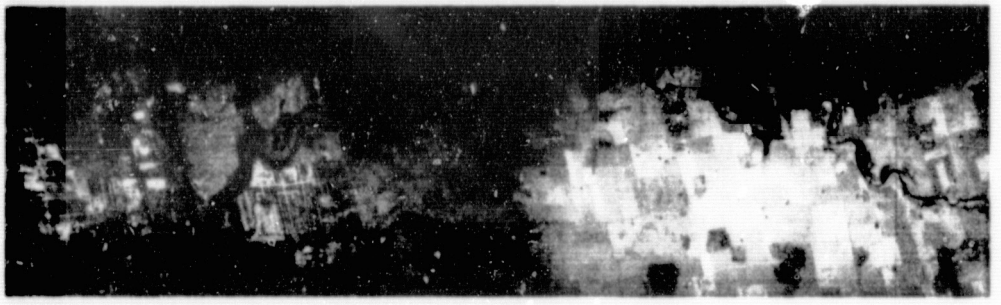
---

*Modified charts are available from authors.

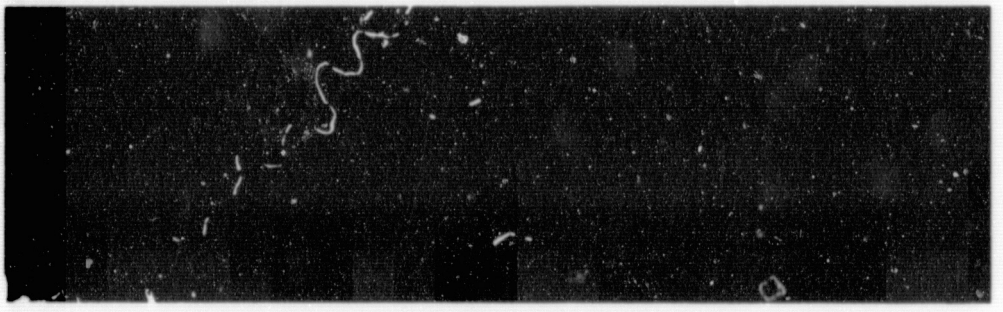
31. Malila, W. A., R. B. Crane, W. Richardson, and R. E. Turner. 1972. "Information Extraction Techniques for Multispectral Scanner Data", in 4th Annual Earth Resources Program Review, Vol. II, MSC-05937,Manned Spacecraft Center, Houston, Texas, January 17-21, 1972. pp. 29-1 thru 29-33.

32. Malila, W. A., 1972. Radiation Balance Mapping with Multispectral Scanner Data. in Remote Sensing of Earth Resources, Vol. 1, edited by F. Shahrokhi, The University of Tennessee. Space Institute, Tullahoma, Tennessee.

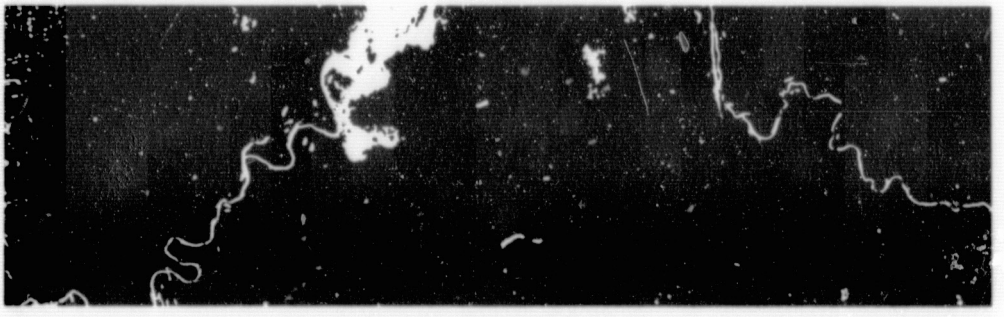
33. Griggs, M., 1968. Aircraft Measurements of Albedo and Absorption of Stratus Clouds, and Surface Albedos, J. Appl. Meteor., 7:1012-1017.



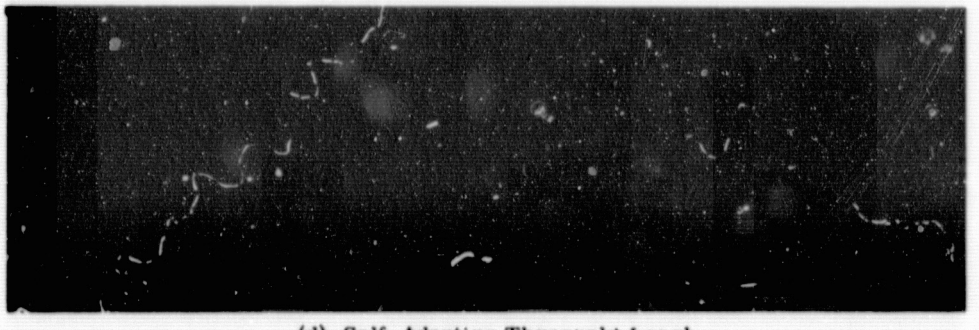
(a) Video Image (1.5 to 1.8-μm)



(b) High-Threshold Level

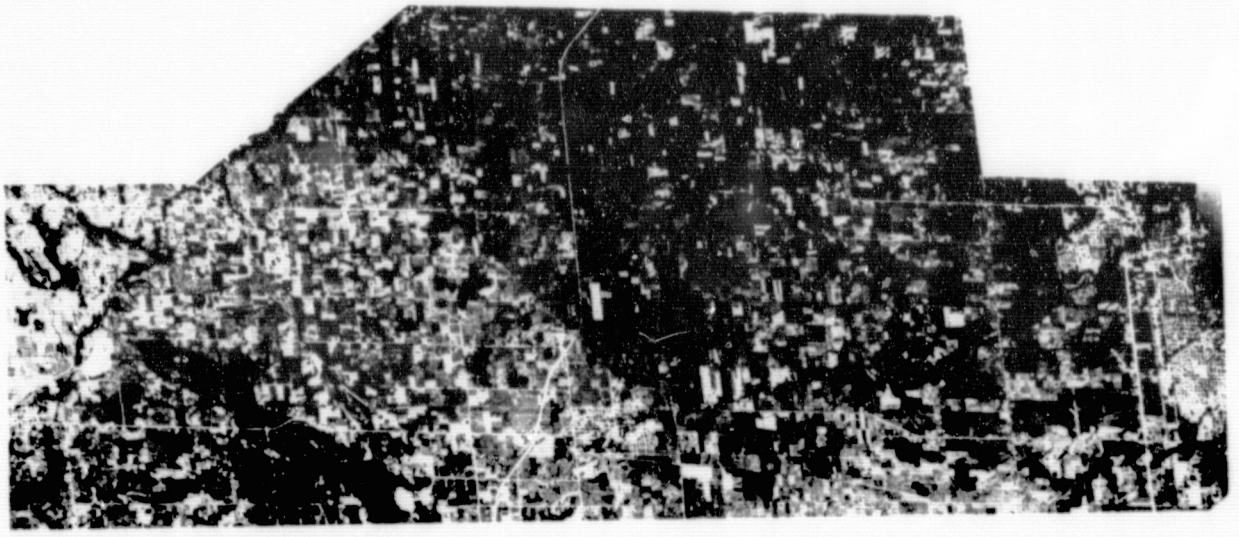


(c) Low-Threshold Level

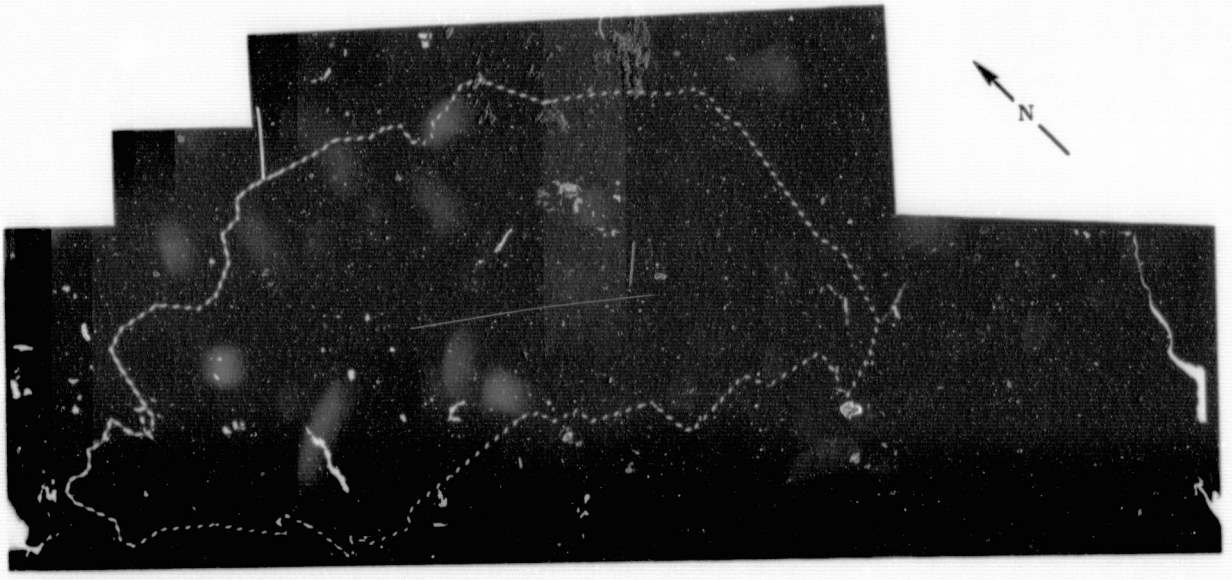


(d) Self-Adapting Thresnold Level

FIGURE 1. SURFACE WATER DISCRIMINATION USING 1.5 TO 1.8-μm CHANNEL. Oakville Creek, Ontario. 11 May 1971, 8000 ft Altitude.

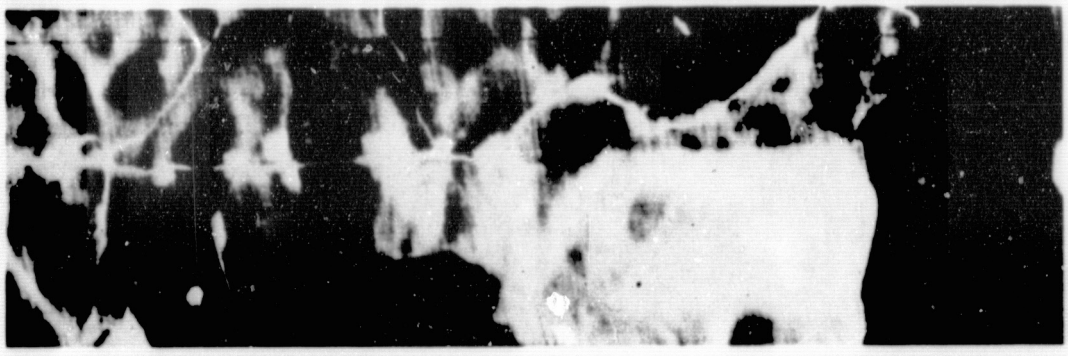


(a) Photo Mosaic



(b) Standing Water Discrimination

FIGURE 2. 1.5- TO 1.8-μm IMAGE MOSAIC OF OAKVILLE REPRESENTATIVE BASIN, ONTARIO, FOR DISCRIMINATION OF SURFACE WATER. Basin area: 81 sq miles. Surface water: 0.61 sq miles.



(a) 1.5-1.8 μm Video of July Data



(b) May Distribution of Ponds



(c) July Distribution of Ponds

FIGURE 3. CHANGES IN POND AREA BETWEEN MAY AND JULY.

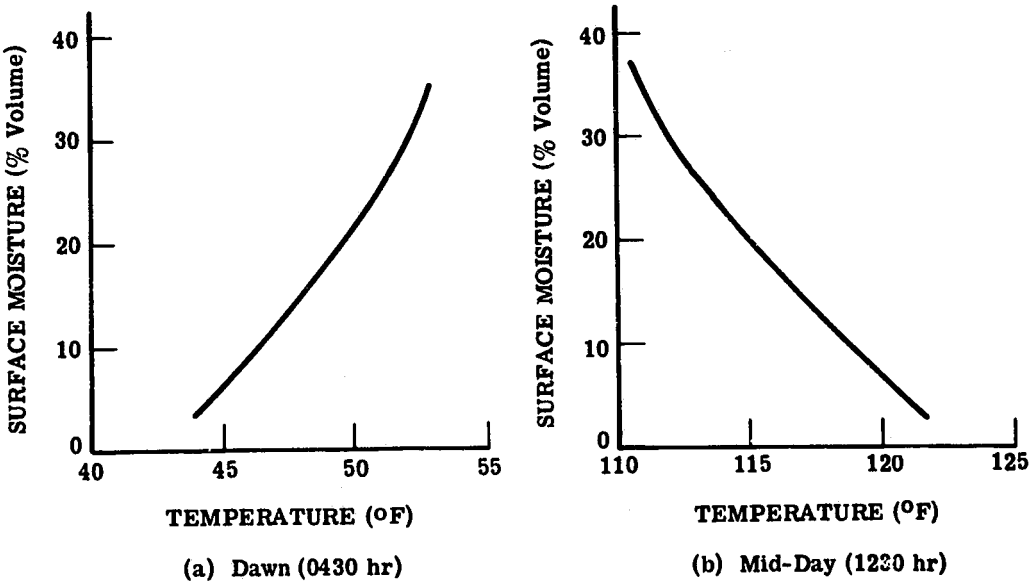
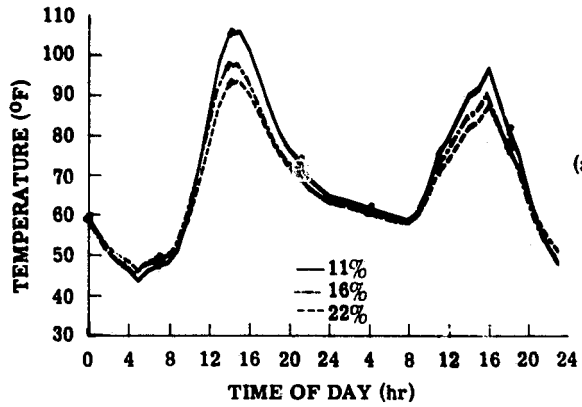
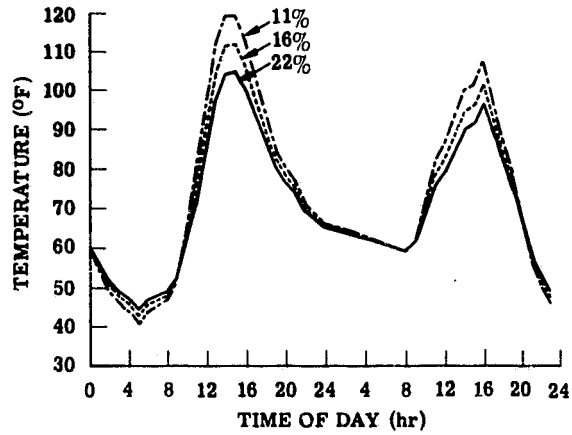


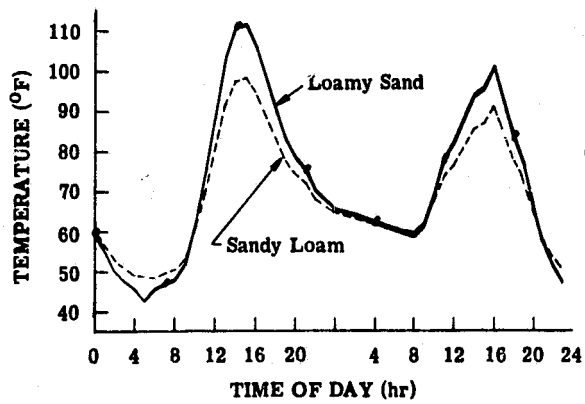
FIGURE 5. PREDICTED SOIL SURFACE TEMPERATURES FOR A LOAM SOIL AT TWO TIMES OF DAY



(a) Variations in Diurnal Temperature For Sandy Loam Soil

(b) Variations in Diurnal Temperature for Loamy Sand Soil



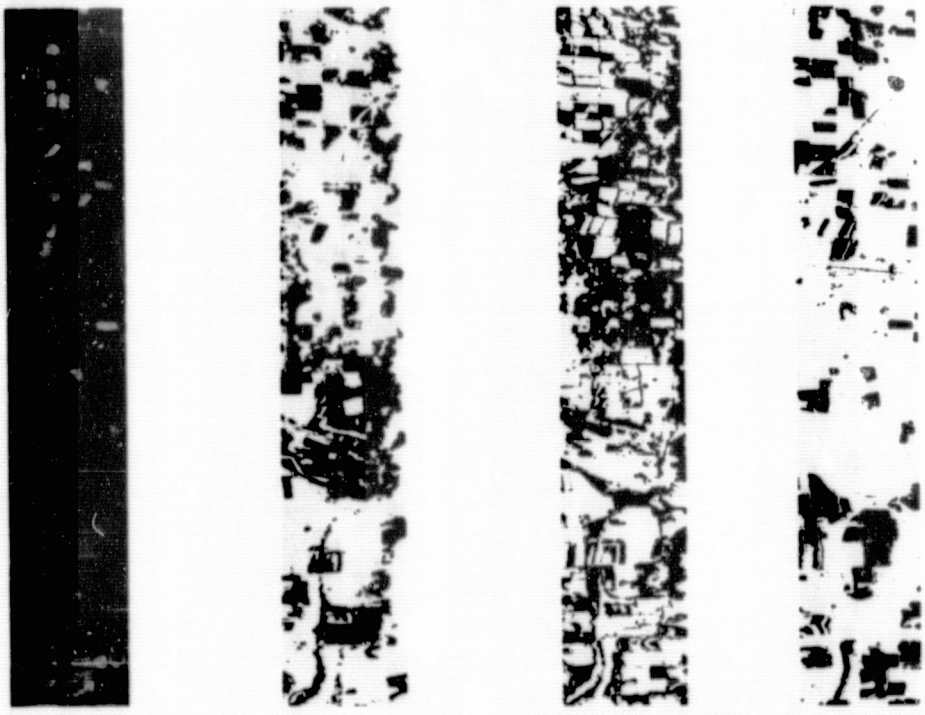


(c) Variations in Diurnal Temperature of Two Soils with the Same Surface Moisture Content

FIGURE 4. PREDICTED VARIATIONS IN DIURNAL TEMPERATURE WITH SOIL TEXTURE AND SURFACE MOISTURE CONTENT. [12].

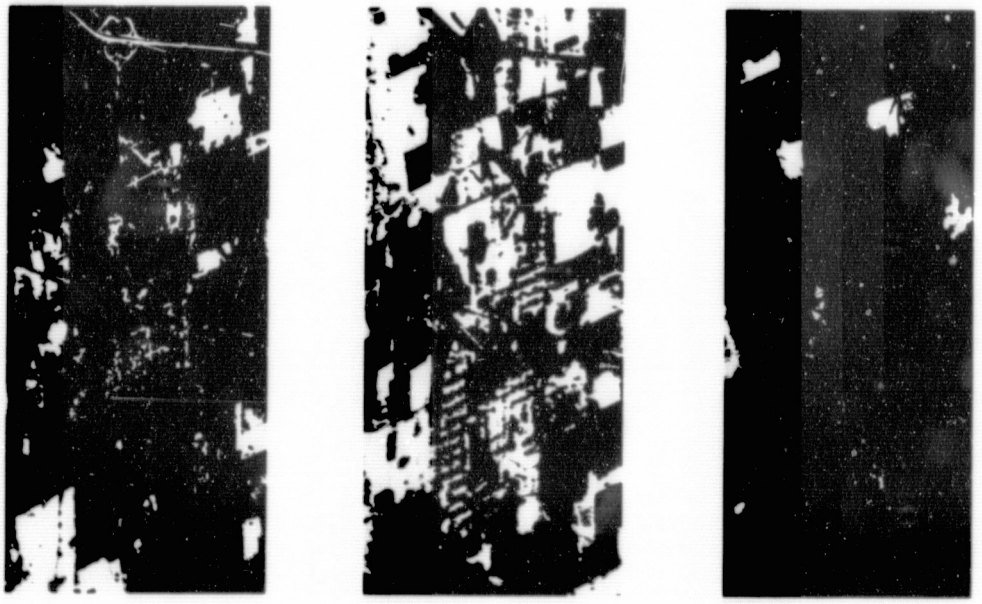


FIGURE 6. COMPARISON OF THERMAL MOSAIC AND GLACIAL MAP OF MOUNT RAINIER, WASHINGTON

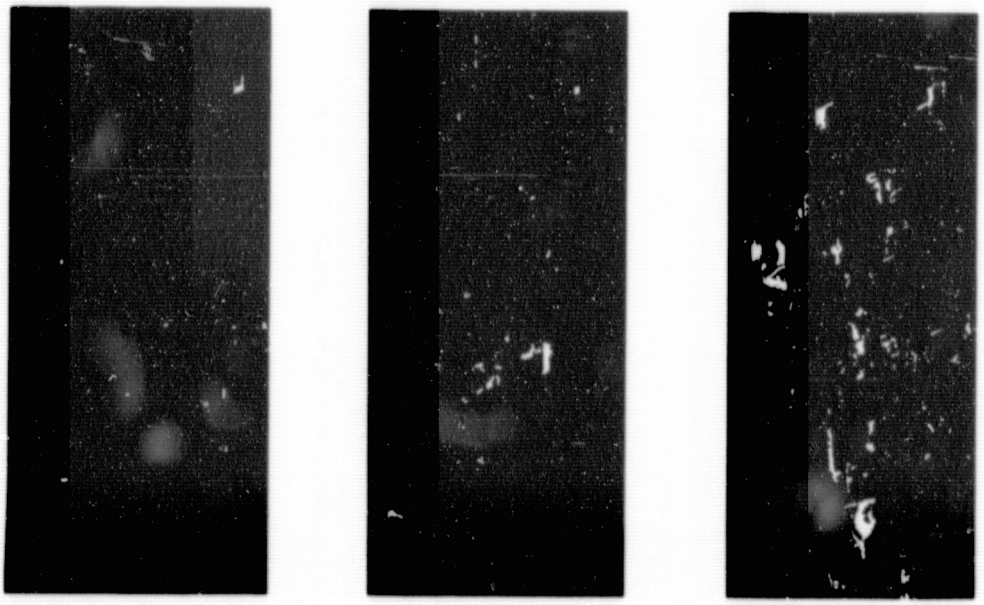


(a) Thermal Video (8.2-13.5 μm) (b) Forest Vegetation (c) Crop Vegetation (d) Bare Soils

FIGURE 7. VEGETATION AND BARE SOIL DISCRIMINATION USING LEVEL-SLICED MID-DAY THERMAL IMAGERY. Blue Springs Basin, Ontario.



(a) Bare (b) Crop and Urban Vegetation (c) Woodlots



(d) Concrete (e) Asphalt (f) Gravel

FIGURE 8. RECOGNITION IMAGES OF SIX DIFFERENT LAND-USE CLASSES IN THE OAKVILLE CREEK BASIN AREA

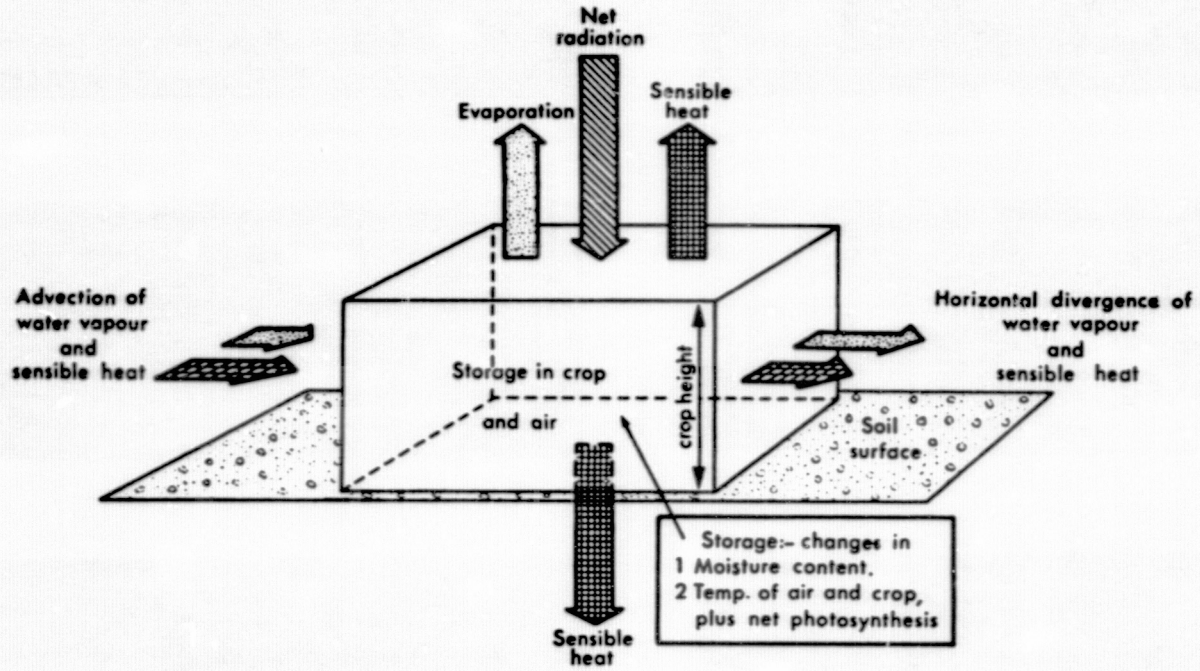


FIGURE 9 The energy balance at the surface (After King, 1961).

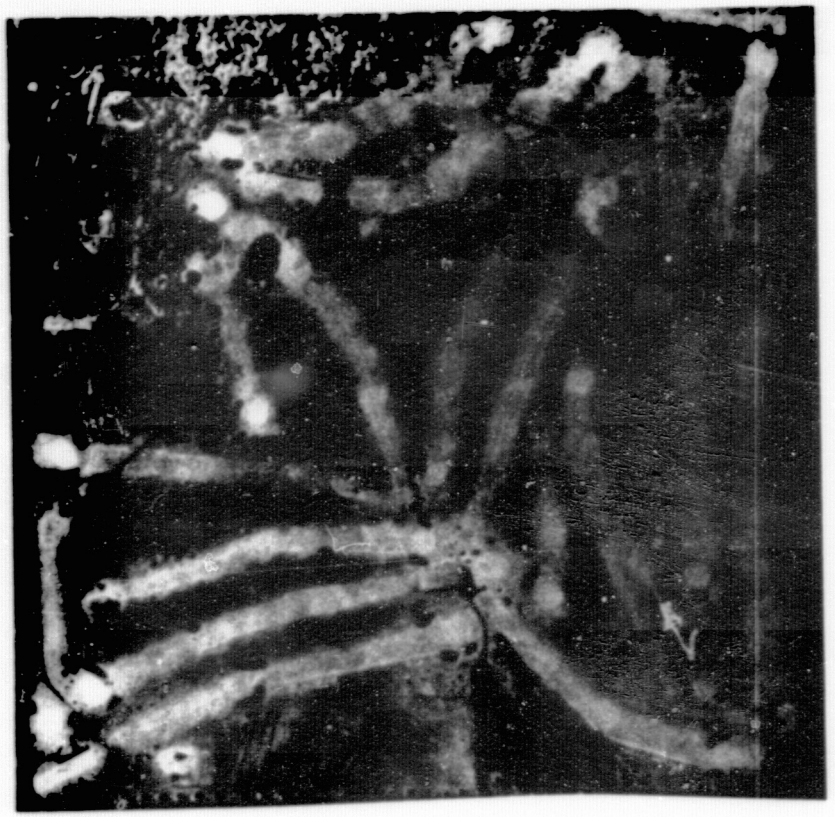


FIGURE 10a PHOTOGRAPH OF GOLF COURSE
(6 Aug 71. Alt = 5000 Ft. 9:57 EST. MSU)



FIGURE 10b EXITANCE MAP FOR GOLF COURSE
(6 Aug 71. Alt = 5000 Ft. 10:57 EST, MSU)



FIGURE 11a PHOTOGRAPH OF APARTMENT COMPLEX
(6 Aug 71, Alt = 5000 Ft, 9:57 EST, MSU)

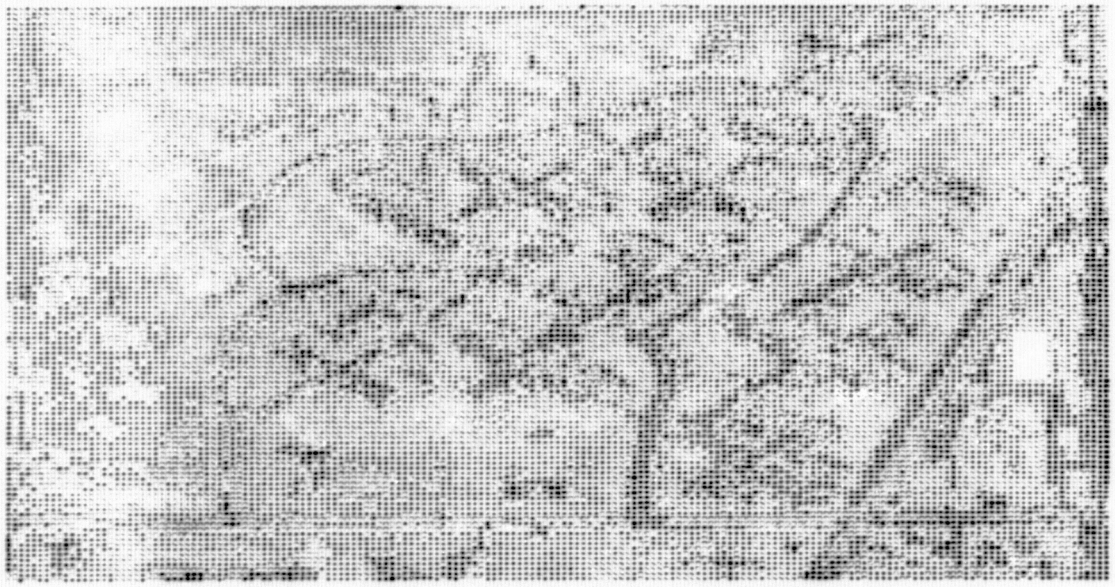
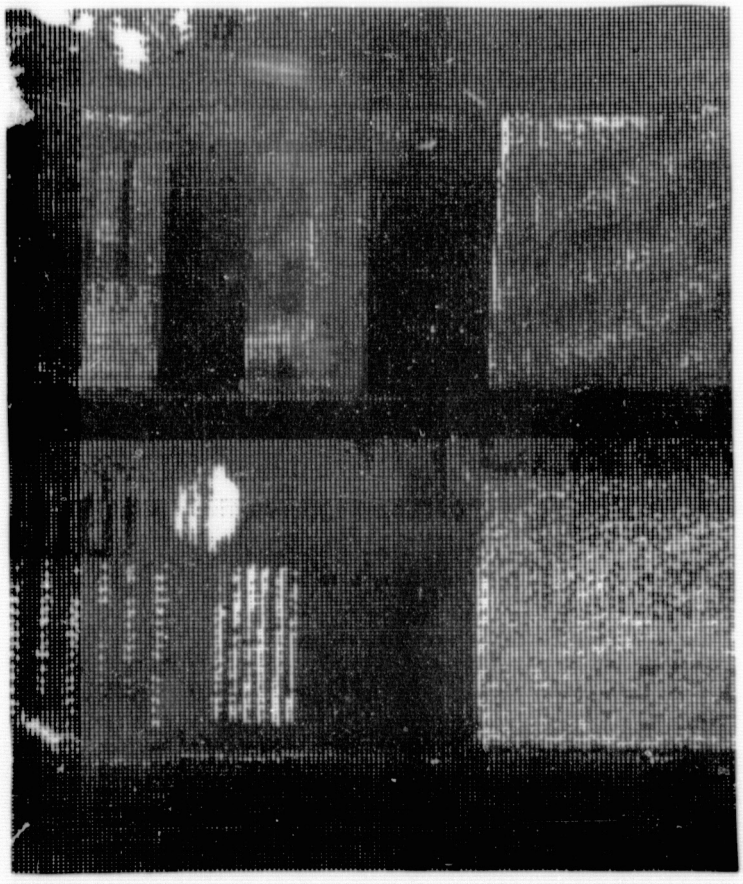


FIGURE 11b EXITANCE MAP FOR APARTMENT COMPLEX
(6 Aug 71, Alt = 5000 Ft, 10:57 EST, MSU)



RADIATION BALANCE
MAP

FIGURE 12

SALINITY SURVEYS USING AN AIRBORNE MICROWAVE RADIOMETER

J. F. Paris

Lockheed Electronics Company, Inc.
Earth Observations Department
Houston, Texas

ABSTRACT

Surface water salinity is an important parameter to be measured and surveyed in many environmental quality and resource inventory programs. These include coastal circulation, river outflow, marine ecological, salt springs pollution, disease vector and fisheries studies.

Studies of the electric properties of water with dissolved salts revealed that the thermal microwave emission of surface water is affected significantly by changes in water salinity for microwave frequencies less than 3 GHz. Surface water temperature affects the relationship also.

An L-band (1.42 GHz) microwave radiometer was on the NASA 927 (NP-3A) aircraft as a part of the multifrequency microwave radiometer (MFMR). Also, an airborne infrared radiometer (PRT-5) was available on the NASA 927 aircraft. It was therefore feasible to use these two remote sensors to conduct surveys of water surface temperature and salinity using the NASA 927 aircraft.

An error analysis of the MFMR system was made. As a result, it was determined that large systematic errors were present in the determination of (1) the scale factor for the response curve of the radiometer and (2) the antenna transmission factor. To remedy this problem, a scheme was developed such that MFMR data taken during a flight could be used along with a supporting surface measurement and an atmospheric sounding of temperature and humidity to determine the correct values of scale factor and antenna transmission factor. This scheme involved the use of computer models for water surface emission and reflection, atmospheric absorption, transmission, and emission; and sensor transmission and self-emission.

It was further determined that the same models could be used to obtain the salinity of the surface water from a given set of MFMR and PRT-5 data. In general, this information is gained from the remotely sensed data by a three-step process. First, measurements of sky brightness and water brightness over a selected surface-truth point are used to determine the correct values of scale factor and antenna transmission factor. Second, the PRT-5 measurement is used to determine water surface temperature. Last, the L-band measurement of water brightness is used with the surface temperature measurement to determine surface water salinity. An iteration technique is used for the latter step with the use of the computer models of the microwave properties of water and of the atmosphere.

Preceding page blank

These methods were tested by using MFMR and PRT-5 data taken over a line intersecting South Pass and Southwest Pass, La., in the region of the outflow of the Mississippi River into the Gulf of Mexico. The flight took place at 262 meters above the sea surface in November 1971 during Mission 190 on a clear day with light winds. A computer program incorporating the above methods was used to produce a plot of water surface temperature and salinity along the aircraft flight line. The surface-truth point was taken to be the outflow area at Southwest Pass, La., where the salinity and temperature had been measured to be 8.0 PPT and 22.2° C. A surface survey of the line was conducted shortly after the aircraft survey. The surface measurements showed good agreement with the airborne measurements. Also, gradients in the remotely determined salinity were associated with surface convergence fronts marked by foam lines.

These investigations showed that water surface salinity and temperature may be surveyed accurately with an airborne infrared radiometer and an L-band microwave radiometer.

1. INTRODUCTION

Surface water salinity and temperature measurements are useful to studies of coastal processes such as bay circulation and river outflow. Marine organisms are affected by the salinity and temperature of their water habitat. Marine ecologists and biologists thus need the capability for conducting surveys of salinity and temperature. Also, fish forecasting by the National Fisheries Service of the National Oceanic and Atmospheric Administration (NOAA) requires information on the temperature and salinity of breeding grounds of marine organisms.

Past investigations have shown that the microwave emission of water is affected significantly by changes in the salinity of the water surface layer for microwave frequencies less than 3 GHz [refs. 1-3]. So, the possibility existed for making surveys of the water surface salinity from aircraft through the use of an L-band microwave radiometer. A multifrequency microwave radiometer was installed on the NASA 927 (NP-3A) aircraft in 1969. One channel of the MFMR operates in the L-band at 1.42 GHz. This paper is a report on the development of an analysis technique whereby the distribution of surface water temperature and salinity along the flight line may be calculated by computer from MFMR and infrared radiometry (PRT-5) data taken along the flight track of the NASA 927 aircraft.

To recover the salinity of the water surface from MFMR measurements, one must consider carefully the effects of a number of other parameters, such as variations in water surface temperature, absorption and emission by the intervening atmosphere, absorption and emission by the MFMR radome antenna and waveguide, and departures in the calibration constants from the values determined before the aircraft flight. These considerations are discussed in section 2.

A computer program was developed to analyze the MFMR and PRT-5 data and to produce profiles of water surface salinity and temperature along the aircraft flight track. The development of the computer program is discussed in section 3.

The computer program was used with flight data acquired during a flight of the NASA 927 over the outflow of the Mississippi River into the Gulf of Mexico in November 1971. The results are given in section 4.

2. THEORETICAL DEVELOPMENTS

2.1 EMISSION AND REFLECTION OF WATER

In the determination of salinity from measurements of the microwave emission of water, a computationally simple mathematical model is needed that may be used to predict the microwave emissive and reflective properties of water, given the observable conditions of the water and trial values of salinity. It is known that

the microwave emission of water is affected, in general, by changes in water temperature, water salinity, water surface roughness (wind waves and swell), and by the presence of other materials on the surface, such as sea foam and oil [refs. 1-7].

Mathematical models exist for predicting the microwave properties of sea foam and oil on water. These models require, however, a knowledge of the thicknesses of foam and oil, of the dielectric constant of the oil, and of the air-to-water ratio of the foam. These parameters are not available through the use of remotely sensed data. Visual or photographic data may be used, however, to determine the presence or nonpresence of oil or foam on the water surface. Thus, in the mathematical model, it is assumed that there is no foam or oil on the water surface.

Mathematical models exist also for predicting the effect of water surface roughness on the microwave emission of water. These models require a knowledge of the spectrum of water slopes which, in turn, may be inferred from a knowledge of the fetch, duration, and speed of the wind over the water. Again, these parameters are not available from remotely sensed data. Studies [refs. 4 and 6] have shown, however, that the effect of the water surface roughness is small for viewing angles near nadir and for vertical polarization. In the mathematical model developed for use in this paper, the effects of water surface roughness can be ignored.

With the elimination of the above effects, only the effects of temperature and salinity remain. To model the microwave properties of water, the water is assumed to be a homogeneous, semi-infinite dielectric bounded by a plane surface and overlaid by air. Since the water is an absorbing and emitting medium of large depth, the radiation impinging upon the air-water interface from below is the same as that emitted by a blackbody at the temperature of the water. That is, the brightness temperature of the radiation just under the air-water interface is equal to the absolute themometric temperature of the water.

At the air-water interface, a fraction, r, of the radiation impinging from below is reflected back into the water mass. The rest of the radiation is transferred through the air-sea interface and emerges as emitted radiation. Thus, the brightness temperature of the emitted radiation, T_e (°K), is

$$T_e = (1 - r)T_w \tag{1}$$

where T_w is the water temperature in °K.

The reflectivity, r, for a flat semi-infinite dielectric of dielectric constant, $\varepsilon'-j\varepsilon''$, is given in ref. 2 as

$$r_v = \left| \frac{(\varepsilon' - j\varepsilon'') \cos\psi - \sqrt{(\varepsilon' - j\varepsilon'') - \sin^2\psi}}{(\varepsilon' - j\varepsilon'') \cos\psi + \sqrt{(\varepsilon' - j\varepsilon'') - \sin^2\psi}} \right| \tag{2}$$

or

$$r_h = \left| \frac{\cos\psi - \sqrt{(\varepsilon' - j\varepsilon'') - \sin^2\psi}}{\cos\psi + \sqrt{(\varepsilon' - j\varepsilon'') - \sin^2\psi}} \right| \tag{3}$$

where ψ is the zenith angle of observation, and the subscripts v and h refer to vertical and horizontal polarization.

The microwave radiation directed downward impinging upon the air-water interface is characterized by a sky brightness temperature, T_{sky} (°K), which is the sum of the transmitted cosmic background brightness and the katabatic emission by the atmosphere.

A portion of the sky radiation is reflected from the air-water interface toward the observer so that the total radiation leaving the air-water interface and traveling toward the observer has a brightness temperature of

$$T_o = r\,T_{sky} + (1 - r)\,T_w \tag{4}$$

To compute the reflectivity for a given angle of observation and polarization, one must be able to specify the dielectric constant, $(\varepsilon'-j\varepsilon'')$ of the water.

Studies [refs. 8 and 9] have shown that the values of ε' and ε'' for water with dissolved salt (NaCℓ) may be predicted for the microwave spectrum through the use of the Debye model. That is,

$$\varepsilon' = \varepsilon_\infty + \frac{\varepsilon_s\,\varepsilon_\infty}{1 + \omega^2\,\tau^2} \tag{5}$$

and

$$\varepsilon' = \frac{\omega\tau(\varepsilon_s - \varepsilon_\infty)}{1 + \omega^2\,\tau^2} + \frac{\sigma_i}{\omega\varepsilon_o} \tag{6}$$

where ε_∞ is 4.9, ε_s, τ, and σ_i are functions of water temperature and salinity only, and ω is the circular frequency, $[2\pi\nu$, where ν is the electromagnetic frequency (Hz)].

To predict the values of ε' and ε'' for any water temperature and salinity, interpolation among given values of Debye constants is necessary. Interpolation formulas for this purpose are indicated in table 1 [ref. 8].

TABLE I. REGRESSION COEFFICIENTS FOR THE DEBYE PARAMETERS OF AQUEOUS SODIUM CHLORIDE

Independent Variable	Regression Coefficients		
	ε_s	$\tau_t \times 10^{12}$ (sec)	$\sigma_i\,(\Omega m^{-1})$
constant	0.88195 E02	0.19390 E02	----------
T_{sea}	-0.40349 E-00	-0.68020 E-00	----------
S	-0.43917 E-00	-0.11370 E-00	0.87483 E-01
$T_{sea}S$	0.43269 E-02	0.58629 E-02	0.45802 E-02
T^2_{sea}	0.65924 E-03	0.95865 E-02	----------
S^2	0.16738 E-02	0.11417 E-02	00.25662 E-04
$T^2_{sea}S$	-0.92286 E-05	-0.87596 E-04	-0.16914 E-04
$T_{sea}S^2$	-0.42856 E-04	-0.54577 E-04	-0.37158 E-04
$T^2_{sea}S^2$	0.44410 E-07	0.82521 E-06	0.39288 E-06
$\exp(T_{sea})$	----------	-0.65303 E-17	----------

With these interpolation formulas and the use of equations 2-6, one has a mathematical model that may be used to predict the emissive and reflective properties of water at 1.42 GHz for any given water temperature, water salinity, angle of viewing and polarization. This model was used to compute the microwave emission for vertical and horizontal polarization, for a viewing angle of 0 degrees, for water salinities of 0, 5, 10, 15, 20, 25, 30, and 35 0/00*, and for water temperature ranging from 0° to 30° C. The results of the calculations are shown in figure 1 for the nadir case.

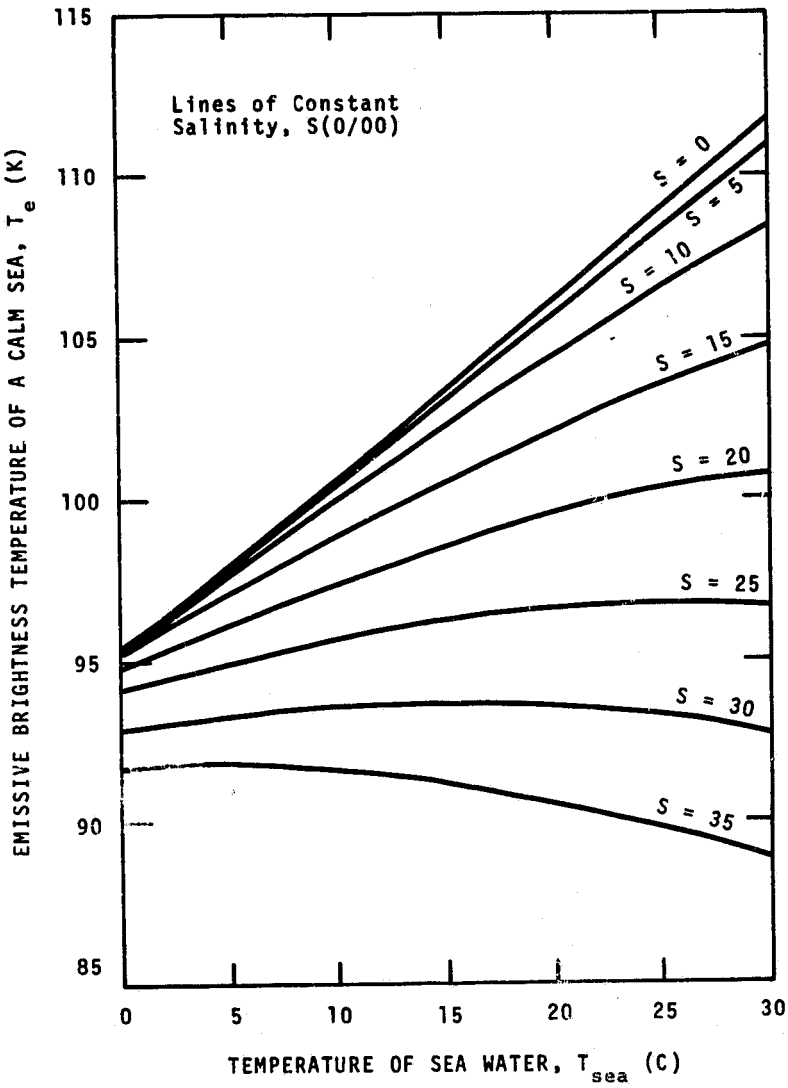


FIGURE 1. MICROWAVE EMISSION OF A CALM SEA: ν = 1.42 GHz, θ_a = 0 deg, VERTICAL OR HORIZONTAL POLARIZATION.

*0/00 means parts per thousand (gm kg^{-1})

2.2 EMISSION AND ABSORPTION BY THE ATMOSPHERE

A mathematical model that may be used to predict the effect of the atmosphere on the transfer of microwave radiation is needed to allow the proper consideration of this effect. For a given aircraft flight, soundings of atmospheric temperature and humidity are available, usually through the use of radiosondes released at National Weather Service stations. At 1.42 GHz, the atmosphere is practically transparent for all conditions, including clouds and rain [ref. 8]. However, the surface water would be disturbed and diluted by rainwater. Also, the aircraft radome would be covered by liquid water and would create large and unpredictable losses. For these reasons, rainy weather conditions must be ruled out for the measurement of salinity by the MFMR. The emission and transmission of the atmosphere may be computed from the knowledge of the vertical distribution of temperature and humidity in the atmosphere [ref. 8].

In addition, the effects of refraction and a spherical geometry may be included easily in the calculation [ref. 9]. As a result, the relationship between the brightness temperature of the radiation impinging upon the MFMR radome, T_b, and T_o, the brightness temperature of the radiation leaving the air-water interface, is

$$T_b = T_o t + T_{atm} \tag{7}$$

where t is the transmission coefficient for the intervening atmosphere, and T_{atm} is the brightness temperature of the radiation emitted by the intervening atmosphere toward the observer.

2.3 TRANSMISSION OF SENSOR COMPONENTS

If the radiation received is neglected in the side lobes of the L-band radiometer of the MFMR, then the equivalent radiometric temperature of the radiant power received by the radiometer is given by

$$T_r = \frac{T_b}{L_r L_a L_w} + \frac{(L_r - 1)}{L_r L_a L_w} T_{rd} + \frac{(L_a - 1)}{L_a L_w} T_a + \frac{(L_w - 1)}{L_w} T_w \tag{8}$$

where

L_r is the loss factor for the radome,
L_a is the loss factor for the antenna
L_w is the loss factor for the waveguide,
T_{rd} is the thermometric temperature of the radome,
T_a is the thermometric temperature of the antenna, and
T_w is the thermometric temperature of the waveguide.

2.4 CALIBRATION EQUATION

The microwave radiometer is a linear device such that the output, C (counts)*, is given by

$$C = C_{b\ell} - \frac{T_{b\ell} - T_r}{S} \tag{9}$$

where

$C_{b\ell}$ is the output of the radiometer when the power emitted by the reference load is being monitored (counts),

*The output of the MFMR is voltage; however, it is recorded as PCM counts.

$T_{b\ell}$ is the thermometric temperature and equivalent radiometric temperature of the reference load, °K, and

S is the response of the instrument or scale factor, °K per count.

In the MFMR, the scale factor may be determined before or after a data run by injecting a known amount of argon noise that has an equivalent noise temperature, T_n (°K), and observing the change in output, ΔC (counts). In this case,

$$S = \frac{T_n}{\Delta C} \tag{10}$$

2.5 SUMMARY OF MATHEMATICAL MODELS

Mathematical models were developed to predict the effects of all measurable parameters and salinity on the output of the MFMR. These models are valid only for the following conditions.

- Smooth water surfaces free from foam and oil
- Nonraining atmospheres
- Matched radiometer systems
- Linear radiometer systems

3. PROGRAM DEVELOPMENT

3.1 DATA AVAILABLE FOR ANALYSIS

The data available for analysis consists of the following:

1. One-second averages of the thermometric temperature of the radome, the antenna, and the waveguide of the MFMR and of the equivalent radiometric temperature of the radiation measured by the L-band radiometer as determined from the calibration equations (eqs. 9 and 10).
2. Averages taken over 0.792 sec. of the equivalent radiometric temperature of the radiation measured by the PRT-5 infrared radiometer.
3. Radiosonde measurements of atmospheric temperature and humidity from the surface to the 10-mbar level (approximately 31 km).
4. Flight logs for the aircraft flight.
5. Location (latitude, longitude, and altitude), attitude (heading, drift, roll, pitch), and speed of aircraft sampled once each ten seconds.
6. Surface measurements of salinity and temperature at selected points under the aircraft surface track.
7. Photographic coverage (10 percent overlap) along the flight line.
8. Scale factors, baseline counts, and baseline temperature used to reduce raw MFMR data to produce data in 1 above.
9. Equivalent argon noise temperature, radome loss factor, and waveguide loss factor.

3.2 ADEQUACY OF THE AVAILABLE DATA AND MATHEMATICAL MODELS

It has been noted that some minor effects, such as surface roughness and side lobe contributions, have been ignored in the development of the mathematical models. There is also some evidence that they are systematic errors in the values of injected argon noise and of the antenna loss factor for the MFMR. All of these factors could create a significant bias in the data if not properly treated. To insure consistency in the analysis and to eliminate the effects of systematic errors, a new set of calibration constants (scale factor and antenna loss factor) is obtained through the flight data and the mathematical models. Two portions of the flight data are taken, the first over water of known temperature and salinity and the second when the radiometrically cold sky is being viewed.

3.3 DETERMINATION OF THE NEW CALIBRATION CONSTANTS FOR THE MFMR

Combining and rearranging equations (8) and (9) gives the expression,

$$T_b = L_r L_a L_w [T_{b\ell} - S\,(C_{b\ell} - C)] - (L_r - 1)T_{rd}$$

$$- (L_l - 1)L_r T_a - (L_w - 1)L_r L_a T_w \qquad (11)$$

The actual output of the radiometer, C, may be obtained from the given values of radiometric temperature through the use of equation (9) and the old calibration constants.

If T_{bw} is the brightness temperature corresponding to the radiometer reading, C_w, obtained when the known water target is being viewed, and T_{bs} is the brightness temperature of the sky corresponding to the radiometer reading, C_s, then from equation (11),

$$T_{bw} - T_{bs} = L_r L_a L_w S(C_w - C_s) \qquad (12)$$

or

$$S = \frac{T_{bw} - T_{bs}}{L_a L_r L_w (C_w - C_s)} \qquad (13)$$

Inserting equation (13) into (11) and solving for L_a gives the expression

$$L_a = \frac{a_1}{a_2} \qquad (14)$$

where

$$a_1 = T_b + \frac{(T_{bw} - T_{bs})(C_{b\ell} - C)}{C_w - C_s} + (L_r - 1)T_r - L_r T_a \qquad (15)$$

and

$$a_2 = L_r L_w T_b - (L_w - 1)L_r T_w - L_r T_a \qquad (16)$$

In equations (14) through (16), either C_w and T_{bw} or C_s and T_{bs} may be used to determine L_a. With the knowledge of L_a, one may obtain the value of the scale factor, S, from equation (13).

The effect of the above determinations is to force the MFMR measurements to agree with the mathematical model at two points, namely, for a selected water point and for a cold sky point. Since all of the radiometric measurements are made for water conditions close to the selected water point, there should be consistency in the values of the derived salinities.

3.4 COMPUTATIONAL PROCEDURE FOR OBTAINING SALINITY AND TEMPERATURE FROM MFMR AND PRT-5 DATA

After receipt of all of the flight data and surface and atmospheric measurement data obtained in support of the aircraft flight, the following procedure was followed:

1. A homogeneous area of water with known water temperature and salinity was selected.
2. From an inspection of the surface measurement and PRT-5 tabulations, the difference between the two temperatures was determined for the selected water area. In general, there will be a fixed difference due to the cool skin of the water, the nonunity value of the emissivity of water, and the absorption and emission of the intervening atmosphere.
3. The radiation properties of the atmosphere were calculated through the use of the Microwave Atmospheric and Oceanic Data Analysis Program (MAODAP). The MAODAP uses radiosonde data taken during the flight [ref. 10].
4. The salinity and temperature analysis program (STANL) was then employed. In the STANL, the following operations are performed:
   - Control cards are read.
   - Data are read from PRT-5 and MFMR data tapes supplied by the Computation and Analysis Division (CAD) of the NASA Manned Spacecraft Center.
   - Eleven-second running averages are computed for needed MFMR and PRT-5 parameters.
   - The new calibration constants are determined by use of the flight data and the equations (13) through (16).
   - The salinity and temperature are determined from the MFMR and PRT-5 data through the following procedure:
     (1) First, the microwave radiometric temperatures are corrected for the change in scale factor, that is

$$T_r' = T_{b\ell} + S' \frac{(T_r - T_{b\ell})}{S} \tag{17}$$

     (2) Second, the PRT-5 infrared radiometric temperature is used with the correction factor in 2 above to determine the water temperature (°K).
     (3) Last, the value of salinity is determined through iteration so that the predicted radiometric temperatures agree with the corrected radiometric temperature determined in (1) above

4. PROGRAM APPLICATION

4.1 MISSION 190, FLIGHT 3

Mission 190, flight 3, was flown over the outflow of the Mississippi River into the Gulf of Mexico (Site 128) on November 11, 1971. Nine data runs were made over line 1 (see figure 2) at about 242 m (860 ft) above the water surface. The first eight data runs were made with the MFMR antennas pointing 4.8 degrees from nadir in vertical polarization. The last run was made with the antennas pointing 45 degrees from the zenith in vertical polarization. The first data run began at the ENE end of line 1 at 0935 CST; the last data run ended at the ENF end of line 1 at 1803 CST. Two KA-62 cameras, the PRT-5 infrared radiometer, the MFMR boresite camera, the MFMR, and the navigation equipment were used on the NASA 927 (NP-3A) aircraft during the flight, and all sensors functioned normally.

Flight support consisted of a radiosonde released at Boothville, Louisiana, (approximately 25 nautical miles north of the aircraft flight line) and a surface survey along the aircraft flight line. The surface survey was made through the use of a 65-foot crewboat leased at Venice, Louisiana. The surface measurements consisted of *in situ* measurements of salinity and temperature with an *in situ* salinometer. The measurements were taken at stations approximately every nautical

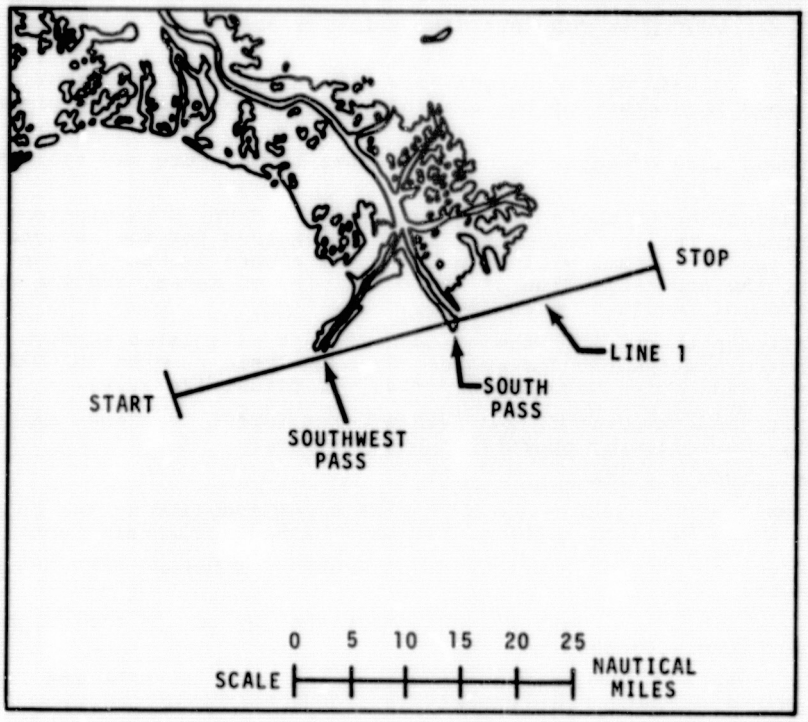


FIGURE 2. FLIGHT LINE FLOWN DURING MISSION 190, FLIGHT 3, SITE 128, NOVEMBER 11, 1971.

mile along the flight line. In addition, water samples were taken approximately every 10 stations. As originally planned, the surface survey was to take place during a time period centered upon the time interval of the aircraft flight. Unfortunately, the crewboat ran into the dock the evening before the day of the aircraft flight and had to undergo repairs before leaving the morning of the flight. The accident did not come to the attention of the mission manager since the aircraft crew and sensor operators had left for the airport before the surface survey team arrived at the docks in Venice to leave on the crewboat. As a result, the surface survey boat arrived at Southwest Pass and began the survey at 1157 CST just before the aircraft survey was being completed. The surface survey proceeded toward the WSW end of line 1 and returned to Southwest Pass at 1641 CST. In general, the atmosphere was clear and dry, and surface winds were from the ENE at 5 knots.

4.2 DATA PREPARATION

The water area at the Southwest Pass outflow was selected as the calibration point for the water data. The surface measurements of water surface temperature at this point were compared with the PRT-5 radiometric temperatures, and the radiometric temperatures, were found to be 3.5° C lower than the bucket temperature of the water surface.

The MAODAP was used to calculate the microwave parameters of interest for the later analysis. The parameters of interest from the MAODAP program are listed in table II.

The analysis program (STANL) developed for the study was then used to determine the new calibration constants and to produce a plot of surface water salinity and temperature along the flight track.

TABLE II. LIST OF PARAMETERS FROM MAODAP NEEDED FOR THE ANALYSIS PROGRAM

Parameter	Value
Temperature of selected water area	22.2° C
Salinity of selected water area	8.0 0/00
Equivalent radiometric temperature of sky (at a 45-degree zenith angle)	7.06° K
Atmospheric transmission factor for intervening atmosphere	0.99982
Emissive brightness temperature of intervening atmosphere	0.1° K
Sky brightness temperature at surface for the viewing angle of the MFMR	5.15° K
Zenith angle of viewing	4.8 deg

4.3 RESULTS

The plot of surface water salinity and temperature along the flight track during run 8 is shown in figure 3. The symbols in the figure indicate the values of surface temperature and salinity obtained by the surface survey that was conducted shortly after the aircraft flight. In general, there is good agreement. The times of passage over the river mouths are indicated by the symbol M and the time of passage over surface foam lines as seen in the photography are indicated by the symbol F .

These data confirm the usefulness of L-band measurements of water microwave emission in determining the surface salinity of water.

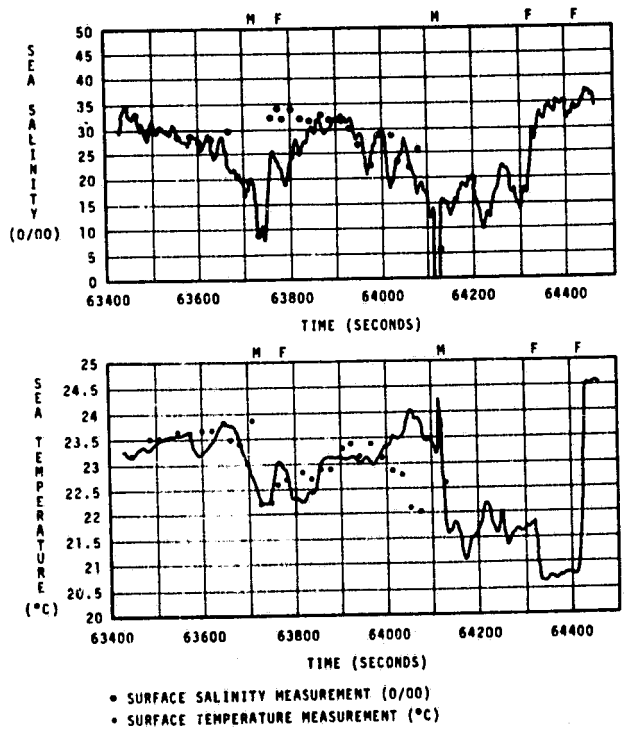


FIGURE 3. RESULTS OF MISSION 190, FLIGHT 3, RUN 8, OVER SITE 138, LINE 1.

5. REFERENCES

1. Sirounian, V., 1968: "The Effect of the Temperature, Angle of Observation, Salinity, and Thin Ice on the Microwave Emission of Water." *J. Geophys. Res.*, 73, 4481-4486.

2. Paris, J. F., 1969: "Microwave Radiometry and Its Applications to Marine Meteorology and Oceanography." Ref. No. 69-II, Contract Nonr 2119 (04), College Station, Texas A&M University, 210 pp.

3. Droppleman, J. D., R. A. Mennella, and D. E. Evans, 1970: "An Airborne Measurement of the Salinity Variation of the Mississippi River Outflow." *J. Geophys. Res.*, 75, 5909-5913.

4. Stogryn, A., 1967: "The Apparent Temperature of the Sea at Microwave Frequencies." *IEEE Trans., Ant. Prop.*, AP-15, 278-286.

5. Williams, G. F., Jr., 1969: "Microwave Radiometry of the Ocean and the Possibility of Marine Wind Velocity Determination From Satellite Observation." *J. Geophys. Res.*, 74, 4591-4594.

6. Hollinger, J. P., 1970" "Passive Microwave Measurements of the Sea Surface." *J. Geophys. Res.*, 75, 5209-5213.

7. Nordberg, W., J. Conaway, D. B. Ross, and T. Wilheit, 1971: "Measurements of Microwave Emission from a Foam-Covered, Wind-Driven Sea." *J. Atmos. Sci.*, 28, 429-435.

8. Paris, J. F., 1971: "Transfer of Thermal Microwaves in the Atmosphere." Vols. I and II, NASA Grant NGR-44-001-098, Dept. of Meteorology, Texas A&M University, College Station, Texas, 468 pp.

9. Paris, J. F., 1971: "A Program for Computing the Brightness Temperature of a Clear Atmosphere from Radiosonde Data." Tech. Rpt. LEC/HASD 649D.21.068, NASA Manned Spacecraft Center, Houston, Texas, under contract NAS 9-10950, 38 pp.

10. Paris, J. F., 1971: "MAODAP – Microwave Atmospheric and Oceanic Data Analysis Program." Earth Observations Division, NASA Manned Spacecraft Center, Houston, Texas, under contract NAS 9-12200, AD 63-0117-3334-15, 150 pp.

APPLICATIONS OF REMOTE SENSING IN PUBLIC HEALTH

C. M. Barnes*, C. E. Fuller*, H. J. Schneider*
E. E. Kennedy*, D. R. Morrison**, and H. G. Jones***

*NASA Manned Spacecraft Center
Life Sciences Directorate, Health Services Division
Health Applications Office
Houston, TX 77058

**National Research Council Fellow
NASA Manned Spacecraft Center
Houston, TX 77058

***The Boeing Company
Houston, TX 77058

ABSTRACT

Since August 1970, a small staff at the Manned Spacecraft Center and the University of Texas, School of Public Health at Houston has studied the feasibility of using remote sensing in public health applications. Practical applications of remote sensing have been discussed with representatives of various health organizations and directed toward potential applications on an experimental scale.

Currently, detailed research is underway to determine the habitat of mosquito vectors of disease in the United States. Advanced interpretative processes have enhanced the recognition of the breeding areas of salt marsh mosquitoes in a joint project with the New Orleans Mosquito Control District and studies in suburban Harris County are being conducted to determine the efficiency of remote sensing to determine the breeding sites of Culex quinquefasciatus, the mosquito responsible for transmission of St. Louis strain of encephalitis and of human filariasis. Remote sensor data has also been useful to scientists studying the habitat of endemic strains of Venezuelan encephalitis virus in Florida.

Research on the use of remote sensing in the public health aspect of air, water, and urban degradation has just begun. Preliminary data is encouraging and it is believed that remote sensing will play a significant role in future health programs, particularly those which have relationships with distinctive characteristics of the environment.

---

1. INTRODUCTION

The foundation for modern geographic and environmental study of disease is deeply rooted in medical history. About 400 years before Christ, Hippocrates, the father of medicine, wrote in his treatise, AIRS, WATERS AND PLACES, the following remarks:

> Whoever wishes to investigate medicine properly should proceed thus: in the first place to consider the seasons of the year, and what effects each of them produces. Then the winds, the hot and the cold, especially such as are common to all countries, and then such as are peculiar to each locality. In the same manner, when one comes into a city to which he is a stranger, he should consider its situation, how it lies as to the winds and the rising of the sun; for its influences is not the same whether it lies to the north or the south, to the rising or the setting sun. One should consider most attentively the waters which the inhabitants use, whether they be marshy and soft, or hard and running from elevated and rocky situations, and then if saltish and unfit for cooking; and the ground, whether it be naked and deficient in water, or wooded and well watered, and whether it lies in

> a hollow, confined situation, or is elevated and cold; and the mode in which the inhabitants live, and what are their pursuits, whether they are fond of drinking and eating to excess, and given to indolence, or are fond of exercise and labor.

It is said that in his practice of medicine, Hippocrates utilized field observations along with his bedside diagnosis. Thus the Hippocratic method and philosophy has influenced medicine for over 2000 years. However, the complexity of the earth and its interaction with the disease process has continued to be an enigma. Only recently, with the use of modern analytical procedures has it begun to be understood.

The Health Applications Office (HAO) of the Earth Observations Program was formed to study in detail those conditions of the environment and other earth processes which influence the mal-being of man. We believe that the remote sensing technology presently available will allow us to discover some basic principles never before obvious to health workers. We are particularly intrigued that these studies will not only contribute to our basic understanding of environmental disease but that through such research, unique methods of combatting plagues and infection will also become obvious. We do not claim that remote sensing will become a panacea for all public health work. Only that its use will present a new and unique overview of such problems.

In establishing a work plan and research program for the Health Applications Office, it was decided that our activities should be limited to health studies. In defining "health", the definition of the World Health Organization (WHO) was used for this purpose. Paraphrased, the WHO purports that health is the sum of those factors which relate to the physical, social, and mental well being of man--not just the absence of disease. We have thus adopted a philosophy which permits us to broadly look at a large segment of man's activities including those which cause industrial pollution of water and air, urban public health problems, health aspects of natural disasters, as well as diseases influenced by the environment.

Previous reports (1, 2, 3) have indicated the scope of activities of our organization as well as preliminary data resulting from such research. We have been supported contractually with scientists from the School of Public Health, University of Texas at Houston and the Lockheed Electronics Company. Numerous local, state, and federal health entities have also contributed to our thinking and participated in cooperative programs.

2. PROBLEM AREAS UNDER STUDY

A simple listing of current projects both large and small is given in Figures 1 and 2.

While time will not permit lengthy discussion of each research effort, I do wish to comment briefly on typical approaches that the HAO has made to some of the broad problems outlined.

Shell fish contamination in Texas estuaries is caused primarily from uncontrolled sewage effluents from towns and villages. This is detected by coliform bacterial concentrations indicating the presence of fecal-related disease organisms. This can cause illness in persons consuming shell fish from such areas. For example, control of oyster beds in Texas began in late 1920's directly as a result of a major typhoid epidemic. To determine clean waters where shell fish may be harvested requires significant resources of the health and fish and game departments in all of the coastal states. The process of examination is tedious, expensive, and extrapolative.

The HAO in conjunction with the Texas Department of Health and the University of Texas, School of Public Health is exploring the possibilities of using thermal and other imagery to (a) point out offending effluent systems and (b) test thermal dilution as a tracer for disease causing microorganisms.

If successful, such a system could materially reduce the resources necessary to detect and map contaminated estuaries, and perhaps render more precise information relative to changes in bacterial concentrations due to winds and water current activity.

Studies in air quality degradation, in addition to the usual air filtration system and particle sizers for ground truth, are attempting to determine several improved methods for studying suspended particulates in aerial surveillance. It is believed that such overview of large geographic regions can more accurately determine the true geographic dispersion and dose limits for several noxious substances in the Houston area. Recently publicized epidemiologic data from the M. D. Anderson Hospital and Tumor Institute indicates that citizens living within polluted areas of Houston are subject to a death rate considerably higher than that of persons in rural areas of Texas. It is expected that together with a ground truth work supported by the Environmental Protection Agency, the State of Texas, and the City of Houston that NASA supported efforts can (a) further define sources of pollutants, (b) quantify and identify types of pollutants, and (c) assist in estimation of illness factors or increased death rate within the test site.

Just as Hippocrates hypothesized, modern investigation have found that terrain characteristics can severely modify the presence of disease. Most living things including organisms which either cause disease or transmit disease require a few common environmental factors—food, moisture, appropriate temperature, shelter, etc. These factors, many of which can be directly monitored with remote sensing instrumentation are the key to the presence or absence of disease.

A case in point - Anthrax, a disease known for centuries as a killer of man and animals but one which has never been observed in its total environmental context. At the request of the Center for Disease Control (CDC), Public Health Service, the HAO responded to a request for environmental surveillance of Ascension Parish, Louisiana, in which numerous animals and man had been affected with Anthrax this past year. NASA photography supplied for the epidemiologic survey has been favorably received by CDC, who stated, "We found that a meaningful survey could not have been conducted without the aid of the color infrared mosaic and the assistance of the MSC technical staff."

While the final result of this survey is not yet complete, it is only fair to point out the importance of what was accomplished by HAO liaison with the Public Health Service--more complete and accurate analysis coupled with a geographic overview to permit an understanding of the interrelationships existing between the disease and the animals, man, plants, waterways, marshlands, crops, and the total ecological set. Without such overview from remote sensing, these studies would have been impossible (Figure 2).

Many of the urban public health problems under study by Health Applications are equivalent to those currently underway at other population centers. However, one unique feature concerns the combination of studies with the air and water degradation efforts of the staff at the University of Texas. In addition, the sixth largest city in the U. S., Houston, Texas, does have peculiar problems of climate, and unique petroleum, petro chemical, and other industries. Another aspect of urban public health studies has resulted in a simple plan to aid firemen and other emergency service personnel in the performance of their jobs. Aerial photography, when properly indexed can provide the fire fighter necessary information relative to the immediate operation. For example, such aerial views can easily pinpoint adjacent outbuildings sometimes hidden from line-of-sight view and permits the fire director to immediately understand not only the immediate fire but the potential incendiary region surrounding it. It also can quickly indicate, (of great importance to suburban fire departments) the location of surface water for refilling booster trucks. A similar analogy can be utilized for ambulance and police services which respond to urgent calls for service.

The important role of remote sensing, particularly aerial photography in analysis of the impact of natural disasters has been demonstrated many times in the past. From our single experience in this area, Hurricane Celia, at Corpus Christi, Texas, it was determined that it could be effectively used to quickly point out rotting and decaying animal bodies, ruptured chemical lines, and damaged water and sewage system, all of which are of immediate importance to public health. We are continuing to study hurricane, tornado, and earthquake data retrospectively such that when disaster strikes again an indoctrinated, well grounded team of public health specialists can quickly respond—an action that could save lives at a time when the right decision is quickly required.

Perhaps of greatest importance to health is the current HAO effort with vector-borne disease.

Schistosomiasis, a disease affecting over 200 million people in tropical areas of the world may be more amenable to control through use of recently reported data from the U. S. Public Health Service in Puerto Rico. The Schistosoma organism, a parasite of blood and several organs in man and birds uses a snail as a mandatory intermediate host. Without the snail, the life cycle is broken and the disease is erased. One of the problems concerns the location of snails within a suburban-rural environment. The Puerto Rico investigators have reported an extensive relationship of snails with a plant, Calladium sp., which grows in shallow streams and in the same ecological set as the snail. Find Calladium and you probably have found the snail causing Schistosomiasis in Puerto Rico. This information would point the way for application of molluscicides for snail control. HAO proposes to utilize radar to topographically locate appropriate streams in remote areas and multiband photography for identification of Calladium infested streams. Our University of Texas team will be working this fall within a Schistosoma test area of the British West Indies and reports of these endeavors shall be forthcoming at future meetings.

The ability of multiband photography to identify precise fall vegetation types within marshlands of the New Orleans Mosquito Control District has been previously reported (1). The New Orleans staff have reported significant correlations between the ecological set supporting the production of the Aedes sollicitans species of mosquito and certain plant communities of the test site. Subsequent flights over the same test site in the spring have resulted in similar detailed data acquired by the same method effectively identifying changes in vegetation due to season. A 24 channel multispectral sensor system was also utilized during the same spring flight and comparable results were achieved. Early results comparing multiband photography and multispectral sensor data indicates no major advantage in using 24 channel MSS equipment over multiband, false color enhanced photography. It was

necessary only to utilize bands 8, 9, and 10 (.76 to 1.05 micrometers) of the NASA MSS system to conveniently separate plant communities. For practical use of remote sensing systems for the average mosquito control district multiband photography is apparently the method of choice due to cost considerations.

The introduction of fire ants (Solenopsis geminata and saevissiama) into Alabama in 1933 has led to an infestation of major areas of the southern United States. These ants have been known to attack newborn animals, livestock and small children. Unwary field workers have often been incapacitated by the painful stings of the fire ants and it is reported that 13 human deaths have occurred in Louisiana, Mississippi, and Alabama as a result of massive fire ant stings.

The control and eradication measures instituted by federal and various state agencies have been severely hampered by the lack of an adequate and economical method of assessing the geographical boundaries of the infestation and the distribution of fire ant mounds within an infested area.

The USDA is spending $1 million annually in Florida to make a ground survey of only 2 percent of the land in an attempt to establish the boundaries of fire ant infestation.

Preliminary studies by USDA investigators have shown that aerial photography could be used to survey 100 percent of the infested land in Florida at one-tenth the present cost for the 2 percent surveys. The HAO is engaged in more sophisticated aerial assessment techniques (s.a., multiband photography) and automatic data scanning and processing which may provide a more practical and economic method of identifying the location and limits of fire ant infestation. This information is crucial to any successful program for eradication or control of these pests.

The screw worm fly (Cochliomyia hominovorax) has been known to infest the temperate zones of the Americas for at least 125 years causing serious losses to livestock and wild animal life. In brief, this insect lays its eggs in wounds or navels of warm blooded animals. Shortly thereafter the eggs hatch and the larval or maggot stage emerges and eats live meat, causing death or serious crippling in affected species. In Latin America, this loss concerns irreplaceable protein resources vital to human health. In the United States, the estimated economic losses to the animal industry was at one time believed to be several hundred million dollars annually.

In recent years a method of sexually sterilizing flies has been employed to combat this pest. When released in sufficient numbers within infested areas the sexually sterile males compete with local males and mate with the monogamous female flies resulting in production of sterile egg masses and the gradual decrease in total numbers of screw worm flies in the environment. By this method, during a 10 year period of time, the United States has been liberated from overwintering populations of this insect menace. However, immense populations of flies exist in Mexico and annually there is a migration of flies into the Southwestern United States.

To combat this invasion, a barrier of sterile flies is seeded by aircraft along the Mexican-American border extending some 300 miles into Mexico. The cost for this operation is 8.5 million dollars annually. The U. S. Department of Agriculture has signed an agreement with Mexico to move this barrier within southern Mexico to the Isthmus of Tehuantepec where it can be maintained at a lesser dollar figure. Further, Mexico would be liberated from the fly with this effort and Texas and the Southwestern United States would be forever rid of costs associated with combatting this fly. (Texas rancher costs in 1972 were approximately $100 million dollars.)

Pupating insects such as the screw worm fly are greatly dependent on environmental factors which either promote or degrade their populations. Proper moisture, temperature, and shade are all important factors.

During the U. S. eradication campaign, entomologists responsible for the program gained considerable detailed climatological information from the daily weather reports from the extensive U. S. network, allowing them to liberate sterile flies in a favorable environment. As the program of eradication proceeds to Mexico, it is perhaps even more important that this detailed climatological information be available due to the varied topography of the Republic. Terrain features include vast areas of jungle huasteca along the gulf coast changing to upper highlands of 2000 meters altitude or more in the central regions. This is interspersed with mountain peaks topped with snow. In all regions there is considerable seasonal variation in rainfall, humidity, soil moisture, and temperature. These factors cause considerable difficulty for the eradication team since the number of weather reporting stations is extremely meager, and it is necessary to have such data if one is to intelligently drop from aircraft the 500 million sterile flies on a weekly basis in the eradication campaign.

The Health Applications Office is making orderly progress toward assisting the governments concerned with local climatology information. By the use of Nimbus E data, it is proposed that a daily detailed map may be provided of the Mexican subcontinent highlighting environmental factors important in the life cycle of the screw worm fly. When used in conjunction with maps of vegetation

cover and other information from the ERTS satellite, it is contemplated that program managers can make intelligent decisions on where to drop flies, when to drop flies, and perhaps predict the effectiveness of such aerial seeding.

A most important point is that when the technology for this application is developed, it may likely be applied to campaigns for eradicating other pupating insects wreaking havoc in this world of ours.

3. CONCLUSION

The Health Applications Office of NASA sincerely believes that the technology of remote sensing can be of great importance to the field of public health. The time scale when applications of such technology is actually in major use, is materially dependent on funding and support for this rather basic developmental effort. We are reminded that another technology, the use of the compound microscope in medical research, was not begun until 300 years after its invention. We trust that we shall not wait a similar time period to put the modern technology of remote sensing to work in solving some of the health problems in man and his supporting biota.

FIGURE 1. PROBLEM AREAS UNDER STUDY
HEALTH APPLICATIONS OFFICE, NASA-MSC

POLLUTION

WATER QUALITY
- SHELL FISH CONTAMINATION

AIR QUALITY
- SUSPENDED PARTICULATES
- HARMFUL GASES
- MORBIDITY (ILLNESS) - MORTALITY

DISEASE RELATED TERRAIN CHARACTERISTICS

SOIL: MOISTURE, TYPE, PH, TEMPERATURE, VEGETATION COVER, MINERALS, OTHER RELATIONSHIPS

ANTHRAX

FIGURE 2. PROBLEM AREAS UNDER STUDY
(CONT'D)

PUBLIC HEALTH PROBLEMS - URBAN COMMUNITIES

PLANNING AND OPERATIONAL CONTROL

INDUSTRY, RECREATION, NOISE, HEALTH CARE, EMERGENCY SERVICE - FIRE, POLICE

NATURAL DISASTERS

VECTORS OF DISEASE

SNAIL (SCHISTOSOMIASIS)

MOSQUITO

FIRE ANT

SCREW WORM

BIBLIOGRAPHY

(1) Fuller, C. E., PUBLIC HEALTH APPLICATIONS OF REMOTE SENSING, Fourth Annual Earth Resources Program Review, Section 22, Vol. 1, Document MSC 05937, (January 17-21, 1972) NASA Manned Spacecraft Center, Houston, Texas.

(2) The University of Texas, School of Public Health at Houston, PUBLIC HEALTH APPLICATIONS OF REMOTE SENSING OF THE ENVIRONMENT (AN EVALUATION) - Final Report, (January 1972).

(3) Fuller, C. E., Barnes, C. M.,and Jones, H. G., PUBLIC HEALTH IMPLICATIONS OF NASA'S EARTH OBSERVATIONS PROGRAM, 98th Annual Meeting of the American Public Health Association, Houston, Texas (1970).

WATER QUALITY DETERMINATIONS IN THE VIRGIN ISLANDS FROM ERTS-A DATA

W. G. Egan

Research Department, Grumman Aerospace Corporation
Bethpage, New York 11714

ABSTRACT

The harbor at Charlotte Amalie on St Thomas, Virgin Islands, has a concentration of many factors affecting water quality: untreated sewage effluent, sediment from navigation and dredging operations, runoff from a garbage dump, and hot effluent from a desalination/power plant. Imagery from ERTS-A in association with aircraft imagery and ground truthing permits the characterization of water quality in terms of absolute color values. This necessitates the establishment of photometric standards resolvable by the ERTS-A sensors in order that atmospheric effects, which generally vary on sequential overpasses, may be determined and subtracted. The overall program is described together with typical numerical results.

INTRODUCTION

The Virgin Islands ERTS-A experiment has the object to determine the feasibility of using both airborne and spacecraft sensors quantitatively in coastal zone water quality management by establishing the boundaries of applicability of each technique separately. In order to sense water quality remotely, two requirements must be fulfilled: 1) the optical properties of the water must be affected by the pollutants in a predictable way; and 2) the remote sensor must be capable of distinguishing these variations. There are thus two aspects associated with the program, the first requiring measurements of the optical properties of the polluted water itself with the ultimate aim of correlating these with the biological, chemical and other physical properties of the water. It would be expected that generally there would be an average level of pollution with temporal variations caused by tides, winds, and miscellaneous local effects, and these variations would cause corresponding related changes in the optical, biological, chemical and other physical properties of the water. The second aspect deals with two types of remote sensors, the first being aircraft and the other being those in the ERTS-A. The ERTS-A system has been thoroughly described in the user's manual (Ref. 1), and the present operating sensor is the MSS (multispectral scanner). The remotely sensed light reflected and scattered by polluted water is significantly affected by absorption and scattering in the atmosphere. In order to quantitatively account for this atmospheric absorption and scattering so that precision remote sensing measurements of color may be made, optical calibration standards must be utilized. These standards take the form of calibrated optical test panels placed on the ground for aircraft measurements, and a sufficiently large calibrated optical target for the ERTS-A.

By knowing the true color of these targets from laboratory measurements and the response of the aircraft photographic or satellite sensing system, the absorption and scattering of the atmosphere may be deduced.

The study of water quality in the Virgin Islands, and in particular the Harbor at Charlotte Amalie in St. Thomas is being carried out by Grumman Ecosystems under NASA sponsorship on Experiment No. 589, and in association with the Marine Resources and Development Foundation of the Virgin Islands.

STUDY AREA

The harbor of St. Thomas (Fig. 1), which is the study area, appears to be a gem of the Carribbean, but in reality is more akin to an open sewer. The view is to the south; prevailing winds are from the east to southeast, and a small tidal effect (about one foot) exists. A dredge is seen operating in the channel at the left, acquiring sand for building construction while concurrently filling the nearby water with sediment. Another cause of sediment is the daily docking of between 2 and 3 cruise ships, generally at the West Indian Dock (at the right in the photograph, Fig. 2; the section of an oblate spheroid visible in the photograph at the left is part of the aircraft structure). The water depth in the harbor near the dock is about 30 feet, and during docking and departing much of the bottom coral sand is stirred up by the ships propellers and bow thrusters. A track of suspended sediment in the wake of the docked ship, as well as a sediment eddy off the port side ahead of the bow of the ship, is shown in Fig. 2.

Raw sewage is discharged into the harbor at the rate of about a million gallons per day. Since there is no aquifer on the Island of St. Thomas, drinking water is obtained from catch basins and a desalination plant. Sanitary sewage (toilet waste) is flushed using bay water pumped inland through a separate water system. The raw sewage is presently discharged into the bay along the sea wall (Fig. 3) at the north rim. A sewage treatment plant is under construction and is expected to be operational by the end of 1972. The discharge from this plant will be in 70 feet of water at a location southwest of the airport.

A land fill for garbage exists off the southwest end of the airport runway, and land runoff into the sea would occur from it during rain. A combination desalination and power plant discharges hot saline water into Lindbergh Bay just south of the airport.

Thus we have in this small area a concentration of many factors affecting water quality, and this provides an opportunity for convenient study. The study then has general application to coastal zone water quality management.

SURVEY PROGRAM

The water quality program necessary to accomplish the objectives outlined in the Introduction consists of three aspects: 1) the optical, biological, chemical and physical ground truth program; 2) aerial imagery - acquisition, calibration, and interpretation; and 3) ERTS-A imagery - calibration and interpretation. By such a thorough program we expect to delineate the range of applicability of ground measurements, aerial imagery and ERTS-A.

The ground truth program presently in progress is depicted in Fig. 4. A grid of 17 stations is shown, where samples will be acquired weekly for optical, biological, chemical and physical measurements. Also shown are 70 benthic quadrats. The weekly measurements consist of dissolved oxygen, pH, optical transmission between 0.4 and 0.7μm, chlorophyll a, chlorophyll b and xanthophyll, nitrates, nitrites, phosphates, turbidity, total and fecal coliform, BOD, temperature, depth, salinity, and ambient light versus depth. Recording current meters are also located at the 17 stations. Measurements will also be made during the aircraft and

ERTS-A overflights. Primary untreated effluent locations are marked as arrows along the shore line on Fig. 4.

In order to establish the range of variation of the optical water quality parameters, initial in situ optical measurements of the spectral transmission of the harbor water were made on September 5, 1972 at 9 stations during the afternoon (Fig. 4), and 3 stations at night (Fig. 4), all shown as triangles. Initial benthic quadrats (bottom study areas) are indicated (as hexagons) where a diver acquired bottom samples. The optical locations were chosen to include a variety of physical conditions such as: adjacent to a sewer outfalls; near where the docking cruise ships stirred up sediment; out in deep clearer water; and intermediate points.

The aerial imagery is acquired during the ERTS-A overflight by a four lens I^2S camera with spectral filters to match the MSS bands 4, 5, and 6. Preliminary aerial imagery was acquired in the morning of September 5, 1972 using type EH high speed Ektachrome and Type 8443 false color infrared Ektachrome films. In the initial imagery on September 5, 1972 precision ground photometric procedures are included, and this will continue in future work. This involves the use of accurately controlled color test panels on the ground at the Brewers Bay Beach, and laboratory spectrophotometric measurements of the Brewers Bay Beach sand. The Brewers Bay Beach has a sufficient size to be resolvable from the ERTS-A by the MSS as well as from an aircraft.

Since no imagery has been obtained as yet of St. Thomas Harbor, as a substitute some initial ERTS-A imagery of other water areas will be used for preliminary assessment of the radiance levels of relatively clean and lower quality water. Subsequent imagery from St. Thomas Harbor, hopefully using the high gain mode of the MSS on bands 4 and 5 for finer resolution, will permit detailed analysis of the harbor water quality.

EXPERIMENTAL APPROACH

The approach we use on the aircraft and ERTS-A data is new, involving absolute color measurement and combining that with contrast measurements. Past analyses have emphasized contrast (Ref. 2) and the utilization of training areas for the sensors for recognition with certain limitations (Ref. 3). An important benefit is achieved by combining an absolute ground reflectance standard with the measurement of apparent target radiance at aircraft and the MSS: the determination of the effect of the atmosphere. Incident solar radiation upon a ground target is filtered by the atmosphere, which includes molecular and dust scattering, that reduces the blue end of the spectrum as compared to the red. The scattered radiance by ground targets is similarly attenuated more highly at the blue end of the spectrum as compared to the red, and in addition, a veil of blue haze intervenes between the ground target and aircraft and ERTS-A sensors due to directly atmospherically scattered incident sunlight; the scattered sunlight is highest in the blue and the over-all effect is to reduce contrast in aircraft and satellite imagery. While there is theoretical concern for this problem (Ref. 4), our approach is empirical utilizing precision ground color test panels previously described (Ref. 5).

The optical analysis of the atmospheric effects proceeds as follows: measurements of the incident solar radiance are made in five bands 0.433, 0.533, 0.633μm, broadband blue, and white; also irradiance is measured on a diffusely reflecting white panel on the ground in these bands. The first series of radiance measurements yield information on the filtration of the sun's direct radiation, while the second series of measurements yield information about the filtration of the incident solar radiation plus the scattered sunlight. These measurements must be made concurrently with the acquisition of aircraft and satellite imagery. For aircraft imagery, large test panels must be used sufficient to be resolved by the aerial cameras; and for the satellite a large and relatively homogeneous optical target

must exist to be resolved by the satellite. The photographic and satellite sensors must be calibrated in terms of incident radiance upon them. Then the photographic sensors will quantitatively sense the incident solar and sky radiance scattered by the ground test panels; and the ERTS-A satellite MSS will quantitatively sense the solar and sky radiance scattered by another selected optically homogeneous large ground target. These measurements will be in the spectral bands of operation of the sensors. Then by knowing the radiance on the ground test panels (or satellite targets), the difference sensed photographically by the aircraft (or by the MSS on the ERTS-A) is the effect of atmospheric scattering.

The next step in the optical analysis is the interpretation of true water color as an index of water quality. Essentially, the color of water is the result of light backscattered by the water. For pure water, molecular scattering dominates, producing a blue color similar to the effect with the atmosphere. When impurities or pollutants occur in the water, these will generally backscatter longer wavelengths. For a detailed analysis of the backscattering properties of impure water, angular scattering measurements as a function of wavelength and viewing geometry must be made. However, a rough indication of scattering may be obtained by measuring the attenuation coefficient of water; the attenuation index is composed of scattering and absorption, and both are wavelength dependent. Hence, in our initial optical measurements of the St. Thomas Harbor water, the attenuation coefficient was measured in the same 5 bands just as was the solar radiance. The test panels necessary for the implementation of the optical ground truthing and aerial photography were placed on an open coral sand area on Brewers Bay Beach (see Fig. 3 for location) as shown in Fig. 5. The ground color panels were then used for ground irradiance measurements, to monitor color bias by the atmosphere, to make in situ relative measurements of the beach sand reflectance and to monitor the response of the aerial color films. During the aerial photography, the 6 foot color panels and adjacent beach areas (Fig. 6) were photographed on at least one frame in 12. The beach area on which the panels were placed has a size of 350 by 900 feet. Although some trees and a road exist, 200 by 900 feet are relatively clear and sufficiently resolvable by the ERTS-A, in at least one line element, to serve as a ground calibration to permit atmospheric effects to be subtracted. It is to be noted that the placement of the panels on a white sand area is detrimental as far as using the panels for aerial photography; a dark background would be better because the solar radiation scattered by the sand into the atmosphere above the panels adds to that scattered directly by the atmosphere above the panels.

The spectral reflectance of the test panels was determined in the laboratory (Fig. 7) and the associated photometric properties similarly determined (Fig.8); from these the apparent spectral reflectance for the given incident solar and sky radiation was determined. Also, the coral beach sand to be used as a calibration standard, for the ERTS-MSS, was similarly determined spectrometrically (Fig. 9) and photometrically (Fig. 10). (Note that the phase angle is the angle between the incident radiation and the scattered ray.) However, the determination of the specific atmospheric constituents causing the observed optical filtration depends upon a knowledge of the optical complex index of refraction of the possible dust and aerosol particles in the atmosphere and an appropriate scattering theory, neither of which exist at present. However, for a pure molecular atmosphere, Rayleigh scattering occurs, and this is well understood. For the water attenuation measurements a portable 3 degree acceptance angle Minneapolis-Honeywell photometer with interchangeable filters was mounted on a submarine viewing tube. The tube had a watertight plexiglass window that permitted photometric measurements under water without interference from the surface waves. Optical filters used in the measurements were peaked at 0.433, 0.533, and 0.633μm; they were Optics Technology narrow band interference filters with a bandpass of 0.02μm; also used was a 0.4μm wideband filter consisting of 8 mm Corning CS5-56 glass; and also white consisting of the band between 0.4 and 0.7μm. These measurements are then correlated, as a function of position, with aircraft and ERTS-A imagery. The calibrated aircraft photography is additionally used as an interim step in the interpretation of the

ERTS-A MSS imagery since we then have a synoptic representation, spot ground truthed at selected locations and imaged at relatively low resolution by the MSS.

RESULTS

The results will be presented in the following order: ground optical properties and circulation characteristics of the St. Thomas Harbor water; calibration panel measurements necessary for interpretation of aerial photography; application of calibration procedures to aerial imagery of harbor water areas; the effect of temporal atmospheric changes; and finally an example of ERTS-A imagery of a water area.

The initial *in situ* optical attenuation results for the St. Thomas Harbor water are presented in Table 1. Near the sea wall in the vicinity of sewer outfalls (Stas. 5, 6, 7, 8, 9 - Table 1) the water is observably polluted which is consistent with the higher attenuation coefficients. As one proceeds seaward (Sta. 4), the attenuation coefficient decreases, and the water is observably less polluted; however, the condition of pure water (Ref. 6) is not reached. At night the attenuation increased (compare green Sta. 9 day with Sta. 1 night and green Sta. 3 day with Sta. 2 night; these aforementioned stations are at corresponding locations [see Fig. 4]). It is to be noted in Table 1 that the blue and green produce the greatest range of values whereas the red and white have a more restricted range for the locations considered, particularly for Sta. 9 of high pollution and Sta. 4 of low pollution. From this we infer that blue and green absorption are most indicative of sewage pollution in this harbor water.

In order to determine whether the circulation conditions in the St. Thomas harbor would permit sludge deposits to accumulate, bottom samples were obtained by a skin diver at the 5 initial benthic quadrats shown in Fig. 4. The samples were obtained on September 7, 1972 and were remarkably free from sludge, being at least 90% white coral sand. Table 2 lists the sampling locations, the depth at which the sample was acquired, the diver's visibility estimate, and a visual description of the sample. The harbor appears to be reasonably clean considering the quantity of untreated sewage dumped into it. The wind driven surface current extends down perhaps 15 feet with a velocity of the order of a few knots, more or less depending upon the harbor location and geometry (Ref. 7); this plus the bottom agitation by the docking ships appears to be cleansing the harbor. Tidal effects are of the order of 11 inches (Ref. 7), and thus do not strongly affect water flow in the harbor.

The diver's visibility estimates in Table 2 follow the general trend indicated in Table 1; Station B is of lowered visibility as a result of a dredge operating in the harbor.

The results of the calibration panel photography at ground level, 2000 and 4000 foot altitudes is presented in Table 3. The ground panels (and beach sand) were photographed using type EH high speed Ektachrome film, and subsequent densitometric measurements were made on a Joyce-Loebl microdensitometer. The lightest gray ground panel (shown as G_1 in Fig. 7 was not placed in position during the aircraft runs). The densitometric measurements were made at wavelengths of 0.440, 0.530, and 0.63μm, corresponding to the three emulsion transmission peaks in the transparency. Also tabulated are the density differences between green and blue (G - B), and red and green (R - G). The reason for the tabulation of density differences is that they correspond to color ratios; this is because a density value is the logarithm of the light transmission in one of the three wavelengths of measurement (0.440, 0.530, or 0.630μm), and the difference between densities (which is the difference between the logarithms of light transmission in two wavelength regions) corresponds to a color ratio by virtue of the mathematical properties of logarithms. Thus these density differences represent ratios that demon-

strate changes in color contrast as a function of altitude for the calibration panels and the sand.

By perusing Table 3, it is seen that the darker panels (at ground level) apparently become brighter as the altitude is increased, this being the result of sunlight scattering by the atmosphere, and secondary scattering of light reflected from the bright beach sand. In comparison, the brighter white panel and the beach sand become darker because of the competing attenuation of the atmosphere in comparison with the scattering. In general, however, the contrast, as represented by the density differences, becomes smaller, or even reverses sign [G_2 in (R - G)].

By making densitometric measurements on the transparencies, and using the integral density curves for type EH Ektachrome film (Fig. 11), the equivalent exposure may be deduced. As an example, using the densitometric measurements on the white panel (Table 3), its spectral reflectance (Fig. 7) and goniometric properties (Fig. 8), and the black body curves (Fig. 12; from Ref. 8), an equivalent apparent color temperature may be deduced for the white panel at an altitude of 4000 feet; this turns out to be 5200°K. If we use the Brewers Bay Beach sand (Table 3, Figs. 9 and 10), we proceed to deduce the same apparent effective color temperature of the sand illuminant at 4000 feet altitude of 5200°K. While this specification of color temperature is only an artifice aimed at representing a complicated absorption and scattering process of the atmosphere in a simple way, it does yield a way of specifying absorption by the atmosphere. Generally it is an approximation given by a best fit to the black body curves (Fig. 12), but would more properly be represented as a spectral distribution, independent of black body curves. This identical technique of specification of color temperature may be applied to ERTS-A and other satellite imagery.

If we now apply these analysis procedures to aerial imagery of the ground truth stations of Fig. 4, using absolute photometric calibration measurements of the panels and sand, we obtain equivalent exposure values for the harbor water areas which may be converted into reflectance and radiance. The reflectance values are presented in Table 4 and the equivalent radiance values are presented in Table 5. The reflectances and radiances quantitatively agree with those in Table 1, with a notable exception that illustrates the strength of the photographic technique: the Sta. 4 measurements in Table 1 were made in midafternoon on September 5 and indicated relatively clean water; however, during the prior early morning aerial photography, a dredge was operating in the area acquiring sand for construction operations. A combination of an incoming tide, a wind driven northwest current, and sediment settling had reduced the level of sediment contamination by the afternoon to yield the values shown in Table 1.

The H. S. Truman airport runway reflectance (away from the landing aircraft skid marks) is listed in the event that a lower reflectance standard than the beach is desired as a reference as when the MSS is operated on the high gain mode on bands 4 and 5. High gain operation is advantageous to resolve finer differences in ground target reflectance at low reflectance levels, as is the situation with the water targets. The airport runway is large enough to be resolved by the ERTS-A imagery, and thus serve as a standard.

In another specific application, consider Fig. 13, which is an aerial photograph of Crown Bay with a sewer outfall. Figure 13 is a black and white copy of the original three color positive transparency. A transect 9a and 9d is shown in the figure with the radiance values also listed in Table 5. The region 9a is west of the outfall and 9b east; 9c is an area where the sand bottom is seen and 9d an area where deeper water (about 30 feet) exists, and the bottom is invisible.

A remark is in order with respect to Tables 4 and 5; the first data columns in these tables indicate what would be sensed by the RBV (Return Beam Vidicon) if it were operated and the other columns indicate the response of the MSS. Since

the MSS does not sense the spectral region between 0.4 and 0.5μm, and this is a region that appears to be useful for water pollution analyses, albeit at low reflectance levels, but the RBV would sense these levels, the RBV would be of value if it were operational.

The radiance values in Table 5 are those existing at 4000 foot altitude, which is about half way through the low altitude aerosol and dust layer. Referring to Table 2, and comparing the darker panels, the scattering amounts to ≈ 0.2D at $\lambda = 0.633\mu m$ and ≈ 0.5D at 0.433μm, depending strongly on the ground level reflectance. The absorption effects due to the atmosphere are relatively small, but the aerosol and dust particles have varying effects.

Other optical conditions which affect the aerial and satellite imagery are those of the time dependent filtering of the incident sunlight by the atmosphere (including dust and aerosols) producing a reddening by scattering, and the time dependent effect of sky light (including clouds).

Table 6 illustrates the time dependent effects of atmospheric scattering of sunlight as the sun rises, producing a bluer sun as it ascends (the values for radiance have been normalized to a value of 13.6 at $\lambda = 0.633\mu m$ to facilitate analysis of color changes). In comparison, the diffuse white test panel (with the reflectance shown on Fig. 7) produces a higher blue irradiance because it is illuminated by blue sky light in addition to sunlight. At 1030 hrs on Signal Mountain (St. Thomas) scattered cumulus clouds began to form which decreased the blue sky light, together with the total sky light, moving the color balance toward the red. Later measurements, also with scattered clouds, showed increased blue. These effects occurred on the previous day during the aerial photography.

Another indication of the time dependent sky effects is presented in Table 7, which is the sky radiance as a function of viewing angle above the horizon. At 0745 hrs, at low elevation angles, particularly toward the sun, the high scattering effect of the aerosol haze is noted. There was an unusual atmospheric haze condition existing on the 5 September 1972 in the Virgin Islands: generally the visibility is of the order of 60 miles, but was 8 to 10 miles during the measurements. The San Juan weather bureau conjectured that the low visibility was the result of dust from storms over the Sahara carried west by trade winds.

The elevation angles in Table 7 are measured toward or away from the sun, and the N and S indication are measurements perpendicular to this direction. The haze effect persisted throughout the morning. The values listed in Table 7 are referenced to absolute radiance measurements through the calibrations listed at the bottom of the table.

Since appropriate ERTS-A imagery is not yet available for St. Thomas Harbor, the values of radiance indicated in Table 5 may be compared with those obtained by the MSS on scans of representative water areas such as at the Pyramid Lake Area, California - Nevada. The MSS imagery was obtained on Orbit 28, July 25, 1972. The digital levels of clear water areas of Pyramid Lake are (Ref. 9) (compared to full scale radiance values of digital level 63)

Band	Digital Level
4 (0.5 to 0.6μm)	7 and 8
5 (0.6 to 0.7μm)	2 and 3
6 (0.7 to 0.8μm)	2 and 3

But, where the water is shallow and silty as in Honey Lake, the digital level on band 6, for instance, rises to 12 and 13 (Ref. 9). These levels are comparable

with those indicated in Table 4 for the polluted water of St. Thomas Harbor and are therefore detectable. A problem with poor signal to noise ratio occurs at the lower radiance levels with the MSS, with the ratio dropping below 10:1 on bands 4, 5, and 6 for a signal 0.1 or less of the maximum.

Since the bottom of St. Thomas Harbor is predominantly sand, with coral formations in shallower water, it is possible to infer depth from aircraft or satellite imagery. Where the bottom is seen, a structure is generally evident. Thus, knowing the reflectance of the bottom sand (under water), an estimate of the depth may be made when the attenuation coefficient of the water is known.

CONCLUSIONS

Initial ground truth optical measurements indicate an appreciable variation of the optical attenuation coefficient (absorption plus scattering) in the harbor water as a function of location relative to known sewer outfalls and visible causes of silt contamination. The variation is greatest in the green and blue spectral regions for the St. Thomas Harbor. By using ground color calibration panels together with ground based measurements of sun and sky radiance, the radiance and reflectance of water areas in St. Thomas Harbor may be determined. The ground color calibration panels provide a means for the separation of the effects of atmospheric aerosol and dust scattering in aerial and ERTS-A imagery. The reflectance and radiance sensed from St. Thomas Harbor water areas correlate well with the in situ measurements of attenuation coefficients, even to the extent of relatively rapidly changing harbor conditions. Ground based measurements of sun and sky radiance are useful in areas containing unusual atmospheric contamination conditions in order to properly interpret data. Benthic topography may also be inferred when a knowledge of the optical reflectance properties of the bottom is known along with the absorption properties of the overlying water. The ERTS-A appears capable of resolving the variations noted in the St. Thomas Harbor, permitting long term monitoring of the conditions subsequent to the new Charlotte Amalie sewage plant going operational at the latter part of 1972. Cloud cover poses a problem, but with repetitive flights and the possibility of imagery acquisition on overlapping adjacent frames, the situation is helped.

Finally, while only a brief outline of our photometric procedures has been presented designed to resolve and especially to quantify color differences in aircraft and ERTS-A imagery, it appears that ultimately the most precise determinations will be made from tape outputs rather than their photographic representation. Some contrasts can be seen visually, and that is quite satisfying, but the tape information is the basis for precise quantification of color, together with the proper photometric calibrations.

The 300 foot spatial resolution of ERTS-A imposes a limit on the detail of the flow patterns that may be established, but has the advantage of a synoptic presentation over a large area (100 nautical miles square). In comparison the aircraft imagery has a resolution of the order of a few feet and is thus amenable to detailed studies of flow patterns of the order of magnitude of a few feet.

ACKNOWLEDGMENTS

The author wishes to thank E. Medlicott for his assistance in the field measurement program; D. Bertolet for excellent pilotage during the aerial photography; P. Blackwell and B. Glanville for assistance in the benthic sampling operation; W. Coulbourn, program manager and his staff in Grumman Ecosystems; the Research Department, Grumman Aerospace Corporation; and NASA under Experiment No. 589 for their support and assistance.

REFERENCES

1. ERTS Data Users Handbook, Prepared by EROS Program, U.S. Geological Survey, 1972.

2. Anuta, P. E., Kristof, S.J., Levandowski, D. W., Phillips, T. L., and MacDonald, R. B., Crop, Soil, and Geological Mapping from Digitized Multispectral Satellite Photography, Proceedings of Seventh International Symposium on Remote Sensing of Environment, Institute of Science and Technology, The University of Michigan, Ann Arbor, May 1971, pp. 1983-2016.

3. Smedes, H. W., Spencer, M. M., and Thomson, F. J., Preprocessing of Multispectral Data and Simulation of ERTS Data Channels to Make Computer Terrain Maps of a Yellowstone National Park Test Site, Proceedings of Seventh International Symposium on Remote Sensing of Environment, Institute of Science and Technology, The University of Michigan, Ann Arbor, May 1971, pp. 2073-2094.

4. Turner, R. E., Malila, W. A., and Nalepka, R. F., Importance of Atmospheric Scattering in Remote Sensing, or Everything You've Always Wanted to Know About Atmospheric Scattering But Were Afraid to Ask, Proceedings of Seventh International Symposium on Remote Sensing of Environment, Institute of Science and Technology, The University of Michigan, Ann Arbor, May 1971, pp. 1651-1698.

5. Egan, W. G. and Hair, M. E., Automated Delineation of Wetlands in Photographic Remote Sensing, Proceedings of Seventh International Symposium on Remote Sensing of Environment, Institute of Science and Technology, The University of Michigan, Ann Arbor, May 1971, pp. 2231-2252.

6. Jerlow, N. G., Optical Oceanography, Elsevier Publishing Company, New York, 1968, p. 51.

7. Van Eepoel, R., Carribbean Research Institute, St. Thomas, U.S. Virgin Islands, Private Communication, September 6, 1972.

8. Joos, G., Theoretical Physics, Blackie and Son Ltd, London, 1951, p. 615.

9. Bachofer, B., Mgr. Systems Engineering, General Electric Co. Space Division, Valley Forge, Pa., Private Communication, October 9, 1972.

Table 1

Charlotte Amalie Harbor Water Attenuation

September 5, 1972

Location	$\alpha_{.433/cm}$	$\alpha_{.533/cm}$	$\alpha_{.633/cm}$	$\alpha_{.4WB/cm}$	$\alpha_{white/cm}$
1	.0020	.0034	.0040	.0024	----
2	.0051	.0040	.0051	.0029	.0032
3	.0009	.0029	.0040	.0029	.0026
4	.0006	.0009	.0026	.0020	.0026
5	.0026	.0031	.007	.004	.0026
6	.0050	.0027	.006	.0046	.0031
7	.006	.007	.012	.007	.008
8	.007	.0016	.00?	.00?	.006
9	.016	.0029	.008	.006	.008
1	----	.011	----	----	.0075
2	----	.0057	----	----	.0052
3	----	----	----	----	.0055
Pure Water (from Ref. 6)	.00033	.00041	.00228	~.0003	~.001

Table 2

Benthic Samples

	Location	Estimated Visibility	Depth	Sample Description
A	(W. of Long Bay near optical Sta. 5)	5 Ft.	30 Ft.	Sandy with a thin (1mm) muck layer on top and interwoven in layers
B	(Scorpion Rock) (Strong surface current into channel)	20-25 Ft.	35 Ft.	Black particulates in sand and fine silt (probably due to dredge)
C	(East Gregerie Channel) (near optical Stas. 3 and 3)	50 Ft.	45 Ft.	Black particulates in sand; a live snail in a shell and a live green leaf plant
D	(Crown Bay) (Strong surface current appears half way up)	35 Ft.	35 Ft. hole	Many black particulates in sand; similar to B
E	(East Gregerie Channel)	20 Ft.	50 Ft.	Coarser sand and black particulates

Table 3

CALIBRATION PANEL DENSITOMETRY

(Brewers Bay Beach, Sept. 5, 1972)

Altitude	Target/ Panel Color	λ = .440μm Transparency Density	ΔD (G - B)	λ = .530μm Transparency Density	ΔD (R - G)	λ = .630μm Transparency Density
0 ft	Sand	0.405	-.217	0.188	.008	0.196
	White	0.430	-.230	0.200	-.02	0.180
	Red	1.677	-.520	1.157	-.957	0.200
	Blue	1.036	.111	1.147	.433	1.580
	Green	1.285	-.524	0.761	.279	1.040
	Gray 2	0.614	-.156	0.458	.156	0.614
	Gray 3	1.090	-.263	0.827	.238	1.065
2000 ft	Sand	0.370	-.068	0.302	-.037	0.265
	White	0.248	.001	0.249	-.071	0.178
	Red	0.933	-.191	0.742	-.450	0.292
	Blue	0.708	.050	0.758	.146	0.904
	Green	0.826	-.232	0.594	.042	0.636
	Gray 2	0.521	-.099	0.422	-.057	0.365
	Gray 3	0.723	-.091	0.632	.016	0.648
4000 ft	Sand	0.470	-.040	0.430	.020	0.450
	White	0.325	-.045	0.280	-.050	0.230
	Red	0.870	-.200	0.670	-.250	0.420
	Blue	0.670	-.155	0.515	.318	0.833
	Green	0.780	-.128	0.652	.166	0.818
	Gray 2	0.480	-.045	0.435	-.135	0.300
	Gray 3	0.720	-.050	0.670	.146	0.816

Table 4

APPARENT REFLECTANCES OF ST. THOMAS HARBOR WATER TARGETS

(Altitude 4000 feet; 1000 hrs; Sept. 5, 1972)

Location	Percent Reflectance		
	λ = 0.440μm	λ = 0.530μm	λ = 0.630μm
Brewers Bay Beach Sand	36.5	41.0	43.0
1	3.5	4.6	1.7
2	6.6	6.1	2.6
3	2.9	3.4	0.8
4	8.3	5.7	1.6
5	9.4	9.3	2.8
5a	12.0	12.9	5.0
6	10.3	11.6	5.4
7	5.2	6.9	4.3
8	3.7	3.9	1.6
9a	14.6	11.6	6.2
9b	12.4	11.6	6.1
9c	9.4	9.4	2.7
9d	5.9	5.2	1.8
Airport Runway (West End)	5.2	6.7	8.0

Table 5

RADIANCE LEVELS OF ST. THOMAS HARBOR WATER TARGETS

Location	RBV Band 1 (.4 to .5μm) Radiance (mw/cm^2/sr)	MSS Band 4 (.5 to .6μm) Radiance (mw/cm^2/sr)	MSS Band 5 (.6 to .7μm) Radiance (mw/cm^2/sr)
Brewers Bay Beach Sand	0.70	1.00	1.30
1	0.067	0.19	0.057
2	0.13	0.25	0.086
3	0.056	0.14	0.027
4	0.16	0.23	0.052
5	0.18	0.38	0.094
5a	0.23	0.53	0.17
6	0.20	0.47	0.18
7	0.10	0.28	0.14
8	0.07	0.16	0.051
9a	0.28	0.47	0.21
9b	0.24	0.47	0.20
9c	0.18	0.38	0.090
9d	0.11	0.21	0.059
Airport Runway (West End)	0.10	0.27	0.26

Table 6

TARGET ILLUMINATION COLOR EFFECTS

Sun Observations - Signal Mountain; 10/6/72

	0725 hrs	0850 hrs	0920 hrs	0950 hrs	6100°K Black Body
λ = 0.433μm	11.8	11.5	12.2	12.4	13.8
λ = 0.533μm	12.5	12.3	12.6	12.5	13.5
λ = 0.633μm	13.6	13.6	13.6	13.6	13.6
Sun elevation above horizon	21°	39.5°	47°	55°	—

Diffuse White Plate Observations

	Signal Mt; 10/6/72			Brewers Bay Beach	Sta. 1
	0920 hrs	0950 hrs	1030 hrs	10/5/72; 1100 hrs	10/5/72; 1448 hrs
λ = 0.433μm	12.3	13.3	12.2	12.7	12.7
λ = 0.533μm	12.5	12.3	12.4	12.4	12.5
λ = 0.633μm	13.6	13.6	13.6	13.6	13.6
Sun elevation above horizon	47°	55°	61.7°	64°	79°

Note: The tabulated values are to a base of 2, as in photographic exposure specifications (i.e., $13.6 \equiv 2^{13.6}$)

Table 7

SKY RADIANCE MEASUREMENTS - SIGNAL MOUNTAIN, 9/6/72, ALTITUDE = 1510 FEET

0745 hrs: Sun Elevation = 28°; Magnetic Bearing = 90°

Sight Elevation Angle		λ = 0.633μm	λ = 0.533μm	λ = 0.433μm
2°	toward sun	14.7	13.4	13.9
8½°	↓	15.5	14.2	14.0
34°	↓	14.6	13.3	14.3
45°	↓	13.6	12.2	12.7
57°	↓	13.5	12.3	12.9
90°	↓	10.1	9.2	11.0
45°	away from sun	10.1	9.3	11.3
9½°	—	11.5	10.0	12.9
N 10½°	—	12.5	11.4	12.2
S 16°	—	10.8	10.0	11.7

0900 hrs: Sun Elevation = 47°; Magnetic Bearing = 105°

11°	toward sun	14.0	9.7	16.6
27½°	↓	14.7	10.4	17.2
56½°	↓	14.4	10.3	16.4
90°	↓	10.9	9.0	13.7
23½°	away from sun	10.7	9.2	14.2
16°	—	11.6	9.7	14.4
N 1°	—	12.0	8.5	15.0
7½°	—	12.6	9.3	15.2
S 20°	—	10.6	8.8	14.1

0930 hrs: Sun Elevation = 55°; Magnetic Bearing = 110°

13½°	toward sun	12.8	10.0	15.6
34½°	↓	14.2	10.2	16.7
90°	↓	11.2	9.2	14.6
N 1°	—	11.6	8.7	14.5
N 9°	—	11.7	8.7	14.7
S 16½°	—	11.0	8.3	13.2

Absolute Calibration

λ = 0.633μm

16.7 ≡ 1.3 mw/cm^2/ster for RBV Band 1

λ = 0.533μm

16.6 ≡ 1.0 mw/cm^2/ster for MSS Band 4

λ = 0.433μm

16.9 ≡ 0.7 mw/cm^2/ster for MSS Band 5

Note: The tabulated values are to a base of 2, as in photographic exposure specifications (i.e., $13.6 \equiv 2^{13.6}$).



FIGURE 1. VIEW OF THE HARBOR AT CHARLOTTE AMALIE, ST. THOMAS, LOOKING SOUTH

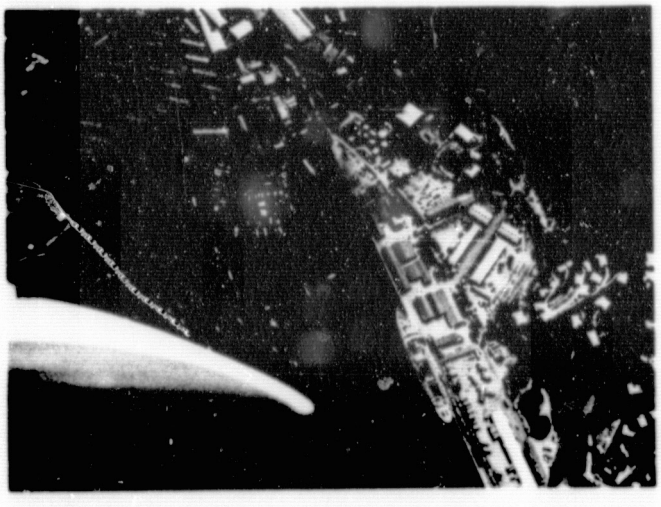


FIGURE 2. AERIAL PHOTOGRAPH OF HARBOR AT CHARLOTTE AMALIE, ST. THOMAS, SHOWING CORAL SAND SEDIMENTS STIRRED UP BY DOCKING SHIP AT RIGHT

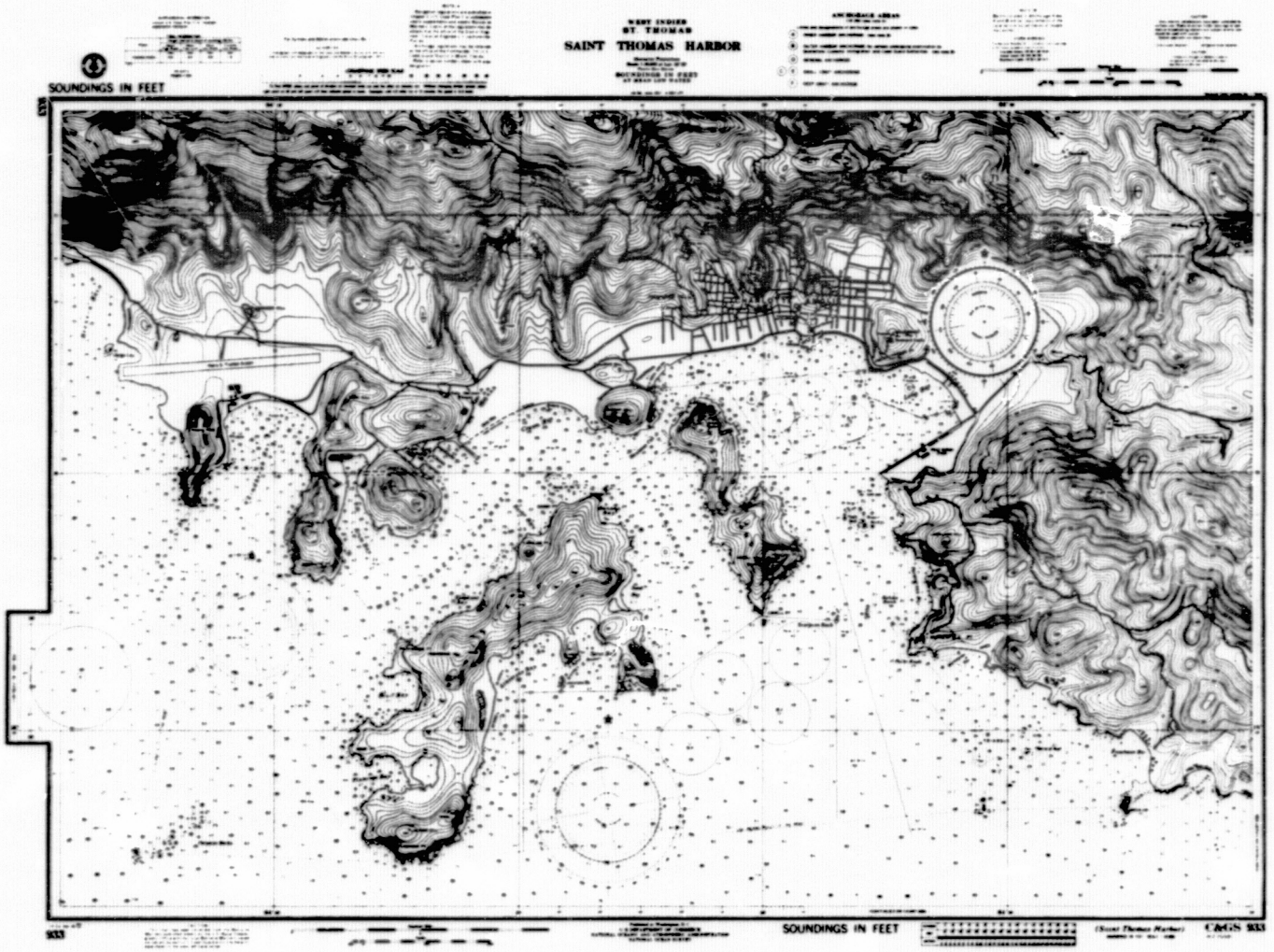


FIGURE 3. C AND GS CHART NO. 933 OF THE ST. THOMAS HARBOR, WEST INDIES SHOWING ENTRANCE CHANNELS AND THE URBAN AREAS

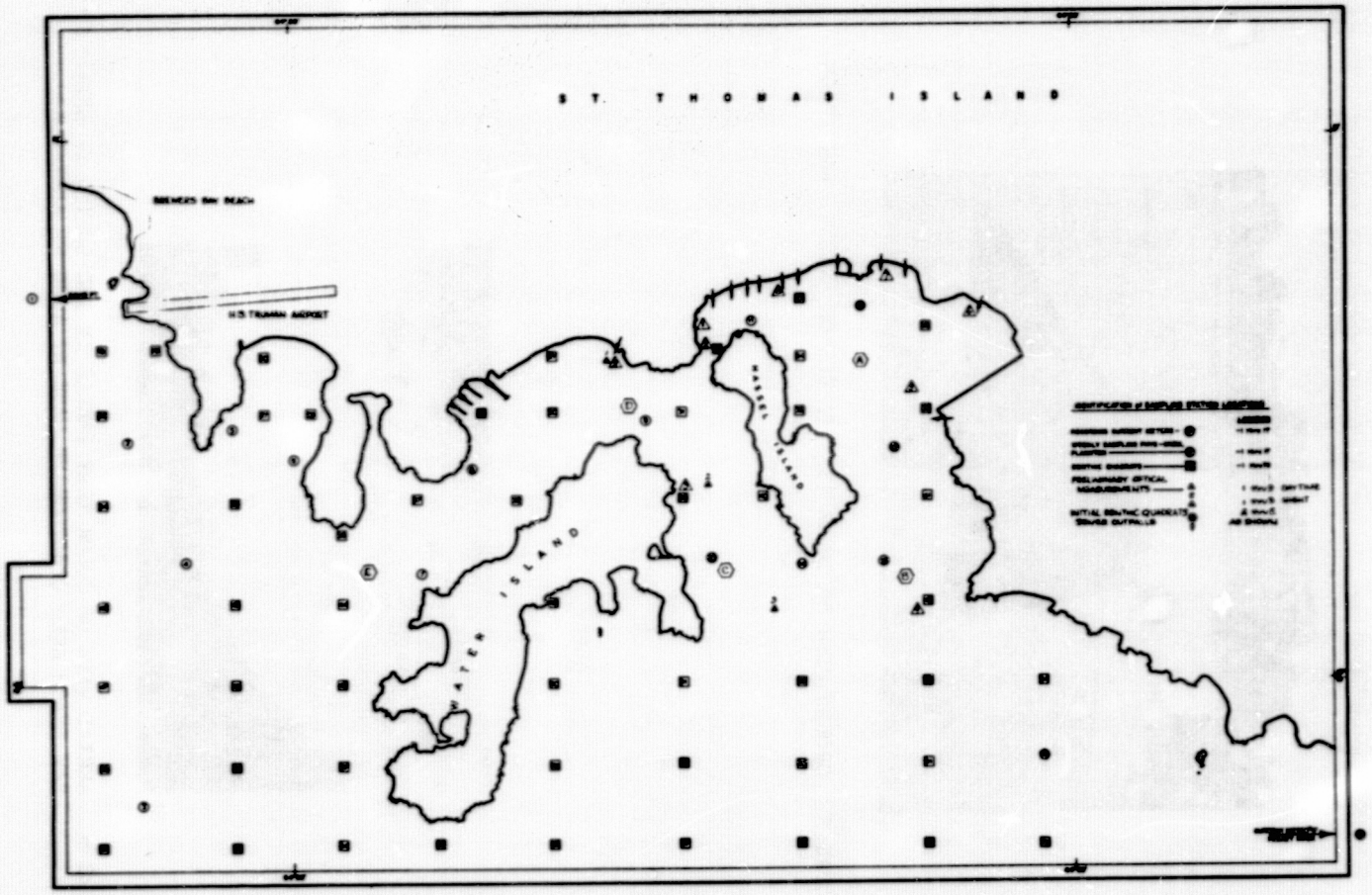


FIGURE 4. OVERLAY FOR C AND GS CHART NO. 933 SHOWING LOCATIONS OF SAMPLING STATIONS FOR GROUND TRUTH PROGRAM

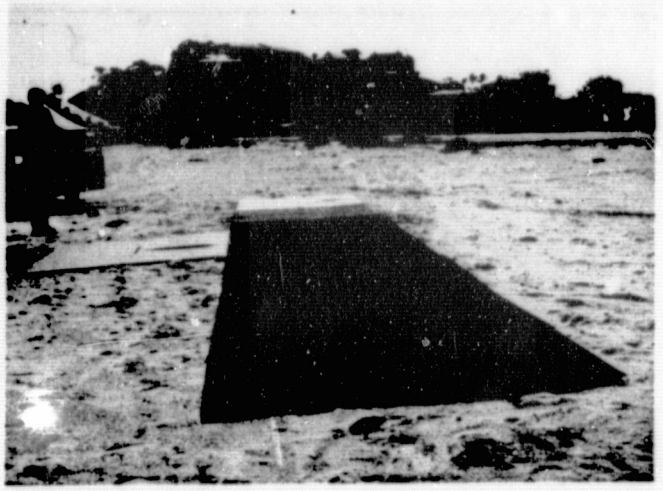


FIGURE 5. GROUND VIEW OF COLOR TEST PANELS ON BREWERS BAY BEACH

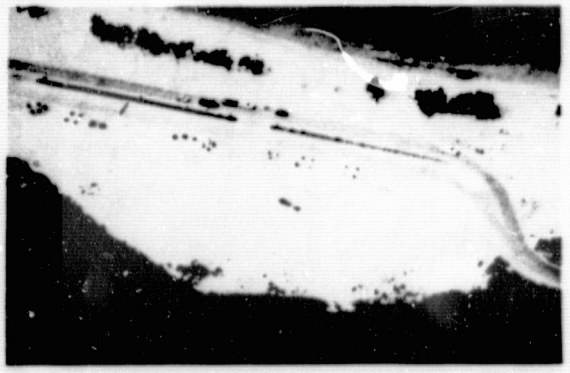


FIGURE 6. AERIAL VIEW OF COLOR TEST PANELS IN THE CENTER OF BREWERS BAY BEACH AREA (PHOTOGRAPH MADE AT 4000 FT ALTITUDE)

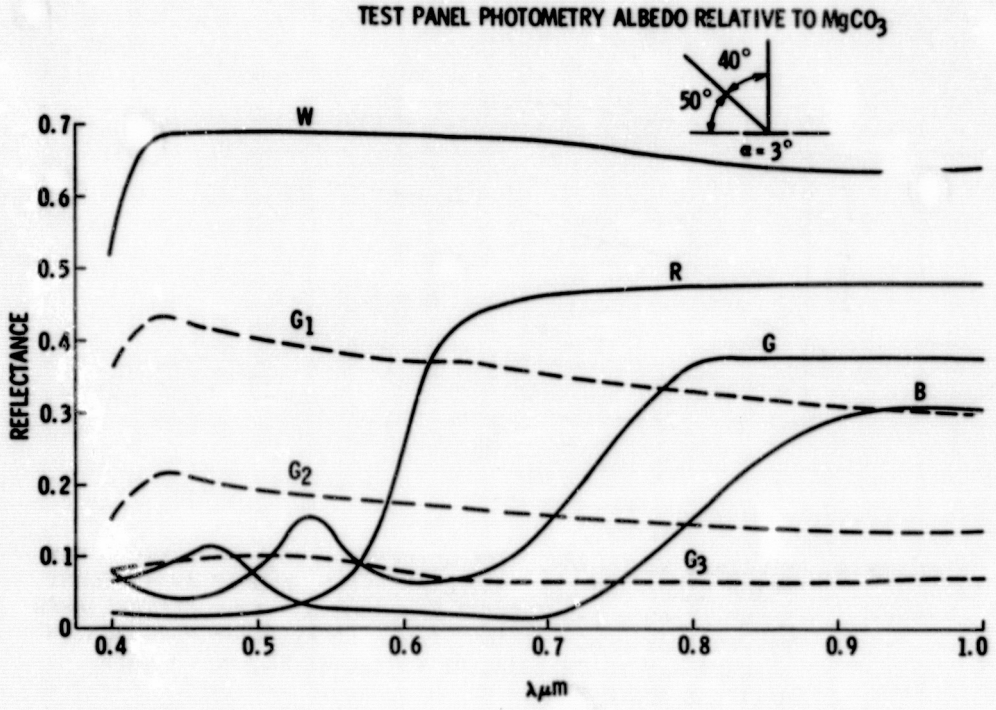


FIGURE 7. SPECTRAL REFLECTANCE (RELATIVE TO $MgCO_3$) OF TEST PANELS AT AN INCIDENT ANGLE OF 40°, AND A PLASE ANGLE OF 3° (W - WHITE; G_1, G_2, G_3 - GRAY SHADES; R - RED; G - GREEN; B - BLUE) (FROM REF. 5)

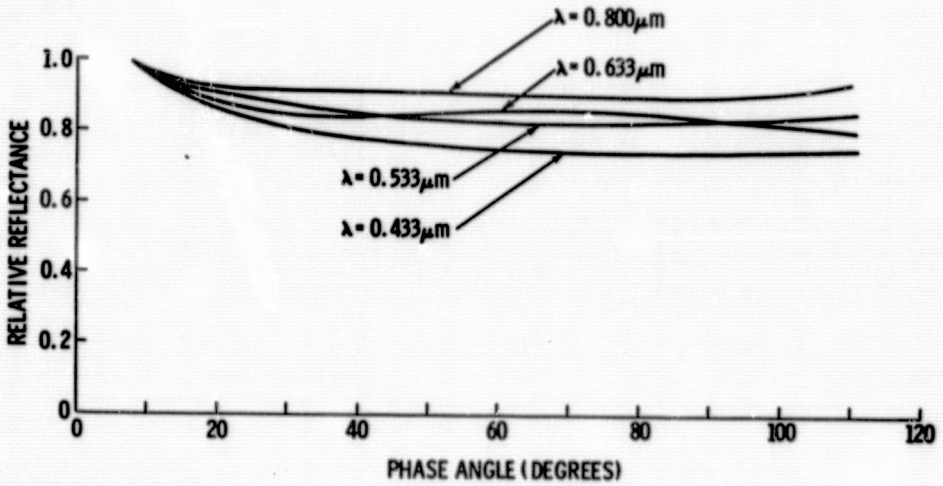


FIGURE 8. SPECTROPHOTOMETRIC PROPERTIES OF 3-M NEXTEL WHITE 110-A-10 PAINT AS A FUNCTION OF PHASE ANGLE AND WAVELENGTH FOR AN INCIDENT ILLUMINATION ANGLE OF 40° (FROM REF. 5)

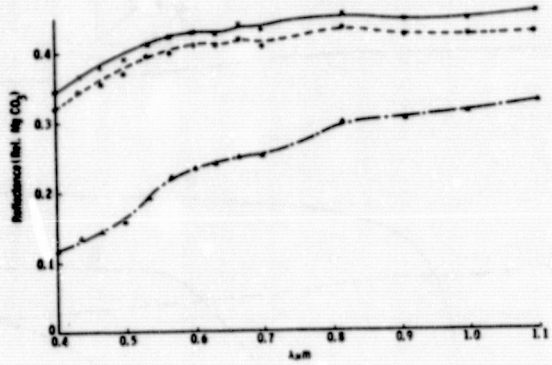


FIGURE 9. SPECTRAL REFLECTANCE (RELATIVE TO $MgCO_3$) OF BREWERS BAY BEACH SANDS AND CAPE HATTERAS BEACH SAND AT AN INCIDENT ANGLE OF 40°, AND A PHASE ANGLE OF 3° (—— CENTRAL AREA BREWERS BAY BEACH AT TEST PANEL LOCATION; – – – AREA ON BREWERS BAY BEACH ADJACENT TO THE WATER; – · – CAPE HATTERAS BEACH SAND)

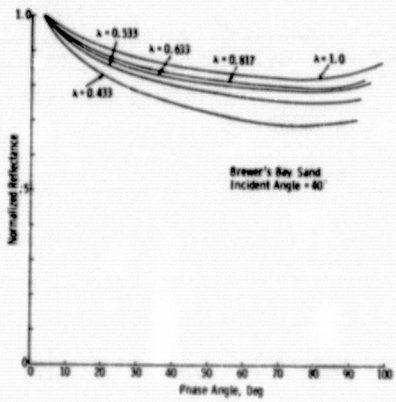


FIGURE 10. SPECTROPHOTOMETRIC PROPERTIES OF BREWERS BAY BEACH SAND FROM TEST PANEL LOCATION AT AN INCIDENT ANGLE OF 40° AND A PHASE ANGLE OF 3°

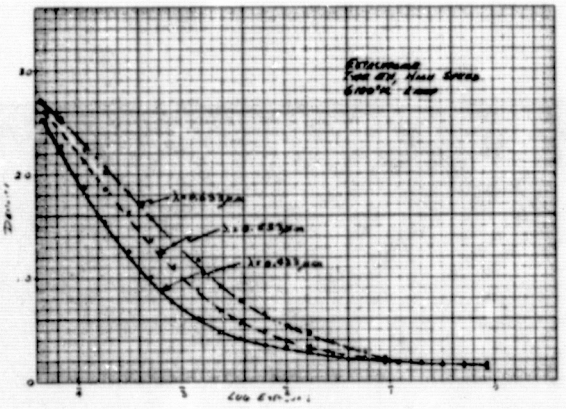


FIGURE 11. INTEGRAL DENSITY CURVES FOR KODAK HIGH SPEED EKTACHROME FILM, TYPE EH OBTAINED ON JOYCE-LOEBL MICRODENSITOMETER

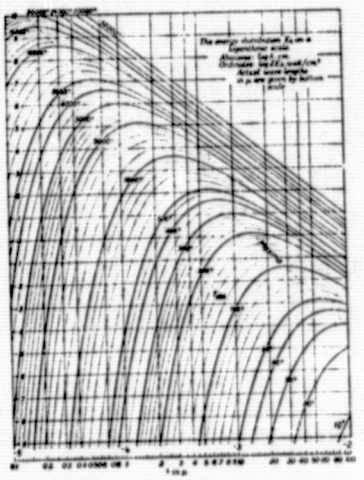


FIGURE 12. BLACK BODY ENERGY DISTRIBUTION CURVE (FROM REF. 8)

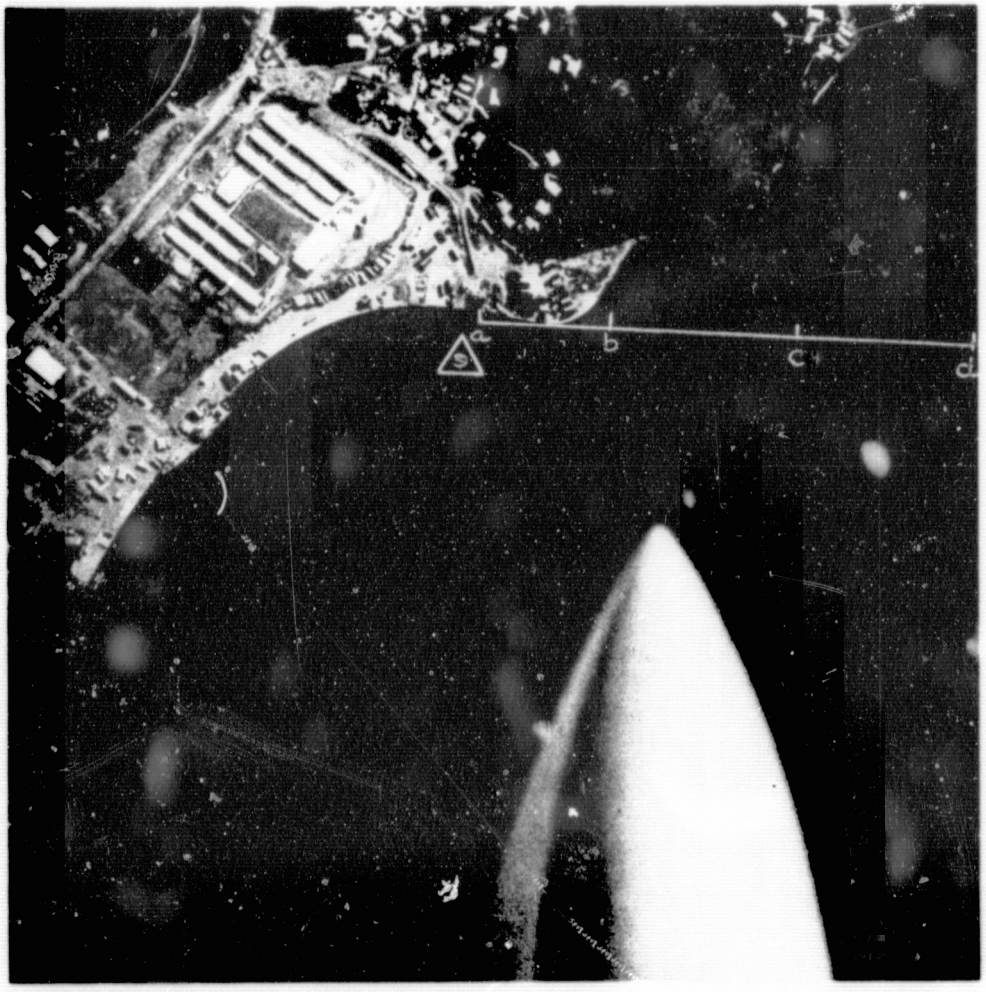


FIGURE 13. TRANSECT LOCATION AT CROWN BAY AND EAST GREGERIE CHANNEL IN ST. THOMAS HARBOR SHOWN ON TRUE COLOR EKTACHROME AERIAL PHOTOGRAPH (BLACK AND WHITE RENDITION)

UTILIZATION OF THERMAL INFRA-RED GROUND MEASUREMENTS

FOR DETERMINATION OF ADEQUATE SURVEYING PERIODS IN REMOTE SENSING

F. Bonn, P. Clément and collaborators:
J.F. Gadbois, C. Jalbert, M. Lajeunesse, C. Trudel

Laboratoire de géographie physique
Université de Sherbrooke
Sherbrooke, Québec, Canada

ABSTRACT

This paper deals with daily and seasonal variations of emissivities in the 9.5 - 11.5 microns spectral range on grass covered and bare ground areas in Southern Quebec, and their consequences on the interpretation of documents.

RESUME

Les variations journalières et saisonnières de l'émissivité dans la bande spectrale 9.5 - 11.5 microns ont fait l'objet d'observations sur des surfaces nues et couvertes de végétation herbacée dans le sud du Québec. Ces dernières montrent de considérables variations dépendant de leur état hydrique et biotique, alors que le comportement des premières se rapproche de celui d'un corps noir. Les conséquences de ces faits sur l'interprétation des documents sont examinées.

METHODS

The outgoing thermal infrared radiation has been measured by means of a Barnes PRT 5 special radiation thermometer in the 9.5 - 11.5 microns spectral range, on two experimental plots located on the Sherbrooke University Campus.

The 9.5 - 11.5 microns spectral range has two advantages compared to the 8 - 14 microns standard execution: 1) it is less sensitive to atmospheric moisture variations, 2) the bolometer filter transmittance curve sharply cuts the spectrum, without any internal minimum under 0.95.

The experimental plots have been chosen because they are representative of the surrounding area and equipped with soil moisture and temperature measuring devices.

Measurements have been taken in order to compare a semi natural meadow with a bare ground area. Both plots are located on a southwest facing slope mantled byasilty till deposit.

The following datas have been measured, along with the outgoing thermal radiation:
- incident solar radiation,
- soil temperature profiles,(thermistor probes 0,5, 10, 20 and 30 cm depths.)
- soil moisture (gypsum resistor blocks at 5 cm depth).
- dry and wet bulb air temperatures
- environmental changes (runoff, surface and subsurface sediment exportation, surface modifications).

Day and night measurements have been made at short intervals (2 hours or less) during the following periods:

May 11-15 1971, July 9-13 1971, September 29-October 2 1971, May 17-23 1972, July 09-14 1972, July 31-August 05 1972, August 27-September 01 1972.

RESULTS

Until now, the most instructive results have been obtained from comparison between blackbody temperatures (T_{bb} and true surface temperatures T_s).

Regression equations between T_{bb} and T_s vary

a) from one plot to the other
b) according to the season (Table 1).

TABLE 1

Regression equations, and correlation coefficients (r)

(T_{bb} vs T_s)

	P.C. (grass covered plot)		P.D. (bare plot)	
May 1971	y: - 15.29 + 2.42 x	r: 0.86	y: - 4.51 + 1.27 x	r: 0.92
July 1971	y: 0.95 + 0.78 x	r: 0.90	y: - 7.96 + 1.27 x	r: 0.93
Sept. 1971	y: - 2.01 + 1.12 x	r: 0.94	y: 0.40 + 0.92 x	r: 0.91
May 1972	y: 5.21 + 1.62 x	r: 0.91	y: - 0.99 + 1.12 x	r: 0.94
July 1972	y: - 9.45 + 1.54 x	r: 0.90	y: - 1.30 + x	r: 0.96
August 1972	y: - 14.89 + 1.68 x	r: 0.84	y: - 3.02 + 1.03 x	r: 0.92
Aug.-Sept. 1972	y: - 18.97 + 1.97 x	r: 0.89	y: - 7.26 + 1.29 x	r: 0.95

In most cases regression slopes for the grass covered plot are steeper excepted for July 1971. At this time, the soil moisture was very low whereas for all other periods, it was around field capacity (F. Bonn, P. Clément, 1972).

During all measuring periods, the bare plot reacts as a quasi blackbody. The regression slopes vary only slightly with the season.

On the opposite, the grass covered plot shows much more variations. During spring, emissivities are maximum. At this time following the snowmelt, the soil watertable is very high, and a wet straw mat lies on the ground (Fig. 1 and 2).

Hourly variations patterns show that T_{bb} rises and decreases faster than T_s on both plots, like a hysteresis type phenomenon (Fig. 3). This effect is stronger in May. No verified explanation has been yet found.

SUGGESTED APPLICATIONS

Thermal infrared datas can be used for two different purposes: differenciation of bodies and ecognition of true surface temperatures.

According to our observations on grass covered and bare ground terrain the first goal can be more efficiently obtained by measurements around noon, when maximum T_{bb} values are attained. However, the differences are smoothed out during scattered shower periods. During very dry soil conditions, peak readings are higher on the bare ground plot. The opposite occurs when the soil is humid. The knowledge of previous climatic conditions is therefore necessary for correct interpretation.

On the other hand, for recognition of true surface temperature, measurements appeared to be more suitable at night in May, in the evening in July, around noon in August, and in the early afternoon in the beginning of September, for grass covered surfaces. Most of the time, the bare ground surface was at a temperature which showed only little difference with the emitted T_{bb}. (Table II).

CONCLUSIONS.

These observations show the great variability of emissivities on vegetation covered surfaces, and incite to caution when interpretating thermal infrared datas. For example, we noticed that wind speed variations were associated with rapid T_{bb} fluctuations, the amplitude of which could attain 2 to 5 degrees K, on the grass covered plot. More information is needed about various terrains and their seasonal behaviour.

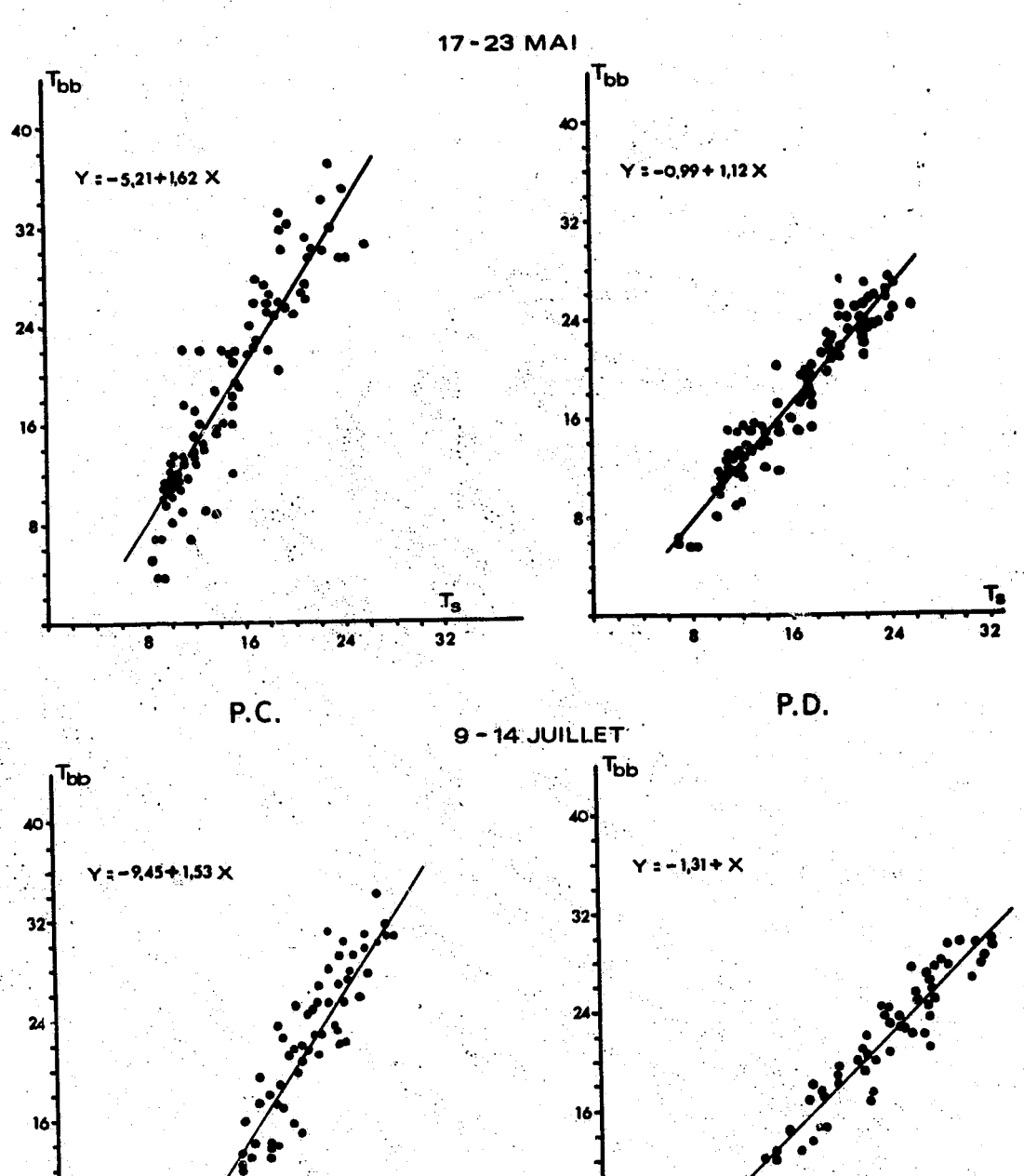


Figure 1: Blackbody temperatures vs surface temperatures, May and July 1972.
PC: grass covered plot PD: bare ground plot Temperatures in °C

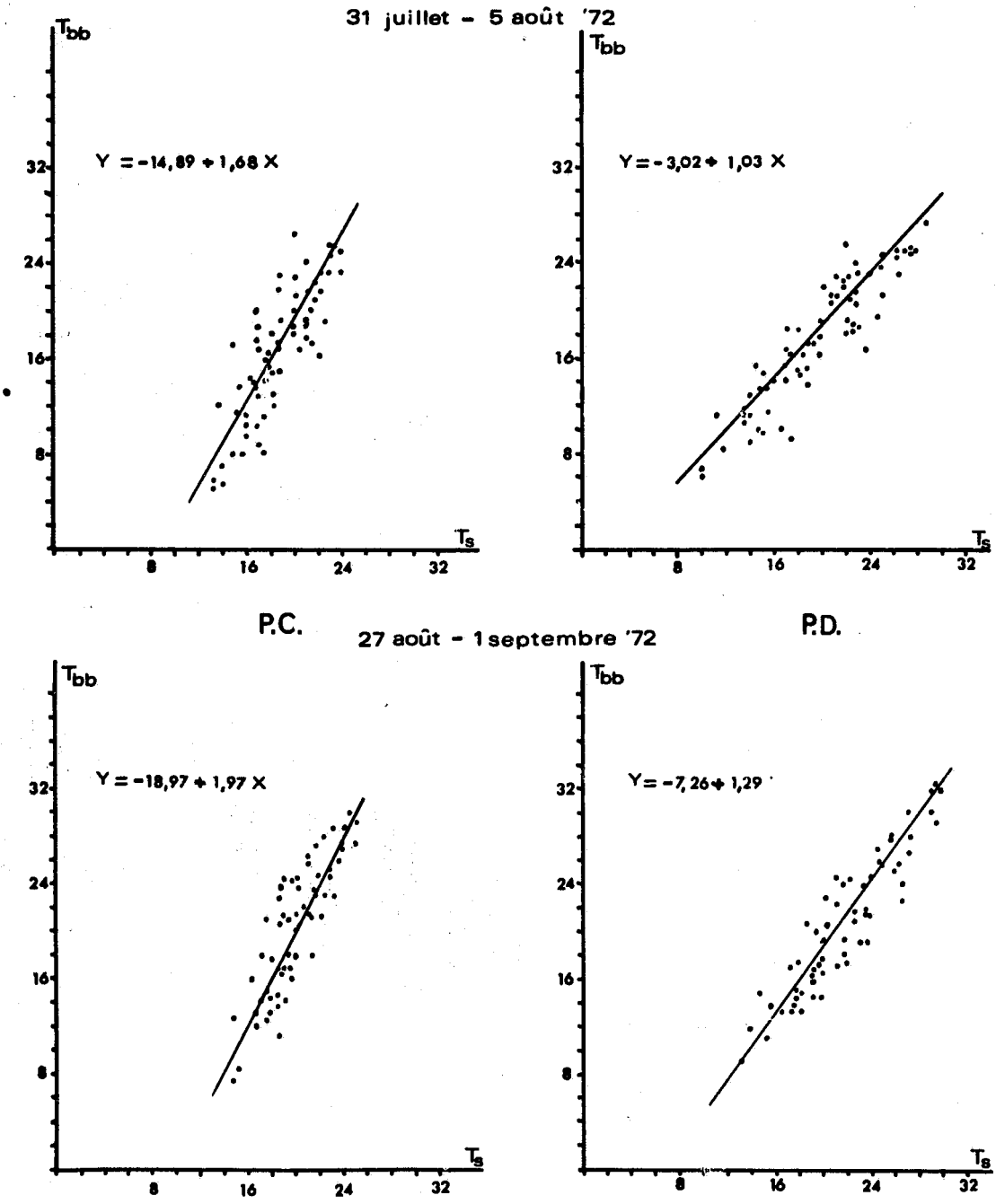


Figure 2: Blackbody temperatures vs surface temperatures, July-August and August-September 1972.
PC: grass covered plot PD: bare ground plot Temperatures in °C.

REFERENCES

(1) D. Auding, R. Kanth, Estimation for Sea Surface Temperature from Space, Remote Sensing of Environment. 1, pp. 217-220, 1970.

(2) F. Bonn, Applications de la radiométrie infra-rouge thermique à la détection de phénomènes géomorphologique superficiels, Comm. 39e Congrès de l'ACFAS, Sherbrooke, 1971.

(3) F. Bonn, et P. Clément, Etalonnage au sol sur parcelles expérimentales d'un radiomètre Barnes PRT 5 dans la fenêtre 9.5 - 11.5 microns, 1er colloque canadien de télédétection, Ottawa, février 1972.

(4) A. Hadni, Elements of Modern Physics applied to the study of the Infrared, Pergamon.

(5) K.J.K. Buettner, C.D. Kern, The Determination of Infra-Red Emissivities of Terrestrial Surfaces, Jal of Geophysical Research, Vol. 70, #6, March 1965.

(6) J.O. Mattson, Thermal Pattern in the Landscape recorded with Infra-red Technique and Simulated in Model Experiments, Geografiska Annaler, 51 A, #4, 1969.

(7) R.B. Platt, J.F. Griffiths, Environmental Measurement and Interpretation, Reinhold, 235 p., 1965.

(8) J. Pouquet, Géomorphologie et Ere Spatiale, Zeitschrift für Geomorphologie, 13, #4, p. 414-471, 1969,

(9) J. Pouquet, Les Sciences de la Terre à l'heure des Satellites, Coll. Sup., P.U.F., 259 p., 1971.

(10) C.W. Rose, Agricultural Physics, Pergamon, 230 p. 1966.

(11) J. Tricart et A. Husson, Quelques apports des enregistrements infra-rouges à la connaissance du milieu physico-géographique, Annales de Géographie, été 1972.

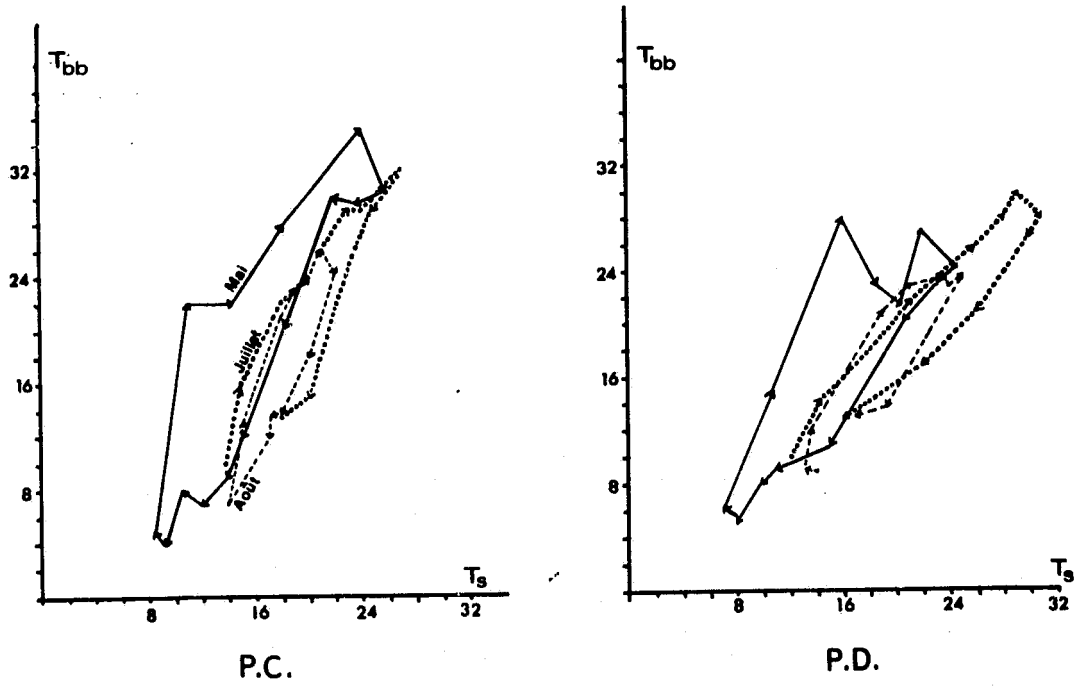


Figure 3: Sample days showing different behaviours during rising and decreasing temperatures (hysteresis effect)

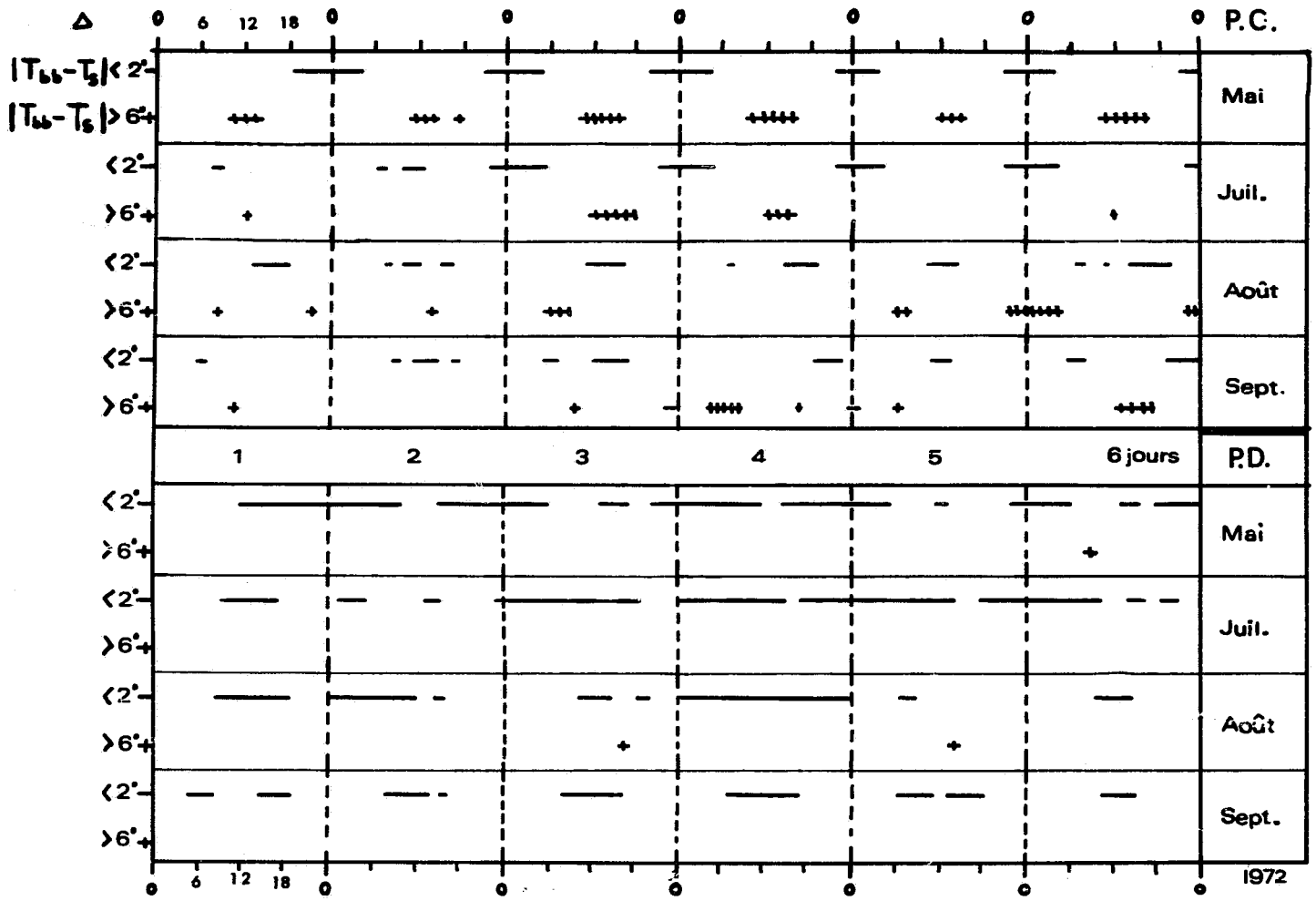


TABLE II : Differences between T_{bb} and T_S

REMOTE SENSING FOR DEFINING AQUIFERS IN GLACIAL DRIFT

by

Victor I. Myers and Donald G. Moore
Remote Sensing Institute
South Dakota State University
Brookings, South Dakota

INTRODUCTION

The economy of much of the glaciated portion of the middle western states is greatly influenced by the availability of ground water. Shallow aquifers, containing extensive ground-water reserves which are continually recharged to varying degrees, occur throughout the region. The bottoms of many of these shallow aquifers are less than 30 m below the surface. Their thickness may vary from only a few meters to as much as 25 m or more. The water quality is generally good. Application of remote sensing techniques may provide part of the information required to map these shallow ground-water reserves.

Aquifers can seldom be detected directly by using remote sensing. However, there are certain properties of aquifers and their associated features which influence reflected and emitted radiant energy. Mapping surficial geology by interpreting surface features is an important part of ground-water surveys. Also, thermodynamic considerations show that a shallow aquifer might form a heat sink that influences and modifies the temperature effects of heat at the land surface and within the crust.

This project is supported by the U. S. Geological Survey under Contract No. 14-08-0001-12510. The District USGS office at Huron, South Dakota, the South Dakota State Geological Survey and U.S. Bureau of Reclamation furnished well logs and historical information and provided valuable consultation. The National Aeronautics and Space Administration provided high altitude photographic coverage of the sites.

The objectives of this study were to determine the properties of shallow aquifers and related features that influence electromagnetic energy, to determine how these properties can be detected remotely, and to establish remote sensing procedures for aiding in ground-water mapping.

Historical Ground Water Studies

Aerial photography has been used for some time as a geohydrologic mapping tool for locating ground water. Howe (1958) lists six steps for locating ground water by photo-interpretation. Procedures were outlined by Quinn (1963) for using aerial photos for locating ground water in remote and inaccessible areas.

Vegetation vigor may be useful as an indicator of ground water for near-surface water. Certain types of vegetation, particularly phreatophytes, show a contrast in vigor in accordance with depth to water (Robinson, 1958).

In recent years a number of investigators have used thermal measurements for ground-water mapping, although most of these have been ground-based surveys, and temperature measurements have been made below the surface. Birman (1969) reported on investigations of a number of geologic terrains and climates. He found that shallow earth temperatures can be related to the occurrence of ground water. Significant studies were made by Cartwright (1968, 1970) in Illinois, in which he related thermal anomalies measured under the ground surface to characteristics of aquifers and overburden.

Applications of geothermal techniques to exploration of ore deposits by Lovering and Goode (1963) and Lovering and Morris (1965) point to the difficulties in interpreting shallow temperature measurements within the zone affected by surface-derived effects (diurnal and annual temperature variation).

Numerical modeling of a ground water thermal regime in a glacial complex was conducted by Parsons (1970). He found differences in temperature of ground water in two environments, and

through modeling concluded that the variations are related to differences in thermal conductivities of the flow media, to variations in the magnitude of the ground-water flux, and to spatial variations in the water table temperature.

PROCEDURE

Description and Location of Study Areas

Two areas are being studied having contrasting aquifer conditions. Shallow aquifers in the James River Basin (Beadle County) are intermittent with intermingled layering of sands and gravels and finer materials. Hedges (1968) and Howells and Stephens (1968) have written complete descriptions of Beadle County geohydrology. The aquifer in the Sioux River Basin (between Sioux Falls and Dell Rapids) on the other hand, consists of fairly coarse unconsolidated materials in well-defined layers (Flint, 1965). Figure 1 is a map of eastern South Dakota showing where shallow aquifers are known or suspected to occur, and delineating the study areas.

Remote Sensing Data Collection

Aircraft missions were flown over lines selected by the project cooperators. Flightlines for the James River Basin study (Beadle County) covered select areas representative of geohydrologic conditions. Flightlines for the Sioux Basin cover the entire watershed from north of Dell Rapids to south of Sioux Falls.

Low altitude missions were flown as required with the Remote Sensing Institute (RSI) aircraft at an altitude of about 3040m AGL. High altitude missions were flown by NASA at an altitude of 18,300m AGL with the RB-57F aircraft. Scheduling of aircraft missions for timely coverage is very difficult. For example ideal conditions for conducting predawn flights to obtain thermal imagery for identifying aquifers are rare in areas away from arid deserts and cannot be predicted more than a few hours prior to flight time. Therefore it is necessary to have an aircraft available on a standby basis to obtain a successful predawn mission. Missions for thermal mapping were scheduled in accordance with guides as presented by Moore and Myers (1972). The sensors and spectral ranges used to collect the aerial data are shown in Table.1.

Table 2. Aerial data collection.

Variables	Spectral Range	Method of Collection
Photography - Four Cameras		70mm Hasselblads (50mm F.L.)
Black & White Film-filtered		
Green - 58	0.47μm → 0.61μm	2402 Film
Red - 25A	0.59μm → 0.70μm	2402 Film
Near Infrared - 89B	0.68μm → 0.90μm	2402 Film
Color Reversal Infrared 15G/30m	0.51μm → 0.90μm	2443 Film
Incoming Radiation	0.35μm → 1.15μm	2443 Film
Reflected Radiation Filtered		Solameter
Blue - 47B	0.37μm → 0.50μm	
Green - 58	0.47μm → 0.61μm	
Red - 25A	0.59μm → 0.70μm	
Near Infrared - 89B	0.68μm → 0.90μm	
Thermal Infrared Radiation	4.5 μm → 5.5 μm 8.7 μm →11.5 μm	Daedalus Line Scanner
Surface Temperature	8.0 μm →14.0 μm	Precision Radiation Thermometer
Haze Condition		Evaluate
Cloud Type and Condition		Evaluate
Cloud Cover		Evaluate

No single remote sensing sensor or method is sufficient for locating aquifers. Therefore, this report describes several approaches, all of which compliment one another. Investigation procedures using photography and thermal infrared were utilized. Multistage imagery from high and low altitudes were included Indirect indicators of aquifers investigated included geohydrologic units, soil associations, vegetation type and vigor, thermal patterns on the land surface, ice melt on streams, and temperature changes in streams.

Seasonal missions were flown to assess time-dependent phenomena that may help define aquifer and related plant and soil conditions. Diurnal flights were made at two times: (1) predawn for soil moisture and thermal characteristics of aquifers and recharge areas, and (2) midday for photography and thermal sensing of plants.

The most valuable ground-truth data available were the results of various geology and water-resources investigations, along with profile data contained in well logs. Ground truth data gathered at the time of overflights included the following: temperature and depth to water table in selected observation wells, vegetation and soil type and condition, soil moisture, soil temperature, and climatological information.

A temperature log has been recorded monthly by USGS District Office Personnel in an artesian well (155 m depth) located in Beadle Co. The temperature profile measurements were to monitor changes in water temperature with depth and time. Since the well remained capped between measurements, it was likely that water profile temperatures were very close to soil profile temperatures. The artesian well flows very slowly, when uncapped, during periods of measurement.

Streams in the glaciated area under study often intersect shallow aquifers. Under certain optimum conditions, flow of ground water from an aquifer into a stream may cause an increase in the water temperature that may permit detection using a thermal scanner. Also, inflow of warm ground water to a stream may cause ice melt. This may provide evidence of the stream intersection with an aquifer. These hypotheses were investigated as part of the studies.

Soil temperature data for studying the occurrence of aquifers were obtained from predawn missions flown on May 7, July 21, August 26 and October 12, 1971. The locations of logged exploration wells were plotted on thermal imagery and optical densities of transparencies measured at those points. Statistical correlations were computed using simple linear correlation techniques to determine the dependence of surface temperature on the independent variable, aquifer thickness.

RESULTS AND DISCUSSION

Photography As An Indicator Of Surficial Geology

Identifying land forms in a glacial complex commonly defines the transport mechanism involved in their development. The transport mechanism usually limits the type and sorting of materials present which indicates the transmissibility and water storage characteristics of the various water-bearing units. Reflectance properties of various geohydrologic units vary with type of material, topographic position, moisture content, vegetative cover, etc., which also vary with time. The type of material and topographic position are relatively constant. The land-surface moisture content will frequently be masked by the crop canopy; however, the soil moisture content may be revealed indirectly through reflectance of the crop canopy. This portion of the research program was to determine if land-surface reflectance (reflectance from crop canopy with associated background reflectance) could be used in machine-density analysis to discriminate surficial geologic materials using ERTS and other satellite data.

The type of vegetation adapted to a specific area has limits basically set by the climate of the region. Soils developing from specific parent-geologic materials then impose local edaphic restrictions on the type of vegetation adapted to these various land forms. Table 2 defines the major soil associations in Beadle County. In addition, it presents some of their physical properties and the type of crops generally adapted to these soils.

The time-dependent planting, growth, and harvesting characteristics of crops should yield reflectance patterns on imagery which may discriminate among types of supporting land forms. Two methods for evaluation of reflectances from selected areas in Beadle County were used to determine if land-surface reflectance can be used to discriminate among various surficial geologic classes.

Table 1. Soil associations, their physical characteristics and general crop capabilities.

Feature	Soil Association*				
	Beadle	Houdek-Prosper	Peever-Cavour	Blendon-Enet	Lamo
Soil texture					
surface	loam	loam	clay loam	loam to sandy loam	silty clay loam
subsoil	clay loam	clay loam	heavy clay loam	loam to sandy loam	silty clay loam
Land form	ground ε end moraine	ground ε end moraine	ground ε end moraine	terraces and outwash plains	alluvium
Topography	nearly level to gently undulating	gently undulating to undulating	nearly level to gently undulating	nearly level to gently undulating	level
Parent material	till	till	till	alluvium & outwash	alluvium
stoniness	yes-local	yes-local	yes-local	no	no
Occurrence of claypans	yes	yes	yes	no	no
Drainage (gen.)	well drained	mod. well to well drained	mod. well drained	well drained	poorly drained
runoff	slow-medium	mod. to rapid	slow to medium	slow	
permeability	mod. to mod. slow	mod. to rapid mod.	mod. slow	mod. rapid to rapid	
Estimated infiltration rates (in./hour)(after Moxon 1965)	0.1 → 0.2	0.1 → 0.2	<0.1	>0.7	0.2 → 0.7
Crops generally adapted	small grains row crops	cropland hayland	small grains hayland pasture	cropland hayland pasture corn legumes	hayland pasture

*After Westin et al (1967) and Derscheid and Westin (1968)

The first method utilized color-encoding density slicing of Ektachrome infrared (2443) 70-mm transparencies which were collected May 6, May 27, June 22, July 2, and July 16, 1971 by the RSI aircraft at 3030 m AGL. The geologic settings were an end-moraine complex, outwash plain, and alluvium (James River trench). Each frame was analyzed in total so the resolution elements were frame size (3.2 km on a side). An analysis of variance of the data revealed that significant differences occurred between geologic units. The greatest spread in reflectance differences among geologic units was for the June 22 date when a red band-pass filter (corresponds approximately to the infrared layer) was used on the color analyzer. In addition, significant interactions of geologic material with time and filters occurred indicated that both of these factors could be varied to derive more information. Changes in snow cover, reflectance changes after a rainfall, seasonal variations in crop growth, and other time-dependent reflectance changes may all be evaluated for broad regions using low resolution data such as Nimbus, ITOS, etc. For these applications, analysis of data for many times will probably yield more information than a single analysis of higher resolution data.

The second analysis procedure utilized resolution elements corresponding approximately to ERTS-1 (60-m diameter circular land measurement). The analysis pursued incorporation of procedures which evaluated more than one feature at a time. Six fields (3 alfalfa and 3 grass) from each of seven different geologic classes (as mapped by Hedges, 1968) were selected. Twenty random density measurements were taken with a Macbeth TD404 spot densitometer for each of four densitometer filters (red, blue, green, neutral). The fields selected for analysis of the May data were again used for August. The features used for classification are presented in Table 2.

Table 2. Features and their transformations used for classification (densitometer filters used with Ektachrome infrared film).

Band-pass densitometer filters	Transformations	
a. Neutral (N)	e. B/R	i. (R - B)/N
b. Red (R)	f. B/G	j. (G - B)/N
c. Green (G)	g. R/G	k. $\frac{(R - G - B)}{N}$
d. Blue (B)	h. $\frac{(R - B)}{G}$	l. $\frac{(R - G)}{(R+B+G)}$

Various combinations of the feature sets were used to determine the optimal classification results utilizing the preceding procedures. Up to 94.4% correct classification was obtained using the K-class classifier (Zagalsky 1968)when all twelve features were used for the August grass-covered fields. Increasing the number of features, increasing the number of data collection times, and using data averages all increased classification results. This type of data analysis can be incorporated into computer data processing with the final product a thematic map of the region in question. It depends on first recognizing the crops in different fields. Then the fields are classified into their various geologic settings.

Emittance as an Indicator of Aquifer Properties

Seasonal flights were made over the Sioux Basin study area to determine the optimum season for conducting thermal sensing studies. Figure 2 shows thermograms which exhibit surface temperature contrasts as observed seasonally. The August 26 imagery is an illustration of the thermal response that can be recorded under favorable weather and water table conditions. The depth to water table varied from 1.5-4.5 m in August. It shows a broad cool pattern within the flood plain. This anomaly was not present on the thermograms for the other dates. Correlations of film to density to well log data indicate that for the August thermogram a significant correlation (0.05 significance level) was obtained for gravel thickness in the 0-15 m layer (81 degress of freedom).

The response of the land-surface temperature to aquifer properties, as indicated on the August 26 imagery, is mainly a function of ΔT, (the temperature difference between the surface and depths less than annual damping), the thermal diffusivity, and meteorological conditions. The latter consists mainly of radiation conditions and wind that produces produces turbulent mixing of air at the ground-air interface and resultant transfer of heat from the soil to the air (Landsberg and Blanc, 1958).

From both theoretical predictions and observed anomalies, it appears that late August or early September is the period most applicable for temperature sensing of shallow aquifers.

Surface Plant and Soil Conditions Influencing Temperatures

Seasonal and diurnal fluctuations of soil temperature greatly depend on the plant cover, its character and changing height. Land use patterns thus have an effect on temperature anomalies, as can be seen in Fig 2. However, the anomaly present on the August predawn imagery that is apparently due to aquifer properties extends over farms with a diversity of land use and tends to override those anomalies due to land use. It was observed by Bouyoucos (1916) and Chang (1958) that the mean annual temperature of extremely contrasting conditions, such as a wet bog and a well-drained sand, are practically identical. From these and other studies it seems that land use does not influence the mean annual soil temperature appreciably and that land use temperature patterns are diurnal or seasonal in nature.

Daytime thermal anomalies present quite a different pattern than night time anomalies. Daytime surface heating is directly or indirectly provided by incoming solar radiation. Due to differential evapotranspiration rates, ground shadings, and albedos of various soil and crop surfaces, thermal patterns associated with subsurface conditions (if present) are masked. The response of surface temperature to incoming radiation for the same area shown in Figure 2 is illustrated in Figure 3. The daytime imagery shows little or no evidence of thermal anomalies that could be associated with aquifer properties.

Soil Temperature Fluctuations and Variability With Depth

Carson (1961) presented results from theoretical calculations which indicate that the depth of penetration of annual temperature fluctuations should exceed the depth of penetration of diurnal temperature oscillations by a factor of 19. However, the actual ratio is greater, because thermal conductivity normally increases with depth since porosity usually decreases with depth.

Field investigations of the depth of damping of temperature fluctuations have been conducted by Penrod and Stewart (1967) and Lovering and Goode (1963). The suggested depths to which air affects ground temperatures varied considerably between investigations (from 9 to 39 m). At northern latitudes depth of penetration of annual temperature oscillations is greater than at temperate and southern latitudes. Theory predicts the time of maximum and minimum temperature is delayed by 20-30 days per meter of depth. The depth of damping of the annual wave cannot be determined in this case until several test wells can be drilled and temperature-measuring devices installed at various depths for frequent monitoring.

Thermal Regime of Well

Temperature measurements of soils and geologic materials, such as those described above, are difficult to obtain to any considerable depths and thus are nearly non existent. An indirect method of making temperature profile measurements is to measure temperature of relatively undisturbed water in a well. Such measurements were made periodically to depths of 30 m or more in a well near Huron.1/ The well is a capped artesian well, cased to a depth of 158 m. When the well is uncapped, water barely runs over the top of the casing. Water temperature is measured at various depths by lowering a temperature logger into the well. Figure 4 shows an example of the temperature logs.

A number of factors may influence the temperature of the water in the well such as density mixing of water, thermal conductivity of the well casing, and other factors; however, the temperature logs give qualitative data that are helpful for (1) checking theory and (2) planning the optimum times for conducting remote sensing missions when maximum gradients for heat flow to the land surface exist.

Spatial Variability in Surface Temperatures

Some differences in surface temperatures appear between areas of the same logged aquifer thickness in the August 26 imagery of Figure 2. Any one of several phenomena could be responsible for this apparent inconsistency. The location of an area with respect to the principle recharge sources is likely to influence the ground water temperature. Shallow ground water generally becomes warmer as it moves away from its source.

In the general case, water is in motion, and its thermal effects are increased by its history from the source. Two very important aspects are that water moves down gradient and that in many

1/ Data gathered by Mr. E. LeRoux of U.S. Geological Survey State Office, Huron, South Dakota

regions the maximum precipitation occurs in early spring. For both of these reasons, moving ground water has a cooling effect, and lower temperature can probably be related to higher transmissibilities and more rapid movement of the ground water.

It may be possible for material, logged as unconsolidated material with high transmissibility, to be relatively isolated from a recharge area by intervening fine-textured materials. Ground water in such an area would not be continuously cooled by recharge.

Most computations and measurements of temperature with depth have been under nearly static ground-water conditions, or for non-saturated unconsolidated materials. Birman (1969) has shown that the presence of ground water creates an enormous effect in the thermal environment. Water has very large specific heat and higher conductivity that does dry unconsolidated sediment. The presence of water in unconsolidated materials of high porosity markedly changes the thermal constants of the material. Whether or not the water is in motion must be considered in the interpretation of its effect. If completely stagnant and shallow enough to be within the penetration zone of the annual wave, the effect will be a more severe attenuation of the annual cycle and a larger time lag than would occur in dry material. This would appear as a low rate of temperature advance during a warming cycle as compared with that in dry materials or where the water table is very deep.

Ice Melt on Streams

Many streams in the glaciated regions of the upper midwest intersect shallow aquifers. During periods of high runoff which, in South Dakota and surrounding areas, generally occurs in the spring when the accumulated winter snow melts, water is lost from streams to aquifers. During periods of low flow water may be lost from shallow aquifers and picked up in streams. Low flows occur in late summer, fall, and winter. Frequently, those areas where water from an aquifer which is warmer or cooler than the water in the stream, can be delineated by directly measuring water temperatures, or by observing an indirect indicator such as the occurrence of ice or non-ice conditions.

An example of icemelt as an indicator of an aquifer losing water to a stream is shown in the thermogram of Figure 5. A quartzite outcrop, a natural barrier to ground water flow, occurs at section (QB). Figure 6 shows an ice melt area just below dam (X), then a frozen sigment (Y), and again a melt portion (Z) below the outcrop.

During late summer months, the inflow of water from an aquifer may be substantial in relation to the magnitude of stream flow, and thus may create a thermal anomaly which is measureable by direct or remote means. In late fall the first hard freeze will generally result in a solid ice cover except in reaches where warmer water enters from a dissected aquifer. Although the ice in a stream may melt in a reach where water enters, unless the added water volume is sufficient to increase the temperature of the entire streams more than a degree or two above freezing, the temperature of the river will be reduced to a level that will permit freezing of the surface a short distance downstream

Conclusions

The research studies described are underway in areas of South Dakota where intensive geology and water resources investigations have been conducted. Thus a great deal of data are readily available for correlation with remote sensing imagery. Upon successful completion of the studies in areas of known aquifers, they will be expanded to a pilot study in an area where a ground-water investigation is in its early stages, and procedures developed here will be used to predict the occurrence of aquifers.

This report describes the surface geohydrologic, soils, and vegetative features that are indirect indicators of shallow aquifers. Also, the physical laws governing the range of temperatures at various depths and the rate of penetration are discussed. Other indirect indicators of buried aquifers described are ice and snow melt, and temperature changes in stream – both of which can be measured remotely.

These investigations have advanced the knowledge of the possibilities as well as the limitations in remote detection of buried aquifers. There is still a great deal to be learned concerning the influence of climatic, hydrologic, geologic, and land use characteristics on the surface responses of electromagnetic energy. Undoubtedly the growing number of complex water management problems and the increasing awareness by planners of the need for comprehensive data on ground-water resources will accelerate research and application programs in this segment of water development.

BIBLIOGRAPHY

Birman, Joseph H. 1969. Geothermal exploration for ground water. Geological Society of America, Bulletin 80:617-630.

Cartwright, Keros. 1968. Temperature prospecting for shallow glacial and alluvial aquifers in Illinois. Illinois State Geological Survey, Circular 433. Urbana, Illinois. 41 p.

Cartwright, Keros. 1970. Ground-water discharge in the Illinois Basin as suggested by temperature anomalies. Water Resources Research 6:912-916.

Derscheid, L. A. and F. C. Westin. 1968. North Central South Dakota Soil Atlas and Crop Production Guide. Cooperative Extension Service Circular 660. South Dakota State University, Brookings, South Dakota.

Flint, R. F. 1955. Pleistocene geology of eastern South Dakota. Geological Survey Professional Paper No. 262. U. S. Government Printing Office, Washington.

Hedges, L. S. Geology and water resources of Beadle County, South Dakota; Part I: Geology. South Dakota Geological Survey Bulletin No. 18, Vermillion, South Dakota.

Howe, Robert H. L. 1958. Procedures of applying air photo interpretation in the location of ground water. Photogrammetric Engineering 24:35.

Howells, L. W. and J. C. Stephens. 1968. Geology and water resources of Beadle County, South Dakota; Part II: Water resources. South Dakota Geological Survey Bulletin No. 18, Vermillion, South Dakota.

Kerr, F. F. and Merlin J. Tipton. 1964. South Dakota ground water supplies. South Dakota State University Extension Circular FS-201. Brookings, South Dakota.

Lovering, T. C. and H. D. Goode. 1963. Measuring geothermal gradients in drill holes less than 60 feet deep, East Tintic District, Utah. U. S. Geological Survey Bulletin 1172:1-48.

Lovering, T. C. and H. T. Morris 1965. Underground temperatures and heat flow in the East Tintic District, Utah. U. S. Geological Survey Professional Paper 504:1-28.

Landsberg, H. E. and Milton L. Blanc. 1958. Interaction of soil and weather. Soil Science Society of America Proceedings 22:491-495.

Moore, Donald G., and Victor I. Myers. 1972. Environmental factors affecting thermal ground water mapping. Interim Technical Report No. SDSU-RSI-72-06. South Dakota State University, Brookings, South Dakota.

Moxon, V. W. 1965. Preliminary general soil map of Beadle County, South Dakota. In Howells, L. W. and J. C. Stephens. 1968. South Dakota Geological Survey Bulletin, No. 18, Vermillion, South Dakota.

Myers, Victor. I. 1971. Remote sensing for defining aquifers in glacial drift. Interim Technical Report SDSU-RSI-71-07.

Parsons, Myles L. 1970. Ground water thermal regime in a glacial complex. Water Resources Research 6:1701-1720.

Penrod, E. B. and O. W. Stewart. 1967. Determination of the thermal properties of a soil and the periodic transfer of solar energy in the earth. Presented at the 1966 winter meeting of ASAE.

Quinn. A. O. 1963. Photogrammetry to locate water. Civil Engineering 33 : 8:50-53.

Robinson, T. W. 1958. Phreatophytes. Geological Survey Water-supply Paper No. 1423. U. S. Government Printing Office, Washington.

Westin, F. C., L. F. Puhr, and G. J. Butley. 1967. Soils of South Dakota. Agricultural Experiment Station, Soil Survey Series No. 3., Brookings, South Dakota.

Zagalsky, N. 1968. A new formulation of a classification procedure. M. S. thesis, University of Minnesota, Minneapolis, Minnesota.

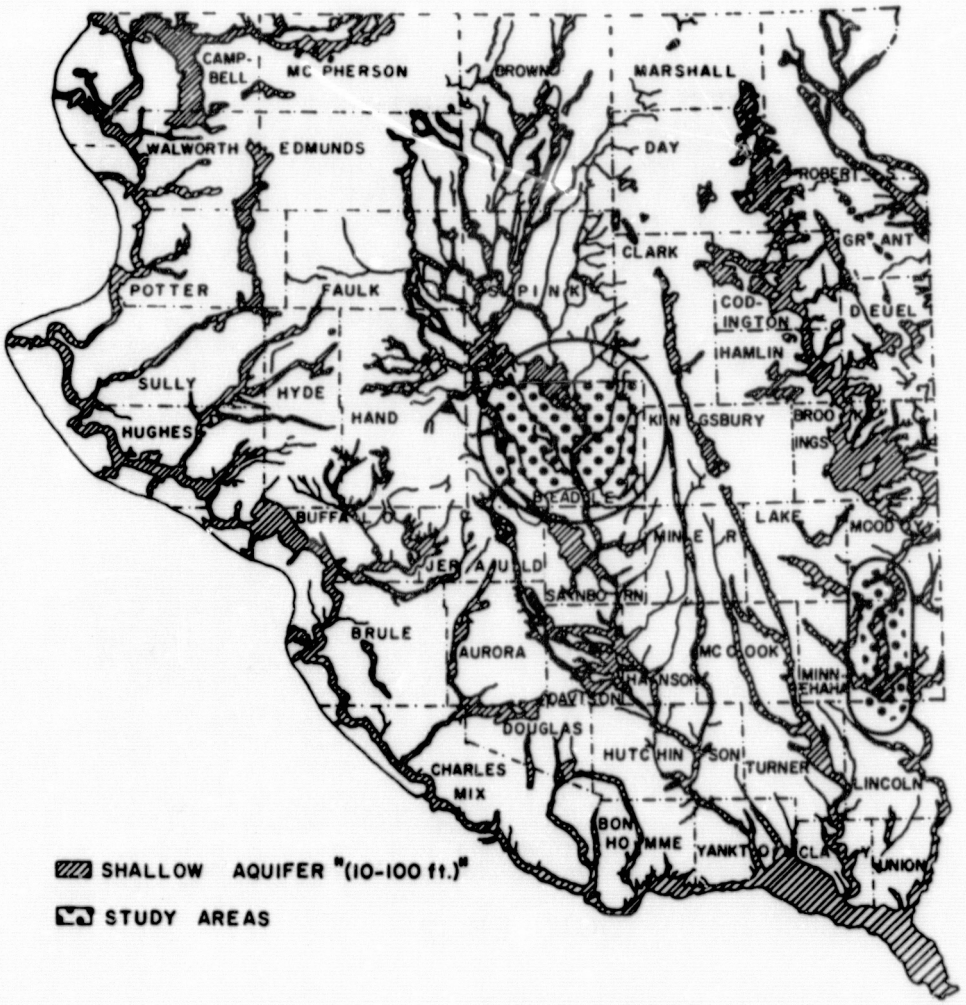
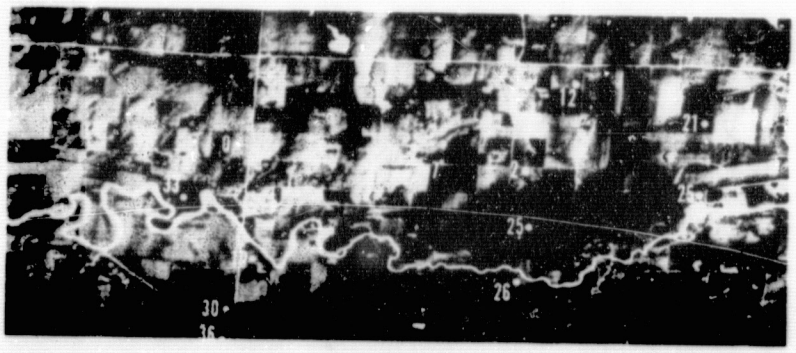


Fig. 1 - LOCATIONS OF REMOTE SENSING GROUNDWATER STUDY AREAS IN SOUTH DAKOTA
after Kerr and Tipton, 1964

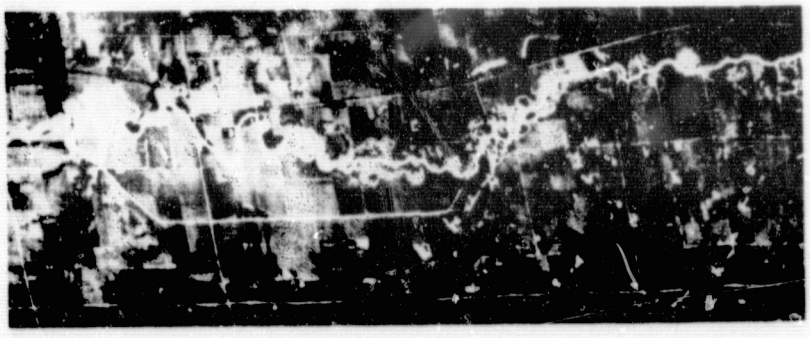


AUGUST 26

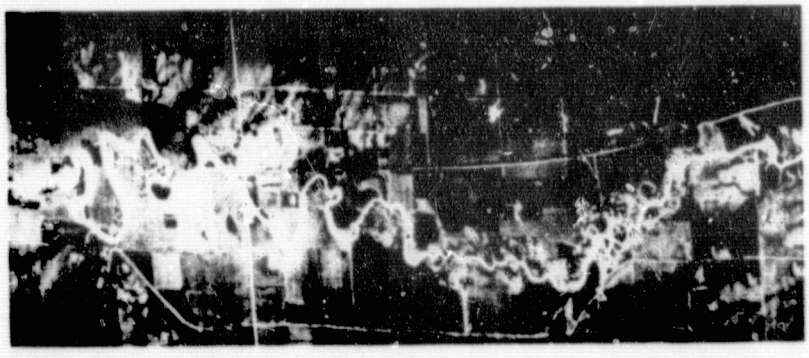


OCTOBER 12

Fig. 2 - NUMBERS DENOTE THE AQUIFER THICKNESS (FT). APPROX. SCALE, 1:63,400

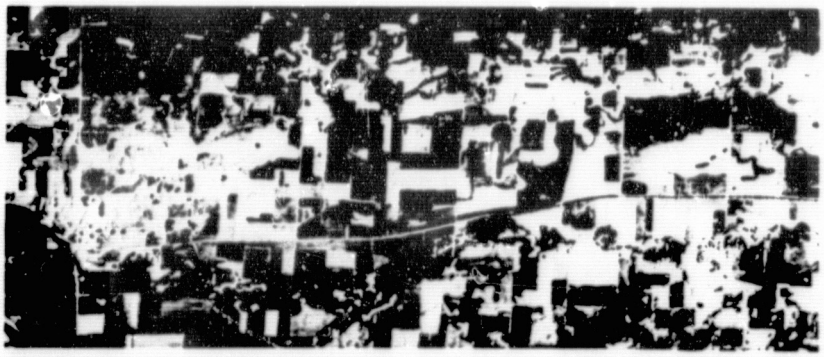


MAY 7

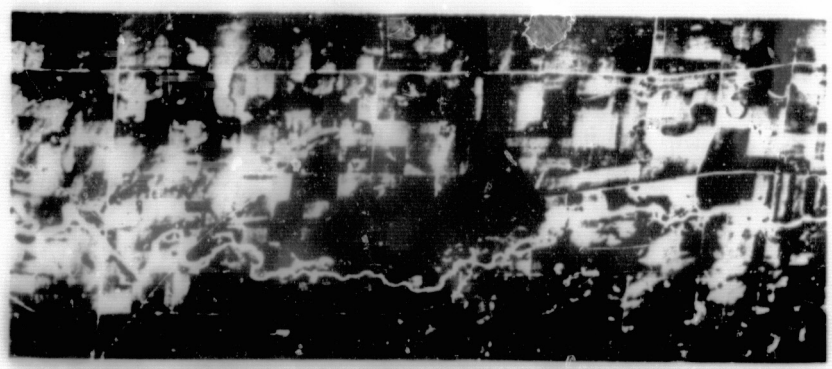


JULY 21

Fig. 2 - SEASONAL DETECTION OF BURIED AQUIFERS IN THE SIOUX BASIN.



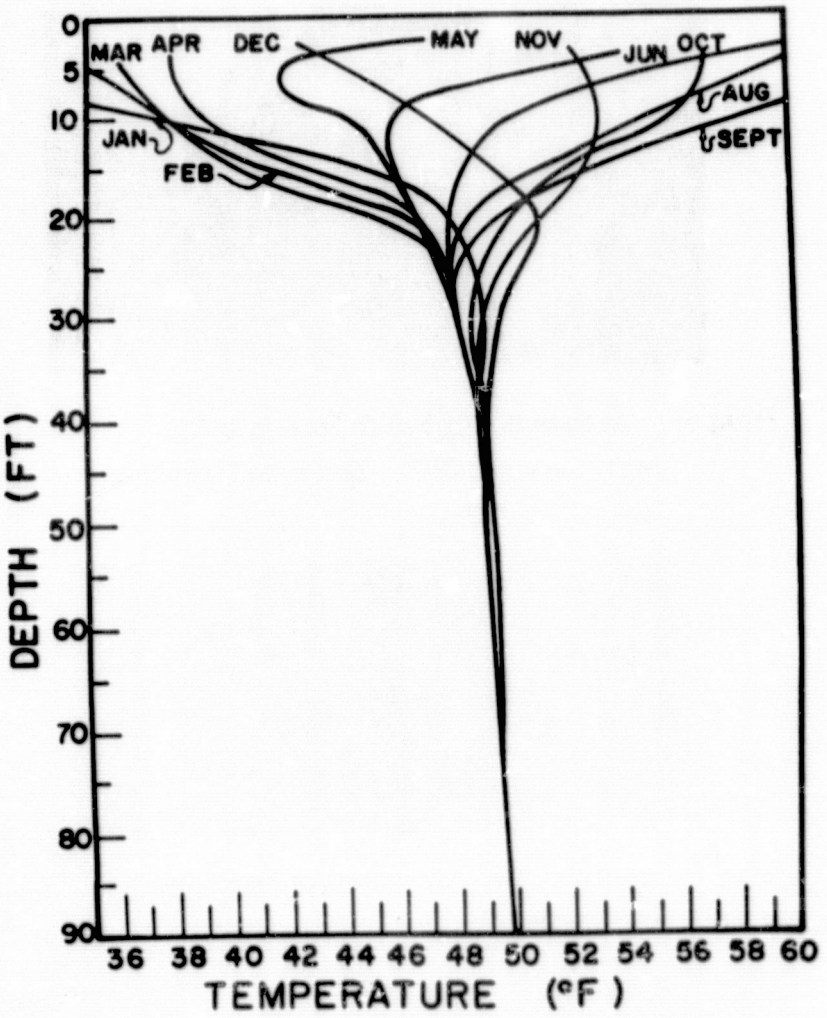
DAY, AUGUST 28, 1971
4.5–5.5 μm



NIGHT, AUGUST 26, 1971
4.5–5.5 μm

R.S.I.–S.D.S.U.

Fig. 3 - DAY AND NIGHT THERMOGRAM CONTRASTS ASSOCIATED WITH LAND USE



DATA FROM U S G S, HURON S.D.

Fig.4 - ANNUAL PROGRESSION OF TEMPERATURES WITH DEPTH IN WELL, HURON, SO. DAK.

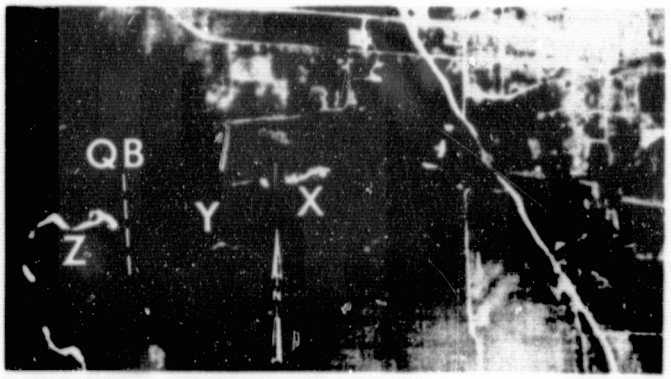


FIGURE 5: THERMOGRAM (8.7-11.5μm) OF SIOUX RIVER ICE MELT, JANUARY 2, 1972. (DARK = COOL; APPROXIMATE SCALE = 1:20,000)

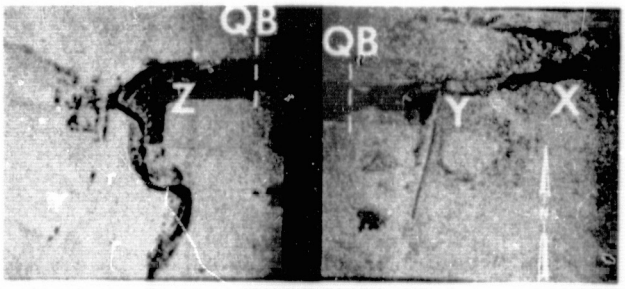


FIGURE 6: HASSELBLAD 70MM COLOR IMAGERY OF SIOUX RIVER ICE MELT, DECEMBER 16, 1971. (APPROX. SCALE = 1:18,000)

FIGURES 5 AND 6: X = MELTED ICE BELOW DAM; Y = ICE; Z = MELTED ICE; QB = QUARTZITE BARRIER

THERMAL STRUCTURE OF THE SAND DESERT FROM THE DATA OF IR AEROPHOTOGRAPHY

B. V. Vinogradov
A. A. Grigoryev
V. B. Lipatov
A. P. Chernenko

Moscow Institute
Aerospace Methods
Moscow, USSR

At present a number of experiments conducted in the domain of the airborne IR survey in the first (λ = 3.5-5.5 μm) and second (λ = 8-12 μm) atmospheric transmission windows have shown various possibilities of studying thermal structure of the underlying surface [11, 12, 13, 14, 15, 16, 17, 18, 19]. A number of papers contain ground-based microclimatic measurements combined with airborne IR imagery photography, data on the soil surface distribution of temperature contrasts and their determining factors [16, 17]. The present work is devoted to the application of airborne IR imagery to the study of thermal structure of the sand desert. Similar investigations have not been undertaken earlier. The current publication presents the results only for daylight IR survey which was synchronized with measurements by other methods of investigating the radiation balance of the terrain according to the CAENEX-70 programme [5].

1. MICROCLIMATIC STRUCTURE OF THE THERMAL FIELD DISTRIBUTION FOR THE SAND DESERT SURFACE

To study the thermal regime in the Repetek region we have conducted microclimatic temperature measurements over two types of land.

(1) Large sand ridges, 15-20 m high, of NE-SW orientation, unfixed or weakly fixed by vegetation and dissected at the tops by barchanes, 4-5 km high.

(2) Small, sand hillocks up to 1 m high, semi-fixed by vegetation and situated in flat depressions between the barchanes and ridges.

On each type of land the most characteristic observational points have been chosen depending on the orientation and steepness of slopes. In the first type of locality, these were situated on different barchane features: (1) on the south slope, (2) on the top, (3) in the depressions between barchanes, (4) on the north slope, and (5) on the west slope. In the second type of locality, the points have been selected on different features of small hillocks: (1) in the depression, (2) at the top, (3) on the south slope, (4) in the saxaul shadow, and (5) on the west slope. From October 13 to 27, 1970, sand surface temperature measurements with a mercury thermometer were conducted simultaneously at all the points within a 1-hr interval. Also, the velocity and direction of the wind and the air temperature were measured every hour.

The analysis permitted the study of sand desert temperature contrasts peculiar to different types of underlying surface in the early autumn period characterized by periodic cold intrusions ("wave activity"). As seen from the published data, the temperature regime of sand deserts is not sufficiently studied.

Slope exposition. Temperature and its contrasts vary depending on the slope exposition. The maximum day temperature, +58° - +61°, slightly varying from day to day, was observed in the anticyclonic period at 14 hr on the steepest south slopes of the barchanes. Second highest maximum temperatures were measured in the depression and were +35° - +45°. Lower maximum day temperatures were on the west and north slopes, +35° - +40°. The lowest maximum temperature was fixed at the barchane tops, +30° - +38°. In the case of small sand hillocks, the highest temperatures at 14 hr were also observed on the south slopes of the hillocks, +54° - +58°. On the west slopes they attained +42° - +49°, at the tops +39° - +43°, and in the depressions between hillocks +35° - +45°.

Solar elevation In general, the diurnal temperature variation of different surfaces of the desert is slightly different from that of the soils in other physico-geographical conditions [1, 7, 9]. The largest spatial temperature contrasts (ΔT) were observed at about 14 hr (Figure 1). At this time ΔT between the south slopes of barchanes and other land features unshaded by vegetation on an average, was +15° - +23°. ΔT between the areas shaded by saxaul and the south slope of barchane reached, at 14 hr, +30° - +35° (Figure 1a).

In the morning and evening hours with a lower solar elevation, the ΔT's are much smaller. For example, temperature contrasts between the south slope of barchane and the unshaded and shaded areas constituted, on 16 October 1970, at 10 hr, +17° and +22°, respectively. Still smaller ΔT (+9° - +11°) were observed at 18 hr.

On the whole, at about 18 hr the temperatures of different surfaces (with the exception of the south slope) were nearly equal and decreasing, and only the south slope temperature remained above that of other surfaces (Figure 1). After sunset ΔT diminished still more and at 22 hr constituted about 6°C. At night, temperatures were uniform. On 19 October 1970 at 02 hr with 100% cloud coverage and lack of wind, the temperature of the depression was +10°, that of the south slope +12°, of the top +9°, and of the north slope +10°.

While analysing the values of the day temperature variation, it is necessary to allow for both the cumulative temperature contrasts between all main land features expressed through the variation coefficient ($\sqrt{\ }$%) and the temperature contrast frequency (Fn) exceeding the empirical limit of the surface temperature distinction (i.e., > 2°C) in the IR pictures. The maximum of the temperature variation coefficient of different land features (Figure 1b) falls on the antemeridian and noon time (12 - 14 hr). The maximum of temperature contrast frequencies $\geq$ 2° (Figure 1c) was observed in the late morning and antemeridian hours (11 - 12 hr). Comparing the graph frequencies (Figure 1b) and the variation coefficients of the contrasts (Figure 1c) we arrive at the conclusion that the optimum time when the largest number of temperature gradations with the greatest contrast can be observed falls on the antemeridian hours.

Wind The wind effect is particularly pronounced on the leeward slopes and the ridge tops. With the wind the temperatures appreciably decrease as compared to the windless hours. Hence ΔT increase between the tops and depressions exposed to the wind. Thus, on all the days of observations, the ridge top temperature at mid - and noonday was higher than those at other barchane points (Figure 2). In the case of small hillocks, ΔT between the south slopes and other unshaded points was 5 - 7° lower than on barchanes, which is connected with a lesser relief dissection and a stronger wind effect on the decrease of temperature contrasts of the small hillock area of the desert. Variability of the surface heating on windy days can be seen in Table 1.

TABLE 1

Influence of the wind direction and velocity on the surface temperature of different features of the sand desert

	Depression	South slope	The top	North slope	West slope
14 October 1970 South Wind V = 0	44°	54°	39°	41°	39°
15 October 1970 North Wind V = 8m/sec	43°	56°	35°	37°	41°

As seen from the graphs (Figure 2), the temperature regime is affected not only by the wind velocity but also by its direction. For example, on all days (except for 14 October 1970, when a weak south wind was blowing) the temperature of the north slope at 14 hr was 4 - 5° lower than that of the west slope, which is related to the prevalence of the north wind.

Cloudiness Cloudiness always decreases surface temperature thus reducing temperature contrasts. As an example, compare measurements carried out on different days at the same time (10 hr) with a different cloud coverage (Table 2).

TABLE 2

Cloud effects on the surface temperatures of different features of the sand desert

	Depression	South Slope	The Top	North Slope	West Slope	Under the saxaul bush
16 x 70 cloud coverage 10%	27°	38°	24°	29°	29.5°	17°
17 x 70 cloud coverage 80%						

The south slope temperature undergoes the strongest decrease and resulted in reducing the contrasts.

Change of air masses Temperature contrasts are greatly influenced by the change of air masses, in particular, by the intrusion of the transparent cold air. Thus, on 16 October 1970 after the passage of a cold air wave, ΔT on the barchane (south slope) top increased from 16° - 19°C to 20° - 23°C while those between the barchane tops, and the areas shaded by saxaul rose from +20° to +37°, whereas, the air temperature at 14 hr decreased from 32° to 20°C.

Precipitation Temperature differences after rain are always reduced. For instance, on 19 October 1970 at 07 hr 30 min after a short night rain with the amount of cloud coverage equal to 10% and lack of wind, the following temperatures were observed: 9.5° in the depression, +11°C on the south slope of barchane, +9°C at the top, +9.5°C on the north slope, while on 26 October 1970 after a longer night rain at 07 hr the temperatures at all the points of barchane were uniform at +8°C.

Influence of the plant canopy With other conditions being equal, the sand ridges and hillocks less covered by vegetation are more heated and have higher temperatures. Thus, the exposed sand temperature at 11 hr (14 October 1970) amounted to 38.1°C, while the area shaded by saxaul had 27.5°C (i.e. ΔT = 10°), still larger T were observed at 14 hr constituting +45.9 and 31.8°C, respectively, i. e., ΔT = 14°C. The air temperatures at 11 hr were +27.7° and at 14 hr were +31.8°C.

The time of the temperature maximum was also different: 13 hr - for the exposed sand (46.8°C) and 16 hr (+32.3°C) - for the area shaded by saxaul.

2. BRIEF CHARACTERISTIC OF THE TECHNICAL DATA OF THE AIRBORNE IR SURVEY AND THE OBTAINED IMAGES

IR imagery was collected from the instrumented aircraft of the Main Geophysical Observatory with the help of the airborne IR scanner STV-60m operating in the wavelength range of 3 - 5.5μm [3, 8]. IR pictures have been obtained at two heights; middle-scale photos with the resolution of 8.5 x 8.5m at 2 850m, and large-scale photos with the resolution of 4 x 4m at 1 300m. Also, radiative temperatures of the area were measured at a height of 300m from aircraft.

3. PECULIARITIES OF IR IMAGES OF THE UNDERLYING SURFACE

Different types of the underlying surface are observed in the IR pictures (Figures 3a, 4). From the brightnesses of the individual land features varying according to their integral temperature and from the pattern of the IR image, a number of terrestrial features are differentiated (Figure 3b).

Large structural features of the surface such as extensive barchane ridges, depressions with the hillock relief, and sand hillocks and ridges are well recognized in the medium resolution IR pictures, the details of their structure being seen in the large-scale pictures.

(1) The landscape of unfixed barchane ridges with scarce vegetation is, on the whole, recognized in the medium resolution IR picture by a light (in parts very light) image tone due to the highest surface temperatures and the strip pattern reflecting the presence of barchane chains.

Surface temperatures measured during the IR survey were as follows: the highest temperatures, 54°C, were observed on the south slope at 12 hr (at 13 hr - 57°C), which is due to the solar exposure, the steepness of the slope, substrate dryness, and the lack of vegetation. The depressions between barchanes with rather dense vegetation and the barchane tops devoid of vegetation had at 12 hr much lower temperatures, +35.5°C (at 13 hr +37.5 - 40°C). At the top, the temperatures were somewhat lower because of the wind (west wind with the velocity of 3m/sec). Finally, the lowest temperatures were observed on the north slope +25°C at 12 hr and +33°C at 13 hr, respectively. It is to be remembered that the time of the survey (12 hr 30 min) corresponds to the time of the maximum T between different land features (see above). This accounts for a rather clear-cut differentiation of the nonuniformities of the thermal background of the earth's surface in the IR pictures. Distinctly identified in the medium resolution picture is a ridge structure expressed as a sequence of subparallel strips of different tone. Not less than 5 gradations of tone may be visually distinguished in the medium resolution picture - from the lightest (the most heated south slopes) to the very dark (the coldest north slopes). A landscape of this type is seen in more detail in the high resolution IR picture. Not less than 9-10 gradations of tone are distinguished. A large detailing of thermal nonuniformities in the large-scale IR images is due to its smaller spatial resolution.

(2) A landscape consisting of depressions with small sand hillocks and denser vegetation is recognized in the middle of the medium-scale IR image by the prevailing dark hues and the nonoriented spot structure.

On the whole, this type of landscape is characterized by lower surface temperatures. A weaker west wind - to 1m/sec (at the tops the wind velocity was three times that of the depression) noticeably affects the heating of different land features - leeward west slopes and tops have higher temperatures as compared to those of large sand barchanes and ridges.

A smaller relief structure on the most heated south slopes leads to a lower heating of this type of landscape on the whole (as compared to barchanes) and a lesser contrast in its thermal imagery.

Also, the landscape of sand hillocks is characterized by a stronger fixation of the surface by vegetation which considerably reduces heating of the surface (measured temperatures in the shadow of the white saxaul bush were 16°C at 12 hr and 17°C at 18 hr).

The medium scale IR pictures of the sand hillock type of landscape are characterized by the nonoriented contours of the image constituting mosaics of different configuration spots. The lighter spots correspond to the more heated sand hillocks, the latter being more elevated and less fixed by vegetation. The darker ones correspond to the colder cell depressions fixed by vegetation. Bright light spots peculiar to the image of sand barchanes are almost lacking. Narrow spots of light tone and indistinct orientation (from NNW to SSE) corresponding to the more heated south and south-west slopes are rarely encountered.

The boundary between the two above described thermal patterns is well pronounced, particularly, in the medium scale IR picture. The latter reflects the division of two large unequally heated types of the underlying surface corresponding to the natural contact of two landscape types: sand barchanes and ridges, on the one hand, and sand hillocks on the other.

(3) Fixed in the southern part of the middle-scale IR picture is the landscape of transitional type with the hillock-ridge relief less fixed by vegetation as compared to the hillock sands. In the middle-scale IR image, the landscape of the weakly fixed sand hillocks and ridges is distinguished by the integral lighter tone of the image as compared to the landscape with semifixed sand hillocks. This is due to the intermediate heating of the surface.

CONCLUSIONS

Thermal nonuniformities of the airborne IR images reflect the structural peculiarities of the fixed landscape of both the macro and meso forms. These are due to the various changes in the landscape structure, viz., in the type of relief (barchane-ridge, hillock-ridge, and small hillock), in slope steepness and dissection, in the density and composition of the plant canopy, in the solar elevation and the direction and velocity of the wind. Similar investigations of thermal nonuniformities of the underlying surface are important for the solution of a number of problems set before the CAENEX-70 [4], viz., detection of the statistical relations between the radiation field and its parameters; measuring of the heat balance of the underlying surface and its spatial nonuniformity, in particular, determination of the space-time meso and macro structure of the component fields. And finally, the investigations of the thermal structure of the Earth's fields in the sample sites are necessary for the development of a theory of the satellite IR imagery with a considerable geometrical integration of the nonuniformities [9, 13].

REFERENCES

1. Aizenshtat, B. L., Ogneva, T. A., Borushko, I. S., Influence of Irrigation on the Distribution of the Meteorological Elements in the Surface Layer. Trudy GGO, 39, 1958.

2. Vinogradov, B. V., Grigoryev, A. A., Gunin,P. D., Physico-Geographical Characteristic of the CAENEX-70 Area, Trudy GGO, 276, 1972.

3. Dyachenko, L. N., Chernenko, A. P., Binenko, B. I., Possibilities of IR Survey for the Detection of Forest Fires from Vehicles, Trudy GGO, 252, 1970.

4. Zholtaya, N. N., Influence of the Locality on the Thermal Regime of Air and the Upper Soil Layer, Trudy NIIAK, 33, 1965.

5. Kondratyev, K. Ya., Orlenko, L. R., Rabinovich, Yu. I., Ter-Markaryants, N. E., Shlyakhov, V. I., The Complex Energetic Experiment (CAENEX) Bull. WMO, v. 19, No. 4, 1970.

6. Orlov, B. P., On the Sand Temperature From the Observations at the Repetek Sand-Desert Station, Met. vestnik No. 6, 1922.

7. Sapozhnikova, S. A., Micro-and Local Climate, Gidrometeoizdat 1950.

8. Sokolsky, B. P., Chernenko, A. P., Some Results of the Airborne IR Scanner Application to the Investigation of the Underlying Surface Radiation, Trudy GGO, 252, 1970.

9. Shulgin, A. M., The Soil Climate and Its Regulation, Gidrometeoizdat, 1967.

10. Dorfman, S. D., Gastaldo, J. R., Exner, W. L., Some Experimental Results on Earth Resources Data Transmission BOMEX 1969, AIAA Paper, No. 328, 1970.

11. Estas, J. E., Some Geographic Applications of Aerial Infrared Imagery, Proc. of the Fourth Symposium on Remote Sensing of Environment, 1966, Michigan.

12. Fagerlund, E., Kleman, D., Sellin, L., Svensson, H., Physical Studies of Nature by Thermal Mapping, Lund Studies in Geography, Ser., A, Phys. Geogr., No. 47, 1970.

13. Harris, D. E., Woodbridge, C. L., Terrain Mapping by Use of Infrared Radiation, Photogramm, Engng., v. 30, No. 1, 1964.

14. Langley, P. G., New Multi-stage Sampling Techniques Using Space Aircraft Imagery for Forest Inventory, Proc. of the Sixth International Symposium on Remote Sensing of Environment, 1969, Michigan, 1970.

15. Mattson, J. O., Infrared Thermography - A New Technique in Microclimatic Investigations, Weather, v. 24, No. 3, 1969.

16. Mattson, J. O., Thermal Patterns in the Landscape Recorded With Infrared Technique and Simulated Model Experiments. Geografiska Ann., v. 51

17. Myers, V. J., Heilman, M. O., Thermal Infrared for Soil Temperatures Studies. Photogramm. Engng., v. 33, No. 10, 1969.

18. Sabins, F. F., Infrared Imagery and Geological Aspects. Photogramm. Engng., v. 33, No. 7, 1967.

19. Williams, R. S., Ory, Th. R., Infrared Imagery Mosaics for Geological Investigations, Photogramm. Engng., v. 33, No. 12, 1967.

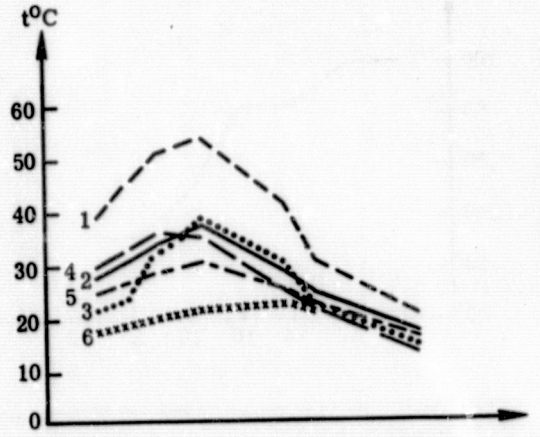


Figure 1 a Day temperature variation of the soil surface of the main features of the large barchane and small hillock landscape on the day of "CAENEX-70" 16.X. 1- the south slope, 2- inter-ridge lowland, 3 - the west slope of the barchane ridge, 4 - the north slope of the barchane ridge, 5 - the top of barchane, 6 - the shadow of the white saxaul bush.

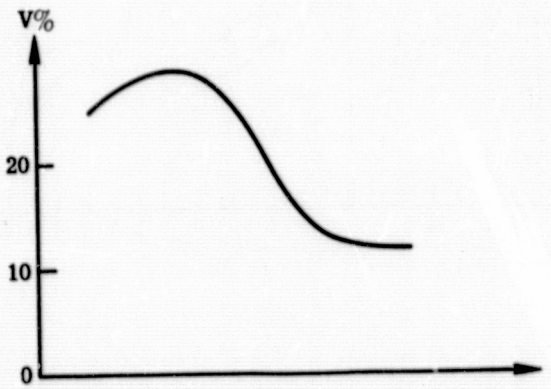


Figure 1 b Day variation of the temperature coefficient

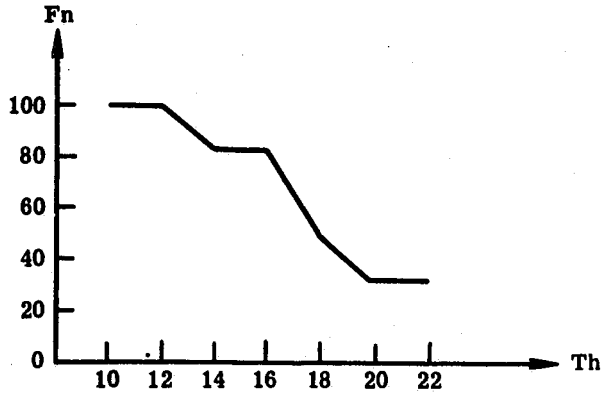


Figure 1 c Day frequency variation of the effective temperature differences $\geq$ 2°. Local time is used.

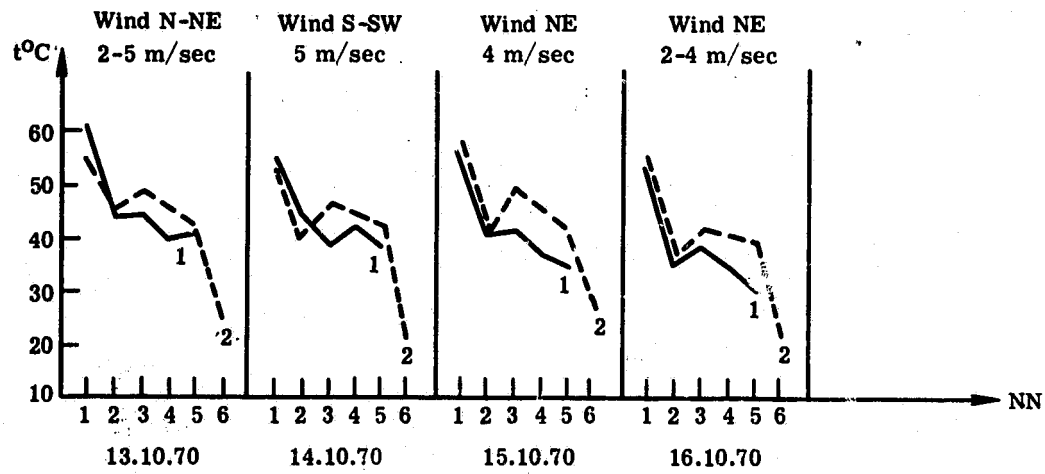


Figure 2 Graph of temperature distribution of the soil surface of the main landscape features at the early postmeridian hours (14 hr) on the days with different wind regimes and different air masses. 1 - large barchane relief, 2 - small hillock relief.

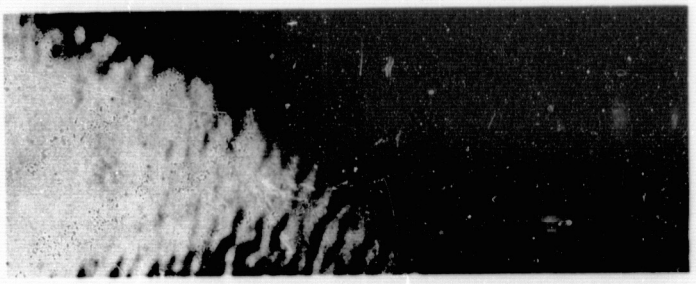


Figure 3 a The middle-scale IR picture of sand landscape in the wavelength range of λ = 3.0 - 5.4 μm at H = 2850 m at 12 hr 35 min (as obtained from the instrumented aircraft of the Main Geophysical Laboratory with the help of the IR scanner STV - 60M.

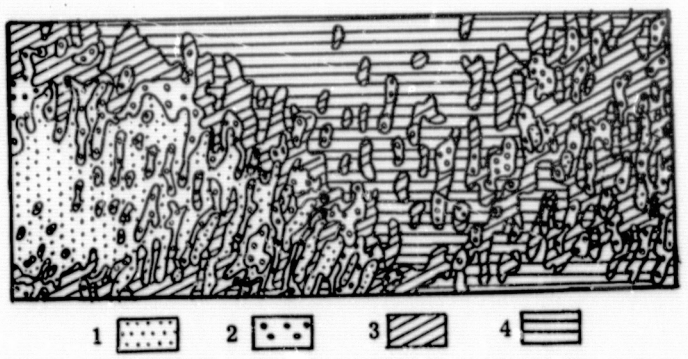


Figure 3 b The isodensitometric map-scheme of the positive IR image of sand landscape as compiled from 4 levels of the density corresponding to the temperature gradations of the soil surface from 55° on the sunlit slope of the barchane chain to 16°C in the shadow of the white saxaul bush.

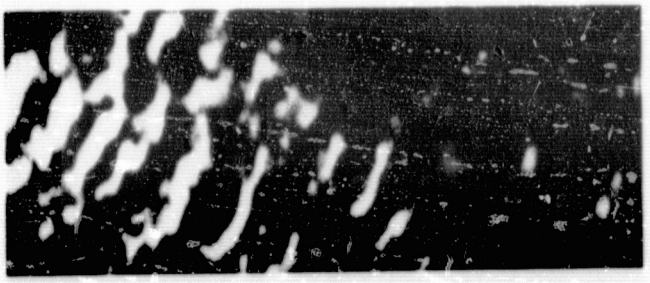


Figure 4 The large-scale IR picture of the sand landscape in the wavelength range of 3.0 - 5.4 μm at H = 1300m at 12 hr 20 min.

RADIOMETRIC TERRAIN MAPPING AT 3 MM WAVELENGTH

E. Schanda, G. Schaerer, M. Wüthrich

Institute of Applied Physics
University of Berne
Berne, Switzerland

ABSTRACT

A narrow beam (10 arcminutes) microwave scanning radiometer, operating at 92 GHz has been used for thermal mapping. Real time display of the sceneries is performed on a TV screen. Radiometric images of distant areas, urban sceneries and single buildings are presented and some special features are discussed. The data acquisition system of the radiometer is equipped with a calculator which performs the subtraction of the informations of different images, thus enabling the display of the changes within a certain scenery.

1. INTRODUCTION

In a contribution to an earlier Remote sensing symposium [1] a description of our three millimeter radiometer for terrain mapping purposes has been given. The operational specifications are: Center frequency 92 GHz, temperature resolution 3 K for a 1 second integration time and a bandwidth of 1 GHz; angular resolution (half power points of the antenna beam) 10 arcminutes achieved by a Cassegrain antenna of 1.5 meter diameter. The antenna motion can be programmed to sweep a certain field of view continuously line by line. A Dicke-type receiver is used with a square wave modulation at 10 KHz and a single ended Schottky-barrier mixer converts a one GHz bandwidth down to an intermediate frequency of 10 GHz. A phase sensitive detector in a digital operation mode is triggered by the reference frequency of the input modulator and synchronized by the antenna drive. Integration times between 1 ms and 1000 ms are possible. The real time display is capable of showing up to 160 lines, each consisting of 256 spots on a TV-screen, corresponding a view of 16° x $25{,}6^{o}$. The compilation of a full size image with a measurement every 6 arcminute can last between several minutes and several hours due to the different integration times used in our scans. A memory system is not only feeding the information to the display but is also used in a calculator for comparison of different scans of the same scenery (e.g. presentation of differences in a changing scenery). The total intensity range of the radiometer is divided into 256 output steps, which can arbitrarily be combined into 32 groups corresponding to 32 gradations of brightness or 32 color and brightness values on a color display. Any response curve between radiation temperature and image gradation can be achieved. On a successful use of this instrument for microwave imaging of detailed sceneries has already been reported [2] .

Preceding page blank

2. THE MICROWAVE THERMAL IMAGES

We discuss now a number of thermograms which show the capability of our three millimeter wavelength scanning radiometer. We optionally associate low radiation temperatures with bright points on the display and high radiation temperatures with dark points.

Figure 1a shows the radiometric image of a mountaineous horizon line at a distance of 7 to 8 km from the radiometer. Figure 1b gives the photographic identification, which has been taken at the time of scanning. The overcast sky-deteriorated the resolution of the horizon line only slightly. Figure 2 shows the result of a scan through a complex urban scenery. A number of metallic constructions - partly on very distant roofs - are the most conspicuous parts on the microwave thermogram of Figure 2a. The traffic on the foreground (Figure 2b) was moving continuously through the scans and appears blurred on the thermogram. The photograph has unfortunately not been taken at the hour of the microwave scan, therefore the situation at the car-parc was different. During the days of scanning this scenery (February 1972) the weather has been unfavourable: humid air masses at lower levels and snow-clouds at larger distances. This is the reason for a bad resolution of the horizon line at a distance of 6.5 to 7 km. The trees left to the street (Figure 2b) - at that time leafless - are randomly scattering any radiation in a very effective way and are therefore appearing as a rather uniform region with a mean gradation on the thermogram (Figure 2a). By a slightly extrafocal arrangement of our antenna feed we were able to produce microwave thermal images of single buildings at short distances (Fresnel zone of the antenna). In Figure 3a the microwave radiometric image is presented of a corner of the main building of the University of Berne (Figure 3b). The closest distance between the radiometer and the building is about one hundred meters. The area of the bigger windows is only about 1.5 times larger than the area of the antenna. Again the metallic parts - even those of rather small size - are distinguished very sharply if they are arranged under favourable angles with regard to the cold sky.

3. MICROWAVE IMAGERY OF CHANGING SCENERIES

The capacity of the display memory is sufficient to store the information of several images. A calculator enables us to use the stored information of a specific scenery for combinations with the informations of a new thermal image of the same scenery. Specifically the operation of subtraction yields directly the changes within a given scenery. Presentation of the difference of two images on the display is possible. The alternate observation of the original thermal image and the difference image can produce an easy identification of the areas of changed microwave radiation. Figure 4a represents the radiometric appearence of a truck in the terrain (Figure 4c) at a distance of about 200 meters. After removing the truck and subtracting the new image information from the previous one the result is the difference image of Figure 4b.

4. SOIL SIGNATURES ATMOSPHERIC AND RAIN ATTENUATION

In earlier papers [3] [4] [5] we have reported on the thermal radiation properties of a large number of media at a wavelength of 3 cm. Experiments are now going on for establishing the 3 mm-wavelengths signatures of a number of media which are important for remote sensing purposes. The dependence of the emissivities on observational angle, the polarization and the moisture content for smooth surfaces are under investigation. One of the goals is to compare the results with those obtained at 3 cm wavelength in order to establish a multispectral microwave sensor. The wavelength should serve as an additional dimension in the identification of different materials, which show the same radiation temperature at one specific wavelength but not in a different part of the microwave spectrum.

The differences of the emissivities of water (moisture content) between these different wavelengths offer an important tool for the remote sensing of natural resources. The emissivity as a function of the polarization is another dimension in the identification problem as already shown in an earlier investigation [3] . An important part of the experiments on signatures is devoted to the problems of surface roughness and mixtures of different solid media. The atmospheric absorption is already considerable in the used frequency band. This results for a ground based radiometer in a bad resolution of a far horizon line (see e.g. Figure 2a) but in specific situations the atmospheric radiation can be used advantageously.

An atmospheric temperature of 280° K results in a radiation temperature of the order of 50° K from the zenith but in about 250° K from an elevation of 5 degrees which can be shown by measuring through this range of elevation angles. This latter value is hardly discernible from objects with an emissivity of about 0.9. The effects of atmospheric radiation and elevation angle on the detectability is clearly demonstrated in Figure 3a.

The contrast between the sky and the roof is very sharp because at the elevation angle of about 30° the sky temperature is only about 90 K for clear weather. On the original images of this scan some metallic parts appear "colder" than the sky background because they reflect the atmospheric temperature contribution by steeper paths than 30°.

For cloudy sky the far horizon lines become blurred - see e.g. in Figure 2a and to a much lesser extent in Figure 1a - because of the larger optical depth of the overcast sky for short millimeter waves.

The effect of rain on the radiometric visibility is serious at this wavelength. A systematic study of the relation between the rain parameters (rain rate, size and shape of the droplets) and the radiation temperature is in progress. For wavelenghts comparable to the droplet size the distinction between the effects of scattering and absorption is important because of their different contributions to the radiation temperature. Roughly speaking a rain rate of about 10 mm/hour reduces the differences of the radiation temperatures of the various objects in the sceneries down to below the thermal resolution of our instrument (∿ 3° K).

5. REFERENCES

1 K. Künzi, M. Wüthrich, E. Schanda

A mm-wave scanning radiometer for terrain mapping, Proc. 7th internat. Symp. Remote Sensing of Environment, 17-21 May 1971, University of Michigan, Ann Arbor, p. 865-868

2 G. Schaerer, E. Schanda

Thermal imaging by a 3-mm wavelength radiometer, Zeitschr. Angew. Math. Phys., 23 (1972) Nr. 3

3 C. Mätzler

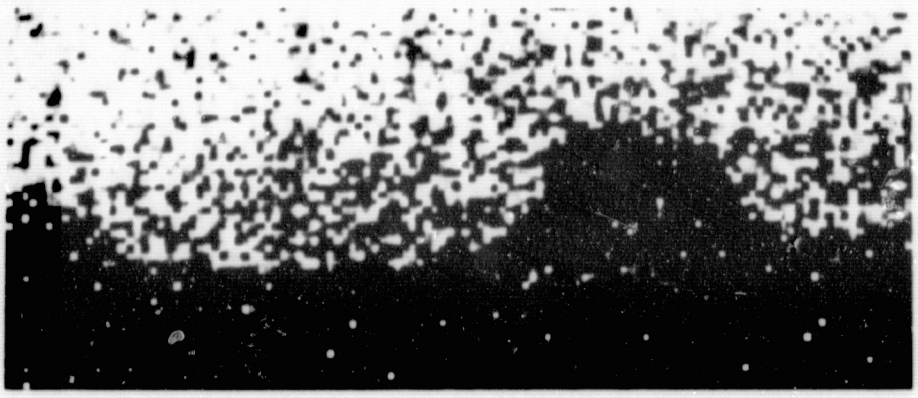
Messung der Wärmestrahlung der Erdoberfläche im Mikrowellengebiet, Diploma-thesis, Institute of Applied Physics, University of Berne, 1970

4 K. Künzi, A. Magun, C. Mätzler, G. Schaerer, E. Schanda

Passive microwave remote sensing at the University of Berne, Switzerland, Proc. 7th internat. Symp. Remote Sensing of Environment, 17-21 May 1971, University of Michigan, Ann Arbor, p. 1819-1826

5 E. Schanda

Remote sensing of earth resources by microwave radiometry, Industries atomiques et spatiales, 16 (1972) Nr. 4, p. 65-80



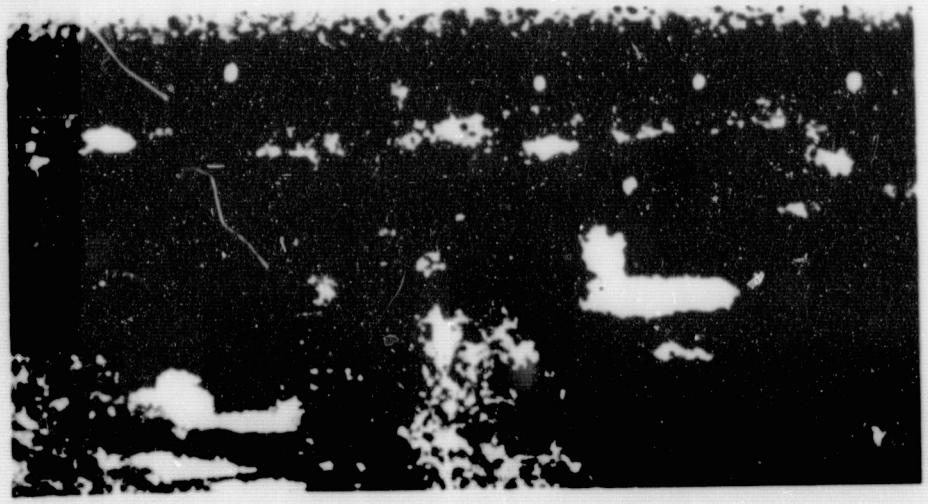
a)



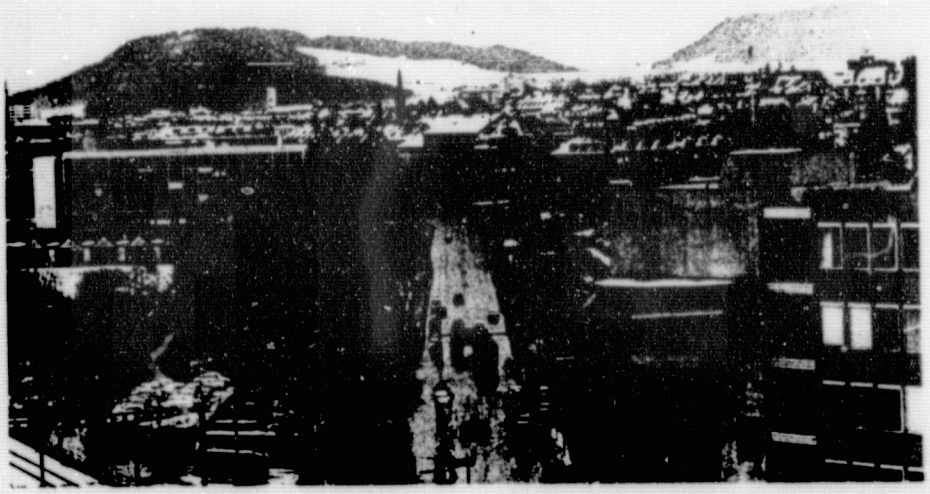
b)

Fig. 1. a) Radiometric microwave image of a distant (7 to 8 km) mountaineous horizon line

b) Photographic identification of a)



a)

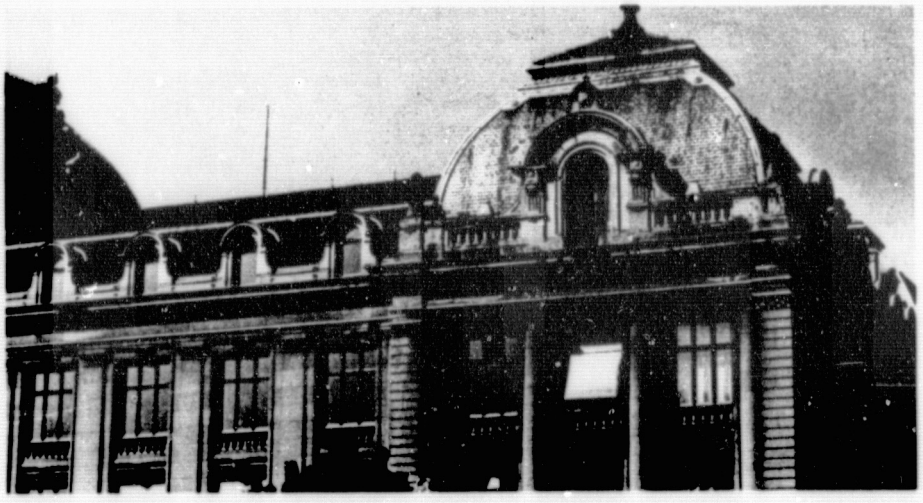


b)

Fig. 2. a) Microwave thermogramm of an urban scenery
b) Photographic identification of a)



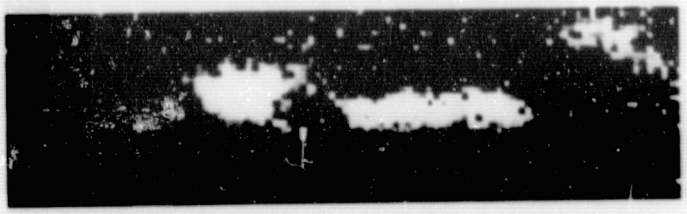
a)



b)

Fig. 3. a) Microwave thermal image of a single building at short distance (about 100 meter)

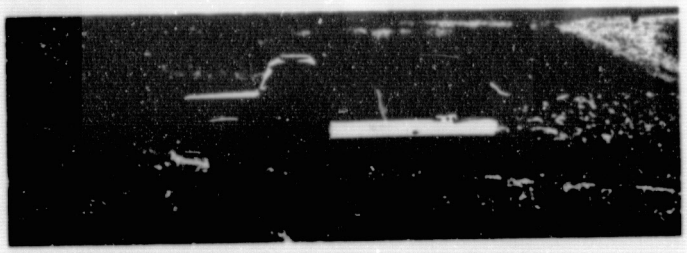
b) Photographic identification of a)



a)



b)



c)

Fig. 4 a) Microwave radiometric image of a truck in the terrain

b) The result of the subtraction procedure between the stored image information a) and the thermal image information of the same terrain without the truck

c) Photographic identification of a)

PROGRESS REPORT ON AIRCRAFT GAMMA-RAY SURVEYS FOR SOIL-MOISTURE DETECTION AT A NOAA TEST SITE NEAR PHOENIX, ARIZONA

Donald R. Wiesnet
National Environmental Satellite Service/NOAA
Washington, D.C.

Eugene L. Peck
National Weather Service/NOAA
Silver Spring, Maryland

Introduction

Recent experimentation and research by the National Weather Service (NWS) have been centered about remote-sensing measurements of areal snow cover conditions. Peck et al. (1971) have reported on the use of terrestrial gamma-ray measurement from low-flying aircraft (100 m above ground level) in non-mountainous areas as a method of measuring the water equivalent of snow. The results of this research are rather encouraging and additional test sites are being flown to evaluate the technique under varying climatic terrain and geographic conditions. Research on this method has been conducted for several years in the Soviet Union and Norway (Kogan et al., 1965; Zotimov, 1968; Dahl and Odegaard, 1970). Kogan et al. (1971) have reported that the technique is currently used in the Soviet Union on an operational basis.

The technique for measuring the water equivalent of snow cover is based on the attenuation effect of the total water mass interposed between the source of the natural gamma radiation--that is, the underlying soil--and the detectors in the aircraft. The attenuation of the gamma radiation depends only on the total mass of water, regardless of state, i.e., whether snow, ice, or free water. The amount of moisture in the soil affects the amount of radiation that emanates from the soil and therefore the measurement of the water equivalent of the snow cover. Investigators in the Soviet Union regard this variation as low in winter and disregard its effect (Dmitriev, et al., 1971), while those in the United States (Peck et al., 1971) have developed methods to correct for soil moisture variations.

The National Environmental Satellite Service (NESS) and the National Aeronautics and Space Administration (NASA) are engaged in research in the remote sensing of soil moisture, primarily in the microwave region.

Acknowledgements. The authors would like to thank Zolin G. Burson of EG&G, Inc. for the reduction of the radioactivity data and for his helpful advice.

Soil Moisture

Soil moisture is an important parameter in hydrology, and one which is difficult to measure. Its practical relevance to agricultural hydrology is rather obvious, but it is also relevant to many other facets of hydrology. Soil moisture values affect ground-water recharge rates, road and site construction, forest and water management operations, and calculations for water-level or flood forecasting. It is the last-mentioned use that is our primary concern at NOAA.

Remote sensing of soil moisture for our purposes means detecting and measuring, at least semi-quantitatively, the moisture present in the uppermost 20 cm of soil. Ideally, a daily assessment of soil moisture in large river basins or subbasins could be made by a satellite system and fed into existing computer conceptual forecast models as those used by the National Weather Service.

Conventional gravimetric measurements of soil moisture are made by taking soil samples by auger, then weighing the sample in the laboratory, heating it for 24 hours at 105°C, and then reweighing the dessicated sample. The percent soil moisture is then calculated by use of the formula

$$\text{soil moisture (percent)} = \frac{\text{Weight of wet sample-weight of dry sample}}{\text{dry weight}} \times 100$$

Preceding page blank

Obviously, this technique is costly and time consuming. Synoptic observations of soil moisture are all but impossible. If samples are poorly located or are nonrepresentative, erroneous estimates of soil moisture will result. For these reasons the agricultural, hydrologic, and hydrometeorological communities have been seeking a remote sensing technique that would permit rapid assessment of soil moisture over large areas.

Inadequacy of Ground Truth Measurements

One of the primary limitations in evaluating methods for remote sensing of hydrologic factors such as soil moisture and water equivalent of snow cover is the high degree of difficulty in determining areal averages for these factors using conventional ground truth methods. Soil moisture methods have been used only very little in the field of hydrology for operational purposes, as point measurements or sets of point measurements are of limited value for estimating areal conditions.

The prospect of utilizing the gamma radiation aerial measurement techniques as used for measuring water equivalent of snow cover in order to provide an improved estimate of average soil-moisture conditions appears very promising. The coupling of the ground truth point measurements with the areal measurements of the gamma-ray survey should provide a more suitable indication of average conditions that would be viewed by the microwave system.

Test Site Ground Truth

The ground truth measurements for this experiment (and for the related microwave overflights) were made by Biospherics, Inc. The test site is located in Maricopa County, Arizona, several miles west of Phoenix. (See index map, fig. 1)

A majority of the fields along the north-south line were without vegetative cover on Feb. 25, 1971. The fields are irrigated by canals and ditches, and this type of field-by-field irrigation creates a rather spotty or heterogeneous soil-moisture distribution pattern. The relation between irrigation date and soil moisture is apparent in figure 2, which shows the variation of mean soil moisture with time since the last irrigation.

Table 1 shows the precipitation that was recorded at the Phoenix Airport in February. Note that six days had elapsed with no measurable rainfall prior to the test.

TABLE 1.

Date	Precipitation (inches)
1 - 16	0
17	0.30
18	0.04
19	0.01
20	Trace
21	0
22	0
23	Trace
24	0
25*	0
26	0
27	0
28	0

* Date of aerial surveys.
Table.--Record of precipitation at Phoenix, Arizona, for February 1971.
Source: National Weather Service.

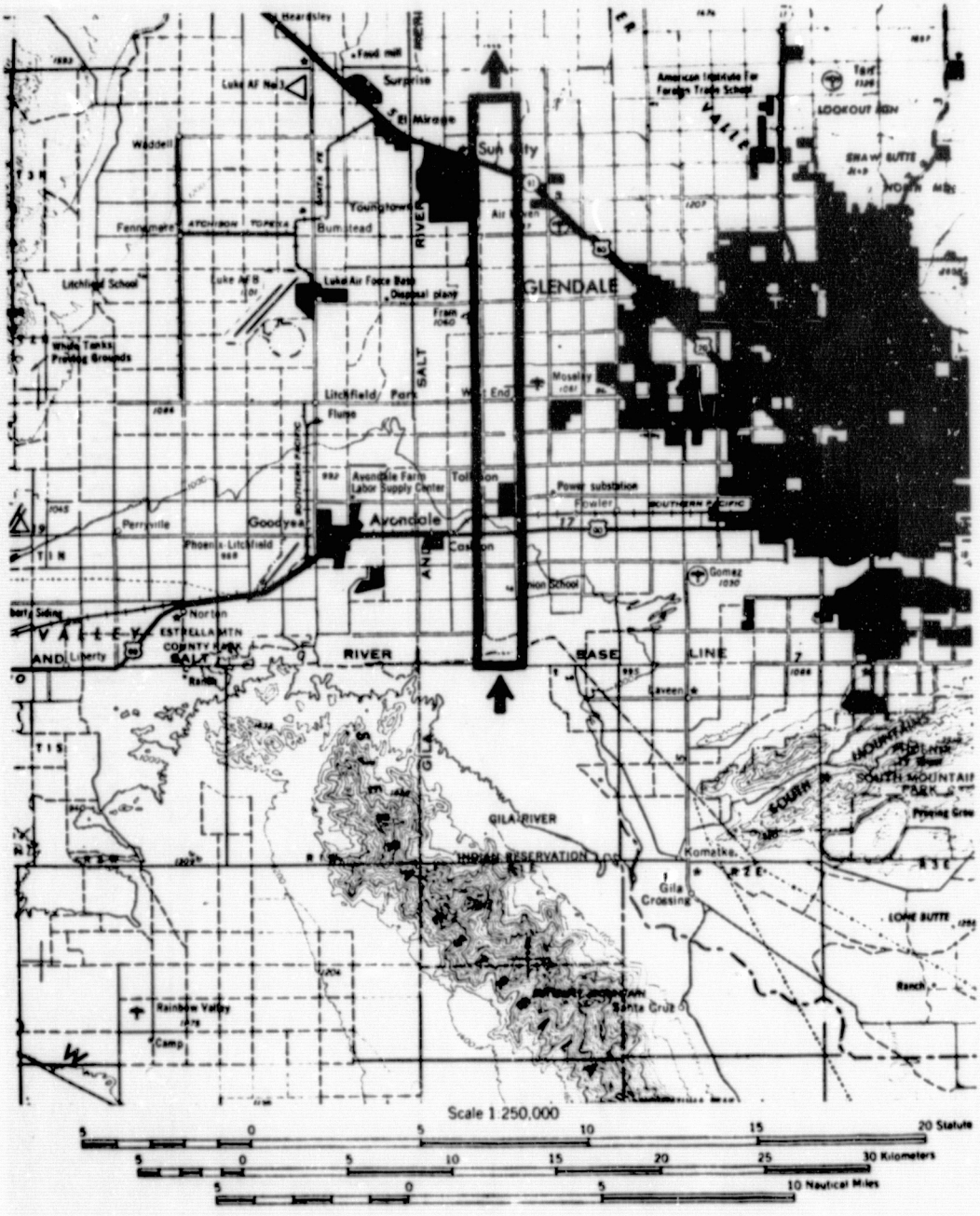


FIGURE 1. Index map showing the test site for this study.

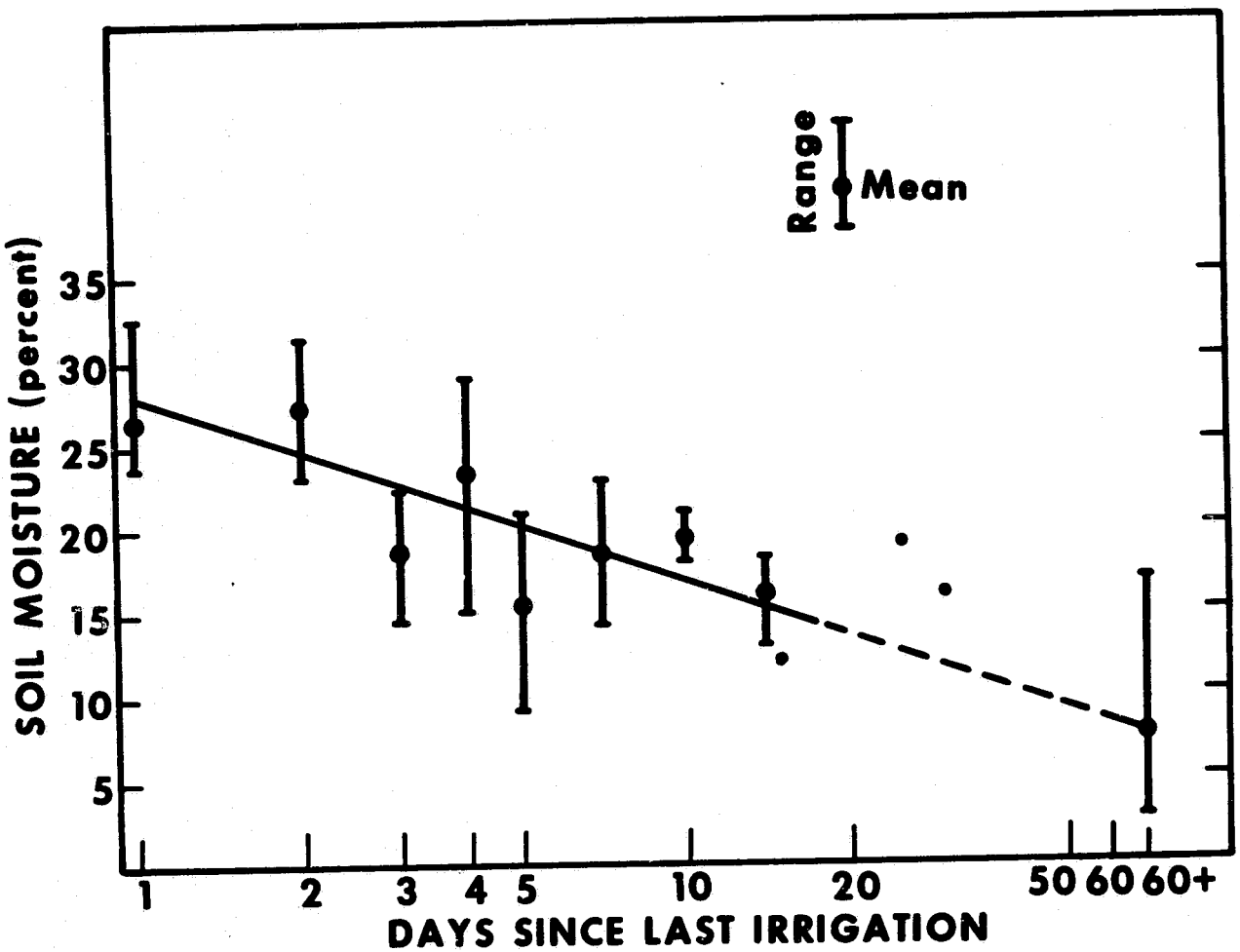


FIGURE 2. Graph showing the variation in soil moisture as a function of the number of days since the last irrigation.

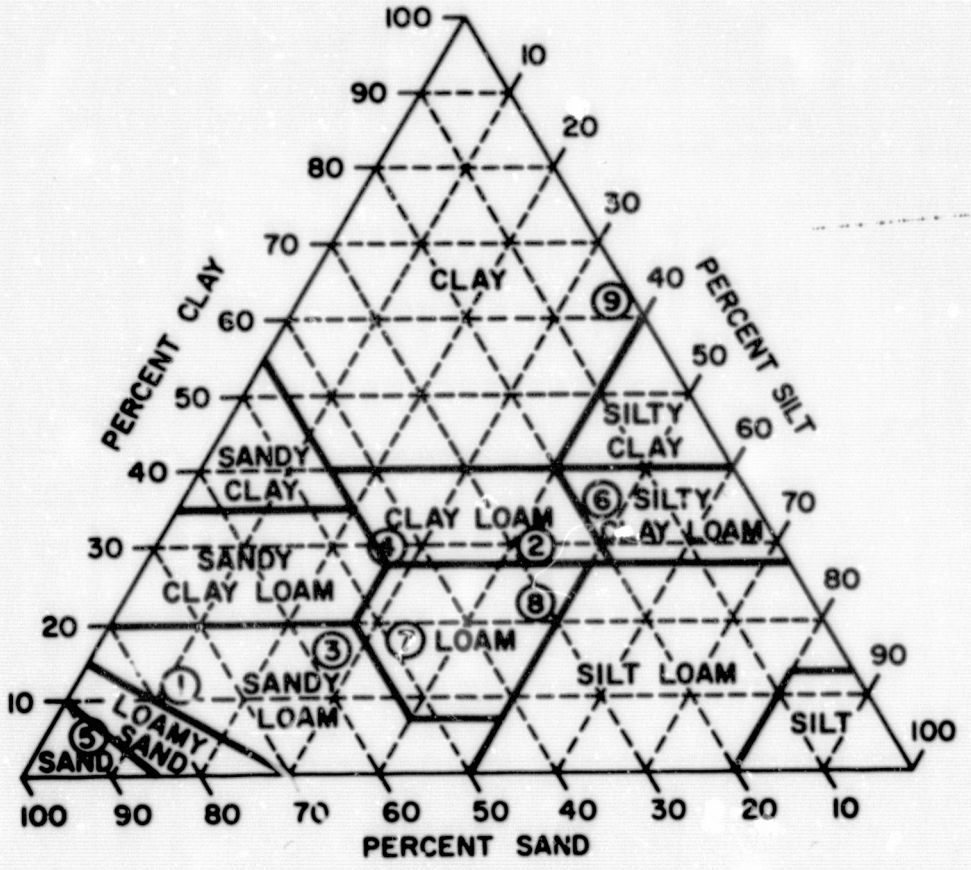


FIGURE 3. Soil samples from the Phoenix test site are shown in a textural matrix. (From Schmugge, et al., 1972). Samples 3-8 are from the Phoenix Test Site.

As pointed out by Schmugge et al. (1972) the type of soil texture is rather inportant in soil-moisture studies. In general, the clayey soils can hold more moisture than sandy soils which have greater permeability. Textural data on the soils at the test site are combined on figure 3.

One hundred fields were sampled on the north-south flight line. Four 6-inch samples were taken in each field. From the four soil-moisture values a mean was obtained for each field.

The test site is relatively homogeneous geologically. It is uniformly underlain by basin-fill deposits, although modern flood plain deposits of silt, sand, and gravel occur in mile segment one and from mile 14 to mile 16. (Thor Karlstrom, personal communication).

Soil texture can have a considerable affect on the distribution of moisture in the upper 30 cm of soil. The sample shown on figure 3 as sand (no 5) is probably from the flood plain. Such a sandy soil would drain quickly while less permeable silty soils would retain water much longer. A zone of moisture slowly draining downward would have a pronounced effect on gamma radiation originating in that soil at first, but as the moisture moves deeper into the soil, its effect drops off exponentially.

The Aerial Radiological Measuring System (ARMS)

The system employed in this experiment was designed and operated by EG&G, Inc. and was used with the permission of the Atomic Energy Commission. The Aerial Radiological Measuring System (ARMS) is installed in a Beechcraft Twin Bonanza, which is also equipped with a precise positioning system that measures radar altitude, ground speed, drift angle and heading.

The gamma-ray detection package consists of 14 four-inch by four-inch sodium iodide (NaI) scintillation crystals, thermally insulated and shock-mounted. The large volume of the crystals provides a sensitivity to gamma radiation several thousand times greater than that of a common Geiger-Mueller counter. An on-board computer produces a paper tape record of all flight and radiation data. A complete description of the system has been given by Anderson et al. (1969).

Initial Investigation

An initial investigation of soil moisture has been conducted over flight lines in the vicinity of Phoenix, Arizona, during February and March 1971. Gamma-ray surveys were flown with the Atomic Energy System's ARMS equipment by EG&G, Inc. Concurrent missions were flown by the NASA Convair 990 aircraft with multiband passive microwave radiometers at frequencies of 1.42, 4.99, 19.35, 37, and 94 GH_z. A description of the microwave experiment and its results has recently been published (Schmugge, Gloersen, and Wilheit, 1972). Ground truth measurements were collected over two selected flight lines, the 16-mile north-south line previously mentioned and a 30-mile east-west line by Biospherics, Inc. Radiometric data from the east-west line are not yet available for analysis.

As seen in fig. 1, the flight lines were selected to parallel the road net in this area. This selection was made to insure accurate identification from the air and to facilitate collection of ground truth data. Two passes at 300 feet (90 m) and one at 500 ft (150 m) above ground level were made.

Date	Leg No.	Altitude
2-25-71	102	500'
	108	300'
	111	300'
3-2-71	119	500'
	125	300'
	127	300'

Figure 4 indicates excellent reliability of the ARMS system during one day's operation, but in order to determine a correct base-line background count an additional flight is required during wet conditions. The prolonged record drought in the Phoenix area has forced postponement of this investigation.

Variations in the total gamma count from one day to another are also affected by the radon gas daughter products (^{214}Bi) in the atmosphere. The spectral information collected for selected flight line lengths provide a better measurement of the temporal variations in the soil moisture for the spatial averages. Investigations being conducted for improvement of the snow water equivalent measurements to develop techniques to overcome the adverse effects due to the

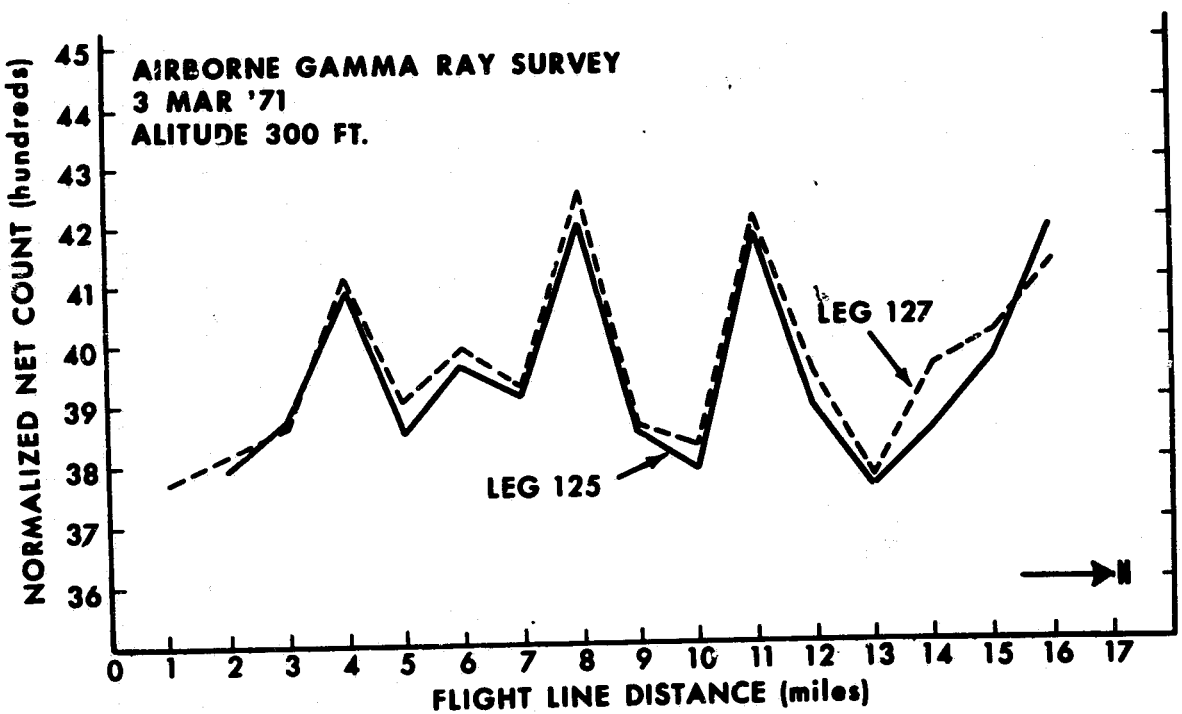


FIGURE 4. Graph showing the variation in gamma count of two flight legs flown a few minutes apart over the NOAA/NASA test site.

radon gas variations should also improve the total count method.

Other Investigations

Test sites in other parts of the country have also been flown, notably Luvernne, Minn., and near Syracuse, N.Y. Both sites were flown in June 1972. Data are not yet available for these flights, but at Luvernne the background count baseline is well established and the Syracuse sites will be reflown next week in conjunction with an ERTS-1 investigation for soil-moisture studies in the Lake Ontario basin. The earlier June flights were concurrent with microwave surveys flown for NOAA by Aerojet Electrosystems. The microwave data collected at Syracuse are reportedly of excellent quality (Al Edgerton, personal communication).

Summary

The Phoenix gamma-ray survey is incomplete. It lacks one additional flight under wet conditions to enable calculation of the radioactivity background count. The ARMS system has proved to be reliable for measuring the moisture equivalent of snow and seems to have worked very well in the first Phoenix flights, demonstrating excellent reproducibility of data.

The Phoenix test site has several drawbacks: 1) its soil moisture depends primarily on irrigation of local fields; 2) the unexpected severe drought that has plagued it. It also has several advantages: 1) it has excellent access; 2) it is uniformly underlain by the same basin-fill deposits except for two small areas, thus making it less susceptible to extreme radioactive variation.

Data from a similar experiment, completed in June 1972 for Luvernne, Minn., are being reduced by EG&G. A third similar experiment will be flown next week near Syracuse, N.Y. NOAA/NESS believes the gamma-ray technique will provide the kind of synoptic ground truth necessary to evaluate the ability of microwave sensors to measure soil moisture from high-altitude aircraft and satellites.

References

Anderson, C.N., Bundy, D.H., Cleland, J.R., and Weissman, V.F., 1969, Aerial Radiological Monitoring Surveys (ARMS) Systems and Procedures employed through FY 69. Tech. Rept. No. EGG-1183-1457, EG&G Inc., Las Vegas, Nev., 49 pp.

Biospherics, Inc., 1971, Soil Moisture Ground Truth for Correlation with Microwave Radiation Data, Contract No. NAS5-21610, Rockville, Md.

Dahl, J.B., and Odegaard, H., 1970, Aerial Measurements of Water Equivalent of Snow Deposits by Means of Natural Radioactivity in the Ground, in Isotope Hydrology, 1970, IAEC, Vienna, pp. 191-210.

Domitriev, A.V., Kogan, R.M., Nikiforov, M.B., and Fridman, Sh. D., 1971, Aircraft Gamma-ray Survey of Snow Cover, Nordic Hydrology, v. 2, pp. 47-56.

Kogan, R.M., et al., 1965, Determination of Water Equivalent of Snow by Method of Aerial Gamma-Ray Survey, Sov. Hydrol. Selec. Pap. [Engl. Transl.] No. 2, pp. 183-187.

Kogan, R.M. Nazarov, I.M., and Fridman, S.D., 1971, Gamma Spectrometry of Natural Environments and Formations, TT 70-50092, [transl. from Russian] 337 pp. Israel Prog. for Sci. Transl., Jerusalem.

Peck, E.L., Bissel, V.C., Jones, E.B., and Burge, D.L., 1971, Evaluation of Snow Water Equivalent by Airborne Measurement of Passive Terrestrial Gamma Radiation, Water Resources Research, v. 7, No. 5, pp. 1151-1159.

Schmugge, T., Gloersen, P., and Wilheit, T., 1972, Remote Sensing of Soil Moisture with Microwave Radiometers, Goddard Space Flight Center preprint X-652-72-305, 31 pp.

Zotimov, N.V., 1968, Investigation of a Method of Measuring Snow Storage by using the Gamma Radiation of the Earth, Sov. Hydrol. Sel. Pap. [Engl. transl.] No. 3, pp. 254-266.

THE RELIABILITY OF THE INTERPRETATION OF SOILS FROM AERIAL PHOTOGRAPHS IN HIGHWAY PLANNING PRACTICE

Ulf Kihlblom

Techn. Dr., B.A.

VBB - member of SWECO, Stockholm

SUMMARY

In cooperation with the Swedish Road Administration, a method of soil interpretation from aerial photographs combined with geotechnical investigations has been developed during 1965-1969 (Kihlblom 1970). The method is primarily applicable under the conditions prevailing in the Scandinavian countries and in other glaciated areas such as Canada, northern USA and Russia. In a later investigation, the reliability of the interpretation process - the determination of soil types and soil boundaries - has been tested (Viberg 1972).

A comprehensive investigation of the use of interpretations of aerial photographs for highway planning followed in 1969-1971. Among the goals of the investigation was the introduction of the method to the National Swedish Road Administrations and the checking of the reliability of the results obtained by different categories of interpreters. This paper will report on this part of the investigation only.

The quality of the interpretation results is of decisive importance for use in planning work. To test the reliability of the method and the quality of various categories of interpreters, an area outside Stockholm, characteristic of the soil conditions prevailing in middle and southern Sweden, was chosen.

The results of the reliability test were analyzed in two different ways, namely by interpreting test areas and by interpreting boundaries. The staff involved in the investigation was divided into three categories due to different knowledge of interpretation.

Determinations of soil types show very good results in regard to sandy, silty moraine and coarse sediments. The three groups have correctly identified 80-93 %. The interpretation of clay areas gives a rather large dispersion between the groups. The correctly interpreted areas vary within the range 59-90 %. A significant difference between the groups was obtained with regard to the interpretation of a few areas where the soil consists of clay with dry crust extending to the firm strata below. Thus the correct values vary between 40 and 91 %. Organic deposits are correctly interpreted by Group 1, while the variations are rather considerable in the other groups. The values of Group 1 and Groups 2-3 are 84-93 % and 59-66 % respectively.

The interpretation results of rocks are divided into three classes, namely: large rock areas, marked rock outcrops in woodland or open terrain and very small outcrops in open terrain. As may be expected, difficulties increase as the size of the outcrops decreases. The variation between the test groups is very considerable. Thus for the three types of rock which were correctly interpreted the values are 66-100 %, 35-93 % and 30-75 % respectively.

The analysis of the interpretation of boundaries shows that the boundaries between outcrops and moraine or coarse sediments are difficult to identify. The correct values for Groups 1-3 are as low as 60-65 %, 20 and 50 % respectively. All other types of boundaries within the area such as rock/clay, friction soil/clay, friction soil/organic soil and clay/organic soil were quite easy to interpret. The correct result varies between 80 and 100 %.

GENERAL

Since 1965 work has been carried out to develop methods of interpretation of soil types from black and white aerial photographs. The work has been carried out in collaboration with the Swedish Road Administration for use during geotechnical soil investigations in connection with highway and urban planning in Sweden. To introduce the method in routine road planning, a large number of designers, photogrammetrists and geotechnicians have been given short courses in the interpretation of soil types from aerial photographs.

This paper will report on the third step of a long-term programme to develop and introduce the interpretation of soils from aerial photographs for highway location and design studies. The main purposes of this investigation, which took place in 1969-1971, were to:-

- Estimate the value of the method and adapt the method to the present planning practice.
- Write instructions concerning the use of interpretation methods for the National Swedish Road Administration.
- Continue the training of the staff of the National Swedish Road Administration in connection with the planning of 17 highways.
- Develop an applicable combination of interpretation and soil exploration.
- Study costs and time requirements for different parts of the interpretation process.
- Develop a suitable reporting technique.
- Investigate the reliability of the results obtained by different categories of interpreters.

In this paper only the last item will be discussed. A 4 km^2 test site outside Stockholm was chosen for the purpose, FIGURE 1. The area is characteristic of the soil conditions prevailing in middle and southern Sweden. The staff involved in the investigation can be divided into three categories, namely:-

Group 1 Four experienced aerial photograph interpreters.

Group 2 Eleven interpreters with 1-4 weeks of training in the interpretation of soils.

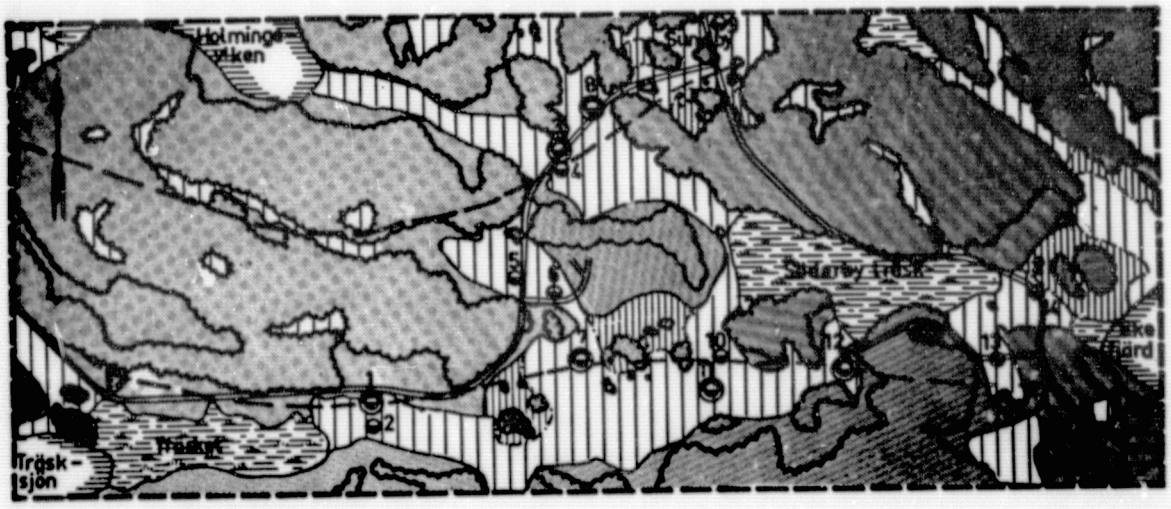
Group 3 Eleven interpreters, students at the Royal Institute of Technology, with one day of training each.

The types of soil in the test site are comparatively easy to interpret. Exceptions are clayey areas which were sometimes difficult to identify, while boundaries of other soil types are clearly indicated on the photographs. An aerial photograph and a general soil type map of the area on a scale of approximately 1:13 000 is presented in FIGURE 1.

The interpretation was carried out using black and white photographs on a scale of 1:13 000. Group 1 also used 1:30 000 to compare the influence of different scales. No aids, such as maps or geological reports, were used. Groups 1 and 2 were not allowed to check the result of the interpretation in the field. Group 3 was in the field for only three hours. The results for Groups 2 and 3 are therefore somewhat confusing if the differences in field checks are not considered. As could be expected, the results were poor in some cases, but many of the discrepancies could easily be corrected during field work.

To study the results obtained by the three groups, the interpretations have been analyzed with regard to both the determination of soil types in number of test areas chosen at random and the determination of soil boundaries along certain test lines.





LEGEND :

- WATER
- ROCK
- FRICTION SOIL
- DRY CRUST CLAY
- CLAY
- ORGANIC SOIL

FIGURE 1. AERIAL PHOTO AND GENERAL MAP
OF SOIL TYPES IN THE LADVIK AREA
Scale approximately 1:13 000.

RESULT OF INTERPRETATION OF TEST AREAS WITHIN THE LARVIK AREA

For the interpretation of soil types the following categories were used:-

- Friction soils (moraine and coarse sediments).
- Clay.
- Dry crust clay.
- Organic soil.
- Rock.
- Rock with thin soil cover.

Results of the interpretations of each group are given in TABLES 1-4. The interpretation of soil types is summarized in FIGURE 2.

Determinations of soil types show very good results in regard to sandy, silty moraine and coarse sediments, here grouped under the heading "friction soil". The three groups have correctly identified 80-93 %. The remaining 7-20 % were misinterpreted as clay areas. Most of the mistakes were caused by the fact that the boundary is drawn too high up in the terrain and thus somewhat inside the moraine or coarse sediment areas.

The interpretation of clay areas gives a rather large dispersion between the groups. The correctly interpreted areas vary within the range 59-90 %. Some clay areas, 1-6 %, were interpreted as organic deposits. This error can be regarded as small, since in some cases there is a gradual transition between the two soil types. 4-37 % clay areas were classified as moraine or coarse sediments. From the geotechnical point of view this is a serious mistake, as all these areas occur in parts where clay depths are greatest. However, in an ordinary interpretation followed by the necessary field check, this kind of mistake is easily corrected.

GROUP 1 1:50 000

SOIL TYPE	INTERPRETED SOIL TYPE: Friction soil	Clay	Dry crust clay	Organic soil	Large rocks areas	Marked rock outcr.	Small outcrops	Number of obs
Friction soil	93	7	-	-	-	-	-	14
Clay	6	89	-	5	-	-	-	44
Dry crust clay	25	-	75	-	-	-	-	16
Organic soil	-	7	-	93	-	-	-	28
Large rocks areas	-	-	-	-	100	-	-	24
Marked rock outcrops	34	-	-	-	-	66	-	44
Small outcrops	62	9	-	-	-	-	29	32

GROUP 1 1:15 000

SOIL TYPE	INTERPRETED SOIL TYPE: Friction soil	Clay	Dry crust clay	Organic soil	Large rocks areas	Marked rock outcr.	Small outcrops	Number of obs.
Friction soil	93	7	-	-	-	-	-	14
Clay	4	90	-	6	-	-	-	44
Dry crust clay	9	-	91	-	-	-	-	16
Organic soil	-	16	-	84	-	-	-	28
Large rocks areas	-	-	-	-	100	-	-	24
Marked rock outcrops	7	-	-	-	-	93	-	44
Small outcrops	25	-	-	-	-	-	75	32

GROUP 2 1:15 000

SOIL TYPE	INTERPRETED SOIL TYPE: Friction soil	Clay	Dry crust clay	Organic soil	Large rocks areas	Marked rock outcr.	Small outcrops	Number of obs.
Friction soil	80	20	-	-	-	-	-	40
Clay	40	55	-	5	-	-	-	109
Dry crust clay	51	-	49	-	-	-	-	35
Organic soil	8	23	-	65	-	-	4	57
Large rocks areas	38	-	-	-	62	-	-	53
Marked rock outcrops	71	-	-	-	-	29	-	110
Small outcrops	60	13	-	-	-	-	27	71

GROUP 3 1:15 000

SOIL TYPE	INTERPRETED SOIL TYPE: Friction soil	Clay	Dry crust clay	Organic soil	Large rocks areas	Marked rock outcr.	Small outcrops	Number of obs.
Friction soil	86	14	-	-	-	-	-	44
Clay	29	70	-	1	-	-	-	111
Dry crust clay	60	-	40	-	-	-	-	40
Organic soil	17	24	-	59	-	-	-	77
Large rocks areas	7	-	-	-	93	-	-	66
Marked rock outcrops	43	2	-	-	-	55	-	121
Small outcrops	42	27	-	-	-	-	31	88

TABLES 1-4. INTERPRETATION OF SOIL TYPES

Result of Group 1-3 in per cent.

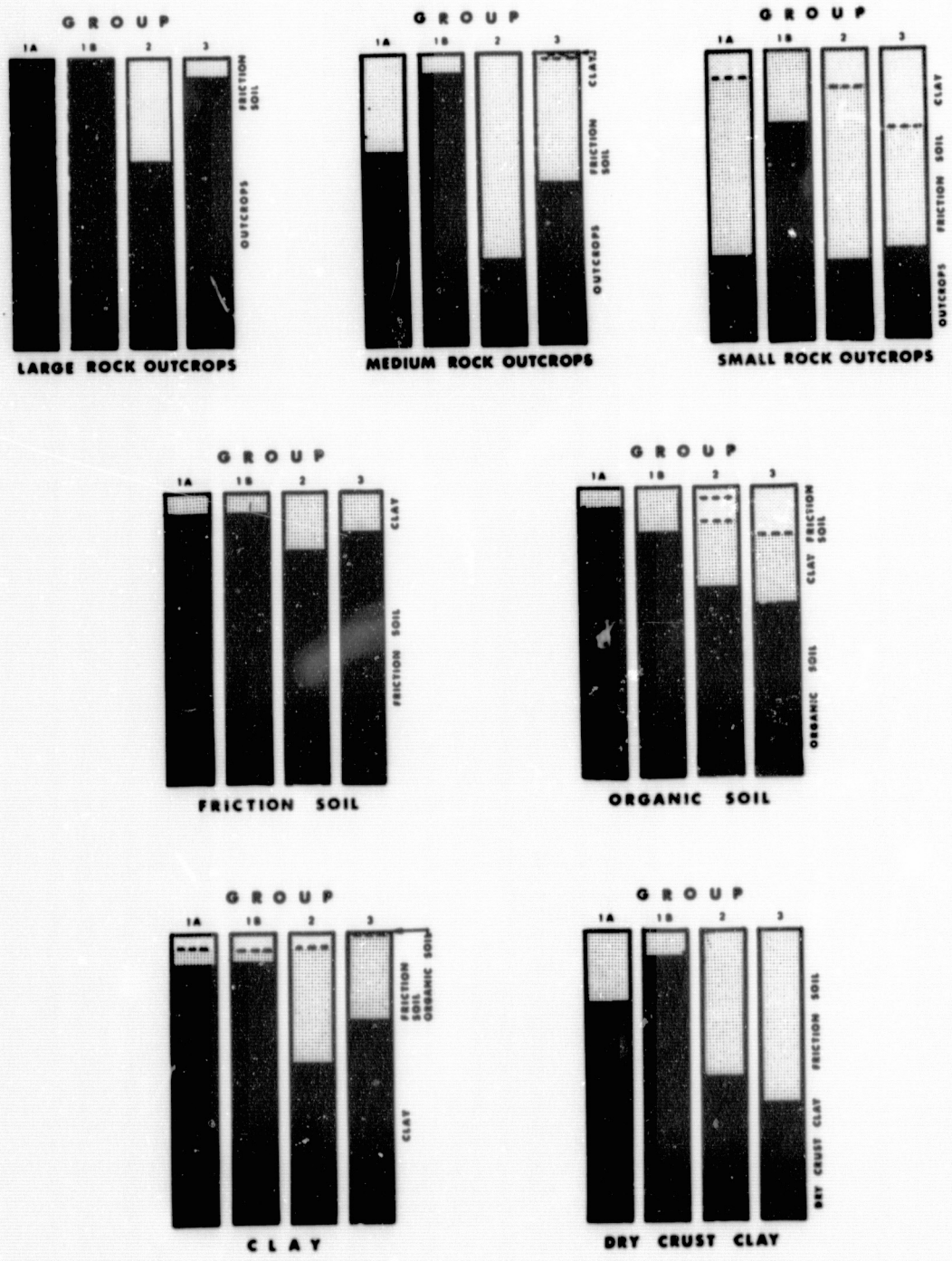


FIGURE 2. IDENTIFICATION OF SOIL TYPES.

Number of correctly (black) and incorrectly identified soil types in per cent. Group 1_A has used photographs to a scale of 1:30 000. Groups 1_B, 2 and 3 have used 1:13 000.

In a small number of areas the soil consists of clay with dry crust, including some silt and sand, extending to the firm strata below. A significant difference between the groups was obtained. Thus the correct values vary between 40 and 81 %. However, the mistakes are not so serious in highway planning, because the only alternative interpretation was moraine or coarse sediments.

Organic deposits are correctly interpreted by Group 1, while the variations are rather wide in the other groups. The values of Groups 1 and 2-3 are 84-93 % and 59-66 % respectively. The most dominant organic deposits have been identified with high accuracy. Most of the misinterpretations concern very thin peat cover or small peat or marshy areas in elevated forest terrain.

The interpretation results of outcrops are divided into three classes depending on their size, namely: large rock areas, marked rock outcrops in woodland or open terrain and very small outcrops in open terrain.

The identification of easily recognizable, quite large rocky areas with typically marked ranges is surprisingly low in Group 2. The aerial photographs show the characteristic features of rock such as landform, fissures and gray-tones. Sparse and low forests or vegetation appear only in large fissures and minor depressions. The large rock areas are at least 10 000-20 000 m^2 while the small outcrops are of a size of 5-10 m^2. As may be expected, difficulties increase as the size of the outcrops decreases. The variation between the test groups is very wide. Thus for the three types of outcrop which were correctly interpretated the values for Group 1 was 66-100 %, for Group 2 was 35-93 % and for Group 3 was 30-75 %. The most serious mistakes are found in the class of outcrops of 5-10 m^2, where as much as 13-25 % were interpreted as clay.

RESULT OF INTERPRETATION OF BOUNDARIES WITHIN THE LADVIK AREA

The analysis of results of interpretations of soil type boundaries included the following:-

- Rock/friction soil.
- Rock/clay.
- Friction soil/clay.
- Friction soil/organic soil.
- Clay/organic soil.

To demonstrate the reliability of the method, some examples of interpreted rock boundaries are given in FIGURE 3 and boundaries of organic soil in FIGURE 4, as produced by interpreters in Group 1. The largest deviations between rock boundaries occur mainly because clearly defined ranges gradually turn to moraine.

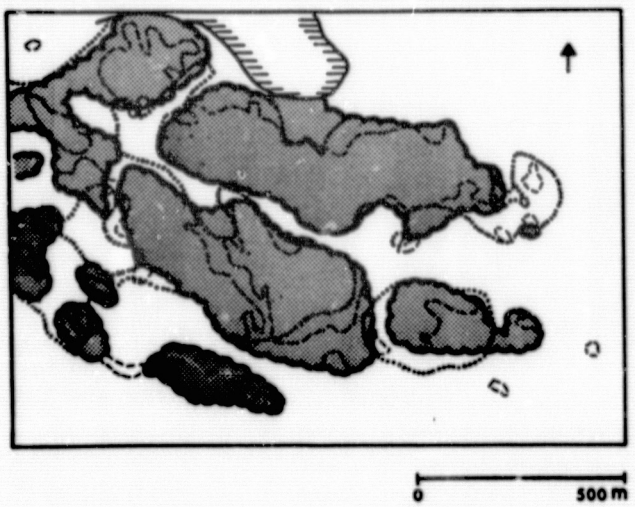


FIGURE 3. ROCK BOUNDARIES
Maximum deviation between interpreters.

As organic soil borders on rock and moraine, variation is small. Boundaries against clay, however, vary to a much larger extent, a condition which can be explained by the gradual thinning down of the thickness of the organic soil layers.

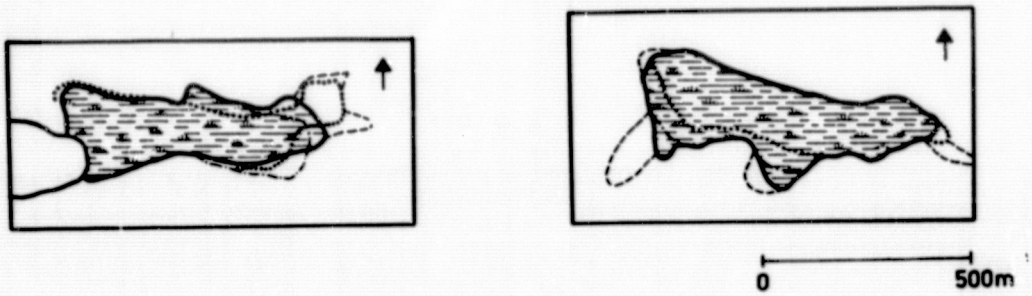


FIGURE 4. ORGANIC SOIL BOUNDARIES

Maximum deviation between interpreters.

The precision test showed that interpreters use various degrees of generalization. To illustrate, the results of three different interpreters in Group 1 are shown in FIGURE 5. None of them can be said to be really incorrect. The same results can be obtained by field surveys. The differences occur therefore in the varying opinions as to the degree of detail required. Opinions as to the spread of the moraine layers and the thickness of clay around rock ranges in the southern part of the area cause the differences in results within the area chosen. All interpretations, however, express rather similar ideas of the soil conditions and can be used for general planning purposes. The most detailed interpretations of the three may give an impression that all rocks were mapped, which is impossible to carry out in the forest-covered upper part of the area. The most generalized interpretation of rock and clay only may be sufficient for very general planning. The time required for rough generalization is less than for other types of interpretations. Results thus show that there should be rules for determining a degree of generalization in geotechnical interpretations of photographs similarly to geological mapping.

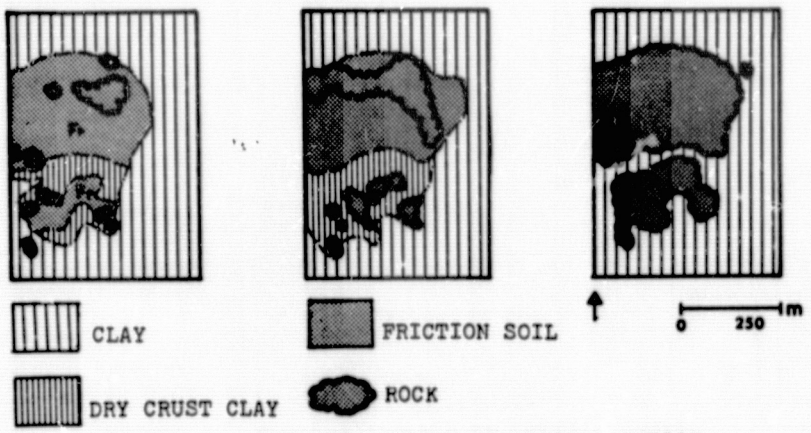


FIGURE 5. VARIOUS DEGRESS OF GENERALIZATION

Maximum deviation between three different interpretations of soil.

FIGURE 6 also shows two different interpretations of rock on a scale of 1:30 000. They give a completely different picture. One is very detailed, the other more generalized, although it gives a better idea of the small and large rock zones in the area. When rock and moraine are put together, the two interpretations are identical. The interpretations show extremes in judgements of rock and moraine. Between these extremes there are large variations in Groups 1-3. It should be pointed out that there are various opinions as to where on a field the boundaries between rock and moraine should be drawn.

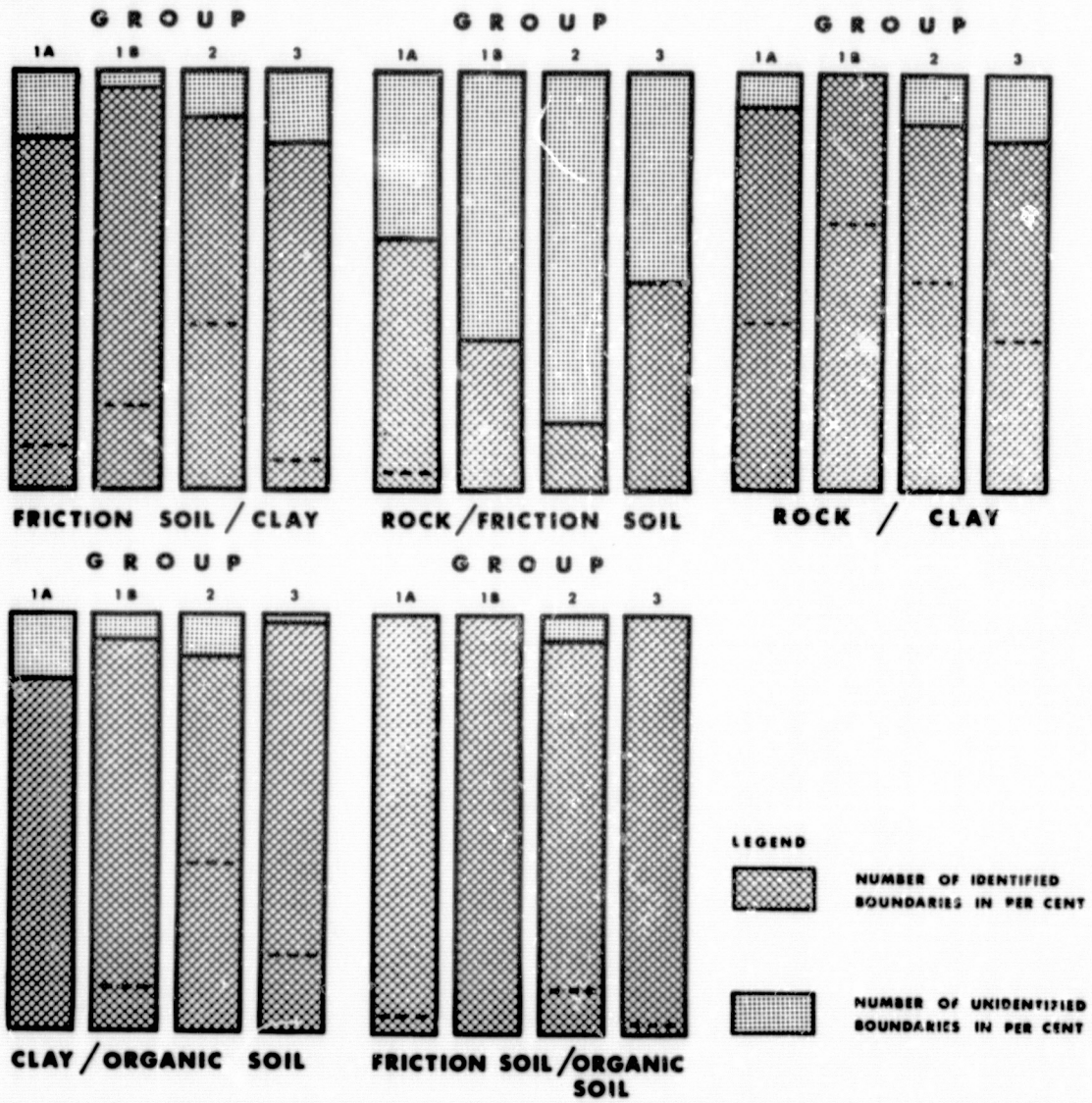


FIGURE 7. IDENTIFICATION OF BOUNDARIES

Number of identified boundaries in per cent. Group 1_A has used photographs to a scale of 1:30 000. Groups 1_B, 2 and 3 have used 1:13 000. Broken times indicated the number of correctly identified boundaries wher one or both soil types on each side of the boundary were incorrectly identified.

The identification of boundaries by Groups 1-3 has been checked in several sections. The results are summarized in a diagram in FIGURE 7. The results show that boundaries between rock and friction soil are difficult to interpret, while boundaries between rock/clay, friction soil/clay, friction soil/organic soil and clay/organic soil are in most cases correctly identified.



FIGURE 6. VARIOUS DEGRESS OF GENERALIZATION IN THE INTERPRETATION OF ROCKS

A large proportion of boundaries between rock and friction soil are not identified, as boundaries between moraine and fluvial outwash or coarse sediments have been identified in different ways. In a number of cases reservations were made, for example "minor zones of moraine and fluvial outwash of a thickness of 0.5 and 1 m respectively may occur within areas marked rock" or "minor outcrops may occur within moraine zones".

The results in FIGURE 7 illustrate the possibilities of using aerial pictures for geological and geotechnical purposes in highway planning. Identified boundaries seldom need to be corrected, though it is often necessary to check interpretations of soil types.

This third investigation of the long-term programme presented in this paper is followed by an analysis in 1971-1973 of the comparison between colour and black and white photographs. The schedule is similar, i.e. to test accuracy in the two types of film. The number of interpreters will be increased to approximately 70-80. The deviation in metres between the interpreted boundaries and the real boundaries will also be measured.

REFERENCES

Damgaard, J.J., Kihlblom, U., Kolhinen, M., and Melleby, L., 1970. Aerial Photographic Interpretation of Soils in the Nordic Countries. Nordic Association of Road Engineers.

Forsell, M., 1972. Remote Sensing Activities in Sweden. Svensk Lantmäteritidsskrift No 2:1972.

Kihlblom, U., 1970. Determination of Soils by Aerial Photographic Interpretation. Stockholm. Textbook in Swedish with summary in English.

Kihlblom, U., Viberg, L., et al. 1971. Geobildtolkning vid vägprojektering. Rapport från försöksverksamhet 1969-1971. Swedish Road Administration. Stockholm.

"Remote Sensing Symposium" Stockholm 24.11.1969. Swedish Board for Technical Development.

Viberg, L., 1972. Geotechnical interpretation of Aerial Photographs - A Study of the Reliability of the Method. Svensk Lantmäteritidsskrift No 2:1972, Stockholm.

DEFINITION OF SPECTRALLY SEPARABLE CLASSES FOR SOIL SURVEY RESEARCH

J. E. Cipra
P. H. Swain
J. H. Gill
M. F. Baumgardner
S. J. Kristof

Laboratory for Applications of Remote Sensing, Purdue University
West Lafayette, Indiana 47906

ABSTRACT

Spectral classes defined by a Euclidean distance criterion have shown similarity to soil classes as mapped by the National Cooperative Soil Survey (local, state, and federal governments cooperating). However, two problems have occurred in past studies:

1) The number of spectral classes defined by the researcher is arbitrary.
2) Spectral properties of nonvegetated soils are modified by rainfall, cultivation, and other factors not directly related to the classes of interest for soil survey purposes.

This research outlines a procedure for defining spectral classes such that the differences between classes can be quantified. It also facilitates determination of a number of classes such that the classes are spectrally discriminable. This is accomplished by partitioning the data into many classes and then combining similar spectral classes on the basis of appropriate criteria.

Multispectral data were collected over a 12-mile flightline in White County, Indiana, in connection with the 1971 Corn Blight Watch Experiment. Data were collected in May by the University of Michigan airborne scanning spectrometer at an altitude of 5000 feet. Spectral maps resulting from the analysis were compared to existing soil surveys of the National Cooperative Soil Survey.

This method should help determine the extent to which spectral properties of soil surfaces can be associated with morphologic and topographic differences of interest to soil surveyors engaged in operational soil mapping.

1. INTRODUCTION

Several researchers have shown that the spectral properties of nonvegetated soils correlate with other physical and chemical soil properties of interest (1, 2, 4). It has also been shown that spectral classes of soils, as mapped using computer-implemented pattern recognition techniques, correlate with National Cooperative Soil Survey mapping units to some degree (5). However, it is also known that surface conditions can affect spectral properties of soils as measured by an airborne multispectral scanner, and that these effects can sometimes mask the effects of interest to soil surveyors. It is also known that if there were a 1:1 correspondence between soil classes as mapped by the National Cooperative Soil Survey and the spectral classes as mapped using remote sensing that this would be extremely valuable information.

Preceding page blank

2. OBJECTIVES

The objectives of this research were to 1) find spectral classes in the data which could be discriminated; 2) define a repeatable method for obtaining these discriminable spectral classes; 3) compare the resulting spectral classes with the National Cooperative Soil Survey mapping units; 4) determine the extent to which the National Cooperative Soil Survey mapping units could be discriminated spectrally.

3. MATERIALS

The study area was a 12-mile flightline in White County, Indiana (Segment 208 of the 1971 Corn Blight Watch Experiment). The soils are of glacial origin being composed largely of glacial till and outwash. Windblown silts occur in parts of the study area. The soils have a range in surface textures from silty clay loam to sandy loam. The soils in this study area are described briefly in Table 1.

Multispectral data were collected on May 17, 1971 at 1:29 p.m. by the University of Michigan aircraft at an altitude of 5,000 feet, with a ground heading of 180°.

4. PROCEDURES

For the analysis, the flightline was divided longitudnally into two halves, east and west, to minimize the effects of look angle and sun angle. Each half was analyzed separately. Exhaustive samples which represented areas of bare soil were selected from multispectral imagery. These samples were pooled, and a cluster analysis was conducted using the LARSYS program NSCLAS (8). Fifteen classes were specified in the cluster analysis in order to be sure to define at least as many spectral classes as there were soil mapping units. It was anticipated that from six to ten soil mapping units might exist in such an area in this length of flightline. Seven wavelength bands in the visible region (0.40-0.70 μm) were used throughout the analysis.

A set of test fields was selected using a systematic random procedure. Each test field was assigned to the soil survey mapping unit which it represented. This was the first stage in the analysis at which ground information regarding mapping units was employed. Prior to this stage only spectral information was used in the definition of classes.

After having defined the spectral classes using the clustering program, the entire area was classified using the cluster classes as the basis for training. This classification procedure utilized a maximum-likelihood algorithm (6).

The distribution of the soil mapping units (represented by the test fields) into the 15 spectral classes was examined. Mapping units were combined if they were not spectrally distinct, and the distribution of the test field data into grouped spectral categories was examined. Grouping was accomplished using Figure 1, as described in the following paragraphs, and was based on an average quotient of less than 1.0 within groups.

Cluster classes were combined into groups by first combining those classes which were most similar, based on the quotient value. In the example (Figure 1), this was classes 14 and 15 which had a quotient of 0.50. Then the next most similar class, 10 and 11, (quotient = 0.56) were combined. This was followed by combining classes 4 and 5, then 6 and 7, then 12 and 13. etc. At each step the possibility of a single class combining with an existing group of two or more classes was checked. Likewise, as the procedure continued, groups were combined with other groups. A consistent rule was employed at every step, which may be stated as follows. Classes or groups were combined to yield the smallest quotient or average quotient for all pairwise comparisons within the new group. This procedure is described and discussed more fully by other researchers (3, 7).

Figure 2 shows the distribution of the test field data for one-half of the flightline into the 7 groups which were derived from the information in Figure 1.

On the left is the soil series which was mapped by the soil survey. Prior to combining 15 classes into 7 classes, Dana and Parr were not found to be spectrally

discriminable; so they were grouped in this table. The table shows the number of points (resolution elements) which occurred in each of the new spectral groups which were defined. The Miami soil had a rather small sample, only 8 points, but these were all classified into Group 1, the brightest group. The Plainfield soil had 40 points, all of which were classified into spectral Group 1, also. The Dana and Parr occurred primarily in spectral groups 2 and 3. This means that Dana and Parr soils are slightly darker in tone than the Miami and Plainfield soils and that this fact was detected by the scanner and the analysis procedure.

The Chalmers soil occurred almost entirely in cluster group 7, the darkest spectral group. It is possible to reduce this table still further by grouping together Miami and Plainfield samples, since these two were not found to be spectrally discriminable from one another, and considering groups 2 and 3 as being related to the Dana and Parr soils.

Figure 3 shows the recognition of soil types based on these criteria. By this grouping, the three groups of soils were recognized 91.6% correct on the average.

5. CONCLUSIONS

Three groupings of soil mapping units were differentiated spectrally by these procedures. Five different mapping units had been delineated by the soil survey in this area. Clusters were not sharply defined in the data. This is reasonable when considering the continuous nature of soils and their occurrence on the landscape. Soils often grade from one into another on the landscape rather than having sharply defined boundaries between them. Some soil mapping units were quite similar to one another and had a rather large amount of spectral variability within a mapping unit. From this analysis, we conclude that one to one correspondence between soil survey mapping units and discriminable spectral classes is unlikely for glacial soils of Western Indiana.

The three groups which were separated in this study correspond to some extent to management groups. The Chalmers soil occurs in depressions and is usually tile drained to make it agriculturally productive. It also has limitations for urban and other purposes.

Dana and Parr can be cultivated without tile drainage, and are often more productive soils than Miami and Plainfield.

Finding Dana and Parr soils spectrally similar was not an unlikely result. Apparent nondiscriminability of Miami and Plainfield, however, was not anticipated since these two soils are quite different in terms of surface texture and other properties. It seems possible that future investigations may explain this phenomenon, or at least achieve greater spectral separability for such soils.

6. REFERENCES

1. Baumgardner, M. F., S. J. Kristof, C. J. Johannsen, and A. L. Zachary. 1970. Effects of organic matter on the multispectral properties of soils. Proc. of Indiana Acad. of Science, 79:413-422.

2. Bowers, S. A., and R. J. Hanks. 1965. Reflection of radiant energy from soils. Soil Science, 100:130-138.

3. Cipra, J. E. 1967. Application of cluster analysis and centroid factor analysis to the numerical taxonomy of some soils of the world. M.S. Thesis. Kansas State University, 162 p.

4. Cipra, J. E., M. F. Baumgardner, E. R. Stoner, and R. B. MacDonald. 1971. Measuring radiance characteristics of soil with a field spectroradiometer. Soil Science Soc. of America Proc. 35:1014-1017.

5. Kristof, S. J., and A. L. Zachary. 1971. Mapping soil types from multispectral scanner data. International Symposium on Remote Sensing of Environment, Proc. 7th Institue of Science and Technology, University of Michigan, Ann Arbor, 3:2095-2108.

6. Nilsson, N. J. Learning Machines. McGraw-Hill, 1965.

7. Sokal, R. R., and C. D. Michener. 1958. A statistical method for evaluating systematic relationships. University of Kansas Sci. Bull. 38:1409-1438.

8. Wacker, A. G., and D. A. Landgrebe. 1971. Minimum distance classification in remote sensing. LARS Information Note 030772. Laboratory for Applications of Remote Sensing, Purdue University, West Lafayette, Indiana 47907.

TABLE I. SOILS OF THE STUDY AREA.

Soil Series and Surface Texture	Typical Surface Color (Munsell)	Natural Drainage
Plainfield sand	10 YR 4/2	well drained
Miami silt loam	10 YR 4/2	well drained
Parr silt loam	10 YR 3/2	well drained
Dana silt loam	10 YR 3/2	moderately well drained
Chalmers silty clay loam	10 YR 3/1	very poorly drained

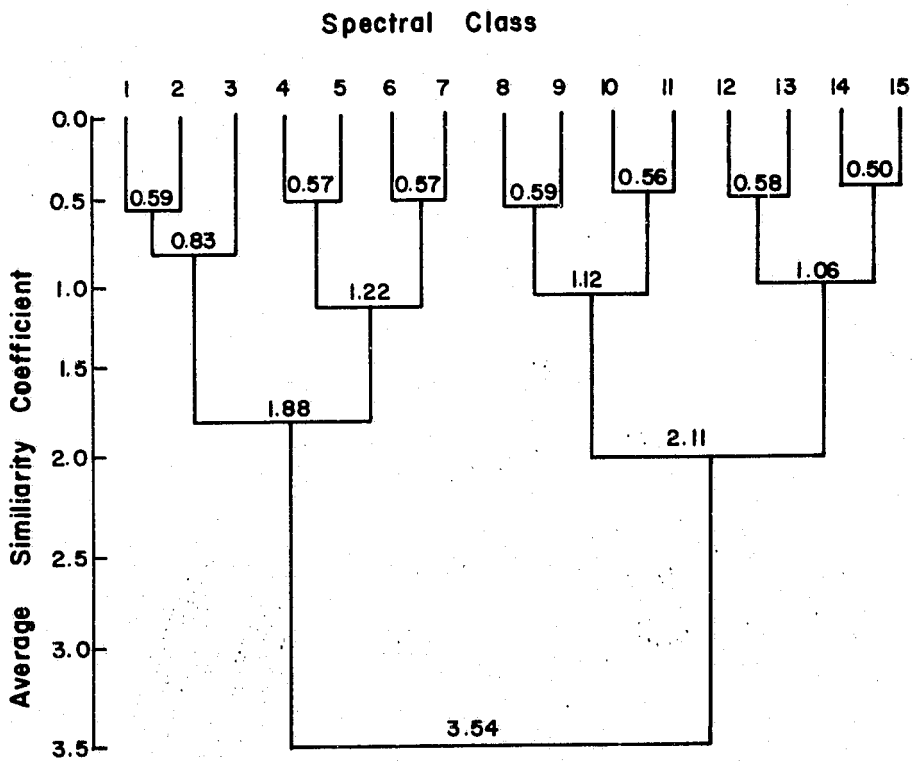


FIGURE 1. DIAGRAM SHOWING GROUPING OF 15 CLUSTER CLASSES BASED ON SIMILARITY COEFFICIENT.

Soil Series	Spectral Group 1	2	3	4	5	6	7
Miami	8	0	0	0	0	0	0
Plainfield	40	0	0	0	0	0	0
Dana-Parr	16	100	92	4	0	0	0
Chalmers	0	12	16	0	0	32	304

FIGURE 2. DISTRIBUTION OF TEST SAMPLE POINTS INTO SEVEN SPECTRAL GROUPS.

Soil Series	% Correct
Plainfield, Miami	100.0 %
Dana, Parr	88.6
Chalmers	92.2
Overall	91.6 %

FIGURE 3. PERCENT CORRECT RECOGNITION OF FIVE SOIL TYPES WHEN COMBINED INTO THREE GROUPS.

AUTOMATIC TERRAIN MAPPING BY TEXTURE RECOGNITION

E. E. Triendl

Institut für Satellitenelektronik
Oberpfaffenhofen, Germany

ABSTRACT

Black and white air photos of forest areas are processed into maps by the recognition of forest textures. Only two features are used: the moving average of the grey value and its second derivative. Borderline behavior, a more general approach and the connections to multispectral image recognition are discussed.

1. TEXTURES

Texture is a local property of an image, it can be calculated from features measured over a certain area (determined by the coarseness of the texture) of the image. These features describe the texture at every point of the image, and bear a certain resemblance to the color components of a color image or a multispectral scan. Recognition of texture from texture features is therefore similar to the recognition of color from color components.

2. GENERAL PROCEDURE OF TEXTURE RECOGNITION

Texture recognition is performed by multiple local filtering of a digitized image. For every picture element a label is calculated, which names the texture. This is done by local operations which take into account only a certain neighborhood (e.g. 9x9 picture elements) of each picture element.

Texture recognition is performed in four steps (fig. 1):

2.1 Multiple filtering of the original image produces a set of corresponding images in each of which a certain feature pertinent to textures is enhanced. Such features are lines, edges, dots, of various with, acuity and direction.

2.2 Linear or nonlinear averaging of these filtered images produces a new set of images lacking high frequency detail, which can be considered as texture components of a composite image (as are the spectral ranges in a multispectral scan image). Every picture element in the composite image consists of a vector whose components are the corresponding picture elements of the averaged images.

2.3 Partitioning of this vector space into classes of textures, either in a non supervised mode using a clustering algorithm, or by supervised learning. Every point in the image is now assigned to a certain class without regard to geometrical contiguity. However the averaging performed in step 2.2 results in areas with a certain size and a smooth borderline.

2.4 Generation of a terrain map consisting of the borderlines of areas whose texture has been recognized and of computer generated texture such a hatching, crosses, etc. replacing the original image.

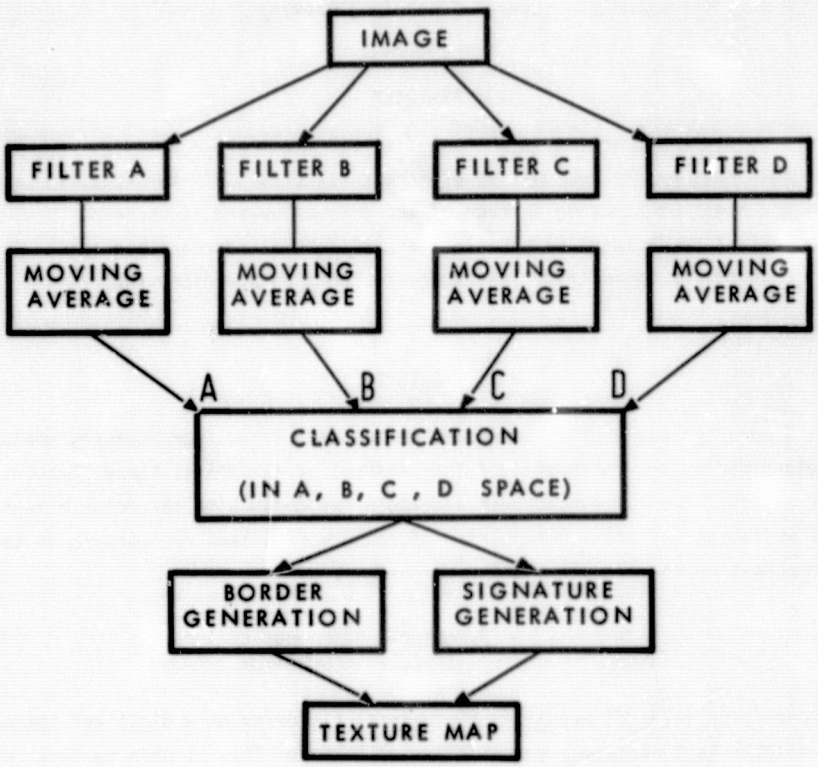


FIGURE 1. PRINCIPLE OF TEXTURE RECOGNITION

Result has been obtained using only a twodimensional features space, whose base vectors are the values "brightness" and "roughness", on artificially generated textures. Since the twodimensional feature space can be printed as a picture, clustering points can be picked by hand and the results of clustering algorithms can be checked by visual comparision. Border line behavior and texture separation can be studied in this twodimensional case.

3. FOREST TEXTURES

For the recognition of forest textures an air photograph of a recultivation forest with various types of shrubs, deciduous trees and conifers planted in rows or at random on a lignite mine is used. The picture has been digitized with 240 x 500 picture elements, which results in a distance of not more than 5 or 6 picture elements between trees. Figure 2 shows the digitized picture.

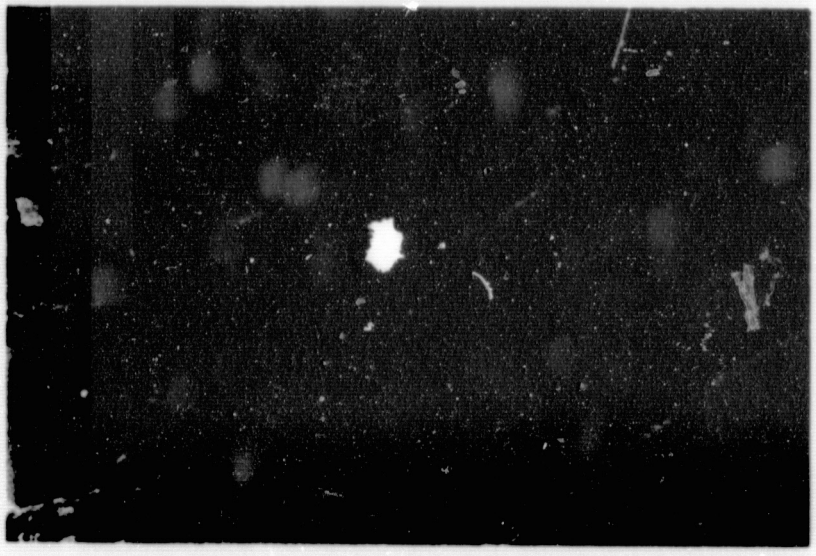


FIGURE 2. RECULTIVATION FOREST. Digitized with a resolution of 240 by 500 picture elements.

The digitized picture has been subjected to two local filters:

a) a low frequency filter (3x3 average) and a greyscale expansion
b) a high frequency filter (3x3 Laplacian derivative), with negative picture elements set to zero

The images a) and b) are shown overleaf (fig. 3).

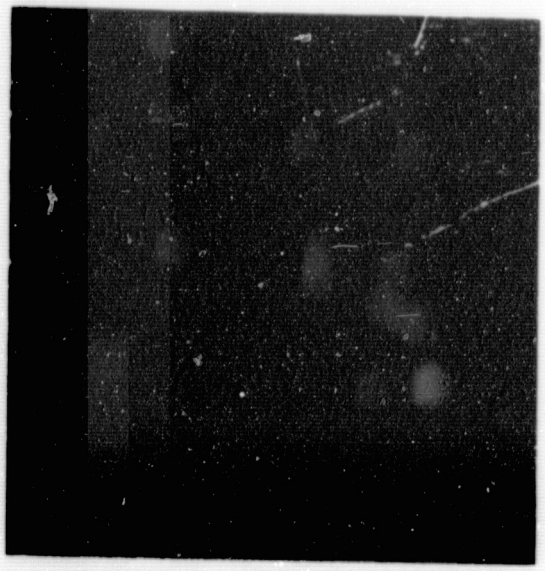


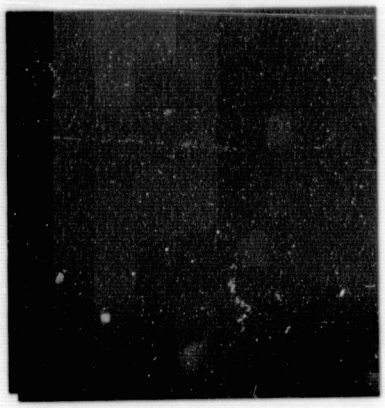
FIGURE 3. AFTER DOUBLE FILTERING.
a: low frequency and grey scale manipulation.
b: positive part of the Laplacian derivative.



FIGURE 4. FEATURES "BRIGHTNESS" and "ROUGHNESS".
The result of unsharpening figure 3.

A moving average over 11 by 11 picture elements of the pair of filtered images produces features fit for a recognition algorithm. A corresponding pair of points in the feature images defines a spot with a certain value of "brightness" (low frequency content) and of "roughness" (high frequency content) in the (twodimensional) feature space. Points from the same type of forest tend to group together and produce a population maximum. Figure 5 shows the population density of the feature space displayed as grey value. The maxima which can be distinguished are used to classify the picture into 6 types of textures. Every point of the picture is assigned tc the class of the nearest (in city block measure) maximum in feature space. The texture map shown in figure 6 is produced by substituting a different hatching or grey level for each texture class.

brightness



roughness

FIGURE 5. POPULATION DENSITY IN FEATURE SPACE.

4. DISCUSSION

This stripped down version of a texture classification method is still capable of differentiating between various types of forest and land. However a closer look at the resulting maß reveals that obvious misclassifications occur.

The process can be enhanced by:

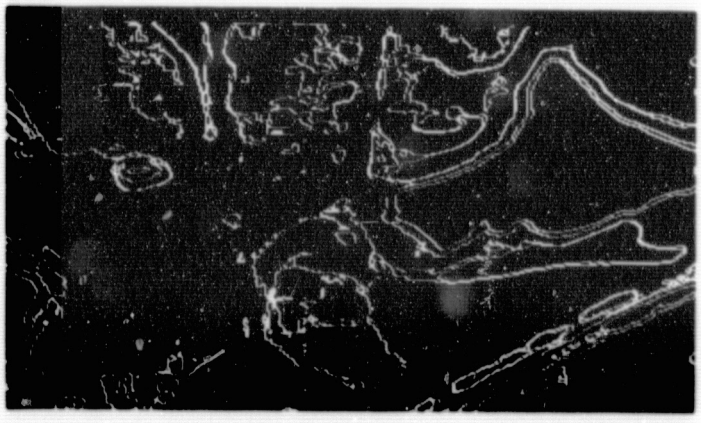
a) using more than two feature filters (matched to the expected textures)

b) using an elaborate clustering algorithm, which does not only take into account neighborhood in the feature space but also local contiguity of potential cluster candidates.

A mayor problem is the influence of non areal features such as lines and edges on the averaging process. Since remedying this requires the extraction of these features before averaging, texture recognition becomes feasible in conjunction with line, edge and object recognition, which is needed anyway to produce a map. It is also suggested that texture recognition may be a supplement to the recognition of multispectral color signatures.



FIGURE 6. TEXTURE MAP. Textures are classified by minimum distance to maxima in feature space.



REMOTE SENSING FROM

AN EARTH RESOURCE ROCKET

B. S. E. BEATTIE

British Aircraft Corporation Ltd.
Electronics and Space Systems.
Bristol, England.

1. INTRODUCTION

The use of rockets as platforms for Earth Resource Survey sensors is a comparatively recent concept. The employment of aircraft and satellites for this purpose has been the subject of considerable work since the Gemini series highlighted the possibilities of such techniques. Rockets on the other hand have only been seriously considered over the past two or three years.

The main conceptional initiative in this development is due to Commodoro Tasso of the Argentine Space Research Committee. The Royal Aircraft Establishment of Farnborough in collaboration with the British Aircraft Corporation Sounding Rockets Department at Bristol after consultations in the Argentine have designed and constructed a number of prototype earths resource rockets based on the well proven Skylark sounding rocket. The first of these was launched at the Woomera rocket range in Australia on 27th March 1972.

Although the primary purpose of this first flight was to prove the earth resource rocket as a sensor platform the opportunity was used to carry out additional trials covering handling techniques and flight use of photographic sensors. This involved the establishment of ground truth and helicopter borne sensors operated in accordance with a programme devised and implemented by Reading University in collaboration with the Commonwealth Scientific and Industrial Research Organisation.

The choice of Woomera for the first flight was dictated by the requirements for safety during the trial of a prototype. The modifications to the standard Skylark sounding rocket to allow for its use as an Earth Resource Rocket have been designed to allow operations outside established rocket firing ranges and the next trials in this series are planned to take place in such areas in the Argentine.

The development of this rocket is aimed at providing a complementary system to the primary sensor platforms represented by satellites and aircraft.

2. THE SKYLARK ROCKET

Approximately 300 Skylark Sounding Rockets have been launched with a cumulative flight reliability for the rocket exceeding 98%. Comprising two major sections, the motor and the payload, the rocket is 44 cm in diameter and approximately 12 m long when maximum payload volume is required. The design is modular in concept and in manufacture takes the form of a wide range of interchangeable components which allow considerable flexibility in build and therefore in application. Thus payloads are built up using tubular self-aligning cast magnesium body sections of various standard lengths up to 51 cm which, after the assembly of details, are clamped together by manacle rings. As shown in fig.1 the various marks of Raven motor used singly or in combination with the Goldfinch and Cuckoo boost motors provide a wide coverage in terms of performance relative to payload weight.

Continuous development of the Skylark Sounding Rocket has taken place over the last fifteen years. The changing requirements of scientific research in geophysics and astrophysics has demanded the ability to lift heavier payloads to greater altitudes, to stabilise and control the attitude of

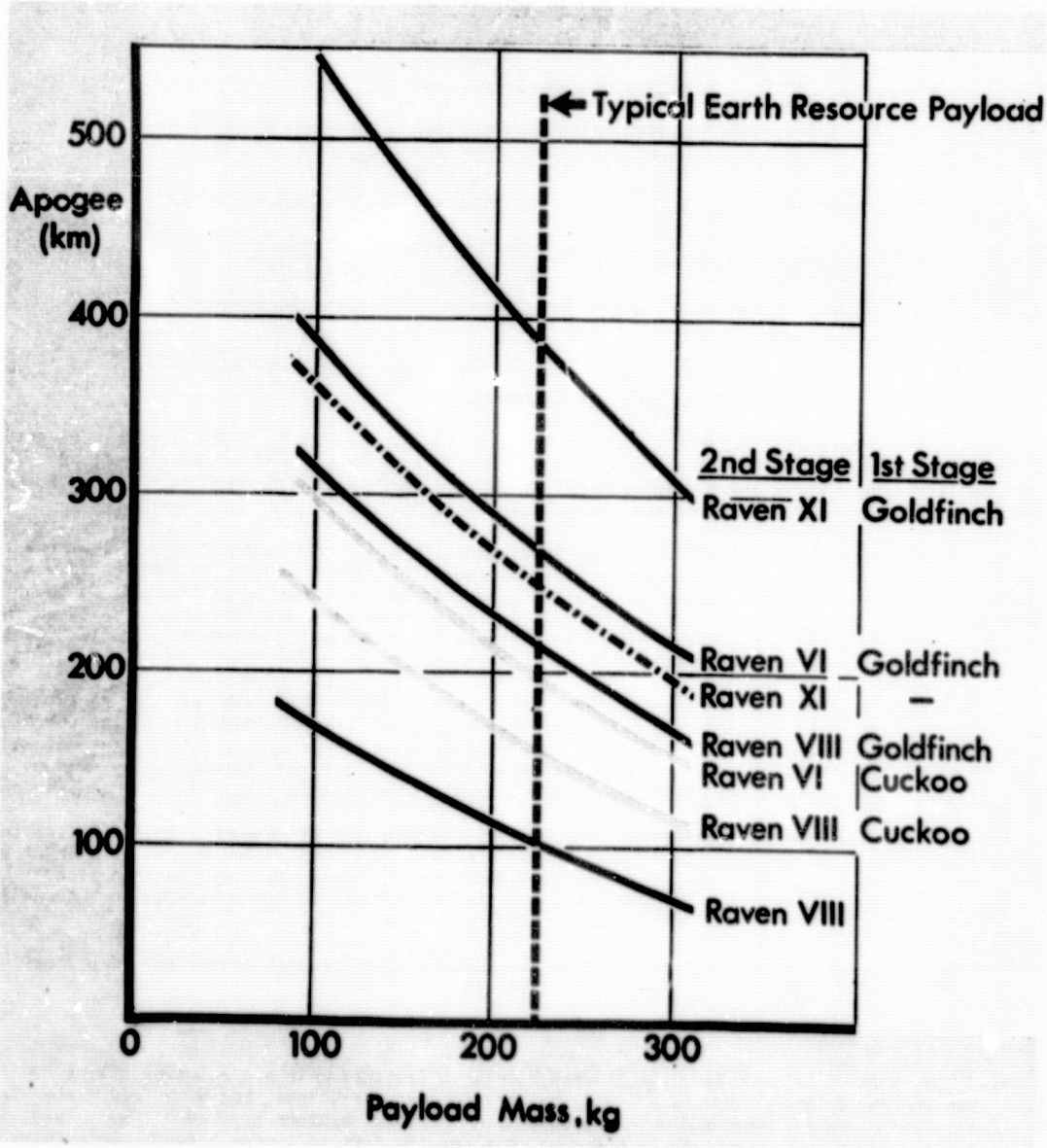

Typical Earth Resource Payload
500
Apogee
(km)
400
300
200
100
0
100
200
300
Payload Mass, kg
2nd Stage
1st Stage
Raven XI
Goldfinch
Raven VI
Goldfinch
Raven XI
—
Raven VIII
Goldfinch
Raven VI
Cuckoo
Raven VIII
Cuckoo
Raven VIII

FIGURE 1

payloads in flight and to effect reliable recovery by parachute. The same considerations have dictated flexibility in the choice of launch site with the consequential use of transportable launchers and the need to achieve the accuracy in timing and trajectory necessary for high altitude observation of lunar occultation of cosmic X-ray sources.

An Earth Resource version of the Skylark rocket has become a practical possibility due to these developments. This does not mean that the Earth Resource application can only be achieved by employing the most advanced components in the Skylark range but that the unique compromise between simplicity, safety and performance which this application demands is now feasible. For this reason it is now possible to overcome the operational and sociological problems involved in launching high altitude rockets away from the established rocket firing ranges in areas which may vary from comparatively highly developed regions containing centres of population to those which are under-developed and inaccessible. At the same time the rocket retains the flexibility inherent in the basic design of Skylark thereby allowing a wide range of earth resource survey requirements to be met.

3. THE PROTOTYPE EARTH RESOURCE ROCKET

The build standard of the earth resource Skylark designated SL 1081 which made the trial flight at Woomera is in many ways typical of the rockets currently being launched for upper atmospheric and space research. The motor combination, Goldfinch boosted Raven 6 with its triple fin assembly and ignition unit, is a normal Skylark configuration. The payload section, however, whilst utilising many standard items, has a number of features which have been developed specially for this application.

One such feature is the attitude control system which has been developed by the Royal Aircraft Establishment. In this instance existing units utilising sun pointing or inertial platforms were considered unnecessarily complex and expensive. In the earth resource Skylark two earth albedo horizon sensors set into the surface of the forward body section produce outputs in the form of staircase signals dependant upon the position of the sensors relative to the earth's horizon. These signals are then processed in the electronics sub-system to control high pressure nitrogen jets, positioned at the base and the tip of the stainless steel nose-cone. The jets at the base stabilise the payload in roll and those at the tip place and maintain it in a horizontal attitude. Its direction in azimuth is controlled similarly through the operation of a further set of jets disposed laterally at the nose-cone tip which are activated by outputs controlled by a rate gyroscope.

Another special unit developed for the earth resource rocket is the roll rate control unit which operates during the Raven motor burn period. It is normal practice with rockets using high performance motors to avoid roll/yaw instability problems by using canted or off-set stabilising fins to spin the rocket during the period of motor thrust. Unfortunately fins canted for this purpose tend to be ripped away by the severe aerodynamic forces operative during re-entry. This partial disintegration is unacceptable for safety reasons on flights outside rocket firing ranges and therefore in the earth resource rocket the alternative approach must be adopted which is to use straight fins and control the roll to very low rates which are equally effective in avoiding roll/yaw instability. The simple and robust roll rate control unit devised by B.A.C. to carry out this function uses a roll rate gyro to control the position of three small aerodynamic vanes.

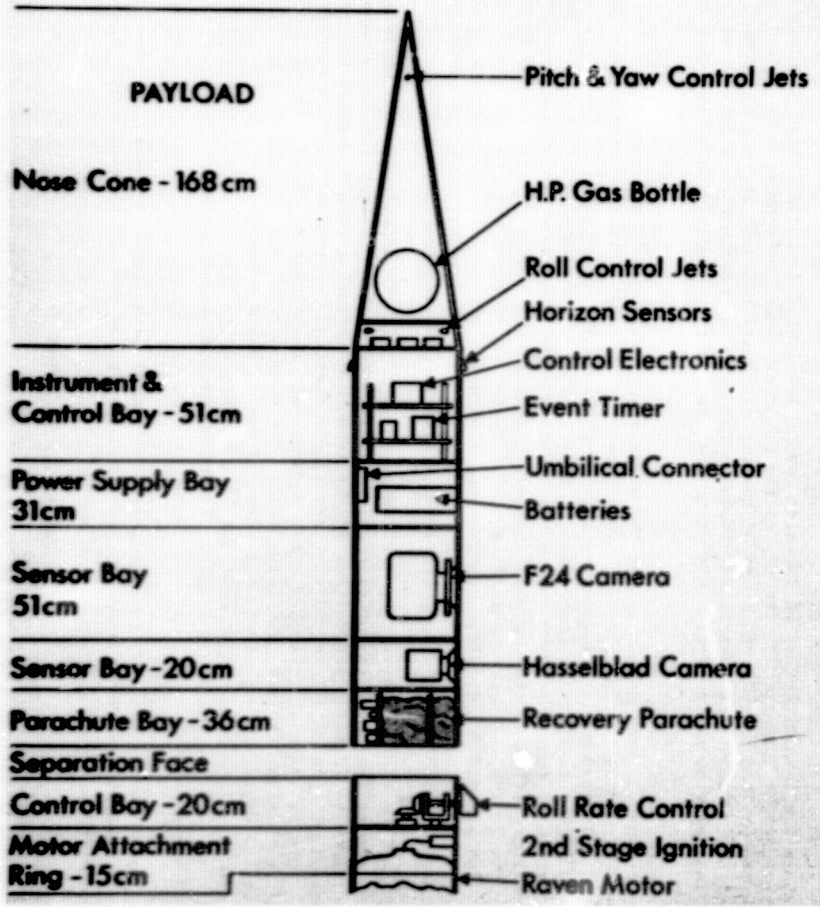
The configuration of Skylark SL 1081 is shown in fig.2. In addition to the units already mentioned, the payload service bays include telemetry and instrumentation for flight analysis, a programme timer to initiate the various flight sequences including camera operations, power supplies and an umbilical connector to facilitate pre-flight testing. A standard payload recovery system is used. This is barostat initiated after re-entry at an altitude of about 3 Km deploying a large parachute which slows descent to 9 metres/sec. The parachute panels are alternating radar reflective and dayglow orange to assist tracking during descent and location on the ground. The limited camera installations specified for this proving trial were accommodated easily in two standard bays of 51 cm and 20 cm length. For more complex sensor installations up to three 51 cm bays could be utilised.

The Skylark motor recovery parachute is still under development and was not programmed for SL 1081. A balasted bay was substituted for trials purposes and the total payload weight including this was 218 Kg.

4. CAMERA INSTALLATION

The decision to control the earth resource payload to maintain a horizontal attitude in flight was mainly determined by considerations of space utilisation in the sensor bays. It was recognised that sensor installation and operation could be simplified with resulting savings in

SL1081 CONFIGURATION



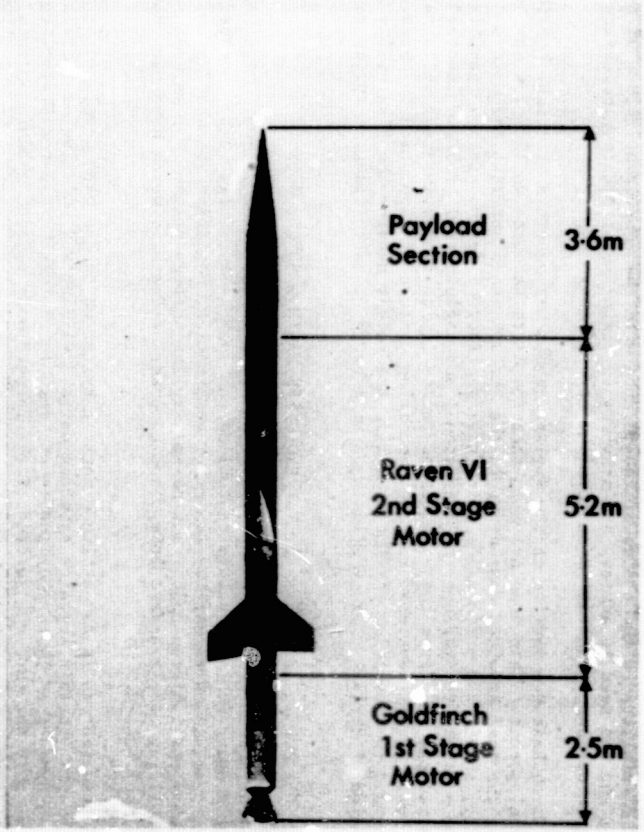


FIGURE 2

weight and space if the field of view was arranged to be normal to the longitudinal axis of the payload. The horizontal attitude is also advantageous for re-entry when as a result of increased drag the payload decelerates more rapidly at higher altitudes with a consequential reduction in kinetic heating.

As the primary purpose of the SL 1081 flight was to prove Skylark as a sensor platform it was decided to limit the installation to a pair of cameras chosen to allow correlation with results of surveys using aircraft and the ERTS series. It was also decided to off-set the mounting of the cameras from the vertical and programme the attitude control unit to rotate the payload in azimuth on to headings at 60° intervals thereby obtaining a significant increase in coverage..

It will be appreciated that the only limitation on camera selection is that of size in relation to the capacity available in a Skylark bay (428 mm internal diameter). The performance of the attitude control system is ±0.5 degrees in position and ±0.25 degrees per second in rate and this is well within the values required to achieve the maximum resolution accuracies available from existing cameras and films. The largest standard format which could be accommodated albeit with a modified low capacity film magazine is 230 mm square. However for SL 1081, considerations of availability and the programme timescale led to a decision to install as the larger format camera an F24, which approximates to the present standard 115 mm format.. The second camera, a Hasselblad 500, was selected mainly on account of the wide range of lenses available. It was also decided to use panchromatic film in the F24 and infra-red false colour in the Hasselblad.

Selection of lenses for the two cameras was influenced by considerations of definition and coverage requirements taking into account the facility provided to rotate the platform and the varying altitude of the payload during trajectory. For the F.24 a Ross EMI f/4 mm focal length lens was chosen. This gives a 70° field of view and the camera was therefore offset 25° from the vertical. For the Hasselblad a Zeiss f/2.8 Planar with 127 mm focal length was employed and the offset was set at 18°.

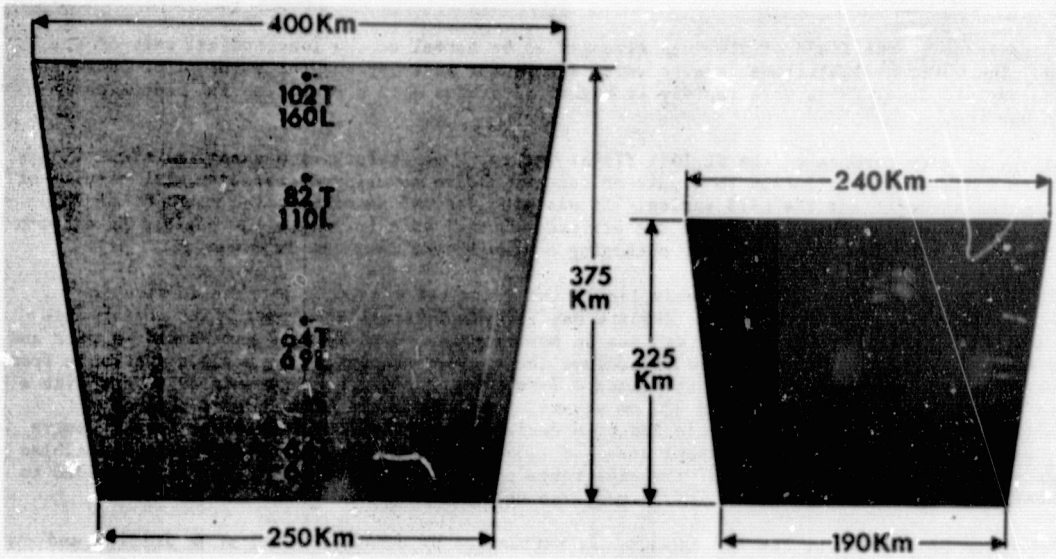
In order to obtain results at different spectral levels the F24 is provided with a filter wheel carrying six filters at three different wavebands which is rotated continuously at 24 degrees/sec. The filters are chosen to have similar light transmission factors so that exposure is kept constant and the rotation of the wheel is phased so that exposures through each of the three filters can be made on each of the headings on which the payload is stabilised. The Hasselblad installation on SL 1081 uses a fixed filter.

The estimated ground coverage and resolution of the two cameras for a single exposure at an altitude of 290 Km are shown in fig.3. Assumptions made include aperture f/8, apparent contrast of the subject reduced by a factor of 2 by atmospheric absorption and scatter, the area a flat plane and the film type as specified. The diagrams show the non-linear degradation in resolution between the nadir and the most oblique edge of the coverage: from 65 m to 160 m in the case of the F24 and from 118 m to 183 m for the Hasselblad. The estimated area coverage of the two cameras assuming 360° rotation of the payload at a height of 260 km is shown in fig.4.

5. TRIALS PREPARATION

Preparation of SL 1081 followed the normal practice for Skylark sounding rockets launched at Woomera under the British Science Research Council's programme. This involves prior shipment of rocket motors and other explosives by sea and a comprehensive payload assembly integration and test programme in the United Kingdom to prove the flight worthiness of the payload followed by partial dismantling for despatch by air. After arrival in Adelaide payloads are transported by road some 500 km to the Weapons Research Establishment at Woomera where re-assembly and re-testing is carried out. In the case of SL 1081 the payload was ready for flight within five days of arrival on the range.

Preparation for the sensor evaluation aspects of the trial was planned by the University of Reading, and carried out by them jointly with the South Australian Department of Mines and the Commonwealth Scientific and Industrial Research Organisation. This involved a preliminary reconnaissance of the ground coverage and the selection of test areas for the ground truth and low altitude tests. Four test areas of about 4 x 10 km were selected at Woomera, Mirakata, Tarcoola and Wilmington (see Fig.4) and within these areas sites of approximately 300 metres square were designated for highly detailed examination. During a period immediately prior to the launch of SL 1081 geological surveys of the test areas were prepared and about 107 of the small test sites within these areas were visited. These were surveyed for location, slope and aspect and reflectance readings at various wavelengths were taken. Surface details were recorded photographically and in writing and samples of rocks, soils and vegetation collected where appropriate. Aerial photographs from a helicopter using cameras and films comparable with those



Camera:	F24	Camera:	Hasselblad
Lens:	Ross E.M.I.127mm	Lens:	Zeiss Planar 80mm
Emulsion:	Kodak Plus X Aerographic 2648	Emulsion:	Kodak Aerochrome 2443

Resolution Values are in Metres Transversely (T) and Longitudinally (L)

FIGURE 3

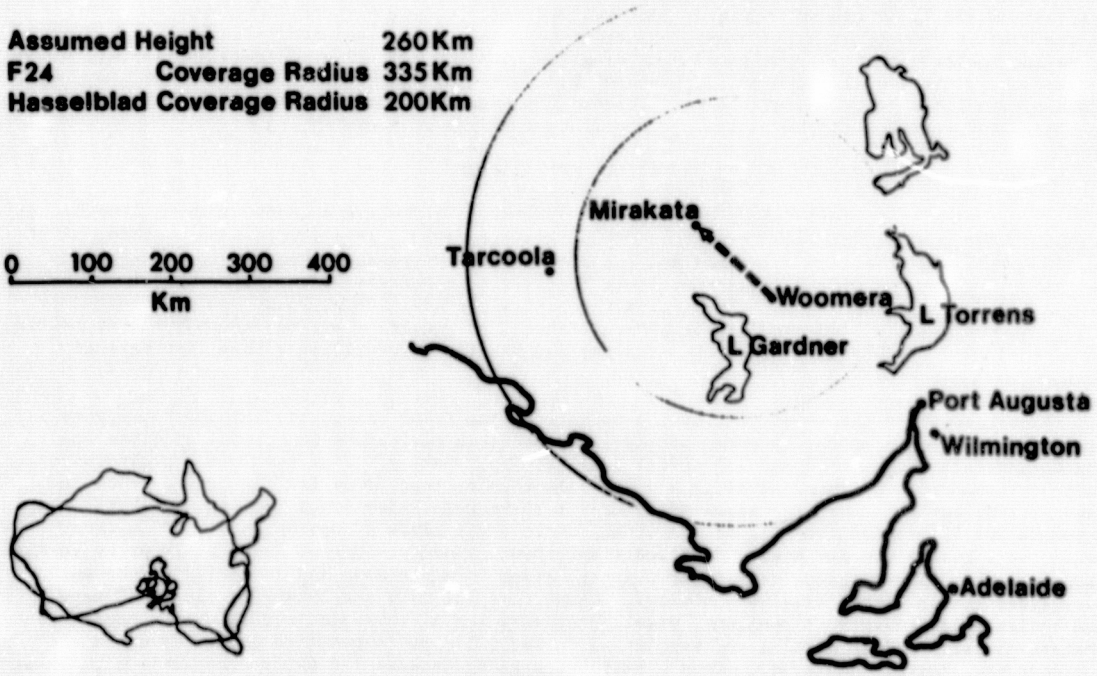


FIGURE 4

to be used in SL 1081 were also obtained just before the rocket firing. These cover the four test areas and were taken at heights of 800 and 6000 metres.

The specification for the actual flight trial called for launch early in the day with sun elevation between 35 and 55 degrees, good visibility and as little cloud as possible. Rapid recovery of the film magazines was considered essential with storage in a cool container to be effected immediately on removal from the camera bay.

6. FLIGHT SEQUENCE AND RECOVERY

Skylark SL 1081 was launched at Woomera at 09.00 hrs. Australian Central Time on 27th March 1972. The sequence of main events and resulting pattern of photographic coverage is illustrated diagramatically in fig.5. Weather conditions were good with less than ⅛ cloud over the whole coverage area.

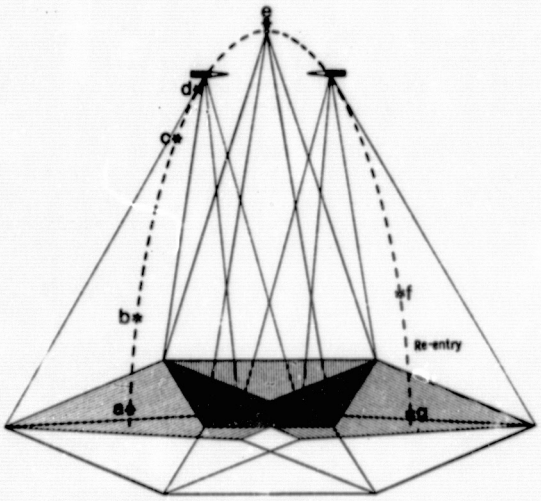
All operations took place as planned. Nineteen seconds after ignition of the Raven motor the roll rate control system was activated and maintained the rate of roll within the required limits during the remainder of the burn. The attitude control unit was programmed to stabilise the payload 103 seconds after payload/motor separation in order to preclude any possibility of losing photographic coverage at or near apogee due to any abnormal gas consumption in this prototype unit. In fact the system operated perfectly throughout the remaining trajectory. The cameras were started 212 seconds after launch at a height of 261 Km. Sixteen seconds later the payload rotated 60° and stabilised on the new heading, this manoeuvre taking 4 seconds. The sequence then repeated every 20 seconds. The first full 360° rotation was thus completed in 2 minutes during which period the payload tracked 45 Km and at the mid-point reached apogee at 278 Km. The camera shutters were controlled to operate as soon as the payload was stabilised on each heading and to repeat every 2½ seconds in the F24 and every 5 seconds in the Hasselblad. For one complete 360°manoeuvre this resulted in a total of 36 exposures by the F24 and 18 by the Hasselblad. Rotation of the payload and camera operation continued for a further 2 mins 50 seconds until the payload had descended to an estimated 60 Km. Re-entry took place with the attitude control system still maintaining a horizontal attitude until the recovery parachute deployed. Landing took place approximately 13 minutes after launch 150 Km down range and within 30 minutes the recovery team had located the payload which as indicated in fig.6 was almost undamaged. Two hours 45 minutes after launch the film magazines had been returned to refrigerated storage at the launching site.

7. RESULTS ANALYSIS

The results of the trial are considered in relation to the primary and secondary aims already mentioned. Analysis of the telemetry records and inspection of the recovered payload confirm that the primary, rocket proving, aspects of the trial have been satisfactorily accomplished . The only requirement for modification before the next flight in the programme is for an increase in the available torque in the roll rate control system. The attitude control system which must be considered the most important item undergoing trial has completely fulfilled the design aims. Stabilisation took place as programmed and all manoeuvres were carried out within the prescribed tolerances. The SL 1081 flight is therefore adjudged to be completely successful as a proving trial for the Skylark rocket as a remote sensing platform.

Evaluation of the photographic data obtained from the secondary, sensor proving aspects of the trial is still being carried out and it is therefore too early to assess the level of success achieved. However from the work done to date it seems that this part of the trial can not be considered entirely satisfactory. In terms of coverage the results are gratifying although the photographic overlay at nadir might prove inadequate. This would be rectified on future flights by adjustment of camera off-set angle. A typical example of the imagery obtained is shown in Fig.7.

The Commonwealth Scientific and Industrial Research Organisation (C.S.I.R.O) and Reading University are carrying out separate analysis programmes which differ in their aims and approach. Thus the C.S.I.R.O. programme aims to correlate spectral reflectance measurements taken at a number of levels with terrain types. The levels to be used include ground level, 800m and 6 km (helicopter), 180-270 km (SL 1081) and a 900 km (ERTS A). The basic aim of this work is to aid the interpretation of ERTS imagery. The Reading University programme has two phases. The first aims to produce land system mapping for the whole area coverage by applying normal visual recognition techniques to the SL 1081 imagery. The second phase is to carry out an accuracy assessment of this land system mapping, utilising the helicopter survey material and the results of pre-flight and post-flight ground truth sampling. Here the aim is the development of photographic analysis techniques most appropriate to the earth resource rocket.



a	2nd Stage Motor Ignition	6	
b	2nd Stage Motor Separation	60	
c	Attitude Control System On	162	
d	Cameras On	217	Sec
e	Apogee	272	
f	Cameras Off	502	
g	Parachutes Deployed	713	

FIGURE 5

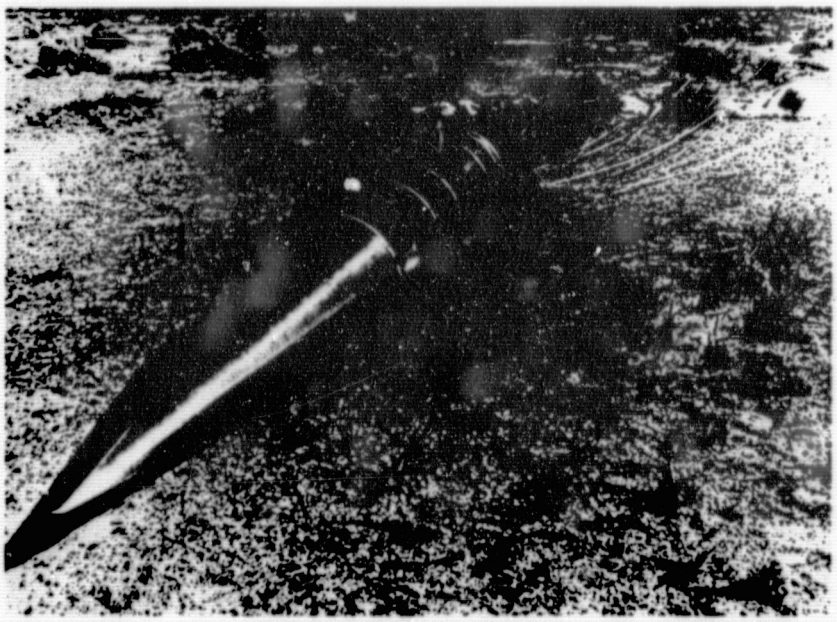


FIGURE 6

Progress on both of these programmes has been retarded by difficulties which have arisen in the production and distribution of processed imagery. In the case of C.S.I.R.O. the resolution values of copy photographs has been lower than expected and this together with the complications which are introduced by changing scale and obliquity have reduced the value of the imagery for the purpose of interpreting the ERTS data. Reading University, on the other hand, have already obtained some encouraging results particularly in land system mapping in the cultivated region near Ceduna which is situated near the most oblique limit of the F24 coverage (see Fig.7). On a visit to this area, land use for some 70 fields was established and typed as scrub, fallow, stubble and bare soil with the percentage content of each field noted. Then, using the data for 5 of the fields as control, the land use type and percentage for the remainder were estimated visually from the SL 1081 imagery. Standard deviations in the results of this exercise are 20 - 30%. For the land system mapping in the semi desert areas there are indications that correlation of the photographic data from the two cameras will prove productive. The degradation of resolution which has proved troublesome to C.S.I.R.O. is fortunately absent from the Reading University material and the work to date indicates that resolution on both types of film is in the order of 100m. It is expected that the SL 1081 sensor analysis programmes will be completed by the end of 1972.

8. DEVELOPMENT AND APPLICATION

Skylark 1081 is the first of a small number of earch resource rockets which have been designated for the development programme. The trial at Woomera has given proof that the rocket is a suitable vehicle from which to carry out remote sensing. The next requirement is to prove the techniques of rocket operations away from established rocket ranges and at the same time to develop further the sensor installations. In fulfilment of these aims a further firing is scheduled to take place under co-operative agreement between the British and Argentinian Governments in March 1973. The build standard of the rockets is very similar to that of SL 1081 with the addition of the motor recovery parachute. The camera installation will comprise one F24 and three Hasselblad units. Launch is planned to take place at Mercedes in the province of San Luis using a transportable single rail launcher and ancillary equipment designed to simplify launching and recovery procedures. The trajectory flown is expected to produce photographic data of particular interest in the agricultural sphere. The development of sensor installations optimised for rocket use in meeting the wide range of earth resource survey applications is a vital requirement. Progress on the SL 1081 imagery analysis will give added impetus to this work.

The application of the earth resource rocket in remote sensing operations will be determined by a comparison of the characteristics of this system with those of aircraft and satellites. Obviously each system has a unique combination of such characteristics and this lends weight to the assumption that they are complementary in terms of the total requirement. However circumstances have determined that the rocket is a late-comer in this field and for this reason alone its selection may, at first, only be made if aircraft and satellites are unable to meet a particular requirement. Such a situation appears almost inevitable. The combination of a requirement for synoptic sensing over large areas and a requirement for freedom of choice in timing is extremely likely when regional earth resource survey is needed in parts of the world having high probability cloud cover (see fig.8). The rocket alone has characteristics which meet this combination of requirements.

9. CONCLUSION

The flight of Skylark 1081 at Woomera achieved the primary objective of proving the earth resource rocket as a platform for remote sensing. The experimental camera installation operated satisfactorily, and photographic analysis is producing some commendable results. The next firing in the test programme is planned to take place in the Argentine and this will complete the development of the basic earth resource rocket. Refinement of the rocket/sensor combination will continue thereafter in accordance with user requirements.

Mt. Eba
Kingoonya
Tarcoola
Poochera
Streaky Bay
Ceduna
Penong
N
E
S
W

FIGURE 7

The Shaded Area indicates regions in which
the average annual Cloud Cover exceeds 40%

FIGURE 6

AUTHOR INDEX

Ahl, J. G., 23
Aldrich, R. C., 351
Allen, R. D., 157
Anderson, D. M., 1511
Atwell, B. H., 1491

Barnes, C. M., 677
Basharinov, A. E., 291
Bashilova, I. I., 1199
Bauer, M. E., 157
Baumgardner, M. F., 765
Beattie, B. S. E., 777
Beaver, G., 553
Benson, A. S., 1467
Bertram, C. L., 241
Bessis, J. L., 225
Binenko, V. I., 1297
Blansjaar, P. W. H., 229
Bonn, F., 709
Borgese, D., 1017
Boylan, M. G., 23
Bradford, R., 441
Brown, W. L., 563, 583
Brown, W. M., 1
Butler, R. W., 1093
Buznikov, A. A., 505
Byrne, R., 1311

Campbell, K. J., 241
Carey, R. L., 375
Carneggie, D. M., 1471
Chang, C. H., 1049
Chase, P., 569
Chelyshev, K. B., 279, 1083
Chernenko, A. P., 729, 1297
Cipra, J. E., 765
Clapp, J. L., 1429
Clément, P., 709
Clifton, J. W., 157
Coffeen, D. L., 515
Coiner, J. C., 1477
Collins, W. G., 103
Conitz, M. W., 99
Conrod, A., 569
Crane, R. B., 815
Cummings, R. E., 861

Dakshinamurti, C., 1327
DeGloria, S. D., 1471
DeRycke, R. J., 1069
Dinelli, G., 1017
Dornbach, J. E., 53
Draeger, W. C., 1467
Driscoll, R. S., 1259
Dunn, D. R., 311
Dyachenko, L. N., 1297

Eckhart, D., 229
Egan, W. G., 685
Egorov, S. T., 291
Eremin, V. K., 1199
Ericksen, G. E., 1523
Erickson, J. D., 157
Estes, J. E., 317, 1093

Falbel, G., 409
Felsher, M., 153
Fernandopullé, D., 1159
Ferriano, O. J., Jr., 1509
Frazee, C. J., 375
Friedman, E. J., 617
Fuller, C. E., 677

Gadbois, J. F., 709
Gallagher, J. L., 1287
Gatto, L. W., 1511
Geerders, P. J. F., 229
Ghovanlou, A. H., 617
Gill, J. H., 765
Gordon, M., 833
Gorodezky, A. K., 291
Grigoryev, A. A., 463, 729
Gryc, G., 1209
Gurvitch, A. S., 291
Gusev, N. A., 1147

Halajian, J., 523
Hallock, H., 523
Hallum, C. R., 951
Hansen, J. E., 515
Harries, J. E., 475
Harris, J. B., 53
Haugen, R. K., 1511
Hayden, J., 553
Hebard, F., 1121
Heinemann, L. R., 47
Helbig, H. S., 959
Henry, H. R., 21
Hickman, G. D., 617
Hodder, D. T., 999, 1017
Hogg, J. E., 617
Holtzman, J., 1279
Horwitz, H., 833
Hsu, S., 1195
Hyde, P. D., 935

Imhoff, E., 569

Jalbert, C., 709
James, G. W., 1477
Jones, H. G., 677

Karizhenski, E. J., 1147
Kedar, E. Y., 1195
Kelly, M., 969
Kennedy, E. E., 677
Kiefer, R. W., 1429
Kihlblom, U., 755
Knepper, D. H., Jr., 1127
Kondratyev, K. Y., 505, 1297
Kriegler, F. J., 833
Krishen, K., 1105
Kristof, S. J., 765
Kurskaya, A. A., 291
Kutuza, B. G., 291

Lajeunesse, M., 709
LaMoreaux, P. E., 21
Landgrebe, D. A., 157
Lathram, E. H., 1209
Leese, J., 441
Lewis, L. V., 983
Lindgren, D. T., 299
Lins, H. F., Jr., 325
Lipatov, V. B., 463, 729
Loshchilov, V. S., 279, 1083
Lundholm, B., 191

MacDonald, R. B., 157
Magnuson, L. M., 1477
Makhin, G. V., 1199
Malila, W. A., 639
Mallon, H. J., 61
Marrs, R. W., 1127
Marshall, R. E., 833
Marzolf, G. R., 1477
Matveev, D. T., 291
Maughan, P. M., 1491
McCarthy, M. M., 1385, 1429
McCauley, J. R., 1477
McCue, G. A., 999
McDonough, G., 21
McGinnis, D. F., 231
McKim, H. L., 1511
McKimmy, J. R., 563
Melentyev, V. V., 217
Milazzo. V. A., 325
Miller, L. D., 1355
Moe, R., 1279
Mokma, D. L., 23
Moore, D. G., 715
Moore, R. K., 1279
Morgenstern, J. P., 881
Morrison, D. R., 677
Mower, R. D., 789
Munday, J. C., Jr., 1311
Myers, V. I., 47, 715
Myers, W. L., 23

Nalekpa, R. F., 881, 935
Nichols, M., 969
Niemann, B. J., Jr., 1429
Novak, C., 441

Offield, T. W., 1237
Oliver, R. E., 1333
Olson, C. E., Jr., 1381
Orlov, A. P., 291
Orlov, V. M., 505
Osterhoudt, F. H., 297

Paludan, C. T. N., 345
Paris, J. F., 665
Parrini, F., 1017
Passerello, J. B., 7
Pearson, R. L., 1355
Peck, E. L., 747
Phillips, D. M., 983
Pohn, H. A., 1237
Polcyn, F. C., 541, 563, 583
Poulton, C. E., 393
Prewett, O. E., 563

Rabinovich, Y. I., 217
Raina, B. N., 1213
Reimold, R. J., 1287
Richardson, A. J., 1249
Richardson, W., 815
Rose, G. C., 261
Rudzki, J. E., Jr., 487
Ryerson, J. M., 1093
Ryland, D. W., 553, 603

Sadowski, F. G., 351
Sandler, S. S., 241
Sattinger, I. J., 23
Schaerer, G., 739
Schanda, E., 739
Schar, S. W., 23
Scherz, J. P., 35
Schmer, F. A., 553, 603
Schneider, H. J., 677
Schumann, H., 3
Schwartz, D. E., 7
Senger, L. W., 317
Sevastyanov, V. I., 505
Seyhan, M. E., 229
Sharma, R. D., 137
Shaw, E., 1497
Shilin, B. V., 1147
Shutko, A. M., 291
Sidran, M., 1121
Simpson, R. B., 299
Smith, J. A., 1333
Smotky, O. I., 505
Spencer, M. M., 895, 1259
Steller, D. D., 983, 1017
Stevenson, W. H., 1491
Stewart, S. R., 583
Stoertz, G. E., 1523
Strome, W. M., 1497
Strong, A. E., 1069
Stumpf, H., 1069
Su, M. Y., 861
Summanwar, A. S., 1327
Swain, P. H., 765

Taranik, J. V., 11
Tarrant, J. R., 1425
Thaman, R. R., 1093
Thompson, D. E., 1287
Thomson, F. J., 351
Tipton, M. J., 553
Torline, R. J., 1249
Triendl, E. E., 771
Trudel, C., 709
Turner, R. E., 895
Tuthill, S. J., 11
Tzschupke, W., 959

Ulaby, F. T., 1279

van Genderen, J. L., 117
Van Kuilenburg, J., 229
Vasilyev, O. B., 505
Vavilov, E. I., 1147
Vickers, R. S., 261
Vincent, R. K., 1239
Vinogradov, B. V., 463, 729
Vlasin, R. D., 23
Vogel, M., 199

Wacker, A. G., 851
Wagner, T. W., 639
Walker, A. S., 1137
Waltz, F. A., 47, 603
Waters, J. W., 467
Watson, K., 1237
Weber, F. P., 351
Welch, R., 1411
Westin, F. C., 375
Wezernak, C. T., 541
Wiegand, C. L., 1249
Wiesnet, D. R., 747
Williams, R. S., Jr., 1159
Winikka, C., 3
Wüthrich, M., 739

Yarger, H. L., 1477
Young, L. A., 1049
Yuill, R. S., 299

Zagorodnikov, A. A., 279, 1083

789